BJR

THE BRITISH JOURNAL OF RADIOLOGY

Volume 65 Number 774 June 1992

CUK-H06084-29-P25863.

29

ray Diagnosis • Ultrasound • Interventional Radiology
Radiotherapy • Oncology • Hyperthermia
Nuclear Medicine • Nuclear Magnetic Resonance
adiation Physics • Radiobiology • Radiation Protection

JR is published by The British Institute of Radiology BIR

"IS THERE A WAY TO VERIFY PATIENT DOSAGE DELIVERED DURING RADIATION THERAPY...ACCURATELY, RELIABLY AND INSTANTANEOUSLY?"

THERE IS WHEN YOU USE THE NUCLEAR ASSOCIATES' RAINBOW PATIENT DOSE VERIFICATION SYSTEM.

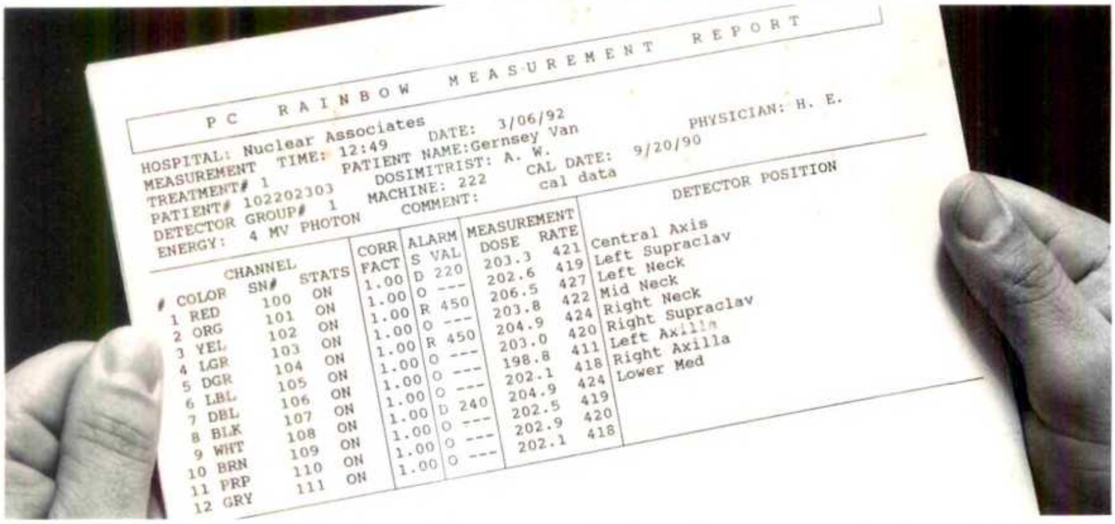

```
P C   R A I N B O W   M E A S U R E M E N T   R E P O R T

HOSPITAL: Nuclear Associates      DATE:  3/06/92
MEASUREMENT  TIME: 12:49    PATIENT NAME:Gernsey Van      PHYSICIAN: H. E.
TREATMENT# 1              DOSIMITRIST: A. W.
PATIENT# 102202303        MACHINE: 222       CAL DATE:  9/20/90
DETECTOR GROUP#  1          COMMENT:           cal data
ENERGY:   4 MV PHOTON
                         CORR|ALARM|MEASUREMENT |    DETECTOR POSITION
      CHANNEL            FACT|S VAL| DOSE   RATE|
# COLOR  SN#   STATS     1.00|D 220| 203.3   421|Central Axis
 1 RED   100    ON       1.00|O ---| 202.6   419|Left Supraclav
 2 ORG   101    ON       1.00|R 450| 206.5   427|Left Neck
 3 YEL   102    ON       1.00|O ---| 203.8   422|Mid Neck
 4 LGR   103    ON       1.00|R 450| 204.9   424|Right Neck
 5 DGR   104    ON       1.00|O ---| 203.0   420|Right Supraclav
 6 LBL   105    ON       1.00|O ---| 198.8   411|Left Axilla
 7 DBL   106    ON       1.00|O ---| 202.1   418|Right Axilla
 8 BLK   107    ON       1.00|D 240| 204.9   424|Lower Med
 9 WHT   108    ON       1.00|O ---| 202.5   419|
10 BRN   109    ON       1.00|O ---| 202.9   420|
11 PRP   110    ON       1.00|O ---| 202.1   418|
12 GRY   111    ON
```

We call it the PC-RAINBOW. You'll call it great! The PC-RAINBOW System uses an IBM™ PC computer (or equivalent) and ties it to the proven strengths of Nuclear Associates' diode dosimetry systems. Results: Patient dose monitoring and QC beam analysis in radiation therapy, performed easily, accurately and reliably — across a wide range of treatment modalities — with up to 12 detector channels.

PC-RAINBOW consist of a high-speed, microprocessor-controlled electrometer mounted on a "goes anywhere" mobile stand. Controller software for an IBM PC compatible computer and a 30-meter interface cable complete the system. And when it comes to the features, PC-RAINBOW:

- Provides up to 12 detector channels plus a trigger channel for maximum measurement verification.
- Alerts the operator to possible dose misadministration.
- Provides for storage of calibration factors for up to 20 sets of 12 diodes.
- Lets you apply individual correction factors to any or all diodes at the time of measurement.
- Is suitable for whole body treatment at dose rates below 5 rads/min.
- Has user-selectable alarms for any combination or number of channels.
- Allows you to store patient exposure data on floppy disk, or print out on any PC-compatible printer.

So when you're looking for the way to verify patient dosage accurately, and reliably, look to the PC-RAINBOW System from Nuclear Associates.

IBM™, International Business Machines, Inc.

And for more information, request Bulletin 4451-14

NUCLEAR ASSOCIATES

VICTOREEN

Division of VICTOREEN, INC.
100 VOICE ROAD • P.O. BOX 349
CARLE PLACE, NY 11514-0349
(516) 741-6360 • FAX (516) 741-5414

I 25 263

BJR THE BRITISH JOURNAL OF RADIOLOGY
Established 1896

The Editorial Board
Honorary Editors
D. G. Shaw, FRCP, FRCR
F. A. Duck, BSc, MSc, PhD

Deputy Editors
C. K. Bomford, BSc, MPhil, FInstP
D. M. King, MB, BS, FRCR, DMRD
D. M. Tait, MB, ChB, MRCP, FRCR
J. W. Hopewell, BSc, PhD

Associate Editors
H. Baddeley, MB, BS, DMRD, FRCR, MRACR
R. Beaney, BSc, MB, ChB, MD, MRCP, FRCR
J. B. Bingham, MA, MRCP, MSc, FRCR
P. R. Blake, MD, MB, BS, BSc, FRCR
D. J. Cole, MB, BS, MRCP, FRCR
D. R. Dance, MA, PhD, FIPSM
A. M. Davies, MB, ChB, DMRD, FRCR
P. Dawson, BSc, PhD, MB, BS, MRCP, MInstP, FRCR
A. H. Freeman, MB, BS, FRCR
J. Glaholm, BSc, MRCP, FRCR
R. M. Harrison, BSc, MSc, PhD, FInstP
D. Hirst, BSc, PhD
H. C. Irving, MB, BS, DMRD, FRCR
P. C. Jackson, BSc, PhD, FInstP, CPhys, FIPSM
B. Karani, FRCR
A. M. Peters, BSc, MSc, MB, ChB, MD, MRCPath
D. W. Pilling, MB, ChB, DCH, DMRD, FRCR
J. F. Reidy, MB, BS, FRCP, FRCR
M. B. Rubens, MB, BS, LRCP, MRCS, DMR, FRCR
R. A. Shields, PhD
P. J. Shorvon, MB, BS, MRCP, FRCR
J. Tudor, MB, BS, FRCR
A. R. Valentine, MB, BS, MRCS, LRCP, FRCR, DMRD
J. Virjee, MB, ChB, FRCR
T. E. Wheldon, BSc, PhD, FInstP
G. H. Whitehouse, MB, BS, FRCP, FRCR, DMRD

Associate Editors Overseas
S. G. A. Chenery, PhD, FCCPM (North America)
B. J. Cremin, MD, FRCR, FRACR (South Africa)
R. Fox, DPhil (Australia)
M. Takahashi, MD (Japan)

Managing Editor: T. R. Hogan, BSc, PhD

The British Journal of Radiology is published monthly by the British Institute of Radiology, 36 Portland Place, London W1N 4AT. Telephone 071-580 4189 (editorial); Facsimile 071-255 3209. Editorial communications should be addressed to the Honorary Editors in accordance with the Instructions to Authors published in the January issue each year, copies of which may be obtained from the Managing Editor upon request.

Advertisements. Communications should be addressed to the Advertising Manager at the above address. Tel. 071-631 1168.

Subscriptions. The monthly fulfilment is carried out by BJR Subscriptions, PO Box 500, Leicester LE99 0AA, UK. Telephone 0858 410510; Facsimile 0858 434190.

The 1992 annual subscription to *The British Journal of Radiology* is £152 for EEC (incl. UK) readers and £167 for readers in the rest of the world.

These prices include delivery by sea mail; airmail rates are £10 extra for Europe and £30 extra for the rest of the world, effective from March 1992. Copies of this journal sent to subscribers in Bangladesh, Canada, India, Japan, Pakistan, Sri Lanka and USA are air-speeded for quicker delivery at no extra cost. Subscriptions are on a calendar year basis only.

Back issues prior to the current volume can be ordered from the British Institute of Radiology at the address above.

US mailing agents: Mercury Airfreight International Ltd Inc. Second class postage paid at Rahway, NJ, USA. Postmaster: send address corrections to The British Journal of Radiology, c/o Mercury Airfreight International Ltd Inc., 2323 Randolph Avenue, Avenel, NJ 07001, USA.

THE BRITISH INSTITUTE OF RADIOLOGY
BIR

Founded 1897
Incorporated by Royal Charter
Patron: Her Majesty The Queen

The British Institute of Radiology is an association of persons interested in radiology and allied subjects. Meetings are held monthly from October until May. Particulars of membership and other information may be obtained on application to the General Secretary at the Institute, 36 Portland Place, London W1N 4AT. The British Institute of Radiology is a registered charity, no. 215869.
Telephone: 071-580 4085 and 071-580 4189
Fax: 071-255 3209.

President
S. C. Lillicrap, DSc, PhD, FInstP, FIPSM
Honorary Secretaries:
N. W. Garvie, MAMB, BChir, MRCP, DMRD, FRCR, MSc
M. P. Law, BSc, PhD
Honorary Treasurer
D. S. McIntosh, BSc, PhD, MRPharmS, MRSC, MIMC
General Secretary
Mary-Anne Piggott, BSc, MBA, MBIM

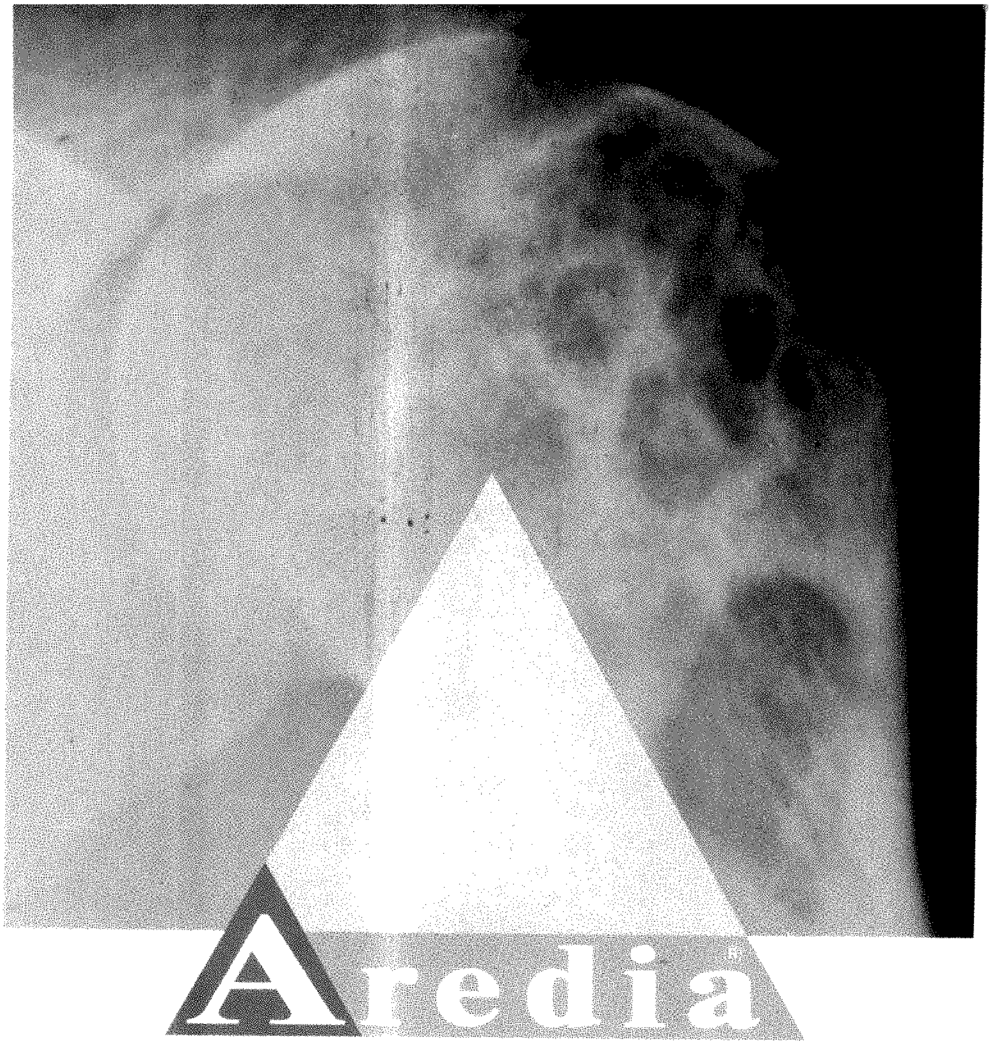

pamidronate disodium

for the treatment of tumour-induced hypercalcaemia

- **Reliable response**
  "Calcium concentration fell in all patients [n=30] and was restored to normal in all but two"[1]
- **Sustained effectiveness**
  Normocalcaemia maintained for an average of 3 weeks[1]
- **Well tolerated**
  Reported side-effects not of clinical relevance[1,2]
- **Effective as a single infusion**

Ciba

Prescribing Notes Aredia® (pamidronate disodium) **Presentation** Ampoules of 5ml aqueous injectable concentrate containing 15mg pamidronate disodium (calculated as the anhydrous form) for intravenous infusion. **Indication** Tumour-induced hypercalcaemia. **Dosage** Adults and elderly : Depending on the initial calcium plasma level, 15-90mg by slow intravenous infusion in sodium chloride 0.9%. Infusion rate should not exceed 30mg/2hrs, and concentration should not exceed 30mg/250ml. Total dose can be given either as a single i.v. infusion or divided over 2-4 consecutive days. Rehydration with normal saline before treatment is recommended. Not recommended for children. See full prescribing information. **Contraindications** Known hypersensitivity to pamidronate disodium or other bisphosphonates. **Precautions** Monitor clinical and biochemical effects. Do not administer as a bolus injection. Do not co-administer with other bisphosphonates, plicamycin (mithramycin) or calcium containing infusion solutions. Caution in patients with severe renal insufficiency (multiple dosing recommended); haemodialysis; pregnancy. Theoretical interference with bone scintigraphy examinations. **Side-effects** Asymptomatic hypocalcaemia and transient pyrexia. Occasionally transient lymphocytopenia and hypomagnesaemia. Less frequently reactions at infusion sites and gastrointestinal effects. For further information see full prescribing information. **Packs** Ampoules 15mg/5ml (PL0001/0138) in packs of 4, basic NHS price £96.62. ® denotes registered trademark. Full prescribing information is available on request from Ciba Laboratories, Horsham, West Sussex RH12 4AB. **References :** 1. Morton AR, et al. Single Dose Versus Daily Intravenous Aminohydroxypropylidene Bisphosphonate (ADP) for the Hypercalcaemia of Malignancy. Br Med J 1988; 296: 811-814. 2. Ralston SH, et al. Treatment of Cancer Associated Hypercalcaemia with Combined Aminohydroxypropylidene Diphosphonate and Calcitonin. Br Med J 1986; 292: 1549-1550.

VOL 65 NO 774 JUNE 1992

The British Journal of Radiology
Contents

Page

Editorial 469

Papers

Increasing patient throughput in magnetic resonance imaging: a practical approach 470
N. R. Moore and S. J. Golding

Radiological features during and following treatment of spinal tuberculosis 476
D. I. Boxer, C. Pratt, A. L. Hine and M. McNicol

The musculoskeletal manifestations of epidermolysis bullosa: an analysis of 19 cases with a review of the literature 480
W. L. Wong and J. Pemberton

Intramuscular myxoma: magnetic resonance features 485
A. F. Abdelwahab, S. Kenan, G. Hermann, M. M. Lewis and M. J. Klein

Scintigraphic abnormalities in patients with painful hip replacements treated conservatively 491
K. A. Miles, W. M. Harper, D. B. L. Finlay and I. Belton

Magnetic resonance imaging of pulsatile cerebrospinal fluid flow by spatial modulation of magnetization 495
S. C. Wayte, T. W. Redpath and D. J. Beale

The value of magnetic resonance relaxation time in staging ovarian endometrial cysts 502
K. Sugimura, M. Takemori, M. Sugiura, H. Okizuka, M. Kono and T. Ishida

Audit in action: significant reduction of double-contrast barium enema screening time with no loss of examination quality 507
D. Horton, A. M. Cook and A. D. Taylor

Radiotherapy to the surviving kidney after unilateral nephrectomy in bilateral Wilms' tumour 510
P. Kirkbride and P. N. Plowman

Output factors for blocked fields 517
E. M. Dean and J. B. Davis

The application of microdosimetry in clinical bone densitometry using a dual-photon absorptiometer 523
A. J. Waker, B. Oldroyd and M. Marco

A preliminary investigation of the imaging performance of photostimulable phosphor computed radiography using a new design of mammographic quality control test object 528
A. R. Cowen, D. S. Brettle, N. J. Coleman and G. J. S. Parkin

Technical notes

A manual afterloading technique for the treatment of patients with bronchial carcinoma using iridium-192 wire 536
A. J. Vinall and P. J. Mulvey

Technique for steel coil embolization of biopsy track for use with the "Biopty" needle 538
P. Dawson, A. Adam and R. Edwards

Case reports

Splenic cyst: demonstration of the relationship between subcapsular haematoma and false cyst by imaging 541
O. Dourthe, P. Maquin, B. Pradere and J.-J. Railhac

Juxtaglomerular cell tumour of the kidney as cause of hypertension: a case report 542
J. C. van den Berg, A. R. M. M. Hermus and G. R. Rosenbusch

Contrast extravasation from a Pulse-Tec graft: a complication of high-dose recombinant tissue-type plasminogen activator therapy 545
T. M. Buckenham, R. S. Taylor, D. Reiff and J. E. Page

Pancreatic metastasis from renal cell carcinoma 547
F. Rypens, D. Van Gansbeke, J. P. Lambilliotte, G. Van Regemorter, A. Verhest and J. Struyven

Case of the month

Contralateral thinking 549
S. Mehta and R. Whitehouse

Erratum 551
R. Miettunen

Correspondence

Radiation protection associated with well women breast cancer screening 552
B. M. Moores and E. T. Henshaw

Mistaken hilar mass 553
F. W. Wright

Author's reply 553
R. J. Thomas

Results from the HAD psychometric questionnaire in 54 breast cancer patients treated with breast conservation 553
A. S. Bulman

Author's reply 554
A. R. Bull

Measurement of tissue perfusion by dynamic computed tomography 554
S. Rees

Author's reply 555
K. A. Miles

Mesenteric lymphadenopathy in idiopathic retroperitoneal fibrosis 555
F. Pombo, J. Pérez-Fontán and E. Rodriguez

Now you see it . . . now you don't 556
D. Kessel and P. E. Bearn

BIR Bulletin *facing page* 556

© 1992 The British Institute of Radiology. This publication is copyright under the Berne Convention and the Universal Copyright Convention. All rights reserved, apart from any relaxations permitted under national copyright laws, no part of this publication may be reproduced, stored in a retrieval system or transmitted in any form or by any means without the prior permission of the copyright owners. Permission is not, however, required to copy abstracts of papers or of articles on condition that a full reference to the source is shown. Multiple copying of the contents of the publication without permission is always illegal. Published by The British Institute of Radiology, 36 Portland Place, London W1N 4AT. Origination by BPCC Whitefriars Ltd, Tunbridge Wells, and printed and bound in Great Britain by BPCC Wheatons Ltd, Exeter.
ISSN 0007 1285

VOL 65 NO 775 JULY 1992

The British Journal of Radiology

Contents

Page

Foreword iv

Papers

A comparison of ultrasound exposure in therapy and pulsed Doppler fields 557
H. C. Starritt and F. A. Duck

Routine radiographer screening for fetal abnormalities by ultrasound in an unselected low risk population 564
I. M. Shirley, F. Bottomley and V. P. Robinson

A study of the relationship between routine ultrasound quality assurance parameters and subjective operator image assessment 570
S. C. Metcalfe and J. A. Evans

A role for ultrasound in limb lengthening 576
N. D. J. Derbyshire and A. H. R. W. Simpson

An audit of ultrasound diagnosis of gallbladder calculi 581
J. Walker, R. T. A. Chalmers and P. L. Allan

The ultrasound appearances of intramural bowel gas: the bright ring appearance and the effervescent bowel. A report of three cases 585
R. A. Bloom, E. Craciun, P. D. Lebensart, P. Levy and J. Bar Ziv

The value of ultrasound in the assessment of bone 589
G. M. Steiner and A. Sprigg

Conventional 15 G needle technique for renal biopsy compared with ultrasound-guided spring-loaded 18 G needle biopsy 594
N. J. A. Cozens, J. T. Murchison, P. L. Allan and R. J. Winney

Case reports

Two cases of isolated deficiency of all four limbs diagnosed antenatally with a review of the literature 598
W. L. Wong, O. Clarke, J. Bhattacharya and L. M. MacDonald

Ultrasound demonstration of a leaking hydatid cyst of the liver causing "cyst within a cyst" appearance 604
B. Banerjee, A. Rennison and Q. M. Haque

The thread and streak sign of portal vein tumour thrombus demonstrated by colour Doppler imaging 607
K. McBride and J. Masterson

Prenatal ultrasonographic diagnosis of an aneurysm of the vein of Galen 609
L. Worswick, R. F. Lamont, R. Thomas and H. Gordon

Epitheloid haemangioendothelioma of liver: a vascular tumour easily mistaken for metastatic carcinoma on ultrasound imaging 611
B. Banerjee and A. Rennison

Proceedings

Proceedings of the British Medical Ultrasound Society 23rd Annual Meeting (Abstracts) 614

BIR Bulletin *facing page* 648

© 1992 The British Institute of Radiology. This publication is copyright under the Berne Convention and the Universal Copyright Convention. All rights reserved, apart from any relaxations permitted under national copyright laws, no part of this publication may be reproduced, stored in a retrieval system or transmitted in any form or by any means without the prior permission of the copyright owners. Permission is not, however, required to copy abstracts of papers or of articles on condition that a full reference to the source is shown. Multiple copying of the contents of the publication without permission is always illegal. Published by The British Institute of Radiology, 36 Portland Place, London W1N 4AT. Origination by BPCC Whitefriars Ltd, Tunbridge Wells, and printed and bound in Great Britain by BPCC Wheatons Ltd, Exeter.

ISSN 0007 1285

Foreword

Every year the BJR has published the abstracts of all the papers accepted for presentation at the Annual Scientific Meeting of the British Medical Ultrasound Society.

It has been pleasing to see the quality and breadth of these papers improving year by year and Council of BMUS has recently been anxious to encourage the authors of these papers to submit them for publication in a well respected refereed journal. We were delighted when the editors of the BJR agreed to accept BMUS derived papers for consideration and in 1991 all authors whose papers were accepted for presentation at the annual BMUS meeting were invited to offer full manuscripts of their papers.

In this issue of the BJR are included all those papers which, after the normal refereeing process, were accepted for publication. BMUS is very grateful to the editorial staff of the BJR who have seen these papers through so quickly and efficiently.

We hope that this new venture will be found useful and instructive, that larger numbers of future BMUS authors will be encouraged to offer their papers for consideration and that this special ultrasound issue will become a regular feature and will grow in value and stature.

Hylton B Meire (President of BMUS)

VOL 65 NO 776 AUGUST 1992

The British Journal of Radiology
Contents

Page

Papers

Use of ultrasound in osteomyelitis 649
A. K. Nath and A. U. Sethu

Direct and CT measurements of canals and foramina of the skull base 653
A. Berlis, R. Putz and M. Schumacher

Subluxation of the patella: evaluation of patellar articular cartilage with MR imaging 662
K. Nakanishi, M. Inoue, K. Harada, J. Ikezoe, T. Murakami, H. Nakamura and T. Kozuka

What is the clinical disadvantage of discarding old radiographs? Survey of patients not re-examined for a long time 668
Y. Oyama, K. Imamura, H. Ashida, Y. Nakajima, T. Itoh, M. Saeki, Y. Kikuchi, H. Matsumoto and T. Ishikawa

Intracardiac metastases from germ cell tumours—an unusual but important site of metastasis 672
D. Pickuth, R. Eeles, M. Mason, C. Pumphrey, P. Goldstraw and A. Horwich

The radiology and terminology of cryptogenic organizing pneumonia 674
J. A. A. Haddock and D. M. Hansell

The radiological imaging of bronchial atresia 681
D. Kinsella, G. Sissons and M. P. Williams

An alternative approach to contrast-detail testing of X-ray image intensifier systems 686
C. J. Kotre, N. W. Marshall and K. Faulkner

Accelerated fast neutron therapy: a pilot study 691
D. J. Husband, R. D. Errington, S. Myint, J. A. H. Littler and H. M. Warenius

Low oxygen extraction fraction in tumours measured with the oxygen-15 steady state technique: effect of tissue heterogeneity 697
A. A. Lammertsma and T. Jones

Image comparison techniques for use with megavoltage imaging systems 701
P. M. Evans, J. Q. Gildersleve, E. J. Morton, W. Swindell, R. Coles, M. Ferraro, C. Rawlings, Z. R. Xiao and J. Dyer

Asymptomatic temporal lobe injury after radiotherapy for nasopharyngeal carcinoma: incidence and determinants 710
S. F. Leung, L. Kreel and S. Y. Tsao

Technical notes

Anal endosonography: which endoprobe? 715
M. Papachrysostomou, S. D. Pye, S. R. Wild and A. N. Smith

Virtual source distances and field geometry independent output factors for 5–14 MeV electron beams from a Siemens Mevatron M7145 717
J. H. Plane and M. M. Trevor

Case reports

Gadolinium-DTPA enhanced MRI in neonatal osteomyelitis of the cervical spine 720
A. Martijn, A. M. van der Vliet, W. M. van Waarde and W. M. C. van Aalderen

Patellar metastasis: a rare presentation 722
R. K. Sur, D. P. Singh, M. S. Dhillon, B. D. Gupta, D. Murali and R. Sidhu

Renal ultrasonographic appearances at presentation in an infant with Lesch–Nyhan syndrome 724
C. N. Ludman, C. Dicks-Mireaux and A. J. Saunders

Small cell carcinoma of the prostate 726
J. Sule-Suso and A. M. Brunt

Case of the month

A rare cause of a common symptom 729
P. J. Close and P. L. Monks

Correspondence

Spontaneous disappearance of staghorn calculus 731
L. Sheppard

Author's reply 731
D. S. Grant

Radiation damage to mouse skin and oesophagus 731
A. Michalowski

Proceedings

Proceedings of the British Institute of Radiology
The new legislation—friend or foe (after the White Paper and into Europe), 13 June 1991 733

Book reviews

Introduction to Radiobiology. *M. Tubiana, J. Dutreix and A. Wambersie* 736
The Visible Human Body: An Atlas of Sectional Anatomy. *G. Von Hagens, L. J. Romrell, M. H. Ross and K. Tiedemann* 736
Easily Missed Fractures and Corner Signs in Radiology. *H. O. Riddervold* 736

BIR Bulletin *facing page* 736

© 1992 The British Institute of Radiology. This publication is copyright under the Berne Convention and the Universal Copyright Convention. All rights reserved, apart from any relaxations permitted under national copyright laws, no part of this publication may be reproduced, stored in a retrieval system or transmitted in any form or by any means without the prior permission of the copyright owners. Permission is not, however, required to copy abstracts of papers or of articles on condition that a full reference to the source is shown. Multiple copying of the contents of the publication without permission is always illegal. Published by The British Institute of Radiology, 36 Portland Place, London W1N 4AT. Origination by BPCC Whitefriars Ltd, Tunbridge Wells, and printed and bound in Great Britain by BPCC Wheatons Ltd, Exeter.
ISSN 0007 1285

VOL 65 NO 777 SEPTEMBER 1992

The British Journal of Radiology

Contents

Page

Invited Review

Permanent radiation myelopathy 737
T. E. Schultheiss and L. C. Stephens

Papers

Primary choroid plexus papilloma of the cerebellopontine angle: magnetic resonance imaging, computed tomographic and angiographic appearances 754
A. Jackson, B. J. Panizza, D. Hughes and H. Reid

How frequent is chronic lumbar arachnoiditis following intrathecal Myodil? 758
D. G. Hughes and I. Isherwood

The prognostic importance of CT features in primary intracranial lymphoma 761
J. Namasivayam and E. Teasdale

Transverse geniculate ligament of the knee: appearance and frequency on plain radiographs 766
S. A. Sintzoff Jr, B. Stallenberg, I. Gillard, P. A. Gevenois, C. Matos and J. Struyven

Macrodystrophia lipomatosa: radiographic observations 769
S. K. Gupta, O. P. Sharma, S. V. Sharma, B. Sood and S. Gupta

Fatty infiltration of the liver: analysis of prevalence, radiological and clinical features and influence on patient management 774
A. Y. El-Hassan, E. M. Ibrahim, F. A. Al-Mulhim, A. A. Nabhan and M. Y. Chammas

Accuracy of ultrasound and oral cholecystography in assessing the number and size of gallstones: implications for non-surgical therapy 779
K. Brakel, J. S. Laméris, H. G. T. Nijs, A. Z. Ginai and O. T. Terpstra

The optimum pressure of oxygen for radiotherapy of a mouse tumour 784
P. M. Perry and A. H. W. Nias

Treatment planning for ^{131}I-mIBG radiotherapy of neural crest tumours using ^{124}I-mIBG positron emission tomography 787
R. J. Ott, D. Tait, M. A. Flower, J. W. Babich and R. M. Lambrecht

A pilot study of accelerated fractionation in the radiotherapy of invasive carcinoma of the bladder 792
D. J. Cole, K. R. Durrant, J. T. Roberts, P. J. T. K. Dawes, H. Yosef and J. W. Hopewell

An investigation into the effect of protective devices on the dose to radiosensitive organs in the head and neck 799
N. W. Marshall, K. Faulkner and P. Clarke

Evaluation of skeletal metastases 803
M. V. Merrick, J. S. M. Beales, N. Garvie and R. C. O. Leonard

Errors due to non-uniform distribution of fat in dual X-ray absorptiometry of the lumbar spine 807
P. Tothill and D. W. Pye

Technical notes

An afterloading technique utilizing The Royal London Hospital caesium-137 brain needle in an oral obturator 814
A. M. Tierney and B. S. Mantell

A flexion and extension device for dynamic MR imaging of the neck 816
D. M. Hadley, B. R. Condon and W. Richardson

Digital cardiac imaging—the death knell of cineangiography? 818
J. F. Dyet, W. Hartley, A. R. Cowen and C. P. Aber

Case reports

Tuberculosis of the ribs: computed tomographic findings 822
R. FitzGerald and C. E. Hutchinson

External carotid angioplasty in the treatment of developing stroke 825
A. H. Troughton, R. A. Morgan, R. M. Paxton and I. P. Wells

Osteosarcoma metastatic to the kidney with invasion of the inferior vena cava 827
C. M. P. King, R. H. Reznek, A. J. Norton and J. E. Kingston

Case of the month

The third dimension 831
A. D. King and A. L. Hine

Short communications

Radiation-induced hearing impairment—a pilot study in patients treated for malignant parotid tumours 833
P. Kirkbride, F.-F. Liu and M. K. Wax

Historical experiments predating commercially available computed tomography 835
S. Webb

Erratum 838
M. R. Gandhi, P. Brown, C. A. J. Romanowski, S. K. Morcos, S. Campbell, A. M. El Nahas and T. A. Gray

Proceedings

Proceedings of the British Institute of Radiology. Progress in MRI: scientific and clinical developments in the United Kingdom, 14 October 1991 839

BIR Bulletin *facing page* 844

© 1992 The British Institute of Radiology. This publication is copyright under the Berne Convention and the Universal Copyright Convention. All rights reserved, apart from any relaxations permitted under national copyright laws, no part of this publication may be reproduced, stored in a retrieval system or transmitted in any form or by any means without the prior permission of the copyright owners. Permission is not, however, required to copy abstracts of papers or of articles on condition that a full reference to the source is shown. Multiple copying of the contents of the publication without permission is always illegal. Published by The British Institute of Radiology, 36 Portland Place, London W1N 4AT. Origination by BPCC Whitefriars Ltd, Tunbridge Wells, and printed and bound in Great Britain by BPCC Wheatons Ltd, Exeter.
ISSN 0007 1285

1992, *The British Journal of Radiology*, *65*, 469

Editorial

From its emergence as a diagnostic tool about three decades ago ultrasound has expanded and continues to grow in importance and influence as a unique diagnostic device whose potential has yet to be fully explored and exploited. Next month, July 1992, the *British Journal of Radiology* is devoting its complete issue to diagnostic ultrasound. Whilst it remains the editorial policy of the Journal to maintain its multidisciplinary scientific and clinical spectrum, we believe that highlighting this one area of interest in a special issue will be appreciated by all users of the BJR. Those whose special interest is in ultrasound will find a substantial content of direct application to their specialty. For others, this single issue will enable a quick current perspective to be obtained of contemporary research and development in diagnostic ultrasound.

A second, and perhaps more important, aspect relating to this issue is that it marks an important milestone in the development of closer relationships between the British Institute of Radiology and the British Medical Ultrasound Society. The papers to be published in the July issue of BJR have been selected from submissions first presented orally at BMUS '91, held in Bournemouth in December last year. We believe that by devoting a special issue of the BJR to publishing the best papers from the BMUS meeting, we will be able to serve the wider scientific radiological community in a unique and effective way.

It is intented that future occasional issues of the BJR will likewise be devoted to topics of single special interest. These will be carefully selected to ensure that they combine a substantial contribution of new research and development in the specialist area with sufficient substance of interest to inform and educate the wide spectrum of scientific interests of the readers of this Journal. In this way the British radiological community, both clinical and scientifc, will be able to communicate effectively with one another original, creative and innovative work. Furthermore, the BJR will continue to contribute to the dissemination of knowledge to the broader European, American and world radiological scientists.

Francis Duck
Honorary Editor (Scientific)

Don Shaw
Honorary Editor (Medical)

1992, *The British Journal of Radiology*, 65, 470–475

Increasing patient throughput in magnetic resonance imaging: a practical approach

By N. R. Moore, MA, MRCP, FRCR and S. J. Golding, MA, DMRD, FRCR, on behalf of the Oxford MRI group*

Department of Radiology, University of Oxford, The Oxford MRI Centre, John Radcliffe Hospital, Oxford OX3 9DU, UK

(*Received 2 August 1991 and in revised form 2 December 1991, accepted 14 January 1992*)

Keywords: Magnetic resonance imaging, Throughput

Abstract. A major factor governing the throughput of patients in a magnetic resonance imaging (MRI) service is the number and length of sequences employed. This study investigated the feasibility of prospectively selecting patients for whom a pre-planned examination of the brain, spine or knee could be applied with a high chance of success. The implications on throughput of using these pre-planned examinations were determined. 173 patients were studied. A successful outcome was defined as an examination in which a diagnosis could be made with 100% confidence and without the need for further sequences. Examinations of the brain (n = 113), knee (n = 23) and lumbar spine (for disc degeneration, n = 14) were performed with success rates of 96%, 87% and 64%, respectively. Examinations of the lumbar spine (for radicular symptoms, n = 20) and cervical spine (n = 3) were performed with success rates of 85% and 66%, respectively. The examinations of the brain, knee and lumbar spine (for disc degeneration) were completed within the target time of 20 min in 92%, 95% and 69% of cases, respectively. Examinations of the lumbar spine (for radicular symptoms) and cervical spine were completed within 30 min in 75% and 33% of cases, respectively. Analysis of our results suggests that success rates could be improved by minor changes in sequence design. Carefully selected patients can be successfully examined in short examination times. Instituting these practices would increase the efficiency of MR machine time and improve patient throughput by 80–125%. This would have a marked effect on the length of waiting lists, and would increase the general availability of MRI.

Magnetic resonance imaging (MRI) has already become one of the most powerful diagnostic techniques in craniospinal and musculoskeletal imaging and may replace conventional tests in many aspects of body imaging. The excellent soft-tissue contrast and the ability to image in any plane give an unrivalled display of anatomy and disease.

The original spin–echo and inversion–recovery sequences are time consuming and may take as long as 15 min per sequence to perform. The gradient-recalled-echo techniques may provide similar information with shortened examination times. The wide choice of pulse sequences and imaging planes often results in prolonged studies and there is the general belief that magnetic resonance imaging (MRI) is a slow technique.

Although it is conventional to tailor examinations to individual patients, experience has shown that standardized examinations may be carried out for certain common indications. This study was carried out to assess examination duration and the implications on throughput of applying a standard set of sequences to pre-selected groups of patients.

Patients and methods

Selection of patients

173 patients were selected from the waiting list on the basis of the information provided on the request form. All patients were asked to arrive 30 min before their appointment time, and were informed of the high throughput nature of the study. All examinations were performed on a Signa Advantage machine (IGE Medical Systems Ltd, Slough) operating at 1.5 T. Dedicated head and knee extremity coils were used for the cranial and knee studies; examinations of the spine were performed using 5 in. circular or 11 in. × 5 in. rectangular surface coils.

Indications

Patients were selected if there was a clear-cut clinical problem that was thought to be soluble by a standardized MRI examination of two or three sequences. The indications in these patients for MRI examinations of the brain, cervical spine, lumbar spine and knee are summarized in Table I.

The patients in the lumbar spine category were divided into two groups. The first group of patients had symptoms of back pain and sciatica and were thought, on clinical grounds, to have a prolapsed intervertebral disc (referred to as "radicular"). The second group of

---

*Members of the Oxford MRI group: P. Anslow, J. V. Byrne, D. Dobson, E. W. L. Fletcher, S. J. Golding, L. Irvine, A. J. Molyneux, N. R. Moore, S. J. Ostlere, E. M. Warren and D. J. Wilson.

Address correspondence to Dr N. R. Moore, Department of Radiology, University of Oxford, The Oxford MRI Centre, John Radcliffe Hospital, Headley Way, Headington, Oxford OX3 9DU, UK.

Table 1. Indications for MRI examination

Examination	*n*
Cranial (*n* = 113)	
Multiple sclerosis	61
Mass	10
Thalamic (1)	
Temporal lobe (1)	
3rd ventricle (1)	
Posterior fossa (7)	
Vascular	10
AVM (4)	
Vasculitis (2)	
Dural venous thrombosis (2)	
Infarction (2)	
Foramen magnum lesion	9
Epilepsy	8
Psychiatric disorder	4
Movement disorder	3
Symptoms	8
Trigeminal neuralgia (3)	
Migraine (2)	
Vertigo (1)	
Hemifacial spasm (1)	
Dysphagia (1)	
Cervical (*n* = 3)	
Radiculopathy	2
Myelopathy	1
Lumbar – radicular (*n* = 20)	
Prolapsed intervertebral disc	15
Canal stenosis	2
Tumour	2
Retained disc fragment	1
Lumbar – degeneration (*n* = 14)	
Discogenic low back pain	13
Annular tear	1
Knee (*n* = 23)	
Meniscal tear	13
Patellar lesion	3
Knee pain and locking	3
Cruciate ligament tear	2
Discoid lateral meniscus	1
Pre-arthroscopy	1

patients had symptoms of back pain only, which was attributed to disc degeneration (referred to as "degeneration"). Those in this latter group were being investigated for evidence of disc dehydration as a prelude to spinal fusion, preceded by discography if the MRI revealed multiple-level disc degeneration.

Examinations of the brain, knee and lumbar spine ("degeneration") were allocated 20 min machine time. The cervical spine and lumbar spine ("radicular") examinations were allocated 30 min.

Protocols

Sequences were designed to optimize signal-to-noise ratio (SNR), spatial resolution and number of slices per acquisition and to combine these factors with a short acquisition duration. Software options were chosen to increase SNR and reduce artefact. The principal features of each sequence are recorded in Table II.

Timing

The following times were recorded for all patients as illustrated in this two-sequence examination (see Fig. 1).

1. *Examination time*: the difference between entry to, and exit from, the examination room.
2. *Sequence time*: the duration of all the sequences.
3. *Set up time*: the time elapsed between the entry time and the time recorded for the first sequence time ("set up 1"). This is the time for positioning, entry into the bore and the automatic pre-scan procedure. The time to prescribe and initiate a subsequent sequence ("set up 2, etc.") was determined from the start of the previous scan, the previous scan duration and the start of the subsequent scan.
4. *Removal time*: the difference between the start of the final scan plus scan duration and the time the patient left the room.
5. "*Dead*" *time*: the interval between patient exmination times.

The radiographers also recorded the presence of anxiety, claustrophobia or immobility to determine the effects of these factors on throughput.

Radiological assessment

All examinations were reported by a radiologist experienced in MRI. The radiologist was asked to assess:

1. whether the examination provided a diagnosis;
2. the degree of confidence in the ability to make a diagnosis (recorded on a percentage scale: 100%, 75%, 50%, 25%, 0%);
3. whether the patient needed to be recalled;
4. the reason for any recall.

Results

149 of 173 patients (86%) were examined within the target times during these high-throughput sessions. The examinations of the brain, knee and lumbar spine (for

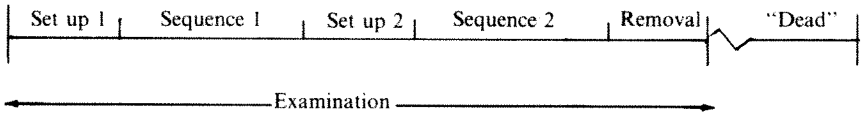

Figure 1. An example of a two-sequence examination showing the total examination time, and the components of sequence, set up and removal times. Also shown is the time between patients ("dead" time).

Table II. Details of the protocols used in this study

		Pulse sequence	Imaging options	TR (ms)	TE (ms)	Matrix	NEX	FOV (cm)	Slice thickness (mm)	Slice gap (mm)	No. slices	Imaging time (min : s)
Brain	Localizer Sagittal	MEMP	SAT I	500	10	256 × 192	2	24	5	2.5	11	3 : 14
	Transaxial	VEMP	SAT I FC VB	2700	30/90	256 × 192	0.75	24	5	2.5	20	7 : 01
Spine, cervical and lumbar (radicular)	Localizer Sagittal	GRE 60 deg. flip	FC	33	15	256 × 128	1	24	5	2.5	3	0 : 13
	Sagittal and transaxial (lumbar)	MEMP	SAT R/L NP	4–500	13	256 × 192	4	20	4	1	9–12	5 : :09 to 6 : 26
	Sagittal	MPGR 20 deg. flip	SAT A/P RT FC	440	15	256 × 256	6	24	4	1	11	5 : 40
	Transaxial (cervical)	MPGR 20 deg. flip	SAT R/L RT FC	440	15	256 × 256	4	20	4	1	11–14	7 : 43 to 9 : 00
Lumbar (degeneration)	Localizer Sagittal	MEMP	SAT A	200	10	256 × 128	1 or 2	24	5	2.5	3	0 : 28 or 0 : 52
	Sagittal (1)	VEMP	SAT S/I/F CL FC NP VB	2000	30/80	256 × 192	1	24	4	1	11	7 : 20
	(2)	VEMP	SAT S/I/F CL FC NP VB	2000	30/80	256 × 128	2	24	4	1	11	8 : 56
Knee	Localizer Transaxial	GRE 60 deg. flip	FC	33	15	256 × 128	2	20	5	2.5	1	0 : 09
	Sagittal	SPGR/Vol 35 deg. flip	SAT S/I	35	10	256 × 256	1	16	1.5	0	64	9 : 34

MEMP, multi echo multi planar; VEMP, variable echo multi planar; GRE, gradient recalled echo; MPGR, multi planar gradient recalled (echo); SPGR/Vol, spoiled gradient recalled acquisition in the steady state, volume acquisition; SAT, pre-saturation pulse; S,I,A,P,R,L, superior, inferior, anterior, posterior, right, left; F, fat; CL, classic; FC, flow compensation; NP, no phase (wrap); VB, variable bandwidth (sampling); TR, repetition time; TE, echo time; NEX, number of excitations; 0.75 NEX, fractional NEX. An IGE software option in which the number of phase encoding steps is reduced (undersampled). The matrix size is maintained by interpolation of data in K-space; FOV, field of view; RT, rectangular field of view.

Table III. Duration of the examination, sequence, set up, removal and "dead" times (all times given in minutes)

Region	Number of examinations	Examination time range (mean)	Sequence time (mean)
Brain	113	15–22 (18.5)	10.3
Cervical spine	3	20–33 (28.0)	14.2
Lumbar (radicular)	20	21–40 (28.1)	13.2
Lumbar (degeneration)	14	13–29 (18.3)	7.8
Knee	23	15–21 (17.2)	9.7
Set up 1 (mean)		3.5	
Set up 2 (mean)		3.2	
Removal (mean)		2.0	
Dead time		11 h 38 min	
Total scan time		56 h 28 min	

disc degeneration) were completed within the target time of 20 min in 92%, 95% and 69% of cases, respectively. Examinations of the lumbar spine (for radicular symptoms) and cervical spine were completed within 30 min in 75% and 33% of cases, respectively. The duration of the examinations, sequences, set up and removal are given in Table III.

The total time taken to perform these 173 examinations was 56 h 28 min. Within this time, 11 h 38 min were identified as "dead" time, *i.e.* time when there was no patient in the examination room (Table III). This equates to a further 16–24 patient examinations (depending on the part being examined) that could have been performed in the time available.

The effects of anxiety, claustrophobia and immobility on examination times were assessed in the largest group of patients, who had cranial MRI. The mean examination time for patients who had no delay was 17.8 min ($n = 65$, SD = 1.1 min). The examinations in those patients identified as anxious lasted 19.8 min ($n = 8$, SD = 1.0 min), and in those patients who were immobile lasted 19.3 min ($n = 15$, SD = 1.0 min). These patients need special care and encouragement, but it is clear that even very anxious patients can be successfully examined without major delay.

The results of the radiologist's assessments are given in Table IV. The fixed protocols provided all the information with which to make a diagnosis in 156 out of the 173 (90%) examinations. In three further patients, the radiologist was able to make a diagnosis, but with less confidence.

12 patients had to be recalled and were given early appointments for re-examination. Four patients (2.3%) experienced sufficient claustrophobia to require an examination with sedation. Five patients required a repeat examination for technical reasons: (i) insufficient signal to noise gave poor images in three patients; (ii) the volume acquisition of the knee in one patient did not include the area of abnormality; and (iii) the wrong lumbar spine protocol was applied in one patient; this was considered a failure even though the images were of perfect quality.

In two patients it was not possible to make a complete diagnosis. One patient had a cervical spine examination, but the clinical features suggested a brachial plexus lesion. This was not included in the examination area. In another patient who had hemifacial spasm, the sagittal and transaxial images demonstrated an ectatic vertebral artery. However, a facial nerve neuroma had not been excluded with complete confidence. These two patients

Table IV. Results of the radiologist's assessments

	Brain	Cervical	Lumbar (radicular)	Lumbar (degeneration)	Knee
Number	113	3	20	14[a]	23
Diagnosis obtained	110	2	18	9	20
Confidence level					
100%	108	2	17	9	20
75%	2	1	2		1
50%					1
25%				2	
0%	3		1	2	1
Recall	4	1	2	4	1

[a] One patient was too obese to fit in the bore of the machine and could not be examined.

were considered to have been incorrectly selected for this study.

In one patient the sagittal and transaxial images of the brain revealed a cervical syrinx. This patient was recalled for a cervical spine examination to demonstrate the full extent of the syrinx. One patient was too large to fit in the magnet.

Overall successful examinations, as defined by a diagnosis made with 100% confidence, were performed in 96% of brain, 87% of knee, 85% of lumbar spine (for radicular symptoms), 64% of lumbar spine (for disc degeneration) and 66% of cervical spine examinations.

Discussion

This study was designed to assess examination duration and patient throughput, and to investigate the range of indications for which standard protocol examinations could be applied. We have shown that examinations of carefully selected patients can be performed with a high degree of success in the brain, knee and lumbar spine ("degeneration") using examination times of 20 min. The lumbar spine "radicular" patients were successfully examined in 30 min. The small number of patients in the cervical spine group makes detailed assessment difficult.

The principal factor that determines the duration of an MRI examination, and hence the overall patient throughput, is the number of sequences performed. Many radiologists choose to view the images from one sequence before deciding on the next sequence. This is thought to give greater flexibility to unravel a complicated clinical problem, but the process of viewing and prescribing new sequences is time consuming. In this study the initial and subsequent sequences took 3.5 and 3.2 min, respectively, to prescribe and initiate. Even though the supervising radiologist was not allowed to use additional sequences, only 12 of 173 patients had to be recalled and 90% of all the varied clinical problems were solved successfully by a pre-planned MRI examination.

The reason for this high success rate is the accurate selection of patients suitable for this high-throughput type of MRI examination. It might be thought that this selection is time consuming, but these patients were selected during the routine process of vetting request forms. In addition to accepting the request, each radiologist indicated the suitability for a high-throughput examination. We informed the referring clinicians of the directed nature of these examinations and the possible need for recall in some patients. In many cases this resulted in more specific requests, which facilitated the process of vetting and increased the number of suitable patients. Approximately 30% of all our MRI requests are for patients for whom a high-throughput examination could be performed.

It is interesting to compare our approach with national trends. Average appointment times of 30 min for cranial MRI and 45 min for MRI examinations of the spine and knee are common. Using these times it could have taken approximately 101.5 h to examine the patients in this study. The use of the Oxford protocols represents an increase in throughput of 80%, and the release of 45 h scanning time. These assumptions do not take account of the 11.5 h in the study identified as "dead time". If this is included, the potential increase in throughput is 125%.

This study also shows that the protocols on which these fixed examinations are based should be subject to regular review. It was clear that the sagittal spin–echo T_2-weighted sequence provided insufficient signal to noise in some patients in the lumbar spine ("degeneration") group. Following three failures, the protocol was adjusted to increase the number of excitations (NEX) from one to two, and reduce the number of phase encode steps from 192 to 128. The change in matrix size and number of excitations increased the SNR by 73% but reduced the spatial resolution. The aim of the sequence was to demonstrate disc hydration, for which high spatial resolution was not necessary. If the modified sequence had been applied successfully in the three failures the success rate would have improved to 92%. The sequence time changed from 7 min 20 s to 8 min 56 s so the mean examination time increased from 18.0 to 19.5 min.

The diagnostic failures in the knee examinations can also be attributed to relative inexperience of this technique. The volume acquisition involved a 60-section block of 1.5 mm slice thickness and positioning this volume was critical. If a larger volume were prescribed, *e.g.* 124 slices at 0.9 mm thickness with a 256 × 192 matrix, the whole knee could be covered with ease, obviating diagnostic failure. This potentially would result in 23 out of 23 complete examinations (100% success). A further benefit is that the larger, thinner slice volume acquisition would result in voxels 20% smaller in size and a significant improvement in resolution in one of the reformatted planes. The larger volume would, however, take longer to acquire and would increase the sequence time to 14.3 min, and the mean examination time to 22.2 min.

All the requests for a particular anatomical area (*e.g.* brain or knee) were aggregated into one session. This avoids the need to change the surface or extremity coil between patients, which is time consuming. The radiographers thought that these sessions were easier to manage, even though more patients were examined, because they knew exactly which sequences to perform and no time was lost in selecting the sequences and viewing the images.

The patients participating in this study were highly motivated, as indicated by the high attendance rate (99%). During their examination, patients were seen by the receptionist, by a nurse who performed the safety screening procedure and finally by the radiographer who took the patient into the examination room. There were no adverse comments from any patients during the study period.

In conclusion, this study has shown that it is possible to perform pre-planned examinations with a high degree of success in selected groups of patients. By using these protocols, throughput rates can be increased by 80–125%. If our approach were extended nationally, there would be a major impact on the efficiency of use of MR machine time. In turn this would lead to greater availability of a scarce and expensive imaging procedure. We are continuing this study to identify more areas in which this approach is viable.

1992, *The British Journal of Radiology*, 65, 476–479

Radiological features during and following treatment of spinal tuberculosis

By D. I. Boxer, FRCR, *C. Pratt, MRCP, A. L. Hine, FRCR and *M. McNicol, FRCP

Departments of Radiology and *Thoracic Medicine, Central Middlesex Hospital NHS Trust, London, UK

(Received 3 October 1991 and accepted 6 December 1991)

Keywords: Spinal tuberculosis, Radiography, Therapy

Abstract. A retrospective study was performed in order to document the sequence and time scale of radiological changes occurring during the healing of spinal tuberculosis. 28 episodes occurred in 26 patients, of whom only two were Caucasian. All demonstrated good response to conventional chemotherapy. Soft-tissue masses increased in size for up to 1.5 months and took about 12 months to resolve. Bone destruction was seen in all cases and progressed in 70% of patients, whilst on treatment. There was loss of vertebral body height in 79%, which progressed for up to 14 months; any recovery of height was a very late feature. Sclerosis was seen at presentation in 52% and developed in most of the remaining patients within 5 months of instigating treatment. It progressed for up to 14 months and took, on average, 31 months to return to normal. Reduction in disc height was commonly seen and the vertebrae fused in three-quarters of those affected, the time of onset of fusion being very variable. To manage patients with spinal tuberculosis, an appreciation of the variability of radiological changes that can occur during treatment is necessary.

Spinal tuberculosis is an ancient disease, in existence for at least 5000 years, having been demonstrated within mummified remains from Northern Egypt dating from 3400 B.C. The association of spinal deformity with paralysis, as was so often seen in this disease, was described by Sir Percival Pott in 1779 (Lifeso et al, 1985).

The prevalence of pulmonary tuberculosis has been declining within the United Kingdom in recent years. However, the notification of bone and joint tuberculosis has remained fairly constant (Communicable Diseases Surveillance Centre, personal communication).

Most patients with spinal tuberculosis are managed conservatively with combination chemotherapy. Disease response is monitored clinically and radiologically. We have analysed the radiographs of 28 cases of vertebral tuberculosis that have demonstrated a good clinical response, in order to document the sequence and range of radiological changes that can be expected.

Patients

28 sites of spinal tuberculosis occurring in 26 patients were identified. All patients attended the Willesden Chest Clinic. 13 patients were male and 13 female. Average age at presentation was 39 years (range 12–79 years). 21 patients originated from the Indian subcontinent, two were Afro-Caribbean, two Caucasian and one unknown. 11 patients also had tuberculous disease at other sites (three pulmonary, four abdominal, four skeletal and one nodal). Diagnosis was made on a combination of clinical and radiological criteria; confirmatory tests, such as percutaneous biopsy, were only performed if other features were atypical.

Patients were routinely treated with combination chemotherapy, consisting of isoniazid and rifampicin for 1 year with pyrazinamide for the initial 3 months. Only one patient also underwent surgery. Patients were followed up in the clinic for up to 73 months (average 33 months). Clinical outcome was universally good. Only one patient had a residual neurological deficit: persistent foot drop. This had developed following spinal biopsy and was attributed to that procedure rather than the disease.

Radiographs, including tomograms, taken on presentation and during follow-up were obtained and analysed. The presence or absence and progression or resolution of the following features were sought:

1. Soft-tissue paravertebral mass visible on plain radiograph;
2. Bone destruction;
3. Bone sclerosis;
4. Loss of vertebral height;
5. Reduction in disc height;
6. Fusion of adjacent vertebrae.

Results

On average, two vertebrae were involved. Two cases spanned the thoraco-lumbar junction and therefore appear in both regions. The thoracic spine was the commonest region of the spine involved (17/26) followed by the lumbar region (9/26), the cervical spine being least commonly involved (4/26). The vertebral body alone was involved in 17 cases, the body and

---

Address correspondence to Dr D. I. Boxer, Department of Radiology, St Mary's Hospital, Praed Street, London W2 1NY, UK.

Table I. Distribution of disease

Region	No. of cases	Body alone	Body + posterior elements	Posterior alone
Cervical	4	3	—	1
Thoracic	17	9	7	1
Lumbar	9	6	3	—

posterior elements in nine and the posterior elements alone in two (Table I).

Soft-tissue mass (Fig. 1)

Cervical spine. A soft-tissue paravertebral mass was clearly seen at presentation in all three cases in which the vertebral body was involved. It took 8–12 months to resolve.

Thoracic spine. A mass was seen in 13 cases, in all but one at presentation. Increase in size of the mass was seen for an average of 1.5 months. Resolution took 12 months on average. Two patients were left with residual slight widening of the paraspinal lines, which did not change on long-term follow-up.

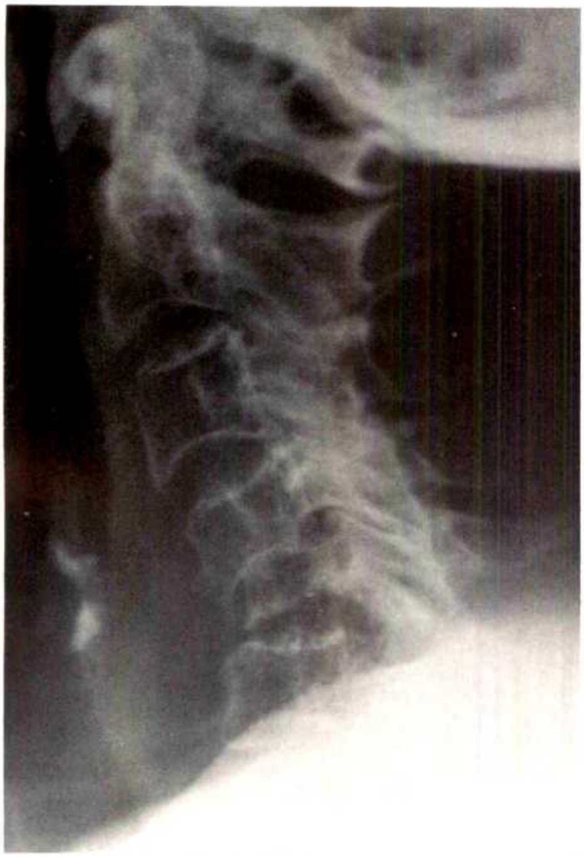

Figure 1. Lateral view of the cervical spine in a 63-year-old female patient showing advanced destruction of the vertebral body of C5. A prevertebral soft-tissue mass is present.

Lumbar spine. On plain radiographs it was not possible to consistently demonstrate either the presence or absence of a soft-tissue mass.

Bone destruction (Fig. 1)

This was seen in all cases and was visible at presentation in all but four cases; in these it developed within 3 months. Destructive changes progressed on treatment in 70% (20/28) for, on average, 6.5 months. Loss of vertebral body height occurred in 79% (22/28) and progressed for up to 14 months. Only three cases demonstrated recovery of body height; the earliest this occurred was after 15 months (Fig. 2).

Sclerosis (Fig. 3)

This was seen in 90% of cases (25/28). It was demonstrated at presentation in 52% (13/25) and appeared within 5 months in the remainder. It progressed for up to 14 months. Bone density returned to normal in 44% (11/25), taking, on average, 31 months (range 12–59 months).

Disc changes

Reduction of disc height occurred in 77% of those cases in which the vertebral body was involved (20/26). The vertebrae fused in 75% (15/20) of these, starting anteriorly in all. The earliest that evidence of fusion was seen was after 3 weeks and the latest 27 months (average 9 months).

Discussion

Bone and joint tuberculosis is an uncommon condition. In recent years, however, the incidence in England and Wales has remained fairly constant. From 1981 to 1986 between 59 and 92 cases were notified each year to the Communicable Diseases Surveillance Centre, Colindale (Communicable Diseases Surveillance Centre, personal communication). Tuberculous spondylitis accounts for 6% of all new cases of extrapulmonary tuberculosis notified (Mann & Cole, 1987). Most cases are treated conservatively with combination chemotherapy. The majority of patients respond well to such treatment and surgery is only infrequently required (Lifeso et al, 1985; Fancourt et al, 1986). Response to treatment is primarily judged by clinical criteria. However, an appreciation of the normal pattern and time course of healing seen radiologically is required. This paper documents these changes.

Typically, vertebral tuberculosis begins in the anterior part of the body, either superiorly or inferiorly. With spread, the adjacent intervertebral disc and adjoining vertebral body become involved (Patton, 1986). Occasionally vertebral tuberculosis spreads below the anterior longitudinal ligament, involving several levels and causing scalloping of the anterior margin of the vertebral bodies.

The radiological features may vary with the race of the patient. Caucasian patients usually demonstrate bone destruction of the anterior portion of the vertebral body, narrowing of the adjacent disc space and involve-

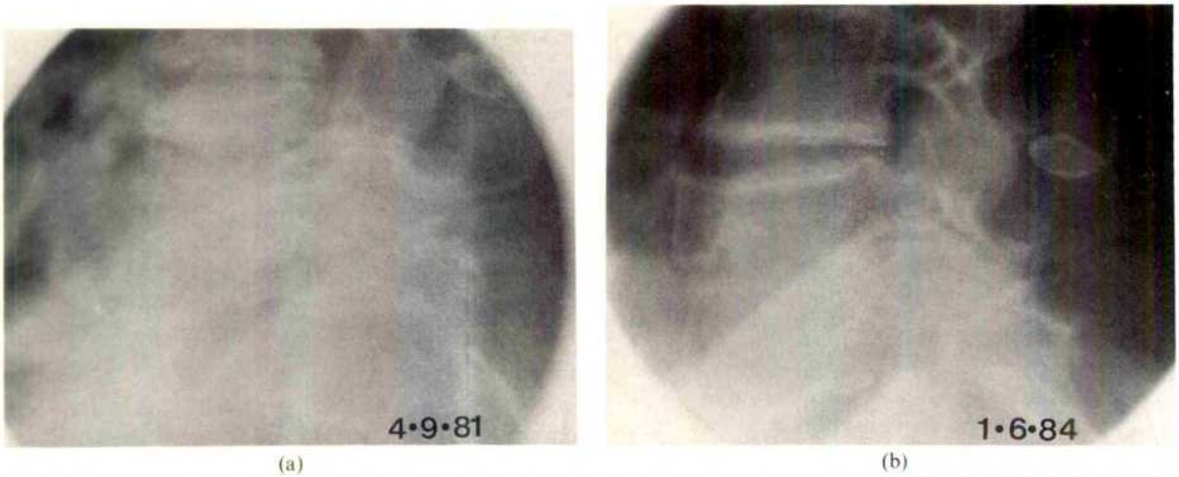

(a) (b)

Figure 2. (a) Lateral view of the lumbar spine in a 68-year-old female patient, showing marked loss of height of the body of the L4 vertebra. (b) 33 months later there has been partial recovery of vertebral height.

ment of contiguous vertebral bodies. Reactive sclerosis, at presentation, is not a feature. Untreated patients develop progressive vertebral collapse with anterior wedging, leading to gibbus formation (Gorse et al, 1983). Associated soft-tissue masses are common and most easily demonstrated on plain radiographs of the dorsal spine. In non-Caucasian patients the appearances may vary. Infection may be confined to a single vertebral body and early sclerosis may be a feature. Involvement of the posterior elements of the vertebra are not uncommon and may be the only sites of involvement (Chapman et al, 1979).

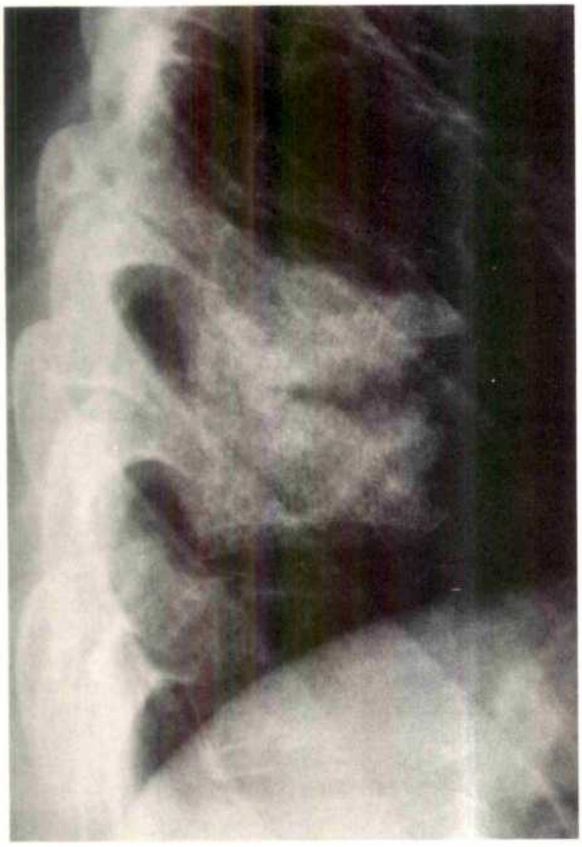

Figure 3. Lateral view of the thoracic spine at presentation in a 30-year-old male patient. There is marked sclerosis of the vertebral bodies of T9 and T10.

Since the advent of effective chemotherapy, little has been published on the radiological changes of successful treatment. It is recognized that radiological evidence of healing occurs late on routine radiographs (Gorse et al, 1983). In our series we found that evidence of bone destruction or loss of vertebral height could progress for up to 14 months and recovery of vertebral body height was not seen earlier than 15 months after starting treatment. These findings agree well with those of the Medical Research Council (MRC) trials of treatment for spinal tuberculosis (MRC, 1976, 1978, 1982). In these series, loss of vertebral height was seen for up to 18 months, but thereafter there was little change. Recovery of vertebral body height, if it occurred, was seen between 18 and 36 months. Thus progression of bone destruction whilst on treatment should not, necessarily, be considered an adverse feature.

Sclerosis was present in half of our patients at presentation (a reflection of the high proportion of patients of Afro-Caribbean and Indian sub-continent origin) and in these patients its progression provides little information about disease activity. In those patients with initially purely lytic changes, sclerosis is a feature of healing and should be seen within 5 months. It can progress for over 1 year. Although we saw a return to normal bone density in less than one-half of these patients, it took up to 5 years to occur and if our follow-up period had been longer it is likely that in most patients it would have returned to normal density.

The presence of a soft-tissue paravertebral mass is a useful feature for follow-up in patients with involvement of thoracic or cervical vertebral bodies. These masses reached maximum size within 1.5 months of presentation, although they could take up to 15 months to resolve. We were unable reliably to demonstrate soft-tissue masses in patients with lumbar spinal involvement or in those patients with disease at other sites which only involved the posterior elements. If confirmation of an abscess is required in the lumbar region, an ultrasound examination may be sufficient (Rubaltelli et al, 1990). Alternatively, these patients may be assessed by computed tomography (Lin-Greenberg & Cholankeril, 1990) or magnetic resonance imaging (De Roos et al, 1986). These techniques are of particular value in any patient in whom there is doubt about the diagnosis (Azzam & Tammawy, 1988), extent of disease or the presence of complications such as spinal cord involvement (Lin-Greenberg & Cholankeril, 1990; Bell et al, 1990).

Reduction in disc height is common, reflecting the nature of the infection, and fusion of contiguous vertebrae is seen in many of these patients. Calcific debris, which was seen on serial radiographs to progress to fusion, was seen as early as 3 weeks after initiation of treatment, although it could take up to 27 months for any evidence of fusion to appear. Fusion of contiguous vertebrae has long been regarded as the surest evidence of healing of spinal tuberculosis, although there is no actual proof of this (MRC, 1978). Ultimately vertebral fusion occurred in over 50% of all our cases.

Spinal tuberculosis remains an important cause of morbidity within the United Kingdom. Monitoring of response to treatment is based on a combination of clinical and radiological features. It is therefore vital that the radiologists and clinicians involved in the care of these patients are aware of the variable radiological changes that may occur during successful treatment of this disease.

References

AZZAM, N. I. & TAMMAWY, M., 1988. Tuberculous spondylitis in adults: diagnosis and treatment. *British Journal of Neurosurgery*, *2*, 85–91.

BELL, G. R., STEARNS, K. L., BONUTTI, P. M., & BOUMPHREY, F. R., 1990. MRI diagnosis of tuberculous vertebral osteomyelitis. *Spine*, *15*(6), 462–465.

CHAPMAN, M., MURRAY, R. O. & STOKER, D. J., 1979. Tuberculosis of the bones and joints. *Seminars in Roentgenology*, *14*(4), 266–282.

DE ROOS, A., VAN MEERTEN, E. V., BLOEM, J. L. & BLUEMM, R. G., 1986. MRI of tuberculous spondylitis. *American Journal of Roentgenology*, *147*, 79–82.

FANCOURT, G. J., EBDEN, P., GARNER, P., COOKSON, J. B., WALES, J. M. & STOYLE, T. F., 1986. Bone tuberculosis: results and experience in Leicestershire. *British Journal of Diseases of the Chest*, *80*(3), 265–272.

GORSE, G. J., PAIS, M. J., KUSSKE, J. A. & CESARIO, T. C., 1983. Tuberculous spondylitis: a report of six cases and a review of the literature. *Medicine (Baltimore)*, *62*, 178–193.

LIFESO, R. M., WEAVER, P. & HARDER, E. H., 1985. Tuberculous spondylitis in adults. *Journal of Bone and Joint Surgery*, *67*, 1405–1413.

LIN-GREENBERG, A. & CHOLANKERIL, J., 1990. Vertebral arch destruction in tuberculosis: CT features. *Journal of Computer Assisted Tomography*, *14*(2), 300–302.

MANN, J. S., & COLE, R. B., 1987. Tuberculous spondylitis in the elderly: a potential diagnostic pitfall. *British Medical Journal*, *294*, 1149–1150.

MRC, 1976. Medical Research Council Working Party on Tuberculosis of the Spine. A five-year assessment of controlled trials of in-patient and out-patient treatment and of plaster-of-Paris jackets for tuberculosis of the spine in children on standard chemotherapy. *Journal of Bone and Joint Surgery*, *58B*, 399–411.

MRC, 1978. Medical Research Council Working Party on Tuberculosis of the Spine. Five-year assessments of controlled trials of ambulatory treatment, debridement and anterior spinal fusion in the management of tuberculosis of the spine. *Journal of Bone and Joint Surgery*, *60B*, 163–177.

MRC, 1982. Medical Research Council Working Party on Tuberculosis of the Spine. A 10-year assessment of a controlled trial comparing debridement and anterior spinal fusion in the management of tuberculosis of the spine in patients on standard chemotherapy in Hong Kong. *Journal of Bone and Joint Surgery*, *64B*, 393–398.

PATTON, J. T., 1986. Bone & joint infection. In *Diagnostic Radiology*, ed. by R. G. Grainger and D. J. Allison (Churchill Livingstone, Edinburgh), vol. 2, pp. 1349–1367.

RUBALTELLI, L., DE GERONE, E. & CATERINO, G., 1990. Echographic evaluation of tubercular abscesses in lumbar spondylitis. *Journal of Ultrasound in Medicine*, *9*, 67–70.

P 25863

1992, *The British Journal of Radiology*, *65*, 480–484

The musculoskeletal manifestations of epidermolysis bullosa: an analysis of 19 cases with a review of the literature

By Wai Lup Wong, MRCP(UK), FRCR and James Pemberton, MRCP(UK), FRCR

Department of Clinical Radiology, St Thomas' Hospital, Lambeth Palace Road, London SE1 7EH, UK

(*Received 5 March 1991 and in final form 16 December 1991, accepted 13 January 1992*)

Keywords: Epidermolysis bullosa, Musculoskeletal manifestations

Abstract. Epidermolysis bullosa encompasses a group of rare disorders characterized by marked skin fragility and blister formation. In patients with dystrophic epidermolysis bullosa, skeletal and soft-tissue abnormalities are an important feature. An analysis of the musculoskeletal manifestations in 19 patients is presented. In the hands and feet, features included generalized osteoporosis, wedge-shaped thinning and hooking of distal phalanges, overconstricted bones, acro-osteolysis, flexion contractures, metatarsal and metacarpal subluxation, distal trophic changes, webbing of digits, encasement of the whole extremity in a pouch of skin, soft-tissue calcification and retarded skeletal maturity. Previously undescribed findings in the hands and feet are bony ankylosis of the proximal interphalangeal joints, resorption of the metatarsal and metacarpal heads, shortened metatarsal bones, carpal and tarsal fusion and destruction, and cystic changes of the distal radius and ulna. In the remainder of the skeleton, hip dysplasia with premature osteoarthritis, knee joint bony ankylosis and thoracic and thoraco-lumbar scoliosis are other undescribed findings.

Epidermolysis bullosa (EB) encompasses a group of rare diseases characterized by marked skin fragility and blister formation following seemingly minor trauma to the skin. Most of the diseases that meet these criteria are hereditary, though some non-hereditary diseases or diseases of uncertain heredity also qualify (Pearson, 1988).

Since the term was first introduced by Kobner in 1886, more than 20 different forms of EB have been described, differing in mode of transmission, clinical morphology and the level of blister formation (Kobner, 1886; Gedde-Dahl Jr, 1971; Gedde-Dahl Jr, 1981). However, each of these clinical variants can be placed in one of three general groups based on the level at which the skin separates:

1. Epidermolytic, designating separation within the epidermal layer;
2. Lamina lucidolytic, indicating separation in the plane of the lamina lucida of the basement membrane;
3. Dermolytic (dystrophic), designating separation beneath the basement membrane (Cooper & Bauer, 1984b; Pearson, 1988).

Of these three groups, only the dystrophic variants are associated with severe scarring.

Dystrophic EB includes at least five variants with a wide range of clinical severity and involvement. They are all transmitted in a simple autosomal mode of inheritance and are typified by the presence of generalized or primarily acral (distal extremity) blisters, which heal with scarring and milia formation (white cystic nodules of skin composed of densely packed keratin). Both squamous and basal carcinomas can complicate areas of scarring (Schwartz et al, 1981; Fine, 1986). Other cutaneous features can include dystrophic nails and albopapuloid, plaque and papular scars lighter than surrounding skin. The latter is a typical feature of the Pasini variant of the disorder (McKee, 1989).

Non-cutaneous features include keratitis, premature dental decay and lesions of the mucous membranes resulting in difficulty in opening the mouth, dysphagia and oesophageal strictures, with some infants succumbing eventually to terminal respiratory infections. Anaemia and developmental growth retardation with a shortened lifespan may occur in severely involved individuals (Pearson, 1988).

In this paper we describe the musculoskeletal manifestations and quantify the incidence of these changes in 19 patients with dystrophic EB, the largest single series in the world literature.

Materials and methods

Radiographs of 19 patients with a diagnosis of dystrophic EB were reviewed. The group studied consisted of 10 male and 9 female patients ranging in age from 2 to 41 years, with a mean of 17 years and a median of 13 years. 16 patients had radiographs of their hands, five of whom also had radiographs of their feet. Chest radiographs were obtained in eight patients, knee radiographs in three patients, plain abdominal radiographs in two patients and pelvis and femora radiographs in one patient.

Radiological findings

Hands/feet

Tables I and II list the abnormalities identified, together with their frequencies.

Soft tissue. Extensive distal soft-tissue atrophy was a very common feature (Fig. 1). Webbing of the fingers and toes with soft-tissue digital fusion was also often

Table I. Musculoskeletal features of EB

Recognized features of EB in the hands and feet	Number of patients	
	Hands	Feet
Osteoporosis	16	5
Wedge-shaped thinning and hooking of distal phalanges	16	5
Distal trophic changes; acro-osteolysis	15	5
Flexion contracture of the MCP/MTP and IP joints	14	2
Webbing of fingers/toes and digital fusion	13	1
Overconstricted slender bones	11	1
MTP/MCP subluxation	7	3
Retarded epiphyseal growth	4	—
Encasement in a pouch of skin	4	1
Soft-tissue calcification	1	1

Hand radiographs were reviewed in a total of 16 patients and feet radiographs were reviewed in five patients.

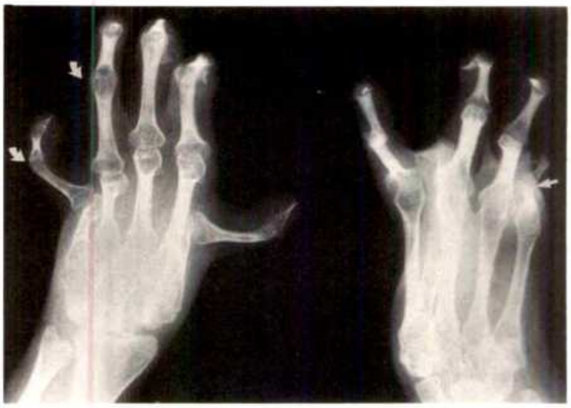

Figure 1. Soft-tissue atrophy, generalized osteoporosis with coarsened subarticular trabecular pattern, bony ankylosis of the proximal IP joints (curved arrows), shortened left ring and little finger metacarpals and destruction of the distal end of the proximal phalanx of the little finger on the right are present (arrow). Wedge-shaped thinning is seen in most distal phalanges.

seen (Figs 2, 4). In a few cases the whole hand was encased in a complete pouch of skin (Figs 3, 5). Clusters of punctate calcification distributed in the subcutaneous layer of the skin were present in two of the cases (Fig. 2).

Bones. All cases demonstrated generalized osteoporosis with coarsened subarticular trabeculation and wedge-shaped thinning or hooking of the distal phalanges (Figs 1, 2). Acro-osteolysis with tuft resorption was a very common feature (Fig. 1). In many of the patients the shafts of the radius and ulna and tibia and fibula were slender and overconstricted.

Other features seen included carpal and tarsal bone destruction, resorption of metacarpal, metatarsal or phalangeal heads and shortened metacarpals (Figs 1, 2, 5). In two cases, there was bilateral shortening of the little finger metacarpals and in one case there was shortening of the left ring and little finger metacarpals (Fig. 1). In addition, in the distal radius and ulna, cystic changes were present in one case and a grossly tapered ulna styloid in another.

Joint alignment. Flexion contractures of the metacarpophalangeal (MCP) and interphalangeal (IP) joints were a common finding (Fig. 2). In some cases subluxation or dislocation of the carpometacarpal/metatarsophalangeal (MTP)/MCP joints with ulna deviation was seen (Fig. 3).

Bony ankylosis of the proximal IP joints was present in six patients (Figs 2, 3). Carpal fusion was observed in two cases and tarsal fusion in another two, one each of

Table II. Occurrence of previously undescribed findings of EB in the hands and feet

EB findings in hands and feet	Number of patients	
	Hands	Feet
Bony ankylosis of PIP joints	6	—
Resorption of metacarpal/metatarsal heads	3	1
Short metacarpal bones	3	—
Carpal/tarsal fusion	2	2
Carpal/tarsal destruction	1	1
Cystic changes in the distal radius and ulna	1	—
Tapered ulna styloid	1	—

Hand radiographs were reviewed in a total of 16 patients and feet radiographs were reviewed in five patients.

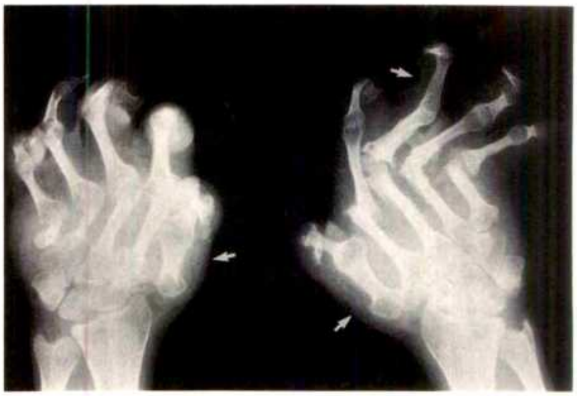

Figure 2. Webbing of the fingers with soft-tissue digital fusion and subcutaneous calcification is present (arrows). Resorption of the metacarpal heads, flexion contractures of the IP joints, dislocation of the MCP joints with ulna deviation and bony ankylosis of both middle-finger PIP joints are seen. In addition, there is wedge-shaped thinning and hooking of the terminal phalanges of both ring fingers.

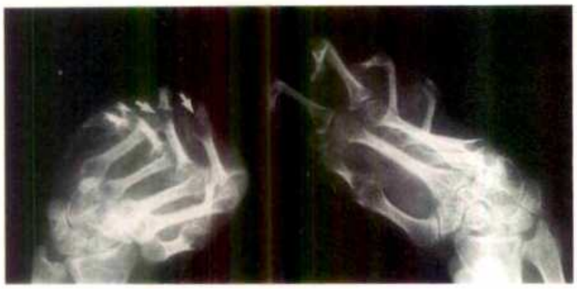

Figure 3. The left hand is enclosed in a pouch of skin. Bilateral capitate-hamate coalition is present. In addition, there is generalized osteoporosis, dislocation of the MCP joints with ulna deviation and bony ankylosis of the PIP joints (arrows).

capitate–hamate coalition, total carpal fusion, total tarsal fusion and cuneiform coalition (Figs 3, 4). Both cases of carpal coalition were associated with ankylosis of the proximal interphalangeal (PIP) joints.

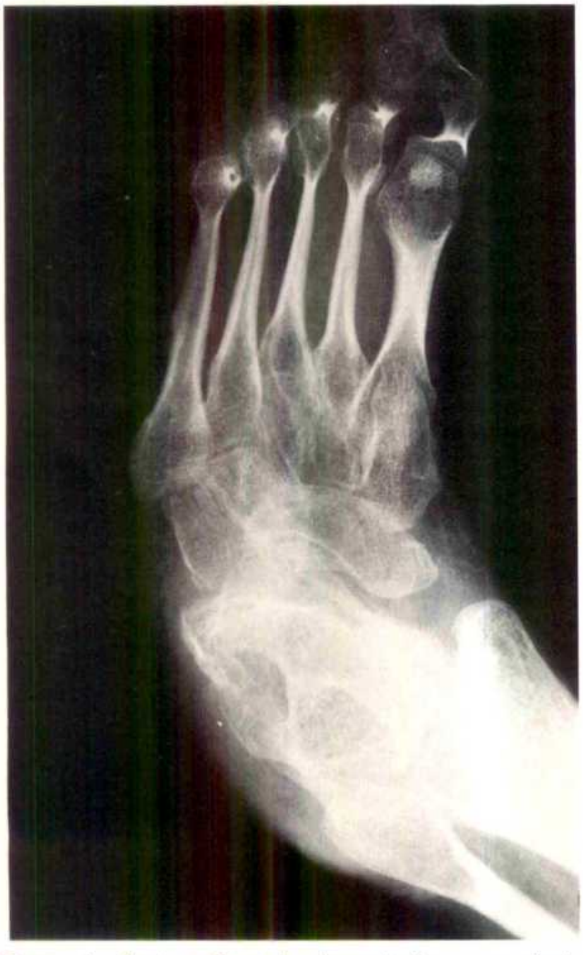

Figure 4. Foot radiograph demonstrating generalized osteoporosis, coalition of the cuneiform bones and soft-tissue webbing of the toes.

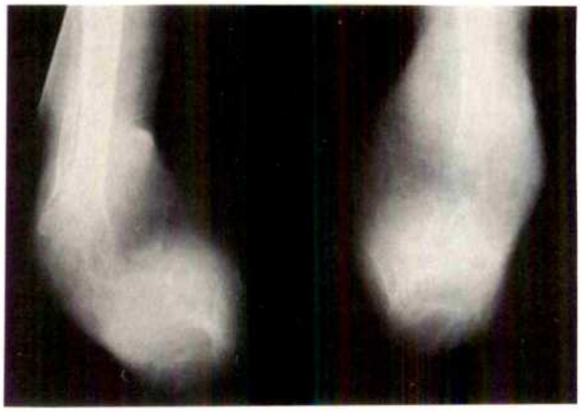

Figure 5. The feet are enveloped in pouches of skin. There is, in addition, destruction of the tarsal bones and severe disorganization of all the bones of both feet.

Abnormal feet radiographs were all associated with severe abnormalities of the hands. Retarded epiphyseal development was present in four patients.

Other musculoskeletal features

Table III lists the abnormalities identified, together with their frequencies.

Pelvis. In one case the right hip joint was dysplastic with signs of premature osteoarthritis.

Knees. Bony ankylosis across the knee joint was seen in one of the cases.

Spine. Thoracic scoliosis was observed in one case and a thoraco-lumbar scoliosis was seen in another.

Discussion

In 1908, Nobl found that radiological diagnosis was a useful adjunct in the examination of a patient with EB. The radiographs revealed shortening and atrophy of the terminal phalanges of the hand (Nobl, 1908).

Since then, various authors have described other radiological findings associated with EB involving the extremities (Thoroczkay, 1940; Roach, 1946; Kitlowski & Banfield, 1948; Hadley & MacDonald, 1960; Brinn & Khilnani, 1967; Becker & Swinyard, 1968; Mauro et al, 1987).

Table III. Other musculoskeletal features of EB

Musculoskeletal features	Number of patients
Hip dysplasia with premature osteoarthritis	1
Bony ankylosis across the knee joint	1
Thoracic scoliosis	1
Thoraco-lumbar scoliosis	1

Chest radiographs were reviewed in eight patients, knee radiographs in three patients, plain abdominal radiographs in two patients and pelvis and femora radiographs in one patient.

In 1957, Alpert reviewed the radiological manifestations of EB. Together with cases from previous reports and his own case, he discussed the radiological changes involving the hands and feet in 14 patients (Alpert, 1957).

Many of the features seen in the hand and feet radiographs of our patients concur with the findings of previous authors. Several previously undescribed features were also noted. These include subluxation of the MCP and MTP joints, bony ankylosis across the proximal IP joints, resorption of the metacarpal heads, shortened metacarpals, cystic changes in the distal radius and ulna, carpal and tarsal fusion and destruction.

In the rest of the skeleton, other features not previously described include hip dysplasia with premature osteoarthritis, bony ankylosis of the knee joint and thoracic and thoraco-lumbar scoliosis.

The abnormalities in the hands and feet may be explained by extensive blister formation, first appearing at an early stage, leading to severe scarring and obliteration of blood vessels (Alpert, 1957; Brinn & Khilnani, 1967; Mauro et al, 1987).

Generalized osteoporosis and slender, overconstricted long bones are most likely due to malnutrition and disuse since many of these patients are reluctant to move about and eat poorly (Becker & Swinyard, 1968).

The underlying pathophysiological mechanisms that result in the common skin findings of marked skin fragility and blister formation are still unclear. In recessive dystrophic EB, dermal fibroblasts have been shown to function abnormally as well as to produce excessive amounts of chemically and structurally abnormal collagenase (Bauer, 1977; Bauer & Eisen, 1978; Ehrlich et al, 1983). Presumably, excessive amounts of this enzyme facilitate dissolution of collagen in the region of the basement membrane (possibly anchoring fibril related), thereby leading to blister formation. Furthermore, anchoring fibrils are absent and KF-1 and LH 7:2 antigens, normal structural components of the human skin, are either absent or markedly reduced in amount (Briggaman et al, 1985; Eady et al, 1987). The significance of these features and how they tie up with the collagenase and fibroblast abnormalities is unknown.

In dominant dystrophic EB, both KF-1 antigen and the number of anchoring fibrils are reduced in quantity, though collagenase levels appear to be normal. Since subepidermal blisters develop in both dominant and recessive forms of dystrophic EB, the latter feature suggests that elevated collagenase facilitates, but is not solely responsible for, blister formation (Fine, 1986).

With regard to treatment, phenytoin has been found to be partly successful in patients with recessive dystrophic EB, reducing blistering by up to 45% in some cases (Eisenberg et al, 1978; Bauer et al, 1980; Cooper & Bauer, 1984a). It probably acts by reducing collagenase synthesis.

In some patients, newer techniques of reconstructive hand surgery may lead to significantly increased function, though unfortunately such procedures may have to be performed repeatedly (Horner et al, 1971). The mainstay of management of most patients with dystrophic EB remains symptomatic and supportive therapy.

In summary, the radiological features of EB include musculoskeletal changes that can often be severe. These abnormalities are commonly seen in the extremities but may also be present in the spine, hips and knees.

Acknowledgments

We would like to thank Mr B. Mayou for allowing us to publish details of these cases and Miss Karen Kemmett for preparing the manuscript.

References

ALPERT, M., 1957. Roentgen manifestations of epidermolysis bullosa. *American Journal of Roentgenology, 78*, 66–72.

BAUER, E. A., 1977. Recessive dystrophic epidermolysis bullosa: evidence for an increased altered collagenase in fibroblast cultures. *Proceedings of the National Academy of Sciences, USA, 74*, 4646–4650.

BAUER, E. A. & EISEN, A. Z., 1978. Recessive dystrophic epidermolysis bullosa: evidence for increased collagenase as a genetic characteristic in cell culture. *Journal of Experimental Medicine, 148*, 1378–1387.

BAUER, E. A., COOPER, T. W. M. D., TUCKER, D. R. & ESTERLY, N. B., 1980. Phenytoin therapy of recessive dystrophic bullosa: clinical trial and proposed mechanism of action on collagenase. *New England Journal of Medicine, 303*, 776–781.

BECKER, M. H. & SWINYARD, C. A., 1968. Epidermolysis bullosa dystrophica in children: radiological manifestations. *Radiology, 90*, 124–128.

BRIGGAMAN, R. A., DALLDORF, F. G. & WHEELER, C. E., 1971. Formation and origin of basal lamina and anchoring fibrils in adult human skin. *Journal of Cell Biology, 51*, 384–395.

BRINN, L. B. & KHILNANI, M. T., 1967. Epidermolysis bullosa with characteristic hand deformities. *Radiology, 89*, 272–274.

COOPER, T. W. & BAUER, E. A., 1984a. Therapeutic efficacy of phenytoin in recessive dystrophic epidermolysis: a comparison of short and long term treatment. *Archives of Dermatology, 120*, 490–495.

COOPER, T. W. & BAUER, E. A., 1984b. Epidermolysis bullosa: a review. *Paediatric Dermatology, 1*, 181–188.

EADY, R. A. J., TIDMAN, M. J., HEAGERTY, A. H. M. & KENNEDY, A. R., 1987. Approaches to the study of epidermolysis bullosa. *Current Problems in Dermatology, 17*, 127–141.

EHRLICH, H. P., BUTTLE, D. J., TRELSTAD, R. L. & HAYASHI, K., 1983. Epidermolysis bullosa dystrophica recessive fibroblasts altered behaviour within a collagen matrix. *Journal of Investigative Dermatology, 80*, 56–60.

EISENBERG, M., STEVENS, L. H. & SCHOFIELD, P. J., 1978. Epidermolysis bullosa: new therapeutic approaches. *Australasian Journal of Dermatology, 19*, 1–8.

FINE, J. D., 1986. Epidermolysis bullosa: clinical aspects, pathology and recent advances in research. *International Journal of Dermatology, 25*, 143–157.

GEDDE-DAHL, JR, T., 1971. *Epidermolysis Bullosa: a Clinical, Genetic and Epidemiological Study* (Johns Hopkins Press, Baltimore).

GEDDE-DAHL, JR, T., 1981. Sixteen types of epidermolysis bullosa. *Acta Dermato-Venereologica (Stockholm), 95* (Suppl.), 74–87.

HADLEY, M. & MACDONALD, A. F., 1960. Epidermolysis bullosa. *British Journal of Radiology, 33*, 646–649.

HORNER, R. L., WIEDEL, J. D. & BRALLIAR, F., 1971. Involvement of the hand in epidermolysis bullosa. *Journal of Bone and Joint Surgery, 53A*, 1347–1356.

KITLOWSKI, E. & BANFIELD, E., 1948. Epidermolysis bullosa hereditaria. Report of a case with unusual associated deformities. *Plastic and Reconstructive Surgery, 3*, 481–488.

KOBNER, H., 1886. Anlage zur Blasenbildung. (Epidermolysis bullosa hereditaria). *Deutsche Medizinische Wochenschrift, 12*, 21–22.

MAURO, M. A., PARKER, L. A., HARTLEY, W. S., RENNER, J. B. & MAURO, P. M., 1987. Epidermolysis bullosa: radiographic findings in sixteen cases. *American Journal of Roentgenology, 149*, 925–927.

MCKEE, P. H., 1989. *Congenital Diseases. Pathology of the Skin with Clinical Correlations* (J. B. Lippincott, Philadelphia), Ch. 2, 2.2–2.40.

NOBL, G., 1908. Dystrophia bullosa congenita. *Ikonographica Dermatologica, 3*, 107–111.

PEARSON, R. W., 1988. Clinicopathological types of epidermolysis bullosa and their nondermatological complications. *Archives of Dermatology, 124*, 718–725.

ROACH, R. D., 1946. Recessive epidermolysis bullosa. *Canadian Medical Association Journal, 55*, 122–125.

SCHWARTZ, R. A., BIRKRANT, A. P., RUBENSTEIN, D. J., KIM, U., BURGESS, G. H., STOLL JR, H. L., CHAI, S. W., SOUTHWICK, G. J. & MILGROM, H., 1981. Squamous cell carcinoma in dominant type epidermolysis bullosa dystrophica. *Cancer, 47*, 615–620.

THOROCZKAY, M., 1940. Csontelvaltozas epidermolysis bullosa hereditaria. *Esetebengen Magyar Rontgen Kozlozy, 14*, 14–18.

1992, *The British Journal of Radiology*, *65*, 485–490

Intramuscular myxoma: magnetic resonance features

By Abrahim Fikry Abdelwahab, MD, *Samuel Kenan, MD, George Hermann, MD, *Michael M. Lewis, MD and †Michael J. Klein, MD

Departments of Radiology, *Orthopaedic Surgery and †Pathology, Mount Sinai Medical Center, New York, USA

(Received 2 September 1991 and in revised form 2 January 1992, accepted 13 January 1992)

Keywords: Soft-tissue tumours, Intramuscular myxoma, Magnetic resonance imaging

Abstract. Magnetic resonance imaging (MRI) was performed in six cases of intramuscular myxoma of the extremities and revealed the following characteristics. All tumours were confined to muscle and had a sharply defined border. All had a signal intensity lower than skeletal muscles on T_1-weighted images and brighter than fat on T_2-weighted images. The signals were homogeneous on both T_1- and T_2-weighted images. This study did not include contrast enhancement. The diagnosis was confirmed by an open biopsy. All tumours were resected with no recurrence. Diagnosis based on these MRI characteristics was incorrect in two cases of intramuscular ganglia and in a case of intramuscular cysticercus cellulose. MRI features of intramuscular myxoma are typical in the majority of cases. Benign intramuscular lesions that contain mainly fluid can mimic intramuscular myxomas.

Intramuscular myxoma is a distinct benign tumour. The diagnostic efficacy of magnetic resonance imaging (MRI), a multiplanar imaging technique, compared with computed tomography (CT) has proved to be superior in the detection and evaluation of soft-tissue masses (Petasnick et al, 1986; Petterson et al, 1987; Wetzel et al, 1987). Certain criteria favour benign soft-tissue tumours, which include sharp definition of the margin, lack of septation and homogeneity in signal intensity (Sundaram et al, 1988; Kransdorf et al, 1989a; Berquist et al, 1990).

Materials and methods

These cases were referred over a five-year period to our orthopaedic tumour service, which functions as a tertiary referral centre for patients with bone or soft-tissue tumour in New York City. These patients were investigated, including MRI scans, by their private physicians before they were referred to us. There were two male and four female patients ranging in age from 36 to 65 years, with a mean of 49 years. The MRI scans were performed by different scanners ranging from 0·5 T to 1.5 T. Scanning sequences included spin-echo T_1-weighted 300–600/20–30 TR/TE (time to repeat/time to echo) and T_2-weighted, 2000–2600/80–100 pulse sequences. Section thickness varied from 4 to 10 mm. At least two orthogonal planes were imaged, and in two patients imaging was in three planes. All the MRI scans were without contrast enhancement or short T_1 inversion–recovery sequence (STIR). The scans were reviewed by a musculoskeletal radiologist. Open biopsies and the resected tumours were studied by a bone pathologist.

The diagnosis of intramuscular myxoma was considered from the MRI scans and was based on the intramuscular site of the lesions, the sharp definition of the margin, the characteristic signal intensities and the homogeneity of the signals. All the patients had an open biopsy followed by total excision of the tumour. All patients were followed up every 3 months. Three patients were followed for more than 3 years, two for less than 2 years and the sixth patient for more than 6 months with no evidence of recurrence.

Case histories

Case 1

A 40-year-old white female noticed a painless lump in the left shoulder for 2 weeks. Physical examination revealed a non-tender, 2 cm × 4 cm well demarcated mass in the region of the deltoid muscle. There were no skin changes. The MRI scan revealed an oval mass lesion in the left deltoid muscle (Fig. 1).

Case 2

A 65-year-old white female presented with a lump in the posterior aspect of the right shoulder, which she noticed 3 weeks earlier. Physical examination revealed a non-tender, 6 cm × 8 cm mass in the infraspinatus region of the right scapula. There was full range of movement of the right shoulder. MRI revealed a well circumscribed oval mass in the infraspinatus muscle.

Case 3

A 48-year-old white female noted a painless left gluteal mass for 1 year, which grew slowly during this period. Clinical examination revealed a 3 cm × 5 cm, non-tender, deeply seated left gluteal mass. There was

---

Address correspondence to Ibrahim Fikry Abdelwahab, MD, Department of Radiology, Box 1234, Mount Sinai Medical Center, 1 Gustave L. Levy Place, New York, NY 10029–6574, USA.

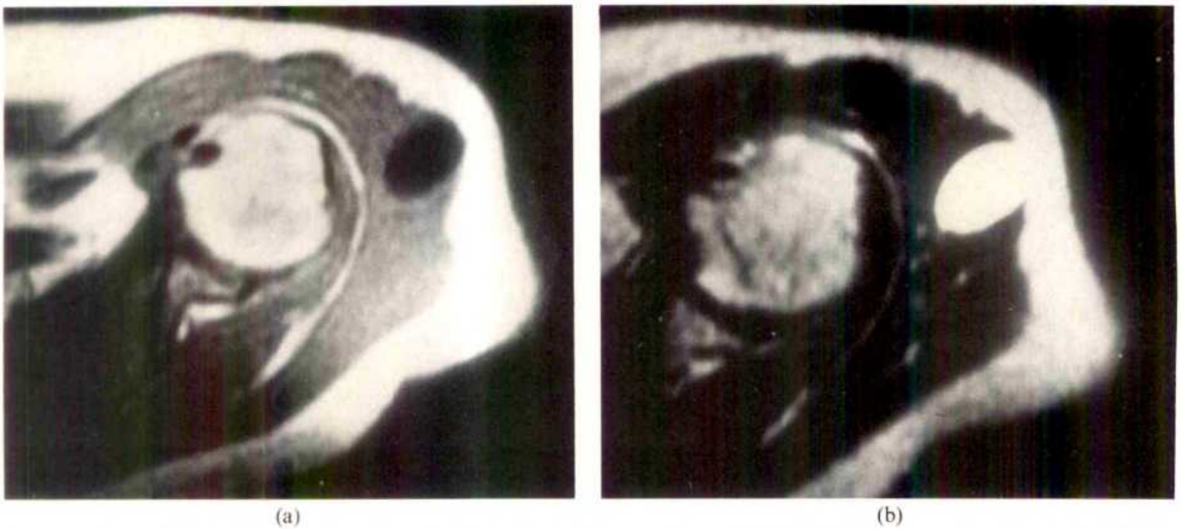
(a) (b)

Figure 1. MRI of the left shoulder. (a) Axial T_1-weighted image (TR 400/TE 20) and (b) axial T_2-weighted image (TR 2000/TE 80). MRI reveals an oval, sharply defined lesion in the left deltoid muscle with hypointense signal on the T_1-weighted image and bright signal on the T_2-weighted image. Both signals are homogeneous.

no neurovascular deficit. MRI revealed an oval mass in the left gluteus maximus (Fig. 2).

Case 4

A 38-year-old black female noted 3 months earlier a painless, deeply seated mass in the proximal part of the right thigh. Physical examination revealed full range of movement of the right hip and knee without neurological deficit. A firm, mobile, non-tender mass, 4 cm × 8 cm, was felt in the proximal anteromedial part of the right thigh. MRI showed the mass to be in the vastus medialis (Fig. 3).

Case 5

A 65-year-old Asian male presented with a 6-month history of a firm, painless mass on the medial aspect of the left thigh. Physical examination revealed an oval, non-tender mass approximately 4 cm × 5 cm in its greatest diameter located in the mid-thigh in the region of the adductor muscles. The overlying skin and the neurovascular bundle were intact. MRI revealed the mass to be in the semimembranosus muscle (Fig. 4).

Case 6

A 36-year-old white male presented with a mass in the anterolateral aspect of the left knee just proximal to the patella, noticed 1 year earlier. Lately the mass became painful during walking and climbing stairs. A laminectomy had been performed 12 years earlier. Physical examination revealed a firm nodule on the lateral aspect of the quadriceps tendon approximately 3 cm proximal to the patella. The mass was mobile and slightly tender

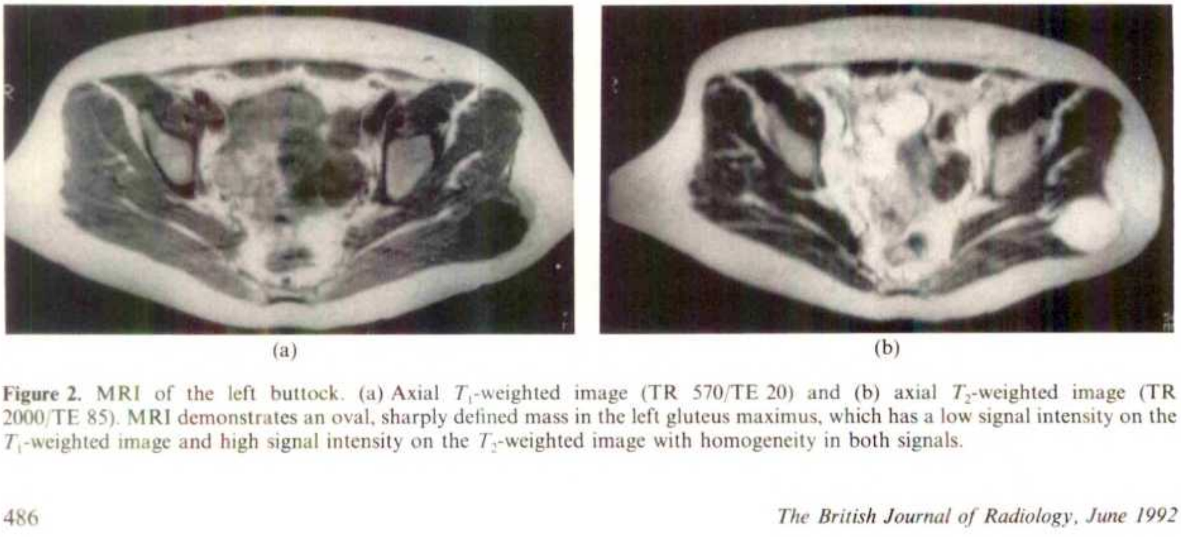
(a) (b)

Figure 2. MRI of the left buttock. (a) Axial T_1-weighted image (TR 570/TE 20) and (b) axial T_2-weighted image (TR 2000/TE 85). MRI demonstrates an oval, sharply defined mass in the left gluteus maximus, which has a low signal intensity on the T_1-weighted image and high signal intensity on the T_2-weighted image with homogeneity in both signals.

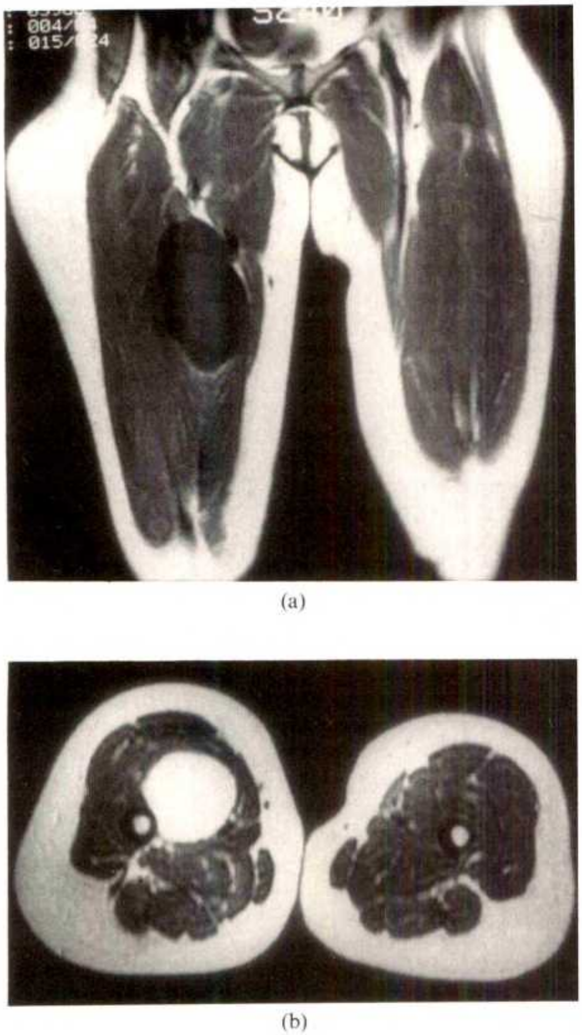

(a)

(b)

Figure 3. MRI of the right thigh. (a) Coronal T_1-weighted image (TR 600/TE 20) and (b) axial T_2-weighted image (TR 2000/TE 60). MRI shows an oval lesion that has sharp borders in the vastus medialis muscle with homogeneous hypointense signal on the T_1-weighted image and homogeneous bright signal on the T_2-weighted image.

on deep palpation. It was attached neither to the skin nor to the bone. There was a full range of movement in the hip and knee. MRI revealed the mass to be in the quadriceps muscle.

Discussion

Although the superiority of MRI over CT in evaluating soft-tissue masses is well established, the specificity of MRI in the histological diagnosis of these tumours is less than 20% (Kransdorf et al, 1989a). Tumours with substantial amounts of myxoid tissue may be benign as intramuscular myxomas or they may be malignant tumours undergoing myxomatous degeneration.

The majority of intramuscular myxomas occur between the fourth and seventh decades They are less commonly encountered in young adults and rarely in children (Ireland et al, 1973; Canalis et al, 1976; Kransdorf et al, 1989b). The mean age in our cases was 49 years. There is a slight female predominance (Canalis et al, 1976); four of our six patients were women. The most common site of myxoma is the heart (Stout, 1948). If we eliminate bony myxomas, which are almost exclusively in the jaws with only a few cases reported in the long tubular bones and pelvis (Stout, 1948; Ireland et al, 1973; Canalis et al, 1976; McClure & Dahlin, 1977; Abdelwahab et al, 1991), the majority of extracardiac soft-tissue myxomas occur in the musculature of the extremities, particularly of the thigh and shoulder girdle (Stout, 1948; Enzinger, 1965; Ireland et al, 1973). Three of our cases occurred in the thigh and two in the shoulder. To date, the total number of intramuscular myxomas is less than 150 (Canalis et al, 1976; McCook et al, 1981). The tumour usually presents as a painless mass. About 20% of patients are symptomatic, complaining of pain and/or tenderness (Enzinger, 1965). The rate of tumour growth is variable, and occasionally there is no apparent growth over long periods of time (Kransdorf et al, 1989b). It is rare for the tumour to be clinically diagnosed before MRI or biopsy. There has been no documented case of metastasis (Shugar et al, 1987).

In 1948, Stout defined the myxoma as a true mesenchymal neoplasm composed of undifferentiated stellate cells in myxoid stroma. Enzinger (1965), reviewing soft-tissue myxomas but excluding cardiac myxomas, found that one of every six myxomas was located in muscle. On gross inspection, the tumour is oval or spherical in shape, and when cut open presents a white or grey-white mucoid, gelatinous surface. Small cyst-like spaces or traversing trabeculae are not uncommon. On close inspection, the delicate fibrous capsule is usually incomplete and practically all lesions infiltrate adjacent muscles. Microscopically, myxoma is composed of stellate cells and a meshwork of reticulum fibres in a matrix of mucoid material that contains hyaluronic acid (Stout, 1948; Kindbloom et al, 1974) (Fig. 5). Although Stout stated that the recurrence rate was high after resection of these tumours, other reports, including ours, have not confirmed this (Enzinger, 1965; Kindbloom et al, 1974; Feldman, 1979). There is an association between intramuscular myxomas and fibrous dysplasia (Ireland et al, 1973; Sundaram et al, 1989). Wirth et al (1971) described this association as a syndrome in which intramuscular myxomas are an extraskeletal manifestation of fibrous dysplasia. The majority of tumours are associated with polyostotic fibrous dysplasia (Wirth et al, 1971; Logel, 1976; Dahlin, 1987). The intramuscular myxomas are usually located in the vicinity of the most severely affected bones and most often occur in the thigh and may be multiple. Half of the patients had some manifestation of Albright's syndrome (Logel,

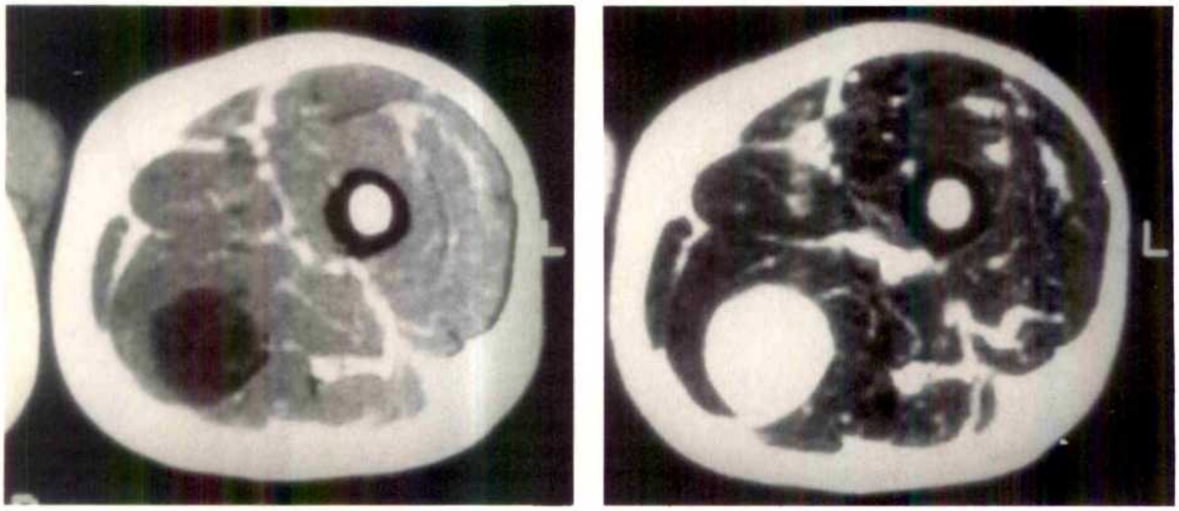

(a) (b)

Figure 4. MRI of the left thigh. (a) Axial T_1-weighted image (TR 500/TE 30) and (b) axial T_2-weighted image (TR 2000/TE 60). MRI reveals an oval lesion with sharp borders in the semimembranosus muscle, which has low signal intensity on the T_1-weighted image and high signal intensity on the T_2-weighted image. Both signals are uniform.

1976). To date, there are less than 20 cases of intramuscular myxomas associated with fibrous dysplasia. Of these, only two cases were associated with monostotic fibrous dysplasia (Ireland et al, 1973; Sundaram et al, 1989). The possibility of associated fibrous dysplasia when an intramuscular myxoma is discovered should always be considered. Our six cases were not associated with fibrous dysplasia.

Intramuscular myxomas are rare tumours. In three large series of soft-tissue tumours studied by MRI, totalling 258, there were only three intramuscular myxomas (Sundaram et al, 1988; Kransdorf et al, 1989a; Berquist et al, 1990). There are also sporadic case reports of intramuscular myxomas in which MRI was performed (Kransdorf et al, 1989b; Sundaram et al, 1989). Our series of six intramuscular myxomas seems to be the largest studied by MRI.

The characteristic pattern of MRI was typical in all our cases. However, our experience differed from other authors. In a recent report by Peterson et al (1991), although three of their four cases of intramuscular myxomas demonstrated the typical MRI characteristics, one case that was homogeneous on both T_1- and T_2-weighted images demonstrated, only after contrast enhancement, an irregular contrast enhancement in only one of the two components of the lesion. Part of the

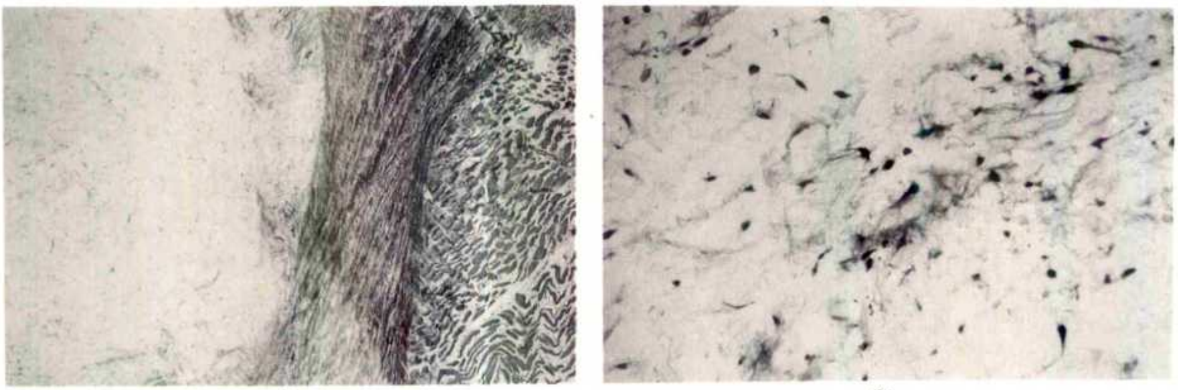

(a) (b)

Figure 5. Photomicrographs. (a) A low-power view demonstrating loose textured, avascular myxoid tissue of the tumour (left and centre). A fibrous capsule separates the lesion from the skeletal muscle fibres (right) (× 11). (b) A high-power view reveals spindle and stellate cells with long processes in a loose acellular myxoid stroma (× 113).

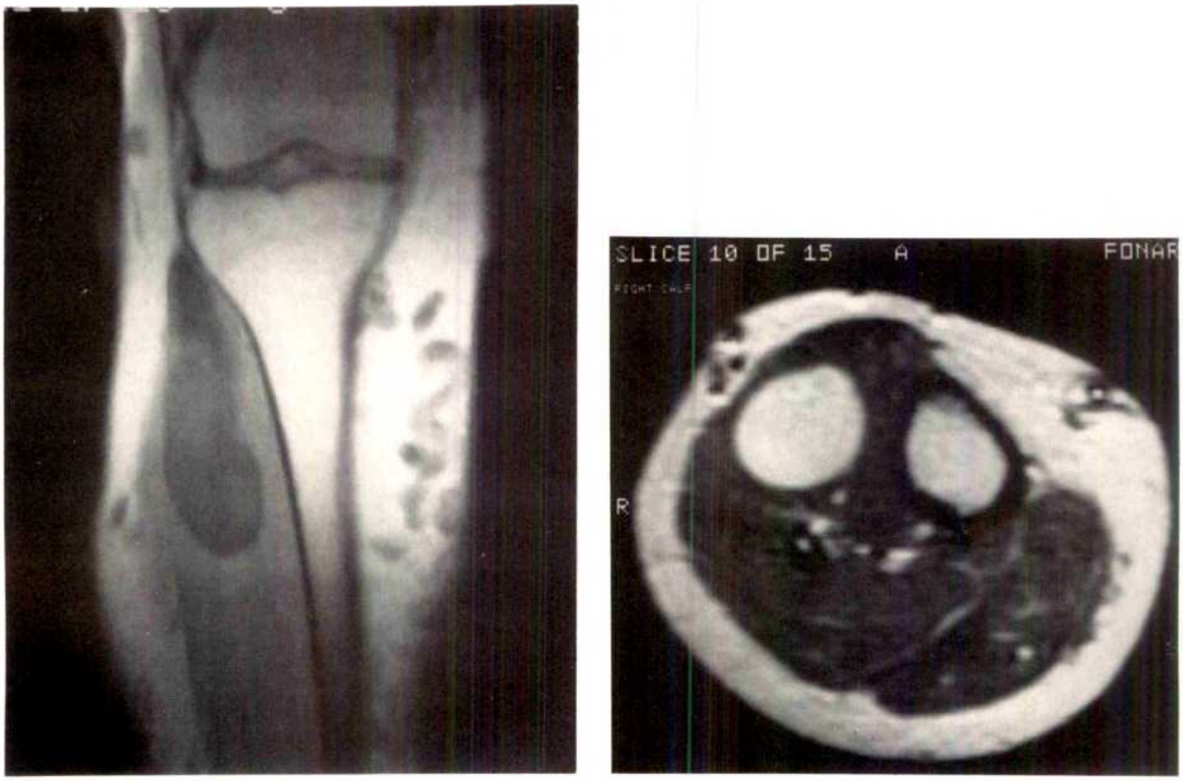

(a)

(b)

Figure 6. MRI of the right leg. (a) Coronal T_1-weighted image (TE 400/TE 20) and (b) axial T_2-weighted image (TR 1800/TE 60). The coronal slice reveals an oval, sharply defined lesion in the proximal part of the right leg with low signal intensity. Note the stalk between the lesion and the superior tibiofibular joint. The signal is bright on the T_2-weighted image. The above appearances are characteristic of an intramuscular ganglion.

border was also not sharply defined. In one of two cases of intramuscular myxomas reported by Kransdorf et al (1989b), MRI revealed on T_1- and T_2-weighted pulse sequences an area of increased signal intensity in the distal aspect of the tumour similar to subcutaneous fat.

As fluid and myxoid tissue have the same MRI characteristics, our diagnosis was incorrect in three rare benign lesions that contained mainly fluid. Two were intramuscular ganglia in the proximal part of the leg, which communicated with the synovium of the knee joint by a thin duct-like structure lined by single, flattened endothelial cells. Retrospective study of the MRI of the intramuscular ganglia revealed, in the cuts performed in the coronal plane, the tract between the ganglion and the knee joint (Fig. 6). We, therefore, emphasize performing MRI in the coronal planes, particularly when fluid-containing lesions are close to the joints. The third lesion was an intramuscular cysticercus cellulose located in the brachioradialis muscle of the right forearm in a Middle Eastern young male. The lesion contained gelatinous fluid. Acute haematoma containing fresh blood can mimic myxoma, although there is usually a history of trauma with a painful tender swelling. Intramuscular abscess usually has inhomogeneous signal intensity, depending on the amount of protein and necrotic debris within the abscess, with oedema in the surrounding tissue. Schwannomas are attached to the nerve roots outside the muscles, but if large, may compress the surrounding muscles and may simulate myxoma. However, they are usually more hyperintense than the muscle on T_1-weighted images and have areas of decreased signal intensity on T_2-weighted images. Some malignant soft-tissue tumours, namely liposarcomas, chondrosarcoma and malignant fibrous histiocytomas, may undergo myxomatous degeneration and may demonstrate a high signal intensity on T_2-weighted images, simulting intramuscular myxomas. However, these tumours usually lack the uniformity of the signal intensity and usually have septations on T_2-weighted images (Kransdorf et al, 1989a; London et al, 1989). Myxoid liposarcomas constitute approximately 50% of liposarcomas. They show amorphous or linear foci of high signal within a low signal mass on T_1-weighted images and one should consider this possibility even if the tumour otherwise appears benign (Sundaram et al, 1990). Occasionally, a malignant tumour may have a homogeneous signal intensity with a sharply defined margin. A signal intensity on a T_1-weighted image greater than muscle or if the tumour is extramuscular, may differentiate them from myxomas.

We conclude that MRI characteristics of intramuscular myxomas are typical in the majority of cases and that benign lesions which contain mainly fluid may mimic intramuscular myxomas. On the other hand, malignant soft-tissue tumours with myxomatous degeneration can be differentiated by the heterogeneity of the signal intensity on both T_1- and T_2-weighted images and the presence of septations.

Acknowledgments

The authors wish to thank Thomas A. Einhorn, MD, for Case 1 and Herbert S. Sherry, MD, for Case 3.

References

Abdelwahab, I. F., Hermann, G., Klein, M. J., Kenan, S. & Lewis, M. M., 1991. Fibromyxoma of bone. *Skeletal Radiology*, *20*, 95–98.

Berquist, T. H., Ethan, R. L., King, B. F., Hodgman, C. G. & Ilstrup, D. M., 1990. Value of MR imaging in differentiating benign from malignant soft tissue masses: study of 95 lesions. *American Journal of Roentgenology*, *155*, 1251–1255.

Canalis, R. F., Smith, G. A. & Konrad, H. R., 1976. Myxoma of the head and neck. *Archives of Otolaryngology*, *102*, 300–305.

Dahlin, D. C., 1987. Polyostotic fibrous dysplasia associated with myxoma of the soft tissues. Presented at the closed meeting of the International Skeletal Society, Cannes, France, September 1987.

Enzinger, F. M., 1965. Intramuscular myxomas, a review and follow-up study of 34 cases. *American Journal of Clinical Pathology*, *43*, 104–113.

Feldman, P. S., 1979. A comparative study including ultrastructure of intramuscular myxoma and myxoid liposarcoma. *Cancer*, *43*, 512–525.

Ireland, D. C. R., Soule, E. H. & Ioins, J. E., 1973. Myxoma of somatic soft tissues. A report of 58 patients, 3 with multiple tumors and fibrous dysplasia of bone. *Mayo Clinic Proceedings*, *48*, 401–410.

Kindbloom, L. G., Stener, B. & Angervall, L., 1974. Intramuscular myxoma. *Cancer*, *34*, 1737–1744.

Kransdorf, M. J., Jelinek, J. S., Moser, R. P., Jr, Utz, J. A., Brower, A. C., Hudson, T. M. & Berry, B. H., 1989a. Soft tissue masses: diagnosis using MR imaging. *American Journal of Roentgenology*, *153*, 541–547.

Kransdorf, M. J., Moser, R. P., Jr, Jelinek, J. S., Weiss, S. W., Benton, P. C. & Berry, B. H., 1989b. Intramuscular myxoma: MR features. *Journal of Computer Assisted Tomography*, *13*, 836–839.

Logel, R. J., 1976. Recurrent intramuscular myxoma associated with Albright's syndrome. Case report and review of the literature. *Journal of Bone and Joint Surgery*, *58A*, 565–568.

London, J., Kim, E. E., Wallace, S., Shirkoda, A., Coan, J. & Evans, H., 1989. MR imaging of liposarcoma. Correlation of MR features and histology. *Journal of Computer Assisted Tomography*, *12*, 832–835.

McClure, D. K. & Dahlin, D. C., 1977. Myxoma of bone. Report of three cases. *Mayo Clinic Proceedings*, *52*, 249–253.

McCook, T. A., Martinez, S., Korobkin, M., Ram, P. C., Bowen, J. H., Breiman, R. S., Harrelson, J. M. & Gehweiler, J. A. Jr, 1981. Intramuscular myxoma. Radiographic and computed tomographic findings with pathologic correlation. *Skeletal Radiology*, *7*, 15–19.

Petasnick, J. P., Turner, D. A., Charters, J. R., Gitelis, S. & Zacharias, C., 1986. Soft tissue masses of the locomotor system: comparison of MRI with CT. *Radiology*, *160*, 125–133.

Peterson, K. K., Renfew, D. L., Feddersen, R. M., Buckwalter, J. A. & El-Koury, G. Y., 1991. Magnetic resonance imaging of myxoid containing tumors. *Skeletal Radiology*, *20*, 245–250.

Petterson, H., Gilepsy, T., Hounlin, D. J., Enneking, W. F., Springfield, D. S., Andrew, R. E., Spanier, S. & Stone, R., 1987. Primary musculoskeletal tumors: examination with MR imaging compared with conventional modalities. *Radiology*, *164*, 237–241.

Shugar, J. M., Som, P. M., Meyers, R. J. & Chaeffer, B. T., 1987. Intramuscular head and neck myxoma. Report of a case and review of the literature. *Laryngoscope*, *97*, 105–107.

Stout, A. P., 1948. Myxoma, a tumor of primitive mesenchyme. *Annals of Surgery*, *127*, 706–719.

Sundaram, M., Baren, G., Merand, G. & McDonald, D. J., 1990. Myxoid liposarcoma: magnetic resonance imaging appearances with clinical and histologic correlation. *Skeletal Radiology*, *19*, 359–362.

Sundaram, M., McDonald, D. J. & Merand, G., 1989. Intramuscular myxoma: a rare but important association with fibrous dysplasia of bone. *American Journal of Roentgenology*, *153*, 107–108.

Sundaram, M., McGuire, M. H. & Herbold, D. R., 1988. Magnetic resonance imaging of soft tissue masses. An evaluation of fifty-three histologically proven tumors. *Magnetic Resonance Imaging*, *6*, 237–248.

Wetzel, L. H., Levine, E. & Murphey, M. D., 1987. A comparison of MR imaging and CT in the evaluation of musculoskeletal masses. *Radiographics*, *7*, 851–874.

Wirth, W. A., Leavitt, D. & Enzinger, F. M., 1971. Multiple intramuscular myxomas. Another extraskeletal manifestation of fibrous dysplasia. *Cancer*, *27*, 1167–1173.

1992, *The British Journal of Radiology*, *65*, 491–494

Scintigraphic abnormalities in patients with painful hip replacements treated conservatively

By K. A. Miles, FRCR, *W. M. Harper, FRCS ED, D. B. L. Finlay, MRCP, FRCR and †I. Belton, BSc, MSc, MIPSM

Departments of Radiology, *Orthopaedics and †Medical Physics, Leicester Royal Infirmary, Infirmary Square, Leicester, UK

(Received 1 July 1991 and in revised form 30 October 1991, accepted 14 January 1992)

Keywords: Hip, Prosthesis, Radionuclide, Imaging, Management

Abstract. A retrospective review of the scintigraphic appearances of 98 painful hip replacements was made. 16 patients (16%) underwent revision surgery whereas in the remaining 82 hips (84%), symptoms settled with conservative management. 73 of these (89%) had at least one area of increased activity on delayed diphosphonate scintigraphy with 27% having increased activity in three or more areas around the femoral component. Hips with increased activity at the lesser trochanter and tip were less likely to undergo spontaneous resolution of symptoms. Uncemented prostheses were more likely to have multiple areas of increased activity. Abnormalities in dynamic bone scintigraphy and gallium studies were also seen in patients whose symptoms resolved without surgery. Whereas a normal bone scintigram indicates that loosening or infection is most unlikely, the presence of increased activity does not necessarily indicate a need for revision surgery, even when multiple areas are present. A period of conservative management should be considered before operative intervention is undertaken.

Bone scintigraphy is a widely used and sensitive means of detecting loosening and infection of hip replacements. Normal post-operative appearances have been established in control groups of painless prostheses (Utz et al, 1986) but in clinical practice the decision is whether or not a painful hip replacement requires revision surgery, which can often be prolonged and technically demanding.

We have noticed that some patients with painful hip prostheses have areas of increased activity on bone scintigraphy and yet their symptoms have resolved with conservative management. A retrospective analysis of patients investigated by bone scintigraphy for painful hip prostheses was undertaken to see how often this occurred and to determine those patterns of activity associated with spontaneous resolution.

Patients and methods

98 hips were studied in 80 patients having bone scintigraphy for a painful prosthesis between January 1982 and October 1988. 32 of these were also investigated by dynamic bone scintigraphy and 42 by gallium-67 studies. All these studies were reviewed along with the radiographs and the clinical notes.

Bone scintigraphy was performed using 400 MBq of a ^{99}Tc^{m}-labelled diphosphonate. Anterior and posterior images were obtained 3 h after injection using a large field-of-view gamma camera and a general-purpose collimator. For dynamic studies, immediate arterial images and a blood pool image at 2 min were also obtained. Anterior and posterior gallium images, when obtained in cases of suspected infection, were performed at 48–72 h after injection with 75 MBq of gallium-67 citrate.

The scintigraphic appearances were reviewed by a consultant radiologist with experience in bone scintigraphy (D.F.) without knowledge of the clinical findings. Any sites of increased activity were observed and recorded as being localized in the acetabulum, greater trochanter, lesser trochanter, prosthetic shaft or tip.

The clinical review was made using the hospital notes and radiographs. The date of operation and operative technique, including surgical approach and prosthetic type for the original hip replacement, were noted. The time of second presentation with pain and subsequent outcome were recorded. If revision was performed, the operative findings were reviewed. The presence of infection at surgery was diagnosed by the macroscopic presence of pus or a subsequent positive culture. The component or components loose were recorded. The scintigraphic appearances in those hips undergoing revision surgery and those settling with conservative management were compared.

Results

All radionuclide studies were performed at least 12 months after the primary surgery and the minimum time of follow-up was 1 year. The decision to revise a painful prosthesis had been primarily dependent on the patient's symptoms, the results of scintigraphy being considered in association with the results of other investigations and the clinical findings. Of the 98 hips studied, 16 (16%) subsequently underwent revision surgery. 13 of these were loose and three were infected.

Address correspondence to W. M. Harper, Department of Orthopaedics, Glenfield General Hospital, Glenfield, Leicester, UK.

Table I. The incidence of increased activity at various sites (figures in parentheses are percentages)

	Sites of activity					
	Acet	Tip	Shaft	G. Troch	L. Troch	All sites
Operated	7 (44)	12 (75)	6 (38)	10 (63)	13 (81)	48 (60)
loose	7 (54)	10 (77)	5 (38)	8 (62)	11 (85)	41 (63)
infected	0 (0)	2 (67)	1 (33)	2 (67)	2 (67)	7 (47)
Non-operated	35 (43)	41 (50)	25 (30)	41 (50)	37 (45)	179 (44)
cemented	32 (43)	35 (47)	21 (28)	36 (49)	29 (39)	153 (41)
uncemented	3 (38)	6 (75)	4 (50)	5 (63)	8 (100)	26 (65)

Acet, acetabulum; G. Troch, greater trochanter; L. Troch, lesser trochanter.

The incidence of increased activity at the different sites around the prosthesis for the various patient groups is given in Table I. The total number of sites affected was significantly greater in the operated group than the non-operated group ($p < 0.01$) and, amongst the non-operated hips, there were more abnormal sites in the uncemented prostheses ($p < 0.005$). No significant difference in the total number of sites affected was observed when comparing loose and infected prostheses. Comparison of individual sites in the operated and cemented non-operated groups showed no significant difference in the incidence of increased activity for the acetabulum, greater trochanter or shaft whereas the lesser trochanter and tip were more likely to be affected in those patients who underwent revision surgery ($p < 0.005$, $p < 0.05$, respectively; Fisher's exact test was used in all cases).

The number of sites around the femoral component with increased activity for various patient groups are summarized in Table II. The predictive value of a normal scintigram (*i.e.* no sites affected) was found to be high at 95% whereas of the 79 hips with one or more sites of increased activity, only 13 (16%) underwent revision surgery. When comparing the operated and non-operated groups, there were significantly more hips with two or more areas of increased activity in the operated group ($p < 0.05$, χ^2 test). There was even greater statistical significance when uncemented prostheses were excluded ($p < 0.02$). Uncemented prostheses not requiring revision surgery all had two or more areas of increased activity and all demonstrated increased activity at the lesser trochanter. The most discriminant criteria for no need of revision surgery are outlined in Table III, giving a sensitivity of 81% and specificity of 66%, when uncemented prostheses are excluded. Yet, 18 of 74 (24%) patients with a cemented prosthesis, whose symptoms settled with conservative management, had three or more areas of increased activity.

42 (43%) of the 98 prostheses demonstrated increased activity related to the acetabulum. Seven of these subsequently had revision surgery performed but in only two (5%) was the acetabulum found to be loose. Two further hips demonstrating acetabular loosening at surgery and the three infected prostheses had no increase in activity at this site. Three prostheses with increased acetabular activity were Thompson's hemiarthroplasties and such activity is known to be a feature of acetabular migration (Rushton & Wraight, 1981). Considering two part prostheses only, increased acetabular activity as an indication for revision surgery would give a sensitivity of 50% and specificity of 58%.

32 hips were studied by dynamic bone scanning. A positive study was considered as suggesting infection rather than aseptic loosening. 28 were normal of which five subsequently had revision surgery with one hip infected (false negative). Four dynamic studies were abnormal with three of these undergoing revision for loosening; one was treated conservatively (all false positives).

42 of the prostheses studied also had gallium images available but none of these had revision surgery for infection. 26 gallium scans were normal but 16 (38%) demonstrated areas of increased activity. Three of these

Table II. The number of patients (%) and the number of sites around the femoral component with increased activity for various patient groups

	Number of sites affected					
	0	1	2	3	4	Total
Infected	1 (33)	0 (0)	0 (0)	1 (33)	1 (33)	3
Femoral loosening	0 (0)	2 (18)	2 (18)	2 (18)	5 (45)	11
Not operated	18 (21)	24 (29)	19 (11)	8 (10)	15 (18)	84
uncemented	0 (0)	0 (0)	3 (38)	3 (38)	2 (25)	8
cemented	18 (24)	24 (32)	16 (21)	5 (7)	13 (17)	76

Table III. The most discriminating patterns of activity around the femoral component for painful cemented prostheses (sensitivity 85%, specificity 66%)

Conservative management	Revision surgery
No increased activity	
Activity limited to one site only (especially the greater trochanter)	Activity in three or four sites
Activity in: (a) greater trochanter and shaft (b) greater trochanter and tip (c) tip and shaft	Activity in the lesser trochanter and one other site

showed incongruous uptake when correlated with the diphosphonate images and hence were falsely positive for infection.

Discussion

The normal scintigraphic appearances of a hip replacement have been derived from studies on painless prostheses and it is generally considered that activity should not exceed that of surrounding osseous structures 9 months post-operatively. However, the largest reported study of asymptomatic prostheses (Utz et al, 1986) describes increased activity at a number of sites persisting for more than 1 year in a significant number of patients. In clinical practice, bone scintigraphy is often used to help decide whether a painful hip prosthesis requires revision surgery and this group may demonstrate abnormalities on bone scintigraphy that are not due to loosening or infection but may reflect another process that causes pain. Taylor et al (1989) described scintigraphic abnormalities in 29% of hips not requiring revision but do not consider in detail the patterns of abnormality in these patients and the criteria for loosening and infection are not clearly defined. Williamson et al (1979) observed causes, other than loosening or infection, for increased activity on bone scintigraphy including heterotopic calcification and non-specific synovial inflammation.

In 84% of the hips in our series, the pain settled without operative intervention and 81% of these had at least one area of increased activity related to the prosthesis, with 27% having three or more areas around the femoral component affected (Fig. 1). Uncemented prostheses were particularly likely to have extensive activity around the femoral component, accounting for 22% of those with three or more affected areas but only 10% of the total number of hips studied. This is in accordance with the experience of Rushton and Wraight (1980) when studying uncemented Thompson's hemiarthroplasties. Our series also included some newer designs of uncemented total hip replacement, including porous coated prostheses, and these demonstrated similar abnormalities in keeping with the findings of Oswald et al (1989). Such prostheses are being used with increasing frequency and the diagnosis of loosening or infection in these patients will be particularly difficult.

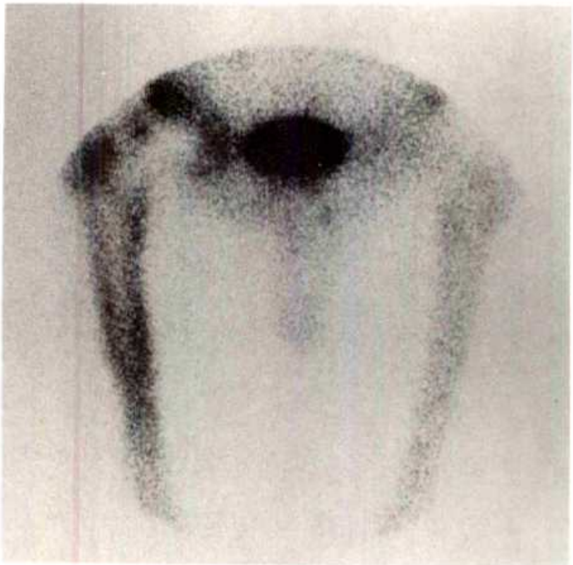

Figure 1. Anterior ^{99}Tc^{m}-diphosphonate image at 3 h, demonstrating widespread increased activity around the femoral component with focally increased activity in the acetabulum. The patient's symptoms settled with conservative management.

We found a low probability that a hip replacement would require revision if the bone scan demonstrated no area of increased activity, activity localized to the greater trochanter, tip or shaft, or in the greater trochanter and tip, greater trochanter and shaft, or tip and shaft. Abnormalities at the greater trochanter were very common, occurring in 45% of hips studied. Causes for activity in this area may be readily appreciated from plain radiographs, including heterotopic bone formation or previous trochanteric osteotomy, an un-united osteotomy being well recognized as a cause for post-operative pain. Utz et al (1986) report in asymptomatic prostheses 1 year post-operatively, that 35% will have significantly increased activity in the greater trochanter and 9% show persistent activity at the tip. Weiss et al (1979) also describe increased activity in the greater trochanter in asymptomatic patients.

Increased activity in the acetabulum was very common, occurring in 43% of cases, and is a poor indicator of acetabular loosening with low sensitivity and specificity. Lower accuracy for acetabular loosening has been reported by other authors (Aliabadi et al, 1989) and Utz et al (1986) found 30% of asymptomatic prostheses had significantly increased activity in the acetabulum 1 year post-operatively. The diagnosis of acetabular loosening by scintigraphy will thus remain difficult.

We have found that abnormalities on dynamic bone studies and gallium-67 citrate scintigraphy also occur in hip replacements with symptoms that settle spontaneously. Arterial and blood pool diphosphonate images that demonstrate increased blood flow are not specific for infection, occurring in up to 30% of loose prostheses (Pearlman, 1980), but could also reflect other causes of prosthetic pain. The increased activity seen on gallium scintigraphy was predominantly non-specific bone uptake, parelleling the diphosphonate activity, but we did have three gallium scans falsely positive for infection and this is also reported by other authors (Rosenthall et al, 1979; Horoszowski et al, 1980; Mountford et al, 1986).

In the management of a patient with a painful hip replacement, the absence of any abnormality on bone scintigraphy or increased activity at limited sites around the femoral component, particularly the greater trochanter or shaft, will be of high value in deciding if operative intervention is not required. If any scintigraphic abnormality is present, causes other than loosening and infection should be considered. The plain radiographs, and a knowledge of the type of prosthesis and whether cemented, are essential for full assessment as they may account for the scintigraphic appearances. Such information should be available at the time of reporting. More extensive abnormalities, particularly if the lesser trochanter or tip are involved, suggest that symptoms are less likely to resolve spontaneously but the decision to perform revision surgery should be made considering the clinical features and radiographic appearances; further investigation may be required. This may include arthrography for loosening and gallium-67 citrate or labelled white cell studies for infection. Unless there is a clear indication for immediate surgery, a period of conservative management should be considered.

References

Aliabadi, P., Tumeh, S. S., Weissman, B. N. & McNeil, B. J., 1989. Cemented total hip prosthesis: radiographic and scintigraphic evaluation. *Radiology*, *173*, 203–206.

Horoszowski, H., Ganel, A., Kamhin, M., Zaltaman, S. & Farine, I., 1980. Sequential use of technetium-99m MDP and gallium-67 citrate imaging in the evaluation of painful total hip replacement. *British Journal of Radiology*, *53*, 1169–1173.

Mountford, P. J., Hall, F. M., Wells, C. P. & Coakley, A. J., 1986. ^{99}Tc^{m}-MDP, ^{67}Ga-citrate and ^{111}In-leucocytes for detecting prosthetic hip infection. *Nuclear Medicine Communications*, *7*, 113–120.

Oswald, S. G., Nostrand, D. G., Savory, C. G. & Callaghan, J. J., 1989. Three-phase bone scan and idium white blood cell scintigraphy following porous coated hip arthroplasty: a prospective study of the prosthetic tip. *Journal of Nuclear Medicine*, *30*, 1321–1331.

Pearlman, A. W., 1980. The painful hip prosthesis: value of nuclear medicine imaging in the diagnosis of late complications. *Clinical Nuclear Medicine*, *5*, 133–142.

Rosenthall, L., Lisbona, R., Hernandez, M. & Hadjipaviou, A., 1979. ^{99m}Tc-PP and ^{67}Ga imaging following insertion of orthopaedic devices. *Radiology*, *133*, 717–721.

Rushton, N. & Wraight, E. P., 1980. Technetium-99m methylene diphosphonate scanning in Thompson hemiarthroplasties. *British Journal of Radiology*, *53*, 781–783.

—— 1981. The early detection of acetabular migration after Thompson hemiarthroplasty using technetium bone scanning. *Nuclear Medicine Communications*, *2*, 345–350.

Taylor, D. N., Maughan, J., Patel, M. P. & Clegg, J., 1989. A simple method of identifying loosening or infection of hip prostheses in nuclear medicine. *Nuclear Medicine Communications*, *10*, 551–556.

Utz, J. A., Lull, R. J. & Galvin, E. G., 1986. Asymptomatic total hip prosthesis: natural history determined using Tc-99m MDP bone scans. *Radiology*, *161*, 509–512.

Weiss, P. E., Mall, J. C., Hoffer, P. B., Murray, W. R., Rodrigo, J. J. & Genant, H. K., 1979. ^{99m}Tc-methylene diphosphonate bone imaging in the evaluation of total hip prostheses. *Radiology*, *133*, 727–729.

Williamson, B. R. J., McLaughlin, R. E., Wang, G. J., Miller, C. W., Teates, C. D. & Bray, S. T., 1979. Radionuclide bone imaging as a means of differentiating loosening and infection in patients with a painful total hip prosthesis. *Radiology*, *133*, 723–725.

1992. *The British Journal of Radiology*, *65*, 495–501

Magnetic resonance imaging of pulsatile cerebrospinal fluid flow by spatial modulation of magnetization

By S. C. Wayte, BSc, T. W. Redpath, PhD and *D. J. Beale, FRCR

Departments of Clinical Physics and Bioengineering and *Radiology, Walsgrave Hospital, Clifford Bridge Road, Coventry CV2 2DX, UK

(*Received 22 August 1991 and in revised form 8 January 1992, accepted 11 January 1992*)

Keywords: MRI, Flow measurement, CSF

Abstract. Various orders of binomial spatial modulation of magnetization sequences up to (1 4 6 4 1) have been tested to find the optimum sequence for clinical application. Stripe width, stripe sharpness and the tolerance of the sequences to radiofrequency non-linearity have been investigated. The (1 3 3 1) sequence was found to be a good compromise between competing design criteria, and its application to viewing pulsatile cerebrospinal fluid motion is described.

Spatial modulation of magnetization (SPAMM) is a technique to show motion in magnetic resonance imaging (MRI), and was first introduced by Axel and Dougherty (1989). The SPAMM pulses can be placed in front of any normal imaging sequence. The sequence produces periodic spatial modulation of the longitudinal magnetization in the direction of one of the gradients in the image plane, resulting in a stripe pattern in the final image. Any movement between the time of application of the modulation of the magnetization and the time of data collection causes a displacement of the stripes along the direction of movement.

The other commonly used technique for imaging flow in MRI is phase-encoding. This method was first reported by Moran (1982) and uses bipolar pulse gradients to produce isochromats with a phase that is dependent on their velocity. Phase-encoded imaging requires calibration using a flow phantom. Acceleration and higher orders of motion introduce errors (Nayler et al, 1986).

As well as steady cerebrospinal fluid (CSF) movement resulting from its production in the ventricles and reabsorption in the arachnoid villi, the flow also has a pulsatile component because of the cardiac cycle (Du Boulay, 1966). MRI is the only technique that can be used to image the pulsatile flow of CSF non-invasively.

In cases of hindbrain herniation with associated syringomyelia, the pulsatile movement of the CSF is often severely affected (Williams, 1990). The SPAMM sequence can be used to investigate whether corrective surgery for this condition has restored pulsatile flow, as this is an indicator that the potentially damaging pressure difference between intra- and extracranial CSF has been reduced.

Theory

The SPAMM sequence uses a series of non-selective radiofrequency (RF) pulses separated by gradient pulses. These RF pulses have amplitudes that follow the binomial distribution in a method analogous to that used by Hore (1983) for solvent suppression in nuclear magnetic resonance (NMR) spectroscopy. Thus, RF pulses with relative amplitudes (1 1), (1 2 1), (1 3 3 1), (1 4 6 4 1), etc. can be used in the SPAMM sequence. The SPAMM sequences up to (1 3 3 1) are shown in Fig. 1. The RF pulse magnitudes were set to give a total SPAMM flip angle of 90°.

The strength and duration of the gradient between each binomial RF pulse dictates the separation between stripes according to the equation:

$$\delta x = \frac{2\pi}{\gamma \int_0^t G(t)\mathrm{d}t} \qquad (1)$$

where δx is the stripe separation, γ is the gyromagnetic ratio, $G(t)$ is the gradient amplitude as a function of time and t is the duration of a single gradient pulse (see Fig. 1a).

A series of $(n+1)$ RF pulses separated by a time interval of $2T$ with their amplitudes following the binomial distribution, if regarded as delta pulses, can be represented mathematically by the formula:

$$H(t) = \tfrac{1}{2} \sum_{k=0}^{n} \binom{n}{k} \delta[T(n-2k)+t] \qquad (2)$$

where $H(t)$ is the RF pulse amplitude as a function of time. This formula has the Fourier transform:

$$H(\omega) \alpha \cos^n(\omega T) \qquad (3)$$

as given by Hore (1983).

Thus, in the frequency domain, a cosinusoidal modulation of magnetization, or stripe pattern, would be produced.

If the phase of the RF pulses are alternated between 0° and 180°, to produce (1 $\bar{1}$), (1 $\bar{2}$ 1), (1 $\bar{3}$ 3 $\bar{1}$), etc.

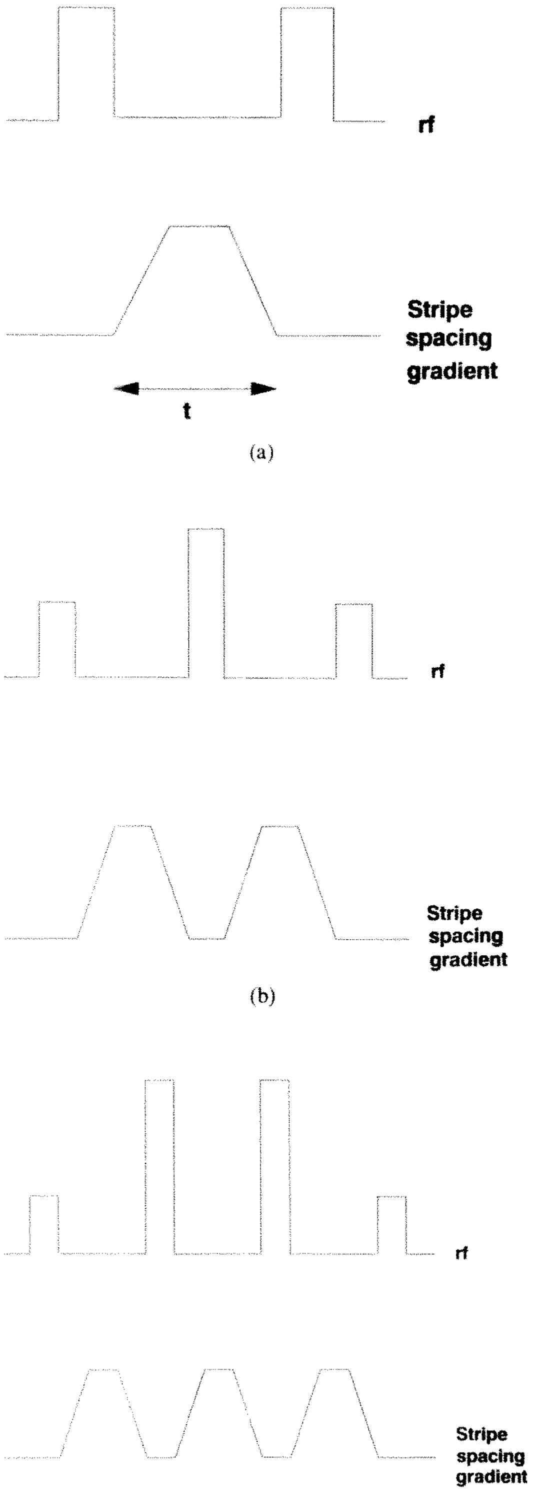

Figure 1. Various order SPAMM RF pulses and stripe spacing gradients are depicted. The relative RF amplitudes shown are (a) (1 1), (b) (1 2 1), and (c) (1 3 3 1).

sequences, the corresponding mathematical representation for these RF pulses is:

$$H(t) = \tfrac{1}{2} \sum_{k=0}^{n} (-1)^k \binom{n}{k} \delta[T(n-2k)+t], \tag{4}$$

which has the Fourier transform:

$$H(\omega) \alpha \sin^n(\omega T). \tag{5}$$

The modulation of magnetization produced in the image is given by the modulus of $H(\omega)$. Thus, according to Fourier theory, the only effect the phase alternation of the RF pulses has on the image is to offset the phase of the stripes by half a cycle.

Equations 3 and 5 show that the order of the sine and cosine functions in the frequency domain increases as the number of RF pulses increases. As the sine and cosine functions are raised to higher powers, the gradients between their peaks and troughs will become steeper. Fourier transform theory, therefore, implies that as the number of RF pulses is increased the stripes will become sharper.

The response of the imaging systems to RF excitation is not linear, so that Fourier transform theory is only an approximation. Therefore, the effect of the SPAMM imaging pulses was modelled using a computer program based on the Bloch equations in the rotating frame. Relaxation was not taken into account.

Owing to RF transmission non-linearity the RF pulses applied during imaging might not be those specified by the pulse amplitudes. Any RF transmission non-linearity in the system will result in an alteration of the ratio between the RF pulse amplitudes. Consider the flip angles produced by the ideal (1 $\overline{2}$ 1) sequence on resonance. The first RF pulse, which is applied along the x axis, rotates the isochromat through an angle of 1, in units where 4 ($=1+2+1$) corresponds to 90°. The second RF pulse, which is applied along the $-x$ axis, acts on the isochromat to produce a final angle of -1 to the B_0 field. The final RF pulse applied along the x axis returns the isochromat to an angle of 0°. Following the same steps for the other phase-alternated sequences with ideal RF amplitudes, it can be verified that they all produce a final isochromat angle of 0°. Thus, any altered ratio sequences that result in a final alignment of the isochromat along B_0 will be least affected by non-linearities.

Table I. Calculation of the intermediate and final angle of an isochromat to B_0 for non-linear RF pulses

Amplitude of RF pulse	1		$\overline{2.5}$			1					
Intermediate flip angle		1			$\overline{1.5}$						
Final flip angle							$\overline{0.5}$				
Amplitude of RF pulse	1		$\overline{3.75}$				3.75	$\overline{1}$			
Intermediate flip angle		1			$\overline{2.75}$			1			
Final flip angle									0		
Amplitude of RF pulse	1		$\overline{5}$		9.375			$\overline{5}$		1	
Intermediate flip angle		1		$\overline{4}$			5.375		0.375		
Final flip angle											1.375

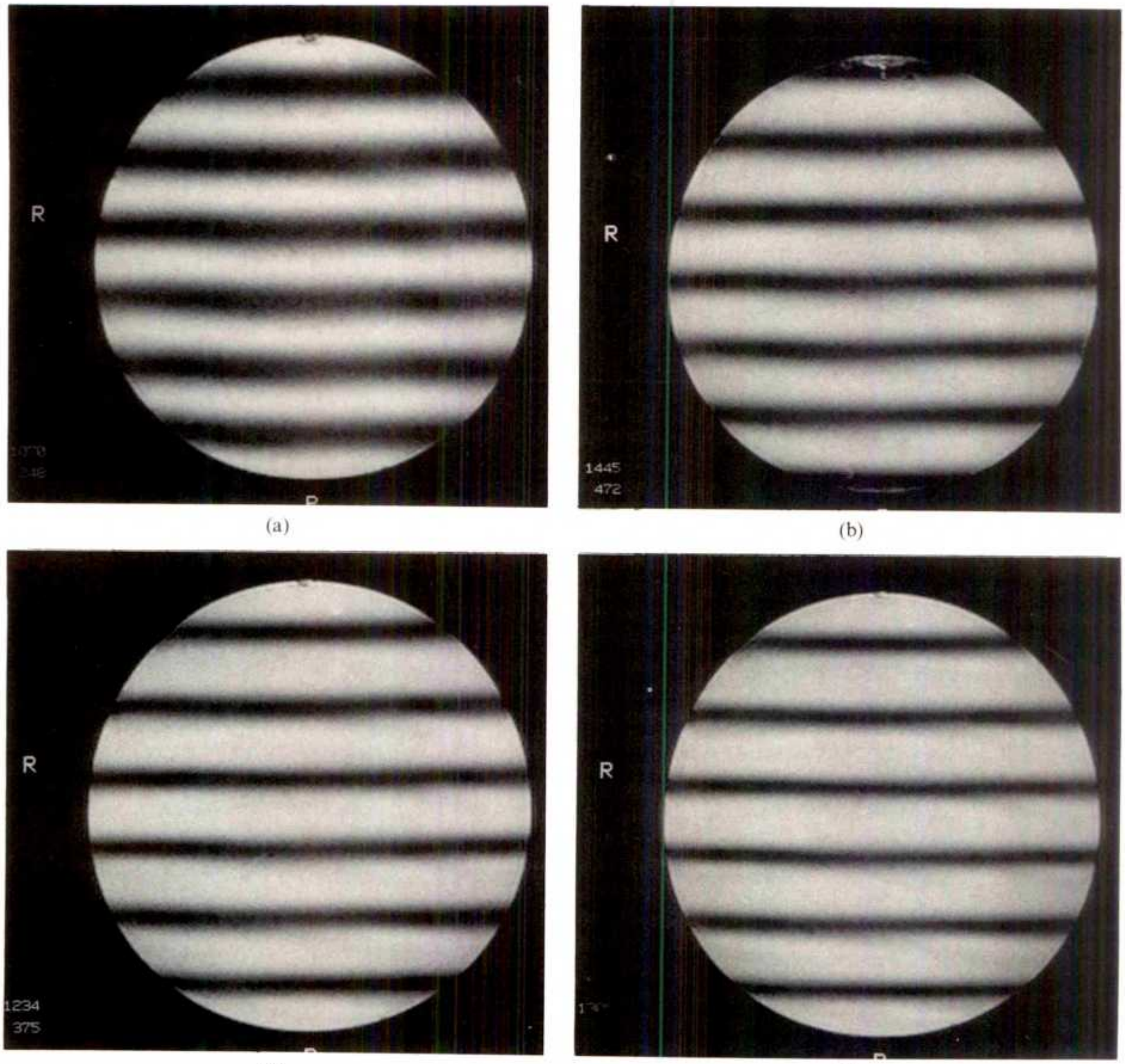

(a) (b) (c) (d)

Figure 2. Images obtained of a $CuSO_4$ doped phantom using the various SPAMM pulses in front of a field echo sequence. The RF pulse amplitudes used to produce the images were (a) (1 1), (b) $(1\ \bar{2}\ 1)$, (c) (1 3 3 1), and (d) (1 4 6 4 1). The stripes are displaced by half a cycle in the $(1\ \bar{2}\ 1)$ sequence owing to its phase alternation.

To computer-simulate RF transmission non-linearities, the binomial sequences $(1\ \bar{2}\ 1)$, $(1\ \bar{3}\ 3\ \bar{1})$ and $(1\ \bar{4}\ 6\ \bar{4}\ 1)$ had the ratios of their pulse amplitudes all increased progressively by 20% to form $(1\ \overline{2.5}\ 1)$, $(1\ \overline{3.75}\ 3.75\ \bar{1})$ and $(1\ \bar{5}\ 9.375\ \bar{5}\ 1)$ sequences. It was assumed that the sequences still produced an overall flip angle of 90°. The final angle of the isochromat to B_0 for all these sequences is shown in Table I.

Only the $(1\ \overline{3.75}\ 3.75\ \bar{1})$ sequence has a final flip angle of 0° in Table I, and is therefore expected to be the least affected by RF non-linearity. It can be seen that the maximum signal intensity of the $(1\ \bar{3}\ 3\ \bar{1})$ sequence will be unaffected, whatever non-linearity were introduced into the sequence, owing to its inherent symmetry (*i.e.* for each RF pulse in the sequence there is another pulse of exactly the same amplitude that negates the effect of the first pulse). This is also true for a $(1\ \bar{5}\ 10\ \overline{10}\ 5\ \bar{1})$ sequence, or any sequence with an even number of phase-alternated pulses. These conclusions also apply to the sequences without phase alternation of the RF pulses, since phase alternation only has the effect of shifting the stripe pattern by half a cycle.

For SPAMM sequences with RF pulses of identical lengths, giving a composite 90° flip angle, the energy

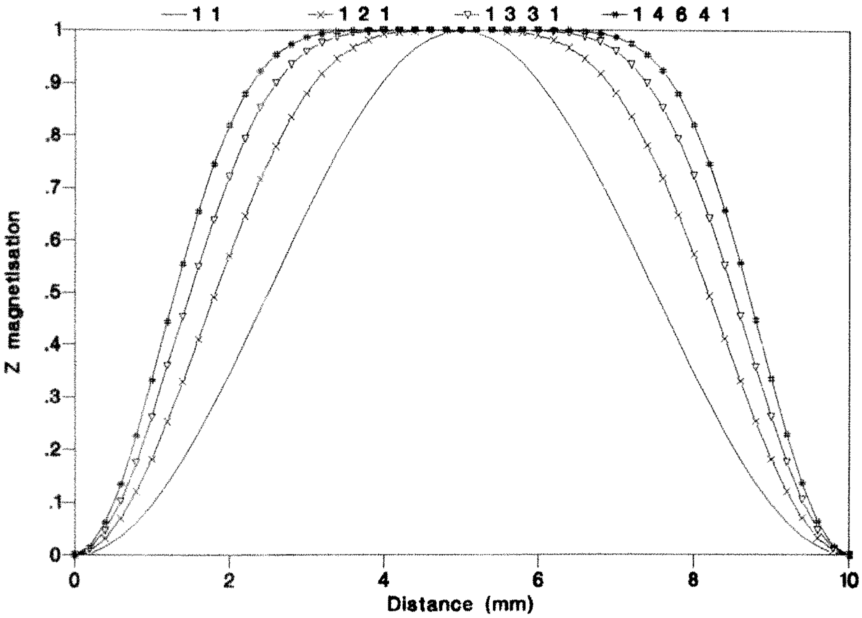

Figure 3. Computer model prediction of the variation of longitudinal magnetization with distance, over one cycle, for the different order SPAMM sequences up to (1 4 6 4 1).

deposited by the sequences decreases as the number of RF pulses increases (*e.g.* the (1 3 3 1) sequence deposits 15% more energy than the (1 4 6 4 1) sequence).

Materials and methods

SPAMM sequences using RF amplitudes in the ratio (1 1), (1 $\bar{2}$ 1), (1 3 3 1) and (1 4 6 4 1) were implemented on a phantom using a 0.5 T MRI system (Picker 2055HP). The phantom contained water doped with $CuSO_4$ to give $T_1 = T_2 = 200$ ms. All the SPAMM RF pulses used were non-selective square pulses with a duration of 0.6 ms and a separation of 4 ms between the pulse centres. In the gap between each pulse, 3 ms read gradient pulses were used to produce the stripe spacing. The amplitude of these gradient pulses was set to give a stripe separation of 1 cm, so that the normal maximum pulsatile caudal flow velocity of the CSF, which is of the order of 3 cm/s (Ridgway et al, 1987), would not produce a displacement of more than half a stripe separation within the echo time (TE = 100 ms), thus avoiding ambiguities. For convenience, in order to reduce the performance time for the phantom tests, the SPAMM pulses were placed in front of a conventional gradient-echo sequence. The time interval between the end of the last SPAMM pulse and start of the imaging gradients of the gradient-echo sequence was 1 ms.

The effect of RF transmission non-linearities was investigated using the computer simulation program. It was assumed that the non-linear RF pulses still produced a total overall flip angle of 90°, since the total flip angle of the sequences are calibrated on the MRI scanner to be 90°, prior to the sequences being used for imaging. The ratios of the RF pulses were increased progressively by 20%, to produce the sequences (1 2.5 1), (1 3.75 3.75 1) and (1 5 9.375 5 1).

The SPAMM (1 3 3 1) pulses, with the same pulse timings as the SPAMM pulses used to image the phantoms, were used clinically preceding a T_2-weighted spin-echo sequence with second-order motion compensated gradients. Cardiac gating was applied and data were collected every other heart beat. 150 ms after the R wave, the SPAMM pulses were applied, followed by a gap of 1 ms before the imaging sequence. The spin-echo, therefore, occurred 250 ms after the R wave. CSF motion was thus imaged over a period of 150–250 ms after the R wave, which corresponds to the region of peak CSF displacement (Ridgway et al, 1987).

Results and discussion

The images obtained using the SPAMM sequences with various amplitude RF pulses on the phantom containing $CuSO_4$ are shown in Fig. 2. The (1 $\bar{2}$ 1) sequence has its stripes offset by half a cycle with respect to all the other images, since the SPAMM RF pulses were phase alternated.

The graphs obtained from the computer simulation program, using the same pulse timings and amplitudes as those used in the phantom images, are shown in Fig. 3, but without phase alternation being used. This plot shows that as the number of RF pulses increases, the width of the troughs decreases, and the trough edges become steeper. Thus, the greater the number of RF pulses used to produce the stripes, the larger the area of the image there will be at the full signal level, which will facilitate image interpretation. This is visually confirmed by Fig. 2.

The higher the order of the RF sequence the greater the time required to produce the modulation of magnetization. As this time period increases so does the amount of relaxation of magnetization and the chance of tissue movement. These two effects may lead to stripe degradation.

The plots produced by the computer programs to test non-linearity are shown in Fig. 4. The altered ratio sequences are plotted along with the original SPAMM pulses as a comparison. It can be seen that, as predicted, the non-linearity has the least effect on the symmetrical sequences. In the other sequences the non-linearity reduces the height of the peaks, thus reducing the maximum signal intensity. The width of the peaks is also reduced, thus decreasing the area of the image at the maximum signal intensity. The (1 3 3 1) sequence has its peak width slightly reduced by non-linearity, but the height of the peaks remains the same, so that the maximum signal intensity is unchanged.

Clinical images obtained using the (1 3 3 1) sequence preceding a T_2-weighted spin-echo sequence, with motion compensating gradients, are shown in Fig. 5.

Figure 5a shows the mid-line sagittal T_1-weighted image of a volunteer, Fig. 5b is the corresponding SPAMM image. CSF flow can be seen in the cervical region below the foramen magnum, in the pre-pontine region and, to a lesser extent, in the fourth ventricle.

Figures 5c and 5d show the T_1-weighted and SPAMM images, respectively, of a patient with hindbrain herniation. In the SPAMM image there is evidence of CSF flow in the cervical region, but no flow is visible in the fourth ventricle or in the pre-pontine region.

Figures 5e and 5f depict a mid-line sagittal T_1-weighted image and the corresponding SPAMM image of a patient who has had successful corrective surgery for hindbrain herniation. During the surgery the tonsils were pinned back, and a pouch opened up to allow the CSF to flow around the cervical region of the spinal cord. It can be seen that the CSF flow pattern is very similar to that in the normal patient, with CSF flow occurring in the fourth ventricle, the pre-pontine region and the cervical region.

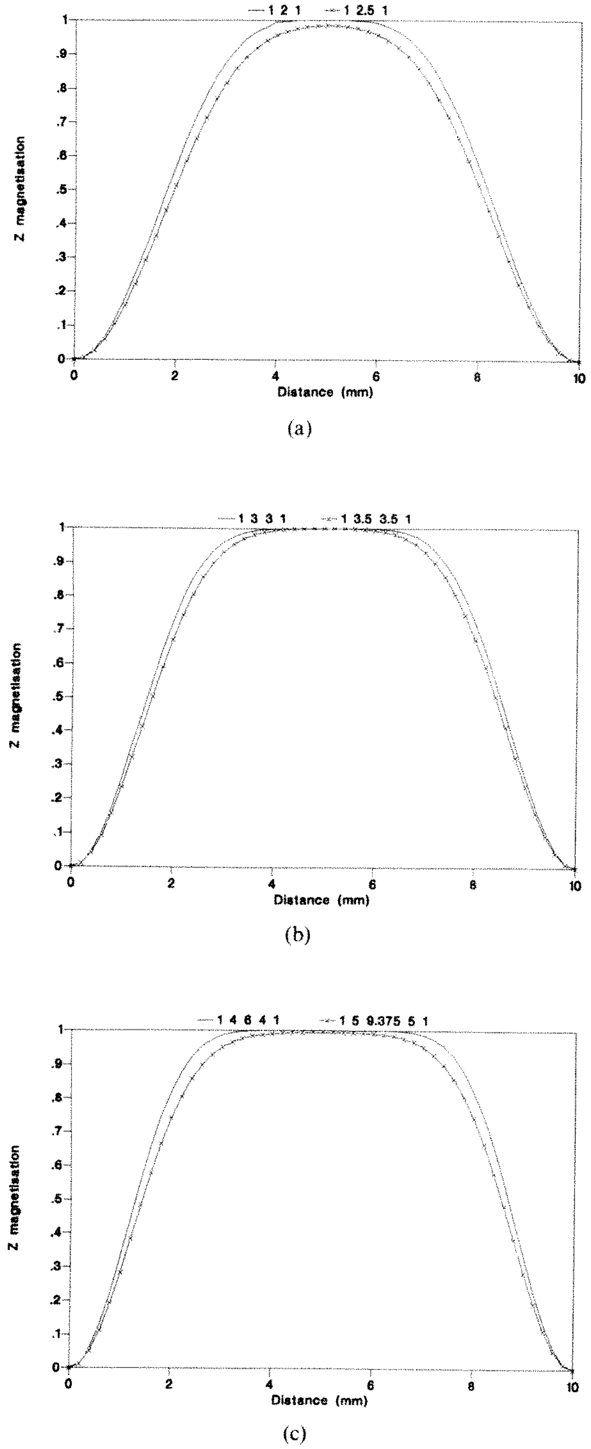

Figure 4. Computer model prediction of the variation of longitudinal magnetization with distance from the point of resonance for the SPAMM sequences with ideal RF amplitudes and those with altered ratios. The RF amplitudes used to produce the plots were (a) (1 2 1) and (1 2.5 1), (b) (1 3 3 1) and (1 3.75 3.75 1), and (c) (1 4 6 4 1) and (1 5 9.375 5 1).

Conclusion

Our results suggest that the (1 3 3 1) sequence is the best sequence to implement clinically since it has almost as sharply defined troughs as the (1 4 6 4 1) sequence, is more tolerant of RF non-linearity, and takes less time to produce the stripe pattern than other higher ordered sequences. However, it does have a higher energy deposition than the (1 4 6 4 1) sequence.

The SPAMM images obtained clinically using the (1 3 3 1) sequence give useful information about the distribution of pulsatile CSF flow around the upper cord and brain stem. However, an insufficient number of patients has been imaged to draw any firm conclusions about the expected CSF flow pattern in patients with hindbrain herniation.

Acknowledgment

We thank Mr Bernard Williams of the Midland Centre for Neurosurgery and Neurology for his co-operation in this study, Dr Ray Dupree of the University of Warwick for his advice and encouragement, and Mr A. McIntosh, Director of Clinical

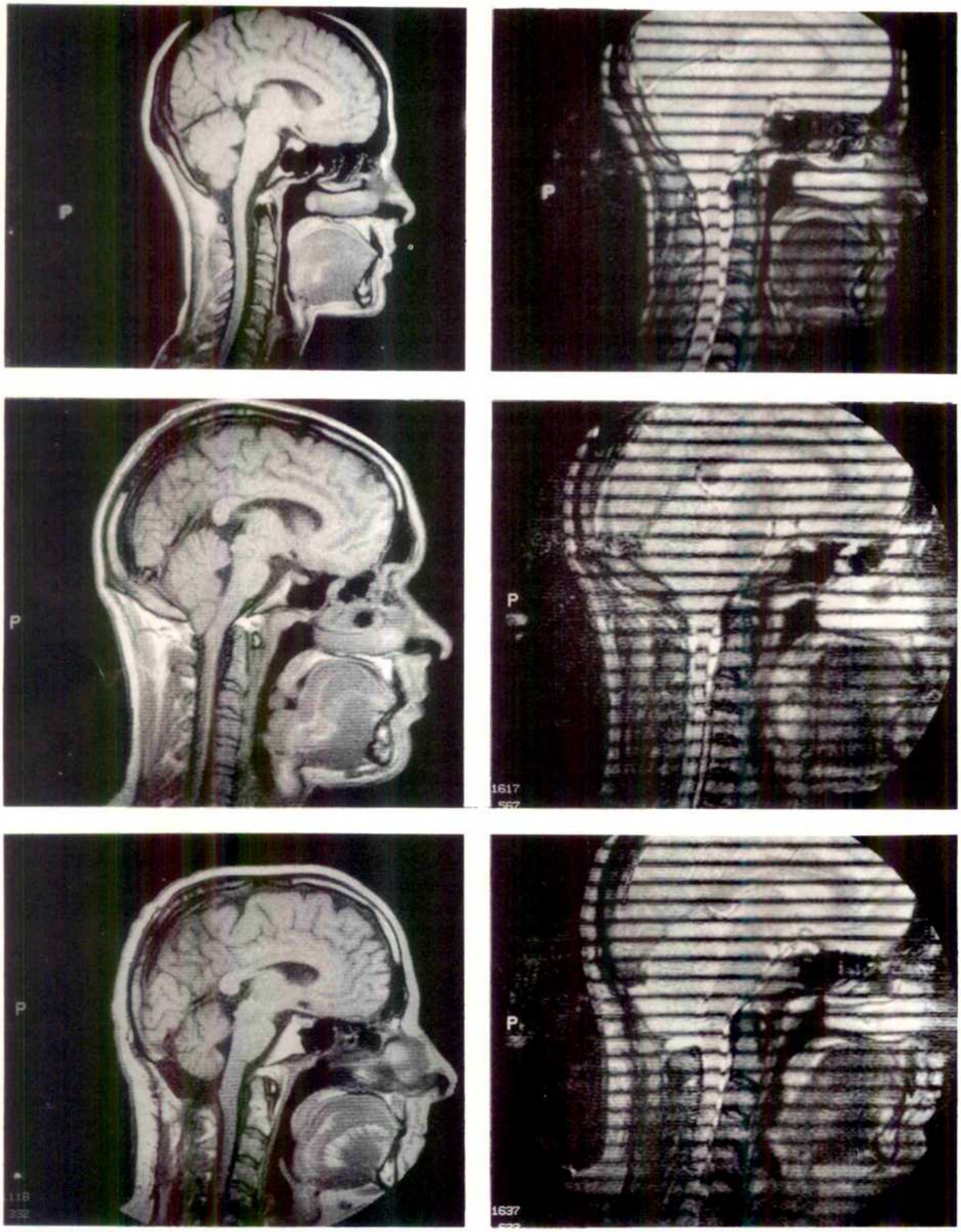

(e) (f)

Figure 5. Pairs of midline sagittal images with (a, c, e) a T_1-weighted sequence and (b, d, f) a (1 3 3 1) SPAMM sequence preceding a T_2-weighted spin-echo (TE = 100 ms) sequence. (a) and (b) are for a normal volunteer, (c) and (d) are for a patient with hindbrain herniation, and (e) and (f) are for a patient with corrective surgery for hindbrain herniation.

Physics and Bioengineering, Walsgrave Hospital, for his support.

We are grateful to Picker International Inc. for the use of their sequence generating software, which has been supplied under a mutual research agreement.

References

AXEL, L. & DOUGHERTY, D., 1989. MR imaging of motion with spatial modulation of magnetization. *Radiology, 171,* 841–845.

DU BOULAY, G. H., 1966. Pulsatile movements in the CSF pathways. *British Journal of Radiology, 39,* 255–262.

HORE, P. J., 1983. A new method for water suppression in the proton NMR spectra of aqueous solutions. *Journal of Magnetic Resonance, 54,* 539–542.

MORAN, P. R., 1982. A flow velocity zeugmatographic interlace for NMR imaging in humans. *Magnetic Resonance Imaging, 1,* 197–203.

NAYLER, G. L., FIRMIN, D. N. & LONGMORE, D. B., 1986. Blood flow imaging by cine magnetic resonance. *Journal of Computer Assisted Tomography, 10,* 715–722.

RIDGWAY, J. P., TURNBULL, L. W. & SMITH, M. A., 1987. Demonstration of pulsatile cerebrospinal-fluid flow using magnetic resonance phase imaging. *British Journal of Radiology, 60,* 423–427.

WILLIAMS, B., 1990. Syringomyelia. *Neurosurgery Clinics of North America, 1,* 653–685.

THE SOMERSET
MRI
COURSE

THE FIFTH SOMERSET MAGNETIC RESONANCE IMAGING COURSE

SUNDAY, OCTOBER 25th – THURSDAY 29th 1992

St Pierre Hotel Golf and Country Club
Chepstow, Gwent

This five day course consists of a comprehensive series of lectures and workshops covering all aspects of Magnetic Resonance Imaging and is aimed at Radiologists who are practicing MR as well as to introduce other Radiologists to the technique.

The international faculty will include:

DAVID STARK (Massachusetts), MURRAY SOLOMON (California), GEORGE HARTNELL (Massachusetts), GRAEME BYDDER (London), JANET HUSBAND (London),

Residential Registration £600 Non-Residential Registration £325

This Course is approved by the Royal College of Radiologists.

For further information contact:

Rachel Amesbury, Course Secretary, The Somerset MRI Centre, The Kerland Clinic, Marsh Lane, Nr Bridgwater, Somerset, TA6 6LQ. Telephone: 0278 429094. Fax: 0278 429622.

The Second Annual

INTRODUCTORY MRI COURSE

THE
ROYAL MARSDEN
HOSPITAL

18th - 21st January 1993

Course organisers –
V. T. Ayton DCRR
Dr J. E. Husband FRCR
Dr R. L. Guy FRCR

The course will consist of formal lectures as well as tutorials, practical workshops and a quiz.

Emphasis will be placed on active participation and the number of delegates will therefore be limited to fifty. Early application is advised.

For further information and application form contact
Miss P. Johnston,
Department of Diagnostic Radiology,
The Royal Marsden Hospital, Downs Road,
Sutton, Surrey SM2 5PT,
United Kingdom
Tel: 081-642 6011
Extn: 3215.
Fax No: 081-770 1643

One Day Teaching Seminar

STEREOTACTIC EXTERNAL BEAM RADIOTHERAPY
RADIOSURGERY
using Linear accelerator

The Royal Marsden Hospital, London, SW3
Friday, 16th October 1992

Do you wish to set up radiosurgery in your hospital ? Do you know what is involved ? Why do you need it ?

Intensive one day teaching seminar for the neurosurgeon, radiation therapist, physicist and neuro-oncologist providing a detailed insight into the practical aspects of the technique and application of radiosurgery using conventional radiotherapy equipment. Topics will include methods of fixation, imaging, treatment planning, treatment delivery and the role in the management of brain tumours and AVM's.

Course fee £110.00
Enquiries and applications to:
Dr M Brada, Neuro-oncology Unit
The Royal Marsden Hospital
Downs Road, Sutton, Surrey, SM2 5PT, UK
Tel: 081 642 6011 Ext. 3272 Fax: 081 643 5468

Bielefeld

– Ihr Arbeitgeber –

Municipal Hospital of Bielefeld

Our Clinic of Radiology and Nuclear Medicine offers a vacancy as a

Technician for Radiology

Knowledge of the German language is required.

Bielefeld, a town in West Germany between Dortmund and Hannover, has 300,000 inhabitants. It is situated in a wonderful landscape near the Teutoburger Forest.

Bielefeld has excellent cultural facilities: two theatres, the Oetkerhalle Concert Hall and the Municipal Music Hall.

We can offer an apartment in our hostel for nurses.

The Clinic of Radiology and Nuclear medicine supplies 356 beds. They are divided between the Medical Clinic, the Surgical Clinic and the Gynaecological Clinic.

For more information do not hesitate to contact the Head of the Clinic, **Dr. Bockslaff. Tel. (0049 521) 4474-340**

Please send your CV (school reports, licence of your profession and a short personal record) for the attention of: **Mrs.. Fortmann, Administration of the Municipal Hospital, Teutoburger Str. 50, 4800 Bielefeld 1, Germany**

Die freundliche Stadt am Teutoburger Wald

BIR THE BRITISH INSTITUTE OF RADIOLOGY

Where there's a will
there's a way

Remembering the British Institute of Radiology in your Will is a lasting and ever important way to ensure the continued development of the BIR.

Full details on giving by way of a legacy and donation may be obtained from:

The Administration Manager
British Institute of Radiology
36 Portland Place
London, W1N 4AT

With your help we will succeed

The Future of Human Radiation Research (BIR Report 22)

Editors: G B Gerber, D M Taylor, E Cardis and J W Thiessen.

Contains the full review papers presented at a workshop held at Schloss Elmau on 4th-8th March 1991 under the joint sponsorship of the US Department of Energy, the Radiation Effects Research Foundation of Japan, the International Agency for Research on Cancer and the Commission of the European Communities.

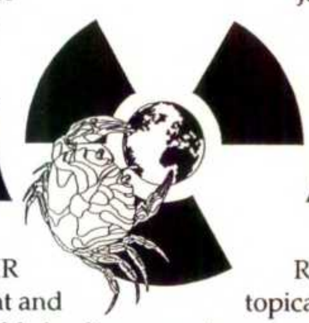

This publication complements BIR Report 21 Risks from Radium and Thorotrast. It covers the important and topical subject of cancer risk prediction and contains papers from the worlds leading experts.

ISBN 0 905749 27 8, 174pp, 265mm x 197mm, Illustrated, Softcover, £27.50
(25% discount for BIR members)

BIR MERCHANDISE

BIR T-Shirts are available to members at **£7.50** each (including postage). They come in black and fluorescent with a white skeleton on the front and back. We also have children's sizes at only **£4.00.**

100% silk BIR ties are **£15.00** each (including postage). Available in navy, they carry the rays from the Institute's logo, in gold.

Please send your remittance to: Helen Smith, Sales and Promotions Manager, 36 Portland Place, London W1N

Buy yours now!

BIR **NYCOMED**

The British Institute of Radiology
Nycomed Scandinavian Scholarships 1993

The British Institute of Radiology invites applications for two Nycomed Scandinavian Scholarships.

These scholarships — generously funded by Nycomed (UK) Ltd — are to enable diagnostic radiologists of senior registrar or junior consultant status, preferably members of the British Institute of Radiology, interested in diagnostic or interventional procedures concerned with intravascular contrast media, to visit one or more academic departments of Radiology in Scandinavia (Norway, Sweden, Finland, Denmark) for in-depth radiological experience. A maximum of £5,000 will be available for each scholarship to permit **two months** of concentrated study free of financial constraints. The recipients will be responsible for their itinerary, travel, accommodation and insurance arrangements, subject to the approval of the BIR.

A condition of the scholarships is that a report of work undertaken, in a form suitable for publication in the Bulletin of the British Institute of Radiology, shall be submitted.

Applications are invited and should be submitted by **31 August 1992.** The application, containing a detailed CV, should detail both the purpose of the visit and the costings and indicate that agreement has been reached with the Scandinavian department(s) concerned. Interviews will take place in October.

For further information please write to:
The General Secretary
The British Institute of Radiology
36 Portland Place
London W1N 4AT

BRISBANE NORTH REGIONAL HEALTH AUTHORITY

Royal Brisbane Hospital

FELLOW IN DIAGNOSTIC RADIOLOGY

Department of Radiological Sciences

Vacancy No: 44/92

Applications are invited for the above position from recently accredited Radiologists or Registrars who have passed the FRCR examinations but who have to gain further experience before accreditation.

The period of the Fellowship is from 1st July 1992 for a period of 12 months or 2 years.

The Royal Brisbane Hospital is a 1100 bed Teaching Hospital associated with the University of Queensland. The Division of Radiological Sciences provides radiological services for all sections of the Hospital which involves most medical specialties.

Last year the Department of Radiological Sciences performed one or more examinations on 96,833 patients, including 11,598 special and interventional procedures. There were 8,597 CT scans, and 5,031 Ultrasound examinations. In addition to the 4 staff Radiologists there are 12 Radiology Registrars in training. The Department is accredited for postgraduate training in Radiology. A 1.5 Teslar MRI facility will be operational in July 1992.

Appointees will be responsible to the Director of Radiological Sciences. There will be the opportunity for experience in body CT, MRI, general ultrasound, neuroradiology, gastrointestinal radiology, interventional radiology, chest radiology, bone and joint radiology and uroradiology. Appointees will be required to contribute to the general out of hours radiological cover at the Hospital.

Salary range will be A$60,641.93 to A$69,574.90 per annum depending on period of eligibility for Specialist Registration.

Further details regarding the Department may be obtained from Dr P D Mowatt, Director, Department of Radiological Sciences and regarding the Hospital and terms of employment from Dr I Wilkey, Medical Superintendent, Royal Brisbane Hospital, Herston Road, Herston Qld 4029, Australia

Closing date: Wednesday, July 1st 1992

Application kits for the position listed may be obtained from the Industrial/Personnel Section on 61 7 253 7456

Applications for the position listed should give full details of qualifications, experience and the names and contact numbers of two professional referees and should be addressed to:

The Acting Chief Executive Officer, Royal Brisbane Hospital, Herston Road, Herston Qld 4029 Australia.

WANTED

Small Kodak or Fuji table-top film processor in good working order.

Image Intensifier, Philips TV system and/or spares.

Intensifying screens.

Reply with details to Box No. 16, BJR, 36 Portland Place, London W1N 4AT.

National Heart and Lung Institute
Royal Brompton Imaging Research

CARDIOTHORACIC IMAGING IN THE 90'S
CLINICAL PROBLEMS AND IMAGING SOLUTIONS
9 and 10 July 1992

A symposium on imaging techniques and their application to clinical problems in diseases of the heart and lungs.

The techniques (9 and 10 July): digital radiography and arteriography, new radiographic techniques, high resolution and ultrafast CT, echocardiography, nuclear medicine, positron emission tomography, magnetic resonance imaging

The problems (9 July)	*The problems (10 July)*
myocardial infarction	the pulmonary nodule
stable angina	suppurative lung disease
heart failure	haemoptysis
valvular disease	diffuse lung disease
congenital heart disease	pulmonary vascular disease
coronary function and atheroma	asbestos exposure
cardiovascular stress	assessing new technology

Course organisers: Richard Underwood and David Hansell.
Fee: £100 for one day, £150 for both days (incl catering).
Details: Postgraduate Medical Centre, National Heart and Lung Institute, Dovehouse St, London SW3 6LY, Tel: 071-351 8172, Fax: 071-376 3442

New *Information Service*
...for everyone involved with radiology.

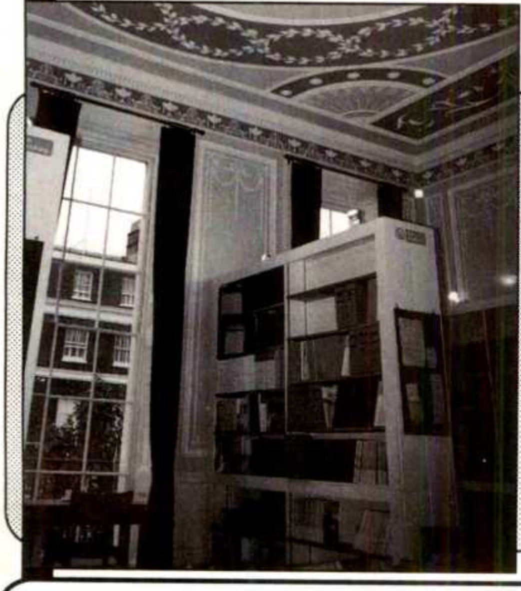

The British Radiological Library scheme covers all aspects of Radiology and related areas. The *Information Service* is based on the internationally significant collection of the Bernard Sunley Library housed in the British Institute of Radiology.

Services Available

An intake of 100 International Journal titles

A comprehensive collection of current radiological textbooks and reference works

A unique historical collection.

A Current Awareness Service
Study facilities

Access to Online searching and CD ROM

Postal, fax and telephone service UK wide

Photocopying facilities

Services of Professional Librarians

Links with other libraries

K. C. Clark collection from the College of Radiographers

Archived books

Do you have an information need in radiology? If so, you should contact the BIR Information Service.

For further details please contact: Stephen Johnson, Systems Librarian, The British Institute of Radiology, 36 Portland Place, London, W1N 4AT. Tel: 071-580 4189. Fax: 071-255 3209.

1992, *The British Journal of Radiology*, 65, 502–506

The value of magnetic resonance relaxation time in staging ovarian endometrial cysts

By Kazuro Sugimura, MD, *Masayuki Takemori, MD, †Makiko Sugiura, PhD, Hiromi Okizuka, MD, ‡Michio Kono, MD and Tetsuya Ishida, MD

Department of Radiology, Shimane Medical University, *Department of Gynecology, Kobe Kawasaki Hospital, †Kobe Women's College of Pharmacy, and ‡Department of Radiology, Kobe University, Japan

(*Received 28 August 1991 and in revised form 2 January 1992, accepted 13 January 1992*)

Keywords: MRI, ovarian endometrial cyst, relaxation time, staging

Abstract. We evaluated the use of magnetic resonance imaging (MRI) in the pre-operative staging of 15 endometrial cysts. The effect of the iron content on the T_1 and T_2 relaxation times was assessed in confirmed endometrial cysts employing a 0.15 T MR system and a 200 MHz spectrometer. There was a positive linear correlation ($r = 0.93$) between the T_1 values of the lesions obtained using the MR system (T_1) and those of the resected cyst contents obtained using the spectrometer (sp-T_1). A similar relationship was found between T_2 and sp-T_2 ($r = 0.87$). There was a negative linear relationship between the T_1 value and the cyst iron content ($r = -0.81$), but there was no relationship between the T_2 value and the iron content. T_1 was 412 ± 91 ms for Stage II cysts ($n = 3$), 356 ± 126 ms for Stage III cysts ($n = 3$) and 208 ± 30 ms for Stage IV cysts ($n = 9$). The T_1 value for Stage IV cysts was significantly shorter than that for Stages II and III cysts ($p < 0.05$). Thus, the T_1 value was useful in distinguishing fresh from old endometrial cysts, suggesting that the MRI T_1 relaxation time might be useful for staging ovarian endometrial cysts before surgery.

Endometriosis is a condition in which tissue similar to the endometrium occurs aberrantly in various locations in the pelvic cavity (Tindall, 1987). It is occasionally also found in adolescent women. Endometrial cysts often develop in the ovary and are known as chocolate cysts. In the early stages of cyst growth, few adhesions are seen, but as the condition progresses adhesions to the surrounding structures develop and can eventually form a "frozen pelvis". The surgical removal of such advanced cysts is difficult owing to the risk of severe haemorrhage. Consequently, it is important to determine the state of such cysts prior to surgery and to stage the disease accurately. In addition, it is necessary to make a differential diagnosis of endometrial cysts. Changes in the cyst fluid occur as the condition progresses, with the iron concentration increasing exponentially and the viscosity also rising.

If the cyst fluid could be analysed non-invasively, it would be possible to determine whether or not a cyst was at an early stage of development. However, it is not possible to stage these cysts using conventional imaging techniques like computed tomography (CT) and ultrasonography. Magnetic resonance imaging (MRI) is a useful diagnostic method, but there have been few detailed studies on its value for the assessment of ovarian cysts (American Fertility Society, 1985; Michell et al, 1989). In the present study, we investigated the relationship between the relaxation time of surgically proven endometrial cysts and their iron content. We also evaluated MRI as a diagnostic technique by comparing the MRI findings with those obtained during surgery.

Materials and methods

Fifteen surgically proven endometrial cysts were included in this prospective study. We employed a 0.15 T resistive magnet system (Picker International, Highland Hts, Ohio), in which the number of gradient increments was 3 mT/m, and the pulse sequences used were inversion–recovery (IR) and spin–echo (SE) techniques. There were four data acquisitions per imaging period and two-dimensional Fourier transformations were used for image reconstruction. We also employed a Varian XL-200 spectroscopic (proton 200.06 MHz) nuclear magnetic resonance (NMR) unit. All patients were studied in the axial plane with one IR pulse sequence (2100/500 ms; repetition time [TR]/inversion time [TI]) and two SE sequences (2100/40 ms and 2100/80 ms; TR/echo time [TE]). A calculated T_1 or T_2 image was obtained when possible. T_2 calculations were obtained with the SE sequences at the same attenuator setting, and T_1 calculations were obtained with the IR sequence and the 2100/40 SE sequence. Operator-defined regions of interest larger than 100 pixels were drawn in the centre of each endometrial cyst. T_1 and T_2 values for cysts were measured four times and the average was determined (Fig. 1). We excluded one case each in which the respective T_1 and T_2 values could not be obtained owing to physical movement.

The cyst fluid was collected after surgery or, if the cyst could not be removed, the fluid was aspirated at operation taking care not to include blood or exudate. The

---

Address correspondence to Kazuro Sugimura, MD, Department of Radiology, Shimane Medical University, 89-1 Enya Izumo, 693 Japan.

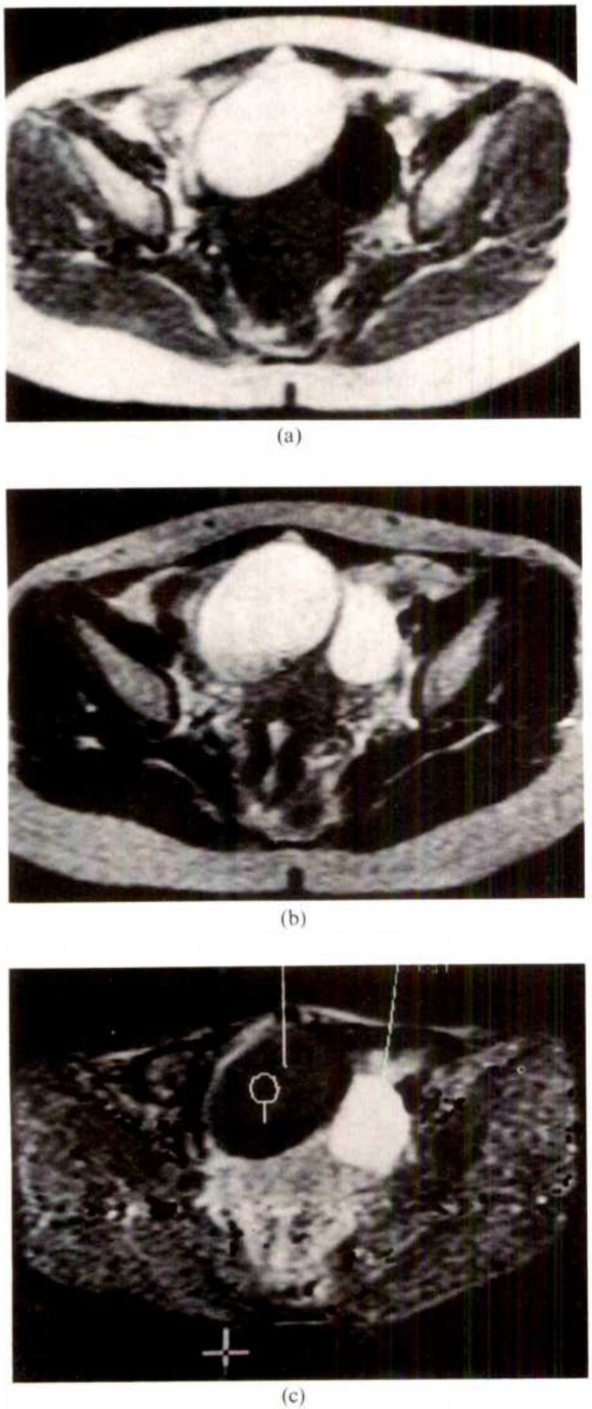
(a)

(b)

(c)

Figure 1. Right endometrial cyst and left simple ovarian cyst. (a) Transaxial T_1-weighted image (IR pulse sequence, TR 2100 ms, TI 500 ms). (b) T_2-weighted image (SE sequence, TR 2100 ms, TE 80 ms) and calculated T_1 image obtained with the IR sequence and the 2100/40 SE sequence. (c) A calculated T_1 image and operator-defined regions of interest are shown. The endometrial cyst demonstrates high signal intensity on both T_1 and T_2-weighted images and a short T_1 value on the T_1 calculated image. The serous cyst demonstrates low signal intensity on the T_1-weighted image and high signal intensity on the T_2-weighted image, which reflects prolonged relaxation time.

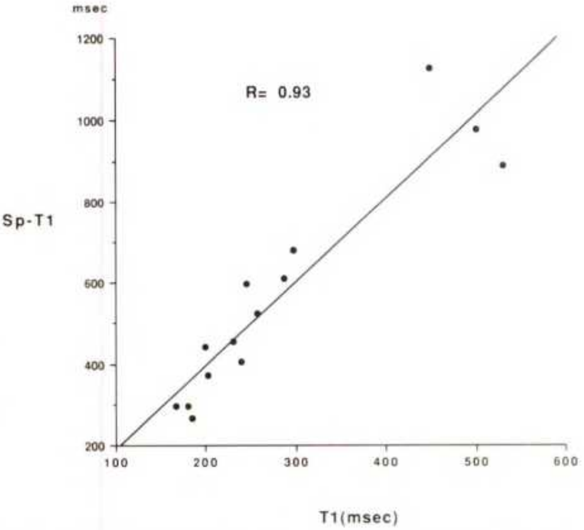

Figure 2. Correlation between the T_1 and sp-T_1 values for endometrial cysts. The T_1 and sp-T_1 values correlate very strongly and the T_1 values obtained using this MRI system are found to be reliable (the correlation coefficient is 0.93, $p < 0.01$).

iron content of the cyst fluid was then measured by the nitroso-PAT method.

Cyst fluid was placed in an NMR sample tube 5 mm in diameter for measurement using the XL-200. The IR method was used to obtain sp-T_1 and the Carr-Purcell-Meiboon-Gill (CPMG) method was used for sp-T_2. Sp-T_1 and sp-T_2 values of the cysts were measured three times and the average was determined. Staging of the endometrial cysts by clinical examination was performed according to the American Fertility Society classification system (AFS, 1985), in which each stage indicates the severity of the endometriosis (minimal, mild, moderate, or severe). Table I shows the relaxation times, cyst fluid iron concentrations, and AFS grades for all 15 patients. Analysis of variance was used statistically.

Results

Reliability of the MRI T_1 and T_2 values

Figures 2 and 3 show the relationship between the T_1 and T_2 values for the endometrial cysts obtained by MRI and spectroscopy. The correlation coefficient for T_1 and sp-T_1 was 0.93 ($p < 0.01$) and that for T_2 and sp-T_2 was 0.87 ($p < 0.01$). In particular, the T_1 and sp-T_1 values correlated very strongly and the T_1 values

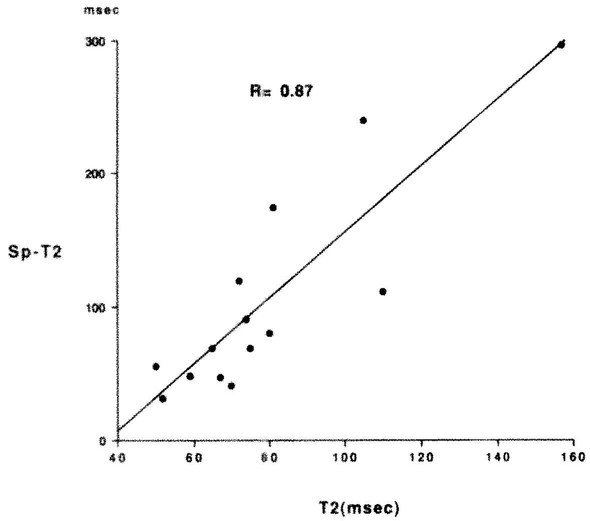

Figure 3. Correlation between the T_2 and sp-T_2 values for endometrial cysts. The correlation coefficient for T_2 and sp-T_2 is 0.87 ($p < 0.01$).

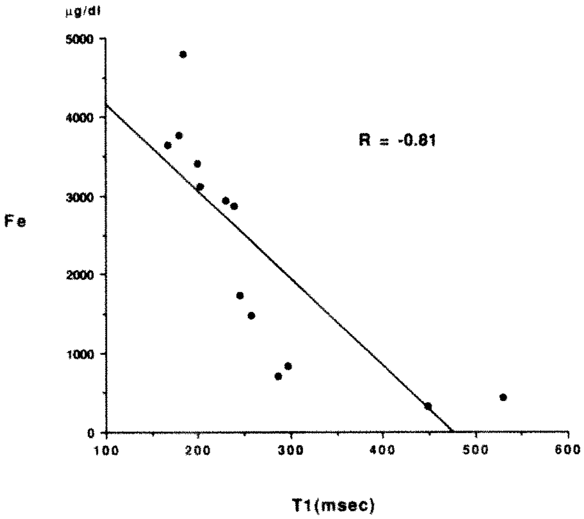

Figure 4. Correlation between the T_1 value and the cyst fluid iron content. A negative linear relation was found between the two parameters ($r = -0.81$, $p < 0.01$).

obtained using this MRI system were found to be reliable.

Utility of relaxation times

T_1 values and the cyst fluid iron concentration showed a negative correlation ($r = -0.81$, $p < 0.01$), suggesting an inverse relationship between the two factors (Fig. 4). T_2 values and the iron concentration also correlated negatively, but the relationship was not significant.

Table II shows the cyst fluid iron concentrations, relaxation times and AFS stages. The disease was Stage II in three cases, Stage III in three cases, and Stage IV in nine cases. An increased iron concentration and a reduction of T_1 and T_2 values was noted in higher-stage cysts. It is crucial to distinguish Stage IV from the other stages, because surgery becomes difficult owing to extensive adhesions in this stage. Therefore, iron concentrations and relaxation times were compared between Stages II and III and Stage IV. The T_1 value was 384 ± 124 in Stages II and III and 208 ± 32 in Stage IV, a

Table I. T_1 and T_2 relaxation times obtained using MRI and spectrometry, and the cyst fluid iron content for all the endometrial cysts

Patient age (years)	T_1 (ms) Mean	SD	T_2 (ms) Mean	SD	sp-T_1 (ms)	sp-T_2 (ms)	Fe (µg/dl)	Stage (AFS)
42	500	23	157	22	978	297	—	II
28	287	12	—	—	610	198	696	II
54	449	18	81	18	1127	174	320	II
42	530	24	105	21	890	241	431	III
24	298	11	72	11	680	119	830	III
40	239	7	65	11	405	69	2870	III
43	167	4	59	7	95	48	3640	IV
43	184	8	67	7	265	47	4800	IV
51	257	11	74	6	525	90	1480	IV
51	230	15	75	9	455	69	2940	IV
42	180	7	50	7	296	55	3780	IV
36	245	9	110	14	599	111	1740	IV
36	200	11	80	9	442	80	3420	IV
45	—	—	52	8	162	31	5720	IV
45	203	13	70	15	372	40	3120	IV
41 ± 8	284 ± 116		80 ± 27		540 ± 269	111 ± 78	2556 ± 1621	

SD = standard deviation.

Table II. T_1 values, T_2 values and cyst fluid iron content for cysts of each stage. An increased iron concentration and a reduction of T_1 and T_2 values were noted in higher-stage cysts

Stage	T_1 (ms)	T_2 (ms)	Fe (μg/dl)
II	412 ± 111 ($n = 3$)	119 ± 54 ($n = 2$)	508 ± 266 ($n = 2$)
III	356 ± 154 ($n = 3$)	81 ± 21 ($n = 3$)	1377 ± 1308 ($n = 3$)
II + III	384 ± 124	96 ± 37	1029 ± 1049
IV	208 ± 32 ($n = 8$)	71 ± 18 ($n = 9$)	3404 ± 1336 ($n = 9$)

statistically significant difference ($p < 0.05$). The cyst fluid iron concentration was 1029 ± 1049 in Stages II and III and 3404 ± 1336 in Stage IV, again a statistically significant difference ($p < 0.05$).

Discussion

In recent years, the use of MRI to diagnose endometrial cysts has been reported, but previous studies did not investigate the cyst contents as we did (Nishimura et al, 1987; Arrive et al, 1989; Michell et al, 1989). Characterization of the cyst fluid is possible by measuring the intensity of its signal, although this intensity is affected by the pulse sequence used, the size of the patient or the position of the lesion. For this reason, comparison between different patients is difficult, even if the imaging methods used are identical. Secondly, more iron concentration and viscosity causes higher signal intensity on both T_1 and T_2-weighted images. However, prominent concentration of iron causes magnetic susceptibility inhomogeneity and prominent viscosity causes marked T_2 shortening, especially in old endometrial cysts. Therefore, the older endometrial cyst does not always demonstrate the higher signal intensity on T_1- or T_2-weighted images. However, relaxation times may be compared, provided that the magnetic field intensity is constant. When relaxation times obtained using MRI have been compared with those obtained by *in vitro* spectroscopy, the T_1 value has appeared to be reliable in some cases (Terrifer et al, 1985). The NMR signal is influenced in a complex way by blood flow and tissue pH, so the relaxation times of resected specimens are thought to provide inaccurate results for solid lesions.

However, endometrial cysts exist in the body as a relatively isolated entity and the resected specimen is therefore considered to have similar characteristics to the *in situ* cyst. We found a strong correlation between the relaxation time obtained using MRI and those obtained using spectroscopy in the present study, indicating that the MRI relaxation time for endometrial cysts has a high reliability.

It is possible to compare the relaxation time obtained from different patients, but since the relaxation time is itself dependent on the magnetic field, accurate comparison will only be possible when the field intensity can be controlled precisely and field uniformity is improved. In addition, the algorithms for calculating the relaxation time vary with the type of MRI equipment used, further compounding the difficulty in obtaining an accurate comparison of patient data. Absolute relaxation time should thus only be compared with data obtained from the same type of MRI unit. However, it is possible to compare relative relaxation times obtained from different types of MRI units because the relaxation time is closely correlated to the magnetic field strength (Lynch, 1983).

MRI has been advocated as the method of choice for evaluating endometrial cysts, although there are some limitations on detecting small peritoneal implants. The limitations of MRI in demonstrating small implants and adhesions, as well as the absence of known correlations between MRI findings and severity of the disease, appear to preclude the accurate staging of endometriosis by MRI. Small peritoneal implants cannot be demonstrated even using superconducting MRI. MRI was previously found to be not useful in staging endometrial cysts because the diagnosis of adhesions to adjacent organs was based on indirect findings. A more accurate diagnostic method was thus needed to stage endometrial cysts (Arrive et al, 1989). This study focused on the contents of endometrial cysts because changes of the contents might correlate with the aging of endometrial cysts. Previous reports on intracranial haematomas have shown that the methaemoglobin content of haematoma, free Fe^{3+} ions, haematocrit, protein and lipids are all related to the T_1 and T_2 values. In particular, the concentrations of methaemoglobin and free Fe^{3+} ions are related to the T_2 value and the haematocrit to the T_1 value (Stark et al, 1985; Bradley & Schmidt, 1986). Endometrial cysts can be graded with respect to their contents, since the long-term nature of the intracystic haemorrhage results in an iron concentration approximately 10–20 times greater than that of a chronic subdural haematoma. Consequently, an endometrial cyst is very different from an intracranial haematoma, and the cyst contents show a marked increase in iron concentration and viscosity with time because of the degradation of old blood. The present study revealed that the T_1 value and the iron concentration were correlated negatively, indicating that a smaller number of factors influence the relaxation time for endometrial cysts when compared with intracranial haematomas (Bradley & Schmidt, 1986). As the iron concentration and the viscosity of the cyst fluid increased, a corresponding decrease in relaxation time was observed (Fullerton, 1988).

In conclusion, we have investigated the clinical application of MRI in staging endometrial cysts by measuring relaxation times (Sugimura et al, 1987), and found that the T_1 value might be useful for assessing cyst progression. It was especially useful for identifying Stage IV cysts, for which surgical management is very difficult. This novel application of MRI will hopefully prove to be of value in the future diagnosis of endometrial cysts.

References

AFS, 1985. Revised American Fertility Society classification of endometriosis: 1985. *Fertility and Sterility, 43*, 351–352.

ARRIVE, L., HRICAK, H. & MARTIN, M. C., 1989. Pelvic endometriosis: MR imaging. *Radiology, 170*, 687–692.

BRADLEY, W. G. & SCHMIDT, P. G., JR, 1986. Effect of methemoglobin formation on MR appearance of subarachnoid hemorrhage. *Radiology, 156*, 99–103.

FULLERTON, G. D., 1988. Physiologic basis of magnetic relaxation. In *Magnetic Resonance Imaging*, ed. by D. D. Stark and W. G. Bradley (Mosby, St. Louis), pp. 36–55.

LYNCH, L. J., 1983. Water relaxation in heterogeneous and biological systems. In *Magnetic Resonance in Biology*, ed. by J. S. Cohen (John Wiley and Sons, Chichester), pp. 251–255.

MICHELL, D. G., MINTZ, M. C., SPRITZER, C. E., GUSSMAN, D., ARGER, P. H., COLEMAN, B. G., AXEL, L. & KRESSEL, H. Y., 1989. Adnexal masses: MR imaging observations at 1.5T, US, and CT correlation. *Radiology, 162*, 319–324.

NISHIMURA, K., TOGASHI, K., ITOH, K., FUJISAWA, I., NOMA, S., KAWAMURA, Y., NAKANO, Y., ITOH, H., TORIZUKA, K. & OZASA, H., 1987. Endometrial cyst of the ovary. *Radiology, 162*, 315–318.

STARK, D. D., MOSELEY, M. E., BASCON, B. R., MOSS, A. A., GOLDBERG, H. I., BASS, N. M. & JAMES, T. L., 1985. Magnetic resonance imaging and spectroscopy of hepatic iron overload. *Radiology, 156*, 137–142.

SUGIMURA, K., YAMASAKI, K., KITAGAKI, H., TANAKA, Y. & KONO, M., 1987. Bone marrow disease of the spine: differentiation with T_1 and T_2 relaxation times in MR imaging. *Radiology, 165*, 541–544.

TERRIFER, F., REVEL, D., PAJANNEN, H., RICHARDSON, M., HRICAK, H. & HIGGINS, C. B., 1985. MR imaging of body fluid collections. *Journal of Computer Assisted Tomography, 10*, 953–962.

TINDALL, V. R., 1987. Endometriosis and allied states. In *Jeffcoate's Principles of Gynaecology* (Butterworth, London), pp. 355–370.

1992, *The British Journal of Radiology*, 65, 507–509

Audit in action: significant reduction of double-contrast barium enema screening time with no loss of examination quality

By D. Horton, MB, BS, A. M. Cook, FRCR and A. D. Taylor, FRCR

Department of Radiology, Hull Royal Infirmary, Anlaby Road, Kingston upon Hull HU3 2JZ, UK

(*Received 27 August 1991 and in revised form 25 November 1991, accepted 14 January 1992*)

Keywords: Barium enema, Screening time

Abstract. The double-contrast barium enema is an examination of high radiation exposure to the patient. As part of a departmental audit, our own fluoroscopic screening times were being recorded. A study was undertaken to see if a determined effort could reduce the screening time without having a detrimental effect on the quality of the examinations. Methods of screening time reduction were identified and then implemented by two radiologists. In the period before the study the average screening time for radiologists A and B was 2.6 min and 3.2 min, respectively (over 56 examinations). After implementation of the changes, the average screening time for both was 0.9 min (over 50 examinations). This is a statistically significant reduction ($p < 0.01$). The examinations were assessed independently by a gastroradiologist. No difference in the quality of the examinations was identified. We conclude that a significant reduction of screening time for the double-contrast barium enema can be achieved without loss of examination quality.

As part of the departmental audit programme, screening times were being recorded for a number of fluoroscopic examinations. The aim was to make each radiologist aware of their own screening times and to consider it an integral part of the examination.

The joint National Radiological Protection Board and Royal College of Radiologists (NRPB-RCR) report (1990) has highlighted the potential for patient dose reduction for a number of radiographic procedures, and the need for work in this area. It was shown that several methods could be used to reduce radiation exposure to the patient during screening procedures. A general reduction of screening time was one suggestion, but as far as we are aware no work has been carried out to establish if a more deliberate effort to lower screening times can succeed without loss of useful diagnostic information.

This paper examines ways in which screening times can be reduced in the double-contrast barium enema examination, and looks at the effect this may have on the examination quality.

Method

The total double-contrast barium enema screening time, as recorded on the equipment timers, was noted for all radiologists. At the end of each month the figures were transferred to a computer for analysis. The same screening table, a Phillips Diagnost 73, was used throughout.

Tables were produced giving the average screening time for each radiologist, as well as the number of examinations and the average number of radiographs taken.

Correct use and appropriate removal of the anti-scatter grid, and collimation of the beam to the area of interest, were used throughout the study. It was, however, the screening time reduction techniques that were the main direction of effort.

During the barium-filling phase of the examination, screening was pulsed to short intervals with longer gaps between. Any delays in the passage of the barium were easy to detect and that area of bowel was examined more closely, with spot radiographs being taken as necessary.

Much of the barium enema examination involves a pattern of patient rotation usually differing little between individual patients. This rotation was performed without screening, with short pulses of screening being used afterwards to check the effectiveness of barium coating. When coating and air insufflation had been achieved, the patient was positioned for the spot radiographs. This was carried out without screening during the actual movement. The position was checked with a short pulse of screening. If the positioning was inadequate, repositioning was carried out without screening control, before being checked by pulsed screening again. In this way the screening times were kept as low as possible.

Hyoscine-*n*-butylbromide (20 mg) (Boehringer Ingelheim) was used routinely for each patient. The barium used was barium 520 disposable (E-Z-EM).

The results from the month after the changes were implemented were taken and compared with the figures from the month before the changes were implemented. All of the radiographs taken in those 2 months by the two radiologists were recalled and independently

Table I. Average screening time (in minutes) before and after implementation of changes

Radiologist	Screening time			
	Month before		Month after	
	Average	Range	Average	Range
A	2.6	1.2–3.9 (n = 19)	0.9	0.3–2.5 (n = 26)
B	3.2	1.8–5.0 (n = 37)	0.9	0.1–3.5 (n = 24)

There was a significant reduction in screening time between the 2 months ($p < 0.01$). The average number of film exposures taken remained unchanged throughout the study at 11 per examination (n = number of examinations).

reviewed by a gastroradiologist who did not know when or by whom the examinations were performed. Each examination was assessed for quality on the basis of whether a confident report could be given for all the areas of the large bowel. The examination was then graded as acceptable or non-diagnostic. The 2-months results were compared. 11 months later, the patient case note were recalled to assess the outcome of the enemas performed in the 2 months. The enema findings were compared with subsequent patient progress and investigations to discover if any lesions had been missed.

Results

Results of the study are summarized in Table I. A total of 106 double-contrast barium enemas were performed in the months before and after the changes were implemented by the two radiologists. There was no significant difference in the pattern of disease detected by the two radiologists. The average screening time for each radiologist fell significantly between the two months ($p < 0.01$, modified Z-test). Before the changes, the average screening time for radiologist A (a consultant) was 2.6 min; the average time for radiologist B (a registrar) was 3.2 min. The department average at this time was 3.3 min. After the changes, both radiologists had an average screening time of 0.9 min. The number of radiographs taken did not change over the 2 months, remaining at 11 per examination for both radiologists. No difference was found in the quality of the radiographs produced between the 2 months using the definition of diagnostic acceptability set out above. Three enemas from each month were considered non-diagnostic. This was due to factors such as residual faeces, incontinence of the barium or numerous overlapping loops of bowel with diverticula, and not due to the technique itself. Of the 106 examinations, no lesion has been discovered in the 11 months follow-up that was not shown on the radiographs taken during the examinations.

Discussion

Patient radiation exposure has been a point of increased interest over recent years in the lay press (*Which?*, 1990), the general medical press (Nolan, 1991) and within the radiology professions (DeLacey, 1987; Kerr, 1991). Efforts to reduce patient radiation exposure have been highlighted by the NRPB-RCR (1990).

We were concerned that any efforts directed at reducing patient radiation exposure further would have a detrimental effect on the quality of the examination, believing our techniques to be adequate as they were.

The departmental audit programme had the aim of almost subconsciously effecting a screening time reduction, and so reducing patient radiation exposure, by making the figures available for assessment and comparison. We believe that this study shows a more direct effort can reduce screening time and radiation exposure without reducing the quality of the examination.

A previous report based on a survey of 20 different hospitals looked at patient radiation exposure during various radiological procedures and found an average screening time for barium enemas of 3.7 min (Shrimpton et al, 1986). However, it included an unspecified number of single-contrast enemas within the group and is therefore not directly comparable.

The assumption that a change in screening time results in a change in patient radiation exposure, all else being equal, is not new (Harrison et al, 1983). Direct exposure measurements were not taken during the study as a dose–area monitor was not available at that time. After the study period we were able to assess exposure more quantitatively. An estimate was made of the fraction of the patient exposure attributable to the screening time by averaging readings taken over a separate group of enema examinations. We estimated that on our equipment, before the screening time reduction changes, around 25% of the total patient exposure was attributable to the screening time. After the changes, this had

Table II. Estimated exposure levels (air kerma × area product) on our equipment for each of the screening times based on readings taken using a dose–area monitor. Exposure levels are rounded up to the nearest whole number

Average screening time (min)	Total area exposure product (mGy × cm^2)	Screening area exposure product (mGy × cm^2)	Screening exposure as percentage of total
0.9	10428	1130	10.8%
2.6	11870	2572	21.7%
3.2	12470	3172	25.4%

fallen to just under 11% of the total. There had, therefore, been approximately a 14% reduction in the total patient radiation exposure by reduction of screening time alone (Table II).

The amount of radiation reaching the patient may be modified by a number of well recognized factors (Harrison, 1991). The performance of fluoroscopy equipment such as image intensifiers has improved, but the expense of purchasing new equipment has limited the overall effect of this method of reducing patient radiation exposure. The radiologist has available a number of ways to alter patient exposure. The use of the lowest exposure factors compatible with a reasonable image, the appropriate use of the antiscatter grid, collimation of the beam to the minimum size required and attempts to reduce the number of radiographs taken are all recognized methods of reducing radiation exposure. Reduction of the screening time has been suggested alongside these measures, but, as far as we are aware, has not been assessed previously in its own right in this way.

It is important to note that the primary consideration for all examinations is to achieve a diagnostically acceptable result with minimum disturbance of the patient. Allowing for the above, efforts can be made towards screening time reduction and we conclude that it is possible to reduce screening time by a significant amount without affecting the overall quality of the examination.

References

De Lacey, G. 1987. Overexposure to radiology (Editorial). *British Medical Journal, 295,* 1162–1163.

Harrison, R. M., 1991. Radiation protection of the patient: the impact of new technology. *Advanced Hospital Technology, 2,* 37–43.

Harrison, R. M., Clayton, C. B., Day, M. J., Owen, J. P. & York, M. F., 1983. A survey of radiation doses to patients in five common diagnostic examinations. *British Journal of Radiology, 56,* 383–395.

Kerr, I. H., 1991. Patient dose reduction in diagnostic radiology (Editorial). *Clinical Radiology, 43,* 2–3.

NRPB-RCR, 1990. *Patient Dose Reduction in Diagnostic Radiology. Documents of the NRPB, 1, 3* (HMSO, London).

Nolan, D. J., 1991. Minimizing radiation in diagnostic radiology. *British Journal of Hospital Medicine, 45,* 337.

Shrimpton, P. C., Wall, B. F., Jones, D. G., Fisher, E. S., Hillier, M. C., Kendall, G. M. & Harrison, R. M., 1986. Doses to patients from routine diagnostic X-ray examinations in England. *British Journal of Radiology, 59,* 749–758.

Which?, 1990. January issue (Consumers Association, London).

1992, *The British Journal of Radiology*, 65, 510–516

Radiotherapy to the surviving kidney after unilateral nephrectomy in bilateral Wilms' tumour

By *P. Kirkbride, FRCR and *†P. N. Plowman, FRCR

*Department of Radiotherapy, St Bartholomew's Hospital, West Smithfield, London EC1A 7BE and
†Department of Oncology, The Hospital for Sick Children, Great Ormond Street, London WC1N 3JH, UK

(*Received 30 September 1991 and in revised form 2 January 1992, accepted 15 January 1992*)

Keywords: Wilms' tumour, Surviving kidney, Renal radiation tolerance

Abstract. Despite an improving overall survival rate for children with Wilms' tumour, four out of seven patients with bilateral tumours died in the period from 1952 to 1960 and five out of eight died in the period from 1971 to 1989, at St Bartholomew's Hospital and the Hospital for Sick Children. More aggressive chemotherapy with both adriamycin and actinomycin D and concern over young age being predisposed to late radiation morbidity prompted us to keep radiotherapy dose prescriptions to the surviving kidney below the quoted renal radiation tolerance dose equivalent. In three long-term survivors treated with daily fractions up to 167 cGy and total doses of 1000–1200 cGy, we have found renal function and growth to be within the "normal" range at follow-up and the patients to be normotensive 6–8 years later. As four of the eight patients reported here died from local disease progression within the kidney (albeit despite slightly larger dose prescriptions), we discuss the potential for larger total doses to be delivered in this situation.

Bilateral (Stage V) nephroblastoma (Wilms' tumour) may arise synchronously or metachronously, and accounts for approximately 5% of all cases (Bishop et al, 1977). The management of these patients is difficult and controversial. Cases involving both kidneys at presentation are currently managed either by nephrectomy to the predominantly affected kidney, wedge excision of small contralateral tumours, post-operative chemotherapy and radiotherapy to the surviving kidney, or by bilateral renal biopsies, chemotherapy and, usually, low-dose radiotherapy to both kidneys. Relapse in the contralateral kidney may be salvaged by employing combination chemotherapy, radiotherapy and occasionally surgery (Plowman, 1988).

It is well established that the kidney is a radiosensitive organ, and the syndromes of acute and chronic radiation nephropathy are well described and have recently been reviewed by Robbins and Hopewell (1991). As radiosensitivity of an organ is usually maximal at times of high proliferation, it was thought likely that a growing, immature kidney is at highest risk; the clinical observations of Zuelzer et al (1950) and Zeigerman et al (1957) and the experimental work of Pheimster & Thomassen (1973) appear to support this. Therefore, original National Wilms' Tumour Study Group (NWTS) protocols varied doses of abdominal radiation given, using an age-related scale (D'Angio et al, 1976). However, more recent work with rodents suggests that young and adult kidneys are equally radiosensitive (Jongejan et al, 1987) and radiation tolerance in humans may be similar (Rubin et al, 1982), although the subject remains controversial and the volume of kidney irradiated with respect to age may be relevant.

Chemotherapeutic agents commonly used in the treatment of Wilms' tumours are known radiosensitizers and any radiation toxicity may be enhanced. Arneil et al (1974) described two children with Wilms' tumour who developed acute renal failure following chemotherapy with actinomycin D and vincristine and post-nephrectomy radiation (1500 cGy and 2000 cGy) to the surviving kidney. In addition, Moskowitz et al (1980) observed a lack of normal compensatory renal hypertrophy in two children following whole abdominal irradiation and combination chemotherapy. These observations have naturally influenced our dose prescription (*vide infra*) in patients receiving renal radiotherapy in combination chemo-radiotherapy protocols for Wilms' tumour patients.

At the Hospital for Sick Children, Great Ormond Street, 178 patients have been treated for Wilms' tumour since 1971, of which 30 have been Stage V. In this paper we review the eight patients, usually having synchronous advanced bilateral tumours, whose treatment has involved irradiation of their only surviving kidney, and discuss in detail the three long-term survivors. We examine the effect of radiation to a sole kidney, review the role of chemotherapy and radiotherapy, and discuss the possible dose regimes employed.

Methods

Between 1971 and 1986, eight children aged between 9 months and 6 years were referred from Great Ormond Street to St Bartholomew's Hospital for radiotherapy to

---

Address reprint requests to Dr P. N. Plowman, Department of Radiotherapy, St Bartholomew's Hospital, West Smithfield, London EC1A 7BE, UK.

Table I. Details of treatment and outcome on all eight patients studied, with synchronous or metachronous bilateral Wilms' tumours, whose treatment involved nephrectomy and irradiation of the remaining kidney

Patient (sex)	Age at presentation (years)	Bilateral or recurrence	Histology	Radiation to surviving kidney			Outcome after R/T	Survival	Notes
				Dose (cGy)	Fractions	Time (days)			
S.M.(F)	2	Bilat.	FH	1000	6	8	CR	A/W 6 years	See text
J.T.(F)	6	Recur.	FH	1500	10	12	PD	†3 months	Died in ARF (urea = 46) with progressive local disease in kidney
M.A.(F)	5	Bilat.	FH	1000	12	16	CR	A/W 8 years	See text
R.S.(F)	2	Recur.	FH	1200	13	17	CR	A/W 13 years	See text
M.P.(M)	2	Recur.	UH	1800	15	19	PR	†4 years	Normal urea, electrolytes, BP before death, but ultrasound showed recurrence in kidney 4 years post R/T
R.O'R(F)	9 months	Bilat.	FH	1350	9	19	PR	†1year	Died in ARF (urea = 82) but progressive local disease in kidney
M.L.(M)	1	Bilat.	FH	1782 to whole abdomen and then 1 year later: 500 to remaining kidney Total dose = 1282 cGy	8 5	12 7	PD	†18 months	Normal urea, electrolytes, but raised BP before death. Died of local recurrence in kidney
J.M.(F)	4	Bilat.	FH	750	15	20	PD	1 year	Residual disease post-nephrectomy in right flank. Relapsed during R/T with ascites and died of ARF secondary to PD

R/T = radiotherapy; FH = favourable histology; UH = unfavourable histology; CR = complete remission; PD = progressive disease; PR = partial remission; A/W = alive and well; ARF = acute renal failure.

the surviving kidney following nephrectomy for Wilms' tumour (Table I). All either had bilateral disease or had developed recurrence in the remaining kidney. All patients had also been given combination chemotherapy: all received vincristine and actinomycin, six received additional adriamycin, two cyclophosphamide, and one etoposide and ifosfamide.

The patients were treated through parallel opposed megavoltage X-ray portals, and received doses ranging from 500 to 1800 cGy given over 6–15 fractions over periods ranging from 8 to 19 days. Following treatment, patients were followed up at Great Ormond Street and Bart's with physical examinations, blood pressure measurements and assessment of renal function by serum urea and electrolytes and in some cases DMSA, DPTA and ultrasound scans. Follow-up varies from 3 months to 11 years.

Case histories of three long-term surviving patients are recorded.

Case reports

Case 1

This girl (Patient S.M. in Table I) presented at age 2 years, with abdominal swelling. Laparotomy disclosed bilateral Wilms' tumours. There was a well circumscribed tumour replacing the lower pole of the left kidney and a suspicious area at the lower pole of the right kidney.

Left nephrectomy was performed and biopsies of the right kidney taken. Histology showed both tumours to be Wilms' tumours of favourable histology. Post-operatively, her renal function was normal (serum urea 4.2 mmol/l, serum creatinine 43 μmol/l) and her blood pressure was 110/60 mmHg.

Adjuvant chemotherapy with vincristine, adriamycin and actinomycin, according to the UKCCSG protocol current at that time, was commenced, which the child received for 3 months.

At this time (20 days after this last chemotherapy

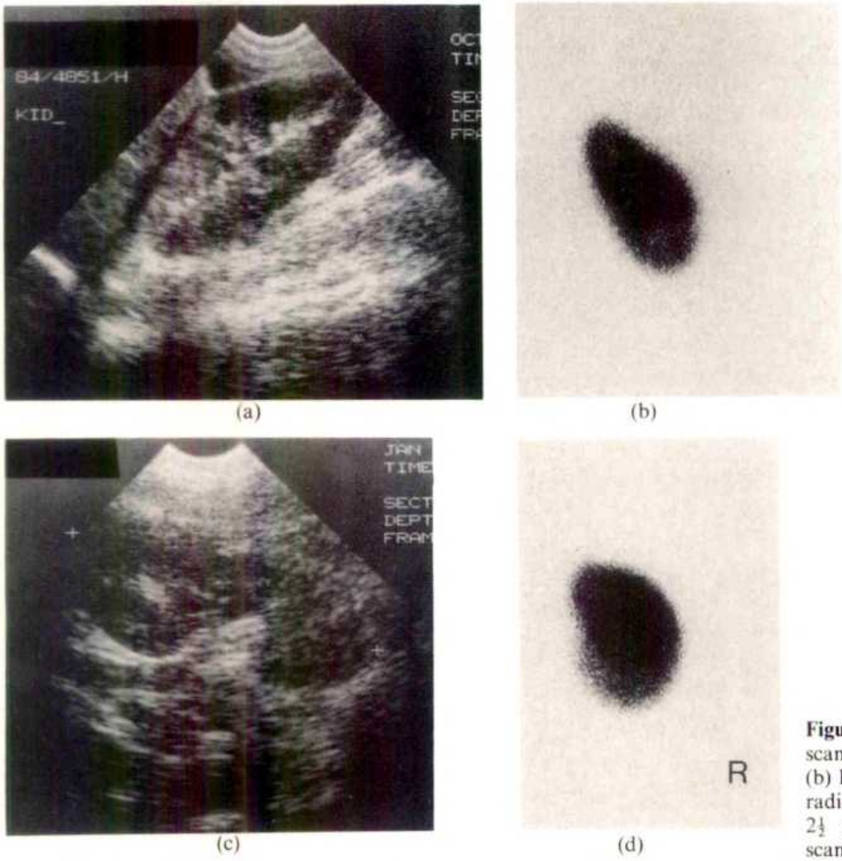

(a) (b) (c) (d)

Figure 1. *Case 1.* (a) Renal ultrasound scan 1 month post-radiotherapy. (b) DMSA scan 1 month post-radiotherapy. (c) Renal ultrasound scan 2½ years post-radiotherapy. (d) DMSA scan 3½ years post-radiotherapy.

dose) radiotherapy to the right flank, encompassing the whole right kidney, was delivered. Using 6 MV X rays and parallel opposed anterior and posterior portals, a mid-plane dose of 1000 cGy in 6 fractions over 8 days was delivered. Further chemotherapy was then given for another 8 months, using the same drugs, starting 2 weeks after completion of radiotherapy.

The child is now 6 years from renal radiotherapy and is aged 8 years. Her renal growth and function has been assessed by serial ultrasound and DMSA scans (see Table II and Fig. 1). Renal size has always been within the normal limits for her age using the nomogram of Han and Baldock (1985) (Fig. 2), and all DMSA scans have been normal. (The nomogram predicts growth in normal children with both kidneys present; therefore, in a nephrectomized patient compensatory hypertrophy may be expected, but no data are available to predict normal renal growth in such a situation.) Her current renal function is normal, as evidenced by the following investigations: serum urea 5.3 mmol/l, creatinine 50 μmol/l, renin 790 ngAI/l/W (normal 131–834), haemoglobin 12.0 g/dl. Other serum electrolytes were normal, urinalysis showed no proteinuria and glomerular filtration rate, measured by EDTA clearance, was 110 ml/min/1.73 m^2. Renal ultrasound showed a normal-sized kidney and blood pressure was 118/68 mmHg.

Table II. Results of serial ultrasound and DMSA scans on Case 2

Time of scans	Findings
1 month post-R/T	Ultrasound: normal right kidney (Fig. 1a) Renal length: 7.8 cm DMSA: normal (Fig. 1b)
1 year post-R/T	Ultrasound: normal right kidney Renal length: 8.0 cm DMSA: normal
2½ years post-R/T	Ultrasound: normal right kidney Renal length: 9.4 cm (Fig. 1c)
3½ years post-R/T	DMSA: normal (Fig. 1d)
4 years post-R/T	Ultrasound: normal right kidney Renal length: 8.7 cm
6 years post-R/T	Ultrasound: normal right kidney Renal length: 9.6 cm

R/T = radiotherapy.

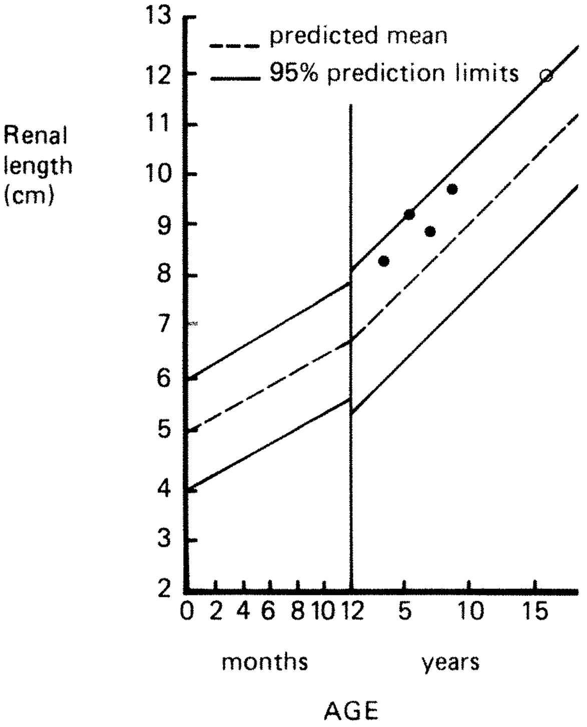

Figure 2. Nomogram for normal renal size in children, as measured by ultrasound (Han & Baldock, 1985). Following nephrectomy and irradiation of the sole surviving kidney, all measurements on Case 1 (●) have been within 95% confidence limits, and the length of the surviving kidney of Case 3, 15 years after treatment, is also illustrated (○).

Case 2

This girl (Patient M.A. in Table I) presented aged 5 years with haematuria and a mass palpable in the right flank. At operation the right kidney was massively enlarged by nephroblastoma. Nephrectomy was performed, complete with the entire tumour, which extended along the renal vein into the vena cava. The left kidney was also found to be extensively involved with tumour, especially in the upper pole, and a representative nodule was biopsied. Histology of the right tumour showed "favourable histology" Wilms' tumour and that of the left, necrotic tumour with features of nephroblastoma.

Post-operative renal function and blood pressure were normal and she was commenced on chemotherapy with alternating etoposide, vincristine, adriamycin (EVA) and vincristine, actinomycin D, cyclophosphamide (VAC), with weekly vincristine for 10 weeks. She also received radiotherapy to a field encompassing the left kidney to a total mid-plane dose of 1000 cGy using ^{60}Co γ rays by parallel opposed fields in 12 fractions over 16 days. Chemotherapy recommenced 2 days after radiotherapy and was continued for 2 years.

She is now aged 13 years, more than 6 years post-completion of treatment and is completely well with no evidence of disease. Her blood pressure is 90/60 mmHg. Her haemoglobin is 11.6 g/dl, and her other renal function tests including serum urea and electrolytes and urinalysis are normal. Her last DTPA scan performed 2 years ago showed a glomerular filtration rate (GFR) of 123 ml/min and was reported as normal, and no further radioisotope scans are planned for 5 years, as the child lives in Greece.

Case 3

This girl (Patient R.S. in Table I) was found to have a Stage I "favourable histology" left-sided Wilms' tumour at 2 years of age, when she presented with haematuria and loin pain. She had a left nephrectomy and then 4 months chemotherapy with single-agent vincristine.

Two years later she again developed haematuria and a right kidney could be palpated. An intravenous pyelogram (IVP) showed multiple unresectable tumours in the right kidney and the clinical diagnosis of recurrent Wilms' tumour was made. She was treated with 6 courses of vincristine, adriamycin and actinomycin D, during which she also received 1200 cGy to her entire right kidney by parallel opposed fields with ^{60}Co γ rays, given in 13 fractions over 17 days.

Eleven years later she is alive and disease-free. During this time there has never been any disturbance of her renal function tests, and recent investigations show good renal function: serum urea 6.8 mmol/l, creatinine 77 μmol/l, blood renin 526 ngAI/l/W (normal range 55–899) and haemoglobin 12.5 g/dl. GFR measured by EDTA was 81.2 ml/min/1.73 m^2, urinalysis showed no evidence of proteinuria and blood pressure was 116/70 mmHg. Ultrasound of the kidney shows a mass resulting from a long-standing calcified haematoma, but otherwise the kidney is of normal appearance and meaures 12 cm in length, within the expected limits for her age according to the nomogram of Han and Baldock (Fig. 2).

Other cases

A summary of the treatments and outcomes of the other five patients is shown in Table I. Two patients were treated for recurrent disease in the surviving kidney up to 4 years following primary therapy with surgery and chemotherapy; the other three patients had bilateral disease at presentation. One of these had a nephrectomy and chemotherapy, followed by radiotherapy to the surviving kidney; the second received whole abdominal radiotherapy and chemotherapy and then, on relapse, nephrectomy, chemotherapy and low-dose radiation. The third had whole abdominal radiotherapy following chemotherapy and nephrectomy because of residual disease in the nephrectomized flank, the dose of radiation to the contralateral kidney being attenuated by a partial transmission block (Fig. 3).

Discussion

The radiosensitivity of renal tissue has long been appreciated, although there are many manifestations of renal damage and the exact pathogenesis of renal radia-

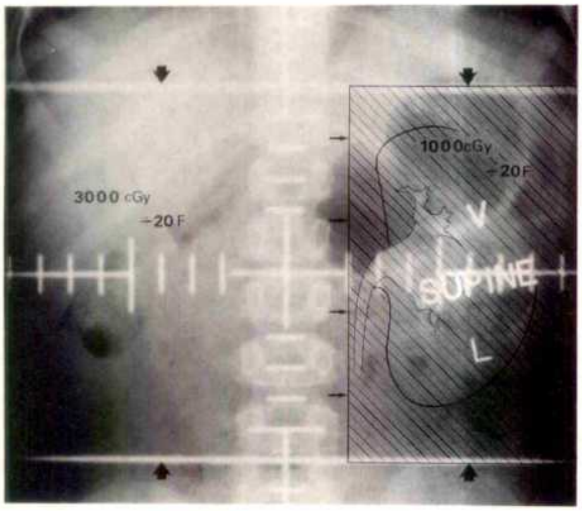

Figure 3. Partial transmission block technique used for Patient J. M., enabling a dose of 1000 cGy to be given in 50 cGy fractions to the surviving kidney, simultaneously to the rest of the abdomen (unshielded) receiving 3000 cGy.

tion injury remains poorly understood. Domagk (1927) described a 9-year-old girl who received abdominal radiation for tuberculous mesenteric adenitis and who developed fatal renal failure 6 months later. Kunkler et al (1952) clarified the clinical radiosensitivity of the human kidney in his analysis of patients receiving total abdominal irradiation as therapy for testicular tumours. He concluded that doses exceeding 2300 cGy in 5 weeks carried a significant risk of renal damage.

Of particular note was the low daily dose fraction size used (necessitated by the acute gastrointestinal tolerance) given the current experimental and clinical evidence demonstrating the importance of fraction size in the late tolerance of the kidneys to radiotherapy (Williams & Denekamp, 1984; Stewart et al, 1984).

In the following years, Grossman (1955) and Redd (1960) extended these observations, and several syndromes of radiation "nephritis" were described (Luxton, 1953). Avioli et al (1963) studied 10 patients who were given whole abdominal irradiation (the kidneys receiving 2000–2400 cGy over 3–4 weeks) and noted that subclinical changes occurred in renal plasma flow and GFR within 12 months of treatment, although more routine tests such as blood urea levels, urinalysis and IVPs were normal. Subsequent studies such as those of Kim et al (1980) have confirmed these observations and shown that such changes persist for up to 8 years after treatment, although spontaneous recovery may occur.

More severe and clinically significant changes may also develop to give the picture of acute radiation nephropathy, with oedema, dyspnoea and hypertension. These patients generally have a poor prognosis and may develop malignant hypertension. Late radiation nephrosis (Luxton, 1953) characterized by proteinuria, raised blood pressure, decreased renal function and anaemia may occur, but generally has a better prognosis.

Isolated proteinuria or hypertension (usually mild but occasionally malignant) are other possible sequelae of renal irradiation. Clinical studies suggest the involvement of the renin–angiotensin system, probably as a result of ischaemia of the juxtaglomerular apparatus causing increased renin production (Shapiro et al, 1977). The development of malignant hypertension is a poor prognostic sign, and usually necessitates nephrectomy, although a case has been reported where a patient was successfully treated by the excision of a renal artery stenosis (Thomas et al, 1983).

Of particular relevance when irradiating kidneys in paediatric patients is the effect on renal hormone production. The consequences with respect to the renin–angiotensin system have already been mentioned. There is little evidence on the influence on erythropoietin production, but Fisher et al (1964) found that irradiation of the dog kidney resulted in significant suppression of the expected rise in erythropoietin production 6 weeks after stimulation by injection of cobalt. However, baseline plasma erythropoietin levels and haematological values did not change. The clinical significance of these observations is unknown.

There appears to be no evidence for an effect of irradiation on renal hydroxylation of vitamin D.

In the management of bilateral Wilms' tumour, or recurrence in the contralateral kidney, the radiotherapist is faced with the consequence of irradiating a sole surviving kidney following unilateral nephrectomy or irradiating both kidneys as part of the primary treatment. In this paper we have looked at a group of predominantly bad-risk Stage V Wilms' tumour patients, who were referred for radiotherapy to the surviving kidney following nephrectomy to the worst affected side since 1971. In the period from 1952 to 1960, 70 patients with Wilms' tumour presented to our hospitals. Seven patients had had bilateral disease and, where the second tumour was not removed, Williams (1972) found 1500 cGy in 2–3 weeks to the surviving kidney to be a safe dose in conjunction with chemotherapy. Three of those seven patients were alive 6–19 years later. Subsequently the NWTS adopted the same dose: Bishop et al (1977) analysed 33 bilateral cases who received post-operative radiotherapy with doses ranging from 1000 to 2000 cGy. Although the higher doses appeared to be safe, they recommended a dose of 1500 cGy in 10 fractions as being effective, well tolerated and not associated with clinically apparent late renal damage.

Vaeth (1964) reported doses of up to 3800 cGy (maximum) and 2100 cGy (average) as being well tolerated by the surviving unaffected kidney in unilateral cases, but two of three Stage IV cases reviewed by Thomas et al (1983) developed renal complications following lower doses; one child developed radiation nephritis after 2050 cGy, although renal function was only transiently abnormal. The second patient suffered hypertension after a dose of 2200 cGy, but the renal artery received

3000 cGy, and it was a segment of this vessel that developed stenosis leading to hypertension, which reversed after excision of the stenosis.

With the introduction of more aggressive chemotherapy in Wilms' tumour protocols it is now worth reviewing the safety of "sandwich" radiotherapy in such a programme. The radiation-enhancing effects of adriamycin and actinomycin D in particular (Lieber, 1962; Arneil et al, 1974; Phillips & Fu, 1976) have been described, and some evidence suggests that such combination therapy may inhibit the future growth of the treated kidney (Donaldson et al, 1980). The scheduling of the drugs may be particularly important, bearing in mind recent observations that the administration of radiosensitizing agents prior to radiotherapy is less morbid than when the drugs are given simultaneously or immediately following irradiation (Horwich, 1989).

Such aggressive chemotherapy prompted us to use radiotherapy doses lower than Williams' recommended 1500 cGy in four of the seven patients who completed therapy. In the three long-term survivors, who received 1000–1200 cGy in 150–167 cGy fractions, the renal fraction tests including GFR, renal growth, haemoglobin and urinalysis have shown no discernible abnormality. (Although renal growth has been normal in the two patients for whom we have data, a caveat needs to be expressed in that the normal size ranges and growth curves apply only to children with two normal kidneys, and may not account for the compensatory hypertrophy in the remaining kidney of a nephrectomized child). Considering the fact that four patients died from local relapse in the kidney, it is now worth reviewing the total renal dose, although all four children who died received 1500 cGy or more. The recent demonstration of extreme radiosensitivity of childhood tumours to small dose fractions (Deacon et al, 1985; Kelland et al, 1989), and the results of experimental studies that suggest there is a marked increase in renal tolerance with decreasing fraction size (Robbins & Hopewell, 1991), has prompted a move in this department away from "shrinking field" techniques. We have moved towards "partial transmission block" techniques (rationale reviewed by Plowman, 1991) and this led to the treatment prescription given to the last patient in Table I, as shown in Fig. 3. The right flank required the UKCCSG recommended dose prescription of 3000 cGy in 20 fractions; we used the 20 fractions to deliver 1000 cGy to the surviving kidney, a fraction size of 50 cGy. Unfortunately the child died from the development of generalized abdominal relapse and ascites during radiotherapy. Nevertheless, the concept of small daily dose fractions, which we might now take to a higher overall total dose of 1500–1750 cGy, was being explored in this case.

In conclusion, the survival of patients with Stage V Wilms' tumour in the period from 1971 to 1989 was similar to that in the period from 1952 to 1960, the only stage for which survival figures have not dramatically improved at this centre (Plowman, 1988). Although more conservative surgery is now often preferred to unilateral nephrectomy, radiotherapy to the surviving kidney bearing active Wilms' tumour remains an important part of management. We were originally swayed from delivering doses as high as recommended by Williams (1972), because of radiosensitizing chemotherapy and data on age-related renal radiation tolerance, but we have now reviewed our practice. Our own observations on patients treated with 1000 cGy in 6 fractions to 1200 cGy in 13 fractions sandwiched into a chemotherapy programme (preferably at a time when the surviving kidney's compensatory hypertrophy has largely finished) and the more recent evidence of less age dependence in renal radiation morbidity (*vide supra*), suggest that higher doses in these cases may be well tolerated and safe.

However, in our series the four children receiving larger doses died of uncontrollable local disease, and further work is required to determine whether more intensive local radiotherapy will improve local control. Although our current practice is to return to the original prescription recommended in 1972 by Williams, viz. 1500 cGy in 10 fractions, it may be possible to exploit the capacity of renal tissue for repair of sublethal damage by using smaller fraction sizes to achieve higher doses, as exemplified by the case illustrated here in Fig. 3.

Acknowledgments

We are grateful to Dr C. D. Mireaux at the Hospital for Sick Children for her assistance, and to Tracy Cocks for typing the manuscript.

References

Arneil, G. C., Emmanuel, G. C., Flatman, G. E., Harris, F., Young, D. G. & Zachary, R. B., 1974. Nephritis in two children after irradiation and chemotherapy for nephroblastoma. *Lancet*, *i*, 960–963.

Avioli, L. V., Lazor, M. Z., Cotlove, E., Brace, K. C. & Andrews, J. R., 1963. Early effects of radiation on renal function in man. *American Journal of Medicine*, *34*, 329–337.

Bishop, H. C., Tefft, M., Evans, A. E. & D'Angio, G. J., 1977. Survival in bilateral Wilms' tumor—review of 30 national Wilms' tumor study cases. *Journal of Pediatric Surgery*, *12*, 631–638.

D'Angio, G. J., Evans, A. E., Breslow, N. et al, 1976. Treatment of Wilms' tumour. Results of national Wilms' tumour study. *Cancer*, *38*, 633–646.

Deacon, J. M., Wilson, P. A. & Peckham, M. J., 1985. The radiobiology of human neuroblastoma. *Radiotherapy and Oncology*, *3*, 201–211.

Domagk, G., 1927. Roentgenstrahlenschädigungen der Niere beim Menschen. *Medical Klinics*, *23*, 345–347.

Donaldson, S. S., Moskowitz, P. S., Canty, E. L. & Fajardo, L. F., 1980. Combination radiation-adriamycin therapy: renoprival growth, functional and structural effects in the immature mouse. *International Journal of Radiation Oncology, Biology, Physics*, *6*, 851–859.

Fisher, J. W., Roh, B. L. & Shenep, K., 1964. Influence of X-irradiation of the dog kidney on erythropoietin production. *Sangre*, *9*, 112–117.

Grossman, B. J., 1955. Radiation nephritis. *Journal of Pediatrics*, *47*, 424–433.

HAN, B., & BALDOCK, D., 1985. Sonographic measurements and appearance of normal kidneys in children. *American Journal of Roentgenology, 145*, 611–616.

HORWICH, A., 1989. Combined radiotherapy-chemotherapy in clinical practice. In *The Biological Basis of Radiotherapy*, 2nd edn, ed. by G. G. Steel, G. E. Adams and A. Horwich (Elsevier, Amsterdam), pp. 279–290.

JONGEHAN, H. T.-M., VAN DER KOGEL, A. J., PROVOOST, A. P. & MOLEVAAR, J. C., 1987. Radiation nephropathy in young and adult rats. *International Journal of Radiation Oncology, Biology, Physics, 13*, 225–232.

KELLAND, L. R., BINGLE, L., EDWARDS, S. & STEEL, G. G., 1989. High radiosensitivity of a newly established and characterised human embryonal rhabdomyosarcoma cell line. *British Journal of Cancer, 59*, 160–164.

KIM, T. H., FREEMAN, C. R. & WEBSTER, J. H., 1980. The significance of unilateral radiation nephropathy. *International Journal of Radiation Oncology, Biology, Physics, 6*, 1567–1571.

KUNKLER, P. B., FARR, R. F. & LUXTON, R. W., 1952. The limit of renal tolerance to X-rays. *British Journal of Radiology, 25*, 190–210.

LIEBLER, E. J., 1962. Actinomycin D and radiation therapy. *American Journal of Roentgenology, 87*, 94–105.

LUXTON, R. W., 1953. Radiation nephritis. A long term study of 54 patients. *Lancet, ii*, 1221–1224.

MOSKOWITZ, P. S., DONALDSON, S. S. & CANTY, E., 1980. Chemotherapy-induced inhibition of compensatory renal growth in the immature mouse. *American Journal of Roentgenology, 134*, 491–496.

PHEIMSTER, R. D. & THOMASSEN, R. W., 1973. Renal failure in perinatally irradiated beagles. *Radiation Research, 55*, 399–410.

PHILLIPS, T. L., & FU, K. K., 1976. Quantification of combined radiation therapy and chemotherapy on critical normal tissues. *Cancer, 37*, 1186–1200.

PLOWMAN, P. N., 1988. Radiotherapy of pediatric genitourinary tumours. In *Pediatric Tumours of the Genitourinary Tract* (Alan R. Liss, New York), pp. 263–281.

PLOWMAN, P. N., 1991. Minimizing the morbidity of radiotherapy. In *Complications of Cancer Management*, ed. by P. N. Plowman, T. J., McElwain and A. T. Meadows (Butterworths, London), pp. 474–486.

REDD, B. L., 1960. Radiation nephritis. Review, case report and animal study. *American Journal of Roentgenology, 83*, 88–106.

ROBBINS, M. V. & HOPEWELL, J. W., 1991. Renal and genitourinary system morbidity of radiotherapy. In *Complications of Cancer Management*, ed. by P. N. Plowman, T. J. McElwain and A. T. Meadows (Butterworths), pp. 193–212.

RUBIN, P., VAN HOUTTE, P. & CONSTINE, L., 1982. Radiation sensitivity and organ tolerance in pediatric oncology: a new hypothesis. *Frontiers of Radiation Therapy Oncology, 16*, 62–82.

SHAPIRO, A. P., CAVALLO, T., COOPER, W., LAPENAO, D., BRON, K. & BERG, G., 1977. Hypertension in radiation nephritis. *Archives of Internal Medicine, 137*, 848–851.

STEWART, F. A., SORANSON, J. A., ALPEN, E. L., WILLIAMS, M. V. & DENEKAMP, J., 1984. Radiation induced renal damage: the effects of hyperfractionation. *Radiation Research, 98*, 407–420.

THOMAS, P. R. M., GRIFFITH, K. D., FINEBERG, B. B., PEREZ, C. A., & LAND, V. J., 1983. Late effects of treatment for Wilms' tumour. *International Journal of Radiation Oncology, Biology, Physics, 9*, 651–657.

VAETH, J. M., 1964. The remaining kidney in irradiated survivors of Wilms' tumour. *American Journal of Roentgenology, 92*, 148–151.

WILLIAMS, I. G., 1972. *Tumours of Childhood: a Clinical Treatise* (W. Heinemann, London), pp. 88–107.

WILLIAMS, M. V., & DENEKAMP, J., 1984. Radiation induced renal damage in mice: influence of fraction size. *International Journal of Radiation Oncology, Biology, Physics, 10*, 885–893.

ZEIGERMAN, J. H., TULSKY, E. G. & MAKLER, P., 1957. Post-irradiation nephritic syndrome. *Obstetrics and Gynecology, 9*, 542–548.

ZUELZER, W. W., PALMER, H. D. & NEWTON, N. A., 1950. Unusual glomerulonephritis in young children, probably radiation nephritis; report of three cases. *American Journal of Pathology, 26*, 1019–1039.

1992, *The British Journal of Radiology*, *65*, 517–522

Output factors for blocked fields

By *E. M. Dean, BSc, MSc and J. B. Davis, BSc, MSc

Department of Radio-Oncology, University Hospital Zurich, Raemistrasse 100, 8091 Zurich, Switzerland, and *Department of Radiation Physics, St Bartholomew's Hospital, West Smithfield, London EC1A 7BE, UK

(*Received 17 June 1991 and in revised form 24 October 1991, accepted 6 December 1991*)

Keywords: Output factors, Blocks, Scatter

Abstract. This study investigates the output from blocked treatment fields with 6 MV and 18 MV photons. Square fields, defined by collimators, were blocked down to smaller symmetrical square, rectangular and asymmetrical rectangular fields using blocks on a tray beneath the collimators. Up to 7.5% difference was found between the output measured for the blocked field and the output calculated using a collimator output factor for the surface field size. A method is described by which output factors for the blocked fields can be measured and used in practice. Three methods of approximating these output factors are also presented.

The variation in linear accelerator output with collimator field size (CFS) is well documented. When the output of a 10 cm × 10 cm field at 100 cm source–surface distance (SSD) is measured at the depth of maximum dose and normalized to 1.00, the output of 5 cm × 5 cm and 30 cm × 30 cm fields will be less than and greater than 1.00, respectively. The variation in collimator output factors (OF_c's) with field size for our Varian Clinac 2100c with 6 MV and 18 MV photons is shown in Fig. 1.

It has been assumed in this department that the OF_c's for the surface field size (SFS) could also be used for fields defined by blocks, placed on a tray beneath the secondary collimators. Taking an extreme case of a 30 cm × 30 cm CFS blocked down to a 5 cm × 5 cm SFS, the output factor for the blocked field would be taken to be the same as the output factor of a 5 cm × 5 cm field defined by the collimators. However, the blocks are closer to the patient than are the secondary collimators and will provide a different scatter contribution to the measuring point. Some of the scattered radiation from the secondary collimators will be stopped by the blocks and the blocks themselves will create additional scatter (Fig. 2). This paper describes work carried out in this department to measure output factors for symmetrically and asymmetrically blocked fields and, if possible, to combine the results into a single output factor table for all blocked fields. Meli (1986) has also measured output factors for 6 MV photons; this paper extends the results to 18 MV photons and, because of the length of time needed for such measurements, suggests approximations that could be used to calculate output factors for blocked fields using OF_c's.

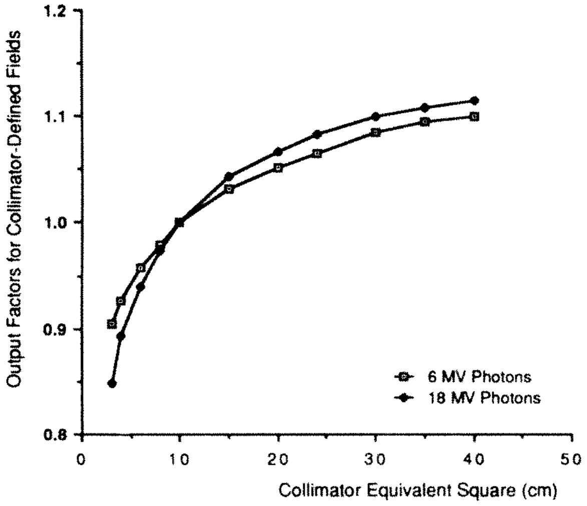

Figure 1. Variation in output factors for collimator-defined fields with field size for 6 MV and 18 MV photons.

Equipment

The following equipment was used in the measurements reported below:

Varian Clinac 2100c with 6 MV and 18 MV photons
Varian Clinac 6/100 with 6 MV photons
Dosetek water phantom 33 cm × 33 cm × 33 cm

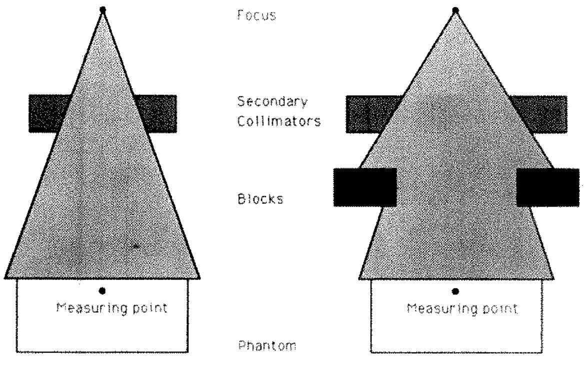

Figure 2. Effects of blocks on scatter to the measuring point.

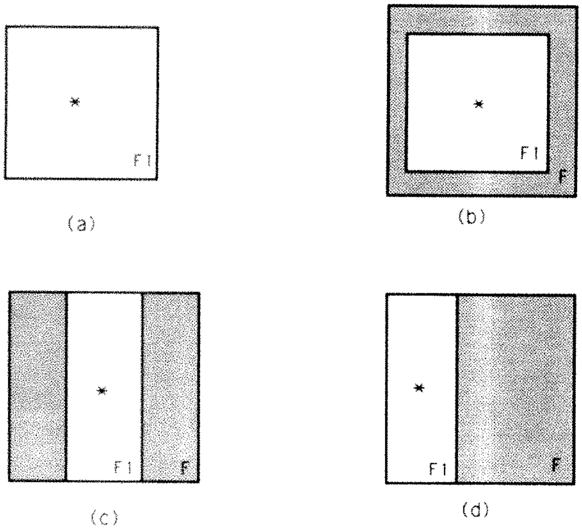

Figure 3. Symmetrical and asymmetrical blocked fields. (a) Open field, with (b) symmetrical square block, (c) symmetrical rectangular block, and (d) asymmetrical rectangular block. (*Denotes the measuring point.)

Farmer 0.6 cm^3 chamber (type 2571) in waterproof sheath
Farmer electrometer (type 2570)

Theory

In the following equations, the equivalent square of the SFS at 100 cm SSD is always F1. The CFS without blocks is also F1 and with blocks the CFS is increased to F (Fig. 3).

All equivalent squares were calculated using the sector integral method (Clarkson, 1941; Johns & Cunningham, 1983) employed by the Target treatment planning system (Cunningham et al, 1972; Cundiff et al, 1973; Hallberg, 1976; Hallberg et al, 1977). The electrometer readings obtained from the ionization chamber are denoted R1 (Reading 1), R2 (Reading 2), etc. All output factors are calculated relative to a 10 cm × 10 cm collimator-defined field.

Symmetrical fields

For a field defined by the secondary collimators (Fig. 3a), an electrometer reading contains primary output P (which is defined to include scatter from the head but exclude collimator scatter), an output factor OF_c, which includes collimator and phantom scatter S_c and S_p, respectively, and a block tray attenuation factor T, which is minimally field-size dependent.

$$\text{(Open field)} \quad R1 = (P \times T) \times OF_c \quad (1)$$

P is independent of collimator scatter by this definition, and T is only dependent on the SFS. Therefore, for any given SFS F1, $(P \times T)$ is constant whether the field is defined by the collimators or blocks. Adding blocks to a field to define a new SFS (Fig. 3b,c) modifies the collimator scatter to S_c' and adds scatter from the blocks S_b, therefore changing the output factor to OF_b. The phantom scatter contribution depends only on the SFS, and so remains the same for open or blocked fields.

$$\text{(Blocked field)} \quad R2 = (P \times T) \times OF_b \quad (2)$$

The output factor OF_c is known, having already been measured during commissioning. Therefore, dividing Equation 2 by Equation 1 gives OF_b, the output factor of the symmetrically blocked field.

Asymmetrical fields

Output factors for symmetrical fields are defined in the beam central axis, which coincides with the centre of the irradiated field. These central-axis output factors (OF_c) can be modified by an off-axis ratio (OAR) (Chui & Mohan, 1986) to provide an off-axis output factor OF_{coa} for the collimator-defined field. The OAR is defined as the ratio of outputs at positions off and on the beam central axis. The output factor in the centre of the asymmetrically blocked field is defined as OF_{boa} and the factor on the beam central axis is OF_{bcax}. The equations to calculate the output factors for asymmetrically blocked fields are given below.

$$\text{(Open field)} \quad R3 = (P \times T) \times OF_{coa} \quad (3)$$
$$\text{where } OF_{coa} = OAR \times OF_c$$

$$\text{(Blocked field)} \quad R4 = (P \times T) \times OF_{boa} \quad (4)$$
$$\text{where } OF_{boa} = OAR \times OF_{bcax}$$

Dividing Equation 4 by Equation 3 gives OF_{boa}, since the OAR and OF_c for the open field are known. As one of the aims of this study was to investigate the possibility of having a single table of output factors for the blocked fields, whether symmetrical or asymmetrical, the output factors in both cases need to be measured at the same point: on the beam central axis. This can be achieved in the asymmetrical case by dividing the output factor OF_{boa} by the open field OAR to find the collimator central-axis output factor OF_{bcax}. Using an OAR from the open field and not the blocked field includes off-axis scatter from the blocks in the value of OF_{bcax}.

Measurement technique

The measuring point of the Farmer chamber (2.4 mm nearer the source than the chamber axis) was positioned at the depth of maximum dose: 1.5 cm deep for 6 MV photons and 2.5–3.5 cm deep for 18 MV photons, depending on the CFS. All measurements were corrected to standard temperature and pressure. Collimator and gantry positions were 0°, source-to-water-surface distance was 100 cm and each measurement was taken after setting 100 monitor units. Readings were obtained for a range of CFS from 5 cm × 5 cm to 30 cm × 30 cm with the block tray in position. For a fixed collimater setting, the field area at 100 cm SSD was then reduced by placing blocks on a tray and readings were obtained in the centre of the irradiated field.

Table I. Output factors for symmetrically blocked fields

Unblocked fields		Blocked fields			% Difference (OF_b/OF_c)
CFS (cm)	Output factor OF_c	CFS (cm)	SFS (cm)	Output factor OF_b	
6 MV Photons					
5 × 5	0.943	30 × 30	5 × 5	1.013	+7·4
10 × 10	1.000	30 × 30	10 × 10	1.041	+4.1
15 × 15	1.032	30 × 30	15 × 15	1.068	+3.5
20 × 20	1.052	30 × 30	20 × 20	1.083	+2.9
30 × 30	1.085	30 × 30	30 × 30	1.085	0.0
18 MV Photons					
5 × 5	0.918	30 × 30	5 × 5	0.987	+7.5
10 × 10	1.000	30 × 30	10 × 10	1.037	+3.7
15 × 15	1.044	30 × 30	15 × 15	1.083	+3.8
20 × 20	1.068	30 × 30	20 × 20	1.114	+4.3
30 × 30	1.100	30 × 30	30 × 30	1.100	0·0

Results

The output factors for 6 MV and 18 MV photons with symmetrical blocking are shown in Table I. If a 30 cm × 30 cm field, defined by the secondary collimators, is blocked down to produce an SFS of 5 cm × 5 cm, there is a 7.4% and 7.5% difference between the output factors for a given SFS, defined by collimators or blocks, for 6 MV and 18 MV, respectively. The results for 6 MV confirm the results of Meli (1986).

Although blocking down to a 5 cm × 5 cm is unlikely during patient treatments, blocking down to an equivalent square of 20 cm × 20 cm might be done in order to keep the same isocentric position when a target volume is decreased, for example, in a second course of treatment. In this latter case, there is a 2.9% and 4.3% error in the dose delivered by using OF_c rather than OF_b for 6 MV and 18 MV, respectively. Using blocks to produce a square field is also not a very likely clinical situation; far more likely is blocking one or both sides of a field to produce either an asymmetrical or a rectangular field.

The discrepancies shown in Table II for asymmetrically blocked fields are of approximately the same magnitude as in the symmetrical case, with a tendency to be less. The variation in output factor comparing symmetrically and asymmetrically blocked fields is shown in Fig. 4 for 18 MV photons and a 10 cm × 10 cm collimator setting. This shows only a small difference with blocking arrangement (typically within ±1% of the mean when blocking down to 75% of the open field size). Therefore, it was deemed reasonable to calculate a table of average output factors to be used for all blocked fields, whether symmetrical or asymmetrical. Figure 5 shows the average output factors for blocked fields calculated in this way, with

Table II. Output factors for asymmetrically blocked fields

Unblocked fields		Blocked fields			% Difference (OF_{bcax}/OF_c)
CFS (cm)	Output factor OF_c	CFS (cm)	SFS (cm)	Output factor OF_{bcax}	
6 MV Photons					
5 × 5	0.943	30 × 30	5 × 5	—	—
10 × 10	1.000	30 × 30	10 × 10	1.041	+4.1
15 × 15	1.032	30 × 30	15 × 15	1.059	+2.6
20 × 20	1.052	30 × 30	20 × 20	1.065	+1.2
30 × 30	1.085	30 × 30	30 × 30	1.085	0.0
18 MV Photons					
5 × 5	0.918	30 × 30	5 × 5	—	—
10 × 10	1.000	30 × 30	10 × 10	1.057	+5.7
15 × 15	1.044	30 × 30	15 × 15	1.075	+3.0
20 × 20	1.068	30 × 30	20 × 20	1.091	+2.2
30 × 30	1.100	30 × 30	30 × 30	1.100	0·0

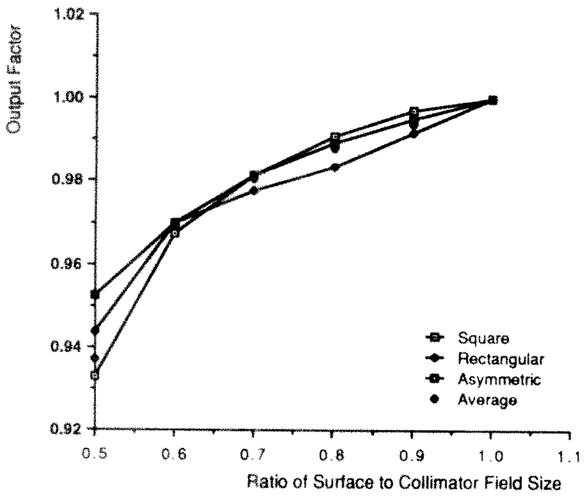

Figure 4. Output factors for various blocked field types for 18 MV photons and a collimator setting of 10 cm × 10 cm.

CFS dimensions of 5–30 cm, compared with the output factors for open fields. These curves show the discrepancies that would occur if the OF_c for the SFS was used to calculate dose given (open field values) rather than the more correct values of OF_b.

Discussion

From measurements in a water phantom, the output of a given SFS defined by blocks is always higher than the output of the same field size defined by the secondary collimators. Three possible components creating this change in output factor are: (i) the collimators are open wider in the blocked field case, contributing fewer backscattered electrons to the ion chamber in the head of the accelerator and allowing a longer "beam-on" time; (ii) the blocks are cutting out some of the forward scatter from the collimators; and (iii) the blocks themselves are producing scatter to the measuring point of a greater magnitude than the forward scatter from the collimators would have been, owing to their proximity to the phantom surface. The increases in output factor resulting from (i) and (iii) are the predominant components, with the decrease in output factor resulting from (ii) having less effect. The difference in output factors from open and blocked fields, shown in Tables I and II, is greater for 18 MV photons than for 6 MV photons. This is probably due to a relatively higher forward scatter component off the blocks at the higher energy.

With current treatment planning techniques, the aim is to give a patient dose within 5% of the planned dose. An error of up to 7.5% as a result of inaccurate output factors should therefore be avoided. In practice this would mean having to calculate an equivalent square for every treatment field with blocks and then look up or measure an output factor for that field. This is impractical for most radiotherapy departments and three methods of approximating the blocked output factor are now considered in order to avoid this. An analysis of patient data is shown in Fig. 6, in which the output factors calculated for the equivalent squares of the SFS (Fig. 6a) and the collimator jaw setting (Fig. 6b), looked up in the collimator output factor tables, are compared with the correct output factors for the blocked field.

These graphs show that most treatment fields are blocked down to no less than 65% of the collimator setting. Using the OF_c for the SFS gives a smaller

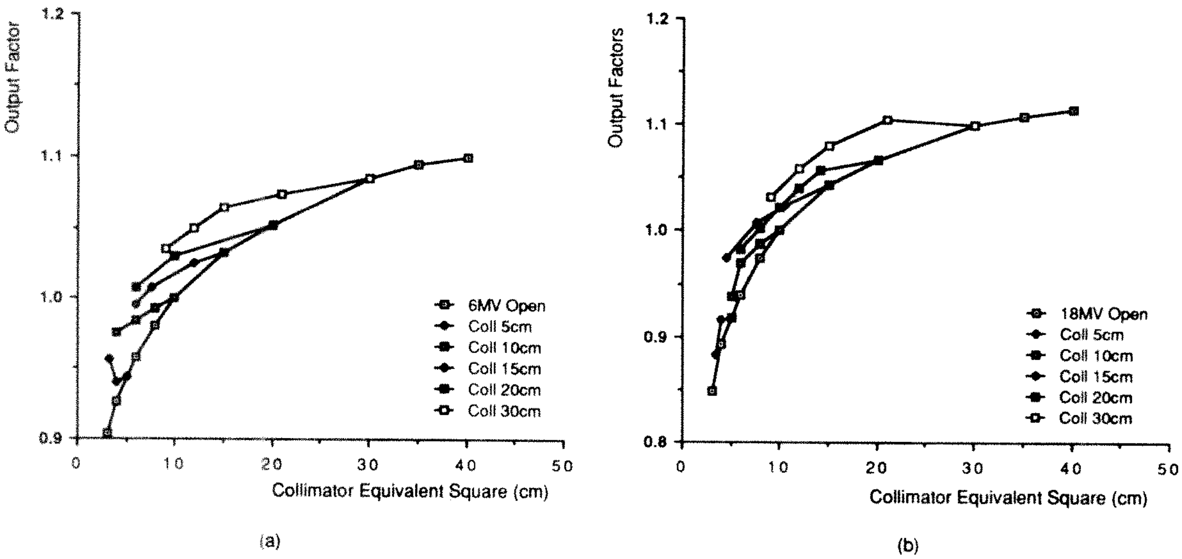

(a) (b)

Figure 5. Output factors for open and blocked fields with (a) 6 MV and (b) 18 MV photons. [The curve Coll 5 cm shows the output factors when blocking a collimator field size of 5 × 5 cm etc.]

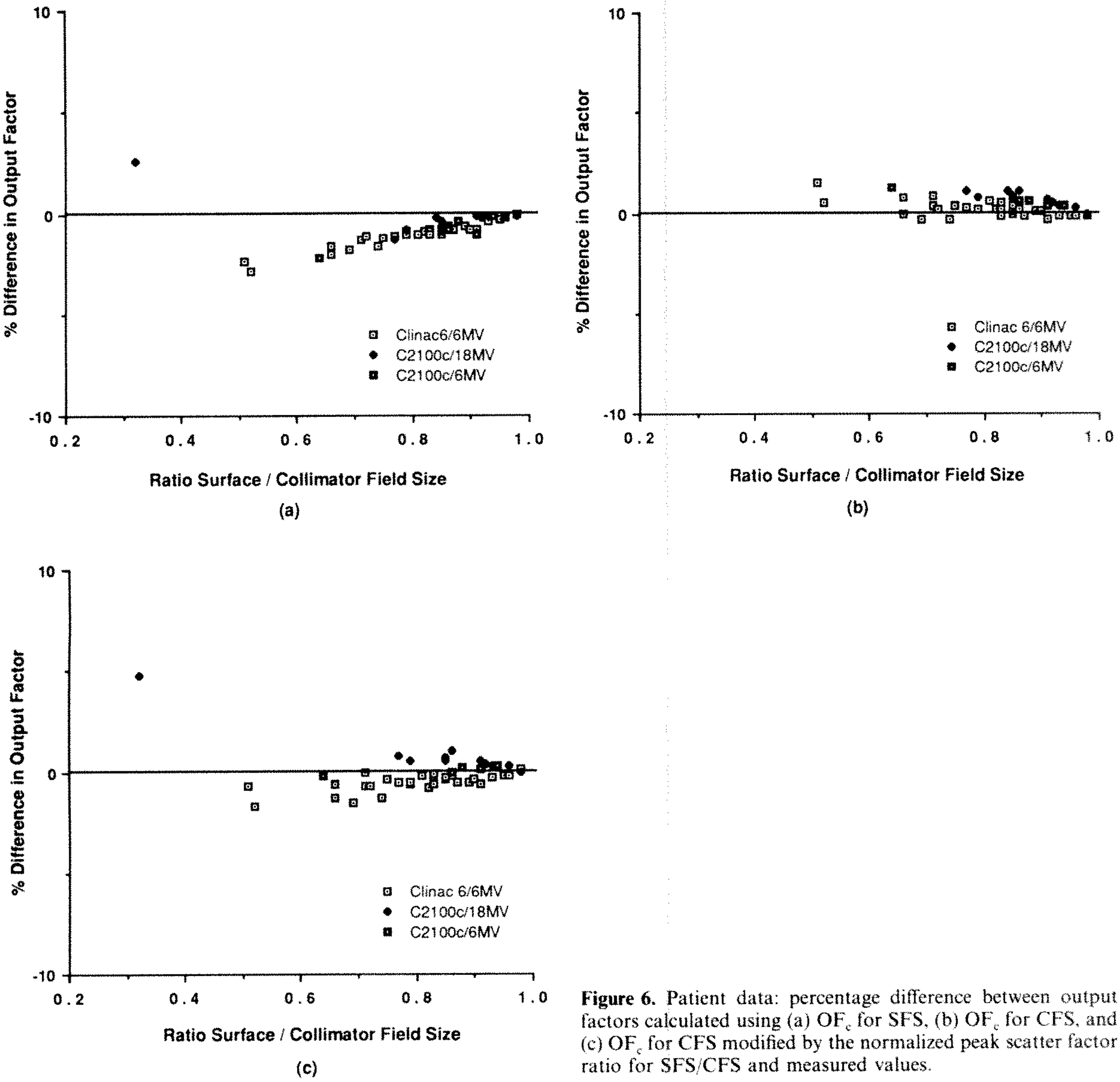

Figure 6. Patient data: percentage difference between output factors calculated using (a) OF_c for SFS, (b) OF_c for CFS, and (c) OF_c for CFS modified by the normalized peak scatter factor ratio for SFS/CFS and measured values.

output factor and hence a greater dose to the patient by up to 2.5% than if the OF_b was used (Fig. 6a), confirming the measurements in the phantom. Figure 6b shows that using the OF_c for the CFS, not the SFS, reduces the error to 1.2% in dose given to the patient.

Using the larger CFS to calculate a value of OF_c offsets the increased scatter from the blocked field, so reducing the error in dose given. Also evident from these graphs is the dependence of the results on the source-to-block-tray distance, the output factors for the Clinac 6/100 being slightly different from those for the Clinac 2100c. Lambert (personal communication, 1991) has suggested a modification of the OF_c by the ratio of normalized peak scatter factors for the surface and collimator field sizes. This method also produces output factors that are within ±2% of the correct values, with a tendency for 6 MV and 18 MV output factors to be too high and too low, respectively (Fig. 6c).

Conclusion

Output factors have been measured for symmetrically and asymmetrically blocked fields and found to be up to 7.5% greater than the output factors for the same SFSs defined by collimators. However, an analysis of patient data suggests that treatment fields are not usually blocked down to be more than 65% of the open field size. With this extent of blocking, the output factors can be sufficiently well approximated from the output factor for the CFS to within 1.2% of the correct value.

The output factors calculated from the SFS, or from the OF_c of the CFS modified by a ratio of normalized peak scatter factors, lie within 2.5% and 2% of the correct value, respectively.

If the blocked field size is less than 60% of the open field size, we recommend that an output factor should be measured for the particular block configuration, in order to avoid an error of between approximately 3% and 7.5% in dose given using an open field output factor for the CFS or SFS. The OF_b is dependent on the block-to-patient-surface distance, and should be measured for other treatment machines with different block-to-surface distances. The use of asymmetrical and multileaf collimators will certainly reduce the number of blocks needed to conform a field to a target volume, and hence the problem of additional scatter to the patient from the proximity of the blocks, but the challenge of output factor measurement for each field remains.

References

Chui, C. S. & Mohan, R., 1986. Off-center ratios for three-dimensional dose calculations. *Medical Physics*, *13*, 409–412.

Clarkson, J. R., 1941. A note on depth doses in fields of irregular shape. *British Journal of Radiology*, *14*, 265–268.

Cundiff, J. H., Cunningham, J. R., Golden, R., Lanzl, L. H., Meurk, M. L., Ovadiá, J., Pope, R. A., Sampiere, V. A., Saylor, W. L., Shalek, R. J. & Suntharalingham, N., 1973. A method for the calculation of dose in the radiation treatment of Hodgkin's disease. *American Journal of Roentgenology and Radium Therapy*, *117*, 30–44.

Cunningham, J. R., Shrivastava, P. N. & Wilkinson J. M., 1972. Program IRREG—Calculation of dose from irregularly shaped radiation beams. *Computer Programs in Biomedicine*, *2*, 192–199.

Hallberg, J. R., 1976. Concepts and accuracy of an improved irregular fields dosimetry computer program. MSc Thesis, University of Colorado Medical Center.

Hallberg, J. R., Ibbott, G. S., Carson, P. L., Hendee, W. R. & Aymar, M. A., 1977. Computational analysis and dosimetric evaluation of a commercial irregular-fields computer program. *Medical Physics*, *4*, 528–534.

Johns, H. E. & Cunningham, J. R., 1983. The interaction of single beams of X and gamma rays with a scattering medium. In *The Physics of Radiology*, 4th edn, ed. by C. Thomas (Springfield, Illinois), pp. 341–347.

Meli, J. A., 1986. Output factors and dose calculations for blocked X-ray fields. *Medical Physics*, *13*, 405–408.

1992, *The British Journal of Radiology*, *65*, 523–527

The application of microdosimetry in clinical bone densitometry using a dual-photon absorptiometer

By *A. J. Waker, PhD, B. Oldroyd and †M. Marco

Department of Medical Physics, University of Leeds, The General Infirmary, Leeds LS1 3EX, UK and
†Instituto de Estudios de la Energia, CIEMAT, Avenida Complutense 22, 28040 Madrid, Spain

(*Received 10 April 1991 and in revised form 29 October 1991, accepted 14 January 1992*)

Keywords: Microdosimetry, Dosimetry, X-rays, Absorptiometry

Abstract. Experimental microdosimetric methods have been used to determine absorbed dose values for a scanning dual-photon absorptiometer. Absorbed doses within the scanned field have been obtained for three different scanning speeds. For the normal speed setting used clinically, measurements have also been carried out in a water-filled phantom in order to estimate typical patient entrance, exit and midline doses. The results agree well with values obtained using thermoluminescence dosimetry and support the claims of the manufacturers with regard to upper limits placed on patient dose levels. The microdosimetric method enables changes in radiation quality to be followed and comparisons to be made with other low-energy photon fields used in medical diagnosis.

In recent times, new dual-photon absorptiometers have become commercially available, enabling selected site and whole-body scans of bone density to be carried out in the clinical environment. These devices facilitate the study of bone mineralization in groups of patients suffering from conditions known to affect bone loss. As part of one such study recently carried out in Leeds, 270 normal women between the ages of 20 and 80 years were scanned using a Lunar DPX scanner (Lunar, Madison-Wisconsin) in order to establish a set of control data for bone mineral density (BMD).

In this paper we present data on the dosimetry of the scanner determined experimentally using microdosimetric techniques. As an absorbed dose integrating technique, microdosimetry is a suitable method for making measurements in a scanning beam and so can provide direct comparative data to more conventional thermoluminescent dosimetry (TLD), which has an associated uncertainty in its response to low-energy photons (Delgado et al, 1987). Furthermore, although it is currently not considered helpful to allocate different quality factors to photon fields of different energy (International Commission on Radiological Protection (ICRP), 1990), nevertheless at the secondary electron interaction level, differences in quality do exist (International Commission on Radiation Units and Measurements (ICRU), 1986a). These differences are directly revealed in microdosimetric measurements, which can then be used as input data in radiological risk analysis of the type described by Brenner and Amols (1989).

Experimental methods

The DPX scanner (Fig. 1a) is based on the use of a cerium-filtered and highly collimated beam from an X-ray generator operated at 76 kVp, in effect supplying a dual-energy photon beam with narrow energy bands centred about 38 and 70 keV (Lunar, 1988a). The X-ray tube and sodium iodide detector are scanned across the patient over a pre-selected field size. Three

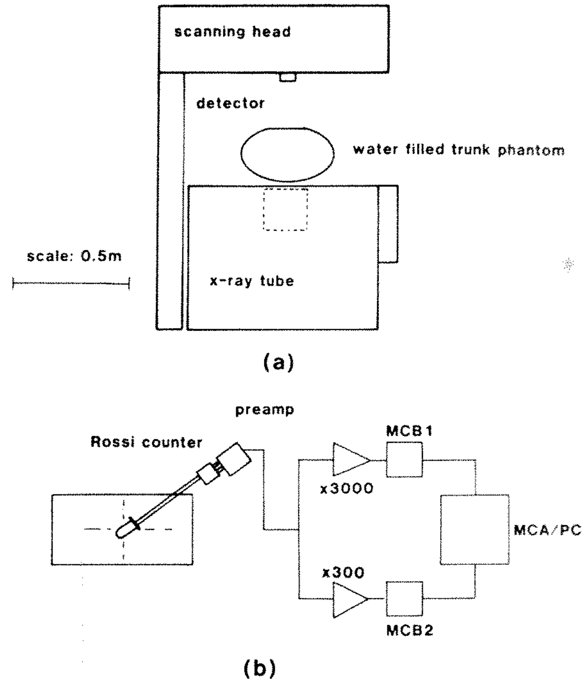

Figure 1. (a) An end view of the Lunar DPX scanning dual-photon absorptiometer. (b) Schematic diagram of the microdosimetric measuring system with the tissue-equivalent proportional counter positioned in the water-filled phantom. MCB1 and MCB2 are the multichannel buffer cards and MCA/PC is a computer-based multichannel analyser.

---

*Present address: AECL Research, Chalk River Laboratories, Chalk River, Ontario, Canada, K0J 1J0.

Table I. Absorbed dose values and microdosimetric averages derived from data recorded with a tissue-equivalent proportional counter free-in-air at three different scan settings of a dual-photon-energy X-ray absorptiometer

Measurement name (No. of scans)	Scan data		Absorbed dose		Microdosimetric averages	
	Speed (mm/s)	Pixel (mm)	Dose per scan (μGy)	Dose-rate (μGy/s)	$\bar{y}_F$ (keV/μm)	$\bar{y}_D$ (keV/μm)
DPX1 (4)	38.4	1.2	12.9	47.3	1.59	3.20
DPX2 (5)	76.8	1.2	6.4	47.0	1.58	3.18
DPX3 (8)	153.6	2.4	1.6	46.3	1.60	3.19
DPX4 (5)	38.4	1.2	13.0	47.7	1.58	3.14
DPX5 (5)	76.8	1.2	6.4	47.0	1.57	3.14
DPX6 (5)	153.6	2.4	1.6	46.3	1.57	3.17

scanning speeds are available. For the slow and medium scanning speeds the incremental step between each scan line is 1.2 mm and for the fast speed the step is 2.4 mm. Table I lists the linear velocities of the beam for the three settings. Differential absorption between the higher- and lower-energy photons provides the raw data for mapping out the bone density in the scanned field.

The microdosimetric measuring system employed in the investigation is shown schematically in Fig. 1b. The tissue-equivalent proportional counter (TEPC) used was a commercially available $\frac{1}{2}$ inch Rossi counter (Far West Technology, Goletha, California) filled with propane-based tissue-equivalent gas. Most of the measurements were carried out with the counter gas pressure set such that the TEPC simulated a unit density site size of 2 μm, a few measurements being carried out at a 10 μm site size. Signals from the proportional counter were recorded using two amplifiers with a gain factor of 10 between them and two multichannel buffer cards (EG&G Instruments). In this manner the complete range of pulse heights from the TEPC can be recorded in the form of two subspectra, which are subsequently joined, as part of the data analysis, to form a single microdosimetric event-size spectrum. The two multichannel buffer cards are part of an integrated pulse-height analysis and microcomputer system enabling full analysis of the microdosimetric data at the site of measurement.

After calibration of the TEPC, by means of an internal ^{244}Cm alpha source depositing a known amount of energy, the pulses from the TEPC are scaled in terms of imparted energy and the absorbed dose can be obtained by integration of the measured pulse height spectrum. In effect this is a measurement of the absorbed dose on an event-by-event basis where in this context an event is the deposition of energy in the tissue-equivalent counter by a single interacting electron that has been generated in the counter wall or gas cavity by the primary X-ray field.

The scan dimensions were set up by placing lead markers above and below the TEPC and observing the image on the DPX output monitor. Field sizes 5 cm by 10 cm ensured that the TEPC was completely scanned.

In the study, two sets of measurements were carried out with the TEPC free-in-air and with the DPX operated at three different scanning speeds. Measurements were also made with the DPX operated at the medium scanning speed and the TEPC placed at three different depths in the trunk section of a Bush phantom filled with water. A Bush phantom consists of hollow circular and elliptical polythene cylinders simulating the various regions of the human body (Bush, 1946). This set of measurements provided an estimate of patient entrance, midline and exit doses. Further measurements were also carried out in the phantom with the TEPC operated with a 10 μm simulated diameter.

Results

Table I provides the free-in-air absorbed doses and microdosimetric averages derived from the measured event-size spectra, an example of which is shown in Fig. 2. The microdosimetric spectra recorded for the three different scan settings were found to be identical and so only the spectrum for the medium speed is shown. For presentation purposes it is usual for the TEPC pulses to be scaled in terms of lineal energy, y, which is the imparted energy divided by the mean chord length of the TEPC simulated site and has the units of keV/μm. The recorded pulse-height spectrum from the TEPC is then displayed as the fraction of the absorbed dose per logarithmic interval of lineal energy. In this format, equal areas under the spectrum represent equal contributions to the absorbed dose (ICRU, 1986b) and the event-size spectrum is known as a dose distribution. Microdosimetric spectra can be characterised by two average quantities, the frequency mean, $\bar{y}_F$, and the dose mean, $\bar{y}_D$. The frequency mean is the first moment of the measured event-size frequency spectrum and the dose mean is the first moment of the recorded data converted to a dose distribution. Both these quantities are used to express the average microdosimetric quality of a radiation field.

Table II provides a summary of the dosimetric data obtained from the phantom measurements that were carried out at the medium-scan-speed setting. Also shown in Table II are the dosimetric data derived from

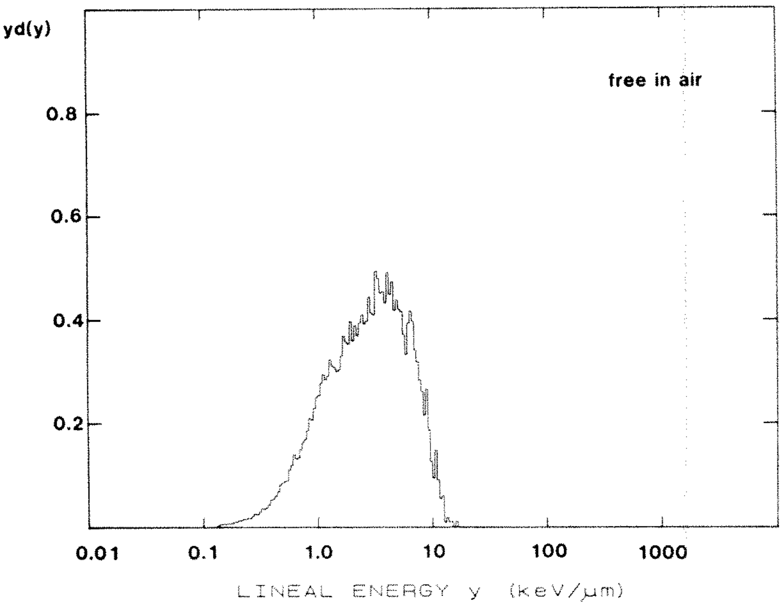

Figure 2. Microdosimetric event size spectrum $yd(y)$ giving the absorbed dose fraction per logarithmic interval of lineal energy y for a measurement made free-in-air at the position of the couch top and for a TEPC 2 μm simulated diameter. Equal areas under the curve represent equal dose fractions.

measurements carried out in the phantom at the beam entrance and exit with a 10 μm TEPC simulated diameter.

Discussion

Examination of Table I shows that for the two independent sets of measurements made, the dosimetric results are in good agreement.

For a stationary beam the absorbed dose to a layer of uniform density and unit thickness will be given by the intrinsic dose-rate of the beam $\dot{D}$, multiplied by the time of exposure. For a scanning beam, however, during an identical time interval, the same imparted energy is deposited in a much larger mass and therefore the absorbed dose, D_{scan}, in a scanned field will be less by a factor given by the ratio of the beam area, A_{b}, to the total scanned area A_{scan}, thus:

$$D_{\mathrm{scan}} = \dot{D} \times t_{\mathrm{scan}} \times (A_{\mathrm{b}}/A_{\mathrm{scan}})$$

For a fixed scanning speed the beam sweeps out equal areas of field in equal time intervals, so D_{scan} will be the same everywhere within the scanned field although the total imparted energy to the patient does of course increase in direct proportion to the field size scanned. As A_{scan} is proportional to the scan velocity and scan time, the dose per scan will, for a fixed pixel size, be inversely proportional to the scan velocity. This is seen to be the case in Table I.

Using the relation between the dose per scan and the intrinsic beam dose-rate given above, the beam dose-

Table II. Dosimetric and microdosimetric quantities derived from measurements made with a tissue-equivalent proportional counter using two different simulated diameters in a water phantom scanned by a dual-photon-energy X-ray absorptiometer

Measurement data			Scan data			Absorbed dose		Microdosimetric averages	
Name	Position	ϕ (μm)	No.	Speed (mm/s)	Pixel (mm)	Dose/scan (μGy)	Dose rate (μGy/s)	$\bar{y}_{\mathrm{F}}$ (keV/μm)	$\bar{y}_{\mathrm{D}}$ (keV/μm)
DPX7	ENT	2	5	76.8	1.2	7.4	54.3	1.63	3.04
DPX8	ML	2	5	76.8	1.2	1.9	13.9	1.50	2.99
DPX9	EX	2	10	76.8	1.2	0.36	2.64	1.45	3.21
DPX10	ENT	10	6	76.8	1.2	7.2	52.8	1.06	1.88
DPX11	EX	10	18	76.8	1.2	0.43	3.16	0.99	1.81

ENT = entrance, base of phantom: 17 cm depth in water.
ML = midline, centre of phantom: 8.5 cm depth in water.
EX = exit, surface of phantom: centre line of counter at zero depth.
ϕ Tissue-equivalent proportional counter simulated unit density diameter.

rate can be determined from the measured scan doses. The ratio (A_{scan}/A_b) has been estimated from the DPX manufacturer's data concerning the beam size and, for the field sizes used, is 396.3. Derived beam dose-rates are given in Table I and to within less than 2% a constant value is found, as should be the case for a machine parameter independent of the selected scanning velocity.

At the edges of the field the beam is almost stationary as it increments forward before commencing the next line. Therefore at the field edges the dose-rate will be higher than the scan dose and will approach that of the intrinsic beam dose-rate.

The microdosimetric event-size spectrum corresponding to the free-air measurements is shown in Fig. 2. Although the beam is composed of two principal photon energies around 70 keV and 38 keV, because of the change in proportion of photoelectric effect to Compton scattering that takes place between these two energies, the mean energy of the secondary electrons produced in tissue-like materials remains almost the same for the two energies at around 12 keV. At these energies and for a 2 μm simulated diameter, the electrons are mostly crossing the counter and the device still behaves as a good lineal energy spectrometer with a peak in the event-size spectrum at round 3.9 keV/μm. This is in agreement with that found with other measurements recorded in this range of photon energies (Schmitz et al, 1989). The constancy of the microdosimetric averages for the various scanning conditions shown in the final columns of Table I is a consequence of the similarity between the measured spectra and indicates no change in the beam microdosimetric quality.

As the beam passes through a phantom the proportion of the 70 keV X-ray energy peak changes from about 20% to 60% of the total influence (Sorenson et al, 1989). However, as discussed above, the mean secondary electron energy does not change significantly and therefore the microdosimetric spectra for the in-phantom measurements are the same regardless of depth of measurement. Comparison of the microdosimetric averages for the 2 μm measurements in Table II shows that the beam quality is indeed the same as for the free-air measurements. The absorbed dose per scan, however, is reduced by a factor of around 20 as one moves from the beam entrance to the exit on the far side of the phantom. It is interesting to note that the dose per scan at the phantom entrance is higher than that recorded in air for the same speed by around 14%, owing to the presence of scattering material above the point of measurement.

In previous work carried out to investigate the energy response of the TEPC to measure absorbed dose at low photon energy (Evazi, 1990), it was seen that with a 10 μm simulated diameter the TEPC had a marginally flatter energy response than with a 2 μm site size. This prompted the measurements to be made at 10 μm, and these were found to be in very good agreement with those given for the 2 μm simulated diameter.

Conclusions

The objective of the work reported in this paper has been to investigate the application of a tissue-equivalent proportional counter and microdosimetric technique to the dosimetry of a dual-photon absorptiometer

The scan absorbed doses agree well with TLD dosimetry carried out by hospital radiation protection staff, who measured scan doses of between 8 and 9 μGy for eight measurements at the medium speed. These measurements were made at the base of an aluminium spine phantom set in a block of wax, and so correspond most closely with the measurements reported here for the phantom entrance dose. The recorded doses-per-scan are significantly lower than the DPX manufacturer's data of upper limits: 15 μGy for the medium speed, 30 μGy for the slow speed and 5 μGy for the fast setting (Lunar, 1988b).

The measurement of dose using microdosimetric methods has the advantage that changes in radiation quality can be followed and comparisons made with other applications of low-energy X rays in medicine. A comparative quality factor to that of mammography X rays can be derived in the manner suggested by Brenner and Amols (1989) and discussed by Waker and Marco (1991), by incorporating the ICRU 40 quality factor versus lineal energy function (ICRU, 1986a) into the measured event-sized spectra. Quality factors derived in this way are 1.18 and 0.88 for the mammography beam and DPX beam, respectively.

Acknowledgments

This work has been funded by the British Council, whose support is gratefully acknowledged, under the Acciones Integradas scheme.

References

Brenner, D. J. & Amols, H. I., 1989. Enhanced risk from low energy screen-film mammograph X-rays. *British Journal of Radiology*, *62*, 910–914.

Bush, F., 1946. Energy absorption in radium therapy. *British Journal of Radiology*, *19*, 14–21.

Delgado, V., Gonzalez, L., Marco, M., Moran, P. & Vano, E., 1987. Experimental determination of the relative TL response of TLD-100 chips for 60 kVp X- and ^{60}Co gamma-rays. *Nuclear Instruments and Methods*, *A255*, 238–241.

Evazi, M. T., 1990. Application of experimental microdosimetric techniques to the dosimetry of X-rays in the diagnostic energy range. PhD Thesis, University of Leeds.

ICRP. 1990. Recommendations of the International Commission on Radiological Protection, Publication 60. *Annals of the ICRP*, *21*(1–3), 81.

ICRU, 1986a. *The Quality Factor in Radiation Protection*, Report 400 (International Commission on Radiation Units and Measurements, Bethesda, Maryland).

—— 1986b. *Microdosimetry*, Report 36 (International Commission on Radiation Units and Measurements, Bethesda, Maryland).

Lunar, 1988a. *Technical Note No. 1. Introduction to DPX and Basic Principles*. (Lunar, 313 W. Beltline Hwy, Madison, Wisconsin 53713, USA).

—— 1988b. *Technical Note No. 3. DPX Performance: Dose* (Lunar, 313 W. Beltline Hwy, Madison, Wisconsin 53713, USA).

SCHMITZ, TH., KRAMER, H. M. & BOOZ, J., 1989. Assessment of the photon response of a TEPC: implementation of operational quantities for dose equivalent. *Radiation Protection Dosimetry*, *29*, 69–74.

SORENSON, J. A., DUKE, P. R. & SMITH, S. W., 1989. Simulation studies of dual energy X-ray absorptiometry. *Medical Physics*, *16(1)*, 75–80.

WAKER, A. J. & MARCO, M., 1991. The application of microdosimetry to the metrology of low-energy X rays used in mammography. *British Journal of Radiology*, *65*, 258–261.

1992, *The British Journal of Radiology*, *65*, 528–535

A preliminary investigation of the imaging performance of photostimulable phosphor computed radiography using a new design of mammographic quality control test object

By A. R. Cowen, BSc, D. S. Brettle, BSc., N. J. Coleman, BA and *G. J. S. Parkin, BSc, DMRD, FRCR

FAXIL, The University of Leeds, Department of Medical Physics, Wellcome Wing and *Department of Diagnostic Radiology, The General Infirmary, Leeds LS1 3EX, UK

(Received 18 June 1991 and in revised form 11 November 1991, accepted 14 January 1992)

Keywords: Mammography test object, Computed radiography

Abstract. Leeds Test Object TOR[MAM] has been designed to supplement the current FAXIL mammography test object TOR[MAX]. It contains a range of details that have a more natural radiographic appearance and has been designed as a test that more closely approximates the image quality achieved in clinical mammography. Physical aspects of the design and implementation of TOR[MAM] are presented. The TOR[MAM] has been used in a preliminary physical evaluation of the comparative image qualities produced by conventional (screen–film) and photostimulable phosphor computed mammography and the results are discussed. TOR[MAX] results are also presented. The influence of digital image processing (enhancement) on the image quality of computed mammograms is also considered. The results presented indicate the sensitivity of TOR[MAM].

In 1987 FAXIL developed a test object TOR[MAX] to coincide with the launch of the Forrest screening programme (Cowen & Coleman, 1990). This test object was designed to address the basic aspects of mammographic imaging performance and meet the needs of commissioning trials, acceptance inspections and routine quality control. This test object contained test patterns and details required to measure grey-scale rendition, high-contrast spatial resolution and both large and small area detail detectability (see Fig. 1) (Cowen et al, 1988). The device was designed as a calibrated test device that could be accurately reproduced in large numbers. This was an important aspect of the design, as the Pritchard Committee Report on Quality Management in the Screening Programme (Pritchard, 1989) emphasized the need for a uniformly high standard of performance across the whole country. The screening programme is now well established and therefore the emphasis on quality control is expanding to cover the overall clinical aspects of image quality management. FAXIL has recently developed a new type of mammographic test object that may help to satisfy some of these requirements whilst continuing to satisfy the recommendations of the Pritchard Committee. The TOR[MAM] can be used to supplement (not replace) the current FAXIL mammography test object TOR[MAX]. It contains test details that have a more "natural" appearance aimed at more closely approaching the conditions pertaining during a real mammographic examination. The design and initial applications of the TOR[MAM] are described below. The designation TOR denotes the test object is also intended for application in routine quality control. This implies a simple design with limited complexity such that the test images can be assessed quickly and conveniently in the field.

It is generally intended that TOR[MAX] be used to provide quantitative information for quality control purposes, whereas TOR[MAM] is designed to provide a qualitative result based on details more closely representing genuine clinical features. In this way TOR[MAM] is more suited for use by clinical staff rather than the physics/technical staff required for TOR[MAX]. The two test objects in conjunction should cover most aspects of mammographic quality control, satisfying both clinical and technical demands.

TOR[MAM] was developed for internal purposes to support a preliminary investigation into computed radiography in mammography; it was also simultaneously developed as a routine quality control test object. This paper presents the results of the preliminary investigation, which indicates the sensitivity of TOR[MAM] to different image modes.

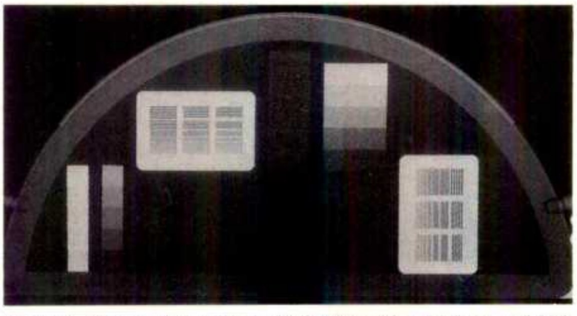

Figure 1. Conventional film of TOR[MAX] acquired at 28 kV.

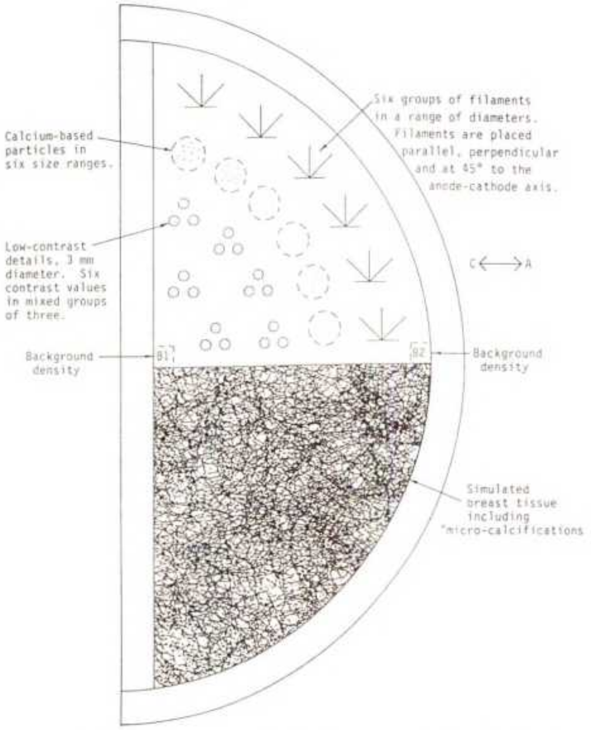
Calcium-based particles in six size ranges.
Six groups of filaments in a range of diameters. Filaments are placed parallel, perpendicular and at 45° to the anode-cathode axis.
Low-contrast details, 3 mm diameter. Six contrast values in mixed groups of three.
C⟷A
B1
B2
Background density
Background density
Simulated breast tissue including "micro-calcifications

Figure 2. Detail layout of Leeds Mammographic Test Object type TOR[MAM].

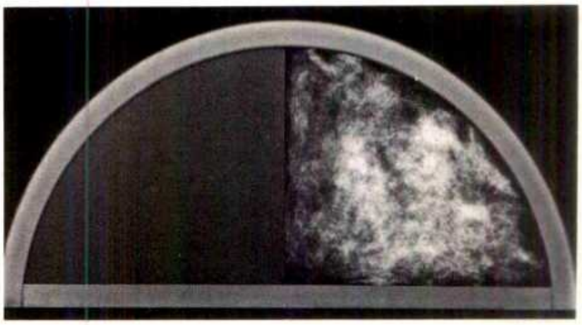

Figure 3. Photostimulable phosphor computed mammogram of Leeds TOR[MAM]: test image acquired at 28 kVp and 64 mAs.

Design of TOR[MAM]

TOR[MAM] comprises a D-shaped Perspex container divided into two sectors and includes three types of test details (see Figs 2, 3). The test plate is used in conjunction with a stack of three 1 cm thick Perspex plates, which provide the base attenuation of the radiation beam, and also introduce scatter and geometric unsharpness effects. The thickness of Perspex in TOR[MAM] itself is 1.1 cm giving a total of 4.1 cm base attenuation. The average compressed breast thickness for the purposes of quality control recommended by the Institute of Physical Sciences in Medicine (IPSM) Report 59 (1989) is 4.5 cm. The amount of Perspex necessary to simulate the effects of 4.5 cm of tissue is 4.15 cm (Dance, 1990). Therefore, TOR[MAM] plus the base plates closely represents the average compressed breast in physical imaging terms. The image quality is assessed by subjective review of the detectability/visibility of large-area, low-contrast circular details, low-contrast filaments and groups of pseudo microcalcifications from which an "image quality score" can be derived. The main *physical* factors involved in image quality assessment are grey-scale rendition, unsharpness and noise. These are determined by the physical characteristics of the mammography system (X-ray spectrum, focal spot size, exposure factors, etc.) together with those of the image detection device (characteristic curve, modulation transfer function (MTF), Wiener spectrum, etc.). These factors act, individually or in conjunction, to influence the visibility of the various test details in different ways and to different degrees. The accumulated detail-visibility scores provide a convenient measure of overall image quality. The full detail specifications are presented in Fig. 4. The three types of test details are each presented in an array of six groups denoted A, B, C, D, E, F. In general, detail visibility diminishes from Group A through to Group F.

Low-contrast details

The low-contrast details provide a subjective test that is different from the standard FAXIL layout used in TOR[MAX], *i.e.* rows of single details regularly spaced

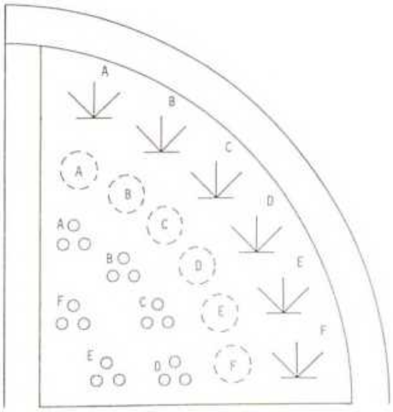

TOR [MAM] detail specifications

	A	B	C	D	E	F	
Filament diameters (length 10 mm)	0.40	0.35	0.30	0.25	0.225	0.20	mm
Particle size range	354 to 224	283 to 180	226 to 150	177 to 106	141 to 90	106 to 63	μm
Nominal contrasts (detail size 3 mm) ○ ○ ○	4 3 2	3 2 1½	2 1½ 1	1½ 1 ½	1 ½ 4	½ 4 3	%

Figure 4. List of test details used with TOR[MAM].

and decreasing progressively in contrast. The new arrangement includes three details at each subject contrast placed at different locations, thereby reducing the spurious results that can occur if noise artefacts happen to coincide with a single detail close to the threshold of visibility. There are six contrast values, and the details are arranged in six groups, each containing three details of differing contrast.

The low-contrast details in TOR[MAM] comprise circular discs 3 mm in diameter made of plastic of six thicknesses producing six contrast values. The nominal X-ray contrast at 28 kVp using a molybdenum anode X-ray tube with 0.03 mm Mo tube filtration are 4%, 3%, 2%, 1.5%, 1%, 0.5%. These details approximate the mean size of detail recommended by Kimme-Smith (1989) of 2 mm to 5 mm diameter, but are significantly lower in contrast than their suggested levels of 8–12%. This is in order to provide test contrasts overlapping the threshold of visibility for details on a uniform background.

Filaments

The low-contrast filaments are laid out in a fixed pattern comprising details at three orientations. It is important to position the test filaments in a number of directions, as their visibility can vary with their orientation with respect to the anode–cathode axis, owing to differences in the dimensions (length : width) of the X-ray focal spot projected at different points within the image field. The filament groups are arranged so that the finest details lie closest to the central axis where the focal spot size is smallest. It is claimed that differences in the Mach effect (Lane et al, 1976) can also influence the relative visibility of filaments (see Kimme-Smith, 1989) but this is unlikely to be significant in TOR[MAM] because of the comparatively low contrasts of the filaments. The filaments comprise lengths of monofilament material with a range of six diameters as follows: 0.4, 0.35, 0.30, 0.25, 0.225, 0.20 (mm). For each diameter, four filaments 10 mm long are arranged so that they lie parallel, perpendicular and at 45° to the anode–cathode axis of the X-ray tube. Since the visibility of filaments may be dependent on their orientation, the filaments should be examined individually and not simply as a group of four.

Particles

The particles (pseudo-microcalcifications) are made of a calcium-based mineral substance. Several particles comprise each individual test group, simulating a cluster of microcalcifications. The particles are of irregular shape and are graded into the following ranges of size (μm): 354 to 224, 283 to 180, 226 to 150, 177 to 106, 141 to 90, 106 to 63.

The actual figures denote the upper and lower limits of sizes in each group and not the actual particle size. The size ranges are based on the test sieves used to grade the particles; these sieves satisfy the international test sieve standard ISO 565 and 3310/1 for accuracy and regularity of layout. In order to verify the upper limits of the size ranges, random samples of particles were measured using a Vernier microscope.

Breast tissue morphology

One half of the test object was designed to simulate the appearance of breast tissue and is constructed from a material chosen for its malleability, physical stability and non-degradability. *It must be noted that we do not claim that this pseudo-breast structure is tissue-equivalent either in the radiological or anatomical sense.* This feature has been included in an attempt to simulate the noise contribution of breast morphology itself to overall image quality. Responses from the consultant radiologist involved with this work indicate that the result obtained does achieve this. The authors believe that testing mammographic imaging performance exclusively under homogeneous (featureless) imaging conditions may lead to an overestimation of the minimum detail visibility compared with that found in practice. In clinical mammography, anatomical structure noise adds to that of the external (physical) noise process and the internal (visual) noise mechanisms of the observer. The amalgam of these various contributions of noise power set the ultimate limit to the level of detail conspicuity. Clearly, anatomical structure noise will vary from breast to breast and exhibit a wide diversity in texture, shape, intensity, etc. In this test object we have attempted to address this important aspect of mammographic image quality. Six further groups of microcalcifications have been placed within this test area. These groups have the same specifications as those used in the upper (homogeneous) half of the test object but are distributed pseudo-randomly and not in an arc-shaped pattern. The other features (fibres and low-contrast details) have not been included in this section in an attempt to simplify its use. Although this section is constructed with exactly the same amount of material, packed into the same volume and laid down the same way in every test object, some variation in the resultant structure is inevitable. However, extreme care is taken to ensure that the particle clusters are always placed in similar areas in all devices. It is emphasized that this area is intended to give a quick subjective *impression* of image quality and not a measurable result.

Background density measurements

Two areas, B1 and B2, indicated in Fig. 2 are for the measurement of the background density to allow control between films.

Implementation of TOR[MAM]

The TOR[MAM] was originally developed for internal purposes to support a preliminary investigation of the image quality of mammograms produced by a photostimulable phosphor computed radiography (CR) system. This installation comprises a Philips Graphics II Compact (7000 Series) CR system employing third-generation Fuji high-resolution storage phosphor screens. This system is operated in conjunction with a Philips Diagnost UC mammography unit. The X-ray

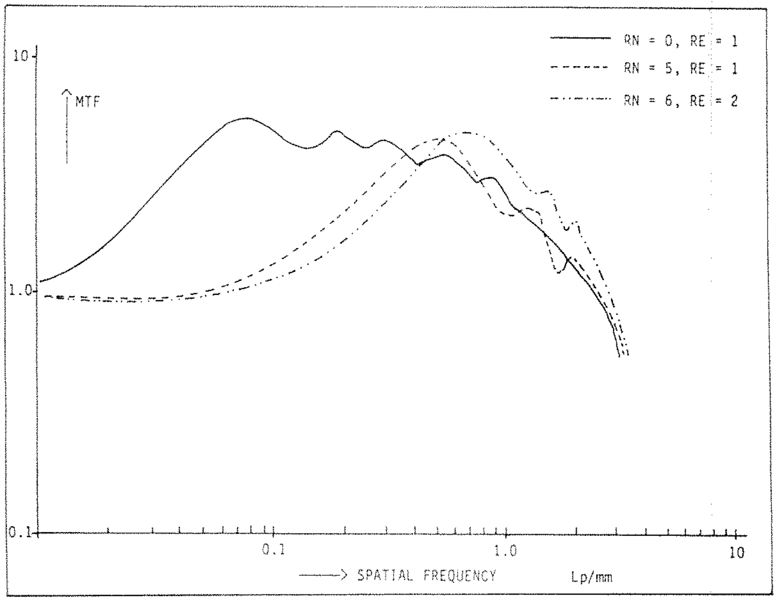

Figure 5. The MTFs of the CR system for default, IP1 and IP2 image processing selections.

unit underwent a rigorous commissioning trial, which included checks of radiographic exposure factors, automatic exposure control and focal spot dimensions prior to the study. These aspects of performance all fell within acceptable operating limits (Department of Health, 1990). A Fuji MA screen cassette combined with Fuji MI-NH film was used as the reference screen/film system in this study. 12 each of CR and film/screen test images of TOR[MAM] were acquired. In all cases radiographic exposure factors were set at 28 kVp and 60 mAs to ensure an identical image receptor entrance exposure. All films were processed in a Kodak M8 automatic film processor using a standard 90 s development plus fix cycle and a development temperature of 34°C. All the CR images were archived on an optical disk store using (2:1) reversible image data compression. The CR test images were reviewed from laser-printed hard-copy films (soft-copy assessment of CR images from the display workstation (DMS 20) will feature in a follow-up study). In order to ensure reproduction of the CR images at full spatial resolution (2370 × 1770 pixels), hard-copy images were presented using the single-image format, rather than the more familiar default presentation of two images, one normal "film-like" image and one more heavily enhanced image. The single-format hard-copy images are essential for mammography as it is only then that the image data are reproduced at full spatial resolution. The spatial resolution limit of the CR system is 5 cycles/mm compared with the 15 cycles/mm exhibited by the screen–film combination.

The computed mammographic images undergo digital image enhancement prior to display/hard copy. The image processing environment used in the CR system comprises a set of routines to manipulate image contrast rendition (using grey-scale look-up tables) and spatial-frequency filtering using the unsharp mask technique (the algorithm has been fully described by Tateno et al (1987) and Blume (1986)). The latter can be tuned to one of 10 spatial frequency selections to enhance preferentially details of specific ranges of size; this is achieved using a parameter $R_n(i)$ where $i = 0 \rightarrow 9$). The manufacturer provides a default image processing routine, which is applied to all mammographic images. The image processing can be adjusted subsequently at the DMS 20 to produce a user-defined presentation prior to hard-copy. A series of test hard-copy images were produced, firstly using the default image processing setting and then with two variants selected by the authors. The two variants are denoted IP1 and IP2. IP1 was a slightly modified version of the default setting, which was developed to improve the apparent sharpness of the CR images without materially changing the grey-scale rendition. Essentially IP1 features an unsharp mask tuned to a higher spatial frequency ($R_n = 6$) rather than the standard ($R_n = 5$). The degree of spatial frequency enhancement was also increased using the parameter R_e from the default setting of $R_e = 1$ to $R_e = 2$ (the full range of R_e is $R_e = 0 \rightarrow 16$). It must be stressed that IP1 had been developed to improve the aesthetic quality of the image, in particular the presented sharpness of microcalcifications. IP1 was included in the study following a subjective ranking study on a number of image processing options. Subjectively, the radiologist much preferred IP1 to the default setting.

IP2 was included in the study as previous work had indicated that this option offered the greatest contrast detectability. The IP2 selection ($R_n = 0$) provides signal enhancement over a wide band of spatial frequencies. The equivalent MTFs of the three CR image processing options (the default, IP1 and IP2) are reproduced in Fig. 5 (see also Blume, 1986).

Table I. Score sheet used with TOR[MAM]

TOR[MAM] SCORE SHEET

DATE: / / MARKERS NAME:
HOSPITAL/LOCATION:
DEPARTMENT:
X-RAY MACHINE:
FILM/SCREEN:
EXPOSURE: kV mAs FOCAL SPOT, GRID: Y/N
BACKGROUND DENSITY: B1 B2 PERSPEX cm
ADDITIONAL NOTES:

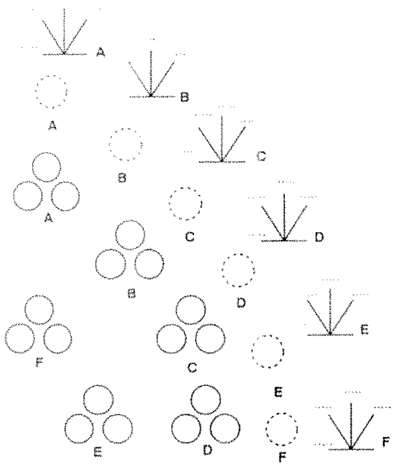

FILAMENTS TOTAL:
PARTICLES TOTAL:
CONTRASTS TOTAL:
GRAND TOTAL:

The four sets of test images, one standard film and three CR hard copy (default, IP1 and IP2) were evaluated by five observers. One observer was inexperienced in viewing test object images while another was a consultant radiologist with many years experience in reading mammograms; the other three observers were experienced in viewing test objects. The test images were presented in random order and viewed in four batches of 12 images, three from each of the four modes. At the outset of the study all observers underwent a training session using a representative batch of 12 images. Images were viewed in subdued background lighting and a ×2 magnifying lens was provided to improve visualization of the particles and fine filaments.

For each test film, individual test details were examined and given a detail visibility rating according to the following criteria:

Detail not visible	score 0
Barely visible/at threshold	score 1
Faintly visible	score 2
Clearly visible	score 3

A standard score sheet (see Table I) was used to record the results. The accumulated score for all details provided a measure of "overall" image quality.

Results and discussion

The results of the study are summarized in Table II, which presents the mean and standard errors of the accumulated scores from the 12 films in each category averaged over all five observers ($n = 60$). The equivalent mean and standard error for each of the types of details are also presented. Using TOR[MAM] we found that the default image processing produced a significantly lower score than screen–film mammography. This was reflected in inferior scores for all types of test detail. Although IP1 presented images in an aesthetically more acceptable way, no material improvement in detail visualization was discerned compared with the default setting. IP2, on the other hand, produced a significant improvement in overall contrast and detail visualization, such that the total score approached that of screen–film mamography. IP2 did not however, materially improve the visualization of the calcification particles, which remained inferior to conventional mammography. It should be noted that the number of groups of particles detected in the simulated breast structure (*i.e.* number of scores of unity or greater) was almost identical in screen–film mammography and CR. Specifically, on film an average of 41 clusters were correctly located, for the default setting the number of correct locations was 41, for IP1 42 and IP2 40. This result closely agrees with the findings of Oestmann et al (1989) who reported that the ROC detectability of groups of microcalcifications is identical in standard and computed mammography. Our TOR[MAM] study indicates that provided the image data are displayed in an optimum manner through the use of appropriate image processing, the image quality of CR mammography

Table II. Results of the study including mean scores plus standard errors ($n = 60$) accumulated for all observers and for each type of test detail

Feature	Film	Default CR	CR IP1	CR IP2
Fibres	41.67±1.20	39.02±0.99	39.74±1.00	40.76±0.97
Particles	12.36±0.16	11.11±0.15	11.23±0.17	11.25±0.16
Contrast	28.18±0.71	27.15±0.66	26.75±0.61	28.75±0.61
Total	82.28±1.56	77.16±1.26	77.68±1.57	81.93±1.17

Errors indicated are ±standard error (absolute).

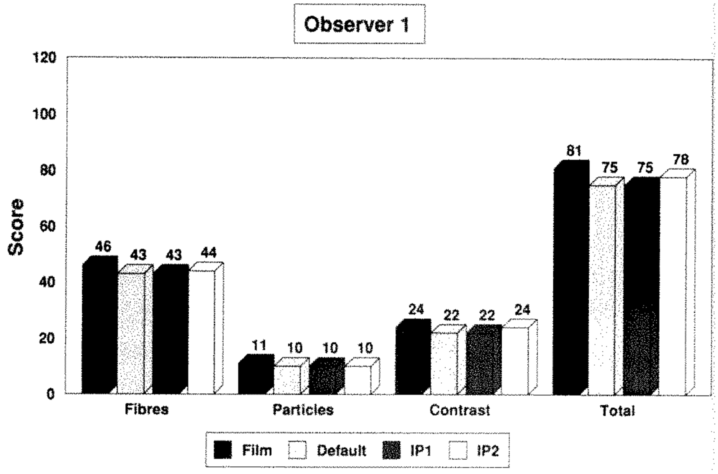

(a)

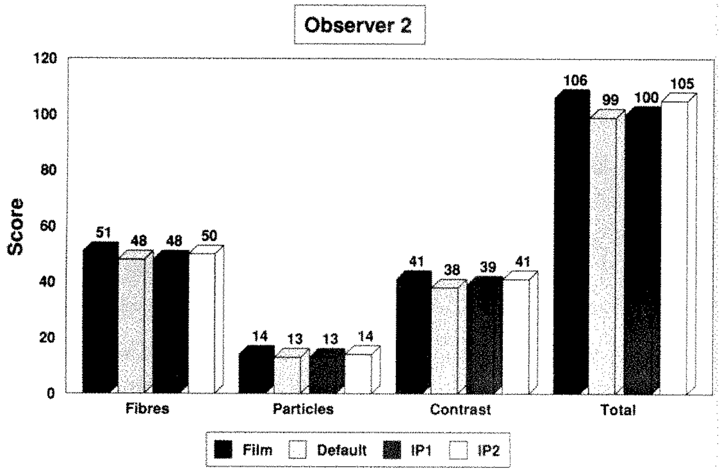

(b)

(Figure 6 continues overleaf)

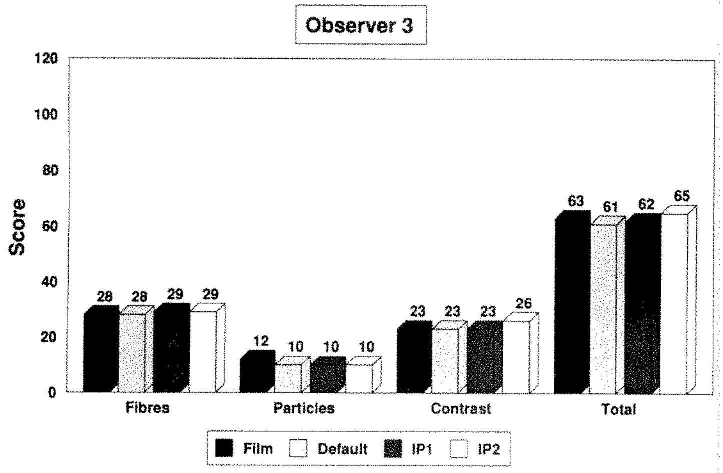

(c)

approaches that of a screen–film technique of equivalent radiographic speed.

All observers produced a pattern of response similar to that of the accumulated mean; this can be seen in the individual observers' scores (Fig. 6a–e). The mean response of each observer did, however, vary widely (for the film–screen presentation one observer scored a mean of 105.5 while another observer scored 63.58).

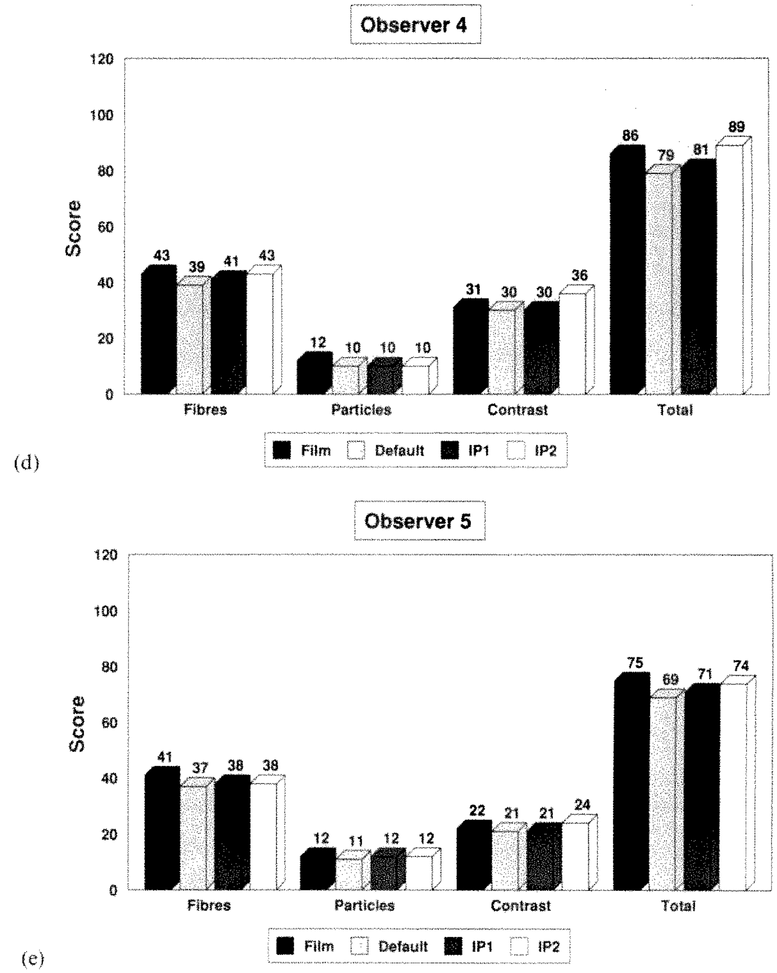

Figure 6. (a–e) Results for each of the observers.

Mechanisms to control this variation are being investigated by the authors. Clearly, if test objects such as TOR[MAM] are to be used to compare image quality measured by different observers, the results must be treated with great care. We also recommend that control films should always be included in any programme of image quality assessment using TOR[MAM]. A control film is one that has been viewed by each observer and is then introduced to each viewing session in order to allow the observer to recalibrate their scoring criteria. Despite the wide differences in subjective results between observers, the same overall pattern of response showed through with IP2 always producing the best score for CR.

Images of TOR[MAX] obtained in exactly the same way as for TOR[MAM] were also considered. The images were examined as recommended by Cowen et al (1988) with the results shown in Table III. It can be seen from these results that there is no difference between CR images with regard to the high-contrast bar patterns, with CR giving an estimated limiting resolution of 5

Table III. Results for TOR[MAX] films. All TOR[MAX] films were obtained in exactly the same way as the TOR[MAM] films

Feature	Film	Default CR	CR IP1	CR IP2
Mean background density (OD)	1.43	1.32	1.32	1.32
High density test point (OD)	1.98	1.77	1.77	1.98
Base + fog (OD)	0.24	0.28	0.28	0.24
Contrast index	0.70	0.53	0.52	0.76
Visual contrast	0.10	0.06	0.05	0.08
RHS grating (cycles/mm)	12.0	5.0	5.0	5.0
LHS grating (cycles/mm)	14.3	5.0	5.0	5.0
Low-contrast grating (cycles/mm)	3.0	2.6	2.6	2.6

All density measurements (OD) were measured on a MacBeth densitometer.

cycles/mm, against a limit of 12.0/14.3 cycles/mm for film. It was only possible to estimate the limiting resolution of the CR images using the Hüttner high-contrast resolution test pattern owing to aliasing artefacts. The low-contrast bar patterns produced a limiting resolution of 2.6 cycles/mm for all CR images against a limit of 3.0 cycles/mm for film. With regard to the optical density measurements, it is shown that although the background density for all CR images did not change, there was an overall increase in contrast for IP2. There was also a slight difference between default and IP1 images, but only IP2 approached the results for film. It is therefore concluded that the TOR[MAX] results presented correlate closely with the results obtained using TOR[MAM], indicating that TOR[MAM] is a valid clinical companion for the technical TOR[MAX].

This (albeit limited) study illustrates the important and subtle influence of digital image processing on detail visualization. Much more work is required to define rigorously the physical quality of PCR images and identify the digital image processing algorithms that optimize information transfer to the observer. Studies of these subjects represent fundamental elements of our current programme of investigation in computed mammography.

Acknowledgments

We are grateful to the UK Department of Health (MDD) and Philips Medical Systems (UK and USA) for their support of this study and Stewart McArdle for his excellent craftsmanship in constructing the TOR[MAM].

References

Blume, H., 1986. Digital processing of diagnostic images. *Medica Mundi*, *31*(3), 96–107.

Cowen, A. R. & Coleman, N. J., 1990. Design of test objects and phantoms for quality control in mammographic screening. In *Physics in Diagnostic Radiology*, IPSM Report No. 61 (Institute of Physical Sciences in Medicine, York), pp. 30–36.

Cowen, A. R., Coleman, N. J. & Workman, A., 1988. *Leeds Mammographic Test Objects–Instruction Manual.* FAXIL, The University of Leeds, Department of Medical Physics, Wellcome Wing, The General Infirmary, Leeds, LS1 3EX, UK.

Dance, D. R., 1990. Monte Carlo calculation of conversion factors for the estimation of mean glandular breast dose. *Physics in Medicine and Biology*, *35*(9), 1211–1219.

Department of Health, 1990. *Report on the Use of the Philips Mammo Diagnostic Mammography Unit for the Assessment of Women Referred from Breast Screening*, DH STD Report 90/23 (Department of Health, London).

IPSM, 1989. *Commissioning and Routine Testing of Mammographic X-ray Systems*, IPSM Report 59 (Institute of Physical Sciences in Medicine, York).

Kimme-Smith, C., 1989. A review of mammography test objects for the calibration of resolution, contrast and exposure. *Medical Physics*, *16*(5), 758–765.

Lane, E. J., Proto, A. V. & Philips, T. W., 1976. Mach bands and density preception. *Radiology*, *121*, 9–17.

Oestmann, J. W., Kopans, D., Hall, D. A., McCarthy, K. A., Rubens, J. R. & Greene, R., (1989). Equivalent diagnostic performance of digitised storage phosphors and conventional mammography in the detection of malignant microcalcifications. *Investigative Radiology*, 23, 725–728

Pritchard, J., 1989. *Guidelines on the Establishment of a QA System for the Radiological Aspects of Mammography Used for Breast Screening.* (Department of Health, London).

Tateno, Y., Iinuma, T. & Takano, M., 1987. *Computed Radiography.* (Springer-Verlag, Tokyo, Berlin, New York and London).

Technical notes

A manual afterloading technique for the treatment of patients with bronchial carcinoma using iridium-192 wire

By A. J. Vinall, MSc, MIPSM and P. J. Mulvey, MSc, FIPSM

Department of Medical Physics, University College Hospital, Gower St, London WC1E 6AU, UK

(Received 6 June 1991 and in revised form 4 October 1991, accepted 23 October 1991)

Keywords: Afterloading, Endobronchial

The difficulties of effective palliative treatment of patients with bronchial and oesophageal tumours have long been under consideration. For a brachytherapy technique the generally accepted way to treat such patients is using a remote afterloading machine such as the Mico-Selectron and some early results have already been reported (Burt et al, 1989). In the absence of funding for such a machine we have developed a technique for manually inserting a single iridium wire, mounted in a dual-catheter system, through a mini-tracheotomy tube. This treatment has been facilitated by the recent availability of high-specific-activity iridium wire (up to 370 MBq/cm).

Technique

A week prior to the planned insertion date, the patient is reviewed at bronchoscopy. Here a specially constructed catheter of alternate 1 cm lengths of radio-opaque wire and coloured plastic marker thread is passed down the bronchoscope in order to make an assessment of the length of the tumour, and hence the length of iridium wire required. If possible, this is assessed visually through the bronchoscope, but may be performed radiographically if necessary.

Prior to the insertion, a nylon catheter is sealed at one end (diameter ~ 1.6 mm) and cut to a suitable length ready for the insertion. Two inner catheters (diameter ~ 0.85 mm) are cut to 4 cm longer than the outer catheter and marked such that it is quite clear when the inner catheter is pushed fully into the outer. The outer catheter is visually marked to indicate where the iridium wire will eventually lie, and this can be viewed through the bronchoscope.

One of the inner tubes is loaded with 1 cm of coloured marker thread, followed by the predetermined length of iridium wire, and then more marker thread in the remaining length of the catheter. Both ends of the catheter are crimped with the non-active end being crimped so as to fall within the length of the outer catheter when inserted. The second inner catheter is then loaded in exactly the same configuration, but using non-active iridium-192 wire, to form a dummy source train for checking purposes.

A schematic diagram of the catheter system is shown in Fig. 1. The inner catheter containing the predetermined length of iridium wire and marker thread is contained within the outer catheter. The outer catheter is passed through a specially constructed screw collet, which is attached to the tapered end of the mini-tracheotomy tube. When the screw collet is tightened it grips and retains the outer catheter but allows the inner catheter to pass freely through it. Once the inner catheter has been inserted, it is cut off flush with the end of the outer catheter. An end-stop locking device is fixed over the ends of both catheters effectively sealing them and preventing any relative movement between the two.

At insertion the patient is given a general anaesthetic in the endoscopy suite and the mini-tracheotomy is performed. The advantage of insertion through the tracheotomy tube is that the iridium wire catheter does not pass through the oral or nasal passages, thus the patient is able to breathe, and to eat and drink normally during the treatment. Also, the catheters themselves can be made relatively short and with fewer bends, thus facilitating the insertion procedure.

The screw collet is attached to the end of the mini-tracheotomy tube and the outer catheter is threaded through it. It is guided into the correct lobe and to the correct position using the bronchoscope and the visual marker. When the correct position is reached the screw collet is tightened so that it grips the catheter and retains it in position. A visual check along the length of the catheter is made using the fibre-optic bronchoscope to ensure that there are no kinks and that the catheter is in the correct position.

The dummy inner catheter containing the non-active wire is inserted, and is known to be in the correct position when the end mark is level with the end of the outer catheter. Any problems encountered can be rectified at this stage without the hazards of the active wire. Once the dummy catheter has been successfully inserted with no problems it is then withdrawn, and the active catheter is immediately inserted in its place. When the inner catheter is fully in position, the end of the inner catheter is cut off flush with the end of the outer catheter. The end-lock is fixed over the ends of both catheters and tightened. The excess external tubing can then be taped to the patient's shoulder out of the way.

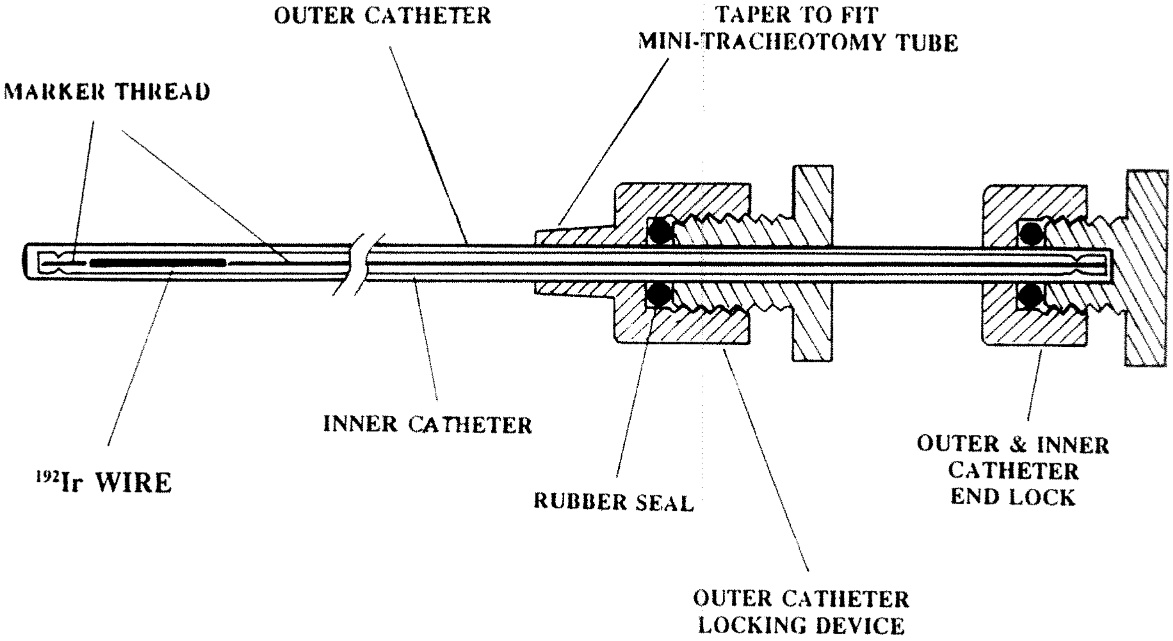
OUTER CATHETER
TAPER TO FIT MINI-TRACHEOTOMY TUBE
MARKER THREAD
INNER CATHETER
^{192}Ir WIRE
RUBBER SEAL
OUTER & INNER CATHETER END LOCK
OUTER CATHETER LOCKING DEVICE

Figure 1. Schematic diagram of the catheter system.

On recovery, the patient is returned to the ward and nursed subject to the usual precautions for radioactive insertions.

At removal of the wire, which is carried out on the ward, the end-lock is unscrewed, the end of the inner catheter containing the iridium is grasped using forceps and withdrawn. The wire is immediately placed in a portable lead safe. After suitable monitoring the outer catheter is removed and disposed of, followed by the mini-tracheotomy tube. The insertion wound is dressed and the patient is discharged. The wound closes of its own accord in a few days.

Discussion

To date, we have treated a total of 18 patients using this method. With one exception all patients have tolerated the treatment remarkably well. The exception was a young girl whose cough reflexes were such that the catheter had to be removed after several hours. Each patient has received a dose of 40 Gy specified at 1 cm radius from the centre of the iridium wire. Typical lengths of wire have been of the order of 4.5–8.0 cm to treat tumours 3.5–7.0 cm in length. This has led to treatment times of between 1.5 and 2 days using the highest activity wire available (370 MBq/cm or 10 mCi/cm) or 3.0–3.5 days using wire of activity 185 MBq/cm (5 mCi/cm) (supplied by Amersham International plc in 50 cm coils). In the early stages we were concerned that the patient would not tolerate the wire *in situ* for extended periods, and therefore our aim was to reduce the treatment times by using the highest-activity wire available. However, because the technique has proved so successful the necessity for the highest-activity wire is not so acute as was originally thought. There is probably an optimum activity of wire of ~ 240 MBq/cm (6.5 mCi/cm), which would give a treatment time of approximately 50–55 h but would ensure that extremity doses to staff were kept to a minimum.

Because of the high specific activity and the half-life of iridium (74 days), we have found it possible to treat several patients from one coil of wire, treating one new patient each week. This makes this form of treatment very cost effective. Indeed, the cost of equipment per patient has averaged out at about £90 combined with only a 3-night stay in hospital. This compares very favourably with repeated laser surgery.

The disadvantage of any manual loading brachytherapy technique is, of course, the doses received by staff involved in the procedure. We have carried out whole-body film-badge monitoring and extremity thermoluminescent dosemeter (TLD) monitoring for all personnel involved. The whole-body doses to all staff have been negligible; the average extremity doses are detailed in Table I. The average dose received by the clinician at insertion is 0.42 mSv. The average total dose received by the physicist at insertion and removal is 0.31 mSv, whilst the extremity finger doses during loading are, on average, 1.28 mSv per physicist per insertion. It is also our normal practice to involve at least two physicists so that doses can be spread between staff. The monthly pro rata extremity dose limit for a non-classified worker is 12.5 mSv and hence it is normally possible to keep doses to well below half of this limit even with a maximum workload of one patient per week.

Table I. Average TLD extremity doses

	Physicist	Clinician
Loading	1.28 mSv	—
Insertion and removal	0.31 mSv	0.42 mSv
Total	1.59 mSv	0.42 mSv

Conclusions

The major disadvantages to this treatment technique are two-fold. First, the patient has to undergo a general anaesthetic and two routine bronchoscopy procedures in the space of a week, with attendant risks, and, secondly, there is the radiation exposure to associated staff primarily at loading and insertion. With regard to the second part we are confident that doses received are well within acceptable limits as indicated above.

We therefore offer this technique as a low-cost method of palliative treatment for patients with bronchial or oesophageal lesions, where the purchase of expensive remote afterloading equipment is not immediately possible. The long-term clinical effectiveness of such treatments has yet to be established, particularly in relation to the Micro-Selectron; however, to date, there have been no adverse effects encountered and patients tolerate the treatment very well. The advantages of remote afterloading equipment have already been mentioned and this would normally be the preferred choice whenever possible.

Reference

Burt, P. A., Notley, H. M. & Stout, R., 1989. A simple technique for intraluminal irradiation in oesophageal tumours using the high-dose-rate Microselectron. *British Journal of Radiology*, *62*, 748–750.

Technique for steel coil embolization of biopsy track for use with the "Biopty" needle

By Peter Dawson, MRCP, FRCR, Andreas Adam, MRCP, FRCR and *Richard Edwards, MRCP, FRCR

Department of Diagnostic Radiology, Hammersmith Hospital, Du Cane Road, London W12 0HS and
*Department of Diagnostic Radiology, Western Infirmary, Glasgow G11 6NT, UK

(*Received 27 June 1991 and in revised form 2 October 1991, accepted 20 November 1991*)

Keywords: Coil embolization, Biopsy, "Biopty" needle

Percutaneous biopsy is quick, usually relatively easy to perform with a minimum of special equipment and, with its high diagnostic yield and low associated morbidity and mortality, is a key tool in the radiologist's armamentarium. Indeed, it is the single most frequently performed interventional procedure. A number of risks have been enumerated (Perrault et al, 1978; Westaby, 1980; Reichert et al, 1983; Whitmire et al, 1985; Lees, 1987), the most serious being severe bleeding, particularly, but not exclusively, in patients with a bleeding diathesis. The bleeding is thought to be related to needle size, and fine-needle aspiration cytology (FNAC), which, with improvements in cytology, is a reliable procedure (Lees et al, 1985), is thought to be safer than histological biopsy. However, there are frequently circumstances, such as diffuse organ disease, suspected unusual or benign neoplasms and lymphoma, where a core biopsy using a larger cutting needle is desirable in spite of some increased risk.

For liver biopsy, in particular, a number of alternative techniques to the percutaneous approach have been developed, the transjugular approach being the most favoured (Hanafee & Winer, 1967; Korshin et al, 1978; Bull et al, 1983; Colapinto, 1985). However, this is cumbersome and time consuming, requires high technical skill and, most importantly, frequently yields inadequate samples. It is not, in any case, without its own risks such as accidental carotid artery puncture, neck haematoma and intraperitoneal bleeding (Bull et al, 1983). The recent trend has consequently been towards improving the safety of the essentially straightforward and well established percutaneous biopsy technique by embolization of the biopsy track following the procedure with, variously, Gelfoam particles (Riley et al, 1984; Chuang & Alspaugh, 1988; Tobin & Gilmore, 1989), steel coils (Allison & Adam, 1988), fibrin sealant (Chisholm et al, 1989) or haemostatic protein-polymer sheath (Gazelle et al, 1990).

These have been developed for patients at high risk for bleeding, but, since there is no consensus on the criteria for the definition of high risk (*e.g.* platelet count, prothrombin time, etc.), it is difficult to assess from published series the efficacy of the different embolization materials. However, some practical points of importance clearly emerge.

1. Gelfoam and other particulate materials are not radio-opaque and are difficult to see fluoroscopically

during the procedure even when mixed with contrast medium. They are, therefore, difficult to position optimally in relation to the vessel responsible for the bleeding. In addition such materials may be flushed out of the biopsy track if bleeding is severe and, if injected forcefully, may pass into the portal venous system, which is undesirable in patients with hepatic function impairment, or into the hepatic venous system and, subsequently, the lungs.

2. Fibrin sealant (Chisholm et al, 1989) is not commercially available.

3. The haemostatic protein polymer sheath device described by Gazelle et al (1990) is of 8F gauge to fit over a 14-gauge "Trucut" needle, making an even larger and undesirable track than the original needle. It is not commercially available as yet.

4. The most practical and, in our experience, the most effective technique is that of steel coil embolization. However, as previously discussed (Allison & Adam, 1988), it too uses a larger flexible outer sheath of 8F over a 14-gauge "Trucut" style needle and therefore, in itself, increases the likelihood of bleeding.

Some of these shortcomings of established techniques are theoretical and they have nevertheless been remarkably successful in practice even in patients with a severe bleeding diathesis.

Crummy et al (1989) have suggested that embolization may be performed without an outer sheath and simply through the cannula of a cutting needle after the biopsy has been removed on the inner stylet. This is attractively simple and would avoid the problem of increasing the size of the biopsy track more than that of the needle but would involve leaving in place in the patient's liver a relatively rigid metallic cannula for the period of embolization during which time it would, naturally, be necessary for the patient to breathe.

The recently introduced "Biopty" system (Jennings et al, 1989) largely overcomes the problem of decreased reliability in the production of good specimens by smaller cutting needles by its rapid, controlled spring-powered delivery mechanism and it may be used reliably for core biopsy with smaller 18-gauge "Trucut" style needles. These are intrinsically safer than the 14-gauge needle and are, importantly, quite flexible. We describe here a simple technique for steel coil embolization for use with this system.

Technique

The "Biopty" gun–needle assembly kit is illustrated in Fig. 1. The simple use of this device has been described in detail elsewhere (Jennings et al, 1989). We prefer to use the version with a 1 cm rather than 2 cm movement as we consider this safer. The procedure is carried out in a fluoroscopy suite. Most patients with abnormal blood coagulation undergoing liver biopsy have diffuse liver disease and no localization is necessary. However, if a focal lesion is to be biopsied and the patient has disordered coagulation or if a lesion is suspected of being vascular on the basis of computed tomography, magnetic resonance imaging or angiographic appearances, an ultrasound-guided biopsy may be performed in the fluoroscopy suite, followed by embolization of the track.

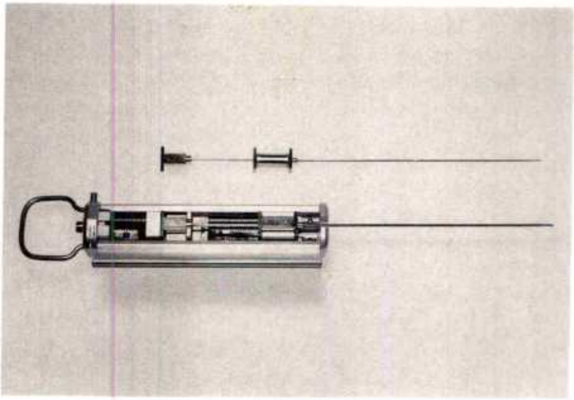

Figure 1. The "Biopty" gun assembly with 18-gauge "Tru-cut" style needle.

The biopsy is performed during suspended respiration and the gun assembly is then simply separated from the needle. The patient may then resume breathing as the needle is relatively flexible and is unlikely to cause laceration of the liver parenchyma. It is important in making the initial skin puncture not to position the needle immediately above or below a rib to avoid a "cheese wire" effect through the liver owing to splinting of the needle by adjacent bone. Following the biopsy procedure the sample is removed on the inner needle stylet leaving the outer cannula (18-gauge) in the liver. Contrast medium is then injected through the cannula. For this purpose a 16-gauge (white) needle neatly makes a leak-free connection between the contrast syringe and the "Biopty" cannula. In our experience, if bleeding follows a liver biopsy, the source of the blood is usually either a tributary of a hepatic vein or a portal venous radicle. Bleeding from a branch of the hepatic artery is rare, probably because of the resilience of arterial walls. The injection of contrast medium through the cannula will demonstrate the precise point of communication between the track and the vessel responsible for the bleeding.

The cannula is then withdrawn slightly and a modified version (William Cook Delivery Stylet DPES/18/16 carrying a 38-4-3 coil) of the 20-gauge embolization stylet described in a previous communication (Allison & Adam, 1988) is used to deposit a coil in the track immediately adjacent to the bleeding vessel. The embolization needle assembly is 1 cm longer than the previously commercially produced device (William Cook) because the needle employed with the Biopty gun is longer than the one included in the biopsy and embolization set we have described previously (Allison & Adam, 1988). When the new embolization needle is fully inserted in the Biopty cannula and the central wire removed, the coil is released precisely at the needle tip,

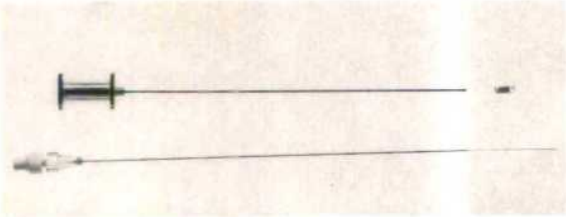

Figure 2. The 18-gauge "Biopty" cannula shown with the coil delivery stylet. Note that these are the same length so that the coil may be released reliably at the very tip of the cannula.

which can be seen clearly on fluoroscopy (Fig. 2). The cannula is then withdrawn in small steps and further injections of contrast medium are made to demonstrate any other vessels traversed by the needle. If such vessels are found, more coils are deposited until the bleeding stops (Fig. 3). In most cases, haemostasis results 2–3 min following completion of the embolization.

We cannot claim, any more than can the proponents of other techniques of plugged biopsy, that our enthusiasm is supported by comparative trials against alternatives or by carefully controlled assessment of relative bleeding diathesis in different patients. However, the technique described has theoretical advantages over others, is very simple and easy to learn and is now in routine use in our department for patients with bleeding diathesis.

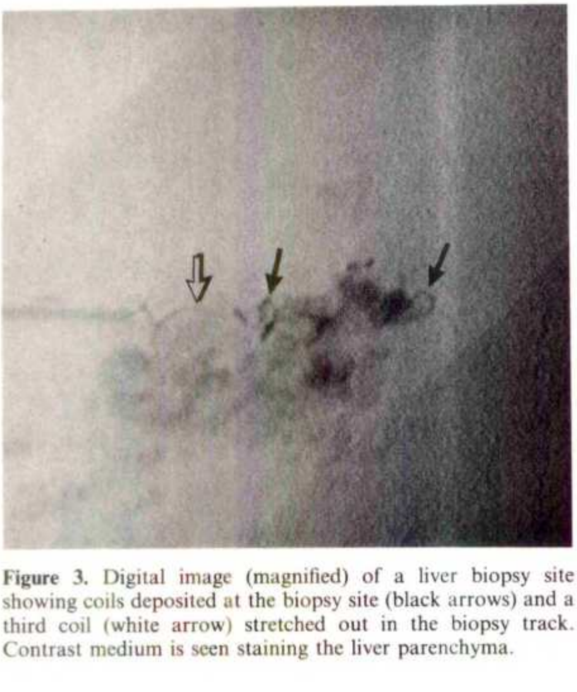

Figure 3. Digital image (magnified) of a liver biopsy site showing coils deposited at the biopsy site (black arrows) and a third coil (white arrow) stretched out in the biopsy track. Contrast medium is seen staining the liver parenchyma.

References

Allison, D. J. & Adam, A., 1988. Percutaneous liver biopsy and track embolisation with steel coils. *Radiology, 169*, 261–263.

Bull, H. J., Gilmore, I. T., Bradley, R. D., Marigold, J. G. & Thompson, R. P., 1983. The transjugular route as an alternative to direct percutaneous needle biopsy of the liver. *American Journal of Gastroenterology, 70*, 653–656.

Chisholm, R. A., Jones, S. N. & Lees, W. R., 1989. Fibrin sealant as a plug for the post-liver biopsy needle track. *Clinical Radiology, 40*, 627–628.

Chuang, V. P. & Alspaugh, J. P., 1988. Sheath needle for liver biopsy in high-risk patients. *Radiology, 166*, 261–262.

Colapinto, R. F., 1985. Transjugular biopsy of the liver. *Clinical Gastroenterology, 14*, 451–467.

Crummy, A. B., McDermott, J. C. & Wojtowycz, M., 1989. A technique for embolisation of biopsy tracts. *American Journal of Roentgenology, 153*, 67–68.

Gazelle, G. S., Haaga, J. R. & Neuhanser, D., 1990. Hemostatic protein–polymer sheath: new method to enhance hemostasis at percutaneous biopsy. *Radiology, 175*, 671–674.

Hanafee, W. & Winer, M., 1967. Transjugular percutaneous cholangiography. *Radiology, 88*, 35–39.

Jennings, P. E., Donald, J. J., Coral, A., Rode, J. & Lees, W. R., 1989. Ultrasound-guided core biopsy. *Lancet, i*, 1369–1371.

Korshin, P. V., Klauber, P. V., Christensen, V. & Scorsted, P., 1978. Percutaneous catheterization of the internal jugular vein. *Acta Annaesthesiologica Scandinavica, 67*, 27–33.

Lees, W. R., 1987. Transcutaneous biopsy and drainage procedures. In *Complications in Diagnostic Imaging*, ed. by G. Ansell and R. A. Wilkins (Blackwell Scientific Publications, Oxford), pp. 247–255.

Lees, W. R., Hall-Craggs, M. A. & Manhire, A., 1985. Five years' experience of fine-needle aspiration biopsy: 454 consecutive cases. *Clinical Radiology, 36*, 517–520.

Perrault, J., McGill, D. B., Ott, B. J. & Taylor, W. F., 1978. Liver biopsy: complications in 1,000 inpatients and outpatients. *Gastoenterology*, **74,** 103–106.

Reichert, C. M., Weisenthal, L. M. & Klein, H. G., 1983. Delayed hemorrhage after percutaneous liver biopsy. *Journal of Clinical Gastroenterology, 5*, 263–266.

Riley, S. A., Irving, H. C., Axon, A. T. R., Ellis, W. R., Lintott, D. J. & Losowsky, M. S., 1984. Percutaneous needle biopsy with plugging of needle track: a safe method for use in patients with impaired coagulation. *Lancet, ii*, 436.

Tobin, M. V. & Gilmore, I. T., 1989. Plugged liver biopsy in patients with impaired coagulation. *Digestive Diseases and Sciences, 34*, 13–15.

Westaby, D., MacDougall, B. R. D. & Williams, R., 1980. Liver biopsy as a day-case procedure: selection and complications in 200 consecutive patients. *British Medical Journal, 281*, 1331–1332.

Whitmire, L. F., Galambos, J. T., Philips, V. M., Sewell, C. W., Erwin, B. C., Torres, W. E., Gedgandas-McClees, R. K., Bernardino, M. E., 1985. Imaging guided percutaneous hepatic biopsy: diagnostic accuracy and safety. *Journal of Clinical Gastroenterology, 7*, 511–515.

1992, *The British Journal of Radiology*, *65*, 541–542

Case reports

Splenic cyst: demonstration of the relationship between subcapsular haematoma and false cyst by imaging

By Olivier Dourthe, *Pierre Maquin, †Bernard Pradere and *Jean-Jacques Railhac

CREIM, Villantipolis 8, 06560 Sophia-Antipolis, France, *Radiologie Centrale and †Chirurgie Générale, CHU Purpan, Place A. Baylac, 31059 Toulouse cedex, France

(*Received 13 May 1991 and in revised form 6 August 1991, accepted 20 September 1991*)

Keywords: False cyst of the spleen, Post-traumatic haematoma, Computed tomography, Ultrasound

Splenic cysts form a heterogeneous group, classified in 1953 by Fowler. Excluding cystic neoplasms and parasitic cysts, splenic cysts can be classified as "true" cysts lined by an epithelium, and "false" cysts without epithelial lining. It has been postulated that the latter are post-traumatic (Dachmann et al, 1986). In the described case, we record the evolution on ultrasound (US) and computed tomography (CT) of a post-traumatic subcapsular haematoma of the spleen that resulted in cyst formation.

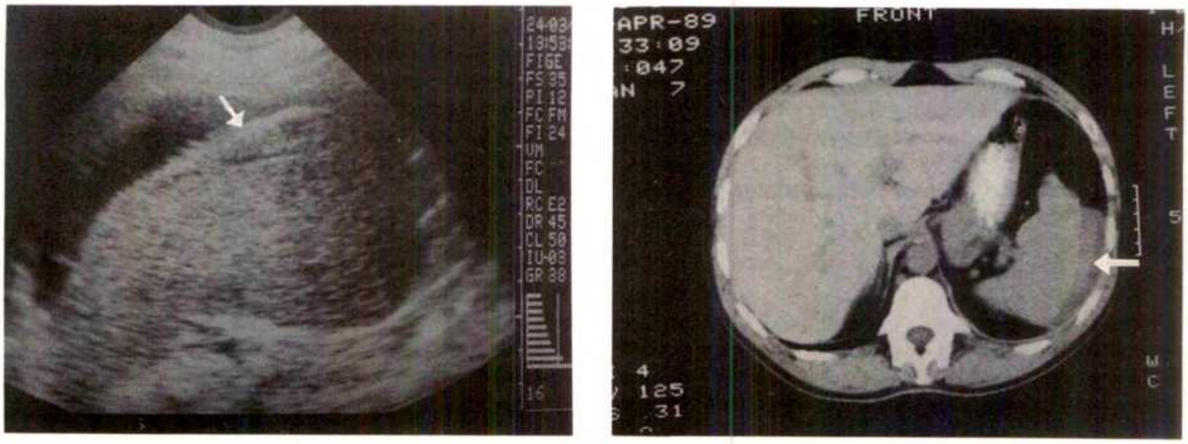

(a) (b)

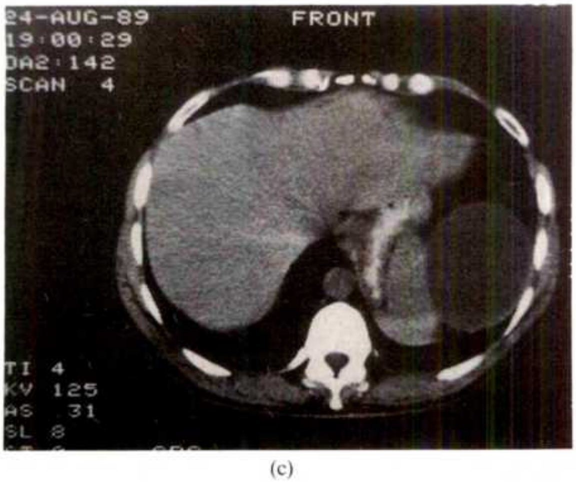

(c)

Figure 1. (a) US scan on admission showing a subcapsular collection with internal echogenic (arrow) and peripheral anechoic components. (b) Unenhanced abdominal CT scan 7 days later at the centre of the collection of increased density (arrow). (c) Enhanced abdominal CT scan 5 months after admission: cystic aspect.

Case report

A 39-year-old man was seen in the emergency department with acute left lower thoracic pain. There was a history of intermittent trauma. Physical examination revealed no obvious abnormality. US examination on admission (Fig. 1a) showed a subcapsular splenic collection with internal echogenic and peripheral anechoic components. CT (Fig. 1b), performed a week later, confirmed the diagnosis of subcapsular haematoma and showed its complex structure of an internal dense area (30 Hounsfield units (HU)) and a low-density, probably liquefied, peripheral zone (15 HU). A US scan performed 1 month after admission again revealed a heterogeneous collection with an alteration in morphology showing a decrease of the echogenicity of the internal part and an increase in volume of the liquefied peripheral component.

A CT scan (Fig. 1c), performed 5 months after admission, showed a typical, 7 cm, non-enhancing round lesion of liquid density (17 HU) consistent with a subcapsular cyst. This appearance is typical of a "false" cyst of the spleen (Dachmann et al, 1986).

Discussion

Splenic haematomas would be the main cause of false cyst. The relationship resolving haematoma into splenic cysts was shown in surgical specimens (Economides et al, 1980) and on US and CT (Dachmann et al, 1986). Our case illustrates the transformation of a subcapsular collection to a cyst in 5 months.

A history of trauma is found in one-quarter to one-half of cases of "false" cyst (Garvin & King, 1981), but the trauma is often in the distant past and not recalled. More than 50% of false cysts are diagnosed in the 3 years following trauma, and this corresponds with the delay seen in our case.

Diagnosis of splenic cysts is mainly based on US and CT. Once a splenic mass is shown as a large cystic lesion with a relatively thin wall, and if echinococcus is excluded, a false cyst or true cyst is the likely diagnosis (Dachmann & Magid, 1987).

The evolution of the false cyst as illustrated by this case includes slow growth (Ross et al, 1977). Rupture, infection and rapid increase in size (Dibble & Weigent, 1965) may lead to acute presentation. The usual treatment is surgical excision of the symptomatic cyst. Percutaneous puncture, laparoscopic cyst puncture and creation of a cyst–peritoneal window have been successfully performed.

US demonstration of a splenic cyst at the time of acute abdominal pain may pose a diagnostic dilemma. The major role of imaging following diagnosis is to document the morphological evolution of splenic cysts and haematomas as a complement to clinical evaluation in the determination of the need and timing of surgical and percutaneous drainage procedures.

References

DACHMANN, A. H. & MAGID, D., 1987. Splenic focal disease. In *Radiology of the Liver, Biliary Tract, Pancreas and Spleen*, ed. by A. C. Friedman (Williams and Wilkins, Baltimore), pp. 947–984.

DACHMANN, A. H., ROS, P. R., MURARI, P. J., OLMSTEDT, W. W. & LICHTENTSTEIN, J. E., 1986. Nonparasitic splenic cysts: report of 52 cases with radiologic-pathologic correlation. *American Journal of Roentgenology*, *147*, 537–542.

DIBBLE, J. B. & WEIGENT, C. E., 1965. Epidermoid cyst of the spleen presenting as an abdominal emergency. *Journal of the American Medical Association*, *194*, 1144–1146.

ECONOMIDES, N. G., BENTON, B. F., FORTNER, T. M. & MILES, R. M., 1980. Splenic pseudocysts: report of two cases and review of the literature. *American Surgeon*, *46*, 644–648.

FOWLER, R. H., 1953. Collective review: nonparasitic benign cystic tumors of the spleen. *International Abstracts of Surgery*, *96*, 209–227.

GARVIN, D. F. & KING, F. M., 1981. Cysts and non-lymphomatous tumours of the spleen. *Pathology Annual*, *16*, 61–80.

ROSS, M. E., ELLWOOD, R., YANG, S. S. & LUCAS, R. J., 1977. Epidermoid splenic cysts. *Archives of Surgery*, *112*, 596–599.

Juxtaglomerular cell tumour of the kidney as cause of hypertension: a case report

By Jos C. van den Berg, MD, *Ad R. M. M. Hermus, MD and Gerd R. Rosenbusch, MD

Departments of Radiodiagnosis and *Internal Medicine (Division of Endocrinology), St Radboud Hospital, University of Nijmegen, Geert Grooteplein Zuid 18, 6525 GA Nijmegen, The Netherlands

(Received 3 June 1991 and in final form 28 November 1991, accepted 14 January 1992)

Keywords: Hypertension, Kidney neoplasms, Renin, Reninoma

Benign renin-secreting juxtaglomerular cell tumours of the kidney (reninomas) are recognized but rare causes of hypertension.

Although 46 well documented cases have been described since the first report by Robertson et al (1967) there has been little emphasis on the radiological aspects of this clinical entity (Conn et al, 1973; Davidson & Clark 1974; Dunnick et al, 1983). The radiodiagnostic criteria and diagnostic investigations will be dealt with in this case report.

Address reprint requests to Dr J. C. van den Berg.

Case report

A 33-year-old woman was referred to our hospital because of hypertension (230/130 mmHg) uncontrollable by β-blocking agents. There were no complaints of increased thirst, polyuria or muscular weakness. On physical examination, no abnormalities except for the hypertension were found. The chest radiograph together with an intravenous urogram were normal.

Laboratory examination of the blood showed a lowered serum potassium level, a normal creatinine clearance and no indications of phaeochromocytoma. Plasma-renin activity (PRA) was elevated and there was a markedly increased aldosterone secretion rate. A secondary form of aldosteronism was suspected.

Abdominal aortography showed no stenoses of the renal arteries and a barely visible radiolucent area in the lower pole of the right kidney. A subsequent selective study of the renal arteries revealed a hypovascular, smoothly delineated lucent area in the lower pole of the right kidney with a diameter of approximately 3 cm. No calyceal deformity was seen in the excretion phase (Fig. 1).

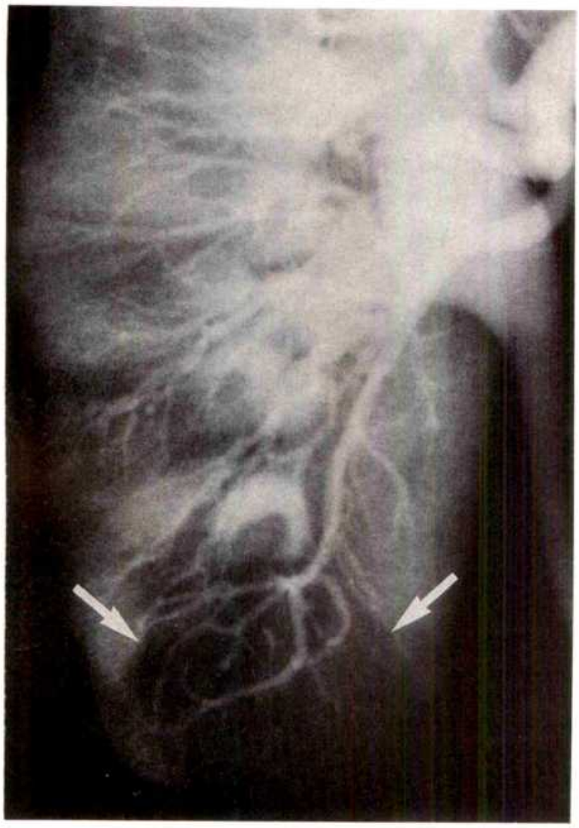

Figure 1. Selective right renal arteriography shows sparse vascular structures in the lower pole with a sharply defined radiolucent area (arrows); note the absence of calyceal deformity.

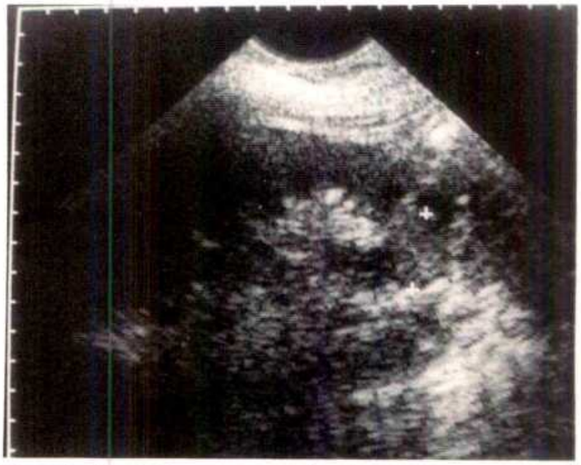

Figure 2. Renal ultrasound scan showing a homogeneous, well delineated echogenic lesion in the right lower pole.

On ultrasound examination this lesion was echogenic (Fig. 2). Computed tomography (CT) was performed and showed an isodense structure in the lower pole of the right kidney, which appeared to be hypodense as compared with the normal parenchyma after intravenous administration of contrast medium (Fig. 3).

Selective renin sampling of the renal veins showed a markedly elevated plasma renin activity on the right side, with a ratio of 24.6 to 16.7 ng/ml/h (for comparison: PRA in the lower inferior caval vein was 11.2 ng/ml/h). Renal radionuclide scanning was not performed.

All these findings suggested a renin-secreting tumour in the lower pole of the right kidney and a right lower pole resection was performed, revealing a well encapsulated tumour with a diameter of 2 cm. Histologically it was composed of neoplastic juxtaglomerular cells. Histological and immunocytochemical aspects of this tumour, which are described extensively elsewhere (Hermus et al, 1986), were typical of a benign juxtaglomerular cell tumour.

Immediately after extirpation of the tumour, blood pressure fell dramatically to 120/80 mmHg. In the subsequent period the blood pressure stabilized in a range of 130/90 to 160/100 mmHg (this high value is most probably due to essential hypertension) with normal values of PRA.

Discussion

A renin-producing tumour is characterized clinically by a syndrome of (severe) hypertension, hypokalaemia and hyperaldosteronism. Patients may have complaints of headache, polyuria and/or polydipsia or muscle weakness (Robertson et al, 1967; Lam et al, 1982). Patients are usually young, with an age range of 6 to 53 years (mean age 21.5 years) (Corvol et al, 1988). PRA is always elevated (Hirose et al, 1974). These tumours are solitary and are almost always solid on macroscopic examination (only one partly cystic, partly solid tumour has been described; Hanna et al, 1979), with a diameter ranging from 0.2 to 0.8 cm (mean diameter 2.3 cm) (Lam et al, 1982). Juxtaglomerular cell tumours are always located just below the renal capsule and are equally distributed throughout upper and lower pole. Histologically most of the renin-producing tumours originating from the juxtaglomerular apparatus of the kidneys are benign and of the haemangiopericytoma or

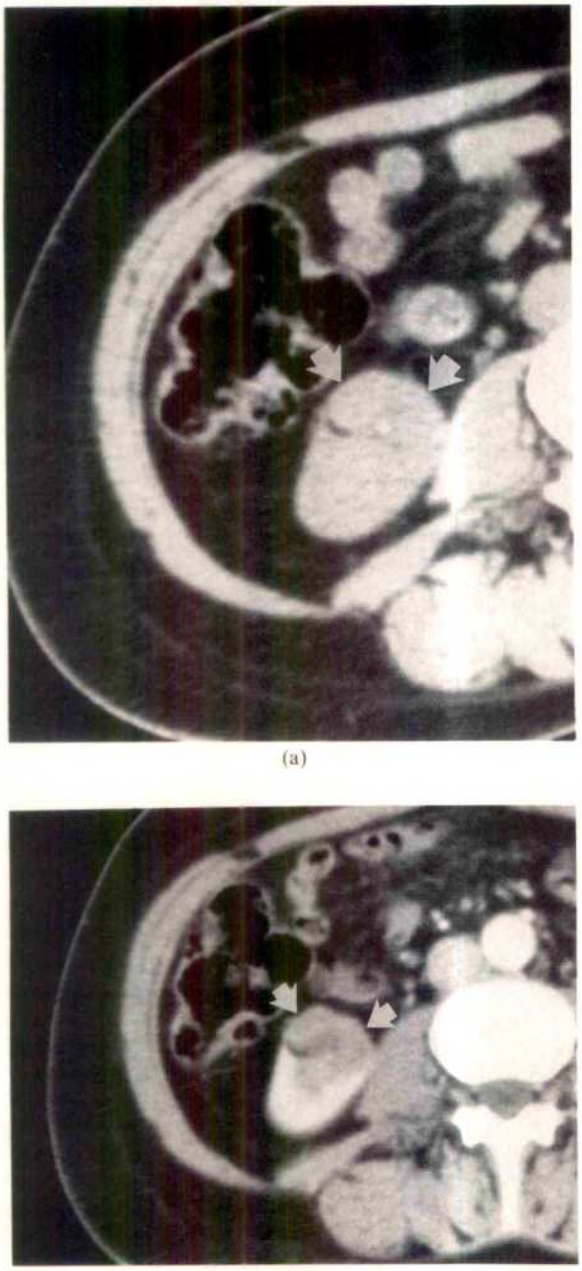

(a)

(b)

Figure 3. CT scan: the tumour (arrows) appears to be isodense on the native scan (a) and non-enhancing after intravenous administration of contrast medium (b).

hamartoma type (Hirose et al, 1974; Dunnick et al, 1983). Malignant renin-producing tumours of renal origin, such as Wilms tumour, renal cell carcinoma and mesoblastic nephroma (Dunnick et al, 1983; Malone et al, 1989), as well as extrarenal primary tumours (*e.g.* lung, pancreas and ovary) (Anderson et al, 1989) causing hypertension have also been described, but these are even more rare.

Intravenous urography may show stretching or displacement of calices or the mere presence of a mass, (Takahashi et al, 1976; Dunnick et al, 1983; Pedrinelli et al, 1987; Remynse et al, 1989) but in most cases no abnormalities are seen (Robertson et al, 1967; Davidson & Clark, 1974; Lam et al, 1982). With only one cystic (Moss et al, 1982) and only one partly cystic/partly solid mass (Lee, 1971) having been reported in 10 cases, the findings at ultrasound most commonly suggest a solid mass (Dunnick et al, 1983; Pedrinelli et al, 1987). Most of these masses are echogenic, although hypoechoic and isoechoic masses (sometimes surrounded by a hyperechoic rim corresponding to a pseudocapsule) are known (Dunnick et al, 1983).

CT scanning may reveal an isodense or hypodense solid tumour (Dunnick et al, 1983; Corvol et al, 1988), which may be surrounded by a small rim of haemorrhage or may show increased density centrally resulting from haemorrhage (Moss et al, 1982; Dunnick et al, 1983). After intravenous administration of contrast medium, the tumour may be non-enhancing owing to hypovascularity (Lee, 1971) or only slightly enhancing (Dunnick et al, 1983; Remynse et al, 1989).

Although aortography may be inconclusive or even normal, it is usually able to show a hypovascular mass (Hanna et al, 1979; Lam et al, 1982; Moss et al, 1982; Pedrinelli et al, 1987; Corvol et al, 1988). Despite the presence of well developed vascular spaces microscopically the angiographic features consist of tortuous and sparse, poorly defined vasculature (Conn et al, 1973; Davidson & Clark, 1974; Dunnick et al, 1983; Remynse et al, 1989) with or without abnormal calibre, course or displacement (Takahashi et al, 1976). Cases with an arteriovenous shunt are unknown, but early staining of the renal vein has been described (Takahashi et al, 1976). The renal parenchyma usually shows an area of translucency, sometimes surrounded by a zone of increased density caused by a rim of compressed renal parenchyma (Davidson & Clark, 1974; Takahashi et al, 1976). Selective renin sampling of the renal veins shows lateralization with elevated renin levels on the affected side (Conn et al, 1973; Davidson & Clark, 1974; Pedrinelli et al, 1987). A ratio of more than 1.5 to 1 is considered to be significant and in this way even very small tumours (down to 0.2 cm) can be detected (Hirose et al, 1974).

A renal radionuclide scan is usually normal (Hirose et al, 1974; Lam et al, 1982), but a focus of diminished activity may be seen (Takahashi et al, 1976).

In establishing the diagnosis of a renin-producing tumour of the kidney, ultrasound and CT together with selective renin sampling of the renal veins is essential. Aortography performed because of suspicion of renal artery stenosis should always look for a mass as described in this case report. Whenever a mass is suspected, selective renal arteriography should be performed in order to confirm and delineate the lesion. Intravenous urography and renal radionuclide scanning have a low sensitivity for the detection of small renal masses such as renin-producing tumours but are usually helpful in excluding other pathological processes.

Acknowledgments

The authors would like to thank Miss Mariska Ebbelink and Miss Tineke van IJzendoorn for their secretarial assistance in the preparation of this manuscript.

References

Anderson, P. W., Macaulay, L., Do, Y. S. Sherrod, A., d'Ablaing, G., Koss, M., Shinagawa, T., Tran, B., Montz, F. J. & Hsueh, W. A., 1989. Extrarenal renin-secreting tumors: insights into hypertension and ovarian renin production. *Medicine*, *68*, 257–268.

Conn, J. W., Bookstein, J. J. & Cohen, E. L., 1973. Renin-secreting juxtaglomerular cell adenoma. *Radiology*, *106*, 543–544.

Corvol, P., Pinet, F., Galen, F. X., Plouin, P. F., Chattelier, G., Pagny, J. Y., Corvol, M. T. & Ménard, J., 1988. Seven lessons from seven renin-secreting tumours. *Kidney International*, *34* (Suppl. 25), 3–44.

Davidson, J. K. & Clark, D. C., 1974. Renin-secreting juxtaglomerular-cell tumour. *British Journal of Radiology*, *47*, 594–597.

Dunnick, N. R., Hartman, D. S., Ford, K. K., Davis, C. J. & Amis, E. S., 1983. The radiology of juxtaglomerular tumors. *Radiology*, *147*, 321–326.

Hanna, W., Tepperman, B., Logan, A. G., Robinette, M. A., Colapinto, R. & Phillips, M. J., 1979. Juxtaglomerular cell tumour (reninoma) with paroxysmal hypertension. *Canadian Medical Association Journal*, *120*, 957–959.

Hermus, A. R. M. M., Pieters, G. F. F. M., Lamers, A. P. M., Smals, A. G. H., Hanselaar, A. G., Van Haelst, U. J. & Kloppenborg, P. W., 1986. Hypertension and hypokalaemia due to a renin-secreting kidney tumour. *Netherlands Journal of Medicine*, *29*, 84–91.

Hirose, M., Arakawa, K., Kikuchi, M., Kawasaki, T., Omoto, T., Kato, H. & Nagayama, T., 1974. Primary reninism with renal hamartomatous alteration. *Journal of the American Medical Association*, *230*, 1288–1292.

Lam, A. S. C., Bédard, Y. C., Buckspan, M. B., Logan, A. G. & Steinhardt, M. I., 1982. Surgically curable hypertension associated with reninoma. *Journal of Urology*, *128*, 572–575.

Lee, M. R., 1971. Renin-secreting kidney tumors. *Lancet*, *2*, 254–255.

Malone, P. S., Duffy, P. G., Ransley, P. G., Risdon, R. A., Cook, T. & Taylor, M., 1989. Congenital mesoblastic nephroma, renin production, and hypertension. *Journal of Pediatric Surgey*, *24*, 599–600.

Moss, A. H., Peterson, L. J., Scott, C. W., Winter, K., Olin, D. B. & Garber, R. L., 1982. Delayed diagnosis of juxtaglomerular cell tumour hypertension. *North Carolina Medical Journal*, *34*, 705–707.

Pedrinelli, R., Graziadei, L., Taddei, S., Lenzi, M., Magagna, A., Bevilacqua, G. & Salvetti, A., 1987. A renin-secreting tumor. *Nephron*, *46*, 380–385.

Remynse, L. C., Begun, F. P., Jacobs, S. C. & Lawson, R. K., 1989. Juxtaglomerular cell tumor with elevation of serum erythropoietin. *Journal of Urology*, *142*, 1560–1562.

Robertson, P. W., Klidjian, A., Harding, L. K. & Waters, G., 1967. Hypertension due to a renin-secreting renal tumour. *American Journal of Medicine*, *43*, 963–976.

Takahashi, T., Miura, T., Sue, A., Sáito, K., Sakane, M., Yamagata, Y., Fukuchi, S., Sato, Z., Hirai, T., Terashima, K., Oka, K. & Imai, Y., 1976. A case of juxtaglomerular cell tumor diagnosed preoperatively. *Nephron*, *17*, 483–495.

Contrast extravasation from a Pulse-Tec graft: a complication of high-dose recombinant tissue-type plasminogen activator therapy

By T. M. Buckenham, FRACR, *R. S. Taylor, MS, FRCS, D. Reiff, MRCP and J. E. Page, MRCP, FRCR

Departments of Radiology and *Surgery, St George's Hospital, Blackshaw Road, London SW17 0QT, UK

(Received 1 August 1991 and in revised form 17 October 1991, accepted 20 November 1991)

Keywords: Thrombolysis, Extravasation, Recombinant tissue plasminogen activator (rt-PA), Pulse-Tec

Transmural contrast extravasation through both knitted Dacron and Gore-Tex grafts is well documented. Reports have appeared associating this complication with the use of both streptokinase and urokinase (Rabe et al, 1982; Becker et al, 1984; Rosner & Doris, 1984; Perler et al, 1986). We report a case of extravasation through a Pulse-Tec (Newtec Vascular Products Ltd, UK) graft in association with the use of high-dose recombinant tissue plasminogen activator (rt-PA) therapy. This complication has not previously been reported in this type of graft or with this particular thrombolytic agent.

Case report

A 75-year-old woman with a long history of peripheral vascular disease presented with an ischaemic ulcerated fore-foot. Ankle–brachial indices were 0.4 on the left and 0.6 on the right, which was asymptomatic. A diagnostic arteriogram

---

Address correspondence to Dr T Buckenham, Department of Radiology, St George's Hospital, Blackshaw Road, London SW17 0QT, UK.

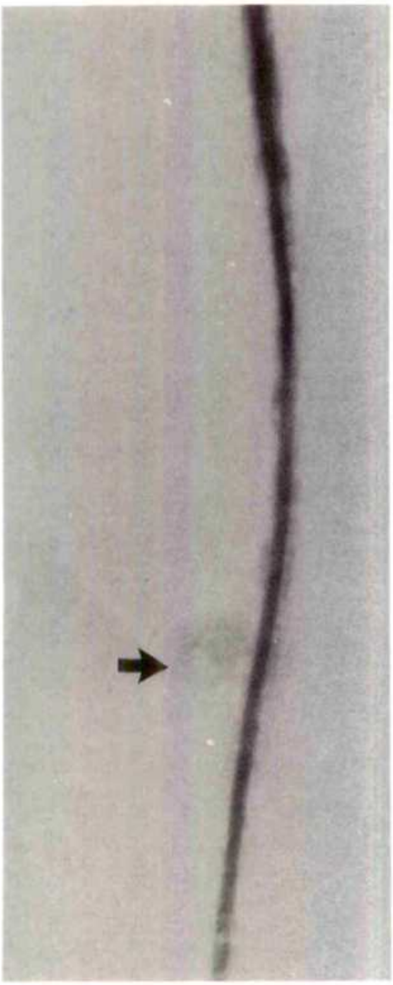

Figure 1. Digital subtraction angiogram showing initial focal contrast extravasation (arrow).

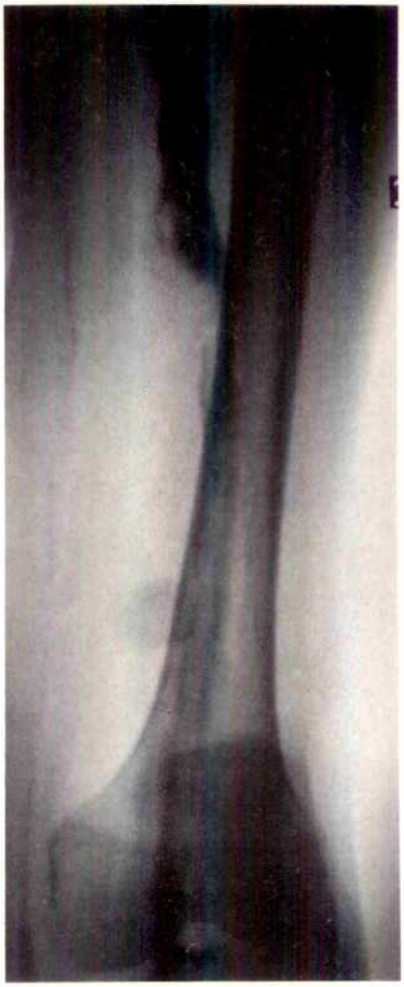

Figure 2. Digital subtraction angiogram demonstrating diffuse contrast extravasation along the length of the graft.

showed a segmental 7 cm superficial femoral artery occlusion with a good popliteal artery and posterior tibial and peroneal arteries patent to the ankle. Percutaneous transluminal angioplasty was attempted but the occlusion could not be traversed and she went on to surgical reconstruction with a Pulse-Tec femoro-popliteal bypass graft. The graft was subcutaneous in position and extended from the common femoral to the below-knee popliteal artery. Peroperative angiography showed good flow and no abnormality. 11 days post-operatively her leg became ischaemic and an intravenous digital subtraction arteriogram showed the graft to be occluded. Thrombolytic treatment with rt-PA was then attempted. The graft was accessed via the right femoral artery using a 5F Simmons catheter, with the tip positioned in the proximal graft. High-dose pulsed intrathrombic rt-PA was given as three 5 mg boluses at 10 min intervals. The catheter was advanced after each bolus to ensure the tip lay within the thrombus. Intercurrent angiography initially showed focal contrast extravasation (Fig. 1), and after the third bolus injection extramural contrast could be seen along the entire length of the graft (Fig. 2). The procedure was abandoned at this point. The patient remained haemodynamically stable and no clinical abnormality was apparent. Her recovery was uneventful and she underwent a successful revision of the graft, which has remained patent.

Discussion

The Pulse-Tec graft is a relatively new vascular prosthesis constructed from a biocompatible polyurethane, polytetrafluoroethylene. This material does not depend on pre-clotting to ensure the absence of leaks, although on insertion the prosthesis may sweat a little blood (less than 35 ml). Unlike the extravasation seen with the Gore-Tex graft, where it is limited to a localized area and may be due to surgical manipulation (Becker et al, 1984; Rosner & Doris, 1984), in our case extravasation was from the entire length of the graft, similar to that seen in the knitted Dacron grafts (Rabe et al, 1982; Perler et al, 1986).

The explanation for this may be related to the porous nature of the polyurethane material used in the construction of the graft. These pores may pass indirectly from the luminal aspect to the exterior, but in the normal situation may be occluded by thrombus. With the application of a thrombolytic agent such as rt-PA, the blood in the pores may well be thrombolysed permitting extravasation. We are unsure of the clinical significance of this phenomenon and we do not know if it would occur in a well established graft, but recommend caution in the use of thrombolytic agents in the Pulse-Tec graft.

References

Becker, G. J., Holden, R. W., & Rabe, F. E., 1984. Contrast extravasation from a Gore-Tex graft: a complication of thrombolytic therapy. *American Journal of Roentgenology*, *142*, 573–574.

Perler, B. A., Kinnison, M. & Halden, W. J., 1986. Trans-graft haemorrhage: a serious complication of low-dose thrombolytic therapy. *Journal of Vascular Surgery*, *3*, 936–938.

Rabe, F. E., Becker, G. J., Richmond, B. D., Yune, H. Y., Holden, R. W., Dilley, R. S. & Klatte, E. C., 1982. Contrast extravasation through Dacron grafts: a sequela of low-dose streptokinase therapy. *American Journal of Roentgenology*, *138*, 917–920.

Rosner, N. H. & Doris, P. E., 1984. Contrast extravasation through a Gore-Tex graft: a complication of low dose streptokinase therapy. *American Journal of Roentgenology*, *143*, 633–634.

Pancreatic metastasis from renal cell carcinoma

By F. Rypens, MD, D. Van Gansbeke, MD, *J. P. Lambilliotte, MD, †G. Van Regemorter, MD, ‡A. Verhest, MD and J. Struyven, MD

Departments of Radiodiagnosis, *Surgery, †Urology and ‡Pathology, Hôpital Erasme, Cliniques Universitaires de Bruxelles, B-1070 Brussels, Belgium

(*Received 15 July 1991 and accepted 20 September 1991*)

Keywords: Pancreas, Neoplasms, Renal cell carcinoma

Pancreatic metastasis from renal cell carcinoma is exceptional, but may appear many years after initial diagnosis and radical nephrectomy of an apparently limited tumour. We report one case of an asymptomatic isolated pancreatic metastasis discovered fortuitously, 21 years after right radical nephrectomy for a low-grade renal cancer.

Case report

In 1969, a 47-year-old man underwent right nephrectomy for renal cell carcinoma of "low-grade malignancy". At this time, no metastases were evident and he remained well on follow-up.

In June 1990, he complained of prostatism and a fine-needle biopsy disclosed a well differentiated prostatic carcinoma. Abdominal sonography demonstrated a hyperechoic heterogeneous mass measuring 5 cm × 4 cm × 3 cm in the pancreatic tail (Fig. 1). On computed tomography (CT), the pancreatic tail appeared enlarged by a hypodense mass. The lesion was limited to the pancreatic parenchyma, and remained hypodense and heterogeneous after intravenous contrast medium enhancement. No other abnormality was identified (Fig. 2). Endoscopic retrograde cholangiopancreatography revealed a pancreatic duct stenosis with overhanging of secondary pancreatic canaliculi. Fine-needle aspiration was haemorrhagic and inconclusive, hence partial pancreatectomy was performed. Histological examination of the mass showed neoplastic clear cells containing glycogen and fat but no prostatic specific antigen (Fig. 3). Comparison with the histology slides from the previous right renal tumour confirmed similarity of the two tumours. Final diagnosis was therefore of a solitary asymptomatic pancreatic metastasis from renal cell carcinoma 21 years after radical nephrectomy.

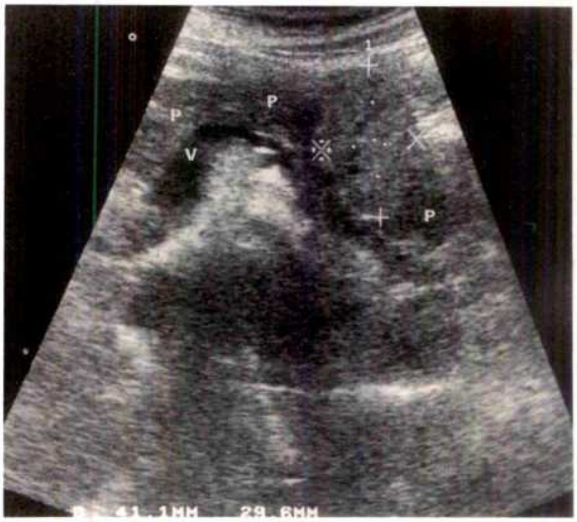

Figure 1. Sonography shows a hyperechoic heterogeneous mass (between crosses) in the pancreatic tail (P: pancreas, V: splenic vein).

Address correspondence to Dr F. Rypens, MD, Department of Radiodiagnosis, Hôpital Erasme, Cliniques Universitaires de Bruxelles, route de Lennik 808, B-1070 Brussels, Belgium.

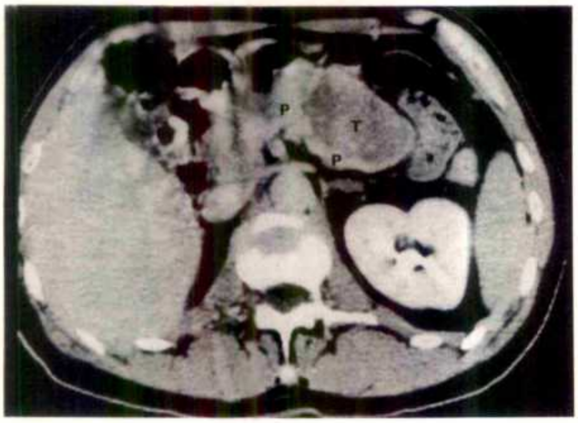

Figure 2. CT scan after intravenous contrast medium enhancement demonstrates a hypodense mass limited to the pancreatic tail, without adenopathy (P: pancreas, T: tumour).

Discussion

Metastatic disease to the pancreas is rare, being described at autopsy in only 3% of patients with generalized malignancies. Generally, the primary tumour is melanoma, breast carcinoma or bronchogenic carcinoma but rare cases have been reported in association with oesophageal, gastric, hepatocellular, biliary, colonic, renal, prostatic and ovarian carcinomas and also in various sarcomas (leiomyosarcoma, Merkel spindle cell sarcoma) (Friedman & Edmonds, 1989; Rumancik et al, 1984). In most cases the pancreatic metastasis is part of widespread nodal and visceral involvement (Malek & Madsen, 1969; Strijk, 1989). About half the patients have pancreatic symptoms or signs including pancreatitis, endocrine or exocrine dysfunction, pain, biliary obstruction or gastrointestinal bleeding. In the other patients, symptoms are absent or masked by the presence of other symptomatic metastasis and pancreatic involvement is only discovered during a staging procedure in advanced tumour. Two sonographic patterns are described: multiple small lesions disseminated throughout the pancreas or large solitary pancreatic lesions. Sonographically, these metastases appear generally more hypoechoic than the pancreatic parenchyma (Strijk, 1989). In our case, the fatty tumoral content may be responsible for the hyperechoic heterogeneous aspect. The CT scan usually shows a hypodense mass sometimes associated with pancreatic or bile duct dilatation. Differentiation from a primary pancreatic tumour will be impossible without tissue sampling; however, the prognosis of these metastases is better than that for primary pancreatic cancer. Here diagnosis was made more difficult because the lesion was solitary and because the renal cell cancer was treated so many years earlier. Cytological examination initially was non-contributory because the sample was heavily blood-stained, but on review neoplastic clear cells similar to those of the pathological specimen were identified.

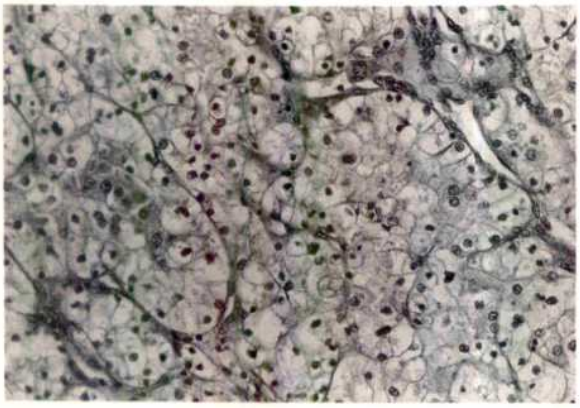

Figure 3. Histological examination shows a tubular clear-cell pattern, typical of renal cell carcinoma.

To our knowledge, only one case of pancreatic metastasis from renal cell carcinoma has been reported, discovered 17 years after the initial diagnosis but in that case it was associated with retroperitoneal lymph node enlargement and melaena (Werneke et al, 1986). Our case illustrates the difficulties in the diagnosis in such a late solitary lesion.

References

Friedman, A. C. & Edmonds, P. R., 1989. Rare pancreatic malignancies. *Radiologic Clinics of North America, 27(1)*, 177–190.

Malek, G. H. & Madsen, P. O., 1969. Carcinoma of the prostate with unusual metastases. *Cancer, 24*, 194–197.

Rumancik, W. M., Megibow, A. J., Bosniak, M. A. & Hilton, S., 1984. Metastatic disease to the pancreas: evaluation by computed tomography. *Journal of Computer Assisted Tomography, 8(5)*, 829–834.

Strijk, S., 1989. Pancreatic metastases of renal cell carcinoma: report of two cases. *Gastrointestinal Radiology, 14*, 123–126.

Werneke, K., Peters, P. E. & Galanski, M., 1986. Pancreatic metastases: US evaluation. *Radiology, 160*, 399–402.

1992, *The British Journal of Radiology*, *65*, 549–550

Case of the month

Contralateral thinking

By S. Mehta, MRCP, BSc and *R. Whitehouse, FRCR

Department of Diagnostic Radiology, University of Manchester, Stopford Building, Oxford Road, Manchester M13 9PT, UK

(*Received 25 April 1991, accepted 4 June 1991*)

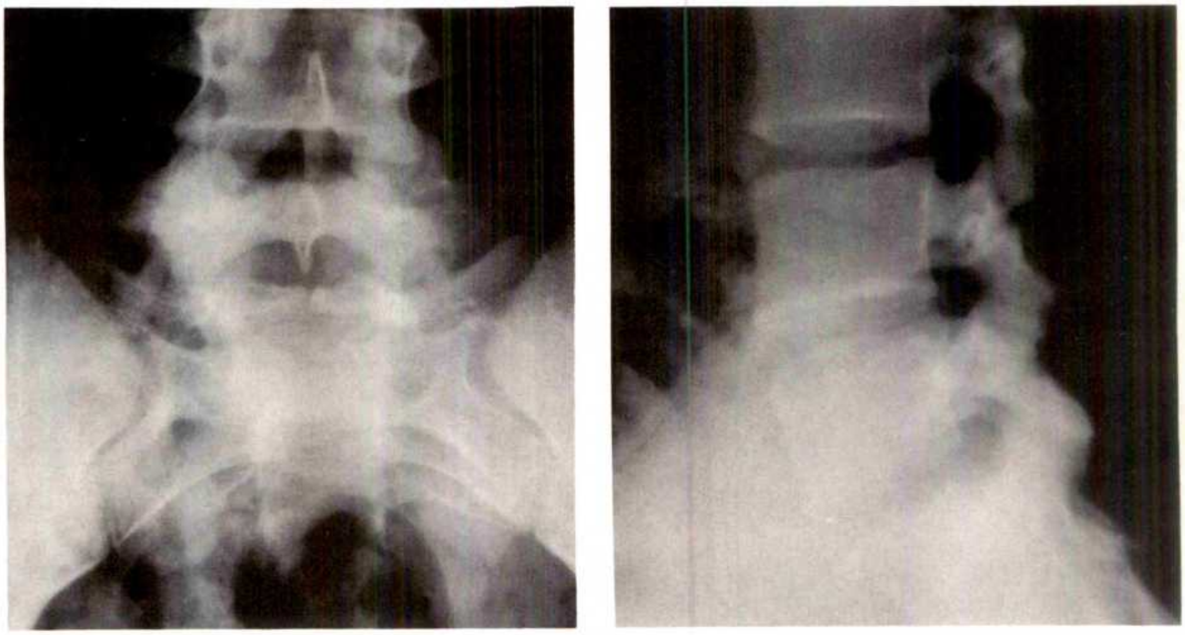

(a) (b)

Figure 1. (a, b)

A 23-year-old man presented to a sports injury clinic with a 6 month history of exercise induced low back pain with radiation to his right buttock. 18 months previously he had been treated for osteomyelitis of the right medial malleolus. On examination there was no neurological deficit. Initial investigations consisted of antero-posterior (AP) and lateral lumbar spine films (Fig. 1) and a $^{99}Tc^{m}$ HDP bone scan (Fig. 2). Haematological and biochemical investigations were normal.

What is the differential diagnosis and what further investigations are appropriate?

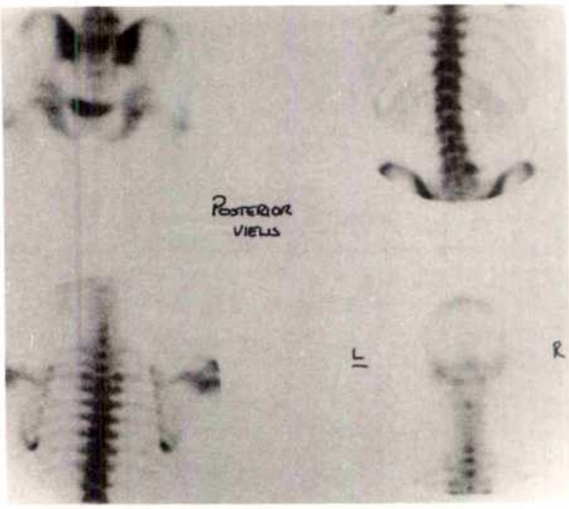

Figure 2.

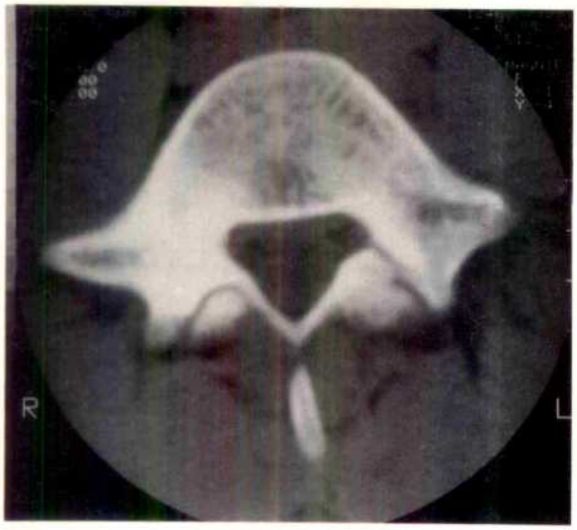

Figure 3.

The lumbar spine films showed a right sided localized area of sclerosis of the neural arch of the L5 vertebra and spina-bifida occulta at S1. The bone scan confirmed increased uptake in the region of sclerosis but no other focal abnormality.

The patient was referred for computed tomography (CT) with a differential diagnosis of an osteoid osteoma or possibly metastatic osteomyelitis. CT was performed with a GE 9800 scanner using contiguous 5 mm sections through the region of interest with the beam parallel to the end plate. Sclerosis of the pedicle and lamina on the right side of the L5 neural arch was confirmed. There was thickening and elongation of the lamina but no evidence of bone destruction, fracture or a nidus of an osteoid osteoma. On the left there was discontinuity of the neural arch anterior to the facet joint confirming a unilateral spondylolysis (Fig. 3).

Sclerosis is a recognized change in the lamina and pedicle opposite a unilateral spondylolysis, reflecting increased stress (Wilkinson & Hall, 1974). Elongation of the lamina on CT has also been described (Rothman & Glenn, 1984).

Table I. Sclerosis of the pedicle

Agenesis or hypoplasia of the contralateral neural arch
Ipsilateral or contralateral spondylolysis
Osteoid osteoma or osteoblastoma
Metastases, myeloma or lymphoma
Infection
Idiopathic

Discussion

Sclerosis of the pedicle in the lumbar spine has a wide differential diagnosis. Important causes are listed in Table I. A comprehensive review of causes has been published recently (Yochim et al, 1990). These include the major differentials in this case: osteoid osteoma, infection and spondylolysis. The incidence of spondylolysis has been shown to be zero at birth with an increasing incidence as childhood progresses. Symptomatic spondylolysis often occurs in relation to exercise and there is a familial incidence. Spondylolysis is therefore considered to develop as a stress fracture in patients with a congenital predisposition. Standard AP and lateral plain films will miss up to 20% of cases. Oblique views are generally considered to be the most useful additional view, but a coned lateral view has been found to be the single most sensitive view identifying 84% of defects. The lateralization, however, cannot be defined and the combination of standard AP, lateral and oblique views remains most sensitive identifying 96.5% of all defects visible on plain film (Amato et al, 1984).

CT involves a higher radiation dose and defects obvious on plain films may not be easily visible as the pars defect merges with the adjacent facet joint. A CT examination may, however, prove necessary, as in this case, to exclude other pathology such as an osteoid osteoma, osteoblastoma or sclerotic metastases. Failure to detect a complete ring on any section has been suggested as a simple method for detection of spondylolysis on CT (Langston & Gavant, 1985). 13% of patients with spondylolysis or spondylolisthesis in one study were found to have a unilateral defect. There was often found to be contralateral sclerosis of the neural arch with elongation attributed to healing of microfractures (Rothman & Glenn, 1984).

Conclusion

Unilateral spondylolysis may not be obvious on clinical or initial radiological investigation. The presence of unilateral sclerosis of the neural arch requires careful evaluation of the contralateral pars interarticularis.

References

Amato, M., Totty, W. G. & Gilula, L. A., 1984. Spondylolysis of the lumbar spine: Demonstration of defects and laminal fragmentation. *Radiology*, *153*, 627–629.

Langston, J. W. & Gavant, M. L., 1985. "Incomplete ring" sign: a simple method for CT detection of spondylolysis. *Journal of Computer Assisted Tomography*, *9*, 728–729.

Rothman, S. L. & Glenn, W. V. 1984. CT: multiplanar reconstruction in 253 cases of lumbar spondylolysis. *American Journal of Neuroradiology*, *5*, 81–90.

Wilkinson, R. H. & Hall, J. E., 1974. The sclerotic pedicle: tumour or pseudotumour? *Radiology*, *111*, 683–688.

Yochum, T. R., Sellers, L. T., Oppennheimer, D. A., Peterson, C. K., Kirton, D. C., Dal Mas, E. C. & Anderson, A. L., 1990. The sclerotic pedicle—how many causes are there? *Skeletal Radiology*, *19*, 411–417.

1992, *The British Journal of Radiology*, *65*, 551

Erratum

Measurement of extrafocal radiation by computed radiography

THE EDITOR—SIR,

Please note that there was an error in the formula contained in the paper entitled Measurement of extrafocal radiation by computed radiography, published in the March 1992 issue of the *British Journal of Radiology*. The error occurred in the formula on p. 240, the correct formula is shown below.

$$\frac{EF}{F} = \frac{1}{10^{\{[(\text{focal value} + 1115) - \text{extrafocal value}]/465\}}}$$

The Publisher apologizes to both the author and the readers for this error.

R. H. MIETTUNEN

Department of Diagnostic Radiology,
Helsinki University Central Hospital,
Helsinki,
Finland

(*Received 23 March 1992*)

Reference

MIETTUNEN, R. H., 1992. Measurement of extrafocal radiation by computed radiography. *British Journal of Radiology*, *65*, 238–241.

1992, *The British Journal of Radiology*, *65*, 552–556

Correspondence

(The Editors do not hold themselves responsible for opinions expressed by correspondents)

Radiation protection associated with well women breast cancer screening

The Editor—Sir,

We wish to raise a number of issues concerning radiation protection aspects associated with well women breast cancer screening programmes now established throughout the UK.

Does irradiation of well women for screening purposes constitute a medical exposure and, therefore, fall within the terms of the 1988 Ionizing Radiation (Protection of Persons Undergoing Medical Examination or Treatment) Regulations? If so, then according to section 4 part 3, persons physically directing a medical exposure shall select procedures such as to ensure a dose of ionizing radiation to the "patient" as low as reasonably parcticable in order to achieve the required diagnostic or therapeutic purpose. In the case of well women breast cancer screening what is the required diagnostic purpose and what is the upper level of dose considered acceptable to achieve this purpose? Is this the level which corresponds to a detection of 5 cancers per 1000 women on the first screen, but what about subsequent screening rounds?

If irradiation of well women does not fall within the framework of the 1988 Regulations then perhaps it falls within the framework of Chapter 2 section 2.16–2.29 of the Guidance Notes to the 1985 Ionizing Radiation Regulations which is concerned with irradiation of volunteers for medical research purposes or screening programmes. In effect the UK Breast Screening Programme would be classed as a research project whose intention was to assess the risk-benefit arising from the widespread application of mammography. Obviously the well women involved are indeed volunteers.

The exposure guidelines for this type of irradiation are presented in the Guidance Notes namely: wherever possible the effective dose equivalents to normal control subjects should be no greater than those for a Category II irradiation with an upper limit effective dose equivalent corresponding to dose limits for memebers of the general public. These limits are now 1 mSv.

In order to evaluate the breast dose which corresponds to this dose equivalent we can employ the most recent tissue or organ weighting factor provided by ICRP for the breast, namely 0.05. However, since this figure assumes a population of both men and women, and it is predominantly females who are at risk from breast cancer, there is a strong case for taking the weighting factor to be 0.1 (see ICRP 34 p. 8).

It is not at all clear, however, whether this factor constitutes a tissue or organ weighting factor. In Table B-8 of the 1990 ICRP Recommendations (Vol. 21 p. 124) the risk factor for the breast employing a multiplicative risk model is indicated as 0.6×10^{-2} Gy^{-1} for a population of males and females. Notwithstanding that in this publication the Tables employ units of Grays and the text refers to Sieverts, this value must be divided by 2 to calculate "the total and other organ probability values". Thus the risk per organ (*i.e.* to each breast) would be 0.3×10^{-2} Gy^{-1} (Sv^{-1}) which is roughly 5% of the total, all organ, risk factor quoted, namely 7×10^{-2} Gy^{-1} (Sv^{-1}) consequently the weighting factor of 0.05 quoted above would appear to be a single organ factor and irradiation of each breast would involve an additive overall risk. This difficulty obviously arises when attempting to employ organ risk factors calculated from whole body irradiation, which involves integral doses throughout a single distributed organ like red bone marrow or additive doses for multiple organs of a particular type, like the breast. Whole body irradiation will involve the whole organ (or tissue) whereas radiological irradiation will involve partial body or single organ exposure. Incidentally there is evidence in ICRP 21 Table B-14A that in the UK the relative organ risk factor for the breast might be 60% higher than the average value indicated by the organ weighting factor of 0.05 quoted above.

Assuming an organ weighting factor of 0.1 for women, the maximum absorbed breast dose corresponding to the recommended upper limit for a Category II exposure of volunteers would appear to correspond to 10 mSv for the same risk as a whole body exposure of 1 mSv. If we assume a conversion factor for entrance surface dose to absorbed breast dose of approximately 0.25 for the beam qualities normally employed in mammography, then the entrance surface dose corresponding to the upper limit for Category II exposures would be 40 mGy, assuming numerical equivalence between absorbed dose and equivalent dose quantities.

For a breast screening mammographic examination comprising two views per breast, the upper limit entrance surface dose would correspond to 10 mGy per image. The outputs of mammographic X-ray units are in the dose range 0.05–0.2 mGy/mAs. Consequently the upper limit X-ray exposure would correspond roughly to 100 mAs per image or 400 mAs per examination.

The Commission of European Communities has issued guidelines for the upper limit entrance surface dose of 7 mGy per image for a breast examination (CEC, 1990). These guidelines were deduced from the results of a UK mammography physics group study involving approximately 30 screening centres. These measurements were not performed on actual patients but on a 4.5 cm thick Perspex phantom. Nonetheless, 25% of centres demonstrated an entrance surface dose value per image to the phantom which exceeded the value of 7.5 mGy. During the first European trial of the image quality criteria document which presented the entrance surface dose guidelines for the breast, over 25% of dose measurements made on actual patients exceeded 10 mGy per image. There is no evidence to indicate that the situation within the UK is any different.

If this is the case then up to 25% of women undergoing mammographic breast screening examination comprising two views of each breast may be receiving a dose which exceeds the upper limit for a Category II exposure of volunteers. At this level of exposure the benefit/risk ratio expressed in terms of cancers detected to cancers induced for a women 50–54 years of age would be approximately 50 for a single screen, with a lifetime benefit/risk decreasing markedly with subsequent screens.

A number of questions obviously need to be addressed.

1. What is the precise radiation protection frame work which covers the exposure of well women in breast screening programmes?
2. What are the actual levels of radiation being employed as distinct from measurements employing phantoms?
3. Why have Perspex phantom measurements been employed in assessing actual breast doses when this approach is not employed for other radoilogical examinations?

4. What constitutes an acceptable upper limit dose for an examination?
5. What action needs to be taken and by whom if any upper limit is exceeded?
6. What are acceptable benefit-risk ratios for well women screening?
7. Are there particular groups within the population, *i.e.* women with large and/or dense breasts who should be considered separately?
8. If women continue to receive doses from multiple screening rounds what is an acceptable lifetime benfit-risk ratio?
9. What are the specific diagnostic purposes in an ongoing breast screening programme?
10. To whom should these questions be addressed?

A great deal of material has been published in both the popular press and scientific journals extolling the virtues of breast screening programmes for the early detection of cancer. However, it would appear that a number of fundamental radiation protection aspects have not yet been resolved. Their resolution would help greatly in providing a balanced appraisal of the acceptable levels of risks arising from breast screening programmes employing mammography. Hopefully this letter will prompt further discussion on these issues.

Yours etc.,

B. M. Moores
E. T. Henshaw

Integrated Radiological Services Ltd,
Unit 188, Centuary Building,
102 Tower Street,
Liverpool L3 4BJ
(Received 29 January 1992, accepted 8 April 1992)

References

CEC, 1990. *Quality Criteria for Diagnostic Radiographic Images*, 2nd edn (Brussels).

Mistaken hilar mass

The Editor—Sir,

R. Thomas discusses the possibility of hilar enlargement due to a dilated oesophagus on a supine radiograph taken on a radiotherapy simulator apparatus and states that this is "well known"!

Two radiographs, one supine and one in the erect position were published with his letter to "prove" the point. However, the oesophagus is not a hilar structure as it lies behind it, and in the absence of a barium examination showing a mid-oesophageal diverticulum lying behind the hilum, I find the explanation very difficult to believe.

Two likely explanations are: (a) the soft tissue mass of the chest wall tumour being treated; or more likely (b) the right venous confluence of the pulmonary veins where this joins the left atrium.

Yours etc.,

F. W. Wright

X-ray Department,
The Churchill Hospital,
Oxford OX3 7LJ
(Received 20 January 1992, accepted 8 April 1992)

Reference

Thomas, R., 1991. Mistaken hilar mass. *British Journal of Radiology, 64*, 977.

Author's reply

The Editor—Sir,

F. Wright's comments further consolidate my point that simulator radiographs should not be used for diagnostic purposes and the expertise of radiologists is essential to give a broader differential diagnosis. However, with respect, the mass in question, seen on the supine but not the erect radiographs, was in the anterio-posterior (AP) projected region of the right hilum. As the title suggested this may have been "mistaken" for a hilar mass without further lateral or barium studies. In a man with a long history of severe oesophageal reflux, oesophageal dilation in the posterior mediastinum is by far the most likely diagnosis. A soft tissue chest wall mass or prominent pulmonary vessels are less likely to demonstrate such dramatic postural changes.

Oesphageal dilation in the differential diagnosis of paramediastinal radiographic masses is well established (Grainger, 1980; Hoffner, 1989) and is often discussed in medical teaching sessions and, hence, although not common is well known.

Yours etc.,

R. J. Thomas

Department of Oncology,
University College London,
The Middlesex Hospital,
London W1N 8AA
(Received 7 February 1992, accepted 8 April 1992)

References

Grainger, R., 1980. *Textbook of Radiology and Imaging*, ed. by D. Sutton, 3rd edn (Churchill Livingstone, Eastbourne), p. 444.
Hoffner, J., 1989. *Textbook of Internal Medicine*, ed. by W. Kelley, p.1960.

Results from the HAD psychometric questionnaire in 54 breast cancer patients treated with breast conservation

The Editor—Sir,

Following the report in this journal by Bull and Campbell (1991) on the use of the HAD psychometric scale to detect anxiety and depression in women attending for breast screening which turned out to be negative, it may be of interest to compare the results with those obtained in patients with established breast cancer.

57 patients with operable breast cancer presented in 1 year to a single surgical firm at the Westminster Hospital and were treated by uniform breast conservation policy (Bulman et al, 1987). 54 completed the HAD scale after local tumour excision, after radical radiotherapy, at 6 months and at 12 months. Standard criteria were used for normal, borderline and abnormal scores. Mean scores, range of scores and the proportion of patients with borderline and abnormal scores are shown in Table I for anxiety and Table II for depression. A total of 15 out of 54 patients scored abnormally anxious at least once, four of these 15 patients scored both abnormally anxious and depressed. There were no cases of depression without anxiety.

All 54 patients were also interviewed by a senior consultant psychiatrist at 6 months. One of the 15 patients with an abnormal HAD score received psychiatric treatment, as did one other patient who did not score as abnormal or borderline on HAD. This treatment rate was lower than we had anticipated based on more

Table I. HAD scale results for anxiety in patients with breast cancer

	Post-operative	Post-radiotherapy	6 months	12 months
Mean HAD score	6.31	5.04	5.02	3.41
Range HAD scores	0–16	0–17	0–17	0–15
% borderline	15	8	12	22
% abnormal	17	12	12	6
Number of patients	53	49	51	54

Table II. HAD scale results for depression in patients with breast cancer

	Post-operative	Post-radiotherapy	6 months	12 months
Mean HAD score	2.96	2.82	2.61	2.30
Range HAD scores	0–17	0–18	0–12	0–7
% borderline	6	6	8	2
% abnormal	6	2	2	0
Number of patients	53	49	51	54

rigorous studies in which about one third of women are consistently reported to show psychiatric morbidity, but in which the practical therapeutic implications of this finding are seldom discussed (Fallowfield et al, 1990).

A comparison of the mean HAD scores from the cancer patients and from the screened patients described by Bull and Campbell shows remarkably little difference, for anxiety 4.95 (cancer) 4.50 (screened) and for depression 2.67 (cancer) and 4.33 (screened). The percentage of patients abnormally depressed was the same in the cancer/screened groups, 0–6%. The only marked difference was the higher proportion (17–12%) of abnormally anxious cancer patients in the first 6 months after diagnosis, falling to the same range of 6% as the screened patients by 12 months.

The reliance which can be placed on the HAD scales in quantifying psychiatric morbidity, and what the results mean to non-pyschometrists, should become clearer as further data on well defined groups of patients are published.

Yours etc.,

A. S. Bulman

Regional Radiotherapy Centre,
Cookridge Hospital,
Leeds LS16 6QB

(*Reveived 15 July 1991, accepted 10 April 1992*)

References

Bull, A. R. & Campbell, M. J., 1991. Assessment of the psychological impact of a breast screening programme. *British Journal of Radiology, 64*, 510–515.

Bulman, A. S., Zieitman, A., Phillips, R. H. & Ellis, H., 1987. Interim results of treatment of breast cancer with breast conservation for all patients. *Surgery, 101*, 395–399.

Fallowfield, L. J., Hall, A., Maguire, G. P. & Baum, M., 1990. Psychological outcomes of different treatment policies in women with early breast cancer outside a clinical trial. *British Medical Journal, 301*, 575–580.

Author's reply

The Editor—Sir,

The letter from A. Bulman makes an interesting point that the HAD scale results were similar amongst cancer patients as among our non-cancer patients. The HAD scale is designed to detect overall psychological state rather than anxieties focussed on a particular problem which would explain a lack of sendsitivity in these circumstances.

Our main conclusions were drawn from reported frequency of breast self-examination and self-reported anxieties. Dr Bulman's observations do not alter our suggestion that at least 10% of women proceeding to open surgery of a benign lesion as a result of the screening programme require professional counselling and support.

Yours etc.,

A. R. Bull

The Queen Building,
Park Parade,
Harrogate HG1 5AH

(*Received 31 July 1991, accepted 10 April 1992*)

Measurement of tissue perfusion by dynamic computed tomography

The Editor—Sir,

While finding the paper by Miles (1991) extremely interesting, I was surprised by the comment in the discussion where it is claimed that "absolute values for tissue perfusion from CT have not been previously reported". There is substantial literature from North America in which the measurement of absolute perfusion with computed tomography has been compared with radiolabelled microspheres, and I think the author should be aware of the following key references.

Jaschke, W. R., Gould, R. G., Cogan, M. G., Sievers, R. & Lipton, M. J., 1987. Cine-CT measurement of cortical renal blood flow. *Journal of Computed Assisted Tomography, 11*(5), 779–784.

Jaschke, W., Cogan, M. G., Sievers, R., Gould, R. & Lipton, M. J., 1987. Measurement of renal blood flow by cine computed tomography. *Kidney International, 31*(4), 1038–1042.

Gould, R. G., Lipton, M. J., McNamara, M. T., Sievers, R. E., Koshold, S. & Higgins, C. B., 1988. Measurement of regional myocardial blood flow in dogs by ultrafast CT. *Investigational Radiology, 23*(5), 348–353.

Rumberger, J. A., Feiring, A. J., Lipton, M. J., Higgins, C. B., Ell, S. R. & Marcus, M. L., 1987. Use of ultrafast computed tomography to quantitate regional myocardial perfusion: a preliminary report. *Journal Am Coll Cardiology, 9*(1):59–69.

Wolfkiel, C. J., Ferguson, J. L., Chomka, E. V., Law, W. R., LABIN, I. N., TENZER, M. L., BOOKER, M. & BRUNDAGE, B. H., 1987. Measurement of myocardial blood flow by ultrafast computed tomography. *Circulation, 76*(6): 1262–1273.

Yours etc.,

S. REES

National Heart & Lung Hospital,
Sydney Street,
London SW3 6NP

(*Received 6 January 1992, accepted 10 April 1992*)

Reference

MILES, K. A., 1991. Measurement of tissue perfusion by dynamic computed tomography. *British Journal of Radiology, 64*, 409–412.

Author's relpy

THE EDITOR—SIR,

I am most grateful for the references S. Rees has supplied on the measurement of blood flow using computed tomography (CT) in response to my paper (Miles, 1991). My comment in the discussion should have stated that absolute values for tissue perfusion from CT have not been reported previously in man. All of the papers listed by S. Rees describe work performed only in animals and I remain unaware of any reports of human studies.

The method for calculating tissue perfusion that I have described also benefits from being applicable to a wide range of different tissues. This is not so for the renal work of Jaschke et al (1987) whose technique requires data from the renal vein.

I am grateful for the opportunity to correspond on this topic as the ability of CT to provide functional information is poorly recognized.

Yours etc.,

K.A. MILES

Departments of Radiology and
Nuclear Medicine,
Addenbrookes Hospital,
Hills Road,
Cambridge CB2 2QQ

(*Received 2 March 1992, accepted 10 April 1992*)

Reference

JASCHKE, W., COGAN, M. G., SIEVERS, R., GOULD, R. & LIPTON, M. J., 1987. Measurement of renal blood flow by cine computed tomography. *Kidney International, 31*(4), 1038–1042.
MILES, K. A., 1991. Measurement of tissue perfusion by dynamic computed tomography. *British Journal of Radiology, 64*, 409–412.

Mesenteric lymphadenopathy in idiopathic retroperitoneal fibrosis

THE EDITOR—SIR,

Bilateral ureteral obstruction in a 54-year-old man was diagnosed as idiopathic retroperitoneal fibrosis (IRF) on the basis of surgical biopsy and treated with bilateral ureterolysis 8 years ago. 5 years later, the patient presented with symptoms of colonic partial obstruction and mild renal failure. Relapse involving the perivascular retroperitoneum and the pelvis extending to the mesosigmoid colon was evident on an abdominal computed tomography (CT) study. A new surgical biopsy revealed IRF. The patient was treated with bilateral percutaneous nephrostomy and steroids. Repeat CT after 4 months revealed almost complete resolution of the fibrotic process. 1 year later, abdominal CT disclosed again a soft tissue homogeneous para-aortic mass and mesenteric lymph adenopathy (Fig. 1a). To rule out malignancy CT-guided percutaneous biopsy of the adenopathy was performed and histology showed non-specific inflammatory changes. No organisms were identified from the specimen. CT at 6 and 12 months, after steroid treatment revealed reduction of the retroperitoneal mass and almost complete resolution of the adenopathy (Fig. 1b).

IRF is considered an autoimmune periaortitis resulting from leakage of ceroid from atheromatous plaques in the aortic wall (Mitchinson, 1984). CT and magnetic resonance are the imaging modalities of election in the diagnosis of IRF (Brooks et al, 1987;

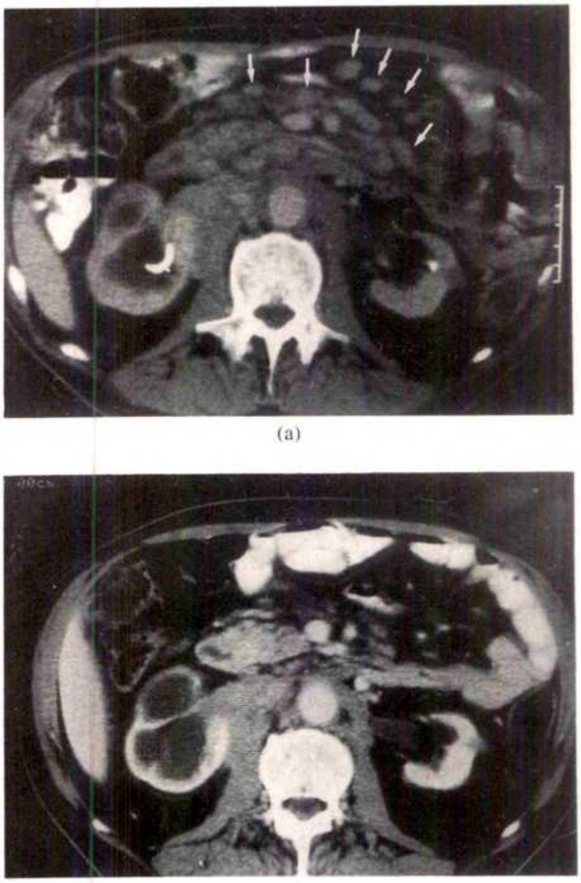

(a)

(b)

Figure 1. (a) Contrast-enhanced abdominal CT shows multiple homogeneous enlarged mesenteric lymph nodes (arrows) measuring 1–1.5 cm. There is a soft tissue mass (representing the IRF) surrounding the aorta and inferior vena cava. Note the hydronephrotic right kidney and nephrostomy catheters in both renal plevis. (b) Contrast-enhanced abdominal CT 1 year later demonstrated nearly complete resolution of mesenteric lymphadenopathy and marked reduction of the retroperitoneal mass. Note the persistent bilateral hydronephrosis.

Amis, 1991). Typically IRF appears on CT as a well-defined periaortic retroperitoneal soft tissue mass (Brooks et al, 1987). However, this appearance can be similar to that found in malignant retroperitoneal fibrosis (Brooks et al, 1987). Atypical cases of IRF are not infrequent. The fibrotic mass can grow in the peripancreatic or periduodenal regions or present as an isolated mass in a paravertebral or mesenteric location (Inaraja et al, 1986; Brooks, 1990; Amis, 1991).

Mesenteric lymphadenapathy can represent another unusual manifestation of IRF which, to our knowledge, has not been reported previously.

Yours etc.,

F. Pombo
J. Perez-Fontan
E. Rodriguez

Department of Radiology,
Hospital Juan Canalejo,
Xubias de Arriba, 84,
15006 La Coruna, Spain

(*Received 3 March 1992, accepted 10 April 1992*)

References

Amis, E. J., 1991. Retroperitoneal fibrosis. *American Journal of Roentgenology, 157*, 321–329.

Brooks, A. P., 1990. Computed tomography of idiopathic retroperitoneal fibrosis ("periaortitis"): variants, variations, patterns and pitfalls. *Clinical Radiology, 42*, 75–79.

Brooks, A. P., Reznek, R. H., Webb, J. A. W. & Baker, L. R. I., 1987. Computed tomography in the follow-up of retroperitoneal fibrosis. *Clinical Radiology, 38*, 597–601.

Inaraja, L., Franquet, T., Caballero, P., Encabo, B. & Humbert, P., 1986. CT findings in circumscribed upper abdominal idiopathic retroperitoneal fibrosis: case report. *Journal of Computer Assisted Tomography, 10*, 1063–1064.

Mitchinson, M. J., 1984. Chronic peri-aortitis and peri-arteritis. *Histopathology, 8*, 589–600.

Now you see it...now you don't

The Editor—Sir,

We were interested to read the case report by J. S. Millar (1992) showing the unusual appearance of a para-umbilical hernia. In the discussion the author states that the diagnosis of a diaphragmatic hernia is usually obvious. McHugh et al (1991) makes the point that plain radiographic findings of diaphragmatic hernia are often nonspecific and that when suspected a contrast study should be performed. We present a case in which the diaphragm could not be seen but in which the presence of a stricture suggested the correct diagnosis.

A 78-year-old lady was referred with constipation, abdominal pain and distention. A chest radiograph showed a left pleural effusion and free gas under the right hemidiaphragm. The supine abdominal radiograph revealed distention of both large and small intestine.

A gastrografin enema (Fig. 1) demonstrates a short extrinsic stricture in the region of the splenic flexure and a healed rib fracture (from an accident 20 years previously). A diagnosis of incarcerated diaphragmatic hernia was suspected and confirmed at laparotomy. The free air was due to caecal perforation.

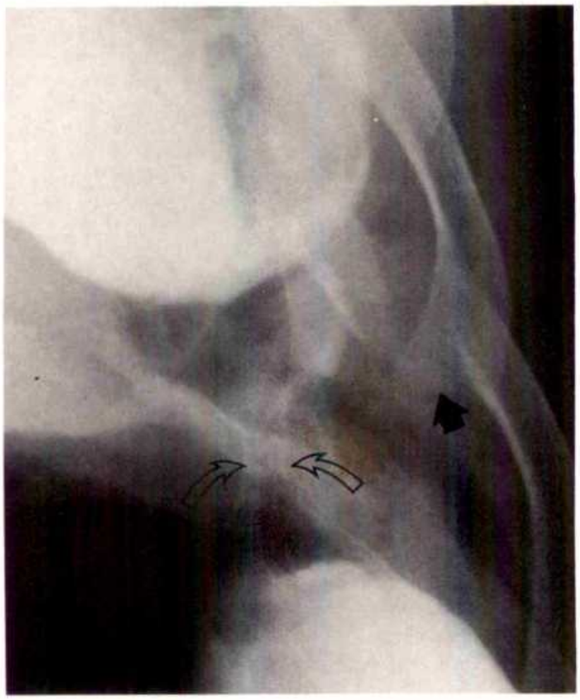

Figure 1. Spot view from the gastrografin enema. Open arrows mark the short extrinsic stricture in the splenic flexure. Closed arrow indicates the healed rib fracture of the left 9th rib. The diaphragm cannot be seen.

90% of traumatic herias of the diaphragm are left sided, they usually result from blunt abdominal injury. Approximately one third of cases will have a delayed presentation. The diagnosis is straight forward if there is an appropriate history and the combination of an elevated hemidiaphragm and high splenic flexure or, if bowel loops are visible in the chest. In fact this is not often the case. A spectrum of radiological appearance exists, changes are often minimal. Even a large diaphragmatic defect may be difficult to recognize with herniated bowel mimicking diaphragmatic contour. Pleural effusion or basal shadowing are frequently present but, if the diaphragm is obscured, may mask the true diagnosis.

Yours etc.,

D. Kessel
*P.E. Bearn

Departments of Radiology and *Surgery,
Middlesex Hospital,
Mortimer Street,
London W1N 8AA

(*Received 9 March 1991, accepted 15 April 1992*)

References

McHugh K., Ogilvie, B. C. & Brunton, F. J., 1991. Delayed presentation of traumatic diaphragmatic hernia. *Clinical Radiology, 43*, 246–250.

Millar, J. S., 1992. Now you see it... now you don't. *British Journal of Radiology, 65*, 183–184.

1992, *The British Journal of Radiology*, 65, 557–563

VOLUME 65 NUMBER 775 JULY 1992

The British Journal of Radiology

A comparison of ultrasound exposure in therapy and pulsed Doppler fields

By H. C. Starritt, PhD and F. A. Duck, PhD

Department of Medical Physics, Royal United Hospital, Combe Park, Bath, Avon BA1 3NG, UK

Based on a paper presented at the BMUS 23rd Annual Meeting in Bournemouth, on 10–12 December 1991

Keywords: Diagnostic ultrasound, Therapeutic ultrasound, Exposure, Measurement

Abstract. A detailed comparison of the ultrasound exposure in water from a therapeutic beam and a pulsed Doppler beam was carried out. A significant overlap in acoustic power was found between therapy intensity levels used clinically and the upper end of the diagnostic range, between approximately 100 mW and 200 mW. In addition, pulse pressure amplitudes in the range 0.5–1.0 MPa were measured close to the transducer on both units. It is common to use physiotherapy equipment at pulse average intensities of 0.5 W/cm^2 or less, and at these levels exposures of similar magnitude may be obtained with beams currently defined as therapeutic and those available from pulsed Doppler equipment.

In recent years the exposure levels available for pulsed Doppler operation have steadily increased. For example, the mean spatial peak temporal average intensity (I_{SPTA}) was observed to have increased by a factor of almost 5 in the time period 1985 to 1989 (Duck, 1989). Similarly, increases in total power and peak negative pressure were also observed over the same period. Conversely, in physiotherapy applications it has become more common to operate ultrasound equipment clinically at spatial average intensities that are at the lower end of the available range (ter Haar et al, 1987). It has been argued that the treatment is effective at low intensities, while potentially harmful thermal effects are avoided. Further, Dinno et al (1989), amongst others, have suggested that cellular changes that are non-thermal in nature can be induced by low-intensity ultrasound. Thus, while the trend for diagnostic ultrasound has been towards higher available powers and intensities, in physiotherapy there has been encouragement to reduce the spatial average intensities used for treatment. Williams (1991) has noted that patients are occasionally being subjected to higher time-averaged ultrasonic intensities during some diagnostic procedures than they might receive during a typical therapy procedure. Until now, a detailed comparison of exposures has not been reported in the literature. In this paper the acoustic beams produced by equipment designed for use in physiotherapy are quantitatively compared with beams produced by diagnostic ultrasound equipment operating in pulsed Doppler mode. Modern diagnostic Doppler equipment is highly complex with many factors affecting the total power output and the spatial peak intensity generated at any point in the field. One aim of the study was to carry out a detailed investigation of exposure levels over the total range of control settings in order to compare the ranges of values available in pulsed Doppler mode with those available from physiotherapy equipment.

Ultrasound equipment

Two commercial ultrasound units were selected for this study. Each was representative of equipment that is widely used clinically. The therapeutic equipment used was a Therasonic-1032 (Electromedical Supplies (EMS), Wantage, Oxon). Two transducers were supplied with this unit, one large (nominal radiating area 390 mm^2 at 3 MHz) and one small (nominal radiating area 60 mm^2 at 3 MHz). Each transducer could be driven at 1 MHz or at 3 MHz, either continuously or in tone bursts with mark-to-space ratios of 1:2, 1:4 or 1:9. Exposure measurements were made on three Therasonic-1032 units in order to take account of the variation in output between different units. It is noted that a variation of ±30%, in the measured intensity compared with the stated intensity, is permitted by British Standard 5724 (British Standards Institution (BSI), 1985). Therasonic ultrasound equipment is widely used in physiotherapy departments in the United Kingdom and can be taken to typify physiotherapy equipment in general since there is little variation between manufacturers.

The diagnostic equipment investigated was an Acuson-128 scanner. This unit was selected because it was capable of operating towards the upper end of the range of output powers available from commercial diagnostic scanners. (A review of diagnostic exposure levels currently available from modern ultrasound equipment has been produced by Duck & Martin (1991).) Measurements were made using a V328 phased array transducer, with a nominal frequency of 3.5 MHz, oper-

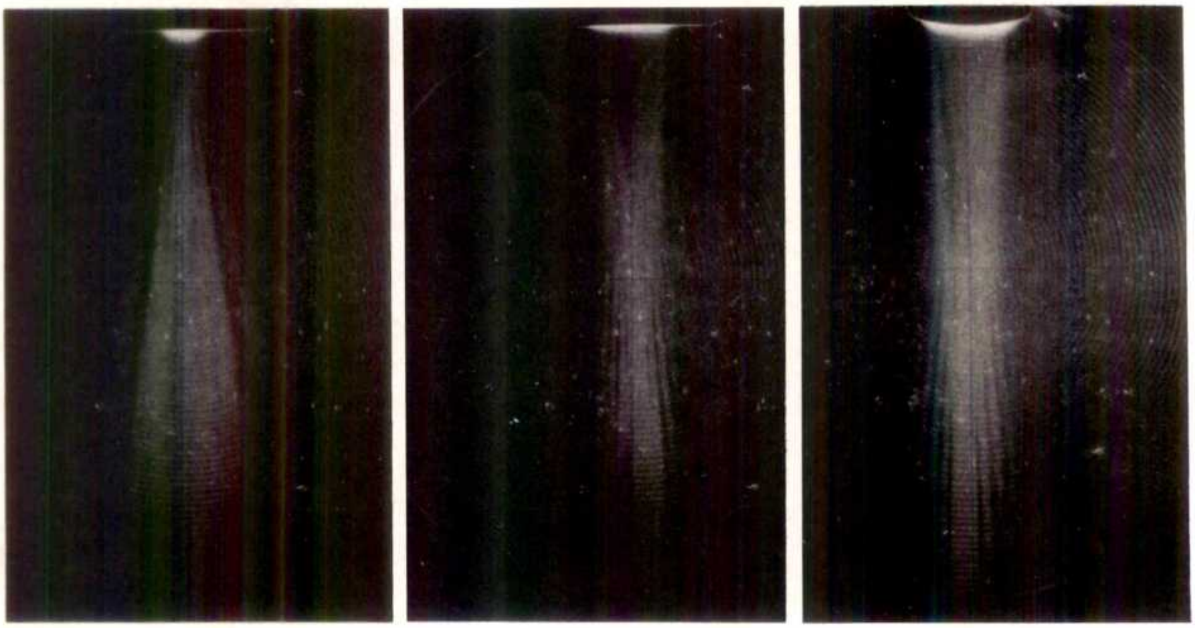

Figure 1. Schlieren images of the pulsed Doppler beam: (a) range gate setting 19 mm, (b) range gate setting 40 mm and (c) perpendicular direction showing geometric focus. The vertical length of each photograph is 100 mm.

ating in pulsed Doppler mode. The exposure delivered by this unit was dependent on a number of control settings. For example, it depended on the output control, labelled PWR, which could be set at <500, <100 or <50 (no units are given), on the velocity range selected, on the range gate location, labelled PWD, which could be varied between 8 mm to 240 mm, and on the gate width.

The two devices differed in the fact that the diagnostic beam was weakly focused, with a maximum pressure gain of approximately 8.0, while the therapy beams were unfocused. The gain of the diagnostic beam varied between 2.2 and 8.0 as the range gate location was altered with the highest values occurring at PWD settings in the middle of the range. The maximum gain occurred at a range gate setting of 89 mm and when the range gate was located closer to the transducer or further away the gain was reduced. A number of the exposure measurements on both types of equipment were made in the region close to the transducer, for example source pressure amplitude and radiating area. At this location more similarities were observed between the beams than were found at greater depth, when focusing of the diagnostic beam resulted in a decrease in the beam area and an increase in the pressure amplitude and spatial average intensity.

Measurements and results

Schlieren observation of the beams

A portable Schlieren system (see Acknowledgments) was used to visualize the acoustic beams. In this technique a change in the refractive index of water, caused by the passage of an acoustic wave, is used to produce an image of the wavefront by transverse illumination of the propagation fluid. Figure 1 shows a series of images of the pulsed Doppler beam demonstrating the location of the electronic focus at range gate settings of 19 m and 40 mm in turn. In Fig. 1c the geometric beam fo in the orthogonal plane is imaged. Schlieren imag the therapy beam are shown in Fig. 2. The beams respectively, (a) large transducer, 3 MHz; (b) small transducer, 3 MHz; (c) large transducer, 1 MHz; and (d) small transducer, 1 MHz. It can be seen from these images that in the region close to the transducer the therapy beams can be of similar dimensions to the diagnostic beams. In particular, the source area of the large therapy transducer is similar to the Acuson operating with a long focal length and the source area of the small therapy transducer is similar to the Acuson operating with a short focal length. The unfocused nature of the therapy beams can also be seen.

Acoustic power

Measurement of acoustic power was carried out using a calibrated radiation force balance (Perkins, 1989). The output of the pulsed Doppler beam was affected primarily by two of the scanner controls, the PWR (transmit power control) and the PWD (range gate control). Each was varied in turn throughout its range and the total acoustic power measured under a range of conditions. Figure 3 shows how the acoustic power varied when the range gate setting was systematically increased from 8 mm to 240 mm for each of the three available transmit power settings. At the maximum

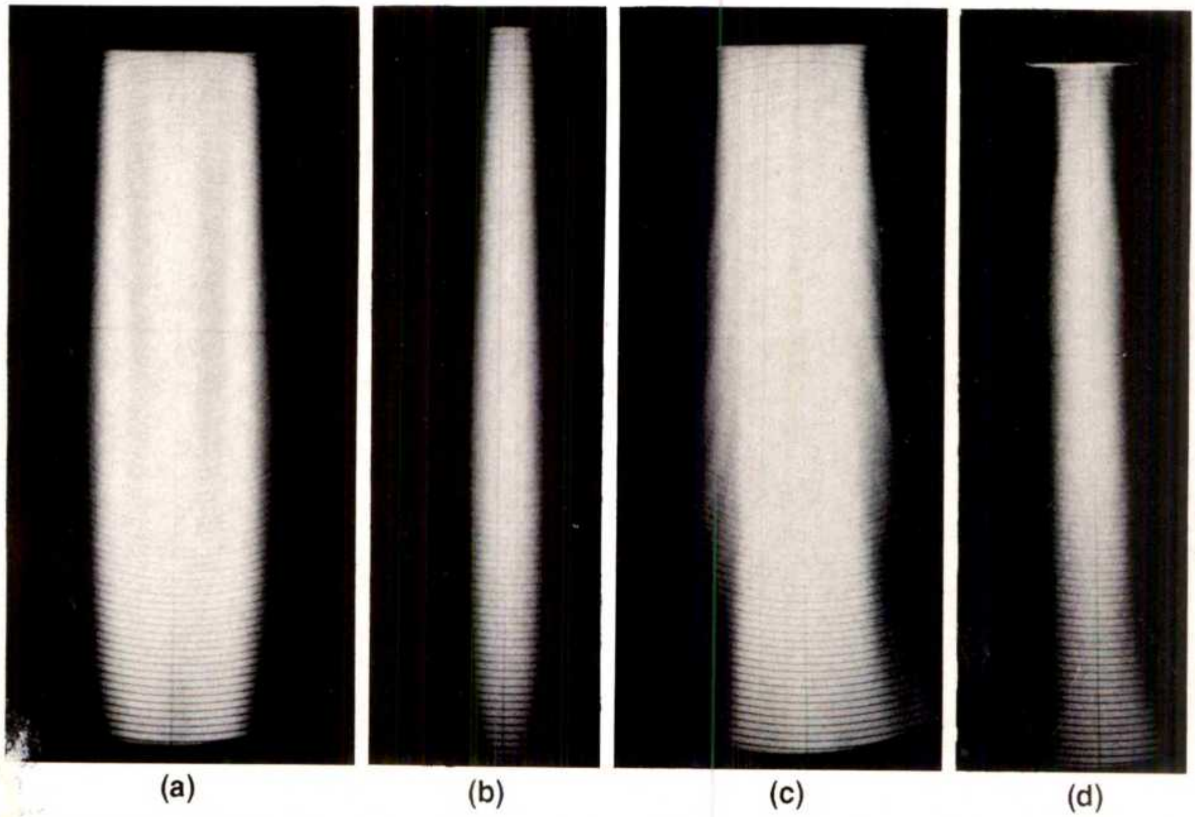

ure 2. Schlieren images of the therapy beam: (a) large transducer, 3 MHz; (b) small transducer, 3 MHz; (c) large transducer, Hz; and (d) small transducer, 1 MHz (scale as Fig. 1).

setting, PWR < 500, the acoustic power ranged 22 mW to 195 mW with the highest measured value occurring at a range gate (PWD) setting of 110 mm.

Figure 4 shows a representation of the ranges of total acoustic power available in the pulsed Doppler beams and the therapeutic beams under investigation. The lower end of each therapy range in this figure indicates the acoustic power levels measured at pulse intensity settings of 0.25 W/cm². Lower powers were available

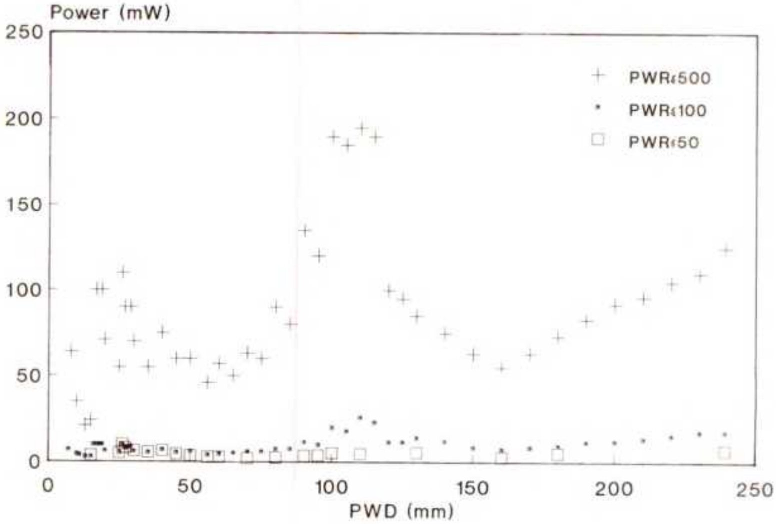

Figure 3. Variation in total acoustic power with range gate setting (PWD) for the pulsed Doppler beam.

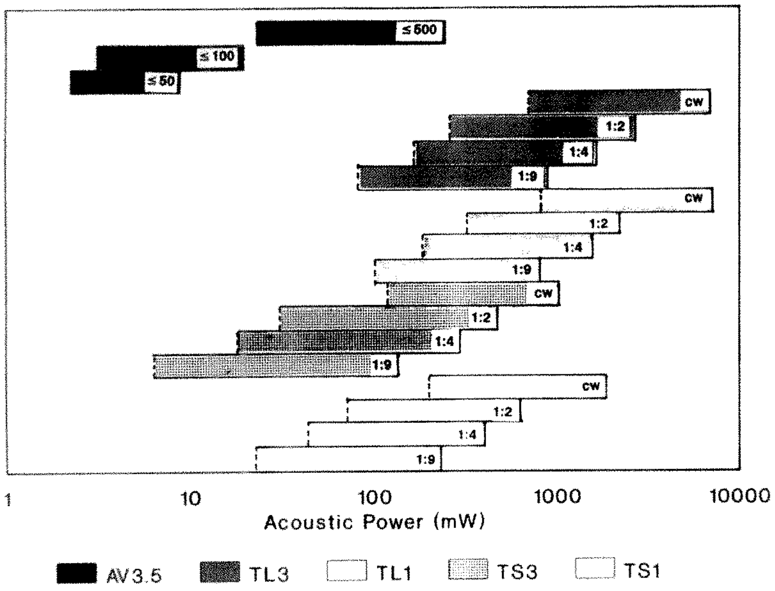

Figure 4. Range of acoustic power available from each transducer; AV3.5 = Acuson-128, V328, 3.5 MHz transducer; TL3 = Therasonic-1032, large transducer, 3 MHz; TL1 = Therasonic-1032, large transducer, 1 MHz; TS3 = Therasonic-1032, small transducer, 3 MHz; TS1 = Therasonic-1032, small transducer, 1 MHz. Ratios of on–off times for the therapy transducers operating in pulsed mode are shown as 1:2, 1:4 and 1:9; CW represents continuous mode.

from the Therasonic-1032, but measurements were not made at settings below this. Some considerable degree of overlap can be seen between the power levels measured in the pulsed Doppler beam generated at maximum output settings and in the therapy beams operated at or below 0.5 W/cm^2 in pulsed mode.

Hydrophone measurements

An NPL (National Physical Laboratory) Ultrasound Beam Calibrator (UBC) (Preston, 1988) was used for measurement of pressure amplitude, beam cross-sectional area and pulse duration. Measurement of the peak pressure amplitudes generated in water at the face of the transducer were made in each acoustic beam with the hydrophone array positioned as close as possible to the transducer face. In all cases the hydrophone array was less than 0.5 mm from the transducer. The magnitudes of the peak positive source pressure (p^+) and the peak negative source pressure (p^-) measured in the acoustic beam are given in Table I.

For the therapy beams the maximum source pressures were generated at the maximum output setting, 2.54 W/cm^2, spatial average intensity. In the pulsed Doppler beam the pressure amplitude at the transducer varied with range gate setting, between 0.38 MPa and 0.98 MPa as shown in Fig. 5. The maximum pressure amplitude at the source was obtained at the maximum output setting, PWR < 500, and at a range gate setting of PWD = 8 mm. The range of pressure amplitudes generated close to the transducer in the therapy beams and in the highest output pulsed Doppler beam were very similar. Therapeutic intensities of 0.5 W/cm^2, spatial average intensity, are common in clinical practice and resulted in a maximum positive pressure amplitude of 0.28 MPa and maximum negative pressure amplitude of 0.27 MPa. In the pulsed Doppler beam, at reduced output setting, PWR < 100, maximum pressures of 0.44 MPa (p^+) and 0.43 MPa (p^-) were measured.

Table I. Maximum pressure amplitudes at the transducer face for each acoustic beam

	p^+ (MPa)	p^- (MPa)
Doppler	0.98	0.90
Therapy		
Large, 3 MHz	0.77	0.69
1 MHz	0.65	0.59
Small, 3 MHz	0.70	0.69
1 MHz	0·53	0·49

Considerably higher pressure amplitudes were measured at the focus of the pulsed Doppler beam. The maximum focal pressure amplitudes were 5.4 MPa (p^+) and 2.4 MPa (p^-). No significant increase in pressure amplitude was observed with depth in the unfocused therapy field.

Temporal average intensities measured for the pulsed Doppler beam ranged from 20 mW/cm^2 to 190 mW/cm^2 (I_{SATA}) at the source, depending on the location of the range gate. At the focus the spatial peak temporal average intensity (I_{SPTA}) was 5.05 W/cm^2 and the I_{SATA} was 2.93 W/cm^2. The maximum intensity (I_{SATA}) obtained with the large Therasonic transducer at 3 MHz was 2.49 W/cm^2.

The beam area at the transducer, the radiating area, was calculated for each beam from the −6 dB beam widths measured in two orthogonal directions using the UBC. The Doppler beam was assumed to be rectangular close to the transducer, while the therapy beams were circular in cross section.

As the depth of the range gate was increased, the

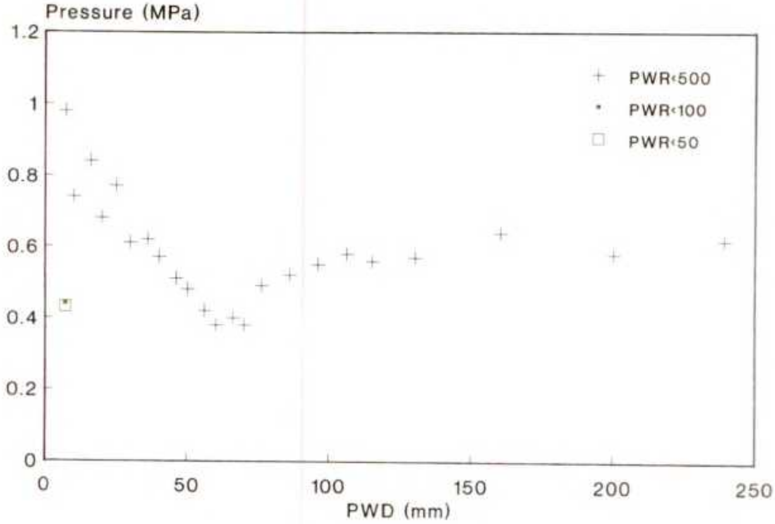

Figure 5. Variation in peak positive pressure amplitude at the transducer with range gate setting for the pulsed Doppler beam.

radiating area of the pulsed Doppler beam increased from 33 mm^2 to 380 mm^2, beyond which no further increase occurred. The shape of the beam also varied from an elongated rectangle to one that was more square, with the cross-sectional area of the "squarest" beam being 209 mm^2 at the transducer. Therapy beam areas measured at the transducer (−6 dB level) were 67 mm^2 and 63 mm^2 for the small transducer and 380 mm^2 and 282 mm^2 for the large transducer, each operating at 3 MHz and 1 MHz, respectively. The range of pulsed Doppler beam areas measured at the transducer therefore encompassed most of the therapy beam areas, with the maximum cross-sectional area of the pulsed Doppler beam possibly exceeding that of the therapy beam.

The mark-to-space ratio of the pulsed therapy beams was measured by displaying the acoustic waveform detected by a single element of the UBC hydrophone array on an oscilloscope. Figures 6 and 7, obtained in this way, give a visual comparison of the pulse lengths typical with pulsed Doppler and pulsed therapy beams, respectively. In Fig. 6, 1.8 μs pulses are shown at a pulse repetition frequency of 1.6 kHz. The output of the therapy transducer could be pulsed with tone bursts of 2 ms duration and off-times of 4 ms, 8 ms or 18 ms. Figure 7 shows the output on the 1:2 pulse setting.

Discussion

This study has shown that for physiotherapy applications in which spatial average intensities of 0.5 W/cm^2

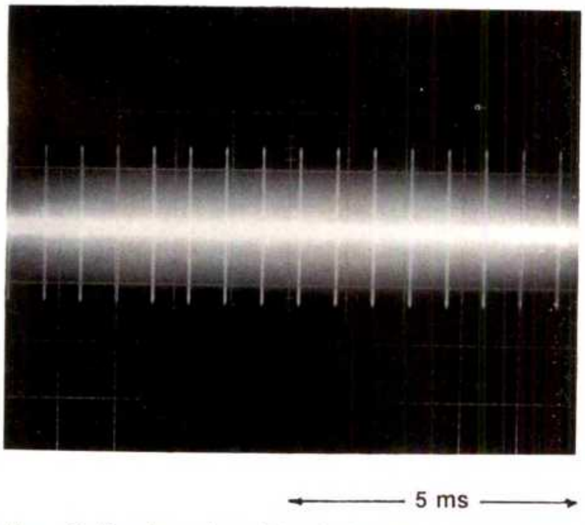

Figure 6. Doppler pulses, 1.8 μs in length, at 1.6 kHz pulse repetition frequency.

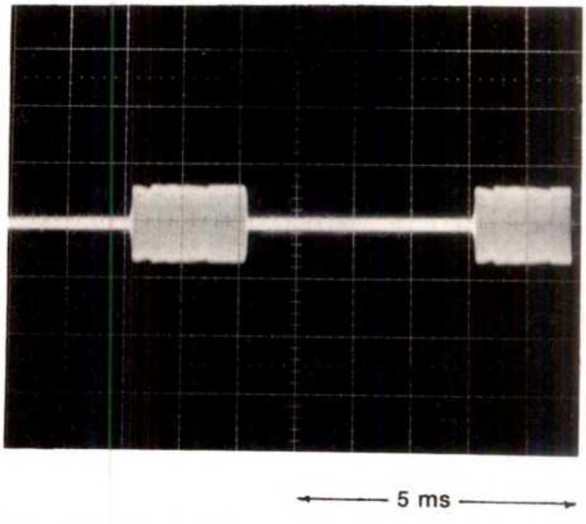

Figure 7. Therapy pulses, 2 ms in length, at a mark-to-space ratio of 1:2.

or less are employed, the total acoustic power delivered to a patient may be less than that delivered during a diagnostic pulsed Doppler examination with the equipment operating under "worst case" conditions. It has also been shown that source pressures from both types of equipment can be equivalent, as can the radiating areas, although the transducers may be different shapes. Under these conditions the main difference between two such systems lies in the way in which the power is delivered. In physiotherapy applications the exposure is either continuous and low in amplitude, for example 0.3 MPa at 0.5 W/cm^2, or of the same amplitude but pulsed with long tone bursts of 2 ms and a high mark-to-space ratio. For example, a mark-to-space ratio of 1:4 is equivalent to a pulse repetition frequency of 100 Hz. In pulsed Doppler applications an equivalent total power may be delivered with higher amplitude pulses, for example 1 MPa source pressure and with a low mark-to-space ratio. In the study described here, for example, 2 μs duration pulses and a pulse repetition frequency of 6.1 kHz resulted in the highest measured value of total acoustic power.

Total power is the exposure variable associated most closely with thermal effects, although beam dimensions are also important. This study has shown that both units are capable of delivering equivalent powers with equivalent beam areas. Measurements of temperature elevation in tissue have been reported by a number of authors. In a pulsed Doppler beam, for example, a temperature rise of 2°C in excised bovine liver has been reported (ter Haar et al, 1989). Measurements were made under "worst case" conditions in which the maximum available power generated by the ultrasound equipment was used. Carstensen et al (1990) have demonstrated greater heating of mouse skull, *in vivo*, at comparable intensities. Temperature rises of the order of 3°C per W/cm^2 were reported. Using physiotherapy equipment, a temperature elevation of approximately 3°C after 10 min was reported in live, exteriorized rat fetuses, using an intensity of 1.3 W/cm^2, at a frequency of 1 MHz (Abraham et al, 1989). Carnes et al (1991) have measured temperature rises *in vivo* in the mouse fetus using implanted thermocouples and a 1 MHz, unfocused transducer. At 0.5 W/cm^2, spatial average intensity, a temperature rise of 2°C was recorded after 400 s exposure. At lower intensities, such as those used clinically, the temperature elevation produced in tissue by physiotherapy equipment might be expected to be very similar to that produced by high-level pulsed Doppler beams for the reasons stated above. If thermal effects are not important at the power levels used clinically, then physiotherapy ultrasound treatments must rely for their effectiveness on a non-thermal mechanism, be it from direct mechanical vibration, cavitation or streaming. Since there is a clear overlap in exposure levels available from pulsed Doppler equipment and those levels used by physiotherapists in the treatment of patients, it is important that the possible mechanisms of interaction of ultrasound with tissue are considered carefully for each case. A detail investigation of thermal effects and acoustic streaming produced by both types of equipment will form the basis of a future publication.

The total absorbed energy depends on the time for which the ultrasound beam is applied to a patient. In physiotherapy applications, treatment times range from 5 to 25 min with the transducer being moved over the area of interest throughout that time (Benwell & Bly, 1987). For the physiotherapy ultrasound unit used in this study, in common with other units, the treatment duration must be selected before commencement. A maximum of 19 min is permitted with the Therasonic-1032 and after this time the ultrasound output is automatically terminated. This acts as a safeguard in limiting the duration of any single exposure. A similar situation occurs in diagnostic radiology where fluoroscopic exposures are limited in the same way. For pulsed Doppler applications, no such safeguard exists, but examination times are likely to be shorter, of the order of a few minutes at maximum at any one location.

Throughout this discussion it has been assumed that pulsed Doppler equipment is operated under conditions that produce the highest exposure levels, whereas in practice, it is generally used at reduced power levels whenever possible. The rationale behind this is one of increased safety and, in particular, of reducing any thermal effects. Nevertheless, commercial Doppler equipment has the ability to produce higher exposures and these levels may be used in a diagnostic examination apparently without affecting the patient in any way. The question of how ultrasound "works" in physiotherapy treatments, what the mechanism of interaction is, and hence how it is effective at low intensities remains the subject of much study.

Acknowledgments

We thank the staff of the Radiology Department, Salisbury General Infirmary, for allowing us the opportunity to make measurements on the Acuson-128. We also acknowledge the contribution of Mr D. Follet of the Medical Physics Department in Bristol, who designed and built the portable Schlieren system used in this study.

References

ABRAHAM, V., ZISKIN, M. & HEYNER, S., 1989. Temperature elevation in the rat fetus due to ultrasound exposure. *Ultrasound in Medicine and Biology, 15*, 443–449.

BENWELL, D. A. & BLY, S. H. P., 1987. Sources and applications of ultrasound. In *Ultrasound, Medical Applications, Biological Effects and Hazard Potential*, ed. by M. H. Repacholi, M. Grandolfo and A. Rindi (Plenum Press, New York), pp. 29–47.

BSI, 1985. *Medical Electrical Equipment Part 2. Particular Requirements for Safety. Section 2.5: Specification for Safety of Ultrasonic Therapy Equipment*, British Standard BS 5724 (BSI, London).

CARNES, K. I., DREWNIAK, J. L. & DUNN, F., 1991. *In utero* measurement of ultrasonically induced fetal mouse temperature increases. *Ultrasound in Medicine and Biology, 17*, 373–382.

CARSTENSEN, E. L., CHILD, S., NORTON, S. & NYBORG, W., 1990. Ultrasonic heating of the skull. *Journal of the Acoustical Society of America, 87*, 1310–1317.

DINNO, M. A., DYSON, M., YOUNG, S. R., MORTIMER, A. J., HART, J. & CRUM, L. A., 1989. The significance of membrane changes in the safe and effective use of therapeutic and diagnostic ultrasound. *Physics in Medicine and Biology, 34*, 1543–1552.

DUCK, F. A., 1989. Output data from European studies. *Ultrasound in Medicine Biology, 15 (Suppl. 1)*, 61–64.

DUCK, F. A. & MARTIN, K., 1991. Trends in diagnostic ultrasound exposure. *Physics in Medicine and Biology, 36*, 1423–1431.

PERKINS, M. A., 1989. A versatile power balance for ultrasound measurement. *Physics in Medicine and Biology, 34*, 1645–1652.

PRESTON, R. C., 1988. The NPL Ultrasound Beam Calibrator. *IEEE Transactions on Ultrasonics, Ferroelectrics and Frequency Control, 35*, 122–139.

TER HAAR, G., DYSON, M. & OAKLEY, E. M., 1987. The use of ultrasound by physiotherapists in Britain, 1985. *Ultrasound in Medicine and Biology, 13*, 659–663.

TER HAAR, G., DUCK, F. A., STARRITT, H. C. & DANIELS, S., 1989. Biophysical characterisation of diagnostic ultrasound equipment—preliminary results. *Physics in Medicine and Biology, 34*, 1533–1542.

WILLIAMS, A. R., 1991. In *The Safe Use of Diagnostic Ultrasound*, ed. by M. F. Docker and F. A. Duck (British Institute of Radiology, London), pp. 1–6.

1992, *The British Journal of Radiology*, *65*, 564–569

Routine radiographer screening for fetal abnormalities by ultrasound in an unselected low risk population

By *Isabel M. Shirley, FRCR, Fiona Bottomley, DMU and Victor P. Robinson, MRCOG
The Hillingdon Hospital, Uxbridge, Middlesex UB8 3NN, UK

Based on a paper presented at the BMUS 23rd Annual Meeting in Bournemouth, on 10–12 December 1991

Keywords: Ultrasound screening, Fetal abnormalities, Radiographers

Abstract. A screening programme for fetal abnormalities began at The Hillingdon Hospital in July 1986. Second trimester ultrasound scans are performed by radiographers. A combined prospective and retrospective study of the ultrasound findings and outcome in all pregnancies delivered in 1989–1990 was undertaken. 6412 babies were born during this period, of whom 6183 (96%) were examined by ultrasound in the second trimester; 29 pregnancies were terminated for fetal abnormality. Of the 89 fetuses who were abnormal at birth or at induced termination of the pregnancy (1.4%), 84 were scanned in the second trimester. In 51 cases the abnormality was detected before 22 weeks gestation (sensitivity, 60.7%). 56 of these 84 abnormal fetuses scanned had potentially lethal or major handicapping abnormalities of which 41 were detected by ultrasound before 22 weeks gestation (sensitivity, 73%). There was one false positive diagnosis of abnormality which did not affect outcome. 6352 babies were normal at delivery or on discharge from hospital (specificity, 99.98%).

About 2% of newborn infants have congenital or genetically determined abnormalities (Royal College of Physicians, 1989). The number of such infants born annually in the UK is currently around 14000. In a district general hospital with a delivery rate of 3000 babies per annum, approximately 60 malformed babies can be anticipated each year. Congenital abnormalities acccount for 20–30% of perinatal deaths (Morrison, 1985) and 90% of infants with congenital malformations and chromosome disorders are born to healthy young women with no identifiable risk factors (Royal College of Physicians, 1989).

An ultrasound scan is relatively cheap and safe and provides much useful information during pregnancy, including gestational age, number and viability of fetuses and placental position (Royal College of Obstetricians and Gynaecologists, 1984; Wells, 1987). The majority of pregnant women in the UK now receive at least one ultrasound scan, most of which are performed by radiographers (Witcombe & Radford, 1986).

There have been a number of recent reports of the ability of pre-natal ultrasound to detect fetal abnormalities (Nicolaides & Campbell, 1987; Romero et al, 1988; Nyberg et al, 1990). Studies of ultrasound screening of low-risk populations have demonstrated the ability of scanning to detect between 40% and 85% of fetal abnormalities (Campbell & Smith, 1983; Rosendahl & Kivinen, 1989; Saari-Kemppainen et al, 1990; Chitty et al, 1991; Levi et al, 1991). In particular, three studies have shown that 39.4%, 21% and 74.4% respectively of malformations were detected before 24, 23 and 24 weeks of gestation (Rosendahl & Kivinen, 1989; Chitty et al, 1991; Levi et al, 1991) thus allowing parents the option of termination of pregnancy.

This report gives our experience of prenatal ultrasound screening of an unselected low risk population in a District General Hospital, the scans being performed by radiographers.

Patients and methods

Since July 1986 all women booking for ante-natal care and delivery at The Hillingdon Hospital have been offered a second trimester detailed ultrasound scan using standard real-time equipment. No routine biochemical screening for fetal abnormality is available. Approximately 3000 women are delivered annually. Scans are performed at 19 weeks gestation by radiographers holding the Diploma of Medical Ultrasound and who have an average of 4 years' experience of obstetric ultrasound. Supervision is given by a consultant Radiologist with wide experience of obstetric ultrasound (I.M.S.).

Scans are performed in the ante-natal clinic to an agreed protocol (Table I). Approximately 15 min is available for each scan and allows assessment of fetal gestational age, viability, number and anatomy and placental position. The fetal anatomical check list is detailed in Table I and recorded in the obstetric notes by the radiographer at the time of scanning. It is important to note that during the period of this study only the fetal facial profile was examined to detect severe bilateral facial clefting. In addition, the presence of limbs was confirmed but they were not studied in detail. If the fetus is less than 18 weeks gestation on scanning, the patient is recalled for a further scan. When the anatomical check cannot be completed for technical reasons, for example unfavourable fetal lie or excessive fetal movement, the patient is recalled during the session

---

*Address correspondence to: Isabel M. Shirley, Consultant Radiologist, The Hillingdon Hospital, Uxbridge, Middlesex UB8 3NN.

Table I. Fetal anomaly scan at 19 weeks

Measurement of biparietal diameter, head and abdominal circumference, femur length, cerebellar diameter and thickness of nuchal soft tissues
Head: anterior and posterior ventricular/hemisphere ratios, cerebellum, facial profile and neck, exclusion of intra-cerebral cysts and defects in cranial vault
Spine: longitudinal and transverse sections
Heart and chest: four chamber view
Diaphragm: stomach below on left
Abdominal wall and cord insertion. Three vessel cord
Exclusion of abdominal masses and cysts. Echogenicity of bowel.
Kidneys and bladder present and normal size
Limbs present
Assessment of amniotic fluid volume
Placental site and appearance

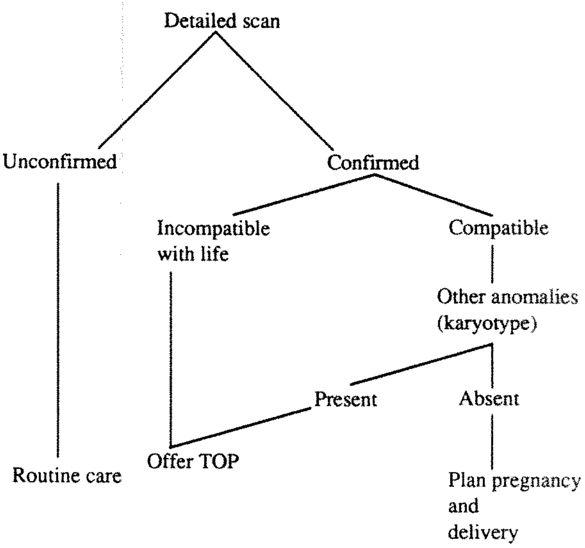

Figure 1. Management of pre-natally diagnosed fetal anomalies.

or on another day. Women are encouraged to bring their partners to share the scan experience and radiographers are trained to communicate with parents to reduce the anxiety produced by screening, as far as is possible. All scans are recorded on video tape for later review if necessary and there is a facility to allow parents to purchase fetal photographs at the time of scanning. If no fetal abnormality is found parents are immediately reassured.

When a fetal abnormality is detected or suspected the mother is referred for further detailed scanning by a radiologist (I.M.S.), in most cases on the same or the following day. As indicated in Fig. 1 if no abnormality is found the mother continues in routine care. If an abnormality is found, parents are counselled as to the findings and prognosis. Some cases are referred to tertiary centres for late karyotyping and/or advice on diagnosis, management and treatment. Most patients return the day after initial counselling for discussion with their consultant obstetrician. All pre-natal diagnoses of fetal abnormality are followed up by photography, plain film radiography, occasional ultrasound imaging of the fetus after delivery and post-mortem examination in the event of fetal demise. Fetal material is routinely obtained for karyotyping when certain abnormalities have been shown (Table II). All newly born babies are examined by midwives and paediatricians prior to discharge from hospital.

Table II. Fetal abnormalities where karyotyping is advised

Abnormality	Possible karyotype
Abnormal nuchal soft tissues	(Trisomy 21, Turner's)
Omphalocele	(Trisomy 13, 18)
Dilated upper renal tracts	(Trisomy 13, 21)
Bilateral facial cleft ± other stigmata	(Trisomy 13)
Diaphragmatic hernia	(Trisomy 18)
Pleural effusions	(Trisomy 21)
Duodenal atresia	(Trisomy 21)
Abnormal fetal heart	(Trisomy 13, 18, 21)
Ventriculomegaly	(Trisomy 21)

We count as congenital abnormalities all anatomical or structural abnormalities present at birth, including malformation, deformation, disruption and dysplasia (Nyberg et al, 1990) and abnormal karyotype. The minor anomalies listed below are excluded (De Wals et al, 1984):

Minor deformity of face or ears
Club foot of postural origin
Clicking hip
Phimosis and hypospadias
Skin lesions
Absent or hypoplastic umbilical artery with no other abnormality
Isolated polydactyly and syndactyly
Functional cardiac murmur
Uncomplicated spina bifida occulta
Congenital hernias

Our various records have been reviewed to ascertain the sensitivity and specificity of our ultrasound screening programme for the detection of congenital abnormalities in 1989–1990.

Results

The annual number of deliveries at The Hillingdon Hospital since 1985 is shown in Table III with the annual totals of abnormal fetuses detected by ultrasound at any stage during the pregnancy and terminations of pregnancy for fetal abnormality. 1.4–1.8% of all babies delivered are congenitally abnormal; the prevalence of congenital abnormalities in our health

Table III. Hillingdon ultrasound programme

	1985	1986	1987	1988	1989	1990
Total babies born	2860	2843	3130	3341	3096	3316
Abnormal fetuses detected	4 (0.14%)	12 (0.4%)	18 (0.57%)	19 (0.57%)	27 (0.87%)	31 (0.93%)
Terminations of pregnancy for abnormality	1	8	12	7	15	14
Perinatal mortality rate	12.9	8.8	7.1	7.8	7.7	7.2

region (North West Thames) in 1989 was 2.3 per 100 births in a total of 40 189 births.

A total of 6441 babies were delivered during the study period. There were 29 terminations of pregnancy for fetal abnormality (Table IV). In 23 (79%) of these cases the fetus had a lethal abnormality. 89 fetuses (1.4%) were abnormal at birth or at induced termination of the pregnancy. One pregnancy, which resulted in the delivery of an infant with spondylo-epiphyseal dysplasia and congenital heart disease, was never scanned in our hospital as a diagnosis of limb shortening had been made elsewhere before booking. A second case of a small sacrococcygeal teratoma was also never scanned owing to maternal anxiety. Therefore, of the 89 abnormal fetuses, 87 were scanned at some stage in our hospital, and fetal abnormality found in 58 (sensitivity, 66.7%). 84 abnormal fetuses (Table V) had a detailed screening scan before 22 weeks gestation and abnormalities were detected in 51 (sensitivity, 60.7%).

During the study period, 14 fetuses with abnormal karyotype were delivered (Table V), all of whom were scanned during pregnancy. Of the 10 cases of Trisomy 21, six had no detectable anatomical abnormality. Of the remaining four cases of Trisomy 21, three were detected before 22 weeks by the screening programme. Two cases, associated with hydrocephaly and abnormally thick nuchal soft tissues respectively, were karyotyped. In the third case, a cardiac defect was found at 19 weeks (atrio-ventricular septal defect), strongly indicating the possibility of Trisomy 21. The mother aged 45 refused fetal karyotyping and continued the pregnancy, delivering a baby with Down's Syndrome and the expected cardiac defect. The fourth case appeared normal at 19 weeks, even on review of the video tape, and was diagnosed by karyotyping in the third trimester following the ultrasound detection of fetal hydrops on scanning for an obstetric indication. The three cases of Trisomy 18 were all detected before 22 weeks following the detection of fetal anatomical abnormalities (see Table V). The single case of triploidy was detected by the finding of severe symmetrical fetal growth retardation in the second trimester. If the six cases of Trisomy 21 with no associated anatomical abnormality are deducted from the 84 abnormal fetuses screened before 22 weeks, sensitivity of detection of abnormality becomes 65.4% (51 of 78). If the 12 cases of facial abnormality and talipes which could not have been detected in our screening programme during the study period are also excluded, sensitivity of detection of abnormality before 22 weeks becomes 77.3% (51 of 66).

Table IV. Termination of pregnancy for fetal abnormality 1989–1990

Neural tube defect	12
Central nervous system	1
Cardiovascular	5
Skeletal (same patient)	2
Syndrome	1
Cystic hygroma	2
Multiple abnormalities	1
Abnormal karyotype	5
Total	29

In addition to these seven cases with abnormal fetal karyotype, a further 12 abnormal fetuses were karyotyped during pregnancy and the karyotype found to be normal.

During the study period, 56 of the 84 abnormal fetuses scanned before 22 weeks had lethal or major handicapping abnormalities, of which 41 were correctly detected by ultrasound before 22 weeks gestation (sensitivity, 73%).

There was one false positive diagnosis of abnormality during the study period. A fetus of 19 weeks gestation was noted to have a 15 mm lesion of the anterior abdominal wall, which was thought to be a small omphalocele. There was no other fetal abnormality. The patient was counselled on the need for karyotyping and referred to a tertiary centre where the diagnosis was changed to haemangioma of the root of the umbilical cord. The lesion became smaller as the fetus grew and the baby was normal at delivery, although the cord was unfortunately not examined histologically. 6352 babies were normal at delivery or on discharge from hospital giving a specificity of 99.98%.

During the study period, there were 73 multiple pregnancies of which two were abnormal. Of the 6366 women delivered or having termination of pregnancy, 26 women were referred to tertiary centres for a second opinion on diagnosis and/or for fetal karyotyping or other investigation or treatment. The diagnosis was confirmed in all cases. An additional eight women at increased risk of fetal congenital heart disease due to maternal diabetes or history were referred to a tertiary centre for confirmation of fetal cardiac normality, which was given in all cases. Our tertiary referral rate was therefore 34 of 6366 (0.5%).

Several cases of minor abnormality were noted in addition to the abnormalities detailed in Table V. There were four cases of mild dilatation of the renal pelvis, in

Table V. Fetal abnormalities in pregnancies screened before 22 weeks

Abnormalities diagnosed	Abnormalities not diagnosed
Neural tube defects	
3 spina bifida and hydrocephaly	
8 anencephaly (1 twin)	
2 anencephaly and spina bifida	
1 encephalocele	
Central nervous system	
2 hydrocephaly	1 hydrocephaly
Cardiovascular	
1 tricuspid atresia	1 tricuspid atresia and transposition
1 dysplastic tricuspid	1 truncus
1 double outlet RV and VSD and pulmonary stenosis	1 pulmonary atresia
1 coarctation	1 total anomalous pulmonary venous drainage
1 double inlet, double outlet single ventricle	
Pulmonary	
2 diaphragmatic hernia	1 diaphragmatic hernia and bowel malrotation (twin)
1 congenital cystic adenomatoid malformation (Type 3)	
1 pulmonary hypoplasia (PROM)	
Face	
2 bilateral cleft lip and palate	3 unilateral cleft lip and palate
1 unilateral cleft lip and palate	2 cleft palate
	1 cleft lip
Gastro-intestinal tract	
1 omphalocele	1 ileal atresia
1 gastroschisis	
Renal	
1 multicystic kidney and PUJ	1 bilateral renal dysplasia
2 unilateral moderate hydronephrosis	1 posterior urethral valves
4 bilateral moderate hydronephrosis	
Skeletal	
1 achondrogenesis	4 unilateral talipes
1 unilateral femoral hypoplasia	2 bilateral talipes
Syndrome	
1 Meckel's	
Other	
2 cystic hygroma	4 multiple abnormalities
2 multiple abnormalities	1 hydrops fetalis
Abnormal karyotype	
3 Trisomy 18	
1 omphalocele	
1 omphalocele and CHD	
1 non-immune hydrops	
3 Trisomy 21	7 Trisomy 21
1 hydrocephaly	6 normal anatomy
1 congenital heart disease	1 fetal hydrops
1 abnormal nuchal soft tissues	
1 triploidy	
Total = 51 + 33 = 84	

RV, right ventricle; VSD, ventricular septal defect; PROM, premature rupture of membranes; PUJ, pelviureteric junction obstruction; CHD, congenital heart disease.

two cases bilateral. All were confirmed post-natally and are probably within normal limits, according to present knowledge. A further six cases had choroid plexus cysts which resolved by 26 weeks gestation. All these babies are included in the 6352 normal babies delivered and have been excluded from the abnormalities in the sensitivity and specificity calculations.

Discussion

There are differing views on the efficacy of routine ultrasound screening in pregnancy. Screening enables the early detection of multiple pregnancies (Grennert et al, 1978), determination of true gestational age (Campbell et al, 1985), assessment of fetal growth (Rosendahl & Kivinen, 1988), and detection of congenital abnormalities (Campbell & Smith, 1983; Rosendahl & Kivinen, 1989; Saari-Kemppainen et al, 1990; Chitty et al, 1991; Levi et al, 1991). Early studies (Bennett et al, 1982; Bakketeig et al, 1984; Neilson et al, 1984) showed no improvement in pregnancy outcome with routine ultrasound. By contrast, Eik-Nes et al (1984) and Waldenstrom et al (1988) showed a decrease in the rate of labour inductions in the screened group. Waldenstrom et al also found that babies in the screened group had higher birth weights relative to controls. The failure of all these randomized trials to show a significant decrease in peri-natal mortality suggests limited sample size according to Thacker (1985), poor detection of congenital abnormalities or a low rate of termination of pregnancy for fetal abnormality. A recent controlled study of 9310 women by Saari-Kemppainen et al (1990), has shown that peri-natal mortality was significantly lower in the screened than in the control group (4.6/1000 *vs.* 9.0/1000) and that this 49.2% reduction in peri-natal mortality in the screened group was mainly due to improved early detection of major fetal malformations leading to termination of pregnancy.

In our study peri-natal mortality was 7.5/1000. Of the 29 terminations of pregnancy for fetal abnormality, 23 (79%) were associated with lethal abnormalities (3.6/1000). Of the 48 peri-natal deaths 11 were due to congenital abnormality (1.7/1000). In 10 cases this had been detected by ultrasound during the pregnancy and the parents were counselled with consequent opportunity for some emotional adjustment. In six of these 10 cases the diagnosis had been made before 22 weeks gestation and termination of pregnancy refused. We therefore believe that ultrasound screening of all pregnancies at 19 weeks gestation has the potential to reduce peri-natal mortality by allowing consideration of termination of pregnancy for major fetal abnormality.

In this study eight babies had early neonatal surgery with a good outcome in five. In six of these eight cases the diagnosis had been made by ultrasound pre-natally, in four cases by the screening scan at 19 weeks. This suggests that there is the potential for peri-natal mortality to be further reduced by appropriate management of the delivery and early neonatal care, when abnormality has been detected pre-natally. In the future pre-natal treatment of some of these disorders may also be possible.

This study has shown that routine ultrasound screening by radiographers at 19 weeks gestation of women at normal risk of fetal abnormality has a sensitivity of 60.7% in detecting all abnormal fetuses, including those with abnormalities at the more minor end of the spectrum and those with abnormal karyotype without structural abnormality. The sensitivity of detection of lethal or major handicapping abnormalities was 73%. Specificity was 99.98%.

There are no other studies in the literature which allow direct comparison of results, as there are differences in the reporting of congenital abnormalities. Campbell and Smith (1983) reported the detection of 85% of major fetal anomalies between 1978 and 1983 in a unit with a special interest in obstetric ultrasound. The study of Rosendahl and Kivinen (1989) ran from 1980 to 1988 and reported a sensitivity of detection of fetuses with major malformations of 41.7% by ultrasound at 18 weeks gestation and specificity of 99.9%. Sensitivity rose to 63.8% when a second scan at 34 weeks gestation was added. Saari-Kemppainen et al (1990) found a sensitivity of detection of 76.9% of major fetal abnormality in one of the two hospitals in the Helsinki trial between 1986 and 1988. Levi et al (1991) have published the results of the Belgian Multicentre Trial (1984–1989) in which scanning between 12 and 20 weeks had a sensitivity of detection of abnormality of 21%. When later scans were added sensitivity of detection rose to 40.4%. The specificity was 99.9%. Most recently Chitty et al (1991) have reviewed the efficacy of routine ultrasonography for detecting fetal structural abnormalities in a low risk population in a British District General Hospital. The sensitivity of detection of fetal structural abnormality by ultrasound before 24 weeks gestation was 74.4%. This study did not include babies with abnormal karyotype but no structural abnormality in the sensitivity calculations. From the data given, if these 15 babies are added, sensitivity of detection of fetuses with congenital abnormality was 66% in this study.

Levi et al (1991) have described the criteria which routine ultrasound screening must meet. These may be summarized as:

The sensitivity must be high enough.
The specificity must be high.
Patients should find it comfortable and convenient.
It must be safe for mother and fetus.
Effective therapy should be available for problems detected.
It should be cost effective.

We suggest that the sensitivity and specificity of our programme are sufficiently high for screening purposes. Analysis of abnormalities not detected by screening scans at 19 weeks in our study suggests that the detection of a further 15 abnormal fetuses might have been possible with our current extended protocol. Therefore, we disagree with the recent conclusion of Pitkin (1991) that ultrasound seems to be of little potential as a means of screening for congenital malformation because of relatively low sensitivity. We agree that the cost effectiveness of programmes like ours has not yet been proven and hope to study this soon.

Could the results of this study and that of Chitty et al (1991) be obtained in other District General Hospitals in the UK? With appropriate training for radiographers and supervising doctors and the necessary equipment and conditions of work, we think that the answer is probably yes. Since most patients are already being scanned by radiographers (Witcombe & Radford, 1986), there is the potential for a national screening programme in the future. However, since a fetal anatomical survey adds approximately 10 min to each scan, further resources would be required. Studies of the effectiveness of programmes like ours, including cost benefit analyses, are urgently needed.

Acknowledgments

We would like to thank Dr Samuel Ashebu, Commonwealth Medical Fellow, for his help in collecting data for this study, all radiographers involved in the Hillingdon scanning programme and obstetricians at The Hillingdon Hospital.

References

Bakketeig, L. S., Eik Nes, S. H., Jacobsen, G., Ulstein, M. K., Brodtkorb, C. J., Balstad, P., Eriksen, B. C., Jorgensen, N. P., 1984. Randomised controlled trial of ultrasonographic screening in pregnancy. *Lancet, II*, 207–211.

Bennett, M. J., Little, G., Dewhurst, J. & Chamberlain, G., 1982. Predictive value of ultrasound measurement in early pregnancy: a randomised controlled trial. *British Journal of Obstetrics and Gynaecology, 81*, 338–341.

Campbell, S. & Smith, P., 1983. Routine screening for congenital abnormalities by ultrasound. In *Pre-natal Diagnosis. Proc. 11th Study Group of the Royal College of Obstetricians and Gynaecologists*, ed. by C. R. Rodeck & K. N. Nicolaides (Royal College of Obstetricians and Gynaecologists, London), pp. 325–330.

Campbell, S., Warsof, S. L., Little, D. & Cooper, D. J., 1985. Routine ultrasound screening for the prediction of gestational age. *Obstetrics and Gynecology, 65*, 613–620.

Chitty, L. S., Hunt, G. H., Moore, J. & Lobb, M., 1991. Effectiveness of routine ultrasonography in detecting fetal structural abnormalities in a low risk population. *British Medical Journal, 303*, 1165–1169.

De Wals, P., Mastroiacovo, P., Weatherall, J. A. C. & Lechat, M. F., 1984. *Eurocat Guide* (Catholic University, Louvain) p. 65.

Eik Nes, S. H., Okland, O., Aure, J. C. & Ulstein, M., 1984. Ultrasound screening in pregnancy: a randomised controlled trial. *Lancet, I*, 1347.

Grennert, L., Persson, P. H. & Gennser, G., 1978. Benefits of ultrasonic screening of the pregnant population. *Acta Obstetrica et Gynecologica Scandinavica (Supplement), 78*, 5–17.

Levi, S., Hyjazi, Y., Schaaps, J. P., Defoort, P., Coulon, R. & Buekens, P., 1991. Sensitivity and specificity of routine ante-natal screening for congenital anomalies by ultrasound: The Belgian Multicentric Study. *Ultrasound in Obstetrics and Gynecology, 1*, 102–110.

Morrison, I., 1985. Perinatal mortality: basic considerations. *Seminars in Perinatology, 9*, 144–150.

Neilson, J. P., Munjanja, J. P. & Whitfield, C. R., 1984. Screening for small for dates fetuses: a controlled trial. *British Medical Journal, 289*, 1179–1182.

Nicolaides, K. H. & Campbell, S., 1987. Diagnosis and management of fetal malformations. *Baillieres Clinical Obstetrics and Gynaecology, 1*, 591–622.

Nyberg, D. A., Mahony, B. S. & Pretorius, D. H., 1990. *Diagnostic Ultrasound of Fetal Anomalies* (Yearbook Medical Publishers, Chicago).

Pitkin, R. M., 1991. Screening and detection of congenital malformation. *American Journal of Obstetrics and Gynecology, 164*, 1045–1048.

Romero, R., Pilu, G., Jeanty, P., Ghidini, A. & Hobbins, J. C., 1988. *Pre-natal Diagnosis of Congenital Anomalies* (Appleton and Lange, Norwalk).

Rosendahl, H. & Kivinen, S., 1988. Routine ultrasound screening for early detection of small for gestational age fetuses. *Obstetrics and Gynecology, 71*, 518–521.

Rosendahl, H. & Kivinen, S., 1989. Ante-natal detection of congenital malformations by routine ultrasonography. *Obstetrics and Gynecology, 73*, 947–951.

Royal College of Obstetricians and Gynaecologists, 1984. *Report of a Working Party on Routine Ultrasound Examination in Pregnancy* (Royal College of Obstetricians and Gynaecologists, London), pp. 29–49.

Royal College of Physicians, 1989. *Pre-natal Diagnosis and Genetic Screening. Community and Service Implications.* (Royal College of Physicians, London).

Saari-Kemppainen, A., Karjalainen, O., Ylostalo, P. & Heinonen, O. P., 1990. Ultrasound screening and perinatal mortality: controlled trial of systematic one-stage screening in pregnancy. *Lancet, 336*, 387–391.

Thacker, S. B., 1985. Quality of controlled clinical trials. The case of imaging ultrasound in obstetrics: a review. *British Journal of Obstetrics and Gynaecology, 92*, 437–444.

Waldenström, U., Axelsson, O., Nilsson, S., Eklund, G., Fall, O., Lindeberg, S., Sjodin, Y., 1988. Effects of routine one stage ultrasound screening in pregnancy: a randomised controlled trial. *Lancet, II*, 585–588.

Wells, P. N., 1987. The prudent use of diagnostic ultrasound. *Ultrasound in Medicine and Biology, 13*, 391–400.

Witcombe, J. B. & Radford, A., 1986. Obstetric ultrasonography: wider role for radiographers? *British Medical Journal, 292*, 113–115.

1992, *The British Journal of Radiology*, 65, 570–575

A study of the relationship between routine ultrasound quality assurance parameters and subjective operator image assessment

By S. C. Metcalfe, HNC and J. A. Evans, BSc, MSc, PhD

Department of Medical Physics, Leeds General Infirmary, Leeds LS1 3EX, UK

Based on a poster presented at the BMUS 23rd Annual Meeting in Bournemouth, on 10–12 December 1991

Keywords: Ultrasound, Quality assurance, Subjective perception

Abstract. Comparisons have been made between a number of routine quality assurance (QA) measurements and a number of related subjective aspects of image quality. These comparisons between lateral resolution and perceived definition, dynamic range and subjective grey-level assessment, and slice thickness and overall image quality appraisal showed very poor correlation. We deduce from this that other QA parameters are needed to quantify good image quality as defined by the operators.

Ultrasound quality assurance (QA) techniques have been reported widely for many years, and many groups have suggested protocols (American Institute for Ultrasound in Medicine and Biology (AIUM), 1974; Brendel et al, 1976; Goldstein, 1980; Banjavic, 1983; International Electrotechnical Commission (IEC), 1986). Comments on the identification and nature of appropriate parameters have also been published (Powis & Powis, 1984; DHSS, 1987) and these have cited high resolution and wide dynamic range as being fundamental requirements for good image quality. The most recent development has been the publication of a British Standard, BS 5724 (British Standards Institution (BSI), 1990), which relies heavily on the principle of tissue-mimicking test objects and identifies a number of quantities such as penetration, dynamic range, resolution, dead zone and magnification error as being important.

However, assessment of the efficacy and relevance of ultrasound QA procedures is rare. One example is the work of Donofrio et al (1984), who looked at the effectiveness of a number of QA tests in the diagnosis of scanner malfunction. An "Ultrasound Equipment Evaluation Project" (UEEP) report (Common Services Agency (CSA), 1991) explored the relationship of technical tests to clinical assessment, but this was specific to cardiac ultrasound scanners and did not compare individual parameters. Hill et al (1991) have recently reviewed the physical factors responsible for ultrasonic image formation and compared them with knowledge in the fields of visual physiology and psychophysics. They concluded that echography may benefit from the application of some of this knowledge and the use of some parameters developed in these fields.

In this study, we have examined the correlation between objective QA parameters, as specified by BS 5724 (BSI, 1990), with a number of subjective assessment parameters. In order to reduce some of the variabilities inherent in any subjective evaluation, the study has been restricted to assessment of specific aspects of the quality of a number of images. These images, of the same anatomy of a normal volunteer, were obtained by only two experienced operators on a number of systems, using normal scanning procedures. These images have been evaluated by 43 ultrasound users. The results of this subjective evaluation were then compared with QA measurement results carried out on the same scanners.

Methods

Subjective image assessment

Images were acquired by two experienced operators from a normal female volunteer. Two anatomical regions were scanned: the liver and right kidney [illegible] 1a) and the uterus (Fig. 1b). The first image obtai[illegible] each case was used as a reference and the operat[illegible] to replicate that anatomical section as closely as p[illegible] on all subsequent scans. Within this constraint[illegible] operator was asked to obtain the "best" image usi[illegible] their own subjective judgment. A total of nine scanners was used and a selection of the available transducers employed where appropriate. This gave a total of 14 different scanner/transducer combinations.

The liver and uterus images were digitized and stored using a video frame grabber (PCVISION*plus*, Imaging Technology, Woburn, MA) controlled via a model 286 PC. The frame grabber has dual 512 × 512, 8-bit frame stores, and a digitization rate of 10 MHz. Gain and offset adjustments were used to ensure that the same peak white and background black were maintained for all scanners. The same hard-copy device (with constant settings) was then used to obtain transparencies of the images on standard radiographic film. It is apparent that the range of echo brightness levels obtained from different scanners is quite variable. The possibility of operator inconsistency cannot be ruled out, but it was

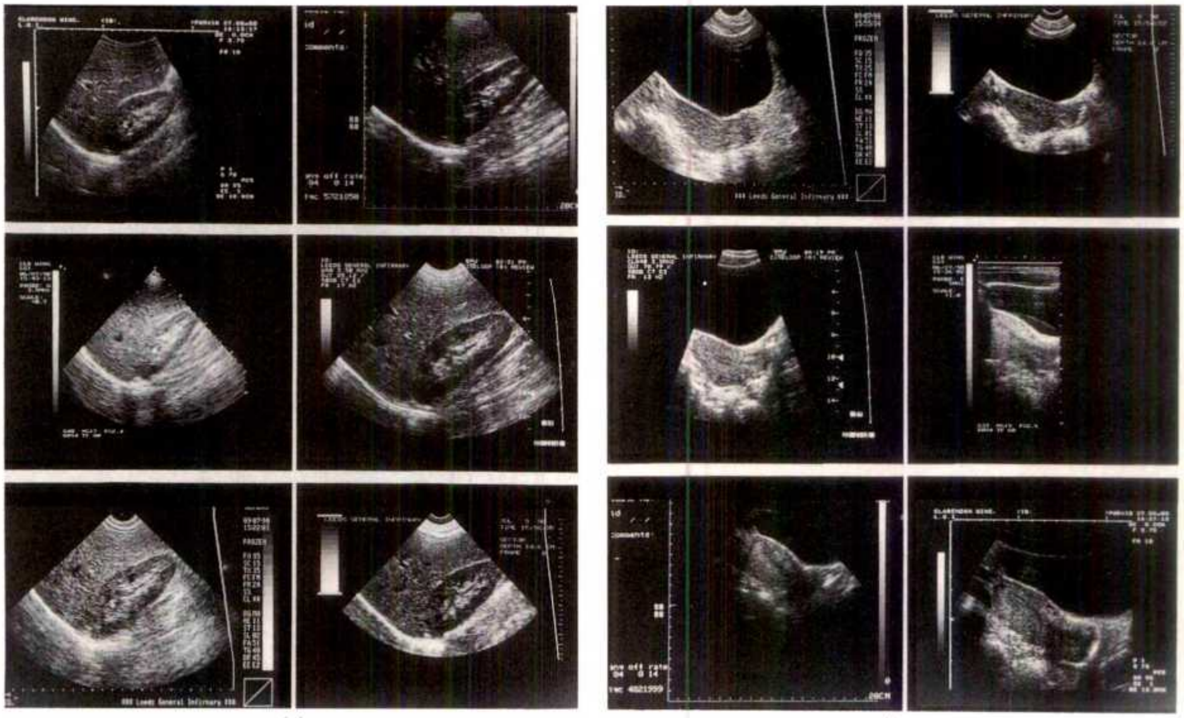
(a) (b)

Figure 1. A selection of typical images presented for subjective assessment showing (a) the liver and kidney and (b) the uterus of a normal volunteer. Note: The grey-level brightness levels are not faithfully reproduced in the photographs used for this figure.

felt that the procedures adopted minimized such variations. The transparencies presented to each observer contained images from several scanners and therefore it is assumed that each image was viewed under the same conditions. The possibility of different viewing conditions between observers was not allowed for, but it is nlikely that this would introduce any systematic achine bias.

f the images obtained, 20 were chosen (12 uterus d eight liver images) to represent a cross-section of canners (ranging in age from about 10 years to just a few months) and transducers used (including mechanical sectors and electronic curved, phased and linear arrays). These 20 images were then presented in a questionnaire in which participants were asked to rate the images in terms of a number of parameters (discussed later).

The questionnaire consisted of four sections requesting information regarding (i) level of experience; (ii) details of scanner use and operator assessment; (iii) assessment of the images presented; and (iv) other comments. For this study, only data from sections (ii) to (iv) were required, although further work is planned to examine the possible influence of operator experience.

The scanners and images were assessed in terms of the following categories:

Overall image quality;
Definition/resolution;
Range of grey levels;
Noise and artefact;
Graininess.

These categories were selected following preliminary discussion with ultrasound users to determine subjective performance evaluators. Therefore no attempt was made to produce precise definitions of these terms and this remains an important area for future investigation.

Overall image quality was included to record the participant's general impression of the image. This was the baseline category to determine if the image was considered "good" or "bad"; the subsequent categories were used to explore the basis for this judgment.

Definition and resolution are considered by some to be synonymous. Resolution is thought to be important in determining visibility of fine detail and small structures, but definition is perhaps a much broader parameter describing detectability, particularly of edges (Rosenfeld & Thurston, 1971).

Range of grey levels was included as a category to cover the effects of contrast, dynamic range and transfer curve characteristics, which are thought to be important for diagnoses of tissue pathology.

Noise and artefact and "graininess" (a term used to describe speckle texture) were included as other features that may determine image quality, but are not common QA parameters and so are not analysed as part of this initial study.

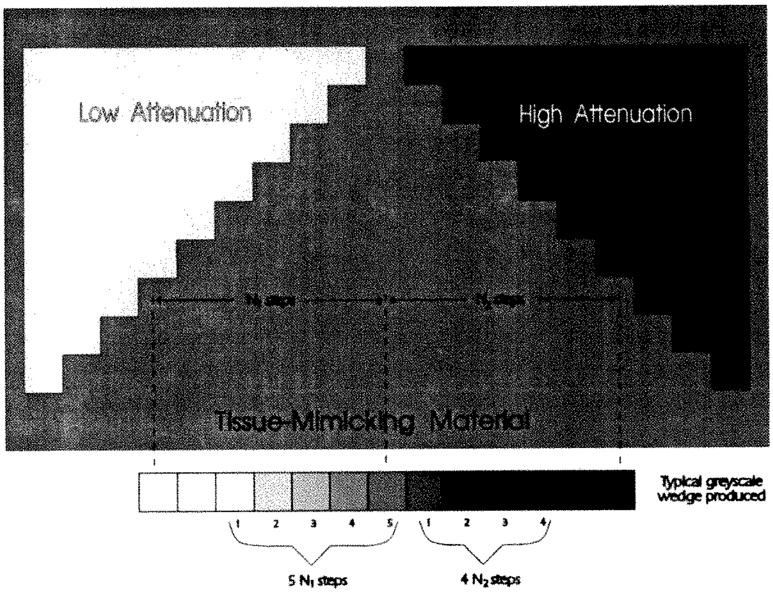

Figure 2. The Cardiff Grey-scale Test Object showing identification of N_1 and N_2 steps on a typical image.

Penetration, although a common QA measurement, was not included as a category because it was considered unlikely to be a major contributing factor to operator assessment. The work of Donofrio et al (1984) supports this view. Calliper accuracy and dead zone were also excluded for similar reasons.

The participants were asked to rate performance in each of the above categories on a 5-point scale: 5, very good; 1, very poor.

Objective QA assessment

Routine QA measurements are conducted on ultrasound scanners throughout west Leeds using Cardiff Grey-scale and Resolution Test Objects (Gammex RMI, Nottingham). These measurements are performed by a single operator who was not involved in the acquisition or subjective assessment of the *in vivo* images. Records of QA results were therefore available for the scanner/transducer combinations used for the questionnaire images. The parameters routinely measured include: penetration, dynamic range, dead zone, slice thickness and lateral and axial resolution. The measurement methods used are similar to those described in BS 5724 (BSI, 1990) except that all measurements are made at "scanning gain settings" (to give an even mid-grey speckle to the maximum penetrable depth when imaging an homogeneous region of tissue-mimicking material). These settings were not identical to those used for the *in vivo* images, but the mean speckle pattern brightness was similar to that obtained from parenchymal echoes. The "70% dark threshold" criteria required for "measurement gain" settings has been found difficult to implement reproducibly and is considered not representative of clinical settings.

Of the parameters measured, it was suggested that the following correlations may be expected with the subjective categories assessed in the questionnaire:

1. Dynamic range measurement: "range of grey levels" assessment.
2. Lateral resolution measurement: definition/resolution assessment.
3. Slice thickness measurement: overall image quality assessment.

The reason for the first two comparisons was to check the commonly held belief that these subjective and objective parameters are linked. The decision for inclusion of the latter comparison follows a recent UEEP report (CSA, 1991). This was aimed at evaluating cardiac ultrasound scanners (both subjectively and objectively) and concluded that slice thickness was a significant factor in distinguishing good image quality in such machines. We were interested to see if this applied to other, more general ultrasound systems.

The dynamic range, lateral resolution and slice thickness for each scanner/transducer combination under test were recorded and each was scored using a system described below.

Dynamic range was recorded as the number of N_1 and N_2 steps visualized under the low- and high-attenuation inserts of the Cardiff Grey-scale Test Object, respectively (Fig. 2). These numbers are converted to a dynamic range expressed in decibels using the following equation:

$$\text{Dynamic range} = N_1(1.4f+0.3)+N_2(0.6f+0.1)\ \text{dB}$$

where f is the measured peak frequency (in MHz) of the pulses generated by the ultrasound system, found by spectrum analysis.

Lateral resolution and slice thickness were scored

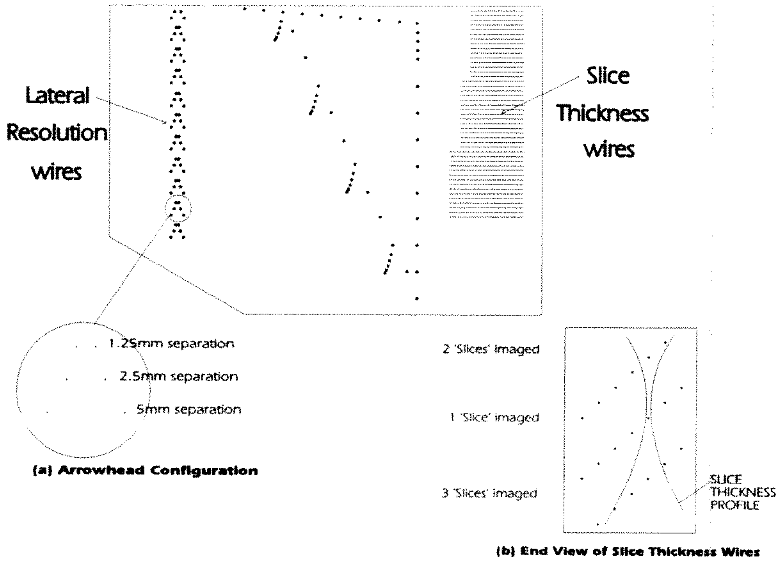

Figure 3. The Cardiff Resolution Test Object showing groups of wires used for measurement of (a) lateral resolution (arrowhead configuration) and (b) slice thickness.

according to the range of depths over which resolution/slice thickness was $\leqslant 3$ mm. Lateral resolution is assessed using the arrowhead arrangements of wires in the Cardiff resolution test object (Fig. 3a) and is estimated to ±1 mm depending on the separation perceived between imaged wires. Local tests have shown that inter- and intra-observer reproducibility is adequate for this method. Slice thickness is recorded as the maximum number of "slice thickness wires" (Fig. 3b) imaged at a number of depths. The wires are positioned 3 mm apart, therefore allowing slice thickness to be quoted in millimetres (*e.g.* 1 wire $\equiv <3$ mm; 1–2 wires $\equiv$ 3 mm; 2 wires $\equiv$ 3–6 mm).

Results and discussion

Comparisons of lateral resolution *vs.* "definition", dynamic range *vs.* "grey levels" and slice thickness *vs.* "overall image quality" all showed poor correlation (Fig. 4).

It was expected that the lateral resolution would be strongly correlated with "definition" as this is often considered to be an important factor in determining perception of detail. It is possible that the interpretation of "definition" was not the same for all observers, although the relative consistency of the responses (standard error typically, 0.12, see Fig. 4a) indicated that this was not the case. It is likely that parameters other than resolution, such as edge detection algorithms, contrast and noise, contribute to the overall perception of definition. The quantification of these parameters would therefore seem to be a reasonable objective for further work in this area. The relationship between spatial resolution and the perception of speckle may also merit further study. Good resolution tends to be associated with a fine speckle pattern (Wagner et al, 1988) and it might be hypothesized that this makes the image appear too "grainy" or "noisy". In clinical practice, temporal smoothing of the ultrasound image, to reduce the graininess of the speckle pattern, may be preferred despite loss of spatial information.

The correlation between dynamic range and assessment of grey levels was found to be even poorer (Fig. 4b). This is not surprising as dynamic range is just one feature of the grey-level characteristics of a system. Grey-level transfer curves are therefore currently being evaluated to try to quantify other characteristics that correlate better with the users' grey level assessment. Further work is also proposed to investigate whether increased dynamic range systems are also more susceptible to electronic noise, therefore compromising image quality.

The correlation between slice thickness and image quality reported in the recent UEEP survey (CSA, 1991) was not confirmed in this assessment of general purpose scanners used for imaging abdominal organs (Fig. 4c). Good spatial resolution is of great importance for ultrasound cardiac studies and most modern cardiac machines generally have good lateral and axial resolution although the slice thickness is perhaps more variable. In ultrasound examination of the abdomen, it is important to image the grey-scale characteristics of soft-tissue organs and contrast resolution is a more significant factor. Contrast resolution may not be linked with slice thickness and this could account for the discrepancy in results between this study and the UEEP report.

Further work is needed to see if some measure of overall image quality can be found for other ultrasound cases. In particular, the possible contribution of contrast-detail measurements (Smith et al, 1985) should be examined. Hill et al (1991) suggest that factors used in image science may be useful, and specific mention is made of the "modulation transfer function area"

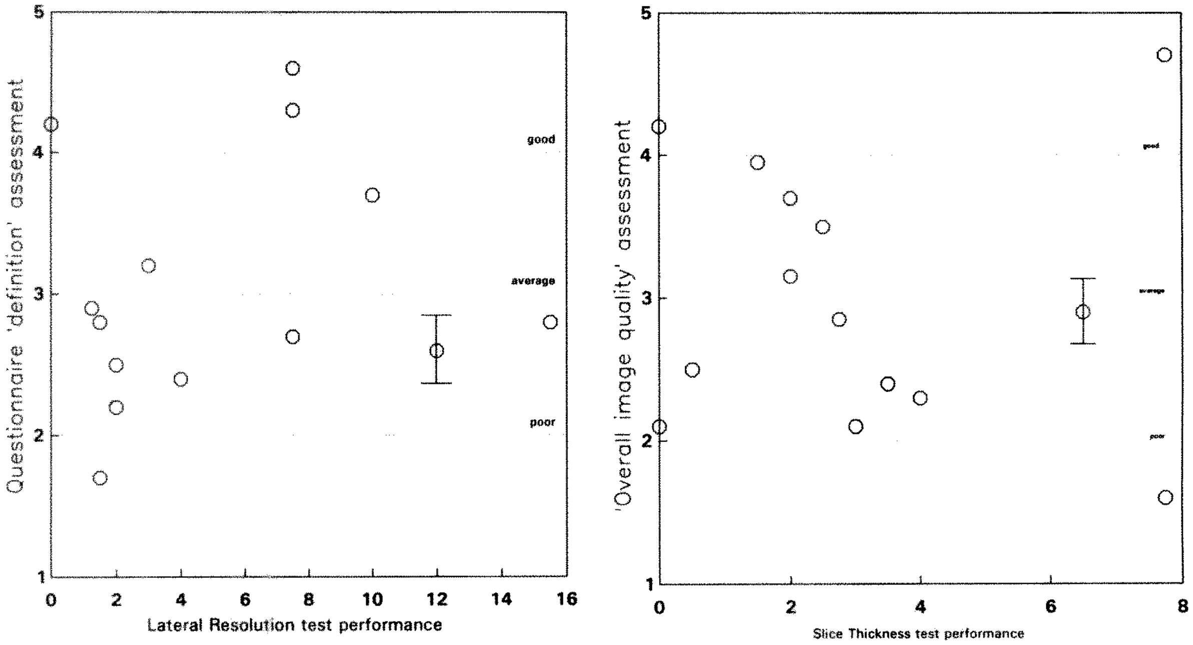

(a)

(b)

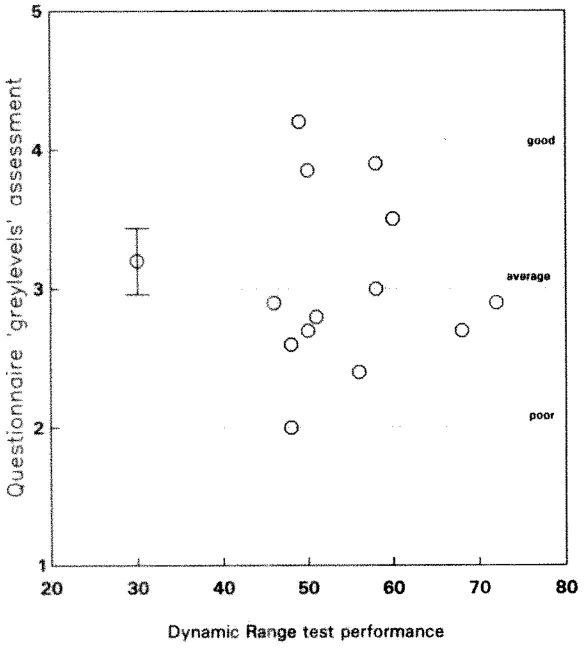

(c)

Figure 4. Scatter plots of objective QA measurements *vs.* subjective image assessment categories. (a) Lateral resolution measurement *vs.* "definition" assessment; (b) slice thickness measurement *vs.* "overall image quality" assessment; (c) dynamic range measurement *vs.* "range of grey levels" assessment. A single vertical error bar is shown in each graph representing ±2 standard errors, typical of all points.

(MTFA) parameter, which has been successfully used elsewhere.

Conclusions

The hypothesis that measurements of resolution (including slice thickness) and dynamic range are necessary and sufficient components for assuring ultrasound image quality is not supported. Although these are undoubtedly important characteristics, the results obtained in this study suggest that they are not adequate to describe good image quality as perceived by the operator. It would appear that more (or perhaps different) parameters are needed for quality assurance. There is a need for further work to identify appropriate parameters and measurement methods.

Acknowledgment

We would like to gratefully acknowledge the participation of all 43 observers who took the time to fill in the questionnaires. In particular, we would like to thank the two operators, Miss S. Kell and Mrs M. Ward, for their assistance in compiling the selection of *in vivo* images.

References

AIUM, *Standard 100 mm Test Object Manual* AIUM Publication 331, (AIUM, Bethesda, Maryland, USA).

Banjavic, R. A. 1983. Design and maintenance of a quality assurance program for diagnostic ultrasound equipment. *Seminars in Ultrasound, 4*(1), 10–26.

Brendel, K., Filipczynski, L. S., Gerstner, R., Hill, C. R., Kossoff, G., Quentin, G., Reid, J. M., Saneyoshi, J., Somer, J. C., Tcherneko, A. A. & Wells, P. N. T., 1976. Methods of measuring the performance of ultrasonic pulse-echo diagnostic equipment. *Ultrasound in Medicine and Biology, 2,* 343–350.

BSI, 1990. British standard medical electrical equipment: Particular requirements for performance—Methods for declaring parameters for ultrasonic diagnostic equipment using test objects, BS 5724 part 3, section 3.26. Obtainable from BSI, 2 Park Street, London W1A 2BS, UK.

CSA, 1991. *Comparative Evaluation of Imaging and Doppler Ultrasound Systems for the Examination of the Heart,* CSA Report EEV/91/3. Available from CSA, Supplies Division, Trinity Park House, South Trinity Road, Edinburgh EH5 3SH, UK.

DHSS, 1987. *Explanatory Notes for Interim Reports of the Ultrasonic Equipment Evaluation Project.* In *Assessment of Ultrasound Scanners,* Report STD/87/8 (Department of Health and Social Security, London).

Donofrio, N. M., Hanson, J. A., Hirsch, J. H. & Moore, W. E., 1984. Investigating the efficacy of current quality assurance performance tests in diagnostic ultrasound. *Journal of Clinical Ultrasound, 12,* 251–260.

Goldstein, A., 1980. *Quality Assurance in Diagnostic Ultrasound: A Quality Assurance Manual for the Clinical User,* HHS Publication, FDA 81-8139, Oklahoma.

Hill, C. R., Bamber, J. C., Crawford, D. C., Lowe, H. J. & Webb, S., 1991. What might echography learn from imaging science? *Ultrasound in Medicine and Biology, 17*(6), 559–575.

IEC, 1986. *Methods of Measuring the Performance of Ultrasonic Pulse-Echo Diagnostic Equipment,* IEC publication no. 854 (IEC, Geneva).

Powis, R. L. & Powis, W. J., 1984. *A Thinker's Guide to Ultrasonic Imaging* (Urban & Schwarzenberg, Baltimore).

Rosenfeld, A. & Thurston, M., 1971. Edge and curve detection for visual scene analysis. *IEEE Transactions on Computers, C-20,* 562–569.

Smith, S. W., Lopez, H. & Bodine, W. J., 1985. Frequency independent ultrasound contrast-detail analysis. *Ultrasound in Medicine and Biology, 11*(3), 467–478.

Wagner, R. F., Insana, M. F. & Smith, S. W., 1988. Fundamental correlation lengths of coherent speckle in medical ultrasound images. *IEEE Transactions on Ultrasonics, Ferroelectrics and Frequency Control, 35*(1), 34–44.

1992, *The British Journal of Radiology*, *65*, 576–580

A role for ultrasound in limb lengthening

By N. D. J. Derbyshire, MRCP and A. H. R. W. Simpson, FRCS

Departments of Radiology and Surgery, Nuffield Orthopaedic Centre NHS Trust, Windmill Road,
Headington, Oxford OX3 7LD, UK

Based on a paper presented at the BMUS 23rd Annual Meeting in Bournemouth, on 10–12 December 1991

Keywords: Ultrasound, Limb lengthening, Callotasis

Abstract. The distraction gap at eight sites in six patients undergoing limb lengthening was monitored by both standard radiographs and ultrasound. Using the measurements obtained we were able to assess the rate and quality of callus formation at the distraction site, something that radiographs alone do not enable one to do. We suggest that ultrasound has a valuable role to play in gauging the optimum rate of lengthening for a particular patient and commend it as a technique to complement radiographs in the follow-up of the increasing numbers of patients undergoing distraction osteogenesis.

An increasing number of patients now present to orthopaedic surgeons with short stature or unequal leg lengths in the hope of benefiting from limb lengthening procedures, which have become more popular with improvements in their success rate. The technique pioneered in Russia by Ilizarov is now widely used in Europe and America. This method involves stabilizing the limb with an external fixation frame and dividing the bone. After a post-operative period of 5–14 days, controlled distraction of the bone is produced by the external frame usually at a rate of 1 mm per day. The distraction is continued until the required length is achieved, and then a period of consolidation allows the new bone to strengthen.

Accurate imaging is required to monitor this process. Traditionally, radiographs have been used to monitor new bone formation and measure the bone gap at the corticotomy site; however, callus formation in the bone gap is typically not seen on radiographs within the first month and in some cases considerably longer (Fig. 1). This limitation results in uncertainty during the initial stages of the procedure as to the success and appropriate rate of the osteogenesis. The clinician, therefore, cannot tell whether good quality bone is forming and he/she may stop, slow down or even reverse the lengthening, or conversely proceed at too rapid a rate.

This study was designed to evaluate the role of ultrasound during limb lengthening with the aim of optimizing the procedure in terms of duration and outcome.

Materials and methods

We studied eight lengthening gaps in six patients, four males and two females, with ages between 8 and 28 years, who were undergoing limb lengthening by the Ilizarov technique. The indications for limb lengthening procedures were post-traumatic growth arrest (1), Ollier's disease (1), infantile bone infection (1), congenital hemiatrophy (2) and adult bone infection (1). Ultrasound examinations of the distraction site using a 10 MHz or 7.5 MHz transducer were performed at regular intervals as described by Young et al (1989). Measurements were made of the gap between the

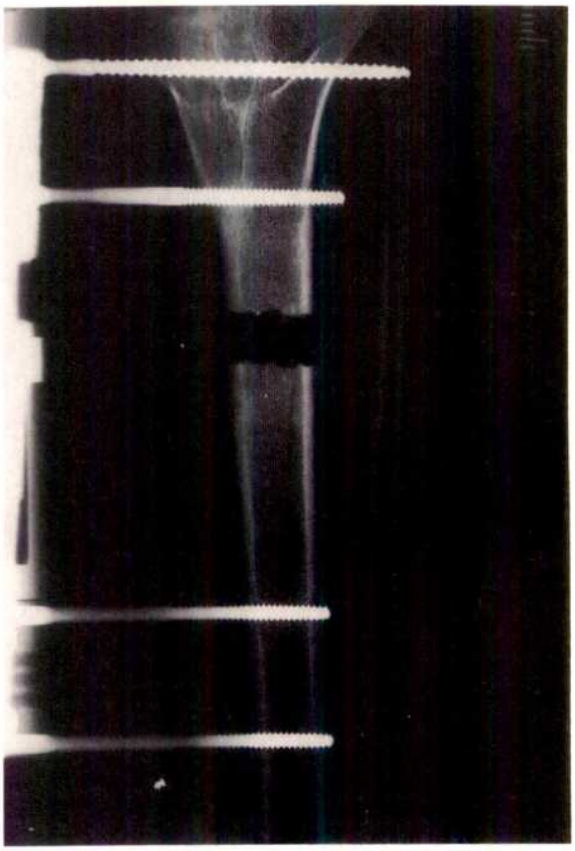

Figure 1. Radiograph of distraction site with minimal callus formation.

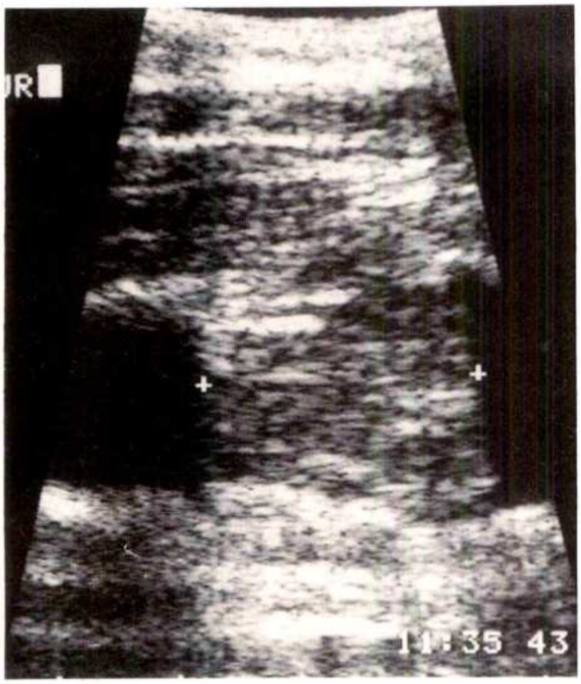

Figure 2. Sonographic appearance of distraction site showing a uniform lamellar pattern of echoes. The markers indicate the margins of mature callus.

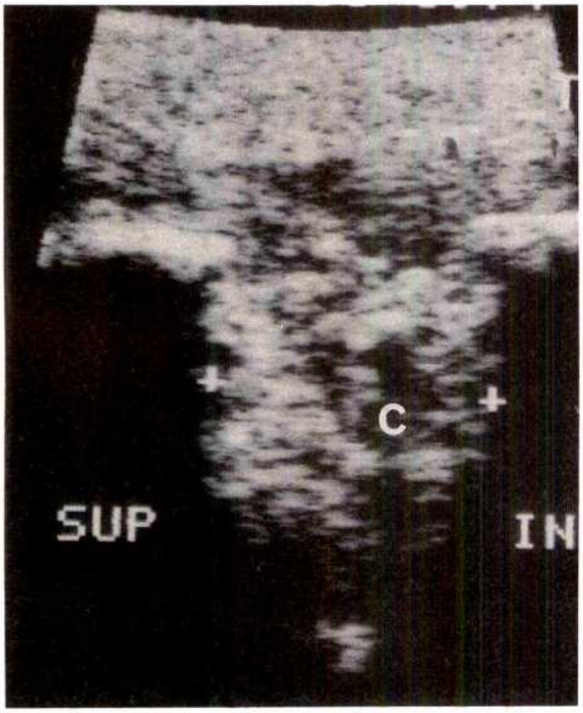

Figure 3. Sonographic appearance of the distraction site showing a small area of reduced echogenicity resulting from early cyst (C) formation.

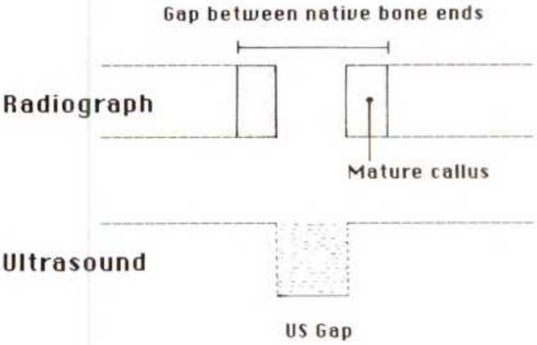

Amount of callus = Gap between native bone ends minus ultrasound gap

Figure 4. Diagram to illustrate the relationship between the native bone ends, mature callus and the ultrasound gap.

margins of maturing callus, which is seen as a well marginated reflective zone (Fig. 2). A note was made of the presence and size of any low-reflectivity areas thought to be fluid-filled cysts (Fig. 3). Radiographs were also obtained and the gap between the native bone ends measured by placing a radio-opaque ruler in the same plane as the bone. The measurements obtained were displayed graphically, the bone gap and the ultrasound gap being plotted against time since the operation. The ultrasound gap was subtracted from the bone gap and this was judged to indicate the amount of new bone produced (Fig. 4) and this was also plotted against time. Ultrasound assessment was continued during the consolidation period after the distraction had ceased.

Results

All the patients showed an initial lag phase before the production of measurable callus. During this phase the measurement of the gap on ultrasound and that between

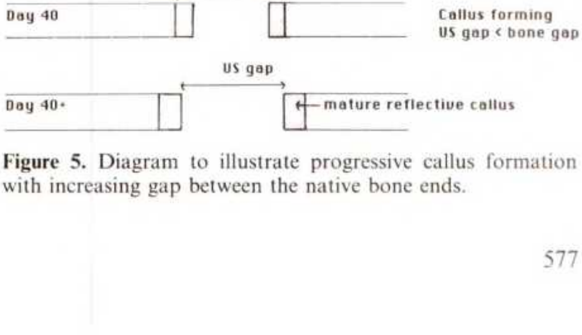

Figure 5. Diagram to illustrate progressive callus formation with increasing gap between the native bone ends.

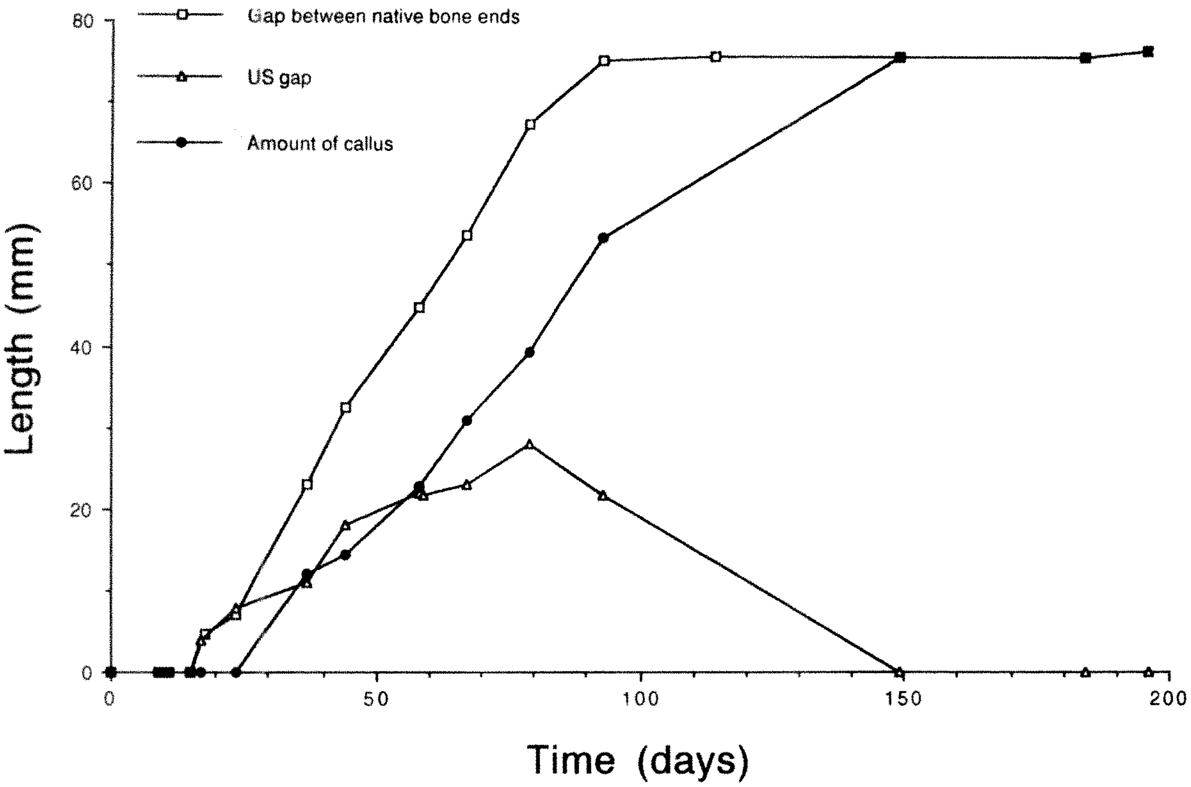

Figure 6. Graph from a patient in whom the rate of callus formation parallelled the rate of bone lengthening.

the native bone ends was the same. After this period it was not possible to detect the original bone ends as the callus had now matured sufficiently to be reflective. Usually the lag phase was of the order of 10 days but, in the three patients that had delayed healing, a prolonged lag period in excess of 25 days of lengthening was found. After the initial lag period the measurements obtained on ultrasound differed from the gap between the native bone ends as seen on the radiograph, the difference being the amount of mature callus that had formed (Fig. 5). The rate that this callus formed fell into three groups:

1. Equal rates of callus formation and limb lengthening (Fig. 6). Four lengthening sites displayed this optimum pattern. All these sites healed well with the frames in place for a minimum length of time.
2. Rate of callus formation less than rate of limb lengthening (Fig. 7). Three sites fell into this category. For two of the three sites the rate of limb lengthening had to be reduced from 1 mm to 0.5 mm a day. The frame had to be on for a prolonged period of time both during the lengthening phase and during the consolidation phase. Cysts were detected in two of these patients.
3. Rate of callus formation faster than limb lengthening. The rate of limb lengthening of one patient had to be reduced and even stopped at one stage because of pain and stiffness of the soft tissues. The rate of callus formation in this patient exceeded the rate of limb lengthening.

Discussion

In this study serial ultrasound examinations enabled the gap between the margins of the corticotomy or mature callus to be measured quickly and accurately. The quality of maturing callus was assessed and judged to be good if there was a uniform lamellar pattern of echoes and no echo-free regions. This concurs with the findings of Blane et al (1991). As in our study, areas of decreased echogenicity in the ultrasound gap were found by Young et al (1989). They aspirated these and found them to be fluid-filled cysts, the aspiration of which they felt improved osteogenesis. In this study we found that the smaller cysts disappeared by stopping or reversing distraction for 1 week.

To obtain a satisfactory result during the distraction osteogenesis, the rate of callus formation should parallel the rate of bone lengthening. The four sites that achieved satisfactory bone lengthening had such curves. There were three sites in which the outcome was deemed to be unsatisfactory. In these cases there is a prolonged lag period and the curve of callus formation is seen to be shallow, *i.e.* too slow a rate of callus formation for the rate of bone lengthening. Three patients who had such

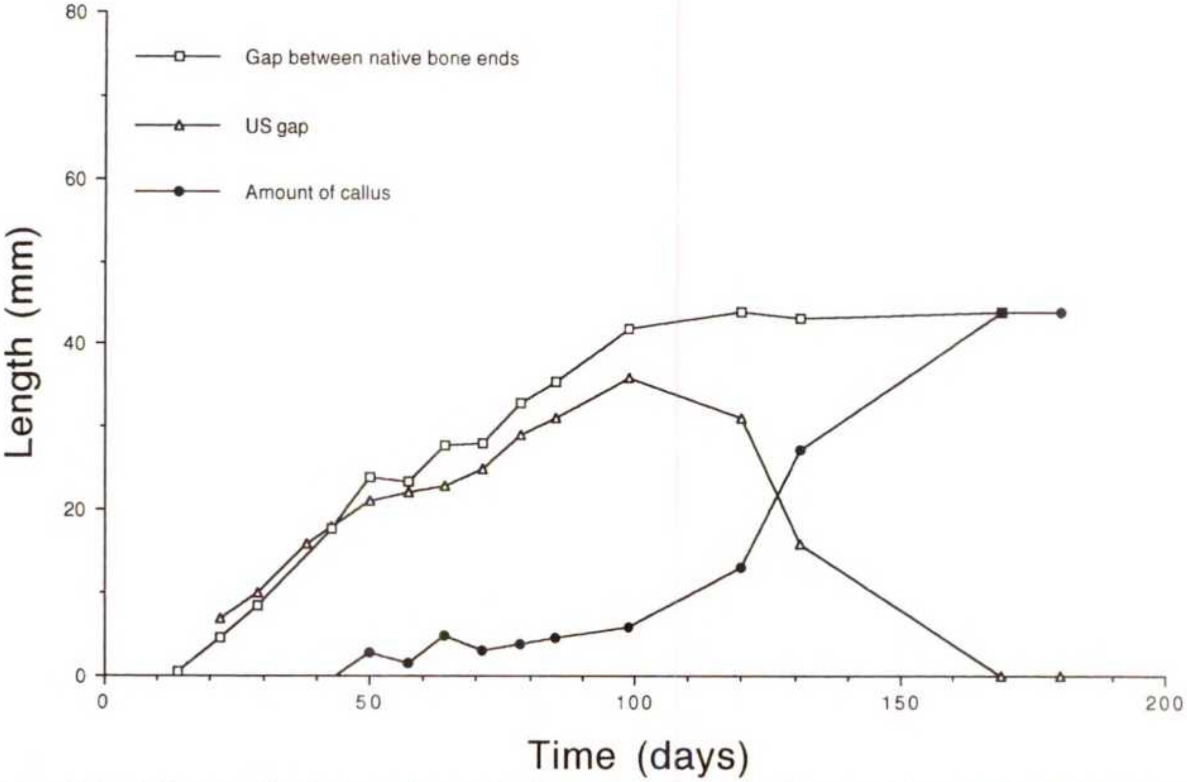

Figure 7. Graph from a patient in whom the rate of callus formation fell short of the rate of bone lengthening following a prolonged lag period.

curves were also the ones to develop cysts within the gap (Fig. 8). When such results are seen to be developing, the rate of distraction needs to be slowed. It is hoped that this will enable the optimum rate of lengthening to be chosen before cysts have had a chance to develop, and therefore pre-empt the problem of poor quality callus formation. Finally, in one patient the rate of callus formation was seen to be faster than the rate of distraction. Too slow a rate of distraction may result in premature consolidation and failure to achieve the target increase in length. However, the patient in our study did not suffer this complication, and it may be that so long as an ultrasound gap of sufficient width is maintained, premature consolidation will not occur.

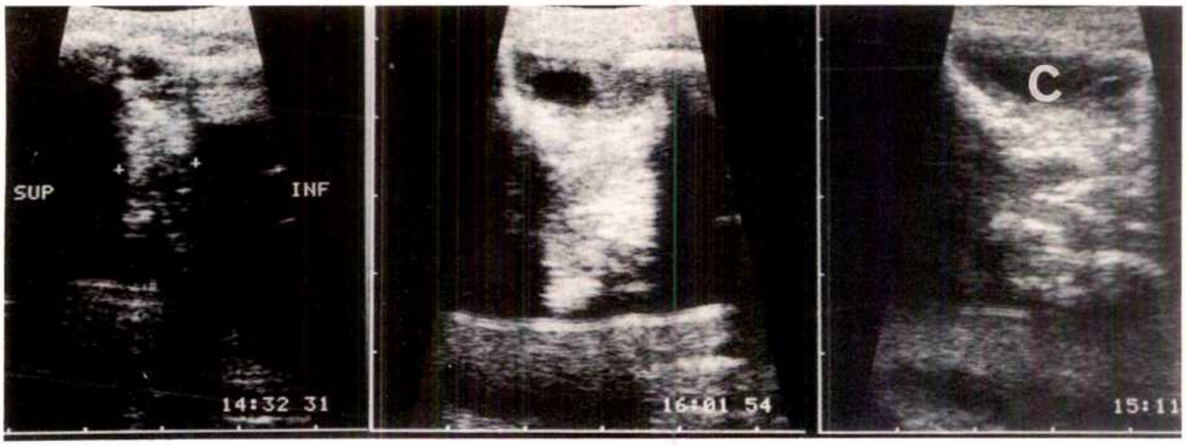

Figure 8. Serial ultrasound pictures from the patient illustrated in Fig. 7 (all same magnification) showing progressive enlargement of a cyst (C), from 4 mm to 22 mm, within the gap indicating poor quality callus formation.

Radiographs may not show any evidence of callus formation in the first 4 weeks of lengthening, sometimes longer, whereas following a relatively short lag period we found that ultrasound can indicate whether callus is forming satisfactorily. Radiography is still required at intervals during distraction to ensure that there is no angulation at the lengthening site; however, the number of films can be reduced.

Ultrasound thus provides a means of monitoring the quality and the rate of new bone production from the time of the initial corticotomy. The distraction can thus confidently proceed, the rate can be optimized, and the time that the patient has to wear the fixator minimized. It is a valuable technique, which complements radiography in the follow-up of patients undergoing limb lengthening procedures.

References

BLANE, C. E., HERZENBERG, J. E. & DIPIETRO, M. A., 1991. Radiographic imaging for Ilizarov limb lengthening in children. *Pediatric Radiology, 21,* 117–120.

YOUNG, J. W. R., KOSTRUBIAK, I. S., RESNIK, C. S. & PALEY, D., 1989. Sonographic evaluation of bone production at the distraction site in Ilizarov limb lengthening procedures. *American Journal of Roentgenology, 154,* 125–128.

1992, *The British Journal of Radiology*, *65*, 581–584

An audit of ultrasound diagnosis of gallbladder calculi

By J. Walker, BSc, MRCP, DMRD, *R. T. A. Chalmers, MB, ChB, FRCS and
P. L. Allan, BSc, FRCPE, FRCR

Departments of Radiology and *Surgery, Royal Infirmary, Lauriston Place, Edinburgh EH3 9YW, UK

Based on a paper presented at the BMUS 23rd Annual Meeting in Bournemouth, on 10–12 December 1991

Keywords: Gallstones, Ultrasound, Cholecystectomy

Abstract. Many series suggest that ultrasound is an accurate method for demonstrating cholelithiasis. However, these series were often prospective and the examinations performed by experienced sonographers. This audit addresses whether the accuracy is maintained in daily practice. We reviewed the ultrasound scans of 128 patients who underwent cholecystectomy for cholelithiasis and compared the findings. The operative and ultrasound findings were at variance in eight of the 128 patients (6.2%). Five were reported as having gallstones on ultrasound but none were found at cholecystectomy, a false positive rate for ultrasound of 3.9%. Three had abnormal gallbladders with no gallstones on ultrasound but gallstones were found at operation, a false negative rate of 2.3%. To avoid false positive diagnoses, suboptimal examinations should be repeated and the scan should be repeated immediately pre-operatively if only small calculi are seen. Alternative imaging should be performed if necessary, either cholescintigraphy in the acute situation or elective oral cholecystography. Some false negative examinations may be avoided by performing repeat examinations if the gallbladder is thick-walled and tender. With these provisos we conclude that ultrasound correctly diagnoses cholelithiasis in daily practice.

In the Royal Infirmary of Edinburgh, ultrasound is used as the standard pre-operative investigation in patients presumed to have cholelithiasis. It was suggested to us by one general surgical unit in the Royal Infirmary that on occasion there is some disparity between the ultrasound findings and those of cholecystectomy. We therefore reviewed the published literature and performed an audit of our own results.

Cooperberg & Burhenne (1980) first suggested that real-time ultrasound was the diagnostic technique of choice for calculous gallbladder disease. In 313 patients they achieved an accuracy of 96%. They reported five false negative results, one definite false positive result and two others as possible false positives; six examinations were inadequate. Other published series also quote an accuracy of 96% or greater (Crade et al, 1978; Hessler et al, 1981). However, often these figures relate to prospective series where the examinations are performed by a senior, highly motivated sonographer. In our retrospective review, we sought to audit the daily practice of an ultrasound department where sonographers of varying experience are scanning routine and emergency referrals.

Methods

Using the Lothian Surgical Audit database, every patient who had undergone cholecystectomy for cholelithiasis in one general surgical unit in the Royal Infirmary of Edinburgh between March 1988 and March 1991 was identified. Individual patient case notes and copies of the pre-operative ultrasound reports were reviewed. The ultrasound findings, the grade of the radiologist performing the scan and operative details were noted. The ultrasound scanners used were an Acuson 128, a Siemens AC or a Siemens Sonoline SX using 3.5 or 5 MHz transducers.

In cases where the ultrasound report was found to be at variance with the findings at cholecystectomy, the report and hard-copy films from the scan were reviewed by a consultant radiologist (P.L.A.). The pathologist's report on the excised gallbladder was also reviewed.

Results

A total of 144 cholecystectomy patients were reviewed. Of these, 35 were male and 109 female; seven were emergency operations. 128 had pre-operative ultrasound scans performed (see Table I). Of the others, 14 underwent oral cholecystography and two had calcified gallstones noted on plain radiographs.

Table I. Comparison of the ultrasound detection of gallstones with the findings at cholecystectomy

	Ultrasound	
	Stones	No stones
Cholecystectomy		
Stones	115[a]	3
No stones	5	5
Total	120	8

[a] At cholecystectomy, two of these patients had no stones in the gallbladder but stones were found in the common bile duct.

Address correspondence to Dr J. Walker.

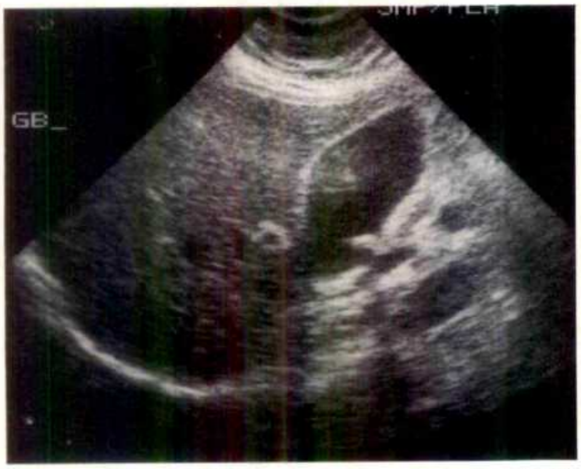

Figure 1. False positive ultrasound examination. A highly reflective structure casting an acoustic shadow is present in the gallbladder. This is still felt likely to represent a gallstone.

There was a false positive rate for ultrasound of 5.4% (7/128) for calculi in the gallbladder and a false negative rate of 2.3% (3/128). In two of the seven false positives, however, though there were no calculi in the gallbladder, calculi were found in the common bile duct at surgery. It is considered likely that these stones had migrated in the interval between ultrasound and surgery, the interval being 10 days in one case and 21 days in the other. Therefore, excluding these as false positives because of the presence of gallstones, the revised false positive rate was 3.9% (5/128). The overall error rate for this audit is 6.2% (8/128).

Of the 128 pre-operative scans performed, 65 were performed by consultants, 48 by senior registrars and 15 by registrars. Of the erroneous scans, three were performed by a consultant radiologist, four by a senior registrar and one by a registrar. Respectively, 4.6% (3/65) of the consultants' scans were erroneous, 8.3% (4/48) of the senior registrars' and 7% (1/15) of the registrars'. These results were not statistically significantly different by a χ^2 test.

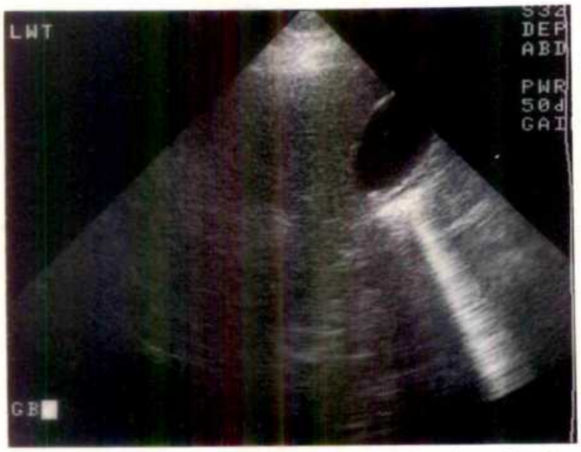

Figure 2. False positive ultrasound examination. A small reflective structure is present in the gallbladder, which may or may not represent a gallstone.

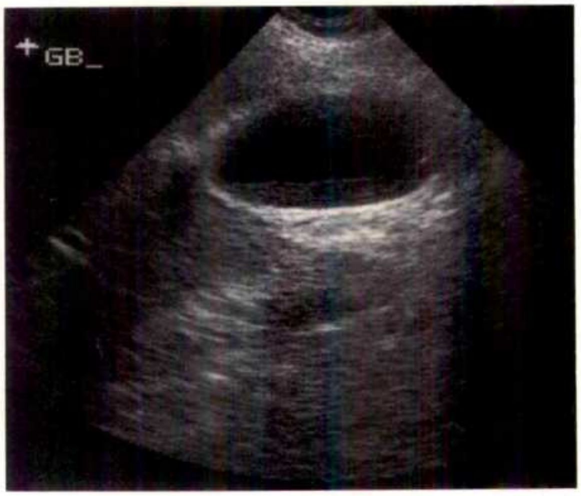

Figure 3. False positive ultrasound examination. Only sludge is seen to be present in the gallbladder; an error may have been made.

The hard-copy films of the incorrect scans and the pathology reports on the excised gallbladders of those patients were reviewed. All five of the false positives had chronic cholecystitis. The hard-copy films of three of the five patients were available. In one, an opacity that had definite characteristics of a gallstone was present (Fig. 1). The common duct was dilated at 14 mm and, though the interval between ultrasound and operation was only one day, it was possible that the stone had been passed. In the second case, a small opacity without an acoustic shadow was present, which had been interpreted as a gallstone (Fig. 2). In the third, sludge and calculi were reported but only sludge was present on review (Fig. 3).

The three false negative examinations were all in acutely ill patients and, though no gallstones were seen, all three gallbladders were reported as abnormal and dilated. In addition, one was commented on as having a thick and oedematous wall, one as being tender with a thick wall, and one as tender and oedematous. The first two patients were given the diagnoses of acute cholecystitis (Fig. 4) and acalculous cholecystitis, respectively; the third was given no specific diagnosis. Thus, although no gallstones were identified, the site of the patient's pathology was correctly identified and appropriate surgery performed.

Discussion

Ultrasound is commonly used as the imaging investigation of choice in calculous gallbladder disease (Cooperberg & Burhenne, 1980) and is used routinely in our department. It is convenient and safe (merely requiring an 8 h patient fast and involving neither radia-

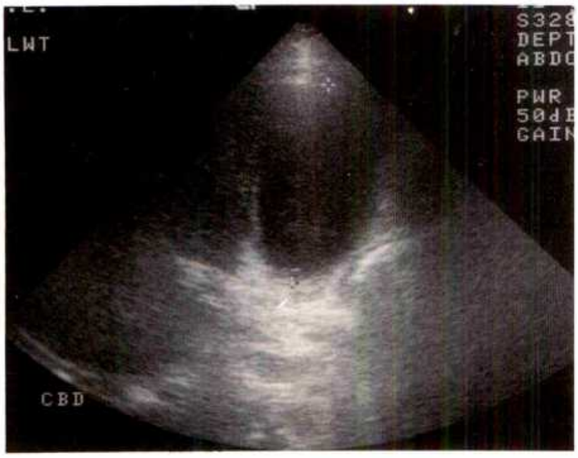

Figure 4. False negative ultrasound examination. At ultrasound no gallstones were identified but the gallbladder was described as being oedematous and thick-walled and the diagnosis of acute cholecystitis was given.

tion nor drugs), can be extended to visualize the biliary tree and other upper abdominal organs, and is accurate. This accuracy has been determined previously and has been reported as 96% or greater, but these were mostly prospective studies in which the examinations were performed by highly experienced sonographers (Cooperberg & Burhenne, 1980; Crade et al, 1978; Hessler et al, 1981). Our audit of the day-to-day work in a department where both emergency and elective patients are scanned by sonologists of varying experience gave an overall error rate of 6.2% for patients coming to surgery. This compares favourably with the previously reported series and confirms the ability of ultrasound to correctly diagnose cholelithiasis. However, the audit only includes patients coming to surgery and no information is available on those false negative results where gallstones were missed on ultrasound and no surgery has been performed.

In our series we diagnosed gallstones in five patients where no gallstones were found at cholecystectomy. These false positive diagnoses must be avoided (Hessler et al, 1981) as unnecessary surgery may be performed. They may arise because gallstones are passed in the interval between ultrasound and surgery. They may also arise because of the mistaken identification of other structures, such as the spiral valve of Heister, polyps or folds in the gallbladdder wall, as calculi. Technically difficult examinations, such as in obese or ill patients, can result in inadequate, erroneous examinations. Thus, an optimal ultrasound examination should be performed when the patient is adequately fasted and can be moved into different positions. It may also be prudent to repeat the ultrasound immediately pre-operatively if there is an interval of several days between the scan and operation, especially if only small calculi are seen initially (Cooperberg & Gibney, 1987). If doubt still persists as to whether highly reflective foci are calculi or not, an alternative imaging investigation should be performed; in an elective situation oral cholecystography is recommended. This has recently been reported as having a detection rate for biliary calculi differing little from ultrasound (Gelfand et al, 1988), although it requires more rigorous patient preparation, the ingestion of contrast medium and the use of radiation. In a patient presenting as an emergency with the suspected diagnosis of acute cholecystitis and in whom the ultrasound is equivocal or suboptimal, cholescintigraphy is the alternative imaging technique of choice. Failure of uptake by the gallbladder confirms cystic duct obstruction and is strongly suggestive of acute cholecystitis (Samuels et al, 1985).

In our three patients with false negative diagnosis of calculi, all three gallbladders had been reported at ultrasound as abnormal, with dilatation, thickened, oedematous walls and tenderness. A recent paper (Ekberg & Weiber, 1991) has recognized the clinical importance of thick-walled, tender gallbladders without stones on ultrasound. In their series of 31 patients, follow-up was available in 28. They reported that further imaging (oral cholecystography, intravenous cholangiography or ultrasound) demonstrated calculi in 14 patients. Thus, to avoid some (possibly 50%) of false negative diagnoses, when the gallbladder is abnormal but no stones are seen, either a repeat examination at a later date or an oral cholecystogram will be helpful.

We conclude from this audit that ultrasound, as performed daily in our department, correctly diagnoses cholelithiasis. It should remain the diagnostic imaging technique of choice. However, if false positive diagnoses are to be avoided, the examination should be adequate, repeated if necessary and, if doubt persists, oral cholecystography or cholescintigraphy should be performed as indicated. Some false negative diagnoses may be avoided by repeating the scan or performing an oral cholecystogram if, at the initial examination, no stones are demonstrated but the gallbladder is tender and thick-walled.

Acknowledgments

We thank Mr I. F. McLaren and Mr K. Fearon for their help and advice.

References

Cooperberg, P. L. & Burhenne, H. J., 1980. Real-time ultrasonography. Diagnostic technique of choice in calculous gallbladder disease. *New England Journal of Medicine, 302,* 1277–1279.

Cooperberg, P. L. & Gibney, R. G., 1987. Imaging of the gallbladder. *Radiology, 163,* 605–613.

Crade, M., Taylor, K. J. W., Rosenfield, A. T., De Graff, C. S. & Minihan, P., 1978. Surgical and pathological correlation of cholecystosonography and cholecystography. *American Journal of Roentgenology, 131,* 227–229.

Ekberg, O. & Weiber, S., 1991. The clinical importance of a thick walled, tender gallbladder without stones on ultrasonography. *Clinical Radiology, 44,* 38–41.

Gelfand, D. W., Wolfman, N. T., Ott, D. J., Watson, Jr, N. E., Chen, Y. M. & Dale, W. J., 1988. Oral cholecystography

1992, *The British Journal of Radiology*, *65*, 585–588

The ultrasound appearances of intramural bowel gas: the bright ring appearance and the effervescent bowel. A report of three cases

By Ronald A. Bloom, MD, Eli Craciun, MD, Pinchus D. Lebensart, MD, *Pavel Levy, MD and Jacob Bar Ziv, MD

Departments of Radiology and *Surgery, Hadassah University Hospital, Jerusalem, Israel

Based on a paper presented at the BMUS 23rd Annual Meeting in Bournemouth, on 10–12 December 1991

Keywords: Ultrasound, Bowel necrosis, Mesenteric thrombosis, Intestine

Abstract. Bowel necrosis is a serious condition with a very high mortality rate. The earlier the diagnosis is made, the better chance for survival. Ultrasound is a primary imaging technique in the diagnosis of the acute abdomen. Three cases are presented in which bowel wall gas could be demonstrated on ultrasound. In all cases there was computed tomographic and either operative or post-mortem correlation. In each case there was a "bright ring" appearance of the affected bowel when the ultrasound examination was carried out in transverse section. In one case, small bubbles were seen arising from the deep surface of the bowel.

Bowel infarction is an illness resulting from diverse pathological conditions and results in necrosis of the intestine, which is uniformly fatal if left untreated (Sak & Aldrete, 1984). It is one of the common causes of abdominal crises in the adult population and the incidence is increasing along with the mean age of the population. It currently accounts for about one in every 1000 hospital admissions in the USA and has a very high mortality rate (Singh et al, 1975). Diagnosis by clinical and radiological examination is often difficult, and diagnosis and effective treatment remain challenging problems. Bowel wall gas in the correct clinical setting is accepted as being highly suggestive, if not diagnostic, of intestinal necrosis. This diagnosis is rarely made on plain radiography but has been variously described as being seen in from 22 to 71% of proven cases by means of computed tomography (CT) (Federle et al, 1984; Alpern et al, 1988; Smerud et al, 1990).

Only two cases of intramural bowel wall gas demonstrated on ultrasound have been recorded (Vernacchia et al, 1985; Vijayaraghavan, 1990). We present three further cases, each with CT and operative or post-mortem correlation.

Case reports

Case 1

A 75-year-old man was admitted via the Casualty Department with an intertrochanteric fracture of the right hip. This was treated surgically; 3 weeks later, while the patient was still in the Orthopaedic Department, he complained of abdominal pain. On ultrasound no upper abdominal pathology was seen, but in the left lower quadrant, fluid-filled loops of bowel with thickened walls were found. In one of these loops bright echoes of the same intensity as the gas in the adjacent bowel lumen were seen. These gave the appearance of a bright ring. Intramural gas was diagnosed (Fig. 1). A subsequent CT examination confirmed these findings (Fig. 2). At laparotomy a length of necrotic bowel was found and the diagnosis of mesenteric vein thrombosis made; 2.5 m of necrotic and compromised bowel were removed. The post-operative course was complicated and led to a second laparotomy some days later. A further 5 cm of ileum and the ascending and proximal half of the transverse colon were removed owing to vascular compromise. A month later, following another vascular event, further small bowel resection was performed. The patient was eventually returned to his Old Age Home with a Hickman catheter *in situ* for intermittent parenteral nutrition.

Case 2

A 37-year-old woman was admitted for bone marrow transplantation (BMT) owing to disseminated non-Hodgkin's lymphoma. Following BMT she became neutropenic and developed fever. Blood cultures were negative and she was treated with broad-spectrum antibiotics. On the eighth post-operative day she developed diffuse abdominal pains, purpura and abdominal distension with tenderness. Paralytic ileus developed over the next few hours and the bilirubin level, already high, continued to rise. Abdominal ultrasound demonstrated portal vein gas bubbling into the distal intrahepatic branches. In the lower abdomen, thickened fluid-filled bowel loops were seen with bright intramural echoes indicative of gas (Fig. 3). In one such loop small gas bubbles were seen arising from the deep surface and rising anteriorly (Fig. 4). No bowel peristalsis was seen

---

Address correspondence to Professor Ronald A. Bloom, Department of Radiology, Hadassah University Hospital, Ein Kerem, Jerusalem, Israel.

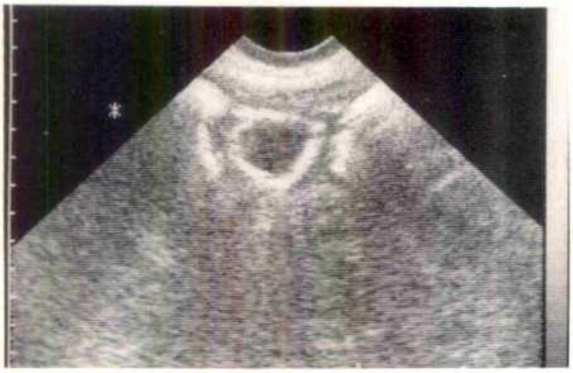

Figure 1. The ultrasound appearance of the "bright ring" of highly reflective gas situated in the bowel wall when the bowel is scanned transversely (Case 1).

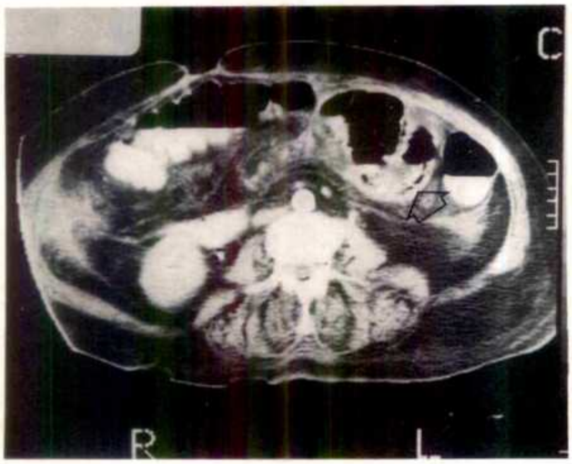

Figure 2. CT scan of the same case showing intramural bowel gas (arrow).

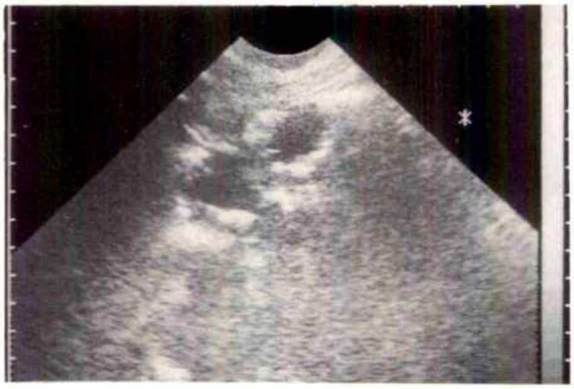

Figure 3. Abdominal ultrasound scan of Case 2 showing the bright echoes of gas in the thickened bowel wall in transverse section.

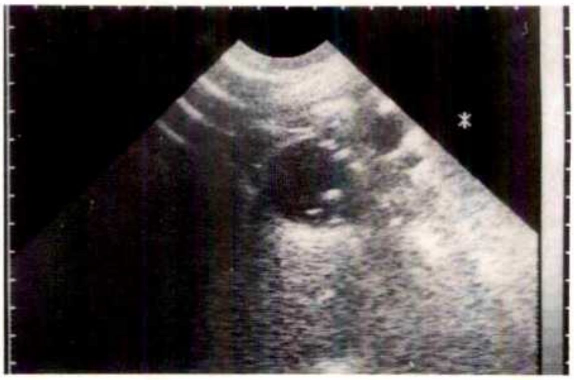

Figure 4. Small gas bubbles rising from the deep surface of the bowel: "the effervescent bowel" (Case 2).

and the bubbles did not move along the lumen as would be seen in peristaltic propagation. A subsequent CT scan demonstrated gas in the bowel wall extending from the stomach to the colon (Fig. 5). The patient was treated conservatively and died the next day. Necrotizing enterocolitis extending from the stomach to the colon was demonstrated at post-mortem examination.

Case 3

A 79-year-old man was admitted to the Internal Medicine Department with diarrhoea, weight loss and anorexia. He had a 1 week history of abdominal pain related to food and a previous history of hypertension, chronic renal failure and chronic heart failure. While in hospital he developed acute abdominal pain and fever. A CT scan demonstrated gas in the portal vein and its intrahepatic branches, and also in the mesenteric vessels and the wall of contrast medium-filled bowel loops (Fig. 6). An ultrasound examination was performed immediately prior to laparotomy. Fluid-filled bowel loops with the bright echoes of gas in the bowel wall were noted. When the affected bowel was scanned in the transverse projection, a "bright ring" appearance was seen (Fig. 7). At laparotomy mesenteric arterial occlusion was noted. The small bowel was totally necrotic. The patient died the next day.

Discussion

Ultrasound is a primary technique in the examination of the acute abdomen and its efficacy in demonstrating pathology in the upper abdominal parenchymal organs is well established. Less information is available on the ultrasound findings in acute bowel disease, and intraluminal bowel gas often precludes adequate imaging. Small bowel wall thickening may, however, be detected even when relatively large amounts of gas are present, and the symmetry or otherwise of the thickening may help determine its nature (Matos et al, 1986).

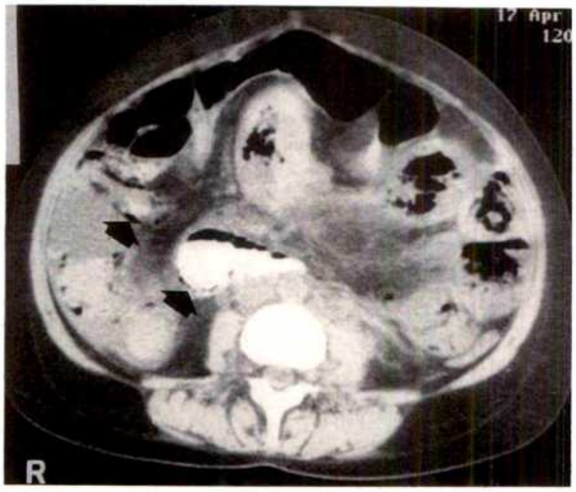

Figure 5. Intramural gas seen on CT (arrows) (Case 2).

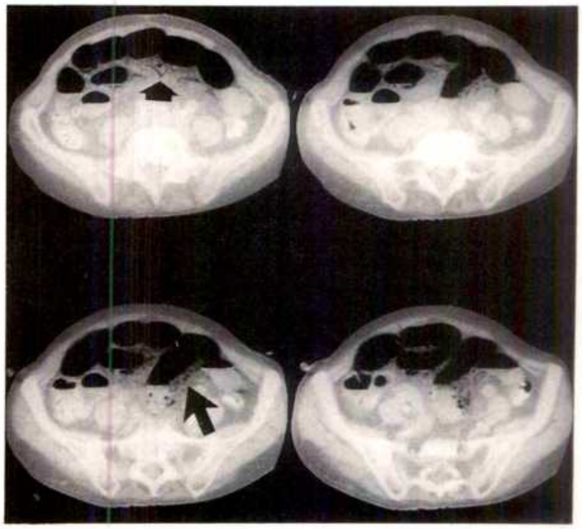

Figure 6. CT scans of Case 3 demonstrating mesenteric vascular gas (arrowhead) and intramural bowel gas (arrow).

Gas in the bowel wall is a reliable sign of bowel necrosis in the correct clinical setting, and its prevalence in two retrospective studies of CT findings in patients with proven ischaemic or infarcted bowel have been published (Alpern et al, 1988; Smerud et al, 1990). Combining the two series, there were 588 cases with ischaemic or necrotic bowel of which 46 cases had a CT examination shortly before surgery or death. A specific diagnosis of ischaemic bowel was made at the time of initial CT interpretation in only 15 patients. The diagnosis depends on demonstrating pneumatosis intestinalis, portal venous or mesenteric vascular gas, or "thumb printing" of the bowel wall. Of these 15 cases, 11 showed intramural bowel wall gas and six mesenteric or portal venous gas.

The sensitivity of CT diagnosis of bowel infarction in these two series was only 28%, with bowel wall gas observed in 24%. The 23 cases in the series of Smerud et al (1990) had correlative plain film radiographs. Only one of these showed evidence of intramural bowel wall gas, but, in conjunction with other plain radiographic findings, seven cases (30%) were thought to be suggestive of bowel infarction.

In view of these somewhat disappointing results, any additional help in the diagnosis of this deadly disease is to be welcomed. The ultrasound appearances of bowel wall gas have been described in only three cases. One of

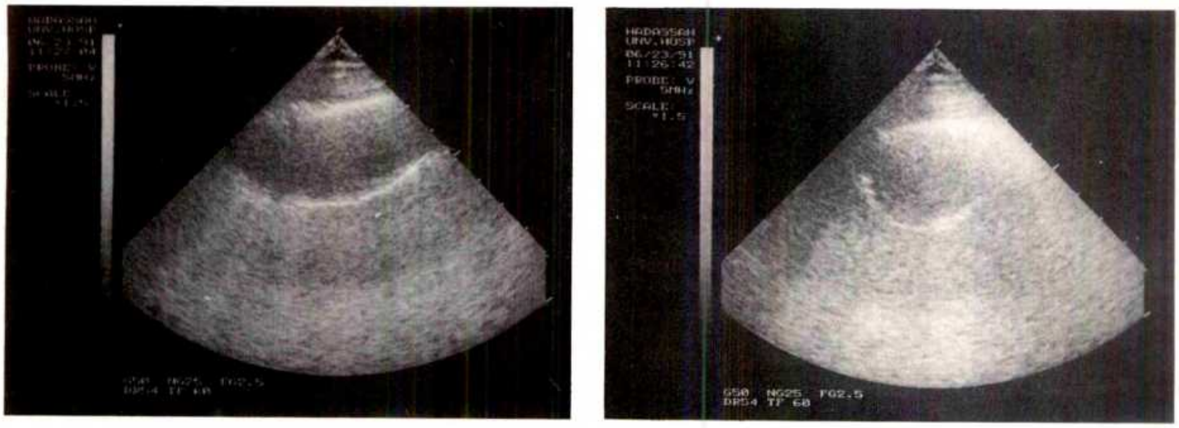

(a)

(b)

Figure 7. Ultrasound scans of Case 3 showing (a) bowel wall gas in longitudinal section and (b) the "bright ring" appearance in transverse section.

these was an intraoperative examination of the gas-filled cysts of benign pneumatosis intestinalis (Sigel et al, 1985). A second case demonstrated gas in the colonic wall in idiopathic ulcerative colitis with superimposed shigellosis (Vernacchia et al, 1985), while the third showed intramural gas in a gangrenous jejunal wall. This gas shifted when the patient was placed in a decubitus position (Vijayaraghavan, 1990), analogous to the shifting intramural gas sometimes seen in emphysematous cholecystitis (Bloom et al, 1984).

In two of our three cases the diagnosis of bowel wall gas was made with a fair degree of confidence by ultrasound examination. Bright reflections were seen emanating from the bowel wall, the appearances being identical to one of the findings seen in emphysematous cholecystitis (Bloom et al, 1989). In one case, tiny gas bubbles were seen rising from the dependent portion of the bowel, reminiscent of rising champagne bubbles (Fig. 4). This appearance, seen in emphysematous cholecystitis, has been described as the "effervescent gallbladder" (Nemcek et al, 1988). In our case it could with equal aptness be called the "effervescent bowel". In the third case, the diagnosis of intramural bowel gas had already been made by CT (Fig. 6). The bowel wall gas was easily demonstrated by ultrasound performed shortly afterwards (Fig. 7).

In each of our three cases a "bright ring" appearance was seen, similar to that described in emphysematous cholecystitis (Bloom et al, 1989). This is caused by the strong echoes from the gas in the wall, surrounding the fluid-filled viscus (Figs 1, 3, 7). When the bowel is scanned longitudinal to the bowel, its tubular shape becomes obvious (Fig. 7). Intramural bowel gas is often associated with intrahepatic portal vein gas, which can be seen easily by ultrasound when present (Bloom et al, 1988), and in Case 1 it was the presence of portal vein gas that led to a search for bowel wall gas.

We suggest that when an ultrasound examination of the acute abdomen is being performed, the bowel should be carefully examined, particularly when a mesenteric occlusion is suspected in an elderly patient or when portal venous gas is seen.

References

Alpern, M. B., Glazer, G. M. & Francis, I. R., 1988. Ischemic or infarcted bowel: CT findings. *Radiology, 166*, 149–152.

Bloom, R. A., Fisher, A., Pode, D. & Asaf, Y., 1984. Shifting intramural gas—a new ultrasound sign of emphysematous cholecystitis. *Journal of Clinical Ultrasound, 12*, 40–42.

Bloom, R. A., Craciun, E., Jurim, O. & Lebensart, P. D., 1988. Sonographic demonstration of hepatic venous gas in mesenteric arterial thrombosis. *Journal of Clinical Gastroenterology, 10*, 226–228.

Bloom, R. A., Libson, E., Lebensart, P. D., Craciun, E., Klin, B., Fields, S. I. & Haskell, L., 1989. The ultrasound spectrum of emphysematous cholecystitis. *Journal of Clinical Ultrasound, 17*, 251–256.

Federle, M. P., Chun, G., Jeffrey, R. B. & Rayor, R., 1984. Computed tomographic findings in bowel infarction. *American Journal of Roentgenology, 142*, 91–95.

Matos, C., Van Gansbeke, D., Zalcman, M., Ansay, J., Delcour, C., Engelholm, L. & Struyven, J., 1986. Mesenteric vein thrombosis: early CT and US diagnosis and conservative management. *Gastrointestinal Radiology, 11*, 322–325.

Nemcek, A. A., Gore, R. M., Vogelzang, R. L. & Grant, M., 1988. The effervescent gallbladder: a sonographic sign of emphysematous cholecystitis. *American Journal of Roentgenology, 150*, 575–577.

Sack, J. & Aldrete, J. S., 1984. Primary mesenteric venous thrombosis. *Surgery, Gynecology, and Obstetrics, 154*, 205–208.

Sigel, B., Machi, J., Ramos, J. R., Serota, A. I. & Robertson, A. L., Jr, 1985. Ultrasonic features of pneumatosis intestinalis. *Journal of Clinical Ultrasound, 13*, 675–678.

Singh, R. P., Shah, R. C. & Lee, S. J., 1975. Acute mesenteric vascular occlusion: a review of 32 patients. *Surgery, 78*, 613–617.

Smerud, M. J., Johnson, C. D. & Stephens, D. H., 1990. Diagnosis of bowel infarction: a comparison of plain films and CT scans in 23 cases. *American Journal of Roentgenology, 154*, 99–103.

Vernacchia, F. S., Jeffrey, R. B., Laing, F. C. & Wing, V. W., 1985. Sonographic recognition of pneumatosis intestinalis. *American Journal of Roentgenology, 145*, 51–52.

Vijayaraghavan, S. B., 1990. Sonographic features of pneumatosis of the small bowel. *Journal of Clinical Ultrasound, 18*, 579–581.

1992, *The British Journal of Radiology*, *65*, 589–593

The value of ultrasound in the assessment of bone

By G. M. Steiner, FRCP, FRCR and A. Sprigg, FRCR

Department of Diagnostic Radiology, Sheffield Children's Hospital, Western Bank, Sheffield S10 2TH, UK

Based on a paper presented at the BMUS 23rd Annual Meeting in Bournemouth, on 10–12 December 1991

Keywords: Ultrasound, Bone

Abstract. The impenetrability of bone to ultrasound can be turned to advantage and the effects of bony lesions on the adjacent soft tissues can be analysed. Fractures, bone destruction, inflammation, distraction of bone and new bone formation can be diagnosed.

We wish to draw attention to the value of ultrasound in the diagnosis of lesions of bone and encourage its use as an adjunct to radiography. There are reports of the ultrasound diagnosis of fractures in infancy (Graif et al, 1988), separation of epiphyses (Dias et al, 1988; Broker & Burbach, 1990), osteomyelitis (Yousefzadeh & Ramilo, 1986; Howard & Einhorun, 1991), measurement of distraction in leg lengthening and of fracture healing (Leitgeb et al, 1990).

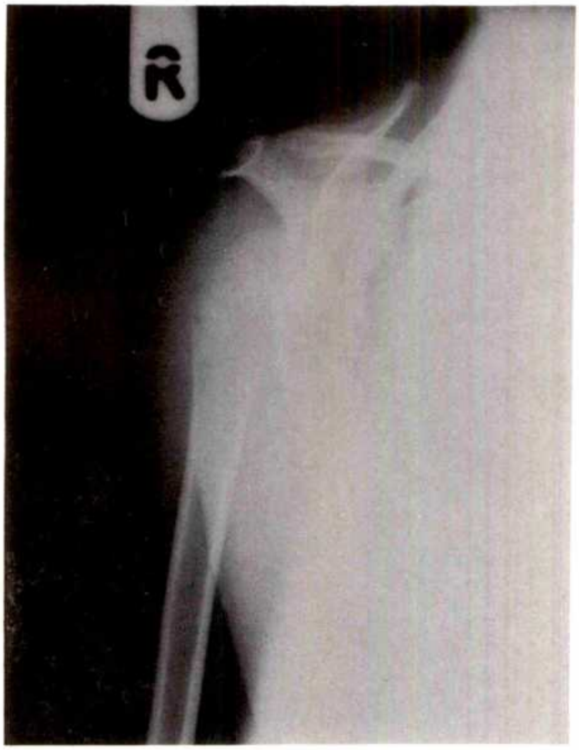

(a)

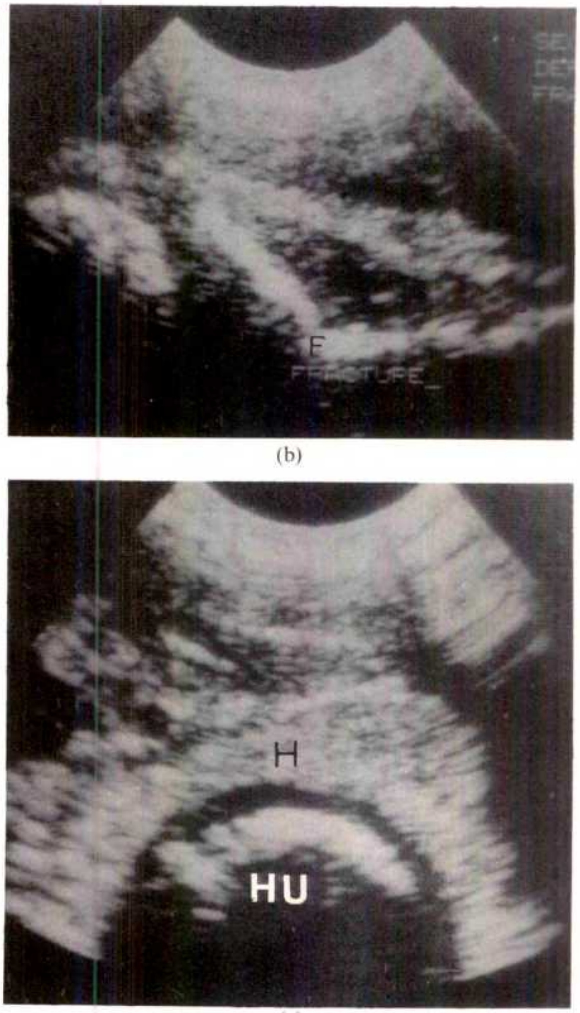

(b)

(c)

Figure 1. The shoulder is dislocated and the neck of the humerus fractured. (b) Longitudinal scan of the upper humeral shaft. The surface of the humerus is kinked at the fracture site (F). (c) Transverse scan of the humerus. The reflective layer (H) represents intra-articular blood. HU, humeral head.

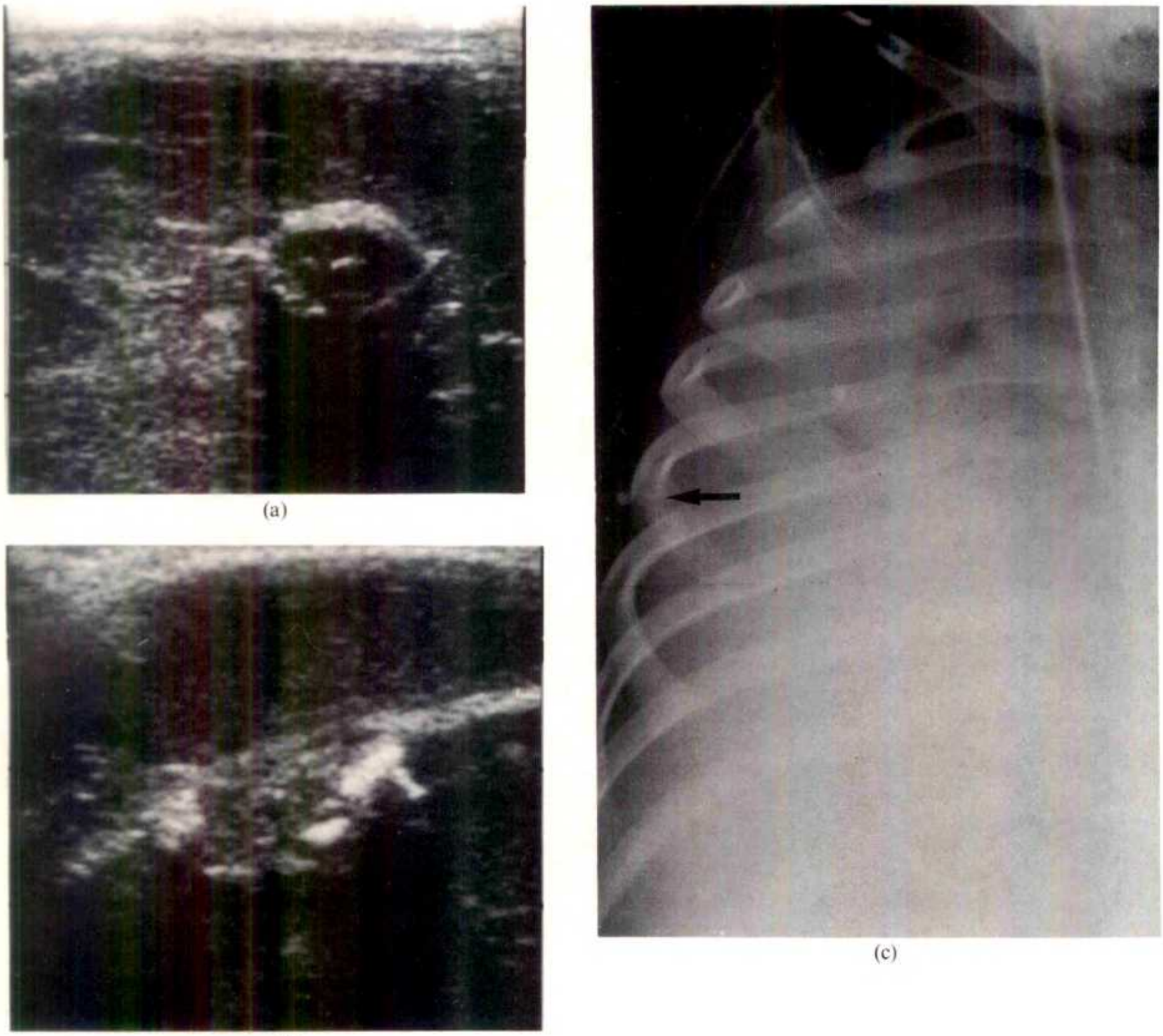

(a)

(b)

(c)

Figure 2. Transverse scan of a normal rib showing the oval appearance. (b) Longitudinal scan of an abnormal rib showing destruction of its anterior surface and reflective material (presumably tumour) within the shaft. (c) Chest radiograph showing rib destruction (arrow).

Method

An ATL 4 machine was used to scan the area of interest using 5 MHz or 7.5 MHz sector probes or a 7.5 MHz linear array probe.

Case reports

Case 1

The right shoulder of an 8-year-old boy became very swollen following a fall. Radiography revealed a dislocated shoulder and a fracture of the neck of the humerus (Fig. 1a). Ultrasound indicated the swelling was due to a haemarthrosis (Fig. 1b) and confirmed the presence of the fracture (Fig. 1c). Five millilitres of clotted blood were aspirated from the joint.

Case 2

A 2½-year-old boy with known neuroblastoma presented with a soft-tissue swelling on the right chest wall. Ultrasound demonstrated the soft-tissue swelling but also revealed a discontinuity in the cortex of the underlying rib (Fig. 2a, b). The presence of bone destruction resulting from metastasis was confirmed by radiography (Fig. 2c).

Case 3

An 8-year-old girl presented with a painful right knee and was found to be very tender over the proximal tibia. Radiography showed a very small area of lucency in the proximal tibial metaphysis (Fig. 3a). Ultrasound showed a small area of abnormal reflectivity over the

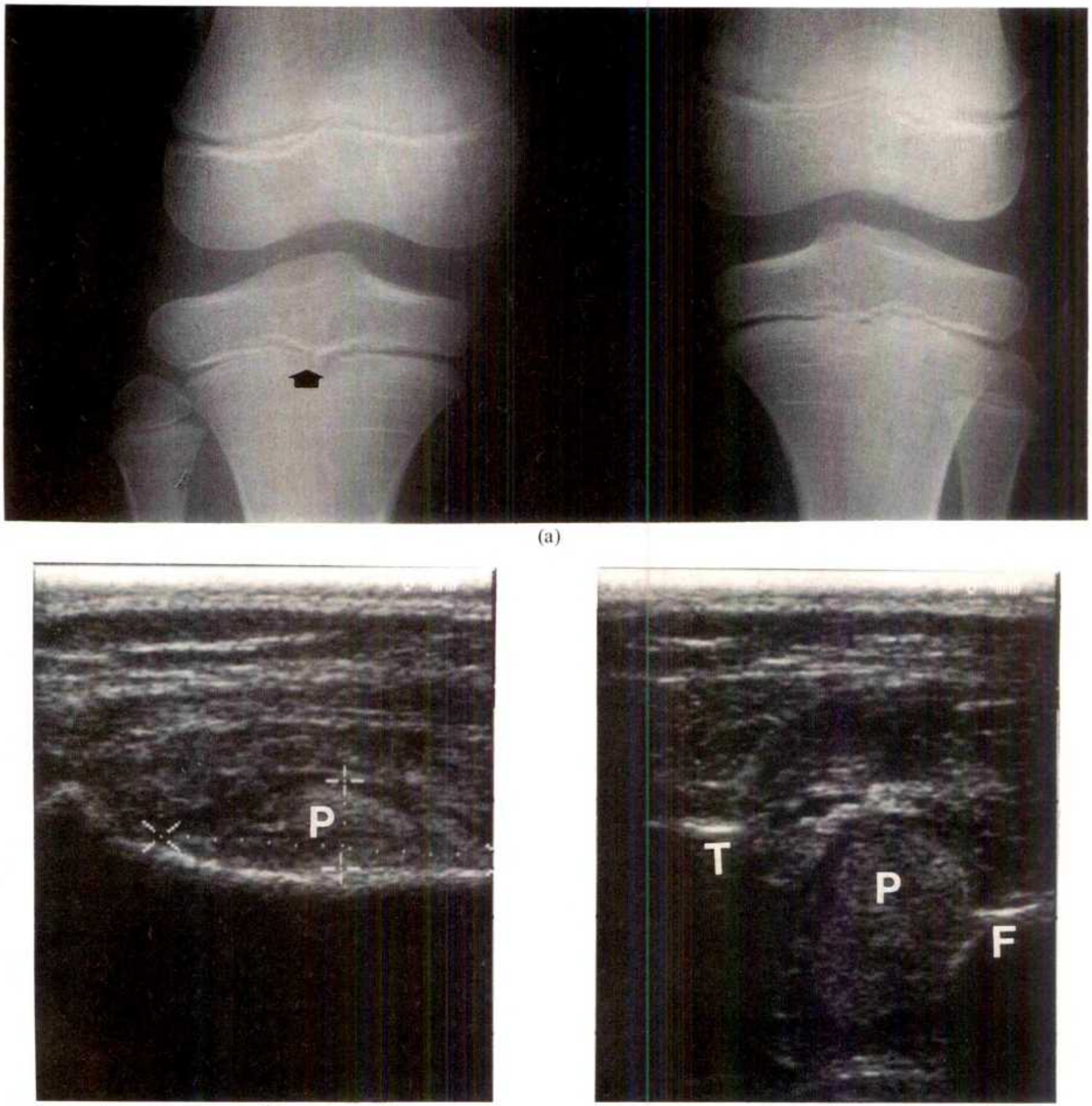

(a)

(b)

(c)

Figure 3. Small ill-defined lucency in metaphysis of the right tibia (arrow) is the site of osteomyelitis. (b) Longitudinal scan of the right tibial shaft. The pus collection (P) adjacent to the tibial shaft confirms the presence of osteomyelitis. (c) Transverse scan of the right tibia and fibula. The collection of pus (P) is seen to track between the tibia (T) and fibula (F) down to the interosseous membrane.

same area (Fig. 3b). This was assumed to lie under the periosteum and could be followed laterally and distally to a large collection lying deep adjacent to the interosseous ligament (Fig. 3c). The diagnosis of a large collection of pus secondary to osteomyelitis due to *Staphylococcus aureus* was confirmed at operation.

Case 4

Osteotomies for leg lengthening were performed on a boy with achondroplasia and held in place by Orthofix leg lengthening devices (Fig. 4a). The increasing gap between the bone segments was easily measured with ultrasound (Fig. 4b, c, d).

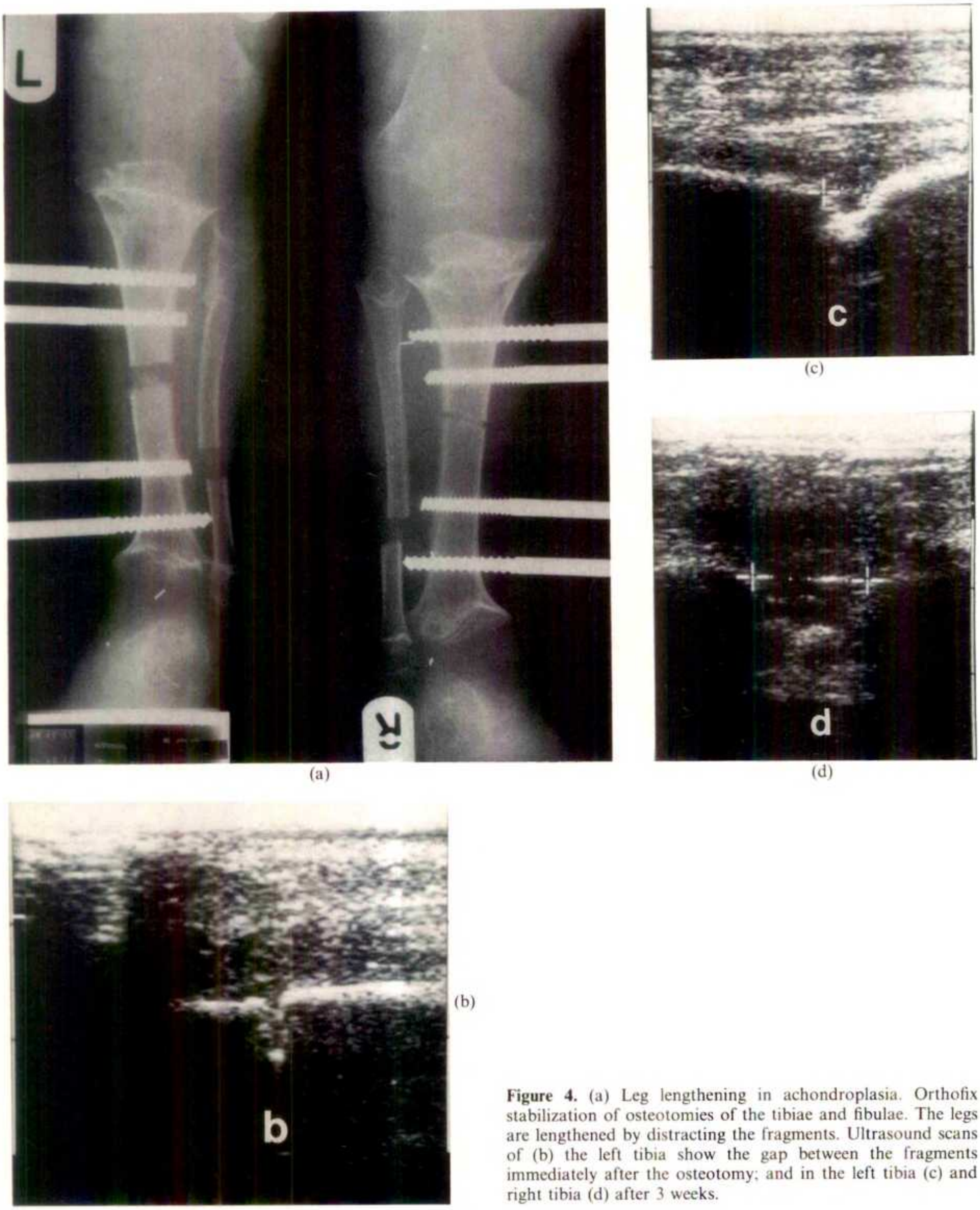

(a) (b) (c) (d)

Figure 4. (a) Leg lengthening in achondroplasia. Orthofix stabilization of osteotomies of the tibiae and fibulae. The legs are lengthened by distracting the fragments. Ultrasound scans of (b) the left tibia show the gap between the fragments immediately after the osteotomy; and in the left tibia (c) and right tibia (d) after 3 weeks.

Discussion

Ultrasound can help the clinician by making or confirming the diagnosis of damage to bone and by adding further useful information on the presence of associated soft-tissue injury or articular effusion. In Case 1 the presence of a large haemarthrosis was diagnosed on the evidence of the reflectivity of the intra-articular fluid. The fracture, which could have been confused with the humeral epiphyseal line, was confirmed. The presence of overt bone metastases had not been clinically suspected in Case 2. In Case 3 osteomyelitis was strongly suspected on clinical grounds and was confirmed by the fluid collection adjacent to the bone. The extent of the abscess tracking to lie on the interosseous membrane could not be appreciated without the use of ultrasound.

In cases of leg lengthening the Orthofix apparatus makes radiography of the underlying bone difficult, and ultrasound provides a safe and accurate way of determining the gap at the osteotomy sites without the use of radiation (Case 4). Ultrasound can also be used to assess new bone formation and fracture healing (personal observation and Leitgeb et al, 1990) but this application requires further investigation. Its value in trauma to unossified bone is well documented (Dias et al, 1988; Broker & Burbach, 1990). Our cases illustrate the value of ultrasound in the assessment of the continuity of bone surfaces and the condition of adjacent soft tissues. The examination is quick, simple, radiation-free and painless.

Acknowledgment

We wish to acknowledge the help of Mrs A. Allen with the ultrasound investigations.

References

BROKER, F. H. L. & BURBACH, T., 1990. Ultrasonic diagnosis of separation of the proximal humeral epiphysis in the newborn. *Journal of Bone and Joint Surgery, 72A* (2), 187–191.

DIAS, J. J., LAMONT, A. C. & JONES, J. M., 1988. Ultrasonic diagnosis of neonatal separation of the distal humeral epiphysis. *Journal of Bone and Joint Surgery, 70B* (5), 825–828.

GRAIF, M., STAHL-KENT, V., BEN AMI, T., STRAUSS, S., AMIT, Y. & ITZCHAK, Y., 1988. Sonographic detection of occult bone fractures. *Pediatric Radiology, 18*, 383–385.

HOWARD, C. B. & EINHORUN, M. S., 1991. Ultrasound in the detection of subperiosteal abscesses. *Journal of Bone and Joint Surgery, 73B*, 175–176.

LEITGEB, N., BODENTEICH, A., SCHWEIGHOFER, F. & FELLINGER, M., 1990. Ultrasonic diagnosis of fractures. *Ultraschall in der Medizin, 11*, 206–209.

YOUSEFZADEH, D. K. & RAMILO, J. L., 1986. Ultrasound diagnosis of osteomyelitis. In *Report of 23rd Congress of the European Society of Paediatric Radiology, Barcelona.* (ESPR, Hôpital Saint Vincent de Paul, 74 Avenue Denfert Rochereau, F-75674, Paris.)

1992, *The British Journal of Radiology*, 65, 594–597

Conventional 15 G needle technique for renal biopsy compared with ultrasound-guided spring-loaded 18 G needle biopsy

By N. J. A. Cozens, DMRD, J. T. Murchison, MRCP, P. L. Allan, FRCR and
*R. J. Winney, FRCP (Ed)

Departments of Radiology and *Renal Medicine, Royal Infirmary of Edinburgh, Edinburgh, UK

Based on a paper presented at the BMUS 23rd Annual Meeting in Bournemouth, on 10–12 December 1991

Keywords: Needle biopsy, Kidney, Ultrasound

Abstract. Two techniques for percutaneous renal biopsy were retrospectively reviewed to assess their relative safety and efficacy. Ultrasound localization of the kidney by a radiologists, with subsequent biopsy performed by a renal physician using a hand-held 15 G cutting needle (Tru-Cut), was compared with biopsy performed by a radiologist using an 18 G cutting needle with a spring-loaded biopsy device (Biopty) and real-time ultrasound guidance. The smaller needle with real-time ultrasound is more reliable at retrieving an adequate specimen for histological examination (93%) than the "conventional" technique (79%). Fewer complications occurred in the Biopty group although the difference did not reach statistical significance. The average length of stay in hospital was significantly shorter for elective biopsies with the Biopty device (1.80 compared with 2.93 nights, $p < 0.01$). We recommend the use of the Biopty device with an 18 G needle and real-time ultrasound guidance as the method of choice for percutaneous renal biopsy.

Percutaneous renal biopsy is an important procedure for many patients with renal disease. It was first reported in 1934 (Ball, 1934) and became routine during the early 1950s. The kidney was originally localized by correlating plain radiographs with anatomical landmarks (Kark & Muerck, 1954). Subsequent developments have focused on localization of the kidney rather than on modifications to the method of obtaining tissue. Plain radiographs, image intensification fluoroscopy with pyelography, radioisotope scanning, retrograde pyelography, static or real-time ultrasound and computed tomography have all been used to localize the kidney for subsequent biopsy (Madaio, 1990). Renal biopsy using these techniques is, however, not free of morbidity and is not always successful in obtaining a diagnostic specimen.

A recent modification to the technique of obtaining tissue has been possible since the introduction of an automated biopsy instrument, the "Biopty" gun (Lindgren, 1982). The safety and efficacy of this technique has not been compared with conventional renal biopsy (Madaio, 1990; Morrison et al, 1990). We initially started using the Biopty gun for difficult renal biopsies and subsequently for routine biopsies. This study compares our experience with conventional renal biopsy and the Biopty gun technique.

Method

We examined retrospectively the case notes of the first 100 patients on whom we performed renal biopsies using an 18 G needle with the Biopty device and of 50 consecutive patients on whom "conventional" renal biopsies had been performed with ultrasound localization. All the biopsies were performed between August 1988 and March 1991. Information was obtained regarding the indication for renal biopsy, whether the biopsy was elective or urgent, the frequency with which diagnostic tissue was obtained, the number of glomeruli in the specimen, complications and length of hospital stay.

The conventional technique for performing percutaneous renal biopsies in our hospital is similar to the method described recently by Beaman (1989). The patient lies prone with a rolled-up blanket placed under the abdomen to fix the kidney. The kidney (usually the right) is then localized by a radiologist using ultrasound and a suitable puncture site marked on the skin. Information on depth and direction is also given to the renal physician who is performing the biopsy. After infiltrating the subcutaneous tissues with local anaesthetic, the renal physician introduces a standard 20 G spinal needle along the planned track of biopsy, to locate the kidney, to and fro movement of the needle with respiration confirming renal puncture. The locating needle is then withdrawn and replaced by a 15 G Tru-Cut needle. Considerable patient co-operation is required as their breath must be held while advancing the needle, while the needle enters the kidney and during

---

Address correspondence to Dr J. T. Murchison.

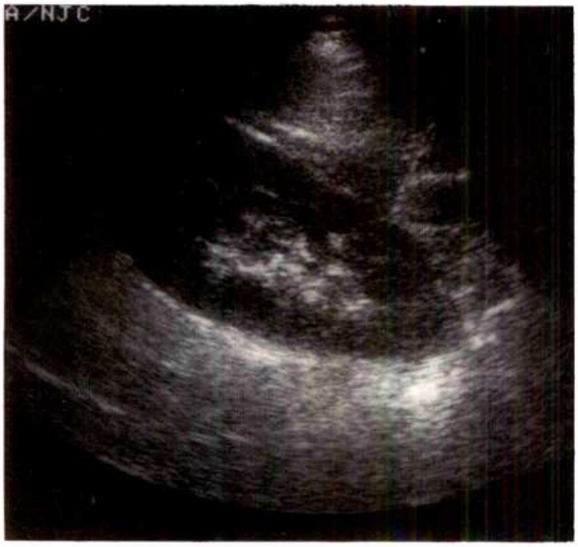

Figure 1. Biopty needle tip touching the renal capsule.

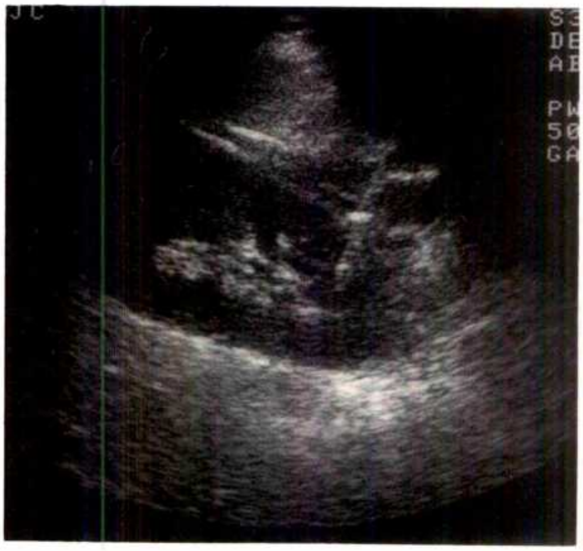

Figure 2. Biopty needle within renal cortex during biopsy.

the biopsy. Normally, using this technique, the aim is to obtain two cores of tissue.

For biopsy with the spring-loaded Biopty device and 18 G needle, the patient lies prone with a blanket roll or pillow under the abdomen, and the operator locates either the right or left kidney depending on which is more accessible for biopsy. The ultrasound transducer is then covered in a sterile plastic sheath containing a little ultrasound gel and sterile contact jelly is applied to the outside to provide ultrasound coupling. The operator can now use real-time control to guide the needle to the correct region of the kidney. After infiltration of skin and subcutaneous tissues with local anaesthetic, a small incision is made in the skin with the point of a scalpel blade. The 18 G needle is advanced through the tissues under direct ultrasound control and its relation to the kidney is assessed either from identifying the needle directly or by assessing the movement of the tissues as the needle is passing through them. The needle is a modified Tru-Cut design with an inner notched component and an outer sheath. When the needle is considered to be in the correct position, touching the renal capsule (Fig. 1), the device is triggered and the inner, notched part advances 1.1 cm into the kidney, followed almost immediately by the outer cannula. Often the needle can be identified on ultrasound within the cortex while the specimen is being obtained, thus confirming the location of biopsy (Fig. 2). The patient only needs to hold their breath for a short time whilst the Biopty device is triggered. Three to five passes are usually made.

Details of the two patient groups are shown in Table I, and the indications for renal biopsies for the patients in each group are recorded in Table II. The Biopty procedures were performed by a single radiologist with experience in biopsy techniques. The Tru-Cut biopsies were performed by experienced senior renal physicians (senior registrar or consultant). 10 of the Biopty patients had had previously unsuccessful

Table I. Patient details

	18 G Biopty	15 G Tru-Cut
Male	58	31
Female	42	19
Total	100	50
Age range (years)	14–79	15–74
Mean age (SD) (years)	49.3 (17.70)	43 (17.88)
Mean (SD) serum creatinine (μmol/l)	414 (471.8)	309 (321.0)
Elective admission for biopsy	51	28
Inpatient requiring biopsy	49	22
Mean (SD) length of stay in hospital for all elective biopsies (nights)	1.80 (1.11)	2.93 (1.94)

Table II. Indication for biopsy

	18 G Biopty: number of patients	15 G Tru-Cut number of patients (%)
Asymptomatic proteinuria	28	12 (24)
Microscopic haematuria	15	8 (16)
Acute renal failure	21	9 (18)
Chronic renal impairment	19	10 (20)
Nephrotic syndrome	16	10 (20)
Hypertension	1	0 (0)
Assessment of potential kidney donor	0	1 (2)
Total	100	50

Tru-Cut biopsies; two of these patients are in our 15 G Tru-Cut group, the others were initially biopsied elsewhere. One patient in the Tru-Cut biopsy group had previously undergone unsuccessful Biopty biopsy.

Comparison between groups was by χ^2 or unpaired Student's t-test with significance at the 5% level.

Results

Patients in the Biopty group were older (49.3 years compared with 43 years, two-sided t-test, $t = 2.044$, $p < 0.05$). There were no significant differences in mean serum creatinine (414 μmol/l versus 309 μmol/l, $t = 1.61$, not significant), ratio of males to females, elective to urgent biopsies or indications for biopsy (Tables I and II).

Table III shows the rates for histologically adequate and non-diagnostic biopsies as well as for failures when no renal tissue was obtained. Of the patients with non-diagnostic biopsies, one 18 G Biopty and three 15 G Tru-Cut biopsies were repeated using the same technique; therefore 100 patients underwent 101 biopsies, and 50 patients had 53 biopsies in the respective groups. Of these four repeated biopsies, all were diagnostic except for one of the 15 G Tru-Cut biopsies. Renal tissue and diagnostic biopsies were obtained significantly more often (χ^2, $p < 0.01$ and χ^2, $p > 0.05$, respectively) in the 18 G Biopty group. When biopsies were successfully obtained the average number of glomeruli per specimen was slightly greater with the 15 G Tru-Cut needle. The average length of time for the 18 G Biopty procedure (from entering to leaving the procedure room) was 24 min (range 15–45 min). This included an initial ultrasound examination of the patient's kidneys to assess them and confirm their suitability for biopsy. No accurate figures are available for the conventional biopsy group but our overall impression is that the time taken is considerably longer.

The average number of passes using the 18 G Biopty technique was 4.07 (range 2–8). Figures were only recorded in four cases of 15 G Tru-Cut biopsy with an average of 3.25 (range 2–4). It is difficult to know how representative these four cases are but it is the experience of one of the authors (R.J.W.) that it is not uncommon for a number of unsuccessful passes to be made before tissue is obtained.

Table III. Results of biopsies

Histological result of biopsy	18 G Biopty: number of biopsies	15 G Tru-Cut: number of biopsies (%)
Diagnostic biopsy obtained	93	42 (79)
Renal tissue obtained not diagnostic	7	4 (8)
No renal tissue obtained	1	7 (13)
Total	101	53
Total glomeruli per biopsy	1–25 (mean 9.0)	2–45 (mean 12.5)

This table combines both initial biopsies and repeat biopsies.

Complications generally tended to be more common (26% compared with 15%) in the 15 G group compared with the 18 G Biopty group (Table IV), but none of these differences was statistically significant (χ^2). Two patients in the Biopty group and one in the Tru-Cut group with back pain also had visible haematuria. The two patients who required transfusion after 15 G Tru-Cut biopsies also required renal angiography with embolization to control bleeding. None of the 18 G Biopty patients required angiography or surgical intervention. The single patient who required transfusion after 18 G Biopty had pre-existent cirrhosis with ascites and abnormal clotting. In this patient it was felt imperative to the management to confirm a suspected vasculitic cause for acute renal failure. Despite fresh frozen plasma and platelet cover for the biopsy, a large retroperitoneal haematoma developed 3 days post-biopsy; this was treated successfully with transfusion and conservative management. He had received 750 units/h of heparin for continuous venovenous haemofiltration after the biopsy and this may have been a contributory factor.

The length of stay in hospital after 15 G Tru-Cut biopsies is greater than after 18 G Biopty biopsies (2.93 nights compared with 1.80 nights, two-sided t-test, $t = 2.82$, $p < 0.01$, 95% confidence interval 0.34 to 1.92 nights difference).

Discussion

When we started using the 18 G Biopty gun technique for renal biopsy we hoped to confirm, as has already been shown with renal allograft biopsy (Ubhi et al, 1987; Bogan et al, 1990), that adequate diagnostic material would be obtained and to show that the complication rate would be reduced compared with a conventional biopsy technique.

This retrospective study has found that despite a smaller specimen size, diagnostic renal tissue is obtained in a significantly higher proportion of patients using the Biopty technique compared with the conventional technique. Real-time ultrasound guidance, giving more accurate localization of the needle in relation to the kidney and subsequent biopsy site in the renal cortex, would seem to be the reason for this. The Biopty system

Table IV. Complications

	18 G Biopty ($n = 101$)	15 G Tru-Cut ($n = 53$)
Nil	85 (85)	39 (74)
Back pain	12 (12)	11 (21)
Visible haematuria + clots	5 (5)	2 (4)
Transfusion required	1 (1)	2 (4)
Intervention required (embolization/surgery)	0 (0)	2 (4)

Data are expressed as numbers (percentages) of biopsies resulting in complications.

also results in less crush artefact or obscuring blood in the specimen obtained (Parker et al, 1989). The slightly smaller number of glomeruli per specimen obtained with the 18 G Biopty needle was unlikely to alter significantly the accuracy of the histological diagnosis (Corwin et al, 1988). In allograft kidneys, which lie superficially and are not affected by respiratory movement, real-time ultrasound localization may be less important and, indeed, Bogan et al (1990) found no improvement in the diagnostic biopsy rate using 18 G Biopty with real-time ultrasound localization.

Although there was no statistically significant difference in the complication rates between the two groups, each of the complications occurred less frequently in the 18 G Biopty group, and several factors may have spuriously increased the relative complication rate in this group. The patients biopsied were not matched precisely; indeed, those in the 18 G Biopty group were significantly older and had a higher mean serum creatinine. This tends to confirm our impression that since the introduction of the Biopty technique we are increasingly prepared to biopsy patients who in the past we were reluctant to biopsy because they were regarded as high risk. This has resulted from the more accurate localization with the 18 G Biopty technique, the impression that the elastic capsule is penetrated with greater ease and the rapid speed of the Biopty action, patient co-operation in breath holding thus being less critical. Our confidence in the technique means that the biopsies are now carried out on the severely ill, the very obese, the very anxious, patients with smaller kidneys, and patients who have some difficulty in co-operating for various reasons, such as language problems or mental retardation. This has the advantage that diagnosis may be established at an earlier stage in the patient's illness enabling the institution of appropriate early therapy. It is also our strong impression that the technique produces less pain and is much more acceptable to the patient.

The difference in length of stay in hospital for elective biopsies has important cost-saving implications. The length of stay in hospital after 15 G Tru-Cut biopsies was significantly longer than after the 18 G Biopty biopsies; this may be due to the development of complications requiring longer inpatient stay after elective biopsy in the 15 G Tru-Cut group. It has been suggested that percutaneous renal biopsy might be used in selected patients on a day-patient basis (Murphy & MacIsaac, 1989). Our results suggest that use of the Biopty gun may make this a more feasible and safer proposition.

We recommend use of the Biopty with an 18 G needle guided by real-time ultrasound as the method of choice for percutaneous renal biopsy.

References

BALL, D. P., 1934. Needle (aspiration) biopsy. *Journal of the Tennessee Medical Association, 27,* 203–206.

BEAMAN, M., 1989. How to perform a renal biopsy. *British Journal of Hospital Medicine, 41,* 158–160.

BOGAN, M. L., KOPECKY, K. K., KRAFT, J. L., HOLLADAY, A. O., FILO, R. S., LEAPMAN, S. B. & THOMALLA, J. V., 1990. Needle biopsy of renal allografts: comparison of two techniques. *Radiology, 174,* 273–275.

CORWIN, H. L., SCHWARTZ, M. M. & LEWIS, E. J., 1988. The importance of sample size in the interpretation of renal biopsy. *American Journal of Nephrology 8,* 85–89.

KARK, R. M. & MUEHRCK, R. C., 1954. Biopsy of kidney in prone position. *Lancet, i,* 1047–1049.

LINDGREN, P. G., 1982. Percutaneous needle biopsy. *Acta Radiologica (Diagr.), 23,* 653–656.

MADAIO, M. P., 1990. Renal biopsy. *Kidney International, 38,* 529–543.

MORRISON, R. T., BARR, J. G., WILKOWSKI, M. J., CAMPBELL, J. A. & NOLAN, C. R., 1990. A new technique for percutaneous renal biopsy (abstract). *Kidney International, 37,* 281.

MURPHY, B. F. & MACISAAC, A., 1989. Percutaneous renal biopsy as a day patient procedure. *American Journal of Kidney Disease, 14,* 77.

PARKER, S. M., HOPPER, K. D., YAKES, W. F., GIBSON, M. D., OWNDBEY, J. L. & CARTER, T. E., 1989. Image-directed percutaneous biopsies with a biopsy gun. *Radiology, 171,* 663–669.

UBHI, C. S., IRVING, H. C., GUILLAN, P. J. & GILES, G. R., 1987. A new technique for renal allograft biopsy. *British Journal of Radiology, 60,* 599–600.

1992, *The British Journal of Radiology*, 65, 598–604

Case reports

Two cases of isolated deficiency of all four limbs diagnosed antenatally with a review of the literature

By *W. L. Wong, MRCP(UK), FRCR, O. Clarke, DRC(R), DMU, J. Bhattacharya, MB, BS and L. M. MacDonald, MB, BS, FRCR

Clinical Radiology Department, St Thomas Hospital, London SE1 7EH, UK

Based on a paper presented at the BMUS 23rd Annual Meeting in Bournemouth, on 10–12 December 1991

Keywords: Congenital limb reduction anomalies, Amelia, Sonography, Prenatal diagnosis, Associations, Classification

Congenital absence of a limb (amelia) is extremely rare with an incidence ranging from between 0.05 to 0.15 per 10 000 live births with total absence of an upper limb having an incidence of between 0.02 to 0.07 per 10 000 live births (Birch-Jensen, 1949; Bod et al, 1983; Froster-Iskenius & Baird, 1990; Kallen et al, 1984). The different rates quoted probably reflect the different periods over which the cases were collected in the various studies, ranging from 3 to 32 years, rather than a true variation.

Complete absence of all four limbs is particularly unusual. Froster-Iskenius and Baird identified two cases amongst 1 213 913 consecutive live births in British Columbia between 1952 and 1984, one of which was associated with thalidomide exposure (Froster-Iskenius & Baird, 1990). In their search of the world literature, Dresher and MacDonell identified only 11 cases, including one described in 1886. To these they added a further two cases (Dresher & MacDonell, 1965).

We present two cases of severe limb reduction diagnosed by ultrasound scanning during the second trimester. In one case all four limbs were absent and in the other one limb was absent and there was severe reduction of the other three.

Case 1

A 37 year old Indian (G7, P6) presented for a routine ultrasound examination at 19 weeks. She had no family history of congenital abnormalities. There were no complications to the pregnancy at this time.

Ultrasound findings

A single live fetus of 19½ weeks gestation was demonstrated. All intracranial and intra-abdominal structures were normal and correctly sited. There was complete absence of both upper limbs (Fig. 1a). In addition, two soft tissue vestigial stumps were seen arising from the pelvis (Fig. 1b). The axial skeleton was normal. Liquor volume was normal.

The diagnosis of complete transverse deficiency (amelia) of all four limbs was made.

After discussion with the parents an elective termination of pregnancy was performed.

Autopsy findings

External examination showed the fetus to be female and confirmed the absence of all four limbs (Fig. 1c). No other external or internal anomalies were identified and the chromosome studies confirmed a normal 46XX karyotype.

Post-mortem radiographs of the fetus further verified the prenatal findings.

The patient became pregnant again and an ultrasound examination at 12/40 weeks revealed a normal fetus.

Case 2

A 26 year old single Jamaican (G2, P1) presented to the antenatal clinic with an uncertain last menstrual period date and a fundal height equivalent of 23/40 weeks. There was no family history of congenital abnormalities. An ultrasound scan was requested to date the pregnancy.

Ultrasound findings

A single fetus with a breech presentation was demonstrated. Measurements of biparietal diameter, head circumference and abdominal girth correlated with 24 weeks gestation. The major intracranial and intra-abdominal structures were normal and correctly sited. The left upper limb, however, terminated at the level of the elbow (Fig. 2d) and the right upper limb consisted of a soft tissue stump measuring 13 mm by 8 mm. In addition, there was marked foreshortening of both lower limbs with no detectable tibial or fibular ossification centres. The left femur was short and measured 9 mm. The other femur was not identified (Fig. 2b,c).

The diagnosis of complete transverse deficiency of the right arm, left forearm, right thigh and left leg was made.

On close questioning, the patient admitted to taking tablets in Jamaica for her pregnancy but the nature of these was not known.

The patient elected for a therapeutic abortion.

Autopsy findings

External examination showed the fetus to be male and confirmed the abnormalities of the upper limbs. In the lower limbs clubbed feet (talipes) with three toes were present attached to the femoral stumps (Fig. 2d). No other external or internal anomalies were identified. Chromosomal analysis of the fetal skin demonstrated a normal 46XY karyotype.

The post-mortem radiograph of the fetus further verified the prenatal findings in the upper limbs. It confirmed the ultrasound suspicion that the left femur was dysplastic with no

---

*Author to whom correspondence should be addressed.

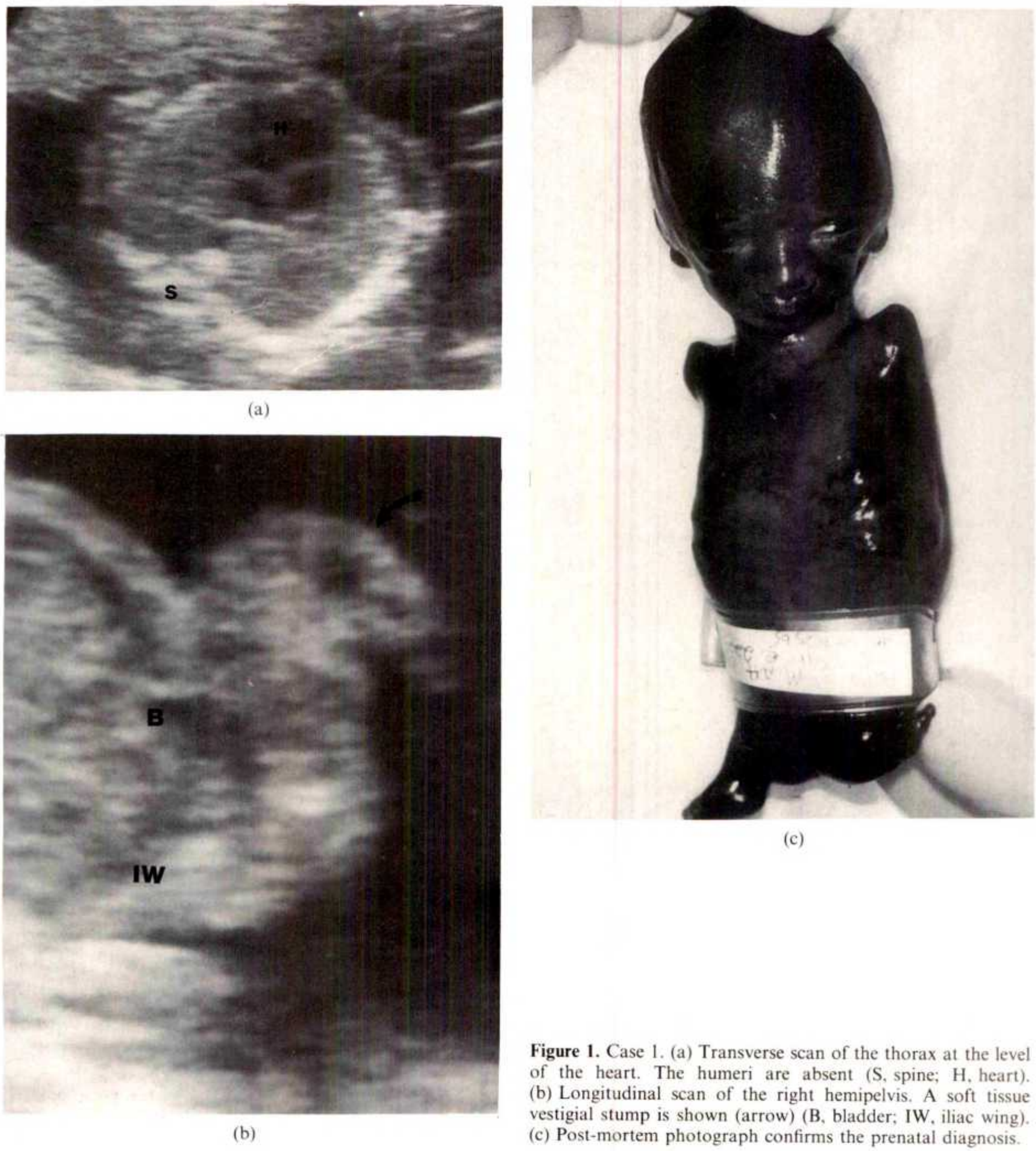

(a)

(b)

(c)

Figure 1. Case 1. (a) Transverse scan of the thorax at the level of the heart. The humeri are absent (S, spine; H, heart). (b) Longitudinal scan of the right hemipelvis. A soft tissue vestigial stump is shown (arrow) (B, bladder; IW, iliac wing). (c) Post-mortem photograph confirms the prenatal diagnosis.

bones distally. It also demonstrated complete longitudinal deficiency of the right femur, tibia, fibula and tarsal bones, together with the first and second metatarsals and phalanges. In addition dysplasia of the pelvis was observed.

Discussion

Advances in ultrasound imaging have allowed more accurate and earlier detection of congenital limb reduction anomalies. This is important as it gives both parents and physicians the opportunity to consider the full implications of continuing with the pregnancy and permits consideration of a therapeutic abortion. Our own experience, and that of others, suggest that the diagnosis may be established during the second trimester (Kaffe et al, 1977; Gollop et al, 1987; Romke et al, 1987; Robins et al, 1989). Interestingly as far as we are aware there have been no previous reports on the ultrasound diagnosis of the absence of all four limbs not

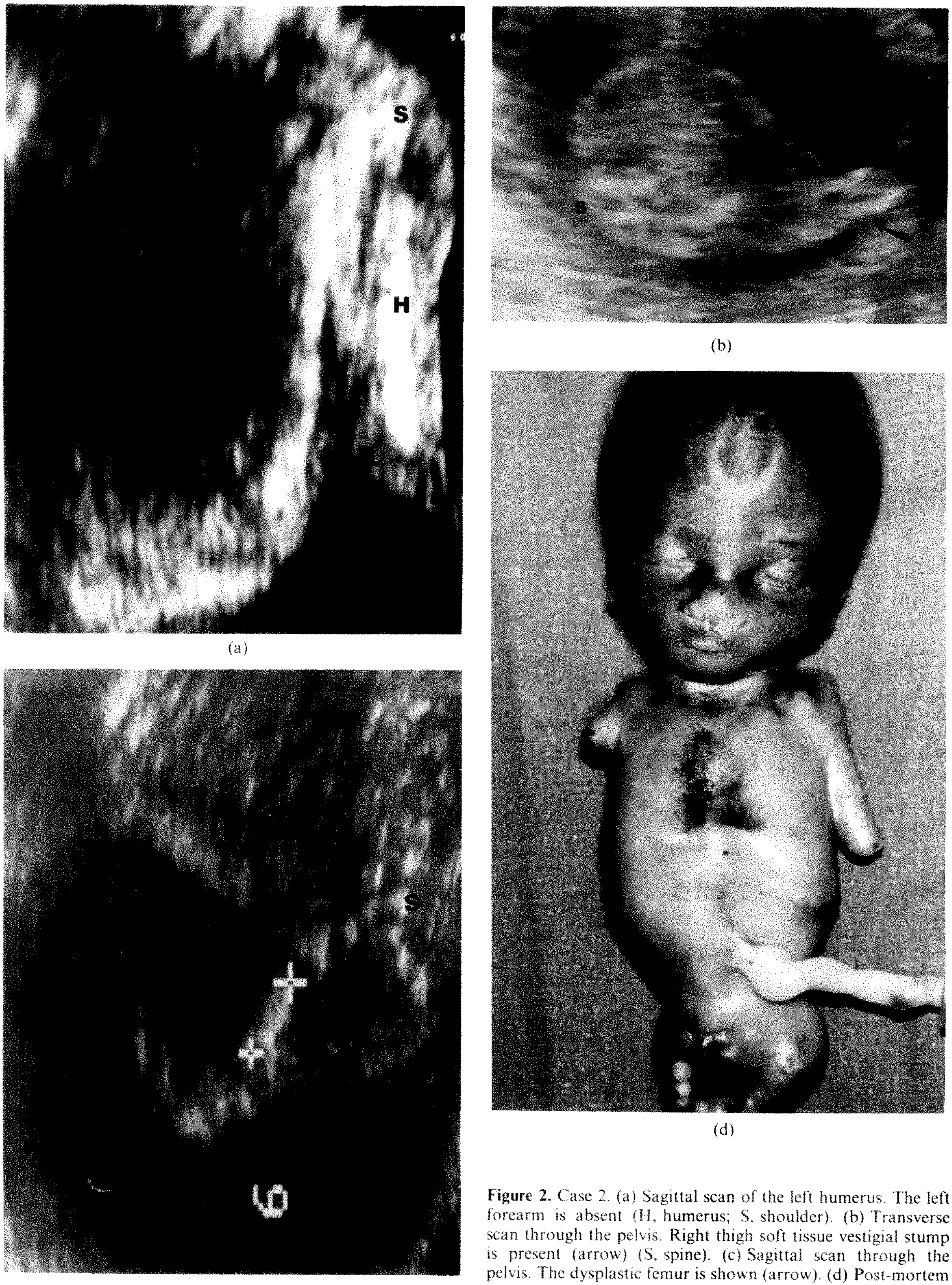

(a) (b) (c) (d)

Figure 2. Case 2. (a) Sagittal scan of the left humerus. The left forearm is absent (H, humerus; S, shoulder). (b) Transverse scan through the pelvis. Right thigh soft tissue vestigial stump is present (arrow) (S, spine). (c) Sagittal scan through the pelvis. The dysplastic femur is shown (arrow). (d) Post-mortem photograph confirms the prenatal diagnosis.

Table I. Conditions associated with complete absence of a limb

Syndrome/chromosomal anomaly	Non-limb defects	Comment
Amniotic band sequence[a] (Higginbottom et al, 1979; Chen & Gonzalez, 1987)	Craniofacial, cutaneous, thoraco-abdominal wall	Probably related to limb–body–wall complex
Femur/fibula/ulna complex (Kuhne et al, 1967)	—	Unilateral or bilateral complete absence of the upper limbs with incomplete reduction of the femur and fibula
Limb–body–wall complex (Van Allen et al, 1987a,b)	Vertebral, CNS, lungs, thoraco-abdominal wall, intestinal and renal atresia, diaphragmatic defects	—
Spleno-gonadal fusion[a] (Pauli & Greenlaw, 1982)	Orofacial, anal stenosis	
45, XX, C−[a] (Pawlowitzki et al, 1973)	Craniofacial, cardiac, abdominal, severe developmental retardation	Single case report, aborted fetus, 95 days post last menstrual period
(Falek et al, 1968)	Ipsilateral scaly skin, cardiovascular, ribs	1 case report
(Oertel, 1962)[a]	Gastrointestinal, lung	Male identical twins, all four limbs absent in both
(Ohdo et al, 1987)[a]	Hypertrichosis, facial, developmental retardation	2 cases, possibly AR homozygous
(Rindenz, 1939)	Mid-line maxillary cleft	Consanguinity
(Zimmer et al, 1985)[a]	Craniofacial, vertebral	6 male fetuses with absence of all four limbs in a family with consanguinity

[a] Syndromes associated with absence of all four limbs.
AR, autosomal recessive.

associated with other congenital anomalies. This is not entirely surprising as this constellation of abnormalities is extremely rare and it has only been within the past decade that resolution of ultrasound imaging has been adequate for the diagnosis of these anomalies.

In 61% of cases of complete absence of the limbs there are associated cardiovascular, gastrointestinal, urogenital, neural tube and respiratory anomalies, together with defects of other parts of the skeletal system and these are usually multiple (Froster-Iskenius & Baird, 1990). We found only four such cases of complete absence of limbs in the English language literature which had only one other defect. These were cleft palate, anencephaly, patent ductus arteriosus and vertebral malformations (Rogala et al, 1974; Herring, 1985; Froster-Iskenius & Baird, 1990).

There are a number of rare syndromes including the Roberts syndrome, some variants of the thrombocytopenia, absent radius (TAR) syndrome and Grebe syndrome associated with severe limb reduction anomalies (Filkins et al, 1984; Hall, 1987; Jones, 1988; Robins et al, 1989). However, in the majority of these, although limb reduction anomalies were severe, there was usually some skeletal structure present within the abnormal limb. As Brent and Homes noted the aetiologies for complete absence of a limb are much more restricted compared with those for limb reduction anomalies (Brent & Holmes, 1988). This is probably because absence of a limb or limbs results from a very early abnormal event in human development prior to the eighth embryonic week (10 weeks after the last menstrual period). The limb buds in the human embryo first appear in the third week, the upper limb buds appearing a few days before the lower ones. Complete absence of a limb is a result of either arrest or severe disruption of the normal development, owing to a vascular, teratogenic or mechanical accident to the limb bud (Moore, 1982). Table I lists some of the syndromes associated with complete limb absence.

Congenital absence of a limb may also be caused by exposure to thalidomide during pregnancy. Although it is no longer widely available, it is still used for the treatment of leprosy and may cause the thalidomide syndrome where such therapy is not supported by efficient contraceptive care (Gollop et al, 1987; Crawford, 1991). The limb reduction defects present in our second case, although characteristic of thalidomide exposure, could not be ascribed with certainty to this cause.

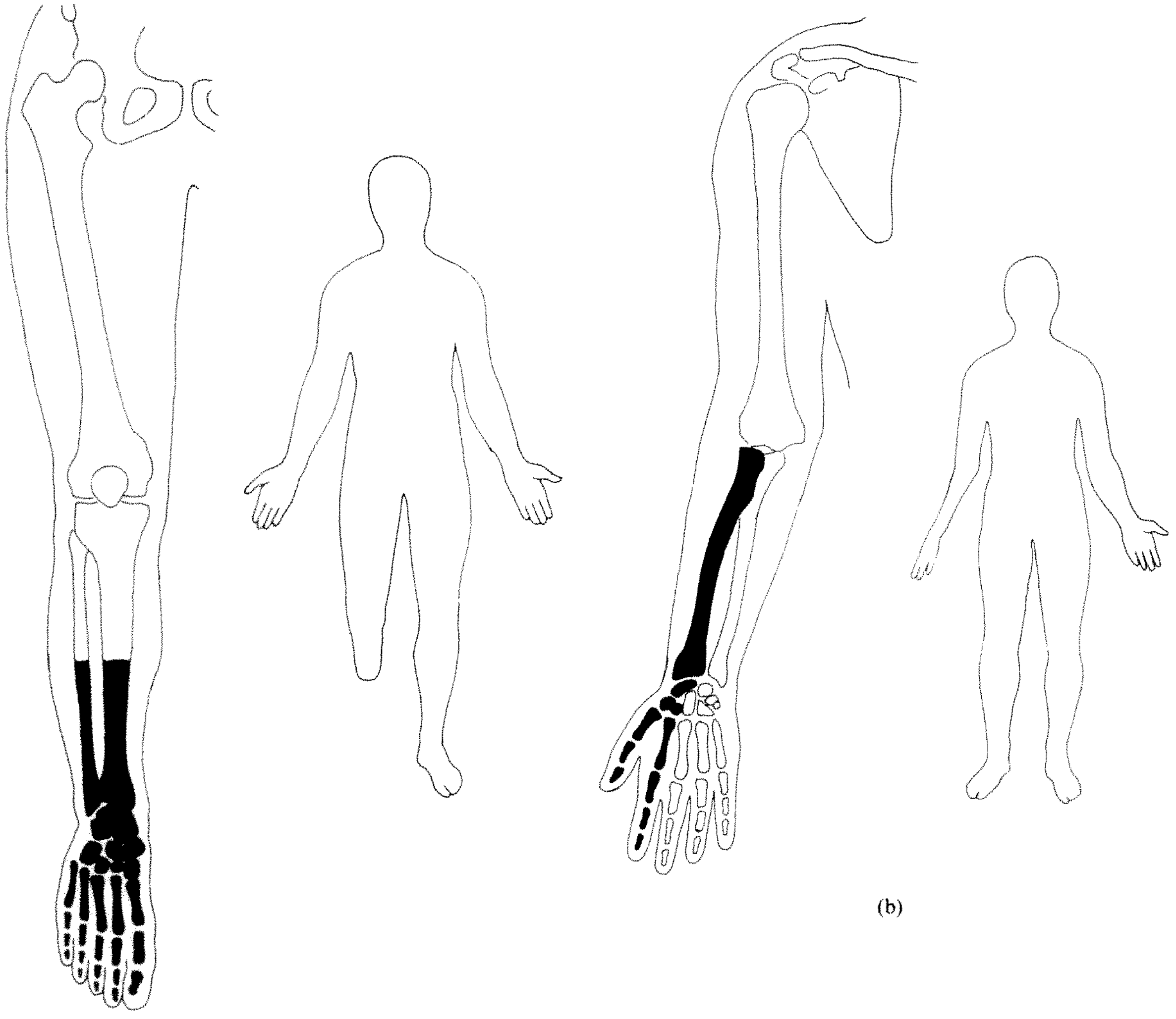

(a)

(b)

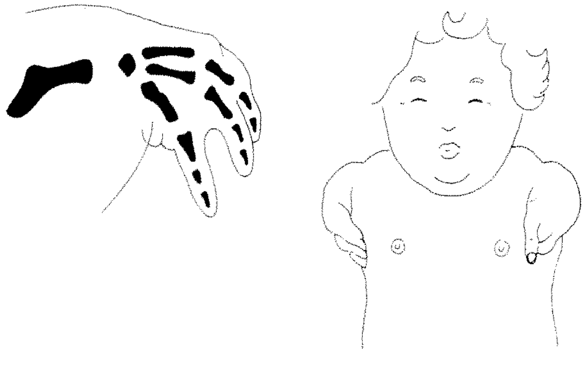

(c)

Figure 3. (a) Transverse deficiency of the middle third of the right leg (transverse deficiency—right, Le, middle). (b) Complete longitudinal deficiency of the right radius with partial longitudinal deficiency of the carpus and complete longitudinal deficiency of the thumb and index finger metacarpals and phalanges (longitudinal deficiency—right, Ra, complete; Ca, partial; MC 1, 2, complete; Ph 1, 2, complete). (c) Longitudinal deficiency of the left arm with complete absence of the humerus, partial absence of the radius and ulna with synostosis, partial absence of the carpus, complete absence of the thumb and index finger metacarpals and phalanges (longitudinal deficiency—left, Hu, complete; Ra and Ul, partial with synostosis; Ca, partial; MC 1, 2, complete; Ph, 1, 2, complete). The parenthensized version and abbreviations used are those suggested by the ISPO working party, (Ca, carpus; Hu, humerus; Le, leg; MC, metacarpals; Ph, phalanges; Ra, radius; Ul, ulna).

Other drugs, including pyridoxine (vitamin B6) in high doses, Debendox and the oral contraceptive pill have all been implicated in severe congenital limb reduction anomalies (Gardner et al, 1965; Nora & Nora, 1974; Jaffe et al, 1975; Janerich et al, 1975; Hughes & Cavanagh, 1983). Unfortunately many of these associations have been based on individual case reports or small series of patients and hence any apparent link may be entirely spurious (Brent & Holmes, 1988). Furthermore, none of these have been associated with complete absence of a limb.

Accurate classification of complex limb deficiencies should use a terminology that is clearly understood by all working in the field. The terminology used to date has often been confusing. Words such as ectromelia or meromelia do not always have the same meaning to those who use them and are incomprehensible to many others.

In 1975 a simplified classification was introduced by a working party sponsored by the International Society for Prosthetics and Orthotics (ISPO). Unfortunately it is still not widely used. With this system every limb deficiency is considered as either transverse or longitudinal. The transverse defects encompass all so-called congenital amputation-type conditions. These deficiencies are further characterized by the level at which the limb terminates, all skeletal elements distal to that level being absent. At the level of the arm, forearm, thigh and leg complete, upper, middle and lower third are used to describe the precise level of termination. Distally, the terms partial and complete are used.

For example if one row of carpal bones is present the limb reduction anomaly would be described as a partial transverse carpal deficiency. Complete transverse deficiency of the carpus would indicate no bones distal to the radius and ulna.

The second major category includes all deficiencies not in the transverse category. With these longitudinal defects each deficiency is described by naming the bone(s) affected and indicating whether they are completely or partially absent. In cases where hypoplasia is found the bone(s) so involved is named (ISPO, 1975). Figure 3a,b,c illustrates the application of this classification procedure.

An editorial article in the *Lancet* around the time of publication of this classification system suggested that terms such as amelia and phocomelia were so well established in ordinary clinical practice in the UK that they were unlikely to be dropped immediately. Nevertheless it urged us to adopt this system in case records and reports, as universal adoption of this system, it felt, would go a long way to promote international understanding of limb reduction anomalies and all that can be done to help those who suffer from them (Lancet, 1975).

We conclude that total absence of a limb may be diagnosed in the second trimester of pregnancy. When such a diagnosis has been established it is important to exclude other skeletal anomalies as well as those involving other organ systems. Exposure to drugs during the pregnancy, especially thalidomide, have also to be considered. All limb reduction anomalies should be classified according to the ISPO recommendations.

Acknowledgment

We acknowledge the kind secretarial assistance of Karen Kemmett.

References

Birch-Jensen, A., 1949. Congenital deformity of the upper extremities. *Opera ex Domo Biologica Heredita Humana, 19,* 31–43.

Bod, M., Czeizel, A. & Lenz, W., 1983. Incidence at birth of different types of limb reduction abnormalities in Hungary 1975–1977. *Human Genetics, 65,* 27–33.

Brent, R. L. & Holmes, L. B., 1988. Clinical and basic science lessons from the thalidomide tragedy: what have we learned about the causes of limb defects? *Teratology, 38,* 241–251.

Chen, H. & Gonzalez, E., 1987. Amniotic band sequence and its neurocutaneous manifestations. *American Journal of Medical Genetics, 28,* 661–673.

Crawford, C. I., 1991. Use of thalidomide in leprosy. *British Medical Journal, 303,* 1404.

Dresher, C. S. & MacDonell, J. A., 1965. Total amelia. *Journal of Bone and Joint Surgery, 47A,* 511–516.

Falek, A., Heath, C. W., Ebbin, A. J. & McClean, W. R., 1968. Unilateral limb and skin deformities with congenital heart disease in two siblings: a lethal syndrome. *Journal of Pediatrics, 73,* 910–913.

Filkins, K., Russo, J., Bilinki, I. & Searle, B., 1984. Prenatal diagnosis of thrombocytopenia, absent radius syndrome using ultrasound and fetoscopy. *Prenatal Diagnosis, 4,* 139–142.

Froster-Iskenius, U. G. & Baird, P. A., 1990. Amelia: incidence and associated defects in a large population. *Teratology, 41,* 23–31.

Gardner, L. I., Welsh-Sloan, J. & Cady, R. B., 1985. Phocomelia in an infant whose mother took large doses of pyridoxine during pregnancy. *Lancet, I,* 636.

Gollop, T. R., Eigher, A. & Guidugli Neto, J., 1987. Prenatal diagnosis of thalidomide syndrome. *Prenatal Diagnosis, 7(4),* 295–298.

Hall, J. G., 1987. Thrombocytopenia and absent radius (TAR) syndrome. *Journal of Medical Genetics, 24,* 79–83.

Herring, 1985. Amelia and scoliosis. *Journal of Paediatrics, 5,* 605–609.

Higginbottom, M. C., Jones, K. C., Bryan, D. H., Smith, D. W., 1979. The amniotic band disruption complex: timing of amniotic rupture and variable spectra of consequent defects. *Journal of Pediatrics, 95,* 544–549.

Hughes, D. T. & Cavanagh, N., 1983. Chromosomal studies in children with phocomelia exposed to Debondex during early pregnancy (letter). *Lancet, II,* 399.

ISPO, 1975. The proposed international terminology for the classification of congenital limb deficiencies. *Developmental Medicine and Childhood Neurology, 17, Supplement 34.*

Jaffe, P., Liebermann, M. M., McFadyen, I. & Valman, H., 1975. Incidence of congenital limb reduction deformities (letter). *Lancet, I,* 526–527.

Janerich, D. T., Piper, J. M. & Glebatis, D. M., 1975. Congenital limb reduction deficiencies (letter). *Lancet, I,* 931.

Jones, K. L., 1988. Grebes syndrome. In *Smiths Recognisable Patterns of Human Malformation,* ed. by K. L. Jones (W. B. Saunders, Philadelphia) p. 258.

Kaffe, S., Rose, J. S., Godmilow, L., Walker, B. A., Kerenyi, T., Beratis, N., Reyes, P. & Hirschhorn, K., 1977. Prenatal diagnosis of renal anomalies. *American Journal of Medical Genetics, 1,* 241–251.

Kallen, B., Rahmani, T. M. Z. & Wimberg, J., 1984. Infants with congenital limb reduction registered in the Swedish register of congenital malformation. *Teratology, 29,* 73–85.

Kuhne, D. W., Lenz, K., Peterson, D. & Sconberg, L., 1967. Defekt von femur und fibula mit amelia promelia oder ulnaren. *Strahldefekten der Arme Humangenetik, 3,* 244–263.

LANCET, 1975. Nomenclature of congenital limb deficiencies (editorial). *Lancet*, *II*, 117.

MOORE, K. L., 1982. *The Developing Embryo*, 3rd edn (W. B. Saunders, Philadelphia).

NORA, J. J. & NORA, A. H., 1974. Can the pill cause birth defects? (editorial). *New England Journal of Medicine*, *291*, 731–732.

OERTEL, O., 1962. Amelia bei Zwillingen. *Monatschrift Kinderheilkunde*, *11*, 481–484.

OHDO, S., MADOKORO, H., SONODA, T., TAKEI, M., YASUDA, H. & MORI, N., 1987. Association of tetra-amelia ectodermal dysplasia hypoplastic lacrimal ducts and sacs opening towards the exterior peculiar face and developmental retardation. *Journal of Medical Genetics*, *24*, 609–612.

PAULI, R. M. & GREENLAW, A., 1982. Limb deficiency and splenogonadal fusion. *American Journal of Medical Genetics*, *13*, 81–90.

PAWLOWITZKI, I. H., CENANI, A. & FRISCHBIER, H. J., 1973. Autosomal monosomy (45, XX, C−) in the human embryo with total amelia and further malformations. *Clinical Genetics*, *4*, 193–202.

RINDEZ, 1939. Uber doppelseitige aplasie freien oberen Gliedmasse (brachiale amelia). *Zeitungen Geburtschrifte Gynäkologie*, *118*, 442–447.

ROBINS, D. B., LADDA, R. L., THEIME, G. A., BOAL, D. K., EMANUEL, B. S. & ZACKAI, E. H., 1989. Prenatal detection of Roberts-SC phocomelia syndrome—report of 2 sibs with characteristic manifestations. *American Journal of Medical Genetics*, *32*, 390–394.

ROGALA, E. J., WYNNE-DAVIES, R., LITTLEJOHN, A. & GORMLEY, J., 1974. Congenital limb anomalies: frequency and aetiological factors. *Journal of Medical Genetics*, *11*, 221–233.

ROMKE, C., FROSTER-ISKENIUS, U., HEYNE, K., HOHN, W., HOF, M., GRZEJSZCK, G., RAUSKOLB, R., REHDER, H. & SCHWINGER, E., 1987. Roberts syndrome and SC phocomelia—a single genetic entity. *Clinical Genetics*, *31*, 170–177.

VAN ALLEN, M. I., CURRY, C., WALDEN, C. E., GALLAGHER, L. & PATTEN, R. M., 1987b. Limb body wall complex: II. Limb and spine defects. *American Journal of Medical Genetics*, *28*, 549–565.

VAN ALLEN, M. I., CURRY, C. & GALLAGHER, L., 1987a. Limb reduction wall complex: I. Pathogenesis. *American Journal of Medical Genetics*, *28*, 529–548.

ZIMMER, Y., SOVA, M. Y., DIVON, M., PERY, M. & PERETZ, B. A., 1985. Tetra-amelia with multiple malformations of one kindred. *European Journal of Pediatrics*, *144*, 412–414.

Ultrasound demonstration of a leaking hydatid cyst of the liver causing "cyst within a cyst" appearance

By B. Banerjee, FRCS, DMRD, FRCR, A. Rennison, BSc(Hons), DCRR and *Q. M. Haque, DMRD, FRCR

Department of Diagnostic Radiology & Imaging, Tameside General Hospital, Ashton-Under-Lyne, Lancashire OL6 9RW and *Ormskirk District General Hospital, Wigan Road, Ormskirk, Lancashire L39 2AZ, UK

Based on a poster presented at the BMUS 23rd Annual Meeting in Bournemouth, on 10–12 December 1991

Keywords: Unilocular hydatid cyst, Simple liver cyst, endocyst, "Cyst within a cyst"

Echinococcal disease may affect any part of the body; the liver is the most frequently affected organ (75%) (Saidi, 1976). Although a cyst with internal septation or loculation is the classical ultrasound description of hydatid cyst of the liver, in reality unilocular cysts are more frequently encountered (Sciarrino et al, 1991). On ultrasound unilocular hydatid cysts are usually indistinguishable from innocent simple hepatic cysts, which are common incidental findings during ultrasound examination of the liver. Moreover, in a non-endemic area the index of suspicion is low and the possible diagnosis of hydatid disease may not be entertained when unilocular cysts are detected in the liver. On rare occasions, however, the thin internal membrane, the endocyst, of a unilocular hydatid cyst may separate spontaneously from the thick outer ectocyst, giving rise to the appearance of a cyst with a membrane-like structure beneath its wall. Demonstration of the internal membrane is considered to be pathognomonic of hydatid disease (Beggs, 1983; Garcia et al, 1988) and allows a firm diagnosis of hydatid disease by ultrasound alone. We present a case to illustrate the above mechanism.

Case report

A 42-year-old woman presented with dyspepsia and vague right upper quadrant discomfort and underwent ultrasound examination of the abdomen for suspected calculous disease of the gallbladder. Her past medical history was unremarkable and her whole blood count and urine analysis were normal. On ultrasound no calculus was detected in the gallbladder or bile ducts and the gallbladder appeared normal. A thin-walled unilocular echo-free cystic space of 2.7 cm diameter was noted in the right lobe of the liver (Fig. 1). This was diagnosed as a

---

Address correspondence to Dr B. Banerjee.

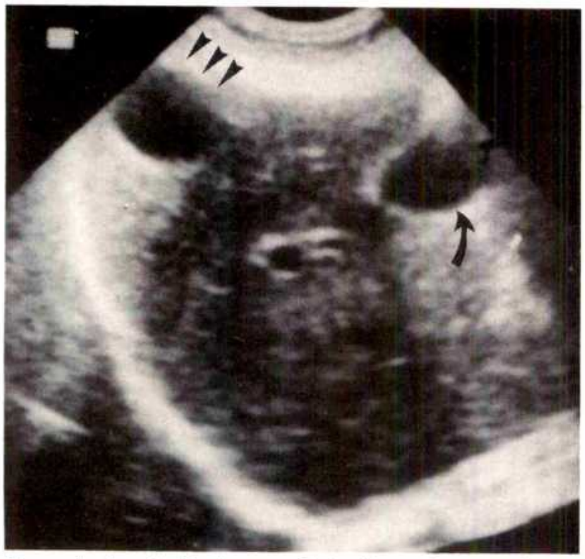

Figure 1. Longitudinal scan of the liver, demonstrating a unilocular cyst in the right lobe of the liver (arrowheads). There is no evidence of internal echo and there is distal enhancement. A normal gallbladder is seen (curved arrow).

simple liver cyst and considered to be an innocent incidental finding.

Several days later, the patient attended the Accident and Emergency Department with an acute exacerbation of her symptoms and a clinical diagnosis of acute cholecystitis was made. A repeat ultrasound examination, performed within a short time of her arrival, revealed no evidence of gallbladder disease, but there was a striking change in the appearance of the cystic lesion in the right lobe of the liver. There was now a membrane-like structure partially separated from the inner wall of the capsule of the cyst (Fig. 2) and, while scanning was still in progress, the sonographer witnessed the complete separation of the internal membrane from the capsule of the cyst, producing a "cyst within a cyst" appearance (Fig. 3).

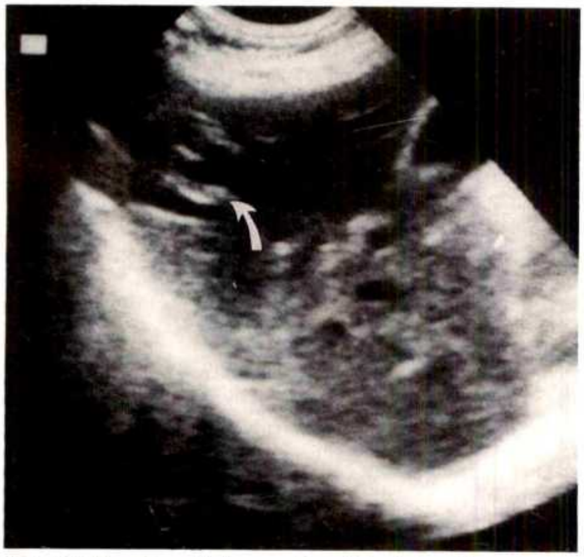

Figure 2. There is partial separation of the internal membrane, the endocyst (curved arrow), from the outer cyst wall, the ectocyst.

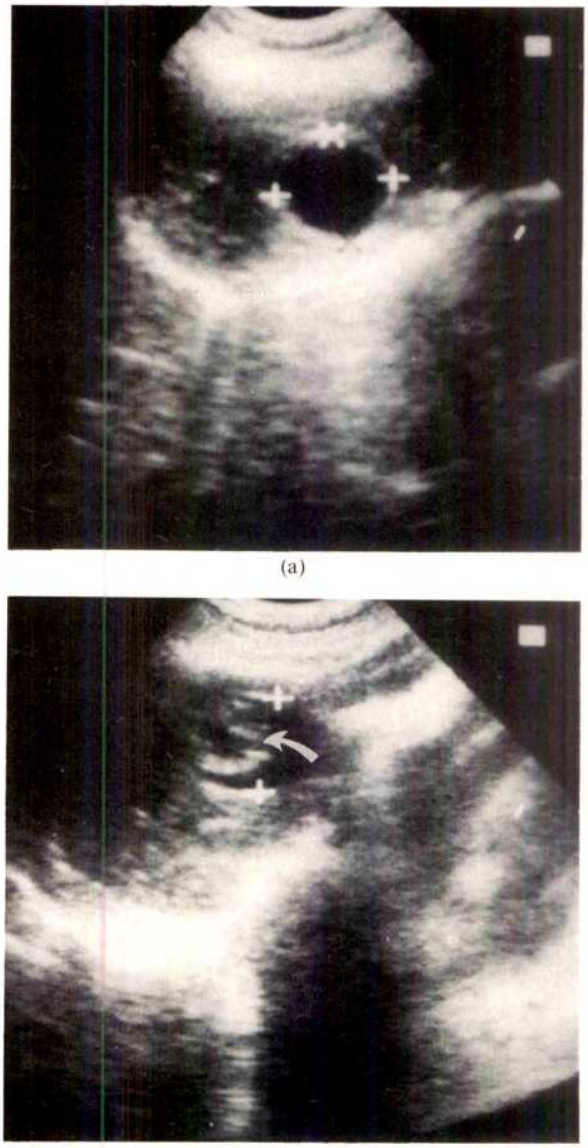

(a)

(b)

Figure 3 caption and part (c) overleaf.

During and after the completion of the separation of the internal membrane the patient did not experience any increased discomfort. A complement fixation test for hydatid disease was positive, confirming the diagnosis. The blood count and liver function tests were normal and on enquiry no definite association with endemic areas of hydatid disease was revealed. The patient was discharged from the hospital within a few days following improvement of her acute symptoms but some vague discomfort persisted.

Discussion

The ultrasound appearance of hydatid cysts of liver is varied. The diagnostic difficulty of "solid" forms of

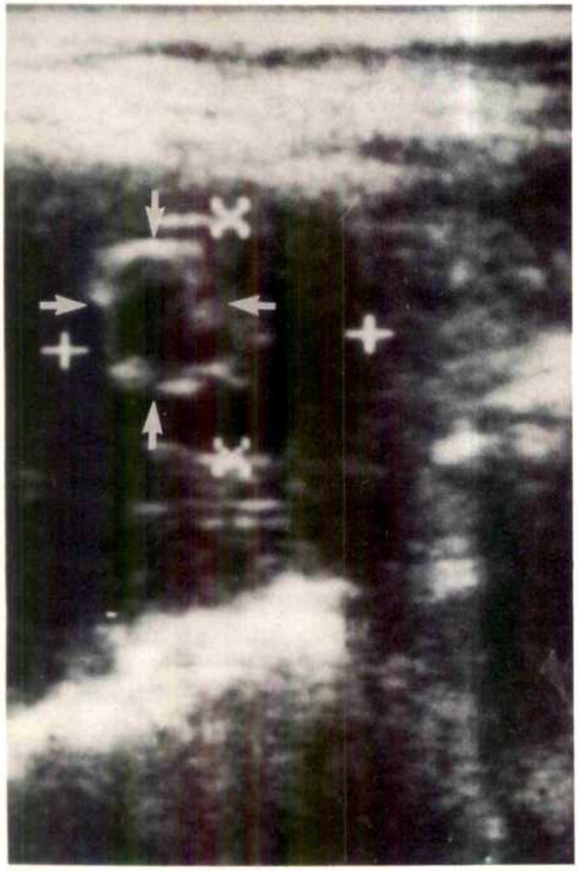

(c)

Figure 3. (a) Oblique sagittal view of the right lobe of the liver showing the intact wall of the hydatid cyst. (b) Partial separation of the internal membrane of the cyst (curved arrow) is noted at the beginning of the examination. (c) There is now complete separation of the internal membrane, giving rise to a "cyst within a cyst" appearance (arrowheads) while the ultrasound examination is still in progress.

hydatid cyst is well documented (Garcia et al, 1988). Unilocular echo-free hydatid cysts may be indistinguishable from simple hepatic cysts by ultrasound. However, demonstration of an internal membrane in such a cyst is considered to be pathognomonic of hydatid; therefore, when serology is negative, demonstration of an internal membrane may be the only indicator of the true nature of the cyst. Detachment of the internal membrane is most likely due to a host defence mechanism or ageing of the parasite (Lewall & McCorkell, 1986).

Some authors believe that the univesicular cyst represents the fully developed form of the parasite, and the subsequent stages after rupture of the cyst, namely separation of the internal membrane and formation of daughter cysts, are attempts at survival by the parasite (Barriga et al, 1983).

This case illustrates that echinococcal disease should be considered in the differential diagnosis of every cyst in the liver, even though the patient may not have lived in an endemic area.

Acknowledgment

Thanks to Mr R. Biggs for the photography.

References

Barriga, P., Cruz, F. V. & Lathrop, R., 1983. An ultrasonographically solid, tumor-like appearance of echinococcal cysts in the liver. *Journal of Ultrasound in Medicine* 2 (3), 123–125.

Beggs, I., 1983. The radiological appearances of hydatid disease of the liver. *Clinical Radiology*, *34*, 555–563.

Garcia, F. J., Marti-Bonmati, L., Menor, F., Rodrigues, B. & Ballesta, A., 1988. Echogenic forms of hydatid cysts: sonographic diagnosis. *Journal of Clinical Ultrasound*, *16*, 305–311.

Lewall, D. B. & McCorkell, S. J., 1986. Rupture of echinococcal cysts. *American Journal of Roentgenology*, *146*, 391–394.

Saidi, F., 1976. *Surgery of Hydatid Disease* (Saunders, Philadelphia), Ch. 3, pp. 31–155.

Sciarrino, E., Virdone, R., Loiacono, O., Fusco, G., Ricca, T., Cottone, M., Maringhini, A. & Della Monia, A., 1991. Ultrasound changes in abdominal echinococcosis treated with Albedozole. *Journal of Clinical Ultrasound*, *19*, 143–148.

1992, *The British Journal of Radiology*, *65*, 607–609

The thread and streak sign of portal vein tumour thrombus demonstrated by colour Doppler imaging

By K. McBride, FRCR, FFRRCSI and J. Masterson, FRCR

Department of Diagnostic Imaging, St Vincents Hospital, Elm Park, Dublin 4, Ireland

Based on a poster presented at the BMUS 23rd Annual Meeting in Bournemouth, on 10–12 December 1991

Keywords: Portal vein tumour thrombus, Colour Doppler imaging, CT portal venography

The angiographic, computed tomographic (CT) and real-time ultrasound demonstration of portal vein invasion and tumour thrombus is well documented, particularly in association with hepatocellular carcinoma (Gregg et al, 1975; Miller & Thomas, 1979; Freeny, 1980). One sign of portal vein tumour thrombus is the "thread and streak" sign first described angiographically in 1975 (Okuda et al, 1975). In this paper, we describe an unusual case of portal vein tumour thrombus first suspected by colour Doppler imaging (CDI). There have been no previously documented cases to show the thread and streak sign using this technique.

Case report

A 73-year-old man presented with a 4-month history of back pain, anorexia, weight loss and dyspnoea. He had a history of left pneumonectomy for squamous cell carcinoma of the bronchus 12 years previously, and a more recent history of drainage of left empyema 9 months earlier. On examination he had hepatomegaly, finger clubbing and ankle oedema. Chest radiography showed signs of previous surgery, but no suspicion of malignant recurrence. Real-time abdominal ultrasound revealed multiple large masses within the liver and an irregular mass within the portal vein. The portal venous flow was hepatopetal. CDI with an Acuson 128 unit displayed disturbed flow within and around the mass (Fig. 1). On biopsy, the liver masses proved to be poorly differentiated squamous cell carcinoma consistent with multiple metastases from a presumptive chest recurrence. Portal venous phase angiography and CT portography (Fig. 2) confirmed the thread and streak appearance seen at CDI. The patient died 6 months later but postmortem examination was refused.

Discussion

The first description of the "thread and streak sign" was in 1975 (Okuda et al, 1975). In all their cases the patients had hepatocellular carcinoma (HCC). The streaks shown angiographically correspond to the blood spaces and vessels that run longitudinally in and around a tumour cast growing in the portal vein or one of its large branches.

Since then, many authors have shown the propensity for HCC to cause portal vein tumour thrombus (Gregg et al, 1975; Freeny, 1980; Vigo et al, 1980). The first ultrasound demonstration of portal vein invasion with HCC was described in 1979 by Miller and Thomas, but other ultrasound studies have followed (Brunelle & Chaumont, 1984; Subramanyam et al, 1984; Miller & Berland, 1985; Van Gansbeke et al, 1985; Price et al, 1990). The "thread and streak" sign has also been

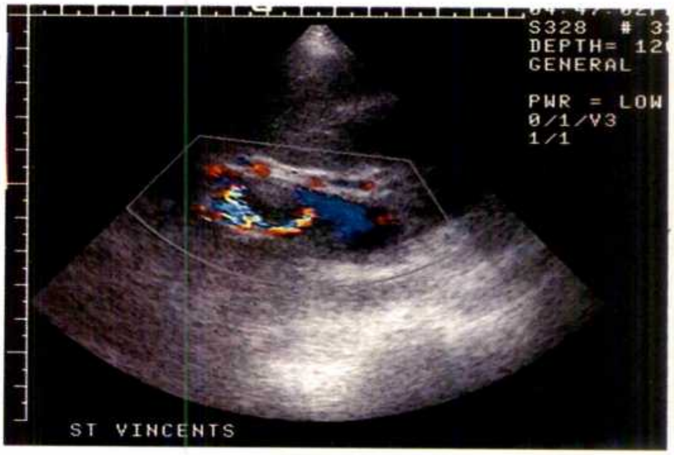

Figure 1. Colour Doppler scan of the main portal vein. There is disturbed, mainly hepatopetal, flow within the portal vein. Flow through the tumour is demonstrated. The thread and streak sign can be seen.

Address correspondence to Dr K. McBride, Department of Diagnostic Imaging, Northern General Hospital Trust, Herries Road, Sheffield S5 7AU, U.K.

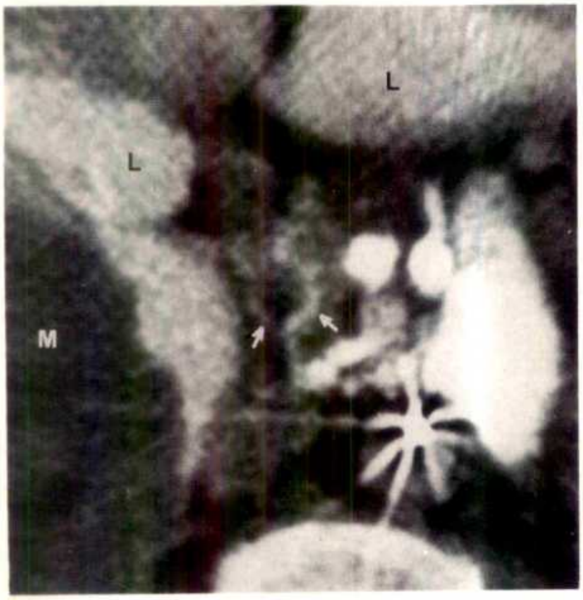

Figure 2. CT portography showing streaky enhancement within the portal vein (arrows). L, liver; M, unenhanced metastasis.

described using CT angiography (Suzuki et al, 1982), but never before on CDI. This sign is indicative of portal vein tumour extension, though not exclusively of HCC. Other malignant lesions have been implicated in causing portal vein involvement, including gastric carcinoma (Takayasu et al, 1989; Araki et al, 1990), pancreatic carcinoma (Van Gansbeke et al, 1985; Garra et al, 1987), childhood hepatic tumours (Brunelle & Chaumont, 1984), cholangiocarcinoma (Gold et al, 1979), renal and colonic hepatic metastases (Heaston et al, 1981) and leiomyosarcoma of the portal vein (Wilson & Hine, 1987). Liver metastases from lung have never been definitely proven to cause portal vein tumour thrombus (Heaston et al, 1981). Magnetic resonance imaging (MRI) has shown promise in identifying portal vein thrombosis and may even be able to differentiate between tumour thrombus and blood clot (Hricak et al, 1985).

There has been no previously documented demonstration of the thread and streak sign using CDI, but its usefulness had been predicted (Alpern et al, 1987). They suggested that CDI would allow clearer differentiation between artefactual intraluminal echoes and soft thrombus and also allow for quicker determination of branch patency. These predictions have been borne out in this report. The normal variations of portal appearance on CDI are well described (Ralls, 1990).

This case report serves as a reminder that portal vein tumour thrombus is seen not only with hepatocellular carcinoma, but also with metastatic disease. It also demonstrates intraluminal tumour by a non-invasive method, previously shown only by angiography and CT portography.

References

Alpern, M. B., Rubin, J. M., Williams, D. M. & Capek, P., 1987. Porta hepatis: duplex Doppler US with angiographic correlation. *Radiology*, *162*, 53–56.

Araki, T., Suda, K., Sekikawa, T., Ishii, Y., Hihara, T. & Kachi, K., 1990. Portal venous tumor thrombosis associated with gastric adenocarcinoma. *Radiology*, *174*, 811–814.

Brunelle, F. & Chaumont, P., 1984. Hepatic tumors in children: ultrasonic differentiation of malignant from benign lesions. *Radiology*, *150*, 695–699.

Freeny, P. C., 1980. Portal vein tumor thrombus: demonstration by computed tomographic arteriography. *Journal of Computer Assisted Tomography*, *4*, 263–264.

Garra, B. S., Shawker, T. H., Doppman, J. L. & Sindelar, W. F., 1987. Comparison of angiography and ultrasound in the evaluation of the portal venous system in pancreatic carcinoma. *Journal of Clinical Ultrasound*, *15*, 83–93.

Gold, J. A., Sostman, H. D. & Burrell, M. I., 1979. Cholangiocarcinoma with portal vein obstruction. *Radiology*, *130*, 15–20.

Gregg, F. P., Goldstein, H. M., Wallace, S. & Casey, J. H. (1975. Arteriographic demonstration of intravenous tumor extension. *American Journal of Roentgenology*, *123*, 100–105.

Heaston, D. K., Chuang, V. P., Wallace, S. & de Santos, L. A., 1981. Metastatic hepatic neoplasms: angiographic features of portal vein involvement. *American Journal of Roentgenology*, *136*, 897–900.

Hricak, H., Amparo, E., Fisher, M. R., Crooks, L. & Higgins, C. B., 1985. Abdominal venous system: assessment using MR. *Radiology*, *156*, 415–422.

Miller, E. I. & Thomas, R. H., 1979. Portal vein invasion demonstrated by ultrasound. *Journal of Clinical Ultrasound*, *7*, 57–59.

Miller, V. E. & Berland, L. L., 1985. Pulsed Doppler duplex sonography and CT of portal vein thrombosis. *American Journal of Roentgenology*, *145*, 73–76.

Okuda, K., Musha, H., Yoshida, T., Kanda, Y., Yamazaki, T., Jinnouchi, S., Moriyama, M., Kawaguchi, S., Kubo, Y., Shimokawa, Y., Kojiro, M., Kuratomi, S., Sakamoto, K. & Nakashima, T., 1975. Demonstration of growing casts of hepatocellular carcinoma in the portal vein by celiac angiography: the thread and streaks sign. *Radiology*, *117*, 303–309.

Price, J., Chan, M., Hamilton-Wood, C., Chronos, N. A. F., Mok, S. D. & Metreweli, C., 1990. Sonographic diagnosis of portal vein invasion in patients with hepatocellular carcinoma: comparison with arterial portography. *Clinical Radiology*, *41*, 9–12.

Ralls, P. W., 1990. Color Doppler sonography of the hepatic artery and portal venous system. *American Journal of Roentgenology*, *155*, 517–525.

Subramanyam, B. R., Balthazar, E. J., Hilton, S., Lefleur, R. S., Horii, S. C. & Raghavendra, B. N., 1984. Hepatocellular carcinoma with venous invasion. Sonographic–angiographic correlation. *Radiology*, *150*, 793–796.

Suzuki, M., Itoh, H., Konishi, H., Ida, M., Matsui, O. & Takashima, T., 1982. Hepatocellular carcinoma involving the portal vein. *Journal of Computer Assisted Tomography*, *6*, 831–832.

Takayasu, K., Tajiri, H., Noguchi, M., Ishikawa, T. & Maruyama, K., 1989. Imaging diagnosis of portal tumor thrombus secondary to gastric cancer. *Gastrointestinal Radiology*, *14*, 161–163.

Van Gansbeke, D., Avni, E. F., Delcour, C., Engelholm, L. & Struyven, J., 1985. Sonographic features of portal vein

1992, *The British Journal of Radiology*, *65*, 609–610

thrombosis. *American Journal of Roentgenology*, *144*, 749–752.

VIGO, M., DE FAVERI, D., BIONDETTI, P. R. & BENEDETTI, L., 1980. CT demonstration of portal and superior mesenteric vein thrombosis in hepatocellular carcinoma. *Journal of Computer Assisted Tomography*, *4*, 627–629.

WILSON, S. R. & HINE, A. L., 1987. Leiomyosarcoma of the portal vein. *American Journal of Roentgenology*, *149*, 183–184.

Prenatal ultrasonographic diagnosis of an aneurysm of the vein of Galen

By L. Worswick, HDCR, DMU, R. F. Lamont, MD, MRCOG, R. Thomas, MRCP and H. Gordon, FRCS, FRCOG

Department of Obstetrics and Gynaecology, Northwick Park Hospital, Watford Road, Harrow, Middlesex HA1 3UJ, UK

Based on a poster presented at the BMUS 23rd Annual Meeting in Bournemouth, on 10–12 December 1991

Keywords: Prenatal, Ultrasound, Doppler, Aneurysm of the vein of Galen

Case report

A 31-year-old white woman, gravida 2, para 1 was admitted to hospital because of pre-term labour at 29 weeks gestation. An ultrasound scan at 18 weeks gestation at the referring hospital had shown normal fetal anatomy.

On admission, an ultrasound scan revealed a midline, fusiform, echo-free area measuring 35 mm × 20 mm × 20 mm in the fetal brain, superior to the thalamus and extending posteriorly (Fig. 1). The remainder of the fetal anatomy was normal, except for mild left-sided renal pelvic dilatation. There were no signs of fetal hydrops or ascites. An aneurysm of the vein of Galen (AVG) was suspected and Doppler studies were performed which revealed arterial type flow within the cystic structure (Fig. 2).

Serial ultrasound scans were carried out at weekly intervals and there was no evidence of any development of hydrocephaly. At 35 weeks gestation, cardiomegaly and polyhydramnios were diagnosed and at 36 weeks gestation scalp oedema was detected.

Full discussion took place between the parents, paediatricians and neurosurgeons and, as a result of these discussions, the parents expressed a wish for non-intervention and non-aggressive management. At 38 weeks gestation the patient went into spontaneous labour and had a normal vaginal delivery of a female infant weighing 2650 g with Apgar scores of 4 at 1 min and 8 at 5 min. Physical examination was normal and neonatal cerebral ultrasound confirmed the prenatal diagnosis. The baby died at 48 h of congestive heart failure.

Discussion

The vein of Galen is a major cerebral vein running superoposterior to the thalami within the subarachnoid space. It joins the inferior sagittal sinus, which runs along the lower edge of the cerebral falx, to form the straight sinus. Aneurysmal dilatation of the vein of Galen is usually found in close association with a variety of patterns of arterio-venous communication.

Prenatal diagnosis and visualization of this condition has been reported (Hirsch et al, 1983; Vintzileos et al, 1986; Evans & Twining, 1991). The first reported case in the British literature was not a true antenatal diagnosis but was made neonatally and retrospectively matched with antenatal ultrasound (Mao & Adams, 1983).

Usually, AVG presents during the neonatal period with congestive cardiac failure secondary to the large arterio-venous communication. Occasionally, symptoms may not develop until after the first year of life when seizures, syncope and subarachnoid haemorrhage occur.

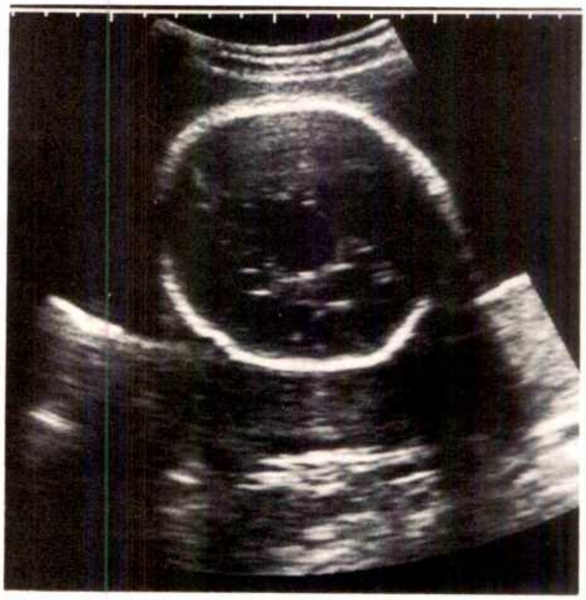

Figure 1. Transverse section through the fetal head demonstrating a midline echo-free area.

Address correspondence to R. F. Lamont.

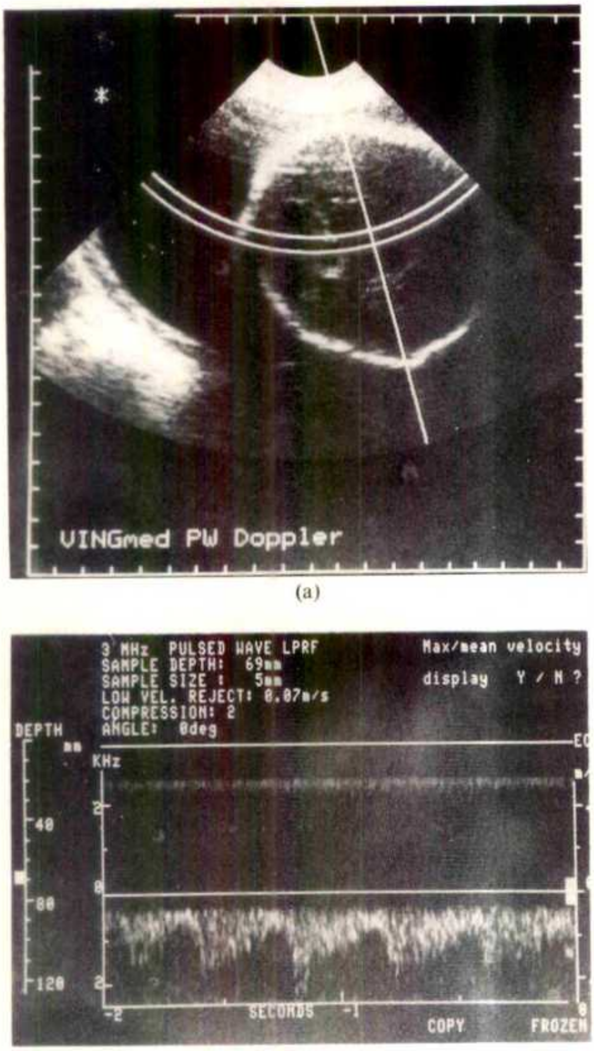

(a)

(b)

Figure 2. (a) Transverse section through the fetal head showing the Doppler gate placed within the aneurysm. (b) Doppler trace of the flow through the aneurysm of the vein of Galen.

It is likely that only severe forms of AVG will be detected in utero and, in these cases, careful evaluation of fetal anatomy and search for non-immune hydrops and destructive lesions of the cerebral parenchyma are recommended as these have important implications for the prognosis. Serial scans should be performed to detect signs of hydrops or the development of hydrocephaly, as these conditions are associated with a very bad prognosis. As this condition has so rarely been diagnosed prenatally we cannot be sure whether it is possible to diagnose it early enough to offer termination of the pregnancy. No data exist with respect to the optimal mode and timing of the delivery and much would depend on the decision of the parents about how aggressive the management should be.

In this case prenatal diagnosis permitted full discussion between the parents and all the health professionals likely to be involved with the care of the infant, and permitted conscious and structured decisions about the future management to be made. This case emphasizes the importance of ultrasound evaluation of women admitted in pre-term labour and also the importance of Doppler flow studies used in conjunction with ultrasound imaging.

References

EVANS, A. J. & TWINING P., 1991. Case report: *In utero* diagnoses of a vein of Galen aneurysm using colour flow Doppler. *Clinical Radiology, 44*, 281–282.

HIRSCH, J. H., CYR, D., EBERDHART, H. & ZUNKEL, D., 1983. Ultrasonic diagnosis of an aneurysm of the vein of Galen *in utero* by duplex scanning. *Journal of Ultrasound in Medicine, 2*, 231–233.

MAO, V. & ADAMS, C., 1983. Antenatal diagnosis of intracranial arteriovenous fistula by ultrasonography. Case report. *British Journal of Obstetrics and Gynaecology, 80*, 872–875.

VINTZILEOS, A. M., EISENFIELD, L. I., CAMPBELL, W. A., HERSON, V. C., DILEO, P. E. & CHAMEIDES, L., 1986. Prenatal ultrasonic diagnosis of AV malformation of the vein of Galen. *American Journal of Perinatology, 3*, 209–211.

1992, *The British Journal of Radiology*, *65*, 611–613

Epitheloid haemangioendothelioma of liver: a vascular tumour easily mistaken for metastatic carcinoma on ultrasound imaging

By B. Banerjee, FRCS, FRCR and A. Rennison, BSc(Hons), DCRR

Department of Diagnostic Radiology & Imaging, Tameside General Hospital, Ashton-Under-Lyne, Lancashire OL6 9RW, UK

Based on a poster presented at the BMUS 23rd Annual Meeting in Bournemouth, on 10–12 December 1991

Keywords: Epitheloid haemangioendothelioma, Focal hepatic lesions, Hepatic metastasis, Factor VIII related antigen

Epitheloid haemangioendothelioma is a rare neoplasm of vascular origin that may occur in the liver. Although there have been sporadic reports of this tumour in the past, the term "epitheloid haemangioendothelioma" was first suggested by Weiss and Enzinger only recently (Weiss & Enzinger, 1982). The tumour usually affects adults and pursues a relatively benign course intermediate between haemangioma and angiosarcoma; long-term survival with chemotherapy, hepatic resection and hepatic transplant has been documented. Scant reference can be found to its radiographic appearances. We present a case to illustrate the ultrasound appearances of this tumour and emphasize its potential confusion with metastatic disease.

Case report

A 29-year-old woman presented with persistent right upper quadrant abdominal pain and anorexia over a period of 2 months. She had undergone laparotomy and repair of a liver laceration 16 years earlier, following a riding accident, but had been in good health in the intervening period. Physical examination revealed a tender and slightly enlarged liver. Total blood count, haematocrit, ESR, liver function tests and urine analysis were normal.

Ultrasound examination of the liver revealed multiple, well defined, echo-poor lesions of varying sizes (Fig. 1), the largest of which was somewhat lobular in outline with a maximum diameter of 3 cm (Fig. 2). There were also a few lesions with slightly increased central reflectivity mimicking "target" lesions (Fig. 3). The liver was not unduly enlarged and its contour was normal. On ultrasound, diagnosis of multiple hepatic metastases was made, but meticulous ultrasound search for a primary lesion was negative. A radiograph of the chest revealed two small lung metastases (Fig. 4). At laparotomy a firm liver with multiple white nodules in both lobes was found, but there was no evidence of a primary lesion in any other abdominal organs.

Histological examination of the liver biopsy revealed widespread fibrosis with effacement of acinar architecture. There was proliferation of "strands" and "nests" of tumour cells and

Address correspondence to Dr B. Banerjee.

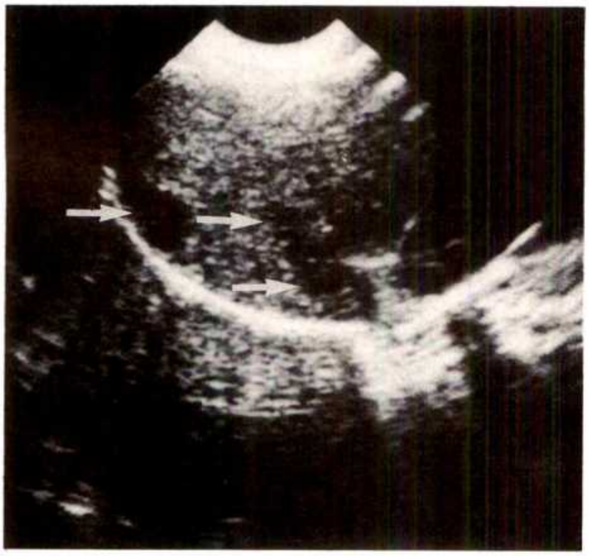

Figure 1. Longitudinal scan through the right lobe of the liver demonstrating multiple echo-poor areas of varying sizes (arrows).

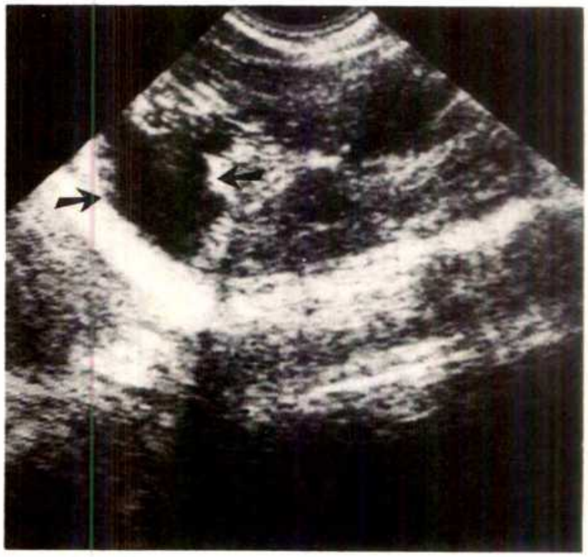

Figure 2. Sagittal section through the lateral clavicular line, demonstrating the largest of the echo-poor lesions, which has a lobulated outline (arrows).

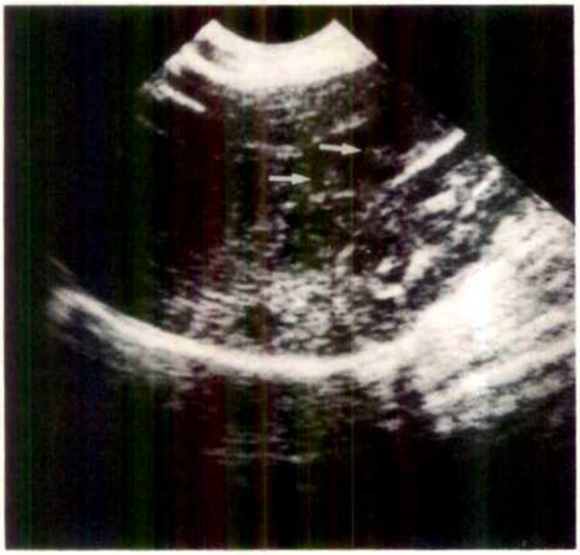

Figure 3. A few small focal areas of slight increase in reflectivity are present in some of the echo-poor lesions, producing a "target" appearance (arrows).

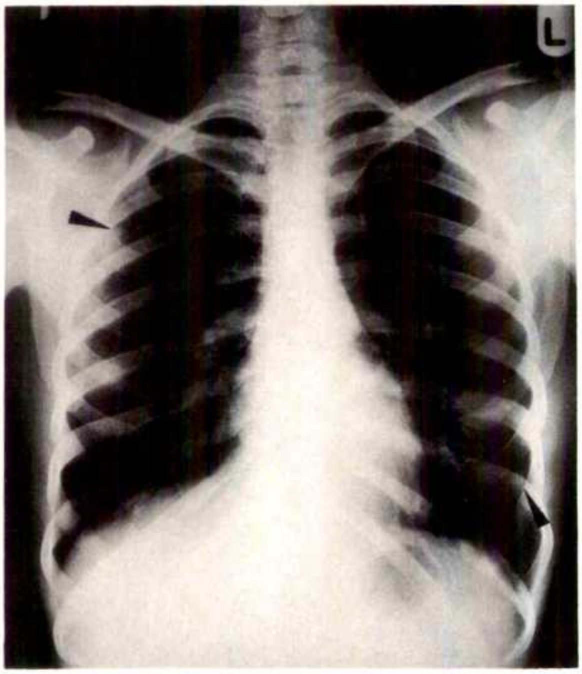

Figure 4. Radiograph of the chest revealing two small lung metastases (arrowheads).

vascular channels in the fibrotic area. The endothelial lining showed hyperplasia but scant evidence of mitosis. The tumour cells were rounded or polygonal in shape and many contained a sharply defined cytoplasmic vacuole (Fig. 5a, b). A histological diagnosis of epithelial haemangioendothelioma was made. Factor VIII related antigen was identified in the neoplastic endothelial cells by the peroxidase-antiperoxidase (PAP) technique, further confirming the diagnosis. Owing to the presence of pulmonary metastases the patient was treated with chemotherapy alone and is still alive and ambulant 5 years after the initial diagnosis, although the primary tumour and pulmonary metastases have increased in size.

Discussion

Epitheloid haemangioendothelioma is a distinct form of vascular tumour. It may occur in superficial and deep soft tissues but quite often the liver is the primary site. It is composed of rounded or spindle-shaped endothelial cells that can synthesize factor VIII related antigen. The pattern of solid growth and epitheloid appearance of endothelial cells may lead to a mistaken histological diagnosis of metastatic carcinoma (Weiss & Enzinger, 1982). Immunohistochemical identification of factor VIII in such cases should indicate the vascular origin of the tumour and distinguish it from metastasis.

There are several possible aetiological factors known to contribute to certain hepatic neoplasms. These

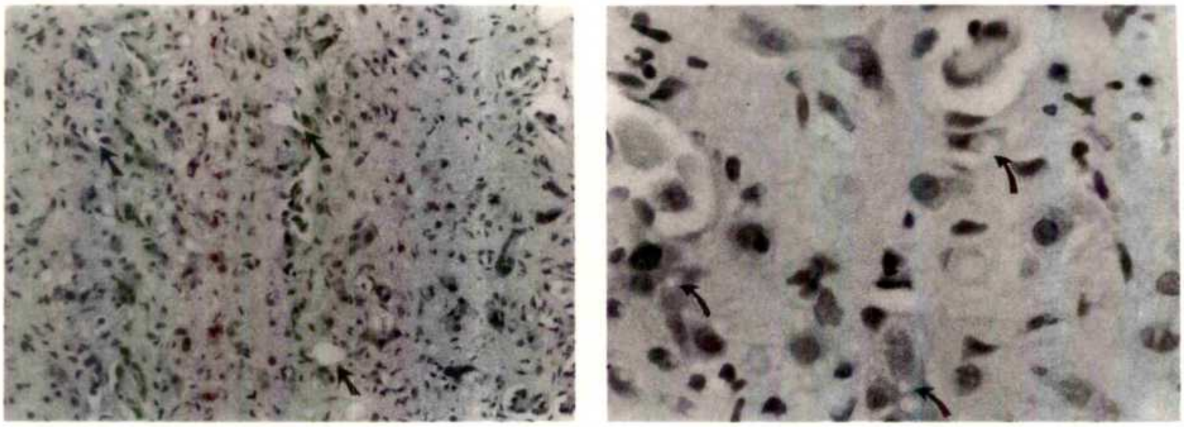

(a)

(b)

Figure 5. (a) Histological section of the tumour demonstrating abundant fibrous stroma in which tumour cells occur singly and in small clusters or stands, in places enclosing a small lumen (arrows). (b) Magnified view of tumour cells, which are spindle-shaped, rounded or oval; a few contain sharply defined cytoplasmic vacuoles (arrows).

include hepatitis B, alcoholism, previous Thorotrast administration, oral contraceptives, anabolic steroids, vinyl chloride and arsenic (Falk et al, 1981; Ishak et al, 1984) but none has been clearly linked with epitheloid haemangioendothelioma of liver. However, two patients with pulmonary epitheloid haemangioendothelioma have been reported to have had prior exposure to occupational contaminants (Dail et al, 1983). The patient in our case report sustained major trauma to her liver, requiring surgical repair. The possibility of trauma as an aetiological factor has not been previously suggested.

The radiographic features of this tumour have been poorly documented. Plain radiographs may show calcification in the liver and pulmonary metastases. The tumours are seen as hypodense areas in the liver substance on computed tomography. Angiography may demonstrate neovascularity in the tumour with distortion of vessels by multiple segmental expansions (Ishak et al, 1984). Splenoportogram and hepatic venograms may demonstrate displacement of intrahepatic venous tributaries and scintigraphy may reveal multiple photon deficient areas (Chowdhury et al, 1977). The ultrasound features of this tumour have not yet been formally documented. On ultrasound imaging, the tumours in our patient were seen as multiple, well defined, echo-poor areas of varying sizes in both lobes of the liver. One or two larger lesions had a somewhat lobulated outline and a few smaller lesions demonstrated a "target" appearance.

Long-term survival in epitheloid haemangioendothelioma of the liver, even without antimitotic treatment, has been well documented (Chowdhury et al, 1977; Ishak et al, 1984). In the absence of metastases, treatment by wide excision of the tumour, and even hepatic transplant, is justified as a curative procedure. As this tumour has a good prognosis and even a chance of cure, it is important that every attempt should be made to differentiate it from hepatic metastases, so that correct advice can be given with respect to prognosis and treatment.

Acknowledgment

Our thanks to Mr R. Biggs for the photography.

References

Chowdhury., A. R., Black, M., Lorber, S. H. & Chey, W. Y., 1977. Hemangioendotheliomatosis of the liver. A 12-year follow up. *Gastroenterology*, *72*, 157–160.

Dail, D. H., Leibow, A. A., Gmelich, J. T., Friedman, T. J., Miyai, K., Myer, W., Patterson, S. D. & Ammar, S. P., 1983. Intramuscular, bronchiolar and alveolar tumor of lung (IVBAT): an analysis of twenty cases of a peculiar sclerosing endothelial tumor. *Cancer*, *51*, 542–564.

Falk, H., Herbery, J., Crowley, S., Ishak, K. G., Thomas, L. B., Popper, H. & Caldwell, G. G., 1981. Epidemiology of hepatic angiosarcoma in the United States (1964–1974). *Environmental Health Perspectives*, *41*, 107–113.

Ishak, K. G., Sesterhenn, I. A., Goodman, M. Z. D., Rabin, L. & Stromeyer, F. W., 1984. Epitheloid haemangioendothelioma of liver: a clinicopathologic and follow-up study of 32 cases. *Human Pathology*, *15*, 839–852.

Weiss, S. W. & Enzinger, F. M., 1982. Epitheloid haemangioendothelioma. A vascular tumor often mistaken for a carcinoma. *Cancer*, *50*, 970–981.

1992, *The British Journal of Radiology*, *65*, 614–648

Proceedings of the British Medical Ultrasound Society

Twenty-third Annual Meeting, held at the Bournemouth International Centre, Bournemouth, December 10–12, 1991

List of sections

	Page
General and interventional	614
Paediatrics	620
Abdominal and endoluminal	622
Physics and safety	623
Neurology	626
Veterinary session	627
Cardiovascular	630
Antenatal counselling	633
Obstetrics and gynaecology	634
Fetal biometry	638
Obstetrics	638
Posters	641

General and interventional

Chairmen: R. Frost and R. Hill

Normal lymph nodes in the abdomen: the hepatic artery "daisy chain", by C. Metreweli
The ultrasound appearance of the normal psoas muscle, by A. D. King and A. L. Hine
Duplex measurement of the mesenteric blood flow dose response to feeding, by K. M. Carlisle, D. Parker, A. E. Read and P. N. T. Wells
The ultrasound appearance of visceral gas—introducing the "effervescent bowel" and the "bright ring sign", by R. A. Bloom, P. D. Lebensart and E. Craciun
Abdominal ultrasound in Noonan syndrome. A study of 45 patients, by C. D. George, E. J. Adam, M. Sharland and M. A. Patton
Ultrasound-guided percutaneous laser, by S. G. Bown
Quantitative analysis of renal transplant collecting system dilatation to improve the diagnostic accuracy of obstruction, by S. H. Kashi, C. Romaniuk, G. R. Giles and H. C. Irving
Ultrasound or urography for assessment of adults with haematuria? Results of follow up, by J. Spencer, T. Meagher and D. Lindsell
Statistical correlation of ultrasound and histology in renal parenchymal disease—its clinical significance, by J. E. Page, S. H. Morgan, J. B. Eastwood, S. Dilly, J. Chow, A. Pottier and A. E. A. Joseph
Improvement in ultrasound images by adaptive speckle smoothing, by D. C. Crawford, D. O. Cosgrove, W. E. Svensson, E. Tohno, B. Al-Murrani, D. S. Bell, K. Stepniewska and J. S. Bamber
Paracholecystic sparing of the fatty liver frequency and aetiology, by C. Metreweli, M. Arnold, Y. F. Lo and L. Kreel
Ultrasound findings in sclerosing cholangitis, by L. J. Yeoman, J. de Caestecker, T. C. Northfield and A. E. A. Joseph
The effect of prostaglandins on human gallbladder contractility assessed by dynamic biliary ultrasound, by S. J. Stinchcombe, F. E. Murray and C. J. Hawkey
Ultrasound and gallbladder calculi: an audit. Are we as good as we think we are? by J. Walker, R. T. A. Chalmers, P. L. Allan and I. F. McLaren
Sequential abdominal ultrasound and the development of biliary sludge on the intensive care unit, by S. J. Stinchcombe, F. E. Murray and C. J. Hawkey
Evaluation of ultrasound assessment of lean body mass in normal volunteers, by D. Withers, T. Watt, I. T. Campbell and D. Martin
Advances in endoscopic ultrasonography, by P. J. Shorvon

Normal lymph nodes in the abdomen: the hepatic artery "daisy chain"

C. Metreweli
Department of Diagnostic Radiology & Organ Imaging, Prince of Wales Hospital, Chinese University of Hong Kong, Shatin, N.T., Hong Kong

The presence of normal lymph nodes is rarely reported in abdominal ultrasonography, two reasons being that many small paraortic nodes are difficult to visualize in large and or gassy patients, and that ultrasonographers are unaware that some of the structures visible on the images are actually lymph nodes. Furthermore the fortuitous visualization of these nodes in indeterminate cases may sway the ultrasonographer in favour of reporting disease that is not there. It has been reported that hilar nodes can be found in chronic hepatic disease. It is particularly in this area that normal lymph nodes are easiest to demonstrate, especially around the distal hepatic artery: the "hepatic artery daisy chain". This is seen in some 85% of patients without any local disease whereas medial portal nodes are seen in only 15% of patients and lateral portal in only 2%. As always, as appreciation of normal appearance is essential for accurate diagnosis.

The ultrasound appearance of the normal psoas muscle

A. D. King and A. L. Hine
Department of Radiology, Central Middlesex Hospital, London, NW10 7NS

The psoas muscle is involved in several pathological processes and, as ultrasound is non-invasive, it is often one of the first investigations to be performed. Interpretation of the findings requires a knowledge of the anatomy and variations in the normal appearance, and therefore 144 psoas muscles were scanned in 72 subjects in whom there were no clinical symptoms or findings to suggest retroperitoneal pathology. An Acuson 128 or Ultramark 5 scanner with a 3.5 MHz sector transducer was used. The examination took about 15 min although in the more obese subjects or those with overlying bowel gas prolonged pressure using the probe was required, so increasing the scanning time up to 45 min. The psoas was divided into three sections for the purpose of description. The first section of the muscle from its origin to the lower pole of the kidney was visualized in all subjects and in 129 (89.6%) demonstrated hyperechoic muscle bundles on a hypoechoic background. Fifteen (10.4%) showed focal areas of echogenicity or echogenic planes. The second section from the lower pole of the kidney to the iliac crest was visualized in all but two subjects. 77 (54.2%), once again, demonstrated hyperechoic bundles on a hypoechoic background, but 65 (45.8%) showed echogenic planes and areas of focal echogenicity, some of which contained hypoechoic centres. These findings were not always symmetrical and may cause confusion with early psoas pathology, although the overall size and contour of the muscle was never altered in the normal subject. The third section of the psoas muscle from the iliac crest to its fusion with the iliacus was not visualized in seven subjects (eight psoas muscles) due to overlying bowel gas. The most common finding was a prominent oblique echogenic plane in the transverse section which occurred in 96 (70.5%). Comparison with cadaver anatomical studies is presented to demonstrate the cause of these echogenic planes, which can also be seen on computed tomography and magnetic resonance imaging. The appearance and contour of both psoas muscles was symmetrical in 49 subjects with 23 showing minor asymmetry in one of the three sections.

Duplex measurement of the mesenteric blood flow dose response to feeding

K. M. Carlisle, D. Parker, A. E. Read and P. N. T. Wells
Department of Medical Physics and Bioengineering, Bristol General Hospital, Guinea Street, Bristol BS1 6SY

The large increase in superior mesenteric artery (SMA) blood flow after both liquid and solid meals has been measured using duplex ultrasound but no quantification of this response has been made. The objectives of this study therefore were to determine the minimal and maximal measurable responses to a liquid meal and to establish the relationship between the calorific content of the food and the percentage rise in SMA blood flow. Six normal healthy male volunteers were studied. They were of average weight for their height and were rested, supine and fasting. A single blind study was undertaken administering a mixed liquid meal on four separate occasions to each volunteer. The meals were isovolumic but of varying calorific values. Both pre- and post-prandial blood flow meaurements were made using a duplex system in each volunteer on each of the four separate occasions. The peak percentage rise in blood flow was found to be linearly proportional to the calorific content of the liquid meal. In each individual the peak rise occurred at approximately the same time after the meal was administered in each individual, indicating that it is the calorific content of the meal which stimulates dilation of the mesenteric vessels reducing the impedance and allows the diastolic flow to rise accordingly.

The ultrasound appearance of visceral gas—introducing the "effervescent bowel" and the "bright ring sign"

R. A. Bloom, P. D. Lebensart and E. Craciun
Department of Radiology, Hadassah University Hospital, Ein Kerem, Jerusalem, Israel

Air or gas is a barrier to propagation of ultrasonic waves, often precluding adequate visualization of intra-abdominal structures. In certain instances the presence of gas in an abnormal position may provide valuable information regarding pathology. This presentation is of the various appearances of emphysematous cholecystitis, intramural gallbladder abscesses, and gas in the bowel wall. Emphysematous cholecystitis is a rare condition, with under 200 cases reported. We have made this diagnosis ultrasonically on five occasions and illustrate the various appearances. Intramural gallbladder gas may produce a "bright ring" appearance that is quite characteristic and differs somewhat from that seen in a porcelain gallbladder. With lesser amounts of gas the bright intramural echoes can be induced to shift in position. This is in contradistinction to intramural abscesses which are small and may be seen as a very narrow band of echoes which maintain a constant positon within the bowel wall. A correct diagnosis of gas in the bowel wall has been made by us in two cases of necrotic bowel. The appearances are very similar to the "bright ring sign" in emphysematous cholecystitis. In one of the two cases bubbles of gas were seen rising from the bowel wall within the fluid luminal content. This "effervescent" bowel is analogous to the "effervescent" gallbladder previously reported in one case of emphysematous cholecystitis.

Abdominal ultrasound in Noonan syndrome. A study of 45 patients

C. D. George, E. J. Adam, M. Sharland and M. A. Patton
Department of Radiology, St George's Hospital, Blackshaw Road, London SW17 0QT

Purpose: To establish the abdominal ultrasound findings in Noonan syndrome; in particular to assess the frequency of renal abnormalities which are well described in Turner's syndrome, a condition with a similar phenotype. *Method:* 45 patients with Noonan syndrome were scanned. The age range was 7 months–37 years, there were 16 males and 29 females. *Results:* 17 scans were normal and 28 abnormal. Five patients had renal abnormalities, consisting of: one unilaterally absent kidney, one ectopic and malrotated kidney, one duplex kidney, bilateral cysts and scarring and one dialted renal pelvis. 23 patients had splenomegaly, and six of these had associated hepatomegaly. In all cases the echo texture of the liver and spleen was normal. One patient was found to have a choledochal cyst in addition to an ectopic and malrotated kidney.

Conclusion: The frequency of renal abnormalities in Noonan syndrome is low but splenomegaly, with or without hepatomegaly is a common finding. In view of the normal morphological appearance of both liver and spleen, the aetiology of the enlargement is obscure.

Ultrasound-guided percutaneous laser therapy

S. G. Brown
National Medical Laser Centre, University College and Middlesex School of Medicine, The Rayne Institute, 5 University Street, London WC1E 6JJ

Interstitial laser hyperthermia is a simple new technique for the treatment of tumours within solid organs. A needle is inserted into the target tumour, a thin laser fibre passed through the needle and the needle withdrawn a few millimetres to leave the bare fibre in the tumour. The Nd:YAG laser is activated at low power for a long exposure time (typically 10–15 min) and the fibre is then removed. The heated tissue is necrosed by gentle thermal coagulation and the dead tissue is left *in situ* to be resorbed or replaced by normal healing mechanisms. The keys to successful therapy are choosing lesions where there is adequate surrounding normal tissue to ensure safe healing and being able to image the tumour, the fibre positions and the real-time changes as the laser is firing. Most work has been done on isolated hepatic metastases monitoring therapy with ultrasound. This technique can produce a necrotic zone of about 15 mm diameter around each treatment point, so for lesions larger than this, multiple fibre sites are required. At present, the maximum number that can be treated simultaneously is four. About 30 s after the laser is switched on, a bright echo pattern appears around each fibre tip and outside this, an expanding darker zone, the outer limits of which correspond approximately to the limits of necrosis (the correlation is better in normal than in tumour tissue). Lesions are followed up after treatment with further ultrasound (US) or computed tomography scanning. 10 patients with a total of 18 isolated secondaries have been treated. Cessation of tumour growth has been documented in most lesions up to 20 mm in diameter, but treatment has had little effect on larger lesions despite US evidence of coagulation of the entire lesion. It is not yet clear why this is. It may be due to insufficiently accurate three-dimensional imaging or to problems interpreting US changes in inhomogeneous tumour tissue. Nevertheless, the technique is simple and safe, and if carefully developed has great potential for treating small tumours within solid organs.

Quantitative analysis of renal transplant collecting system dilatation to improve the diagnostic accuracy of obstruction

S. H. Kashi, C. Romaniuk, G. R. Giles and H. C. Irving
Department of Surgery and Radiology, St James's University Hosptial, Leeds

Dilitation of the pelvicalyceal systems of renal allografts is a common finding but only a small proportion are eventually shown to be obstructed. Quantitative analysis of ultrasound (US) images can be performed to calculate the ratio of the area occupied by the pelvicalyceal system to that of the kidney, on both longitudinal and transverse scans. To investigate whether such quantitative analysis could improve the specificity of the ultrasonographic diagnosis of obstruction, 394 scans in 150 patients were digitized using a Summagraphics tablet. The ratios obtained were compared to both the radiologist's report of the degree of pelvicalyceal dilatation and to the ultimate diagnosis of the presence or absence of obstruction. The results are summarized in the table below. In the grafts where there was ultrasonically visible dilatation, the quantitative analysis revealed statistically significant different ratios for the obstructed and non-obstructed grafts—for mild dilatation $p = 0.08$ on longitudinal scans and $p < 0.005$ on transverse scans (Mann–Whitney *U*-test), while for moderate to severe dilatation $p < 0.01$ and $p = 0.05$, respectively. The diagnostic accuracy can be further improved by using canonical discriminant function to derive an index which combines the ratios for the longitudinal and transverse images of the same kidney. Quantitative analysis of the ultrasound image thus improves upon the radiologist's report and identifies those grafts which require intervention to relieve obstruction.

Final diagnosis	US diagnosis	Ratio of renal area/p-c area (mean ± SEM)	
		Longitudinal	Transverse
Obstructed	Mild dilatation	8.4 (±1.8)	5.18 (0.78)
	Moderate/severe dilatation	5.1 (±0.3)	4.8 (±0.5)
Not obstructed	No dilatation	34.7 (±1.4)	30.5 (±1.6)
	Mild dilatation	13.9 (±1.3)	16.0 (±1.7)
	Moderate dilatation	7.7 (±0.92)	9.7 (±1.9)

Ultrasound or urography for assessment of adults with haematuria? Results of follow up

*†J. Spencer, *T. Meagher and *D. Lindsell
**Department of Radiology, John Radcliffe Hospital, Oxford OX3 9DU and †Division of Ultrasound, Thomas Jefferson University Hospital, Philadelphia PA 19107, USA*

Objective: Prospective double-blind comparison of the diagnostic ability of ultrasound (US) and intravenous urography (IVU) in adults with haematuria. *Patients and methods:* US and IVU were performed, concurrently and independently, as initial tests in 155 consecutive out-patients, 18–93 years, to establish the cause of haematuria. Patients with proven UTI, trauma or acute ureteric colic were excluded. After imaging, all had clinical review and appropriate treatment. 95 patients with unexplained continuing haematuria had further clinical review for a minimum of 1 year (12–23 months). *Initial results:* In 37 of 155 patients (24%), US and/or IVU detected causes of haematuria. US showed bladder tumours in 20 patients, four of which IVU missed (tumours sized 5–21 mm). 15 patients had calculi. US missed ureteric calculi in two cases but showed a radiolucent renal calculus overlooked by IVU. Calculi missed by US were visible on plain abdominal radiographs (AXR). Renal cell carcinoma was demonstrated by both studies in two patients. For 37 patients abnormalities discovered were felt unlikely to fully account for haematuria, *e.g.* simple prostate enlargement. 81/155 patients (52%) appeared normal on both studies. *Follow up:* 50 of 95 patients had continued unexplained haematuria and had cystoscopy. Six bladder tumours, all < 5 mm in size and one urethral tumour were found. Bleeding was felt to be from the prostate in 21 cases and the bladder neck in three cases. In 45 of these 95 patients haematuria ceased during review and was not investigated further.

Conclusion: US proved superior to IVU in the initial imaging of these 155 patients with haematuria principally as a result of improved detection of bladder tumours. The sensitivity of US for detection of all urinary tract tumours discovered was 79% for US and 64% of IVU, with a lower limit of detection of bladder tumour for US of 5 mm in size. US detected fewer ureteric calculi than IVU. US combined with a single AXR should form the initial out-patient imaging assessment of adults with haematuria.

Statistical correlation of ultrasound and histology in renal parenchymal disease–its clinical significance

J. E. Page, *S. H. Morgan, *J. B. Eastwood, †S. Dilly, †J. Chow, †A. Pottier and A. E. A. Joseph
*Departments of Diagnostic Radiology, *Renal Medicine, †Histology and ‡Public Health Sciences, St George's Hospital, Blackshaw Road, London SW17 0QT*

Ultrasound examination of the kidneys were performed in 61 patients undergoing renal biopsy over a 2 year period. Sonographic criteria recorded included renal size, parenchymal echogenicity and prominence of the medullary pyramids. The biopsy specimens were assessd retrospectively for the presence of five histological criteria on light microscopy. These included three glomerular features (sclerosis, proliferation and crescents) and two tubulo-interstitial features (infiltration and atrophy and or fibrosis). Biopsies were considered inadequate in six patients who were excluded from the study. Ultrasound assessment and guided biopsy were performed at the same time without any knowledge of the clinical diagnosis. Statistical analysis was done using the chi-squared test for trend. Increased echogenicity was associated with the presence of sclerosis, crescents, infiltration and atrophy and/or fibrosis; renal size with proliferation and crescents, and prominence of the medullary pyramids and sclerosis. Three patients with mildly increased echogenicity had normal histology. All patients with moderate to marked increase in echogenicity and all patients with prominent medullary pyramids had abnormal histology. Eleven patients considered to have normal kidneys on ultrasound had abnormal histology. In six of these, light microscopy was also normal and the diagnosis was made only on immunofluorescence. Only minor changes were seen in the other five patients using the above histological criteria. Ten of the 11 patients with normal ultrasound findings had a good prognosis with normal renal function on follow up, indicating that in general a normal ultrasound appearance carries a good prognosis. In conclusion, the sonographic appearances in renal parenchymal disease reflect specific histological changes and their severity. Ultrasound was normal only in patients with normal or marginally abnormal light microscopy, and prognosis was good in all but one of those patients.

Improvement in ultrasound images by adaptive speckle smoothing

D. C. Crawford, D. O. Cosgrove, W. E. Svensson, E. Tohno, B. Al-Murrani, D. S. Bell, K. Stepniewska and J. C. Bamber
Departments of Ultrasound and Physics, Institute of Cancer Research, Royal Marsden Hospital, Downs Road, Sutton, Surrey, SM2 5PT

Adaptive speckle smoothing has been designed to improve image contrast, which is likely to be particularly helpful in the diagnosis of malignant disease as the contrast for solid tumours against a background of normal tissue is often low. The processing dramatically alters the familiar appearance of the B-scan display, producing a strong initial impression of blurring. The acceptability to the radiologist of this alternative method of B-scan display has therefore been assessed. Initial clinical trials of this technique have evaluated the ease with which solid lesions can be detected on ultrasound images of the breast and liver. Frozen real-time scans from 83 livers and 71 breasts, all containing focal lesions, were speckle smoothed using a rapid-processing adaptive filter designed to remove the speckle components and replace them by their mean grey level without degrading true anatomical information. Four radiologists took part in the study. The radiologist who performed the clinical examination graded the smoothed images visually by comparison with the unsmoothed scans, scoring for differences in the appearances of the lesions' margins, preception of the texture and echo intensity and in the overall visibility of the lesions as well as effects on artefacts. There were no significant differences in the results of the four radiologists. The definition of the lesion margins was judged to be improved in 38% of cases in both groups while 37% of liver metastases were more clearly demonstrated. Textural information was enhanced in 42% and the images were considered to be generally better in 50%. In the majority of cases artefacts were reduced and there was no significant loss of true anatomical detail. Clinical evaluation of the adaptive speckle smoothed B-scans has demonstrated that image detail is easier to see and interpret, in particular textural detail and soft tissue lesions of low contrast, without loss of significant anatomical detail.

Paracholecystic sparing of the fatty liver frequency and aetiology

C. Metreweli, M. Arnold, Y. F. Lo and L. Kreel
Department of Diagnostic Radiology and Organ Imaging, Prince of Wales Hospital, Chinese University of Hong Kong, Shatin, N.T., Hong Kong

The fatty liver is a well recognized entity in imaging. So also is the phenomenon of sparing of some areas sufficient to cause different acoustic reflectivity for ultrasound and in extreme cases radiographic attenuation in computerized tomography. The resulting imaging can be confusing and cause a misdiagnosis of a primary or secondary tumour of the liver. Paravascular pyramidal distribution, segmental isolation, and lack of a mass effect in an obviously fatty liver guide toward the correct interpretation but occasionally there are smaller areas that do not conform so clearly, prompting unnecessary surveillance, other investigations and even biopsy. One such area is the paracholecystic region of the liver. In this region there is a characteristic hypoechogenic pyramid. We see this in 84% of our patients with fatty livers. In 25% it is very obvious and in 3% marked. As it is easily recognizable awareness will avoid confusion with sinister diagnoses. The aetiology of phenomenon can be explained by the presence of a rich collateral arterial supply to this area from the cholecystic artery which can be seen from post-mortem angiographic studies.

Ultrasound findings in sclerosing cholangitis

L. J. Yeoman, *J. de Caestecker, *T. C. Northfield and A. E. A. Joseph
*Departments of Diagnostic Radiology and *Medicine, St George's Hospital, Blackshaw Road, London SW17 0QT*

There have been very few reports of the sonographic findings in sclerosing cholangitis. We have reviewed the ultrasound (US) scans of 10 patients with sclerosing cholangitis diagnosed by cholangiography, and/or histology, and of one patient with

AIDS-related cholangitis. Amongst the sclerosing cholangitis group a number of US signs were present in all or the majority of patients, including abnormal liver echotexture with multiple pinhead echogenic foci (all patients); ill-defined increased thickness of intrahepatic duct walls (nine patients); irregular beaded appearance of intra- and/or extrahepatic ducts (9); increased thickness of the wall of extrahepatic ducts (9) which resulted in narrowing the lumen in seven patients; and diffuse thickening of the gallbladder wall (6). In five patients there was extensive periductal echogenicity. There is an increased incidence of benign and malignant gallbladder neoplasms in sclerosing cholangitis and in two patients a gallbladder polyp was present. Other signs seen less frequently included a focal stricture of the common bile duct (3), and gallbladder calculi (1) and sludge (1). In two patients a second US examination was performed after an interval of 6 and 21 months and the US appearances showed progression. A number of these findings were also seen in the patient with AIDS-related cholangitis, which is a mimic of sclerosing cholangitis at cholangiography. We illustrate these signs and discuss the differential diagnosis of the appearances. We conclude that the diagnosis of sclerosing cholangitis can be suggested by a combination of the sonographic findings described and discuss the role of US in the investigation of this disease.

The effect of prostaglandins on human gallbladder contractility assessed by dynamic biliary ultrasound

S. J. Stinchcombe, F. E. Murray and C. J. Hawkey
Departments of Radiology and Therapeutics, University Hospital, Queen's Medical Centre, Nottingham NG7 2UH

Impaired gallbladder (GB) contractility is a prerequisite for gallstone formation in animal models. Prostaglandins (PGs) are important mediators of gallstone formation, and may affect GB contractility in animals. The aim of this study was to evaluate the effect of indomethacin, an inhibitor of PG synthesis and misoprostol, a synthetic PG on GB contractility in man. Seven male volunteers (188–33 years, mean age 23 years) were studied blindly during control periods and following oral ingestion of indomethacin 125 mg or misoprostol 800 μg orally. After an overnight fast, GB residual volume (RV) was determined by real-time ultrasonography before and 10, 20, 30, 40, 50 min after ingestion of a standard liquid fatty meal stimulus. Average RV (Rv_{av}), minimum RV (Rv_{min}) and maximal change in gallbladder volume (dV_{max}) were calculated. Gallbladder volumes (ml) are expressed as mean (SEM). Administration of indomethacin and misoprostol had no effect on GB contractility in humans assessed by ultrasonography. The reduced risk of gallstones in NSAID-treated patients must be mediated by a mechanism other than enhanced GB contractility and is likely due to the inhibition of mucin glycoprotein secretion.

Time	Control	Indomethacin	Misoprostol	*P*
0	20.8 (1.6)	20.8 (2.9)	18.3 (1.6)	NS
10	11.7 (2.2)	15.9 (3.2)	12.2 (2.5)	NS
20	8.7 (1.5)	8.3 (2.6)	7.6 (2.4)	NS
30	7.5 (1.4)	7.4 (2.5)	7.6 (2.8)	NS
40	8.3 (1.6)	5.9 (1.3)	7.4 (2.5)	NS
50	8.2 (1.6)	6.4 (1.4)	5.8 (1.4)	NS
RV_{av}	8.9 (1.6)	8.8 (2.0)	8.1 (2.2)	NS
V_{min}	7.0 (1.4)	5.4 (1.1)	4.9 (1.4)	NS
dV_{max}	13.8 (1.8)	15.4 (2.2)	13.3 (1.3)	NS

Ultrasound and gallbladder calculi: an audit. Are we as good as we think we are?

*J. Walker, †R. T. A. Chalmers, P. L. Allan and †I. F. McLaren
**Department of Radiology and †Department of Surgery, Royal Infirmary of Edinburgh, Lauriston Place, Edinburgh EH3 9YW*

Many series suggest that ultrasound is the imaging technique of choice for the detection of cholelithiasis and that it is accurate in doing so. However, these series are often prospective and the examinations performed by experienced sonographers. This audit sought to address whether the accuracy is maintained in the daily practice of a department. We reviewed 128 patients who had had ultrasound scans prior to undergoing cholecystectomy for cholelithiasis. The ultrasound findings were compared with those at surgery. The operative and ultrasonographic findings were at variance in 8 of the 128 patients (6.2%). Five patients were reported as having gallstones on ultrasound though none were found at cholecystectomy; a false positive rate for ultrasound of 3.9%. Three patients had abnormal gallbladders with no gallstones at sonography, however, gallstones were found at operation; a false negative rate of 2.3%. False positive diagnoses are to be avoided as they result in unnecessary operations. They may arise because small stones are passed in the interval between the scan and surgery, or because of the mistaken identification of echogenic foci seen. To avoid them alternative imaging should be performed if there is any doubt regarding the significance of echogenic foci; either cholescintigraphy in a patient with suspected acute cholecystitis or an oral cholecystogram in an elective situation. A sonogram should be repeated immediately preoperatively if only tiny stones are seen and there is an interval between the scan and surgery. Some false negative examinations may be avoided by performing a repeat following clinical improvement should the gallbladder be thick-walled and tender initially but apparently contain no stones. With these provisos we conclude from this audit that ultrasound is an accurate means of diagnosing gallstones in the daily practice of a department.

Sequential abdominal ultrasound and the development of biliary sludge on the intensive care unit

S. J. Stinchcombe, F. E. Murray and C. J. Hawkey
Departments of Radiology and Therapeutics, University Hospital, Queen's Medical Centre, Nottingham NG7 2UH

A large body of experimental and clinical evidence suggests that biliary sludge is the precursor of gallstones in a large number of affected patients. Several risk factors for the development of biliary sludge have been identified including total parenteral nutrition, bone marrow transplantation, AIDS and following abdominal surgery, but no previous study has evaluated the incidence of biliary sludge in intensive care unit (ICU) patients. A prospective study of all patients admitted to the ICU for longer than 2 days was performed over an 11 week period. Patients were studied twice weekly using real-time ultrasonography to determine the presence or absence of biliary sludge. 36 consecutive patients were evaluated (26 male, 10 female, mean age 47 years). Sludge developed in 17 of 36 subjects evaluated (47%), after a mean of 5.5 days. Subjects who developed sludge spent longer in the ICU (14.2 days (± 1.2)), compared with subjects who did not (8.3 days (± 1.2)); $p = 0.01$. Seven sludge-forming subjects had no previously recognized risk factor: five had undergone neurosurgery (and had not received TPN), one multiple trauma, and one had Gram-negative septicaemia. 10 of the sludge-forming subjects had a previously recognized risk factor: TPN (5), abdominal surgery (2) or both (3). All neurosurgical patients ($n = 4$) who received TPN developed sludge. The development of sludge in patients receiving TPN was more rapid than previously recognized (mean 3.1 days). Cholestatic liver biochemistry developed in 5/16 non-sludge-forming subjects and in 13/17 sludge-forming subjects ($p = 0.01$). Biliary sludge develops frequently and very rapidly in subjects admitted to the ICU. Neurosurgical procedures are noted to be associated with sludge formation for the first time. As gallstone formation is a frequent result of biliary sludge formation there is a need to develop a regime to prevent or clear biliary sludge in patients on the ICU.

Evaluation of ultrasound assessment of lean body mass in normal volunteers

D. Withers, T. Watt, I. T. Campbell and D. Martin
Department of Radiology and University Department of Anaesthesia, Withington Hospital, University Hospital of South Manchester, Manchester M20 8LR

The normal anthropometric measurements used to assess lean body mass, which involve the measurement of skinfold thickness and mid-arm circumference, are confounded in critically ill patients by fluid retention which occurs predominantly in subcutaneous tissues and less so in muscle. A non-invasive method is needed to assess lean body mass and its loss in patients on the intensive care unit in order to determine the requirement for nutritional support. In a preliminary study to establish whether ultrasound can be used to assess lean body mass, 31 healthy volunteers (13 males, 18 females, age range 19–86 years, mean 30 years) underwent measurement of skinfold thickness and mid-upper arm circumference. Arm muscle area and arm muscle circumference were calculated. Ultrasound examination using a portable ALOKA SSD 500 machine with 3.5 MHz linear array probe was used to measure muscle thickness in the non-dominant limbs at mid-arm level (biceps), lateral head of triceps, mid-forearm anteriorly, mid-thigh anteriorly and mid-calf posteriorly. The rectus abdominis at the level of the ambilicus was also assessed. Correlation coefficients were calculated for lean body mass assessed by skinfold thickness and body weight compared with (a) total ultrasound muscle thickness (0.95), (b) arm muscle area (0.850), (c) arm muscle circumference (0.841) and (d) mid-arm circumference (0.789). In normal volunteers, ultrasound assessment of muscle thickness measurements are as good an indicator of lean body mass as the established anthropometric measurements. A study is underway using this method to assess loss of lean body mass in critically ill patients.

Advances in endoscopic ultrasonography

P. J. Shorvon
Central Middlesex Hospital, Acton Lane, Park Royal, London NW10 7NS

Whilst the development, in Europe and Japan, of gastroenterological endosonographic techniques over the last decade has been relatively slow, the acceptance of the technology in the USA has created a new surge of interest. Advances in endoscopic ultrasonography (EUS) have been both clinical and technical. There has been a painstaking accumulation of data that has resulted in a number of publications confirming the superior accuracy of EUS over alternative techniques in the local staging of upper gastrointestinal malignancies. EUS has also been shown to be the procedure of choice in identifying recurrent tumour at anastomoses as well as in the follow up of patients with gastric lymphoma. Recent studies with rectally introduced transducers have shown the unique information that can be obtained in patients with pathology in and around the anal sphincters. Data on staging colorectal neoplasia with endosonography are becoming available although the clinical value is unproven. The most commonly used equipment for upper gastrointestinal EUS remains a rotating mechanical sector scanner producing a 360° image in the plane orthogonal to the shaft of the endoscope. However, the equipment now has switchable frequencies (7.5 and 12 MHz) and also a biopsy channel. Miniature high frequency rotating sector scanners which fit down the biopsy channels of standard endoscopes have been developed. Electronic phased array and linear transducers scanning in the line of the shaft of the endoscope have also been developed, some with both duplex and colour Doppler capabilities. Transducers incorporated into colonoscopes are available allowing complete trans-colonic imaging. Three-dimensional reconstruction of EUS images is also under investigation.

Paediatrics

Chairmen: H. Irving and P. Johnston

Infantile torticollis—echographic abnormalities, by C. Metreweli, J. C. Y. Cheng and S. S. Y. Ho
The role of ultrasound in the assessment of suspected ileo-colic intussusception, by S. Pablot
Duplex Doppler ultrasound for the detection of vascular occlusion following liver transplantation in children, by D. J. Lomas, P. D. Britton, R. A. Coulden, A. Egan and P. Farman
Ultrasound in limb lengthening, by N. D. J. Derbyshire and A. H. R. W. Simpson
The value of ultrasound in the assessment of bond, by G. M. Steiner
Sonography of neonatal abdominal masses, by M. J. Siegel
The impact of a screening programme on the incidence of late presenting CDH, by Reinhard Graf

Infantile torticollis—echographic abnormalities

C. Metreweli, J. C. Y. Cheng and S. S. Y. Ho
Department of Diagnostic Radiology and Organ Imaging, Prince of Wales Hospital, Chinese University of Hong Kong, Shatin, N.T., Hong Kong

Infantile torticollis or wryneck may be accompanied by the presence of a 'sternomastoid tumour'. Although well recognized the disease remains a mystery and aetiological explanations are still plentiful and discordant. There is not even agreement whether this condition is a single entity or separate entities producing the same result. Against this background it is not surprising that the therapy of the condition remains controversial with some relying on conservative measures while others operate on 'the tumour'. Imaging of this condition has been virtually non-existent. This is the first echographic study as far as we are aware. We have just completed the initial phase of studying 60 children with this condition to establish the abnormalities that can be demonstrated and it is these findings that we wish to present to the meeting.

The role of ultrasound in the assessment of suspected ileo-colic intussusception

S. Pablot
Department of Radiology, Queen Mary's Hospital for Children, Carshalton, Surrey

We have routinely used ultrasound to confirm or exclude intussusception prior to treatment in 65 consecutive cases. Of these, 41 were positive and 24 were negative. *First presentation:* 39 positive cases—29 were reduced with air enema, six failed reductions went to surgery, four had elective surgery on clinical grounds; 18 negative examinations—10 were confirmed by negative pneumocolon, eight had no further investigation. *Suspected re-intussusception:* eight cases–six negative with no further investigation, two positive reduced by air enema. Although this is a small series so far we have had no false positives or false negatives, and one positive diagnosis missed clinically. We briefly discuss typical ultrasound appearances of intussusception and present one case with inflammed Peyer's patches confirmed at elective surgery on clinical grounds, and one case associated with duplication cyst of the caecum and discuss briefly the role of ultrasound in the differential diagnosis of intussusception, malrotation, colitis and small bowel intussusception. *Conclusion:* We find that ultrasound is a quick non-invasive method of documenting ileocolic intussusception, in assessing underlying pathology, reducing further investigation in negative cases and in the differential diagnosis. This is especially so where air enema is the treatment of choice and the X-rays of the bowel are not of good diagnostic quality, and frequently very rapid reduction of ileocolic intussusception may lead to doubts about the diagnosis.

Duplex Doppler ultrasound for the detection of vascular occlusion following liver transplantation in children

D. J. Lomas, P. D. Britton, R. A. Coulden, A. Egan and P. Farman
Departments of Radiology, Addenbrooke's Hospital, Cambridge CB2 2QQ

Sixty-three children and adolescent patients who received 78 consecutive orthotopic liver transplants and had serial duplex ultrasound monitoring were retrospectively reviewed for episodes of occlusion of the hepatic artery or portal vein. There were 13 documented episodes of complete occlusion of the main hepatic artery or a major branch, of which nine were diagnosed by the absence of flow during duplex ultrasound examination. Four occlusions were not detected, two affected hepatic artery branches, one an accessory hepatic artery, and one the main hepatic artery. The overall sensitivity of the method was 69% and specificity 100%. Six portal vein occlusions were documented in five patients and all six were successfully diagnosed on ultrasound examination, giving a sensitivity and specificity of 100%. Three of the patients had simultaneous occlusions of both vessels. In the early post-operative period, duplex Doppler ultrasound examination has proved an effective non-invasive method for the detection of vascular occlusion, but is not yet sensitive enough to replace angiography fully for the detection of hepatic artery occlusion, particularly when this occurs distal to the main hepatic artery.

Ultrasound in limb lengthening

N. D. J. Derbyshire and A. H. R. W. Simpson
Departments of Radiology and Surgery, Nuffield Orthopaedic Centre NHS Trust, Windmill Road, Headington, Oxford, OX3 7LD

The Ilizarov technique for limb lengthening involves an osteotomy followed by distraction of the two parts of the bone using an external frame. With its more widespread adoption there is an increasing need to develop quick and reliable imaging techniques for monitoring the rate and quality of new bone formation during the distraction osteogenesis. Traditionally plain films have been used to monitor new bone formation and measure the bone gap at the osteotomy site. In our unit, as in others, we have performed serial ultrasound examinations of the distraction site using a 10 MHz or 7.5 MHz transducer. The gap between the margins of mature callus can be quickly and accurately measured and the degree and quality of maturing new bone assessed, as judged by the presence of a uniform lamellar pattern of echoes and the absence of echo-free regions. These areas of decreased echogenicity sometimes seen in the developing new bone have been shown to be fluid-filled cysts, the formation of which is thought to indicate too rapid a rate of distraction. Ultrasound also provides a new form of information not available from plain radiography, namely the ability to calculate the rate of new bone formation during distraction osteogenesis. Measurements obtained from ultrasound and plain films can be used to calculate the amount and rate of new bone formation and when represented graphically it is possible to infer whether the rate of lengthening is too slow potentially leading to premature consolidation, or too fast with the prospect of non-union. Too rapid a rate also correlates with the formation of above mentioned cysts. When seen, lengthening can be slowed or reversed until the cyst disappears. By use of ultrasound we have also found that the number of follow up plain films can be reduced, in some of our patients by 50%. With these benefits we commend ultrasound as a valuable technique, to complement plain film radiography, in the follow up of patients undergoing limb lengthening procedures.

The value of ultrasound in the assessment of bone

G. M. Steiner
Sheffield Children's Hospital, Western Bank, Sheffield S10 2TH

The presence of bone is usually a contraindication to the use of ultrasound. This paper illustrates how bone itself can be assessed for bone regeneration, inflammation, trauma and involvement by tumour. Further investigations can consequently be planned and the patient saved irradiation.

Sonography of neonatal abdominal masses

M. J. Siegel
Mallinckrodt Institute of Radiology, Washington University School of Medicine, 510 South Kingshighway Blvd, St Louis, Missouri 63110, USA

Renal masses account for about 55% of all abdominal masses in the newborn. The most common neonatal renal masses are hydronephrosis and multicystic dysplastic kidney. Polycystic kidney disease and renal vein thrombosis occur but are far less common. Sonographic findings of hydronephrosis include multiple cystic structures of uniform size which communicate with each other and with a dilated renal pelvis, visualization of a dilated ureter in cases with distal obstruction (*e.g.* ureterovesical junction obstruction, duplication with an ectopic ureter or ureterocele, and posterior urethral valves), and visible renal parenchyma. Multicystic dysplastic kidney is characterized by anechoic masses of variable size with a random distribution, no connection between between the cysts, and absence of renal parenchyma. Both autosomal recessive and dominant forms of polycystic kidney disease produce bilateral renal enlargement with increased echogenicity, poor definition of the central pelvocalyceal complex and occasionally discrete cysts. Biopsy and/or family history is required for differentiation of autosomal recessive and dominant forms of the disease. Renal vein thrombosis also causes enlarged, echogenic kidneys early in the course of the disease. As cellular infiltration and fibrosis develop, the kidneys appear hypoechoic and of variable size. An echogenic filling defect representing thrombus may also be identified in the renal vein or inferior vena cava. Non-renal retroperitoneal masses account for 10% of neonatal abdominal masses and are almost entirely comprised of adrenal haemorrhages and rare neuroblastomas. On sonography, both adrenal haemorrhage and neuroblastoma may appear echogenic, complex or cystic. Genital masses (*e.g.* hydrocolpos and ovarian cysts) and gastrointestinal masses (duplications and mesenteric cysts) each account for about 15% of masses. The remainder of neonatal abdominal masses are hepatobiliary masses (5%).

The impact of a screening programme on the incidence of late presenting CDH

Reinhard Graf
A 8852 Clinic Stolzalpe, Austria

Since 1981 hip ultrasound has been routinely performed in our clinic. Up to 1987, 16916 babies were checked and 1990 reviewed. Additionally in the period 1987 to 1988 a general newborn screening programme was performed as a pilot study in 6341 babies. *Results:* In the non-screened pool, the age of the babies at the beginning of treatment decreased steadily from 20 weeks of life to 10:7 weeks. The age at the end of treatment decreased from 48 to 36 weeks. AC and CE angle, checked with X-rays 2 years after the end of treatment, had in this period steadily improved. In the screening pool all babies who needed treatment had been detected before the 6th week of life, treatment could be stopped at the average age of 7.5 months with totally normal hip joints, no head necrosis occurred and no late operations, such as acetabuloplasty, etc., were necessary. The rate of pathological hip joints picked out by ultrasound (US) is 1.5–3%. *Correlation with clinical findings:* This is rather poor. In dislocated joints (Type III/IV) the correlation was 60%/100%, but in the borderline cases (sonographically unstable joints Type IIc/D) 50% looked clinically normal! In the high risk pool (breech position, family history, etc.) only 30% had pathological joints. In order to obtain these excellent results it is necessary to have good organization and a perfect method. *Method:* A strictly standardized examination technique with reproducible plane is used. Exact classification is made into four basic types, the measurement technique classifying the bony and the cartiliage roof. Detection of "clinically normal" but sonographically unstable joints (Type IIc/D) is made using a 5 and 7.5 MHz linear transducer (no sector scanners). The method is of use up to an average age of 12 months. The lateral approach is recommended and gives the best information. Dynamic (= stress) examination is additionally performed in borderline cases (Type IIc/D) to detect unstable joints. *Conclusion:* The aim of US investigation is not only to pick out dislocated joints, but to detect borderline cases which also need treatment and cannot be diagnosed by clinical testing.

Abdominal and endoluminal

Chairmen: R. Frost and R. Talbot

Ultrasonographic assessment of patients with anorectal disorders, by D. Kumar, J. Olliff, C. Hutchinson and J. A. Williams
Rectal endosonography and guided biopsy in the evaluation of recurrent rectal carcinoma, by M. B. Nielsen, J. F. Pedersen and J. Christiansen
Sonography in the evaluation of the male anterior urethra, by P. W. P. Bearcroft and L. H. Berman
Conventional 15G needle technique for renal biopsy compared with ultrasound-guided spring-loaded 18G needle biopsy, by N. J. A. Cozens, J. T. Murchison, P. L. Allan and R. J. Winney

Ultrasonographic assessment of patients with anorectal disorders

*D. Kumar, †J. Olliff, †C. Hutchinson and *J. A. Williams
**Departments of Surgery and †Radiology, Queen Elizabeth Hospital, Birmingham*

Assessment of the anorectum is conventionally made by anal manometry and videoproctography. We have evaluated the usefulness of endo-anal ultrasonography (EAU) in the assessment of anorectal disorders. 20 patients with faecal incontinence, five patients with haemorrhoids, four patients with fissures *in ano* and six other patients with other defaecatory problems were investigated using a 7 MHz probe (Bruel and Kaejer). Subjects were investigated in the left lateral position. Assessments were made at three different levels—lower, mid and upper anal canal. 33 of the 35 patients studied (94%) showed abnormalities in one or more level of the anal canal. Thirteen of the 20 (65%) patients with faecal incontinence showed an anterior deficiency of either EAS, IAS or both. Four patients had a clearly identifiable gap in the subcutaneous EAS anteriorly. One patient had a posterior defect and the other two patients had lateral defects. The site and size of haemorrhoids could be identified in all five patients. Three patients showed evidence of associated mucosal prolapse. The patients with the fissures *in ano* showed a mucosal defect but the sphincters were uniform in shape. In the remaining mixed group of patients two showed rectoceles which were made worse on straining, one had rectal prolapse and three patients with peri-anal Crohn's disease showed gross tissue oedema, but no sphincter damage or localized collections. We conclude that EAU is a useful and relatively non-invasive means of assessment for anorectal disorders. We believe that it will play a major role in not only pre-operative assessment but also evaluation of surgical repair of anal sphincters.

Rectal endosonography and guided biopsy in the evaluation of recurrent rectal carcinoma

M. B. Nielsen, J. F. Pedersen and J. Christiansen
Department of Radiology and Ultrasound and Department of Surgery D, University of Copenhagen, Glostrup Hospital, DK-2600 Glostrup, Denmark

Rectal endosonography was performed in 12 patients who had undergone low anterior resection of the rectum for carcinoma. Endosonography was performed using a 7 MHz axial endoprobe and a 7 MHz multiplanar endoprobe. Local recurrence was suspected by endosonography in eight patients, by rectoscopy in three patients. In five patients an extraluminal recurrence was suspected by endosonography but not by rectoscopy. In these patients transrectal biopsies were performed under sonographic guidance using the multiplanar endoprobe. We used fine needle aspiration biopsies, in some cases combined with core biopsies. In three patients biopsy confirmed the recurrence. In the remaining two patients, repeated endosonography showed no sign of progression of the lesions over an observation time of nine months. These lesions were considered post-operative changes. The biopsy technique and the endosonographic appearances of recurrent carcinomas are discussed.

Sonography in the evaluation of the male anterior urethra

P. W. P. Bearcroft and L. H. Berman
Department of Radiology, Addenbrooke's Hospital, Cambridge CB2 2QQ

Contrast ascending urethrography is considered the imaging technique of choice in demonstrating suspected abnormalities of the anterior urethra. Sonography of the urethra was evaluated in 21 subjects undergoing conventional urethrography. Following the urethrogram, studies were obtained utilising a 7.5 MHz linear array transducer and direct skin contact on the penis, scrotum and perineum. Distention was achieved with a catheter anchored in the navicular fossa infusion of contrast. Normal structures that can be defined include the corpora cavernosa and spongiosum, the urethral lumen and its mucosal lining. Contraction of the bulbo-cavernosus muscle and urogenital diaphragm can be visualized. Sonography was considered normal in nine patients and this was confirmed by the urethrogram. There were two cases of sonographic false negatives: a thin bulbar urethral web and subtle urethrographic mucosal irregularity were not detected in one patient and a small bulbar post-operative diverticulum was overlooked in the other. These errors occurred early in the series when the technique was unfamiliar. Sonography accurately identified all other focal and diffuse urethral strictures as well as two urethral diverticula. Fine urethral irregularity on the contrast study was correctly identified sonographically in four cases and generalized lack of urethral distension in five. Sonography detected a urethral mucosal flap missed on the contrast study. Urethral filling defects thought to be bubbles on urethrography were defined by ultrasound as soft tissue masses. In addition thickening of the periurethral tissues associated with a stricture was visualized sonographically in three studies. These results suggest that ultrasound is a radiation-free alternative in the assessment of the male urethra.

Conventional 15G needle technique for renal biopsy compared with ultrasound-guided spring-loaded 18G needle biopsy

N. J. A. Cozens, J. T. Murchison, P. L. Allan and R. J. Winney
Departments of Radiology and Renal Medicine, Royal Infirmary of Edinburgh, Lauriston Place, Edinburgh EH3 9YW

Two techniques for percutaneous renal biopsy were retrospectively reviewed to assess their relative safety and efficacy.

Ultrasound localization of the kidney by a radiologist with subsequent biopsy performed by a renal physician using a hand-held 15G cutting needle (Tru-Cut) was compared with biopsy performed by a radiologist using an 18G cutting needle with a spring-loaded biopsy device (Biopty) and real-time ultrasound guidance. The 18G Biopty needle with real-time ultrasound is more reliable at retrieving an adequate specimen for histological examination (93%) than the "conventional" technique (79%) (χ^2, $p < 0.05$). This is probably due to the more accurate localization of the needle in the renal cortex which results from the real-time guidance. Fewer complications occurred in the Biopty group (15% *v.* 26%) although the difference did not reach statistically significant levels. The mean length of stay in hospital was significantly shorter for elective biopsies with the Biopty device; 1.80 compared to 2.93 nights ($p < 0.01$), 95% confidence interval 0.34 to 1.92 nights difference). Since the introduction of the Biopty technique we are increasingly prepared to biopsy patients who were previously regarded as high risk. This facilitates an earlier diagnosis expediting appropriate therapy. The technique is associated with minimal pain and appears much more acceptable to the patient. We would recommend the use of the Biopty device with an 18G needle and real-time ultrasound guidance as the method of choice for percutaneous renal biopsy.

Physics and safety

Chairmen: C. R. Hill and J. Aindow

A comparison of exposure and bio-acoustic endpoints in therapy and pulsed Doppler fields, by H. C. Starritt and F. A. Duck
In situ ultrasound exposure in obstetric examinations, by K. V. Ramnarine, D. K. Nassiri, J. M. Pearce, A. E. A. Joseph, R. H. Patel and T. R. Varma
Tinnitus produced during transcranial Doppler sonography of the basilar artery, by T. R. Magee, J. K. Hayward, A. H. Davies, M. Halliwell and M. Horrocks
Directionality and temperature dependence of the ultrasonic properties of bone, by J. A. Evans and M. B. Tavakoli
Ultrasonic bone assessment: is wavefront aberration the principal limitation of current technology? by P. A. Robins, G. Petley, J. D. Aindow and J. Bottle
Correlation between histology and ultrasonic propagation properties of excised human skin, by C. M. Moran, N. L. Bush and J. C. Bamber
Development of an expert system for aiding the ultrasonic diagnosis of solid breast masses, by K. Stepniewska, D. O. Cosgrove, B. Al-Murrani, E. Tohno, W. E. Svensson and J. C. Bamber
Ultrasound resolution enhancement by signal averaging, by R. A. Harris, M. Halliwell and P. N. T. Wells
Three-dimensional colour flow mapping imaging for improved assessment of vascular disease, by K. B. Modaresi, M. G. Taylor and T. S. Padayachee
The development of three-dimensional ultrasound venographic techniques for the lower limb venous system: preliminary report, by K. N. Humphries, R. A. Reynolds, K. Willson and D. O'Keefe

A comparison of exposure and bio-acoustic endpoints in therapy and pulsed Doppler fields

H. C. Starritt and F. A. Duck
Medical Physics Department, Royal United Hospital, Combe Park, Bath BA1 3NG

A detailed comparison of the ultrasonic exposure in water from a therapeutic beam and a pulsed Doppler beam, produced by a Therasonic-1032 and an Acuson-128 scanner, respectively, is presented. A significant overlap in acoustic power was found between therapy intensity levels used clinically and the upper end of the diagnostic range, between approximately 100 and 200 mW. In addition, pulse pressure amplitudes in the range 500–1000 MPa were measured close to the transducer on both units. The streaming velocities generated in water by each beam were measured. In the diagnostic beam, streaming velocities up to $14\ \text{cm}^{-1}$ were seen. Theoretically maximum streaming velocities up to $40\ \text{cm}^{-1}$ were calculated for the therapy beam. However experimentally it was shown that the velocity is limited by turbulence. In the pulsed Doppler beam a maximum temperature rise of 2°C was measured in tissue *in vitro*. This was similar to the heating produced in the therapy beam at intensity levels commonly used clinically. A liquid crystal method was used to visualize the heating distribution. It is common practice to use physiotherapy units at pulse average intensities of 0.5 W/cm or less. At these levels exposures and biophysical effects of similar magnitudes may be obtained with beams currently defined as therapeutic and those available from pulsed Doppler equipment.

In situ ultrasound exposure in obstetric examinations

*K. V. Ramnarine, *D. K. Nassiri, †J. M. Pearce, ‡A. E. A. Joseph, †R. H. Patel and T. R. Varma
**Departments of Medical Physics and Bioengineering, †Obstetrics and Gynaecology and ‡Diagnostic Radiology, St George's Hospital, London SW17 0QT*

Determination of patient exposure to ultrasound is of considerable interest for assessing the safety of ultrasound and establishing standards. A plane layered tissue model has been used to determine fetal exposure to ultrasound during typical obstetric clinical applictions. The model assumes plane homogeneous layers of tissue of known thickness, attenuation and acoustic impedance. Incorporation of measured overlying tissue thicknesses (mean, standard deviation, ranges, etc.) with data on the acoustic properties of tissues in the tissue model enables the *in situ* intensity to be determined. Overlying tissue thicknesses are measured for a selection of routine planes used in obstetric scans. For the first trimester pregnancy, the scan of the crown rump length is collected. Scans for the second and third trimester pregnancies include: the biparietal diameter

(BPD); the cross-section of the fetal abdomen; the mid-line maternal sagittal and transverse scans; the Doppler scans to the left and right maternal uterine artery, and the fetal umbilical cord. Preliminary results from over 50 BPD cases have yielded a minimum and maximum fetal skull depth of 0.9 cm and 5.1 cm, respectively, with a mean of 2.3 cm. The corresponding minimum and maximum attentuation using conservative estimates of attenuation coefficients for overlying tissues are 0.7 dB/MHz and 2.9 dB/MHz, respectively, with a mean of 1.4 dB/MHz. Values calculated for the *in situ* intensity from a comprehensive study of over 50 cases for each of the three trimesters will be presented. The largest source of error in the *in situ* intensity is due to the scarce and unreliable data on the acoustic properties of tissues.

Tinnitus produced during transcranial Doppler sonography of the basilar artery

T. R. Magee, J. K. Hayward, A. H. Davies, M. Halliwell and M. Horrocks
Vascular Studies Unit, Bristol Royal Infirmary, Bristol BS2 8HW

The use of transcranial Doppler sonograph (TCD) to observe changes in velocity of flow in the basal cerebral arteries is well established. The three commonly used approaches are the temporal, basilar and transorbital. Manufacturers of ultrasound equipment and clinicians have set maximum transmitted power levels for transorbital insonation; damage to the retina is a possibility. No other such recommendations exist for the other approaches. During routine use of TCD it was noted that high pitched tones, similar to tinnitus could be heard by the subject when the basilar artery was sought. Ten volunteers with no evidence of hearing impairment were examined. The subjects were asked to identify any noises heard during basilar artery insonation with their ears plugged. The effects of depth gating and transmitted power were noted. All 10 subjects heard high frequency tones. As the pulse repetition frequency changed to allow different depth ranges so did the pitch of the tones. Eight subjects identified the tones increasing as the pulse repetition increased. In all cases, as transmitted power decreased the loudness diminished. The "tinnitus" effect was highly dependent on probe position and direction. This is an example of previously unreported subjective effects of ultrasound. It may be that the tones heard are due to stimulation of the auditory nerve before it enters the internal auditory foramen, by bursts of ultrasound at the pulse repetition frequency. The exact mechanism of this effect must be clarified further; we are carrying out the same experiments on patients with deafness of nerve, and conductive origin. Until further information is available, it would seem prudent to use the minimum transmitted power possible to obtain a satisfactory signal from the basilar artery.

Directionality and temperature dependence of the ultrasonic properties of bone

J. A. Evans and M. B. Tavakoli
Department of Medical Physics, The General Infirmary, Leeds LS1 3EX

There has been increased interest in the use of ultrasound in the diagnosis of bone pathologies, in particular, osteoporosis. A number of parameters such as velocity, attenuation and the slope of attenuation with frequency, have been evaluated as diagnostic tools. However, the dependence of these parameters on temperature and on direction relative to the load-bearing axes is largely unknown. In this study, we have measured the velocity and attenuation of a number of samples of bovine cancellous bone as a function of frequency, direction and temperature. In addition, we have studied the same properities for the major bone constituents; marrow fat, hydroxyapatite and collagen. The results show a significant directional dependence for both the velocity and attenuation of bone but almost no temperature dependence. While the velocity differences are closely linked to the direction of the load-bearing axis, the variations in attenuation are more complex. The data obtained from bone constituents allow a reasonable prediction of velocity to be made but not attenuation. The constitutent materials were found to have both positive and negative temperature coefficients of velocity and it appears that these largely cancel out *in vivo*.

Ultrasonic bone assessment: is wavefront aberration the principal limitation of current technology?

*P. A. Robins, †G. Petley, *J. D. Aindow and ‡J. Bottle
**Dorset County Hospital, Dorchester, Dorset, †Southampton General Hospital, Southampton, Hampshire, and ‡Marconi Underwater Systems, Templecombe, Somerset*

The last decade has seen a rapid growth in interest in assessing bone fracture risk and techniques for the early detection of osteoporosis. Ultrasonic methods such as broadband ultrasonic attenuation and *in vivo* speed of sound estimates have been developed but have so far received limited clinical acceptance. In fact, ultrasonic propagation parameters in scattering media (as bone may be expected to be) are notoriously difficult to assess with accuracy. The almost universal approach of using large aperture receivers may well introduce severe spatial averaging artefacts. In order to determine the magnitude of these uncertainties we have performed a series of *in vivo* measurements using a specially developed small element array. Data from this array enables the emergent wavefronts from bone to be spatially characterized in both amplitude and phase. Preliminary *in vivo* experimental data from this fundamental approach will be presented and its implications for the future of ultrasonic bone assessment discussed.

Correlation between histology and ultrasonic propagation properties of excised human skin

*C. M. Moran, †N. L. Bush and †J. C. Bamber
**Department of Medical Physics and Medical Engineering, Royal Infirmary, Edinburgh, EH3 9YW, and †Physics Department, Institute of Cancer Research, Royal Marsden Hospital, Downs Road, Sutton, Surrey*

We have previously described the apparatus and techniques developed for measuring the acoustic properties of excised skin tissues. This paper reports the results of applying these methods and correlating the acoustic results with the histological properties of sections from excised human skin samples. Eight normal skin samples and one benign compound and intradermal naevus were excised from two cadavers. The samples were taken from four major sites on the body—the upper and lower back, the chest and abdomen. After removal of the excess fat, the skin samples were sutured into 4 cm diameter perspex templates, with sufficient tension to ensure that the samples returned to their *in vivo* dimensions. After scanning, the mounted samples were then frozen in a liquid nitrogen bath to retain their structural and cellular integrity. A series of sections, 4 μm thick, were then taken at the depth of the region of interest and subsequently selectively stained for collagen (picro-sirius stain), and fat (Oil Red-O). The sections were then scanned using a system capable of producing maps of specified quantities, such as percentage content by area of the stained tissue components. The results from this study showed that a positive correlation was obtained between integrated attenuation (over the 20–30 MHz range) and the percentage content of picro-sirius stain. The magnitude of the speed of sound and attenuation values were compared to those in the literature and agreed well with other skin data collected over a wide frequency range of 0.6–100 MHz. Negative, but statistically insignificant, correlations were obtained for all samples between integrated attenuation and fat content. In comparison to extrapolated data from other soft tissues, the magnitude of the calculated backscatter coefficients appeared to be low and no significant correlation was obtained between integrated backscatter and either fat or collagen content.

Development of an expert system for aiding the ultrasonic diagnosis of solid breast masses

*K. Stepniewska, †D. O. Cosgrove, B. Al-Murrani, E. Tohno, W. E. Svensson and *J. C. Bamber
**Joint Department of Physics and †Department of Nuclear Medicine and Ultrasound, The Institute of Cancer Research and The Royal Marsden Hospital, Downs Road, Sutton, Surrey, SM2 5PT*

We previously described a computerized database for storing and quantitatively devaluating diagnostic features of breast cancer obtained from a visual analysis of real-time B-mode images. In this study, 128 cases of solid breast lesions (32 of which were malignant) were used (a) in a preliminary analysis to identify those features which contribute most to the diagnosis and (b) as a training data set for generating classification rules. Two methods of discrimination were used, for comparison of their diagnostic performance and their ranking of the most important features: linear discriminant analysis (LDA) and "classification and regression trees" (CART). LDA makes assumptions about the distribution of data, is strictly valid only for continuous numerical features and produces a classification rule in the form of an equation. CART is a non-parametric method which creates diagnostic decision trees. On the training set, both methods performed well, showing that diagnostic accuracies using 8–10 features was as high as when all the features were used, and producing estimated error rates of 8% for LDA and 7% for CART. However, the specific sub-sets of features selected by each of the two methods were slightly different. Using this information an easy to use on-line expert system, written in C and running on an IBM compatible PC, has been constructed around 12 of the best diagnostic features. The system incorporates both LDA and CART. Diagnostic predictions are provided only after the operator has entered his/her own opinion of the diagnosis. At any time new cases with confirmed diagnoses may be added, enabling the classification rules to be updated and system performance to be improved. Objectives include the evaluation of the usefulness of this system in training radiologists and in helping them to improve their performance in the task of diagnosing breast masses using real-time ultrasonic imaging.

Ultrasound resolution enhancement by signal averaging

R. A. Harris, M. Halliwell and P. N. T. Wells
Department of Medical Physics and Bioengineering, Bristol General Hospital, Guinea Street, Bristol BS1 6SY

All imaging, unless it faithfully reproduces the original object, is imperfect, and a major factor in that imperfection is the presence of undesirable noise. One particular method of reducing artefactual noise from an image is by coherent signal averaging. Theory predicts that this technique has the ability to improve signal-to-noise ratio by an amount proportional to the square root of the number of averages employed. In ultrasonic imaging, this would allow a higher than conventional scanning frequency to be used to investigate a region of interest, or equally, allow increased penetration at a particular frequency. This paper describes current investigations into the practical potential of this approach. Signal averaging has been found to have certain limitations determined by the presence of coherent noise in the radiofrequency echo signal and also by transducer or tissue motion. However, by minimizing these undesirable factors and their effects, it has been shown that averaging techniques can enhance ultrasonic B-mode resolution.

Three-dimensional colour flow mapping imaging for improved assessment of vascular disease

K. B. Modaresi, M. G. Taylor and T. S. Padayachee
Ultrasonic Angiology Research Group, Division of Radiological Sciences, UMDS, Guy's Hospital, London

An IBM-compatible based system for the three-dimensional (SD) representation of ultrasound colour flow mapping (CFM) images has been developed. Serial image slices were frame grabbed from the CFM (ACUSON 128, Mountain View, California) and in conjunction with spatial positioning and cardiac phase information, the image slices were reconstructed into 3D representations. The scanning protocal involved rotating the probe head about a fixed position in space and simultaneously recording the images and the associated angular changes of the probe. An electrocardiogram trigger was used to detect the QRS complex to ensure that all image grab operations were collected at the same point in the cardiac cycle. In addition, by detecting the R wave, it was possible to collect information at different phases in the cardiac cycle and hence record temporal changes in blood flow. They were used to prepare pulsating 3D representations of the two-dimensional (2D) flow maps. By reconstructing the data at different viewing planes/angles, it was possible to generate a cine sequence of the 3D representations. Post-processing of the data allowed for the detection of the edges of the vessels within the regions of interest which were then mapped into 3D space forming a wire frame model of the SD images. The wire frame model was superimposed on to the 3D images thus allowing the user to highlight a specific edge and view the corresponding 2D image and associated velocity profiles along a user chosen path. The system has been validated *in vitro*, and image reconstructions from test rigs and volunteers will be presented. It is envisaged that this 3D format could provide a more accurate and easily comprehensible representation of vessel geometry and associated flow patterns which could in turn improve the sensitivity for detection of vascular disease.

The development of three-dimenstional ultrasound venographic techniques for the lower limb venous system: preliminary report

K. N. Humphries, R. A. Reynolds, K. Willson and D. O'Keefe
Royal Postgraduate Medical School, Hammersmith Hospital, Du Cane Road, London W12 0NN

A study is in progress to investigate the feasibility of using image processing techniques to obtain three-dimensional (3D) displays of arterial and venous morphological and haemodynamic information obtained from ultrasound image arrays.

An Acuson 128 colour Doppler system was used to obtain parallel transverge image planes of 2.5 mm inter-plane spacing for the lower limb venous system, from approximately 3 cm from the medial malleolus to the mid-calf region, in normal volunteers. A video capture card in a 386 microcomputer was used to translate the RGB signal into three colour plane arrays of 640 × 350 pixels, 8 bits per pixel. The data arrays were transferred to a "Context Vision" image processing computer system and were further processed using "Analyze" a 3D software analysis package. Work is in progress to separate the haemodynamic from the morphological information to enable the display of the venous network. 3D displays of the superficial, communicating, deep and anastomotic veins will be shown. Further image manipulation techniques are being investigated to incorporate skeletal information into the vessel displays. The 3D displays obtained from the colour Doppler imaging data indicate the considerable potential of this technique both in the development of ultrasound venography and in assessing the haemodynamics of the venous system.

Neurology

Chairmen: M. Siegel and P. Dubbins

Ultrasound in neurology, by Yu. M. Nitikin and A. I. Trukhanov
Paediatric neurosonography, by T. Jaspan
Multiplanar ("3D") neonatal neurosonography: initial clinical experience, by J. Spencer, A. Alexander, R. Nandekumar and B. Goldberg

Ultrasound in neurology

Yu. M. Nitikin and A. I. Trukhanov
Radiology Department, Scientific-Research Institute of Neurology, The USSR Academy of Medical Sciences, Volokolamsk Highway 80, Moscow 123367, USSR

Nowadays ultrasound is one of the leading diagnostic modalities in angioneurology where it is widely used in detecting cerebrovascular brain damages. The purpose of the paper is to demonstrate new diagnostic possibilities of ultrasound in neurology based on a complex computer archive of the ultrasound patients' data and on functional diagnostic model of the brain blood supply. The work is the result of the authors' Doppler and duplex ultrasound study of extra- and intracranial blood vessels done on more than 20 000 patients with various cerebrovascular pathology. Such complex Doppler diagnosis made it necessary to unite all the ultrasound instruments in a net with a IBM PC/2 386 as a central controlling computer. This allowed us to form a unified patients' data archive and design an expertise system for Doppler ultrasound diagnostics. The archiving of ultrasound study results made it possible to build up a body of data which could be lately used for quick assessment of the patients' cerebrovascular haemodynamics with follow up possibilities. The Doppler diagnostic net has opened a new avenue for a comprehensive non-invasive study of cerebrovascular circulation and helped to design a model of the brain blood supply. The latter is supposed to bridge the gap between the pure theoretical problems of diagnostics and the real vascular pathology of a patient. The brain blood supply computer model and the follow up of the patients will contribute to solving one of the fundamental and disputable questions of the modern angioneurology, that is the choosing of an adequate treatment (surgery, drug therapy) for cerebrovascular patients so that the existing formal system of indications for surgery could be individualized on the basis of the cerebrovascular haemodynamics evaluation of a concrete patient.

Paediatric neurosonography

T. Jaspan
Department of Radiology, University Hospital, Nottingham NG7 2UH

With the advent of more sophisticated technology, the potential value and role of ultrasound (US) in the examination of the infant brain and spine has greatly increased. This paper addresses the wider uses of US for disease states other than the long-established areas of perinatal hypoxiaischaemia, haemorrhagic and hydrocephalic states. The development of colour Doppler imaging has further enhanced the potential for a haemodynamic assessment of the intracranial vasculature as well as permitting vascular mapping and the exciting recent development of cerebrospinal fluid flow assessment in hydrocephalus. High-resolution scanning now provides exquisite detail of normal and pathological anatomy. The role of US in the examination of intracranial trauma and, in particular, non-accidental injury will be discussed with emphasis on near-field high-definition scanning. The value of US in the investigation of congenital malformations, tumours and infection will be reviewed in the context of current neuro-imaging modalities. Spinal sonography is largely limited by the degree of ossification of the posterior neural arches. A potential "window" is maintained for a variable period of up to 6–9 months. Prior to this the intraspinal contents are accessible for the assessment of spinal dysraphic lesions, the commonest indication for spinal sonography in the infant. The advantages and limitations of this technique are discussed.

Multiplanar ("3D") neonatal neurosonography: initial clinical experience

J. Spencer, A. Alexander, R. Nandekumar and B. Goldberg
Division of Ultrasound, Thomas Jefferson University Hospital, Philadelphia, USA

In recent years, three-dimensional (3D) imaging has been achieved with computed tomography using reconstructions from thin contiguous/overlapping sections and with magnetic resonance imaging using acquisition of data from a volume of tissue. Since the beginnings of ultrasound (US) imaging there has been interest in the production of SD images. Recent advances in computer technology and US imaging have led to a renewed interest in this area. We have been evaluating a new US "3D" transducer (Kretztechnik, Austria) which achieves multiplanar imaging following acquisition of a volume of tissue. Firstly an area of interest is localized using the transducer in a single standard US uniplanar mode. The transducer is then switched into "3D" mode and it sweeps through a volume of tissue or organ of interest. In a few seconds the acquired data from this volume of interest is displayed as three orthogonal planar images on the US video monitor. The volume of interest may then be inspected in real time as multiple sequential parallel images in any of these imaging planes—sagittal, coronal or axial. Our experience with this multihertz "3D" sector scanning probe will be reviewed. Initial clinical research with the system has concentrated on its potential role in neurosonography of premature and term infants in a special care nursery. The system achieves production of axial brain images at the cotside from an anterior fontanelle approach. We will discuss the value of this additional axial projection in the management and diagnosis of prevalent conditions such as intracranial haemorrhage and rarer structural anomalies. The limitations of the present system will be discussed.

Veterinary session

Chairmen: J. Boyd and J. Walmsley

Transvaginal ultrasound-guided collection of oocytes in cows, by M. A. M. Taverne, M. C. Pieterse, P. L. A. M. Vos and Th. A. M. Kruip
Ultrasound monitoring of superovulation in cattle, by L. Robertson, J. C. Cattoni and I. A. Jeffcoate
Ultrasonographic features of the healthy and diseased bovine thorax, by P. A. Graham and D. Murphy
Ultrasound imaging of the reproductive tract of the female bottlenose dolphin, Tursiops aduncas, by F. Brook
Ultrasonography in the equine perinatal intensive care unit, by C. M. Marr
Echocontrast agents—their potential use in domestic animals, by J. S. Boyd
Congenital cardiac disease in calves by J. Dukes, C. Marr, C. Patterson and J. Boyd
Ultrasound and histological appearances of the liver in experimentally induced septicaemia in pigs by R. Morgan, C. Finlayson, J. Alexander, K. Edmunds, D. K. Nassiri, A. R. Webb, D. Tighe, R. F. Moss, E. D. Bennett and A. E. A. Joseph

Transvaginal ultrasound-guided collection of oocytes in cows

M. A. M. Taverne, M. C. Pieterse, P. L. A. M. Vos and Th. A. M. Kruip
Department of Herd Health and Reproduction, Veterinary Faculty, University of Utrecht, Yalelaan 7, 3584 CL Utrecht, The Netherlands

A human endovaginal sector transducer (7.5 MHz; scanner SDR 1150, Philips), adapted to the length of the cow's vagina, was provided with a single needle-guide for ovum pick-up (OPU). Detomidine hydrochloride (i.v.) was used to sedate the standing cow and to relax the rectal wall which facilitated the manipulation per rectum of the ovaries. Ovaries were placed against the vaginal wall to the left or to the right of the cervix. A second operator performed the actual transvaginal puncture as soon as a follicle (≥ 3 mm) had been positioned on the puncture line on the monitor of the scanner. Follicular contents were aspirated by a suction pump. In experiment A, immature oocytes were collected repeatedly from natural cycling cows ($n = 10$) three times (on days 3 or 4, days 9 or 10 and days 15 or 16) during successive oestrous cycles ($n = 23$). In experiment B (10 cows) OPU took place on day 3 or 4 from unstimulated follicles and on day 12 or 13 from stimulated follicles (3000 IU PMSG, given on day 9 or 10). Oestrous cycles ($n = 34$) with normal single ovulations were achieved in experiment B by injection of anti-PMSG and PGF2α and insertion of norgestomet ear-implants (for a period of 9 days) on day 12 or 13, immediately after puncturing. Recovery rate and the size of the punctured follicle were negatively correlated. These data demonstrate that with the OPU-technique the potential source of oocytes from non-preovulatory follicles in cows can be utilized, either for research purposes or embryo production *in vitro*. The developmental potency of these oocytes has been explored in a separate, preliminary study: 104 oocytes (from 206 follicle punctures) were matured and fertilized *in vitro* and they were subsequently transferred to the oviducts of sheep. Six days later, 76 oocytes/embryos were recovered; single cells: 32; two-cell stages: 8; 2–32 cells: 18; morulas: 16; blastocysts: 2. This transvaginal puncturing technique can also be used for diagnostic and therapeutic purposes in cases of ovarian disorders.

	Experiment A			Experiment B	
Day of puncture	3/4	9/10	15/16	3/4	12/13
Mean number (±SEM) of Punctured follicles	5.1 (0.7)	3.7 (0.3)	4.3 (0.4)	4.3 (0.3)	7.1 (1.4)
Oocyte recovery rate (%)	58	58	57	61	42

Ultrasound monitoring of superovulation in cattle

L. Robertson, J. C. Cattoni and I. A. Jeffcoate
Department of Surgery and Reproduction, and Department of Veterinary Physiology, Glasgow University Veterinary School, Bearsden, Glasgow G61 1QH

Embryo transfer in cattle is a standard management technique. Cost-effective embryo recovery is dependent upon successful superovulation to increase the embryo yield. Numerous studies have identified problems with repeatability and predictability of response to superovulation which are not attributable to any single cause. Given these problems, an effective method of monitoring follicular growth, ovulation and formation of corpora lutea would be a useful adjunct to the embryo transfer procedure. This study evaluated ultrasound for monitoring follicular growth, ovulation, and formation of corpora lutea in superovulated cows and correlated findings with embryo recovery and post-mortem examination of the ovaries. Cows were studied through a control and superovulated cycle; superovulation was achieved using pregnant mare's serum gonadotrophin (PMSG; 3000 or 1500 i.u.). Ovarian response was monitored using a real-time B-mode scanner equipped with a linear 7.5 MHz rectal transducer. In the control cycle, which was similar in all cows, luteolysis was followed by growth of a single follicle to 1.4±0.2 cm. Ovulation was identified by collapse of the follicle and appearance of a corpus haemorrhagicum and was confirmed by detection of a luteinizing hormone surge and increased plasma progesterone concentration. By day 5 the mature corpus luteum was visible. At the time of PMSG injection the majority of follicles were < 6 mm. Two days later, 6–10 follicles > 8 mm were observed on most ovaries. Ovulation was identified as either disappearance of large follicles or obvious reduction in the size of the ovary (*e.g.* from 3.6 by 3.4 cm to 2.3 by 3.4 cm). It was possible to identify but not to quantify corpora haemorrhagica. It was considered possible to quantify corpora lutea on day 6. However, this estimate of corpora lutea number correlated poorly with the number counted at post mortem. In addition, numerous anovulatory follicles were observed. Ultrasound examination of ovaries in a waterbath showed that anovulatory follicles varied in appearance from follicular structures to luteal structures depending upon the degree of luteinization of the follicular walls. In conclusion, ultrasound is useful for monitoring follicular growth but not accurate for quantifying ovulation and thus predicting embryo recovery.

Ultrasonographic features of the healthy and diseased bovine thorax

P. A. Graham and D. Murphy
Department of Veterinary Medicine, University of Glasgow, Bearsden, Glasgow G61 1QH

Due to economic constraints in farm animal practice, ultrasonography of the bovine patient has been largely limited to reproductive tract examination. However, there is potential value of this technique as an adjunct to existing diagnostic methods in bovine thoracic disease. Equipment should be portable and robust; 3.0 MHz mechanical sector scanheads are ideal but linear array 3.0 MHz scanheads are an acceptable alternative, although they only scan effectively in a plane parallel to the ribs. The bovine thorax is smaller than external appearances would imply. The caudal pleural reflection extends in a curved manner from the proximal part of the 13th rib to the eighth costochondral junction. The caudal borders of the caudal lung lobes lie craniodorsal to and parallel to this reflection, extending from the proximal part of the 12th rib to the sixth costochondral junction. Ventromedially, the diaphragm extends to the level of the sixth rib and contacts the pericardium. The cardiac notch permits the visualization of the heart and pericardium lies ventrally between the third and sixth ribs and is smaller on the right side. To examine structures cranial to the sixth intercostal space, the forelimb must be drawn forward. In health, only the visceral and parietal pleura, myocardium, cardiac chambers, diaphragm, liver and rumen can be consistently identified. In disease states, it is possible to visualize consolidation of peripheral lung lobes due to infection, inflammation, neoplastic infiltrates or compression and also inflammatory or effusive disease of the pleura and pericardium. Solid masses of the body wall, cranial mediastinum or peripheral lung, *e.g.* neoplasms and abscesses, can be characterized or located accurately to allow percutaneous biopsy or aspiration. Vegetative endocarditis of the tricuspid valve is commonly identified and is often associated with right heart failure and pleural effusion. Radiography remains the modality of choice for imaging caudodorsal mediastinal masses, deep pulmonary disease and pneumothorax.

Ultrasound imaging of the reproductive tract of the female bottlenose dolphin, *Tursiops aduncas*

*F. Brook, † D. Chow, †P. Shroeder, †T. Ng, †S. W. Hui, †D. Tam, †P. Ng, †C. Chan and †Y. T. Lam
**Department of Diagnostic Imaging, Hong Kong Polytechnic, and †Ocean Park, Hong Kong*

On-going research and development at Ocean Park, Hong Kong, is aimed towards improved clinical management of captive propagation of cetacean species. This research includes investigation of the use of diagnostic ultrasound and the role it can play in evaluation and monitoring of the reproductive status and performance of the bottlenose dolphin, *Tursiops aduncus*. It has long been recognized that the development of non-invasive techniques, suitable for routine application in marine mammal management, is highly desirable and we are now confident that ultrasound can fulfil that need. Four females of different ages and obstetric histories were scanned at regular intervals to assess uterine and ovarian morphology and follicular activity. Serum progesterone and oestradiol levels were monitored simultaneously to compare the ultrasound appearance with physiological function. The development of examination and training techniques used are explained and the anatomy and ultrasound appearance of the uterus, ovaries and urinary bladder presented.

Ultrasonography in the equine perinatal intensive care unit

C. M. Marr
Department of Clinical Veterinary Medicine, Madingley Road, Cambridge CB3 0ES

Ultrasonography is invaluable in the management of the equine perinatal patient. Current methods of the diagnosis of fetal distress in late gestation are still based primarily on two-dimensional and M-mode ultrasonographic imaging and include the assessment of fetal heart rate and rhythm; aortic root diameter; fetal mobility; and examination of the placenta and amniotic and allantoic fluids. In the neonate, ultrasonography is applied to the investigation of gastrointestinal, urogenital, cardiac and musculoskeletal systems. The absence of a fully functioning large colon facilitates the examination of parts of the gastrointestinal tract which are inaccessible in the adult horse, namely the stomach, small intestine and small colon. In the neonate presenting with signs of abdominal crisis, ultrasonography may compliment radiography and demonstrate small intestinal intussusception, ileus and segmental hypomotility and necrotizing enterocolitis, while also facilitating abdominocentesis. Ultrasonography is the technique of choice for the demonstration of the umbilical arteries and vein, and the urachus. Rupture of the bladder can be determined and periodic assessment of bladder size is useful in the management of micturition problems associated with prolonged recumbency. Echocardiography is mandatory for the diagnosis of congenital cardiac defects and may also confirm bacterial endocarditis in the foal. Echocardiographic examination of foals with neonatal septicaemia demonstrates pericardial effusion, pump failure, hypovolaemia and is an adjunctive guide to the necessity of pressor agents. In myositis and cellulitis, ultrasonography is useful for the demonstration of the precise soft tissue structures involved, for identification of fluid pockets requiring surgical drainage, and for documenting the response to treatment. In summary, ultrasonography has a wide range of uses in diseases commonly encountered in the equine perinatal intensive care unit. The indications for, ultrasonographic features of, these applications will be discussed and recent advances in equine perinatal ultrasonology will be reviewed. The author is grateful for the support of a Fulbright Scholarship and a Miss Aleen Cust Research Fellowship while studying in The George Widener Hospital, New Bolton Centre, University of Pennsylvania.

Echocontrast agents—their potential use in domestic animals

J. S. Boyd
Department of Veterinary Anatomy, University of Glasgow Veterinary School, Bearsden Road, Glasgow

Real-time B-mode echocardiography is of increasing interest in veterinary diagnosis with the wider availability of ultrasound scanners in veterinary practices. However, many cardiac investigations are limited to anatomical definition of structure and measurements of dimensions including M-mode. Doppler analysis of blood flow is becoming more readily available but colour flow mapping is relatively rare in its use in the veterinary field. To expand on the information gained from echocardiography, echocontrast agents have been used to further increase anatomical definition and to detect anomalies in cardiac morphology. The simpler materials used are agitated saline solution or gelatin-based plasma expanders but recent years have seen the introduction of specifically manufactured echocontrast products using sonicated microbubble suspensions of albumin and microspheres of albumin or stabilized saccharides. Such materials can enhance definition, improve Doppler signals and even enhance colour flow mapping. In the human field these agents are proving of advantage in dealing with patients where imaging and signal quality is a problem, *e.g.* due to obesity. This raises the possibility of investigating their administration in domestic animals where imaging may be problematic due to size and difficulty in obtaining convenient scanning planes. The potential application in domestic species will be discussed and illustration of the use of echocontrast agents in echocardiography, Doppler flow analysis and colour flow mapping will be given.

Congenital cardiac disease in calves

*J. Dukes, †C. Marr, C. Patterson and J. Boyd
**Departments of Veterinary Medicine and Veterinary Anatomy, University of Glasgow Veterinary School, Bearsden, Glasgow G61 1QH. *Present address: Department of Clinical Veterinary Medicine, Madingley Road, Cambridge CB3 0ES*

Congenital cardiac anomalies are more common in the bovine than in many other species. They are associated with a failure to thrive or the development of heart failure in some instances but in many cases are incidental to normal health, growth and productivity. A variety of defects are reported, the most common being the ventricular septal defect. A number of complex and bizarre defects have also been recognized. Although not usually economically viable to investigate congenital cardiac disease in this species, a regular throughput of such cases for use in undergraduate teaching is available at the University of Glasgow Veterinary School. The two-dimensional echocardiographic features of some of these defects with their confirmation by spectral and colour flow Doppler echocardiography and contrast echocardiography will be illustrated.

Ultrasound and histological appearances of the liver in experimentally induced septicaemia in pigs

R. Morgan, C. Finlayson, J. Alexander, K. Edmunds, D. K. Nassiri, A. R. Webb, D. Tighe, R. F. Moss, E. D. Bennett and A. E. A. Joseph
Departments of Diagnostic Radiology, Pathology and Medicine, St George's Hospital, Blackshaw Road, London SW17 0QT

Septicaemic shock is commonly seen in intensive care units. Increased capillary permeability with loss of plasma and cellular elements from the circulation is a major factor in the cardiovascular dysfunction in these patients. Sinusoidal occlusion with cell debris and white cells with swelling and disruption of the sinusoidal epithelium has also been described on electron microscopy. We have observed an increased echogenicity of the liver in patients with septicaemic shock. Studies were designed to investigate the mechansism and prevention of shock in severe septicaemia using a pig model. Ultrasound scans were done on these animals to investigate the mechanism for the increased echogenecity of the liver in septicaemia. Septicaemic shock was induced by producing faecal peritonitis in anaesthetized animals. Scans were done pre- and post-infection and matched with histology on liver biopsies obtained at the same times. Results from eight pigs were analysed. Liver echogenicity progressively increased with increasing liver size and the development ascites. Liver biopsies showed progressive expansion of the interlobular septa due to oedema together with distension of the sinusoids. Immunoperoxidase stain for leucocyte common antigen did not show significant focal aggregation of inflammatory cells within the liver parenchyma apart from one animal which developed microabscesses. Measurements of the interlobular septa showed an average increase of 132% in the biopsies post-infection compared to the pre-infection values. These studies show that the increased echogenicity of the liver in the experimental animals is related to the marked septal oedema and the venous congestion rather than to the increased cellularity. A similar explanation may hold for the patients in severe septicaemic shock. This is the first report on a study that has been carried out relating rapid changes in liver texture on ultrasound with histological changes and morphometric measurement on histological specimens and could well prove a useful model in tissue characterization studies.

Cardiovascular

Chairmen: B. Keaton and S. D. Parvin

Left, atrial spontaneous echo contrast and mitral valve disease—occurrence and associated factors assessed by transoesophageal echo, by L. K. Michalis, M. R. Thomas, H. J. F. Why, D. W. Smyth, M. J. Monoghan and D. E. Jewitt

The value of Doppler echocardiographic assessment of diastolic function in hypertension, by H. J. F. Why, M. J. Monaghan, T. Siddique and P. J. Richardson

Upper limb thrombosis: colour Doppler ultrasound *versus* venography, by G. Baxter, W. Kincaid, R. Jeffrey, G. Millar, C. Porteous and P. Morley

Duplex ultrasound assessment of long saphenous vein patency and competence following high ligation for varicosities, by G. Carolan, L. Fliglestone, N. D. Pugh, A. Shandall, A. Thomas and I. F. Lane

The non-invasive assessment of retrobulbar eye flow: a place for colour Doppler ultrasound, by G. M. Baxter, T. H. Williamson, G. McKillop and G. N. Dutton

A role for duplex ultrasound in patient selection for superficial femoral artery angioplasty, by D. M. A. Foy, J. Quinn, J. Hancock and S. D. Parvin

Venous occlusion and duplex scanning in predicting vein graft size for femoro-distal construction, by A. H. Davies, T. R. Magee, J. K. Hayward, D. R. Jones, R. N. Baird and M. Horrocks

Pre-operative Doppler measurement of vein graft capacity and resistance as predictor's of early outcome, by A. H. Davies, T. R. Magee, D. Jones, R. N., Baird and M. Horrocks

The role of bilateral transcranial Doppler and pre-operative carotid compression in patients undergoing carotid endarterectomy, by T. R. Magee, A. H. Davies, J. K. Hayward, R. N. Baird and M. Horrocks

Arterial and venous ghosts, by K. N. Humphries

Left atrial spontaneous echo contrast and mitral valve disease—occurrence and associated factors assessed by transoesophageal echo

L. K. Michalis, M. R. Thomas, H. J. F. Why, D. W. Smyth, M. J. Monaghan and D. E. Jewitt
Department of Cardiology, King's College Hospital, Denmark Hill, London SE5 9RS

Spontaneous echo contrast (SC) is a phenomenon commonly visualized using transoesophageal echocardiography (TOE) in the left atrium (LA) of patients with mitral valve disease (MVD) or prosthetic mitral valves (MVR). The clinical significance of, and factors contributing to, the presence of SC are unknown although it has been previously postulated that red blood cell aggregation is a cause. The presence of SC, and possible associated features, was therefore studied in 97 patients with MVD and MVR by TOE. Thirty-one patients (Group A) had evidence of left atrial spontaneous contrast (SC) while 66 (Group B) were free of SC. The association of SC with left atrial thrombus (T), left atrial size (LAS), atrial fibrillation (AF), mitral regurgitation (MR), mitral stenosis (MS), MVR and warfarin (W) status was studied. The results are given in the table. SC was therefore present in 32% of this group of patients with MVD and MVR. Significant features associated with SC in this study were: AF, the presence of T, and enlarged LA. AF was invariably associated with SC, only 2/31 patients with SC being in sinus rhythm. Significant MR appeared to protect against the development of SC in this study, presumably by increasing systolic flow turbulence within the LA. Warfarin had no influence on the presence of SC. Significant dominant MS or MVD did not appear to be associated with increased SC. The phenomenon is therefore associated with factors that would predispose to increased left atrial haemostasis. This would support the mechanism for SC being the formation of red blood cell aggregate collections large enough to become specular reflectors.

	T	LAS (cm^2)	AF	Moderate/severe MR	Moderate/severe MS	MVR	W
Group A	10/31	5.5	29/31	3/31	11/31	11/31	23/31
Group B	7/66	5.0	25/66	22/66	17/66	22/66	40/66
p	< 0.01	< 0.05	< 0.001	< 0.02	NS	NS	NS

Statistical test = χ^2 and t-test (mean LAS). NS = not significant.

The value of Doppler echocardiographic assessment of diastolic function in hypertension

H. J. F. Why, M. J. Monoghan, T. Siddique and P. J. Richardson
Cardiac Department, King's College Hospital, Denmark Hill, London SE5 9RS

Left ventricular (LV) hypertrophy is a frequent echocardiographic finding in hypertensive patients and may be a cause of reduced LV compliance. The peak 'E' and peak 'A' velocities and E/A ratio of transmitral LV filling on Doppler echocardiography have been described as indicators of LV diastolic function and compliance in hypertensives, with reversal of the normal filling patterns being a frequent finding. A number of other factors, however, may influence this parameter; these include age, heart rate and blood pressure itself. To examine the value of these Doppler parameters in the assessment of diastolic function, 180 serial Doppler echocardiograms were performed on 54 hypertensive patients prior to initiating therapy and at intervals over a six month period. During the follow up period, significant reductions in blood pressure were obtained in all but seven patients. The 'E' and 'A' velocities and E/A ratio were compared to age, heart rate (HR), systolic (SBP) and diastolic (DBP) blood pressures, LV dimensions and LV fractional circumferential shortening (FS) using multiple regression analysis. Significance values for the independent contributions of these variables to the parameters of diastolic function were thus obtained. The results are given in the table. Thus age, heart rate and blood pressure all alter the parameters of diastolic filling significantly whilst neither LV diameters nor FS have any significant effect. LV posterior and septal wall thickness have only a weak effect. In conclusion these parameters of diastolic function may be altered in hypertension but they are only poorly related to the degree of LV hypertrophy. Therefore, caution should be exercised in their interpretation in the individual patient and corrections for age, heart rate and blood pressure are required.

	Peak E	Peak A	E/A ratio
Age	$p < 0.001$	$p < 0.001$	$p < 0.001$
HR	$p < 0.05$	NS	$p < 0.01$
LVESD	NS	NS	NS
LVEDD	NS	NS	NS
PW	$p < 0.05$	NS	NS
IVS	NS	NS	$p < 0.05$
SBP	$p < 0.001$	$p < 0.001$	NS
DBP	$p < 0.001$	NS	$p < 0.005$
FS	NS	NS	NS

LVESD = LV end-systolic diameter; LVEDD = LV end-diastolic diameter; PW = LV posterior wall thickness; IVS = LV intraventricular septal thickness; NS = not significant.

Upper limb thrombosis: colour Doppler ultrasound *versus* venography

G. Baxter, W. Kincaid, R. Jeffrey, G. Millar, C. Porteous and P. Morley
Department of Radiology, Western Infirmary, Glasgow G11 5NT

Colour Doppler ultrasound is a new technique that has recently been shown to be a suitable alternative to venography in the diagnosis of lower limb venus thrombosis. In view of this, and in order to see if this technique is applicable to the diagnosis of central vein thrombosis, we performed a double-blind prospective trial on 19 renal dialysis patients (30 limbs), all of whom had had multiple central venous cannulations. Both colour Doppler and venography were done in all cases, these investigations being within 2 h of each other and performed by different radiologists. Colour Doppler ultrasound was as accurate as venography, with complete correlation between both techniques in the diagnosis of venous occlusion. A positive ultrasonic diagnosis was based on the absence or marked reduction in spontaneous colour flow. A case of subclavian vein stenosis was missed using colour Doppler as it lay directly beneath the clavicle and was thus an ultrasonic blind spot. Apart from the obvious advantage of safety and financial saving, colour Doppler gave more information on the local extent of thrombus within the internal jugular and innominate veins, this information often being absent on venography. In addition, it is a quicker technique than Doppler ultrasound alone and has the advantage of visualizing collateral vessels, adding confidence to the diagnosis.

Duplex ultrasound assessment of long saphenous vein patency and competence following high ligation for varicosities

G. Carolan, *L. Fliglestone, N. D. Pugh, *A. Shandall, *A. Thomas and *I. F. Lane
*Departments of Medical Physics and *Vascular Surgery, University Hospital of Wales, Cardiff*

Stripping of the long saphenous vein (LSV) for management of varicose veins provides excellent cosmetic and symptomatic results. In an ageing population however, demand for revascularization is increasing and prosthetic bypass gives poorer patency rates than autologous vein graft, so preservation of the LSV is desirable for future use in coronary or peripheral artery bypass. The technique of high saphenous ligation would be advantageous if it offered satisfactory results with the additional benefit of preserving the vein. We studied 75 limbs in 44 patients following high saphenous ligation with multiple stab avulsions in order to determine the extent to which the ligated veins were adequately preserved for use as arterial prosthesis. A Diasonics Spectra or Toshiba 270 colour flow system was used to scan the LSV from groin to ankle. Duplex assessment was made of patency, competence, length and diameter of the LSV and also of perforator competence, 12 months post-operatively. Subjective and objective assessment of cosmetic and symptomatic results of surgery was made and recorded using a linear analogue score. Results showed a good subjective and objective outcome in 95% and 97%, respectively. There was a high patency rate of the LSV following its connection from the femoral vein at the groin, with 68% patent from ankle to groin, 72% patient above the knee and 82% patent below the knee. The internal diameter and vessel characteristics were suitable for use as a vascular conduit in all but six (8%) of the patent veins. The LSV below knee is the graft of choice for coronary bypass grafting, and in this series 75% of patients having undergone high saphenous ligation and multiple avulsions have a suitable venous segment below the knee. There was no association between the presence of reflux in the LSV and relief of symptoms or subjective or objective cosmetic result.

The non-invasive assessment of retrobular eye flow: a place for colour Doppler ultrasound

G. M. Baxter, T. H. Williamson, G. McKillop and G. N. Dutton
Department of Radiology, Western Infirmary, Glasgow G11 5NT

Colour Doppler ultrasound is a non-invasive method of blood flow analysis and, as its use has increased, it has become apparent that it may have many applications. One of its potential applications is in the analysis of retrobulbar eye flow. In view of this, we performed a prospective trial to assess if colour Doppler ultrasound could reliably and reproducibly measure retro-orbital blood velocity parameters in 20 normal healthy volunteers. Exclusion criteria included a positive cardiovascular or neurological history, eye disease or current drug therapy. All Doppler velocity waveforms were assessed in three positions, viz. supine, sitting and erect. Three regional vessels arbitarily named vessels 1, 2 and 3 were identified within the eye and Doppler recordings taken from all in each of the above positions. Results showed significant regional variations of blood velocity ($p < 0.001$) within the eye and these were independent of whichever of the four Doppler spectral parameters analyzed (maximum and minimum velocity, pulsatility index and resistive index). In addition, no significant change in these regional measurements was recorded despite a change in posture resulting in a small but significant increase in diastolic blood pressure and pulse rate ($p < 0.05$). In conclusion we feel these results show that Doppler ultrasound of the eye is a reliable non-invasive method of assessing retro-orbital blood flow and can detect significant regional flow variations which may be a useful tool in the detection and management of certain eye diseases.

A role for duplex ultrasound in patient selection for superficial femoral artery angioplasty

*D. M. A. Foy, J. Quinn, J. Hancock and S. D. Parvin
**Department of Medical Physics, Poole General Hospital, Longfleet Road, Poole, Dorset, and Department of Surgery, Royal Bournemouth Hospital*

In an attempt to improve case selection for angioplasty, duplex ultrasound was used to identify occlusions at the origin of the superficial femoral artery. 82 consecutive angiograms of 160 lower limbs performed at the Royal Bournemouth Hospital were recently reviewed. 70 of these limbs had occlusion of the superficial femoral artery (SFA) of which 37 occlusions occurred at the origin. All of these SFA origin occlusions were more than 10 cm in length and were therefore unlikely to be suitable for angioplasty. Following the initial review, a study was undertaken using a new group of patients in which the accuracy of colour duplex in the identification of SFA origin occlusions was assessed. 54 limbs have now been examined. With each limb, the common femoral artery and the origins of the SFA and profunda femoris artery were identified. Where possible, Doppler signals were recorded from these sites. The SFA was traced more distally for a minimum of 10 cm to assess patency. The duplex assessment of the SFA origin and the length of any associated occlusion were then compared with angiography. Duplex ultrasound was found to be a quick, accurate and reliable method for determining patency of the SFA origin. Thus in cases where surgery was not being contemplated it was possible to advise the surgeon and radiologist of the feasibility of SFA angioplasty. Those with long SFA origin occlusions could then be saved the expense and trauma of an initial angiogram. A prospective study is now under way in the hope of establishing this technique as the first choice in the selection of patients with clinically suspected SFA occlusions who are not being considered for surgery but who might be suitable for angioplasty.

Venous occlusion and duplex scanning in predicting vein graft size for femoro-distal reconstruction

A. H. Davies, T. R. Magee, J. K. Hayward, D. R. Jones, R. N. Baird and M. Horrocks
Vascular Studies, Bristol Royal Infirmary, Bristol

The diameter of the long saphenous vein has been shown to affect the outcome of femoro-distal bypass. Many surgeons regard a vein with a diameter of less than 3 mm as being unsuitable despite previous work that suggests that the size of the vein measured pre-operativley may underestimate the size of the subsequent functioning vein graft. Pre-operative duplex assessment has been used to locate and measure vein diameter but to date no attempt has been made to predict pre-operatively the eventual functional size of the graft. 40 patients undergoing femoro-distal bypass have had their long saphenous vein studied. Pre-operatively the diameter of the vein was measured with an ATL duplex scanner at the groin, mid-thigh and knee. At the latter two points, diameter measurements were performed with proximal venous occlusion at minute time intervals. Diameter measurements were subsequently repeated 7 days and 2 months after surgery. The pre-operative mean groin diameter was 4.8 mm (3.2–6.4). Diameter measurements at the other points are given in the table. All six veins with a resting diameter of less than 3 mm dilated with venous occlusion to a diameter greater than 3 mm. These results suggest that by using a technique of venous occlusion at the time of pre-operative vein mapping the ultimate diameter of the vein can be predicted and vein utilization may be significantly increased.

	Non-dilated (mm)	Dilated (mm)	7 days (mm)	2 months (mm)
Mid-thigh	4.1 (2.5–5.7)	5.1 (3.1–7.1)	5.2 (3.7–6.7)	5.4* (3.7–7.1)
Knee	3.9 (2.2–5.6)	4.8 (3.4–6.2)	4.8 (3.1–6.5)	4.99** (3.0–6.8)

(Using analysis of variance: $^*p < 0.01$ and $^{**}p < 0.025$. ( ) 95% confidence interval.)

Pre-operative Doppler measurement of vein graft capacity and resistance as predictors of early outcome

A. H. Davies, T. R. Magee, D. Jones, R. N. Baird and M. Horrocks
Department of Vascular Studies, Bristol Royal Infirmary, Bristol

In the presence of an adequate inflow the quality of the bypass conduit and distal vessels are the two factors important in affecting the early (within 30 days) outcome of bypass surgery for critical ischaemia. Using a combination of a Doppler flowmeter (OPDOP 130 (Scimed UK)) and intra-arterial pressure, the distal resistance has been obtained in 53 femoro-distal reconstructions. The capacity of the vein graft was calculated using flow measurements performed prior to the insertion of the distal anastomosis ($Q1$), after completion of the distal anastomosis ($Q2$) and then after the administration of papaverine hydrochloride 30 mg ($Q3$). The capacity loss ratio after papaverine (CLR_p) was thus calculated, $CLR_p = (Q1-Q3)/Q1$. Of the 10 early failures in 53 femoro-distal bypasses, four were attributable to a conduit problem and six were associated with poor run-off. In the former group this was associated with a significantly lower CLR_p and in the latter group the distal resistance was significantly higher. The run-off failure is shown in the table. A high resistance is suggestive of possible failure secondary to poor run-off. A minimal or no loss in the CLR_p suggests that the graft is running at its maximum capacity and may be inadequate to sustain the reconstruction, and may indicate a poor conduit. Using these measurements it it possible to pre-operatively identify the infrainguinal vein bypass graft at risk of early occlusion and the likely cause of such failure.

	Success	Failure
Resistance	0.72 (0.59–0.85)	1.51* (1.33–1.69)
Conduit failure CLR_p	40 (34–46)	6** (2–10)

(Means, with 95% confidence intervals. $^*p < 0.001$ and $^{**}p = 0.002$; Mann–Whitney U-test.)

The role of bilateral transcranial Doppler and pre-operative carotid compression in patients undergoing carotid endarterectomy

T. R. Magee, A. H. Davies, J. K. Hayward, R. N. Baird and M. Horrocks
Vascular Studies Unit, Bristol Royal Infirmary, Bristol BS2 8HW

Selective shunting of patients with inadequate cerebral perfusion following carotid clamping remains the ideal. Currently transcranial Doppler appears to be the best simple intraoperative technique for monitoring cerebral perfusion. Bilateral transcranial Doppler has not been used intraoperatively before. Therefore, little information exists on the behaviour of the circle of Willis at the time of carotid clamping. 36 patients with symptomatic internal carotid artery stenosis of 70% were examined. Pre-operative common carotid artery compression was performed while a bilateral transcranial Doppler system was used to measure middle cerebral artery velocity (MCAV). Flat 2 MHz transducers were used with headband attachment. During carotid endarterectomy all patients were monitored using the same system. On the ipsilateral side the mean changes in MCAV during pre-operative compression was 19.5 cm/s (9.5–29.5) and during operative clamping was 14.9 cm/s (5.6–24.2). There was good correlation between the changes in MCAV during compression and clamping ($r = 0.852$). The contralateral side acted as a control and surprising changes were seen on occasions following carotid clamping. These included a rise in MCAV on the contralateral side and on two occasions a rise on the clamped side. Common carotid artery compression reproduces the effects of internal carotid artery clamping, and may prove to be a simple method of identifying patients who would benefit from a shunt during carotid endarterectomy. The use of a bilateral transcranial system has been without problems of "crosstalk" or signal loss due to movement of the transducers. Further work is being carried out in this department to quantify changes in Doppler waveforms from both middle cerebral arteries during carotid surgey.

Arterial and venous ghosts

K. N. Humphries
Royal Postgraduate Medical School, Hammersmith Hospital, Du Cane Road, London W12 0NN

A recent addition to carotid Doppler ultrasound artefacts has been the appearance of a carotid artery "ghost". First recorded in 1990 during investigations of the carotid artery using colour Doppler, a duplicate of "ghost" carotid was consistently obtained parallel to and deeper than the true artery. The presence of strong reflective boundary and the vicinity of the artery was hypothesized to be necessary to produce a mirror image. In order to investigate this phenomenon, three normal volunteers were tested using an Acuson 128 colour Doppler system. The L and R subclavian arteries were visualized at the palpation sites at the clavicle. The colour Doppler mirror/virtual image was obtained for each vessel and the Doppler waveform signatures were examined in detail at a number of sites within both the true and mirror vessel images. Similarly the long saphenous vein was imaged antero-medially in a region approximately 3–8 cm from the medial malleolus. Venous signal augmentation was carried out by proximal and distal compression manoeuvres. These examples confirm the necessary conditions for arterial and venous "ghosting" of a strong reflecting surface within the vicinity of the vessel being examined and generally at a greater depth. No carotid artery "ghosting" has been noted during the investigations of several hundred patients undergoing extracranial vascular assessment.

Antenatal counselling

Chairmen: J. Drife and I. M. Shirley

Parental support following termination of pregnancy for congenital heart disease, by S. Lockhart, L. D. Allan, A. Groves and A. Hereward

Routine radiographer screening for fetal abnormalities by ultrasound in an unselected low risk population, by I. M. Shirley, F. Bottomley and V. P. Robinson

Parental support following termination of pregnancy for congenital heart disease

S. Lockhart, L. D. Allan, A. Groves and A. Hereward
Department of Fetal Cardiology, 15th Floor, Guy's Tower, St Thomas Street, London SE1 9RT

Over a 15 month period, 51 women/couples attended counselling following termination of pregnancy for fetal congenital heart disease. Our aim was to assess the factors which influenced their recovery. In order to achieve this, parents were encouraged to discuss the diagnosis, management and care received surrounding the event. They were seen between 2 and 4 months after the event, with a mean of 12 weeks at this stage. Feelings of guilt were common, but only one woman regretted her decision to terminate the pregnancy. Recovery was positively influenced by a supportive partner, family and friends, the facility to talk and work through the grieving experience. However, the practical care by health professionals had an important bearing on the patient's recovery. Those who were carefully prepared prior to being referred to us were usually accompanied and better able to understand and cope with the information given about the pregnancy. There was an individual variation between patients of 1–7 days as to how long they needed before a decision could be made concerning termination. The sensitivity and quality of care during the termination itself was variable and profoundly influenced the patient's speed of recovery. Follow-up care was often neglected both by hospital staff and local practitioners but was very helpful when offered. In summary, honest and accurate information and sensitive care allows patients to make a full recovery from this traumatic experience.

Routine radiographer screening for fetal abnormalities by ultrasound in an unselected low risk population

I. M. Shirley, F. Bottomley and V. P. Robinson
The Hillingdon Hospital, Pield Heath Road, Uxbridge, Middlesex UB8 3NN

About 2% of newborn infants have congenital or genetically determined abnormalities. Congenital abnormalities account for 20–30% of perinatal deaths. 90% of infants with congenital malformations and chromosome disorders are born to healthy young women with no identifiable risk factor. The detection of these disorders will therefore require screening of all pregnant women by methods that are safe, simple, cheap and effective. This study describes our experience of prenatal ultrasound screening of an unselected low risk population in a district general hospital using radiographers. The technique and equipment are described. 6412 babies were born in our hospital during 1989/90. There were in addition 29 terminations of pregnancy for fetal abnormality. An estimated 97% of all pregnancies were scanned in the second trimester in our hospital. 89 fetuses (1.4%) were abnormal at birth or at induced termination of the pregnancy. Of the 89 abnormal fetuses, 87 were scanned in our hospital and 58 were detected by ultrasound during the pregancy (sensitivity 66.7%). 84 fetuses with significant abnormalities confirmed at delivery were scanned in the second trimester in our hospital. In 51 cases, the abnormality was correctly diagnosed by ultrasound before 22 weeks gestation (sensitivity 60.7%). 50 of the 87 abnormal fetuses scanned had potentially lethal or major handicapping abnormalities, of which 43 were correctly detected by ultrasound during the pregnancy (sensitivity 86%). 38 were correctly diagnosed before 22 weeks gestation (sensitivity 76%). 6352 fetuses were normal at delivery or on discharge from hospital. There was one false positive diagnosis of abnormality which did not affect outcome (specificity 99.98%). Routine screening by radiographers of unselected pregnant women at low risk of fetal abnormality by ultrasound in the second trimester can detect the majority of major fetal congenital abnormalities in time to allow parents and obstetricians informed choice about the management of the pregnancy.

Obstetrics and gynaecology

Chairmen: B. Trudinger and J. W. Scott

A comparison of the changes in pelvic blood flow in early intrauterine pregnancies and ectopic pregnancies, by T. H. Bourne, D. Jurkovic, K. Reynolds, S. Campbell and W. P. Collins
Transvaginal *versus* transabdominal scan in measurement of the endometrial thickness in post-menopausal women, by M. N. Nasri
Ultrasound appearances of the endometrium before and after endometrial resection related to clinical response, M. Rymer and M. Creagh-Barry
The incidence and significance of post-hysterectomy pelvic fluid collections, by J. Slavotinek L. H. Berman and D. Burch
Transvaginal colour Doppler ultrasonography for the diagnosis of uterine cancer, by T. H. Bourne, T. Crayford, K. Reynolds, J. Hampson, S. Campbell and W. P. Collins
Vaginal scanning in a district general hospital, by H. Massouh
Transabdominal *versus* transcervical chorionic villus sampling, by D. Maxwell
Choroid plexus cysts—incidence and clinical significance in low-risk pregnancies, by T. Chudleigh, L. Chitty, S. Campbell and M. Pembrey
Incidence, natural history and clinical significance of mild fetal pyelectasis, by L. Chitty, T. Chudleigh, S. Campbell and M. Pembrey
The differential diagnosis of normal size hyperechogenic kidney detected antenatally, by C. Owen and R. De Bruyn
The antenatal ultrasound appearances of gastroschisis and their correlation with neonatal findings of surgical repair, by W. W. Gibbon and C. Hayward
The outcome of fetuses with anterior abdominal wall defects, by F. M. A. Wilson and P. Twining
Fetal nuchal translucency: ultrasound screening for chromosomal defects in the first trimester of pregnancy, by K. N. Nicolaides, G. Azar, D. L. Byrne and K. Marks

A comparison of the changes in pelvic blood flow in early intrauterine pregnancies and ectopic pregnancies

T. H. Bourne, D. Jurkovic, K. Reynolds, S. Campbell and W. P. Collins
The Department of Obstetrics and Gynaecology, Kings College School of Medicine and Dentistry, London

The incidence of ectopic pregnancy is increasing. The availability of relatively non-invasive techniques for the treatment of this disorder has led to some workers advocating a policy of screening early pregnancies to check for their location. A more sensitive and specific test for presence or absence of an ectopic pregnancy would be of value. Transvaginal colour Doppler has been used to study blood flow within the corpus luteum, uterine arteries and developing trophoblast of 20 uncomplicated intra-uterine pregnancies (from 4 to 20 weeks gestation). These data were compared to a further 20 women with ectopic pregnancies. There was no difference between the two groups with regard to indices of blood flow within trophoblast or corpora lutea. Whilst indices of impedance to flow were similar in both groups, there was a significant reduction in peak blood velocity within the uterine arteries of women with ectopic pregnancy. Such a difference is unlikely to be clinically useful. However the corpus lueteum was identified in all cases and was ipsilateral to the ectopic gestation in over 90%; this information may be used as a guide to the identification of an ectopic gestation sac. The blood supply to the corpus luteum and the ectopic sac could usually be identified separately. These subtle vascular changes may be helpful in making the correct diagnosis in the presence of an adnexal mass. These data suggest that there are only limited haemodynamic differences between early normotopic and ectopic pregnancies, but that subtle changes in tubal and ovarian vascularity may have a role in improving the facility with which ectopic pregnancy can be diagnosed.

Transvaginal *versus* transabdominal scan in measurement of the endometrial thickness in post-menopausal women

M. N. Nasri
506 Park West, Park West Place, London W2 2QS

Transvaginal (TVS) and transabdominal (TAS) ultrasound approaches to measure the endometrial thickness in post-menopausal women were compared in two separate groups of patients. The first group consisted of 90 women who had a TAS of the endometrium before dilatation and curettage or hysterectomy for either post-menopausal bleeding or uterine prolapse. The second group consisted of 111 women who had a TVS of the endometrium for similar post-menopausal symptoms. Patients acceptance and image quality were better in the TVS group. The proximity of the transvaginal probe to the endometrium and the absence of a full bladder compressing the endometrium revealed a unique group of patients with atrophic but thick endometrium due to the intracavity fluid. In the presence of uterine fibroids distorting the uterine cavity, TVS was better than TAS in visualizing the endometrium. The transabdominal full bladder approach can be of value in detecting asymptomatic bladder pathology. The disadvantages of TVS are initial difficulty with anatomical orientation and unacceptability in virgins or patients with gross vaginal atrophy. The advantages of TVS in measuring the endometrium in post-menopausal women include excellent tissue characterization, rapid performance, resolution of many of the technical difficulties of TAS and good patient acceptance.

Ultrasound appearances of the endometrium before and after endometrial resection related to clinical response

M. Rymer and M. Creagh-Barry
Poole General Hospital, Longfleet Road, Poole, Dorset BH15 2JB

All patients attending for endometrial resection at a district general hospital were examined by transvaginal ultrasound pre-operatively, 30–40 days after the commencement of patient preparation with Danazol, and post-operatively at 12–14 weeks. Patients were examined by ultrasound to assess endometrial thickness and uterine dimensions together with any incidental or related pathology. The aims of the study were to obtain a pre-operative assessment as a baseline for comparison, to look for incidental pathology and determine a possible relationship with response to treatment, to assess measurement of myometrial thickness as an aid to the procedure. The aims of the post-operative study were to establish "normal" appearances to aid ultrasound assessment when scanning patients with complications following the procedure of endometrial resection, and to document ultrasound appearances of complications. The findings are reported with relation to clinical outcome following endometrial resection.

The incidence and significance of post-hysterectomy pelvic fluid collections

J. Slavotinek, L. H. Berman and D. Burch
The Departments of Radiology, Addenbrooke's Hospital, Cambridge CB2 2QQ

Pyrexia and vaginal discharge are common post-hysterectomy sequelae. Although many febrile patients demonstrate no sonographic abnormality, the authors have observed pelvic fluid collections at the apex of the vagina in some of these symptomatic patients utilizing endovaginal sonography. These collections have usually proved to be sterile when drained under EV sonographic control. There are no previous studies assessing the incidence of post-hysterectomy collections or whether their presence correlates with symptoms or physical signs. Endovaginal scans were obtained four days after hysterectomy in 32 consecutive subjects. Pelvic collections were identified in 19 patients (59%) of whom nine were asymptomatic. There was no correlation between the findings of post-operative pyrexia or discharge and the presence, size or sonographic characteristics of a vault collection. 24 patients consented to a second scan at 7 weeks including 14 of the 19 patients with abnormal initial scans. Five of these patients with abnormal scans demonstrated a persisting but smaller collection at the follow-up scan. In nine patients the collection had resolved by 7 weeks. Surprisingly, in two cases with normal initial scans, collections were detectable on the later study. The authors conclude that most patients undergoing hysterectomy sustain a pelvic collection detectable by EV sonography and that this finding does not correlate with symptoms or signs.

Transvaginal colour Doppler ultrasonography for the diagnosis of uterine cancer

T. H. Bourne, T. Crayford, K. Reynolds, J. Hampson, S. Campbell and W. P. Collins
Department of Obstetrics and Gynaecology, King's College School of Medicine and Dentistry, London

Transvaginal colour Doppler ultrasonography has been used to assess uterine blood flow and morphology in 227 post-menopausal women. 72 had symptoms of abnormal post-menopausal bleeding, and 155 were asymptomatic. Endometrial biopsy was performed after ultrasonography had been performed. There were 119 women whose endometrium was atrophic, 23 with secretory or proliferative changes, three cases of hyperplasia, and 24 women with confirmed endometrial carcinoma. 58 women were taking hormone replacement therapy. All women with endometrial cancer had a significantly thicker endometrium (mean 20.2 mm) than the other groups such as those with atrophic endometrium (1.35 mm). In addition all cases of uterine cancer had a markedly lower pulsatility index (PI) (mean PI 1.00 compared to 3.80 for atrophic endometrium), suggesting reduced impedance to blood flow within the uterine arteries distal to the point of sampling. It is of interest that women taking hormone replacement therapy demonstrated a marked decrease in impedance to blood flow in the uterine arteries (mean PI 2.5) suggesting that oestrogens may have a direct effect on the human vasculature. The difference in PI and endometrial thickness measurements between the groups suggests that discriminatory values may be determined. We are currently assessing the use of transvaginal colour Doppler in a screening programme for early ovarian and uterine cancer.

Vaginal scanning in a district general hospital

H. Massouh
X-ray Department, Frimley Park Hospital, Frimley, Camberley, Surrey

Vaginal ultrasound (VUS) is a well-recognized modality for diagnosing pelvic pathology. Its well-known advantages over the transabdominal ultrasound, plus the availability of vaginal transducers by almost all known ultrasound manufacturers, makes it an important diagnostic tool which should be available to all sonographers at every district general hospital (DGH). VUS is an essential technique in *in vitro* fertilization, monitoring follicular growth during ovarian stimulation and assessing endometrial changes. It is the examination of choice in the first 14 weeks of pregnancy for confirming viability, early confirmation of fetal anatomy and accurately assessing the fetal age. It is an excellent method for visualizing placental anomalies, particularly praevia and succenturiate lobe. VUS clearly visualizes ovaries and uterus and demonstrates their abnormalities. In particular it is an essential technique in diagnosing polycystic ovaries, dermoid cysts, pathologically enlarged cystic or solid ovarian and uterine masses and early detection of ovarian cancer. In our experience, VUS has been extremely helpful in pelvic inflammation like hydrosalpinx, diverticulitis, colitis and their complications. In particular, it is a useful approach for draining/aspirating pelvic abscesses under ultrasound guidance. In certain cases, and following careful criteria, VUS can be used for aspirating simple ovarian cysts, performing fine-needle aspiration on pelvic tumours or suspected recurrence. The use of colour flow ultrasound, subject to availability in a DGH, is used in assessing pelvic varices and pelvic vascular anomalies, studying the ovarian and uterine vasculature and adding new methods for diagnosing pelvic anomalies. This talk will cover and demonstrate the usefulness of vaginal scanning in a variety of pelvic pathologies with special emphasis on its role in DGH.

Transabdominal *versus* transcervical chorionic villus sampling

D. Maxwell
Guy's Hospital, Floor 2, New Guy's House, London Bridge, London SE1 9RT

The aim of chorionic villus sampling (CVS) is reliably to obtain an adequate quantity of clean villus tissue for laboratory analysis. The method chosen should combine the greatest safety with the least discomfort and be acceptable to the individual woman. The technical evolution of CVS has seen utilization of the transabdominal and transcervical routes under ultrasound guidance. There are vigorous advocates of the superiority of each of these methods. Comparative studies by sampling route have not shown convincing evidence that either technique is preferable. Both are comparable for reliability, amount of villus tissue obtained, patient discomfort and patient preference. This analysis with regard to pregnancy risk remains limited. At present, neither techique could claim to be unequivocally safer. The choice of route for CVS can therefore, be made entirely on pragmatic grounds. Free-hand transabdominal CVS can be performed over a wide gestational range and the technique is inherently similar to other ultrasound-guided techniques. It is easy to learn and the performance of any other ultrasound-guided technique reinforces the operator's ability to perform a transabdominal CVS. For these reasons, transabdominal CVS should be considered the primary technique. Not all transabdominal procedures will be easy and not all patients will wish to have the test done by this method. In any centre performing large numbers of CVS, it seems reasonable at the present time to maintain the availability of both transabdominal and transcervical methods.

Choroid plexus cysts—incidence and clinical significance in low-risk pregnancies

*T. Chudleigh, *L. Chitty, †S. Campbell and *M. Pembrey
**Institute of Child Health, Guildford Street, London, and*
†Department of Obstetrics and Gynaecology, King's College Hospital, London

The first prenatal diagnosis of choroid plexus cysts was made in 1984 and since this time many workers have described an association with trisomy 18. Many of these studies refer to high-risk populations or to a relatively small number of pregnancies. We have designed a multicentre study, involving 14 hospitals, to investigate the incidence of choroid plexus cysts and their association with abnormal karyotypes in a large low-risk population. In the first 18 months of this study 287 fetuses with choroid plexus cysts were identified in a total of 45 350 deliveries. In 19 cases there was an associated anomaly. One of these fetuses had trisomy 18. In the remaining 269 fetuses the choroid plexus cysts were an isolated finding. One of these fetuses was found the have trisomy 18 at amniocentesis. Of the remainder there was one intrauterine death and one intrapartum malformed still birth. We will discuss our findings, including size, number, laterality and time of resolution of the cysts and the relevance of prenatal karyotyping in the light of our report and other published papers.

Incidence, natural history and clinical significance of mild fetal pyelectasis

*L. Chitty, *T. Chudleigh, †S. Campbell and *M. Pembrey
**Institute of Child Health, Guildford Street, London and*
†Department of Obstetrics and Gynaecology, King's College Hospital, London

Mild fetal pyelectasis is a relatively common finding but its clinical significance to the neonate remains unclear. Previous reports would suggest that the likelihood of neonatal renal pathology is small if the dilatation of the renal pelvis is less than 10 mm. The other significant association appears to be with Down's syndrome. We have designed a multicentre study, involving 14 hospitals, to define more clearly the normal renal pelvic parameters, to establish the clinical significance of mild fetal pyelectasis to the neomate and to determine the associated risk of an abnormal karyotype. In the first 18 months of the study, 373 fetuses with mild pyelectasis (defined as a mean transverse and antero-posterior pelvic diameter of 5 mm or greater) were identified in 45 350 deliveries. Pyelectasis was an isolated finding of 350 fetuses of which three had an abnormal karyotype. The remaining 23 had an associated structural abnormality, four of these had karyotypic abnormalities. We will discuss the natural history of the pyelectasis in these fetuses. The study is designed to provide paediatric follow up to the age of one year (or more if clinically indicated) for all fetuses recruited into the study. We will present details of this follow up and its relevance of pre-natal counselling.

The differential diagnosis of normal size hyperechogenic kidney detected antenatally

C. Owen and R. De Bruyn
Department of Paediatric Radiology, The Hospital for Sick Children, Great Ormond Street, London WC1N 3JH

The antenatal detection of normal size hyper-reflective kidneys can pose both a diagnostic and counselling dilemma especially when discovered during a routine scan. We present four patients with normal size hyperechoic kidneys detected antenatally and their post-natal follow up. One patient has nephrocalcinosis, another has a large calcified thrombus in the IVC. The remaining two have been diagnosed as renal dysplasia. The literature will be reviewed and the differential diagnosis discussed. A protocol for the post-natal investigation of infants with antenatally diagnosed hyperechoic kidneys is suggested.

The antenatal ultrasound appearances of gastroschisis and their correlation with neonatal findings at surgical repair

W. W. Gibbon and C. Hayward
Department of Diagnostic Radiology, University Hospital of Wales, Heath Park, Cardiff

Gastroschisis is a rare extraumbilical defect of the anterior abdominal wall probably produced by premature obliteration of the right, or more rarely, left umbilical vein. The true incidence has apparently increased over recent years and the incidence of antenatal ultrasound diagnosis has certainly increased and improved sonographic experience and technology. We describe the specific sonographic features of gastroschisis both with regard to differentiation from omphalocoele and the features suggesting intrauterine complications of gastroschisis. The antenatal sonographic findings of 15 cases of proven gastroschisis diagnosed over a 3 year period from 1988 to 1991, were compared with surgical findings at neonatal repair (13) or termination (2). No satisfactory qualitative nor quantitative criteria for the diagnosis of bowel atresia *in utero* and no accurate prognostic indicator of bowel viability or overall survival was found. Early antenatal diagnosis did, however, allow careful parental counselling and obstetric care. It also allowed planned delivery at a specialized centre where surgical repair of the abdominal wall defect and any associated complications could be corrected in the immediate neonatal period. We suggest a rationale for the diagnosis and follow up of such cases over the antenatal period to provide optimum conditions for neonatal surgery.

The outcome of fetuses with anterior abdominal wall defects

F. M. A. Wilson and P. Twining
X-ray Department, University Hospital, Queen's Medical Centre, Nottingham NG7 2UH

In order to assess the outcome of fetuses with anterior abdominal wall defects, a 4 year review was carried out at Queen's Medical Centre, Nottingham. 19 fetuses were available for study. There were nine cases of omphalocoele, eight cases of gastroschisis and two cases of eventration. Six of the eight cases of omphalocoele were associated with other abnormalities and two of these had chromosomal anomalies–one trisomy 13 and one trisomy 18. The three fetuses with an isolated omphalocoele had normal chromosomes. In the omphalocoele group, three patients opted for a termination of pregnancy, three were stillborn, there was one neonatal death and two babies are alive and well. In the gastroschisis group one patient opted for a termination of pregnancy, there were two neonatal deaths and five babies are alive and well. One fetus with gastroschisis developed jejunal atresia later in pregnancy and this patient represented one of the neonatal deaths. Both cases of eventration opted for a termination of pregnancy. Within the total group there were 10 liveborn babies, five were delivered by caesarian section and five by vaginal delivery. In our study, fetuses with omphalocoele have a high incidence of associated anomalies, a high rate of chromosomal defects and a poor prognosis. Isolated defects have a low incidence of chromosomal anomalies. Fetuses with gastroschisis have a good prognosis; however, serial scans are indicated in order to exclude the development of complications such as jejunal atresia which has a poor prognosis. We recommend karyotyping all cases of omphalocoele and serial scanning to exclude the development of complications, particularly in fetuses with gastroschisis.

Fetal nuchal translucency: ultrasound screening for chromosomal defects in the first trimester of pregnancy

K. N. Nicolaides, G. Azar, *D. L. Bryne and K. Marks
*Harris Birthright Research Centre for Fetal Medicine, King's College Hospital, Denmark Hill, London, and *Department of Obstetrics and Gynaecology, St Thomas' Hospital, London*

In a prospective randomized trial comparing the safety and diagnostic accuracy of amniocentesis and chorion villus sampling for fetal karyotype at 10–14 weeks gestation, subcutaneous nuchal translucency was detected by ultrasonography in 72 of the 706 (10.2%) fetuses. The indications for fetal karyotyping were advanced maternal age, parental anxiety or a family history of chromosomal abnormality in the absence of a balanced parental translocation. The incidence of chromosomal defects was 3% (24 of 706 cases). In the 41 (6%) fetuses with nuchal translucency 3–8 mm in thickness, the incidence of chromosomal defects was 37% (14 cases). In contrast, only 9 of the remaining 665 (1%) fetuses (including the 31 with translucency of 2 mm or less) were chromosomally abnormal. Therefore, in an unselected, low-risk population of women having fetal karyotyping the presence of fetal nuchal translucency ≥ 23 mm is associated with a ten-fold increase in the risk for a chromosomal abnormality.

Fetal biometry

Chairman: M. McNay

Fetal biometry charts: which charts and when? by L. Chitty, D. Altman and S. Campbell

Fetal biometry charts: which charts and when?

*L. Chitty, †D. Altman and ‡S. Campbell

**Institute of Child Health, London, †Imperial Cancer Research Fund, London and ‡Department of Obstetrics and Gynaecology, King's College Hospital, London*

Fetal biometry charts are used for a variety of purposes, principally dating, growth and diagnosis of abnormalites. It is important that whichever chart is used has been appropriately constructed and is correctly used for each purpose. We have devised charts for a variety of fetal parameters in both longitudinal and cross-sectional studies in a low-risk population in South East London. We have found that the bi-parietal diameter is slightly, but significantly, small at *all* gestations when the fetus is not in a cephalic position. In contrast, the head circumference is unaltered by fetal position. These findings have particular significance when using charts of bi-parietal diameter alone to estimate gestational age and may result in inaccurate dating. Our studies have also shown that the measurements of head and abdominal circumference vary depending on whether direct plotting or derivation from diameters is used to assess size. This implies that to avoid error in the assessment of fetal size the appropriate chart should be used for the technique employed. Finally, we will discuss any difference between the charts derived from the cross-sectional and longitudinal studies and the significance to the assessment of growth velocity.

Obstetrics

Chairmen: M. Dooley and D. Maxwell

Biophysical fetal assessment, by J. C. Dornan

Prediction of fetal acidemia in pregnancies complicated by maternal diabetes mellitus by biophysical profile scoring and fetal heart rate monitoring, by D. R. Salvesen, M. J. Brudenell and K. H. Nicolaides

The prediction of pre-eclampsia using transvaginal Doppler ultrasound in early pregnancy, by K. F. Harrington and S. Campbell

Pregnancy loss following fetal blood sampling—an evaluation in relation to indication, by D. Maxwell, P. Johnson, P. Hurley, K. Neales, L. Allan and P. Knott

Ultrasound time management: a cost-effective approach, by S. Hasnain, T. Chudleigh and S. Campbell

Doppler studies of the fetal vasculature in the prediction and management of the at risk pregnancy, by K. F. Harrington and S. Campbell

Overview of the current state of obstetric Doppler and new advances, by B. J. Trudinger

Biophysical fetal assessment

J. C. Dornan

Department of Obstetrics and Gynaecology, QUB, Institute of Clinical Science, Grosvenor Road, Belfast BT12 6BJ

Biophysical fetal assessment was introduced to Western obstetrics some 15 years ago by Frank Manning who developed an "intrauterine Apgar score" to be applied to all fetuses at all gestations in all obstetrical conditions. Therein lies its strength and its weaknesses. Each particular fetus has its own obstetrical problem and has individual parameters which are more appropriate to it. The gestation and obstetrical condition must be taken into account, and the observed biophysical features expanded outside the five proposed by Dr Manning. We must further consider keeping the biophysical fetal assessment on apparently low-risk fetuses rather than those just clinically identified as being at high risk. In our own unit at the Royal Maternity Hospital, Belfast (3500 deliveries yearly), 20% of patients are referred to biophysical fetal assessment. Of the 80% not referred, 90% of the perinatal mortality occurs. 77% of intrauterine growth retardation is undetected clinically at the antenatal clinic. The observation of normal liquor volume and an estimated fetal weight of > 10th centile is associated with a 99.8% negative predictive value for PNM. It will be suggested that assessment of liquor volume and estimated fetal weight should be a routine screening assessment for all pregnancies whether previously designated high or low risk.

Prediction of fetal acidemia in pregnancies complicated by maternal diabetes mellitus by biophysical profile scoring and fetal heart rate monitoring

D. R. Salvesen, M. J. Brudenell and K. H. Nicolaides

Harris Birthright Research Centre for Fetal Medicine, King's College Hospital, Denmark Hill, London SE5

In 31 pregnancies complicated by maternal diabetes mellitus, fetal heart rate (FHR) monitoring with computer-assisted analysis and the biophysical profile score were used to investigate the relationship between non-invasive methods of fetal assessment and umbilical venous blood glucose concentration and blood gases. Fetal blood was obtained by cordocentesis up to 24 h before delivery at 27–39 weeks' gestation. The mean umbilical venous pH was significantly lower than the normal mean for gestation, and was below the 5th centile in 15 of the cases. The mean PO_2 was not significantly different from the normal mean for gestation. Both the biophysical profile score and FHR variation provided poor prediction of the degree of fetal acidemia. This data demonstrates that in pregnancies complicated by maternal diabetes mellitus, some fetuses are acidemic. If fetal acidemia is the cause of late unexplained stillbirths in this group of pregnancies, then our present methods of fetal assessment are poor at identifying those pregnancies at greatest risk.

The prediction of pre-eclampsia using transvaginal Doppler ultrasound in early pregnancy

K. F. Harrington and S. Campbell
Department of Obstetrics and Gynaecology, King's College Hospital, London

Doppler ultrasound studies of the uterine artery have shown promise as a predictor of the subsequent development of pregnancy complications, in particular pre-eclampsia, and low-dose aspirin is associated with an improved outcome if commenced before the clinical onset of the disease. In an ongoing study, 600 unselected antenatal patients had transvaginal Doppler studies of the uterine artery performed in the first 15 weeks of pregnancy, to assess its value in identifying a group of patients at risk of developing pre-eclampsia and other pregnancy complications. The examinations were performed using a 5 MHz transducer on an Acuson 128. The pregnancies were dated by crown–rump length. Early pregnancy loss, multiple pregnancy and structurally abnormal pregnancies were excluded from the analysis. The uterine arteries were identified with colour flow imaging at the level of the cervical internal os. Pulsed Doppler was then applied to each artery and measurements obtained from a consistent clear waveform. From 6–15 weeks there is a gradual rise in vessel diameter (2.080 cm ± 0.408 to 2.67 ± 0.3625), mean (12.3 ± 0.5 to 33.4 ± 14.5) and maximum (52.35 ± 14.9 to 103.6 ± 29.8) velocity, there is a reduction in the resistance index (*RI*) (0.857 ± 0.051 to 0.667 ± 0.133) and pulsatility index (2.43 ± 0.567 to 1.43 ± 0.64). There is a fall in the number of bilateral uterine notches from 54% to 38%. Almost 200 patients have delivered, six developing pre-eclampsia. All six patients had bilateral notches in the first trimester, and an RI value > 50th centile. This data may be of use in identifying a group suitable for treatment with aspirin from early pregnancy. The results of the study will be presented.

Pregnancy loss following fetal blood sampling—an evaluation in relation to indication

D. Maxwell, P. Johnson, P. Hurley, K. Neales, L. Allan and P. Knott
Fetal Medicine Unit, Guy's Hospital, London, England

In order to assess pregnancy losses after ultrasound-guided fetal blood sampling, an analysis of 363 samplings was performed in relation to the indication for the procedure. All procedures were performed using identical high-resolution ultrasound equipment and a standard freehand technique. Patients were divided into four groups: pre-natal diagnosis with normal ultrasound findings, structural fetal abnormality, fetal assessment (intrauterine growth retardation, infection, etc.) and non-immune hydrops. Gestational age ranged from 16 to 38 weeks, and blood was taken from the umbilical cord, fetal heart or intrahepatic portion of the umbilical vein. Employing a definition of a loss within 2 weeks as being directly related to the procedure, the losses ranged from 1.1% in the 'low-risk' group being investigated for inherited disease, to 25% in the 'high-risk' group with non-immune hydrops. All pregnancy losses were examined, and of the 65 which occurred, 25 were within 2 weeks. In the pre-natal diagnosis group, one pregnancy loss occurred within 2 weeks (1.1%), nine (7.3%) in the structural abnormality group and five (14.7%) in those undergoing fetal assessment whereas 10 such losses occurred in the non-immune hydrops group (25%). These differences are statistically significant ($\chi^2 = 18.535$). There was no relationship demonstrated between pregnancy loss and gestation at sampling or site of sampling. This study confirms that the risk of ultrasound-guided fetal blood sampling is increased in abnormal pregnancies, reflecting the underlying pathology, and this must be taken into account when counselling prior to the procedure.

Ultrasound time management: a cost-effective approach

S. Hasnain, T. Chudleigh and S. Campbell
Ultrasound Department, 6th Floor, New Ward Block, King's College Hospital, Denmark Hill, London SE5

With the current application of many hospitals for trust status, the role of the sonographer in providing an efficient high-quality obstetric service is placed under close assessment. The obstetric ultrasound examination is dependent on the following: (1) the protocol of the department; (2) the equipment and staff available; and (3) the patient throughput/time availability. The ultrasound examination may be divided into components of time: (a) collection time—the time taken to bring the patient from the waiting area and to prepare her for her scan; (b) scan time—the time taken in assessment and measurement of the fetus and uterus; and (c) administration/discussion time—the time taken to evaluate the information from the scan, record or plot it appropriately, and to discuss the findings and any relevant follow-up with the patient and her partner. We present the results from time studies, carried out during 500 routine 20 week obstetric examinations. We compare these findings to those from a further 50 pregnancies where the partners were not present from the start of the procedure but were invited into the scanning room after the majority of the examination was completed. From our results we assess how the limited time available for individual obstetric ultrasound examinations can be best utilized.

Doppler studies of the fetal vasculature in the prediction and management of the at risk pregnancy

K. F. Harringon and S. Campbell
Department of Obstetrics and Gynaecology, King's College Hospital, London

The use of Doppler ultrasound studies of the umbilical artery in identifying true growth retardation from the constitutionally small fetus is well established. The role of Doppler studies of the fetal vasculature is less clear. The normal changes in fetal blood flow though the latter stages of pregnancy have already been documented, as well as the findings in the fetus with established intrauterine growth retardatin or rhesus disease. We performed serial Doppler studies of the fetal thoracic aorta, renal and middle cerebral arteries in 64 women with a poor obstetric history and/or abnormal Doppler studies of the uterine artery at 24 weeks (and endsystolic notch and/or a resistance index > 95th centile). 15 women subsequently developed pre-eclampsia; the Doppler studies of the fetus did not become abnormal until shortly before or at the onset of the clinical disease. Three patients had evidence of intrauterine growth retardation (IUGR), in the absence of pre-eclampsia. All three fetuses showed a pattern of redistribution at the time IUGR was suspected but not before. One patient retained normal blood flow in the umbilical artery despite severe fetal redistribution, thought to be as a result of having a single umbilical artery, confirmed at Caesarian delivery for fetal acidosis. Doppler ultrasound of the fetal vasculature does not appear to predict the subsequent development of pregnancy complications but is useful in the management of the high risk fetus.

Overview of the current state of obstetric Doppler and new advances

B. J. Trudinger
Department of Obstetrics and Gynaecology, The University of Sydney at Westmead Hospital, Westmead, NSW 2145, Australia

Doppler ultrasound provides unique information about blood flow, and the state of the vascular bed, in locations the obstetrician could only have dreamed of measuring in the past. Information is now available about pregnancy physiology and the pathophysiology of common obstetric problems, particularly hypertension, placental insufficiency and the consequent fetal compromise. The umbilical placental circulation has been most studied and is most developed in terms of clinical utility. A well-defined placental vascular pathology is recognized. The effects on the fetus in terms of growth failure and developing hypoxaemia are established. Recognition of abnormality in the umbilical Doppler study dictates intensive fetal surveillance. It is important to keep in mind that umbilical Doppler identifies a placental lesion and so potential fetal comprise. Fetal studies are needed to confirm this. There is also evidence that the placental lesion may be arrested by low-dose aspirin therapy and this opens new approaches to management. Attention is also focusing on Doppler studies of the fetal circulation in the hope that these will define the extent of fetal compromise. The well-known 'brain sparing' when fetal growth fails has focused attention on the cerebral circulation. All major arteries of the brain can be studied. It does appear that cerebral vasodilatation can be defined in the presence of fetal hypoxaemia, although some caution in interpretation is necessary. Arterial flow in the fetal kidneys and to the limbs has also been studied. Attention is also directed now to the venous side of the fetal circulation. Flow patterns in the fetal inferior vena cava reflect venous filling pressure which changes in fetal compromise. Phasic variations in the umbilical vein flow profile are also seen. Interestingly, these patterns may be used to provide information about fetal breathing and lung maturation. The relationship between fetal umbilical and maternal uterine placental flow remains of major interest and importance. The uterine circulation is being increasingly studied from the view point of prediction of risk of pregnancy hypertension—an issue made important by the opportunity to reduce this risk through aspirin therapy. Controversy in this area is high and will be addressed. It can be confidently predicted that the 1990s will see a quite remarkable change in the way pregnancy well-being is assessed and Doppler ultrasound will lead the way.

Posters

Doppler assessment of fetal wellbeing following external cephalic version, by A. D. Cameron and J. B. Robins
Antenatal ultrasound diagnosis of aneurysm of the vein of Galen confirmed by pulsed Doppler, by L. Worswick and R..F. Lamont
A case of mistaken identity! by Y. Kassam and M. Rymer
Clinical and pathological factors in spontaneous abortion following chorionic villus sampling, by M. J. McCormack, W. E. Mackenzie, D. I. Rushton and J. R. Newton
Sonographic comparison of holoprosencephaly and agenesis of corpus callosum in the fetus, by W. Issa, M. Wright and S. L. B. Duncan
Phocomelia—two interesting cases both diagnosed by ultrasonography during the second trimester, by O. Clarke, W. L. Wong and L. McDonald
Hands, knees and bumps-a-daisy, by L. O'Connor and F. Bottomley
Reproducibility of ultrasonic measurements of fetal growth, by T. C. Chang, S. C. Robson, S. Gallivan and J. A. D. Spencer
Comparison of different ultrasound parameters in the prediction of small for gestational age (SGA) infants, by T. C. Chang, S. C. Robson, J. A. D. S. Spencer and R. Boys
Last menstrual period or ultrasound as a baseline for fetal growth assessment? 'New look' growth curves avoid the dilemma, by N. J. Dudley
Ultrasonographic growth measurements in triplet pregnancies, S. Fountain, M. Elder, S. Bishop and R. Winston
Longitudinal assessment of amniotic fluid index, by C. Nwosu and S. Walkinshaw
The accuracy of the ultrasonic diagnosis of hypertrophic pyloric stenosis by paediatric radiographers: an analysis, by B. E. Kelly, J. McKinstrey and P. S. Thomas
Ultrasound of the infant hip. A review of two year's experience at Queen Mary's Hospital for Children, by N. Joshi, V. Cook and S. Pablot
Periportal cuffing–a sign of infectious mononucleosis on ultrasound of the liver, by P. Guest and A. E. A. Joseph
The thread and streak sign of portal vein tumour thrombus demonstrated by colour Doppler imaging, by K. M. McBride and J. Masterson
Epithelioid haemangio-endothelioma of liver. A rare tumour, easily mistaken for metastatic carcinoma on sonography, by B. Banerjee, A. Rennison and M. Cooper-Wilson
Sonographic demonstration of a leaking hydatid cyst of the liver, causing atypical appearance of a cyst with an internal membrane, by B. Banerjee, A. Rennison and Q. M. Haque
Endoscopic ultrasound of the common bile duct, by S. Campbell and B. J. Rathbone
Ultrasonography of the eye in domestic animals, by C. Paterson, J. S. Boyd and J. R. B. Mould
Anal endosonography: technique and normal anatomy, by M. B. Nielsen, J. F. Pedersen, C. Hauge, O. Rasmussen and J. Christiansen
A non-invasive alternative to angiography in the assessment of the superficial femoral and popliteal artery for angioplasty, by A. H. Davies, T. Magee, D. Jones, S. E. A. Cole, J. K. Hayward, R. Parry, P. Murphy, R. N. Baird and M. Horrocks
Incidence of multiple aneurysms in patients presenting with popliteal aneurysm: is screening worthwhile? by D. R. Jones, R. Parry, A. H. Davies, T. R. Magee, R. N. Baird and M. Horrocks
It must be good: our tests say so! by S. G. Metcalfe and J. A. Evans
Routine ultrasound quality assurance for the sonography, by J. P. Brookes and J. M. Pelmore

Doppler assessment of fetal wellbeing following external cephalic version

A. D. Cameron and J. B. Robins
Perinatal Research Unit, Glasgow Royal Maternity Hospital, Rottenrow, Glasgow

External cephalic version (ECV) is a well-recognized obstetric procedure that is currently enjoying a revival. This is in part due to the use of ultrasound techniques in the assessment of fetal wellbeing. A study has been initiated in this department to investigate the place of pulsed Doppler ultrasound assessment of the feto-placental circulation before and after a version attempt. 20 patients in our initial study group have undergone attempted ECV at term using a standard technique with ritodrine tocolysis and a single operator. Fetal umbilical Doppler assessment was performed pre- and post-procedure with analysis of S/D ratio and resistance index (RI). The results are given in the table. These results demonstrate a slightly significant decrease in the resistance index of the umbilical artery following an attempt at ECV. This may indicate a beta sympathomimetic effect from the administration of rotodrine. To date, no adverse effect of ECV on the utero-placental circulation has been demonstrated, but a larger study is being undertaken in order to confirm these preliminary results.

Pre-version	Umbilical RI 0.58 ± 0.07	Umbilical S/D 2.58 ± 0.56
Post-version	Umbilical RI 0.54 ± 0.08*	Umbilical S/D 2.29 ± 0.47

Antenatal ultrasound diagnosis of aneurysm of the vein of Galen confirmed by pulsed Doppler

L. Worswick and R. F. Lamont
Department of Obstetric Ultrasound, Northwick Park Hospital, Watford Road, Harrow, Middlesex HA1 3UJ

We describe the case of a 32-year-old woman who presented at 39 weeks gestation in her second pregnancy in pre-term labour. Following admission, an ultrasound scan revealed a cystic structure in the midline of the fetal brain, superior to the hypothalamus. A more detailed scan excluded holoprosencephaly or spina bifida. Fetal anatomy was otherwise normal apart from mild unilateral renal pelvic dilation. The position and appearance of the cystic lesion had all the characteristics of an aneurysm of the vein of Galen. Pulsed-wave Doppler examination performed at 32 weeks gestation showed forward arterial flow to be present within the cystic lesion. Further scans demonstrated the development of cardiomegaly, subsequent ascites and other signs of hydrops. The future prognosis of the infant was discussed with the parents and with the paediatric neurosurgeons. The patient went into spontaneous labour at term and was delivered of a live female infant. The antenatal diagnosis was confirmed and the infant died after 60 h of life as a result of heart failure. We present the ultrasound images of the aneurysm of Galen including Doppler. We believe this to be the earliest antenatal diagnosis of aneurysm of the vein of Galen, the first diagnosed antenatally in the UK. It is also the first time that pulsed Doppler has been used to confirm the diagnosis antenatally.

A case of mistaken identity!

Y. Kassam and M. Rymer
Ultrasound Department, West Dorset Hospital, Damers Road, Dorchester, Dorset DT1 2JY

A case of abdominal pregnancy resulting in delivery of a live fetus at 31 weeks. The patient presented initially with irregular bleeding and pain and was clinically considered to have a fibroid uterus. Initial ultrasound demonstrated a viable, apparently intrauterine pregnancy of 18 weeks gestation. Routine ultrasound at 20 weeks demonstrated normal fetal anatomy and the pregnancy progressed unremarkably to 29 weeks when the patient presented with vaginal bleeding and was clinically thought to be small for gestational age. Ultrasound reported a symmetrically small fetus with oligohydramnios and echogenic liquor. The placenta was thought to be of abnormal structure, possibly molar or placental tumour. Referral to a tertiary centre was arranged at 30 weeks for further ultrasound, Doppler studies and possible cordocentesis. The examination confirmed a symmetrically small fetus with oligohydramnios, a bizarre placenta and Doppler studies indicated fetal compromise. The patient declined cordocentesis. Immediate delivery was advised. Delivery was planned by caesarian section. On opening the abdomen, a large cystic mass was found adherent to the uterine fundus. Contained within was a small fetus with marked pressure deformities and moulding, a small volume of blood-stained amniotic fluid and a hard spherical placental mass. The appearances at laparotomy were those of a left tubal pregnancy that had progressed to 31 weeks. A live baby weighing 952 grams was delivered. Subsequent neonatal progress has been good although the baby is awaiting surgery for a congenital hip dislocation. At operation the placenta was removed due to the earlier diagnosis of possible placental tumour. Partial haemostasis was achieved. The patient had a transfusion and conservative treatment postoperatively. The mother is at present symptom free with a slowly resolving organized haematoma.

Clinical and pathological factors in spontaneous abortion following chronic villus sampling

M. J. McCormack, W. E. Mackenzie, D. I. Rushton and J. R. Newton
Department of Obstetrics and Gynaecology, Birmingham Maternity Hospital, Edgbaston, Birmingham B15 2TG

29 cases of spontaneous abortion following first trimester chorionic villus sampling (CVS) were reviewed out of a series of 722 patients. Of the 29 cases there were only four abnormal CVS results. Pathological examination was performed in 79% of cases, and this did not identify any characteristic pathological feature associated with spontaneous abortion after CVS. There was no obvious difference in the pathological feature following the TA or the TC methods. The majority of miscarriages occurred within 4 weeks of the procedure, but 38% of cases aborted between 7 and 14 weeks after CVS. The transcervical (TC) method was used in 22 patients, the transabdominal (TA) is six, and both methods in one patient. The TA method was associated with a significantly lower fetal loss rate than the TC method (TA 2%, TC 9%, $p < 0.001$).

Sonographic comparison of holoprosencephaly and agenesis of corpus callosum in the fetus

W. Issa, M. Wright and S. L. B. Duncan
Department of Obstetrics and Gynaecology, Jessop Hospital for Women, Leavygreave Road, Sheffield S3 7RE

The cerebral ventricles in the fetal brain can be demonstrated by ultrasound in the second and third trimesters of pregnancy. Characteristic features can now be recognized which enable identification of some conditions formerly diagnosed only after delivery. We describe the distinguishing features of holoprosencephaly and agenesis of the corpus callosum. Holoprosencephaly is a condition of failure of development and cleavage of the prosencephalon. This results in a reduction or absence of midline structures with fusion of the thalami and usually absence of the third ventricle and corpus callosum. There can be variable degrees of separation failure with corresponding variation in prognosis. More severe cases are always fatal. Agenesis of the corpus callosum is due to developmental failure of the callosal commissure fibres connecting the cerebral hemispheres. The third ventricle is usually enlarged and displaced upwards. There is separation of the lateral ventricle bodies and dilatation and rounding of the horns of the lateral ventricle. There are usually other associated abnormalities. The features of these conditions follow from the anatomical defect. Though each condition can be of variable degree there are characteristic ultrasound features. Features of one each of these conditions will be described. Case 1—Abnormalities were noted on a "dating scan" at 19 weeks. Characteristic ultrasound features of holoprosencephaly led to termination of the pregnancy. Chromosomes showed trisomy 13. Case 2—The intracranial structures were noted to be abnormal at 24 weeks, with a dilated third ventricle and colpocephaly. Hydrocephaly increased and delivery was induced at 32 weeks. Post-natal scan confirmed the features of agenesis of the corpus callosum. The infant died after a few hours. *Conclusion:* The prognosis of these, and other, intracranial abnormalities varies. Accurate pre-natal diagnosis is improved by awareness of the different characteristic features and may enable refinement of pre-natal management.

Phocomelia—two interesting cases both diagnosed by ultrasonography during the second trimester

O. Clarke, W. L. Wong and L. McDonald
Department of Clinical Ultrasound, St. Thomas' Hospital, London SE1 7EH

Phocomelia is derived from two Greek words: *phoke*, meaning seal, and *melos*, meaning limb. It describes a developmental abnormality characterized by absence of the proximal portions of a limb or limbs, the hand or feet being attached to the trunk of the body by a single small, irregularly shaped bone. This fortunately rare, defect is usually associated with Robert's syndrome, some varieties of thrombocytopenia with absent radius (TAR) syndrome and Grebe syndrome. In addition it may also be caused by thalidomide but this is only of historic interest. Isolated phocomelia with no obvious exposure of the mother to a teratogen is most unusual. We present two cases of isolated phocomelia both made by pre-natal ultrasonography—one at 19 weeks of gestation the other at 21 weeks. In one case, the black mother had been given pills to assist the pregnancy in Jamaica during the first trimester. Tetraphocomelia was diagnosed at ultrasonography. In the other case no predisposing factors were identified. Ultrasonographic diagnosis of isolated phocomelia was made. In both cases therapeutic abortions were performed. Post-mortem examination confirmed the ultrasonographic findings. Chromosomal analysis was normal in both cases. The ultrasound scans, post-mortem photographs and radiographs of fetuses as well as a brief review of the literature of this seldomly found condition will be presented.

Hands, knees and bumps-a-daisy

L. O'Connor and F. Bottomley
The Hillingdon Hospital, Pield Heath Road, Uxbridge, Middlesex UE8 3NN

Recent review of fetal abnormalities in our department has revealed the contribution that detailed examination of fetal limbs and extremities can make to the detection of fetal abnormality in ultrasound screening programmes. This poster details with examples the features that we suggest are important in the assessment of fetal limbs. Criteria considered are: (1) mobility of limbs; (2) position of limbs; (3) presence and length of long bones and extremities; (4) shape of long bones and extremities; (5) flexibility of joints; (6) architecture of joints; (7) relationship of joints; and (8) associated anatomical abnormalities.

Reproducibility of ultrasonic measurements of fetal growth

T. C. Chang, S. C. Robson,*S. Gallivan and J. A. D. Spencer
*Department of Obstetrics and Gynaecology, University College Hospital, Chenies Mew, London WCE 6HX, and *Department of Statistical Sciences, University College London*

Meaningful interpretation of fetal growth necessitates knowledge of the variability of ultrasonic measurements. The aim of the present study was to reassess the reproducibility of ultrasonic morphometric measurements and estimated fetal weight (EFW) in trimester fetuses. Three measurements of biparietal diameter (BPD), head circumference (HC), abdominal circumference (AC), and femur length (FL) were performed by two observers in 40 fetuses (mean gestation 34.5 (SD 3.3) weeks). Observers were blinded to their own measurements and those of the other observers. EFW was also calculated for each set of measurements using the formula of Warsof et al (BPD, AC) and Hadlock et al (BPD, HC, AC, FL). Variability was assessed using analysis of variance. The mean absolute and percentage differences together with 95% prediction intervals (PI) for inter-observer comparisons were also calculated. *Results:* For all measurements, with the exception of FL, the inter-observer variance was greater than the residual (intra-observer): variance F ratios; BPD 15.5 ($p < 0.001$), HC 6.7 ($p < 0.01$), AC 6.85 ($p < 0.01$), FL 0.56, EFW (Warsof) 19.1 ($p < 0.001$), EFW (Hadlock) 15.4 ($p < 0.001$). Other results are shown below:

Measurement	% difference		Absolute difference	
	Mean	95% PI	Mean	95% PI
BPD (cm)	−0.67	−4.74, 3.38	−0.6	4.1, 2.9
HC (cm)	−0.50	−4.33, 3.32	−1.6	−13.2, 10.1
AC (cm)	−0.54	−5.43, 4.34	−1.9	−16.8, 13.0
FL (cm)	−0.14	−4.61, 4.32	−0.1	−2.9, 2.8
EFW (cm)	−0.98	−7.78, 5.82	−23.7	−187.3, 139.8
	−0.69	−6.29, 4.91	−17.8	−159.9, 124.3

Conclusion: With the exception of FL measurements, intra-observer variability is small compared with inter-observer variability. These estimates of variability can contribute to ultrasonic assessment of fetal growth.

Comparison of different ultrasound parameters in the prediction of small for gestational age (SGA) infants

T. C. Chang, S. C. Robson, J. A. D. S. Spencer and R. Boys*
*Department of Obstetrics and Gynaecology, University College Hospital, Chenies Mews, London WC1E 6HX, and *Department of Statistics, Newcastle University*

Many different ultrasonic parameters have been used to predict birthweight below the 10th percentile (SGA). Results have invariably been presented as sensitivity and positive predictive value; the latter being highly prevalence dependent. No previous reports have attempted to present summary statistics for each ultrasound variable for comparison. We have reviewed the literature from the past 15 years (72 studies) regarding the ultrasonic prediction of SGA. Studies were included if: (a) the reported population was high risk; (b) the outcome measure was a birthweight < 10th centile (using appropriate population charts); and (c) the necessary information to construct a 2×2 table was reported. Only ultrasound variables reported in at least two different studies were included. For each variable a pooled sensitivity and common odds ratio with 95% confidence intervals is reported. The results are given in the table. *Conclusion:* In a high-risk population, AC has the highest sensitivity and EFW the highest common odds ratio for the prediction of SGA. Comparable data for low-risk populations and for the prediction of neonatal ponderal index will also be presented.

Ultrasound parameter	Sensitivity	Common odds ratio	95% confidence interval
BPD < 10th centile	63.7	5.83	(3.62–9.37)
HC/AC > 95th	47.6	3.34	(1.55–7.99)
FL/AC > 23	49.1	2.82	(1.71–4.66)
EFW < 10th	77.9	39.0	(28.9 –52.7)
AC > 10th	84.4	18.38	(9.83–34.33)
Grade II placenta	61.7	3.0	(1.7 – 5.25)

BPD = biparietal diameter; HC = head circumference; AC = abdominal circumference; FL = femur length; EFW = estimated fetal weight.

Last menstrual period or ultrasound as a baseline for fetal growth assessment? 'New look' growth curves avoid the dilemma

N. J. Dudley
Department of Medical Physics and Computing, County Hospital, Sewell Road, Lincoln LN2 5QY

Practice for the plotting of ultrasound fetal growth varies between centres. There is evidence to suggest that ultrasound dating of pregnancy is more accurate than a reliable menstrual history and yet the last menstrual period (LMP) is still used as a baseline for ultrasound growth. A common practice is to use the LMP if ultrasound agrees to within ten days, or the ultrasound measurements if there is disagreement. There are pitfalls with this approach since there is a spread of possible conception dates with either dating method, *e.g.* the fifth percentile fetus placed on the 50th centile at dating and thus falling well within the normal range in the third trimester. This paper proposes a different approach which allows reliable plotting of fetal growth measurements without compromising the clinician's freedom to allocate an estimated date of delivery. The proposed chart superimposes all centiles of fetal size at the time of the dating ultrasound at 16–20 weeks. This results in a single line which diverges from about 20 weeks into the 10th, 50th and 90th centiles. The normal range is narrower than those currently used as the baseline is more precisely defined. The x-axis of the chart is divided into weeks but is initially unlabelled. The dating measurements are plotted on the single line at the corresponding figure on the y-axis. The x-axis is then labelled with the number of weeks corresponding to ultrasound or LMP as clinically appropriate. For subsequent measurements the number of weeks elapsed since the dating scan must be added to this figure. The major advantage of this method is that the baseline ultrasound measurement is *always* placed on the correct centile. Examples of how the 'new look' curves overcome the pitfalls of current methods will be shown.

Ultrasonographic growth measurements in triplet pregnancies

*S. Fountain, †M. Elder, *S. Bishop and †R. Winston
**Rosie Maternity Hospital, Robinson Way, Cambridge CB2 2SW, and †Institute of Obstetrics and Gynaecology, Hammersmith Hospital, Du Cane Road, London W12 0HS*

Ultrasonographic measurements of biparietal diameter (BPD), head circumference (HC), abdominal circumference (AC), femur length (FL) and liquor volume were obtained from 27 triplet and three quadruplet pregnancies managed at the Institute of Obstetrics and Gynaecology, Hammersmith Hospital and the Rosie Maternity Hospital. These were compared with the standard singleton growth charts used in the two units. Results show that the BPD measurements do not deviate from those of singletons before 33 weeks gestation. The HC measurements show a fall through the normal centiles but this is probably not significant. The AC measurements fall progressively from the 50th centile from 25 weeks gestation. The FL measurements follow those of the normal singleton fetus but unfortunately there are no measurements beyond 29 weeks in this series. We believe that the growth rate of triplet fetuses is different to those of singleton fetuses and that the most important parameter as an indicator of fetal wellbeing is the abdominal circumference. We believe that this is the largest published series of ultrasound measurements to date.

Longitudinal assessment of amniotic fluid index

C. Nwosu and S. Walkinshaw
Department of Obstetrics, Mill Road Maternity Hospital

The assessment of amniotic fluid volume is a key measurement in many areas of fetal surveillance. However, there remains discussion on the optimal measure of fluid volume. Maximum vertical pool depth (1, 2, or 3 cm limits) and subjective evaluation are most commonly used. Recently the use of four quadrant summation of pool depth (the amniotic fluid index) has been proposed as giving a better overall impression of total fluid volume. Cross-sectional data are available but we have derived a normal range from the longitudinal study of 100 women from 20 to 42 weeks. 50 women underwent four weekly ultrasound examinations at 20, 24, 28, 32, 36 and 40 weeks, and 50 women examination at 22, 26, 30, 34, 38 and 42 weeks. Maximal vertical pool depths, free of umbilical cord or fetal limbs, were recorded from each quadrant of the uterus, keeping the transducer parallel to the patient's sagittal plane. The examination is carried out in the supine position, the uterus being divided at each examination into four equal sections. The amniotic fluid index is the summation of the four values. The results are shown below. The data shows rising AFI to 26 weeks gestation, after which levels are constant until 34 weeks, after which the AFI declines. These data will be compared with cross-sectional data and the lower limits defining oligohydramnios discussed (SEE TABLE).

Gestational age (weeks)	20	22	24	26	28	30	32	34	36	38
Amniotic fluid index (AFI) (median)	14.2	18.7	18.6	19.7	20.0	20.1	21.0	21.0	19.9	17.8
Maximum vertical pool	4.8	5.6	5.5	6.1	6.3	6.0	6.3	6.5	6.3	6.7

The accuracy of the ultrasonic diagnosis of hypertrophic pyloric stenosis by paediatric radiographers: an analysis

B. E. Kelly, J. McKinstrey and P. S. Thomas
Department of Radiology, The Royal Belfast Hospital for Sick Children, Grosvenor Road, Belfast 12

This study analyses the accuracy of pyloric measurement by radiographers over an 18 month period at the Royal Belfast Hospital for Sick Children. 50 patients (35 boys and 15 girls) in whom the diagnosis of hypertrophic pyloric stenosis (HPS) was suspected clinically were referred for ultrasound scanning. HPS was diagnosed if the length of the pyloric channel was greater than 15 mm, and the thickness of the circular pyloric muscle was greater than 3 mm. If both parameters were below these values, the pylorus was considered normal. Elevation of only one parameter was not considered sufficient to make a definite diagnosis. Of this group of 50 patients, 24 were diagnosed ultrasonically as having HPS. All were confirmed surgically and corrective procedure performed in all cases. 16 patients were correctly diagnosed ultrasonically as not having HPS. Six patients were incorrectly diagnosed ultrasonically as having

HPS. All proved normal. None of these underwent surgery. Of these six patients statistical analysis of their parameter measurements confirmed them to be within the normal distribution for HPS diagnosis. In the remaining four cases, all had normal transverse muscle thickness but elongated channel length. None proved to have HPS. We concluded that in 40 of our 50 patients the correct diagnosis was made. When the ultrasound refuted the diagnosis of HPS, complete correlation with clinical findings occurred. No cases of HPS were missed. However, six false positive presumptive diagnoses were obtained ultrasonically and this underlines the case for confirmatory investigations if there is any doubt clinically of the diagnosis of HPS in association with a positive ultrasound scan.

Ultrasound of the infant hip. A review of two years' experience at Queen Mary's Hospital for Children

N. Joshi, V. Cook and S. Pablot
Department of Radiology, Queen Mary's Hospital for Children, Carshalton, Surrey

Ultrasound is a simple, non-invasive, accurate method of assessing the infant hip and has been shown to be of value in CDH and the management of the irritable hip. We describe the techniques involved, diagnostic criteria and role of ultrasound in the detection of paediatric hip abnormalities. 340 infants from an at risk population underwent hip arthrosonography. The symmetry and configuration of the hip joints were classified according to Graf Type I, Type IIA and IIB, Type IIIA and IIIB, Type D and Type IV. All eccentric or unstable hips were assessed by an experienced paediatric orthopaedic surgeon. The results of clinical and ultrasound follow up of these patients will be discussed. 100 children with an irritable hip also underwent arthrosonography of both hips. The pathologies encountered included assumed transient synovitis, Perthe's disease, septic arthritis, clipped epiphysis, osteomyelitis and trauma. The ultrasound features and role of ultrasound in the management of these patients will be described.

Periportal cuffing—a sign of infectious mononucleosis on ultrasound of the liver

P. Guest and A. E. A. Joseph
Department of Diagnostic Radiology, St George's Hospital, Blackshaw Road, London SW17 0QT

It is rarely necessary to perform ultrasound scans on patients with infectious mononucleosis as the diagnosis is usually possible on clinical grounds with the aid of serological tests. On occasion the diagnosis is less clear and scans are requested to investigate deranged liver function, jaundice of splenomegaly, Recognized features on ultrasound of infectious mononucleosis include splenomegaly or thickening of the gallbladder wall. We have observed a striking additional finding on ultrasound in four patients with serologically proved infectious mononucleosis. In these patients we noted increased echoes around the main portal vein and its branches, which we describe as periportal cuffing, giving an impression of thickening of the portal vein walls. These patients were not submitted to liver biopsy, since the diagnosis was confirmed serologically. Nevertheless, the ultrasound appearance has a well-established pathological correlate. Periportal lymphocytic infiltration is the main histological finding in liver biopsy specimens in infectious mononucleosis, particularly at 10–30 days from the onset of infection. This pathological process would explain the changes seen on ultrasound. In one of our patients, follow up scans showed a reduction in the periportal cuffing, as the patient improved clincially, further confirming the validity of this observation. Similar periportal cuffing has also been observed in lymphoma and cholangitis. Nevertheless, identification of this sign on ultrasound, particularly in conjunction with splenomegaly or thickening of the gallbladder wall may suggest the correct diagnosis of infectious mononucleosis enabling simple serological confirmation.

The thread and streak sign of portal vein tumour thrombus demonstrated by colour Doppler imaging

K. M. McBride and J. Masterson
Department of Radiology, St Vincent's Hospital, Dublin, Ireland

The angiographic, computed tomographic (CT) and real-time ultrasound demonstration of portal vein invasion and tumour thrombus is well documented, particularly in association with hepatocellular carcinoma. In this presentation, we describe an unusual case of portal vein tumour thrombus first suspected by colour Doppler imaging (CDI). There have been no previously documented cases using this modality. A 73-year-old man presented recently with a four month history of back pain, anorexia, weight loss and dyspnoea. He had a previous history of left pneumonectomy for squamous cell carcinoma of bronchus 12 years previously, and a more recent history of drainage of left empyema 9 months earlier. On examination he had hepatomegaly, finger clubbing and ankle oedema. Chest radiography showed signs of previous surgery, but no suspicion of malignant recurrence. Real-time abdominal ultrasound revealed multiple large masses within the liver and an echogenic irregular mass within the portal vein. The portal venous flow was hepatopetal, but turbulent. CDI displayed turbulent flow elegantly within and around the mass. Biopsy of the liver masses proved to be poorly differentiated squamous cell carcinoma consistent with multiple metastases from a presumptive chest recurrence. Portal venous phase angiography and CT portography confirmed the thread and streak appearance seen at CDI. CDI can demonstrate portal vein involvement in patients with liver tumours and in this case better than by conventional invasive techniques. If the thread and streak sign is seen, it is more likely to be tumour than thrombosis.

Epithelioid haemangio-endothelioma of liver. A rare tumour, easily mistaken for metastatic carcinoma on sonography

B. Banerjee, A. Rennison and M. Cooper-Wilson
Tameside General Hospital, Ashton-under-Lyme, Lancashire OL6 9RW

Epithelioid haemangio-endothelioma is an unusual and rare neoplasm of soft tissue of vascular origin which can often affect the liver. Although there have been sporadic reports of this tumour in the past, the term "epithelioid haemangio-endothelioma" was first suggested by Weiss and Enziger in 1982. In liver, the tumour is multicentric in origin involving both lobes. Microscopically, the neoplastic cells are vasoformative and synthesize factor VIII-related antigen which can be identified by special tissue staining and used as an aid to diagnosis. The tumour pursues a relatively benign course and long-time survivals without treatment have been recorded. When metastasis is exluded, treatment by hepatectomy and hepatic transplant is considered to be curative. A case report of a 29-year-old female suffering from epithelioid haemangio-endothelioma of the liver is presented. The ultrasonic appearances are illustrated and difficulty in distinguishing this tumour from hepatic metastasis is emphasized. The aim of this presentation is to increase awareness of this relatively benign tumour. Every attempt should be made to distinguish this tumour from metastasis so that correct advice relating to prognosis and treatment can be rendered. It also highlights the importance of searching for a primary source when metastatic liver disease is suspected.

Sonographic demonstration of a leaking hydatid cyst of the liver, causing atypical appearance of a cyst with an internal membrane

B. Banerjee, A. Rennison and *Q. M. Haque
*Department of Radiology, Tameside General Hospital, Ashton-under-Lyme, Lancashire OL6 9RW, and *Ormskirk and District General Hospital, Wigan Road, Ormskirk, Lancashire L39 2AZ*

Sonographic apppearances of hydatid disease of the liver are varied. A single large cyst containing multiple small daughter cysts is a classical presentation. However, a solitary cystic structure, indistinguishable from a simple liver cyst may be encountered. One of the less common forms of presentation is a cyst with a membrane-like structure beneath its wall. Rupture of the cyst is a well-documented complication of hydatid disease of the liver. The cyst may rupture into the peritoneal cavity, alimentary canal, biliary channels or pleural cavity. However, leakage of cyst fluid may take place between the cyst membrane and the compressed liver tissue and this is presumed to be the cause of "a cyst with a membrane-like structure beneath its wall"—as described in the literature. To illustrate this, a case is presented where, during sonography for suspected gallbladder disease in a 42-year-old woman, a cyst was detected in the right lobe of the liver. It was diagnosed as a simple liver cyst and was considered clinically insignificant. Several days later the patient was admitted to the hospital with acute right upper quadrant abdominal pain with a provisional diagnosis of cholecystitis. A second sonography on admission revealed that the solitary cyst had partially collapsed with collection of fluid between the cyst membrane and the compressed liver tissue. Diagnosis of hydatid disease of the liver was entertained and confirmed by specific complement fixation test. This case demonstrates the mechanism behind this atypical appearance of hydatid cyst and also highlights that solitary cysts of the liver do not necessarily represent simple liver cysts.

Endoscopic ultrasound of the common bile duct

S. Campbell and B. J. Rathbone
Departments of Radiology and Gastroenterology, Leicester Royal Infirmary, Infirmary Close, Leicester LE1 5WW

The recent development of laparoscopic cholecystectomy has presented radiologists with the problem of visualizing the entire common bile duct. Transabdominal ultrasound cannot visualize all common bile duct stones. Increasingly, surgeons are requesting intravenous cholangiography, but this procedure has a mortality rate of 1 in 5000 and may be diagnostically inaccurate in up to 40% of cases. ERCP to examine the common bile duct requires the use of an X-ray screening room and radiographers time, in addition to radiation exposure to the patient and the small risk of pancreatitis. In a preliminary study to investigate the use of endoscopic ultrasound in assessing the common bile duct, we show good correlation of this technique with ERCP and transabdominal ultrasound. Examples of normal anatomy and abnormal studies are shown. We conclude that endoscopic ultrasound is a useful technique and, by using this more in the future, we may be able to avoid the more hazardous and time-consuming methods of investigation mentioned previously.

Ultrasonography of the eye in domestic animals

C. Paterson, *J. S. Boyd and †J. R. B. Mould
*Departments of *Veterinary Anatomy and †Surgery, University of Glasgow Veterinary School, Bearsden Road, Glasgow*

Real-time B-mode diagnostic ultrasound is becoming a more extensively used tool in the clinical examination of the eye in domestic animals. This imaging modality permits interrogation of the chambers of the eyeball and of the retrobulbar space in a non-invasive fashion. This is of particular use where opacity of the cornea or lens or intrabulbar haemorrhage has occurred, preventing direct opthalmoscopic examination. The animals are conscious with only the occasional subject requiring sedation and the transducer is applied directly to the corneal surface. The scanners used in this series are the Interspec XL and Interspec Apogee, equipped with a 7.5 MHz transducer with a built-in stand off. Images are recorded on VHS tape and on a thermal copier. The purpose of the work is to demonstrate the technique of ultrasonography of the eye in various species and to illustrate the findings in a number of pathological conditions. These include cataract, lens dislocation, detached retina intrabulbar tumours and haemorrhage and retrobulbar space occupying lesions. The scan images are matched to photographs of the eyes as they are presented clinically and at post mortem, where there was sacrifice of the eye. By displaying the clinical signs and the gross and the sectional pathology alongside each other, it is easier to interpret the ultrasound scan images of the various conditions.

Anal endosonography: technique and normal anatomy

M. B. Nielsen, J. F. Pedersen, C. Hauge, O. Rasmussen and J. Christiansen
Department of Radiology and Ultrasound, and Department of Surgery D, University of Copenhagen, Glostrup Hospital, DK-2600 Glastrup, Denmark

This study describes the endosonography appearance of the anal canal and the ano–rectal junction using multiplanar imaging. Anal endosonography was performed in 14 normal female volunteers, in five of them during EMG registration, and in three patients following lateral internal sphincterotomy. The technique and normal anatomy is described using transverse and longitudinal imaging. In transverse images the internal anal sphincter is a 2–3 mm circular echo-poor band which in longitudinal images can be traced to the muscularis propria layer of the rectal wall. The endosonographic appearance of the external sphincter, which is a broad echogenic band, depends on the level in the anal canal. Proximally the relation to the puborectalis muscle and the levator ani muscle can be visualized. Furthermore the thickness of the internal sphincter, and the thickness, length and cross-sectional area of the external sphincter was measured in 30 volunteers: 10 men, 10 women with no childbirths and 10 women with 1–3 childbirths. There were no significant difference between the size of the anal sphincters in these groups.

A non-invasive alternative to angiography in the assessment of the superficial femoral and popliteal artery for angioplasty

A. H. Davies, T. Magee, D. Jones, S. E. A. Cole, J. K. Hawyard, R. Parry, P. Murphy, R. N. Baird and M. Horrocks
Departments of Vascular Studies & Radiology, Bristol Royal Infirmary, Bristol

Patients who have symptoms of claudication which may be amenable to angioplasty need currently to undergo arteriography. The suitability of a lesion for dilatation depends on its morphology and the distal run-off. Non-invasive assessment of the lower limb vasculature may avoid unnecessary arteriography. Colour Duplex scanning of femoral and popliteal arteries was performed to establish whether the vessels were normal, stenosed or occluded. The pulse generated run-off (PGR) system was used to assess the distal vasculature; in particular the number of distal calf vessels in continuity with the popliteal artery. In 50 lower limbs Duplex gave the following results compared to angiography. PGR and arteriography evaluation of run-off agreed in 41 limbs, however in nine (18%), PGR demonstrated better run-off than arteriography, not an unusual finding in the presence of ischaemia. All 18 limbs suitable for angioplasty were correctly identified and satisfactorily dilated. A combination of Duplex scanning and PGR offers a non-invasive alternative in assessing patients and may thereby restrict anteriography to those patients with a lesion suitable for angioplasty.

	Sensitivity (%)	Specificity (%)	Accuracy (%)
Occlusion (n = 20)	95	100	98
Stenosis (n = 13)	93	97	96
Atheromatous vessel (n = 14)	100	100	100
Disease free (n = 3)	100	100	100

Incidence of multiple aneurysms in patients presenting with popliteal aneurysm: is screening worthwhile?

D. R. Jones, R. Parry, A. H. Davies, T. R. Magee, R. N. Baird and M. Horrocks
Vascular Studies Unit, Bristol Royal Infirmary, Bristol

Although the association between popliteal aneurysm and aneurysm at other sites is known, audit of 21 patients who had previously undergone surgery for popliteal aneurysm in a 6 year period found that more than 50% of patients had not specifically been screened. Those who had not previously been investigated were recalled for bilateral femoro-popliteal Duplex scanning (11 patients) and aorto-iliac B-mode ultrasound (nine patients). Six patients (29%) were identified to have previously undiagnosed arterial dilatations. Common femoral artery dilatation greater than 1.5 cm was identified in nine limbs with aneurysm formation in three. One new abdominal aortic aneurysm of 5 cm diameter was found on screening. No new iliac aneurysms or previously undiagnosed contralateral popliteal aneurysms were seen. Inclusion of this data with that available from the computerized vascular database resulted in a true multiple aneurysm incidence of 57%. The mean age of those patients with a single popliteal aneurysm (69.6 years) was not significantly different from those with multiple aneurysms (65.8 years). 10 patients (48%) had bilateral popliteal aneurysms, five (24%) had femoral aneurysms, bilateral in three cases. Three patients (14%) had aortic aneurysms. The high incidence of contralateral popliteal aneurysm and aneurysms at other sites in patients presenting with popliteal aneurysm is sufficient to warrant ultrasound screening of aorto-iliac and femoro-popliteal arteries as a matter of routine in these patients.

It must be good: our tests say so!

S. G. Metcalfe and J. A. Evans
Department of Medical Physics, The General Infirmary, Leeds LS1 3EX

Anecdotal evidence has suggested that the parameters normally measured for quality assurance purposes (*e.g.* resolution and dynamic range) may fall short of ensuring a good quality image as perceived by the user. A survey was conducted comparing the lateral resolution, slice thickness and dynamic range of scanners with user's perception of scanner performance. Images of the liver and uterus of a single volunteer were obtained by one of only two operators using nine machines with various transducers. This gave 14 combinations, which were then evaluated by 43 observers from eight hospitals. Observers were asked to comment on the image quality in terms of overall performance, definition, graininess, noise and grey levels on a subjective 5-point scale. The machine parameters were measured using standard quality assurance techniques with the Cardiff test system. An overall lateral resolution figure was devised. Generally, the correlations between the objective measures and subjective assessments were poor, for example, an r-value of 0.26 was obtained for the correlation between lateral resolution and assessed definition. However, there was good agreement about which was the poorest machine and in two out of four the best machines. One machine which achieved a high lateral resolution score was poorly rated for 'definition' and 'graininess'. Another which scored well for dynamic range was poorly rated in almost all the observer categories. It is concluded that, in clinical pratice, users prefer a smooth image, even if this excludes real spatial information. In addition, wider dynamic range may not necessarily be welcomed by users if it is associated with an increase in noise.

Routine ultrasound quality assurance for the sonographer

*J. P. Brookes and †J. M. Pelmore
**X-ray Department, Leicester General Hospital, and †Medical Physics Department, Leicester Royal Infirmary*

A method for routine quality assurance of imaging systems is described for use on a weekly or monthly basis. Four parameters are monitored: (1) depth of penetration; (2) uniformity; (3) calliper accuracy; and (4) hard copy performance. For monitoring the first three parameters the Gammex 821 Test Object, the Cardiff Resolution Test Object and the Cardiff Routine Test Object are all suitable. These test objects all contain the well established Cardiff tissue mimicking material and are compatible with BSI 5724 section 3.26 (June 1990). If a flat transducer is used ultrasound couplant gel should be used. For curved transducers ultrasound test solution which gives a velocity of 1540 m/s should be used for the baseline test. For subsequent tests tap water is normally satisfactory. (1) Depth of penetration: high and low contrast penetration should be measured under conditions of maximum transmitter power.

(2) Uniformity: the previous image should be examined for transverse and axial non-uniformity. (3) Calliper accuracy: the gain should be reduced so that the images of the wires are small to facilitate accurate positioning of the cursor. (4) Hard copy performance: initially, the hard copy system should be set up on a clinical image containing the full range of grey levels. For subsequent tests a clinical image or other tests can be used. Illustrations of normal and abnormal images are given. Record keeping is discussed.

1992, *The British Journal of Radiology*, 65, 649–652

VOLUME 65 NUMBER 776 AUGUST 1992

The British Journal of Radiology

Use of ultrasound in osteomyelitis

By Ashok Kumar Nath, MB, BS, DMRD, MD and *Arunchala U. Sethu, MS, FRCS(Edin & Glas), FRCS(Edin)Ortho

Department of Radiology and *Department of Orthopaedics and Trauma, Khoula Hospital, Mina Al Fahal, Muscat, Sultanate of Oman

(Received 3 July 1991 and in revised form 27 November 1991, accepted 14 January 1992)

Keywords: Bone infection, Osteomyelitis, Soft-tissue abscess, Ultrasound

Abstract. The use of ultrasound in osteomyelitis has been studied in 25 patients clinically suspected of osteomyelitis. A sonographic diagnosis of osteomyelitis was made if fluid was present in direct contact with the bone, without intervening soft tissues. This was thought to represent an inflammatory exudate dissecting in a subperiosteal and/or extraperiosteal location. Ultrasonographically 15 patients were found to have osteomyelitis, proved either by surgical drainage or needle aspiration. Seven patients had soft-tissue abscesses, one had cellulitis and two patients had no abnormality.

Osteomyelitis is usually a blood-borne infection, though rarely may be due to direct extension, caused by pyogenic organisms settling in cancellous bone. Serious and chronic complications may follow. Establishing an early diagnosis is important. The clinical diagnosis of osteomyelitis is difficult, especially in the early stages of the disease. A multimodality approach is often needed to establish the diagnosis (Abiri et al, 1989). A good clinical and pathological evaluation, plain radiographs and bone and gallium scintigraphy are commonly used for detection of osteomyelitis. Magnetic resonance imaging (MRI) has also proved a sensitive technique for the diagnosis of osteomyelitis. In general, osseous structures are not well imaged with sonography because of their intrinsic physical properties. To evaluate the use of ultrasound in osteomyelitis, we performed ultrasonography of 25 patients clinically suspected of having osteomyelitis.

Materials and methods

Sonography was performed in 25 patients presenting with pain and swelling of the affected limb. Patients were referred from the emergency room, orthopaedic clinic or as inpatients. They ranged in age from 2 to 45 years (Tables I, II).

All patients underwent a thorough clinical evaluation, chest radiographs, plain radiographs of the affected area and sonography of both the affected and opposite normal area for comparison. Toshiba Ultrasound Diagnostic equipment Model SSA-90A was used. Sonograms were obtained with 7.5 MHz phased linear array transducers. The sonographic criterion for the diagnosis of osteomyelitis was an abnormal collection of fluid adjacent to the bone without intervening soft tissues (Figs 1, 2). The criterion for soft-tissue abscess or pyomyositis was demonstration of an abscess in soft tissues or muscle planes, with no evidence of fluid in contact with the bone (Fig. 3). All patients with a fluid collection, either in soft tissues or adjacent to the bone, underwent needle aspiration or surgical drainage. The fluid obtained was sent for culture and sensitivity. Follow-up sonograms and plain radiographs were carried out until healing was complete.

Results

15 of the 25 patients were thought to have osteomyelitis. Eight of these had both abnormal plain radiographs and fluid adjacent to the bone on ultrasound (Figs 1, 2). In seven patients the initial plain radiograph was normal, and fluid was present adjacent to the bone on ultrasound (Table I). In all 15 patients fluid was removed from the affected area and sent for microbiological culture, 10 by a surgical procedure and five by needle aspiration (Table I). In all cases the fluid was found to be infected with coagulase positive *Staphylococus aureus* and appropriate antibiotic treatment was prescribed. When on conservative management the progress of the disease was assessed by repeated ultrasound scans and radiographs until healing was complete.

The typical plain radiographic findings of osteomyelitis were periosteal reaction or periosteal reaction plus bone erosion. The typical ultrasonographic finding of fluid adjacent to the bone was an anechoic area

---

Address correspondence and reprint requests to Dr Ashok Kumur Nath, Department of Radiology, Khoula Hospital, Post Box No. 51090, Mina Al Fahal, Muscat, Sultanate of Oman.

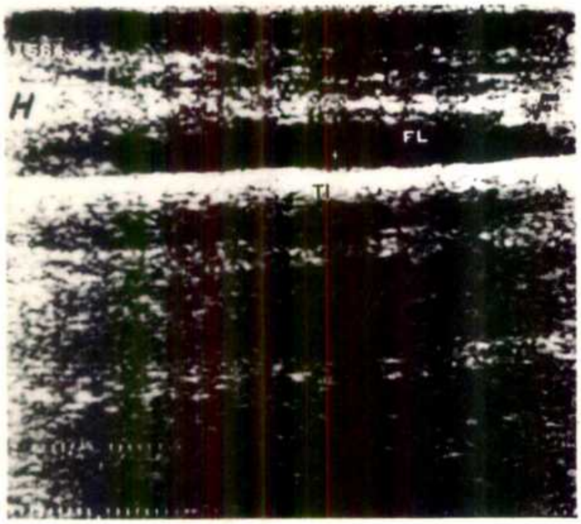

Figure 1. Longitudinal sonogram demonstrating osteomyelitis of the tibia (TI) with anechoic fluid (FL) in contact with the bone.

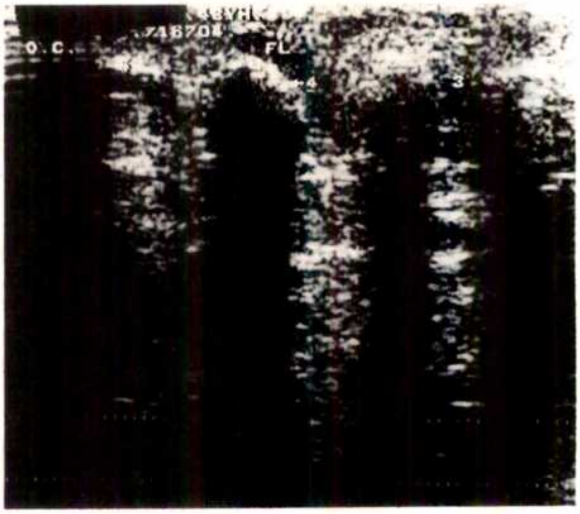

Figure 2. Transverse sonogram demonstrating osteomyelitis of the 4th metatarsal with anechoic fluid (FL) in contact with the bone.

immediately adjacent to the bone with no intervening soft tissues (Figs 1, 2). The fact that eight of the 25 patients had positive radiographic signs of osteomyelitis indicated that our patients were late in reporting their illness to the hospital. The shortest time lag between onset of symptoms and presentation to the hospital was 3 days and the longest was 3 weeks.

10 of our 25 patients did not have either plain radiographic or ultrasonographic evidence of osteomyelitis. Seven of these 10 patients had soft-tissue abscesses or pyomyositis (Table II). The sonographic findings of these patients ranged from well defined anechoic to partially echogenic fluid collections in soft tissues (Fig. 3) with no fluid adjacent to the bone. The diagnosis in these seven patients of soft-tissue abscesses was confirmed either by precutaneous aspiration or surgical drainage (Table II). Of the remaining three patients, who had neither osteomyelitis nor soft-tissue abscess, one patient had cellulitis, treated conservatively, and two patients had no abnormality (Table II). These patients were followed by ultrasound and plain radiography until symptom-free.

Discussion

As osteomyelitis, soft-tissue abscesses and cellulitis may have overlapping clinical signs and symptoms,

Table I. Summary of 15 patients with osteomyelitis

Age (years) and sex	Site	Radiographic findings		Initial US findings of fluid in contact with bone	Proved by	
		Initial	Follow-up		Aspiration	Surgery
9 F	Left femur	−	±	+		+
2 M	Right humerus	+	+	+		+
11 F	Left fibula	+	+	+		+
11 M	Left femur	+	+	+		+
9 F	Right femur	−	+	+	+	
12 M	Left humerus	+	+	+	+	
6 M	Left femur	−	±	+	+	
18 M	Right tibia	+	+	+	+	
16 M	Left tibia	+	+	+		+
43 M	Right metatarsal	+	+	+		+
14 F	Right humerus	−	±	+		+
45 F	Right femur	−	+	+		+
16 M	Left femur	−	+	+		+
11 M	Left tibia	−	±	+		+
6 F	Left tibia	+	+	+	+	

+, Positive findings; −, negative findings; ±, equivocal findings.

Table II. Summary of seven patients with soft-tissue abscess

Age (years) and sex	Site	Radiographic findings		Initial US findings of only soft-tissue fluid collection	Proved by	
		Initial	Follow-up		Aspiration	Surgery
17 M	Right thigh	–	–	+	+	
45 M	Left thigh	–	–	+		+
24 M	Right thigh	–	–	+	+	
20 F	Right leg	–	–	+		+
35 M	Right thigh	–	–	+		+
25 F	Right thigh	–	–	+		+
20 M	Left leg	–	–	+	+	

+, positive; –, negative.
Of the remaining three patients of our series, one had cellulitis and two had no abnormality.

clinical diagnosis of osteomyelitis is difficult. A multimodality approach consisting of good clinical evaluation, pathological investigations, plain radiographs, bone scintigraphy (Paterson et al, 1987) and MRI (Unger et al, 1988) has been used for diagnosis of both soft-tissue abscesses and skeletal infections.

Abiri et al (1989) have shown that sonography of normal soft tissue demonstrates the muscle layers to be hypoechoic, with linear echogenic striations separating the layers. Subcutaneous tissues may appear hypoechoic or echoic. The cortex of the bone is a dense echogenic line with a smooth surface, and throws a strong acoustic shadow. Vascular structures can be identified by their characteristic pulsations. Our sonographic findings of normal limbs corroborate well with the findings of Abiri et al (1989) (Fig. 4).

Osteomyelitis is usually a blood-borne infection, though rarely may be due to direct extension caused by pyogenic organisms. Dissemination of organisms to the bone initiates an acute inflammatory response, resulting in ischaemia, bone liquefaction and necrosis. Resultant pus elevates the periosteum to form subperiosteal abscesses. The periosteum may be eroded, producing extraperiosteal fluid and abscess collection (Blockey, 1980).

It has been our experience that anechoic fluid collections are seen adjacent to the bone or within soft tissues only in pathogenic conditions. The relationship of the sonographically demonstrable fluid to the bone is an important factor in differentiating between osteomyelitis and soft-tissue abscesses. Our results indicate that a fluid collection contiguous with bone is highly suggestive of osteomyelitis (Fig. 1). Our findings are similar to those of Abiri et al (1989) and Kaplan et al (1990) who also demonstrated that if fluid is in direct contact with bone, osteomyelitis can be accurately predicted.

A similar sonographic appearance is also seen in patients with septic arthritis, where fluid is also in direct contact with the bone (Wingstrand et al, 1987). In our study it was impossible to distinguish between septic arthritis and osteomyelitis by means of sonography alone. Hence, all patients with septic arthritis were excluded.

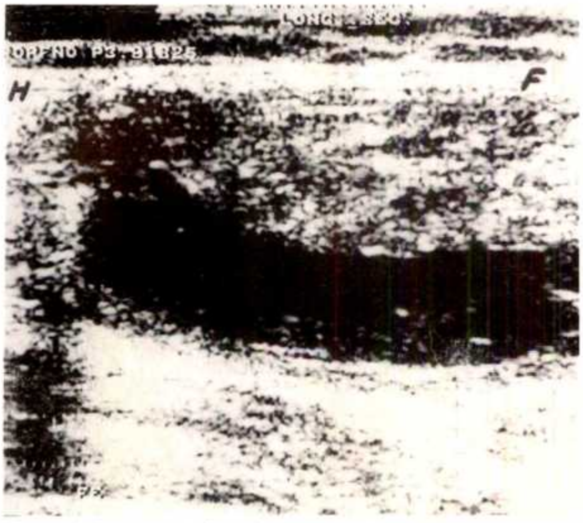

Figure 3. Sonogram of a soft-tissue abscess of the thigh demonstrating an anechoic area in the muscle with no fluid in contact with the bone (longitudinal section).

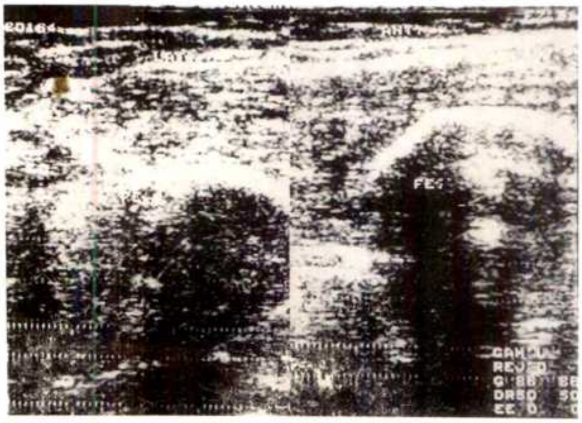

Figure 4. Sonogram of normal thigh demonstrating soft tissues and hypoechoic muscle layers with linear echogenic striations and bone as a dense echogenic line with strong acoustic shadowing (transverse section).

If intervening soft tissues could be demonstrated between the fluid and the bone, a non-osseous origin of the fluid was considered, as in seven patients of our series who proved to have soft-tissue abscesses (Fig. 3). This corroborates well with cases reported by Sarti (1980), Abiri et al (1989) and Kaplan et al (1990).

The higher incidence of positive plain radiographic findings (Table I) in our patients at initial examination is due to delay in presentation. However, in seven of our patients we demonstrated fluid adjacent to the bone before changes were seen on initial radiographs (Table I). In osteomyelitis of the ribs, Zive et al (1985) sonographically demonstrated pericostal fluid in contact with the bone before radiographic changes.

Although Hall et al (1990) showed the importance of diagnosing pyomyositis by computed tomography and bone scintiscan, in our series diagnosing soft-tissue abscess or pyomyositis by ultrasound and confirming by needle aspiration is a simple, rapid and cheap method.

In conclusion, ultrasound is useful in:

1. screening all patients who are clinically suspected of having osteomyelitis;
2. predicting osteomyelitis if fluid is demonstrated in contact with the bone;
3. differentiating osteomyelitis from soft-tissue abscesses;
4. localization of the lesions before aspiration or surgical management; and
5. detecting recurrence of osteomyelitis in patients with chronic osteomyelitis inadequately treated.

References

ABIRI, M. M., KIRPEKAR, M. & ABLOW, R. C., 1989. Osteomyelitis detection with US. *Radiology*, *172*, 509–511.

BLOCKEY, N. J., 1980. Management of bone and joint infections. In *Orthopaedics and Traumatology*, ed. by R. Owen, J. Goodfellow and P. Bullough (William Heinemann Medical Books, London), pp. 481–491.

HALL, R. L., CALLAGHAN, J. J., MOLONEY, E., MARTINEZ, S. & HARRETSON, J. M., 1990. Pyomyositis in a temperate climate. *Journal of Bone and Joint Surgery*, *72A*, 1240–1244.

KAPLAN, P. A., MATAMOROS, JR, A. & ANDERSON, J. C., 1990. Sonography of the musculoskeletal system. *American Journal of Roentgenology*, *155*, 237–245.

PATERSON, D. C., FOSTER, B. K. & SAVAGE, J. P., 1987. The present status of bone scanning in clinical orthopaedic diagnosis. *Recent Advances in Orthopaedics*, *5*, 19–41.

SARTI, D. A., 1980. Ultrasonography of the lower extremity. In *Diagnostic Ultrasound*, 1st edn, ed. by D. A. Sarti and W. F. Sample (G. K. Hall & Co., Boston), pp. 486–501.

UNGER, E., MOLDOFSKY, P. & GATENBY, R., 1988. Diagnosis of osteomyelitis by MR imaging. *American Journal of Roentgenology*, *150*, 605–610.

WINGSTRAND, H., EGUND, N., LIDGREN, L. & SAHLSTRAND, T., 1987. Sonography of septic arthritis of the hip in the child. *Journal of Paediatric Orthopaedics*, *7*, 206–209.

ZIV, J. B., BARKI, Y., MAROKO, A. & MARES, A. J., 1985. Rib osteomyelitis in children: early radiologic and ultrasound findings. *Paediatric Radiology*, *15*, 315–318.

1992, *The British Journal of Radiology*, *65*, 653–661

Direct and CT measurements of canals and foramina of the skull base

By *A. Berlis, R. Putz, MD and *M. Schumacher, MD

Anatomische Anstalt, Ludwig-Maximilians-Universität Müchen, Pettenkoferstrasse 11, D-8000 München and *Abteilung Röntgendiagnostik, Sektion Neuroradiologie, Albert-Ludwigs-Universität Freiburg i.Br., D-7800 Freiburg i.Br., Hauptstrasse 5, Germany

(*Received 9 July 1991 and in revised form 20 November 1991, accepted 14 January 1992*)

Keywords: Skull base, CT, Foramen, Canal, Fissure

Abstract. This investigation is based on measurements of 60 macerated adult European skulls from the Alexander-Ecker Collection at the Anatomy Department of the University of Freiburg. Computer tomographical (CT) and anatomical measurements were compared to assess the accuracy of the CT representation of osseous structures. Nine structures were examined: the optic canal; the superior orbital fissure; the foramen rotundum; the foramen ovale; the foramen spinosum; the foramen Vesalii (venosum); the carotid canal; the internal auditory canal, and the hypoglossal canal. The results show a good and even excellent correlation if the cranial opening is approximately at a right angle to the scanline. For this reason, the results of the coronal examination of the internal auditory canal are less satisfactory, and the coronal and axial measurements of the hypoglossal canal show only a moderately good correlation.

Knowledge of the normal and variant positions of the canals and foramina of the skull base is important for radiologists, neurosurgeons and anatomists, because of the increasingly refined techniques available. Although the effectiveness of computed tomography (CT) in diagnosing bony lesions is uncontested, most of the authors describe optimal positioning without mentioning the correlation between their findings and the actual anatomical position of the osseous structures referred to at the time of writing. CT measurements of the position of the internal auditory porus (Heller et al, 1983), the internal auditory canal (Silverstein et al, 1988) and the foramen Vesalii (venosum) (Lanzieri et al, 1988) are available. Only Silverstein et al (1988), however, have assessed the correlation between CT measurements and those taken from dissections of the temporal bone.

In the following study, anatomical and CT measurements, including length, breadth and height of optic canals, superior orbital fissure, foramen rotundum, foramen ovale, foramen spinosum, foramen Vesalii (venosum), carotid canal, internal auditory canal, and hypoglossal canal, and the distances between these structures, are evaluated. The extent to which anatomical variations can be assessed by CT has also been investigated.

Material and methods

A total of 60 macerated adult European skulls from the Alexander-Ecker Collection at the Anatomy Department of the University of Freiburg were studied.

For the direct anatomical measurements we used digital internal callipers (Mitutoyo 526–153/526–163: 1.50–7.30±0.01 mm), a digital measuring instrument (Mitutoyo 500–110: 0–150±0.02 mm), an anthropometric instrument (Berlis, 1990) of our own construction (0–260±1 mm) and a tintack with a millimetre rule (±1 mm).

The CT scans of the skull base were obtained using a Siemens Somatom DR-H. Continuous 1 mm sections were taken at angles of 10° (axial projection) and 70° (coronal projection) to the radiographic baseline (RB) (Reid's baseline or anthropological baseline). The CT number range was viewed at a window width of 4000 HE. The exposure factors were 550 mA and 125 kV with a scan speed of 9.6 s. The skulls were positioned in plastic on a table and the scanlines were defined by Topo-scan. Double measurements were recorded directly on the monitor using a joystick.

Results

Optic canal (Figs 1 & 8). Following Lang (1981), we divided this canal into three parts: an orbital part (an elongated oval on section), a middle part or "optic waist" (Lang & Oehmann, 1976) and an intracranial part. The mean angle of the axis of the canal and the sagittal plane (SP) was 39.1°, and the RB was −15.5°. This means that the coronal sections met the canal at an angle of 85.5°.

Several variants show asymmetry in the shape of the canal. The so-called keyhole anomaly (Fig. 1) is a result of the absence of the floor at the cranial opening (Potter & Trokel, 1971). This anomaly appears in 3.3% of our material. Another variant is the figure-of-eight optic canal, with a separate canal for the ophthalmic artery produced by a spicule of bone uniting the roots of the lesser wing of the sphenoid. This appeared as a duplicate cranial opening with lengths of 3.0, 2.5 or 1.6 mm and a thickness of 1.4, 1.7 or 1.5 mm. The lumen measured 2.11 × 1.55, 1.76 × 1.00 or 2.50 × 2.00 mm, and

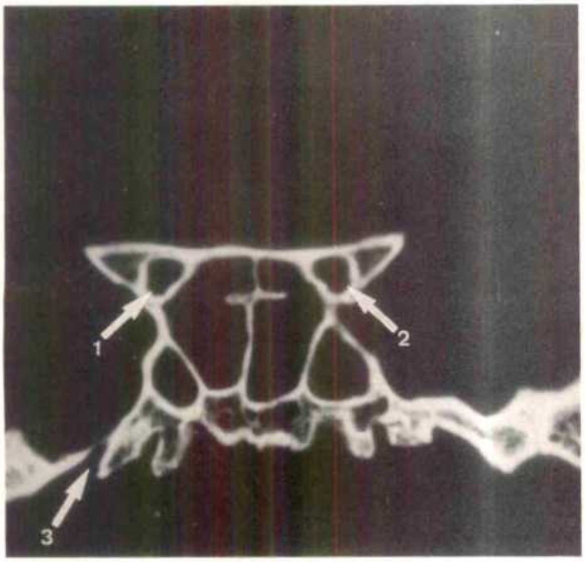

Figure 1. Coronal projection of the optic canal of the skull 42/351. A separate passage for the ophthalmic artery appears on both sides of the skull. 1 = Right optic canal—it appears to be a "keyhole" anomaly, but its "figure-of-eight" character can be seen at a deeper level; 2 = left optic canal of "keyhole" type and 3 = foramen ovale.

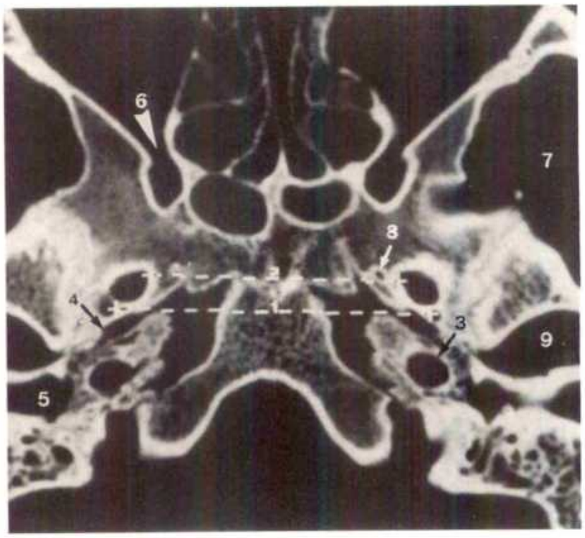

Figure 2. Axial projection of the skull base. 1 = Measuring line between foramina ovalia; 2 = measuring line between foramina spinosa; 3 = carotid canal; 4 = pharyngotympanic tube; 5 = external auditory meatus; 6 = inferior orbital fissure; 7 = middle cranial fossa; 8 = foramen Vesalii and 9 = mandibular fossa.

had an incidence of 2.5% (individual measurements in Table I).

Superior orbital fissure. The superior orbital fissure was explored in coronal projection and could be seen in its entirety (individual measurements in Table II).

Foramen rotundum. The foramen rotundum is, in spite of its name, a short oval canal in the antero-medial portion of the greater sphenoidal wing. According to Lang (1981), the axis lies at a mean angle of −14° to the RB and at 15° to the SP. Consequently, the canal appears in coronal section at an angle of 84° (individual measurements in Table III).

Foramen ovale (Fig. 2). According to Honda et al (1987), the optimal CT plane lies between 0° and 20° to the RB and the foramen can be seen using CT on axial projection. We found the shape of the foramen ovale to be truly oval (56.7%), an elongated oval (31.7%) or semicircular (11.7%). In our material we found two variations in shape. In 12.5% of cases the foramen was partially divided by a thin bony spicule and in one case (0.8%) it was duplicated (individual measurements in Table IV).

Foramen spinosum (Fig. 2). Honda et al (1987) describe the axial projection as a good position for CT examination of this foramen. We found that in 0.8% of cases the foramen spinosum was absent and the foramen ovale was of normal size and shape (individual measurements in Table V).

Foramen Vesalii (or venosum) (Fig. 2). This foramen transmits a small vein connecting the cavernous sinus with the pterygoid venous plexus. According to Lang (1981), the foramen Vesalii is located in the greater sphenoidal wing posterior to the foramen rotundum. In most cases it is postero-medial, and in a few cases postero-lateral, to the foramen rotundum. In 25% of cases we found the foramen on the right side, in 35% on the left side, bilaterally in 15% and completely absent in 64%. The foramen Vesalii was examined in axial projection (individual measurements in Table VI).

Carotid canal (Figs 2 & 3). Following Teufel (1964),

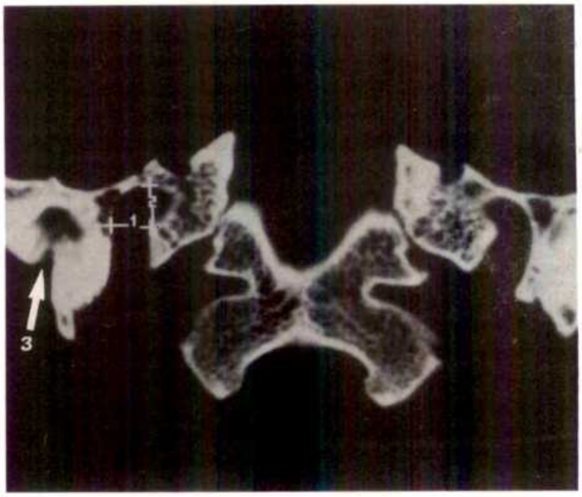

Figure 3. Coronal projection of the carotid canal showing the extracranial aperture and the ascending petrous portion, with the petrous curvature. 1 = Breadth at the petrous curvature; 2 = height at the petrous curvature and 3 = mastoid part of facial canal.

Table I. Measurements of the optic canal (n = 120)

		Mean (mm)	Range (mm)	Standard deviation (SD) (mm)	r^a
Orbital part					
Transverse diameter	CT/70°	5.66	4–10	1.10	0.56
	Skull	4.75	3.40–5.69	0.54	
Vertical diameter	CT/70°	5.01	3–7	0.55	0.53
	Skull	5.46	3.89–7.28	0.54	
Distance of lateral margins	CT/70°	32.83	27–40	2.76	0.73
	Skull	33.13	27.96–40.86	2.77	
Distance of medial margins	CT/70°	20.95	15–30	2.99	—
	Skull	—	—	—	
Optic waist					
Transverse diameter	CT/70°	6.43	4–9	1.08	0.61
	Skull	4.39	3.21–5.47	0.48	
Vertical diameter	CT/70°	5.01	3–7	0.68	0.45
	Skull	4.69	3.04–6.35	0.58	
Intracranial part					
Transverse diameter	CT/70°	7.64	5–11	1.11	0.48
	Skull	6.25	4.21–8.49	0.90	
Vertical diameter	CT/70°	3.63	3–9	0.55	0.73
	Skull	3.70	2.60–5.53	0.60	
Distance of lateral margins	CT/70°	27.97	24–33	2.34	0.73
	Skull	25.15	19.83–30.87	2.51	
Distance of medial margins	CT/70°	12.93	8–19	2.54	0.83
	Skull	14.12	9.35–22.26	2.36	

$^a r$ = Correlation coefficient between direct measurements and CT measurements. (This applies to Tables I–IX.)

we divided the carotid canal into an ascending petrous portion (with the petrous curvature) (Fig. 3), a transverse petrous portion and an ascending cavernous portion. According to Lang et al (1983), the ascending petrous portion encounters the RB at an angle of 80.9° and can therefore be seen in the coronal projection. The horizontal or transverse portion can be seen in the axial projections (individual measurements in Table VII).

Internal auditory canal (Figs 4 & 5). The axis of the canal lies at an angle of 90° ± 6° to the SP (Hassmann, 1975). Because of this "right angle", and because of the frontal orientation of its course in the petrous bone, the canal is best seen in coronal projection (Köster, 1988). The canal, which appears in axial (CT/10°) and coronal (CT/70°) scans, begins at the porus as an oval expanded orifice in the petrous portion of the temporal bone and ends with the falciform crest at the fundus.

The height of the porus, the canal and the fundus, and the length and the distances between the superior and inferior margins on the two sides, can be seen in

Table II. Measurements of the superior orbital fissure (n = 120)

		Mean (mm)	Range (mm)	SD (mm)	r
Length	CT/70°	20.05	13–25	2.72	0.56
	Skull	20.05	12.21–25.29	2.61	
Distance of lateral margins	CT/70°	56.53	46–72	4.65	0.90
	Skull	56.41	45.04–66.57	4.42	
Distance of medial margins	CT/70°	33.00	27–41	3.34	0.95
	Skull	32.81	27.61–40.01	3.29	
Shortest distance	CT/70°	28.20	23–36	2.78	0.93
	Skull	28.18	22.89–36.85	3.08	

Table III. Measurements of the foramen rotundum ($n = 120$)

		Mean (mm)	Range (mm)	SD (mm)	*r*
Breadth	CT/70°	3.11	2–5	0.78	0.69
	Skull	3.29	2.05–5.14	0.63	
Height	CT/70°	3.13	2–5	0.56	0.61
	Skull	3.09	2.08–5.05	0.69	
Intracranial distance	CT/70°	33.00	27–41	3.50	0.98
	Skull	33.39	26.84–41.92	3.63	

Table IV. Measurements of the foramen ovale ($n = 120$)

		Mean (mm)	Range (mm)	SD (mm)	*r*
Breadth	CT/10°	4.20	2–6	0.87	0.75
	Skull	3.91	2.44–6.66	0.77	
Length	CT/10°	7.67	5–12	1.43	0.89
	Skull	7.41	4.61–11.29	1.31	
Distance	CT/10°	44.47	35–59	4.17	0.98
	Skull	45.38	35.36–60.63	4.12	

Table V. Measurements of the foramen spinosum ($n = 119$)

		Mean (mm)	Range (mm)	SD (mm)	*r*
Breadth	CT/10°	1.86	1–4	0.60	0.61
	Skull	2.07	1.23–2.82	0.28	
Length	CT/10°	2.42	1–4	0.71	0.61
	Skull	2.60	1.53–4.35	0.52	
Distance	CT/10°	58.29	48–68	4.28	0.98
	Skull	58.42	48.85–67.61	4.15	

Table VI. Measurements of the foramen Vesalii (or venosum) ($n = 36$)

		Mean (mm)	Range (mm)	SD (mm)	*r*
Breadth	CT/10°	1.04	1–2	0.13	0.25
	Skull	1.33	1.00–2.04	0.35	
Length	CT/10°	1.68	1–3	0.68	0.54
	Skull	1.79	1.00–3.46	0.68	
Distance	CT/10°	35.36	30–42	3.72	0.83
	Skull	36.09	29.25–43.09	3.97	

Table VII. Measurements of the carotid canal ($n = 120$)

		Mean (mm)	Range (mm)	SD (mm)	*r*
Axial projection					
Breadth of extracranial aperture	CT/10°	5.88	3–8	0.64	0.66
	Skull	5.69	3.66–7.05	0.35	
Length of extracranial aperture	CT/10°	7.91	5–12	1.13	0.75
	Skull	7.81	4.45–12.41	1.16	
Extracranial distance	CT/10°	49.88	38–62	4.91	0.95
	Skull	50.58	37.82–62.37	4.77	
Length of horizontal portion	CT/10°	26.97	21–35	2.53	0.85
	Skull	27.90	21.67–35.51	2.52	
Coronal projection					
Length of ascending petrous part	CT/70°	11.10	7–15	1.61	0.57
	Skull	9.49	6–13	1.51	
Length of petrous curvature	CT/70°	6.33	4–8	0.79	
Breadth of petrous curvature	CT/70°	35.36	30–42	3.72	

coronal projection. The length and breadth of the porus, the canal and the fundus, and the distance between the anterior and posterior margins, are better seen in the axial projections (Fig. 4) (individual measurements in Table VIII).

Hypoglossal canal (Figs 6 & 7). The axis of the canal meets the SP at an angle of 44.9° (Schmidt, 1975) and the RB at an angle of $-7°$ (Kirdani, 1967). The canal is seen on both axial (CT/10°) and coronal (CT/70°) scans. The measurement of the height and distance between the inferior and superior margins can be seen on coronal projection. The measurement of breadth, length and distance between the anterior and posterior margins on the two sides is seen on the axial projections. We found that 11.6% were partially divided on the right side and 15% on the left. A complete division into two parts was encountered in 16% (right) and in 10% (left). Complete bilateral division was found in only 3.3% of cases (individual measurements in Table IX).

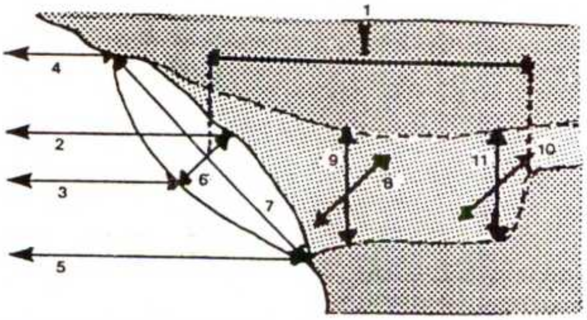

Figure 4. Internal auditory canal including measuring lines between the two sides of the skull (modified from Lang, 1981). 1 = Length of canal; 2 = distance between superior margins; 3 = distance between inferior margins; 4 = distance between anterior margins; 5 = distance between posterior margins; 6 = breadth of the porus; 7 = length of the porus; 8 = breadth of the canal; 9 = height of the canal; 10 = breadth of the fundus and 11 = height of the fundus.

Discussion

Recent advances in CT have produced a growing need for precise information about optimal scanning positions for examining the morphological and metrical details of the foramina and canals in the base of the skull. This study is an attempt to compare CT examina-

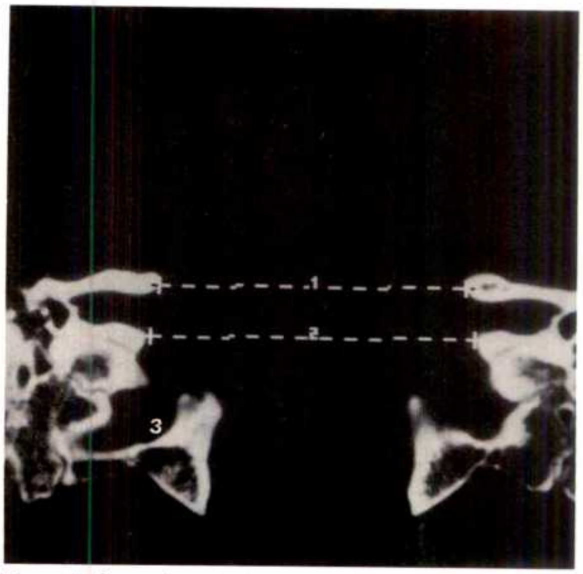

Figure 5. Coronal projection of the internal auditory canal. 1 = Distance between the superior margins; 2 = distance between the inferior margins and 3 = sigmoid sulcus.

Table VIII. Measurements of the internal auditory canal ($n = 120$)

		Mean (mm)	Range (mm)	SD (mm)	*r*
Height of porus	CT/70°	8.05	5–15	1.84	0.27
	Skull	4.77	2.62–8.71	1.00	
Breadth of porus	CT/10°	8.91	5–13	1.72	0.65
	Skull	9.57	6.72–12.90	1.53	
Height of canal	CT/70°	3.95	2–6	0.75	0.51
	Skull	3.70	2.21–5.69	0.71	
Breadth of canal	CT/10°	3.87	2–6	0.80	0.60
	Skull	4.11	2.35–6.36	0.69	
Height of fundus	CT/70°	4.33	3–7	0.92	
Breadth of fundus	CT/10°	3.34	2–5	0.79	
Length of canal	CT/70°	11.98	9–17	1.60	0.61
	Skull	11.68	8–15	1.50	0.55
	CT/10°	10.38	7–14	1.47	
Distance of superior margins	CT/70°	46.05	37–59	4.67	0.82
	Skull	41.42	42.85–62.35	4.81	
Distance of inferior margins	CT/70°	46.30	33–58	5.29	0.77
	Skull	50.48	40.08–59.48	5.02	
Distance of anterior margins	CT/10°	44.66	36–55	4.21	0.90
	Skull	44.43	36.50–53.93	4.13	
Distance of posterior margins	CT/10°	57.47	45–67	4.73	0.98
	Skull	57.57	45.49–66.69	4.82	

tion at two appropriate CT angles with direct measurements made on the macerated skull. Comparison of the two methods allows the accuracy of CT to be assessed and the best angles for viewing the skull to be determined. According to Radü et al (1987), CT examination of small structures is made impossible by the partial volume effect. Against this, Köster (1988) claims that the increased spatial resolution of CT has overcome this difficulty. However, because of this uncertainty, only a few publications listing CT measurements of these foramina and canals have so far appeared (Heller et al, 1983; Silverstein et al, 1988; Lanzieri et al, 1988).

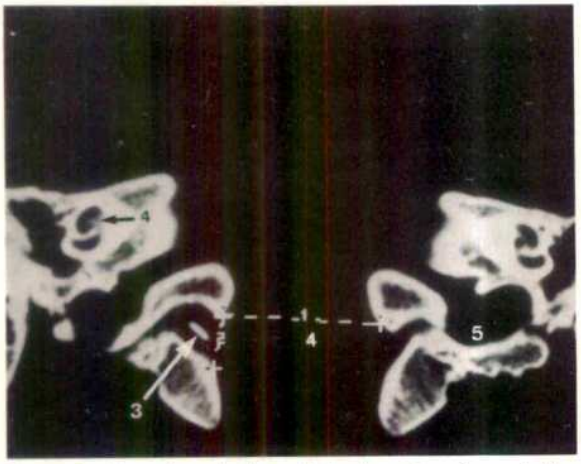

Figure 6. Coronal projection of the hypoglossal canal. The right canal is divided by a bony spicule. 1 = Distance between the superior margins of the porus internus; 2 = height of the porus internus; 3 = bony spicule; 4 = cochlea and 5 = jugular fossa.

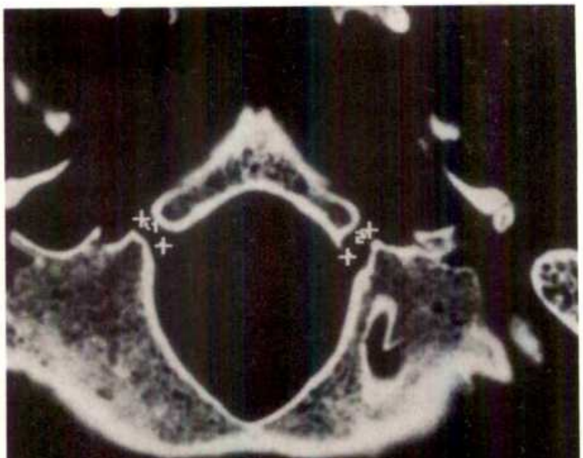

Figure 7. Axial projection of the hypoglossal canal. 1, 2 shows measuring line for the length.

Table IX. Measurements of the hypoglossal canal ($n = 120$)

		Mean (mm)	Range (mm)	SD (mm)	r
Porus internus					
Height	CT/70°	9.08	5–14	1.88	0.24
	Skull	5.41	2.75–12.08	1.58	
Breadth	CT/10°	6.85	3–11	1.69	0.31
	Skull	8.00	3.97–13.39	1.74	
Distance of superior margins	CT/70°	24.39	20–31	2.50	0.69
	Skull	29.30	22.98–35.94	2.93	
Distance of inferior margins	CT/70°	25.97	19–32	2.67	0.56
	Skull	27.21	18.40–33.14	3.22	
Distance of anterior margins	CT/10°	24.63	20–32	2.43	0.76
	Skull	24.38	19.47–32.51	2.42	
Distance of posterior margins	CT/10°	31.98	25–39	3.16	0.88
	Skull	31.95	26.01–38.08	2.70	
Canal					
Height	CT/70°	4.50	3–7	0.84	0.47
	Skull	3.57	2.24–5.28	0.69	
Breadth	CT/10°	4.24	2–8	1.06	0.44
	Skull	5.02	2.29–7.06	1.03	
Length	CT/10°	7.58	4–11	1.61	0.61
	Skull	7.78	5–12	1.46	
Porus externus					
Height	CT/70°	9.08	5–15	2.04	0.22
	Skull	5.70	3.14–8.41	1.12	
Breadth	CT/10°	6.95	3–13	1.61	0.40
	Skull	8.01	3.58–13.69	1.97	
Distance of superior margins	CT/70°	40.05	31–50	4.38	0.45
	Skull	43.14	30.08–51.22	3.71	
Distance of inferior margins	CT/70°	44.57	36–54	4.04	0.64
	Skull	38.91	30.61–47.55	3.71	
Distance of anterior margins	CT/10°	33.50	28–39	3.74	0.90
	Skull	34.00	28.43–39.36	2.53	
Distance of posterior margins	CT/10°	44.38	36–53	3.74	0.76
	Skull	45.50	37.36–56.45	4.48	

There are three main sources of error. First, there is no clinically acceptable plane corresponding to both axes of canals and foramina, and the actual position chosen must therefore represent a compromise. The problems of attaining exact representation and the differences between the two methods of measurement are illustrated by examples taken from the optical canal (Fig. 8). Secondly, there is a greater margin of error to be expected with CT (±0.5 mm) than with direct manual measurement (±0.01 mm). Finally, there is the partial volume effect, which should however have relatively little significance in this study, since sections of 1 mm were used. Furthermore, it will only be operative if the structures are not exactly perpendicular to the scan.

The coronal projection of the optic canal proved to be ideal for CT examination, correlation of direct measurements with CT measurements of the vertical diameters were good, but those of the transverse diameters were poor. This is because the direct measurement is made perpendicular to the course of the canal, whereas the CT measurement is perpendicular to the SP (Fig. 8).

Finally, a qualitative assessment of the correlation between the two methods of measurement and the representation of the canals and foramina at each projection is shown in Table X.

These results show that modern high resolution CT, with 1 mm sections, provides precise measurements which differ little from the actual distances in the anatomical specimen. It is to be assumed, however, that the canals and foramina lie perpendicular to the scanline.

The axial projection is optimal for the foramen ovale,

Table X. Representation of foramina and canals of the skull base, and correlation of direct measurements of breadth, height and length with the corresponding values obtained using CT in coronal (70°) and axial (10°) projection

	Correlation direct and CT/10°	Representation in CT/10°	Correlation direct and CT/70°	Representation in CT/70°
Optic canal			+ +[v] +[t]	+ + +[v] + + +[t]
Superior orbital fissure			+ +	+ + +
Foramen rotundum			+ +	+ +
Foramen ovale	+ + +	+ + +		
Foramen spinosum	+ +	+ +		
Foramen Vesalii	+	+ +		
Carotid canal	+ +	+ + +	+ +	+ + +
Internal auditory canal	+ +	+ + +	+	+ + +
Hypoglossal canal	+	+ + +	+	+ + +

+ = poor ($r < 0.50$), + + = good ($r = 0.51$–0.75), + + + = excellent ($r > 0.76$).
[v] vertical diameter, [t] transverse diameter.

the foramen spinosum, the foramen Vesalii, the horizontal part of the carotid canal and the internal auditory canal, whereas the coronal projection is suitable for the optic canal, the superior orbital fissure, the foramen rotundum and the ascending part of the carotid canal.

A comparison of the derived measurements of the coronal projection of the internal auditory canal, and both projections of the hypoglossal canal, with direct measurement is not possible because of the different measuring lines. Owing to the frontal orientation of its course in the petrous temporal bone, the internal auditory canal is best represented in coronal projection. A good quality picture of the hypoglossal canal can be obtained with coronal projection, whereas the axial projection has the alternative advantage of showing the whole extent of its course.

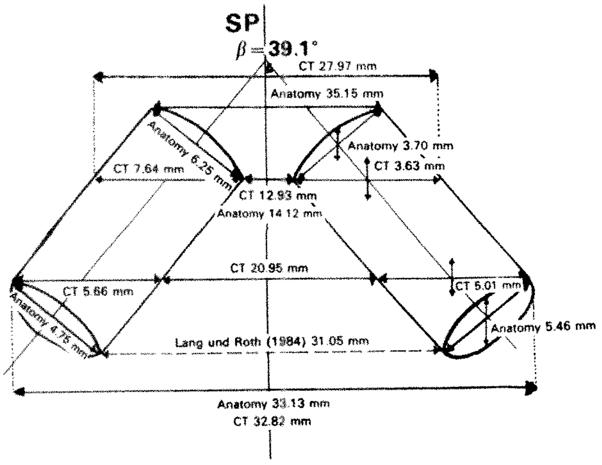

Figure 8. Model of the optic canal showing measuring lines. Difference between the direct and CT measurement is due to the different directions of the measuring lines.

Acknowledgments

We would like to express our thanks to the Wissenschaftliche Gesellschaft of Freiburg i. Br, whose support made this investigation possible, and to Dr Francis Steel for reading the manuscript.

References

BERLIS, A., 1990. Korrelation anatomischer und computertomographischer Maße von Kanälen und Foramina der Schädelbasis. *Medizinische Dissertation Freiburg* i. Br.

HASSMANN, H., 1975. *Form, Maße und Verläufe der Schädelkanäle: Canalis infraorbitalis, Canalis incisivus, Canalis palatinus major, Foramen spinosum und Meatus acusticus internus.* Medizinische Dissertation Würzburg.

HELLER, M., MÖHRLE, M., JEND, H. H., HÖRMANN, K., HELMKE, K., 1983. Anssagekraft der CT in der Diagnostik von Tumoren der Kleinhirnbrückenwinkelregion. *Röfo, 139,* 48–55.

HONDA, H., WATANABE, K., KUSOMOTO, S., HOSHI, H., NISHIKAWA, K., KAHITSUBATA, Y., JINNOUCHI, S., KODAMA, T., NAKAYAMA, S. & ONO, S., 1987. Optimal positioning for CT examinations of the skull base. Experimental and clinical studies. *European Journal of Radiology, 7,* 225–228.

KIRDANI, M. A., 1967. The normal hypoglossal canal. *American Journal of Roentgenology, 99,* 700–704.

KÖSTER, O., 1988. *CT des Felsenbeines* (Thieme Verlag, Stuttgart, New York).

LANG, J., 1981. *Klinische Anatomie des Kopfes* (Springer-Verlag Berlin, Heidelberg, New York).

LANG, J. & OEHMANN, G., 1976. Formentwicklung des Canalis opticus, seine Maße und Einstellung zu den Schädelebenen. *Verhandlungen der Anatomischen Gesellschaft, 70,* 567–574.

LANG, J., SCHAFHAUSER, O. & HOFFMANN, S., 1983. Über die postnatale Entwicklung der transbasalen Schädelpforten: Canalis caroticus, Foramen jugulare, Canalis hypoglossalis, Canalis condylaris, Foramen magnum. *Anatomischer Anzeiger, 153,* 315–357.

LANZIERI, C. F., DUCHESNEAU, P. M., ROSENBLOOM, S. A., SMITH, A. S. & ROSENBAUM, A. E., 1988. The significance of asymetry of the foramen Vesalius. *American Journal of Neuroradiology, 9,* 1201–1204.

POTTER, G. D. & TROKEL, S. L., 1971. In Radiology of the

Skull and Brain. The Skull, ed. by Th. H. Newton and G. D. Potts (C.V. Mosby Company, Saint Louis), pp. 487–506.

RADÜ, E. W., KENDALL, B. E. & MOSELEY, I. F., 1987. *Computertomographie des Kopfes*. (Thieme-Verlag, Stuttgart, New York).

SCHMIDT, Th., 1975. *Der Canalis hypoglossus: Topographie, Form, Länge, Durchmesser und Volumen*. Medizinische Dissertation Würzburg.

SILVERSTEIN, H., NORRELL, H., SMOUHA, E. & HABERKAMP, T., 1988. The singular canal: A valuable landmark in surgery of the internal auditory canal. *Otolaryngology—Head and Neck Surgery, 98*, 138–143.

TEUFEL, J., 1964. Einbau der Arteria carotis interna in den Canalis caroticus unter Berücksichtigung des transversalen Venenabflusses. *Morphologisches Jahrbuch, 106*, 188–274.

1992, *The British Journal of Radiology*, *65*, 662–667

Subluxation of the patella: evaluation of patellar articular cartilage with MR imaging

By Katsuyuki Nakanishi, *Masahiro Inoue, Koushi Harada, Junpei Ikezoe, Takamichi Murakami, Hironobu Nakamura and Takahiro Kozuka

Department of Radiology and *Department of Orthopaedic Surgery, Osaka University Medical School, 1-1-50, Fukushima, Fukushima-ku, Osaka, Japan

(*Received 19 August 1991, accepted 14 February 1992*)

Keywords: Subluxation of the patella, Patellar articular cartilage, MR imaging

Abstract. In patients with subluxation of the patella, injury of the patellar articular cartilage is frequently observed, and correct evaluation of this cartilage injury is extremely important for the management of these patients. Magnetic Resonance (MR) studies were performed on 102 patellofemoral (PF) joints of 51 patients with subluxation of the patella and 20 PF joints of 10 healthy volunteers. In 77 of the 102 PF joints with subluxation, arthroscopy and/or operation were performed. MR images were obtained with spin-echo and FLASH sequences, and para-axial images were obtained. We retrospectively analysed the MR findings of the 77 joints with special attention to the surface and thickness of the cartilage, and classified them into four grades. These MR grades were compared with the grades on arthroscopy, and the following results were obtained: MR grade 0, normal cartilage ($n = 27$, sensitivity 90.9%, specificity 74.2%); MR grade 1, thickening of the cartilage ($n = 24$, sensitivity 50%, specificity 89.1%); MR grade 2, surface irregularity of the cartilage ($n = 20$, sensitivity 85%, specificity 94.7%); MR grade 3, loss of the cartilage ($n = 6$, sensitivity 100%, specificity 100%). Although the early changes observed by arthroscopy were underestimated from the MR images, MR imaging proved to be extremely useful for evaluating moderately or advanced patellar cartilage injury.

Subluxation of the patella is a disorder of recurrent patellar pain, swelling and an unstable sensation of the patella. The onset of the disorder is usually at puberty. When patients are diagnosed as having subluxation of the patella, they usually have a history of giving way of the knees (Hughston, 1968; Merchant et al, 1974; Laurin et al, 1978; Aglietti et al, 1983; Install et al, 1983; Martinez et al, 1983; Inoue et al, 1988). It is very important for the treatment of subluxation of the patella to diagnose correctly the cartilage injury. However, before MR imaging, there was no method to visualize the patellar cartilage itself even when computed tomography (CT) was used. Therefore, invasive methods such as arthroscopy or CT with arthrography were necessary to evaluate the patellar articular cartilage (Boven et al, 1982a,b). Because it enables differentiation between cortical and cancellous bone, and hyaline cartilage and fibrocartilage, MR imaging has proved useful for examining the knee joints non-invasively.

We undertook this study to determine whether MR imaging can accurately demonstrate the patellar articular cartilage, yield a correct grading, or replace arthroscopy.

Materials and methods

MR studies were performed on 20 patellofemoral (PF) joints of 10 normal volunteers (age range 22–27 years; all female) as normal controls and 102 PF joints of 51 consecutive patients (age range 10–55 years; mean 19 years; 3 males, 48 females) who had a history of giving way or dislocation of one or both PF joints and a radiographic diagnosis of subluxation of the patella. The roentgenographic criterion for diagnosing subluxation of the patella was a lateral PF angle of less than 0° on CT, with the knee in full extension (Inoue et al, 1988). From these 102 PF joints, we excluded four PF joints which had previously undergone arthroscopic debridement of cartilage, and 21 PF joints which had not undergone arthroscopy. As a result, 77 PF joints with subluxation were analysed. MR imaging was performed on a 1.5 T unit (Magnetom, Siemens) with a 10 cm planar surface coil. Patients were in the supine position with their knees in full extension. The planar surface coil was placed above the patella. Spin-echo (SE) images (T_1-weighted, spin density, and T_2-weighted parameters) and FLASH images were obtained. T_1-weighted images were obtained with SE 400/26 (repetition time in milliseconds, echo time in milliseconds) pulse sequences and four excitations. The examination time was 6.88 min. Spin density and T_2-weighted images were obtained with dual echo, SE 2000/26, 70 pulse sequences and one excitation. The examination time was 8.80 min. FLASH images were obtained with 320/15/flip angle 90° pulse sequences and four excitations. The examination time was 5.51 min. In all subjects, the image direction was perpendicular to the long axis of the patella. The section thickness was 4 mm with no gap, and the imaging matrix was 256 by 256 with FOV of 14–18 cm.

MR images were prospectively interpreted by independent radiologists without knowledge of the results of

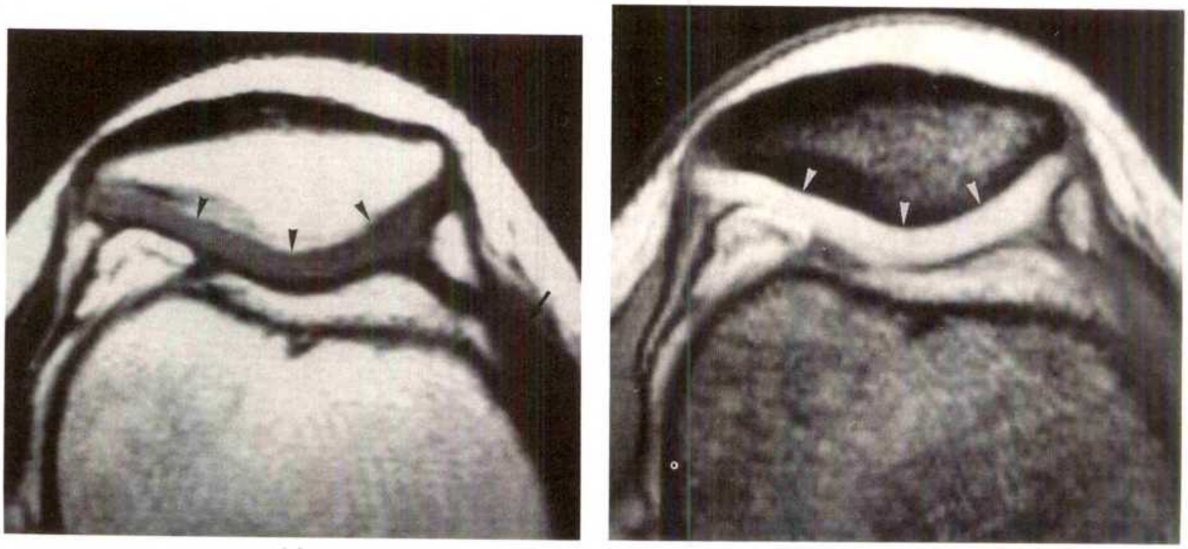
(a) (b)

Figure 1. 25-year-old female with a normal appearance of the left patellar articular cartilage. (a) T_1-weighted image (SE400/26). The patellar articular cartilage (arrowhead) shows a homogeneous appearance, with a slightly higher intensity than skeletal muscle (arrow). (b) FLASH image (320/15, FA90). The patellar articular cartilage (white arrowhead) shows a relatively high intensity because of fat suppression in the bone marrow.

arthroscopy or operation, paying special attention to the surface and thickness of the cartilage. The greatest thickness was measured. If there was some discrepancy among the three observers, agreement was obtained by consensus. We then classified these MR findings into four grades (MR grade 0, normal; MR grade 1, thickening; MR grade 2, surface irregularity; MR grade 3, loss of the cartilage). We compared these MR grades with the arthroscopic grades. Arthroscopy was performed by an experienced orthopaedic surgeon, and the results were recorded by arthroscopic grading, which usually consisted of classification into four grades (arthroscopy (AS) grade 0, normal; AS grade 1, softening and fissure; AS grade 2, fragmentation; AS grade 3, exposure of the subchondral bone) (Table I).

Table I. MR findings and arthroscopic gradings ($n = 77$)

MR grades	Athroscopic (AS) grades				Sensitivity	Specificity
	0	1	2	3		
0: Normal appearance	10	17			90.9%	74.2%
1: Thickening	1	20	3		50%	89.1%
2: Surface irregularity		3	17		85%	94.7%
3: Loss of the cartilage				6	100%	100%

AS grades: grade 0, normal appearance; grade 1, softening and fissure; grade 2, fragmentation; grade 3, exposure of the subchondral bone.

Results

Healthy volunteers

On T_1-weighted images (Fig. 1a), the normal patellar articular cartilage was seen as a homogeneous region with a smooth contour. It had a slightly higher intensity than skeletal muscle. On FLASH images (Fig. 1b), the normal patellar articular cartilage was demonstrated as a relatively high intensity area, because the intensity of the fat in the bone marrow was suppressed on this sequence. The thickness measured from the FLASH image of normal volunteers ranged from 2.8 to 4.4 mm, mean 3.56 mm. There were no significant differences between the right patellar cartilages and the left in each normal volunteer.

Patients with subluxation of the patella

Taking account of the thickness of cartilage in normal volunteers, we defined cartilage with a smooth surface and more than 5 mm thick as "thickening" (MR grade 1), and that with a smooth surface less than 5 mm thick as "normal" (MR grade 0). When irregularity of the surface of the cartilage was observed, we defined it as "surface irregularity" (MR grade 2) regardless of its thickness. If no articular cartilage could be seen on the MR image, we defined it as "loss of the cartilage" (MR grade 3). Using these criteria of MR imaging (Table I), 27 PF joints were diagnosed as MR grade 0, 24 as MR grade 1, 20 as MR grade 2, and six as MR grade 3. 10 (thickness range 2.8–4.7 mm; mean 3.54 mm) of the 27 PF joints visualized as MR grade 0 were also diagnosed as normal AS grade 0 by arthroscopy, but the other 17 (thickness range 2.9–4.8 mm; mean 4.13 mm) were

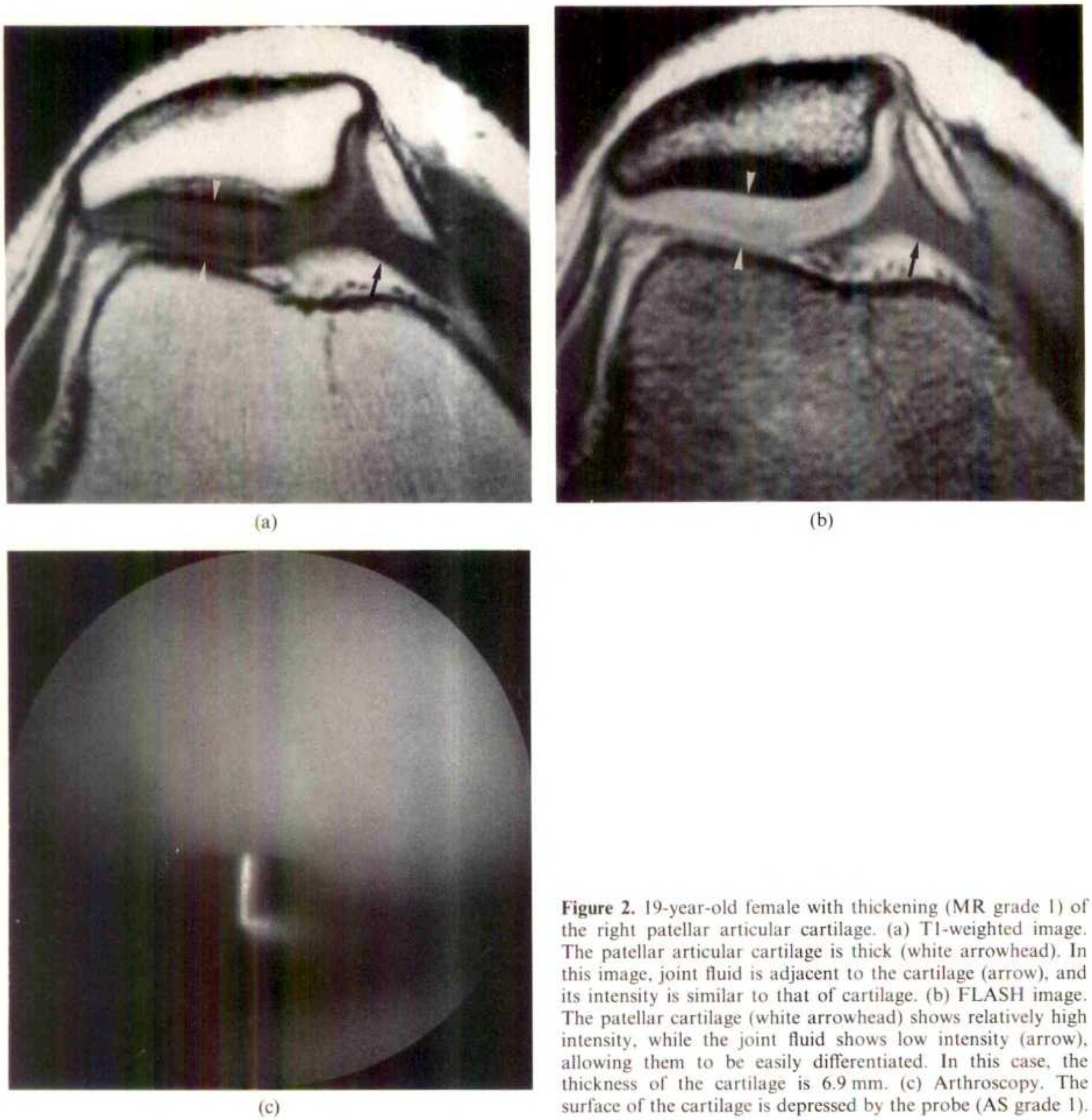
(a)

(b)

(c)

Figure 2. 19-year-old female with thickening (MR grade 1) of the right patellar articular cartilage. (a) T1-weighted image. The patellar articular cartilage is thick (white arrowhead). In this image, joint fluid is adjacent to the cartilage (arrow), and its intensity is similar to that of cartilage. (b) FLASH image. The patellar cartilage (white arrowhead) shows relatively high intensity, while the joint fluid shows low intensity (arrow), allowing them to be easily differentiated. In this case, the thickness of the cartilage is 6.9 mm. (c) Arthroscopy. The surface of the cartilage is depressed by the probe (AS grade 1).

recognized as having softening and fissure (AS grade 1) during arthroscopy. 20 of the 24 PF joints diagnosed as "thickening" (MR grade 1) by MR images were recognized as AS grade 1 (Fig. 2), three as AS grade 2 and the remaining one as AS grade 0 by arthroscopy. The mean thickness of these 24 patellar cartilages was 5.93 mm on the MR images. 17 (range of thickness on MR images 2.9–5.4 mm; mean 4.59 mm) of the 20 PF joints visualized as MR grade 2 were recognized as having fragmentation (AS grade 2) on arthroscopy (Fig. 3). The remaining three (thickness range 5.2–6.5 mm; mean 5.97 mm) were diagnosed as AS grade 1. All six PF joints diagnosed as MR grade 3 were observed as AS grade 3 in arthroscopy (Fig. 4).

Discussion

Cartilage may be classified as hyaline or fibrocartilage. The patellar articular cartilage is hyaline. Cartilage is composed of chondrocytes and matrix. The matrix is composed of collagen fibres and ground substance, which contains various mucopolysaccharides. Hyaline cartilage contains a lot of mucopolysaccharide, which reflects the signal intensity of articular cartilage on MR imaging (Bentley & Dowd, 1984; Shahriaree, 1985).

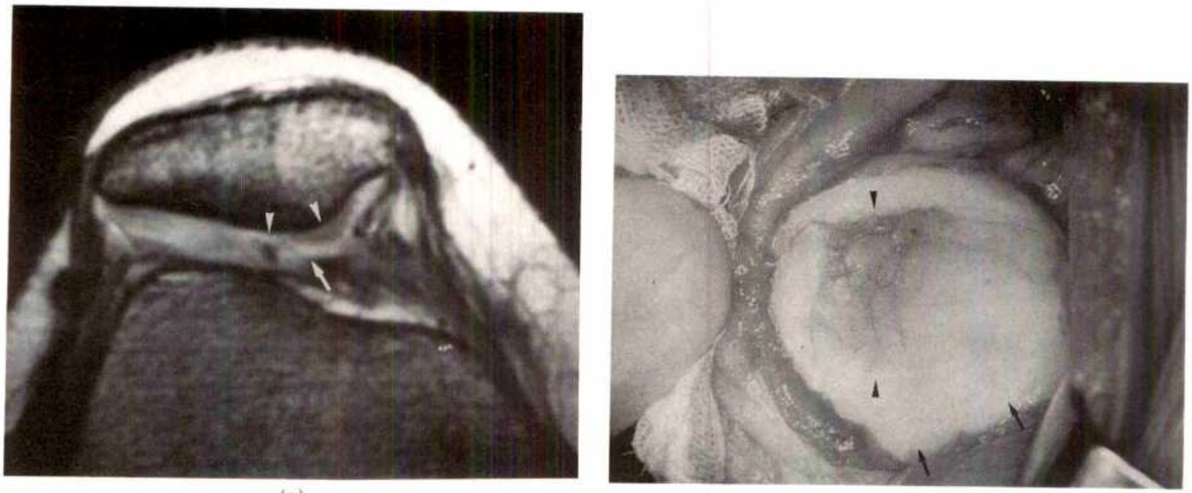

(a) (b)

Figure 3. 19-year-old female with surface irregularity (MR grade 2) of the right knee. (a) FLASH image. From the central ridge to the medial portion, the surface of the articular cartilage is irregular (white arrow), and the cartilage layer is inhomogeneous (white arrowhead). (b) Operative findings. The lateral portion of articular cartilage is almost intact (arrow), but there are many fragmentations of the medial portion (arrowhead). This change corresponds to AS grade 2

Hyaline cartilage shows slightly higher intensity than skeletal muscle on T_1-weighted images (Li et al, 1984; Reicher et al, 1985a,b; Beltran et al, 1986; Konig et al, 1987; Yulish et al, 1987).

All 20 PF joints of 10 normal volunteers showed normal alignment. The thickness was almost equal in all portions of the cartilage. Subluxation of the patella is usually preceded by malalignment of the PF joint. In many cases, the lateral portion of the articular cartilage appears soft on arthroscopy. In this condition, the ground substance in the cartilage has degenerated. Actually, mucopolysaccharide degenerates, and carti-

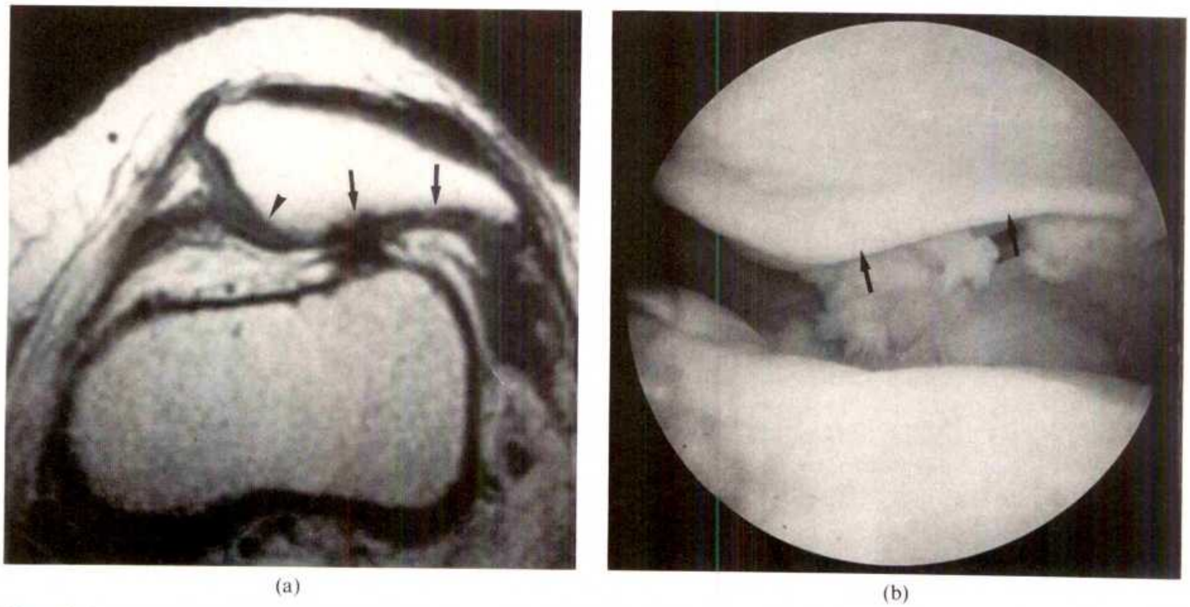

(a) (b)

Figure 4. 50-year-old female with loss of the cartilage (MR grade 3) of the left knee. (a) T_1-weighted image. The lateral portion of the patellar articular cartilage is lost and the subchondral bone is thickened (arrow). The medial portion of the articular cartilage remains, but its surface is irregular (arrowhead). (b) Arthroscopy. In the lateral portion of the petalla, the subchondral bone is exposed (arrow) (AS grade 3).

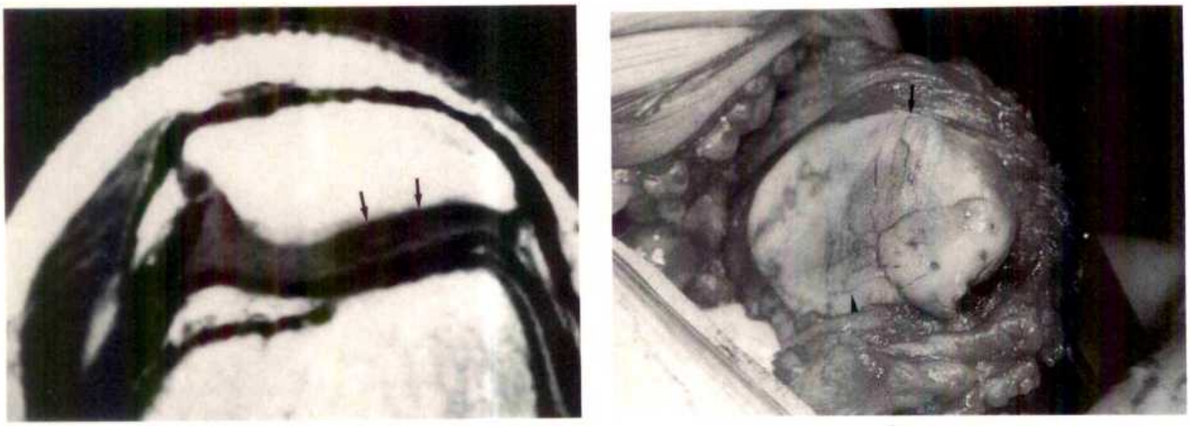
(a) (b)

Figure 5. 19-year-old female with thickening (MR grade 1) of the left patellar articular cartilage. (a) T_1-weighted image. The thickness of the cartilage is 6.2 mm and the surface appears smooth. A low-intensity band is seen in the deep layer of the cartilage (arrow). (b) Operative findings. Many large fragmentations are seen in the cartilage (arrowhead) (AS grade 2).

lage containing a large amount of water as well as vertical collagen fibres is disrupted (Bentley & Dowd, 1984; Shahriaree, 1985). If patients with malalignment of a PF joint suffer from giving way or dislocation, subtle fissures form on the surface of the cartilage. As these episodes repeat, larger fragmentations occur and the surface becomes irregular. With repeated dislocation over a long period, the subchondral bone is finally exposed (condition is observed as exposure of the subchondral bone by arthroscopy).

From the analysis of our results, AS grade 1 lesions were underestimated on MR imaging. 17 PF joints whose thickness did not exceed 5 mm on the MR images (MR grade 0) were evaluated as having softening on arthroscopy. In these 17 PF joints, the mean thickness was 4.13 mm, which was slightly thicker than 10 PF joints seen to be normal (AS grade 0) on arthroscopy. Furthermore, for these 17 PF joints, the mean age was 16.8 years, which was younger than the mean of 23.3 years for the normal volunteers. Since the cartilage thickness of patients at puberty (between 10 and 19 years) might be physiologically thinner than that of normal volunteers, the criteria for "thickening" might be less than 5 mm. Three of the 24 PF joints observed to be thickened on MR images (MR grade 1) showed fragmentation on arthroscopy (AS grade 2). In these three cases, an inhomogeneous appearance was clearly observed around the central ridge of the patella (Fig. 5). The other 21 PF joints diagnosed as MR grade 1 had a relatively homogeneous appearance. Once an obviously inhomogeneous appearance is seen, more advanced changes must be considered. Fragmentation on arthroscopy (AS grade 2) was accurately diagnosed by MR imaging. Although 20 PF joints were observed to have an irregular surface by MR imaging, three of them proved to have many deep fissures around the central ridge of the patella and were diagnosed as AS grade 1. When an irregular surface is observed in this portion by MR imaging, fissure formation or fragmentation must be considered (MR grade 3).

Loss of the articular cartilage (MR grade 3) corresponds to exposure of the subchondral bone (AS grade 3) by arthroscopy. All patients in this group were over 30 years in age and had a long history of giving way or dislocation of the patella.

In some cases, it is difficult to identify the cartilage itself on T_1-weighted images. In such cases, a FLASH image with a flip angle of 90° is useful. This is because when the fluid in the joint capsule is adjacent to the cartilage, it is difficult to differentiate the cartilage from the joint fluid on T_1-weighted images. With FLASH images with a flip angle 90°, however, cartilage shows a relatively high intensity (Konig et al, 1987) while the joint fluid shows a low intensity. For this reason, FLASH images with a flip angle of 90° provide better anatomic detail than T_1-weighted images. However, T_1 and spin-density images are useful for visualizing subtle changes in the cartilage layer. On T_2-weighted images, the cartilage appears as a low intensity region, while the joint fluid shows high intensity (Beltran et al, 1986); however, the imaging time is long.

We conclude that the combination of T_1-weighted images and FLASH images with a flip angle of 90° is extremely effective for detecting abnormalities of the patellar articular cartilage.

In summary, MRI can accurately determine pathological changes in the patellar articular cartilage in patients with subluxation of the patella, especially advanced changes. Cartilage with a thickness exceeding 5 mm (MR grade 1) corresponds to softening and fissure seen in arthroscopy (AS grade 1). An irregular surface observed on MR imaging (MR grade 2) corresponds to fragmentation (AS grade 2) on arthroscopy. Loss of the cartilage observed in MR imaging (MR grade 3) corresponds to exposure of the subchondral bone (AS grade 3). The combination of T_1-weighted images and FLASH images with a flip angle of 90° is extremely effective for detecting abnormalities of patellar articular cartilage.

References

AGLIETTI, P., INSTALL, J. N. & CERULLI, G., 1983. Patellar pain and incongruence. Measurement of incongruence. *Clinical Orthopaedics and Related Research, 176*, 217–224.

BELTRAN, J., NOTO, A. M., HERMAN, L. J., MOSURE, J. C., BURK, J. M. & CHRISTOFORIDIS, A. J., 1986. Joint effusions: MR imaging. *Radiology, 158*, 133–137.

BENTLEY, G. & DOWD, G., 1984. Current concept of etiology and treatment of chondromalacia patellae. *Clinical Orthopaedics and Related Research, 189*, 209–228.

BOVEN, F., BELLEMANS, M.-A., GEURTS, J. & POTVLIEGE, R., 1982a. A Comparative study of the patello-femoral joint on axial roentgenogram, axial arthrogram, and computed tomography following arthrography. *Skeletal Radiology, 8*, 179–181.

BOVEN, F., BELLEMANS, M.-A., GEURTS, J., BOECK, H. D. & POTVLIEGE, R., 1982b. The value of computed tomography scanning in Chrondromalacia patellae. *Skeletal Radiology, 8*, 183–185.

HUGHSTON, J. C., 1968. Subluxation of the patella. *Journal of Bone and Joint Surgery, 50*, 1003–1026.

INOUE, M., SHINO, K., HIROSE, H., HIROBE, S. & ONO, K., 1988. Subluxation of the patella. *Journal of Bone and Joint Surgery, 70*, 1331–1337.

INSTALL, J. N., AGLIETTI, P. & TRIA, A. J., JR., 1983. Patellar pain and incongruence. Clinical application. *Clinical Orthopaedics and Related Research, 176*, 225–232.

KONIG, H., SAUTER, R., DEIMLING, M. & VOGT, M., 1987. Cartilage disorders: comparison of spin-echo, CHESS, and FLASH sequence MR images. *Radiology, 164*, 753–758.

LAURIN, C. A., LEVESQUE, H. P., DUSSAULT, R., LABELLE, H. & PEIDES, J. P., 1978. The abnormal lateral patellofemoral angle. *Journal of Bone and Joint Surgery, 60*, 55–60.

LI, K. C., HENKELMAN, R. M., POON, P. Y. & RUBINSTEIN, J., 1984. MR imaging of the normal knee. *Journal of Computer Assisted Tomography, 8(6)*, 1147–1154.

MARTINEZ, S., KOROBKIN, M., FONDREN, F. B., HEDLUND, L. W. & GOLDNER, J. L., 1983. Diagnosis of patellofemoral malalignment by computed tomography. *Journal of Computer Assisted Tomography, 7*, 1050–1053.

MERCHANT, A. C., MERCER, R. L., JACOBSON, R. H. & COOL, C. R., 1974. Roentgenographic analysis of patellofemoral congruence. *Journal of Bone and Joint Surgery, 56*, 1391–1396.

REICHER, M. A., RAUSCHNING, W., GOLD, R. H., BASSETT, L. W., LUFKIN, R. B. & GLEN, W., JR., 1985a. High-resolution magnetic resonance imaging of the knee joint: normal anatomy. *American Journal of Roentgenology, 145*, 895–902.

REICHER, M. A., BASSETT, L. W. & GOLD, R. H., 1985b. High-resolution magnetic resonance imaging of the knee joint: pathologic correlations. *American Journal of Roentgenology, 145*, 903–909.

SHAHRIAREE, H., 1985. Chondromalacia. *Contemporary Orthopaedics, 11*, 27–39.

YULISH, B. S., MONTANEZ, J., GOODFELLOW, D. B., BRYAN, P. J., MULOPULOS, G. P. & MODIC, M. T., 1987. Chondromalacia patellae: assessment with MR imaging. *Radiology, 164*, 763–766.

1992, *The British Journal of Radiology*, 65, 668–671

What is the clinical disadvantage of discarding old radiographs? Survey of patients not re-examined for a long time

By Y. Oyama, MD, K. Imamura, Dsc, H. Ashida, MD, Y. Nakajima, MD, T. Itoh, MD,
M. Saeki, MD, Y. Kikuchi, H. Matsumoto and T. Ishikawa, MD

Department of Radiology, St Marianna University School of Medicine, Kawasaki, Japan

(*Received 29 July 1991 and in revised form 19 November 1991, accepted 14 January 1992*)

Keywords: X-ray films, Storage, Clinical usefulness, Risk

Abstract. The clinical disadvantage of discarding old radiographs was evaluated in patients who had not been re-examined for more than 8 years after their last radiological examination, 38 772 in total. During the 1 year survey, 158 (0.41%) of them underwent re-examination after a long interval. Retrospective evaluation revealed that in only 12 patients (0.032%) were the old films useful. This survey suggested that the clinical risk of not referring to films more than 8 years old would be less than 0.049%. We consider this acceptable, and have formulated new guidelines of storage of films.

A large number of patients do not undergo another radiological examination for a long time after their last visit. The access rate to stored X-ray films had been surveyed previously in our university hospital (Imamura et al, 1986). We discussed in that paper the access rate to stored films for clinical use and also for research as a function of intervals of X-ray examinations: 90% of retrieved films were of patients who had been examined in the past 5 years. The access rate to films of patients who had not been examined during the previous 6 years or more decreased to a very low level. We found a relationship between the risk of inaccessibility to films and the period of storage.

In this paper, the *clinical* risk caused by inaccessibility to previous films is evaluated.

Subjects and methods

All the radiological images are stored in master jackets for each patient, and filed centrally. They are managed by computer, and data for this investigation were extracted using this system.

The survey was performed during the period between April 1988 and March 1989. The retrieval rates in this period are shown in Table I. Master jackets are classified and stored in three storage areas. The classification is based on the elapsed period since the last examination; 0–2, 3–7 or 8–14 years. The classification was dictated by the available storage space. Patients with an elapsed period of more than 8 years were selected as subjects for this study. 93% (27 240/29 366) of all the jackets requested for clinical use were those of patients with an elapsed period of less than 2 years. Only 0.85% (251/29 366) were those of patients with an elapsed period of more than 8 years. In the group 3–7 years, 1875 out of 103 650 jackets were retrieved in a year for clinical usage, corresponding to 1.8%. 42 649 jackets of 38 772 patients in the third storage space had an elapsed time of 8 years or more. Of these, 158 patients (158/38 772 = 0.41%) underwent radiological examination during the period of survey, and constitute the subjects of this study.

Demographic data of the 158 patients are summarized in Table II. The elapsed period of radiographic examination ranged from 8 to 14 years with an average of 10.3 years. 56 patients (35%) had a comparable previous study. The findings of recent examinations were normal in 86 patients (54%). Abnormal findings were observed in 72 patients (46%), and 29 (18%) of them had previously the same kind of examination.

Table I. Retrieval rates of film jackets in the period of survey: April 1988 to March 1989

Elapsed[a] period (years)	No. of stored jackets	No. of retrieved jackets		
		For research	For clinical use[b]	Total use
0–2	75 592	3964	27 240	31 204
3–7	103 650	3527	1 875	5 402
8–14	42 649[c]	120	251[d]	371
Total	221 891	7611	29 366	36 977

[a] Elapsed since the last visit.
[b] Retrieved automatically on patients' visits.
[c] Number of patients was estimated to be 38 772 (one patient, might have more than one jackets).
[d] Radiological examination was performed in 158 patients.

Corresponding author: Yukio Oyama, MD, Department of Radiology, St Marianna University School of Medicine, 2-16-1 Sugao, Miyamae-ku, Kawasaki, Japan 216.

Table II. Summary of the 158 patients surveyed

Average elapsed period	10.3 years
Previous examinations	
Number	2.9 average
Chest radiograph, present	89 patients
Other plain films	91 patients
Comparable examinations	56 patients
Recent examinations	
Normal findings	86 patients
Abnormal findings	72 patients
With comparable previous examinations	29 patients

Usefulness of the previous films was evaluated retrospectively by two experienced radiologists, independently, as follows.

A: No clinical significance made by reviewing old films.
B: The previous films were useful in the evaluation of the interval change of disease but did not cause change of clinical management.
C: The previous films affected the clinical management.

The films were categorized as C in the following:

(1) An observation made on the new film could be categorized as normal or abnormal with more confidence by reviewing the previous films.
(2) A correct diagnosis could be made or the clinical significance of an observation made on the new film could be confirmed by reviewing the previous films. For example, when benign disease was diagnosed based on the absence of interval change between old and new films, the previous films were categorized as C (Fig. 1).

When there was a disagreement between the two radiologists, five experienced radiologists reviewed and discussed the case together, and a decision was made by consensus.

Results

The results are summarized in Tables III and IV. 146 patients were classified as category A, 6 patients as category B, and 6 as category C (Table III). The previous films were useful in the evaluation of the interval change of disease only in 0.016% and were useful in diagnosis or treatment planning only in 0.016% of 38 772 patients who had not returned for 8 years or more (Table IV). As shown in Table V, the same sites of the body were radiologically examined previously in 44 patients (30%) out of 146 of category A, and in all of the patients of category B or C ($p < 0.05$). The findings of recent examinations (Table VI) were normal in 86 patients (59%) of category A and in none of category B or C ($p < 0.05$).

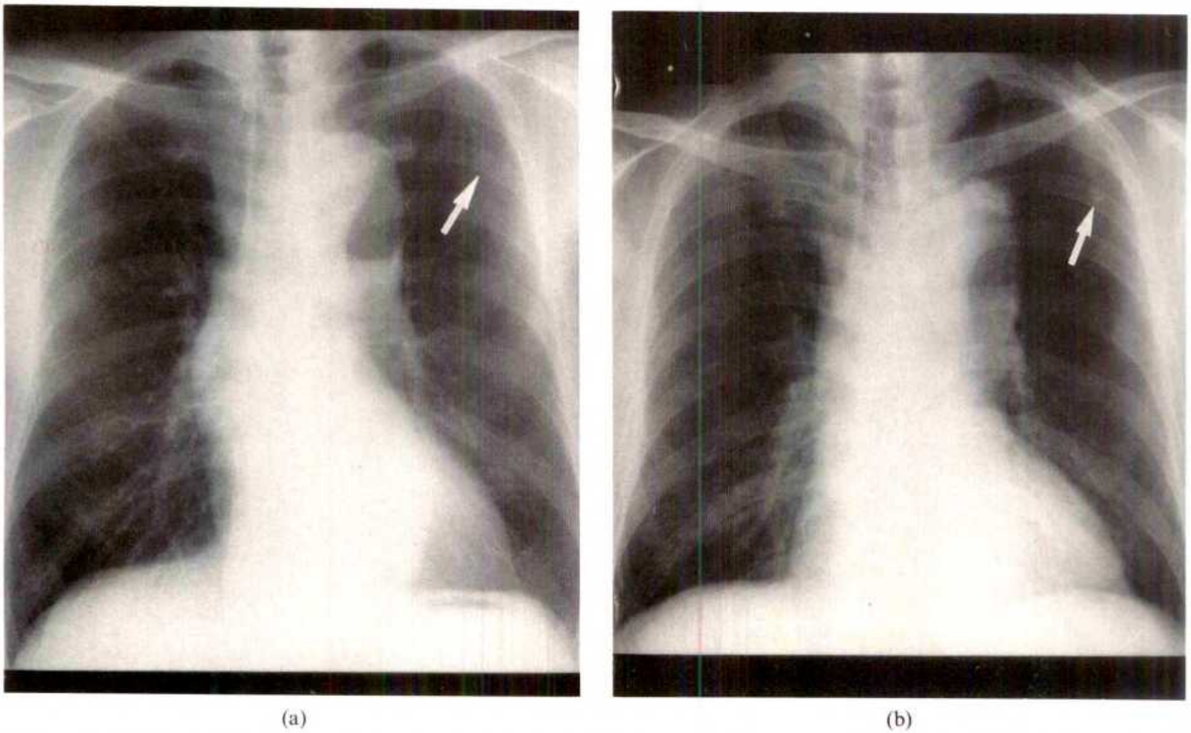

(a) (b)

Figure 1. A lung nodule (case 9), classified as category C. In the chest film (a) of 1988, a nodular shadow is noted in the left upper lung field (arrow). The previous film (b) of 1978 shows a similar lung nodule. Dilatation and elongation of the aorta are also noted with progressive change.

Table III. Patients whose previous films were found clinically useful

No.	Year[a]	Exam[b]	Diagnosis	Interval change
Category B[c]				
1	1979	Chest	Pulmonary emphysema	Worse
2	1979	Chest	Arteriosclerosis of the thoracic aorta	Worse
3	1979	Head CT	Cerebral infarction	No change
4	1979	Abdominal ultrasonography	Intrahepatic cholelithiasis	No change
5	1980	Abdomen, IVP	Urolithiasis	No change
6	1980	Chest	Scoliosis of dorsal spine	Worse
Category C[c]				
7	1976	Chest	Opacity of right apical lung field: normal variation	No change
8	1976	Upper GI series	Gastric ulcer scar	No change
9	1978	Chest	Granuloma of the left lung Arteriosclerosis of the thoracic aorta	No change Worse
10	1978	Chest	Cardiomegaly	No change
11	1978	Head CT	Postoperative residual meningioma	No change
12	1980	Paranasal sinus	Chronic sinusitis	Improved

[a] Year of the last previous examination.
[b] Examination performed in 1988 or 1989.
[c] See text.

A representative case

Case 9—a 71-year-old man with acute myocardial infarction (Fig. 1). A lung nodule of the left upper lung filed was noted. Similar findings were also noted in the film of 1978, suggesting a benign nature of the lesion, such as a granuloma. Therefore, further evaluation was unnecessary to exclude malignancy. This case was classified into category C. Progressive elongation of the thoracic aorta was also noted.

Table IV. Results of evaluation

Category[a]	No. of patients	Risk[b] (%)
Category A	136 (0.35%)	
Category B	6 (0.016%)	0.004–0.028
Category C	6 (0.016%)	0.004–0.028
B+C	12 (0.031%)	0.013–0.049%

[a] See text.
[b] Risks in case the previous films could not be referred to (95% confidence limit).

Discussion and conclusions

Out of 42 649 master jackets of patients who had not undergone radiographic examination for 8 years or more, 371 (0.87%) were requested for clinical use or for research in the period of survey. 99.1% of the jackets remained on the shelves unused. Only 158 of 38 772 patients returned after this long interval. This incidence is 0.041% and is equivalent to the "inaccessibility risk" of previous films, defined simply by the access frequency without any clinical considerations (Imamura et al, 1986).

About two-thirds of the returning patients (102/158) were examined in a different site from the previous examinations. In this situation, the previous films were not clinically useful. In about half of the patients who were examined for the same site (27/56), the examinations were normal and the management of the patients was not significantly affected by the previous films.

Furthermore, reviewing the remaining 29 patients who had examination of the same site previously and also had abnormal findings on the recent examinations, the previous films were not useful in 17 patients; the abnormality was not clinically significant (nine

Table V. Comparison of the incidence of the same kinds of previous examinations between patients of category A and those of category B or C

	Category		Total
	A	B or C	
Present	44	12	56
Absent	102	0	102

Table VI. Comparison of the findings of the new examinations between the patients of category A and those of category B or C

	Category		Total
	A	B or C	
Normal	86	0	86
Abnormal	60	12	72

patients), the interval between the examination was too long to evaluate the significance of the interval change of the abnormality (seven patients), or the estimation of interval change was difficult because of differing projections. Therefore, the old examinations were helpful for clinical care in only 12 patients. Consequently, the inaccessibility risk with any clinical disadvantage was actually 7.6% (12/158) of the simple inaccessibility risk.

In six, the old films were useful in diagnosis or treatment planning (category C). The inaccessibility risk is 0.016% with the upper limit of 0.028% (95% confidence limit) in diagnosis and treatment planning (Table IV). In the remaining six patients, the previous films were useful only in the evaluation of interval change of disease, but did not have any major effect on diagnosis or treatment planning (category B). They might not be absolutely necessary, but information on an interval change may be valuable in assessing the rate of progression and prognosis of a disease. From this point of view, the clinical inaccessibility risk is 0.031% with the upper limit of 0.049% (95% confidence limit).

For management and storage of radiographic images, our results provide a reliable and acceptable basis as the patients' benefit has been carefully considered in this analysis. Whether this risk is serious or not will depend on many factors which might differ according to the philosophy of physicians, to the circumstances of hospitals, to the social concept of the patient's benefit, etc. Limited space for storage, and limited manpower in film management make indefinite film storage impractical.

In our hospital, all films had been stored systematically since the hospital opened. It became necessary to investigate again the policy of the storage of films because of limited space. The problem was discussed with representatives of clinical departments, mainly concerning the risk when the previous films could not be retrieved for patients who did not return for a long time. We came to a consensus that the presumed risk would be acceptable, and consequently the films of patients who had not been re-examined for 10 years were discarded.

Acknowledgment

We are grateful to Dr Yutaka Sato, Ms Sanae Narita and Dr Toshio Yamaguchi for helping us prepare this paper.

Reference

IMAHURA, K., IMANISHI, Y., ISHIKAWA, T., KIKUCHI, Y., ISHII, K. & FUJII, M., 1986. Survey of the access to stored X-ray films in a university hospital. In *MEDINFO 86*, ed. by R. Salamon, B. Blum and M. Jorgensen (Elsevier, Amsterdam), pp. 415–417.

1992, *The British Journal of Radiology*, 65, 672–673

Intracardiac metastases from germ cell tumours—an unusual but important site of metastasis

By Dirk Pickuth, MD, Rosalind Eeles, MA, MRCP, FRCR, Malcolm Mason, MRCP, FRCR, *Charles Pumphrey, DM, MRCP, †Peter Goldstraw, MB, ChB, FRCS and Alan Horwich, PhD, MRCP, FRCR

Academic Unit of Radiotherapy and Oncology, The Royal Marsden Hospital, Downs Road, Sutton, Surrey SM2 5PT; *Department of Cardiology, St George's Hospital, Blackshaw Road, London SW17 0QT and †Department of Thoracic Surgery, The Royal Bromptom Hospital, Sydney Street, London SW3 6NP, UK

(Received 25 September 1991 and in revised form 31 January 1991, accepted 6 March 1992)

Keywords: Germ cell tumours, Testicular neoplasms, Teratoma, Metastases, Heart

Abstract. Two cases of intracardiac deposits from testicular teratomas diagnosed by echocardiography and angiocardiography, respectively, are described. The importance of recognizing this as an uncommon site of metastasis from germ cell tumours is discussed.

The most common sites of metastatic involvement from non-seminomatous germ cell tumours are the locoregional lymph nodes and lungs (Williams et al, 1989). Metastastic deposits from testicular tumours to unusual sites have been described (Husband & Bellamy, 1985). We describe two patients wth intracardiac metastases. The development of a cardiac murmur in a patient with a germ cell tumour should alert the oncologist to this rare, potentially lethal, but treatable site of metastasis.

Case reports

Case 1

A 23-year-old man presented with bilateral pulmonary metastases from a right-sided testicular teratoma (malignant teratoma undifferentiated). He was treated abroad by orchidectomy and chemotherapy with cisplatinum, vinblastine and bleomycin, to which he had a partial response. This was followed by whole lung irradiation. 3 years later his chest disease progressed and he was referred to The Royal Marsden Hospital. Cardiac examination was initially normal, but examination a week later revealed a systolic murmur audible on exercise in the pulmonary area. Subsequently the patient developed an acute episode of right ventricular failure. An echocardiogram showed a large mass filling most of the right ventricle, extending up into the right ventricular outflow tract with a projection reaching towards the tricuspid valve (Fig. 1). There was right atrial enlargement, but no filling defect within the right atrium. In view of the acute cardiac decompensation he began urgent chemotherapy with carboplatin, vincristine and bleomycin. There was an improvement in his dyspnoea and a reduction in the size of the pulmonary metastases. A second echocardiogram showed that the mass in the right ventricle was reduced to half the original size. However, after initial improvement, his condition again deteriorated owing to the development of *Haemophilus influenzae* pneumonia which failed to respond to treatment. He died 1 month after starting chemotherapy. There was no postmortem.

Case 2

A 40-year-old man presented with posterior mediastinal, para-aortic and left-sided cervical lymph node metastases from a left-sided testicular teratoma (malignant teratoma intermediate). He was treated by orchidectomy and chemotherapy with bleomycin, etoposide and cisplatinum followed by excision of residual masses in the left side of the neck and the para-aortic region. He relapsed with para-aortic and mediastinal disease 1 year later and was treated with two further courses of bleomycin, etoposide and cisplatinum, followed by excision of the para-aortic mass. Physical examination before his abdominal surgery revealed a systolic and diastolic murmur in the pulmonary area which had not been noted before. An echocardiogram showed a polypoid tumour arising from the right atrium, or possibly the tricuspid valve. The tumour did not have the appearance of myxoma. Cardiac catheterization was performed prior to open heart surgery and detected a large fimbriated mass arising from the left atrium and passing through the right atrium, the right ventricle into the pulmonary artery (Fig. 2). At operation, a semi-solid tumour mass was found within the right atrium with a tongue of tumour extending into the superior vena cava and the left innominate

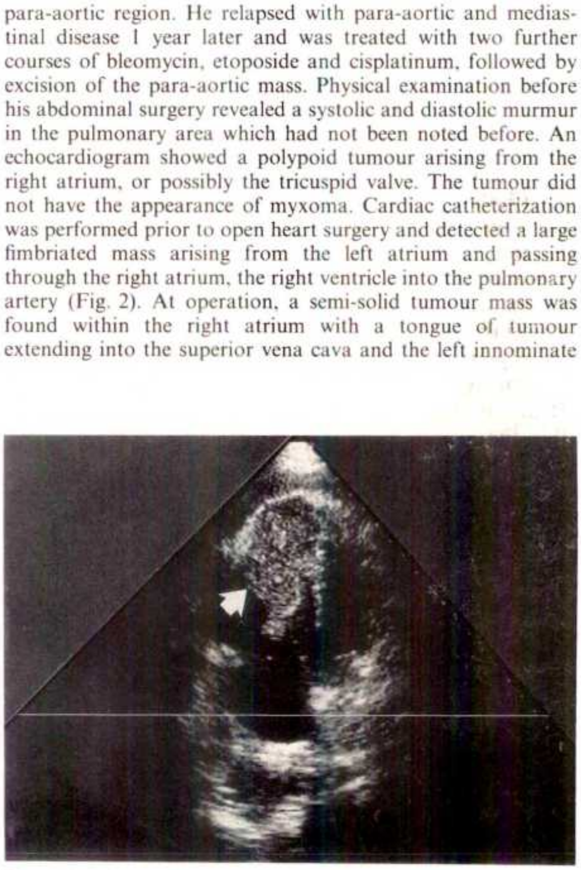

Figure 1. Echocardiogram of Case 1 showing the metastasis in the right ventricle (arrow).

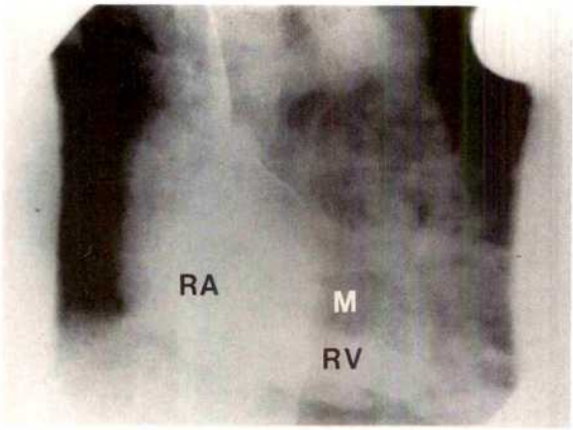

Figure 2. Angiocardiogram of Case 2 showing the metastasis in the right ventricle. M = metastasis, RA = right atrium, RV = right ventricle.

vein. Histology showed differentiated teratoma (Pillai et al, 1986). He subsequently relapsed in the retrocrural area and this was refractory to chemotherapy. He died 3 years after his initial chemotherapy. There was no postmortem.

Discussion

Metastases to the heart are rare, although they account for the majority of cardiac tumours (Colucci & Braunwald, 1991). When they occur, they are usually secondary to locoregional extension and limited to the pericardium or myocardium (Kerbrat et al, 1990). Haematogeneous metastases to the heart usually originate from primaries in the breast or lung (Colucci & Braunwald, 1991). Intracardiac deposits from testicular tumours are extremely uncommon. Melvin et al (1983) reported the first case of an intracardiac metastasis from an embryonal carcinoma of the testis which was successfully removed.

Heart murmurs can be caused by turbulent flow within the heart due to intracardiac metastases. In our cases, signs suggestive of intracardiac involvement, in patients with previously normal cardiac physical examinations, were a systolic murmur in the pulmonary area (Case 1) and a systolic and diastolic murmur in the pulmonary area (Case 2). In both patients the metastases nearly plugged the pulmonary valve. Valvular obstruction and myocardial involvement produced heart failure in one patient (Case 1). Acute obstruction of the blood flow through a valve may also lead to sudden symptoms of convulsions and unconsciousness (Colucci & Braunwald, 1991).

Both the radiologist and oncologist must be aware of all potential sites of residual and recurrent disease. Although rare, it is important to know about the possibility of intracardiac metastases, because teratomas are usually chemo-sensitive and even if residual differentiated teratoma remains after chemotherapy, it can be successfully removed. The sudden development of a cardiac murmur should alert the clinician to the possibility of an intracardiac metastasis which can be diagnosed non-invasively by echocardiography.

Acknowledgements

We should like to thank the staff of the echocardiographic and cardiac catheterization departments at St Helier's Hospital, Carshalton and The Royal Brompton Hospital, London. We should also like to thank Judy Nicholls and Gillian Jay for help with data collection and Christine Evans of the Academic Unit of Radiotherapy and Oncology, Sutton for typing the manuscript.

This work was supported by Cancer Research Campaign, Bob Champion Cancer Trust and The Royal Marsden Hospital.

References

COLUCCI, W. S. & BRAUNWALD, E., 1991. Cardiac tumors, cardiac manifestations of systemic diseases, and traumatic cardiac injury. In *Harrison's Principles of Internal Medicine* 12th edn., ed. by J. D. Wilson, (McGraw-Hill, New York), pp. 988–991.

HUSBAND, J. E. & BELLAMY, E. A., 1985. Unusual thoracoabdominal sites of metastases in testicular tumors. *American Journal of Roentgenology*, *145*, 1165–1171.

KEBRAT, P., TOUSSAINT, C., DEPLACE, C., MARCADE, E., LANCIEN, G. & GEDOUIN, D., 1990. Exerese d'une metastase intra-cardiaque sous chimiotherapie. *Journal de Chirurgie (Paris)*, *127*(3), 164–167.

MELVIN, K. N., HOWARD, R. J., RAKOWSKI, H., GOLDMAN, B. S. & EL-MARAGHI, N. R., 1983. Embryonal carcinoma of the testis with metastases to the right atrium. *Canadian Journal of Surgery*, *26*(1), 86–88.

PILLAI, R., BLAUTH, C., PECKHAM, M., HENDRY, W., BARRETT, A. & GOLDSTRAW, P., 1986. Intracardiac metastases from malignant teratoma of the testis. *Journal of Thoracic and Cardiovascular Surgery*, *92*(1), 118–120.

WILLIAMS, M. P., COOK, J. V. & DUCHESNE, G. M., 1989. Psoas nodes—an overlooked site of metastasis from testicular tumours. *Clinical Radiology*, *40*, 607–609.

1992, *The British Journal of Radiology*, *65*, 674–680

The radiology and terminology of cryptogenic organizing pneumonia

By J. A. A. Haddock, MA, MRCP, FRCR and D. M. Hansell, MRCP, FRCR

Department of Radiology, Royal Brompton National Heart & Lung Hospital, Sydney Street, London SW3 6NP, UK

(*Received 12 November 1991 and in revised form 3 February 1992, accepted 6 March 1992*)

Keywords: Cryptogenic organizing pneumonia, Bronchiolitis obliterans organizing pneumonia

Abstract. The clinical features, radiographic and computed tomographic findings of nine patients with histological proof of cryptogenic organizing pneumonia were analysed. Patients present with cough, dyspnoea and malaise and commonly have bilateral multifocal consolidation on chest radiography, which may show resolution or relapse with or without steroid treatment. A good response to steroids is the rule, usually with complete radiological resolution or minimal residual scarring. The relative merits of the terms cryptogenic organizing pneumonia and bronchiolitis obliterans organizing pneumonia, both currently used to describe this entity, are discussed.

Cryptogenic organizing pneumonia is a condition increasingly recognized with a distinctive, but not unique, constellation of clinical features and radiographic abnormalities. Diagnosis relies on the histological findings of organizing granulation tissue in the air spaces, in the absence of an infective or other aetiological agent. It is important to establish a diagnosis since the majority of patients with cryptogenic organizing pneumonia make a complete and rapid recovery on corticosteroid therapy. The term cryptogenic organizing pneumonia (COP) was first coined in the early 1980s (Davison et al, 1983); at about the same time a large series of patients with so-called bronchiolitis obliterans organizing pneumonia (BOOP) was reported (Epler et al, 1985). Despite the fact that these two descriptions probably relate to the same entity, there has been much confusion over the use of the terms COP and BOOP (Woodhead & du Bois, 1991). The purpose of this study was to describe the clinical features and the radiographic abnormalities in a series of patients with pathologically proven COP. A second objective was to raise awareness of this entity amongst radiologists.

Patients and methods

Nine patients attending the Royal Brompton National Heart & Lung Hospital during the past 9 years with a histologically confirmed diagnosis of organizing pneumonia were studied. The histological criterion for the diagnosis of organizing pneumonia is the demonstration of buds of immature connective tissue (Masson bodies or bourgeons conjunctifs) within alveoli, with some extension into respiratory bronchioles. In addition, lymphocytes, plasma cells, macrophages and fibroblasts are found within buds of granulation tissue (Corrin, 1990) (Fig. 1). An acute infective cause of pneumonia was excluded in all cases. Some patients (4/9) had received one or several courses of antibiotics before referral to the Royal Brompton Hospital. Patients with another primary diagnosis of diffuse lung disease, for example fibrosing alveolitis, were excluded. The clinical features, lung function test results, chest radiographs and computed tomographic (CT) scans (5/9) of these nine patients were analysed.

The majority of chest radiographs were taken at 141 kVp using an air gap and an automatic exposure device. The film/screen combination used was a medium-speed calcium tungstate screen (Kodak regular) with Kodak XL film. Five patients had one or more radiographs taken with an AMBER (Optische Industrie Oldelft, Netherlands) chest unit, also taken at 140 kVp. Radiographic abnormalities were catagorized as upper,

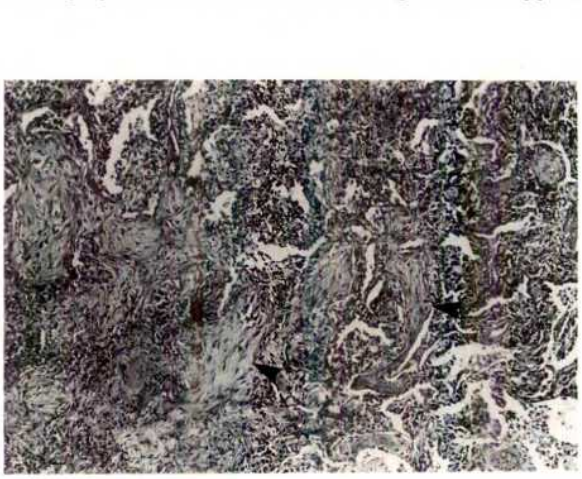

Figure 1. Cryptogenic organizing pneumonia (H & E strain). Buds of granulation tissue occupy the alveoli and stream towards the respiratory bronchioles (arrowheads). (Reproduced by permission, from Corrin (1990).)

Address correspondence to Dr D. M. Hansell.

Table I. Clinical features, lung function test results and biopsy technique

Case	Age (years)	Sex	Presenting symptoms	Past medical history	ESR (mm/h)	Lung function tests: FEV_1/FVC (%) DLCO (% predicted)	Initial diagnosis	Type of biopsy
1	62	F	Dyspnoea, cough, fever and pleuritic pain	Sarcoidosis	Not available	$FEV_1/FVC = 49$ DLCO = 25	—	Percutaneous (Biopty gun)
2	53	F	Cough, haemoptysis and fever	—	30	$FEV_1/FVC = 78$ DLCO = 60	—	Transbronchial
3	47	M	Dyspnoea and pleuritic pain	Ulcerative colitis	12 (on steroids)	$FEV_1/FVC = 81$ DLCO = 75	Cryptogenic fibrosing alveolitis	Transbronchial
4	49	F	Dyspnoea, productive cough and pleuritic pain	—	66	$FEV_1/FVC = 84$ DLCO = 51	Cryptogenic fibrosing alveolitis	Open lung
5	57	F	Dyspnoea, cough and weight loss	Pulmonary tuberculosis	107	$FEV_1/FVC = 60$ DLCO = 36	—	Transbronchial
6	52	M	Dyspnoea and pleuritic pain	—	2 (on steroids)	$FEV_1/FVC = 70$ DLCO = 37	Cryptogenic fibrosing alveolitis	Transbronchial
7	70	M	Dyspnoea, cough, fever and weight loss	—	67	Not available	Pulmonary eosinophilia	Open lung
8	63	M	Dyspnoea, productive cough and haemoptysis	—	63	$FEV_1/FCV = 84$ DLCO = 31	—	Transbronchial
9	67	M	Dyspnoea, productive cough and weight loss	—	40	$FEV_1/FVC = 78$ DLCO = 55	Heart failure	Transbronchial

mid or lower zone. Within the limitations of a two-dimensional postero-anterior (PA) chest radiograph, an estimation of whether the abnormalities were predominantly central or peripheral was made.

CT scan examinations on five patients were performed on an Elscint 2002 scanner with a scanning time of 5.5 s. A standard protocol (contiguous 10 mm sections, normal reconstruction) was used in all cases.

Results

The clinical features, lung function test results and biopsy techniques are summarized in Table I. The presenting symptoms of all patients were similar but non-specific with dyspnoea (8/9) and cough (7/9) being the commonest complaint. Four patients produced white mucoid sputum. Systemic disturbance, manifest as malaise (6/9), fever (3/9) and weight loss (3/9), was also common. Pleuritic pain (4/9) and haemoptysis (2/9) also occurred. None of the patients was on chronic medication known to be associated with COP.

The radiographic abnormalities are recorded in Table II. The predominant radiographic abnormality was of patchy shadowing in seven cases, consistent with multifocal consolidation; in three cases the shadowing had a poorly defined nodular pattern. All patients had lower-zone changes, eight had mid-zone changes and only three had changes in the upper zones. No patient had exclusively upper-zone abnormalities. Changes were bilateral during the course of the disease in all cases. Five patients had predominantly peripheral shadowing (Figs 2, 3).

The peripheral distribution of the shadowing in Case 1 was initially interpreted as pleural disease but a CT scan demonstrated subpleural consolidation with no evidence of pleural disease (Fig. 4). In Case 4 a right-sided pleural reaction was ascribed to a previous open lung biopsy; this remained after the pulmonary changes had completely resolved. In Case 9 the radiographic abnormalities were complicated by the superimposed changes of heart failure: the right pleural effusion was presumed to result from congestive cardiac failure. Of the five patients who underwent CT examination, only three had CT at the time of presentation. These all confirmed that the poorly defined opacities seen on

Table II. Radiographic abnormalities

Case	Zonal predominance (U = upper, M = mid, L = lower zone)			Type of shadowing (all bilateral)	Distribution (p = peripheral, n = no peripheral predominance)	Follow-up (after starting steroids), R = clinical and radiological relapse during follow-up period
1		M	L	Confluent poorly defined nodular shadowing	p	Linear residual changes 14/12
2		M	L	Multifocal consolidation	n	Complete resolution 9/12 R
3		M	L	Multifocal consolidation	n	Linear residual changes 11/12
4	U	M	L	Confluent poorly defined nodular shadowing	n	Linear residual changes 9 years R
5			L	Multifocal consolidation and poorly defined nodular showing	p	Poorly defined residual shadowing 18/12 R
6		M	L	Multifocal consolidation	p	Complete resolution 10/12
7	U	M	L	Widespread dense consolidation	p	Homogeneous residual shadowing 11/12 R
8		M	L	Multifocal consolidation	p	Complete resolution 6/12
9	U	M	L	Widespread dense consolidation	n	Homogeneous residual shadowing 6/12 R

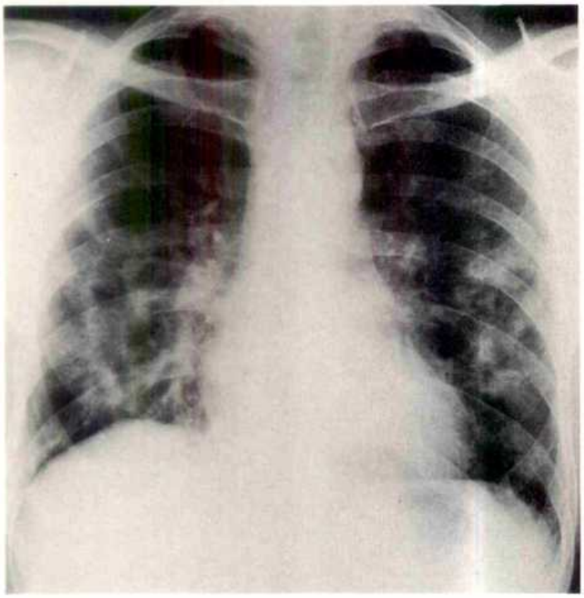

Figure 2. *Case 3.* Patchy bilateral consolidation in the mid and lower zones. These changes resolved completely on steroid treatment.

plain radiography were areas of consolidation with an air bronchogram visible in some of the opacified parenchyma.

Immediate clinical and radiological response occurred with steroids in the majority of patients (7/9); treatment was continued for between 6 months and 1 year.

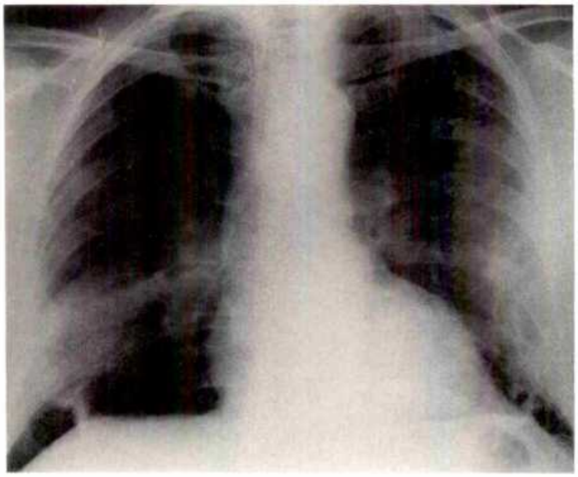

Figure 3. *Case 7.* Bilateral dense consolidation in the left upper zone and both mid and lower zones; note the peripheral distribution.

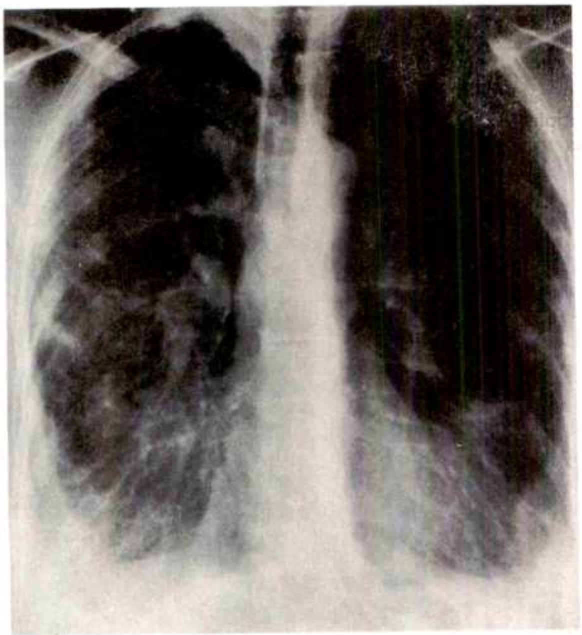

(a)

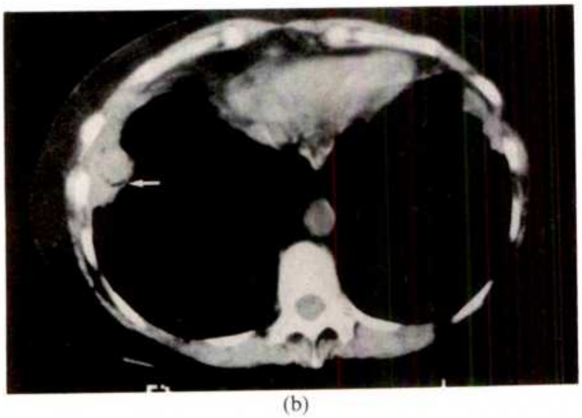

(b)

Figure 4. *Case 1.* (a) Poorly defined multifocal consolidation with nodularity and confluent shadowing at the bases, initially interpreted as pleural disease. (b) CT section through the lower zones confirms the presence of subpleural consolidation containing an air bronchogram (arrow). There is no significant pleural disease.

Relapsing and changing shadows were noted during the course of the disease in five patients. Case 5 was systemically unwell for several months before a diagnosis was made and steroid treatment initiated. During this time, without steroid treatment, changes at the right base cleared and returned; in addition new shadowing developed at the left base (Fig. 5). A similar radiographic sequence was seen in Case 9 (Fig. 6) and 7 while on treatment. One patient (Case 4) inadvertently stopped steroids and relapsed radiographically and clinically 10 weeks later. The shadowing occurred at a site whence it had previously cleared. A similar recurrence of consolidation at the same site occurred in Case 2, despite continued steroid therapy.

Three patients responded to treatment with complete resolution of the radiographic changes. Six patients had residual changes at 6 months to several years after treatment. In three of these the changes were a few linear shadows at the site of the previous consolidation. One patient had persistent bilateral poorly defined opacities at the lung bases. Two patients had residual shadowing at the site of previous larger areas of consolidation 6 and 11 months after starting treatment, respectively.

Discussion

COP was first described in the English literature by Davison (Davison et al, 1983). In this series of eight patients with a history of dyspnoea, cough and malaise, and ill-defined areas of consolidation on chest radiography, no aetiological factor was found. Lung biopsy revealed intra-alveolar buds of organizing fibrous tissue extending some way into the respiratory bronchioles. These patients responded rapidly to steroids with complete resolution of symptoms and radiological abnormalities. Davison grouped these cases together as a distinct entity and suggested the term cryptogenic organizing pneumonitis.

Two years later Epler reported a much larger series of patients with similar features (Epler et al, 1985). In this study 2000 open lung biopsies from the previous 30 years in which the term "bronchiolitis obliterans" appeared in the histological report were reviewed. 50 of these patients had a clinical picture similar to those in Davison's study and, again, no causative factor was identified. Histology was similar to the cases described by Davison with plugs of granulation tissue in the alveoli, alveolar ducts and respiratory bronchioles. This group of patients also responded to steroids, although it is noteworthy that they were labelled as having a pathological component of "bronchiolitis obliterans". Epler felt that a new description was needed to distinguish this condition from "pure" obliterative bronchiolitis in which the prognosis is often extremely poor: in a series of six patients with obliterative bronchiolitis five patients had died within 18 months despite steroid treatment (Geddes et al, 1977). Epler coined the term bronchiolitis obliterans organizing pneumonia, which has since been used by authors in the North American literature (Cordier et al, 1989; Guerry-Fore et al, 1987; Müller et al, 1990).

The terms BOOP and COP describes similar and probably identical clinico-pathological entities (du Bois & Geddes, 1991). BOOP may be the semantically correct term because the distal bronchioles are partially "obliterated" by granulation tissue but the mechanism of bronchiolar obliteration in patients with pure OB is completely different. In contrast to the pathological changes of BOOP and COP there is mucosal thickening in small airways (1–6 mm) with constriction, scarring and finally luminal obliteration; furthermore in oblitera-

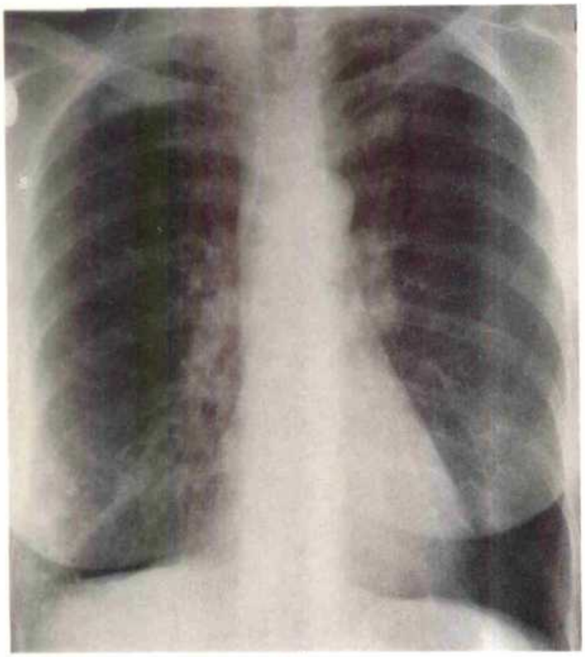

(a)

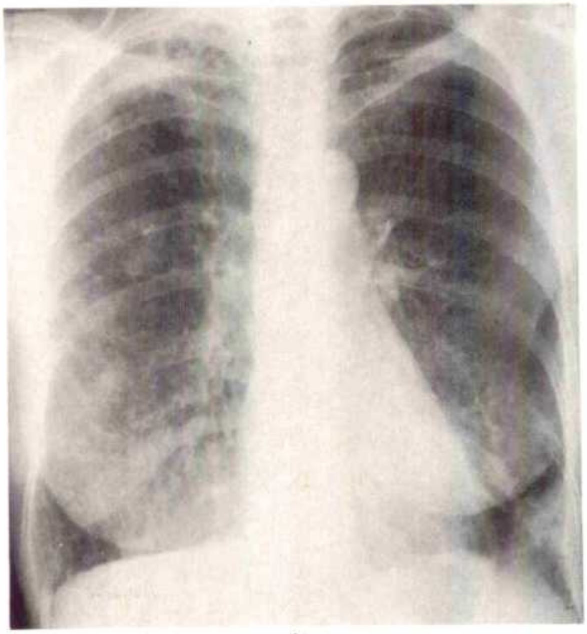

(b)

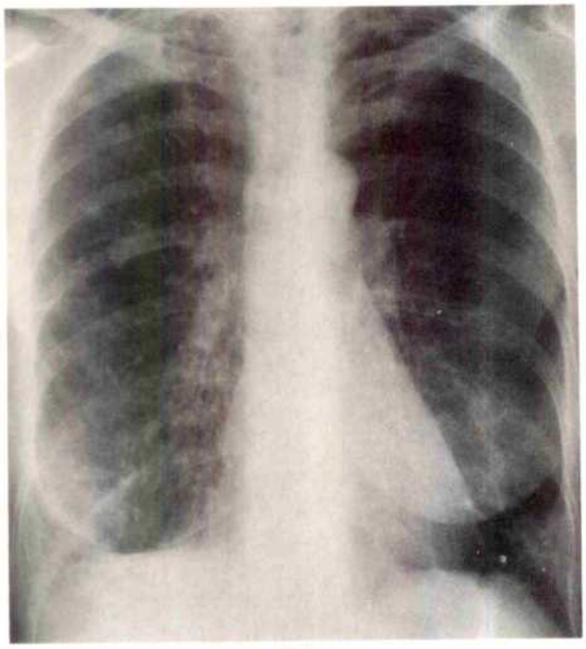

(c)

Figure 5. *Case 5.* (a) Peripheral consolidation at the right base and some poorly defined nodular (5–10 mm) shadowing in the mid and upper zones. (b) Some resolution of the right basal shadowing. The nodular shadowing in the mid and upper zones on the right is more pronounced. New consolidation at the left base (7 months after (a)). (c) Recurrence of consolidation at the right base with some clearing of the shadowing on the left (8 months after (a)).

tive bronchiolitis the alveoli and alveolar ducts are notably spared (Geddes et al, 1977). Although the name BOOP can be seen as an attempt to distinguish this condition from obliterative bronchiolitis, it may be considered a misleading term and the advice of Woodhead and du Bois is to use the term COP (Woodhead & du Bois, 1991). As Geddes points out, it is less fun to pronounce but makes the pathological distinction with greater clarity (Geddes, 1991).

Pathologically the findings in resolving infective pneumonia and COP are similar, although the clinical picture is different and it is likely that COP is yet another way that the lung responds to a variety of insults (Corrin, 1990). A definite aetiological factor remains elusive but various associations are recognized. An association with rheumatoid arthritis has been reported (Rees et al, 1991). Drugs including amiodarone, sulphasalazine, penicillamine and acebutolol have been implicated (Corrin, 1990). There is a single case report of a steroid-responsive organizing pneumonia in a patient with AIDS-related complex (Allen & Wevers, 1989). Ulcerative colitis may be associated (Swinburn et al, 1988) and an environmental agent may play a role as there have been reports of seasonal variations in the severity of the disease (Spiteri et al, 1990).

In this series the presenting symptoms and raised erythrocyte sedimentation rate (ESR) are similar to findings in previous series. The two patients with a normal ESR were already on steroids at the time of referral. Lung function showed a normal FEV_1/FVC ratio except in two patients; one of these was a smoker,

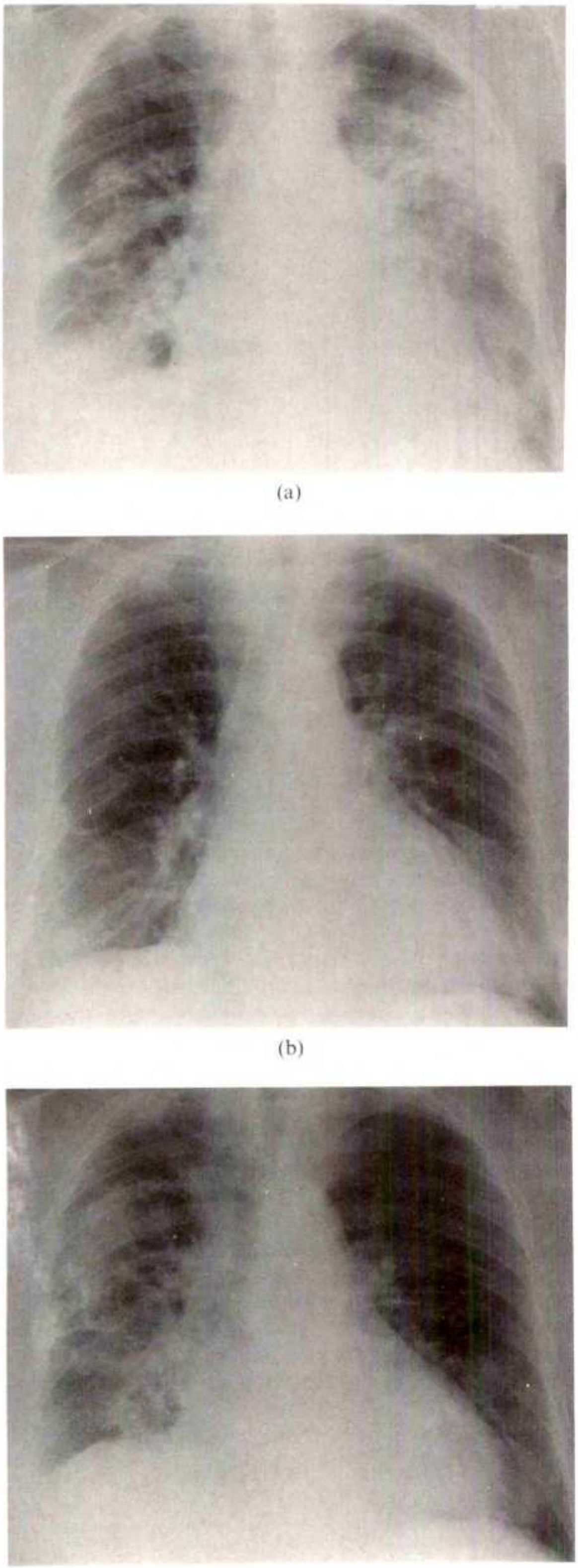

(a)

(b)

(c)

Figure 6. *Case 9.* (a) Bilateral dense consolidation. Right-sided pleural effusion and cardiomegaly: coexisting cardiac failure. (b) Following diuretic treatment, resolution of right pleural effusion. Subsequent steroid treatment also led to the resolution of the bilateral dense consolidation (1 month after (a)). (c) New dense consolidation in the right mid and upper zones (4 months after (a)).

the other was known to have irreversible airways obstruction before the episode of COP. DLCO was reduced in all but one patient. Lung function test results do not reveal a specific or uniform defect. Only one patient had an association that has been noted previously, ulcerative colitis, however patients with a connective tissue disease were deliberately excluded from our series. Some authors advocate open lung biopsy as the method of choice to achieve a definitive diagnosis rather than transbronchial biopsy with the inherent problems of "crush artefact" which can destroy the pathognomonic streams of granulation tissue. However, six of our patients were diagnosed from transbronchial specimens alone.

Radiographic changes within the group were similar with homogeneous mid- and lower-zone shadowing being the most common finding. A peripheral distribution has been noted previously in a CT study of BOOP (Müller et al, 1990) and this accords with our findings of a definite peripheral predominance in just over half of our cases. More than half of our patients had relapsing and changing shadows; it is striking that these may occur with or without treatment. The radiographic abnormalities are all non-specific, however, and may suggest an alternative diagnosis. Given the basal predominance of the changes, it is not surprising that three of the four patients referred to the Brompton arrived with an initial diagnosis of cryptogenic fibrosing alveolitis (CFA). Both COP and CFA are treated with steroids but the prognosis for CFA is very much worse; only 50% of patients are alive at 4.5 years (Turner-Warwick et al, 1980). The peripheral and changing nature of the shadows may be confused with pulmonary eosinophilia and indeed the fourth referral arrived with this diagnosis.

No previous long-term assessment of the radiological changes in COP has been made. In two cases follow-up may not have been sufficiently prolonged and the changes were consistent with a resolving organizing pneumonia. Three cases showed linear shadowing in areas where there had previously been areas of consolidation and these were interpreted as being due to limited fibrosis.

In conclusion, COP is a distinct clinico-pathological entity. In our series, patients presented with increasing dyspnoea, cough and malaise, and chest radiographs showed bilateral multifocal consolidation. Relapsing shadows and new changes may occur during the natural history of the condition or on steroid treatment. It has been suggested that the radiology of COP is too variable to be helpful but our series has demonstrated uniformity in many of the radiographic abnormalities. Although the final diagnosis is one of exclusion and requires histological confirmation, in the correct clinical context the radiographic features should raise the possibility of the diagnosis of COP. Patients responded well to steroids and usually progress to complete recovery although minimal radiographic changes may persist.

References

ALLEN, J. N. & WEVERS, M. D., 1989. HIV-associated bronchiolitis obliterans organizing pneumonia. *Chest, 96,* 197–198.

CORDIER, J. F., LOIRE, R. & BRUNE, J., 1989. Idiopathic bronchiolitis obliterans organizing pneumonia. *Chest, 96,* 999–1004.

CORRIN, B., 1990. *Systemic Pathology: The Lungs,* 3rd edn (Churchill Livingstone, Edinburgh), pp. 174, 210–211, 275.

DAVISON, A. G., HEARD, B. E., MCALLISTER, W. A. C. & TURNER-WARWICK, M. E. H., 1983. Cryptogenic organizing pneumonitis. *Quarterly Journal of Medicine, New Series Lii, 207,* 382–394.

DU BOIS, R. M. & GEDDES, D. M., 1991. Obliterative bronchiolitis, cryptogenic organizing pneumonitis and bronchiolitis organizing pneumonia: three names for two conditions. *European Respiratory Journal, 4,* 774–775.

EPLER, G. R., COLLOY, T. V., MCLOUD, T. C., CARRINGTON, C. B. & GAENSLER, E. A., 1985. Bronchiolitis obliterans organizing pneumonia. *New England Journal of Medicine, 312* (3), 152–158.

GEDDES, D. M., 1991. BOOP and COP. *Thorax, 46,* 545–547.

GEDDES, D. M., CORRIN, B., BREWERTON, D. A., DAVIES, R. J. & TURNER-WARWICK, M., 1977. Progressive airway obliteration in adults and its association with rheumatoid disease. *Quarterly Journal of Medicine, New Series XLVI, 184,* 427–444.

GUERRY-FORE, M. L., MÜLLER, N. L., WRIGHT, J. L., WIGGS, B., COPPIE, C., PARE, P. D., et al, 1987. A comparison of bronchiolitis obliterans with organizing pneumonia, usual interstitial pneumonitis and small airways disease. *American Review of Respiratory Diseases, 135,* 705–712.

MÜLLER, N. L., STAPLES, C. A. & MILLER, R. R., 1990. Bronchillitis obliterans organizing pneumonia: CT features in 14 patients. *American Journal of Roentgenology, 154,* 983–987.

REES, J. H., WOODHEAD, M. A., SHEPPARD, M. N. & DU BOIS, R. M., 1991. Rheumatoid arthritis and cryptogenic organizing pneumonitis. *Respiratory Medicine, 85,* 243–246.

SPITERI, M. A., KLENERMAN, P., SHEPPARD, M., PADLEY, S., CLARK, T. & NEWMAN-TAYLOR, A., 1990. Seasonal cryptogenic organizing pneumonia with intra-hepatic cholestasis: a new clinical entity. *Thorax, 46*(4), 313P.

SWINBURN, C. R., JACKSON, G. J., COBDEN, I., ASHCROFT, T., MORRIT, G. N. & CORRIS, P. A., 1988. Bronchiolitis obliterans organizing pneumonia in a patient with ulcerative colitis. *Thorax, 43,* 735–736.

TURNER-WARWICK, M. E. H., BURROWS, B. & JOHNSON, A., 1980. Cryptogenic fibrosing alveolitis: clinical features and their influence on survival. *Thorax, 35,* 171–180.

WOODHEAD, M. A. & DU BOIS, R. M., 1991. Bronchiolitis obliterans, cryptogenic organizing pneumonitis and BOOP. *Respiratory Medicine, 85,* 177–178.

1992, *The British Journal of Radiology*, *65*, 681–685

The radiological imaging of bronchial atresia

By D. Kinsella, FRCR, *G Sissons, FRCR and M. P. Williams, FRCR

Departments of Radiology, Derriford Hospital, Plymouth and *University Hospital of Wales, Cardiff, UK

(*Received 4 November 1991 and in revised form 3 February 1992, accepted 6 March 1992*)

Keywords: Bronchial atresia

Abstract. The clinical and radiological findings in three cases of bronchial atresia are presented. Bronchial atresia has a characteristic plain radiographic appearance in the majority of cases. Computed tomography may be required to confirm the diagnosis. The condition often presents to the radiologist as an incidental finding on the chest radiograph in a patient undergoing investigation for an unrelated problem.

Bronchial atresia is a rare, congenital anomaly characterized by the presence of a bronchocoele with distal hyperinflation. There is no communication between the bronchocoele and the main bronchial tree. The true incidence is uncertain as some patients are asymptomatic.

We present three cases of bronchial atresia and review the literature on this subject with emphasis on the clinical and radiological features.

Case reports

Case 1

A 14-year-old boy presented to his general practitioner following several episodes of left-sided pleuritic chest pain. Examination revealed decreased air entry on the left. A chest radiograph showed a hyperinflated left lower lobe with air-trapping on expiration (Fig. 1). A branching opacity could be seen within the hyperinflated area. Bronchoscopy was normal. Computed tomography (CT) confirmed the radiographic findings (Fig. 2). At thoracotomy the left lower lobe was excised. Examination of the specimen confirmed the diagnosis of bronchial atresia, which involved the posterior basal segment (Fig. 3).

Case 2

A 55-year-old male smoker presented with increasing breathlessness on exertion. On examination there was reduced air entry at the right base. The chest radiograph showed an area of hyperlucency in the right lower zone with an associated branching structure (Fig. 4). The patient was lost to follow-up for 8 years. He re-presented with increasing dyspnoea. A chest radiograph at this time showed expansion of the area of hyperlucency to fill the whole of the right hemithorax. A CT scan confirmed that the branching structure did not contact with the right hilum. The right lower lobe was excised and the specimen demonstrated atresia of the apical segmental bronchus.

Case 3

A 25-year-old man presented with a history of blackouts for which no cause was found. During investigation a chest radiograph revealed an ovoid density above the left hilum and increased radiolucency in the left upper zone (Fig. 5). Branching structures arising from the mass were clearly seen on plain tomography and a provisional diagnosis of a vascular malformation was made (Fig. 6). Pulmonary arteriograpy showed that the mass was avascular and that there was absent perfusion in the left upper lobe (Fig. 7). A CT scan demonstrated the branching nature of the mass (Fig. 8). There was no evidence of enhancement following administration of intravenous contrast medium (mean attenuation 15 HU). Magnetic resonance imaging was also performed. The bronchocoele was shown to have a moderate signal intensity on the T_1-weighted scan (Fig. 9).

Discussion

Bronchial atresia was first described in 1953 by Ramsay (Ramsay, 1953). Since then, a total of 93 cases have been reported in the world literature (Aalbers et al, 1987; Cohen et al, 1980; Finck & Milne, 1988; Fusonie & Molnar, 1966; Jederlinic et al, 1987; Lau et al, 1987; Simon & Reid, 1963). Most cases have been of young adults. However, the age range is wide and includes a stillborn infant (Bucher & Reid, 1961) and a 66-year-old man (Aalbers et al, 1987). Males predominate by a ratio of 2 : 1. Most of the patients did not have any respiratory symptoms and the diagnosis of bronchial atresia was an incidental finding (as in Case 3). In the remaining 42%, recurrent chest infections, cough and dyspnoea were the most common symptoms. Chest pain is a very uncommon presentation and may have been incidental in our first case. In older patients, as in Case 2, cough and dyspnoea are often secondary to chronic airways disease. The CT scan in this patient did show widespread emphysema, but it is likely that the symp-

---

*Address correspondence to Dr D. Kinsella, Department of Clinical Radiology, Bristol Royal Infirmary, Marlborough Street, Bristol BS2 8HW, UK.

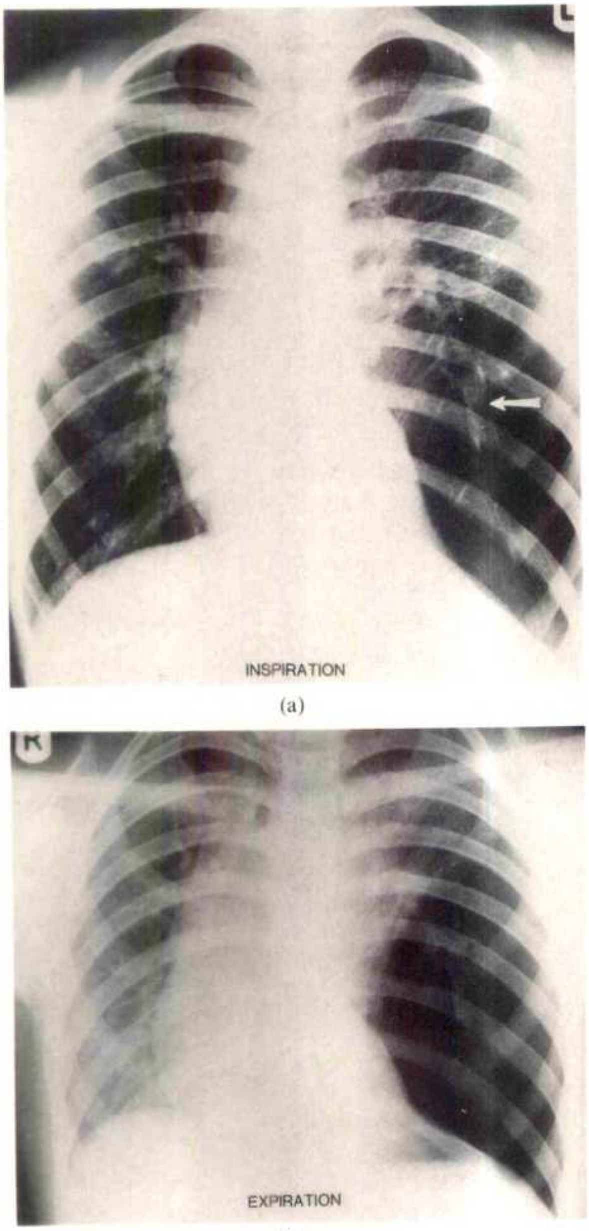

(a)

(b)

Figure 1. (a) Inspiratory chest radiograph of Case 1 showing left lower zone hyperinflation and a bronchocoele (arrow). (b) Expiratory radiograph showing air trapping.

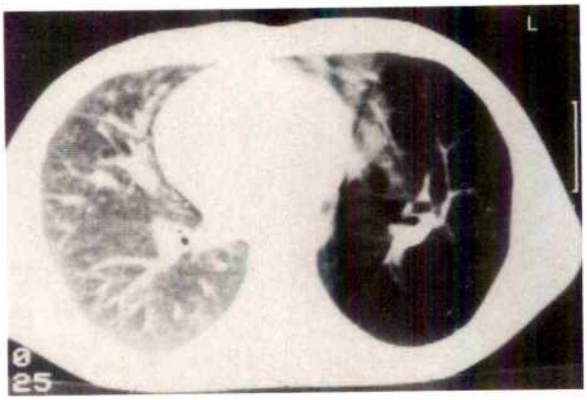

Figure 2. CT scan at a level below the hilum, demonstrating the mass effect of the hyperinflated segment and a fluid level within the bronchocoele.

toms were exacerbated by the compressive effect of the hyperinflated segment. Respiratory embarrassment resulting from the mass effect of the hyperinflated segment can be particularly severe in infancy (Warner et al, 1982). On examination, the only common physical sign is that of reduced air entry over the abnormal segment.

Although bronchial atresia usually involves a segmental bronchus, atresia of a lobar bronchus may rarely occur (Waddell et al, 1965). The segmental bronchi to the left upper lobe are involved in 64% of cases, followed by the left lower lobe in 14% of cases. Involvement of the right lower or middle lobes is seen in only 8% of patients. This predilection for the left lung

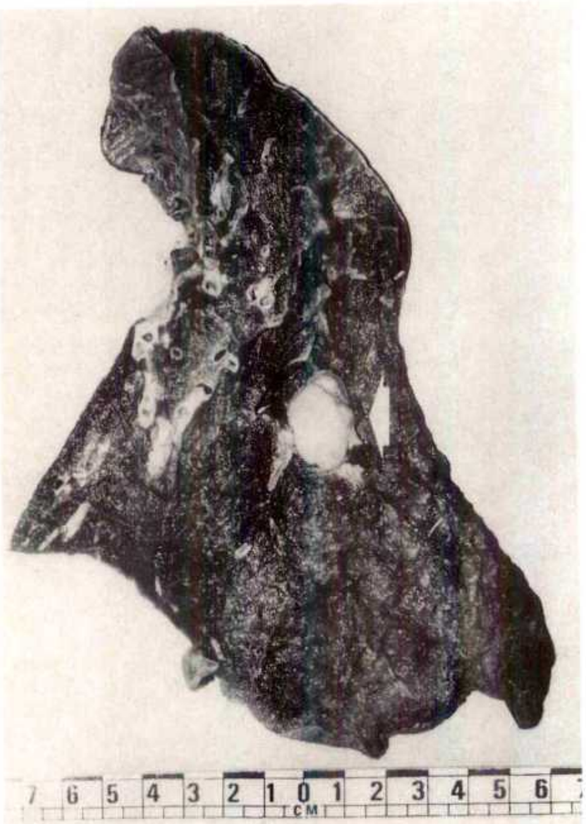

Figure 3. The resected left lower lobe specimen of Case 1. The mucus plug within the bronchocoele is clearly seen (arrow).

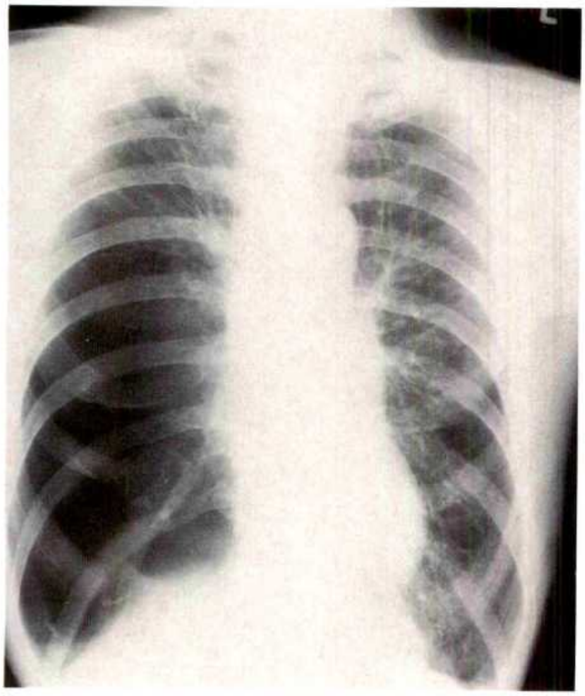

Figure 4. Chest radiograph of Case 2 showing right lower zone hyperinflation with an associated bronchocoele.

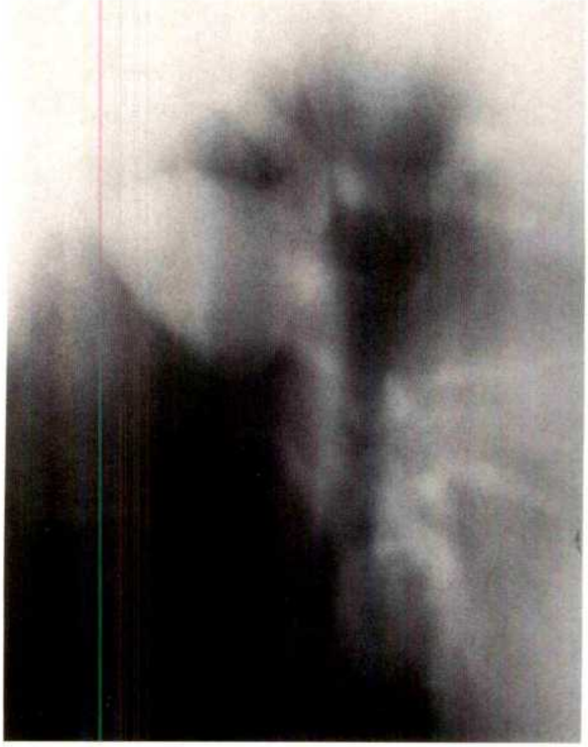

Figure 6. Conventional tomography in an oblique sagittal plane demonstrates the branching nature of the mass.

is shared by other congenital anomalies including agenesis, hypoplasia and sequestration (although other congenital abnormalities, such as scimitar syndrome and oesophageal lung, are commoner on the right). Bronchial atresia has been reported to co-exist with pulmonary sequestration and cystic adenomatoid malformation of the lung (Demos & Teresi, 1975). It has been suggested that some cases of bronchial atresia have been misdiagnosed as congenital lobar emphysema (Schuster et al, 1978).

The aetiology of bronchial atresia is unknown. It most probably occurs as a result of a vascular insult

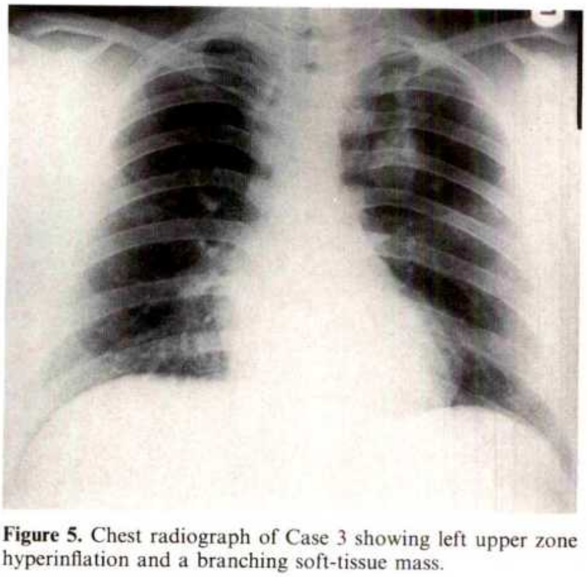

Figure 5. Chest radiograph of Case 3 showing left upper zone hyperinflation and a branching soft-tissue mass.

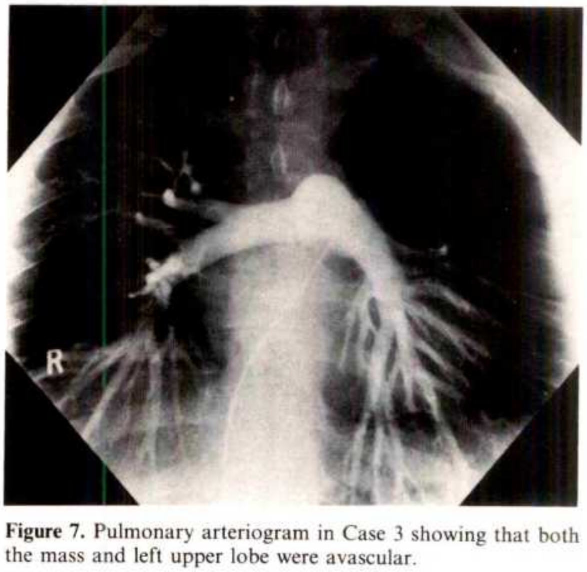

Figure 7. Pulmonary arteriogram in Case 3 showing that both the mass and left upper lobe were avascular.

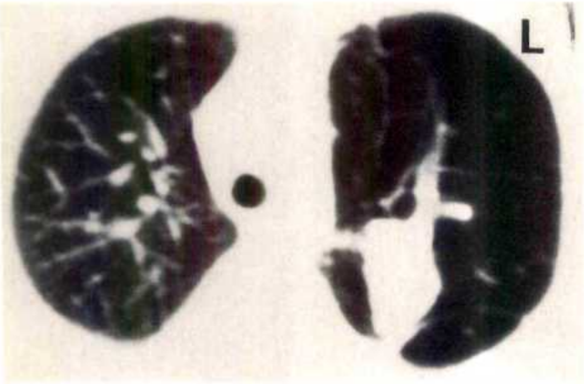

Figure 8. CT scan showing the branching nature of the mass.

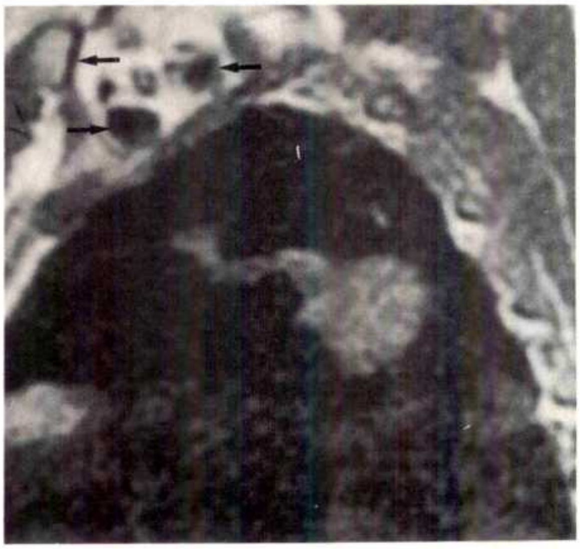

Figure 9. A T_1-weighted (TR 500 ms, TE 25 ms) sagittal MR image. The bronchocoele has a signal intensity greater than that of muscle. Note the signal voids resulting from flowing blood in the mediastinal vessels (arrows).

occurring *in utero*, at approximately 16 weeks gestation. The bronchi distal to the site of atresia develop normally (Curry & Curry, 1966). They have a normal epithelium containing functioning goblet cells. The secreted mucus collects in the closed system and a bronchocoele develops. Aeration of the segment occurs by collateral air drift via the pores of Kohn and the channels of Lambert (Lambert, 1955). The air trapping and resultant hyperinflation may result from the collateral channels acting as check valves (Culiner, 1964). Alternatively, this may result from the smaller alveoli of the normal lung being under higher pressure than the overexpanded alveoli of the abnormal segment, as predicted by Laplace's law.

In up to 75% of the reported cases, both a bronchocoele and a localized area of hyperinflation were visible on the chest radiograph. A bronchocoele can develop as early as 6 days after birth (Oh et al, 1976). Alternatively, mucus accumulation may not become apparent until the third decade (Jederlinic et al, 1987). The bronchocoele may be round, ovoid or branching and may contain an air–fluid level. In a case followed from birth, aeration of the affected segment had occurred by the sixth day (Robotham et al, 1980). Initially in the neonatal period the abnormal segment is fluid-filled (Schuster et al, 1978).

Conventional tomography can be used to define the morphology of the bronchocoele more accurately; however, CT is the diagnostic procedure of choice. CT scanning can demonstrate the lack of communication between the bronchocoele and the hilum and show small bronchocoeles not seen on the plain radiograph. It is more sensitive in the demonstration of segmental hyperinflation and associated mass effect. The mucoid material has a CT number ranging from -5 to $+20$ HU, depending on the degree of inspissation. A dynamic CT scan can be used if required to exclude a vascular anomaly, making pulmonary angiography unnecessary. Depending on the lie of the bronchocoele, the probable site of atresia can be predicted by the CT scan (Lau et al, 1987). However, distortion and displacement of surrounding structures by the hyperinflated segment prevents this in many cases, particularly if the atresia involves the lower lobes.

Lung scintigraphy may show either delayed or absent ventilation in the affected segment with markedly reduced perfusion. Owing to the advantages of CT scanning, more invasive investigational techniques are rarely required. Bronchography can demonstrate nonfilling of the affected bronchus but interpretation is difficult because of distortion of the bronchial tree. Rarely, a short bronchial stump is seen (Lau et al, 1987). Bronchoscopy is only performed if an endobronchial lesion is suspected, particularly in the older age group. Angiography may be required to exclude other possible diagnoses such as sequestration or vascular malformation.

Magnetic resonance imaging has been described in one other case of bronchial atresia (Finck & Milne, 1988). This technique can clearly demonstrate the branching nature of the bronchocoele. Also, the presence of a moderately intense signal within the bronchocoele excludes the presence of rapidly flowing blood. However, such a signal could be produced by a completely thrombosed vascular malformation. A vascular malformation would not be expected to produce an area of distal hyperinflation. This sign cannot be detected on the MR images. CT is very accurate in defining areas of hyperinflation and should therefore be the preferred confirmatory imaging study when performed before and during injection of contrast medium.

The management of patients with bronchial atresia is variable. In children, surgery is recommended to allow the normal development of the surrounding lung. In adults, surgery is reserved for symptomatic patients

(Meng et al, 1978). Owing to the effect of previous infections and irreversible hyperinflation, over 50% of the treated patients undergo a lobectomy rather than a segmentectomy. In older patients with concomitant generalized chronic lung disease, CT scanning can accurately assess the degree of parenchymal disease and thus influence surgery.

In summary, awareness of this rare condition allows the diagnosis of bronchial atresia to be made on the plain radiagraph alone in the majority of cases. This is important, as bronchial atresia often presents as an incidental finding. CT is the most sensitive imaging technique for confirmation of the diagnosis.

References

AALBERS, R., POSTMUS P. E. & JAGT, E. J., 1987. Congenital bronchial atresia in a 66 year old man. *European Journal of Respiratory Diseases*, *71*, 127–129.

BUCHER, U. & REID, L., 1961. Development of the intrasegmental bronchial tree: the pattern of branching and the development of cartilage at various stages of intra-uterine life. *Thorax*, *16*, 207–218.

COHEN, B. M., SOLOMAN, E. A. & AEFIDI, R. J., 1980. Computed tomography in bronchial atresia. *American Journal of Roentgenology*, *135*, 1097–1099.

CULINER, M. D., 1964. Collateral ventilation and the hyperlucent lung. *American Journal of Medicine*, *36*, 395–403.

CURRY, T. S. & CURRY, G. C., 1966. Atresia of the bronchus to the apical-posterior segment of the left upper lobe. *American Journal of Roentgenology*, *98*, 350–353.

DEMOS, N. J. & TERESI, A., 1975. Cogenital lung malformations. *Journal of Thoracic and Cardiovascular Surgery*, *10*, 260–264.

FINCK, S. & MILNE, E. N. C., 1988. A case report of segmental bronchial atresia—radiological evaluation including CT and MRI. *Journal of Thoracic Imaging*, *3*, 53–58.

FUSONIE, D. & MOLNAR, W., 1966. Anomalous pulmonary venous return, pulmonary sequestration, bronchial atresia, aplastic right upper lobe, pericardial defect and intrathoracic kidney. *American Journal of Roentgenology*, *97*, 350–354.

JEDERLINIC, P. J., SICILIAN, L. S., BAIGELMAN, W. & EAENSLER, E. A., 1987. Congenital bronchial atresia: a report of 4 cases and a review of the literature. *Medicine (Baltimore)*, *65*, 73–83.

LAMBERT, M. W., 1955. Accessory bronchial-alveolar communications. *Journal of Pathology and Bacteriology*, *70*, 311–314.

LAU, L., SIMPSON, L. & STREETON, J., 1987. The radiology of bronchial atresia—radiographic, CT and bronchographic correlation. *Australasian Radiology*, *31*, 29–33.

MENG, R. L., JENSIK, R. J., FABER, L. P., MATHEW, G. R. & KITTLE, C. F., 1987. Bronchial atresia. *Annals of Thoracic Surgery*, *25*, 184–192.

OH, K.S., DORST, J. P., WHITE, J. J., HALLER, J. A., JOHNSON, B. A. & BYRNE, W. D., 1976. The syndrome of bronchial atresia or stenosis with mucocele and focal hyperinflation of the lung. *John Hopkins Medical Journal*, *138*, 48–53.

RAMSAY, R. H., 1953. Mucocoele of the lung due to congenital obstruction of a segmental bronchus. *Diseases of the Chest*, *24*, 96–103.

ROBOTHAM, J. L., MENHES, H. A., CHIPPS, B. E., INNERS, C. R., ALDERSON, P. & HUTCHINS, G. M., 1980. A physiologic assessment of bronchial atresia. *American Review of Respiratory Diseases*, *121*, 533–540.

SCHUSTER, S. R., CARRIS, G. B. C., WILLIAMS, A., KIRKPATRICK, J. & REID, L., 1978. Bronchial atresia: a recognisable entity in the paediatric age group. *Journal of Paediatric Surgery*, *13*, 682–689.

SIMON, G. & REID, L., 1963. Atresia of an apical bronchus of the left upper lobe—a report of three cases. *British Journal of Diseases of the Chest*, *76*, 126–132.

WADDELL, J. A., SIMON, G. & REID, L., 1965. Bronchial atresia of the left upper lobe. *Thorax*, *20*, 214–218.

WARNER, J. O., RUBIN, S. & HEARD, B. E., 1982. Congenital lobar emphysema: a case with bronchial atresia and abnormal bronchial cartilages. *British Journal of Diseases of the Chest*, *76*, 177–184.

1992, *The British Journal of Radiology*, 65, 686–690

An alternative approach to contrast-detail testing of X-ray image intensifier systems

By C. J. Kotre, MSc, ACGI, N. W. Marshall, BSc, ARCS, and K. Faulkner, PhD, ARCS

Regional Medical Physics Department, Newcastle General Hospital, Newcastle-upon-Tyne NE4 6BE, UK

(Received 26 June 1991 and in revised form 14 November 1991, accepted 14 January 1992)

Keywords: Fluoroscopy, Image quality, Quality assurance

Abstract. The difficulties of making the results of threshold contrast-detail diameter tests on X-ray image intensifier systems consistent with published performance standards are discussed. The current approach to contrast-detail testing is described and an alternative method intended to give greater consistency for all image intensifier input field diameters proposed. The current and alternative test conditions are compared on two image intensifier systems. The results obtained show that the contrast-detail curves for image intensifier systems with a wide range of input field diameters can be effectively normalized to be directly comparable to a common reference standard by applying the proposed alternative test conditions. The implications of this result on the interpretation of the contrast-detail test are discussed.

Threshold contrast-detail diameter test objects (specifically the "Leeds" test objects) have been a valuable tool for the non-invasive assessment of the image quality of X-ray image intensifier/TV systems since their introduction in the early 1960s (Hay, 1964). Although intended to provide the means for performing serial quality assurance measurements on individual systems, the use of these test objects has often been extended to the distinctly separate task of making measurements of image quality over a wide range of systems. This extension of function, although discouraged in the instructions supplied with the Leeds test objects (Hay et al, 1979), has been necessitated by the need to provide assessments of image quality as part of the acceptance/commissioning tests on new image intensifiers (HPA, 1981; DHSS, 1982; Henshaw, 1989) and to give advice on the replacement of old ones.

The current approach adopted to assess image quality in these situations is to perform contrast-detail tests at pre-determined dose rates, X-ray beam quality and viewing conditions, and to make a comparison between the resulting contrast-detail curves and one of a number of standard curves obtained from surveys of well maintained equipment. The Department of Health and Social Security (now Department of Health) document STB/7/82 (DHSS, 1982) shows the results of two such surveys (for intensifiers with 22–25 cm input field diameters), one for new equipment and one for equipment of average age 5 years, both at an input dose-rate of 0.26 μGy/s. It recommends that the performance level described by the latter curve be used as a reasonable guideline for the performance of new image intensifier systems. This advice was repeated in the subsequent second (1985) and third (1986) editions of this document together with an additional section concerning the application of the Leeds test objects to image intensifiers with larger input field diameters (up to 35 cm) than the 25 cm diameter maximum for which the objects were originally designed. The dose rates recommended for these larger field diameters are, however, manufacturer-dependent and no expected performance curve for these larger intensifiers is given. The document also includes the recommendation from a group of equipment manufacturers that, where performance assessments of larger input field diameter intensifiers are to be performed, the magnified field giving the closest to a 23 cm effective input field diameter should be used for comparison with the standard survey result. This approach, however, does not solve the problem of comparing the performances of systems whose maximum field diameters are less than 23 cm. A curve describing the average performance of smaller field-of-view image intensifiers at 0.87 μGy/s has been published in the Leeds test objects instruction manual, and this is often used as a guideline for acceptable performance of these smaller diameter systems, although the DHSS documents do not recommend this. The Hospital Physicists' Association publication TGR32 (HPA, 1981) gives a range of typical results for input dose-rates of 0.26 μGy/s and 0.87 μGy/s but does not state for what input field diameter the results apply.

The present approach to contrast-detail testing

The approach to contrast-detail testing embodied in the design and instructions for use of the Leeds test objects is to test the image intensifier system under viewing conditions similar to those used by the radiologist in the clinical situation and at clinically realistic dose-rates. When most X-ray image intensifiers were either of single-field 15 cm or dual-field 23/12 cm designs, it was possible to deal with most equipment encountered in two categories: input field diameters of 23–25 cm tested at 0.26 μGy/s, and 12–15 cm tested at 0.87 μGy/s. The recommended viewing distance for both categories is four times the diameter of the TV monitor display. At this distance the visual bias of the observer is expected to be similar to that operating in clinical practice. Cowan et al (1987) suggest that this is an advantage of the conventional test protocol, but while this may be so when the desired result is a simulation of clinical conditions, it will be shown that where the desired result is a quantitative measurement of performance, variations in visual bias with input field diameter can produce misleading results.

The limitations of the present approach emerge when attempts are made to compare the results obtained with the DHSS reference standard. Such comparisons are invalid unless the same test conditions (input field diameter of 23 cm and input dose-rate of 0.26 μGy/s) have been used.

An alternative approach

If the rationale behind the choice of test conditions is altered from an attempt to simulate clinical conditions to an attempt to obtain a quantitative measurement of image intensifier/TV performance, an alternative test protocol can be formulated. Under this protocol it is proposed that the input dose-rate and the visual parameters affecting the observer's ability to detect the test details in noise are maintained constant for all input field diameters. This offers the advantage that the results can be compared directly with the DHSS guideline, but suffers from the disadvantage that the dose-rate used for the test may be different from that being used in clinical practice. Thus, if the constrast-detail measurement is intended to form part of a quality assurance programme, the conventional test protocol should be used at clinically realistic dose-rates.

The X-ray quantum noise present in the image is governed by the dose-rate at the intensifier input plane. To make this comparable to the DHSS guideline it should be set to 0.26 μGy/s. Since the gain of an image intensifier is directly proportional to the ratio of its input and output phosphor areas, an implication of the use of a fixed dose-rate for all intensifiers is that the automatic gain control of the video system must be capable of maintaining the image brightness and video modulation at this dose-rate without increasing the contribution of electronic noise to the extent that the quantum noise no longer dominates.

To minimize variations in the psycho-optical parameters involved in the contrast-detail detection task, the critical variable to be considered is the viewing distance. Other important factors include the ambient room lighting and TV monitor contrast and brightness adjustment. These should, however, be reasonably constant for the task of contrast-detail testing where the room lighting is normally dimmed in line with clinical practice and the TV monitor controls are pre-set using the Leeds grey-scale test object GS1. (The appearance of the GS1 image at 0.26 μGy/s can also be used to establish that the dynamic range of the automatic video gain system has not been exceeded.)

As the viewing distance is changed, the threshold contrast for various sized details will also change. In general, for large diameter details, the threshold contrast decreases with viewing distance as spatial averaging over the sampling aperture of the observer acts to reduce the perceived level of noise, but for small diameter details, the threshold contrast increases with viewing distance owing to the decreasing ability of the eye to resolve them. There is, therefore, no single viewing distance that is optimal for all detail sizes. It is important, however, that a fixed proportionality between the displayed size of the test object and the viewing distance is maintained so that the psycho-optical bias inherent in the contrast-detail test is also kept constant. The conventional viewing distance of four times the diameter of the TV display was originally chosen so that a 625-line TV raster is just not perceptible to a person with normal eyesight (Hay et al, 1985) but this restriction is probably now less important because of improvements in TV monitor design and the increasing use of high-resolution 1000-line TV systems. Whilst the limit of visibility of TV raster lines with distance has been investigated (Siedband, 1981) it is not clear that their perception or otherwise has a significant effect on the detection of low-contrast disks in noise.

The display magnification (*i.e.* the magnification factor between the size of the image displayed on the TV monitor and the original size of the object) and TV screen diameter reported (DHSS, 1981) for a new GEC Kompact 9/5 intensifier/TV system, typical of the equipment on which the 1982 DHSS guideline survey was originally performed, were used to establish a suitable standard viewing distance. The reported display magnification measured at the centre of the 23 cm field (1.025 : 1) was related to the conventionally recommended viewing distance of four times the display circle diameter (23 cm) to establish a standard viewing distance for an unmagnified display of 90 cm. The procedure for setting the viewing distance is therefore to measure the display magnification for the field size under test and multiply this factor by 90 cm. The display magnification can be obtained by measuring the distance on the TV monitor screen across a suitable number of squares on the Leeds M1 matrix test object and dividing by the actual distance as defined by the object. This method of setting the viewing distance has the additional advantage that any geometrical scaling caused by the test object not being at the image intensifier input plane will be automatically corrected for.

Experimental measurements

Threshold contrast-detail diameter tests with the Leeds test objects N3 and TO10 were carried out on two new image intensifer/TV systems to compare the conventional test protocol with the alternative protocol proposed above. In all cases a measured tube potential of 70 kVp and an additional filtration of 1 mm of copper were used. These parameters cannot be altered without invalidating the calibration of the contrasts given by the test object. The systems had input field diameters of 30, 23 and 17 cm and 36, 25 and 15 cm. In each case visual assessments of the contrast-detail test objects were made by two experienced observers.

To test the assumption that the threshold contrast is quantum noise dominated at the proposed standard dose rate of 0.26 μGy/s over a range of intensifier sizes, threshold contrast was measured using the N3 test object over a range of input dose-rates for all field sizes on the two systems. The viewing distance was set in proportion to the display magnification as described above. To compare the contrast-detail results obtained using the conventional and alternative test protocols, the TO10 test object was used with all field sizes on the two systems at a constant input dose-rate of 0.26 μGy/s both with fixed viewing distance and with viewing distance proportional to the display magnification.

In addition, measurements of limiting spatial resolution for each field size were made using a Huttner type 18 test pattern placed at 45° to the direction of the TV raster lines and viewed from close range. Low tube voltage and high tube current were used to produce a high-contrast, low-noise image for this test.

Results

Figure 1 shows the change in threshold contrast with input dose-rate for 11.1 mm diameter details. The figures show individual threshold contrast measurements for the three field sizes on each intensifier as symbols, and a curve fitted to the mean of the three

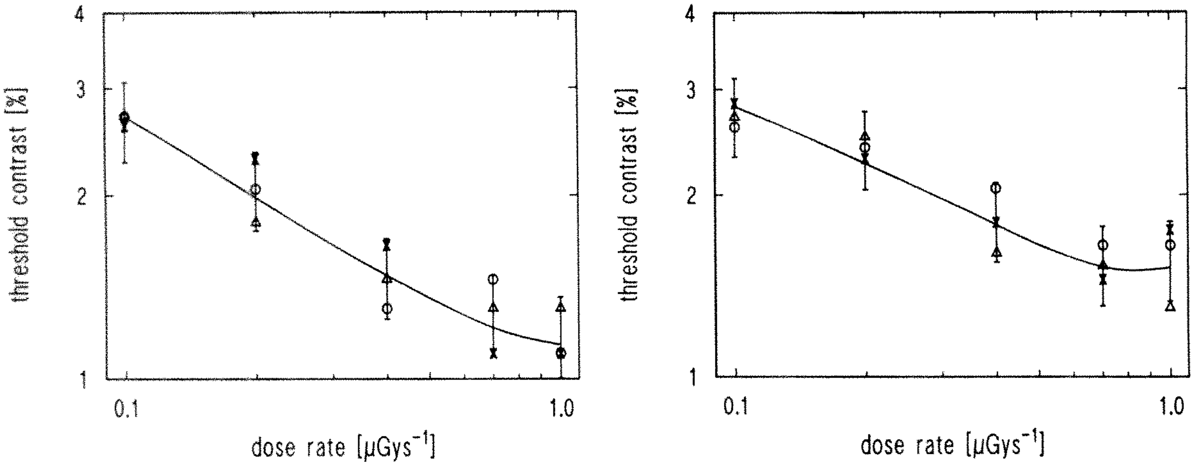

(a)

(b)

Figure 1. Threshold contrasts measured using the N3 test object over a range of input dose-rates for 30 (×), 23 (○) and 17 (△) cm input field diameters (a) and 36 (×), 25 (○) and 15 (△) cm input field diameters (b) of two image intensifier systems tested using viewing distances proportional to the display magnification.

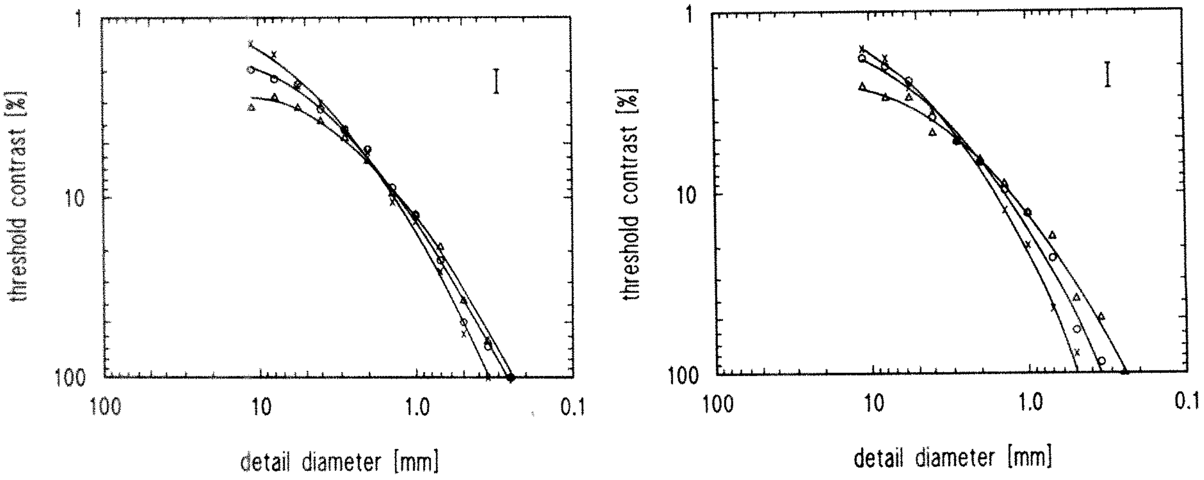

(a)

(b)

Figure 2. Contrast-detail curves for 30 (×), 23 (○) and 17 (△) cm input field diameters (a) and 36 (×), 25 (○) and 15 (△) cm input field diameters (b) of two image intensifier systems tested using the conventional test approach. The example error bar represents a range of ±1 standard deviation.

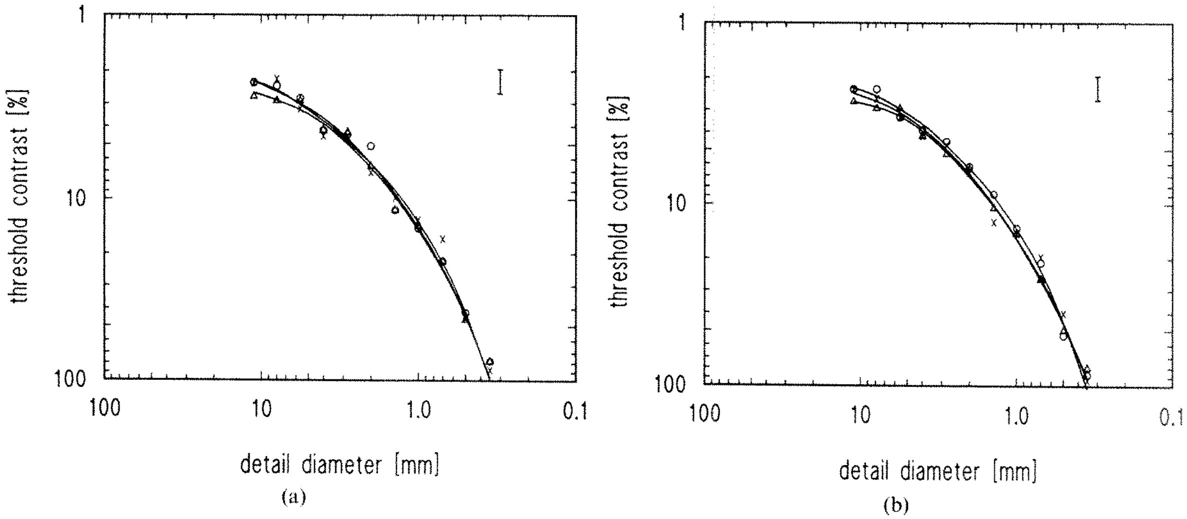

Figure 3. Contrast-detail curves for the same two systems and field sizes as Fig. 2, *i.e.* 30 (×), 23 (○) and 17 (△) cm input field diameters (a) and 36 (×), 25 (○) and 15 (△) cm input field diameters (b), but tested using the alternative approach described in this paper. The example error bar represents a range of ±1 standard deviation.

measurements at each dose-rate. The error bars represent a range of ±1 standard deviation from the mean assuming a relative standard deviation of 0.15 (Hay et al (1985) quote a relative standard deviation of the order of 0.1 to 0.2). The experimental points lie within this error range except for the highest dose rate in Fig. 1b where the image was starting to saturate. Both systems exhibit threshold contrast performance consistent with quantum noise domination up to about 0.7 μGy/s.

Figures 2a and 2b show the contrast-detail curves obtained under the conventional test conditions for the two image intensifiers. Figures 3a and 3b show the results using the alternative test conditions. The results of the limiting spatial resolution measurements are given in Table I. In Fig. 2, the contrast-detail curves for both systems would seem to be consistent with each field size having a different level of performance, with the largest input field being superior at large detail sizes, and the smallest input field being superior at small detail sizes. Such a marked change in low-contrast performance between field sizes would seem to be unlikely since the signal-to-noise ratio for a constant dose-rate should be similar for all field sizes on the same image intensifier at dose-rates where quantum noise dominates. When the visual bias of the observer is kept constant the resulting contrast-detail curves show an effectively identical performance for all field sizes (Fig. 3).

Table I. Measured limiting spatial resolutions

30 cm diameter system		36 cm diamater system	
Input field diameter (cm)	Limiting resolution (lp/mm)	Input field diameter (cm)	Limiting resolution (lp/mm)
30	1.3	36	1.3
23	1.6	25	1.6
17	2.0	15	2.2

Since the dose-rate and relation between viewing distance and display magnification have been set to be in agreement with those typically operative for the DHSS reference performance survey, the results for any size of image intensifier should be directly comparable to the reference standard using this approach.

Discussion

The limiting spatial resolution of an image intensifier/TV system is directly related to the system point spread function (PSF), which is a combination of the individual PSFs of the components of the system. The major contributions to the system PSF are normally made by the TV camera tube and monitor, which therefore limit the spatial resolution of the system (DHSS, 1982). The PSF of the TV system is unchanged for magnified fields, so it might be expected that changing the viewing distance in proportion to the magnification would alter the shape of the contrast-detail curves simply because a closer observer will perceive the system PSF as being wider. Since the shape of the normalized contrast-detail curves are not significantly changed over a wide range of field sizes (Fig. 3), it can be concluded that the shape of the contrast-detail curve is only weakly affected by the resolution of the system. This conclusion is reinforced by the limiting spatial resolution results (Table I), which show that there was a difference in the limiting spatial resolution measured for the various field sizes that was not picked up by the contrast-detail test when the bias of the visual system was maintained constant. Hay et al (1985) have shown the contrast-detail test to be affected by system defocusing for limiting spatial resolutions in the range 0.375–1.45 line-pairs/mm, but the results of Fig. 3 suggest that, for the higher resolutions typical of modern multifield intensifier/TV systems, the sampling aperture of the observer can be dominant over the PSF of the system under test.

Conclusion

It has been demonstrated that the contrast-detail curves for image intensifiers with widely differing input field diameters can be normalized to be directly comparable to a common reference standard by maintaining constant the visual bias of the observer. This is achieved by using test conditions under which the input dose-rate and the relation between the magnification of the displayed image and the viewing distance are held constant.

A comparison of contrast-detail curves measured under the conventional and alternative test conditions shows that features of the curves usually taken as being indicative of differences in the limiting spatial resolution of the system do not appear when changes in the visual bias of the observer are minimized.

Acknowledgments

We would like to thank Dr R. M. Harrison for his comments on the manuscript and Professor K. Boddy for his support and encouragement. This work was partially funded by the European Communities Radiation Protection Programme, contract number B17-0014.

References

COWAN, A. R., HAYWOOD, J. M., WORKMAN, A. & CLARKE, O. F., 1987. A set of X-ray test objects for image quality control in digital subtraction fluorography. 1: Design considerations. *British Journal of Radiology*, *60*, 1001–1009.

DHSS, 1981. *Leeds and Kcare Assessment of the GEC Kompact 9 HD Series 2 Image Intensifier System*. Scientific and Technical Branch Report STB/12/81 (Department of Health, London).

——1982 (2nd edn 1985, 3rd edn 1986). *The Testing of Image Intensifier–Television Systems*. Working Group Report STB/7/82 (Department of Health, London).

HAY, G. A., 1964. A physical assessment of the cinelix electro-optical image intensifier in television fluoroscopy. *Radiology*, *83*, 86–91.

HAY, G. A., CLARKE, O. F., COLEMAN, N. J., COWAN, A. R. & CRAVEN, D. M., 1979. Instructions for the use of the Leeds test objects. (Supplied with each set of test objects).

HAY, G. A., CLARKE, O. F., COLEMAN, N. J. & COWAN, A. R., 1985. A set of X-ray test objects for quality control in television fluoroscopy. *British Journal of Radiology*, *58*, 335–344.

HENSHAW, E. T., 1989. Quality control measurements of X-ray image intensifier television chain systems. In *Technical and Physical Parameters for Quality Assurance in Medical Diagnostic Radiology*, BIR Report 18 (British Institute of Radiology, London), pp. 120–22.

HPA, 1981. *Measurement of the Performance Characteristics of Diagnostic X-ray Systems used in Medicine. Part II, X-ray Image Intensifier Television Systems*, TGR 32, Part 2 (Hospital Physicists' Association, London).

SIEDBAND, M. P., 1981. Fluoroscopic imaging. In *The Physical Basis of Medical Imaging*, ed. by C. M. Coulam, J. J. Erickson, F. D. Rollo and A. Everette James, Jr (Prentice-Hall, London), pp. 75–92.

1992, *The British Journal of Radiology*, 65, 691–696

Accelerated fast neutron therapy: a pilot study

By D. J. Husband, BSc, MRCP, FRCR, R. D. Errington, BSc, DMRT, FRCR, Sun Myint, MRCP, FRCR, J. A. H. Littler, MRCP, FRCR and *H. M. Warenius, FRCP, FRCR, PhD

Mersey Regional Centre for Radiotherapy and Oncology, Clatterbridge Hospital, Bebington, Wirral, Merseyside L63 4JY, UK and *The CRC Oncology Research Unit, University of Liverpool Department of Medicine, Royal Liverpool Hospital, Liverpool, Merseyside L7 8XP, UK

(*Received 29 May 1991 and in revised form 20 December 1991, accepted 11 February 1992*)

Keywords: Neutron therapy, Accelerated fractionation, Late toxicity

Abstract. The clinical role of fast neutron therapy has been limited by excessive late normal tissue damage. A pilot study of accelerated fractionation of fast neutron therapy was performed, based on the rationale that this should result in an increase in the response in acute reacting tissues (normal and malignant), with no change in late damage and a consequent increase in the therapeutic ratio. Further accelerated fractionation should improve the local control of rapidly proliferating tumour, without the potential problem of inadequate reoxygenation inherent in accelerated photon schedules. 6 or 12 fractions of 62 MeV (p-Be) neutrons were given over 12 days to 27 sites in 23 patients with locally advanced tumours. With a dose reduction of 12% (18 Gy), acceptable skin and oral mucosa early reactions were obtained. A larger dose reduction (15%) was required at pelvic sites. The incidence of late EORTC/RTOG grade 4 toxicity was 46%. The overall response rate was 76% with a complete response rate of 16%. For locally advanced breast cancer, the complete response rate was 9%, which compares unfavourably with previous results with conventional neutron fractionation schedules. The combination of a low overall complete response rate and excessive late normal tissue toxicity suggests that accelerated fractionation of fast neutrons does not lead to an improvement in the therapeutic ratio, and that late normal tissue damage will continue to be dose limiting.

Fast neutron therapy has been extensively investigated as a potential means of improving local tumour control, based on a variety of radiobiological rationales (Withers, 1985). The results to date have been contradictory (Catterall & Bewley, 1979; Duncan et al, 1986) and a therapeutic advantage for neutrons may exist in only a limited number of sites (Schmitt & Wambersie, 1990). The major limiting factor in fast neutron therapy has been excessive late normal tissue damage (Withers, 1985; Duncan et al, 1986). It has been suggested that this is due to the poor dose distribution resulting from the low energy neutron beams used in the earlier studies (Griffin et al, 1986) and that the present generation of high energy cyclotron-produced neutron beams will overcome this problem. However, the results from the Fermilab Facility (using a 66 MeV neutron beam) show a crude late toxicity rate (EORTC/RTOG grade 3+) of 18%, and an actuarial complication rate of > 50% at 7–10 years (Cohen et al, 1989). Recent dose optimization studies at five centres in the USA, using 42–66 MeV neutron beams, showed a late toxicity rate (3+) of 11–24%, at 20/20.4 Gy (Griffin et al, 1990). In the neutron arm of the MRC pelvic cancer study, the actuarial late grade 3+ toxicity rate at one year was 24% (Errington et al, 1991), which is consistent with the reports from the USA. There is thus considerable doubt whether high energy neutron beams will overcome the problem of excessive late damage. This is not due to a higher intrinsic neutron relative biological effectiveness (RBE) for late as opposed to early damage, since the RBEs are similar with the exception of neural tissue (Joiner & Field, 1988; Joiner, 1989). It may be explained by the clinical use of photons in relatively small fractions (⩽ 2 Gy) leading to a relative sparing of late compared with early normal tissue damage (because of a differential fractionation response), whereas for neutrons there is only a very limited fractionation effect (Joiner, 1989) with little sparing of late damage as fraction size is reduced (Fowler, 1989). Thus neutrons have a higher clinical RBE for late than for early normal tissue damage (Fowler, 1989). If neutron therapy is given in a shorter overall time than the 4–6 week schedules used hitherto, with fraction size unchanged (*i.e.* accelerated fractionation) there should be an increase in early normal tissue response and in tumour effect, because of the decreased time for compensatory proliferation to occur during treatment. Late normal tissue damage should be unchanged since it depends on total dose, but not overall time (Fowler, 1988). If total dose is reduced to maintain the same acute normal tissue response, then late toxicity should be reduced, for the same or an increased tumour effect (depending on the extent of dose reduction, the radiosensitivity of the tumour, and the tumour clonogen proliferation kinetics). Studies on pig epidermis have suggested that the maximum ratio of acute to late damage by neutrons is produced by using a relatively small number of fractions (6–12) in a short overall time (18 days) (Hopewell et al, 1988).

Reprint requests to: Dr D. J. Husband, Mersey Regional Centre for Radiotherapy and Oncology, Clatterbridge Hospital, Bebington, Wirral, Merseyside L63 4JY.

It has been postulated that the rapid proliferation of tumour clonogens during treatment is an important cause of failure to achieve local control at some sites (Fowler, 1986; Withers et al, 1988), leading to the use of accelerated schedules with overall treatment times reduced to as little as 2 weeks (Fowler, 1986). If such accelerated radiotherapy is to be given, then neutrons have potential advantages compared with photons. Firstly, with very short schedules, there may be a failure to reoxygenate hypoxic cells completely. Failure of reoxygenation may completely negate the benefits of accelerated therapy (Scott, 1990). The lower oxygen enhancement ratio (OER) of neutrons should reduce this problem (Fowler, 1988). Secondly, with accelerated photon schedules, the number of fractions must be significantly reduced, otherwise unacceptable late normal tissue toxicity will occur. This leads to the inconvenient requirement for 20–30 photon fractions in 2–3 weeks. There is no advantage in giving small neutron fractions, and accelerated therapy can be given in a small number of fractions (10–12), possibly less (Fowler, 1983; Withers, 1987).

In view of these considerations, we initiated a pilot study of accelerated fast neutron therapy in late 1987. Most previous experience with neutrons has been with 12 fractions in 4 weeks (treating 3 times weekly) as used in the Hammersmith studies and the present MRC/RTOG protocols. The majority of our patients received 12 fractions, though a subgroup received 6 fractions. The overall time was reduced from 4 weeks to 12 days, as suggested by Fowler (1988). Our initial aim was to determine acute tissue tolerance, since although acute reactions are not dose limiting with the 4 week schedule (Griffin et al, 1990), they might become so with the shortened schedule. To avoid an increase in acute normal tissue reactions, a dose reduction of 10% (Fowler, 1988) to 15% (Hopewell et al, 1988) may be needed. Tumour response and late normal tissue toxicity were other end points.

Patients and methods

Between November 1987 and October 1989, 23 patients received treatment on 25 occasions to 27 sites. Patients were eligible if they had advanced local disease, with a low probability of local control with conventional therapy, and if they were ineligible for concurrent MRC/RTOG Phase III neutron trials in head and neck and pelvic sites. The presence of asymptomatic metastatic disease was not an exclusion criterion. All patients gave informed consent for entry into the study.

19 patients were female, and the age ranged from 41 to 82 years. We accepted patients with tumours of the extremities (melanoma—2; squamous carcinoma—1), pelvis (squamous carcinoma of the cervix—1; adenocarcinoma of rectum—1; squamous carcinoma of the rectum—1), perineum (squamous carcinoma of vulva—1; anus—1; urethra—1), head and neck (squamous carcinoma of oral cavity—2), thorax (squamous carcinoma of bronchus—2; mesothelioma—1) and breast (adenocarcinoma—9). Carcinoma of the breast was treated on 11 separate occasions (two patients having treatment on two occasions). 10 breast tumours were T4, and the other an N2 recurrence. All these patients had failed hormonal therapy, and all but two chemotherapy within the preceding months. Two patients had received prior photon radiotherapy to a limited part of the treated area, but only the previously untreated area was scored for acute tissue toxicity, since full skin build-up was avoided in the retreated areas. Of 27 treated sites, eight had skin ulceration prior to treatment.

Patients were treated using the Clatterbridge 62 MeV (p-Be) neutron beam, which has depth dose characteristics similar to an 8 MV linear accelerator (Shaw et al, 1988). 24 sites were treated by single or parallel opposed fields, and the remaining patients by three field isocentric techniques. Dose was defined at maximum build-up for single fields, and as an intersectional dose for two or more fields. The field sizes used are shown in Table I.

23 sites (in 20 patients) were treated with 12 fractions in 12 days, giving 2 fractions per day, with a minimum 4 h gap, on Monday, Wednesday and Friday (because the cyclotron was available for clinical use only 3 days per week). Four sites (in four patients) received 6 fractions in 12 days, treating three times weekly. The doses used were based on those used in the current MRC/RTOG Phase III studies, *i.e.* 20.4 Gy/12 fractions at head and neck, skin extremity and thoracic sites, and 19.2 Gy/12 fractions at pelvic sites. Four patients were treated at this dose, and the others with varying dose reductions (see results) with 18 Gy (−12% compared with 20.4 Gy) being used at 19/27 sites. Dose is defined as total (neutron plus photon) dose (Shaw et al, 1988).

Acute skin reactions were scored according to the schema shown in Fig. 1, based on that used by Catterall et al (1971). Acute skin reactions were scored at sites where full build-up bolus (2 cm tissue equivalent) was used. The actual skin dose was derived from the treatment plan (in 14 patients) or by calculation (in five patients). When there was prior ulceration, the acute skin reaction was scored for adjacent intact skin only. Other normal tissue responses are reported according to the EORTC/RTOG schema. Local tumour responses are reported according to standard criteria (WHO,

Table I. Field sizes used

Field size (cm^2)	Number of patients		
	All sites ($n = 27$)	Sites at which acute skin reactions scored ($n = 19$)	Sites scored for late skin/subcutaneous toxicity ($n = 14$)
50–100	6	4	5
101–200	6	5	1
201–300	12	7	5
301–400	2	2	2
⩾ 401	1	1	1

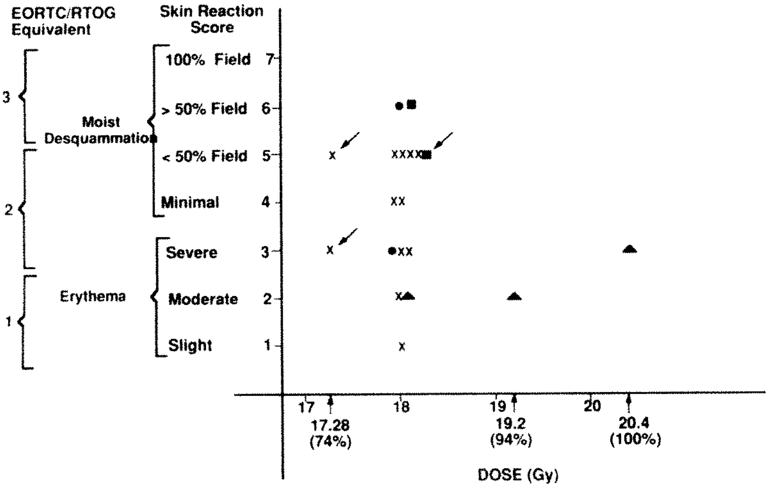

Figure 1. Acute skin reactions in relationship to dose and site: ×, breast/chest wall; ▲, limb; ●, head and neck; ■, inguinal. Treatment was given in 12 fractions (3 times weekly, 2 fractions/day), except at these sites indicated by an arrow, where 6 fractions were given 3 times weekly.

1979). A complete response was defined as disappearance of tumour, and complete healing of any ulceration. A partial response was defined as a 50% or greater reduction in tumour size.

Survival and late complication rates were calculated by actuarial methods (Peto et al, 1977).

Results

Acute skin reactions were assessable at 19 sites at which the skin dose was known because of the use of build-up bolus. This included breast, limb, chest wall, head and neck and inguinal skin. The dose given ranged from 17.28 Gy (−15% compared with 20.4 Gy) to 20.4 Gy with 15 sites receiving 18 Gy (−12%). Peak reaction varied from grade 1 to grade 6 (Fig. 1) without a clear relationship to dose. At 18 Gy, 9/15 sites (60%) developed moist desquamation of some degree. All areas of moist desquamation in previously non-ulcerated skin subsequently healed completely. Perineal skin was irradiated to a dose of 18 Gy/12F in one patient and moist desquamation of > 50% of the field (grade 6) occurred, but subsequently healed.

Oral mucosa was irradiated in two patients (18 Gy/12F); one developed spotted mucositis (EORTC/RTOG grade 2) and one confluent mucositis (EORTC/RTOG grade 3). The oesophagus was irradiated in two patients (18 Gy/12F), one developing a grade 2 and the other a grade 3 reaction (requiring nasogastric feeding). The pelvis was treated in three patients. One who received 19.2 Gy/12F developed a EORTC/RTOG grade 3 acute lower gastro-intestinal tract reaction and required intravenous feeding, but made a full recovery. Patients treated to 15 Gy/12F (−22% compared with 19.2 Gy) and 16.2 Gy (−15%) developed grade 2 and grade 1 lower gastro-intestinal tract reactions respectively. Symptomatic radiation pneumonitis (both grade 2) occurred in 2/9 patients receiving significant lung irradiation who survived more than 3 months post-treatment.

Late normal tissue toxicity was defined as that occurring after more than 3 months. 20 sites in total were followed up for more than 3 months, including 14 skin/subcutaneous sites, at all of which the skin dose was known because of the use of build-up bolus. Four of these sites (29%) developed definite grade 4 toxicity (ulceration in all cases). Two sites received 18 Gy/12F, one 18 Gy/6F and one 20.4 Gy/12F. At a further four sites (three of which received 18 Gy/12F, and one 17.28 Gy/6F) there was residual ulceration, without obvious residual tumour. Healing ceased in these patients, without the progression accompanying ulceration due to residual tumour. If this is scored as grade 4 toxicity, then the total grade 4 toxicity rate is 57% (8/14). Of eight skin/subcutaneous sites with initial ulceration, two had histologically proven radiation necrosis, four failed to epithelialize, one healed completely, and the remaining site was followed up for less than 3 months. For patients receiving a reduced dose (*i.e.* excluding the patient who received 20.4 Gy), the late grade 4 toxicity rates calculated as above are 23% and 54%. Calculation of the cumulative grade 4 toxicity rate for all patients receiving a tumour dose to subcutaneous tissue ($n = 22$) by actuarial analysis (Abratt, 1983) gives a grade 4 toxicity rate of 46% if non-healing is considered a grade 4 toxicity, or 21% if non-healing cases are excluded (with curtailment of the time–failure analysis when there are five subjects at risk (Altman, 1991)) (see Fig. 2). Grade 4 toxicity was not observed in the two retreated areas (which did not receive the full dose because of the avoidance of bolus). Late toxicity was not observed at any other sites.

Tumour response was assessable at 25 sites (two patients being non-assessable owing to early death). There were four complete responses (CR) (16%) and 15 partial responses (PR) (60%) for an overall response rate off 76%. The patient response rate (*i.e.* multiple sites treated concurrently are scored together) was 74% (2 CR, 15 PR). Sites treated with 12F had a response

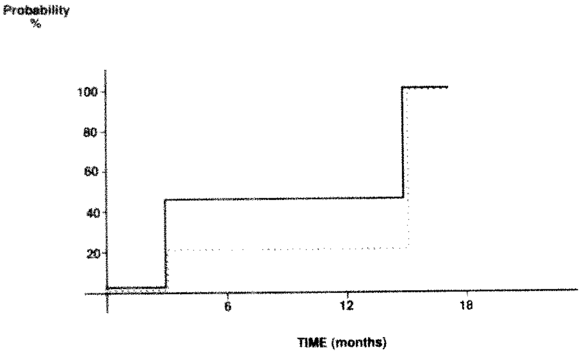

Figure 2. Probability of developing EORTC/RTOG grade 4 late toxicity: broken line, non-healing ulcer not scored as grade 4 toxicity; full line, non-healing ulcer scored as grade 4 toxicity.

rate of 74% (17/22, 3 CR, 14 PR). For sites receiving ⩾ 18 Gy, the response rate was 81% (17/21, 4 CR) and those receiving 18 Gy, 88% (14/16, 4 CR). The response rate for squamous carcinoma was 66% (6/9, 2 CR) and for non-squamous carcinoma 81% (13/16, 2 CR). For adenocarcinoma of the breast the response rate was 91% (10/11, 1 CR) but in four cases ulceration failed to heal after an initial PR. Subsequent infield progression occurred at 3/15 PR, but at none of the sites of a CR. Three patients had complete relief of symptoms at the treated site, 14 partial relief, seven no change and one was not assessable (owing to early death).

22 patients have subsequently died, with a median survival of 6 months (Fig. 3). All deaths were due to progressive disease, usually metastatic, though severe acute radiation oesophagitis may have contributed to the death of one patient with carcinoma of the bronchus 10 weeks after treatment.

Discussion

Accelerated fractionation of fast neutron therapy has previously been reported from two other centres. At the Hammersmith Hospital a group of patients received 13.9 Gy(N) in 6 fractions in 12 days, with three treatments per week (Catterall, 1986). Unfortunately, no details of acute normal tissue reactions are reported, though it is stated that subcutaneous fibrosis and telangiectasis are less (presumably because 13.9 Gy(N) is an 11% reduction from the usual Hammersmith dose of 15.6 Gy(N)). In a second study, patients with advanced head and neck cancer received 10–12 Gy of 5.6 MeV neutrons in 10 daily fractions in 2 weeks (a 9–25% dose reduction compared with their "standard" dose of 13.2 Gy/20F/4 weeks) (Skolyszewski et al, 1988). Four patients received a skin dose of 11–12 Gy/10F and all developed an EORTC/RTOG grade 2 reaction (equivalent to grades 3, 4 and 5 in this paper). We found similar skin reactions in our patients at a dose of 18 Gy (−12% compared with 20.4 Gy), with moist desquamation occurring in 60%. Moist desquamation of > 50% of the irradiated field (grade 6 in this study; EORTC/RTOG grade 3) occurred in 10% of patients receiving skin dose of 18 Gy. This compares with 7% grade 3 EORTC/RTOG early skin reactions at a dose of 20 Gy/12F/28 days (Griffin et al, 1990). Thus if a reaction schedule is shortened from 4 weeks to 12 days, a dose reduction of 12% is associated with similar early skin reactions. Based on the acute skin reactions, a higher dose than 18 Gy might be feasible and indeed two patients treated at 19.2 and 20.4 Gy did not develop excessive acute reactions.

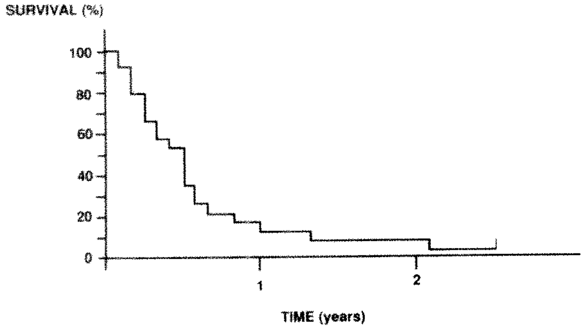

Figure 3. Probability of survival from first day of treatment with accelerated fast neutron therapy.

The oral mucosal reactions in our patients (grades 2 and 3 at 18 Gy/12F) are similar to those reported by Skolyszewski et al (1988) (grade 2 at 75–91% of the 4 week dose). A dose reduction of 10–12% would be reasonable if further studies were planned at this site.

There are no previous data on the use of accelerated neutron fractionation in the pelvis, and the bowel toxicity (at 19.2 Gy) shown by one of our patients, in whom there was no tumour response, illustrates the dangers if high doses are given in this way. Griffin et al (1990) report grade 3 pelvic toxicity in 0/31 patients receiving 20 Gy/12F/4 week and 2/43 at 20.4 Gy. Patients treated with 15% and 22% dose reductions did not develop severe pelvic toxicity (despite large field sizes in both cases). We would recommend an initial dose reduction of 15% as a starting point for further studies.

Late normal tissue toxicity was only observed at skin/subcutaneous sites. The reported incidence of late toxicity is dependent on the methods used to assess and calculate the toxicity. The major assessment problem occurs when the initial tumour is ulcerative, and partial healing occurs post-treatment (resulting in a PR being scored), but an indolent, non-healing ulcer is left, without obvious tumour or progression over several months. This difficulty has been noted by others (Griffin et al, 1990) and occurred in four of our patients. It might be considered that unless a biopsy proves the absence of tumour, this should be considered a tumour effect and not scored as grade 4 late toxicity. However, persistent ulceration is the same to the patient (representing a failure of treatment) whether due to tumour or treatment. Moreover, in one of our patients a large residual ulcer was, on excision, shown to be due to radiation necrosis, with a small area of clinically, and surgically, unsuspected residual squamous cell carcinoma. Finally, ulceration, neither healing nor progressing, is typical of radiation necrosis (Fajardo, 1982). We concur with Griffin et al (1990) that when doubt exists a normal tissue complication should be scored as a treatment effect. The calculation of the rate of late toxicity is affected by early deaths, and the variable latency of late effects (Schultheiss et al, 1986). The observed or crude complication rate is the number expressing injury divided by the number entered into the study. Since late effects are by definition those occurring at 3 months or later, we have used the number surviving 3 months or more in the denominator, giving a grade 4 toxicity rate of 57% (and 54% for those receiving a reduced dose). Alternatively, failure time analysis can be used (Abratt, 1983), but can yield a complication rate of 1 if the last surviving patient expresses the injury (Schultheiss et al, 1986) (see Fig. 2). Curtailment of the analysis when only five subjects are at risk (Altman, 1991) obviates the problems and gives, in our view, the best estimate of the incidence of late toxicity. This leads to an estimated late grade 4 skin/subcutaneous toxicity rate of 46% (or 21% if the patients with residual non-healing ulceration are excluded). For conventional neutron fractionation, late grade 4 toxicity occurs in 9% of extremity sites treated to 20 Gy, and 17% at 22 Gy (Griffin et al, 1990). A number of factors may have contributed to the excessive late toxicity in our study. The advanced nature of the disease studied (with extensive normal tissue destruction by tumour before treatment) may predispose patients to late normal tissue toxicity (Griffin et al, 1990). Secondly, the short median survival may have meant that healing was not complete in some patients (though in all patients with residual ulceration, progressive healing had clearly ceased). Finally, contrary to expectations, accelerated fractionation may have led to an increased incidence of late toxicity. This may be an example of consequential late damage (Peters & Kian Ang, 1988), as previously described in a study of photon irradiation given in 24–27 fractions (2 Gy, three times daily) in 9–11 days (Peracchia & Salt, 1981). In this study, the rate of late oral mucosa necrosis was 55%. Excessive damage to rapidly proliferating clonogens (*e.g.* in skin or oral mucosa) may result in late ulceration because there are insufficient surviving clonogens to repopulate the tissue. Extensive tissue damage by advanced tumours may contribute to this effect. A further factor may have been our use of 2 fractions per day 3 days per week with a minimum 4 h gap. For accelerated photon schedules, a minimum gap of 6 h is recommended to allow for repair of sublethal damage in late reacting tissues (Fowler, 1989). The limited data available for neutrons suggest that whilst recovery is much less complete than for photons, that which does occur occurs more slowly (Field, 1976), implying that a gap of 4 h may be inadequate. If no repair were to occur over the 4 h this would be equivalent to giving 6 fractions rather than 12. There is a small dose-sparing effect from 4–8 fractions in late reacting tissue (kidney) with 62 MeV (p-Be) neutrons (Joiner, 1989) and so an effect is difficult to exlude, though is likely to be minimal. Daily fractions as used in Poland (Skolyszewski et al, 1988) would be a better option.

The overall response rate of 76% is at first encouraging. However, only four complete responses (16%) were obtained and complete response is the relevant end point if radical treatment is given. Skolyszewski et al (1988) reported 5 CR and 6 PR in 12 patients (RR 91%), but 3 of the CR subsequently progressed giving a sustained CR rate of 16%, similar to the present study. The only site for which directly comparable data using the 12F/4 weeks schedule is available is locally advanced carcinoma of the breast (Catterall et al, 1987). Using 7.5 MeV neutrons at a dose of 16.45 Gy ($N+\lambda$) there was a 95% CR rate compared with a CR rate of 9% (and PR rate of 82%) in the present study. Regression of these tumours can however be slow (Catterall et al, 1987) and the short overall survival of our patients may have led to an underestimate of the CR rate. Nonetheless, our fractionation regimen seems unlikely to be more effective than the 4 week schedule.

Our low overall response rate may be partly explained by the short overall survival and selection of patients with very advanced diseases for the pilot study. Further accelerated regimens, with a reduction in total dose, will only be of benefit to tumours with short potential doubling times; for tumours with longer potential doubling times, accelerated regimens may be less effective because of the reduction in total dose required (Tucker & Chan, 1990). We treated a heterogeneous group of tumours without selection based on kinetic parameters. The use of a 3 day/week schedule may have allowed increased time for proliferation or rapidly dividing tumours between fractions, diluting the benefit of shortened overall time (Dische & Saunders, 1990).

In conclusion, we have found that fast neutron therapy could be given in an accelerated schedule in 12 fractions in 12 days with acceptable acute toxicity providing a dose reduction of at least 12% (compared with the 12F/4 weeks schedule) was made. However, a low complete response rate and excessive late normal tissue toxicity suggest limited application for this method of treatment, since further dose reductions would be required to achieve acceptable late toxicity. There is no suggestion of an improved therapeutic ratio and accelerated fractions do not, contrary to predictions, appear to reduce the level of late normal tissue damage of neutrons.

Acknowledgments

We thank Dr M. A. Coe and Dr B. Jones for allowing their patients to be included in this study. We are grateful for the contributions of Sister Rose Dixon, Research Nurse, and Mrs J. Neale, Superintendent Radiographer. Miss S. Minnis is thanked for preparing the manuscript.

References

Abratt, R. P., 1983. Reporting the late complication rate of cancer therapy. *British Journal of Radiology*, *56*, 348–349.

Altman, D. G., 1991. *Practical Statistics for Medical Research* (Chapman and Hall, London), p. 386.

Catterall, M., 1986. Neutron beam therapy. The importance of technique on clinical results. *Nuclear Science Applications, 2*, 235–242.

Catterall, M. & Bewley, D. K., 1979. *Fast Neutrons in the Treatment of Cancer* (Academic Press, London).

Catterall, M., Rogers, C., Thomlinson, R. H. & Field, S. B., 1971. An investigation into the clinical effects of fast neutrons. *British Journal of Radiology, 44*, 603–611.

Catterall, M., Errington, R. D. & Bewley, D. K., 1987. Fast neutrons in the treatment of locally advanced breast cancer. *European Journal of Surgical Oncology, 13*, 315–319.

Cohen, L., Schultheiss, T. E., Hendrickson, F. R., Mansell, J., Saroja, K. R. & Lennox, A., 1989. Normal tissue complications following high energy neutron beam therapy: I Crude response rates. *International Journal of Radiation Oncology, Biology and Physics, 16*, 73–78.

Dische, S. & Saunders, M. I., 1990. The rationale for continuous hyperfractionated, accelerated radiotherapy (CHART). *International Journal of Radiation Oncology, Biology and Physics, 19*, 1317–1320.

Duncan, W., Williams, J. R., Kerr, G. R., Arnott, S. J., Quilty, P. M., Rodger, A., MacDougall, R. H. & Jack, W. J. L., 1986. An analysis of the radiation related morbidity observed in a randomized trial of neutron therapy for bladder cancer. *International Journal of Radiation Oncology, Biology and Physics, 12*, 2085–2092.

Errington, R. D., Ashby, D., Gore, S. M., Abrams, K. R., Myint, S., Bonnett, D. E., Blake, S. W. & Saxton, T. E., 1991. High energy neutron treatment for pelvic cancers: study stopped because of increased mortality. *British Medical Journal, 302*, 1045–1051.

Fajardo, L. F., 1982. *Pathology of Radiation Injury* (Masson, New York), pp. 186–200.

Field, S. B., 1976. An historical survey of radiobiology and radiotherapy with fast neutrons. *Current Topics in Radiation Research Quarterly, 11*, 1–86.

Fowler, J. F., 1983. Rationales for high linear energy transfer radiotherapy. In *The Biological Basis of Radiotherapy*, ed. by G. G. Steel, G. E. Adams and M. J. Packham (Elsevier, Amsterdam), pp. 261–268.

Fowler, J. F., 1986. Potential for increasing the differential response between tumour and normal tissues: can proliferation ratio be used? *International Journal of Radiation Oncology, Biology and Physics, 12*, 641–645.

Fowler, J. F., 1988. What to do with neutrons in radiotherapy: a suggestion. *Radiotherapy and Oncology, 13*, 233–235.

Fowler, J. F., 1989. Heavy particles in radiotherapy. In *The Biological Basis of Radiotherapy*, 2nd ed., ed. by G. G. Steel, G. E. Adams and A. Horwich (Elsevier, Amsterdam), pp. 249–266.

Griffin, T., Pajak, T., Laramore, G. & Davis, L., 1986. Analysis of neutron radiotherapy and treatment complications. *Bulletin Cancer (Paris), 73*, 582–587.

Griffin, T. W., Martz, K. L., Laramore, G. E., Thomas, F. J., Maor, M. H., Hendrickson, F. R., Parker, R. G., Richter, M. P. & Davis, L. W., 1990. High energy (42–66 MeV reactions) fast neutron dose optimization studies in the head and neck, thorax, upper abdomen, pelvis and extremities. *Radiotherapy and Oncology, 19*, 307–316.

Hopewell, J. W., Barnes, D. W. H., Robbins, M. E. C., Sanson, J. M., Knowles, J. F. & Van den Aardwig, G. J. M. J., 1988. The relative biological effectiveness of fractionated doses of fast neutrons (42 MeV d → Be) for normal tissues in the pig. *British Journal of Radiology, 61*, 928–938.

Joiner, M. C., 1989. A comparison of the effects of p(62)Be and d(16)Be neutrons in the mouse kidney. *Radiotherapy and Oncology, 13*, 211–224.

Joiner, M. C. & Field, S. B., 1988. The response of mouse skin to irradiation with neutrons from 62 MV cyclotron at Clatterbridge, U.K. *Radiotherapy and Oncology, 12*, 153–166.

Peracchia, G. & Salt, C., 1981. Radiotherapy with thrice a day fractionation in short overall time. *International Journal of Radiation Oncology, Biology and Physics, 7*, 99–104.

Peters, L. J. & Kian Ang., K., 1988. Accelerated fractionation. In *Innovations in Radiation Oncology*, ed. by H. R. Withers and L. J. Peters (Springer, Berlin), pp. 231–238.

Peto, R., Pike, M. C., Armitage, P., Breslow, N. E., Cox, D. R. & Howard, S. V., 1977. Design and analysis of randomized clinical trials requiring prolonged observation of each patient. II Analysis and examples. *British Journal of Cancer, 35*, 1–39.

Schmitt, G. & Wambersie, A., 1990. Review of the clinical results of fast neutron therapy. *Radiotherapy and Oncology, 17*, 47–56.

Schultheiss, T. E., Thomas, H. D., Peters, L. J. & Dixon, D. U., 1986. Effect of latency on calculated complication rates. *International Journal of Radiation Oncology, Biology and Physics, 12*, 1861–1865.

Scott, O. C. A., 1990. Mathematical models of repopulation and reoxygenation in radiotherapy. *British Journal of Radiology, 63*, 821–823.

Shaw, J. E., Bonnett, D. E. & Blake, S. W., 1988. The Clatterbridge high energy neutron therapy facility: measurement of beam parameters for clinical use. *British Journal of Radiology, 61*, 47–53.

Skolyszewski, J., Fowler, J. F. & Huczkowski, J., 1988. Short course neutron therapy for advanced head and neck cancer. *British Journal of Radiology, 61*, 857–858.

Tucker, S. L. & Chan, K., 1990. The selection of patients for accelerated radiotherapy on the basis of tumour growth kinetics and intrinsic radiosensitivity. *Radiotherapy and Oncology, 18*, 197–211.

WHO, 1979. *Handbook for Reporting Results of Cancer Treatment* (World Health Organisation, Geneva), pp. 22–27.

Withers, H. R., 1985. Neutron radiobiology and clinical consequences. *Strahlentherapie, 161*, 739–745.

Withers, H. R., 1987. Neutrons and other clinical trials: Impossible dreams? *International Journal of Radiation Oncology, Biology and Physics, 13*, 1967–1970.

Withers, H. R., Taylor, J. M. G. & Maciejewski, B., 1988. The hazard of accelerated tumour clonogen repopulation during radiotherapy. *Acta Oncology, 27*, 131–146.

1992, *The British Journal of Radiology*, 65, 697–700

Low oxygen extraction fraction in tumours measured with the oxygen-15 steady state technique: effect of tissue heterogeneity

By Adriaan A. Lammertsma, PhD and Terry Jones, DSc

MRC Cyclotron Unit, Hammersmith Hospital, Du Cane Road, London W12 0HS, UK

(*Received 5 August 1991 and in revised form 9 January 1992, accepted 11 February 1992*)

Keywords: Oxygen extraction fraction, Blood flow, Oxygen-15 steady state technique, Positron emission tomography, Simulation studies

Abstract. Several reports have described decreased oxygen extraction fractions in tumours relative to those in normal tissues as measured with the oxygen-15 steady state technique and positron emission tomography. The present simulation study was carried out to assess the influence of tissue heterogeneity on these measured values. It was found that, within the range analyzed, tissue heterogeneity always resulted in underestimations of mean values of oxygen extraction fraction. It must, therefore, be concluded that the oxygen-15 steady state technique is not an accurate method for the assessment of the oxygen status of tumours. This finding should also apply to other pathological conditions, where a significant degree of tissue heterogeneity can not be excluded. More generally, this study demonstrates the need for detailed analyses of sensitivities of tracer kinetic procedures to tissue heterogeneity.

Using positron emission tomography (PET) and the oxygen-15 steady state inhalation technique (Jones et al, 1976; Frackowiak et al, 1980; Lammertsma & Jones, 1983; Lammertsma et al, 1983), several reports have described the measurement of blood flow (BF), blood volume (BV), oxygen extraction fraction (OEF) and oxygen utilization (MRO_2) in both brain tumours (Ito et al, 1982; Rhodes et al, 1983; Lammertsma et al, 1985; Taki et al, 1985; Mineura et al, 1985, 1986; Tyler et al, 1987) and body tumours (Beaney et al, 1984; Kairento et al, 1985). The striking feature of all these reports was that the OEF in tumour tissue was consistently lower than that in normal tissue.

This finding is in contrast to invasive studies where generally pO_2 in tumours was found to be reduced (for a review of the literature see Vaupel et al, 1989) due to the presence of anoxic or hypoxic cells. As a result of a reduced pO_2 one would have expected an increased rather than a reduced OEF.

It has been shown previously (Lammertsma et al, 1981a; Herscovitch & Raichle, 1983) that in heterogeneous tissue the oxygen-15 steady state technique results in underestimation of mean BF. The present simulation study was carried out to investigate if the low OEF measured in tumours using PET and the oxygen-15 steady state technique could also be explained by tisssue heterogeneity, given that high OEF areas are a result of low delivery rates of oxygen (*i.e.* low BF) and, therefore, their contribution could be masked by the signal originating from high flow areas.

Methods

Based on the standard oxygen-15 steady state equations (Frackowiak et al, 1980; Lammertsma et al, 1983) equilibrium tissue concentrations, which would result from continuous $C^{15}O_2$ and $^{15}O_2$ inhalation, were calculated for given values of BF, OEF and BV. The range of values used was based on previously published data (Lammertsma et al, 1983). Average tissue concentrations were then calculated for various combinations of two different tissues, one of which was taken to have good perfusion and normal or low OEF while the other was considered to be poorly perfused with increased OEF. These average tissue concentrations were in turn used to calculate the mean BF, OEF and MRO_2 that would have been measured with the PET scanner for the various proportions of high and low flow tissues. These calculated values were compared with the actual mean values of BF, OEF and MRO_2.

Although, in the steady state technique, it is usually assumed that the volume of distribution of water (V_d) is unity (Frackowiak et al, 1980), this restriction was not applied to the present simulation studies. This was necessary, since necrotic areas within tumours would represent regions which had a poor effective exchange of water between blood and tissue during the time course of the study and consequently a low value of V_d. In addition, for the calculations of OEF, non-extracted intravascular activity was taken into account as described previously (Lammertsma et al, 1983).

Results

Typical results from the simulation studies are shown in Figs 1 and 2. Fig. 1 illustrates the effect of a changing V_d, the only difference between the three graphs being a

---

Address correspondence and reprint requests to Dr A. A. Lammertsma, MRC Cyclotron Unit, Hammersmith Hospital, Du Cane Road, London W12 0HS.

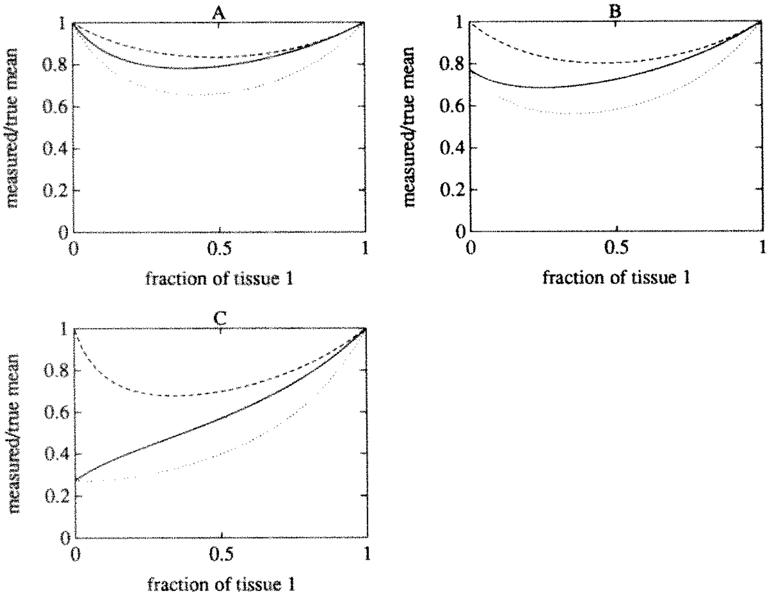

Figure 1. Examples of the effects of tissue heterogeneity on the calculated values of BF (solid line), OEF (dashed line) and MRO_2 (dotted line). Calculated over true ratios are plotted as function of the fraction of the region with the highest BF (tissue 1). All graphs were calculated with BF = 0.5 ml/ml/min, V_d = 1 ml/ml, OEF = 0.4 and BV = 0.05 ml/ml for tissue 1, and BF = 0.1 ml/ml/min, OEF = 0.9 and BV = 0.01 ml/ml for tissue 2. The graphs only differ in the value of V_d used for tissue 2 (A: V_d = 1.0 ml/ml; B: V_d = 0.5 ml/ml; C: V_d = 0.1 ml/ml). Significant underestimation of BF, OEF and MRO_2 is apparent for all heterogeneous tissues. For homogeneous tissue there is only underestimation of BF and MRO_2 if V_d is different from 1.

different V_d for the tissue with low BF and high OEF. Note that, even for homogeneous tissue, there is underestimation of BF (and MRO_2) if V_d is less unity. However, for homogeneous tissue, measured OEF is always correct. Fig. 2 shows some more extreme, but possible (Lammertsma et al, 1983), situations where both BF and BV of the high flow tissue have been varied. Again, OEF is correct if the tissue is homogeneous. However, for a mixture of tissues, an underestimation of mean BF, OEF and consequently MRO_2 can be observed in all cases. Although BV has an effect on the calculation of OEF (and MRO_2), no underestimation of mean BV occurs since the relation between BV and "tissue" concentration of a vascular marker is linear.

Discussion

The results of the present simulation studies confirm previous reports of underestimation of BF (as measured with the oxygen-15 steady state technique) in heterogeneous tissue (Lammertsma et al, 1981a; Herscovitch & Raichle, 1983) and in homogeneous tissue where V_d is less than 1 (Lammertsma et al, 1981b; Herscovitch & Raichle, 1983). However, more importantly, in heterogeneous tissue also an underestimation of OEF is apparent. Consequently, the underestimation of MRO_2

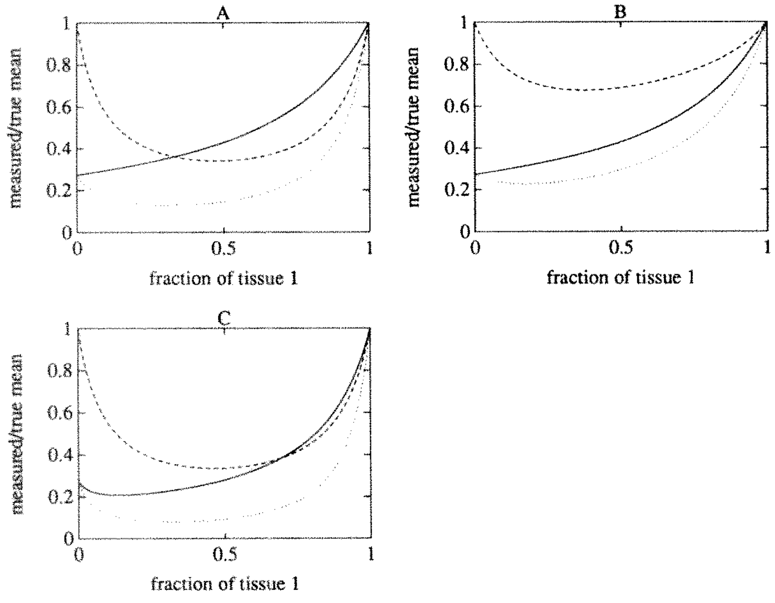

Figure 2. Examples of the effects of tissue heterogeneity on the calculated values of BF (solid line), OEF (dashed line) and MRO_2 (dotted line). Calculated over true ratios are plotted as function of the fraction of the region with the highest BF (tissue 1). All graphs were calculated with V_d = 1 ml/ml and OEF = 0.1 for tissue 1, and BF = 0.1 ml/ml/min, V_d = 0.1 ml/ml, OEF = 0.9 and BV = 0.01 ml/ml for tissue 2. The graphs have been calculated using different BF and BV values for tissue 1 (A: BF = 1.0 ml/ml/min, BV = 0.05 ml/ml; B: BF = 1.0 ml/ml/min, BV = 0.50 ml/ml; C: BF = 2.0 ml/ml/min, BV = 0.10 ml/ml). Compared with Fig 1. underestimations are more severe in these more extreme situations.

is even more severe since it is the product of those for BF and OEF.

The present study was designed to simulate circumstances which are likely to occur in tumours. In all simulations one of the two tissues was considered to have poor perfusion, while the other had normal or increased flow. The well perfused tissue was assumed to have a normal V_d (for simplicity set to 1) and the poorly perfused tissue both a normal and a reduced V_d, since reduced V_d could be associated with necrotic tissue. Although this would not necessarily be the case in all tumours, the present conditions were designed to cover the entire possible range. In all cases analyzed, the poorly perfused (hypoxic) tissue was assumed to have both high OEF (90%) and low BV (1%). OEF in the other tissue was assumed to be normal or decreased (luxury perfusion) with a normal or increased BV (hypervascularity). Again, at least from a biological point of view, this would represent the most likely situation within a tumour. The uncoupling in the well perfused area between BF (high) and OEF (low), which is characteristic of tumours, is the result of an increased rate of glycolysis (Rhodes et al, 1983; Kairento et al, 1985; Mineura et al, 1985, 1986; Tyler et al, 1987).

The underestimation of OEF is due to the fact that the tissue radioactivity signal is weighted towards the contribution from a high flow (delivery) area, which most likely will have a low OEF. In the average signal high OEF areas are masked due to their low delivery rates (low BF).

Using a new kinetic technique (Lammertsma et al, 1990) it has recently been shown that in the case of breast tumours both BF and V_d are higher for the tumours than for normal breast tissue (Wilson et al, 1992). Although these values are not explicitly used in the present simulation study, the higher degree of heterogeneity within the tumours would still result in a higher degree of underestimation of OEF when measured with the steady state technique.

The consistent underestimation of OEF in heterogeneous tissues, as shown in Fig. 1, has serious implications for the interpretation of OEF in tumour studies, since tumours are known to be more heterogeneous than normal tissue (Vaupel et al, 1989). Consequently, care should be taken in assigning the previously measured low tumour OEF values (Ito et al, 1982; Rhodes et al, 1983; Beaney et al, 1984; Kairento et al, 1985; Lammertsma et al, 1985; Taki et al, 1985; Mineura et al, 1985, 1986; Tyler et al, 1987) to luxury perfusion within the tumour as a whole. Although it is perhaps unlikely that all pixels in all studied tumours have a significant degree of tissue heterogeneity, microscopic heterogeneity beyond the spatial resolution of a PET scanner can never be excluded. The present findings indicate that the oxygen-15 steady state technique has only limited value in the assessment of the pathophysiology of tumours. More accurate techniques, which are less sensitive to tissue heterogeneity, are required. Recently, a kinetic technique for the measurement of tumour BF has been described (Lammertsma et al, 1990) which is far less sensitive to tissue heterogeneity. Similar techniques will have to be developed for OEF and MRO_2 in order to assess with more certainty the oxygen status of tumours *in vivo*.

References

Beaney, R. P., Lammertsma, A. A., Jones, T., McKenzie, C. G. & Halnan, K. E., 1984. Positron emission tomography for *in vivo* measurement of regional blood flow, oxygen utilisation, and blood volume in patients with breast carcinoma. *Lancet, i,* 131–134.

Frackowiak, R. S. J., Lenzi, G. L., Jones, T. & Heather, J. D., 1980. Quantitative measurement of regional cerebral blood flow and oxygen metabolism in man using ^{15}O and positron emission tomography: theory, procedure and normal values. *Journal of Computer Assisted Tomography, 4,* 727–736.

Herscovitch, P. & Raichle, M. E., 1983. Effect of tissue heterogeneity on the measurement of cerebral blood flow with the equilibrium $C^{15}O_2$ inhalation technique. *Journal of Cerebral Blood Flow and Metabolism, 3,* 407–415.

Ito, M., Lammertsma, A. A., Wise, R. J. S., Bernardi, S., Frackowiak, R. S. J., Heather, J. D., McKenzie, C. G., Thomas, D. G. T. & Jones, T., 1982. Measurement of regional cerebral blood flow and oxygen utilisation in patients with cerebral tumours using ^{15}O and positron emission tomography: analytical techniques and preliminary results. *Neuroradiology, 23,* 63–74.

Jones, T., Chesler, D. A. & Ter-Pogossian, M. M., 1976. The continuous inhalation of oxygen-15 for assessing regional oxygen extraction in the brain of man. *British Journal of Radiology, 49,* 339–343.

Kairento, A. L., Brownell, G. L., Elmaleh, D. R. & Swartz, M. R., 1985. Comparative measurement of regional blood flow, oxygen and glucose utilisation in soft tissue tumour of rabbit with positron imaging. *British Journal of Radiology, 58,* 637–643.

Lammertsma, A. A., Frackowiak, R. S. J., Lenzi, G. L., Heather, J. D., Pozzilli, C. & Jones, T., 1981a. Accuracy of the oxygen-15 steady state technique for measuring rCBF and $rCMRO_2$: tracer modelling, statistics, and spatial sampling. *Journal of Cerebral Blood Flow and Metabolism, 1,* Suppl. 1, S3–S4.

Lammertsma, A. A. Jones, T., Frackowiak, R. S. J. & Lenzi, G. L., 1981b. A theoretical study of the steady-state model for measuring regional cerebral blood flow and oxygen utilisation using oxygen-15. *Journal of Computer Assisted Tomography, 5,* 544–550.

Lammertsma, A. A. & Jones, T., 1983. Correction for the presence of intravascular oxygen-15 in the steady-state techniques for measuring regional oxygen extraction ratio in the brain: 1. Description of the method. *Journal of Cerebral Blood Flow and Metabolism, 3,* 416–424.

Lammertsma, A. A., Wise, R. J. S., Heather, J. D., Gibbs, J. M., Leenders, K. L., Frackowiak, R. S. J., Rhodes, C. G. & Jones, T., 1983. Correction for the presence of intravascular oxygen-15 in the steady-state technique for measuring regional oxygen extraction ratio in the brain: 2. Results in normal subjects and brain tumour and stroke patients. *Journal of Cerebral Blood Flow and Metabolism, 3,* 425–431.

Lammertsma, A. A., Wise, R. J. S., Cox, T. C. S., Thomas, D. G. T. & Jones, T., 1985. Measurement of blood flow, oxygen utilisation, oxygen extraction ratio, and fractional blood volume in human brain tumours and surrounding oedematous tissue. *British Journal of Radiology, 58,* 725–734.

LAMMERTSMA, A. A., WILSON, C. B., TAYLOR, C. J. V., MCKENZIE, C. G. & JONES, T., 1990. Measurement of blood flow and exchangeable volume of distribution of water in breast tumours using dynamic positron emission tomography. *Journal of Nuclear Medicine, 31*, 746–747.

MINEURA, K., YASUDA, T., KOWADA, M., SHISHIDO, F., OGAWA, T. & UEMURA, K., 1985. Quantitative analysis of regional cerebral hemodynamics and metabolism in gliomas using O-15 and F-18-fluorodeoxyglucose (FDG) PET. In *Proceedings of the International Symposium on Current and Future Aspects of Cancer Diagnosis with Positron Emission Tomography* (Tohoku University, Sendai, Japan), pp. 82–85.

—— 1986. Positron emission tomographic evaluation of histological malignancy in gliomas using oxygen-15 and fluorine-18-fluorodeoxyglucose. *Neurological Research, 8*, 164–168.

RHODES, C. G., WISE, R. J. S., GIBBS, J. M., FRACKOWIAK, R. S. J., HATAZAWA, J., PALMER, A. J., THOMAS, D. G. T. & JONES, T., 1983. *In vivo* disturbance of the oxidative metabolism of glucose in human cerebral gliomas. *Annals of Neurology, 14*, 614–626.

TAKI, W., HANDA, H., ISHIKAWA, M., KOBAYASHI, A., YAMASHITA, J., YONEKAWA, Y., TANADA, S., SENDA, M., YONEKURA, Y., TORIZUKA, K., FUJITA, T., FUKUYAMA, H., FUJIMOTA, N., HARADA, K. & KAMEYAMA, M., 1985. Blood flow and oxygen utilization in brain tumors. In *Proceedings of the International Symposium on Current and Future Aspects of Cancer Diagnosis with Positron Emission Tomography* (Tohoku University, Sendai, Japan), pp. 91–95.

TYLER, J. L., DIKSIC, M., VILLEMURE, J. G., EVANS, A. C., MEYER, E., YAMAMOTO, Y. L. & FEINDEL, W., 1987. Metabolic and hemodynamic evaluation of gliomas using positron emission tomography. *Journal of Nuclear Medicine, 28*, 1123–1133.

VAUPEL, P., KALLINOWSKI, F. & OKUNIEFF, P. 1989. Blood flow, oxygen and nutrient supply, and metabolic microenvironment of human tumors: a review. *Cancer Research, 49*, 6449–6465.

WILSON, C. B. J. H., LAMMERTSMA, A. A., MCKENZIE, C. G., SIKORA, K. & JONES, T., 1992. Measurement of blood flow and exchanging water space in breast tumors using positron emission tomography: a rapid and non invasive dynamic method. *Cancer Research*, in press.

1992. *The British Journal of Radiology*, *65*, 701–709

Image comparison techniques for use with megavoltage imaging systems

By *P. M. Evans, DPhil, †J. Q. Gildersleve, FRCR, *‡E. J. Morton, PhD, *W. Swindell, DSc, *§R. Coles, MSc, *¶M. Ferraro, BSc, †C. Rawlings, DCR, *Z. R. Xiao, MPhil and †J. Dyer, DCR

*Joint Department of Physics and †Department of Radiotherapy, Royal Marsden Hospital and Institute of Cancer Research, Downs Road, Sutton, Surrey SM2 5PT, UK

(*Received 9 October 1991 and in revised form 23 January 1991, accepted 12 February 1992*)

Keywords: Radiotherapy imaging, Patient position verification, Image comparison

Abstract. In this paper we describe software facilities for enabling patient positioning studies using the megavoltage imaging system developed at the Royal Marsden Hospital and Institute of Cancer Research. The study focuses on the use of the system for three purposes: patient position verification (by comparing images taken at treatment simulation with megavoltage images taken at treatment time); reproducibility studies (by analysing a set of megavoltage images); and set-up correction (by adjusting the set-up until the megavoltage image obtained at treatment registers with the simulation image). The need is discussed for suitably presented simulator images, a method of determining field boundaries and the possibility of delineating soft-tissue interfaces. Several algorithms of different types, developed specifically for the purpose of intercomparison of planar projection images, are presented. The techniques employed and their usefulness, in both the qualitative and the quantitative sense, are discussed. The results are presented of a phantom and clinical study, to evaluate the rigour and reproducibility of the algorithms. These results indicate that measurements can be made to an accuracy of about 1–2 mm, with a similar value for interobserver reproducibility for the best image comparison techniques available.

Recent studies have revealed errors of up to several centimetres in patient positioning during radiotherapy (Marks et al, 1974; Byhardt et al, 1978; Rabinowitz et al, 1985; Lam et al, 1987; Huizenga et al, 1988; Graham et al, 1991), a magnitude sufficient both to decrease local control and to increase complications. The most commonly employed method of determining the correctness of the patient's positioning is to take check film images. However, the efficacy of these films is severely limited. The image quality is poor, because of low contrast and the large amount of scatter. Also, a check film has to be removed from the treatment room and developed before the image can be viewed.

With these deficiencies in mind, several groups have developed digital X-ray detection systems for use at megavoltage energies (see, for example, Baily et al, 1980; Meertens et al, 1985; Lam et al, 1986; Leong, 1986; Bova et al, 1987; Leong & Stracher, 1987; Wilenzick et al, 1987; Cheng et al, 1988; Shalev et al, 1988; Reinstein et al, 1988; van Herk & Meertens, 1988; Shalev et al, 1989; Munro et al, 1990; Wong et al, 1990; Antonuk et al, 1991). The intention is that such devices will eventually supersede check films. As the images are digital, they are readily accessible to computerized image processing techniques. Furthermore, images are available within a matter of seconds, rather than minutes as with conventional film.

We have developed a digital megavoltage X-ray system of the type described above (Morton & Swindell, 1987; Morton et al, 1991a). A unique feature of our system is the choice of photon detection medium: a scanning array of 128 $ZnWO_4$ scintillation crystals each of which is optically coupled to a silicon photodiode. The detective quantum efficiency of such a system is very high ($>50\%$), enabling the formation of an image with a relatively small dose (<1 cGy). However, as the device is a scanning system, the total dose delivered to the patient is approximately 25 cGy per frame (Morton et al, 1991a). The portal scanner is reproducibly placed 1 m from the isocentre of a Philips SL25 linear accelerator, ensuring that the megavoltage images all have the same magnification and that the scatter component is minimal (Swindell et al, 1991). Full details of the design, construction and development of this device are given elsewhere (Morton et al, 1991a).

Here we concentrate on work to establish facilities for image comparison using the system. Specifically, a library of software tools for patient image analysis has been developed. Various qualitative and quantitative algorithms have been implemented to enable interimage comparison and hence the determination of set-up and positioning errors. Analyses obtained from such algorithms serve three main purposes: first, comparison of a megavoltage image with a simulation image enables verification of patient positioning relative to the *de facto* standard; second, comparison of a series of images taken at various fractions throughout the course of the treatment regime allows one to establish how reproducible is the patient's set-up; and third, if the results obtained from such an image comparison process conform to the mechanical geometry of the treatment machine (*e.g.* if rotations about the z-axis are calculated about the isocentre, etc.) then such results may be used to correct the patient's positioning during the course of a particular treatment fraction. Clearly, for such a procedure to be practicable, the image comparison process must be both accurate and quick.

---

‡Present address: Department of Radiation Oncology, University of Michigan, Ann Arbor, MI, USA.

§Present address: Department of Medical Physics and Bioengineering, University Hospital of Wales, Cardiff CF4 4XW, UK.

¶Present address: Physics Department, Brunel University, Uxbridge, Middlesex UB8 3PH, UK.

This work was implemented on a μVAX II computer interfaced to a LEXIDATA 3703 image display system.

In the following section the specific requirements for verification and reproducibility studies using a digital imaging system are discussed. In the next section the image comparison algorithms are presented, following which the usefulness of the methods is considered, along with their consistency and ease of use. The conclusions drawn from this study are given in the final section.

General considerations

Qualitative and quantitative comparison techniques

Qualitative techniques of image comparison, although not providing numerical output, still have much use in radiotherapy verification. Analysis of a set of images may yield information on the ways in which a particular treatment procedure is inadequate. For example, it might indicate that there is significant movement in one degree of freedom yet not in another.

Quantitative measurement techniques for use in the radiotherapy clinic have to satisfy certain criteria, the most fundamental of which is numerical accuracy. If the minimum resolvable distance of a measurement system is greater in size than the magnitude of the variability of the position of the patient, then clearly this variability cannot be measured. Our system has a spatial resolution of about 3 mm. However, variations smaller than this may be observed in the images owing to the fact that the human eye is able to average information over several pixels. Reported studies suggest that errors of up to 1 cm will be found on a regular basis (*e.g.* Lam et al, 1987).

The inherently poor contrast in megavoltage energy images makes the use of algorithms to delineate features of interest within the images for automatic analysis difficult. Thus we rely on the user to establish the features of interest. This further optimizes the speed of implementation as required for on-line correction of patient set-up by eliminating the need for complex image-registration software.

The scheme used to implement quantitative image comparison is discussed in the Appendix.

Treatment simulation images

For a radiotherapy portal imaging system to be useful for treatment verification purposes, a reference image has to be available. This will generally be the treatment simulation image. We have described previously how we obtain X-ray image intensifer images from our treatment simulator for incorporation into our imaging system (Morton et al, 1991b). We also digitize simulator films with a CCD camera and use them in the same manner. As our megavoltage scanner is rigidly mounted at a distance of 1 m from the isocentre, the pixel size is constant. Thus, all simulator images may easily be scaled so that they have the same pixel size and, hence, magnification as a megavoltage image. The result is a simulator image that is scaled to the dimensions of a corresponding megavoltage image. Several other groups have discussed the digitization of check film and simulator images (Leong, 1984; Meetens, 1985; Amols & Lowinger, 1987; Grimm et al, 1987).

Regions of interest

We have a facility for specifying a region of interest (ROI). To draw a region of interest, a cursor is moved around the structure to be delineated, tracing out a wire-frame diagram.

Field edge delineation

The quantity that must be measured when evaluating patient set-up is the position of the patient's anatomy relative to the field edge, and so, if two images are to be compared, as a first step their relative position must be adjusted until their field edges coincide. This then constitutes the starting point for any measurement of patient position and may be achieved by adjusting the position of two regions of interest, one corresponding to each field outline, until maximal coincidence is achieved. Any measurements are made from this starting point. This assumes that the absolute positioning of the field is unimportant, *i.e.* that the dose distribution remains constant for small rotations and translations of the collimation system.

It is clear from the above discussion that the field edge must be found. In the case of the simulator images this is easily achieved using field-defining wires which indicate the collimator positioning. A region of interest is drawn manually to trace out the field edge of the simulator and then superimposed on the megavoltage image. The field edge of the megavoltage image is determined (as described below) and also superimposed on the megavoltage image as a region of interest. The operator then adjusts the positioning of the simulator field edge until the two field edges coincide maximally. The adjustment required to achieve this is never more than two pixels. Since the simulator images are obtained by placing a film in front of a camera or from an image intensifier, neither of whose position need be fixed, the above procedure is needed to ensure the simulator field edge in the image registers exactly with the expected megavoltage image field edge. The rigid fixation of our imaging system then enables absolute measurement of field edge positioning as well as patient positioning.

The problem of finding the field edge on a megavoltage image has been discussed in the literature where a dual-exposure technique has been presented (Meertens et al, 1990a,b). We have tried to establish the field edge without the need for dual exposure. The field edge is

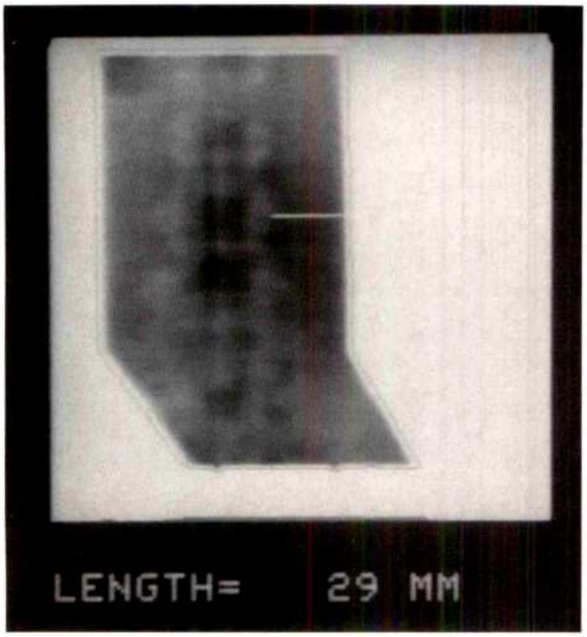

Figure 1. The field edge, defined at the 50% isodose level, determined for a "dogleg" field. Also shown is the use of the ruler technique to establish the distance between the vertebral column and the field edge.

defined at the 50% isodose level. We have used a simple method based on this to estimate the field edge. The brightest region of the image is analysed and the mean intensity there deduced and taken as the 100% level. The image is then scanned line-by-line and the 50% intensity contour established. This contour is then turned into a region of interest for further manipulation. This method relies on the assumption that the distribution of attenuation across the field is uniform. A small amount of non-uniformity will still allow accurate results, as the 50% level coincides with the steepest part of the penumbra cast by the field edge. Hence, a small error in the 100% level still yields the same position for the contour of the 50% level. In order to determine the limitations of this algorithm we have taken a set of phantom images corresponding to an extreme situation—a set of square fields with a 12 cm thickness of Perspex at one end and open field at the other. The error on the measured field edge was no more than 3 mm in the worst case. In practice, however, the calculated field size is in agreement with the collimators' prescribed settings to 1.5 mm or better. In Fig. 1 we present a field edge determination using this method for a "dogleg" field. This technique has been applied to some wedged fields and has yielded results of a similar accuracy to the phantom study described above.

Soft-tissue interfaces

The apparent positioning of soft-tissue/air and soft-tissue/bone interfaces depends critically on the grey-scale window of the displayed image. Furthermore, variations in machine output (particularly fluctuations across the whole field) mean that a given anatomical feature in one image may have a different intensity value compared with the corresponding feature in another image, a fact that compounds the problem of determining soft-tissue interfaces. We have approached this problem by applying histogram equalization to each image to be measured. The assumption is then made that a given anatomical feature has a constant, renormalized intensity in each image. This is only valid if the histogram for each image would be the same were the intensity values identical, a hypothesis that requires that the patient positioning in each image be very similar, if not identical. This method is only valid for comparing megavoltage images with other megavoltage images, as the relative strengths of the Compton scattering and photo-electric interaction processes are different at the diagnostic energies used to produce simulation images, resulting in different image quality.

Image analysis algorithms

Qualitative methods

Side-by-side. This method involves the display of two megavoltage scans, or a megavoltage image and a digitized simulator image, next to one another. Gross differences, such as a large discrepancy in rotation or the absence or misplacing of shielding blocks, would be recognizable immediately. One may also superimpose a chosen region of interest over each image. Deviations between the region of interest outline and the images would indicate the nature of any set-up errors relative to the reference image. This method is included in our system as it is traditionally employed to compare verification and simulator film images manually.

Movies. The human eye is very sensitive to motion. This property of the eye is exploited in the movie procedure. A set of images is displayed, in a temporal sequence, at the centre of the image display system's screen (Reinstein et al, 1988). Differences in anatomical structures and field definition edges between two images are vividly perceived as rapid movement.

Fading between images. In this method two images are displayed superimposed over one another in the form of a composite image whose neighbouring pixel values alternate between those of the first image and those of the second image in a "checker board" fashion. Furthermore, the pixels determined from the second image are given a DC offset so they are written in a different part of the LEXIDATA's grey-scale look-up table to those from the first image, to enable the two components to be windowed independently. The composite image is then windowed in the following manner: as the mean window level for pixels taken from the first image increases, the level for pixels from the second image decreases and vice versa. Thus, as the windowing of the composite image is adjusted, the display visually changes from one input image to the other. In between these two extremes the two are displayed superimposed and with similar brightness. A megavoltage image displayed in this manner superimposed on the corre-

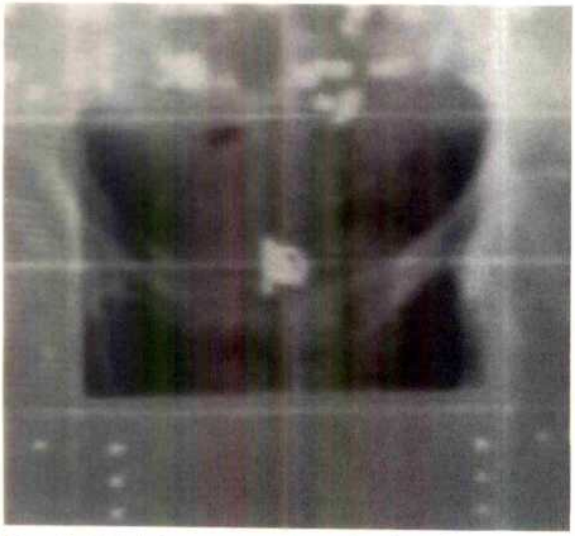

Figure 2. A fade image comprising a simulator image and the corresponding treatment time, megavoltage scan.

sponding simulator image for a pelvic field is shown in Fig. 2.

Quantitative methods

Distance and angle measurement. Conventionally, when two images are compared a ruler and a protractor are used to measure distances and angles mechanically. Such facilities are available on our system. To measure a distance the operator places a cursor at two points of interest. The distance between these points is then calculated. Such a tool may be used to establish the distances between critical structures and the field edge, for example (Fig. 1). A similar facility exists for measuring angles. Two lines are specified and the angle between them is evaluated.

Feature transposition. Two images are displayed side-by-side. A point is marked on one image along with the corresponding point on the other, using a cursor. This procedure is repeated until several points of interest have been indicated. The centre shift (x_t, y_t), rotation (θ_t) and magnification (m_x, m_y) of one image relative to the other are then calculated using the formulae presented in Equations 1–3 (Appendix). This method should give the same results as all of the methods presented below and should indicate unit magnification for all images used on our system. A method similar to this has been implemented by Meertens et al (1990a), as discussed above. The user-interface of this facility is shown in Fig. 3. In practice, the two images are displaced in the y direction to prevent any biasing of results.

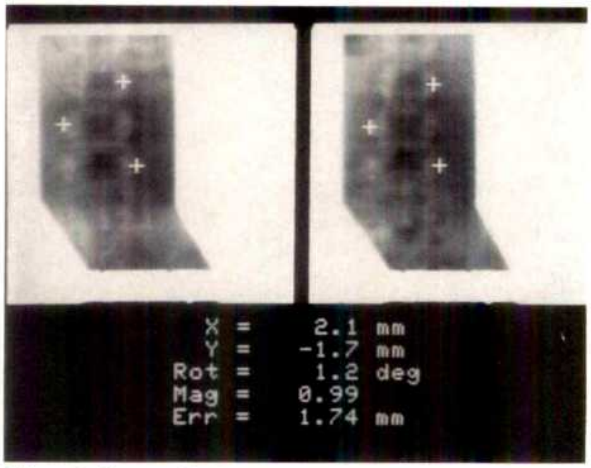

```
  X  =    2.1  mm
  Y  =   -1.7  mm
Rot  =    1.2  deg
Mag  =   0.99
Err  =   1.74  mm
```

Figure 3. The graphical user interface of feature transposition.

Region of interest transposition. In this method a region of interest (obtained from a reference image) is superimposed over the image being analysed. The operator then uses a trackerball interfaced to the LEXIDATA display system to move and rotate the ROI until the best registration with the analysed image is achieved. The shift of the ROI's centre and its rotation (about the isocentre) are displayed (Fig. 4). This routine enables a quick and simple determination of the position of the patient relative to the reference. No magnification parameter is incorporated in this algorithm at present. However, as pointed out above, all images should have the same magnification.

Movie measurement. The philosophy of the movie procedure described above has been applied to the problem of quantitative measurement. The image to be measured and the reference image are displayed in a movie consisting of two images that are displayed alternately at a rate of typically 6 frames per second. During the course of the movie, the operator may adjust the position of the image to be measured by rotation and translation. This is continued iteratively until the features of interest, such as bony structures, are seen to become stationary as the display oscillates from one image to the other. Translations are achieved, in real

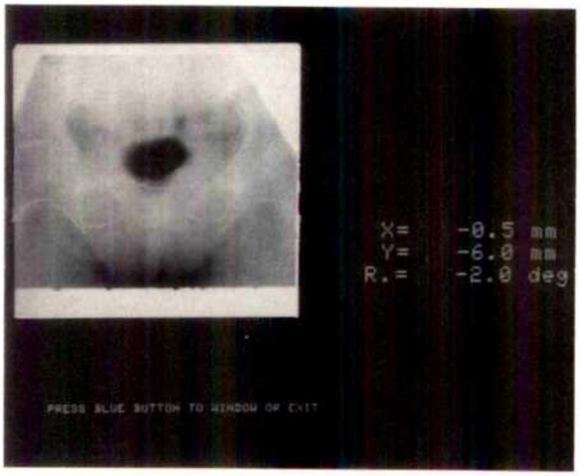

```
X=    -0.5 mm
Y=    -6.0 mm
R.=   -2.0 deg

PRESS BLUE BUTTON TO WINDOW OR EXIT
```

Figure 4. The graphical user interface of region of interest transposition.

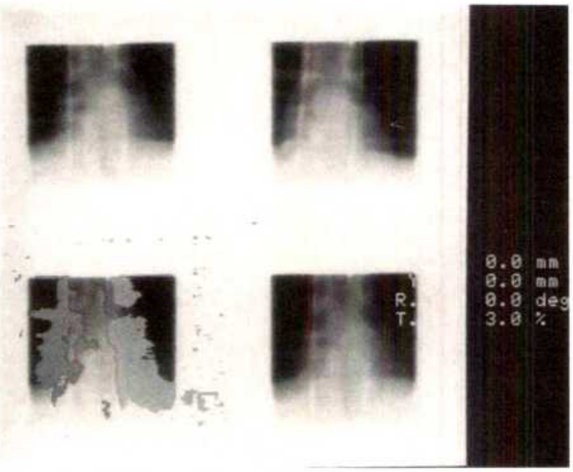

Figure 5. A difference image display. The top two images are under evaluation; the bottom right-hand image is a movie (see text), and the bottom left-hand image is the difference image. The blue region is to the left of the mediastinum (*i.e.* on the right-hand side of the difference image) and the red region is to the right of the mediastinum.

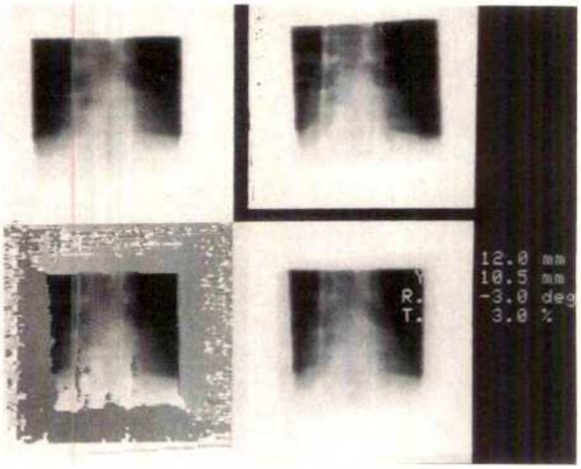

Figure 6. The corresponding image to Fig. 5 with maximal alignment of anatomy. The coloured regions at the edge of the difference image indicate that the collimators now appear in a different position and are caused by penumbra.

time, by adjusting the position at which the image is displayed on the LEXIDATA's screen. All rotations have to be carried out using digital resampling and hence are slightly slower (typically 3 s).

Difference images. The reference image and the image to be measured are normalized, using histogram equalization, as above. A pixel-by-pixel subtraction is then carried out of one image from the other. If the intensity of the first image exceeds that of the second one by more than a chosen threshold value, typically 3% of the mean image intensity, then the difference image is coloured red. Conversely, if the intensity of the second image is greater by more than the threshold, then it is coloured blue. To enable the observer to relate the positioning of these coloured regions to the topology of the original images, if the difference is below the threshold value, then the intensity of the first image is ascribed to the difference image. The two input images are also displayed. The operator then adjusts the relative positioning of the images until the amount of colour present in the anatomical detail within the difference image is minimized. This method cannot be used to compare megavoltage images with simulator images, as the dominant photon interaction process is different for the two image types, resulting in significantly different relative pixel intensities. Figure 5 shows a difference image before image position correction and Fig. 6 shows the same image once the anatomical detail has been aligned.

The source size of a radiotherapy linear accelerator is typically 2 mm at the 4% radius and the primary collimation system is of the order of 40 cm from the source. Our detector is located 2 m from the source and thus the penumbra cast will be of the order of 8 mm. The difference image method will automatically highlight block positioning and field size errors, even for the highest threshold settings, because of the large penumbra region associated with the edge of such features (see Fig. 6).

Evaluation

We grouped the measurement algorithms into two categories, depending on whether the information provided is of a qualitative or a quantitative nature. Of the five quantitative methods presented, four are for the intercomparison of two images, whereas the distance, angle technique provides information on a single image.

The intercomparison techniques may readily be verified by using them to compare images whose differences are known *a priori*. To this end a humanoid phantom was imaged at a set of known rotations, and transverse and longitudinal positions, which were obtained by adjusting the position of the treatment couch. The methods of feature transposition, ROI transposition, movie measurement and difference images were applied by four observers to measure the differences between a reference image and five measurement images. A typical set of results for such a measurement is shown in Table I. The symbol $|\vec{\delta}|$ in Table I denotes the average of the moduli of the difference measurements in x, y and θ for each technique and thus gives an estimate of the error in each case. This suggests that the average error in angle is far less than 1° and that the average error in x or y is no more than 1 mm.

Although the above results suggest that all four techniques fulfil the requirements of accuracy and reliability, the use of humanoid phantom images, in the manner described above, is somewhat different from the real situation encountered in the clinic, in that the phantom is always in the same position relative to the treatment couch. Hence, a perfect match should always be achievable simply by rotating and translating the treatment couch or treatment head (assuming the gantry to be at 0°). However, the position of a real patient on the

Table I. A typical observer's results for the measured deviations from the reference image obtained for a set of phantom images. x_t and y_t are tabulated in millimetres and θ_t is in degrees. "True" denotes the correct difference values. $|\bar{\delta}|$ is the average of the moduli of the differences between the values in each column and the correct value; it thus indicates the relative errors associated with each method

Image	True			Movie			Difference			ROI trans.			Feature trans.		
	x_t	y_t	θ_t	x_t	y_t	θ_t	x_t	y_t	θ_t	x_t	y_t	θ_t	x_t	y_t	θ_t
1	0	0	1	0	0	1	0	0	1	1	−1	1	1	−1	0
2	0	9	−3	−1	10	−3	0	9	−3	2	9	−2	0	11	−1
3	13	9	−3	12	11	−3	12	9	−3	13	11	−2	11	10	−3
4	13	5	−2	12	6	−2	11	5	−3	16	6	−2	13	6	−2
5	13	6	4	12	4	4	12	5	3	11	5	5	12	5	4
$\lvert\bar{\delta}\rvert$				0.8	1.2	0.0	0.8	0.2	0.4	1.6	1.0	0.6	0.8	1.2	0.6

treatment couch will be subject to variations due to rotations out of plane and to anatomical movements, factors that may make a good match between different treatment-time images improbable, if not impossible. Clearly, for a set of real, treatment-time patient images, the variations in position between different images is unknown. However, reproducibility between observers may be tested and is likely to be a good indication of accuracy. To this end, the four techniques have been applied to the analysis of a set of anterior images obtained from a patient being treated in the pelvic region. Four observers made measurements of the differences between a reference image and three other images of this patient. One of the images used is shown in Fig. 4. The results obtained are presented in Table II. For each pair of images, the last row of Table II lists values for the mean deviation and thus is an indicator of reproducibility. Clearly, the movie movement technique displays the best reproducibility.

Of the four intercomparison methods, the movie measurement technique was found to produce the most reproducible results, followed by the difference image, then ROI transposition and feature transposition. The good reproducibility of the movie measurement procedure is brought about by its use of all of the information within the image. Furthermore, it does not require user input to create wire-frame diagrams or to choose specific points of interest, thus removing potential sources of error. For the difference image, because of systematic noise (such as vertical streaks caused by drifts in detector gain) and a non-standard mode of image presentation, it was found necessary to vary the amount of shift quite significantly in order for the observer to establish the component of colour informa-

Table II. Results obtained from the intercomparison of a sequence of clinical images of a patient being treated in the pelvic region (see Fig. 4). Values for the mean deviation obtained from each measurement technique (σ) are also presented. x_t and y_t are in millimetres and θ_t is in degrees.

Image	Observer	Movie			Difference			ROI trans.			Feature trans.		
		x_t	y_t	θ_t	x_t	y_t	θ_t	x_t	y_t	θ_t	x_t	y_t	θ_t
1	1	−2	−3	−2	−2	−3	−1	0	−1	−1	0	−2	−1
	2	−2	−3	−2	−3	−2	0	−2	−2	0	0	0	−2
	3	−2	−3	−2	−2	−3	−2	1	0	−2	−1	−3	−1
	4	−2	−3	−2	−3	−3	0	2	−4	−2	−2	0	−2
σ		0.0	0.0	0.0	0.6	0.5	1.0	1.7	1.7	1.0	1.0	1.5	0.6
2	1	2	−3	1	3	−2	1	2	−2	2	4	1	2
	2	2	−3	1	2	−3	2	4	−2	2	3	4	−1
	3	3	−2	1	3	−2	0	3	−2	1	2	−2	1
	4	3	−3	1	3	−3	1	1	−5	3	1	−2	1
σ		0.6	0.5	0.0	0.5	0.6	0.8	1.3	1.5	0.8	1.3	2.9	1.3
3	1	3	5	−1	3	5	−2	4	3	−1	3	4	0
	2	3	3	0	3	5	−2	3	2	0	3	5	0
	3	3	5	0	3	5	−1	4	2	−1	5	5	3
	4	3	3	0	5	5	−3	3	4	0	3	4	0
σ		0.0	1.2	0.5	1.0	0.0	0.8	0.6	1.0	0.6	1.0	0.6	1.5

tion resulting from systematic noise and to determine which of the colour information is due to shifts and which is due to rotations. Thus, the difference image tool was found to be slow to use for evaluating anatomical shifts. To this end, a movie of the images has been added (Figs 5, 6). Owing to the penumbra effect, this method is, however, extremely sensitive to small variations in field position.

The field edge detection algorithm was evaluated using another set of phantom images, where the field size was set to a series of known values. 10 measurements were taken for each field size. The results indicate an error of no greater than one pixel (1.5 mm) and a standard deviation of typically no more than 0.5 mm.

It is not possible to present a numerical evaluation of the qualitative tools, so we discuss them subjectively. The movie procedure was found to be by far the most useful. It provides good visualization of shifts and rotations of both anatomical structures and the treatment field. Furthermore, it is easy to spotlight features for measurement using a movie sequence. The side-by-side image comparison method was found to be less valuable than the two other qualitative methods, unless used in conjunction with an ROI. In this case it provides a means of detecting image offsets very quickly, unlike the movie technique, which requires time to set up the sequence of images. Rotations are extremely difficult to detect with this method. The process of fading between images has been found to be useful when comparing megavoltage and simulator images, particularly as the simulator images contain information beyond the field edge, whereas the megavoltage images do not.

Summary and conclusions

In this paper we have presented an evaluation of the RMH/ICR megavoltage imaging system for patient position reproducibility studies. Various key considerations pertinent to the use of the system to make measurements have been presented: the need to have access to simulator images; the problem of finding and matching field edges; the delineation of soft-tissue interfaces; the efficacy of using regions of interest; and the desirable properties of a quantitative measurement procedure.

Several algorithms for image measurement were presented. Four provide image intercomparison information: feature transposition, ROI transposition, movie measurement, and difference images. Three are qualitative: movie, side-by-side, and fading between images. A ruler, angle measurement tool was also discussed.

The evaluation of the intercomparison algorithms shows that movie measurement, using the whole image, was the best method, followed by difference images, followed by ROI transposition, typically using the edge of a structure, followed by feature transposition, using a set of points. Thus, we conclude that the usefulness of these algorithms is determined by how much of the information content of the images is used. The difference image technique is useful for determining shifts in megavoltage images, but requires much time to implement (typically several minutes compared with 1 min or less for the other techniques). It also requires significant user familiarity because of its non-standard presentation of the image data.

In conclusion, our megavoltage imaging system is intended for patient position verification studies. A short image acquisition time (< 10 s) coupled to the speed of use of the intercomparison algorithms (no more than 1 min in all but one case) means that, in principle, information on patient set-up may be used on-line for verification of patient position, with the option for correction of this position if required. All of these algorithms may be employed to analyse patient images off-line. This is useful for studying the whole course of treatment given to a particular patient, in order to determine how closely the dose delivered matches the treatment plan. The analysis of a series of images should also provide valuable information on the accuracy and reproducibility of various set-up techniques. We have applied the software facilities discussed in this paper to patient position verification and reproducibility measurements on a day-to-day basis and have acquired data on over 200 patients. We have also investigated the feasibility of treatment intervention using our system. Papers reporting the results of these studies are in preparation.

Appendix

Quantitative image comparison

Consider a patient whose orientation we wish to determine and compare with that in a projection image taken previously (*i.e.* a reference image). Clearly the patient has six degrees of freedom (three translational and three rotational). A projection image will contain information on three of these: two are the position in the plane of the image, which we denote by x_i and y_i and one is rotation within the plane of the image (θ_i). The differences between the images must then be evaluated in order to determine the transformation in x_i, y_i and θ_i required to make the patient's position in each image register correctly.

Information about patient position in the plane orthogonal to x_i, y_i (denoted by z_i) is present in the image magnification, but a large change in z_i is necessary before magnification changes significantly.

The x_i, y_i and θ_i transformations necessary to go from the image being measured to the reference image can be calculated using simple algebra.

Rotation is given by the formula:

$$\begin{pmatrix} x' \\ y' \end{pmatrix} = \mathbf{R} \begin{pmatrix} x_i \\ y_i \end{pmatrix} = \begin{pmatrix} \cos\theta_t - \sin\theta_t \\ \sin\theta_t \cos\theta_t \end{pmatrix} \begin{pmatrix} x_i \\ y_i \end{pmatrix} \tag{1}$$

Translation is given by the formula:

$$\begin{pmatrix} x' \\ y' \end{pmatrix} = \mathbf{T} \begin{pmatrix} x_i \\ y_i \end{pmatrix} = \begin{pmatrix} 1 & 0 \\ 0 & 1 \end{pmatrix} \begin{pmatrix} x_i \\ y_i \end{pmatrix} + \begin{pmatrix} x_t \\ y_t \end{pmatrix} \tag{2}$$

Magnification is given by:

$$\begin{pmatrix} x' \\ y' \end{pmatrix} = \mathbf{M} \begin{pmatrix} x_i \\ y_i \end{pmatrix} = \begin{pmatrix} m_x & 0 \\ 0 & m_y \end{pmatrix} \begin{pmatrix} x_i \\ y_i \end{pmatrix} \qquad (3)$$

where θ_t is the rotation required, x_t, y_t are the translations required and m_x, m_y are the necessary magnifications in x and y to go from the corresponding coordinates in the image being measured (x_i, y_i) to the reference image (x', y'). Equation 1 defines a left-handed rotation such that a clockwise rotation corresponds to a positive angle. Analysis of these matrices reveals certain important features of the image matching process. In general, these operations are non-commutative, the exception being when $m_x = m_y$, in which case $\mathbf{RM} \equiv \mathbf{MR}$. Thus, if these methods are to be used to correct patient positioning, the order in which translations, rotations and magnifications are corrected is vitally important. In our implementations, rotations are carried out before translations.

Previous authors (Meertens et al, 1990a) have determined the rotation about, and translation of, the centre of gravity of a set of points specified in the images. In this case, as the centre of rotation remains fixed relative to the anatomy and not to the image frame as in the discussion above, the operations do, in fact, commute. However, we have not adopted this approach for several reasons: first, it is not clear exactly what relevance the centre of gravity of a set of arbitrarily chosen points has. Specifically, the rotation of the patient may be established unequivocally, but the centre of rotation of the patient will almost certainly not be the centre of gravity of these points and, hence, the positional shift is far more difficult to establish. Second, one may wish to use the results of a measurement to correct set-up parameters on-line. Any correction of patient set-up is carried out in the frame of reference of the accelerator, thus the translation values required are those to yield the correct position if the rotations are carried out about a fiducial point, such as the isocentre. The movement facilities of the treatment head and couch of our SL25 accelerator are designed so that the operations of translation and rotation commute. However, we present the general case here for completeness.

Acknowledgment

This work is supported by the Cancer Research Campaign. We gratefully thank Mr Ian Moore for help with the evaluation work and Mr John Codd and Mr Dave Hill for help with the construction of the detector system.

References

Amols, H. I. & Lowinger, T. 1987. An inexpensive microcomputer based port film image enhancement system. *Medical Physics, 14,* 483.

Antonuk, L. E., Yorkston, J., Morton, E. J., Boudry, J., Kim, C. W. & Longo, M. J., 1991. Flat-panel self-scanning, solid state imagers for real-time radiotherapy and digital fluoroscopy. *Medical Physics, 18,* 610.

Baily, N. A., Horn, R. A. & Kampp, T. D., 1980. Fluoroscopic visualisation of megavoltage therapeutic X-ray beams. *International Journal of Radiation Oncology, Biology, Physics, 6,* 935–939.

Bova, F. J., Fitzgerald, L. T., Mauderli, W. M. & Islam, M. K., 1987. Real time megavoltage imaging. *Medical Physics, 14,* 707.

Byhardt, R. W., Cox, J. D., Hornburg, A. G. & Liermann, G., 1978. Weekly localization films and detection of field placement errors. *International Journal of Radiation Oncology, Biology, Physics, 4,* 881–887.

Cheng, Y. A., Wong, J. W., Binn, W. R., Klarmann, J. & Epstein, J. W., 1988. On-line radiotherapy imaging using fiber-optic image reducers. In Proceedings of the World Congress on Medical Physics and Biomedical Engineering. *Physics in Medicine and Biology, 33* (Suppl. 1), 46.

Graham, M. L., Cheng, A. Y., Geer, L. Y., Binn, W. R., Vannier, M. W. & Wong, J. W., 1991. A method to analyze 2-dimensional daily radiotherapy portal images from an on-line fiber-optic imaging system. *International Journal of Radiation Oncology, Biology, Physics, 20,* 613–619.

Grimm, D. F., Wilson, C. R. & Gillin, M. T., 1987. Digital processing of radiotherapy port films. *Medical Physics, 14,* 483.

Huizenga, H., Levendag, P. C., De Porre, P. M. Z. R. & Visser, A. G., 1988. Accuracy in radiation field alignment in head and neck cancer: A prospective study. *Radiotherapy and Oncology, 11,* 181–187.

Lam, K. S., Partowmah, M. & Lam, W. C., 1986. On-line electronic portal imaging system for external beam radiotherapy. *British Journal of Radiology, 59,* 1007–1013.

Lam, W. C., Partomah, M., Lee, D. J., Wharam, M. D. & Lam, K. S., 1987. On-line measurement of field placement errors in external beam radiotherapy. *British Journal of Radiology, 60,* 361–367.

Leong, J., 1984. A digital image processing system for high energy x-ray portal images. *Physics in Medicine and Biology, 19,* 1527–1535.

Leong, J., 1986. Use of digital fluoroscopy as an on-line verification device in radiation therapy. *Physics in Medicine and Biology, 31,* 985–992.

Leong, J. C. & Stracher, M. A., 1987. Visualization of internal motion within a treatment portal during a radiation therapy treatment. *Radiotherapy and Oncology, 9,* 153–156.

Marks, J. R., Haus, A. G., Sutton, H. G. & Griem, M. L., 1974. Localization error in the radiotherapy of Hodgkin's disease and malignant lymphoma with extended mantle fields. *Cancer, 34,* 83–90.

Meertens, H., 1985. Digital processing of high-energy photon beam images. *Medical Physics, 12,* 111–113.

Meertens, H., van Herk, M. & Weeda, J., 1985. A liquid ionisation detector for digital radiography of therapeutic megavoltage photon beams. *Medical Physics, 30,* 313–321.

Meertens, H., Bijhold, J. & Strackee, J., 1990a. A method for the measurement of field placement errors in digital portal images. *Physics in Medicine and Biology 35,* 299–323.

Meertens, H., van Herk, M., Bijhold, J. & Bartelink, H., 1990b. First clinical experience with a newly developed electronic portal imaging device. *International Journal of Radiation Oncology, Biology, Physics, 18,* 1173–1181.

Morton, E. J. & Swindell, W. 1987. A digital system for the production of radiotherapy verification images. In *Proceedings of the 9th International Conference on the Use of Computers in Radiation Therapy, 375* (Elsevier/North Holland, Amsterdam).

Morton, E. J., Swindell, W., Lewis, D. G. & Evans, P. M., 1991a. A linear array, scintillation crystal-photodiode detector for megavoltage imaging. *Medical Physics, 18*(4), 681–691.

MORTON, E. J., EVANS, P. M., FERRARO, M., YOUNG, E. F. & SWINDELL, W., 1991b. Development of video frame store and distortion correction facilities for an external-beam radiotherapy treatment simulator. *British Journal of Radiology, 64,* 747–750.

MUNRO, P., RAWLINSON, J. A. & FENSTER, A., 1990. A digital fluoroscopic imaging device for radiotherapy localization. *International Journal of Radiation Oncology, Biology, Physics, 18,* 641–649.

RABINOWITZ, I., BROOMBERG, J., GOITEIN, M., MCCARTHY, K. & LEONG, J., 1985. Accuracy of radiation field alignment in clinical practice. *International Journal of Radiation Oncology, Biology, Physics, 11,* 1857–1867.

REINSTEIN, L., SHALEY, S., LESZCZYNSKI, K., COSBY, S. & MEEK, A., 1988. Megavoltage movies. *International Journal of Radiation Oncology, Biology, Physics, 15,* 200–201.

SHALEV, S., LESZCZYNSKI, K. & LEE, T., 1988. On-line portal verification. In Proceedings of the World Congress on Medical Physics and Biomedical Engineering. *Physics in Medicine and Biology, 33* (Suppl. 1), 85.

SHALEV, S., LEE, T., LESZCZYNSKI, K., COSBY, S., CHU, T. & REINSTEIN, L., 1989. Video techniques for on-line portal imaging. *Computerized Medical Imaging and Graphics, 13,* 217–226.

SWINDELL, W., MORTON, E. J., EVANS, P. M. & LEWIS, D. G., 1991. The design of megavoltage projection imaging systems: some theoretical aspects. *Medical Physics 18*(5), 855–866.

VAN HERK, M. & MEERTENS, H., 1988. A matrix ionisation chamber imaging device for on-line patient setup verification during radiotherapy. *Radiotherapy and Oncology, 11,* 369–378.

WILENZICK, R. M., MERRITT, C. R. B. & BALTER, S., 1987. Megavoltage portal films using computed radiographic imaging with photostimulable phosphors. *Medical Physics, 14,* 389–392.

WONG, J. W., BINN, W. R., CHENG, Y. A., GEER, L. Y., EPSTEIN, J. W., KLARMANN, J. & PURDY, J. A., 1990. On-line radiotherapy imaging with an array of fiber-optic image reducers. *International Journal of Radiation Oncology, Biology, Physics, 18,* 1477–1484.

1992. *The British Journal of Radiology*, *65*, 710–714

Asymptomatic temporal lobe injury after radiotherapy for nasopharyngeal carcinoma: incidence and determinants

By S. F. Leung, MB, BS, FRCR, *Louis Kreel, MD, FRCP, FRCR and S. Y. Tsao, MB, BS, FRCR, DMRT

Departments of Clinical Oncology and *Diagnostic Radiology and Organ Imaging, Chinese University of Hong Kong, Hong Kong

(Received 21 October 1991 and in revised form 25 February 1992, accepted 12 March 1992)

Keywords: Brain injury, Hyperfractionation, Nasopharyngeal carcinoma

Abstract. Computed tomography (CT) scans were performed on a cohort of 60 patients for detection of temporal lobe injury (TLI) at 1–3.5 years after radiation therapy for nasopharyngeal carcinoma. Nine cases of TLI were identified, five of which were asymptomatic. The earliest case of asymptomatic TLI was found at 2.2 years after radiation therapy and the earliest symptomatic case at 2.3 years. A significantly higher incidence of TLI was found in patients with decreased temporal lobe shielding consequent to omitted eyeshield to the anterior photon beam and in patients treated with a hyperfractionation schedule giving 67.2 Gy in 42 fractions in 6 weeks. The incidence in these subgroups at 2–3.5 years after radiation therapy was 56% (5/9 patients) and 35% (8/23 patients), respectively. No patient in this study had TLI in the absence of these two factors. The implications of the results are discussed.

The nasopharynx is intimately related anatomically to the sphenoid sinus and the inferior portions of the temporal lobes. Part of the temporal lobes are often included within the radiation portals for treatment of nasopharyngeal carcinoma (NPC). Temporal lobe injury (TLI) is an important dose-limiting late effect of radiation therapy for NPC. The diagnosis of TLI is usually reached by computed tomography (CT) or magnetic resonance imaging (MRI) of patients who present with symptoms suggestive of cerebral dysfunction on follow-up (Lee et al, 1988, 1990). However, the true incidence of this dose-limiting complication has previously not been established because asymptomatic patients with TLI were not included. This information is important for optimization of therapy when different dose-fractionation schedules and treatment techniques are compared.

Method and materials

This is a preliminary report of a prospective study on a cohort of 60 patients with NPC treated by radical radiation therapy at the Department of Clinical Oncology, Prince of Wales Hospital, Hong Kong, between April 1986 and July 1988. All the patients had moderately advanced local disease with either nasal extension and/or skull-base involvement. None had intracranial extension of tumour. The same radiation therapy technique was used for all patients apart from a modification for those with anterior extension of tumour.

The radiotherapy details have been described previously (Ho, 1982). In summary, the primary tumour was treated by a three-field plan comprising one anterior and two lateral wedged portals using 6 MeV photons from a linear accelerator. An anterior 14 MeV electron beam was also included for part of the treatment of cases with anterior extension of disease, with modification of the weighting of the lateral beams. The superior border of the lateral and anterior portals lay at 0.5–2 cm above the roof of the sphenoid sinus, depending on the extent of disease (Fig. 1). The eyeshields in the anterior portal spared most parts of the temporal lobes from the anterior beam, leaving only the inferior and inferomedial parts within the target volume (Fig. 1). In nine patients the disease extent was such that omission of one of the eyeshields in the anterior portal was necessary for adequate tumour coverage. A larger volume of ipsilateral temporal lobe was consequently included in the target volume of these cases. The dose to the temporal lobe in this study refers to the dose in those parts of the temporal lobes within the target volume that received the prescribed tumour dose.

Two different dose-fractionation schedules were used. Thirty-two patients were treated by a conventional fractionation schedule (QD schedule) of either 60 Gy in 24 fractions in 6 weeks or 60 Gy in 26 fractions in 6 weeks. Twenty-five patients were treated by a hyperfractionation schedule (BID schedule), which delivered 67.2 Gy in 42 fractions in 6 weeks using 1.6 Gy per fraction given twice a day 4 h apart, with a 1.5-week rest period after 38.4 Gy. The portals were reduced for the last 6.4 Gy in the BID schedule with the superior borders of the portals lying 1–2 cm below the roof of the sphenoid, leaving smaller portions of the temporal lobes

---

Address correspondence to Dr S. F. Leung, Department of Clinical Oncology, Prince of Wales Hospital, Shatin, Hong Kong.

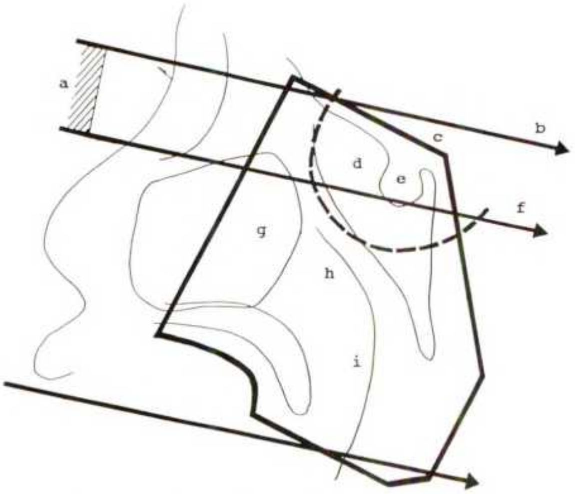

Figure 1. Diagrammatic representation of anatomical structures and projections of radiation portals as seen on a lateral radiograph of the skull. Fine lines outline relevant anatomy. Bold lines represent borders or projections of radiation portals. The dotted line represents the inferior limit of temporal lobes. *Legend*: a, eyeshields on anterior portal—medial borders 1.75 cm from midline, inferior borders 0.5 cm above inferior orbital margins; b, projection of superior border of anterior portal; c, superior border of lateral portals; d, sphenoid sinus; e, pituitary fossa; f, projection of inferior limit of eyeshields—the volume of temporal lobes below this line lies within the target volume; g, maxillary sinus; h, roof of nasopharynx; i, posterior wall of nasopharynx.

within the target volume in this last part of the treatment. Intracavitary booster doses were given to eight patients with residual disease at the nasopharynx 1 month after external radiotherapy. The dose was 24 Gy in 3 fractions in 15 days prescribed at 1 cm from the mid-point of the plane of sources. No patient received chemotherapy treatment.

The diagnosis of TLI was based on the observation of hypodense shadows in temporal lobe(s) in the absence of evidence of recurrent tumour on the cranial CT scan. The characteristic signs of TLI on the CT scan and the factors supporting the diagnosis of TLI have been described previously (Lee et al, 1988). To economize on resources, the timing of the first scan was randomly assigned at 1–3.5 years post-treatment to allow a preliminary assessment of the time-distribution of asymptomatic TLI. Scans were repeated at approximately yearly intervals and 11 patients had a second scan 10–18 months after the first at the time of analysis. Patients were also scanned whenever they developed symptoms suggestive of brain injury.

Results

Five cases of TLI were identified on the first CT scan performed within 3.5 years after radiotherapy for the 60 patients. All were asymptomatic except one. One of the four asymptomatic patients developed symptoms 9 months after the initial scan. Four more cases of TLI (two symptomatic) were found among the 11 second scans performed at 10–18 months after the first. Thus a total of nine patients with TLI were identified within 3.5 years post-treatment, four of whom were symptomatic.

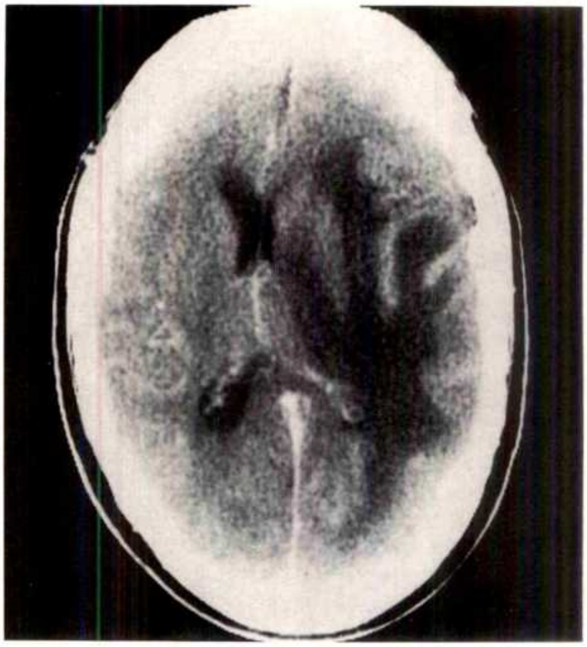

Figure 2. CT scan of a patient with symptomatic temporal lobe injury. A hypodense shadow with a finger-like configuration associated with midline shift is evident.

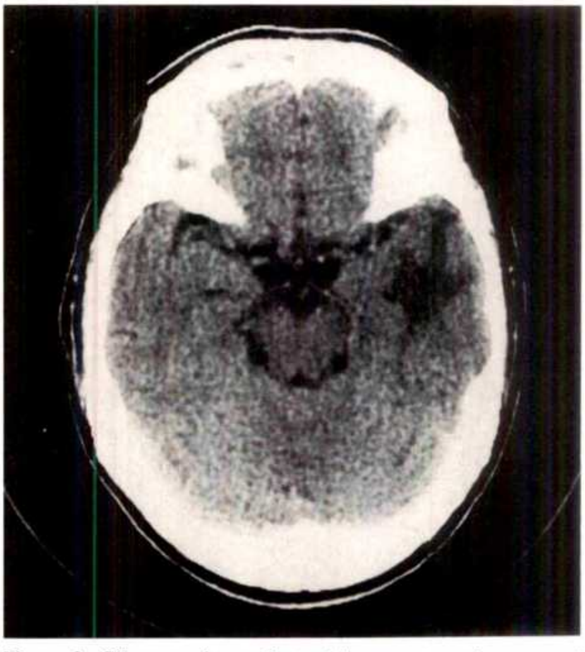

Figure 3. CT scan of a patient with asymptomatic temporal lobe injury. The hypodense area is limited in extent.

All the symptomatic cases had well-developed hypodense shadows in the white matter of the temporal-parietal lobes associated with significant pressure effects such as midline shift (Fig. 2). Two patients presented with significant deterioration of memory, one with an episode of loss of consciousness and the other with episodes of a sensation of coldness associated with aura. The hypodensities in asymptomatic cases were on average less extensive (Fig. 3), and none was associated with midline shift. The earliest case of asymptomatic TLI was found at 26.5 months after radiotherapy and the earliest symptomatic case at 28 months. This suggests that TLI does not manifest within the first 2 years after a single course of radiotherapy.

For the purpose of this preliminary analysis, the incidence of TLI was computed for the interval 2–3.5 years after radiotherapy. The overall incidence was 22% (9/41 cases). Tables I and II show the correlation of TLI with possible contributory factors. A significantly higher incidence was found in patients with omitted eyeshield to the anterior beam ($p = 0.01$, Fisher's Exact test). A higher incidence approaching statistical significance was also found in patients treated by the BID schedule ($p = 0.05$, Fisher's Exact test). In patients with intact eye shields, the rates of TLI in the BID schedule and the QD schedule were 4/17 and 0/15, respectively, while in patients with omitted eyeshields the rates were 4/6 and 1/3, respectively. This suggests that the two risk factors may have an additive effect, although each of the four subcategories contains too few patients for useful statistical comparison. The number of patients with intracavitary booster or medical problems was also too small for interpretation of the significance of these factors.

Table II. Incidence of TLI in different subgroups of patients

Characteristic	No. of patients with CT scan between 2 and 3.5 years follow-up (total = 41)	Incidence of TLI at 2–3.5 years follow-up	p value
BID schedule	23	8/23 = 35%	
QD schedule	18	1/18 = 6%	0.05
Omitted eyeshield	9	5/9 = 56%	
Intact eyeshield	32	4/32 = 13%	0.01
Intracavitary booster	4*	1/4 = 25%	
No booster	37	8/37 = 22%	*
Hypertension/diabetes	2*	1/2 = 50%	
No hypertension/ diabetes	39	8/39 = 21%	*

*Numbers too small for meaningful interpretation.

Discussion

The overall incidence of TLI of 22% in the follow-up interval between 2 and 3.5 years in the present study is alarmingly high. This is, however, not a representative figure since there is a great variation in the incidence in different subgroups of patients. The complication is confined only to patients treated by a plan requiring decreased temporal lobe shielding and/or hyperfractionation. In other words, no patient treated by conventional fractionation with fraction sizes of 2–2.5 Gy by the technique in the present study was affected. In a retrospective analysis of 9606 NPC patients treated by techniques similar to ours, Lee et al found only a 1.6% incidence of symptomatic TLI at 9 months to 16 years after radiation therapy (Lee et al, 1988). All the affected patients in their series had been treated with either large fraction sizes or had received more than one course of radiation therapy. The results of the present study and Lee's study suggest that for patients treated with fraction sizes of 2–2.5 Gy, occurrence of TLI as early asymptomatic or late symptomatic cases is improbable.

The high incidence of TLI in patients with omitted eyeshield suggests that the complication was related to the volume of temporal lobe included within the target volume, especially in view that the involved temporal

Table I. Characteristics of patients with TLI

Patient	BID schedule	No eye shield	Intracavitary booster	Hypertension
1	*			
2	*			
3	*			
4	*			*
5	*	*	*	
6	*	*		
7	*	*		
8	*	*		
9		*	*	

*Represents presence of the factor in the respective patient.

Table III. Estimated biological effective doses (Fowler, 1989) to the temporal lobes in different dose schedules

	Assumed α/β value	Assumed repair half-time (hours)	BED
QD schedule 60 Gy/26 fr/6 wk	3	/	106.7
QD schedule 60 Gy/24 fr/6 wk	3	/	110
BID schedule 67.2 Gy/42 fr/6 wk	3	1.5	108.7
BID schedule 67.2 Gy/42 fr/6 wk	3	2.0	112
BID schedule 67.2 Gy/42 fr/6 wk	3	3.0	117.3
BID schedule 67.2 Gy/42 fr/6 wk	3	4.0	121
QD schedule 60 Gy/26 fr/6 wk	1.5	/	153.3
QD schedule 60 Gy/24 fr/6 wk	1.5	/	160
BID schedule 67.2 Gy/42 fr/6 wk	1.5	1.5	150.8
BID schedule 67.2 Gy/42 fr/6 wk	1.5	2.0	156.8
BID schedule 67.2 Gy/42 fr/6 wk	1.5	3.0	167.3
BID schedule 67.2 Gy/42 fr/6 wk	1.5	4.0	174.7

$BED = D(1 + d[1 + h_m]/\alpha/\beta)$ where BED = biological effective dose, D = total dose, d = dose per fraction, h_m = incomplete repair factor (Thames & Hendry, 1987).

lobe was on the same side as the omitted eyeshield in all these cases. The higher incidence of TLI in patients treated by the BID schedule compared with the QD schedule was, however, unexpected. It is known that the effect of alteration of fraction size is more profound in neural tissue than in other late-reacting tissues. In fact one of the rationales of using hyperfractionation is to decrease the late damage on dose-limiting organs so that the therapeutic ratio can be improved (Thames et al, 1983).

In the modified NSD equation for late effects on the human brain, several authors have established a value for the N exponent in the range of 0.44–0.55 (Cohen & Creditor, 1983; Pezner & Archambeau, 1981; Sheline et al, 1980; Wigg et al, 1981). Applying the btu equation described by Pezner and Archambeau (1981) where $\mathrm{TD} = \mathrm{btu} \times N^{0.45} \times T^{0.03}$, the btu value of 1119 in the BID schedule is *lower* than the btu values of 1240 and 1285 in the QD schedule. Table III gives a range of the estimated biologically effective doses of the BID schedule and QD schedule based on the linear-quadratic formula (Fowler, 1989; Thames et al, 1984; Thames & Hendry, 1987). It is apparent that the relative doses of the BID and QD schedules would be different for different assumed values of α/β and repair half-times of the temporal lobe, although the comparison is complicated by the fact that the target volume was reduced in the last 6.4 Gy of the BID schedule but not in the QD schedule. Assuming the validity of the linear-quadratic formula, the higher incidence of TLI in the BID schedule can be explained if the repair half-time of temporal lobe tissue is longer than 2 h. The implication is that a longer interval between the twice-a-day fractions may be crucial in reducing the incidence of TLI. The importance of the interfraction interval on late effects has also been substantiated by more recent studies of hyperfractionated radiotherapy (Cox et al, 1991).

In an analysis of the results of hyperfractionation radiotherapy treatment of 60 NPC patients followed-up for 6–7 years, Wang did not encounter any case of brain injury (Wang, 1989). The fractionation schedule used by Wang was the same as that used in our patients except that routine booster doses were given in Wang's series but not in our series. The absence of clinical TLI in Wang's series is probably attributable to the radiotherapy technique used, which gives more sparing of the temporal lobes compared with ours. In our experience, however, it is difficult to apply Wang's technique to limit the dose to the temporal lobe in those patients with significant extension of disease to the skull base, since the ethmoid sinus and the anterior part of the skull-base may not be fully covered in the treatment phase using an arc technique.

The natural history of asymptomatic TLI has not been defined. Only one patient in the observation period progressed from the asymptomatic to the symptomatic phase. The lesser extent of CT scan changes in asymptomatic TLI compared with symptomatic TLI suggest that the former is likely to represent an early phase of the latter, although the time of occurrence of the first asymptomatic case (at 26.5 months) and that of the first symptomatic case (at 28 months) were quite similar. Two patients in this study developed symptomatic TLI at 10 and 12 months, respectively, after an initial normal CT scan. This suggests that the duration of the asymptomatic phase in some patients, if it occurs at all, is relatively short. On the other hand, the significant proportion of asymptomatic TLI compared with symptomatic TLI (ratio 5 : 4) in this study and the very low incidence of symptomatic TLI in other studies would suggest that the duration of the asymptomatic phase in some patients may be very long or it may not progress to the symptomatic phase at all. A longer follow-up is required to reveal the evolution and to assess the management of asymptomatic TLI.

Acknowledgments

The results of this study were presented at the 42nd Scientific Meeting of the Royal Australasian College of Radiologists in Adelaide, Australia, 14–18 September, 1991. We would like to thank Drs Wesely Shiu, Peter Teo, Peter Choi and W. H. Kwan of the Department of Clinical Oncology and Professor Metreweli of the Department of Diagnostic Radiology and Organ Imaging, Chinese University of Hong Kong, for their invaluable comments and input of ideas. We would also like to thank Mr Alan Tang for statistical advice. This study was supported by the Chinese University of Hong Kong Research Fund.

References

COHEN, L. & CREDITOR, M., 1983. Iso-effect tables for tolerance of irradiated normal human tissues. *International Journal of Radiation Oncology, Biology, Physics*, *9*, 233–241.

COX, J. D., PAJAK, T. F., MARCIAL, V. A., COIA, L., MOHIUDDIN, M., FU, K. K., SELIM, H., RUBIN, P. & ORTIZ, H., 1991. Interfraction interval is a major determinant of late effects, with hyperfractionated radiation therapy of carcinomas of upper respiratory and digestive tracts: results from Radiation Therapy Oncology Group protocol 8313. *International Journal of Radiation Oncology, Biology, Physics*, *20*, 1191–1195.

FOWLER, J. F., 1989. The linear-quadratic formula and progress in fractionated radiotherapy. *British Journal of Radiology*, *62*, 679–694.

HO, J. H. C., 1982. Nasopharynx. In *Treatment of Cancer*, ed. by K. E. Halnan, J. L. Boak, D. Crowther, C. F. von Essen, J. S. Orr and M. J. Peckham (Igaku-shoin, New York) pp. 249–267.

LEE, A. W. M., NG, S. H., HO, J. H. C., TSE, V. K. C., POON, Y. F., TSE, C. C. H., AU, G. K. H., O, S. K., LAU, W. H. & FOO, W., 1988. Clinical diagnosis of late temporal lobe necrosis following radiation therapy for nasopharyngeal carcinoma. *Cancer*, *61*, 1535–1542.

LEE, A. W. M., CHENG, L. O. C., NG, S. H., TSE, V. K. C., O, S. K., AU, G. K. H. & POON, Y. F., 1990. Magnetic resonance imaging in the clinical diagnosis of late temporal lobe necrosis following radiotherapy for nasopharyngeal carcinoma. *Clinical Radiology*, *42*, 24–31.

PEZNER, R. D. & ARCHAMBEAU, J. O., 1981. Brain tolerance unit: a method to estimate risk of radiation brain injury for various dose schedules. *International Journal of Radiation Oncology, Biology, Physics*, *7*, 397–402.

SHELINE, G., WARA, W. & SMITH, V., 1980. Therapeutic irradiation and brain injury. *International Journal of Radiation Oncology, Biology, Physics*, *6*, 1215–1228.

THAMES, H. D. & HENDRY, J. H., 1987. In *Fractionation in Radiotherapy*, ed. by H. D. Thames and J. Hendry (Taylor & Francis, London), pp. 232–233.

THAMES, H. D., PETERS, L. J., WITHERS, H. R. & FLETCHER, G. H., 1983. Accelerated fractionation vs hyperfractionation: rationales for several treatments per day. *International Journal of Radiation Oncology, Biology, Physics, 9,* 127–138.

THAMES, H. D., WITHERS, H. R. & PETERS, L. J., 1984. Tissue repair capacity and repair kinetics deduced from multifractionated or continuous irradiation regimens with incomplete repair. *British Journal of Cancer, Suppl. VI,* 263–269.

WANG, C. C., 1989. Accelerated hyperfractionation radiation therapy for carcinoma of the nasopharynx: techniques and results. *Cancer, 63,* 2461–2467.

WIGG, D. T. R., KOSCHEL, K. & HODGSON, G. S., 1981. Tolerance of the mature human central nervous system to photon irradiation. *British Journal of Radiology, 54,* 787–798.

1992, *The British Journal of Radiology*, *65*, 715–717

Technical notes

Anal endosonography: which endoprobe?

By Maria Papachrysostomou, MD, *S. D. Pye, PhD, †S. R. Wild, DMRD, FRCR, FRCPEd and A. N. Smith, MD, FRCSEd, FRCPEd

Departments of Surgery, *Medical Physics and †Radiology, Western General Hospital, Edinburgh, UK

(Received 10 July 1991 and in revised form 14 October, accepted 25 October 1991)

Keywords: Anal endosonography, External and internal anal sphincters

Anal endosonography is a simple, minimally invasive technique that can be used to visualize the anal sphincters and can be advantageous in evaluating the anorectum. The first ultrasonographic studies of the human intestinal wall thickness were made many years ago (Wild, 1950). Until recently, technical shortcomings of the equipment have prevented the clinical use of ultrasound as a means of imaging the anal sphincters; so disruption of a sphincter was determined from clinical examination, pressure studies and by concentric electromyogram mapping. Modern endoprobes give high-resolution ultrasound images of the separate sphincter muscles (Law & Bartram, 1989).

When an endoprobe is introduced into the anal canal, it is bound to distend the canal to some extent. Different groups of investigators have used different sizes of endoprobes. We were interested to discover if the larger sizes of probes would have any stretching effect on the sphincters, altering their thicknesses. For this reason, two ultrasound endoprobes of different tip diameter were used in evaluating how the thickness of the anal sphincters might respond to the stretching effects of the probe size.

Materials and methods

Anal endosonography was conducted on 38 patients using two probes: (1) a Bruel & Kjaer 6.5 MHz radial rotating endoprobe of maximum tip diameter 1 cm, and (2) a 7 MHz radial rotating endoprobe of maximum tip diameter 2 cm (Fig. 1). The 1 cm probe tip was fitted with a rigid plastic cone filled with degassed water to provide protection for the rotating probe and effective acoustic coupling within the anal canal. The 2 cm probe tip was protected by a disposable latex tube containing degassed water. Both endoprobes were used in each patient, at the same visit to the hospital.

Each lubricated endoprobe was inserted into the rectum with the patient in the left lateral position and serial images were obtained on slow withdrawal of the endoprobe from the rectum through the anal canal. Video-recordings of the ultrasound scanning were obtained for all patients and were stored for further analysis and study. Hard copy was acquired on single-sided emulsion film and measurements of sphincter thickness were made to ±0.2 mm. The smooth muscle of the internal anal sphincter (IAS) was clearly identifiable as a homogeneous hypoechoic circular band extending caudally to a level just proximal to the anal verge. The striated muscle of the external anal sphincter (EAS) had a different acoustic texture, with mixed echogenicity and linear pattern, giving a "streaky" appearance. Between the two sphincters there was a narrow echogenic band that represented the intersphincteric plane. Immediately adjacent to the endoprobe tip was a hypoechoic layer of mucosa, continuous with the rectal mucosa. Between the mucosa and the IAS was the more echogenic submucosa, which became progressively denser and thicker caudally (Fig. 2). It was possible to identify clearly the hypoechoic layer of the IAS lying

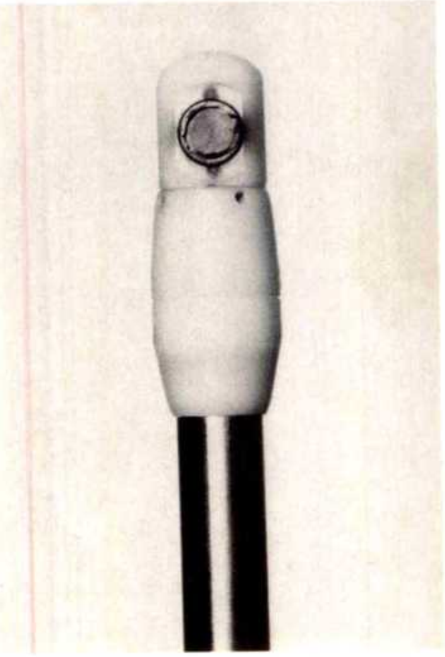

Figure 1. The 7 MHz radial rotating endoprobe, maximum tip diameter 2 cm. The 6.5 MHz endoprobe had a similar appearance, but with a 1 cm diameter.

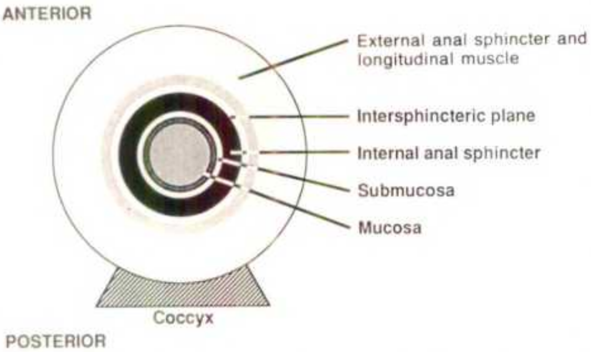

Figure 2. Diagrammatic representation of the different layers of the anal canal as visualized by ultrasonography.

between the two more echogenic structures of the submucosa and the intersphincteric plane. Measurements of the IAS thickness were thus simple and accurate (Fig. 3). On the other hand, the EAS thickness measurements were not as easy to acquire since the EAS was adjacent to the hyperechoic intersphincteric plane, and therefore there is hardly a distinctive line between the two layers of muscle. The solution to this was to measure the thickness of the EAS at the very distal part of the anal canal and to relate its outer border to the anterior border of the coccyx. The thickness of the muscle measured in that way is subjective and depended on individual anatomical considerations. The thickest terminal portion of the internal sphincter was measured at the mid-anal canal. In the lowermost part of the anal canal, the thickness of the EAS was measured using the boundaries of the coccyx shadow.

Results

With the 1 cm endoprobe, results (mean ± SD) were IAS thickness = 0.29 ± 0.11 cm, and EAS thickness = 0.81 ± 0.15 cm. With the 2 cm endoprobe, results (mean ± SD) were IAS thickness = 0.22 ± 0.07 cm, and EAS thickness = 0.83 ± 0.24 cm.

A paired *t*-test was used for comparing the thicknesses of the anal sphincters in the 38 patients using both endoprobes. This showed no difference in the measurements of EAS thickness using either endoprobe ($p > 0.5$), whereas the IAS was found to be thinner in appearance when measured using the 2 cm diameter endoprobe ($p = 0.0003$).

Discussion

We have used ultrasonographic demonstration of the sphincters in patients with various disease states and have measured the thicknesses of both the IAS and EAS using two endoprobes.

The larger 2 cm endoprobe alters the thickness of the IAS by about 30%, but had no measurable effect on the EAS. We would expect the IAS to be more susceptible to stretching than the EAS because of its small size. This is approximately 20 times less than the diameter of the larger probe used. In addition, the difference resulting from stretching may also depend on the IAS smooth muscle "elastance" property. On the contrary, the EAS striated muscle may be less subject to distension effects because of its tonic control, which allows adaptation.

Our conclusion is that a 1 cm diameter endoprobe is preferable for imaging the anal sphincters and for measuring their thickness, since it causes less disturbance than the 2 cm probe.

As various rectal endoprobes with tip diameters ranging from 1 cm to over 2 cm are in common use, it is

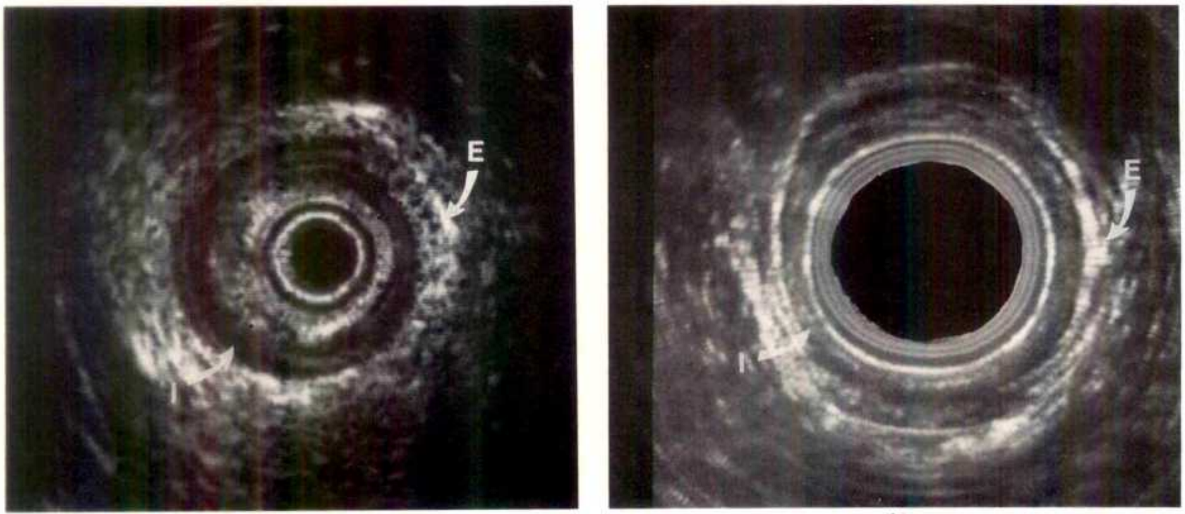

(a) (b)

Figure 3. (a) Anal ultrasonogram using a 6.5 MHz endoprobe of 1 cm diameter. Arrow I indicates the hypoechoic IAS; Arrow E indicates the hyperechoic EAS. (The coccyx is not visible at this level in the anal canal.) (b) Anal ultrasonogram of the same patient as in (a), using the 7 MHz endoprobe of 2 cm tip diameter, detecting a "thinner" IAS.

important that the size of the probe used should be recorded when reporting anal sphincter measurements.

Acknowledgments

Dr M. Papachrysostomou was supported by the Scottish Home and Health Department Clinical and Biomedical Research Grant (K/MRS/5001202). Miss N. Clare is thanked for her technical assistance.

References

Law, P. J. & Bartram, C. I., 1989. Anal endosonography—technique and normal anatomy. *Gastrointestinal Radiology*, *14*, 349–353.

Wild, J. J., 1950. The use of ultrasonic pulses for the measurement of biologic tissues and the detection of tissue density changes. *Surgery*, *27*, 183–188.

Virtual source distances and field geometry independent output factors for 5–14 MeV electron beams from a Siemens Mevatron M7145

By J. H. Plane, BA, MSc and M. M. Trevor, BSc, MSc

Regional Medical Physics Department, South Cleveland Hospital, Marton Road, Middlesbrough, Cleveland TS4 3BW, UK

(*Received 30 October 1991 and in revised form 16 March 1992, accepted 7 April 1992*)

Keywords: Virtual source distances, Output factors, Electron beams

It is well established that an inverse square factor based on virtual source distance (VSD) corrects for an air space between the electron applicator and the skin surface (ICRU, 1972; Almond, 1976). Values of VSD [illegible]ave been measured for electron fields of a Siemens [illegible]evatron M7145. Double scattering foils and collima[illegible]s above the applicator reduce scatter from the applicator walls. As a result some virtual sources are near to the electron window. However, there is some variation with energy and field size.

Output factors for open applicators and those containing irregular shaped fields have been measured for a range of applicators and irregular areas. The output factor for the open applicator is valid for any irregular shape within a given range. Possible reasons for this effect are discussed.

Method

Electrons from a Siemens Mevatron M7145 linear accelerator at South Cleveland Hospital were investigated. The energies of electrons as measured using the HPA protocol (HPA, 1985) were 5.0, 7.2, 9.2, 12.0 and 14.0 MeV. Applicators ranged in size from a 5 cm diameter circle to 10 × 10 cm, 15 × 15 cm, 20 × 20 cm and 25 × 25 cm.

The method used to measure VSD was described by Almond (1976). Ionization readings were made in air using a thimble ionization chamber (Type 2571, NE Ltd) connected to an electrometer (Type 2570, NE Ltd). The chamber was moved using a custom made lead screw driven by a stepper motor. The distances from the end of the applicator were 0, 5, 10, 15, 20, 25 and 30 cm. The transmission ionization chamber of the linear accelerator was used as a reference. The radiation beam was on continuously. Readings were taken by switching the dose meter on for 6 s in each position. This gave adequate ionization readings up to and including 30 cm. The automatic frequency control of the linear accelerator stabilized the output and helped maintain precision. A graph of reciprocal square root of ionization readings against distance from the end of the applicator gave a straight line using linear regression (Klevenhagen, 1985). The interecept on the distance axis gave the value of VSD.

The method used to measure the output factor was that described by HPA (1985). An ionization chamber in a multilayer polystyrene phantom was irradiated. Open applicators in contact with the phantom were used. Regular and irregular fields were produced using the method of Plane and Usher (1990).

Results

The values of VSD are shown in Fig. 1. For high energies at large field sizes the virtual source approaches the electron window. At lower energies and smaller field sizes the VSD was reduced.

The relative outputs of electron fields are shown in Fig. 2. Each output factor is normalized to the 10 cm square open applicator. Fig. 2 shows output factors for regular and irregular shaped fields. Irregular shaped fields may include or exclude the central axis of the applicator. In both cases the output factors are remarkably close to the open applicator.

Application

The absence of significant field geometry dependence permits considerable simplification of irregular field dosimetry. This simplification applies to a Siemens Mevatron M7145. An output factor, OF, can be used depending only on the size of the applicator and the

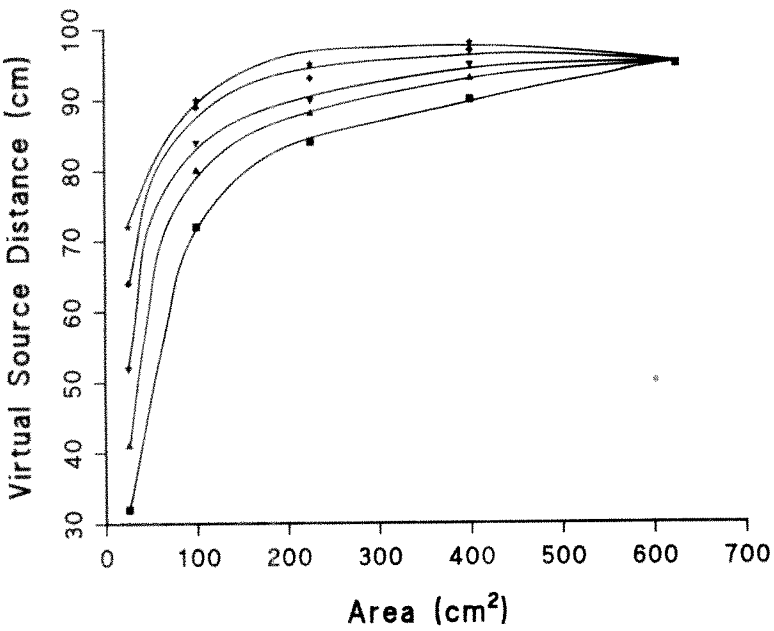

Figure 1. Virtual source distance against area for different applicators and electron energy. ■ 5 MeV, ▲ 7 MeV, ▼ 9 MeV, ◆ 12 MeV, * 14 MeV.

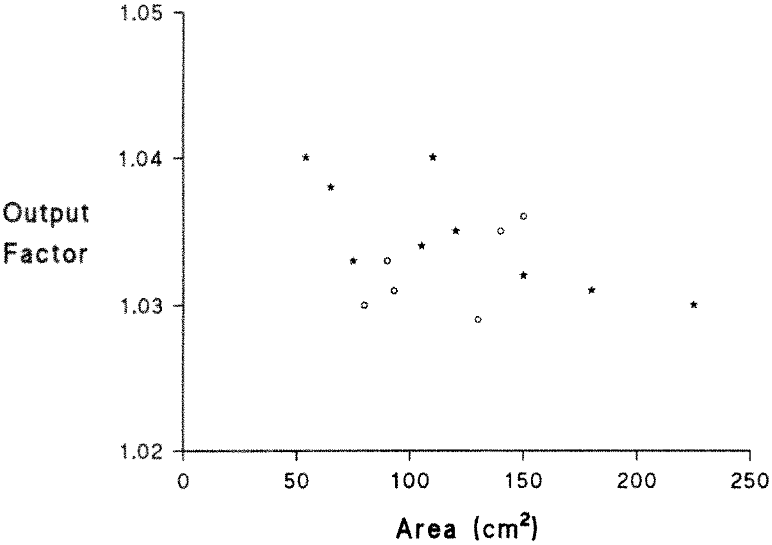

Figure 2. Relative output factors of electron fields for a 15 cm applicator at 9 MeV. * regular, ○ irregular.

electron energy. The mean and standard deviation from the data in Fig. 2 is 1.033±0.005. This compares with 1.030 for the open applicator. The close agreement is typical of all data collected in this study. The number of monitor units (MU) to be set on the dosimetry system is calculated from

$$\mathrm{MU} = \frac{D \times 100 \times (\mathrm{VSD}+s)^2 \times 1}{n \times p \times (\mathrm{VSD})^2 \times \mathrm{OF}}$$

At this centre the radiotherapy prescription defines the total dose (D) the number of fractions (n) and therapeutic range. The last parameter is used to select electron energy, depth of bolus material and the prescribed percentage (p). At the attendance of the patient for the first fraction the stand off (s) between the end of the applicator and the surface of the entry surface is measured.

Output factors are measured to three decimal places but quoted to two decimal places. This does not compromise the tolerance level of 2% required by WHO (1988).

Discussion

In this centre all radiotherapy with electrons comprises single straight on fields. Without the prerequisite of a detailed dose distribution any correction for air gap between the end of the applicator and the skin is made using VSD. Numerical data derived from other centres using accelerators from other manufacturers (*e.g.* Thomas, 1988) do not strictly apply.

It has been verified experimentally that the output of an open field is not sensitive to the change brought about by an electron cut out. An analysis of output factors using different areas failed to produce a curvilinear relationship. This is because regular shaped electron fields have variable size, shape and position with respect to the open area of the applicator. In practice, since irregular electron fields display differences in all three variables, it is surprising that the output could be predicted. It has been the practice in this centre to measure experimentally the output factor of each electron field based on HPA (1985) protocol. As a consequence of the above, this practice has been largely discontinued and is now confined to a small percentage of individual electron fields.

h.
M.
tor
ca

Acknowledgments

The authors thank Dr J. K. Haywood for continuous encouragement and Miss S. Nurse for technical assistance.

References

ALMOND, P. R., 1976. *Clinical Application of the Electron Beam.* Ed. by N. du V. Tapley (Wiley, New York), 34–36.

HPA, 1985. Code of practice for electron beam dosimetry in radiotherapy. *Physics in Medicine andBiology, 30,* 1169–1194.

ICRU, 1972. *Radiation Dosimetry: Electrons with Initial Energies Between 1 and 50 MeV.* (ICRU, Washington DC).

KLEVENHAGEN, S. C., 1985. *Physics of Electron Beam Therapy* (Adam Hilger, Bristol), 173–195.

PLANE, J. H. & USHER, C., 1990. A rapid method of production of irregular shaped fields for use with patients receiving electron radiotherapy. *British Journal of Radiology, 63,* 882–883.

THOMAS, S. J., 1988. Virtual source distances for electron beams between 5 and 20 MeV. *Physics in Medicine and Biology, 33,* 1325–1328.

WHO, 1988. *Quality Assurance in Radiotherapy* (WHO, Geneva), 15–37.

1992, *The British Journal of Radiology*, *65*, 720–722

Case reports

Gadolinium-DTPA enhanced MRI in neonatal osteomyelitis of the cervical spine

By A. Martijn, MD, PhD, A. M. van der Vliet, MD, *W. M. van Waarde, MD and *W. M. C. van Aalderen, MD, PhD

Departments of Radiology and *Pediatrics, University Hospital Groningen, Oostersingel 59, 9713 EZ Groningen, The Netherlands

(*Received 28 August 1991 and in revised form 26 November 1991, accepted 14 January 1992*)

Keywords: Neonate, Cervical spine, Osteomyelitis, MRI

Although the radiographic features of neonatal osteomyelitis are well described, spinal localizations are very rare and occur in about 2–4%. Clinical presentation with paresis and paralysis occurs in less than 1% (Resnick & Niwayama, 1988). In the neonate negative bone scintigraphy in the presence of bony destruction is not inconsistent with osteomyelitis as in the presented case (Swischuk, 1989). Magnetic resonance imaging (MRI) reports of these cases are scarce (Lac et al, 1990) and Gadolinium-DTPA enhanced MRI has not yet been described. Our recent experience with this unusual but characteristic presentation prompted this report.

Case report

A 3-week-old caucasian girl presented with a 1 week history of decreased movements of arms and legs. In the first week of life she suffered from paronychia on both hands. In the 2 weeks thereafter she had two episodes of limpness, the last one causing hospitalization. Neurological examination revealed hypotonic and paratic extremities with absent reflexes. There was no fever and laboratory findings showed an elevation of both sedimentation rate and white blood cell count. Cranial ultrasound examination was normal. Radiography of the lateral cervical spine (Fig. 1) showed destruction of the body of C3. The intervertebral disc space at C2–3 was somewhat decreased in height. There was a large pre-vertebral mass. Non-enhanced coronal and sagittal T_1-weighted MRI (Philips Gyroscan 1.5 T; TR/TE/EX: 650/20/2) (Fig. 2a, sagittal image) showed absence of the normal low intensity signal of the disc spaces C2–3 and C3–4. The body of C3 was hardly distinguishable. An inhomogeneous pre-vertebral mass also involving the spinal canal was present, the latter compressing and displacing the spinal cord posteriorly. The central parts of the masses showed low signal intensity areas surrounded by a rim of higher signal intensity tissue. Contrast-enhanced (Gadolinium-DTPA) coronal and sagittal MRI (650/20/2) (Fig. 2b, sagittal image) showed an increase in signal intensity of the abnormal masses with the exception of the low signal intensity areas. The area of the body of C3 and the surrounding disc spaces showed an increase in signal intensity. Tumour markers for neuroblastoma were negative and bone marrow biopsy showed no abnormality. Bone scintigraphy (^{99}Tc^{m}-MDP) did not show increased activity in the cervical spine or elsewhere. The clinical presentation and radiological findings were very suggestive of osteomyelitis affecting the body of C3 with abscess formation. Blood culture and the culture of the biopsy material showed *Staphylococcus aureus*. Conservative treatment with antibiotics led to a normalization of the neurological symptoms. Follow-up MRI examination showed decreasing abscess size and residual changes of the bodies C2, 3 and 4.

Discussion

Osteomyelitis in the newborn is a seldom encountered entity and vertebral involvement occurs in 2–4% of the cases. The main sites in the spine are the lower thoracic and lumbar vertebrae. In 80–90% *Staphylococcus*

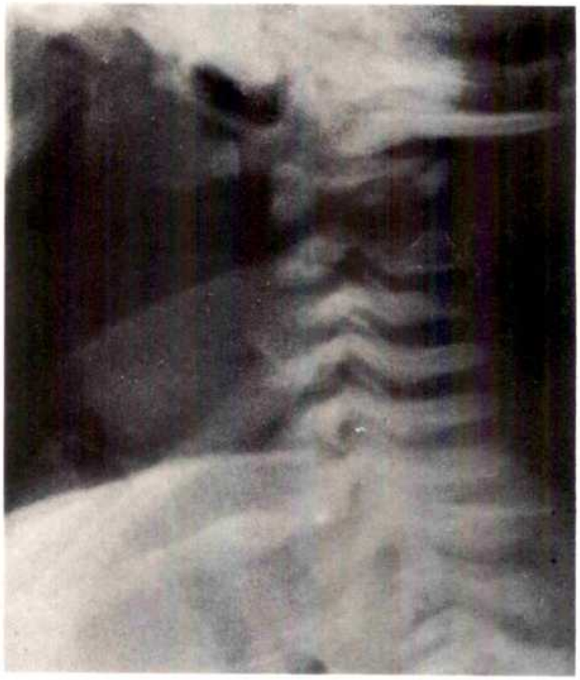

Figure 1. Lateral cervical spine X-ray. Destruction of the body of C3 with a pre-vertebral mass. Slightly narrowed disc space C2–3.

Address correspondence to Dr A. Martijn, Department of Radiology, University Hospital Groningen, Oostersingel 59, 9713 EZ Groningen, The Netherlands.

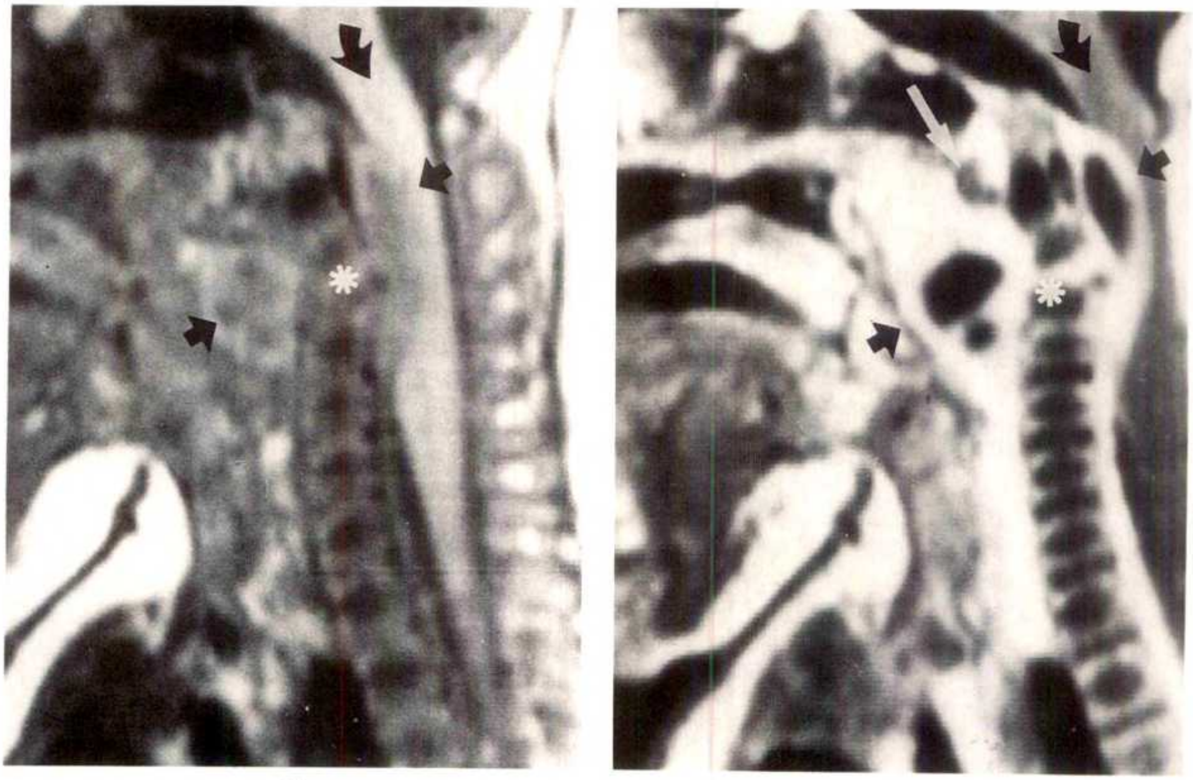

(a) (b)

Figure 2. Sagittal T_1-weighted MRI (650/20/2) obtained (a) pre- and (b) post-Gadolinium-DTPA at the same window and level (W: 1025; L: 416). Abnormal intensity signal of the body of C3 (white asterisk) and the surrounding disc spaces. Inhomogeneous mass pre-vertebral and in the spinal canal (between straight black arrows) with compression and displacement of the spinal cord (curved black arrow). White arrow: anterior arch C1.

aureus is the causative organism (Resnick & Niwayama, 1988; Swischuk, 1989). In the neonatal period osteomyelitis usually occurs as a sequel of sepsis usually following umbilical vessel catherization (Swischuk, 1989). In the present case the sepsis resulted from paronychia. Vertebral osteomyelitis is most often accompanied by disc space involvement seen as narrowing (Resnick & Niwayama, 1988; Swischuk, 1989). In this age group disc space involvement, on plain radiography is the key to differentiating osteomyelitis from metastatic neuroblastoma and histiocytosis X. In these two conditions the disc space is not involved. False-negative bone scintigraphy is not incompatible with the radiological findings as in the presented case (Swischuk, 1989). The findings on the T_1-weighted image in our case are consistent with other descriptions in the literature with respect to the slightly increased signal intensity and the poor discernibility of the vertebral body and disc spaces. Similarly the appearances relating to the abscess formation do not differ from the literature (Lac et al, 1990). However, instead of a T_2-weighted image a Gadolinium-DTPA enhanced T_1-weighted image was made revealing excellent information about the dimensions of the abscess and the relation of the necrotic areas to the cervical spine and the spinal cord. In this way we combined the exquisite anatomical depiction of the T_1-weighted image and the maximum effect of the contrast medium without the problems of the increased signals of oedema on the T_2-weighted image. The first episode of limpness may have resulted from rupture of the vertebral abscess into the spinal canal giving rise to sudden increase of pressure on the spinal cord. The second period leading to more constant neurological findings suggests progressive growth of the intraspinal abscess.

Although osteomyelitis of the cervical spine in the neonatal period is very rare, the clinical examination and the lateral radiograph of the cervical spine are the first important steps in suggesting this diagnosis. MRI is the method of choice for further evaluation. To our knowledge this the first report of Gadolinium-DTPA enhanced MRI in a neonate with proven cervical spine osteomyelitis.

References

LAC, P., PANUEL, M., DEVRED, P., BOLINI, G. & PADOVANI, J., 1990. MRI of disc space infection in infants and children. *Pediatric Radiology*, *20*, 175–178.

1992, *The British Journal of Radiology*, *65*, 722–724

RESNICK, D. & NIWAYAMA, J., 1988. Osteomyelitis, septic arthritis, and soft tissue infection: the axial skeleton. In *Diagnosis of Bone and Joint Disorders*. Ed. by D. Resnick and J. Niwayama (W. B. Saunders Co, Philadelphia), pp. 2619–2646.

SWISCHUK, L. E., 1989. *Imaging of the Newborn, Infant, and Young Child.* (Williams & Wilkins, Baltimore), pp. 751–758; 1018–1021.

Patellar metastasis: a rare presentation

By R. K. Sur, MD, D. P. Singh, MD, *M. S. Dhillon, MS, B. D. Gupta, MD, FRCR, B. Murali, MB, BS and †R. Sidhu MB, BS

Departments of Radiotherapy, †Radiodiagnosis and *Orthopaedics, Postgraduate Institute of Medical Education and Research, Chandigarh, India

(*Received 2 May 1991 and in revised form 30 July 1991, accepted 16 August 1991*)

Keywords: Metastases, Patella, Bronchogenic carcinoma

Primary patellar neoplasms are uncommon and metastasis to the patella is rarer still. Very few reports have been published in the literature (Stoler & Staple, 1969; Keeley, 1973; Gall et al, 1974; Ashby & Dappen, 1976; Hussey, 1976; Kwa & Nade, 1989). We present a case of primary bronchogenic carcinoma presenting as a huge swelling around the knee owing to a metastatic lesion in the patella.

Case report

A 50-year-old man was seen initially in the orthopaedic clinic complaining of pain in the region of the left knee of 2 months duration. Detailed questioning revealed a history of long-term smoking together with persistent cough and occasional blood-tinged expectoration.

Appetite was diminished and there was some loss of weight. Examination revealed 2 cm quadriceps wasting, limitation of knee flexion to 110° and tenderness over the anterior aspect of the patella. There was a significant effusion. Haemoglobin was 9.5 g%, total leucocyte count $11\,000 \times 10^6$/litre with 30% lymphocytes and the erythrocyte sedimentation rate (ESR) was 29 mm/h (Westergren); Mantoux test was positive. A presumptive diagnosis of tuberculosis of the knee was made and the patient was commenced on anti-tubercular therapy consisting of isoniazid, rifampicin and ethambutol. Chest and knee radiographs were advised but the patient did not return for follow-up for 3 months. During this period the knee swelling had dramatically increased to a size of 10 cm × 12 cm and the knee was fixed in a position of 90° flexion (Fig. 1). A biopsy performed by a private practitioner was reported as squamous cell carcinoma, and he was referred to the Department of Radiotherapy in February 1991.

At this time he had severe pain in the knee and the tumour was fungating through the skin. Detailed systemic examination revealed an impaired percussion note and diminished breath sounds at the base of the right lung below the fifth intercostal space. Chest radiographs showed collapse of the right middle and lower lobes as well as a small effusion. Knee radiographs showed complete destruction of the patella (Fig. 2). Computed tomographic (CT) scans at the level of the knee and patella showed complete patellar destruction with only tiny residual fragment of bone (Fig. 3). A radionuclide bone scan was not available at that time.

Histology of a bronchoscopic biopsy revealed a keratinizing squamous cell carcinoma and a review of the patellar biopsy showed similar appearances, thus confirming a metastasis. The patient was treated by palliative radiation therapy, delivering a dose of 30 Gy/10 fractions/2 weeks to the right lung and to the left patella. He improved symptomatically but developed low back pain on the last day of the external radiotherapy. Lumbar spine radiographs revealed collapse of the third lumbar vertebra; this was also treated by external radiotherapy (800 cGy/single fraction) and the patient was discharged.

Discussion

Although the knee is a common site for bone tumours, the patella is not usually involved (Ehara et al,

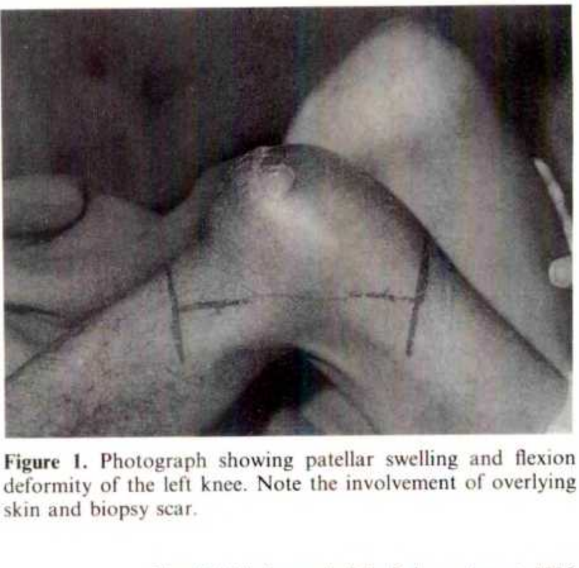

Figure 1. Photograph showing patellar swelling and flexion deformity of the left knee. Note the involvement of overlying skin and biopsy scar.

Address correspondence to Dr M. S. Dhillon, Assistant Professor, Department of Orthopaedics, 1241 Officer's Apartments, Sector 24, Chandigarh 160024, India.

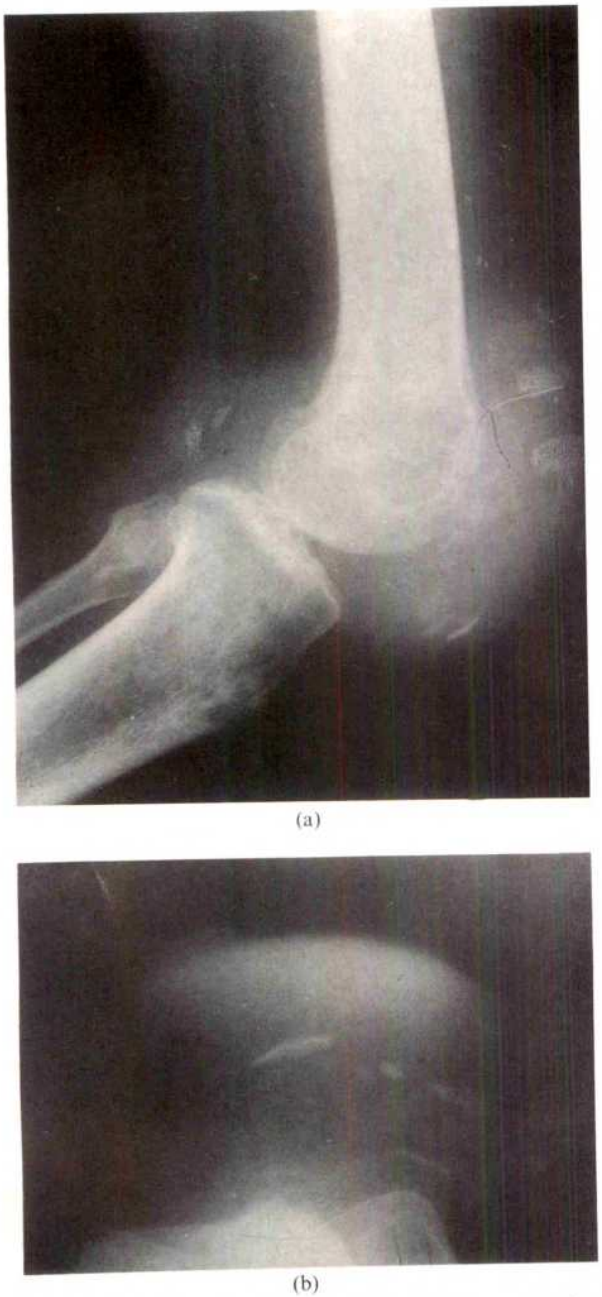

(a)

(b)

Figure 2. (a) Lateral radiograph of the left knee showing complete destruction of the patella. (b) Skyline view of the knee. There is extensive destruction and swelling of the left patella.

1989). Kransdorf et al (1989) reported 42 patellar neoplasms, but found no metastatic lesions. Both the above series stressed vigilance in cases of anterior knee pain. In those cases where patellar destruction is seen on radiographs, rapid increase in size of the lesion and poorly defined margins suggest a metastatic tumour (Kransdorf et al, 1989). Only a handful of reports of patellar metastasis exist in the literature. Keeley (1973) reported bilateral patellar metastasis from carcinoma of the male breast; subsequent radiographs revealed metastatic disease in other bones. Kwa and Nade (1989) described a case of patellar metastasis in renal adenocarcinoma, which also showed increased uptake in the occiput on radionuclide bone scan. Ashby and Dappen (1976) reported a patellar metastasis from oesophageal carcinoma together with a similar lesion in the scapula, and Benedek (1965) described patellar metastasis from bronchogenic carcinoma associated with a second lesion in the scalp. In our patient although a diagnosis of patellar metastasis was entertained once the lung biopsy showed a locally advanced lesion, a radiographic survey of the whole body was not performed. Only when low back pain appeared were further radiographs carried out, which revealed metastatic deposit in the third lumbar vertebra. Patellar metastasis is usually a feature of generalized carcinomatosis when there are sufficient tumour emboli in the circulation. Further investigations to locate other metastatic lesions are thus mandatory.

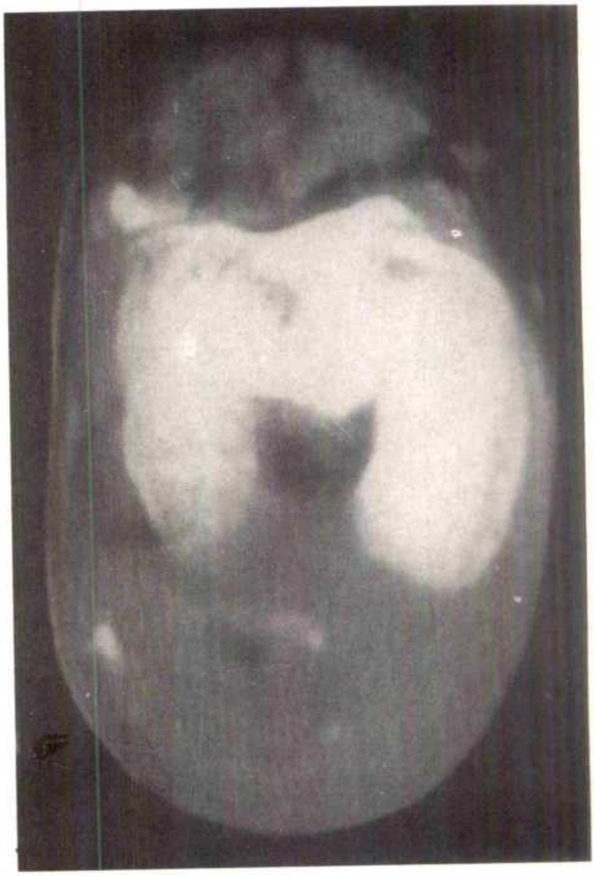

Figure 3. CT scan at the level of the distal femur and patella showing complete destruction of the patella. Only a part of the edge of the patella is seen.

The patella is a sesamoid bone with a relatively poor vascular supply, consisting of a few nutrient branches

1992, *The British Journal of Radiology*, *65*, 724–725

from the collateral vessels of the knee; this seldom provides sufficient access to tumour emboli for metastatic lesions to develop (Goodwin, 1961).

The management of patellar metastasis depends on the size of the lesion. Early deposits without soft-tissue extension may well be treated by patellectomy, whereas larger lesions with soft-tissue extension require palliative external radiotherapy.

References

Ashby, M. E. & Dappen, N., 1976. Esophageal carcinoma metastatic to the patella: a case report. *Journal of the American Medical Association*, *235*, 2519–2520.

Benedek, G. T., 1965. Lysis of the patella due to metastatic carcinoma. *Arthritis and Rheumatism*, *8*, 560–565.

Ehara, S., Khurana, J. S., Kattapuram, S. V., Rosenberg, A. E., El-Khoury, G. Y. & Rosenthal, D. I., 1989. Osteolytic lesions of the patella. *American Journal of Roentgenology*, *153*, 103–106.

Gall, E. P., Didizian, N. A. & Park, Y., 1974. Acute monoarticular arthritis following patellar metastasis. *Journal of the American Medical Association*, *229*, 288–289.

Goodwin, M. A., 1961. Primary osteosarcoma of the patella. *Journal of Bone and Joint Surgery*, *43*, 338–341.

Hussey, H. H., 1976. The vertebral venous system. Editorial. *Journal of the American Medical Association*, *235*, 2524.

Keeley, C. D., 1973. Bilateral patellar metastases from carcinoma of the male breast. *Canadian Journal of Surgery*, *16*, 328–329.

Kransdorf, M. J., Moser, R. P., Jr, Vinh, T. N., Aoki, J. & Callaghan, J. J., 1989. Primary tumours of the patella. A review of 42 cases. *Skeletal Radiology*, *18*, 365–371.

Kwa, S. & Nade, S., 1989. Metastasis in a patella: a rare site. *Australian and New Zealand Journal of Surgery*, *59*, 351–352.

Stoler, B. & Staple, T. W., 1969. Metastasis to the patella. *Radiology*, *93*, 835–836.

Renal ultrasonographic appearances at presentation in an infant with Lesch-Nyhan syndrome

By C. N. Ludman, MB, BS, MRCP, *C. Dicks-Mireaux, MRCP, FRCR and A. J. Saunders, FRCP, FRCR

Department of Radiology, Guy's Hospital, St Thomas Street, London SW1 9RT and *Department of Radiology, The Hospital for Sick Children, Great Ormond Street, London WC1 3JH, UK

(*Received 8 November 1991, accepted 16 January 1992*)

Keywords: Lesch-Nyhan syndrome, Ultrasound, Hyperechoic cortex, Crystal nephropathy

Lesch-Nyhan syndrome, first described in 1964, is an X-linked recessive disorder of purine metabolism. A cellular deficiency or absence of the purine salvage enzyme hypoguanine phosphoribosyl transferase causes purine overproduction and subsequent hyperuricaemia and gout. Clinically the syndrome manifests as neurological disorders, behavioural disturbances characterized by self mutilation and variable mental retardation. In addition, hyperuricaemia results in the clinical features of gout, with gouty arthritis, tophi, urate and uric acid nephropathies.

The previously described renal ultrasonic appearances of Lesch-Nyhan syndrome have referred to patients after they have received allopurinol therapy. We describe a different appearance in a patient with this syndrome, prior to treatment. Allopurinol is a xanthine oxidase inhibitor and leads to an accumulation of the intermediate metabolites xanthine and hypoxanthine. Treated patients develop calculi which appear to be predominantly formed from xanthine secondary to this therapy.

We report on the case of an infant who presented at 3 weeks of age with congenital renal failure, who shortly afterwards developed the features of acute tophaceous gout. The renal ultrasonic appearances at presentation were striking and unusual.

Case report

A 3-week-old male infant in renal failure was transferred to Guy's Hospital. The pregnancy had been unremarkable and the appearance of the kidneys on routine obstetric scanning was reported as normal. Shortly after birth, he developed recurrent vomiting with weight loss and was admitted to his local hospital. He was found to be in renal failure, and was transferred.

On admission to Guy's Hospital, the child's plasma urate was 2.2 mmol/l (n 0.2–0.43) and creatinine was 804 μmol/l. No detectable activity of hypoxanthine guanine phosphoribosyl transferase was found in intact or lysed erythrocytes, thus establishing the diagnosis of Lesch-Nyhan syndrome. On admission an abdominal radiograph was normal with no evidence of renal tract calcification. The renal ultrasonic appearances showed bilateral markedly echogenic cortices. The medullary pyramids were echo poor, but contained streaks of increased echogenicity (Fig. 1).

Discussion

The previously described ultrasonic findings in Lesch-Nyhan syndrome have been seen following long

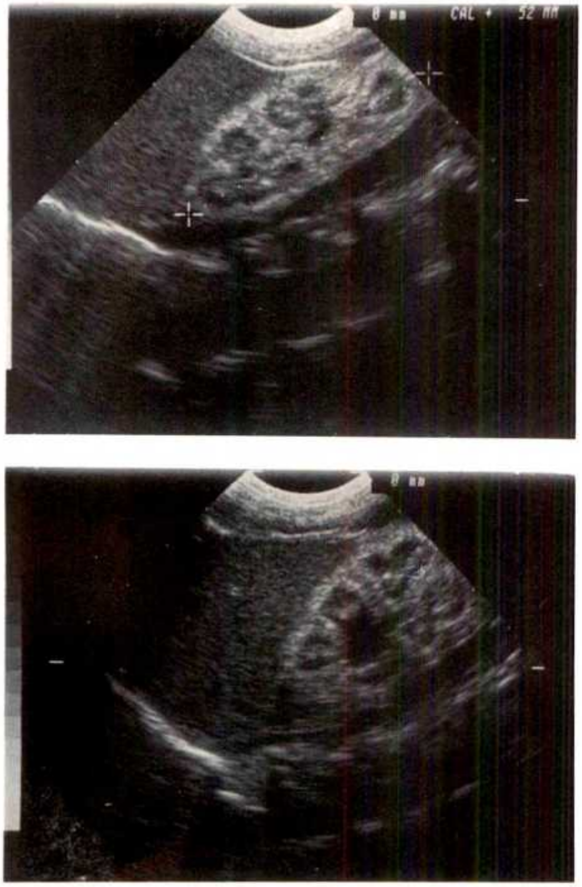

Figure 1. Longitudinal scan of the right kidney, demonstrating the bright cortex and hypoechoic medullary pyramids containing bright streaks.

term treatment with allopurinol and in these cases the appearances have been of a diffuse increase in the medullary echoes, typical of the changes of crystal deposition, as described by Patriquin and Robitaille (1986).

To our knowledge the ultrasonographic features of untreated Lesch-Nyhan syndrome have not been described fully and Kenney (1991) also recently identified the lack of reports of ultrasonic features of Lesch-Nyhan syndrome prior to treatment. Holland et al (1984) refer to bilateral bright renal echo patterns suggestive of crystal nephropathy in their case report of a child at presentation with Lesch-Nyhan syndrome, and therefore prior to treatment. We have reviewed the ultrasonic findings on this child and here too the cortex was found to be hyperechoic with sparing of the medulla. It would seem likely that the ultrasonic differences seen before and after treatment in Lesch-Nyhan syndrome might similarly be seen before and after the treatment of adult gouty nephropathy. There appears to have been little published regarding the ultrasonographic appearances of untreated adult gouty nephropathy, although Tsujimoto and Tada (1985) have described the appearances of biopsy confirmed renal gout and found them to be indistinguishable on ultrasound from medullary nephrocalcinosis.

The striking echogenicity of the cortex in our case is similar to that described by Brennan et al (1982) in a case report of primary hyperoxaluria in infancy, where there was marked cortical echogenicity with medullary sparing. Assessment of cortical echogenicity can be subjective and there are many causes (Rosenfield, 1983); however, in common with Brennan's case the cortical hyperechogenicity in ours was extreme. Of interest in the case described here is the absence of the typical bright medulla seen in cases of crystal deposition (Patriquin & Robitaille, 1986), although unusual, bright streaks within the medulla were seen.

A feature of uric acid deposition is the arousal of a marked inflammatory reaction. This occurrs in the kidney in a similar fashion as the deposition in joints and soft tissues. Although no biopsy was performed in the case presented, the untreated infant described by Holland et al (1984) had an histologically proven widespread inflammatory component. It seems likely that the ultrasonographic changes we have described may have been caused by a combination of crystal deposition and interstitial nephritis and the fact that the infant's renal failure responded to uricosuric drugs would support this. Unfortunately the child returned to the referring hospital before follow-up scans could be performed.

We suggest that prior to treatment the appearances of the kidney in Lesch-Nyhan syndrome may be of a strikingly hyperechoic cortex with an hypoechoic, preserved medulla and the more familiar previously described generalized hyperechogenicity may well develop only after allopurionol therapy. The ultrasonic features described in our case should, therefore, alert sonologists to the possibility of crystal nephropathy even when the medulla is hypoechoic.

References

Brennan J. N., Diwan, R. V., Makker, S. P., Cromer, B. A. & Bellon, E. M., 1982. Ultrasonic diagnosis of primary hyperoxaluria in infancy. *Radiology*, *145*, 147–148.

Holland, P. C., Dillon, M. J., Pincott, J., Simmonds, H. A. & Barratt, T. M., 1984. Hypoxanthine guanine phosphoribosyl transferase deficiency presenting with gout and renal failure in infancy. *Archives of Diseases in Childhood*, *58*, 831–833.

Kenney, I. J., 1991. Renal sonography in long standing Lesch-Nyhan syndrome. *Clinical Radiology*, *43*, 39–41.

Patriquin, H. & Robitaille, P., 1986. Renal calcium deposition in children: Sonographic demonstration of Anderson-Carr progression. *American Journal of Roentgenology*, *146*, 1253–1256.

Rosenfield, A. T., 1983. Letter: Ultrasonic diagnosis of primary hyperoxaluria in infancy. *Radiology*, *148*, 578.

Simmonds, H. A., Cameron, J. S., Barratt, T. M., Dillon, M. J., Meadow, S. R. & Trompeter, R. S., 1989. Purine enzyme defects as a cause of acute renal failure in childhood. *Paediatric Nephrology*, *3*, 433–437.

Tsujimoto, F. & Tada, S., 1985. Ultrasonography of the gouty kidney. *Nippon-Igadu-Hoshasen-Gaddai-Zasshi*, *45* (7), 977–81.

1992, *The British Journal of Radiology*, 65, 726–728

Small cell carcinoma of the prostate

By J. Sule-Suso, LMC and A. M. Brunt, MB, MRCP, FRCR

Department of Clinical Oncology, North Staffordshire Royal Infirmary, Princes Road, Hartshill,
Stoke-on-Trent, Staffs ST4 7LN, UK

(Received 12 June 1991 and in revised form 21 October 1991, accepted 14 January 1992)

Keywords: Small cell carcinoma, Prostate gland

Primary small cell carcinoma of the prostate gland is a rare disease entity with a poor prognosis. Even more unusual than primary disease is a metastasis from a lung primary (Johnson et al, 1974; Hodge & Carson, 1985). We confine ourselves in this paper to primary disease, which has to be differentiated clinically from a pulmonary metastasis.

Primary small cell carcinoma of the prostate has been described as occurring after a diagnosis of adenocarcinoma of the prostate (Schron et al, 1984), as a combination of the two histologies at the time of initial diagnosis (Tetu et al, 1987) or on its own (Sarma & Weilbaecher, 1989). Though it has been suggested that small cell carcinoma of the prostate reflects a terminal aggressive phase of adenocarcinomatous disease (Schron et al, 1984), the occurrence of "pure" small cell carcinoma presents an argument against this in at least a proportion of cases (Tetu et al, 1987; Sarma & Weilbaecher, 1989).

The origin of small cell carcinoma of the prostate is not clear. It has been suggested that this malignancy derives from the argyrophil and argentaffin cells found in the normal prostatic epithelium (Wenk et al, 1977). However, Schron et al (1984) noted that the small cell carcinoma in their three patients developed in association with, and during the course of progression of, "normal" prostatic adenocarcinoma. It, therefore, appeared to represent the emergence of a different clone manifesting the differentiation characteristics of small cell carcinoma rather than an entirely separate tumour. This theory of divergent differentiation is an alternative explanation of aetiology which has other supporters (Vuitch & Mendelsohn, 1981; Jelbart et al, 1988). It is possible that both explanations are correct in a proportion of cases.

We report a further case of small cell carcinoma of the prostate, the first to emanate from the UK.

Case report

A 62-year-old man presented in May 1990 with acute urinary retention. There were no other significant symptoms except for suprapubic pain and dysuria for the prior 2 to 3 weeks. Rectal examination revealed an irregular hard enlarged prostate. A full haematological and biochemical screen was normal except for a mildly lowered serum calcium. It was noted that prostatic specific antigen (PSA) and acid phosphatase (PAP) were normal. 2 days after admission the patient underwent transurethral resection of his prostate gland. Histologically there was fibromyoepithelial hyperplasia, acute and chronic inflammatory foci of prostatitis and no evidence of neoplasia.

He was readmitted 2 months later with a large smooth swelling apparently arising from the prostate and extending to the left pararectal region. His only symptom at the time was a mild degree of tenesmus. He had a further transurethral resection, histological examination of the prostatic tissue revealed a poorly differentiated small cell tumour with hyperchromatic pleomorphic nuclei and little cytoplasm (Figs 1a & b). Immunohistochemistry was weakly positive for neurone specific enolase and negative for PSA and leukocyte common antigen. Appearances were those of a small cell carcinoma. A chest radiograph performed at this time was normal. The alkaline phosphatase and aspartate transaminase levels were

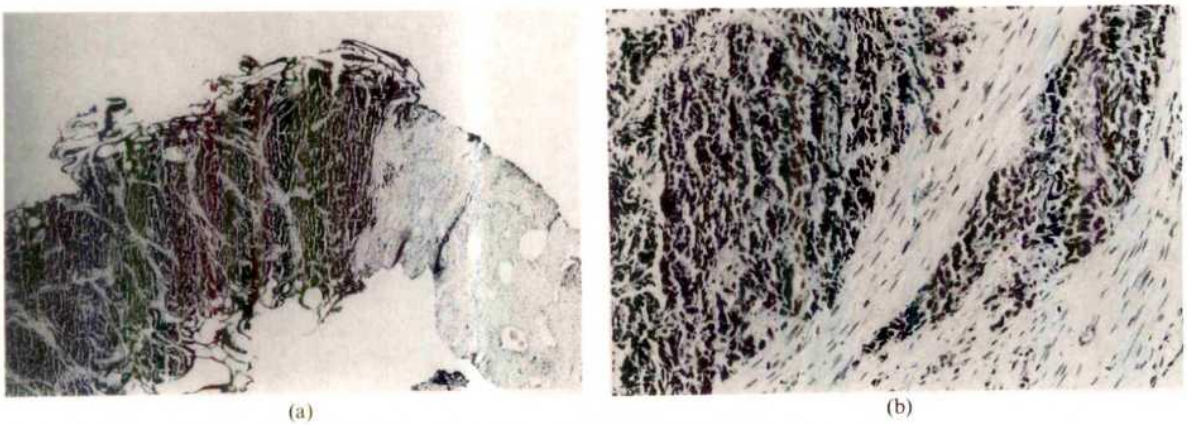
(a) (b)

Figure 1. Biopsy sample from a TURP; (a) ×20 magnification, (b) ×100 magnification.

slighly raised above the upper end of the normal range, but all other routine blood tests were normal. We looked for evidence of peptide hormone secretion, but the adrenocorticotrophic hormone (ACTH), antidiuretic hormone (ADH) and plasma and urine osmolality were normal.

He was commenced on Vincristine, Adriamycin and Cyclophosphamide (VAC) chemotherapy at 3 weekly intervals with the intention of consolidating any response with radiotherapy. 9 days after the second course of VAC he was admitted with a deep venous thrombosis in his left calf. A minimal clinical response to the chemotherapy was observed. Computed tomographic (CT) scanning of his abdomen and pelvis confirmed the presence of a 11 × 12 cm mass involving the prostate and rectum. Irregular extraperitoneal extension towards the inferior aspect of the right sacro-iliac joint was seen, as was the presence of enlarged left iliac nodes. Chest radiographic appearances remained normal.

A month after his second course of VAC he commenced radiotherapy. A large pelvic and perineal field was treated with an anterior and posterior opposed pair to 4500 cGy mid-plane dose in 25 fractions over 5 weeks. Within 10 days of starting radiotherapy a partial response was noted clinically. During treatment he became jaundiced and an ultrasound scan identified multiple enlarged lymph nodes around the head of the pancreas, with common bile duct dilatation. Para-aortic nodes were also seen to be enlarged; all these areas had been normal on the CT scan a month previously.

He received palliative radiotherapy of 3000 cGy in 10 fractions to his porta hepatis. The radiotherapy to his pelvis was completed to try and gain local control. Clinically there was a complete response of the primary at the end of the 5 weeks of radiotherapy.

A follow-up CT scan was arranged but the patient deteriorated rapidly. He died at home 18 days after completing radiotherapy and 3½ months after initial presentation with small cell carcinoma of the prostate. A request for a postmortem examination was declined.

scussion

The main presenting symptoms of small cell carcioma of the prostate are often those of the local disease; dysuria, hesitancy of micturition and then urinary retention (Wenk et al, 1977; Schron et al, 1984; Tetu et al, 1987; Manson et al, 1989; Sarma & Weilbaecher, 1989). Symptoms of systemic disease, such as weakness and weight loss, may also be present (Wenk et al, 1977; Hindson et al, 1985; Hodge & Carson, 1985; Manson et al, 1989). Our patient presented with dysuria, suprapubic pain and then urinary retention, but no systemic symptoms.

Serum PAP levels have been reported as increased, even in patients with pure small cell carcinoma (Tetu et al, 1987; Sarma & Weilbaecher, 1989). PSA is a more recently available serum marker. In the literature we have not identified a pure small cell carcinoma of the prostate with a raised value. Neither marker was raised in our patient.

In our patient the serum ACTH was normal, less than 10 pmol/l (normal range 3.3–15.4 pmol/l). ACTH has been reported as raised in the serum and found to be present at biopsy in tissue of a patient with pure small cell carcinoma (Wenk et al, 1977). A case of Cushing's syndrome has been reported in a patient with mixed disease (Schron et al, 1984) but has also been recorded in pure adenocarcinoma of the prostate (Hall, 1967; Lovern et al, 1975). In our patient ADH was also normal, 1.9 pmol/l (range 0.9–4.6 pmol/l).

Calcitonin, parathormone and bombesin have been raised in some cases of small cell carcinoma of the prostrate. It has been suggested that assays for these should be carried out, if possible, to see if the presence of small cell carcinoma of the prostate is suspected (Jelbart et al, 1988).

These findings indicate that neither the usual serum markers for adenocarcinoma (PAP, PSA) nor the evidence of ectopic production of ACTH can be used to differentiate absolutely between adenocarcinoma or small cell carcinoma of the prostate. The prognosis of patients with small cell carcinoma of the prostate is poor. In the largest reported series of 20 cases, the longest survivors were two patients alive with disease at 18 months (Tetu et al, 1987). In nine other reported cases the mean survival from diagnosis of the small cell component was 3 months, range 0–8 months (Wenk et al, 1977; Vuitch & Mendelsohn, 1981; Schron et al, 1984; Hindson et al, 1985; Manson et al, 1989; Sarma & Weilbaecher, 1989). From the available data it is difficult to form a definite treatment strategy and one could question whether treatment is justified in some patients.

It would be reasonable to base a treatment strategy around the same principles used to manage small cell carcinoma of the lung. We attempted this in our patient with initial chemotherapy followed by consolidative radiotherapy. This was the intention even though the disease appeared limited at presentation. More extensive staging, such as a CT scan of abdomen and pelvis, bone scan and bone marrow aspirate and trephine, could also be performed. These investigations are not mandatory, but can be performed both as a baseline for future comparison and as a way of planning treatment strategy. Unfortunately our patient had only a minimal response to chemotherapy, a response that is assessed as static disease. The responsiveness to radiotherapy was encouraging and it suggests that if effective chemotherapy could be found there may be a role for consolidative radiotherapy.

Responses to chemotherapy have been noted (Tetu et al, 1987). One patient has had a documented complete response (Hindson et al, 1985), but with a duration of only 2 months. He was treated with VAC. It is possible that improved response rates may be achieved with other agents, *e.g.* etoposide and cisplatinum, and it may be reasonable to adopt this approach for treatment of this rare and aggressive tumour.

The only reported use of radiotherapy in the literature is from the M. D. Anderson Hospital, where this modality was used in the treatment of 6 out of 20 cases (Tetu et al, 1987). The precise details and response was not documented. The use of a high dose (60–70 Gy) radiotherapy has been recommended because of the possible admixture of small cell carcinoma and adenocarcinoma (Jelbert et al, 1988). Hormonal manipulation, as used for treatment of adenocarcinoma of the prostate, cannot be expected to produce a worthwhile response, except possibly to an adenocarcinomatous element if present.

It is not feasible to treat patients with such rare tumours on study protocols. However, results of treatment should be reported to enable clinicians seeing isolated cases to try and form a strategy for the individual patient. We believe that it is reasonable to adopt whatever approach would be offered to a patient with a similar stage of disease and primary tumour in the lung. The grim prognosis cannot be overemphasized.

Acknowledgments

We would like to thank Dr J. E. Scoble for allowing us to report on this case and his helpful comments, Dr S. C. Harris for reviewing the histopathology, providing the photographs and for his constructive comments and Miss A. W. Littler for typing the manuscript.

References

Hall, T. C., 1967. Symptomatic hypokalaemic alkalosis in hyperadrenocorticism secondary to carcinoma of the prostate. *Cancer*, *21*, 190–192.

Hindson, D. A., Knight, L. L. & Ocker, J. M., 1985. Small-cell carcinoma of the prostate. Transient complete remission with chemotherapy. *Urology*, *26*, 182–184.

Hodge, G. B. & Carson, C. C., 1985. Oat cell carcinoma of lung masquerading as prostatic carcinoma. *Urology*, *25*, 69–70.

Jelbart, M. E., Russell, P. J., Russell, P. & Raghavan, D., 1988. The biology and management of small cell undifferentiated carcinoma of the prostate. In *Textbook of Uncommon Cancer*, (John Wiley and Sons Ltd, Chichester), pp. 249–262.

Johnson, D. E., Chalbaud, R. & Ayala, A. G., 1974. Secondary tumours of the prostate. *Journal of Urology*, *112*, 507–508.

Lovern, W. J., Fariss, B. L., Wettlaufer, J. N. & Hane, S., 1975. Ectopic ACTH production in disseminated prostatic adenocarcinoma. *Urology*, *5*, 817–820.

Manson, A. L., Terhune, D. & McDonald, G., 1989. Small cell carcinoma of prostate. *Urology*, *33*, 78–79.

Newmark, S. R., Dluhy, R. G. & Bennett, A. H., 1973. Ectopic adenocorticotropin syndrome with prostatic carcinoma. *Urology*, *2*, 666–668.

Sarma, D. P. & Weilbaecher, T. G., 1989. Small cell carcinoma of prostate. *Urology*, *33*, 332–335.

Schron, D. S., Gipson, T. & Mendelsohn, G., 1984. The histogenesis of small cell carcinoma of the prostate. An immunohistochemical study. *Cancer*, **53**, 2478–2480.

Tetu, B., Ro, J. Y., Ayala, A. G., Johnson, D. E., Logothetis, C. J. & Ordonez, N. G., 1987. Small cell carcinoma of the prostate. Part I. A clinicopathologic study of 20 cases. *Cancer*, *59*, 1803–1809.

Vuitch, M. F. & Mendelsohn, G., 1981. Relationship of ectopic ACTH production to tumour differentiation: A morphologic and immunohistochemical study of prostatic carcinoma with Cushing's syndrome. *Cancer*, *47*, 296–299.

Wenk, R. E., Bhagavan, B. S., Levy, R., Miller, D. & Weisburger, W., 1977. Ectopic ACTH, prostatic oat cell carcinoma, and marked hypernatremia. *Cancer*, *40*, 773–778.

1992, *The British Journal of Radiology*, 65, 729–730

Case of the month

A rare cause of a common symptom

By P. J. Close, MRCP, FRCR and *P. L. Monks, FRCOG, FRACOG

Departments of Radiology and *Gynaecology, Princess Alexandra Hospital, Woolloongabba, Brisbane, Queensland 4102, Australia

(Received 7 October 1991, accepted 30 October 1991)

A 34-year-old woman presented with a short history of painless vaginal bleeding. Her last menstrual period was approximately 8 weeks previously and a recent pregnancy test had been positive. She had a history of two previous lower segment Caesarean sections. On general examination she was mildly shocked. Vaginal examination revealed an enlarged dumb-bell shaped 8–10 week uterus. The cervix was enlarged, invaginating the bladder. The external os was closed.

An initial diagnosis of incomplete abortion was made and pelvic ultrasound was requested. A midline sagittal transabdominal ultrasound image is shown (Fig. 1).

What does the image demonstrate? What diagnoses should be considered? How might management be influenced?

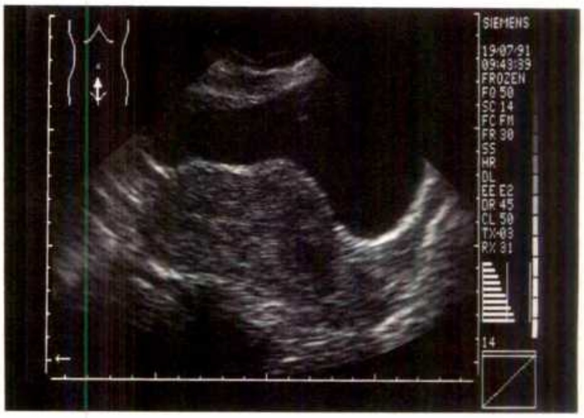

Figure 1. A midline sagittal transabdominal image.

Di

nc

Ultrasound demonstrates a normal midline cavity echo in the body of the uterus. Inferiorly products of conception occupy the lower uterine segment and cervix. The mass bulges into the bladder. No fetal parts are seen and the external os appears closed. No free blood was seen in the pouch of Douglas. The diagnoses to consider are cervical pregnancy or cervical abortion. The former was considered more likely.

At operation products of conception were located in the cervical canal. Gentle removal resulted in brisk haemorrhage which could not be stemmed. Therefore, hysterectomy was performed. The patient made an uneventful recovery. Histological examination of the resected specimen confirmed a cervical ectopic pregnancy.

Discussion

Cervical ectopic pregnancy is a rare occurrence with a reported incidence of between one per 1000 to one per 24 000 pregnancies (Werber et al, 1983; Lobel et al, 1990). Predisposing factors include previous gynaecological surgery and multiparity (Werber et al, 1983), so as the incidence of Caesarean section and other uterine procedures increase, so might the incidence of cervical implantation. Without pre-operative diagnosis, dilatation and curettage for misdiagnosed spontaneous abortion is likely to cause life threatening haemorrhage or rupture the weakened uterine wall. Maternal morbidity rates of 20–50% have been reported (Vas et al, 1984). Emergency hysterectomy is usually required to achieve haemostasis with obvious consequences for future fertility. Clinically, patients present as a miscarriage. A clue to the diagnosis is if pelvic examination reveals a disproportionately enlarged cervix compared with the body of the uterus. Ultrasonic findings include a minimally enlarged uterine fundus with a swollen and bulging cervical canal containing an inhomogenous mass and decidual reaction. Sometimes a poorly defined gestation sac is visible (Vas et al, 1984). Fetal parts may be detected and, if visible, the internal os should appear closed.

Cervical pregnancy is mimicked very closely by cervical abortion, both clinically and ultrasonically. The latter is defined as spontaneous abortion of an intrauterine pregnancy into the cervix where the abortus is retained by a resistant external os. Vas et al (1984) reported four cases of cervical abortion in which the endometrial cavity appeared more prominent than with cervical pregnancies. Blood clots and products of conception rather than a decidual cast were seen. The uterine fundus was larger for the state of gestation, giving less of an "hourglass" appearance, and the internal os was open.

Magnetic resonance imaging (MRI) has been used to aid diagnosis of cervical pregnancy, complementing ultrasound, and confirming the suspicion that implantation had occurred at the site of a previous Caesarean section scar (Bader-Armstrong et al, 1989). Endovaginal sonography (EVS) should be expected to provide further information in cases of cervical pregnancy due to excellent visualization of the cervix. EVS was not available at this institution.

If diagnosed early and accurately, management strategies are available to reduce maternal morbidity and preserve the uterus. Lobel et al (1990) reported two cases of cervical pregnancy detected by ultrasound. Before termination of pregnancy the uterine arteries were successfully embolized using angiographic techniques. As a result, surgical evacuation was performed with minimal haemorrhage. Hysterectomy was not required and the patient's potential fertility was retained. Other reported managment strategies to achieve the same aim include use of feticidal agents (Segna et al, 1990), ligation of internal iliac and uterine arteries, circumsuture and intracervical obturator and intracervical balloon tamponade (Lobel et al, 1990).

In this case the patient exhibited signs of shock and it was not considered prudent to delay surgery any longer than necessary. Also this 34-year-old patient had three previous children, so hysterectomy was not as devastating as for a young nulliparous woman.

References

Bader-Armstrong, B., Shah, Y. & Rubens, D., 1989. Use of ultrasound and magnetic resonance imaging in the diagnosis of cervical pregnancy. *Journal of Clinical Ultrasound, 17*, 283–286.

Lobel, S. M., Meyerovitz, M. F., Benson, C. C., Goff, B. & Bengtson, J. M., 1990. Pre-operative angiographic uterine artery embolization in the management of cervical pregnancy. *Obstetrics and Gynecology, 76* (5 Pt 2), 938–941.

Segna, R. A., Mitchell, D. R. & Misas, J. E., 1990. Successful treatment of cervical pregnancy with oral etoposide. *Obstetrics and Gynecology, 76* (5 Pt 2), 945–947.

Vas, W., Suresh, P. L., Tang-Barton, P., Salimi, Z. & Carlin, B., 1984. Ultrasonic diffentiation of cervical abortion from cervical pregnancy. *Journal of Clinical Ultrasound, 12*, 553–557.

Werber, J., Prasadarao, P. R. & Harris, V. J., 1983. Cervical pregnancy diagnosed by ultrasound. *Radiology, 149*, 279–280.

Keywords: Pregnancy, Ectopic, Ultrasound, Cervix, MRI, Embolization

1992, *The British Journal of Radiology*, *65*, 731–732

Correspondence

(The Editors do not hold themselves responsible for opinions expressed by correspondents)

Spontaneous disappearance of staghorn calculus

THE EDITOR—SIR,
I read with interest the report by McGann et al (1991).

There are earlier reports than theirs of spontaneous disappearance of staghorn calculi. Elliot (1954) reviewed the literature to that date and collected 13 cases of spontaneous dissolution of renal calculi to which he added a further four cases. Not all of these fulfilled McGann's criteria, but all involved large stones which disappeared without treatment.

I append figures of another case given to me by T. H. Cullen, FRCS. They show complete disappearance of a large right staghorn calculus and partial regression of a left staghorn calculus over a period of 4 years and 8 months in an adult female (Figs 1 & 2). She received no treatment.

As Elliot (1954) commented, "it seems likely that spontaneous dissolution of renal calculi occurs more commonly than one might expect from the literature".

Yours etc.,

L. SHEPPARD

Acknowledgment
I am grateful to T. H. Cullen for the radiographs.

Kettering and District General Hospital,
Rothwell Road,
Kettering,
Northamptonshire NN16 8UZ
(Received 2 March 1992 and accepted 8 April 1992)

References

ELLIOT, J. S., 1954. Spontaneous dissolution of renal calculi. *The Journal of Urology*, *72*, 331–336.
McGANN, G., GRANT, D., MILLER, R., 1991. Spontaneous disappearance of a staghorn calculus. *British Journal of Radiology*, *64*, 1161–1162.

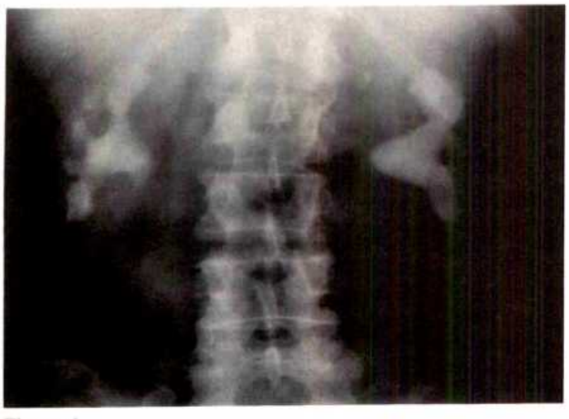

Figure 1.

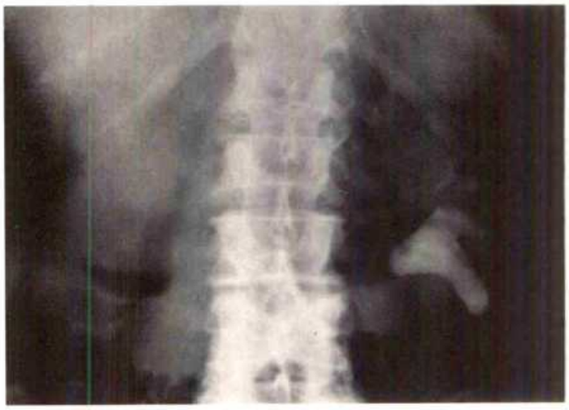

Figure 2.

Author's reply

THE EDITOR—SIR,
We are grateful to Dr Sheppard for drawing our attention to Dr Elliot's (1954) review of the literature. As acknowledged in Dr Sheppard's letter, not all of these cases fulfilled the criteria specified in our report. In particular, the rapidity of dissolution (7 months) was particularly striking in our case. This has implications for the management of patients scheduled for percutaneous nephrolithotomy and emphasizes the need for pre-operative imaging to be performed immediately prior to admission for surgery.

Yours etc.,

D. S. GRANT

Department of Imaging,
Whittington Hospital,
Highgate Hill,
London N19 5NF
(Received 19 March 1992 and accepted 8 April 1992)

Reference

Elliot, J. S., 1954. Spontaneous dissolution of renal calculi. *The Journal of Urology*, *72*, 331–336.

Radiation damage to mouse skin and oesophagus

THE EDITOR—SIR,
I read with great interest the article by Marino et al (1990) and would like to dispute some of the statements and conclusions of it, especially those related to radiation damage to the oesophagus.

Many experimenters either proposed or accepted as true the claim that early cumulative mortality of whole thorax-irradiated rodents is mainly or entirely due to radiation damage to the oesophagus and Marino et al (1990) seem to subscribe to this view. It has, however, been found by autopsy of all succumbing mice so treated followed by light microscopic examination of their thoracic and abdominal organs that radiation-induced ulcerative oesophagitis itself is not a lethal condition, and that only a minority of mice which die do so due to complications of oesophagitis (perforation, also seen by Philliips & Ross (1974), leading to purulent mediastinitis, pleuritis and/or pericarditis) whereas the majority succumb as a consequence of aspiration broncho-pneumonia, pneumonitis, and lesions affecting subdiaphragmatic parts of the alimentary tract (Michalowski, 1981; Michalowski & Hornsey, 1986). A lack of close correspondence between radiation damage to the oesophagus and mortality was further supported by the findings that (1) most of the animal deaths took place after the peak incidence of oesophagitis at the time when, unless the condition was complicated, healing of the oesophagus was well advanced or even completed; (2) a single dose of 27 Gy of X-rays which sufficed to produce ulcerative oesophagitis in all mice (ED 100) was well below LD 50; (3) the mice drank water and consumed some pelleted food at all times and their body weight loss never reached lifetreatening proportions.

As a minor point of order, the paper by Michalowski and Burgin (1982) does not include a statement referred to by Marino et al (1990) that "duodenal ulcers (...) and not acute oesophagitis would be the mechanism of death". This has never been our claim (Michalowski & Hornsey, 1986).

Marino et al (1990) did not see gastric or duodenal lesions in their mice but they do not specify which 17 mm long segment of the oesophagus they were irradiating. In CFLP mice used in the past in this institution for studies on early effects of irradiation of the entire thorax or well defined parts of it, the oesophagus is approximately twice that long, and gastro-duodenal lesions are observed only when the lower mediastinum including the distal part of the organ (corresponding to, and containing, the thoracic vertebrae T5–T10) is irradiated with single X-ray doses in excess of 14 Gy (Michalowski et al, 1983b). Irradiation of the upper mediastinum including the adjacent segment of the oesophagus of the same length (12 mm) never results in duodenal ulcers (ibid) although both parts of the organ are equally radiosensitive (Michalowski et al, 1983a). More recently, duodenal lesions induced in mice by irradiation of the lower mediastinum have proved to be a valuable and illuminating model of peptic ulcer disease in man (Michalowski, 1989; Gompertz, 1990; Gompertz et al, 1991).

A detailed examination of the entire oesophagus by light microscopy coupled with weighing mice daily demonstrated a poor correlation between radiation-induced oesophagitis and body weight loss (Michalowski & Burgin, 1982; Michalowski et al, 1983a) arbitrarily assumed by Marino et al (1990) to hold good for their study. Changes in animal body weight should not, therefore, be relied upon as a means of quanitification of the condition, let alone a basis for conclusions concerning cell kinetics of the epithelial lining of the oesophagus.

It is equally doubtful whether macroscopic lesions in the irradiated composite organ such as skin, including erythema and oedema (*i.e.* changes in dermal blood flow and microvascular permeability), could be interpreted in the fashion of Marino et al (1990) solely in terms of cell kinetics of one of the organ's components, namely, epidermis.

Yours etc.,

A. Michalowski

MRC Cyclotron Unit,
Hammersmith Hospital,
London W12 0HS

(*Received 13 May 1991 and in revised form 21 October 1991, accepted 10 December 1991*)

References

Gompertz, H., 1990. *The Pathophysiology of Duodenal Ulceration —Studies Using the Abscopal Model.* Thesis (Faculty of Medicine, University of London).

Gompertz, R. H. K., Man, W. K., Li, S. K., Spencer, J., Baron, J. H. & Michalowski, A. S., 1991. Acid blockade by omeprazole or ICI 162846 in a chronic duodenal ulcer model. *Agents and Actions, 33*, 161–163.

Marino, C., Hirn-Stadler, B. & Rojas, A., 1990. The influence of a seventy-two hour gap on the acute response of mouse skin and oesophagus. *British Journal of Radiology, 63*, 951–957.

Michalowski, A. S., 1981. Gastrointestinal lesions in thorax-irradiated mice. *British Journal of Radiology, 54*, 713.

——, 1989. Radiopathology of normal tissues: are clonogenic survival and cell kinetics all that matter? In *XVth Berzelius Symposium: Somatic and Genetic Effects of Ionizing Radiation*, ed. by T. Stigbrand (Nyheternas Tryckeri, Umeå), pp. 67–73.

Michalowski, A. & Burgin, J., 1982. Duodenal ulcers as an abscopal effect of thoracic irradiation in mice. In *Progress in Radio-oncology II*, ed. by K. H. Kärcher, H. D. Kogelnik and G. Reinartz (Raven Press, New York), pp. 105–110.

Michalowski, A. & Hornsey, S., 1986. Assays of damage to the alimentary canal. *British Journal of Cancer, 53* (suppl. VII), 1–6.

Michalowski, A., Uehara, S., Yin, W.-B., Burgin, J., Rogers, M. A. & Silvester, J. A., 1983a. Some early effects of thoracic irradiation in mice. In *Proceedings of the VIIth International Congress of Radiation Research*, ed. by J. J. Broerse, G. W. Barendsen, H. B. Kal and A. J. van der Kogel (Martinus Nijhoff, The Hague), abstract D3–28.

Michalowski, A., Uehara, S., Yin, W.-B., Burgin, J. & Silvester, J. A., 1983b. Alternative types of duodenal, ulcer induced in mice by partial X-irradiation of the thorax. *Radiation Research, 95*, 78–86.

Phillips, T. L. & Ross, G., 1974. Time-dose relationships in the mouse esophagus. *Radiology, 113*, 435–440.

1992, *The British Journal of Radiology*, 65, 733–735

Proceedings of the British Institute of Radiology

The new legislation—friend or foe (after the White Paper and into Europe)

Abstracts presented at a meeting organized by the BIR Industry Committee and supported by the European Association of Radiology, held at the Scientific Societies Lecture Theatre, New Burlington Place, London W1 on Thursday, 13 June 1991

Chairman: Professor C. A. Joslin
Dr O. Craig
Miss D. Rigg

The White Paper implications fact from fiction, by J. Roylance. Abstract not received
A model of departmental management, by I. Watt. Abstract not received
What's in it for us? by R. Atkinson
Sharing services—will it work? by J. N. A. Ridyard
Role of the supplies organization, by E. Sutherland. Abstract not received
The impact of the White Paper on the UK radiology market, by R. Meara
New health service—new industry? by C. Robertson
Radiology in Europe, by I. Isherwood
Training for radiotherapists in the UK and Europe, by R. G. B. Evans
Radiographic training in 1992, by P. Richardson. Abstract not received
Training for radiographers in radiotherapy, by S. Williams. Abstract not received

What's in it for us?

B. Atkinson
Norfolk and Norwich Hospital, Brunswick Road, Norwich NR1 3SR, UK

A review of the financial effects on a radiology department in a district general hospital was given and the positive effects of the White paper were discussed. These financial implications were related to particular situations which had arisen at the Norfolk and Norwich Hospital. GP fundholding is often seen as a threat to many but, infact, it can be viewed as an opportunity to expand the service provided by the radiology department. It was proposed that GP fundholders should be targeted in order to ensure that there was some flexibility within the budget; that one should be proactive in looking for opportunities to expand in service by increasing income as this is likely to be the only real opportunity in "The New World". 1991 was a challenging time to be around. There were no problems: only solutions.

Sharing services—will it work?

J. N. A. Ridyard
Lanmark, PO Box 37, Beaconsfield, Bucks HP9 2LR

The recent White Paper and the ensuing legislation has altered the nature of the provision of services between hospitals. The financial implications have to be understood fully. Cross charging for interhospital services is supposed to create a more cost effective environment and enable resources to be acquired and used in the most efficient way. Expensive capital equipment has historically been difficult to fund from within the NHS. Even when the capital element could be found from outside sources, the revenue consequences were large and also had to be provisional from outside since NHS funds were unavailable. Such equipment was therefore initially positioned at locations which were geographically isolated and patients were moved as necessary to the equipment and the necessary clinical resource. Large waiting lists and inconvenience to patients were a common result of this policy. Lack of a means of cross charging for services meant that there was no benefit registered to hospitals who were able to give a service and others without the facility were able to take advantage of this and obtain "free" services. Budgets were therefore difficult to balance correctly and improvements by additional healthcare services difficult to justify. Although many facilities depend upon local availability of clinical support, many non-acute cases can be served by mobile equipment which is scheduled to be on-site for only 1 day per week or even just 1 day per month. This is an excellent way of avoiding under-utilization of equipment and enables all hospital sites to have a local facility without the need for large expenditure of capital, extra space allocation and specialized staff costs. When comparisons are made, fixed site *vs.* mobile facilities are surprisingly similar in operating costs. The need to refer elsewhere or use older procedures which are slower or less clinically advisable can thus be avoided at a viable cost which can easily be budgetted for. Sharing services by mobile equipment is not new in radiology, and mass chest screening and mammography are well known examples. Computed tomography was introduced in the USA in 1977, but is required on an emergency basis for accident and emergency departments and therefore cannot be satisfactorily used in a mobile mode where availability is scheduled. Magnetic resonance imaging is, however, an ideal candidate for mobile use since the majority of clinical applications allow a scheduled availability. The technical difficulties have been solved and a reliable service is no problem. Several such systems are now operating in the UK within the private sector. The NHS has also used these services while building up their own facility. Cardiac catheterization promises a similar benefit since clinicians do not require full local support services on site when using modern techniques. The long waiting lists for patients requiring catheterization presents severe patient risk and a mobile service could reduce this waiting list as well as make the service far more convenient at similar costs to fixed site installations. The financial implications of any expensive capital equipment are surprisingly similar. If a 5 year lifetime is assumed and a total capital budget of £1 million, including building and equipment, the capital repayment represents about 40% of annual costs, interest and insurance costs another 24% while maintenance of the equipment and building or mobile trailer 16%. Administration and other costs add about 20%. Staff costs are additional, but a mobile service with radiographer support can be made available on a daily charge rate of about £2500 for the above example. This is £250 per patient if 10 patients per day can be referred. Therefore, there are many opportunities for sharing services in the new environment within the NHS. We can increase the utilization of high cost capital equipment, minimize transport costs for patients and reduce waiting lists. Facilities can be made available sooner and staff trained in their use prior to acquiring local equipment or during an upgrade or building programme. However, in order to ensure smooth functioning of such a mobile service, the system must integrate with the hospital operation and be seen as a genuine NHS service by all concerned.

The impact of the White Paper on the UK radiology market

R. Meara
Joynings, Seven Hills Road, Cobham, Surrey KT11 1ET

Four key changes arising from the NHS and Community Care Act can be identified. They are (1) the introduction of capital charges; (2) devolved management responsibilities and the independence of Trusts; (3) GP fundholders and the changing role of the acute general hospital; and (4) the management of service departments. Capital charges will force managers to look harder at purchasing expensive equipment and will require a much tougher business case to be made. If a purchase is made, it will have to justify itself in income gained and will have to be used more intensively, during evenings and weekends. Trusts will have greater freedom to purchase outside established channels and will seek to reach deals with manufacturers direct. Local maintenance of equipment may give way to a wider use of service contracts but these will be expected to deliver better value for money against more precisely specified quality standards. The importance of GP fundholders lies in the shift of care from the secondary to the primary setting. This will lead to more treatment being undertaken in health centres and community hospitals. Manufacturers should respond with small scale technology suited to these settings. Finally, is it reasonable to assume that the management of radiology departments will always remain in-house? The X-ray department houses the most costly collection of equipment in the hospital and the departmental manager will have to be prepared to make those assets work hard for the hospital. Some functions could be contracted out to other hospitals on a shared-asset-basis, or to a mobile facility. A facilities management approach may offer lower and more flexible overheads. These changes offer both threats and opportunities to those working in the UK radiology market. Those with the best information and analysis about their customers and competitors are most likely to survive.

"New health service—new industry?"

C. W. Robertson
Private Technical Consultant Maidenhead, Berkshire, UK

The radiological equipment supply industry in the UK must necessarily be geared to the prevailing requirements of its customers and to the economic and legislative climate in which it operates. Major developments are taking place in both these determining factors, but the precise effects of the changes are difficult to predict. The paper discusses, speculatively, the effects that NHS reforms may have on the market environment and the extent to which EEC legislation may create conditions in the UK with which suppliers and users alike are at present unfamiliar. One of the main questions considered is whether the NHS reforms, by generating an element of internal competition for the provision of healthcare services to specified standards of quality, would be likely to increase the rate at which equipment is replaced when it becomes outmoded or relatively expensive to maintain.

Radiology in Europe

I. Isherwood
Department of Diagnostic Radiology, The Medical School, Oxford Road, Manchester M13 9PT

In 1992 the single European Act will be implemented in the 12 nations of the European community. These states have a total population of over 320 million and approximately 600 000 doctors, but represent only part of the Europe for which the European Association of Radiology (EAR) has responsibilities. The EAR is not a society but a federation, representing all 27 national societies of radiology in a Europe which extends from the Urals to the Atlantic and from the Arctic to the Mediterranean. The EAR is especially concerned with establishing and maintaining the highest radiological educational standards throughout Europe. A European College of Radiological Education (EUCORE) is to be established to encourage and advise on standards of training in both teaching programmes and teaching departments and to coordinate continuing education and continuing assessment programmes on a European basis. The importance of this activity in relation to Eastern Europe cannot be overemphasized. Collaboration between EAR and the EC on educational matters is crucial. There are many aspects of EC activity which are likely to influence radiological practice throughout Europe. These include professional opportunities for practice, the standardization and applications of information technology, drug regulations—including approval for and purchase of pharmaceutical products including contrast media, basic science and research—particularly in multinational activities, ethical aspects of medical practice at both national and international levels, medico-legal activities and the effects of a social charter on employees within the health service. The EAR has a most important role in monitoring and coordinating the effects of EC activity to ensure that the wider interests of European radiology are protected.

Training for radiotherapists in the UK and Europe

R. G. B. Evans
Warden of the Faculty of Clinical Oncology, The Royal College of Radiologists

The aims of the Royal College of Radiologists (RCR) are described in its supplemental charter and include the furtherance of instruction and training in radiology and the conduct of examinations and award of certificates and diplomas. For the speciality of radiotherapy, including clinical oncology, this task is delegated to the Warden of the Faculty of Clinical Oncology and the education board of the faculty. Education is conducted by attendance at approved courses. Training is undertaken at a local level, standards being monitored by the RCR through the post-graduate education advisers, and may take place only in departments which have been approved for training by the RCR through its visit panel. Finally, the quality of training is assured by passing the qualification of Fellowship of the RCR. In order to make it easier for persons to pursue activities as self-employed persons, medical directives have been issued by the EC which are concerned with the mutual recognition of formal qualifications and depend upon the harmonization of training conditions, including minimum periods of training, at both undergraduate and post-graduate levels. The advisory committee on medical training as made a number of important recommendations, including regulation of the number of doctors in higher training, supervision and approval by a competent authority, and assessment by a suitable examination or report. In this respect the work of the RCR is a paradigm for many of the goals of the EC. A questionnaire conducted by ESTRO shows varying degrees of uniformity apropos national teaching programmes, their organization, checking the outcome and the requirement or not of examinations. This year, agreement was reached on a minimum curriculum, in radiotherapy, which may raise the standards in some countries in the EC. Finally, some remaining problems were touched on, including the existence of substantial unemployment among doctors in the EC.

1992, *The British Journal of Radiology*, 65, 736

Book reviews

Introduction to Radiobiology. By M. Tubiana, J. Dutreix and A. Wambersie. Translated by D. K. Bewley, pp. 371, 1990 (Taylor & Francis, Hampshire), £50.00 and £19.00 (paperback).
ISBN 0-85066-763-1

This volume represents a translation, with some updating, of a successful book *Radiobiologie* that was first published in French in 1986. The book would be of particular value to trainees in radiotherapy and would also provide a useful introduction to the subject for biologists/radiobiologists entering this field of cancer research. It will also be of considerable value to teachers in the field. The two introductory chapters deal with the initial physical and chemical effects of radiation clearly and concisely. The subsequent chapters build up in a logical way involving radiation effects on DNA, chromosomes, cell and tissues (normal tissues and tumours). The response of tumours includes a particularly valuable chapter on hypoxic cells and their significance for the success or failure of radiotherapy treatment. Given the importance of understanding dose fractionation in radiotherapy the chapter set aside for this problem is perhaps surprisingly brief. However, it does give the reader an insight into the history of the development of dose fractionation models and like other chapters is well referenced so that the reader may delve more deeply into the subject if required.

The book provides a good overview of the field and puts the science of radiobiology into a clearly defined clinical context. At a cost of only £19.00 for the paperback edition it is extremely well worth buying and very good value for money.

J. W. Hopewell

The Visible Human Body: an Atlas of Sectional Anatomy. By G. Von Hagens, L. J. Romrell, M. H. Ross and K. Tiedemann, pp. ix + 150, 1990 (Lea & Febiger UK Ltd, Kent), £23.00.
ISBN 0-8121-1269-5

This atlas of sectional anatomy is a beautifully presented book depicting the body in sagittal, coronal and transverse sections. It follows many others that have appeared in recent years but the preparation of specimens is, in this case, different. The specimens themselves, once produced, have been plastinated where water and lipids have been removed from the tissue sections and replaced with cured epoxy polymers. Also the prepared sections are very thin and the plastination process has resulted in enhanced contrast and sharper definition of structure when compared with the more traditional methods of producing sections of the human body. The photography thereafter employed to produce the illustrations is of high quality, although in some of the sagittal sections the colouration is rather dark.

The atlas is in seven parts and each region of the human body is examined and studied in turn, commencing with the head and neck and leading through to the upper extremity, the thorax, the abdomen, the male pelvis and perineum, the female pelvis and perineum and finally the lower extremity. The number of sagittal and coronal sections is not extensive but the transverse sections are serial and extend through the whole region and are studied in a most detailed fashion. Each illustration is extensively and accurately labelled and in itself the atlas is an excellent reference book for undergraduates or postgraduates studying anatomy in this modality. In certain areas an illustration is accompanied by one or more radiograph, computed tomography scan (CT) and/or magnetic resonance image (MRI). The index is extensive and is a useful search facility.

For a book so beautifully produced and presented I think the major criticism must be that each section of the body is not accompanied by a CT scan, an MRI image and a radiograph. This would allow direct comparison of the three types of image available for comparison with the human body slices. This would be particularly useful for postgraduates studying radiology or a health care specialist seeking a basic understanding of sectional anatomy. Several other works include a comparison of the new technologies that do exist in clinical medicine and relate them directly to the anatomical specimens.

I think this atlas may well have a place in a reference library or in the specialist library of a relevant specialist department. With the restriction in teaching time for undergraduate and gross anatomy, I fear it is probably too detailed to be included as a recommended text although again it may well be used as a reference text. The atlas does, however, prove quite conclusively that plastination has a role to play in the preservation of human tissue specimens for use in teaching at both undergraduate and postgraduate levels.

D. I. Lewis-Jones

Easily Missed Fractures and Corner Signs In Radiology. By H. O. Riddervold, pp. xiii+400, 1991 (Futura Publishing Company, Mount Kisco, NY), $150.00.
ISBN 0-87993-502-2

This 400 page text book is essentially an atlas of trauma radiology with the content almost entirely confined to the plain film. The seven chapters cover the various anatomical sites in a conventional manner; the skull and face, the spine etc. The exception is the first chapter, written by an American lawyer, entitled *Radiology Malpractice in the Emergency Room*. Some of the advice given is peculiar to American practices but may, in due course, become the norm in Europe.

The emphasis in the remaining chapters is on the subtle signs of trauma with the "corner signs" in the title referring to abnormalities present at the periphery of a film which, over here, might be more easily recognized as an "edge of film" diagnosis. While most of the examples are well illustrated, particularly in view of the discrete signs of the abnormality, there are a few cases, such as the clavicular fracture identified on a skull film, which say more about the radiographic coning than the skill of the radiologist. Each chapter commences with a couple of pages of text, half a dozen references and suggested reading followed by numerous figures. This approach means that for the individual radiologist or department this book, on its own, is not an adequate bench book on trauma radiology. Examples of minor deficiencies include the lack of mention of associated vertebral fractures with depressed calcaneal fractures and, in the same context, the mention of Bohler's angle without an explanation of how it is obtained. Nevertheless this book will be of value to trainee radiologists in that, with only a few hours study, they will have seen a large spectrum of fractures; but the cost may deter many.

A. M. Davies

1992, *The British Journal of Radiology*, 65, 737–753

VOLUME 65 NUMBER 777 SEPTEMBER 1992

The British Journal of Radiology

Invited Review: Permanent radiation myelopathy

By Timothy E. Schultheiss, PhD and *L. Clifton Stephens, DVM, PhD

Department of Radiation Oncology, Fox Chase Cancer Center, 7701 Burholme Avenue, Philadelphia, PA 19111 and *Division of Veterinary Medicine and Surgery, MD Anderson Cancer Center, 1515 Holcombe Boulevard, Houston, TX 77030, USA

(*Received 24 October 1991 and in revised form 13 March 1992, accepted 7 April 1992*)

Keywords: Radiation myelopathy, Radiation response, Radiation pathogenesis

Because of the morbidity and mortality associated with radiation myelopathy, radiation injury to the spinal cord has been the subject of more clinical reports than any other normal-tissue injury. The spinal cord is perhaps second only to skin as the organ most frequently studied by radiobiologists. Its response has been investigated in mice, rats, cats, guinea pigs, rabbits, pigs, dogs, and rhesus monkeys—virtually every laboratory animal species. Given this level of attention, it is surprising what is not known about the radiation response of the spinal cord. Relatively few animal studies have been performed on the effect of cytotoxic drugs on the radiation response of the spinal cord, the age effects, the effects of blood pressure or other physiological conditions that are controllable in the laboratory, or the relative response of various anatomical levels of the spinal cord. In addition to these unresolved factors, the dose response in the human is still poorly defined. However, as a result of the attention this injury has received, substantial information is available on the diagnosis, pathogenesis and dose fractionation dependence. This review seeks to establish the facts, expose the myths and define the issues still in dispute regarding radiation-induced myelopathy.

Signs and symptoms

Although several attempts have been made to categorize different syndromes in radiation myelopathy (Innes & Carsten, 1962; Reagan et al, 1968; Schultheiss et al, 1988; Stephens et al, 1983; van der Kogel, 1977b; Verity, 1968; Zeman & Samorajaski, 1971), the various signs and symptoms can occur in almost any combination, depending on the location and severity of the lesion. Symptoms may progress at various rates, even for a specific patient. (One atypical case of which we are aware was stable with mild symptoms for 17 years before a sudden onset of complete paralysis.) Generally, the first signs are hardly noticed by the patient. These may include unilateral sensory deficit and diminished temperature sensation, clumsiness, lower extremity weakness and decrease in proprioception. By the time the patient complains of symptoms, the symptoms will have intensified in severity and could also include signs such as changes in gait and difficulty in walking, hemiparesis, Brown–Sequard syndrome, spasticity, pain, weakness, hyperreflexia and various degrees of incontinence. Babinski signs are common. Although it is usually associated with transient myelopathy, L'hermitte's syndrome accompanies the late developing symptoms of permanent myelopathy more often than is generally appreciated (Dynes, 1960). There is usually an ascending progression of signs or symptoms that can stabilize at any level up to complete quadriplegia, depending on the anatomical level that was irradiated (Holdorff, 1980). These symptoms are often indistinguishable from acute febrile polyneuritis (Guillain-Barré syndrome). Some objective recovery may occur, but any recovery is usually more subjective and is not generally permanent. Neurological symptoms are sometimes initiated by a fall or some other trauma, and the myelopathy progresses from that point.

Again, no specific symptoms are characteristic of radiation myelopathy only. This myelopathy is indistinguishable from many other myelopathies that are a result of, or involve, demyelination. No effective treatment has been found, although symptoms related to swelling from inflammation may respond to corticosteroids (Godwin-Austen et al, 1975).

The prognosis of a radiation myelopathy patient depends primarily on two factors: the degree to which the lesion transects the cord (Holdorff, 1980) and the anatomical level of the lesion (Schultheiss et al, 1986). Complete transection of the cord at any level is a poor prognostic sign, and as the level of the lesion moves superiorly, the prognosis deteriorates. These findings are not peculiar to radiation myelopathy but apply to any traumatic myelopathy. The actuarial mortality from radiation myelopathy is 55% at 18 months for cervical cord injury and 25% at 18 months for thoracic injury (Schultheiss et al, 1986). As in traumatic myelopathy, the younger patient has a better prognosis than older patients with radiation myelopathy.

Address correspondence to Timothy E. Schultheiss, PhD, Department of Radiation Oncology, Fox Chase Cancer Center, 7701 Burholme Ave, Philadelphia, PA 19111, USA.

Diagnosis

The diagnosis of radiation myelopathy is always by a process of exclusion. However, even when myelograms, computed tomography (CT) scans, magnetic resonance imaging (MRI) scans, and plain radiographs are negative for tumour or other aetiology, both the symptomatic presentation and the spinal cord dose must still be consistent with radiation myelopathy before this diagnosis is accepted. Just because no other reason is found to explain the patient's symptoms, one should not adopt a diagnosis of radiation myelopathy as a substitute for an unexplained myelopathy (Zulch & Oeser, 1974; Abadir, 1980). Just as there are no pathognomonic lesions for radiation injury to the spinal cord, diagnostic tests can at most determine the location and extent of injury to the spinal cord but not its cause.

A negative myelogram is almost a requirement for a diagnosis of radiation myelopathy, except that diffuse spinal cord enlargement has been reported (Lechevalier et al, 1973; Marty & Minckler, 1973; Kitamura et al, 1979; Worthington, 1979). Wang et al (1992) reported 10 cases of radiation myelopathy imaged with magnetic resonance. Of eight cases examined 2–8 months after onset of symptoms, they noted spinal cord swelling in six cases and low intensity on T_1-weighted images and high signal intensity on T_2-weighted images in eight cases. Diffuse atrophy was found in two cases examined 36 and 53 months after onset of symptoms. Swelling of the spinal cord (sometimes producing a complete myelographic block) has been associated with particularly poor prognosis in the cases in which it has been reported (Worthington, 1979). Lymphocytes and moderately elevated total protein are commonly found in the cerebrospinal fluid (CSF) of radiation myelopathy cases. Elevated myelin basic protein is a less consistent finding. Measurements of nerve conduction velocities show slowed spinal conduction or complete blocks (Dorfman et al, 1982; Snooks & Swash, 1985).

In making a diagnosis of radiation myelopathy, one should recognize that in an adult, the latency is rarely less than 6 months from the completion of radiation. If the latency is shorter than 6 months, particularly in patients that have received low doses (< 50 Gy in 25 fractions), one should look for alternative diagnoses (including unknown causes), mistakes in dosimetry or factors that could have reduced the patient's radiation tolerance. Paraneoplastic syndromes often have symptoms in common with radiation myelopathy and may be more common in patients who receive radiation therapy. This diagnosis should be considered especially in lymphomas and lung cancer (Feldmann & Posner, 1986; Chouchair, 1991). Both the grey and white matter can be affected by these syndromes, but the grey matter lesions give a somewhat different presentation (Chouchair, 1991).

Pathology and pathogenesis

No pathognomonic characteristics have been identified for the lesions of radiation injury of the central nervous system (CNS). Like many diseases and other forms of injury, radiation shows a predilection for the involvement of white matter. *Selective damage to the grey matter would eliminate radiation as the causative agent of injury.* The white matter is composed of nerve fibres, an inconspicuous vasculature and glial cells. A nerve fibre is an axon surrounded by cytoplasmic processes of oligodendrocytes that form a concentric myelin sheath. Loss of myelin (demyelination) from individual nerve fibres and necrosis (malacia) of groups of nerve fibres are common expressions of white matter injury, regardless of the aetiology. Accordingly, demyelination and malacia are the consistent and dominant morphological features of clinical and experimentally induced radiation myelopathy.

Although damage and loss of nerve fibres are inevitable components of lesions in symptomatic cases, the responses of the vasculature and glial cells are highly variable and, as a result, add controversy to the interpretation of the pathogenesis. The lack of invariant morphological changes resulting from radiation of the CNS is a reflection of the similarities between CNS radiation responses and reactions of the CNS to other causes of damage. These responses are complex and extend beyond the cells that are killed by the initial insult. Some reactions to injury are directed at repair or compensation, while other responses may actually contribute to the damage.

Since our interpretation of the pathogenesis is based on morphological observations, we will begin by describing the lesions encountered in the irradiated spinal cord. The description of the lesions is based on our secondary analysis of the microscopic findings in approximately 60 human cases (Schultheiss et al, 1988), direct observation of autopsy material and our experimental work on non-human primates (Stephens et al, 1983; Schultheiss et al, 1990). To augment these observations, we have scrutinized the pertinent reviews of clinical material by Fajardo (1982), Rubenstein (1972) and Zeman and Samorajski (1971), and experimental studies by Hopewell (1979), Hopewell et al (1987), Myers et al (1986), Rubin et al (1988), van der Kogel (1980, 1986, 1991b) and others that will be specified when we address the pathogenesis.

Pathology

Grossly, the radiation damaged spinal cord may be swollen or atrophic, and the sectioned cord may have areas that are discoloured by necrosis and haemorrhage. However, it is by histopathological examination that radiation myelopathy is confirmed and best characterized. Pathological studies of the irradiated spinal cord are generally restricted to those cases that are symptomatic with neurologic dysfunction. As a result, the available clinical material represents only the more advanced expressions of damage. Animal studies have provided a broader picture of the lesions by affording the opportunity to view milder degrees of injury and, to some extent, they have helped clarify some of the relationships between the changes and such factors as time, dose, fractionation, etc.

Consistent features in all human cases and in animal models are one or more of the white matter lesions that are listed in an estimated order of increasing severity in Table I. (Note, this order does not reflect a possible temporal sequence of these lesions.) Our judgement of severity is strictly related to morphology and not necessarily to morbidity. Clinical consequences are more related to the extent, size and location of the lesions than to specific morphology. The standard terminology of neuropathology used to describe these alterations does not need to be redefined to apply it to radiation myelopathy. Schultheiss et al (1988) have categorized the radiation myelopathy lesions observed in autopsy material. A Type I lesion involves only the white matter parenchyma or has only minor vascular changes assumed to be insufficient to produce symptoms. A Type II lesion is predominantly vascular in nature with any white matter damage judged to be secondary to the vascular damage. A Type III lesion has characteristics of primary damage to both the white matter parenchyma and the vasculature.

The morphological distinction between confluent demyelination and malacia is somewhat arbitrary but when groups of demyelinated axons are either altered to become spheroids or are completely lost, the lesion is designated as malacia. "Inactive" malacia refers to those areas of necrosis comprised of status spongiosus and spheroids and glial scars. These are interpreted to be stable lesions that may remain unchanged for relatively long periods of time. Areas of malacia may be further accentuated by mineral deposits. Coagulative necrosis is a specific class of malacia in which ghosts of nerve fibres and cells can still be recognized. This is "active" malacia, because breakdown of the neuropil is ongoing and ultimately accompanied by accumulations of microglia and an increased prominence of astrocytes. Such lesions, with nerve fibre destruction and prominent glial reactions, are consistent with Wallerian degeneration. Areas that are composed of focal collections of microglia with foamy cytoplasm (gitter cells) provide evidence that liquefactive necrosis has occurred at that site. This severe manifestation of active malacia may also be seen as poorly delineated amorphous areas or as partially or totally empty cystic spaces. Three types of liquefactive necrosis represent the alterations before, during and after the accumulation of foam cells. Blood sometimes fills necrotic areas. These haemorrhages typically appear acutely and may totally obscure the underlying white matter or reside in a cystic space. Such lesions are characteristic of infarction and, as a point of fact, vascular lesions are invariably seen in close association with haemorrhagic necrosis.

Table I. White matter lesions of radiation myelopathy

1. Demyelination of isolated nerve fibres
2. Demyelination of groups of nerve fibres (spongiosis)
3. "Inactive" malacia
    - (a) spongiosis, spheroids
    - (b) scar
4. "Active" malacia
    - (a) coagulative malacia
    - (b) liquefactive malacia
        - (i) amorphous
        - (ii) foam cell fields
        - (iii) cystic
5. Haemorrhagic malacia

Table II. Vasculopathies of radiation myelopathies[a]

1. None
2. Increased vascularity
3. Telangiectasis
4. Hyaline degeneration and thickening
5. Oedema and fibrin exudation
6. Perivascular fibrosis and inflammation
7. Vasculitis
8. Fibrinoid necrosis
9. Thrombosis
10. Haemorrhage

[a] With or without endothelial alterations of hyperchromasia, hypertrophy, anisokaryocytosis and hyperplasia.

The vascular lesions encountered in the irradiated spinal cord are listed in Table II. Reflecting the lack of pathognomonic changes caused by radiation, these vasculopathies are found in other conditions. The irradiated spinal cord, as is the case with other tissues, may contain vascular lesions and no parenchymal changes. The presence of no vasculopathies is listed to emphasize that the converse can also be true. However, vascular lesions, particularly when seen in association with demyelination and malacia, comprise a picture that can be considered to be very characteristic of radiation injury because the combination of lesions is seen in many human cases (Schultheiss et al, 1988) and in the majority of non-human primates (Schultheiss et al, 1990) with radiation myelopathy. The vascular changes most often encountered are endothelial alterations, telangiectasia, hyalinosis and fibrinoid necrosis. Further, albeit indirect, evidence of vascular injury is the common finding of oedema or the accumulation of fibrin in perivascular spaces and in areas of necrosis. Oedema disrupts white matter more than grey matter (Manz, 1974; Feigin & Budzilovich, 1980) and has been proposed as in important feature of radiation injury of the CNS (Feigin & Budzilovich, 1980). Although haemorrhagic necrosis is listed as a white matter lesion, thrombosis and vascular necrosis are essential components of the process. The fact that tissue injury occurs distal to arterial obstruction and proximal to venous obstruction could explain the frequent finding of vascular lesions at levels different from the neuropil lesions.

Clear distinction can rarely be made between arteries and veins in histological sections of the CNS. Even though the vasculopathies associated with radiation injury apparently occur in both arteries and veins, certain features suggest preferential venous compromise. The lack of death of neurons in typical cases of radiation myelopathy argues against arterial impairment. It was noted that monkeys, symptomatic for radiation

Table III. Glial reactions of radiation myelopathy

1. Microglia/macrophages
    - (a) morphology
        - (i) rod-shaped
        - (ii) foam cells
        - (iii) multinucleated
    - (b) patterns
        - (i) diffuse
        - (ii) focal
        - (iii) perivascular
2. Astrocytes
    - (a) morphology
        - (i) inconspicuous
        - (ii) gemistocytic
        - (iii) fibrillary
    - (b) patterns
        - (i) diffuse
        - (ii) focal

myelopathy, consistently had lesions in the lateral corticospinal motor tract (Schultheiss et al, 1990). This is an area that is affected by venous lesions (Gillilan, 1970).

Microglia and astrocytes are normal components of the CNS that commonly exhibit profound alterations in the irradiated spinal cord. As noted in Table III, the pattern of increased numbers and greater prominence of these cells may be diffuse or focally concentrated to areas of white matter destruction. One can see areas of damaged white matter which, instead of being composed of nerve fibres, consist exclusively of microglia/macrophages and astrocytes. The border of a focus of necrosis may be delineated from surrounding intact tissue by a zone of dense gliosis. The close association of microglia and astrocytes with the lesions of demyelination and malacia is accentuated by the overt morphological changes the cells display. Microglia can have abundant foamy cytoplasm that is, in fact, phagocytosed myelin. Multinucleated giant cells are sometimes seen in close association with dystrophic mineral. Astrocytes are increased in both size and number. The morphology varies from that of cells with large, pale-staining nuclei and inconspicuous cytoplasm to that of gemistocytes, which are astrocytes characterized by abundant, eosinophilic cytoplasm. As discussed below, astrocytes and microglia probably play active roles in radiation injury, not just ones of repair and phagocytosis.

Pathogenesis

Identification of a specific target cell and recognition of a consistent pathway of radiation-induced damage of the CNS have not been resolved. Oligodendrocytes and endothelial cells are usually emphasized as the potential target cells. The general view is that these cells have both independent and overlapping roles in the pathogenesis. Their relative contribution is certainly influenced by radiation dose and, most likely, by other factors. An emphasis on oligodendrocyte injury rests on the premise that reproductive death and failure of replenishment of these cells can account for white matter destruction. However, it has been argued that death of oligodendrocytes which slowly turn over cannot alone result in later development of confluent lesions of demyelination and outright malacia (Myers et al, 1986). The accent on oligodendrocyte death has been modified by considering that the loss of these cells may be accentuated by failure of their replenishment owing to killing of glial progenitor cells (van der Kogel, 1991b).

Slowly evolving and late-developing changes in the structure and permeability of the microvasculature were historically emphasized as being primarily responsible for radiation injury of the CNS (Rubin & Casarett, 1968). An essential role for vascular injury cannot be denied in some cases of radiation myelopathy when there are the obvious lesions of vascular necrosis, thrombosis and manifestations of altered permeability seen as oedema, fibrin deposition and haemorrhage. However, an indispensable role for vascular injury might be challenged on the basis of reported cases with malacia but with morphologically normal or minimally altered vessels. Although individual cases can either support or contradict a contribution of vascular changes to the pathogenesis, experimental evidence supports the likelihood of injury to both glial cells and blood vessels. What determines their relative contribution to the destruction of the neuropil is unknown.

It is well recognized that vascular injury can lead to necrosis. However, it seems improbable that white matter necrosis would result from vascular injury without morphological or functional vascular changes somewhere in the irradiated field. Furthermore, no cogent explanation has heretofore been offered for the mechanism by which malacia results from the mitotic death of the oligodendroglia. In many demyelinating diseases, denuded axons are observed without axonal loss characteristic of radiation injury. Furthermore it is not clear why slowly proliferating oligodendrocytes, with as yet unidentified stem cells (in adult animals), should undergo a sudden and dramatic reduction in number at highly variable times following irradiation. In addition, one would expect that mitotic death of oligodendrocytes from radiation would result in diffuse demyelination, but focal necrosis is often observed adjacent to apparently normal white matter. The field of view of the pathogenesis of radiation myelopathy must be broadened to account for these facts.

Consideration of the pathogenesis of radiation myelopathy traditionally ends with a dual focus on changes of nerve fibres and the intramedullary vasculature. Infiltration of the tissue by microglia and proliferations of astrocytes have either been ignored or regarded as a secondary response (Casarett, 1980). However, recently discovered involvement of these cells in a variety of other demyelinating conditions raises the likelihood that they are additional participants in the pathogenesis of radiation-induced injury in the CNS. Infiltration of the tissue by microglia constitutes an inflammatory response, but in more conventional terms inflammation, as represented by lymphoid cells and granulocytes, occurs but is not a predominant feature in radiation myelopathy. Inflammatory cells, when present, are generally found in the Virchow-Robin spaces. Actual inflammation of the parenchyma is seen in lesions that are compatible with recent infarction. Such necrotic areas may also be infiltrated by neutrophils. Although lymphocytes are occasionally admixed with infiltrating microglia, the numbers are usually less than those encountered in inflammatory demyelinating conditions like certain viral encephalitides and multiple sclerosis.

A distinction is drawn between the intensity of traditional inflammation associated with the white matter destruction in radiation myelopathy compared with other conditions. However, parallels can be drawn between the involvement of microglia in the pathogenesis of radiation myelopathy and other CNS conditions, particularly considering the morphological picture presented by the pathophysiological consequences of proliferation, infiltration and activation of these cells. Mildenberger et al (1990) concluded that early responses by microglia in irradiated rat brains heralded the development of destructive lesions. The same has been reported for astrocytes. A combination of changes in blood vessels and adjacent astrocytes was found to precede degeneration and necrosis of white matter in rat brain (Calvo et al, 1988; Reinhold et al, 1990). The narrowest view relegates astrocytes to passive structural roles with the most significant reactive function being involvement in healing by forming a scar. Astrocytes are the most plentiful cell in the CNS and, as is the case with microglia, the diversity of their functional properties in both health and disease, is becoming increasingly apparent, and their role in radiation injury has been appreciated by relatively few investigators (Hubbard & Hopewell, 1979; Myers et al, 1986).

Microglia are the representatives of the mononuclear-phagocyte system in the CNS (Hickey & Kimura, 1988). The reactive microglia associated with demyelination and malacia are from two derivations, *i.e.* resident cells and cells infiltrating from the blood. When tissue destruction is extensive and the blood–brain barrier has been disrupted, most authorities believe that the majority are derived from blood monocytes (Dickson et al, 1991). It is an open question whether microglia actively destroy viable myelin or if they only engage in clearing off debris resulting from myelin destruction. Although direct phagocytic destruction of white matter is disputed, indirect participation in tissue injury (as opposed to the repair process) is becoming clearly established for both microglia and astrocytes (Zucker-Franklin et al, 1987). Astrocytes are normally involved with the formation of the blood–brain barrier and make various contacts with neurons, synapses, ependyma and meninges (Janzer & Raff, 1987; Kimelberg & Norenberg, 1989). Injury and disease cause disruption of these anatomical relationships. In addition, astrocytes assume a variety of immunological and biochemical properties that include characteristics analogous to those of microglia/macrophages (Zucker-Franklin et al, 1987).

The CNS contains a cytokine network that may be important for normal CNS function. Cytokine production and responsiveness are among the characteristics shared by microglia and astrocytes (Dickson et al, 1991; Sawada et al, 1989). An increase in the production or release of cytokines can convert a normal action into a toxic property (Balkwill & Burke, 1989; Brosnan et al, 1988). These substances have actions in inflammation, immunity, coagulation and cellular proliferation and differentiation. Cytokines, such as interleukin-1 (IL-1) and tumour necrosis factor (TNF), have been identified as mediators of the expression of the lesions in a variety of demyelinating diseases. These soluble mediators cause injury to other CNS cells, myelin and endothelium (Dinarello, 1984; Le & Vilcek, 1987; Lieberman et al, 1989; Robbins et al, 1987; Selmaj & Raine, 1988). TNF is unique among cytokines because of its capacity to induce cell death (Laster et al, 1988; Le & Vilcek, 1987). It is implicated in the pathogenesis of demyelination and malacia in conditions as diverse as viral encephalomyelitis (Lieberman et al, 1989), septicaemia and endotoxaemia (Mustafa et al, 1989; Waage et al, 1987), malaria (Grau et al, 1987), Reye's syndrome (Larrick & Kunkel, 1986) and multiple sclerosis (MS) (Brosnan et al, 1988; Hofman et al, 1989). This list includes diseases with infectious, parasitic, unknown and autoimmune aetiologies. The range of stimuli that may evoke TNF production is broad, and its limits are unknown (Beutler & Cerami, 1987). Many conseqences of TNF action have features in common with radiation injury. Regional irradiation causes local exacerbation of experimental allergic encephalomyelitis (EAE) (Love et al, 1987; Oldendorf & Cornford, 1977), and TNF is believed to be a pathogenic component in the EAE model for MS and in the disease itself (Brosnan et al, 1988). Features of radiation lesions that are associated with elevated TNF are astrocyte proliferation (Selmaj et al, 1990), demyelination (Brosnan et al, 1988; Selmaj & Raine, 1988; Robbins et al, 1987), oligodendrocyte cytotoxicity (Robbins et al, 1987) and endothelial cytotoxicity (Pober, 1988; Robaye et al, 1991; Silverman et al, 1990). It is these actions of soluble mediators like TNF from astrocytes and microglia that indicate their potential for participation in the pathogenesis of radiation injury of the CNS. One could hypothesize that radiation directly alters the secretory phenotype of resident astrocytes and microglia to modify cytokine production. Alternatively, astrocytes, microglia and infiltrating macrophages may respond to radiation-induced injury to the tissue by abnormally producing these substances. Whichever is the case, cytokines would be available to augment radiation-induced injury of the neuropil and/or vasculature, with the result being a contribution to the development of lesions in a manner in common with other conditions characterized by white matter destruction.

Perhaps insufficient consideration of participation by microglia, astrocytes and other factors, like the role of cytokines, is a reason that the pathogenesis of radiation injury of the CNS has eluded understanding. The involvement of dynamic components, in addition to the demise of oligodendrocytes and/or endothelial cells, may explain certain features such as the common finding of lesions with "old and new histological ages" in the same section. Observations like this cannot be resolved on the basis of cell kinetic mechanisms alone, but do lend themselves to an interpretation based on the functional waxing and waning of cellular responses like those proposed for microglia and astrocytes.

Dose limits and fractionation studies

Human

Radiation myelopathy was first reported in 1941 by Ahlbom. In 1945, Stevenson and Eckhardt reported the first autopsy on a patient who had developed radiation myelopathy. In 1948, Boden and Greenfield and Stark reported details of radiation myelopathy cases. Boden was the first to recommend safe dose limits. In SI units these limits are approximately 33 Gy in 17 days for large fields (⩾ 15 cm) and 43 Gy in 17 days for small fields (⩽ 10 cm). Fractionation was unspecified (there were no cases with field sizes between 10 and 15 cm) and these limits did not exclude all of the myelopathy cases he reported. Fletcher and Million (1965) suggested a limit of 50 Gy in 25 fractions for head and neck treatments. Atkins and Tretter (1966) found 47.5 Gy in 25 fractions to be well tolerated. However, their treatments were commonly given as a single field per day (P. Tretter, personal communication, 1989). Verity (1968) recommended a limit of 60 Gy in approximately 33 fractions. Schiodt and Kristensen (1978) recommended a tolerance dose for the lumbar cord to be 54 Gy in 30 fractions. Baekmark (1975) suggested that 60 Gy in 30–33 fractions should be well tolerated. Kim and Fayos (1981) concur with this dose if it was applied to small lengths of cord.

Different radiosensitivities for the cervical and thoracic levels of the spinal cord were first suggested by Dynes in 1960. The reasoning for this suggestion was that damage to the vascular supply to the thoracic cord was more likely to induce ischaemia than similar damage to the vascular supply to the cervical or lumbar levels. Kramer (1968) first published different dose limits for the cervical and thoracic levels as 50 Gy in 5 weeks and 45 Gy in 4½ weeks, respectively. The perceived difference in sensitivity probability reflected the facts that (1) the thoracic cord was often irradiated using AP/PA fields in which a single field was treated on alternate days, and (2) the importance of the individual fraction size (Marks et al, 1972) rather than the average fraction size was then not appreciated. Alternatively, Glanzmann et al (1976) stated that cervical cord was said to be *more* sensitive than the thoracic cord, but their analysis could not confirm this. The clinical dogma that the thoracic cord is more sensitive than the cervical cord (and therefore has a lower dose limit) was never established by objective data analysis, has not yet been tested experimentally and has only recently been challenged in the literature (Schultheiss, 1990).

Most of the dose limits for the spinal cord were established by plotting myelopathy cases and controls (cases without myelopathy) on a log dose versus log N (number of fractions) scattergram. The line that excluded all or nearly all of the myelopathy cases while including as many controls as possible was then taken to define a recommended relationship between total spinal cord dose and number of fractions. The scientific insufficiency of this procedure is demonstrated by the facts that (1) the "safe" isoeffect line is established by the outliers, *i.e.* the least representative individuals in the population, (2) the dose per fraction may not have been constant, and (3) the true number of controls is unknown. Furthermore, the slope of this line did not establish the N-exponent for the variable-exponent NSD isoeffect model. However, as an exercise to ensure that a radiotherapist would never experience a case of myelopathy, the procedure was understandable, but incomplete.

It was during the 1970s that radiation therapists became increasingly aware that the late response of the spinal cord did not behave mathematically according to the NSD formula (Wara et al, 1975; van der Kogel, 1977b), although adherence to the NSD formula was still common (Abbatucci et al, 1978). Without invoking any specific isoeffect formula, it can be said that the spinal cord was observed to be relatively more sensitive to large doses per fraction than most other dose-limiting tissues (Phillips & Buschke, 1969), especially those that responded acutely or subacutely. This conclusion was given a mathematical form by Wara et al (1975), when they published that the exponent of the fraction number in an NSD-like isoeffect relationship for spinal cord should be 0.377 rather than 0.24, as given by Ellis (1967) for early-responding tissues. Unfortunately the spinal cord's greater sensitivity to large doses per fraction had to be experienced clinically, as is demonstrated by the considerable number of published reports of myelopathy cases following schedules using 10 fractions of 4 Gy (see Table IV). Several of these reports also served to establish the belief that split course treatments did not reduce the incidence of radiation myelopathy.

The most widely held standard of practice for the dose limit to the spinal cord is 45 Gy in 22–25 fractions. Extensive literature searches have discovered no adequately documented myelopathies following 45 Gy except in cases when one field per day was treated, in patients who had significant medical history that could be contributory to myelopathy, when the chance of a treatment error was significant, or in patients who were treated for a lymphoma (the significance of myelopathies in lymphoma treatments will be addressed below). Several authors have recommended that a dose of 50 Gy in 2 Gy fractions should be safe, whereas others have recommended doses lower than 45 Gy. It should be recognized that the widespread use of lower spinal cord doses will *not* decrease the incidence of radiation myelopathy. Marcus and Million (1990) have clearly demonstrated that 45 Gy, conventionally fractionated, is on the flat region of the dose–response curve, and therefore lower doses will result in an imperceptible decrease in the incidence of myelopathy. Our feeling is that any myelopathies occurring at 45 Gy would also occur at

Table IV. Reports containing radiation myelopathy incidence data for thoracic cord

Reference	Dose	Incidence	Survival
Eichhorn et al (1972)	27 × 2.45 Gy	8/46	12 month minimum
	18 × 2.45 Gy + 9 × 3.16 Gy	5/22	12 month minimum
	1 × 7.6 Gy + 19 × 2.9 Gy	2/33	12 month minimum
Choi et al (1980)	15 × 3 Gy	0/16	51% NED at 5 years
Hazra et al (1974)	15 × 3 Gy	0/75	96% at 1 year to 43% at 2 years
Abramson and Cavanaugh (1973)	10 × 4 Gy	4/103	12 month minimum
Fitzgerald et al (1982)	10 × 4 Gy	6/45	11 month minimum
Miller et al (1977)	10 × 4 Gy	4/97	6.4 month average
Madden et al (1979)	10 × 4 Gy	1/43	7.9 month average
Guthrie et al (1973)	10 × 4 Gy	0/42	6. 8 month average
	20 × 3 Gy	0/32	8.5 month average
Coy et al (1969)	8 × 5 Gy	3/31–97	38% at 9 months
Dische et al (1981)	6 × 5.8 Gy	8/71	6 month minimum
Hatlevoll et al (1983)	3 × 6 Gy + 5 × 4 Gy	43%	Life-table estimate from 157 patients
	3 × 6 Gy + 3 × 4 Gy + 2 × 2 Gy	22%	Life-table estimate from 230 patients

40 Gy, *i.e.* the tolerance of very few patients lies between 40 and 45 Gy.

The fractionation schedules and the associated incidences of myelopathy reported for thoracic and cervical spinal cords are given in Tables IV and V, respectively. In these tables, we have tried to use only those cases where overlapping fields were unlikely, thoracic treatments were given with all fields treated each day and treatments were not given in hyperbaric oxygen. Although these reports only represent a fraction of the published reports of radiation myelopathy, it can be appreciated from these tables that the majority of these cases received radiation doses per fraction considerably larger than 2 Gy.

Based on the series in Tables IV and V, other reports and primate experiments, we estimated that 45 Gy in 22–25 fractions would yield an incidence of myelopathy of $\leqslant 0.2\%$. The conventionally fractionated dose that would result in 5% incidence of myelopathy is probably between 57 and 61 Gy, and the dose resulting in a 50% incidence is probably between 68 and 73 Gy. Because the radiation therapy community has learned to avoid radiation myelopathy, and modern quality assurance programmes decrease the probability of accidental overdoses on a large scale, the establishment of statistically valid estimates of these doses can be obtained only by the analysis of retrospective data. We would respect a lower tolerance for paediatric patients (Knowles, 1983; Schultheiss et al, 1984), especially when radiation is combined with chemotherapy.

Because of the morbidity of radiation myelopathy, spinal cord doses should always be minimized. However, tumour doses should *not* be compromised in curative cases for the purpose of limiting the spinal cord dose to 45 Gy. 50 Gy should be acceptable in an otherwise healthy patient who is being treated for cure and in whom tumour location prohibits limiting the cord to a lower dose. Although 60 Gy carries with it a definite risk of myelopathy, this schedule could be considered in extreme cases since the majority of patients who receive this dose will escape without myelopathy. Because of daily variations in treatment set up, the spinal cord should not be treated to its dose limit (in the judgement of the radiotherapist) if it is also near a significant dose gradient. This situation would arise when off-cord treatment with oblique fields commenced after 45–50 Gy to the cord and the field edges of the boost treatment were in close proximity to the spinal cord.

Just as the spinal cord response revealed the high dose per fraction limitation of the NSD model, the spinal cord was unexpectedly found to be the dose-limiting organ in hyperfractionation studies. The spinal cord's response to multiple daily fractions resulted in the addition of incomplete repair (Thames, 1989; Thames et al, 1988) to the NSD's rival, the linear quadratic (LQ) model. Using the CHART regimen of 1.5 Gy in three

Table V. Reports containing radiation myelopathy incidence data for cervical cord

Reference	Dose	Incidence	Survival
Abbatucci et al (1978)	18 × 3 Gy	8/18	18 month minimum
Atkins and Tretter (1966)	2 × 9.5 Gy	4/10	24 month minimum
McCunniff and Liang (1989)	30 × 2 Gy	3/17	24 month minimum
Marcus and Million (1990)	40–45 Gy	0/91	12 month minimum
(1.8–1.9 Gy per day)	45–50 Gy	0/211	
	50–55 Gy	0/22	
Jeremic et al (1991)	30 × 2 Gy	2/19	24 month minimum
	40 × 1.63 Gy	0/19	

daily fractions for 12 consecutive days, Dische and Saunders (1989) maintained a limit for the spinal cord of about 45–48 Gy. The spinal cord received most of its dose during the large-volume portion of the treatment, 28 fractions of 1.5 Gy, with 3–6 Gy received over the final eight-fraction conedown. Despite what appeared to be a very conservative limit, and similar previous experience indicating a low risk of myelopathy (Van den Bogaert et al, 1986), four cases of myelopathy were observed using this protocol. It appears that during the 6-h interval between the treatments, significantly less repair of radiation damage at the subcellular level occurred than was expected. Wong et al (1991) reported two cases of radiation myelopathy in patients treated four times per day with 1 Gy fractions separated by 3 h. Total hyperfractionated doses were 38 and 43.3 Gy, which were preceded by single fractions of 1.9 and 5 Gy, respectively. Marcus and Million (1990) observed no myelopathies in head and neck patients treated twice daily with 1.2 or 1.0 Gy per fraction to total cord doses of either 40–45 Gy (107 patients) or 45–50 Gy (90 patients). Their interfraction interval was 4–6 h.

To our knowledge, no myelopathies have been reported using 1.2 Gy fractions given twice daily to a total dose of approximately 45 Gy. However, the interval between fractions should be as long as practicable and no shorter than 6 h. It appears unwise at this time to extrapolate from daily fractionation dose regimens to multiple fractions per day using any biomathematical model. If three fractions per day are given, we recommend shielding the cord during the second daily fraction. Dose escalation with hyperfractionation should be undertaken with caution.

Experimental studies

The overwhelming majority of experimental work on spinal cord dose response has been carried out in the rat. Several early studies were aimed at determining the slope of the plot of log isoeffect dose versus log N (van der Kogel, 1977b; Masuda et al, 1977; Hornsey & White, 1980; Ang et al, 1983). It was established that this slope, for the number of fractions used, was larger than the 0.24 of the NSD formula and not much different from the value of 0.377 proposed by Wara et al (1975). More recent studies have shown a linear relationship between log ED_{50} and log N down to doses per fraction of 2 Gy (Ang et al, 1985), and Wong et al (1992) have extended this observation down to 1 Gy per fraction. The data of Ang and Wong do not agree on the extent to which there is sparing below 2 Gy. However, the lack of sparing found by Ang et al (1985) is purportedly due to incomplete repair between twice daily fractions (Thames et al, 1988), whereas Wong et al used daily fractionation. Some of the low-dose-per-fraction studies have used the top-up dose technique to achieve their results while others have not. There is no apparent disagreement between the results obtained with a top-up dose and those without. The value of the slope of the log dose versus log N isoeffect line was in the range 0.33 and 0.44, depending on rat strain, treatment duration, anatomical level of treatment and possibly the length of follow-up. The value of this exponent confirms the clinical observation that the spinal cord is relatively more sensitive to large fractions than many other tissues. However, it is well recognized that the rodent's tolerance expressed in terms of total dose is much greater than that of humans. What is uncertain is whether the dose per fraction effects observed in rodents can be applied without modification to man.

The effect of overall treatment time has also been studied in the rat (White & Hornsey, 1978, 1980). However, one should recognize that clinical treatment durations of approximately 6 weeks generally represent half of the age of the rat at the time of treatment initiation. When treatment durations are comparable to the age of the animal, the interpretation of the results must be viewed with caution, and treatment times shorter than are used clinically may not be relevant to clinical responses. White and Hornsey (1978) observed no increase in the two-fraction, split dose ED_{50} values for lumbar myelopathy as the interfraction interval was increased from 1 day to 16 days. The ED_{50} values ranged from 32 to 33.5 ± 2 Gy. Using a 32-day interval they found an ED_{50} of 36.5 ± 2 Gy. Van der Kogel (1977a) reports no difference in the ED_{50} value in rats treated with 15 Gy and then with varying doses at 1 and 8 weeks after the initial dose. However, there were apparently only five animals per dose group and only one dose point for which the percentage of paralysed rats was neither 0 nor 100%. Using a 16-week interval between the 15 Gy initial dose and the test dose, he found a significant increase in ED_{50}. In 4-month-old mice, Goffinet et al (1976) compared the ED_{50} values after 10 fractions, given as daily fractions, with either a 3-week split after 5 fractions or a 3-month split after 5 fractions. When assessed 6 months after the first day of treatment, there was a clear trend toward higher ED_{50} values with increasing time. However, when assessed 6 months after the last fraction, the ED_{50} values for the split courses decreased. In the case of the 3-month split, the ED_{50} was *less* than that for the daily fractionation. Because of the complexities of the pathogenesis and the dissimilarities between experiments, very little can be asserted with confidence regarding the effect of treatment time on the radiation response of the spinal cord. However, it seems that there is a modest amount of sparing when the treatment time is increased beyond 6 weeks. Certainly most tumours would be spared more than the spinal cord by such extended treatment schedules.

The animal model nearest to the human that has been used in experimental investigation of radiation myelopathy is the rhesus monkey. Innes and Carsten (1962) used large single doses of radiation to study the histopathology of spinal cord lesions. Stephens et al (1983) and Schultheiss et al (1986, 1990, 1991, 1992) have used fractionated treatments to study relative biological effectiveness (RBE), dose response, histopathology and pathogenesis, and latency of radiation myelopathy.

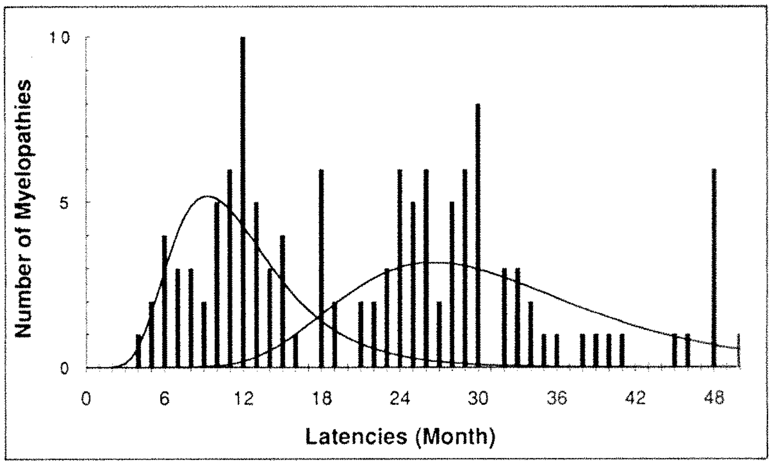

Figure 1. Latencies for patients with cervical or thoracic radiation myelopathy who survived at least 30 months after treatment. The solid curves represent the fit to a bivariate lognormal distribution.

Studies of volume effects, hyperfractionation and retreatment are ongoing. Using 2.2 Gy fractions, the $ED_{50} \pm 1$ SE was 76.1 ± 1.9 Gy. For the logistic dose–response function, the probability (P) of injury after dose D is given by the equation:

$$P = \frac{1}{1 + \left(\frac{ED_{50}}{D}\right)^k} \quad (1)$$

Using this formula, a value of k of 18.7 ± 6.7 was determined (Schultheiss et al 1990). For dogs treated with 4 Gy fractions, $k = 17.5 \pm 5.2$ (data supplied by E. Beck, analysed by us). For pigs treated with single doses, $k = 51 \pm 7$ (data supplied by J. W. Hopewell, analysed by us). For humans treated in six fractions, $k = 43 \pm 16$ (data supplied by S. Dische and M. I. Saunders, analysed by us). Because radiation myelopathy does not result from a known number and type of cells being depleted to a known surviving fraction, the value of k *cannot* be related to Poisson statistics. It is rather a reflection of the heterogeneities in the treated population's response to irradiation. It appears that for a given species and strain, k decreases with increased dose fractionation.

A dramatic field-size effect has been demonstrated in the rat with fields smaller than 1 or 2 cm (Hopewell et al, 1987; van der Kogel, 1991a). It is not clear that such an effect would scale proportionally to the human. Furthermore, van der Kogel (1991b) has reported no field-size effect in rats treated with fields larger than 1 cm. However, Schultheiss et al (1991) observed an increase in the incidence of myelopathy, consistent with the probability model (Schultheiss et al, 1983), in rhesus monkeys when the field size increased from 4 to 16 cm. It is unlikely that the different findings in the rat and the monkey are due to differences in assays (isoeffect dose versus incidence, respectively). The difference is more likely due to species differences or differences in treatment regimens (single dose versus fractionated doses, respectively). Recent findings by Hopewell and van den Aardweg (1992) in pigs show a modest field-size effect for ED_{50}, but no observable field-size effect for ED_{05}. In humans, no field-size effect has been demonstrated with respect to incidence, latency or severity of symptoms.

The latencies for radiation myelopathy have been shown to be bimodally distributed and to follow a lognormal distribution (Schultheiss et al, 1984, see Fig. 1). The bimodality of this distribution has been ascribed to differences in the pathogenesis associated with the lesions that dominate two different peaks (Reinhold et al, 1984; Schultheiss et al, 1984). Although paediatric and adolescent patients appear to have shorter latencies, there is otherwise no correlation between latency and age. Although there is a significant correlation between latency and effective dose, the variations in latencies at any specific dose level are so large that one cannot make inferences about the dose based solely on the latency. No differences exist in latencies between the cervical and thoracic radiation myelopathies. However, it appears that lumbar myelopathies, although relatively rare, have a shorter latency than is observed in higher anatomical levels of the cord (Maier et al, 1969; Schiodt & Kristensen, 1978; Schultheiss et al, 1984).

Rather than the bimodal distribution observed in humans, only a single phase of latencies is observed for the rhesus monkeys. The distribution of latencies for the monkeys corresponds well with the earlier peak of latencies in humans. Furthermore, the types of lesions observed in these monkeys correspond to the types of lesions observed with similar latencies in humans. One may infer that the very late myelopathies (> 24 months) in the human correspond to the late vascular lesions observed in the rat and human but not observed in the monkey. This may be related to the relatively greater age of the rat by the time these lesions are expressed, or to the vascular compromise that may result from the chronic renal disease found in nearly all geriatric rats.

Retreatment

The mouse results from Goffinet et al (1976) with a 3-month interval between irradiations were probably more pertinent to the retreatment issue than to overall retreatment time. Although many clinical cases of radiation myelopathy have been reported after retreatment, only Tan and Khor (1969) have reported on a series of retreatment cases with the spinal cord in both treatments. Their treatment for carcinoma of the nasopharynx was 5500 r or röentgen through laterals and an anterior facial field to the post-nasal space, given over a 6–7 week period in apparently five treatments per week. The spinal cord received about 4000 r, although it is not clear whether all fields were treated at each session. In 22 cases, a second full course was given within a few months to 4 years after the first treatment. Three cases of radiation myelopathy resulted, two of which are reported in detail. The intervals between treatments for the two reported cases were 8 and 52 months. The survival data of the non-myelopathy cases were not reported.

In a review of the clinical literature, Schultheiss et al (1984) found that the latency between the final course of treatment and the onset of symptoms was shorter in retreated myelopathy cases than in those cases resulting from a single treatment course. Although the data are sparse, this effect was not observed in rhesus monkeys that were retreated after 70.4 or 44 Gy in 2.2 Gy fractions (Price et al, 1992). Nonetheless it would seem unwise to rely on a long latency to escape expression of injury when giving a second, palliative treatment.

In a preliminary study on retreatment, rhesus monkeys were given 44 Gy in 20 fractions and were retreated 2 years later to *total* doses of 83.6, 92.4, 101.2 and 110 Gy in 2.2 Gy fractions (Price et al, 1992). There were four animals in each group. One animal in the 110 Gy dose group died during follow-up. One animal in each of the two highest-dose groups showed clinical evidence of radiation myelopathy. These two monkeys were the only animals to develop Type II lesions in any of the rhesus monkey studies performed by these investigators. Three other groups of four animals were retreated to *total* doses of 83.6, 92.4 and 101.2 Gy 2 years after the initial dose of 70.4 Gy. The two animals with signs of radiation myelopathy, one each in the two lower-dose groups, had Type III lesions. Animals without signs had either no lesions or static Type III lesions. The animals in these groups that did not develop signs had minor lesions or no lesions.

Van der Kogel has shown that retreatment tolerance doses increase approximately linearly with time after the initial dose (van der Kogel, 1991a). Although a plateau certainly exists, none could be detected up to 200 days after treatment. Moreover, his data show that the fraction of the effect of the initial dose that is maintained 200 days after retreatment increases with the magnitude of the initial dose. The greater the initial dose, the less recovery there is. However, it may be that the recovery continues for longer times after higher doses. Knowles (1983) found guinea-pigs treated with 10 Gy at age 1 day had only a 1 Gy diminution of their ED_{50} at age 1 year when compared with previously untreated animals.

Because of the life span, latency and dose–response differences, only general guidelines for clinical applications can be offered from the rodent data. These data indicate that substantial recovery of spinal cord tolerance is achieved during a sufficiently long interval after initial radiation therapy. In general, a higher retreatment dose can be given following lower initial doses and longer intervals between treatments. From the sparse clinical and primate data, it appears that at least 50% recovery of 45 Gy would be obtained 2 years after treatment.

Other factors affecting responses

Chemotherapy

The effects of chemotherapy on the incidence of radiation myelopathy are impossible to quantify from literature reports, and the experimental data with cytotoxic agents are sparse. Eight of 10 myelopathies reported by Paulson and Quenemoen (1984) had received multiple chemotherapeutic agents. Abratt et al (1987) observed one case of radiation myelopathy in a series of patients treated with radiation, CCNU, mitomycin C and misonidazole. In similar cases treated without the drug therapy, no myelopathies had been observed. However, the myelopathy patient suffered from alcoholism, the significance of which is not known. Ruckdeschel et al (1979) observed a single case of myelopathy in a small series of patients whose bronchogenic carcinoma was treated with multiagent chemotherapy (cyclophosphamide, adriamycin, methotrexate and procarbazine) following intrapleural BCG and 30 Gy in 10 fractions. The case of myelopathy occurred 12 months after the completion of radiation and 6 months after the completion of chemotherapy. The spinal cord dose was 21 Gy in 10 fractions. Two myelograms were negative. Saunders et al (1982; 1984) found no difference in the rate of myelopathies observed in a large-dose-per-fraction regimen in which patients were randomly assigned to misonidazole or placebo. However, they did observe a significant increase in peripheral neuropathy in the patients who received misonidazole. Likewise, van der Kogel and Sissingh (1983) observed no increase in the ED_{50} of rats when given misonidazole.

Menten et al (1989) found a significant decrease in ED_{50} after both single and two-fraction schedules when Ara C was given intraperitoneally to rats 2 h before irradiation. Using an Ara C dose of 9 g/kg, a dose modifying factor of about 1.2 was determined. They found no apparent difference in the histopathology of the lesions of the animal that received the drug treatment compared with those that did not. Their results compared well with those of van der Kogel and Sissingh (1985) who gave 0.1 g/kg of Ara C intrathecally to the same strain of rats and obtained dose-modifying factors of 1.2 and 1.31 in single-dose and two-fraction experiments, respectively. Ang et al (1986) found no enhancing effect of AZQ given intravenously at a dose of 3 mg/kg 15 min before radiation treatment given as a single dose or a two-fraction regimen. Small dose-modifying factors are probably not detectable in humans who receive less than 50 Gy to the spinal cord.

Many cytotoxic and cytostatic agents are known to be neurotoxic. These include methotrexate (Bleyer & Griffin, 1980), cisplatinum (Walther et al, 1987), vinblastine, Ara C and others (Lee et al, 1986). One can only suggest caution when contemplating the administration of radiation therapy simultaneously with chemotherapy because of the likelihood of diminished spinal cord tolerance. Virtually no data are available on any additivity of effects on the spinal cord of radiation and chemotherapy when given sequentially. Because intrathecal chemotherapy alone is quite capable of producing myelopathy, the combination of radiation and intrathecal chemotherapy must be considered extremely hazardous.

Oxygenation and vascular effects

Treatment in hyperbaric oxygen (HBO) may reduce the tolerance of the spinal cord to radiation. Certainly radiation myelopathy was a common complication of treatment reported by institutions treating patients in hyperbaric oxygen. However, no randomized trials were ever reported in which the frequency of myelopathies with and without HBO were compared. It may be that the increased myelopathies were a result of treating one field per day in some cases and of giving large doses per fraction in general. Coy and Dolman (1971) reported an increased incidence of myelopathy in patients surviving 9 months after radiation treatment for thoracic tumours in HBO at 3 atm with both fields treated at each session (Peter Coy, personal communication, 1986). They found this complication in three of 17 patients who received approximately 39 Gy in 8 fractions in HBO, compared with four of 121 patients who received more than 40 Gy in 8 fractions, twice weekly, in air. We are not surprised by the high incidence of radiation myelopathy in their HBO series, but are by the relatively low incidence in the patients treated in air considering the consistently reported finding of myelopathy in 5–10% of patients who received 40 Gy in 10 fractions (see Table IV). Giving the same or higher total dose in 8 rather than 10 fractions certainly should noticeably increase the observed incidence of myelopathy. In HBO treatments for head and neck cancers, van den Brenk et al (1968) were not able to confirm an increase in the incidence of myelopathy. In comparison to Coy and Dolman, who observed an 18% incidence in patients who survived 9 months after receiving 8 fractions of approximately 5 Gy, van den Brenk et al observed an 18% (7/38) incidence in patients who survived 9 months after receiving only 6 fractions of 5 Gy to the cervical spinal cord. Either the cervical cord enjoys a greater oxygen enhancement ratio or it is more sensitive to radiation.

In a related finding, Dische et al (1986) have demonstrated a significant positive effect of pretreatment haemoglobin level on the incidence of radiation myelopathy after treatment with large doses per fraction. These are somewhat curious findings in an organ as well perfused with oxygen as the spinal cord is reported to be, but can be interpreted as implying a protective effect occurring in patients with lower haemoglobin levels.

The clinical data related to blood pressure are somewhat ambiguous, and the experimental data are very sparse. Certainly many reports contain cases in which hypertensive patients have developed radiation myelopathy. In an early study that has yet to be duplicated or further investigated, Asscher and Anson (1962) found that rats made hypertensive by clipping the renal artery developed radiation myelopathy at lower doses than control rats. Hopewell and Wright (1970) also found increased CNS sensitivity in hypertensive rats. Furthermore, it has been stated that vascular changes in the rat are more prevalent as the time after treatment increases. This phenomenon could correspond to the development of hypertension secondary to renal changes in the geriatric rat. Reinhold et al (1976) found significantly lower blood pressure in their radiation myelopathy cases as compared with controls who were treated with similar doses and who survived a minimum of 30 months. Two of their cases were marginally hypotensive. If the vascular lesions occur with the greater likelihood on the venous or low-pressure side of the vasculature (as we suggest above), then it would be expected that patients with abnormally low blood pressure would be more susceptible to injury than normotensive patients. The fact that radiation lesions occur in the white matter rather than in the grey matter gives some evidence that veins are more likely to be involved than arteries. It is likely, although as yet unproven, that hypotensive as well as hypertensive patients are at greater risk for radiation injury to the spinal cord.

Vascular diseases may also predispose patients to radiation injury, but it is unclear how important atherosclerosis and common cardiovascular diseases are in potentiating radiation damage.

Disease processes

Radiation myelopathy in lymphoma patients should receive special attention. Clearly any radiation myelopathy in these patients will appear to occur at lower doses because these patients receive lower doses than most other cancer patients, and they also survive longer. In addition to the effect of extended survival, misdiagnosis is more likely in these patients. Paraneoplastic syndromes are known to occur with greater frequency in lymphoma than in other diseases (Walton et al, 1968). These syndromes often have a neurological manifestation (Feldmann & Posner, 1986). Such a manifestation could easily be attributed to radiation despite the lack of corroborating clinical data to indicate radiation injury (such as high dose, latency greater than 6 months, proper symptomatology). Furthermore there may be an interaction between these paraneoplastic syndromes and radiation injuries. Consider the example of herpes zoster. It occurs in approximately 10% of Hodgkin's disease patients, it is common in lung cancer patients and it is likely to occur in any immunosuppressed patients. In the series by Ruckdeschel et al (1979), three of the 18 patients completing the treatment developed a localized herpes zoster. Central neurological signs account for approximately 30% of the neurological complications of herpes zoster. Herpes zoster myelopathy is associated with a slightly swollen cord on myelography, slightly elevated total protein and lymphocytes in the CSF, ascending paresis and progressive neurological deficits. This picture could easily be mistaken for radiation myelopathy on symptoms alone if viral assays were not performed. It is feasible that subclinical viral injuries could combine with radiation injury to produce either temporary or permanent spinal cord damage.

Any disease process that has potential CNS effects may be regarded as a candidate for increasing the spinal cord's radiation sensitivity. Among the possibilities are several infectious diseases as well as diseases that affect the mechanical integrity of the spine. Of the 800 cases of cancers of the head and neck reviewed by Marcus and Million (1990), one of the two cases of radiation myelopathy was in a patient who was severely deformed, having had rickets as a child (Weems et al, 1987). We are aware of a case of low-dose radiation myelopathy in a woman with a previously undiagnosed Arnold-Chiari malformation.

Of 13 cervical radiation myelopathy patients diagnosed in one of our institutions (MD Anderson Cancer Center), four had a history of malaria. (The species of plasmodium was not recorded in any of these cases.) The majority of these patients were treated before 1970, and nearly all were over 50 years old. It is possible that this did not exceed the expected incidence of malaria in a cohort of patients who had lived in this region. Despite the fact that malaria is virtually unknown in The Netherlands, Professor Huibert Reinhold at the Rotterdam Radiotherapy Institute has kindly reviewed his published cases and discovered a patient who had contracted malaria in India (H. S. Reinhold, personal communication, 1986). *Falciparum* malaria can be associated with neurotoxicity, haemorrhage and capillaries occluded with infected erythrocytes. Clearly there is the potential for radiation injury given the damage that the small blood vessels may have sustained.

In many cases, it is not possible to implicate a single cause of myelopathy after radiation treatment. A multiplicity of agents can be illustrated by the following case. M.K. received post-operative radiation of 50 Gy in 25 equal fractions for limited small cell carcinoma of the lung. The spinal cord was shielded after 45 Gy. He also received 30 Gy in 10 fractions to the brain. In addition to radiation, he received chemotherapy with six courses of ECHO (etoposide, cytoxan, hydroxydaunorubicin, oncovin) prior to radiation and one course immediately after. Previous medical history included hypertension, moderate to heavy alcohol usage, very heavy cigarette usage, lower sacral spina bifida and a sacral laminectomy. Upon admission he was 182 cm tall and weighed 130 kg. After only 7 months, he developed leg weakness that ultimately progressed to paraplegia. The symptoms were consistent with radiation myelopathy except that a note in the chart had documented a complaint of mild leg weakness only 2 months after completion of treatment. Review of the case revealed no apparent treatment errors. MRI and myelography were normal, and the CSF contained moderately elevated total protein, normal MBP and some lymphocytes and red blood cells. Somatosensory evoked potential was normal in the cervical cord but showed severe disruption of the spinal pathways below the cervical region. He was treated with tiazofurin and two courses of VP-16 and cisplatin for a recurrence 9 months after radiation treatment and developed renal failure. He died 12 months after the completion of his radiation treatment. An autopsy, limited to the spinal cord, showed gross atrophy in 1.5 cm of the mid-thoracic spinal cord, which corresponded microscopically to an area of severe demyelination. There was vascular proliferation with endothelial cell hyperplasia and occasionally thickened vessel walls. There were also reactive gliosis and perivascular chronic inflammation. This case represents a myelopathy for which radiation was a contributory cause but probably was not the only cause. Furthermore, there is little reason to assume that this myelopathy would have been avoided if the dose to the spinal cord had been limi[illegible] to 40 Gy.

Conclusions

Radiation myelopathy continues to occur despite greater appreciation of the necessity to keep the dose per fraction constant and low, to allow for complete interfraction repair, and the tendency toward limiting the cord dose to 45 Gy. Limiting the cord dose to 45 Gy is a reasonable action as long as the tumour is adequately treated. Reducing the dose below this value will not result in overall safer treatments because the dose–response function below 45 Gy is flat, *i.e.* there is virtually no dose effect in the low-dose region of the dose–response curve. Increasing the spinal cord limit is acceptable when it is necessary to do so for adequate tumour coverage.

The incidence of radiation myelopathy can be reduced, not by reducing doses but rather by identifying factors that interact with radiation to enhance its effect or that reduce the tolerance of the spinal cord to radiation. Factors that are likely to increase the risk of myelopathy are chemotherapy treatments, vascular and autoimmune diseases, congenital or acquired spinal abnormalities and any pre-existing CNS damage. Other factors may be certain infectious diseases, alcohol abuse, hypertension, hypotension and elevated haemoglobin. Patients in whom these risk factors are identified could receive specialized treatment planning to avoid the spinal cord, and the remainder of the patient population could potentially be given higher doses if the tumour control probability could be increased through dose escalation.

No definitive data are currently available on the spinal cord's response to retreatment. Animal data suggest that the higher the initial dose, the greater the fraction of initial damage that remains unrepaired at any given time after treatment. Furthermore, repair of occult damage appears to be complete after 1 year. Based on preliminary primate data and sparse clinical data, we believe that the probability of radiation myelopathy is 15–20% after two conventionally fractionated courses of 45 Gy separated by 2 years. This is a crude estimate at best and would probably be increased if neurotoxic chemotherapy were given. Of course in retreatment, the probability of radiation myelopathy must be weighed against the consequences of continued tumour growth.

Multiple daily fractions must be separated by as long an interval as possible. Hyperfractionation has much less effect in sparing spinal cord injury than would be expected on the basis of data for fractionation down to 2 Gy per fraction and an application of the LQ model. Total doses become misleading. A dose of 45–50 Gy in 1.2 Gy fractions separated by 6 h has not been shown to induce radiation myelopathy in humans.

It is unlikely that any diagnostic procedure could yield results that are pathognomonic for radiation myelopathy since most demyelinating myelopathies will produce similar signs, symptoms and test results. Whereas the diagnosis of "demyelinating lesion" may become easier to make with MRI or spectroscopy, ascribing the cause to radiation must be consistent with time and anatomical level. Other causes of demyelination should not be eliminated solely because the patient received radiation. No effective treatment is known, but minimizing the inflammatory response may ameliorate the symptoms. Furthermore, as the multiple factors that contribute to the production of a lesion are identified, including possibly disruption of the blood–brain barrier, cytokine production, etc., some types of intervention may be possible based on disrupting the complex sequence leading to clinical expression of injury.

References

ABADIR, R., 1980. Radiation myelitis: can diagnosis be unequivocal without histological evidence? *International Journal of Radiation Oncology, Biology, Physics, 6*, 649–650.

ABBATUCCI, J. S., DELOZIER, T., QUINT, R., ROUSSEL, A. & BRUNE, D., 1978. Radiation myelopathy of the cervical spinal cord. Time, dose, and volume factors. *International Journal of Radiation Oncology, Biology, Physics, 4*, 239–248.

ABRAMSON, N. & CAVANAUGH, P. J., 1973. Short-course radiation therapy in carcinoma of the lung. A second look. *Radiology, 108*, 685–687.

ABRATT, R. P., WILLCOX, P. A. & HEWITSON, R. H., 1987. Radical irradiation of localized inoperable lung cancer with concurrent chemotherapy and misonidazole: a phase I—II study. *European Journal of Cancer and Clinical Oncology, 7*, 1081–1082.

AHLBOM, H. E., 1941. The results of radiotherapy of hypopharyngeal cancer at the Radium-Hemmet, Stockholm, 1930 to 1939. *Acta Radiologica, 22*, 155–171.

ANG, K. K., VAN DER KOGEL, A. J. & VAN DER SCHUEREN, E., 1983. The effect of small radiation doses on the rat spinal cord: the concept of partial tolerance. *International Journal of Radiation Oncology, Biology, Physics, 9*, 1487–1491.

ANG, K. K., VAN DER KOGEL, A. J. & VAN DER SCHUEREN, E., 1985. Lack of evidence for increased tolerance of rat spinal cord with decreasing fraction doses below 2 Gy. *International Journal of Radiation Oncology, Biology, Physics, 11*, 105–110.

ANG, K. K., VAN DER KOGEL, A. J. & VAN DER SCHUEREN, E., 1986. Effect of combined AZQ and radiation on the tolerance of the rat spinal cord. *Journal of NeuroOncology, 3*, 349–352.

ASSCHER, A. W. & ANSON, S. G., 1962. Arterial hypertension and irradiation damage to the nervous system. *Lancet, ii*, 1343–1346.

ATKINS, H. L. & TRETTER, P., 1966. Time-dose considerations in radiation myelopathy. *Acta Radiologica, 5*, 79–94.

BAEKMARK, U. B., 1975. Neurologic complications after irradiation of the cervical spinal cord for malignant tumour of the head and neck. *Acta Radiologica Therapy Physics Biology, 14*, 33–41.

BALKWILL, F. R. & BURKE, F., 1989. The cytokine network. *Immunology Today, 10*, 299–304.

BEUTLER, B. & CERAMI, A., 1987. Cachectin, more than a tumour necrosis factor. *New England Journal of Medicine, 316*, 379–385.

BLEYER, W. A. & GRIFFIN, T. W., 1980. White matter necrosis, mineralizing microangiography, and intellectual abilities in survivors of childhood leukemia: associations with central nervous system irradiation and methotrexate, In *Radiation Damage to the Nervous System*, ed. by H. A. Gilbert and A. R. Kagan (Raven Press, New York), pp. 155–174.

BODEN, G., 1948. Radiation myelitis of the cervical spinal cord. *British Journal of Radiology, 21*, 464–469.

BROSNAN, C. F., SELMAJ, K. & RAINE, C. S., 1988. Hypothesis: A role for tumor necrosis factor in immune-mediated demyelination and its relevance to multiple sclerosis. *Journal of Neuroimmunology, 18*, 87–94.

CALVO, W., HOPEWELL, J. W., REINHOLD, H. S. & YEUNG, T. K., 1988. Time and dose-related changes in the white matter of the rat brain after single doses of X-rays. *British Journal of Radiology, 61*, 1043–1052.

CASARETT, G. W., 1980. Nervous system. In *Radiation Histopathology*, Volume II, (CRC Press, Boca Raton, FL), Ch. 7, pp. 113–131.

CHOI, N. C. H., GRILLO, H. C., GARDIELLO, M., SCANNELL, J. G. & WILKINS, E. W., 1980. Basis for new strategies in postoperative radiotherapy of bronchogenic carcinoma. *International Journal of Radiation Oncology, Biology, Physics, 6*, 31–35.

CHOUCHAIR, A. K., 1991. Myelopathies in the cancer patient: incidence, presentation, diagnosis and management. *Oncology, 5*, 25–37.

COY, R. & DOLMAN, C. L., 1971. Radiation myelopathy in relation to oxygen level. *British Journal of Radiology, 44*, 705–707.

COY, P., BAKER, S. & DOLMAN, C. L., 1969. Progressive myelopathy due to radiation. *Canadian Medical Association Journal, 100*, 1129–1133.

DICKSON, D. W., MATTIALE, L. A., CURE, K., HUTCHINS, K., LYMAN, W. D. & BROSNAN, C. F., 1991. Microglia in human disease with and emphasis on acquired immune deficiency syndrome. *Laboratory Investigations, 64*, 135–146.

DINARELLO, C. A., 1984. Interleukin-1 and the pathogenesis of the acute-phase response. *New England Journal of Medicine, 311*, 1413–1418.

DISCHE, S. & SAUNDERS, M. I., 1989. Continuous hyperfractionated accelerated radiotherapy (CHART): an interim report upon late morbidity. *Radiotherapy and Oncology, 16*, 67–74.

Dische, S., Martin, W. M. C. & Anderson, P., 1981. Radiation myelopathy in patients treated for carcinoma of the bronchus using a six fraction regime of radiotherapy. *British Journal of Radiology*, *59*, 29–35.

Dische, S., Saunders, M. I. & Warburton, M. F., 1986. Hemoglobin, radiation, morbidity, and survival. *International Journal of Radiation Oncology, Biology, Physics*, *12*, 1335–1337.

Dorfman, L. J., Donaldson, S. S., Gupta, P. R. & Bosley, T. M., 1982. Electrophysiologic evidence of subclinical injury to the posterior columns of the human spinal cord after therapeutic radiation. *Cancer*, *50*, 2815–2819.

Dynes, J. B., 1960. Radiation myelopathy. *Transactions of the American Neurological Association*, *85*, 51–55.

Eichhorn, H. J., Lessel, A. & Rotte, K. H., 1972. Einfluss verschiedener Bestrahlungsrhythmen auf Tumor und Normalgewebe *in vivo*. *Strahlentherapie*, *143*, 614–629.

Ellis, F., 1967. Fractionation in radiotherapy. In *Modern Trends in Radiotherapy*, Vol. 1, ed. by T. J. Deeley and C. Wood (Butterworth, London), pp. 34–51.

Fajardo, L. F., 1982. Nervous system. In *Pathology of Radiation Injury* (Masson, New York), pp. 216–230.

Feigin, J. & Budzilovich, G. N., 1980. The influence of ground substance on the extracellular water of normal and edematous human brain: focal edema and the demyelinating diseases, including multiple sclerosis. *Journal of Neuropathology and Experimental Neurology*, *39*, 13–29.

Feldmann, E. & Posner, J. B., 1986. Episodic neurologic dysfunction in patients with Hodgkin's disease. *Archives of Neurology*, *43*, 1227–1233.

Fitzgerald, R. H., Marks, R. D. & Wallace, K. M., 1982. Chronic radiation myelitis. *Radiology*, *144*, 609–612.

Fletcher, G. H. & Million, R. R., 1965. Malignant tumours of the nasopharynx. *American Journal of Roentgenology*, *93*, 44–55.

Gillilan, L. A., 1970. Veins of the spinal cord. *Neurology*, *20*, 860–868.

Glanzmann, C., Aberle, H. G. & Horst, W., 1976. The risk of chronic progressive radiation myelopathy. *Strahlentherapie*, *152*, 363–372.

Godwin-Austin, R. B., Howell, D. A. & Worthington, B., 1975. Observations of radiation myelopathy. *Brain*, *98*, 557–568.

Goffinet, D. R., Marsa, G. W. & Brown, J. M., 1976. The effects of single and multifraction radiation courses on the mouse spinal cord. *Radiology*, *119*, 709.

Grau, G. E., Fajardo, L. F., Piguet, P.-F., Allef, B., Lanbert, P.-H. & Vassalli, P., 1987. Tumor necrosis factor. Cachectin as an essential mediator in murine cerebral malaria. *Science*, *237*, 1210–1212.

Greenfield, M. M. & Stark, F. M., 1948. Post-irradiation neuropathy. *American Journal of Roentgenology*, *60*, 616–622.

Guthrie, R. T., Ptacek, J. J. & Hass, A. C., 1973. Comparative analysis of two regimens of split course radiation in carcinoma of the lung. *American Journal of Roentgenology*, *117*, 605–608.

Hatlevoll, R., Host, H. & Kaalhus, O., 1983. Myelopathy following radiotherapy of bronchial carcinoma with large single fractions: a retrospective study. *International Journal of Radiation Oncology, Biology, Physics*, *9*, 41–44.

Hazra, T. A., Chandrasekaran, M. S., Colman, M., Prempree, T. & Inalsingh, A., 1974. Survival in carcinoma of the lung after a split course of radiotherapy. *British Journal of Radiology*, *47*, 464–466.

Hickey, W. F. & Kimura, H., 1988. Perivascular microglial cells of the CNS are bone-marrow derived and present antigen *in vivo*. *Science*, *239*, 290–292.

Hofman, F. M., Hinton, D. R., Johnson, K. & Merrill, J. E., 1989. Tumor necrosis factor identified in multiple sclerosis brain. *Journal of Experimental Medicine*, *170*, 607–612.

Holdorff, B., 1980. Dose effect relationships in cervical and thoracic radiation myelopathies. *Acta Radiologica Oncology*, *19*, 271–277.

Hopewell, J. W., 1979. Late radiation damage to the central nervous system: a radiological interpretation. *Neuropathology and Applied Neurobiology*, *5*, 329–343.

Hopewell, J. W. & van den Aardweg, G. J. M. J., 1992. Radiation myelopathy in the pig: a model for assessing volume factors for spinal cord tolerance. *Abstracts of Papers for the Fortieth Annual Meeting of the Radiation Society*, p. 7.

Hopewell, J. W. & Wright, E. A., 1970. The nature of latent cerebral irradiation damage and its modification by hypertension. *British Journal of Radiology*, *43*, 161–167.

Hopewell, J. W., Morris, A. A. & Dixon-Brown, A., 1987. The influence of field size on the later tolerance of the rat spinal cord to single doses of X-rays. *British Journal of Radiology*, *60*, 1099–1108.

Hornsey, S. & White, A., 1980. Isoeffect curve for radiation myelopathy. *British Journal of Radiology*, *53*, 168–169.

Hubbard, B. M. & Hopewell, J. W., 1979. Changes in the neuroglial cell populations of the rat spinal cord after local X-irradiation. *British Journal of Radiology*, *52*, 816–821.

Innes, J. R. M. & Carsten, A., 1962. A demyelinating or malacic myelopathy and myodegeneration—delayed effect of localized X-irradiation in experimental rats and monkeys. In *Response of the Nervous System to Ionizing Radiation*, ed. by T. J. Haley and R. Snider (Academic Press, New York), p. 233.

Janzer, R. C. & Rafe, M. C., 1987. Astrocytes induce blood–brain properties in endothelial cells. *Nature*, *325*, 253–257.

Jeremic, B. J., Djuric, L. & Mijatovic, L., 1991. Incidence of radiation myelitis of the cervical spinal cord at doses of 5500 cGy or greater. *Cancer*, *68*, 2138–2141.

Kim, Y. H. & Fayos, J. V., 1981. Radiation tolerance of the cervical spinal cord. *Radiology*, *139*, 473–478.

Kimelberg, H. K. & Norenberg, M. D., 1989. Astrocytes. *Scientific American*, *260*, 22–76.

Kitamura, H., Kameda, Y., Yoshimura, Y., Nagaoka, S., Takai, S. & Nagatsuka, A., 1979. Delayed radiation myelopathy. *Yokohama Medical Bulletin*, *30*, 61–69.

Knowles, J. F., 1983. The radiosensitivity of the guinea pig spinal cord to X-rays: the effect of retreatment at one year and the effect of age at the time of irradiation. *International Journal of Radiation Biology*, *44*, 433–442.

Kramer, S., 1968. The hazards of therapeutic irradiation of the central nervous system. *Clinical Neurosurgery*, *15*, 301–318.

Larrick, J. W. & Kunkel, S. L., 1986. Hypothesis: Is Reye's syndrome caused by augmented release of tumor necrosis factor? *Lancet i*, 132–133.

Laster, S. M., Wood, J. G. & Gooding, L. R., 1988. Tumor necrosis factor can induce both apoptotic and necrotic forms of cell lysis. *Journal of Immunology*, *141*, 2629–2634.

Le, J. & Vilcek, J., 1987. Tumor necrosis factor and interleukin 1: cytokines with multiple overlapping biological activities. *Laboratory Investigations*, *56*, 234–248.

Lechevalier, B., Humeau, G. & Houtteville, J. P., 1973. Myélopathies radiothérapiques "hypertrophiantes" à propos de cinq observations dont une anatomo-clinique. *Revue Neurologique, Paris*, *129*, 119–132.

LEE, Y.-Y., NAUERT, C. & GLASS, J. P., 1986. Treatment-related white matter changes in cancer patients. *Cancer, 57*, 1473–1482.

LIEBERMAN, A. P., PITHA, P. M., SHIN, H. S. & SHIN, M. L., 1989. Production of tumor necrosis factor and other cytokines by astrocytes stimulated with lipopolysaccharide or a neurotropic virus. *Proceedings of the National Academy of Sciences (USA), 86*, 6348–6352.

LOVE, S., WILEY, C. A., FUJNAMI, R. S. & LAMPERT, P. W., 1987. Effects of regional spinal x-irradiation on demyelinating disease caused by Theiler's virus, mouse hepatitis virus or experimental allergic encephalomyelitis. *Journal of Neuroimmunology, 14*, 19–33.

MADDEN, F. J. F., ENGLISH, J. S. C., MOORE, A. K. & NEWTON, K. A., 1979. Split course radiation in inoperable carcinoma of the bronchus. *European Journal of Cancer, 15*, 1175–1177.

MAIER, J. G., PERRY, R. H., SAYLOR, W. & SULAK, M. H., 1969. Radiation myelitis of the dorsolumbar spinal cord. *Radiology, 93*, 153–160.

MANZ, H. J., 1974. The pathology of cerebral edema. *Human Pathology, 5*, 291–313.

MARCUS, R. G. & MILLION, R. R., 1990. The incidence of myelitis after irradiation of the cervical spinal cord. *International Journal of Radiation Oncology, Biology, Physics, 19*, 3–8.

MARKS, R. D., AGARWAL, S. K. & CONSTABLE, W. C., 1972. Increased rate of complication as a result of treating only one prescribed field daily. *Radiology, 107*, 615–619.

MARTY, R. & MINCKLER, D. S., 1973. Radiation myelitis simulating tumor. *Archives of Neurology, 29*, 352–354.

MASUDA, K., REID, B. O. & WITHERS, H. R., 1977. Dose effect relationship for epilation and late effects on spinal cord in rats exposed to gamma rays. *Radiology, 122*, 239–242.

MCCUNNIFF, A. J. & LIANG, M. J., 1989. Radiation tolerance of the cervical spinal cord. *International Journal of Radiation Oncology, Biology, Physics, 16*, 675–678.

MENTEN, J., LANDUYT, W., VAN DER KOGEL, A. J., ANG, K. K. & VAN DER SCHUEREN, E., 1989. Effects of high dose intraperitoneal cytosine arabinoside on the radiation tolerance of the rat spinal cord. *International Journal of Radiation Oncology, Biology, Physics, 17*, 131–134.

MILDENBERGER, M., BEACH, T. G., MCGEER, E. G. & LUDGATE, C. M., 1990. An animal model of prophylactic cranial irradiation histologic effects at acute, early, and delayed stages. *International Journal of Radiation Oncology, Biology, Physics, 18*, 1051–1060.

MILLER, R. C., ARISTIZABAL, S. A., LEITH, J. T. & MANNING, M. R., 1977. Radiation myelitis following split course therapy for unresectable lung cancer. *International Journal of Radiation Oncology, Biology, Physics, 2* (Suppl. 2), 179–180 (abstract).

MUSTAFA, M. M., RAMILO, O., OLSEN, K. A., FRANKLIN, P. S., HANSEN, E. J., BEUTLER, B. & MCCRACKEN, G. H., 1989. Tumor necrosis factor in mediating experimental Haemophilus Influenza Type B meningitis. *Journal of Clinical Investigations, 84*, 1253–1259.

MYERS, R., ROGERS, M. A. & HORNSEY, S., 1986. A reappraisal of the roles of glial and vascular elements in the development of white matter necrosis in irradiated rat spinal cord. *British Journal of Cancer, 53* (Suppl. VII), 221–223.

OLENDORF, W. H. & CORNFORD, E. M., 1977. A comparison of total body and local spinal cord irradiation in experimental allergic encephelomyelitis. *Journal of Neuropathology and Experimental Neurology, 36*, 50–61.

PAULSON, G. W. & QUENEMOEN, L. R., 1984. Radiation myelopathy. *Ohio State Medical Journal, 80*, 387–389.

PHILLIPS, T. L. & BUSCHKE, F., 1969. Radiation tolerance of the thoracic spinal cord. *American Journal of Roentgenology, 105*, 659–664.

POBER, J. S., 1988. Cytokine-mediated activation of vascular endothelium. *American Journal of Pathology, 133*, 426–433.

PRICE, R. E., FENG, Y., STEPHENS, L. C., SCHULTHEISS, T. E. & ANG, K. K., 1992. Radiation myelopathy in nonhuman primates following conventional fractionation and retreatment. *Abstracts of Papers for the Fortieth Annual Meeting of the Radiation Research Society*, p. 6.

REAGAN, T. J., THOMAS, J. E., COLBY, M. Y., JR, 1968. Chronic progressive radiation myelopathy. Its clinical aspects and differential diagnosis. *Journal of the American Medical Association, 203*, 106–110.

REINHOLD, H. S., CALVO, W., HOPEWELL, J. W. & VAN DEN BERG, A. P., 1990. Development of blood vessel-related radiation damage in the fimbria of the central nervous system. *International Journal of Radiation Oncology, Biology, Physics, 18*, 37–42.

REINHOLD, H. S., KAALEN, J. G. A. H. & UNGER-GILS, K., 1976. Radiation myelopathy of the thoracic spinal cord. *International Journal of Radiation Oncology, Biology, Physics, 1*, 651–657.

REINHOLD, H. S., VAN PUTTEN, W. L. J., HOPEWELL, J. W. & VAN DER KOGEL, A. J., 1984. The latent period in clinical radiation myelopathy. *International Journal of Radiation Oncology, Biology, Physics, 10*, 2385–2387.

ROBAYE, B., MOSSELMANS, R., FIERS, W., DUMONT, J. E. & GALAND, P., 1991. Tumor necrosis factor induces apoptosis (programmed cell death) in normal endothelial cells *in vitro*. *American Journal of Pathology, 138*, 447–453.

ROBBINS, D. S., SHIRAZI, Y., DRYSDALE, B. E., LIEBERMAN, A., SHIN, H. S. & SHIN, M. L., 1987. Production of cytotoxic factor for oligodendrocytes by stimulated astrocytes. *Journal of Immunology, 139*, 2593–2597.

RUBENSTEIN, L. J., 1972. *Radiation Changes in Intracranial Neoplasm and the Adjacent Brain in Tumors of the Central Nervous System* (Armed Forces Institute of Pathology, Washington, D.C.), pp. 346–360.

RUBIN, P. & CASARETT, G. W., 1968. *Clinical Radiation Pathology*, Vol. 2 (W. B. Saunders, Philadelphia), pp. 609–661.

RUBIN, P., WHITAKER, J. N., CECKLER, T. L., NELSON, D., GREGORY, P. K., BAGGS, R. B., CONSTINE, L. S. & HERMAN, P. K., 1988. Myelin basic protein and magnetic resonance imaging for diagnosing radiation myelopathy. *International Journal of Radiation Oncology, Biology, Physics, 15*, 1371–1381.

RUCKDESCHEL, J. C., BAXTER, D. H., MCKNEALLY, M. F., KILLAM, D. F., LUNIA, S. L. & HORTON, J., 1979. Sequential radiotherapy and adriamycin in the management of bronchogenic carcinoma: the question of additive toxicity. *International Journal of Radiation Oncology, Biology, Physics, 5*, 1323–1328.

SAUNDERS, M. I., ANDERSON, P., DISCHE, S. & MARTIN, W. M. C., 1982. A controlled clinical trial of misonidazole in the radiotherapy of patients with carcinoma of the bronchus. *International Journal of Radiation Oncology, Biology, Physics, 8*, 347–350.

SAUNDERS, M. I., BENNETT, M. H., DISCHE, S. & ANDERSON, P. J., 1984. Primary tumor control after radiotherapy for carcinoma of the bronchus. *International Journal of Radiation Oncology, Biology, Physics, 10*, 499–501.

SAWADA, M., KONDO, N., SUZUMURA, A. & MARUNOUCHI, T., 1989. Production of tumor necrosis factor-alpha by microglia and astrocytes in culture. *Brain Research, 491*, 394–397.

SCHIODT, A. V. & KRISTENSEN, O., 1978. Neurologic complication after irradiation of malignant tumors of the testis. *Acta Radiologica Oncology, 17,* 369–378.

Schultheiss, T. E., 1990. Radiation "tolerance" of the spinal cord: doctrine versus data. *International Journal of Radiation Oncology, Biology, Physics, 19,* 219–221.

Schultheiss, T. E., Higgins, E. H. & El-Mahdi, A. M., 1984. The latent period in radiation myelopathy. *International Journal of Radiation Oncology, Biology, Physics, 10,* 1109–1115.

Schultheiss, T. E., Orton, C. G. & Peck, R. A., 1983. Models in radiotherapy: volume effects. *Medical Physics, 10,* 410–415.

Schultheiss, T. E., Price, R. E., Stephens, L. C., Ang, K. K. & Peters, L. J., 1991. Dependence of spinal cord response on irradiated length and level. In *Radiation Research: A Twentieth-Century Perspective,* ed. by J. D. Chapman, W. C. Dewey and G. F. Whitmore (Academic Press, New York), p. 184.

Schultheiss, T. E., Stephens, L. C., Ang, K. K., Jardine, J. H. & Peters, L. J., 1992. Neutron RBE for primate spinal cord treated with clinical regimens. *Radiation Research, 129,* 212–217.

Schultheiss, T. E., Stephens, L. C., Jiang, G. L., Ang, K. K. & Peters, L. J., 1990. Radiation myelopathy in primates treated with conventional fractionation. *International Journal of Radiation Oncology, Biology, Physics, 19,* 935–940.

Schultheiss, T. E., Stephens, L. C. & Maor, M. H., 1988. Analysis of the histopathology of radiation myelopathy. *International Journal of Radiation Oncology, Biology, Physics, 27,* 27–32.

Schultheiss, T. E., Stephens, L. C. & Peters, L. J., 1986. Survival in radiation myelopathy. *International Journal of Radiation Oncology, Biology, Physics, 12,* 1765–1769.

Selmaj, K. W. & Raine, C. S., 1988. Tumor necrosis factor mediates myelin and oligodendrocyte damage *in vitro. Annals of Neurology, 23,* 339–346.

Selmaj, K. W., Farooq, M., Norton, W. T., Raine, C. G. & Brosnan, C. F., 1990. Proliferation of astrocytes *in vitro* in response to cytokines. *Journal of Immunology, 144,* 129–135.

Silverman, P., Goldsmith, G. H., Spitzer, T. R., Rehmus, E. H. & Benger, N. A., 1990. Effect of tumor necrosis factor on the human fibrinolytic system. *Journal of Clinical Oncology, 8,* 468–475.

Snooks, S. J. & Swash, M., 1985. Motor conduction velocity in the human spinal cord: slowed conduction in multiple sclerosis and radiation myelopathy. *Journal of Neurology, Neurosurgery, and Psychiatry, 48,* 1135–1139.

Stephens, L. C., Hussey, D. H., Raulston, G. L., Jardine, J. H., Gray, K. N. & Almond, P. R., 1983. Late effects of 50 $\mathrm{MeV}_{d\rightarrow\mathrm{Be}}$ neutron and cobalt-60 irradiation of Rhesus monkey cervical spinal cord. *International Journal of Radiation Oncology, Biology, Physics, 9,* 859–864.

Stevenson, L. D. & Eckhardt, R. E., 1945. Myelomalacia of the cervical portion of the spinal cord, probably the result of roentgen therapy. *Archives of Pathology, 39,* 109–112.

Tan, B. C. & Khor, T. H., 1969. Radiation myelitis in carcinoma of the nasopharynx. *Clinical Radiology, 20,* 329–331.

Thames, H. D., 1989. Repair kinetics in tissues: alternative models. *Radiotherapy and Oncology, 14,* 321–327.

Thames, H. D., Ang, K. K., Stewart, F. A. & van der Schueren, E., 1988. Does incomplete repair explain the apparent failure of the basic LQ model to predict spinal cord and kidney responses to low doses per fraction? *International Journal of Radiation Biology, 55,* 27–43.

van den Bogaert, W., van der Schueren, E. & Horiot, J.-C., 1986. Early results of the EORTC randomized clinical trial of multiple fractions per day (MFD) and misonidazole in advanced head and neck cancer. *International Journal of Radiation Oncology, Biology, Physics, 12,* 587–591.

van den Brenk, H. A. S., Richter, W. & Hurley, R. H., 1968. Radiosensitivity of the human spinal cord based on analysis of 357 cases receiving 4 MeV X rays in hyperbaric oxygen. *British Journal of Radiology, 41,* 205–214.

van der Kogel, A. J., 1977a. Radiation tolerance of the spinal cord. Dependence on fractionation and extended overall times. In *Radiobiological Research and Radiotherapy: Proceedings of an International Symposium on the Radiobiological Research Needed for Improvement of Radiotherapy* (International Atomic Energy Agency, Vienna), pp. 85–90.

van der Kogel, A. J., 1977b. Radiation tolerance of the rat spinal cord. *Radiology, 122,* 505–509.

van der Kogel, A. J., 1980. Mechanisms of late radiation injury in the spinal cord. In *Radiation Biology in Cancer Research,* ed. by R. E. Meyn and H. R. Withers (Raven Press, New York), pp. 461–470.

van der Kogel, A. J., 1986. Radiation-induced damage in the central nervous system: an interpretation of target cell responses. *British Journal of Cancer, 53* (Suppl. VII), 207–217.

van der Kogel, A. J., 1991a. Central nervous system radiation injury in small animal models. In *Radiation Injury to the Nervous System,* ed. by P. H. Gutin, S. A. Leigel and G. E. Sheline (Raven Press, New York), pp. 91–111.

van der Kogel, A. J., 1991b. The nervous system: radiobiology and experimental pathology. In *Radiopathology of Organs and Tissues,* ed. by E. Scherer, C. Streffer and K.-R. Trott (Springer-Verlag, Berlin), pp. 191–212.

van der Kogel, A. J. & Sissingh, H. A., 1983. Effect of misonidazole on the tolerance of the rat spinal cord to daily and multiple daily fractions of X-rays. *British Journal of Radiology, 56,* 121–125.

van der Kogel, A. J. & Sissingh, H. A., 1985. Effects of intrathecal methotrexate and cytosine arabinoside on the radiation tolerance of the rat spinal cord. *Radiotherapy and Oncology, 4,* 239–251.

van der Kogel, A. J., Sissingh, H. A. & Zoetelief, J., 1982. Effect of X rays and neutrons on repair and regeneration in the rat spinal cord. *International Journal of Radiation Oncology, Biology, Physics, 8,* 2095–2097.

Verity, G. L., 1968. Tissue tolerance: central nervous system. *Radiology, 91,* 1221–1225.

Waage, A., Halstensen, A. & Espevik, T., 1987. Association between tumor necrosis factor in serum and fatal outcome in patients with meningococcal disease. *Lancet, i,* 355–357.

Walther, P. J., Rossitch, E. & Bullard, D. E., 1987. The development of L'hermitte's sign during cisplatin chemotherapy. *Cancer, 60,* 2170–2172.

Walton, J. N., Tomlinson, B. E. & Pearce, G. W., 1968. Subacute "poliomyelitis" and Hodgkin's disease. *Journal of Neurological Sciences, 6,* 435–445.

Wang, P.-Y., Shen, W.-C. & Jan, J.-S., 1992. Magnetic resonance imaging in radiation myelopathy. *American Journal of Neuroradiology, 13,* 1049–1055.

Wara, W. M., Phillips, T. L., Sheline, G. E. & Schwade, J. G., 1975. Radiation tolerance of the spinal cord. *Cancer, 35,* 1558–1652.

Weems, D. H., Mendenhall, W. M., Parsons, J. T., Cassisi, N. J. & Million, R. R., 1987. Squamous cell carcinoma of the supraglottic larynx treated with surgery and/or radiation therapy. *International Journal of Radiation Oncology, Biology, Physics, 13,* 1483–1487.

WHITE, A. & HORNSEY, S., 1978. Radiation damage to the rat spinal cord: the effect of single and fractionated doses of X rays. *British Journal of Radiology, 51*, 515–523.

WHITE, A. & HORNSEY, S., 1980. Time dependent repair of radiation damage in the rat spinal cord after X rays and neutrons. *European Journal of Cancer, 16*, 957.

WONG, C. S., VAN DYK, J. & SIMPSON, W. J., 1991. Myelopathy following hyperfractionated accelerated radiotherapy for anaplastic thyroid carcinoma. *Radiotherapy and Oncology, 20*, 3–9.

WONG, C. S., MINKIN, S. & HILL, R. P., 1992. Linear quadratic model underestimates sparing effect of small doses per fraction in rat spinal cord. *Radiotherapy and Oncology, 23*, 176–184.

WORTHINGTON, B. S., 1979. Diffuse cord enlargement in radiation myelopathy. *Clinical Radiology, 30*, 117–119.

ZEMAN, W. & SAMORAJSKI, T., 1971. Effects of irradiation in the nervous system. In *Pathology of Irradiation*, ed. by C. C. Berdjis (Williams & Wilkins, Baltimore), pp. 213–277.

ZUCKER-FRANKLIN, D., WARFEL, A., GRUSKY, G., FRANGIONE, B. & TEITET, D., 1987. Novel monocyte-like properties of microglia/astroglial cells. *Laboratory Inestigations, 57*, 176–185.

ZULCH, K. J. & OESER, H., 1974. Delayed spinal radionecrosis—a juridical error? *Neuroradiology, 8*, 173–176.

1992, *The British Journal of Radiology*, 65, 754–757

Primary choroid plexus papilloma of the cerebellopontine angle: magnetic resonance imaging, computed tomographic and angiographic appearances

By A. Jackson, PhD, MRCP, FRCR, *B. J. Panizza, MB, BS, MBA, D. Hughes, FRCR and †H. Reid, FRCPath

Departments of Neuroradiology, *Otolaryngology and †Neuropathology, Manchester Royal Infirmary, Oxford Road, Manchester M13 9WL, UK

(*Received 20 November 1991, accepted 6 May 1992*)

Keywords: CT, MRI, Cerebellopontine angle, Choroid plexus papilloma

Abstract. The computed tomographic, angiographic and magnetic resonance imaging (MRI) appearances of a benign primary choroid plexus papilloma of the cerebellopontine angle are reported. Although benign, this tumour showed local invasion of the petrous temporal bone and mastoid air cells. The differential diagnosis of cerebellopontine angle lesions is discussed. Papilloma is suggested by the presence of a vascular, calcified, enhancing extra-axial mass in or around the cerebellopontine angle. MRI may show evidence of high vascularity and internal haemorrhage. Differentiation from other cerebellopontine tumours, most particularly meningioma, may not be possible on radiological features.

Choroid plexus papillomas are benign neoplasms of the neuroectoderm, which are commonest in children where they account for 3% of intracranial tumours. In adults, papilloma accounts for only 0.5% of intracranial tumours and the great majority occur within the ventricular system, predominantly in the lateral and 4th ventricles (Rovit et al, 1970). Primary choroid plexus papilloma of the cerebellopontine angle has been described in only 20 previous cases and the magnetic resonance imaging (MRI) appearances in only one (Martin et al, 1990). The case presented here has a number of distinctive radiological features which are of interest in the differential diagnosis of tumours in the cerebellopontine region.

Case report

A 24-year-old woman presented with a 1-year history of deafness and tinnitus in the left ear. A few months prior to presentation she developed intermittent left-sided hemifacial spasm, which resolved spontaneously. Initial investigations demonstrated a conductive hearing loss but no focal neurological signs were elicited. A computed tomographic (CT) scan (Fig. 1) demonstrated an isodense enhancing mass in the cerebellopontine angle (CPA) with evidence of invasion along the posterior aspect of the petrous bone and into the medial aspect of the mastoid air cells. There was no evidence of tumoral calcification. The adjacent cerebellum showed minor shift but there was no evidence of oedema and no features of parenchymal invasion. An MRI scan performed on a 0.5 T scanner demonstrated a markedly heterogeneous tumour mass on T_1-weighted sequences (Fig. 2a) with areas of focal high intensity around the periphery of the tumour and a heterogeneous internal signal intensity with focal areas of both high and low signal. T_2-weighted sequences showed a high-signal-intensity lesion, again with areas of heterogeneous internal signal (Fig. 2b). Following intravenous gadolinium DTPA (Fig. 2c) the mass showed significant but incomplete enhancement affecting mainly the medial part of the tumour. There was no evidence on any sequence of cerebellar or brainstem invasion or oedema. Angiography (Fig. 3) showed a moderately vascular tumour fed entirely by branches of the external carotid artery arising principally from the occipital branch.

At surgery, the tumour was found to lie predominantly extradurally and to be invading the petrous bone. There was a small *en plaque* element involving the dura. The tumour was removed via a combined suboccipital and translabyrinthine approach. Histological examination demonstrated fronds of fibrovascular tissue covered by uniform cuboidal epithelial cells; immunoperoxidase stains were positive for epithelial membrane antigen S100 and some cells were positive for glial fibrillary acidic protein and carbonic anhydrase. The diagnosis of extradural benign choroid plexus papilloma was made.

Discussion

Choroid plexus papillomas within the CPA usually develop either as a direct extension of 4th ventricular tumours or due to seeding along cerebrospinal fluid (CSF) pathways from an intraventricular papilloma (Rovit et al, 1970; Russell & Rubenstein, 1971). Only 20 cases of primary extraventricular papillomas have previously been reported (Devadiga et al, 1969; Picard et al, 1979; Martin et al, 1990). In the majority of these cases the tumour was shown to originate from the small choroid tuft which normally protrudes from the foramen of Lushka; however, in several cases, including the one reported here, there has been no evidence of a tumour hilum and a primarily extrudural location has

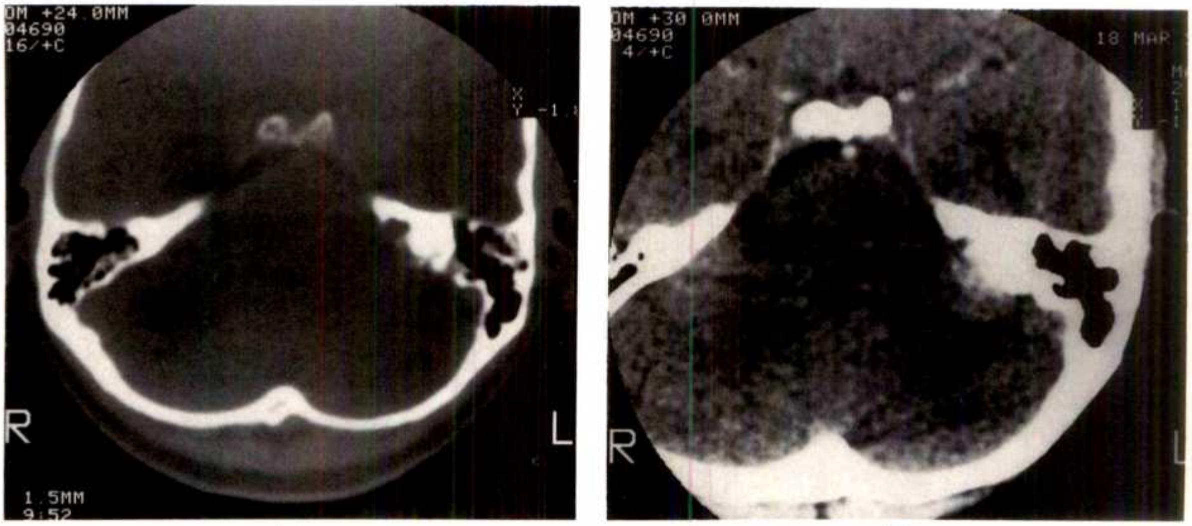

(a) (b)

Figure 1. (a) Pre-contrast scan demonstrates erosion of the left petrous temporal bone and tumour invasion into the mastoid air cells. (b) Post-contrast scan demonstrates a well-defined enhancing mass in the cerebellopontine angle.

been identified (Naguib et al, 1981). The angiographic demonstration of an external carotid supply to the tumour is also in contrast to choroid plexus papillomas of the ventricular system, including those which spread to the CPA, all of which have a predominantly internal carotid or vertebral artery supply (Rovit et al, 1970). These findings support the suggestion that CPA papillomas may develop from an extradural embryonic remnant of choroid tissue (Martin et al, 1990).

CPA papillomas are very slow growing and most commonly present between the 1st and 4th decades. Symptoms are usually slow in onset and include ataxia, V, VII and VIII nerve palsies and sometimes dysphagia. It is interesting to note that the development of hemifacial spasm as seen in the present case has been reported previously following development of a choroid plexus papilloma in the foramen magnum (Domingues et al, 1991). Clinical presentation may occasionally be acute with the development of secondary hydrocephalus due to brainstem compression or secondary extension into the 4th ventricle.

Previous reports have described a non-specific CT appearance of a well-delineated mass with marked enhancement after intravenous contrast medium. In contrast to the current case, intratumoral calcification has been described in the majority of previous reports (Picard et al, 1979; Naguib et al, 1981; Ford et al, 1988; Martin et al, 1990). The finding of tumoral invasion of the adjacent petrous bone is unusual and has been described in only two previous cases. Naguib et al (1981) described a primary papilloma of the CPA invading the petrous bone and mastoid air cells similar to this case. Martin et al (1990) described a similar tumour with invasion of the cavernous sinus. It is important to realize that this invasive tendency, commonly associated with choroid plexus carcinoma, is not necessarily an indicator of malignancy and could provide a useful diagnostic clue.

The MRI appearances of primary choroid plexus papilloma of the CPA have been described in only one previous case and were similar to those presented here (Martin et al, 1990). The presence of areas of signal void on T_1-weighted images seen in both cases presumably corresponds to the rich vascular supply and has been previously described in intraventricular choroid plexus papilloma. The areas of marked hyperintensity at the margin of the tumour on short-TR images were histologically demonstrated to correspond to foci of haemorrhagic necrosis. A single similar focus was seen in the case of Martin et al (1990). The post-gadolinium appearances of these tumours have not been previously described and the presence of marked enhancement is entirely in keeping with the vascular nature of the tumour. The heterogeneity of enhancement presumably reflects regional tumour necrosis.

The differential diagnosis of tumours within the CPA can be difficult when based entirely on radiological features. CPA tumours consist predominantly of acoustic neuromas (75–90% of CPA masses) and meningiomas (2–10%, Russell & Rubenstein, 1971). A large acoustic neuroma may show areas of calcification and significant heterogeneity on MR images; however, evidence of tumoral vascularity and the lack of involvement of the internal auditory meatus made this unlikely in the current case. Differentiation from meningioma on the other hand may be impossible and this was indeed the favoured radiological diagnosis in the present case (Zimmerman et al, 1985; Martin et al, 1990). Tumours metastatic to the CPA may have a similar appearance to that described here and have been mistaken previously

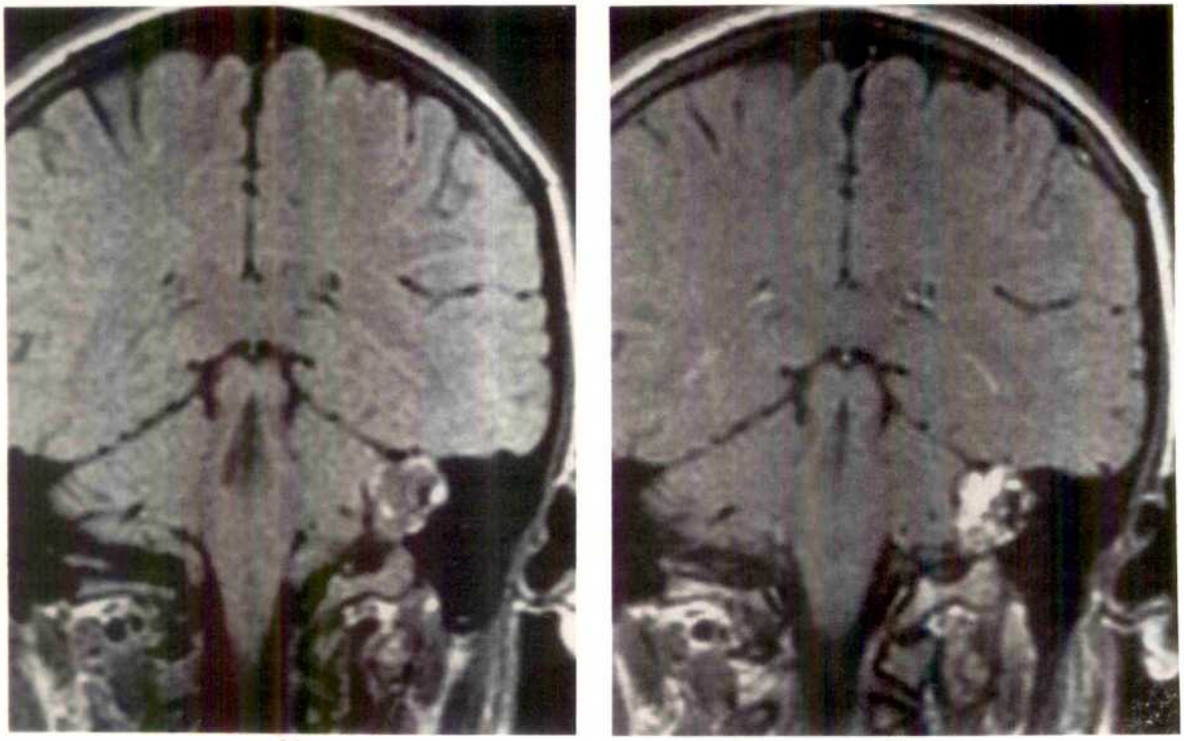

(a)

(c)

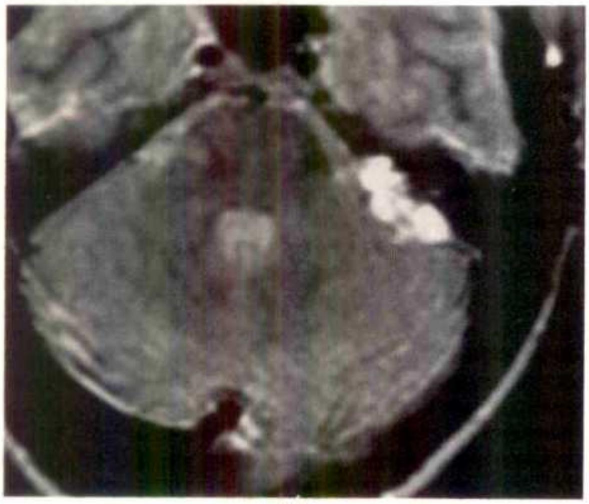

(b)

Figure 2. (a) Coronal T_1 spin-echo image demonstrates a mass in the left CPA with areas of internal signal void and peripheral areas of high signal. (b) Axial T_2 spin-echo image demonstrating heterogeneous high signal intensity. (c) Coronal T_1-weighted image following intravenous gadolinium demonstrates marked but heterogeneous contrast enhancement.

for acoustic neuroma and meningioma. Finally, radiological differentiation from other primary CPA masses such as arachnoid cysts, paragangliomas, epidermoid cysts and lipomas does not pose a problem since these have widely differing appearances on both CT and MRI.

In summary, primary benign choroid plexus papilloma of the CPA is an uncommon lesion which closely resembles meningioma. The presence of features

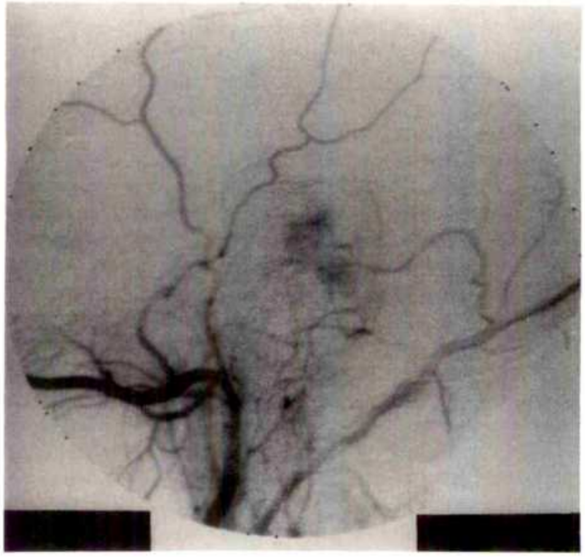

Figure 3. External carotid angiogram shows a vascular tumour fed principally by a branch of the occipital artery.

indicating local invasion, internal ischaemia or haemorrhagic necrosis may provide pre-operative diagnostic indicators.

References

Devadiga, K. V., Abraham, J. & Chandy, J., 1969. Primary choroid plexus papilloma of the cerebellopontine angle. Case report. *Journal of Neurosurgery*, *30*, 286–288.

Domingues, R. C., Taveras, J. M., Reimer, P. & Rosen, B. R., 1991. Foramen magnum choroid plexus papilloma with drop metastases to the lumbar spine. *American Journal of Neuroradiology*, *12*, 564–565.

Ford, W. J., Brooks, B. S., Gammal, T. & Massey, C. E., 1988. Adult cerebellopontine angle choroid plexus papilloma: MR evaluation. *American Journal of Neuroradiology*, *9*, 611.

Martin, N., Pierot, L., Sterkers, O., Mompoint, D. & Nahum, H., 1990. Primary choroid plexus papilloma of the cerebellopontine angle: MR imaging. *Neuroradiology*, *31*, 541–543.

Naguib, M. G., Chou, S. N. & Mastri, A., 1981. Radiation therapy of a choroid plexus papilloma of the cerebellopontine angle with bone involvement. *Journal of Neurosurgery*, *54*, 245–247.

Picard, C., Copty, M., Lavoie, G., Michaud, J. & Bouchard, R., 1979. A primary choroid plexus papilloma of the cerebellopontine angle. *Surgical Neurology*, *12*, 123–127.

Rovit, R. L., Schecter, M. M. & Chodroff, P., 1970. Choroid plexus papillomas: observations on radiographic diagnosis. *American Journal of Roentgenology*, *110*, 608–617.

Russell, D. S. & Rubenstein, L. J., 1971. *Pathology of Tumours of the Nervous System* (Edward Arnold, London), p. 163.

Zimmerman, R. D., Fleming, C. A., Saint Louis, L. A., Lee, B. C. P., Manning, J. J. & Deck, M. D. F., 1985. Magnetic resonance imaging of meningiomas. *American Journal of Neuroradiology*, *6*, 149–157.

1992, *The British Journal of Radiology*, *65*, 758–760

How frequent is chronic lumbar arachnoiditis following intrathecal Myodil?

By *D. G. Hughes, MRCP, FRCR and I. Isherwood, MD, FRCP, FRCR

Department of Neuroradiology, Manchester Royal Infirmary, Oxford Road, Manchester, UK

(*Received 10 January 1992, accepted 12 March 1992*)

Keywords: Myodil, Ventriculography, Lumbar, Arachnoiditis

Abstract. Chronic lumbar arachnoiditis has numerous causes, including the introduction of contrast media into the lumbar subarachnoid space. The oily contrast medium Myodil (iophendylate) is often cited but the true incidence of symptomatic lumbar arachnoiditis due solely to the presence of Myodil is unknown. A retrospective review of 98 patients in whom Myodil was introduced by ventriculography or cisternography, i.e. remote from the lumbar spine, revealed no cases of chronic lumbar arachnoiditis. All patients were monitored closely for periods ranging from 1 to 28 years. We conclude that, in these circumstances, it is rare for Myodil to produce symptomatic arachnoiditis.

Lumbosacral arachnoiditis is a well-defined entity with numerous aetiological factors (Jorgenson et al, 1975; Burton, 1978; Hansen et al, 1978; Quiler et al, 1978). It has characteristic radiological appearances (Irstrom et al, 1974; Jorgenson et al, 1975; Johnson and Burrows, 1978). There is, however, no clear consensus on the clinical features of arachnoiditis (Jorgenson et al, 1975; Quiler et al, 1978; Guyer et al, 1989). The condition is most commonly found in patients with a history of chronic unremitting back pain following surgery and/or after myelography for lumbar disease. Arachnoiditis has been demonstrated after myelography alone and recent interest has been directed towards the role of the oily contrast medium Myodil (iophendylate). How often a myelographic investigation is the cause of symptoms is unknown, as the clinical picture is frequently complicated by the back disease for which the myelogram and possibly subsequent treatment were undertaken.

To investigate the possible incidence of symptomatic Myodil-induced arachnoiditis, we have reviewed a group of patients in whom Myodil was introduced into the cerebrospinal fluid (CSF) pathways remote from the lumbar spine and for reasons other than low back pain.

Method

A retrospective review of clinical notes of patients who had undergone ventriculography, stereotactic thalamotomy or cisternal meatography using Myodil at Manchester Royal Infirmary between the years 1962 and 1977 was carried out. The review was restricted to patients whose notes were readily accessible and to those whose follow-up had been for a minimum of 1 year. All patients had been seen regularly in the neurosurgical outpatient clinic or neurosurgical ward with careful documentation of symptoms, signs and clinical progress.

The practice of Myodil ventriculography during the period considered consisted of the introduction of 1.5–3 ml into a lateral cerebral ventricle via a burr hole, followed by manipulation of the contrast medium into the third and fourth ventricles and thence into the spinal canal unless a total block to the ventricular system was present. The manoeuvre anticipated that the Myodil, being heavier than CSF, would descend to the lumbosacral thecal sac, the most dependent part of the spine. Contrast medium was not aspirated.

The following observations from the clinical notes were specifically recorded: diagnosis at Myodil ventriculography and surgery (if performed), details of Myodil flow in the ventricular system and, if a block was present, subsequent radiological evidence of residual Myodil in the spinal thecal sac. The signs and symptoms were recorded at all stages with specific reference to any patients who developed back pain, leg pain or other problems related to the lumbar region.

Results

The clinical notes of 203 patients were reviewed and 98 patients (47 male and 51 female) had been followed-up for 1 year or more. The mean length of follow-up in this subgroup was 10 years (range 1–28 years).

Seventy-three patients had had diagnostic Myodil ventriculography. In 20 patients, Myodil had been introduced into the ventricular system for stereotactic guidance of thalamotomy. Fifteen patients had had more than one procedure. Five patients had had Myodil meatography where the contrast medium was introduced by cisternal puncture.

Of the 73 patients who underwent diagnostic Myodil ventriculography, no block was present in 52. In six patients there was obstruction to flow of Myodil, but radiographs taken later for other reasons revealed the incidental presence of Myodil in the lumbar thecal sac. In the remaining 15 patients there was an obstruction to flow and no available evidence that Myodil had, subsequently entered the spinal thecal sac. Of the total of 98 patients reviewed, five had ventricular shunts inserted and 46 underwent more complex cranial surgery.

---

*Current address: Department of Radiology, Hope Hospital, Stott Lane, Salford M6 8HD, UK.

Two patients had back pain and leg pain predating the procedures, but no subsequent problems were recorded after 3 and 14 years of follow-up. Three patients were identified as having had symptoms that might have been related to the procedure, of whom details are given below.

Case 1

A 55-year-old man underwent thalamotomy for infantile dyskinesis. The next day he developed an aseptic meningitis with abnormal CSF (protein 1.33 g/l and an elevated white cell count). He made an uneventful recovery and the episode was diagnosed as an acute reaction to Myodil. He underwent a second thalamotomy, which was uneventful, 3 months later.

Case 2

A 30-year-old woman had a Myodil meatogram which demonstrated an acoustic neuroma. This was successfully resected. Two months later she developed backache and cramp in the left leg. Plain radiographs of the lumbar spine revealed residual Myodil. The symptoms were diagnosed clinically as "Myodil effect" as the clinical picture was "not typical of a disc". The condition resolved spontaneously and no further symptomatology was recorded in 7 years of follow-up.

Case 3

A 45-year-old man had a Myodil ventriculogram which demonstrated evidence of an acoustic neuroma, later confirmed at surgery. A year later he developed leg pain. Residual Myodil was observed on plain radiographs of the lumbar spine. A diagnosis of arachnoiditis was made but the pain settled and there was no record of leg or back symptoms in the subsequent 13 years of follow-up.

Discussion

Lumbosacral arachnoiditis is a defined entity, the end stage of which is adhesive arachnoiditis. Marked pial arachnoid proliferation with dense collagen deposition produces encapsulation of nerve roots, which become hyperaemic and undergo progressive atrophy. Numerous aetiological factors have been recorded (Quiler et al, 1978), including myelography, spinal surgery, trauma, spinal stenosis, disc herniation, neurofibroma, subarachnoid haemorrhage and an idiopathic group.

The effects on the arachnoid of contrast agents used in myelography have been well documented in animal studies when volumes of up to five times those used in humans have been employed (Howland & Curry, 1966; Bergerson et al, 1971). Further studies have suggested that blood and contrast medium may combine to produce a higher incidence of arachnoiditis as may myelography followed by laminectomy (Howland & Curry, 1966; Bergerson et al, 1971; Johansen et al, 1984)

Recent interest has focused on the extent to which Myodil used in lumbar myelography could be responsible for chronic arachnoiditis. The commonest clinical features of chronic arachnoiditis are persistent low back pain and radiating leg pain but there is no distinctive syndrome (Jorgenson et al, 1975; Burton, 1978; Quiler et al, 1978; Guyer et al, 1989). Symptoms following myelography may be similar to those for which the patient originally underwent myelography and for which surgery may have then been carried out. The true incidence of symptomatic arachnoiditis resulting from Myodil alone is not known.

To investigate intracranial pathology the group of patients we have reviewed had Myodil introduced by ventriculography or cisternography, remote from the lumbar spine. We have assumed that in patients without obstruction a significant amount of the 1.5–3 ml introduced into the ventricular system gravitated to the lumbar thecal sac. This was demonstrated radiographically in six of the patients who had an apparent block to the flow of Myodil during ventriculography. Only three of the 98 patients developed symptoms that could in any way be attributable to the presence of Myodil. One man had an acute meningeal reaction, which is rare but recognized as occurring in 0.05% of Myodil myelograms (Mayher et al, 1971). This patient did not develop symptoms of chronic arachnoiditis. It is not known whether an acute reaction can indeed lead to chronic arachnoiditis. The other two patients developed back pain and leg pain, which were attributed to Myodil. However, no confirmatory investigation was performed and no long-term symptomatology was recorded. In these circumstances chronic arachnoiditis seems unlikely,

We have not identified any definite case of chronic symptomatic lumbar arachnoiditis in 98 patients who had Myodil introduced remote from the lumbar spine. We conclude that in these circumstances it is rare for Myodil alone to produce symptomatic chronic arachnoiditis.

References

Bergerson, R. T., Rumbaugh, C. L., Fony, H. & Cravisti, H., 1971. Experimental pantopaque arachnoiditis in the monkey. *Radiology*, *99*, 95–101.

Burton, C. V., 1978. Lumbosacral arachnoiditis. *Spine*, *3*, 24–30.

Guyer, D. W., Wiltoe, L. L., Eskay, M. L. & Guyer, B. H., 1989. The long range prognosis of arachnoiditis. *Spine*, *12*, 1332–1341.

Hansen, E. B., Frankenkrug, A. & Praesthom J., 1978. Late meningeal effects of myelographic contrast media with special reference to metrizamide. *British Journal of Radiology*, *51*, 321–327.

Howland, W. L. & Curry, J. L., 1966. Pantopaque arachnoiditis. *Acta Radiologica*, *5*, 1932–1041.

Irstrom, L., Sundtrom, R. & Sigstedt, B., 1974. Lumbar myelography and adhesive arachnoiditis. *Acta Radiologica*, *15*, 356–368.

Johansen, J. E., Barthelemy, C. R., Haughton, V. M., Lipton, B. T. & Ho, K. C., 1984. Arachnoiditis from myelography and laminectomy in experimental animals. *American Journal of Neuroradiology*, *5*, 97–99.

Johnson, A. J. & Burrows, E. H., 1978. Thecal deformity after lumbar myelography with iophendylate (Myodil) and meglumine iothalamate (Conray 280). *British Journal of Radiology*, *51*, 196–202.

Jorgenson, J., Hanson, P. H., Steenskov, V. & Oveson, N., 1975. A clinical and radiological study of chronic lower spinal arachnoiditis. *Neuroradiology*, *9*, 139–144.

Mayher, W. E., Daniel, E. F. & Allen, M. B., 1971. Acute meningeal reaction following pantopaque myelography. *Journal of Neurosurgery*, *34*, 396–404.

Quiler, M., Machisello, P. J. & Tsairis, P., 1978. Lumbar adhesive arachnoiditis. Etiologic and pathologic aspects. *Spine*, *3*, 45–50.

1992, *The British Journal of Radiology*, 65, 761–765

The prognostic importance of CT features in primary intracranial lymphoma

By J. Namasivayam, MRCP, FRCR and *E. Teasdale, MRCP, FRCR

Department of Radiology, Royal Infirmary, Glasgow and *Department of Neuroradiology, Institute of Neurological Sciences, Southern General Hospital, Glasgow G51 4TF, UK

(*Received 3 October 1991 and in revised form 27 November 1991, accepted 6 March 1992*)

Keywords: Primary cerebral lymphoma, CT characteristics, Survival

Abstract. The correlation of computerized tomography (CT) features with survival of 28 patients with primary intracranial lymphoma was analysed retrospectively. Severe perifocal oedema, periventricular tumours and lesions which were non-homogenously enhancing or non-enhancing were found to be associated with a poor prognosis. The prognosis when multiple lesions were present was almost the same as that of a solitary lesion ($p = 0.95$). Ring enhancing lesions had considerably longer survival. Lesions in the frontal region and those close to the meninges, enhancing homogeneously, had a better prognosis.

Introduction

Primary cerebral lymphoma is a relatively rare tumour but occurs more frequently than lymphoma spreading intracranially from other sources (Lee et al, 1986). In the past, these tumours accounted for less than 1% of primary brain tumours but in the last 10 years primary cerebral lymphoma has tripled in frequency even in the non-immune suppressed population (Hochberg & Miller, 1988). Parenchymal intracranial lymphoma is almost exclusively of the non-Hodgkin type, B-cell tumours being more commonly encountered than the T-cell type (Bogdahn et al, 1986). Despite the sensitivity of these lesions to irradiation and chemotherapy (Jiddane et al, 1986) the prognosis remains poor; the average survival of untreated patients is around 6 weeks (Hochberg & Miller, 1988) but following treatment about 50–70% of patients survive for 1 year and between 16%–30% survive for 2 years (Sagerman et al, 1983; Helle et al, 1984).

The aim of our study was to assess the possibility that prognosis could be predicted from features shown by computerized tomography (CT).

Material and methods

We studied the clinical records and CT findings of 28 patients who were shown by histopathological examination to have a primary intracranial lymphoma. The study contained 17 men and 11 women, and covered the period from 1981 to 1990. The median age of the patients was 57 years (range 32–74 years). The common presenting symptoms were personality change, unsteadiness, confusion, weakness and epilepsy. No evidence of systemic lymphoma was identified either at presentation or subsequently. 26 patients had varying regimes of radiation therapy to the whole brain. 13 patients had received a single phase to the whole brain while the remainder had a second phase to the tumour-bearing area in addition. Doses for completed courses ranged from 27 Gy to 54 Gy. Six patients received less than 30 Gy and 14 patients received less than 40 Gy. 24 mg of dexamethasone per day were given in divided doses with radiotherapy in all except two patients, for a period of 8–10 days.

The CT scans were performed with a Philips Tomoscan 350 in 21 patients and an EMI 1010 in seven patients. We assessed the number of lesions, degree of oedema, location of the lesion and the pattern of enhancement. These findings were compared with the patients' known outcome (Table I). The histopathology of the tumour was characterized according to the Kiel classification. Nine were high-grade, large cell lymphomas, of unspecified group; 14 were intermediate/high-grade forms (centrocytic-centroblastic, centroblastic or immunoblastic); and five were low-grade types (lymphoplasmacytoid or centrocytic). All tumours were of B-cell origin.

Results

All 28 patients reviewed presented with a neurological complaint and had their brain tumour confirmed as a lymphoma, either by biopsy or autopsy. At the time of presentation there was no evidence of lymphoma except in the brain. The survival time was calculated from the first presentation up to death or present time. The mean and median survivals of the 28 patients were 48.6 weeks and 16 weeks, respectively. The histopathological features did not significantly influence the survival time in this series. Also there was no correlation between the CT pattern and the histological type.

On CT the majority of patients (78%) had lesions which were well defined, solid and showed homogeneous enhancement (Table I). This is the commonest CT pattern described in the literature (Jack et al, 1986).

Address correspondence to Dr J. Namasivayam, Department of Radiology, Royal Infirmary, Glasgow, G4 0SF.

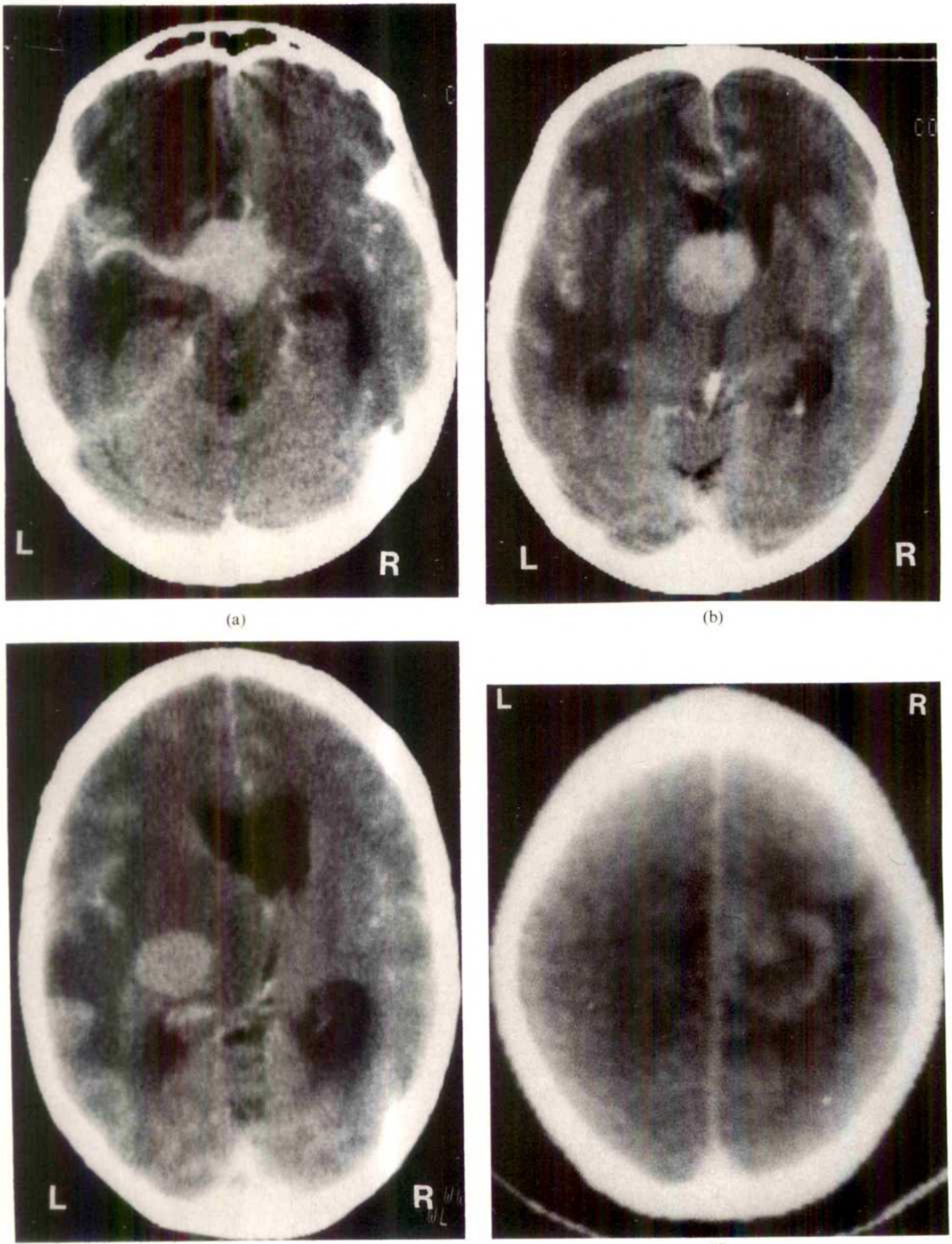

(a) (b)

(c) (d)

Figure 1 caption and parts (e) and (f) opposite.

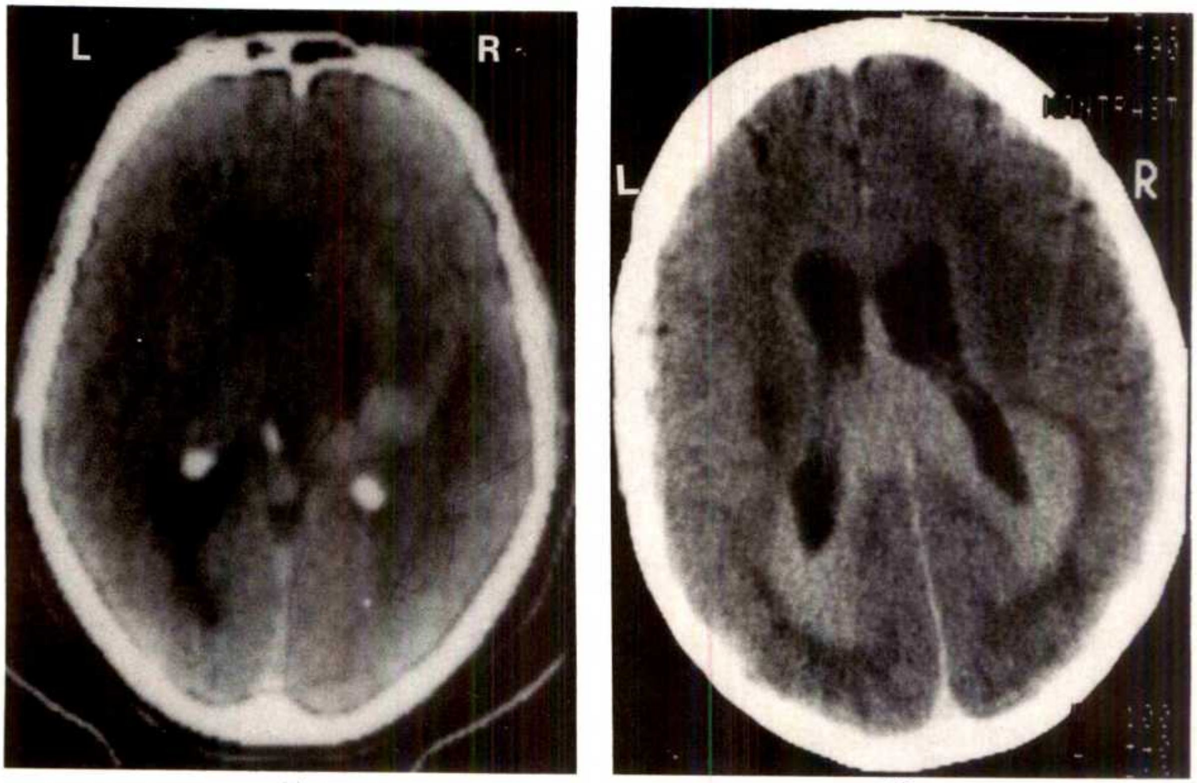

(e) (f)

Figure 1. (a) and (b) Severe oedema associated with a well defined suprasellar mass enhancing homogeneously. Lesion spreads via left Sylvian fissure to the surface of whole hemisphere. There is midline shift to the right. (c) Another patient with a well defined homogeneously enhancing lesion in the left basal ganglia and marked oedema. The following are CT variants of primary intracerebral lymphoma: (d) ring enhancement demonstrated in a solitary lesion lying close to the falx on the right side, (e) non-homogeneous enhancement—a lesion in the right basal ganglia region with ill defined margin and moderate oedema, and (f) periventricular lesion—a symmetrical enhancing lesion around the occipital horns and in the corpus callosum.

Patients with this type of lesion had a mean survival of 41 weeks and a median survival of 16 weeks. Following treatment with steroids and radiotherapy, 15 patients improved clinically and 11 patients remained stable. Recurrent tumour was in the same location in two patients and in a different place in the other patient. Examples of tumour types are given in Fig. 1.

There were eight patients with multifocal lesions. They had mean and median survival time very similar to those of patients with a solitary lesion (Fig. 2). Five patients had severe disproportionate oedema. This was defined as oedema extending over an area with a diameter more than twice that of the tumour (Fig. 1 a–c). These patients had mean and median survival times of 5.6 weeks and 2 weeks, respectively. Patients with periventricular lesions and lesions which either enhanced non-homogeneously or not at all had a mean and a median survival of less than 6 weeks. Each of three patients who had a solitary ring-enhancing lesion survived 3 years and all three had completed the two phases of radiotherapy. There were four patients who had a large, solitary, well-defined lesion based on the meninges. These were situated peripherally and enhanced homogeneously, and meningioma was the first suggested diagnosis. The patients with "meningioma" like lesions and those with frontal lobe lesions had a mean and median survival of about 24 weeks (Table I).

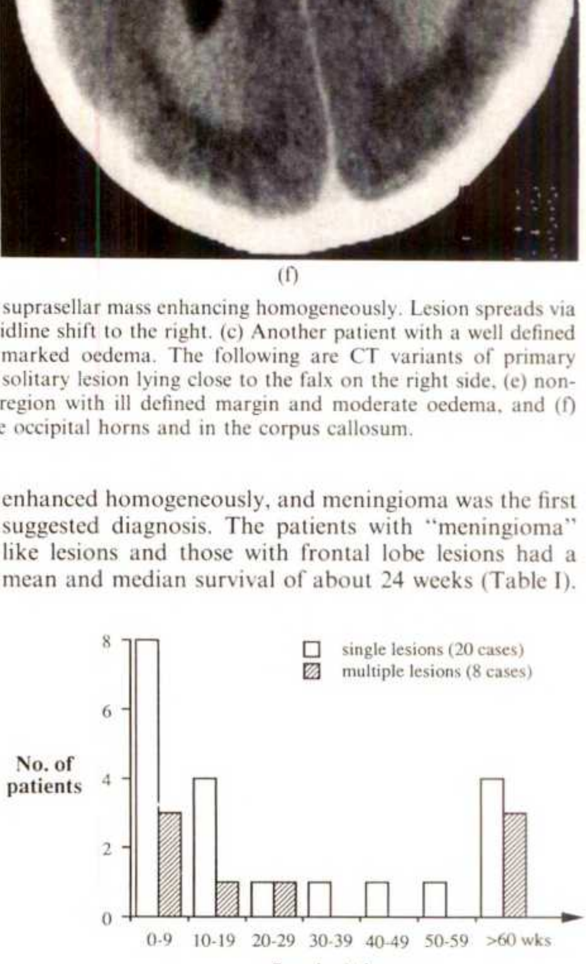

95% confident both groups are not different (student's t test)

Figure 2. Primary intracranial lymphoma:- multiplicity of lesions *vs.* survival time.

Table I. Determinants of survival time in primary intracerebral lymphoma

	Number of patients	Survival time (in weeks)	
		Mean	Median
Number of lesions			
Multiple	8 (30%)	51	17
Single	20 (70%)	49	16
Oedema			
Severe	5 (18%)	5.6	2.0
Mild to moderate	23 (82%)	59.0	21.0
Enhancement			
(a) Homogeneously enhancing, well-defined, solid lesions	22	41.0	16.0
(b) Ring type enhancement	3	156.0	156.0
(c) Non-homogeneous enhancement	2	6.0	6.0
(d) No enhancement	1	1.0	—
Site			
Frontal	9	70.0	24.5
Temporal	2	23.0	23.0
Parietal	4	48.6	4.0
Occipital	2	2.0	2.0
Cerebellum	4	36.6	7.0
Basal ganglia	2	41.3	15.5
Corpus callosum	2	22.0	20.0
Periventricular	3	1.6	2.0
'Meningioma'-like lesions	4	80.0	24.0
Frontal location	2		
Parietal location	2		
Treatment			
Radiotherapy (dose range—27–54 Gy) Steroids (24 mg dexamethasone/day, for 7–10 days)	26	55.6	21.0

There were 10 burrhole and three stereotactic biopsies. Craniotomy was performed in 13 patients; nine for partial resection and four for biopsy only. Of the two patients who died before diagnosis or treatment, one had periventricular haemorrhagic lesions and the other had a diffuse non-enhancing cerebellar lesion.

Discussion

The survival time of patients with primary cerebral lymphoma is better than when lymphomatous deposits occur secondary to systemic disease (Bogdahn et al, 1986). In the present report we studied a range of features that might relate to prognosis in primary lymphoma. The features were: age, histopathology, contrast medium enhancement, multiplicity, excess oedema, frontal location and treatment. Some of the findings both confirm and conflict with previous studies and there are new findings which bear a close relationship to outcome.

Contrary to a previous report (Hochberg & Miller, 1988) we have found that patients with multi-focal lesions have a statistically similar survival time to those with a solitary lesion (Fig. 2). This is an important observation and it emphasizes the fact that patients with multiple lesions may respond to treatment in the same manner as those with a solitary lesion, and multiplicity of tumour does not necessarily indicate a poorer prognosis. Indeed the number of lesions in any individual case may be underestimated by CT. When macroscopic pathological examination suggests a solitary tumour, histological examination will often show collections of tumour cells around vessels in the adjacent tissue and in other distant parts of the brain (Adams and Graham, 1988). The infiltrative nature of lymphoma often means that brain tissue is 'replaced' rather than displaced by an expanding tumour mass. Severe perifocal oedema seen in five of our patients was associated with a very short survival time and all these patients were in a poor physical state at the time of presentation. Although the degree of oedema was assessed beyond the enhancing edge of lesions, this does not necessarily indicate the tumour boundary. Indeed this is suggested by the pattern of tumour spread via the Sylvian fissure into the cerebral hemisphere (Fig. 1(a)).

According to Adams & Howatson (1990) our very high-grade cytological types appeared to show a more aggressive type of growth pattern whilst the low-grade tumours showed a more indolent style of growth. It is perhaps surprising therefore that we could detect no significant influence on survival from the histopathological subtypes. This is in contrast to the report of Hochberg & Miller (1988) in which a series of 66 patients with primary cerebral lymphoma showed a good correlation between histopathology and survival time. However, it is possible that the small number of cases in our study subjected to this subgroup analysis may prevent the identification of a true difference. A further immunoglobin-based pathological study carried out by Kawakami et al in 1985 showed no close relationship with survival time.

Although patients who are young and without prior immunosuppression would be expected to have a longer survival than older patients, in this study as in others (Bogdahn et al, 1986; Hochberg & Miller, 1988) survival time was unaffected by age. The three groups of patients which have been identified as being at risk of developing non-Hodgkin cerebral lymphoma are transplant recipients (Hoover & Fraumeni, 1973), patients with AIDS and other immunodeficiency syndromes (Levy et al, 1985). In our study only one patient who had had a renal transplant fell into a risk group.

30% of the lesions in this study were present in the frontal lobes. This is in agreement with Jiddane et al, (1986) and the percentage is not surprising, because the frontal lobe forms the most substantial single proportion of the brain. The majority of these patients were in good general health and performance status at the time of the diagnosis. Patients' performance status at the outset of treatment has been shown to have a significant influence on the survival time (Jayamohan & Rampling, 1991). There was a longer time interval from the first symptom in these patients to presentation, reflecting the occult nature of frontal masses.

Steroids and radiotherapy were the mainstays of treatment in our patients. Although it is not possible to be certain about the dose–response effect, it may be significant that all three patients with ring-enhancing lesion who received 54 Gy to the tumour had the longest survival. Previous studies have shown improved survival time following irradiation (Rampen et al, 1980) but the median survival time was only 21 weeks in our patients who received radiotherapy.

In summary, although there was no significant influence of histopathology on patients' outcome in our small series, we observed a wide variety of CT patterns few of which relate specifically to overall outcome. The lesions were shown to arise from any part of the brain. We have also observed that the prognosis of patients with multiple lesions was almost the same as for those with a solitary mass and further that lesions associated with severe perifocal oedema carried a grave prognosis. The overall outcome was favourable in patients with ring-enhancing lesions, who had received an optimum dose of radiotherapy.

Acknowledgments

We thank Miss L. Weir for typing the manuscript and Miss M. Mathieson for statistical advice.

References

Adams, J. H. & Graham, D. I., 1988. Primary malignant lymphoma. *An Introduction to Neuropathology* (Churchill Livingstone, Edinburgh), 253–254.

Adams, J. H. & Howatson, A. G., 1990. Cerebral lymphomas: A review of 70 cases. *Journal of Clinical Pathology, 43,* 544–547.

Bogdahn, U, Bogdahn S, Mertens, H. G., Dommasch, D., Wodarz, R, Wunsch, P. H., Kuhl, P. & Richter, E., 1986. Primary non-Hodgkin's lymphoma of the CNS. *Acta Neurologica Scandinavica, 73,* 602–614.

Helle, T. L., Britt, R. H. & Colby, T. V., 1984. Primary lymphoma of the central nervous system. Clinicopathological study of experience at stanford. *Journal of Neurosurgery, 60,* 94.

Hochberg, F. H. & Miller, D. C., 1988. Primary central nervous system lymphoma. Review article. *Journal of Neurosurgery, 68,* 835–853.

Hoover, R. & Fraumeni, J. F., 1973. Risk of cancer in renal transplant recipients. *Lancet, 2,* 55–57.

Jack, C. R., Reese, D. F. & Scheithauer, B. W., 1986. Radiographic findings in 32 cases of primary CNS lymphoma. *American Journal of Radiology, 146,* 271–276.

Jayamohan, J. & Rampling, R., 1991. Primary central nervous system lymphoma in the west of Scotland 1965–1989. Submitted for publication.

Jiddane, M., Nicoli, F., Diaz, P., Bergvall, U., Vincentelli, F., Hassoun, J., & Salamon, G., 1986. Intracranial malignant lymphoma. *Journal of Neurosurgery, 65,* 592–599.

Kawakami, Y., Tabuchi, K., Ohnishi, R., Asari, S. & Nishimoto, A., 1985. Primary central nervous system lymphoma. *Journal of Neurosurgery, 62,* 522–527.

Lee, Y. Y., Bruner, J. M., Tassel, P. V. & Libshitz, H. I., 1986. Primary central nervous system lymphoma: CT and pathologic correlation. *American Journal of Roentgenology, 147,* 747–752.

Levy, R. M., Bredesen, D. E. & Rosenblum, M. L., 1985. Neurological manifestations of the acquired immunodeficiency syndrome (AIDS): experience at UCSF and review of the literature. *Journal of Neurosurgery, 62,* 475–495.

Rampen, F. H. J., Van Andel, J. G., Sizoo, W. & van Unnik, J. A. M., 1980. Radiation therapy in primary non-Hodgkin's lymphomas of the CNS. *European Journal of Cancer, 16,* 177–184.

Sagerman, R. H., Collier, C. H. & King, G. A., 1983. Radiation therapy of microgliomas. *Radiology, 149,* 567–570.

1992, *The British Journal of Radiology*, 65, 766–768

Transverse geniculate ligament of the knee: appearance and frequency on plain radiographs

By Serge A. Sintzoff Jr, MD, Bernard Stallenberg, MD, Isabelle Gillard, MD,
Pierre A. Gevenois, MD, Celso Matos, MD and Julien Struyven, MD

Department of Radiology, Cliniques Universitaires de Bruxelles, Hôpital Erasme, 808 Route de Lennik,
1070 Brussels, Belgium

(Received 2 October 1991 and in revised form 9 March 1992, accepted 2 April 1992)

Keywords: Knee, Anatomy, Normal variant, MR studies

Abstract. The aims of the study were to determine the frequency of visualization of the normal transverse geniculate ligament (TGL) of the knee on lateral plain radiographs with magnetic resonance imaging (MRI) as a reference, and to determine features that make this ligament apparent on plain radiographs. 50 consecutive lateral plain radiographs and sagittal T_1-weighted images of corresponding knees were evaluated prospectively. A TGL was considered visualized on plain radiographs when an opacity of soft-tissue density was apparent in the posterior part of the Hoffa's fat pad. The TGL was identified in 29 of the 50 (58%) sagittal MR images; a TGL was observed on the lateral plain radiographs of six patients (12%). Correlation with the MR images showed that, when visualized on plain radiographs, the ligament is at least 3 mm thick and completely surrounded by fat. Our study shows that the TGL is a normal variant that can be recognized frequently on lateral plain radiographs of the knee.

The transverse geniculate ligament (TGL) of the knee is a normal anatomical variant that has been recently described on lateral plain radiographs of the knee (Sintzoff et al, 1991). It has been described previously on magnetic resonance images as a source of error in interpretation of tears of the menisci of the knee (Herman & Beltran, 1988; Mink, 1987; Watanabe et al, 1989a, b). The TGL runs in the coronal plane anterior to the knee joint capsule, in the posterior part of the Hoffa's fat pad. It connects the anterior horn of the medial meniscus to the anterior margin of the anterior horn of the lateral meniscus. In cadaver studies, this ligament is of variable thickness and may be absent (Williams, 1989). The aims of this prospective study were (a) to evaluate the frequency of the TGL on plain radiographs and on magnetic resonance imaging (MRI), and (b) to determine features that make this ligament apparent on plain radiographs.

Materials and methods

The plain radiographs and MR images of 50 consecutive patients were evaluated prospectively. The MR examinations were performed for suspicion of internal derangements of the knee. The mean age of the patients was 35 years with a range from 12 to 78 years. There were 30 men and 20 women.

The analysis of plain radiographs and MR images was undertaken separately on the basis of consensus by two observers. The lateral plain radiographs were first evaluated without the MR images for the presence of the TGL, which is a rounded opacity of water density surrounded by fat density situated anterior to the knee joint (Sintzoff et al, 1991). The TGL was measured when present. The MR images were T_1-weighted, 4 mm thick and obtained either on a 0.5 or a 1.5 T system (Gyroscan T5, Gyroscan S15, Philips Medical Systems, The Netherlands). On MRI, the TGL is a low-signal-intensity oval or round structure in the posterior part of Hoffa's fat pad (Herman & Beltran, 1988; Mink, 1987; Watanabe et al, 1989a, b). Its presence, shape and thickness (corrected to the nearest whole number) were correlated with the plain radiographic appearance. The fat around the ligament was also evaluated.

Results

A TGL was identified on plain radiographs in six patients (12%). Its mean size was 3.5 mm, ranging from 3 to 5 mm. It was bilobulated in one patient (Fig. 1a), oval in two (Fig. 2a) and rounded in three (Fig. 3a). On MR images the size and shape were comparable and the ligament was completely surrounded by fat in all cases (Figs 1b, 2b, 3b). In the remaining 44 patients, with negative plain radiographs, the ligament was identified on MRI in 23 cases. The ligament was incompletely surrounded by fat in 13 patients. The average size of the ligament was 1.5 mm with a range from 1 to 3 mm. The two ligaments that were 3 mm thick were not completely surrounded by fat. The overall frequency of visualization of the ligament on MRI was 58% (29 of 50 patients).

Discussion

The TGL of the knee lies in the frontal plane anterior to the knee joint capsule, in the posterior part of the Hoffa's fat pad. It connects the anterior horn of the medial meniscus to the anterior horn of the lateral meniscus (Williams, 1989). As the region of confluence of the ligament with the anterior horn of the lateral meniscus and its central tendinous attachments sometimes has the appearance of a high-signal cleft within

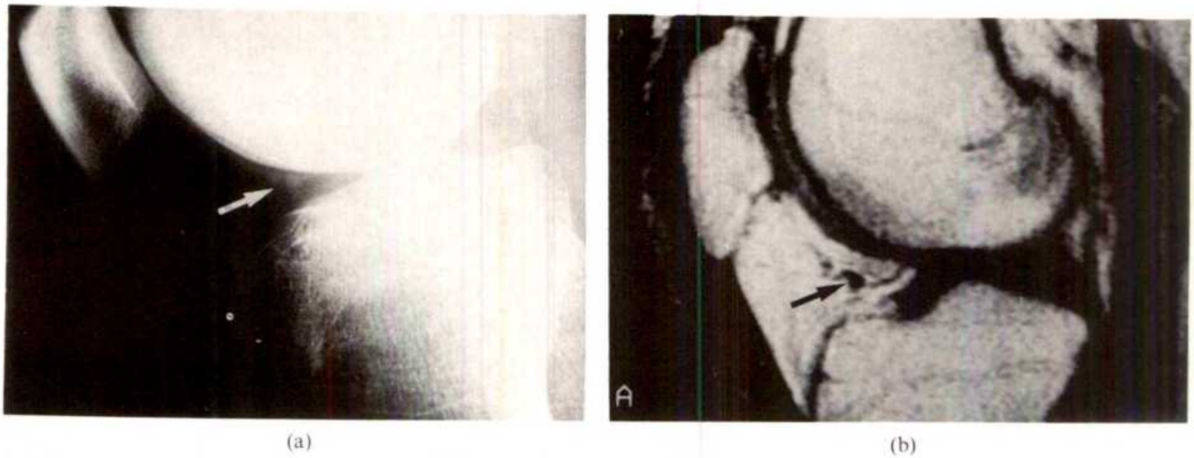

(a) (b)

Figure 1. (a) Lateral plain radiograph of the knee shows a bilobulated opacity (white arrow) anterior to the knee joint, corresponding to the TGL. (b) Corresponding sagittal MRI image (spin-echo TR 440, TE 20) demonstrates a thick TGL of the same shape (black arrow) surrounded by fatty tissue anterior to the knee joint capsule.

the meniscus on sagittal images, it is a source of misinterpretation of oblique tears of the anterior horn of this meniscus (Herman & Beltran, 1988; Mink, 1987; Watanabe et al, 1989a, b). We have observed an opacity on lateral plain radiographs of the knee thought to be this ligament (Sintzoff et al, 1991). The purpose of this study was to determine its frequency and the features that make it apparent on plain radiographs.

The patients were selected on the basis of availability of plain radiographs and MRI. This selection bias should not have influenced the true frequency of visualization of the ligament as it is a normal variant. This could be proved by evaluation of the frequency of the TGL on routine plain knee radiographs but was not carried out in this study.

The TGL was observed in 58% of the T_1-weighted, 4 mm thick, MR images. This frequency may be underestimated as a partial volume effect as the fatty tissue may have hidden very thin ligaments. This frequency could be more accurately determined by the study of thinner slices.

The fact that the opacity apparent on plain radiographs is the TGL is strongly supported by it having the same shape and size on plain radiographs and on MRI (Figs 1–3). When visualized on plain radiographs, the thickness of the ligament, measured on MR images, was in all cases 3 mm or more. It was in all cases completely surrounded by fatty tissue. This feature makes the ligament evident on lateral plain radiographs if the X-ray beam strikes the ligament *en face* and so is tangential to its borders. All ligaments that were not visualized on plain radiographs were 3 mm thick or less. The lack of

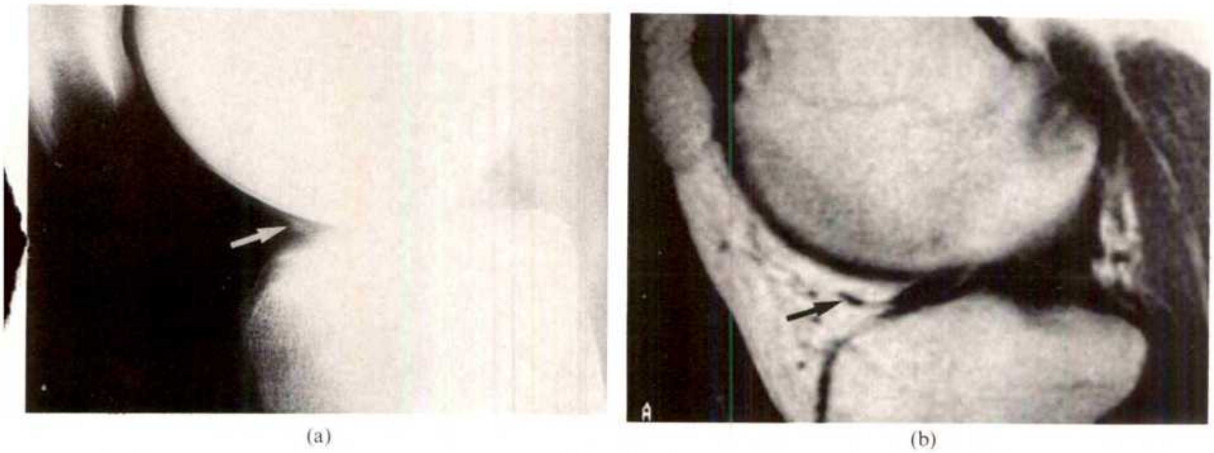

(a) (b)

Figure 2. (a) Lateral plain radiograph of the knee shows an ovoid opacity (white arrow) anterior to the knee joint, corresponding to the TGL. (b) Corresponding sagittal MRI image (spin-echo TR 440, TE 20) demonstrates a thick TGL of the same shape (black arrow), surrounded by fatty tissue anterior to the knee joint capsule.

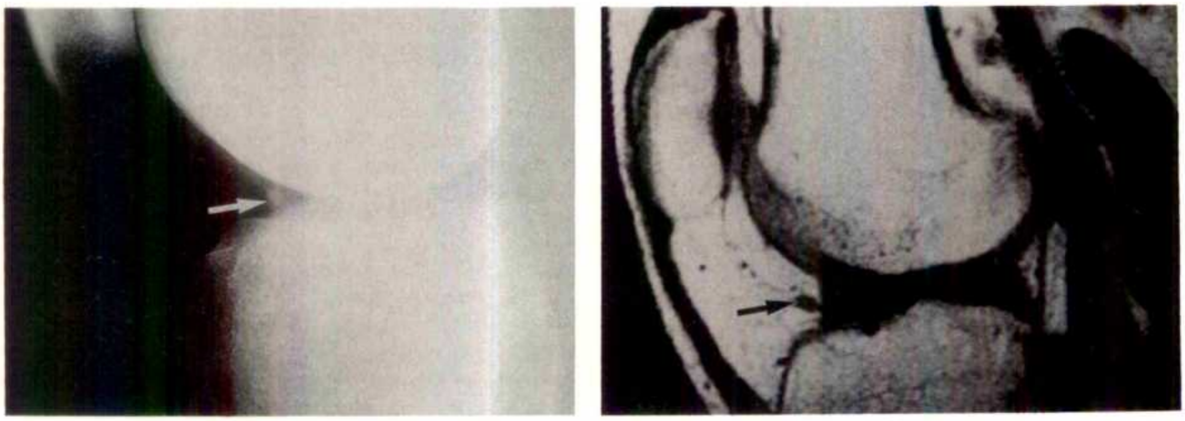

(a) (b)

Figure 3. (a) Lateral plain radiograph of the knee shows a rounded opacity (white arrow) anterior to the knee joint, corresponding to the TGL. (b) Corresponding sagittal MRI image (spin-echo TR 440, TE 20) demonstrates a thick TGL of the same shape (black arrow), surrounded by fatty tissue anterior to the knee joint capsule.

visualization of the TGL on plain radiographs may occur for three different reasons: if the diameter of the TGL is too small, if the X-ray beam is not tangential to the TGL, and or/if the TGL is incompletely surrounded by fat. The last hypothesis is supported by the fact that ligaments 3 mm thick and not visualized were incompletely surrounded by fat.

In conclusion, the TGL of the knee can be recognized on lateral plain radiographs of the knee. Correlation with MRI shows that the TGL is visualized when it is at least 3 mm thick and completely surrounded by fat.

References

HERMAN, L. J. & BELTRAN, J., 1988. Pitfalls in MR imaging of the knee. *Radiology, 167*, 775–781.

MINK, J. H., 1987. Pitfalls in interpretation. In *Magnetic Resonance Imaging of the Knee*, ed. by J. H. Mink, M. A. Reicher and J. V. Crues (Raven Press, New York), pp. 141–155.

SINTZOFF, S. A. JR, GEVENOIS, P. A., ANDRIANNE, Y. & STRUYVEN, J., 1991. Transverse geniculate ligament of the knee: appearance at plain radiographs. *Radiology, 180*, 259.

WATANABE, A. T., CARTER, B. C., TEITELBAUM, G. P., SEEGER, L. L. & BRADLEY, W. G., 1989a. Normal variation in MR imaging of the knee: appearance and frequency. *American Journal of Roentgenology, 153*, 341–344.

WATANABE, A. T., CARTER, B. C., TEITELBAUM, G. P. & BRADLEY, W. G., 1989b. Common pitfalls in magnetic resonance imaging of the knee. *Journal of Bone and Joint Surgery, 71A*, 857–862.

WILLIAMS, P. L., 1989. The genual (knee) joint. In *Gray's Anatomy*, 7th edn, ed. by P. L. Williams (Churchill-Livingstone, London), pp. 528–530.

1992, *The British Journal of Radiology*, 65, 769–773

Macrodystrophia lipomatosa: radiographic observations

By S. K. Gupta, MD, FAMS, FRCR, O. P. Sharma, MD, MNAMS, *S. V. Sharma, MS, MNAMS, B. Sood, MB, BS and †Sanjay Gupta, MD, DNBE

Departments of Diagnostic Radiology and *Orthopedics, Institute of Medical Sciences, Banaras Hindu University, Varanasi-221 005, and †Department of Diagnostic Radiology, Sanjay Gandhi Post-Graduate Institute of Medical Sciences, Lucknow, India

(Received 2 December 1991 and in revised form 10 February 1992, accepted 6 March 1992)

Keywords: Macrodystrophia lipomatosa, Hypertrophy, Gigantism, Fibro-fatty tissues

Abstract. 23 cases of macrodystrophia lipomatosa (MDL) are reported showing a wide spectrum of radiographic findings. Typical findings were hypertrophy of all the mesodermal tissues of the affected digits with dramatic overgrowth of fat. Phalanges were enlarged both in length and transverse diameter, but the trabecular pattern was maintained. In one patient, the phalanges and metatarsals were elongated but thinned. In another case, all the phalanges and metatarsals of the great toe were small. The little toe was also involved in two cases. Articular surfaces were slanting. There was a high incidence of palmar and plantar involvement. In a few cases the forearm and leg were also involved. Other uncommon features observed were early maturation of epiphyseal centres of ossification of phalanges and metatarsals, syndactyly, polydactyly, brachydactyly and symphalangism. Angiography was uncharacteristic.

Macrodystrophia lipomatosa (MDL) is a rare form of localized gigantism of one or more fingers or toes. The overgrowth affects all the mesenchymal elements with a disproportionate increase in the fibro-fatty tissues (Baruchin et al, 1988). It is recognized at birth or in the neonatal period. As the patient grows, the deformity begins to interfere with joint function, vascular supply or innervation. Feriz (1923) coined the term macrodystrophia lipomatosa for localized gigantism of the lower extremity. However, Golding (1960) and later Mikhail (1964) accepted the term as applicable to the hand as well. This congenital anomaly is also called macrodactyly, megalodactyly, congenital localized gigantism, dactylomegaly, gigantomegaly or partial acromegaly. The literature pertaining to MDL is sparse. Barsky (1967) reviewed 64 cases including eight of his own. Other reports in the literature (Minkowitz & Minkowitz, 1965; Ben-Bassat et al, 1966; Rechnagel, 1967; Tsuge, 1967; Thorne et al, 1968; Godman & Kaye, 1977); include two from India by Tuli et al (1969) and Khanna et al (1975).

Our material consists of 23 cases of MDL, the largest series, and describes the radiographic features in detail and emphasizes less reported associated findings such as polydactyly, brachydactyly, early maturation of epiphyseal centres of ossification, thinning of metacarpals or metatarsals, and symphalangism.

Clinical and radiographic observations

Our 23 cases consisted of 16 males and seven females with ages ranging from 2 to 24 years. 20 patients had single limb involvement while in three there was bilateral involvement (Fig. 1a). In five patients, there was upper limb involvement while in the remaining 18 patients there was lower limb involvement. Hypertrophy also affected the forearm and leg in a few cases (Figs 2, 3).

One digit only was involved in two cases, two digits in 10 cases, three digits in five cases, four digits in five cases and five digits in two cases. In 14 cases, the palm of the hand and the sole of the foot were also affected with or without involvement of metacarpals and metatarsals (Figs 4–6, Table I).

Almost any combination of digit involvement was seen, but the commonest involves the second and third digits (seven cases). In bilateral cases, there was no evidence of symmetrical involvement (Figs 1, 6). Affected bones showed an increase in length as well as width. Terminal phalanges often showed a mushroom-like appearance (Fig. 5). The distal phalanx in some

Table I. Macrodystrophia lipomatosa: digital combination

	No. of cases
One digit only	2
1st and 2nd digit	3
2nd and 3rd digit	7
2nd, 3rd and 4th digit	2
3rd and 4th digit	2
3rd, 4th and 5th digit	1
1st, 2nd and 3rd digit	1
2nd, 3rd, 4th and 5th digit	3
1st, 2nd, 3rd and 4th digit	1
1st, 2nd, 3rd, 4th and 5th digit	1

The little toe was also involved in two cases

Address correspondence to Dr S. K. Gupta, 2, G.F. Medical Enclave, Banaras Hindu University, Varanasi-221 005, India.

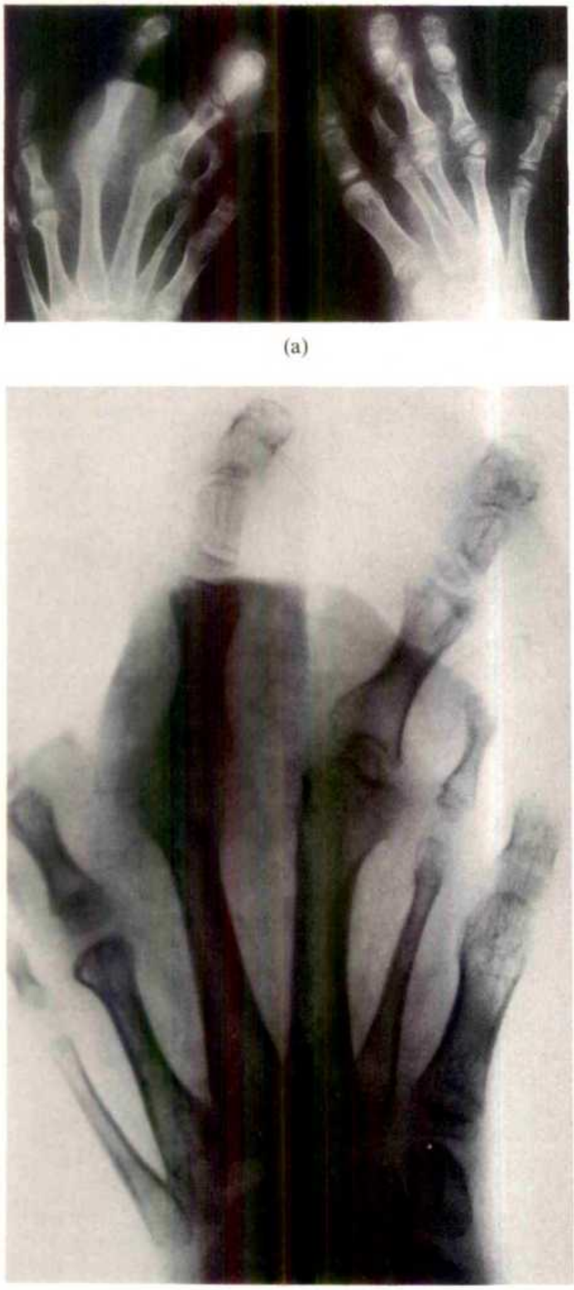

(a)

(b)

Figure 1. (a) Radiographs of both feet showing bilateral involvement and left polydactyly. The first metatarsal and phalanges of the first toe of the left foot are short. The second digit shows soft-tissue hypertrophy but there is thinning of the phalanges and the metatarsal. In the right foot the third, fourth and fifth digits show hypertrophy. There are slanting articular surfaces and dome-shaped terminal phalanges. (b) Contact print of left foot radiograph showing lucent zones of fatty tissue between the third and fourth digit.

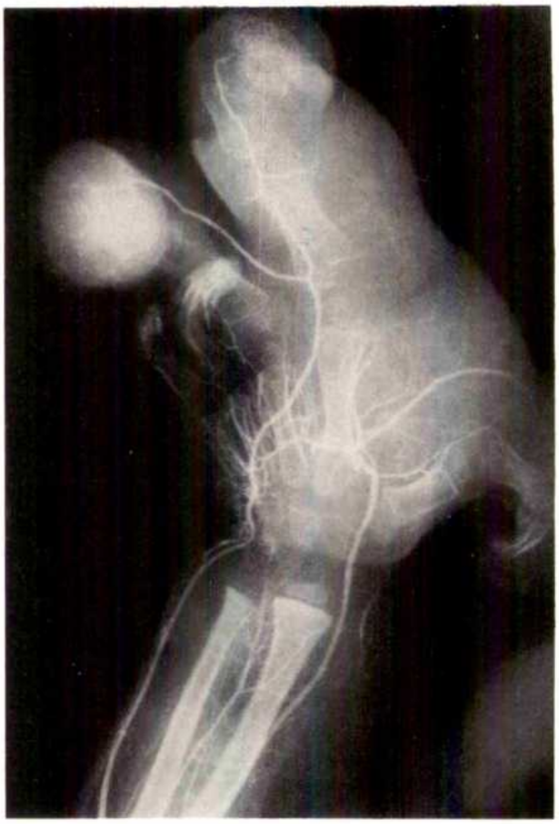

Figure 2. Brachial angiogram showing hypertrophy of the digital vessels of the affected first, second and third hypertrophied digits. There is also involvement of the palm and forearm in this case.

cases was surrounded by a ring of fatty tissue (Fig. 4). Lucent zones of fatty tissue were also discernible in some good radiographs (Fig. 1b). In two patients, the phalanges of the great toe and first metatarsal were smaller than expected. Early bone maturation indicated by the larger size of epiphyseal centres of ossification of phalanges and metatarsals was also present in a few cases (Fig. 5). The articular surfaces of the phalanges were often slanting.

Other uncommon features noted were polydactyly (two cases), syndactyly (three cases), brachydactyly (two cases) and symphalangism (Figs 7, 8). In one case there was metatarsal thinning (Fig. 1a).

On angiography, the digital vessels were proportionately enlarged. There was no indication of arteriovenous fistulae or increased vascularity (Fig. 2). Histological examination of soft tissues in a few cases following operation revealed marked proliferation of fibro-fatty tissue. The nerves were thickened with perineural and endoneural fibrosis. There was proliferation of fibro-fatty tissue between the cortex and periosteum. There was no evidence of cutaneous pigmentation or subcutaneous neurofibromas to suggest a diagnosis of neuro-fibromatosis in any of our cases.

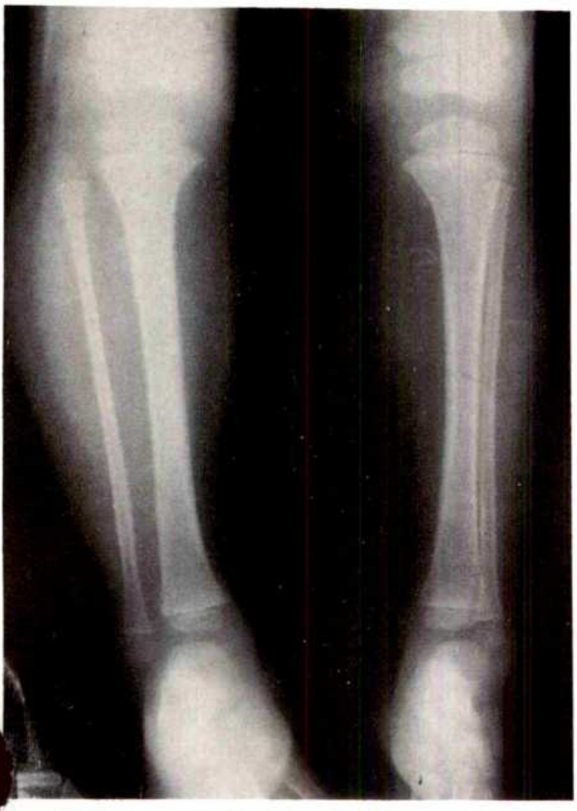

Figure 3. AP radiograph of both legs showing soft-tissue hypertrophy of the right leg. The hypertrophy also affected the sole of the foot in this case.

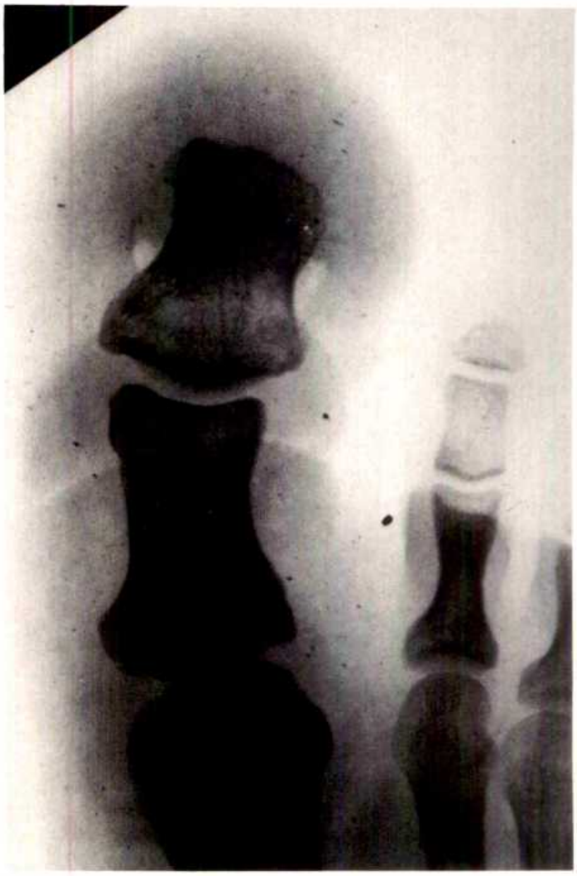

Figure 4. Marked enlargement of phalanges of the great toe. There are areas of fat radiolucency surrounding the terminal phalanx.

Discussion

Typical radiographic findings of MDL are overgrowth of all the tissues of the digits. Broad rings of fatty tissue surrounding the phalanx and lucent zones of fatty tissue in the enlarged digit reflect the dramatic overgrowth of fat characteristic of this anomaly (Godman & Kaye, 1977). The phalanges are also elongated and enlarged in the transverse diameter. The articular surfaces may slant. Although distal phalanges are broadened or expanded with a dome-shaped appearance, the trabecular architecture, however, remains normal. Advanced epiphyseal centres of ossification of phalanges and metacarpals/metatarsals, as reported by Ben-Bassat et al (1966) and Godman and Kaye (1977), were seen in four cases in our series.

Overgrowth of tissues may extend to the sole of the foot or palm of the hand leading to widened intermetacarpal or intermetatarsal spaces. In most of these cases there is enlargement of metacarpals and metatarsals similar to the phalanges. Though the reported incidence of involvement of the palm and soles is low (Dennyson et al, 1977), we had 16 such cases in our series. Involvement of the forearm and leg by soft-tissue hypertrophy in MDL is also low (Tsuge, 1967). Four cases in our series had hypertrophy of the forearm (one case) and leg (three cases). According to most workers (Rechnagel, 1967; Thorne et al, 1968; Kapoor et al, 1988), MDL is almost always unilateral. Barsky (1967), Killinger (1925) and Annandale (1956) have, however, described one case each of bilateral involvement. None of the three cases in our series with bilateral involvement were symmetrical. Symphalangism noted in one case appears to be an unrecorded observation and presumably results from an error of segmentation (Littler et al, 1974). Syndactyly (three cases) and polydactyly (two cases) are rare associations of MDL (Kapoor et al, 1988). Interestingly, in an anomaly where hypertrophy of all the mesodermal components of the digits is the main finding, there was evidence of underdevelopment, in the form of brachydactyly affecting some metatarsals and shortening of phalanges and metatarsals of the great toe. These unreported observations in MDL may be a "vascular steal phenomenon" related to the increased blood supply to the overgrown digits.

In most cases more than one digit is involved and digits affected are always adjacent (Barsky, 1967). Though the commonest digits involved are the second

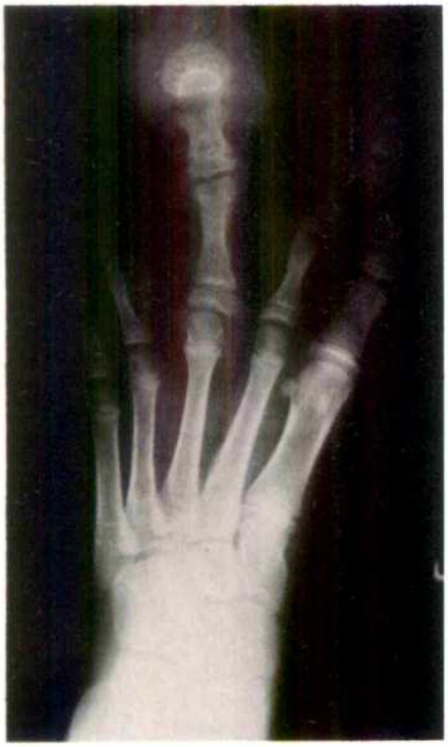

Figure 5. The third digit shows marked enlargement, with a dome-shaped terminal phalanx. The second digit is also enlarged. The epiphyseal centres of ossification of affected phalanges and metatarsals are enlarged; the fourth metatarsal is small.

and third, any combination may be seen in a large series (Table I). Little toe involvement, not previously reported, was found in two of our cases.

On angiography, the digital vessel in each digit is proportionately enlarged in size but there is no indication of arteriovenous fistula or increased vascularity (Ben-Bassat et al, 1966; Khanna et al, 1975).

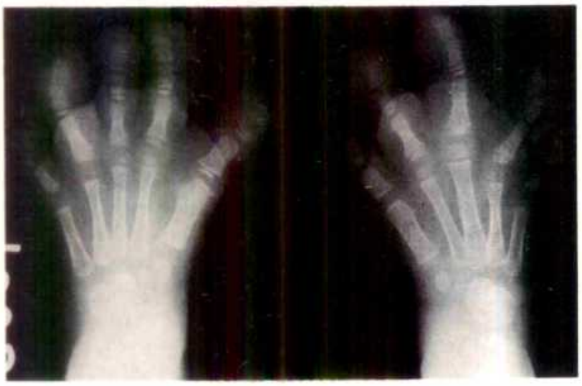

Figure 6. Radiograph showing bilateral involvement. In the left foot all the digits show evidence of soft-tissue hypertrophy. The right foot shows hypertrophy affecting the second, third and fourth digits. The fifth digit is small.

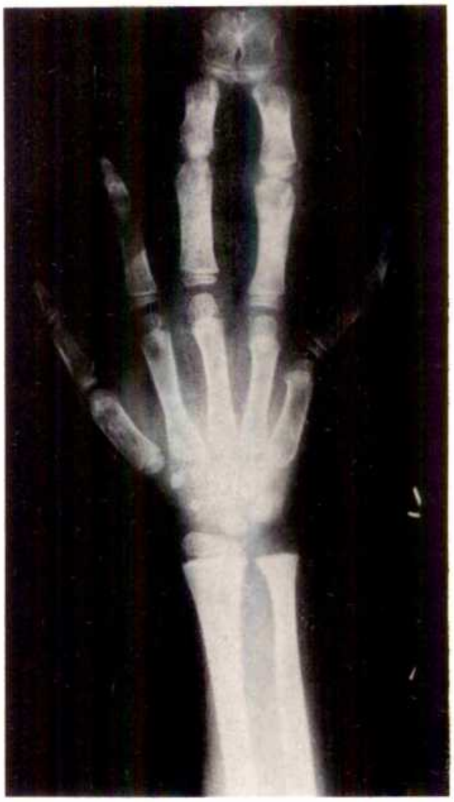

Figure 7. There is (osseous) syndactyly between the third a. fourth fingers.

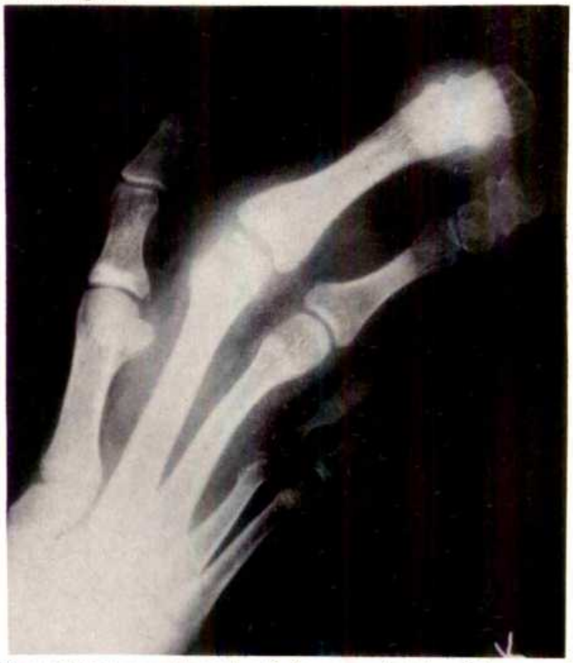

Figure 8. Overgrowth with soft-tissue syndactyly of the second and third digits and involvement of the phalanges and metatarsals. The fourth metatarsal is small. There is symphalangism of the second toe.

The most striking finding on histological examination is an increase in adipose tissue interspersed in a fine mesh of fibrous tissue, involving the bone marrow, periosteum, muscles, nerve sheaths and subcutaneous tissues. The increase in the size of the nerves is due to infiltration of the sheath by fibro-fatty tissue and not by an increase in axons (Ben-Bassat et at, 1966; Tsuge, 1967).

Although overgrowth of all the mesodermal tissues of the digit is a dominant finding in MDL, associated findings of syndactyly, polydactyly, brachydactyly and even underdevelopment in a significant number of cases indicate there is subtle interaction of many factors, some genetic, leading to the wide spectrum of abnormalities in this disorder.

References

ANNANDALE, T., 1956. *The Malformations. Disease and Injuries of the Fingers and Toes and their Surgical Treatment* (Endonston and Douglas, Edinburgh), pp. 3–7.

BARSKY, A. J., 1967. Macrodactyly. *Journal of Bone & Joint Surgery*, *49A*, 1255–1266.

BARUCHIN, A. M., HEROLD, Z. H., SHMUELI, G. & LUPO, L., 1988. Macrodystrophia lipomatosa of foot. *Journal of Pediatric Surgery*, *23*, 192–194.

BEN-BASSAT, M. B., CASPER, J., KAPLAN, I., LARON, Z. & PETAH, T., 1966. Congenital macrodactyly. A case report with a three-year follow up. *Journal of Bone & Joint Surgery*, *8B*, 359–363.

NYSON, W. C., BEAR, J. N. & BHOOLN, K. J., 1977. acrodactyly in the foot. *Journal of Bone & Joint Surgery*, 9, 355–358.

FERIZ, H., 1923. Macrodystrophia lipomatosa progressiva. *Archives of Pathology, Anatomy and Physiology*, *260*, 308–368.

GODMAN, A. B. & KAYE, J. J., 1977. Macrodystrophia lipomatosa Radiographic diagnosis. *American Journal of Roentgenology*, *128*, 101–105.

GOLDING, F. C., 1960. Rare diseases of bone. In *Modern Trends in Diagnostic Radiology*, ed. by J. W. McLaren (Hober, New York, p. 160).

KAPOOR, R., MITTAL, K. P. & JAYA RAM, G., 1988. Macrodystrophia lipomatosa. *Indian Journal of Radiology*, *42*, 237–239.

KHANNA, N., GUPTA, S. K., KHANNA, S. & TRIPATHI, F., 1975. Macrodactyly. *The Hand*, *7*, 215–222.

KILLINGER, R. R., 1925. Dactylomegaly. A bilateral affection. *Journal of the Florida Medical Association*, *12*, 6–10.

LITTLER, W. J., CRAMER, L. M. & SMITH, J. W., 1974. *Symposium on Reconstructive Hand Surgery* (C. V. Mosby Co., St Louis), pp. 218–220.

MIKHAIL, J. K., 1964. Median nerve lipoma in the hand. *Journal of Bone & Joint Surgery*, *46B*, 726–730.

MINKOWITZ, S. & MINKOWITZ, F., 1965. A morphological study of macrodactylism. A case report. *Journal of Pathology and Bacteriology*, *90*, 323–328.

RECHNAGEL, K., 1967. Megalodactylism. Report of 7 cases. *Acta Orthopaedica Scandinavica*, *38*, 57–66.

THORNE, F. L., POSCH, J. L.M.L. & ADICK, R. A., 1968. Macrodactyly. *Plastic and Reconstructive Surgery*, *41*, 232–239.

TSUGE, K., 1967. Treatment of macrodactyly. *Plastic and Reconstructive Surgery*, *39*, 590–599.

TULI, S. M., KHANNA, N. N. & SINHA, G. P., 1969. Congenital macrodactyly. *British Journal of Plastic Surgery*, *22*, 237–243.

1992, *The British Journal of Radiology*, 65, 774–778

Fatty infiltration of the liver: analysis of prevalence, radiological and clinical features and influence on patient management

By Abdulla Y. El-Hassan, DMRD, *Ezzeldin M. Ibrahim, FRCP, Fatma A. Al-Mulhim, MB, BCh,
*Arwa A. Nabhan, MB, BCh and Milad Y. Chammas, ARRT

Departments of Radiology and *Internal Medicine, College of Medicine and Medical Sciences, King Faisal University, Dammam, Saudi Arabia

(*Received 26 June 1991 and in revised form 28 October 1991, accepted 6 March 1992*)

Keywords: Fatty infiltration, Liver

Abstract. Over a 6-year period, in 1425 adult computed tomographic studies, radiological evidence of fatty infiltration of the liver (FIL) was found in 138 patients (9.7%). Patients with FIL had a mean age ±SD of 45.9±15.7 years and 57% were males; the majority were Saudis (73%). Most patients (95%) had one or more underlying aetiological causes. Haematological and non-haematological malignancies with or without liver involvement were the most frequently encountered aetiological factors (66% of patients). FIL contibuted to hepatomegaly or was associated with abnormality in one or more of the liver function tests in 30% and 39% of patients, respectively. Assessment of the various radiological patterns showed diffuse fatty changes in 68% of patients and solitary or multiple focal changes in 9% and 22%, respectively. 13 patients (9%) showed sparing of the caudate lobe within a diffuse fatty process. Patients with diffuse FIL had significantly higher values for alkaline phosphatase ($p = 0.0016$) and serum asparate aminotransferase ($p = 0.0251$) than those who had the focal pattern. FIL in 20 patients (14%) imposed a difficulty in making an appropriate diagnosis, led to inaccurate impressions, or forced unnecessary invasive or non-invasive investigations. We conclude from our large series of patients that FIL is not uncommon in hospital practice and among those at risk should always be considered as an appropriate diagnosis.

Fatty infiltration of the liver (FIL) is a well-recognized histological and radiological entity presenting diffusely or occasionally focally with increased triglycerides in the form of droplets in hepatocytes (Scott et al, 1980; Alpers & Sabesin, 1982; Halvorsen et al, 1982).

Although diffuse FIL can be readily diagnosed radiologically, the condition may lead to diagnostic difficulties or mask a small primary hepatocellular carcinoma (Yoshikawa et al, 1988). While it may have a characteristic radiological pattern (Scott et al, 1980; Halvorsen et al, 1982; Gale et al, 1983), it is not uncommon for focal FIL to simulate liver abscess or metastases (Lewis et al, 1983; Yoshikawa et al, 1987). These diagnostic problems can be complicated further by associated hepatomegaly and abnormal liver function tests. In addition, patients with various forms of cancer are particularly exposed to many factors that favour the development of FIL (Alpers & Sabesin, 1982; Clendeninn et al, 1985).

The intricacy of the subject, its diagnostic implications and the lack of adequate description of the clinical and radiological features of FIL in a large series have prompted this study. Data of adult patients with documented FIL were examined to assess the radiological patterns and associated clinical and biochemical features in a large hospital practice.

Materials and methods

Abdominal computed tomography (CT) studies on adult patients attending King Fahd Hospital of the University over a 5-year period (1985–1989) were retrospectively reviewed independently by two radiologists (A.Y.E. and F.A.M.). Radiologists were unaware of previous reports and patients' clinical data and were required to report on the presence of FIL and its pattern, measured attenuation and other associated radiological findings. Discrepancies between the two radiologists were reconciled by joint review of controversial cases and rejection of those remaining discordant. CT scans were performed with and without i.v. and oral contrast media at a slice thickness of 9 mm, using a Philips Tomoscan 300.

Patients were only considered to have diffuse or focal FIL if their CT scan showed unequivocal radiological evidence with a low attenuation reading of < -10 Hu (Scatarige et al, 1984), if liver biopsy was positive or the clinical and/or radiological follow-up course was appropriate. Focal FIL was defined as the presence of a non-spherical focal area without a mass effect and having a low density as defined earlier. Diffuse low attenuation of the liver was considered compatible with diffuse FIL.

The medical records of all identified patients with FIL were also reviewed.

Address correspondence and reprint requests to Ezzeldin M. Ibrahim, FRCP, Associate Professor of Medicine and Oncology, King Fahd Hospital of the University, Al-Khobar, PO Box 40004, Al-Khobar 31952, Saudi Arabia.

Data analysis and statistical methods

Comparisons of discrete variables were carried out using χ^2 or Fisher's exact test where appropriate. Means of groups of continuous values were compared using an unpaired *t*-test. However, if an assumption of normality and equal variance was not shown by Levene's test, non-parametric Kruskal-Wallis statistics were used (Godfrey, 1985). Values are expressed as mean ±SD. A two-tailed p value < 0.05 was considered significant. For all data analysis the 1DP, 3DP, 4FP and 7DP programs of the BMDP statistical software were used (Dixon et al, 1988).

Results

Of 1425 adult CT scans between January 1985 and December 1990, 142 patients with FIL were identified. However, four were subsequently eliminated owing to lack of agreement between radiologists. The remaining 138 patients constitute the basis of this report. Patients' mean age was 45.9±15.7 years and 57% (79 patients) were male; 73% (101 patients) were Saudis.

Table I shows the distribution of potential aetiological factors for the development of FIL. Patients with underlying non-hepatocellular carcinomas (n-HCC), lymphoma or Hodgkin's disease and hepatocellular carcinoma (HCC) constituted most of our series (66%). Of those with n-HCC (54 patients) or lymphoma (21 patients), only 19 (25%) had documented evidence of involvement of the liver by the primary disease process. FIL developed in some cancer patients after exposure to corticosteroids (11 patients) and/or systemic chemotherapy (32 patients) as evident from their initially normal radiological studies. With the exception of one patient with chronic alcoholic liver disease, no history of alcohol intake was documented in any other patient. While 53% of patients had more than one potential aetiological factor, seven patients (5%) lacked any.

Table I. Distribution of potential aetiological causes for the development of fatty infiltration of the liver

Aetiological factor	Number of patients (%)
n-HCC	54 (39)
High adiposity index (> 2.5)	51 (37)
Anticancer chemotherapy	32 (23)
Lymphoma and Hodgkin's disease	21 (15)
Corticosteroids	18 (13)
Hepatocellular carcinoma	16 (12)
Diabetes mellitus	7 (5)
Tuberculosis[a]	7 (5)
Chronic liver disease	7 (5)
Hyperlipidaemia	1 (0.7)
Cushing's syndrome	1 (0.7)
Biliary disease	1 (0.7)
Rheumatoid arthritis	1 (0.7)
None	7 (5)

The total number of aetiological factors = 217 (53% of patients had more than one aetiological factor). n-HCC, non-hepatocellular carcinomas. [a]Pulmonary or abdominal tuberculosis without tuberculous hepatic involvement.

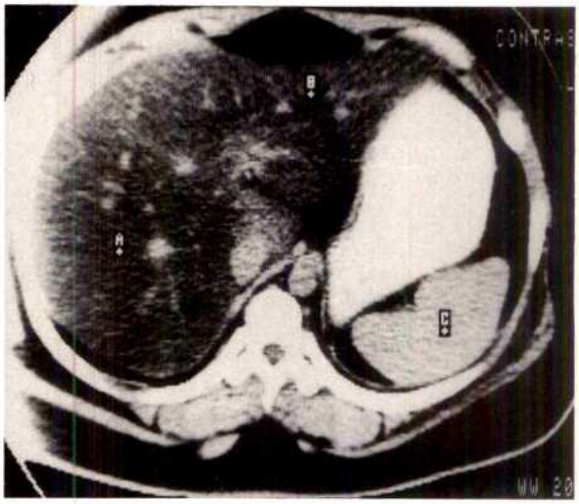

Figure 1. CT scan shows diffuse fatty infiltration of the liver after i.v. contrast medium.

Hepatomegaly was clinically evident in 29 out of 98 patients (30%) in whom the enlarged liver could not be attributed to anything other than FIL. 21 of those 29 patients (72%) had diffuse infiltration while the remaining eight had a multiple focal pattern.

Analysis of CT features of FIL is depicted in Table II. Diffuse fatty metamorphosis (Fig. 1) was evident in 94 patients (68%), of which 13 showed caudate lobe sparing (Fig. 2). Follow-up CT scans were available for 30 patients, with complete or partial resolution of FIL in 17 (57%), progressive fatty deposition in eight (27%) and no change in five (16%). The mean time interval for documentation of radiological changes was 9.4±8.6 months (range 1–30 months). Parallel changes in liver size and liver function tests were also observed. Only in 10 of the 17 patients (59%) who demonstrated complete or partial regression of their fatty liver could the regression be accounted for by the effect of therapy or because of withdrawal of the causative agent. The 10 patients

Table II. Analysis of various radiological features of fatty infiltration of the liver (138 patients)

Radiological feature	Number of patients (%)
Pattern	
diffuse	94 (68)
focal (solitary)	12 (9)
focal (multiple)	30 (22)
focal, progressing to diffuse	2 (1)
Caudate lobe sparing	13 (9)
Radiological evolution	
not assessed	108 (78)
completely resolved	11 (8)
partially resolved	6 (4.5)
increased diffuse pattern	6 (4.5)
no change	5 (4)
focal, progressing to diffuse	2 (1)

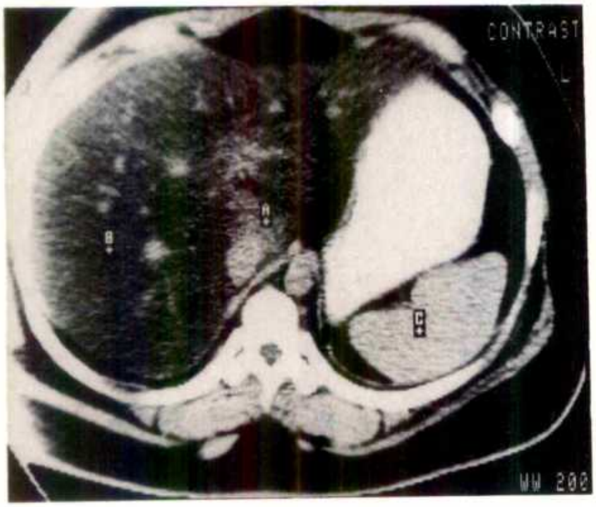

Figure 2. CT scan after i.v. contrast medium shows diffuse fatty infiltration of the liver with an area of sparing in the caudate lobe region (marked A). The CT reading at A was close to splenic attenuation (marked C) and both were significantly higher than areas of dense fatty changes (marked B).

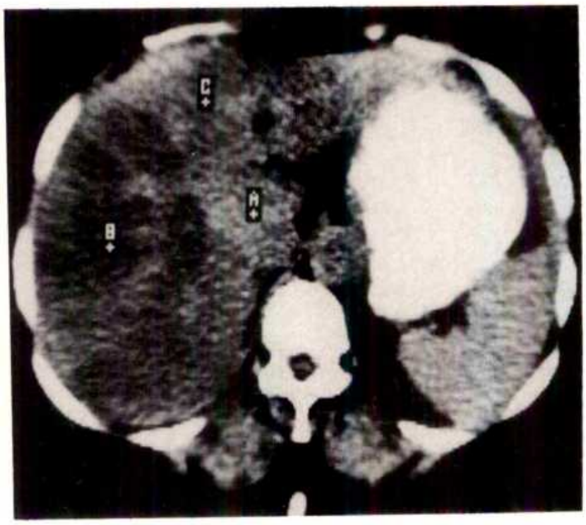

Figure 3. CT scan after i.v. contrast medium shows multifocal fatty infiltration of the liver (marked B and C) with an area (marked A) of relative caudate lobe sparing. Occult metastatic carcinoma was revealed by CT-guided biopsy from area B.

included four who showed partial regression after stopping systemic anticancer chemotherapy, four who showed partial regression after treating their underlying lymphoma, and two tuberculous patients who showed complete regression after completion of their antituberculous therapy.

Comparisons were made between the mean values of biochemical variables for those patients with diffuse and those with focal FIL. Patients with cancer and liver involvement, those with hepatoma and those with chronic liver disease were eliminated from the comparisons made for liver function tests. The analysis showed that patients with diffuse disease had higher levels of alkaline phosphatase (24.5 ± 16.7 *vs.* 13.5 ± 12.8 i.u./ml; normal, up to 14 i.u./ml; $p = 0.0016$) and serum aspartate aminotransferase (53.5 ± 26.6 *vs.* 38.5 ± 24.7 i.u./ml; normal, up to 38 i.u./ml; $p = 0.0251$) than those with a focal pattern. No other significant difference was observed between the two groups for any of the other factors tested. Likewise, no significant difference was detected between those who demonstrated caudate lobe sparing and those who did not.

Table III. Prevalence of abnormal liver function tests attributed only to fatty infiltration of the liver

Test	Number of patients tested (% abnormal)
Total bilirubin	94 (14)
Albumin	93 (31)
Alkaline phosphatase	92 (32)
Aspartate aminotransferase	92 (38)
Alanine aminotransferase	92 (25)
Lactate dehydrogenase	89 (37)
Gamma glutamyl transpeptidase	80 (43)

Table III shows the percentage of patients who had abnormal liver function values that could be attributed only to FIL. Each individual liver function was abnormal in at least one-third of patients. Furthermore, approximately 39% of patients had one or more abnormal liver functions probably accounted for only by FIL.

In a total of 54 patients, liver biopsy was performed for various indications and histopathological evidence of FIL was documented in all cases. In only seven patients, histological features of chronic liver disease were evident (Table I). Of the latter seven patients with chronic liver disease, liver biopsy showed schistosomal periportal fibrosis in four, chronic persistent hepatitis in two, and alcoholic liver disease in one. Conversely, only one of the seven patients without an apparent cause for FIL had a liver biopsy that showed fatty change without other concomitant pathology.

Clinical data were assessed to determine the diagnostic difficulties that were encountered because of the presence of FIL. In 10 of 54 (19%) patients with n-HCC there were difficulties in management. Four patients had hepatomegaly and abnormal liver function tests and were thought to have liver metastases or chemotherapy-related hepatic toxicity. Subsequently, however, diffuse FIL was the only explanation. In the remaining patients the presence of multifocal FIL was mistaken for liver metastases (four patients) or delayed the recognition of hepatic secondaries (two patients) (Fig. 3). Two out of 16 patients (12.5%) with hepatocellular carcinoma had a small primary (< 4 cm) that was diffusely infiltrated by fat, producing a deceptive radiological pattern and delaying diagnosis. Three of 21 patients (14%) with lymphoma or Hodgkin's disease had hepatomegaly and abnormal liver functions due to diffuse (two patients) or unifocal (one patient) FIL that were initially believed to represent liver involvement. In patients with underlying benign conditions, the presence of FIL caused fewer difficulties and forced further invasive investigations in only five patients. Two diabetic patients had focal FIL that required liver biopsy to exclude the existence of malignancy or liver abscess. Similarly, CT-guided liver biopsy was indicated in three out of 13 patients (23%) who had caudate lobe sparing, which radiologically simulated tumours.

Thus, it is estimated that in 20 out of 138 patients (14%) the existence of FIL led to difficulty in making a diagnosis, gave an erroneous impression or forced further invasive and non-invasive investigations. Of those 20 patients, 11 had diffuse and nine had focal fatty deposition. Considering the number of patients in each of the two radiological categories, the difference in the prevalence of problematical cases in the two radiological categories was not statistically significant ($p = 0.25$).

Discussion

Diffuse or focal FIL is a well known entity (Scott et al, 1980; Alpers & Sabesin, 1982; Halvorsen et al, 1982). While in a normal liver, fat accounts for only 5% of the total weight, it may be increased up to 50% in cases of severe fatty change. Nevertheless, there is no evidence that hepatic fat accumulation by itself leads to cirrhosis (Alpers & Sabesin, 1982). Many reports have described the radiological and sonographic patterns and the diagnostic challenges imposed by its presence, particularly in its focal form, but only in a small number of selected patients (Quinn & Gosink, 1985; Baker & Silverman, 1985; Yates & Streight, 1986; Yoshikawa et al, 1987).

We have documented FIL in 138 patients identified from 1425 (9.7%) abdominal CT scans performed over a 6-year period. The mean age (45.9 years) in the current series reflects the average age distribution of the underlying conditions. In our series, concomitant malignant disease was encountered in 66% of patients, and in some (43 patients), corticosteroids and chemotherapy have contributed to the development of FIL. However, the independent contribution of other associated factors that are known to occur in cancer patients, such as protein calorie malnourishment or parenteral hyperalimentation, could not be determined precisely. Obesity, as reflected by a high adiposity index (weight in kg/height in m), was the second most frequent potential association. Mild degrees of FIL have been reported in about 50% of obese persons but only rarely would obesity be associated with gross fatty changes (Kern et al, 1973). The distribution of various aetiological factors among our patients represents the pattern of FIL in Saudi Arabia. In other countries, other factors such as alcoholism may be more prevalent.

Our data have shown that FIL could account for clinical hepatomegaly and abnormal liver function in 30% and 39% of patients, respectively. While in some patients the derangement of liver function could have been attributed to other concomitant or unrecognized factors, hepatomegaly probably would be only explained by FIL after exclusion of other causes. Furthermore, the radiological evolution of FIL was accompanied by parallel changes in liver size and function. Except for higher serum alkaline phosphatase and aspartate aminotransferase levels in patients with a diffuse pattern compared with those with a focal pattern, no other distinguishing clinical features were observed.

In 20 patients (14%) the existence of FIL had created diagnostic problems or erroneous conclusions and in some it caused further unnecessary investigations and invasive procedures. In 19% of patients with n-HCC, the fatty changes either mimicked metastases or camouflaged its existence. The CT (Baker & Silverman, 1985; Yates & Streight, 1986; Yoshikawa et al, 1987) and sonographic (Quinn & Gosink, 1985; Yoshikawa et al, 1987) similarity between focal FIL and liver tumours has been previously described.

While the coexistence of a large hepatocellular carcinoma and FIL was not a diagnostic problem, in two patients with a small primary liver tumour (< 4 cm) the diagnosis was delayed owing to the presence of diffuse fatty changes, as Yoshikawa et al (1988) also recently observed.

Focal caudate lobe sparing in patients with diffuse FIL produced diagnostic problems in three out of 13 patients with this radiological pattern. Radiological and sonographic descriptions of similar sparing of the caudate lobe has been recently reported (Sauerbrei & Lopez, 1986; White et al, 1987; Arai et al, 1988) and explained by the reduction of portal blood flow within the spared areas (Gale et al, 1983; Sauerbrei & Lopez, 1986; Arai et al, 1988).

Other radiological techniques may be useful in clarifying the presence of FIL, particularly in its focal form, and the existence of focal sparing with the diffuse pattern. Dynamic CT-arteriography or CT-arterial portography have been shown to be helpful (Yoshikawa et al, 1988; Arai et al, 1988). Technetium sulphur-colloid scintigraphy may show normal photon activity in areas of fatty infiltration, while metastases usually appear as areas of photon deficiency (Halvorsen et al, 1982). Xenon scintigraphy typically shows photon activity in regions of fatty infiltration, reflecting the solubility of xenon in lipids (Patel et al, 1982). Recently, magnetic resonance imaging has proved valuable in the detection of focal hepatic lesions, including focal FIL (Foley et al, 1987). Unfortunately, these techniques were available to only a few of our patients.

In conclusion, this large series has shown the spectrum of FIL in a hospital practice and has illustrated the scale of its clinical and radiological manifestations. The presence of fatty change substantially influenced diagnosis in 14% of our patients. Radiologists and clinicians alike should be aware of the radiological, clinical and biochemical manifestations of FIL to avoid unnecessary investigations or overlooking more serious pathology.

References

Alpers, D. H. & Sabesin, S. M., 1982. Fatty liver: biochemical and clinical aspects. In *Disease of the Liver*, 5th edn, ed. by

L. Schiff and E. R. Schiff (J.B. Lippincot Company, Philadelphia), pp. 813–845.

Arai, K., Matsui, O., Takashima, T., Ida, M. & Nishida, Y., 1988. Focal spared areas in fatty liver caused by regional decreased portal flow. *American Journal of Roentgenology, 151,* 300–302.

Baker, M. E. & Silverman, P. M., 1985. Nodular focal infiltration of the liver: CT appearance. *American Journal of Roentgenology, 145,* 79–80.

Clendeninn, N. J., Curt, G. A., Allegra, C. J., Weh, J. C., Baram, J. & Chabner, B. A., 1985. Antimetabolites. In *Cancer Chemotherapy,* 7th edn, ed. by H. M. Pinedo and B. A. Chabner (Elsevier, Amsterdam), pp. 1–30.

Dixon, W. J., Brown, M. B., Engelman, L., Hill, M. A. & Jennrich, R. I., 1988. *BMDP Statistical Software Manual* (University of California Press, Berkeley).

Foley, W. D., Kneeland, J. B., Cates, J. D., Kellman, G. M., Lawson, T. L., Middleton, W. D. & Hendrick, R. E., 1987. Contrast optimization for the detection of focal hepatic lesions by MR imaging at 1.5 T. *American Journal of Roentgenology, 149,* 1155–1160.

Gale, M. E., Gerzof, S. G. & Robbins, A. H., 1983. Portal architecture: a differential guide to fatty infiltration of the liver on computed tomography. *Gastrointestinal Radiology, 8,* 231–236.

Godfrey, K., 1985. Comparing the means of several groups. *New England Journal of Medicine, 313,* 1450–1456.

Halvorsen, R. A., Korobkin, M., Ram, P. C. & Thompson, W. H., 1982. CT appearance of focal fatty infiltration of the liver. *American Journal of Roentgenology, 139,* 277–281.

Kern, H. H., Heger, A. H., Payne, J. H. & Dewind, L. T., 1973. Fatty metamorphosis of the liver in morbid obesity. *Archives of Pathology, 96,* 342–346.

Lewis, E., Bernardion, M. E., Barnes, P. A., Parvey, H. R., Soo, C. S. & Chang, V. P., 1983. The fatty liver: pitfalls in the CT and angiographic evaluation of metastatic disease. *Journal of Computer Assisted Tomography, 7,* 235–241.

Patel, S., Sandler, C. M., Rauschbolk, E. N. & McConnel, B. J., 1982. Xe-133 update in focal hepatic fat accumulation: CT correlation. *American Journal of Roentgenology, 138,* 541–544.

Quinn, S. F. & Gosink, B. B., 1985. Characteristic sonographic signs of hepatic fatty infiltration. *American Journal of Roentgenology, 145,* 753–755.

Sauerbrei, E. E. & Lopez, M., 1986. Pseudotumor of the quadrate lobe in hepatic sonography: a sign of generalized fatty infiltration. *American Journal of Roentgenology, 147,* 923–927.

Scatarige, J. C., Scott, W. W., Donovan, P. J., Siegelman, S. S. & Sanders, R. C., 1984. Fatty infiltration of the liver: ultrasonographic and computed tomographic correlation. *Journal of Ultrasound in Medicine, 3,* 9–14.

Scott, W. W., Sanders, R. C. & Siegelman, S. S., 1980. Irregular fatty infiltration of the liver: diagnostic dilemmas. *American Journal of Roentgenology, 135,* 67–71.

White, E. M., Simeone, J. F., Mueller, P. R., et al, 1987. Focal periportal sparing in hepatic fatty infiltration: a cause of hepatic pseudomonas on US. *Radiology, 162* (1), 57–59.

Yates, C. K. & Streight, R. A., 1986. Focal fatty infiltration of the liver simulating metastatic disease. *Radiology, 159* (1), 82–84.

Yoshikawa, J., Matsui, O., Takashima, T., Sugiura, H., Katayama, K., Nishida, Y. & Tsuji, M., 1987. Focal fatty changes of the liver adjacent to the falciform ligament: CT and sonographic findings in five surgically confirmed cases. *American Journal of Roentgenology, 149,* 491–494.

Yoshikawa, J., Matsui, O., Takashima, T., Ida, M., Takanaka, T., Kawamura, I., Kukuda, K. & Miyata, S., 1988. Fatty metamorphosis in hepatocellular carcinoma: radiologic features in 10 cases. *American Journal of Roentgenology, 151,* 717–720.

1992, *The British Journal of Radiology*, *65*, 779–783

Accuracy of ultrasound and oral cholecystography in assessing the number and size of gallstones: implications for non-surgical therapy

By Koen Brakel, MD, Johan S. Laméris, MD, *Huub G. T. Nijs, MD, Abida Z. Ginai, MD and *Onno T. Terpstra, MD

Departments of Radiology and *Surgery, University Hospital Rotterdam/Dijkzigt, Erasmus University Rotterdam, The Netherlands

(*Received 11 September 1991 and in revised form 13 March 1992, accepted 2 April 1992*)

Keywords: Gallstones, Ultrasound, Oral cholecystography

Abstract. Prior to non-surgical therapy of gallstones it is important to assess their number and size. In order to evaluate the accuracy of ultrasound (US) and oral cholecystography (OCG) in counting and measuring gallstones, a prospective blind study was conducted to compare the results of US ($n = 99$) and OCG ($n = 36$), either alone or in combination ($n = 34$), with the number and size of gallstones retrieved after cholecystectomy. The number of gallstones was accurately estimated by US and OCG in 74% and 69% of the cases, respectively. In assessing the presence of up to three, five or 10 gallstones both US and OCG proved reliable. In measuring the size of gallstones, there was 19% accuracy with US compared with only 3% with OCG. With an accepted measurement error of 3 mm these values increased to 80% for US and 44% for OCG. US proved more reliable than OCG in discriminating gallstones smaller or larger than 10 mm and smaller or larger than 20 mm, but with US, detection of gallstones larger than 30 mm was problematic. Both US and OCG underestimated gallstone size. The combination of both techniques did not significantly improve the assessment of either number or size of gallstones compared with the results obtained with US or OCG alone. It is concluded that (1) both US and OCG have some limitations in assessing the number and size of gallstones, (2) the combination of both examinations does not improve acccuracy, and (3) patient selection for non-surgical treatment of gallstones can be started by US alone.

With the introduction of non-surgical treatment of gallstones, the demands for diagnostic imaging of gallbladder disease have changed. It is no longer sufficient to establish only the presence of gallstones. In order to select the proper non-surgical treatment, information is also needed about the number, size and chemical composition of the stones together with the functional status of the gallbladder (Simeone et al, 1989). The primary imaging modalities for gallstone disease are ultrasound (US) (Cooperberg & Burhenne, 1980) and oral cholecystography (OCG) (Gelfand et al, 1988; Maglinte et al, 1991). US has certain limitations in assessing the number and size of gallstones (Simeone et al, 1989; Brandstetter et al, 1989; Brink et al, 1989; Mathieson et al, 1989; Garra et al, 1990), whereas OCG is reported to be more appropriate in this respect (Maglinte et al, 1991). The aim of this investigation was to evaluate the accuracy of US and OCG, in combination and alone, in assessing the number and size of gallstones. For this purpose we correlated, in a prospective blind study, the results of US and OCG with the number and size of gallstones retrieved after cholecystectomy.

Materials and methods

From April 1988 to May 1990, 99 patients (22 male, 77 female, mean age 52 years, range 20–83 years) with symptomatic gallstone disease underwent US and OCG as part of their diagnostic workup for selection for non-surgical treatment. The patients underwent cholecystectomy either because they were randomized for operation in our on-going trial of lithotripsy *vs.* cholecystectomy (den Toom et al, 1992) or because they did not meet the criteria for lithotripsy (den Toom et al, 1992).

US and OCG were performed in the fasting state on the same day by different radiologists and data were recorded on standardized forms, without knowledge of the results of the other examination. US was performed with real-time equipment (Toshiba, Aloka) with 3.5 MHz or 5.0 MHz curved array and sector transducers. Sections of the gallbladder were obtained in different planes with patients in supine, left posterior oblique and erect positions. OCG was performed after oral intake of 4 g iocetamic acid (Cholebrine, Dagra Pharma B.V., Diemen, The Netherlands) the evening before the examination. OCG examinations included supine, prone oblique and erect spot radiographs of the gallbladder, made during fluoroscopy on a Bucky table. Only examinations with diagnostically sufficient opacification of the gallbladder were included (36 out of 53 OCG examinations, 67%). When both US and OCG examinations were available for the same patient ($n =$

Address reprint requests and correspondence to Koen Brakel, MD, Department of Radiology, University Hospital Rotterdam/Dijkzigt, Dr. Molewaterplein 40, 3015 GD Rotterdam, The Netherlands.

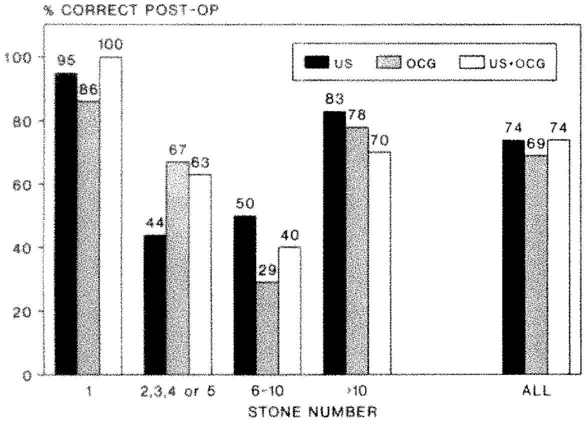

Figure 1. Percentages of correctly assessed numbers of gallstones on US ($n = 99$), OCG ($n = 36$) and combined US and OCG ($n = 34$).

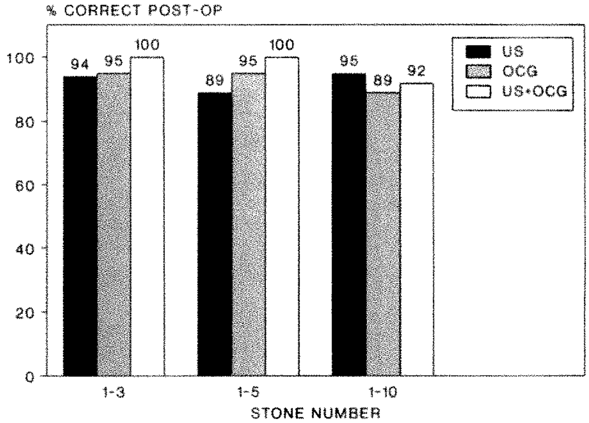

Figure 2. Percentages of correctly assessed presence of up to three, five or 10 gallstones on US ($n = 99$), OCG ($n = 36$) and combined US and OCG ($n = 34$).

34), the largest diameter and largest number of gallstones recorded were considered as the outcome of the combined examinations.

After cholecystectomy, the gallbladder content was collected for analysis. Only stones with a diameter of ⩾ 3 mm were counted. The numbers of gallstones were categorized as 1, 2, 3, 4, 5, 6–10 or more than 10 stones. Only the largest gallstone was measured. In the case of non-spherical stones the largest diameter was recorded. Measurement of stone size by OCG was corrected for an empirically determined magnification factor of 1.3.

Data analysis

The percentage correct was defined as 100 times the proportion of US or OCG that agreed with the post-operative results, divided by the total number of examinations. This proportion is referred to as the positive predictive value. Percentages correct were compared using a standard test to compare two proportions assuming a binomial distribution (Armitage & Berry, 1987). Receiver-operating characteristic (ROC) graphs (Swets, 1979) were used to compare the efficacy of US and OCG in predicting gallstone sizes at various cut-off points.

Results

The results are presented in Figs 1–5. Figure 1 shows the correctly assessed numbers of gallstones on US, OCG and the results of the combined techniques based on the examination revealing the largest number of stones. The number of gallstones was accurately estimated by US and OCG in 74% and 69% of the cases, respectively. In assessing the presence of two, three, four or five gallstones OCG was slightly, but not significantly, more accurate than US: 67% and 44%, respectively. The results did not improve significantly when US and OCG were used in combination.

In assessing the presence of up to three, five or 10 stones the results obtained with US and OCG were similar. Again, combined US and OCG did not significantly improve the results (Fig. 2).

Figure 3 shows accuracy of US and OCG in measuring gallstone diameter and the results of the combined techniques for which the largest measured diameter was used in the analysis. There was 19% accuracy with US compared with only 3% with OCG; with an accepted error of 3 mm the percentage correct increased to 80% for US and 44% for OCG; with an accepted error of 5 mm the percentage increased to 87% for US and 79% for OCG. For up to 4 mm measurement error these results are significantly better for US compared with OCG ($p < 0.05$). The combination of US and OCG did not improve these results compared with either examination performed alone.

The results of the diameter measurements on US were independent of the number of stones. Percentages correct of the predicted measurements on US were not significantly different when the gallstone population was

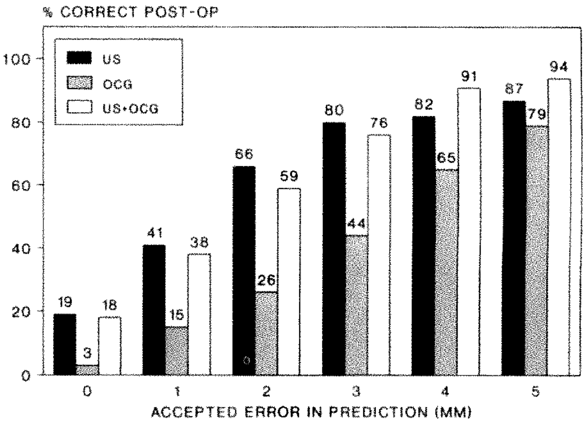

Figure 3. Percentages of correctly measured gallstone diameters on US ($n = 95$), OCG ($n = 34$) and combined US and OCG ($n = 34$).

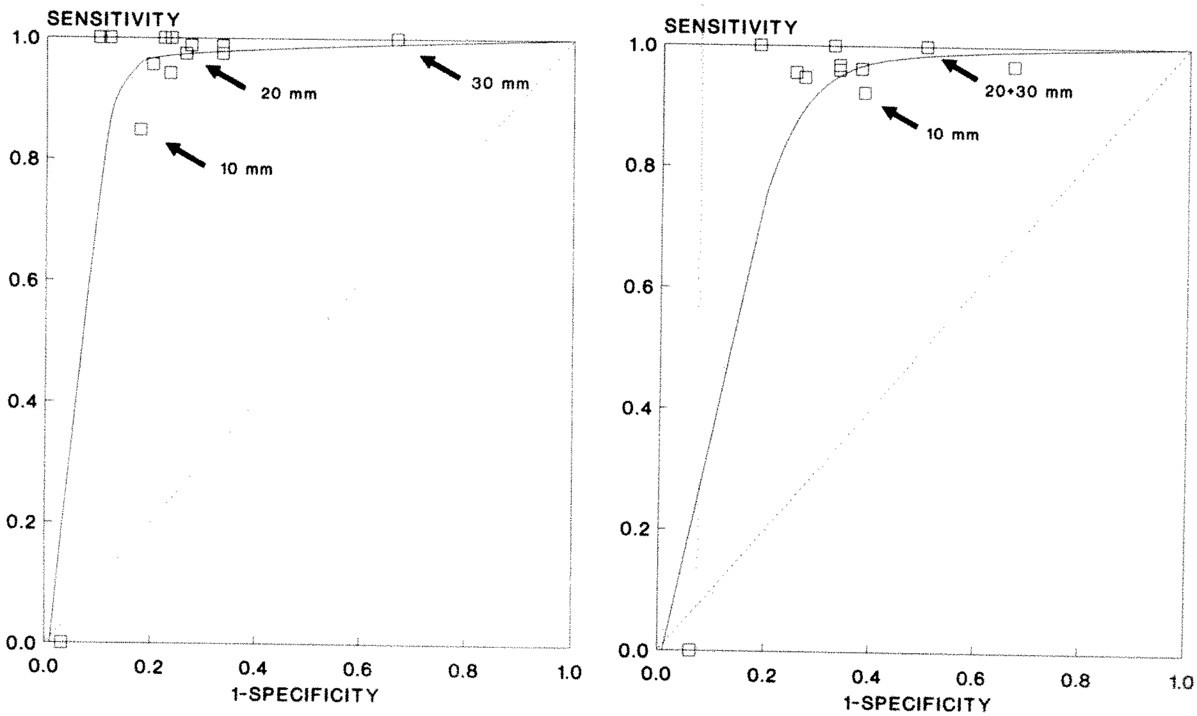

(a)

(b)

Figure 4. ROC graphs for discriminating gallstone diameter with (a) US ($n = 95$) (b) OCG ($n = 34$).

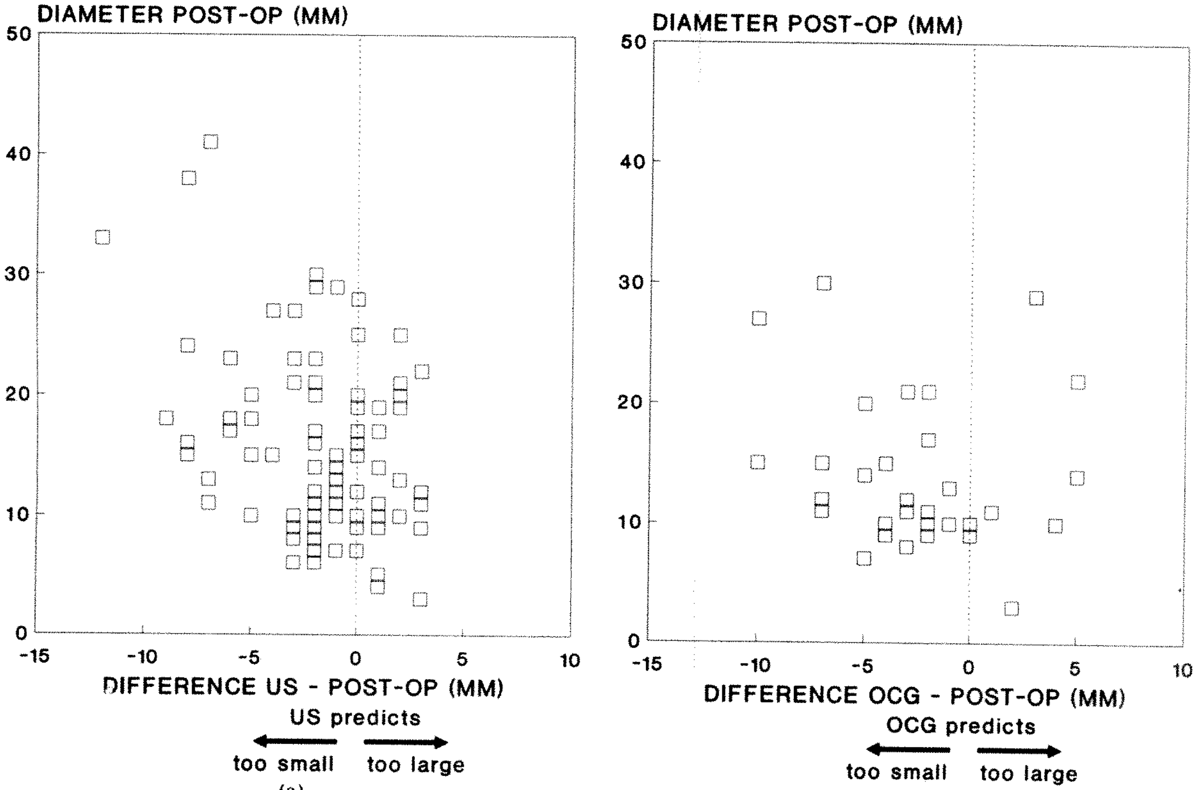

(a)

(b)

Figure 5. Post-operative measurement of gallstones compared with (a) US and (b) OCG.

divided into single *vs.* multiple stones, up to three *vs.* more than three stones, or up to five *vs.* more than five stones. The stone population was also divided into stones up to 15 mm in diameter ($n = 58$) *vs.* larger than 15 mm ($n = 37$). In assessment of stone diameter, US was proved significantly better ($p < 0.05$) with stones up to 15 mm than for larger stones, irrespective of the accepted measurement error.

Figure 4 shows ROC graphs for discriminating gallstone size with US (Fig. 4a) and OCG (Fig. 4b) at various cut-off points. Since the entire curve for US lies closer to the upper left corner than the curve for OCG, US has more discriminating power than OCG, irrespective of the cut-off points. Nevertheless, US missed two out of three cases in detecting gallstones larger than 30 mm.

Figure 5 shows differences in post-operative measurements of gallstone diameter compared with US (Fig. 5a) and OCG (Fig. 5b). Both US and OCG underestimate gallstone size.

Discussion

This study compared the accuracy of US and OCG in assessing the number and size of gallstones. To our knowledge this has not been described previously. The results show some limitations for both US and OCG, either alone or in combination.

With US there were problems in assessing the precise number of stones in the presence of two to 10 stones, which confirms the suggestion by other investigators (Simeone et al, 1989) that US appears to be less accurate in counting stones. With OCG the estimation was slightly more accurate with two to five stones, but the overall results in assessing the number of gallstones were similar to those with US. Simeone and coworkers suggested performing both US and OCG and that the examination revealing the largest number of gallstones should be considered to be correct. As the results of this study did not improve using this method, we cannot support their conclusion. Selection criteria for biliary lithotripsy vary in the number of stones that can be treated (den Toom et al, 1992; Schoenfield et al, 1990; Burhenne et al, 1989; Sackmann et al, 1988). Although in this study both US and OCG showed limitations in counting numbers of stones, these techniques can be used as tools to select patients, independent of the number of stones that are accepted for treatment (Fig. 2).

In assessing stone size, US becomes more reliable with an accepted measurement error of 3 mm, while OCG reaches a reliable standard only at an accepted error of 5 mm. When taking the largest measured diameter on US or OCG as the correct diameter, the results in this study did not improve. This is in contrast to a report by Simeone et al (1989).

In measuring stone size both US and OCG underestimate size and detecting stones larger than 30 mm was problematic with US. This is important, because most protocols for biliary lithotripsy exclude stones larger than 30 mm. Unfortunately this study had no OCG examinations with stones larger than 30 mm proven post-operatively. The accuracy of US and OCG in counting and measuring gallstones will be influenced by patient, technical and observer-related factors. For example, in obese patients the use of 5 MHz transducers in US is limited and can be a cause of less-accurate measurements (Garra et al, 1990). Obesity will also influence the effect of radiographic magnification on OCG examinations.

In this study the measurements were corrected with a magnification factor of 1.3 for all OCG examinations, independent of the weight of the patient, which could have contributed to the less-accurate measurements obtained on OCG. In addition, the stone burden and composition of the stones can influence the level of accuracy. With US, stones can be hidden in the acoustic shadow of other stones, and axial measurements, which are more accurate than transverse measurements, are not always possible. Similarly OCG can miss small and slightly calcified stones or underestimate the size if a calcified rim is missed. The quality of US examination is highly dependent on the expertise of the investigator (Mathieson et al, 1989) as is OCG.

All examinations were performed under routine conditions by different radiologists and therefore this study reflects common radiological practice. Based on the results of this and a previously published study (Brakel et al, 1991), some guidelines are suggested for imaging strategies in patient selection for biliary lithotripsy. In our opinion there are two main options:

1. Patient selection starts with US examination. Patients with a contracted gallbladder (11% in our previously published study) (Brakel et al, 1991) are excluded because this US finding has proven to be highly specific in predicting non-visualization of the gallbladder on OCG (Brakel et al, 1991). Stone impaction in the gallbladder neck or cystic duct (13% in our previously published study) (Brakel et al, 1991) also reliably predicts non-visualization on OCG, but here there could, however, be a role for lithotripsy, because this therapy could re-establish cystic duct patency. Patients with more than three (45% in this study), five (34%) or 10 (24%) stones are excluded depending on the chosen protocol for lithotripsy. The remaining patients (44%, 55% or 65% according to the accepted number of stones) should undergo OCG for the following reasons:
   (a) Visualization of the gallbladder on OCG is mandatory, because this ensures both cystic duct patency and concentration capability of the gallbladder.
   (b) To obtain information about the chemical composition of gallstones, although OCG has limitations for this purpose. Buoyancy is a specific sign for cholesterol stones but unfortunately it is an infrequent finding. Radiolucency versus radio-opacity is unreliable in distinguishing cholesterol stones from pigment stones and computed tomography has proven to be more reliable for

predicting gallstone composition (Brakel et al, 1990).

2. The other option is to perform both US and OCG on the same day and consider it as one examination. Although this option has logistical advantages, the results of this study indicate that this will not improve the outcome and, therefore, some patients (44–65%) will unnecessarily be subjected to OCG.

It is concluded that (1) both US and OCG have some limitations in assessing the number and size of gallstones, (2) the combination of both examinations does not improve the results, and (3) patient selection should start with US, which would exclude ±50% of the patients for biliary lithotripsy.

Acknowledgment
We thank Karin Schoenmaker for help in preparing the manuscript.

References

ARMITAGE, R. & BERRY, G., 1987. *Statistical Methods in Medical Research,* 2nd edn (Blackwell, Oxford), pp. 120–125.

BRAKEL, K., LAMÉRIS, J. S., NIJS, H. G. T., TERPSTRA, O. T., STEEN, G. & BLIJENBERG, B. C., 1990. Predicting gallstone composition with CT: *in vivo* and *in vitro* analysis. *Radiology, 174,* 337–341.

BRAKEL, K., LAMÉRIS, J. S., NIJS, H. G. T., GINAI, A. Z. & TERPSTRA, O. T., 1991. The value of US in predicting non-visualization of the gallbladder on OCG. *Clinical Radiology, 43,* 186–189.

BRANDSTETTER, K., NEUHAUS, H., HAGENMÜLLER, F., GMEINWIESER, J. & ERHARDT, W., 1989. Imaging prior to biliary lithotripsy. In *Biliary Lithotripsy II,* ed. by H. J. Burhenne (C. V. Mosby, Chicago) pp. 57–61.

BRINK, J. A., SIMEONE, J. F., MUELLER, P. R., SAINI, S., TUNG, G. A., SPELL, N. O. & FERRUCCI, J. T., 1989. Routine sonographic techniques fail to quantify gallstone size and number: a retrospective study of 111 surgically proved cases. *American Journal of Roentgenology, 153,* 503–506.

BURHENNE, H. J., BECKER, CH. D., MALONE, D. E., RAWAT, B. & FACHE, J. S., 1989. Biliary lithotripsy: early observations in 106 patients. *Radiology, 171,* 363–367.

COOPERBERG, P. L. & BURHENNE, H. J., 1980. Real-time ultrasonography, diagnostic technique of choice in calculous gallbladder disease. *New England Journal of Medicine, 302,* 1277–1279.

DEN TOOM, R., VERGUNST, H., NIJS, H. G. T., BRAKEL, K., LAMÉRIS, J. S. & TERPSTRA, O. T., 1992. Electromagnetic shock wave lithotripsy of gallbladder stones using a wide range of inclusion criteria. *American Journal of Gastroenterology, 87,* 498–503.

GARRA, B. S., DAVROS, W. J., LACK, E. E., HOZI, S. C., SILVERMAN, P. M. & ZEMAN, R. K., 1990. Visibility of gallstone fragments at US and fluoroscopy: implications for monitoring gallstone lithotripsy. *Radiology, 174,* 343–347.

GELFAND, O. W., WOLFMAN, N. T., OTT, D. J., WATSON, N. E., CHEN, Y. M. & DALE, W. J., 1988. Oral cholecystography vs gallbladder sonography: a prospective blinded re-appraisal. *American Journal of Roentgenology, 151,* 69–72.

MAGLINTE, D. D. T., TORRES, W. E. & LAUFER, I., 1991. Oral cholecystography in contemporary gallstone imaging: a review. *Radiology, 178,* 49–58.

MATHIESON, J. R., SOL, B., MALONE, D. E., BECKER, CH. D. & BURHENNE, H. J., 1989. Accuracy of sonography for determining the number and size of gallbladder stones before and after lithotripsy. *American Journal of Roentgenology, 153,* 977–980.

SACKMANN, M., DELIUS, M., SAUERBRUCH, T., HOLL, J., WEBER, W., IPPISCH, E., HAGELAUER, U., WESS, O., HEPP, W., BRENDEL, W. & PAUMGARTNER, G., 1988. Shock-wave lithotripsy of gallbladder stones. *New England Journal of Medicine, 318,* 393–397.

SCHOENFIELD, L. J., BERCI, G. & CARNOVALE, R. L., 1990. The effect of ursodiol on the efficacy and safety of extracorporeal shock-wave lithotripsy of gallstones. The Dornier National Biliary Lithotripsy Study. *New England Journal of Medicine, 323,* 1239–1245.

SIMEONE, J. F., MUELLER, P. R. & FERRUCCI, J. T., 1989. Non-surgical therapy of gallstones. Implications for imaging. *American Journal of Roentgenology, 152,* 11–17.

SWETS, J. A., 1979. ROC analysis applied to the evaluation of medical imaging techniques. *Investigative Radiology, 14,* 135–140.

1992, *The British Journal of Radiology*, 65, 784–786

The optimum pressure of oxygen for radiotherapy of a mouse tumour

By P. M. Perry, MIST and A. H. W. Nias, DM, FRCR, FRCPath

Richard Dimbleby Department of Cancer Research, United Medical and Dental Schools, St Thomas' Hospital, London SE1 7EH, UK

(*Received 12 June 1991 and in final form 14 January 1992, accepted 11 February 1992*)

Keywords: Hyperbaric oxygen, Mouse, Tumour, Radiosensitivity, Anaesthesia

Abstract. Our previous studies have shown that there is more regrowth delay in mammary tumours irradiated in C3H mice after 25 Gy when breathing normobaric oxygen than in those breathing air, as might be expected. However, in both cases this radiation response was reduced in anaesthetized animals in comparison with unanaesthetized control mice, when a time interval of only 10 min was allowed after anaesthesia. After 25 min, however, the response in air returned to the control level and the oxygen group now showed significantly more radiosensitization. We have now found that when tumour-bearing mice were exposed to different pressures of oxygen for that 25-min period after the induction of anaesthesia, before the tumours were treated with 25 Gy, there was even more regrowth delay with 2 atm pressure than 1, but that there was no further advantage from using 3 atm pressure of oxygen. Our data suggest that 2 atm may be the optimal pressure to use in anaesthetized mice and there is even a small benefit from using this pressure in unanaesthetized animals for a transplanted C3H mammary tumour.

The pioneers who used hyperbaric oxygen (HPO) with radiotherapy worked on the assumption that the higher the oxygen tension the more this would lead to the oxygenation of hypoxic tumour cells. With pressures above 3 atm absolute, however, there was the risk of convulsions unless anaesthesia was used. Churchill-Davidson et al (1957) chose to treat their patients "at three atmospheres absolute not because there is evidence that this is the optimal level, but because it would seem to be near the upper limit of safety, and if there is an oxygen effect it would be likely to be more marked, or at least more consistent, the higher the pressure of oxygen used". They went on to comment that "it is probable that different pressures will be required to produce optimal results in tumours with different circulatory conditions". We have examined this phenomenon using our C3H mouse mammary tumour model.

Previous studies have shown that with HPO at 3 atm absolute, the curative effect of single doses of radiation was enhanced by a factor of 1.7 if the mice had been anaesthetized with ketamine and diazepam (Tozer et al, 1984). More recently, we have asked the question: Which is more important, the pre-irradiation breathing time (PIBT) of oxygen, or the pre-irradiation anaesthetic time? Because the HPO technique requires a minimum pressurization and "soaking" time of 25 min, we had to use normobaric oxygen for this study. This showed that without anaesthesia there was no variation in radiation response whether oxygen was breathed for 0, 15 or 30 min before the commencement of irradiation (Nias & Perry, 1989). On the other hand, we found a marked variation in radiation response in terms of regrowth delay, when ketamine and diazepam anaesthesia was used during normobaric oxygen breathing. There was a small fall in radiation response 10 min after anaesthesia but a large rise in response by 25 min, which was still maintained at 40 min.

We interpreted this on the basis of a reversible vasodynamic response, the vasoconstricting effect of oxygen breathing being reversed by vasodilation owing to anaesthesia. The optimum pre-irradiation time interval was thus 25 min after the induction of anaesthesia when normobaric oxygen was used.

We have now used that time interval to compare the effects of air and oxygen at 1, 2 and 3 atm absolute on the radiation response of the C3H mouse mammary tumour.

Materials and methods

A serially transplanted line of C3H mouse mammary adenocarcinoma (Nias et al, 1980) was used in SPF-derived inbred C3H mice. Single doses of 25 Gy of 250 kVp X rays (0.83 mm Cu half-value thickness) were delivered at 200 cGy/min to mice breathing air or oxygen at various pressures in a chamber used for hyperbaric oxygen studies (Tozer et al, 1984), with all but the tumour shielded by 2 mm of lead. Ketamine (45 mg/kg) and diazepam (0.5 mg mouse) anaesthesia were administered by intraperitoneal injection. Tumour volume was determined from three perpendicular measurements and growth expressed in terms of the mean (± standard error (SE) of the mean) time taken by a group of tumours to reach 3.5 times the initial treatment volume, which was approximately 200 mm^3. The sizes of individual tumours were related to their individual treatment volumes. For unirradiated tumours the time to reach 3.5 times the initial volume was about 6 days for animals sham irradiated but breathing both air and oxygen, with or without anaesthesia.

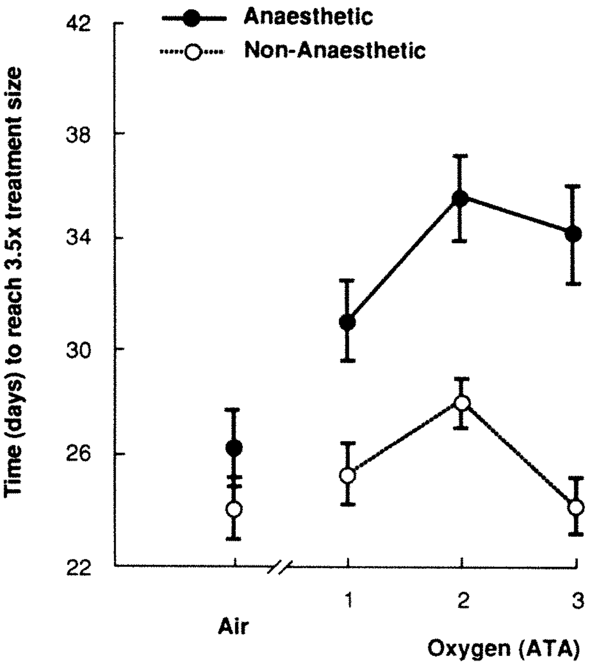

Figure 1. Growth delay of C3H mouse mammary tumours irradiated with 25 Gy in air or various atmospheres absolute (ATA) of oxygen either with or without anaesthesia. Values are shown as the mean ±SE of the mean.

Animals were placed in the hyperbaric chamber and exposed to oxygen at various pressures for 25 min before irradiation. The anaesthetized animals were injected with ketamine and diazepam 10 min before exposure to oxygen to allow time for them to be placed in the hyperbaric chamber. At least 10 animals were used for each experimental point. Statistical comparisons were made using Student's *t*-test.

Results

Figure 1 shows data pooled from two separate experiments that gave very similar results. As might be expected, there was more growth delay of tumours when the animals breathed oxygen at 1 atm absolute rather than air. There was still more growth delay when the animals breathed oxygen at 2 atm absolute but, unexpectedly, oxygen at 3 atm absolute did not lead to any further increase in growth delay.

The effects were more marked in anaesthetized animals but even the unanaesthetized animals showed the most tumour growth delay when breathing oxygen at 2 atm absolute. With 3 atm absolute these unanaesthetized animals showed a significant reduction in tumour growth delay compared with that at 2 atm absolute, which was clearly the optimum pressure of oxygen for radiotherapy in this mouse tumour system.

Discussion

There have been very few studies of the effectiveness of 2 atm absolute of oxygen in the radiotherapy of tumours. All the MRC sponsored clinical trials (Dische, 1979) employed 3 atm absolute of oxygen without anaesthesia, which is rarely used in clinical practice. Anaesthesia was not used by Gray et al (1953) in their studies of growth delay after single doses of X-rays to Ehrlich ascites tumour implanted in the mouse leg. They found an enhancement ratio of 1.5 with 1 atm absolute and 2 with 3 atm of oxygen but did not investigate the effect of 2 atm absolute.

To our knowledge, the only study comparing the effectiveness of 2 atm absolute with that of other oxygen pressures was that of Thomlinson and Craddock (1967) using the RIB5 fibrosarcoma in rats with sodium amytal anaesthesia. They also measured growth delay after single doses of X-rays to tumours implanted in the flank. Compared with a control time of 6 days (to grow from 9 to 25 mm diameter), tumours treated with 3 Gy took 30.1 days when 1 atm absolute of oxygen was used, 40.4 days with 2 atm, 39.3 days with 3 atm and 30.8 days with 4 atm absolute of oxygen. As with our own study, the maximum effect was with 2 atm of oxygen. Increasing the pressure to 3 atm produced no more growth delay and 4 atm actually reduced it.

The studies of tumour oxygenation under various pressures of oxygen made by Mueller-Klieser et al (1983) may explain these findings. They used a cryobiopsy technique to measure oxyhaemoglobin saturation values in tumours implanted into the thigh of rats anaesthetized with sodium pentobarbital. The frequency distribution curve in rats breathing air showed many values with less than 50% oxyhaemoglobin saturation. There were fewer such values with 1 atm of oxygen and even fewer with 2 atm. At that pressure of oxygen most of the oxyhaemoglobin saturation values exceeded 80%. When the rats breathed 3 and 4 atm of oxygen, there was little further change in these frequency distribution curves. These studies seem to confirm the conclusion that there is little advantage, in terms of tumour oxygenation, of increasing the pressure of oxygen breathed above 2 atm absolute, certainly in anaesthetized animals.

There is a physiological explanation for this. There is a limit to the effect of increasing the partial pressure of oxygen inspired. Since haemoglobin is 97% saturated during normal air breathing it will rapidly become saturated as the inspired gas oxygen content is increased to 100%. Once haemoglobin is completely saturated any extra oxygen carried by the blood must be carried in physical solution in the plasma. For this reason, large increases in the pressure of oxygen breathed will only increase the total amount of oxygen carried by the blood by a small amount.

Because anaesthesia was used, there is a further explanation of our findings on the basis of a reversible vasodynamic response, the vasoconstricting effect of oxygen breathing being reversed by vasodilatation as a result of anaesthesia. We had used this hypothesis to explain the results of our earlier studies where we determined the optimum time interval between the induction of anaesthesia and the irradiation of our mouse tumours

(Nias & Perry, 1989). Such a reversible vasodynamic response is even more likely to apply to our present studies: as the oxygen pressure is increased, there should be more radiobiological benefit but also more vasoconstriction, but the latter can be reversed by the vasodilating effect of anaesthesia. With such opposing mechanisms, it is reasonable to suppose that there will be a peak at one particular pressure and this is what we found at 2 atm (and a post-anaesthetic period of 35 min).

In terms of clinical application to radiotherapy practice, there would be an advantage in using the lower pressure of 2 atm of oxygen (compared with 3 atm) in being able to reduce the PIBT and "soaking" time before treatment. Our studies have shown a greater advantage of 2 atm of oxygen in mice anaesthetized with ketamine and diazepam than in unanaesthetized animals. Insofar as clinical radiotherapy is concerned, however, the addition of anaesthesia to hyperbaric oxygen would be a disadvantage.

On the other hand, we have noted a similar advantage when mice were treated using diazepam alone without ketamine (Nias et al, 1989) and that should be a feasible regime in clinical practice.

Acknowledgments

The authors are grateful to Mr J. J. Parker for scientific assistance, Dr O. C. A. Scott for helpful discussion and Mrs Valerie Nunn for typing this manuscript. This study was supported by an endowment from the Richard Dimbleby Cancer Fund.

References

Churchill-Davidson, I., Sanger, C. & Thomlinson, R. H., 1957. Oxygenation in radiotherapy. II: Clinical application. *British Journal of Radiology, 30*, 406–422.

Dische, S., 1979. Hyperbaric oxygen: The Medical Research Council trials and their clinical significance. *British Journal of Radiology, 51*, 888–894.

Gray, L. H., Conger, A. D., Ebert, M., Hornsey, S. & Scott, O. C. A., 1953. The concentration of oxygen dissolved in tissues at the time of irradiation as a factor in radiotherapy. *British Journal of Radiology, 26*, 630–648.

Mueller-Klieser, W., Vaupel, P. & Manz, R., 1983. Tumour oxygenation under normobaric and hyperbaric conditions. *British Journal of Radiology, 56*, 559–564.

Nias, A. H. W. & Perry, P. M., 1989. Variation of tumour radiosensitivity with time after anaesthetic. *British Journal of Radiology, 62*, 932–935.

Nias, A. H. W., Chamberlain, S. M. & Abdelaal, A. S., 1980. The serially transplanted C3H mouse mammary tumour as a clinically relevant model system. *British Journal of Cancer, 41*, Suppl. IV, 157.

Nias, A. H. W., Perry, P. M. & Sandhu, C., 1989. Radiosensitization by diazepam and hyperbaric oxygen. *Proceedings of the 5th European Conference on Clinical Oncology*, P-0258.

Thomlinson, R. H. & Craddock, E. A., 1967. The gross response of an experimental tumour to single doses of X rays. *British Journal of Cancer, 21*, 108–123.

Tozer, G. M., Penhaligon, M. & Nias, A. H. W., 1984. The use of ketamine plus diazepam anaesthesia to increase the radiosensitivity of a C3H mouse mammary adenocarcinoma in hyperbaric oxygen. *British Journal of Radiology, 57*, 75–80.

1992, *The British Journal of Radiology*, 65, 787–791

Treatment planning for ^{131}I-mIBG radiotherapy of neural crest tumours using ^{124}I-mIBG positron emission tomography

By R. J. Ott, PhD, D. Tait, MD, MRCP, FRCR, M. A. Flower, PhD, *J. W. Babich, MSc and †R. M. Lambrecht, PhD

Departments of Physics and Radiotherapy, Institute of Cancer Research and Royal Marsden Hospital, Sutton, Surrey, UK, *Division of Nuclear Medicine, Massachusetts General Hospital, Boston, MA 02114, USA, and †Lucas Heights Research Laboratories, New South Wales, Australia

(*Received 24 October 1991 and in revised form 11 March 1992, accepted 7 April 1992*)

Keywords: Neural crest tumours, mIBG therapy, PET

Abstract. Patients designated to receive ^{131}I-meta-iodobenzylguanadine (mIBG) for the treatment of neural crest tumours have been scanned with ^{124}I-mIBG using the MUP-PET positron camera. Uptake was detected in tumour sites in lung, liver and abdomen. The tomographic images produced have allowed estimates to be made of the concentration of mIBG in both tumour and normal tissue. From these data it is possible to predict the radiation doses that would be achieved using therapy levels (up to 11 GBq) of ^{131}I-mIBG. The levels of tumour uptake are between 0.5 and 2.0 kBq/g indicating that the radiation doses to tumour would be in the range 3 Gy to 7.5 Gy.

Many normal tissues, and tumours that derive from them, are involved in active metabolic processes, the products of which can sometimes be detected in body fluids and tissues. This can have important implications for oncology, providing a possible means of diagnosis, monitoring tumour activity after treatment and even targeting antitumour therapy.

Catecholamines are a group of substances produced by tissues of neural crest origin which act as neurotransmitters in the sympathetic nervous system. Many tumours arising from neural crest-derived structures retain this function, which may provide a method for diagnosis either through urinary catecholamine levels or by meta-iodobenzylguanidine (mIBG) scanning.

mIBG is a synthetic physiological analogue of guanethidine developed in the USA (Wieland et al, 1980). This novel radiopharmaceutical has been successfully used to image neuroblastoma and phaeochromocytoma. The *in vivo* uptake of ^{125}I-mIBG in neuroblastoma tissue has been measured from surgical samples to be in the range 0.002–0.2% of injected dose per gram (Moyes et al, 1988) confirming the possible application of ^{131}I-mIBG as a therapy agent for neural crest tumours. Several authors have reported the use of this agent in the treatment of neuroblastoma (Hoefnagel et al, 1988) and phaeochromocytoma (Khafagi et al, 1991) and their results indicate some therapeutic efficacy. However, the level of radiation dose to tumour achieved in such treatments is difficult to estimate. We have described previously the use of positron emission tomography (PET) using the tracer ^{124}I (Ott et al, 1987; Flower et al, 1989) to determine the radiation dose to thyroid disease obtained using Na^{131}I therapy. We present here the results of measurements with PET and ^{124}I-mIBG leading to estimates of the radiation dose to two patients, one with adult neuroblastoma and a second with phaeochromocytoma, who were designated to receive therapy with ^{131}I-mIBG.

Methods

Patients

Patient P.W. presented in July 1987, at the age of 43 years, with a 3-year history of weight loss. Investigation revealed an abdominal mass and a lesion suggestive of a metastasis within the liver. Biopsy of the mass provided the diagnosis of neuroblastoma with early differentiation. Treatment was instituted as for a child with neuroblastoma and he was given six courses of combination chemotherapy followed by surgical debulking. This was followed by intensive chemotherapy in the form of high-dose melphalan accompanied by autologous bone marrow rescue. Symptomatically he was improved following this, although there was no objective evidence of tumour response. A ^{123}I-mIBG scan, performed at this time as a baseline, demonstrated uptake in a large epigastric mass with a smaller tumour visible in the lower lumbar region.

Over the next 18 months the computed tomography (CT) and mIBG scan appearances were essentially stable but his condition gradually deteriorated with weight loss again being the predominant feature. As a result, he was offered ^{131}I-mIBG therapy and it was at this stage that ^{124}I-mIBG with PET was performed to estimate the likely radiation dose to be delivered to the tumours. Because of his heavy pre-treatment with chemotherapy, bone marrow was harvested and stored in case of severe marrow toxicity following the mIBG treatment.

Patient R.G. presented in 1984, at the age of 62 years, with a right suprarenal mass. This was surgically removed and histology confirmed the suspected diagnosis of phaeochromocytoma. Post-operatively his symptoms improved and over the next 4 years he was well, did not require any further treatment and was monitored for tumour activity by sequential urinary catecholamine examinations. In January 1988 the catecholamine level rose and staging investigations demonstrated two small lung metastases and three lesions in the liver. As these changes were not accompanied by the development of symptoms, he remained on a watch policy. However, by 18 months later he had lost a considerable amount of weight and had abdominal discomfort from hepatic enlargement. A diagnostic mIBG scan showed uptake within the tumour sites and he was therefore given a therapy dose (5.5 GBq) of ^{131}I-mIBG.

There was no firm evidence of tumour response to this initial therapy and when he was referred to this hospital for consideration of a second therapy dose it was felt that some estimate of the likely radiation dose achievable would be important in aiding clinical judgment of the usefulness of such a treatment.

Production of ^{124}I

^{124}I is a proton-rich iodine radioisotope with a half-life of 4.2 days making it a suitable tracer for studying agents with an extended biological action such as mIBG and monoclonal antibodies. The isotope decays via electron capture (75%) and positron emission (25%). The former decay produces several high-energy single photons, the most frequent being of energy 617 keV (62%), 723 keV (10%) and 1690 keV (10%) and these contribute a significant background to the annihilation photon signal via accidentals. The two main positron decays lead to the emission of positrons of mean energy 690 keV and 980 keV, respectively. Whilst the high single/annihilation photon emission is detrimental to the statistical quality of the images obtained, the tracer has been successfully used clinically.

Carrier-free ^{124}I was produced (by the Cyclotron Unit at the King Faisal Hospital and Research Centre in Saudi Arabia) using the ^{124}Te(d,2n)^{124}I reaction. The activity was received as a solution of NaI in aqueous NaOH. Radionuclide purity was > 99.5% at 48 h after irradiation (Lambrecht et al, 1988).

Preparation of ^{124}I-mIBG

^{124}I-mIBG was labelled using the solid-phase exchange reaction initially described by Mangner et al (1982). Cold mIBG and ammonium sulphate were obtained in kit form (CIS, IK4). Prior to the addition of the radioiodine solution to the mIBG reaction mixture, the sodium content was reduced by passing the solution through a cation exchange resin membrane (AG50W-X8, Bio-Rad). This resin had previously been converted to the H$^+$ form using 50 ml of sterile, pyrogen-free 0.1 N HCl and rinsed of residual acid with 50 ml of sterile water for injection. The resulting radioiodine solution was rendered slightly acidic (pH ~ 5). This solution was added to a sterile teflon-capped vial containing 0.3 ml of mIBG solution (3 mg/ml) and 0.3 ml of a 1 M ammonium sulphate solution. The vial was vented to a 60 ml evacuated syringe and heated to dryness in a hot block at 130°C for 1 h.

The reaction product was dissolved in 5 ml of 0.5 M acetate buffer (pH 5). Unreacted radioiodide was removed by passing the solution through a sterile anion exchange membrane (AG1-X8, Bio-Rad) carbonate form. The final product was sterilized by passage through a sterile, pyrogen-free 0.22 μm Millex-GS filter (Millipore). The radiochemical purity of the resulting product was > 95% and the specific activity was > 37 MBq/μmol.

PET imaging

The two patients (P.W. and R.G.) were injected with 22 MBq and 40 MBq of ^{124}I-mIBG, respectively, and scanned at 24 h and 48 h post-injection using the MUP-PET positron camera (Cherry et al, 1989). PET scans were taken of the liver and abdominal tumour for patient P.W. and of tumour in the lungs and liver for patient R.G. Imaging times for each study varied from 18 min to 24 min. In order to obtain an absolute measurement of the radioactivity levels in tissue, an image was acquired of a 25 cm diameter phantom filled with ^{124}I at a concentration of 9 kBq/ml. A further accidentals image of the phantom was obtained to allow for a randoms correction in the calibration.

Basic radiation dosimetry

The formula used to calculate the radiation doses that would be achieved using ^{131}I-mIBG is that described in Loevinger et al (1989). The absorbed dose (D) in Gy in any tissue is given by:

$$D = 1.44 \times Q \times T \times \Delta \times \phi / M \qquad (1)$$

where Q is the maximum activity in the tissue (MBq); T is the effective half-life of the activity in the tissue (h); Δ is the equilibrium dose constant of ^{131}I in kg Gy/MBq h; ϕ is the fraction of radiation absorbed in the tissue; and M is the mass of the tissue (kg).

We assume for the sake of simplicity that the radiation dose to the tissue of interest comes only from radioactivity within that tissue and that the photon component of the absorbed dose can be ignored in comparison to the beta dose. Hence we assume that the value of ϕ is 1.

In this study the effective half-life for therapy is obtained using the ^{124}I-mIBG PET image count density information in the tissues at 24 and 48 h assuming a mono-exponential relationship to obtain the biological half-life of the agent. Any short half-life component associated with rapid renal excretion of the agent is not included. The impracticability of making measurements at longer times post-injection also lead us to ignore any long half-life component in the tissue. Values of Q/M were obtained from the voxel count density levels in the

Table I. ROI analysis results for patient P.W. (22 MBq injected activity)

	Time post-injection (h)		
	24	48	
Abdominal uptake (MBq)	5.7	3.7	
Normal liver uptake (kBq/g)	0.93	0.55	
Abdominal uptake (kBq/g)	1.23	0.68	
	Whole abdomen	Normal liver	Abdominal tumour
Biological half-life (h)	65	53	59

Table II. ROI analysis results for patient R.G. (40 MBq injected activity)

	Time post-injection (h)		
	24	48	
Abdominal uptake (MBq)	6.2	3.0	
Thorax uptake (MBq)	6.9	3.3	
Liver tumour uptake (kBq/g)	1.8	0.9	
L. lung tumour uptake (kBq/g)	1.5	0.6	
R. lung tumour uptake (kBq/g)	1.4	0.7	
	Liver tumour	L. lung tumour	R. lung tumour
Biological half-life (h)	28	24.5	34.5

Table III. Predicted radiation doses for 11 GBq ^{131}I-mIBG

Organ/tissue	Radiation dose (Gy)
Patient P.W.	
Whole body	0.65
Normal liver	4.7
Abdominal tumour	7.4
Patient R.G.	
Whole body	0.38
Liver tumour	3.6
L. lung tumour	3.3
R. lung tumour	3.1

patient images calibrated with those in the phantom images.

Results

All images were reconstructed using the 3D back-projection and deconvolution method described in Clack et al (1984) and corrected for attenuation, detector dead-time and accidentals.

Analysis of the cylindrical phantom data gave a calibration factor of 4370 acquired counts per minute per MBq in the camera field-of-view. The random signal from ^{124}I at these activity levels is ~ 25%. This calibration factor was used to determine the total activity in the field-of-view of the camera for each patient scan.

The PET images of the patients at 24 and 48 h showed uptake in tumours and normal tissue of both patients. Low count rates were indicative of the limited uptake in both tumour and normal tissue. For patient P.W. it is estimated that the total activity remaining in the camera field of view was 5.7 MBq and 3.7 MBq at 24 and 48 h, respectively, leading to an abdominal biological half-life of 65 h. For patient R.G. the equivalent numbers were 6.2 MBq and 3.0 MBq in the thorax and 6.9 MBq and 3.3 MBq in the abdomen leading to biological half-lives of 30 h in both cases.

A region of interest analysis using ANALYSE (Robb, 1990) was carried out to determine the count density and hence uptake in the normal liver and abdominal tumour of patient P.W. and in tumour in left and right lungs and liver of patient R.G. The results of this analysis (Tables I, II) are presented as the maximum values of activity per unit tissue mass (density assumed to be 1 g cm^{-3}) obtained within each region of interest. These values cover the range 0.55–1.23 kBq/ml for patient P.W. and 0.6–1.8 kBq/ml patient R.G. The biological half-lives determined were 53 h (liver) and 59 h (tumour) for patient P.W. and 24.5 h (left lung tumour), 34.5 h (right lung tumour) and 28 h (liver tumour) for patient R.G.

From these data it was possible to calculate the maximum absorbed dose (Table III) that would be achieved using ^{131}I-mIBG for therapy. The values range from 3.1 to 7.4 Gy for an administered activity of 11 GBq. Whole-body absorbed doses were calculated assuming 50% of the activity was removed with an initial 8 h effective half-life (Lashford et al, 1988; Fielding et al, 1991) and the rest with the longer abdominal or thoracic half-lives determined above. The values of predicted whole-body dose obtained for an 11 GBq administration were 0.65 Gy (patient P.W.) and 0.38 Gy (patient R.G.).

Discussion

The major advantages of using PET to provide dosimetry data for this study are the increased sensitivity and spatial resolution of the camera and the intrinsic quantitative nature of the data. The alternative, using SPECT with single photon tracers, gives greatly reduced image quality especially in the abdomen and the quantitative accuracy is correspondingly poorer. The concept of relating the tissue radioactivity concentrations directly to radiation dose is limited by partial volume effects of the method but are again significantly less of a problem using PET. The method obviates the need to measure accurately the functioning tissue volume and allows some estimate of the range of dose achieved if the agent uptake is heterogeneous.

As indicated above, the overall uptake of ^{124}I-mIBG in tumour and normal tissue was not large in these patients, leading to very modest total count levels in the PET images. However, the 3D reconstruction of intrinsically quantitative data allowed us to make estimates of radiopharmaceutical uptake in tissue. Using conventional assumptions about the relationship between time–activity concentration and absorbed dose it was possible to determine the likely macroscopic radiation dose to tumour and normal tissue from therapy levels of ^{131}I-mIBG. The impracticability of imaging patients at longer times has forced us to assume that the activity concentration measurements made at 24 and 48 h are sufficient to describe the major excretion phase of the agent.

In a 70 kg man, a uniform distribution of the agent, assuming no decay or excretion, would lead to an average tissue concentration of 0.0014% dose/g. This number is to be compared with 0.007% dose/g in normal liver and a maximum of 0.01% dose/g in tumour (patient P.W.). These levels are at the lower end of the range of those measured in neuroblastoma tissue samples and indicate a limited specific localization in these particular tissues.

Additionally, the biological half-life of the agent in all tissues was never greater than 65 h over the period of measurement. We have assumed that there is a rapid excretion phase which, in neuroblastoma, removes at least 50% of injected activity in the first 8 h (Lashford et al, 1988). This phase will, however, change the localized tissue dosimetry very little as the majority of activity so excreted is likely to remain firmly in the blood pool.

The main source of error in these measurements is associated with the reconstructed count levels in the images. We estimate that uncertainties from this source may lead to an overestimate of the absorbed dose by 15–25%. However, this is likely to be largely cancelled by the underestimate caused by ignoring any long half-life component.

The combination of relatively low uptake and modest biological half-life leads to estimated absorbed doses to tumour well below those required for effective therapy. The cause of the low uptake may be a combination of high tumour mass, limited vascular access and the variable capacity of phaeochromocytoma and adult neuroblastoma to accumulate mIBG compared with childhood neuroblastoma. It may also be possible that the uptake and half-life of mIBG given at therapy levels (5–11 GBq) may be different, although the values of half-life presented here are totally consistent with those measured for ^{131}I-mIBG therapy of neuroblastoma (Fielding et al, 1991).

The level of radioactivity that can be given to a patient is determined either by the patient tolerance or the safety of the staff handling the activity and nursing the patient. The 11 GBq proposed here as an upper limit is based on the second of these criteria. With this level of activity the whole-body doses to these patients would be well tolerated. It was not possible here to assess bone marrow toxicity, which is likely to be the limiting factor. Hence it may be possible to increase the activity given in some cases. It seems unlikely in the case of these two patients that a significant therapeutic effect could be achieved by increasing the activity given.

In patients where a higher uptake is achieved, especially those with bone marrow involvement, it might be necessary to reduce the activity given to below 11 GBq because of haematological toxicity and here levels of blood activity will be important.

Subsequent to these studies patient P.W. became very unwell and was given 11 GBq of ^{131}I-mIBG as there was no previous clinical experience of response to mIBG with this patient at our centre. However, this patient's condition deteriorated too rapidly to assess whether there was any response. For patient R.G. the ineffectiveness of the initial therapy and the low predicted dose combined with the relatively mild clinical symptoms lead to a decision not to treat further with mIBG.

Conclusions

The first results of attempts to predict the absorbed dose to whole body, normal liver and several tumour sites in two patients with neural crest tumours designated to receive ^{131}I-mIBG therapy are presented. It was concluded that the level of radiation dose achievable with a maximum activity of 11 GBq of this agent would be subtherapeutic for these two patients.

Acknowledgments

The authors would like to acknowledge the contribution of B. Pratt and B. Cronin, especially for their efforts with the PET scanning. This work is supported by the Cancer Research Campaign.

References

Cherry, S. R., Marsden, P. K., Ott, R. J., Flower, M. A., Webb, S. & Babich, J. W., 1989. Image quantification with a large area multiwire proportional chamber positron camera (MUP-PET). *European Journal of Nuclear Medicine, 15,* 694–700.

Clack, R., Townsend, D. & Jeavons, A., 1984. Increased sensitivity and field of view for a rotating positron camera. *Physics in Medicine and Biology, 29,* 1421–1431.

Fielding, S. L., Flower, M. A., Ackery, D., Kemshead, J. T., Lashford, L. S. & Lewis, I., 1991. Dosimetry of iodine 131 metaiodobenzylguanidine for treatment of resistant neuroblastoma: results of a UK study. *European Journal of Nuclear Medicine, 18,* 308–316.

Flower, M. A., Schlesinger, T., Adam, I., Massomi, A. M., Hinton, P. J. & McCready, V. R., 1989. Radiation dose assessment in radioiodine therapy. Part II: practical implementation using quantitative scanning and PET, with clinical results on thyroid carcinoma. *Radiotherapy and Oncology, 15,* 345–357.

Hoefnagel, C. A., de Kraker, J. & Voute, P. A., 1988. Radionuclide treatment of neuroblastoma using I-131 metaiodobenzylguanidine. In *Molecular Biology and Genetics of Childhood Cancers: Approaches to Neuroblastoma,* ed. by M. Sluyser and P. A. Voute (Ellis Horwood, Chichester), pp. 107–120.

Khafagi, F. A., Shapiro, B., Fischer, M., Sisson, J., Hutchinson, R. & Beierwaltes, W. H., 1991. Phaeochromocytoma and functioning paraganglioma in childhood and adolescence: role of iodine 131 metaiodobenzylguanadine. *European Journal of Nuclear Medicine, 18,* 191–198.

Lambrecht, R. M., Sajjad, M., Qureshi, M. A. & Al-Yanbawi, S. J., 1988. Production of iodine-124. *Radioanal Nucl. Chem. Letts, 127,* 143–150.

LASHFORD, L. S., MOYES, J., OTT, R. J., FIELDING, S. L., BABICH, J. W., MELLER, S., GORDON, I., EVANS, K. & KEMSHEAD, J. T., 1988. The biodistribution and pharmacokinetics of metaiodobenzylguanidine in childhood neuroblastoma. *European Journal of Nuclear Medicine, 13,* 574–577.

LOEVINGER, R., BUDINGER, T. F., WATSON, E. E., et al (eds), 1989. *MIRD Primer for Absorbed Dose Calculations* (Society of Nuclear Medicine, New York).

MANGNER, T. J., WU, T. J. & WIELAND, D. M., 1982. Solid-phase exchange radioiodination of aryl iodides. Facilitation by ammonium sulphate. *Journal of Organic Chemistry, 47,* 1484–1488.

MOYES, J. S. E., FIELDING, S. L., FLOWER, M. A., BABICH, J. W., MCCREADY, V. R., MELLER, S. T. & AGRAWAL, M., 1988. Quantitative uptake of ^{131}I-MIBG in neuroblastoma: attempted correlation of two techniques of dose calculation. In *Radioactive Isotopes and Clinical Medicine and Research,* ed. by R. Hofer and H. Bergman (Schattauer), pp. 325–331.

OTT, R. J., BATTY, V., WEBB, S., FLOWER, M. A., LEACH, M. O., CLACK, R., MARSDEN, P. K., MCCREADY, V. R., BATEMAN, J. E., SHARMA, H. & SMITH, A., 1987. Measurement of radiation dose to the thyroid using positron emission tomography. *British Journal of Radiology, 60,* 245–251.

ROBB, R. A., 1990. A software system for interactive and quantitative analysis of biomedical images. In *3D Imaging in Medicine,* ed. by K. H. Hohne, H. Fuchs and S. M. Pizer, NATO ASI Series, Vol. F60, pp. 333–361.

WIELAND, M., WU, J. I., BROWN, L. E., MANGER, T. J., SWANSON, D. P. & BEIERWALTES, W. H., 1980. Radiolabelled adrenergic neuron-blocking agents: adrenomedullary imaging with I-131 iodobenzylguanidine. *Journal of Nuclear Medicine, 21,* 349–354.

1992, *The British Journal of Radiology*, 65, 792–798

A pilot study of accelerated fractionation in the radiotherapy of invasive carcinoma of the bladder

By D. J. Cole, K. R. Durrant, *J. T. Roberts, *P. J. T. K. Dawes, †H. Yosef and §J. W. Hopewell

Department of Radiotherapy and Oncology, Churchill Hospital, Oxford, *Regional Radiotherapy Centre, Newcastle General Hospital, Newcastle upon Tyne, †Beatson Oncology Centre, Belvidere Hospital, Glasgow and §C.R.C. Normal Tissue Research Group, Research Institute (University of Oxford), Churchill Hospital, Oxford, UK

(*Received 14 October 1991 and in revised form 24 February 1992, accepted 26 March 1992*)

Keywords: Bladder cancer, Radiotherapy, Accelerated fractionation

Abstract. 24 patients with muscle invasive carcinoma of the bladder were treated in a pilot study of twice daily fractionation at radiation doses of 1.8–2.0 Gy per fraction to total doses of 54–64 Gy to the bladder and 39.6–44 Gy to the whole pelvis. The treatment aim was to give 32 fractions in 22 days. The interfraction interval was a minimum of 6 h. The principle objective was to record acute and late tolerance, but local control and survival data is also presented. Acute radiation morbidity was scored according to the RTOG system. Grade 2 large bowel effects were seen in 52% of patients, Grade 3 effects in 26% and there was one Grade 4 and one Grade 5 effect. The mean duration of effect was 4.5 weeks although the more severe reactions were also more protracted. Grade 2 urinary effects occurred in 30% and Grade 3 in 17% of patients. The mean duration of effect was 7.2 weeks. There were no Grade 4 or 5 acute urinary effects. Late radiation morbidity was scored according to the EORTC/RTOG system and was assessable in 16 cases who survived more than 6 months. There were two cases (12%) of Grade 1 bowel toxicity, two cases of Grade 1 and three of Grade 2 urinary toxicity. There were no cases of late skin effects. Actuarial analysis at 2 years shows a local control probability of 56% and survival probability of 35%.

The 5-year survival of patients with muscle invasive transitional cell carcinoma of the bladder treated by radical radiotherapy or combined pre-operative radiotherapy and elective radical cystectomy is 40% for T2 tumours (Duncan & Quilty, 1986) and 29–38% for T3 tumours (Bloom et al, 1982). Following radical radiotherapy, complete response in the bladder occurs in up to 56%, but one third of these responders subsequently fail locally (Shearer et al, 1988). Survival in patients treated by irradiation has not been improved by adjuvant methotrexate (Shearer et al, 1988) or cisplatin (Wallace et al, 1991) chemotherapy.

The short latency times to local recurrence after radiotherapy in invasive transitional cell carcinoma of the bladder indicate that the disease is biologically aggressive (Duncan & Quilty, 1986). Moderate or poor histological differentiation is reported in 66% of T2 and 89% of T3 tumours (Duncan & Quilty, 1986), Cell kinetic studies demonstrate rapid proliferation of tumour clonogens with a potential doubling time of 3 days (Trott & Kummermehr, 1985; Sheehan & Newman, 1991). It has been demonstrated that acutely responding normal tissue undergoes accelerated clonogen repopulation starting at between 14 and 28 days following the start of a conventionally fractionated course of irradiation (Morris & Hopewell, 1986). It has also been suggested that rapidly proliferating tumours undergo considerable clonogen repopulation during a lengthy course of irradiation (Trott & Kummermehr, 1985) and that this phenomenon is an important cause of local failure in treatments involving conventional fractionation schedules (Fowler, 1986).

A reduction in the overall treatment time for radiotherapy may reduce the capacity for tumour clonogens to repopulate and thereby improve local control in invasive bladder cancer. However, this cannot be achieved by an increase in the dose per fraction if late responding tissues are to be spared injury (Quilty et al, 1985) and therefore multiple fractions per day are necessary if the required dose is to be delivered in a shorter time. The fractions of radiation must be given at least 6 h apart to allow for the repair of sublethal damage. However, even with this interfraction interval, repair may not be complete (Hopewell and van den Aardweg, 1988, 1989; Turesson and Thames, 1989) and a small decrease in dose per fraction may be required to compensate for this.

This paper presents the results of a pilot study of accelerated fractionation in invasive bladder cancer which was carried out to investigate the potential toxicity of such a schedule. All patients have had a minimum of 12 months follow-up.

Materials and methods

Patients with invasive carcinoma of the bladder with no evidence of nodal or distant metastasis who were suitable for radical irradiation with curative intent were selected for this study. Eastern Co-operative Group (ECOG) performance status 0–2 and normal (or only slightly elevated) serum creatinine were required for entry, but patients over the age of 75 years were generally excluded. Later in the study, those with a history of inflammatory bowel disease, previous lower abdominal or pelvic surgery were excluded.

Patients underwent cystoscopy, biopsy and usually endoscopic resection of tumour, and bimanual examination of the pelvis under anaesthetic. Haemoglobin, serum creatinine and liver function tests were measured. Computed tomography of the abdomen and pelvis was performed to exclude nodal and metastatic disease.

24 patients were entered into this pilot study. There were 18 males and six females. The mean (±SD) age at entry was 66.4±6.3 years. There were 21 cases of transitional cell carcinoma (TCC), two cases of squamous carcinoma (SCC) and in one case the histological type was not stated. There were six T2, 14 T3 and four T4 cases. In 19 cases the grade was reported, three were Grade 2 (moderately differentiated) and 16 were Grade 3 (poorly differentiated).

Radiotherapy was planned using computed tomography localization and treatment was given on linear accelerator machines of energy 6–8 MV. The whole pelvis was treated during the first week of treatment (10 fractions), the bladder alone was treated during the second week (10 fractions) and treatment to the whole pelvis was completed during the third or early fourth week in 10–12 fractions. The pelvic volumes were treated with three or four field techniques in all but three cases in which an anterior and posterior pair of fields were used. The bladder volumes were all treated with three or four field plans. Two treatments were given each day, 5 days per week and these treatments were given not less than 6 h apart. The intention was to deliver a radical dose of radiation in 30–32 fractions in 15–16 treatment days (treating 5 days per week) with an overall time of 19–22 days. Three centres contributed patients to the study and differences in local practice accounted for the slight differences in dose prescription. Of the 24 patients entered into the study, the first 13 were treated at 2.0 Gy per fraction and the remaining 11 received 1.8 Gy per fraction. The dose per fraction (and consequently the total dose) was reduced because of concern regarding acute toxicity. The mean (±SD) dose delivered was 58.85±2.2 Gy with a range of 54–64 Gy. The mean number of fractions was 30.8±1.1 (range 29–32). The mean overall time was 22.7±5.3 days (range 19–44). A protracted skin reaction led to an overall treatment time of 44 days in one patient. Otherwise the maximum treatment time was 29 days. The mean target volume for the whole pelvis was 3030±961 cm^3 (range 1755–5486) and for the bladder 925±313 cm^3 (range 427–1595).

Response was scored at follow-up cystoscopy which was performed at 6-monthly intervals after radiotherapy. Patients with local failure were considered for salvage cystectomy. Normal tissue toxicity was recorded using the RTOG criteria for early effects and RTOG/EORTC criteria for late effects (see Tables I(a) and (b)). Early effects were scored weekly during treatment and then at 4, 6 and 12 weeks after starting treatment. Late effects were scored at 6 months and then annually.

Results

Acute toxicity

Acute large bowel toxicity was assessable in 23 patients and is shown in a histogram in Fig. 1. It can be seen that the majority of patients (78%) encountered Grade 2 toxicity (diarrhoea requiring medication) or Grade 3 toxicity (requiring hospital admission or intravenous fluids). The mean duration (in weeks) of toxicity for each grade is stated on the histogram.

There was one case of Grade 4 large bowel toxicity. This patient completed irradiation to a dose of 57.6 Gy in 32 fractions in 24 days without problems and then 1 week later developed severe diarrhoea, anorexia,

Table I. (a) Radiaton Therapy and Oncology Group (RTOG) acute radiation morbidity scoring criteria

Tissue	Grade 0	Grade 1	Grade 2	Grade 3	Grade 4
Skin	No change	Erythema, dry desquamation	Painful erythema, patchy moist desquamation	Confluent moist desquamation	Ulceration, haemorrhage and necrosis
Small bowel	No change	Nausea	Nausea/vomiting requiring anti-emetics	Requiring i.v. fluids	Requiring surgery
Large bowel	No change	Loose stool	Diarrhoea requiring medication	Requiring i.v. fluids	Obstruction fistula, perforation requiring surgery
Genitourinary	No change	Frequency ×2 baseline	Frequency > hourly, dysuria	Frequency < hourly, dysuria requiring opiate	Haematuria requiring transfusion, ulceration, necrosis

i.v. = intravenous.

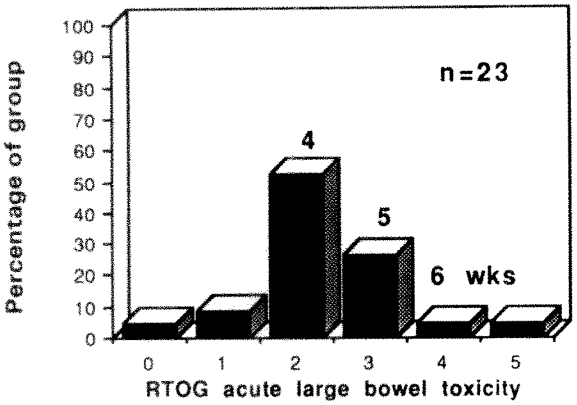

Figure 1. Histogram showing the distribution of acute large bowel toxicity following accelerated fractionation. The number above the columns indicate the mean time to resolution of symptoms after completion of therapy.

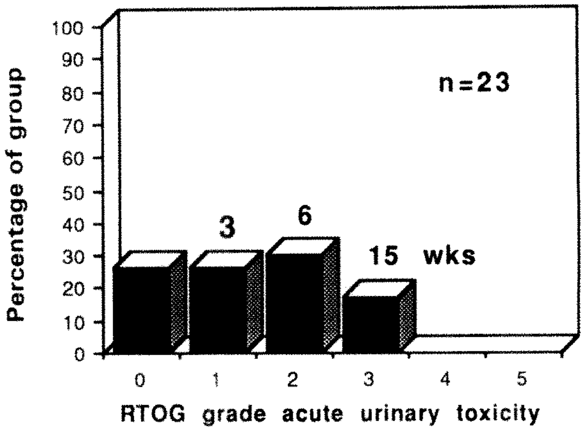

Figure 2. Histogram showing the distribution of acute urinary toxicity following accelerated fractionation. The numbers above the columns indicate the mean time to resolution of symptoms after completion of radiotherapy.

vomiting and weight loss. She was admitted to hospital with intestinal obstruction and at laparotomy found to have an ileus. A defunctioning colostomy was performed and she made a slow but complete recovery over 8 weeks. 18 months later she developed abdominal carcinomatosis and underwent another laparotomy at which time no sequelae attributable to the radiation were found. This patient had a history of appendectomy followed by ureteric surgery for reflux uropathy about 30 years previously.

There was one case of Grade 5 large bowel toxicity. In this case there was an ileo-vesical fistula, probably due to malignancy prior to the start of radiation. Treatment was completed to 60 Gy in 30 fractions in 27 days and 2 weeks later total colectomy was performed for perforated diverticulitis and peritonitis from which the patient succumbed within a month.

The acute urinary toxicity is shown in Fig. 2. It is notable that Grade 3 toxicity (frequency and nocturia < hourly and/or pain requiring strong analgesics) was unusual (17% of cases), but that it was relatively prolonged with a mean duration of 15 weeks. In one of these cases, severe dysuria and frequency persisted for 9 months but was eventually relieved with an antispasmodic agent.

The mean duration of acute urinary effects was 5.4 weeks compared to 3.4 weeks for acute large bowel effects and this difference was significant ($p = 0.045$, *t*-test).

There was one case of Grade 3 skin reaction (confluent moist desquamation). An interruption in treatment was required and the final dose was 58 Gy in 29 fractions in 44 days. Otherwise there were three cases of Grade 2 toxicity and seven cases of Grade 1 toxicity. In all cases the acute skin reaction had healed 3 weeks after the completion of treatment. The remaining 12 cases showed no toxicity.

Table I. (b) RTOG/European Organisation for Research into the Treatment of Cancer (EORTC) late radiation morbidity scoring scheme

Tissue	Grade 0	Grade 1	Grade 2	Grade 3	Grade 4
Skin	None	Mild atrophy, mild alopecia, ± pigmentation	Moderate t'g'ectasis*, complete alopecia	Gross atrophy and t'g'ectasis*	Ulceration
Bowel	None	Mild diarrhoea. Slight rectal bleeding	Diarrhoea > 5/day, requiring surgery	Obstruction or bleeding fistula	Necrosis, perforation
Genitourinary	None	Microscopic haematuria	Frequency, intermittent macroscopic haematuria	Severe frequency, frequent haematuria. Contracted bladder	Necrosis, Contracted bladder (< 100 ml). Severe haemorrhage

*telangiectasis
Any fetal toxicity is Grade 5.

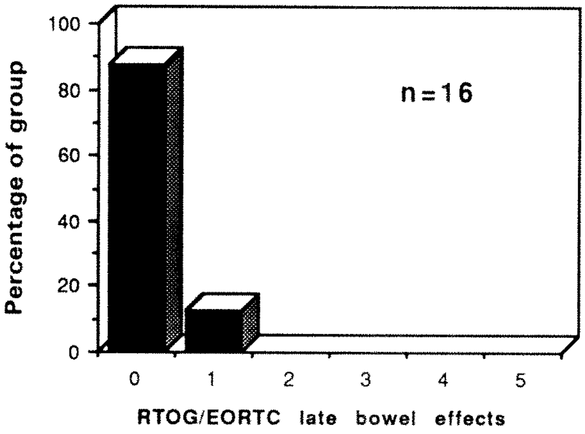

Figure 3. Histogram showing the distribution of late bowel toxicity following accelerated fractionation.

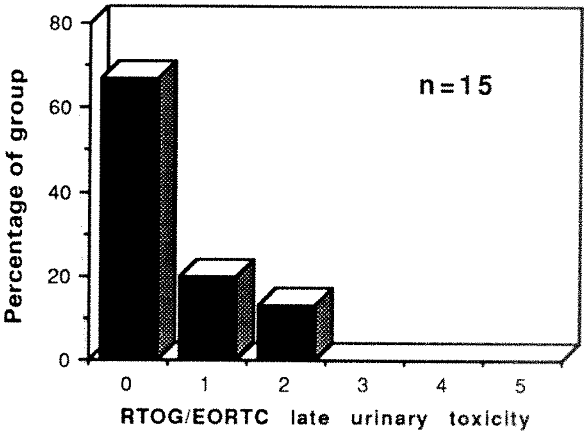

Figure 4. Histogram showing the distribution of late urinary toxicity following accelerated fractionation.

There was only one case of Grade 4 small bowel toxicity. This was the case described above who also had Grade 4 large bowel toxicity. Otherwise, there were three cases of Grade 2 toxicity, 10 Grade 1 and nine Grade 0.

The influence of age, dose, dose per fraction, overall treatment time, pelvis target volume and bladder target volume on severity and duration of acute bowel and urinary toxicity was examined using the Mann-Whitney test for ordinal data, and χ^2 for comparing the two groups treated with 1.8 Gy and 2.0 Gy per fraction. No significant associations were found.

Late toxicity

Late effects were assessable in 16 patients. The distribution of late bowel effects is shown in Fig. 3. Clinical symptoms were recorded in two patients (12% of the group) and in both these cases they were Grade 1. Figure 4 shows the distribution of late urinary effects. Grade 2 effects occurred in 13% and Grade 1 effects in 20% of patients. No late skin effects were seen. There was one patient who developed a non-invasive recurrence which was cysto-diathermied and he proceeded to cystectomy because of suspicion of local relapse with muscle invasive disease. The procedure was complicated by severe fibrosis around the bladder, but the pathological specimen showed no evidence of invasive tumour. This patient subsequently developed lower pelvic sepsis due to a chronic discharging perineal sinus and has undergone three surgical procedures in an attempt to control the problem. This late effect has been categorized as Grade 4 although clearly the morbidity arose from a combination of radiotherapy and surgery. Despite these problems the patient has maintained an ECOG performance status of 1.

Outcome

Local control was evaluable at 6 months or later after the start of treatment in 16 patients. Eight patients were not evaluable for local control: three died within 6 months from metastatic disease, one died shortly after treatment following colectomy for perforated diverticulitis and follow-up information is insufficient in another four. Seven patients had persistent or recurrent disease in the bladder and this was manifest in all cases within 12 months from the start of treatment. Nine patients had durable local control after 12–51 months from treatment. The actuarial local control at 24 months was 56%.

Distant control was assessable in 21 patients. Insufficient follow-up information was available in the other three. There were eight distant failures and six of these died within a year.

Actuarial survival in all 24 patients at 24 months was 35%. There were 14 deaths, eight from metastatic disease, four from local failure (two of whom also had metastatic disease), there was one toxic death, one death from other causes and in two cases the cause of death was unknown. The probabilities associated with local control and survival are illustrated graphically in Fig. 5.

Discussion

The feasibility of reducing the overall time in radical radiotherapy by multiple daily treatments critically depends on the tolerance of the associated acutely responding normal tissues. This "tolerance" is not easily defined and there is considerable variation among patients and radiotherapists as to what degree of toxicity is acceptable.

In this small pilot series the incidence of Grade 3 or greater acute bowel effects was 35%. One patient developed intestinal obstruction secondary to an ileus requiring laparotomy and defunctioning colostomy (Grade 4) and another died after colectomy for perforated diverticulitis (Grade 5). These two patients had prior abdominal surgery and inflammatory bowel disease, respectively and such patients were subsequently excluded from entry to our study. Nevertheless

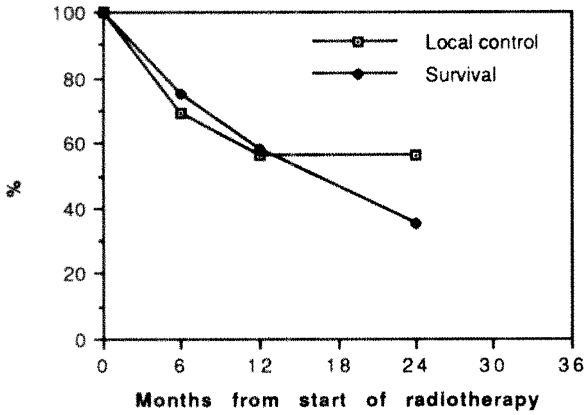

Figure 5. Graph of actuarial local control and survival at 24 months in 24 patients with muscle invasive carcinoma of the bladder treated with twice daily irradiation.

acute radiation reactions requiring operative intervention or those proving fatal are not acceptable unless they are very rare events. A substantial incidence of Grade 3 reactions are acceptable to some patients and radiotherapists provided there is evidence for improved local control and preferably survival.

Grade 3 acute urinary effects occurred in 17% of our patients and in these cases this persisted for a mean of 15 weeks. It is often difficult to separate the symptoms attributable to persistent tumour from those due to radiation effect, but nevertheless it is likely that a significant proportion of this morbidity was radiation related.

There have been other reports of serious reactions to accelerated radiotherapy in bladder cancer. In one case a female aged 77 years received 60 Gy in 30 fractions in 19 days and suffered a perforated sigmoid colon 2 months after the completion of treatment from which she died. Post-mortem confirmed that she had suffered a treatment related death. In another case, a patient developed life-threatening intestinal obstruction after receiving 44 Gy (24 Gy to the whole pelvis) in 22 fractions in 3 weeks. Spontaneous recovery occurred with conservative management. Review of the computed tomography scans showed adhesions of small bowel to the bladder (Horwich, 1991).

The acute toxicity initially seen in the present study and that encountered by others led to a reduction in dose per fraction from 2.0 Gy to 1.8 Gy, although the case of Grade 4 acute bowel toxicity was treated at 1.8 Gy per fraction. This reduction in dose per fraction is supported by the results of recent animal studies which have suggested that sublethal damage is not completely repaired in acutely responding normal tissue even with a 6 hour interfraction interval (van den Aardweg & Hopewell, 1992). It has not been possible to demonstrate a reduction in acute radiation morbidity following this reduction in dose per fraction, although this may be due to the small number of patients in each treatment group.

It is likely that the acute bowel toxicity observed is largely explained by the inclusion of most of the true pelvis in the target volume up to 39.6–44.0 Gy in order prophylactically to treat the regional lymph nodes, although treatment to the larger volume was interrupted for 1 week whilst the bladder boost was delivered. The argument for treating the lymph nodes was based on a series of cases who received pre-operative radiation and cystectomy (Wallace and Bloom, 1976). The incidence of pathologically positive lymph nodes was lower than in a matched group of historical controls treated by surgery alone. However, no survival benefit attributable to nodal downstaging was identified. More recently, a retrospective analysis of 731 patients (Symonds et al, 1990), of whom 395 underwent irradiation to the primary and regional lymph nodes, and 336 historical controls matched for stage and total dose were treated to the bladder only, showed no survival difference. Moreover serious complications occurred in 9.6% of the group receiving nodal irradiation versus 4.3% in the group treated to the bladder only.

A Phase I study of acute toxicity following a similar accelerated fractionation regimen in invasive bladder cancer found a lower incidence of acute bowel toxicity (Horwich, 1991). Maximum acute bowel toxicity was noted at the completion of treatment, at which time 30% of the group had Grade 2 effects and there were no Grade 3 effects, although one patient had had a Grade 3 effect requiring a rest from treatment for 1 week after an accumulated dose of 40 Gy. In this study the maximum bladder toxicity was also seen at the end of treatment, with 10% Grade 2 effects and 20% Grade 3 effects. The Grade 3 bladder toxicity had improved after 4, 3, 5 and 4 weeks, respectively, after onset. Most of the patients in this study were treated to a small volume encompassing the bladder only, thereby excluding a significant volume of small and large bowel.

The importance of clonogen repopulation as a cause of therapeutic failure in clinical radiotherapy has still to be demonstrated in randomized controlled trial. The possible benefits of shortening the overall treatment time could be counterbalanced by recent evidence suggesting that longer overall treatment times may lead to greater cell cycle synchrony and therefore increased radiosensitivity (Hopewell & van den Aardweg, 1991). This work indicates that longer treatment times (*i.e.* 5–6 weeks) may be associated with more severe acute responses for skin than short courses (*i.e.* 2–4 weeks).

The rate of clonogen doubling is in the region of 3–6 days for most invasive transitional cell tumours of the bladder (Trott & Kummermehr, 1985; Sheehan & Newman, 1991). There is evidence in normal tissues that fractionated radiation stimulates an increased rate of clonogen proliferation among surviving cells and that in pig skin this effect occurs at between 14 and 28 days after the start of radiation (Morris & Hopewell, 1986). It is not known whether a similar pattern for the kinetics of repopulation holds for tumours.

A method of comparing the radiobiological effect of different fractionation regimens has been proposed

Table II. Extrapolated response doses for a variety of treatment schedules

Regimen			Extrapolated response doses (Gy)	
Dose (Gy)	Fractions	Days	Tumours	Late responding tissue
"Oxford regimens"				
60	30	40	53.5	99.6
64	32	44	56.5	106.2
54	18	44	51.7	108
"Manchester regimens"				
50	20	26	50.5	91.6
55	22	30	54.9	100.8
"Accelerated regimens"				
57.6	32	24	56.9	92.2
61.2	34	25	60.7	97.9
64.8	36	26	64.5	103.7

(Fowler, 1990). This method uses the linear quadratic formula to obtain an extrapolated response dose (ERD) for a given alpha/beta ratio. It incorporates a time factor which may be used for tumours but omitted for late responding tissues, and uses the potential doubling time as a measure of proliferative capacity in the tumour and is expressed as follows:

$$ERD = \text{Total dose } (1 + d/[\alpha/\beta] - 0.693/a(T/T_{pot}) \quad (1)$$

The following assumptions are made: $a = 0.3$ (*i.e.* 49% survival at 2 Gy); potential doubling time ($T_{pot} = 5$ days); constant proliferation throughout 39 days; $d =$ dose per fraction; $\alpha/\beta =$ alpha/beta ratio for the tissue in question; $T =$ overall time.

Using this method, different fractionation regimens may be compared. The extrapolated response dose is expressed in grays for a given alpha/beta ratio (*e.g.* 10 Gy for tumours and 3 Gy for late responding tissue). The extrapolated response doses for a variety of treatment schedules are shown in Table II. This model predicts that the regimen previously used in Oxford (54 Gy in 18 fractions in 44 days) is associated with the greatest chance of late toxicity, closely followed by the conventional daily regimen of 64 Gy in 32 fractions in 44 days. The accelerated regimens are predicted to have lower late toxicity. The extrapolated dose–response values for tumours are substantially higher for the accelerated regimens than the conventional "Oxford" regimens for a given extrapolated dose–response value for late responding tissue, thus predicting a higher tumour control probability for acceleration. It is also notable that the schedule used in the second half of our study (57.6 Gy in 32 fractions in 24 days) has an extrapolated response dose for tumours that is almost indentical to the conventional daily regimen of 64 Gy in 32 fractions in 44 days. According to this model, therefore, 57.6 Gy in 32 fractions in 24 days does not offer a higher probability of tumour control than a daily regimen of 64 Gy in 32 fractions.

It should be emphasized that this model relies on estimates of alpha/beta ratios and potential doubling times for which there is little conclusive evidence at the present time and more data is awaited. It should be stressed that fractionation regimens should be developed in the light of previous clinical data although in the future it may be possible to tailor regimens to the kinetics of individual tumours.

Based on our clinical experience and bearing in mind these theoretical considerations our next step is to investigate a twice daily regimen over 25–26 days at 1.8 Gy per fraction to a total dose of 61.2–64.8 Gy. The patients will not be treated over the weekend. We will treat the bladder only and there will be 6 h between the twice daily fractions. If this regimen proves to be adequately tolerated, then it is hoped to test its efficacy compared to conventional radiation schedules in a randomized trial.

In summary, the local control and survival in this small pilot series are at least comparable to other published series and this provides a strong stimulus to continuing the investigation of twice daily fractionation schedules in bladder cancer.

References

BLOOM, H. J. G., HENDRY, W. F., WALLACE, D. M. & SKEET, R. G., 1982. Treatment of T3 bladder cancer: controlled trial of pre-operative radiotherapy and radical cystectomy versus radical radiotherapy. *British Journal of Urology, 54*, 136–151.

DUNCAN & QUILTY, P. M., 1986. The results of a series of 963 patients with transitional cell carcinoma of the urinary bladder primarily treated by radical megavoltage X-ray therapy. *Radiotherapy and Oncology, 7*, 299–310.

FOWLER, J. F., 1986. Potential for increasing the differential response between tumours and normal tissues: can proliferation be used? *International Journal of Radiation Oncology, Biology and Physics, 12*, 641–645.

FOWLER, J. F., 1990. Fractionation in radiotherapy. Proceedings of 32nd Annual ASTRO Meeting. *International Journal of Radiation Oncology, Biology and Physics, 19*, Suppl. 1, p. 113.

HOPEWELL, J. W. & VAN DEN AARDWEG, G. J. M. J., 1988. Current concepts of dose fractionation in radiotherapy. Normal tissue tolerance. *British Jounral of Radiology* (Suppl), *22*, 88–94.

HOPEWELL, J. W. & VAN DEN AARDWEG, G. J. M. J., 1989. Kinetics of recovery from sublethal radiation damage. *British Journal of Radiology, 62*, 1009–1010.

HOPEWELL, J. W. & VAN DEN AARDWEG, G. J. M. J., 1991. Studies of dose-fractionation on early and late responses in pig skin: a reappraisal of the importance of overall treatment time and its effects on radiosensitization and incomplete repair. *International Journal of Radiation Oncology, Biology and Physics, 21*, 1441–1450.

HORWICH, A., 1991. Treatment of muscle invasive (T2/T3) disease: the role of radiotherapy. In *Urological Oncology Dilemmas and Developments*, ed. by A. R. Alderson, R. T. D. Oliver, I. W. F. Hanham and H. J. G. Bloom (John Wiley & Sons, Chichester), chap. 13, pp. 137–144.

MORRIS, G. M. & HOPEWELL, J. W., 1986. Changes in the cell kinetics of pig epidermis after repeated daily doses of X-rays.

In *Radiation Damage to Skin, Supplement to British Journal of Radiology* (BIR, London), pp. 34–38.

QUILTY, P. M., DUNCAN, W. & KERR, G. R., 1985. Results of a randomised study to evaluate influence of dose on morbidity in radiotherapy for bladder cancer. *Clinical Radiology*, *36*, 615–618.

SHEARER, R. J., CHILVERS, C. E. D., BLOOM, H. J. G., BLISS, J. M., HORWICH, A. & BABIKER, A. (for THE CO-OPERATIVE UROLOGICAL CANCER GROUP, 1988). A prospective trial: preliminary report. *British Journal of Urology*, *62*, 558–564.

SHEEHAN, T. & NEWMAN, H., 1991. Proliferation characteristics of human bladder tumours *in vivo* determined by bromodeoxyuridine incorporation. *British Journal of Cancer*, *64*, Suppl. XV, 6 (abstract).

SYMONDS, R. P., DAVIDSON, R. P., HABESHAW, T., ROBERTSON, A. G., SNEE, M. P. & WATSON, E. R., 1990. The significance of dose, nodal irradiation and other factors upon the outcome after radiotherapy for bladder cancer (abstract). *British Journal of Cancer*, *61*, 167.

TROTT, K.-R. & KUMMERMEHR, J., 1985. What is known about proliferation rates to choose between accelerated fractionation and hyperfraction? *Radiotherapy and Oncology*, *3*, 1–9.

TURESSON, I. & THAMES, H. D., 1989. Repair capacity and kinetics of human skin during fractionated radiotherapy: erythema, desquamation and telangiectasia after 3 and 5 years follow-up. *Radiotherapy and Oncology*, *15*, 169–188.

VAN DEN AARDWEG, G. J. M. J. & HOPEWELL, J. W., 1992. The kinetics of repair for radiation induced sublethal damage in pig epidermis: an interpretation based on fast and slow components of repair. *Radiotherapy and Oncology*, *23*, 94–104.

WALLACE, D. M. & BLOOM, H. J. G., 1976. The management of deeply infiltrating (T3) bladder carcinoma; controlled trial of radical radiotherapy versus pre-operative radiotherapy and radical cystectomy (first report). *British Journal of Urology*, *48*, 587–594.

WALLACE, D. M. A., RAGHAVAN, D., KELLY, K. A., SANDEMAN, T. F., CONN, I. G., TERIANA, N., DUNN, J., BOULAS, J. & LATIEF, T., 1991. Neo-adjuvant (pre-emptive) cisplatin therapy in invasive transitional cell carcinoma of the bladder. *British Journal of Urology*, *67*, 608–615.

1992, *The British Journal of Radiology*, *65*, 799–802

An investigation into the effect of protective devices on the dose to radiosensitive organs in the head and neck

By N. W. Marshall, BSc, ARCS, K. Faulkner, BSc, MSc, PhD and *P. Clarke, MBBS, MRCP, FRCR

Regional Medical Physics Department, Newcastle General Hospital, Westgate Road, Newcastle-Upon-Tyne, NE4 6BE and *Radiology Department, Royal Victoria Infirmary, Queen Victoria Road, Newcastle-Upon-Tyne, NE1 4LP, UK

(*Received 8 November 1991 and in revised form 3 February 1992, accepted 26 March 1992*)

Keywords: Diagnostic radiology, Protective devices, Radiation protection

Abstract. A series of experiments were performed to determine the dose reduction afforded to radiosensitive organs in the head and neck by various protective devices. These included spectacles with plastic, standard glass, photochromic and lead-glass lenses, a thyroid collar and a lead-acrylic face mask. The measurements were performed using an anthropomorphic phantom loaded with lithium fluoride thermoluminescent dosemeters, in conditions realistic of clinical practice. Irradiations were performed using scattered radiation produced by a pelvic phantom, for X-ray beams generated at 80 kVp and 110 KVp. It was found that the reduction in dose to the lens of the eye ranged between 0% and 97%, whilst the dose to the thyroid and oesophagus was reduced by between 76% and 97%, and was dependent on the protective device and tube potential employed. A reduction in brain dose of up to 81% was also measured, for the lead-acrylic face mask. Also presented is the ratio of organ dose to dose to the bridge of the nose for thyroid, oesophagus, brain and sinuses, as measured for the case of no head or neck protection.

Introduction

A number of workers have studied the radiation dose received by personnel operating fluoroscopy units (Faulkner and Moores, 1982; Jeans et al, 1985; Law, 1985; Palmer and Wright, 1985). These studies have found that the dose to the lens of the eye is particularly important, as in some circumstances (*e.g.* for high workloads or specific interventional procedures) the eye lens dose may be a critical factor in the determination of whether the person becomes a classified radiation worker. In many situations, including those in which eye dose is not the critical factor, it may be necessary to consider protection for the eye.

In the recent report by the International Commission for Radiological Protection (ICRP, 1991), the method of calculating doses to individuals has changed, effective dose replacing the previous quantity effective dose equivalent. In particular, the radiosensitive tissues included in the calculation of effective dose and their weighting factors have been re-evaluated. With the specification of a separate weighting factor for the oesophagus and the inclusion of the brain in the remainder organs, as well as the increase in the weighting factor for the thyroid, the dose to these organs in the head and neck will make an important contribution to the effective dose to workers in radiology who wear a lead apron. The use and effect of various devices worn to protect organs in the head and neck therefore need to be examined. It is important to quantify the dose reduction afforded in situations realistic of those found in radiology departments, both by devices specifically intended for radiation protection purposes and by ordinary spectacles that might be worn by staff.

The protective effects of spectacles (with lead-glass, plastic, glass and photochromic lenses) have been reported before (Richman et al, 1976; Bergstrom et al, 1977; Ardran & Crooks, 1978; Day and Forster, 1981). However, with the exception of Bergstrom et al (1977), the previous work only details the transmission of spectacle lenses directly irradiated. The aim of the present work was to measure the effect of various types of spectacles and protective devices on the dose to the lens of the eye, as well as to specific organs in the head and neck.

Materials and methods

The experimental investigation was performed on two separate three-phase X-ray generators, a Picker Vector 70 and a Picker Vector 100. The X-ray beam (22.5 cm × 22.5 cm as measured at the entrance surface) was centred on a realistic pelvic phantom (3M). A Rando phantom (Alderson Research Laboratories) loaded with lithium fluoride (LiF) thermoluminescent dosemeters (TLD) was positioned within the scattered radiation field thus generated (see Fig. 1). The TLD (packed in thin polythene sachets) were located at positions corresponding to the brain, eyes, bridge of the nose, sinuses, thyroid and the upper portion of the oesophagus, as described in a previous paper (Faulkner and Harrison, 1988).

The protective devices investigated included spectacles with standard glass, plastic, photochromic and lead-glass (0.25 mm Pb equivalent) lenses, a lead-acrylic face mask with side shields (0.35 mm Pb equivalent) (Moti, USA) and a thyroid collar (0.35 mm Pb equivalent). The protective device to be evaluated was attached to the

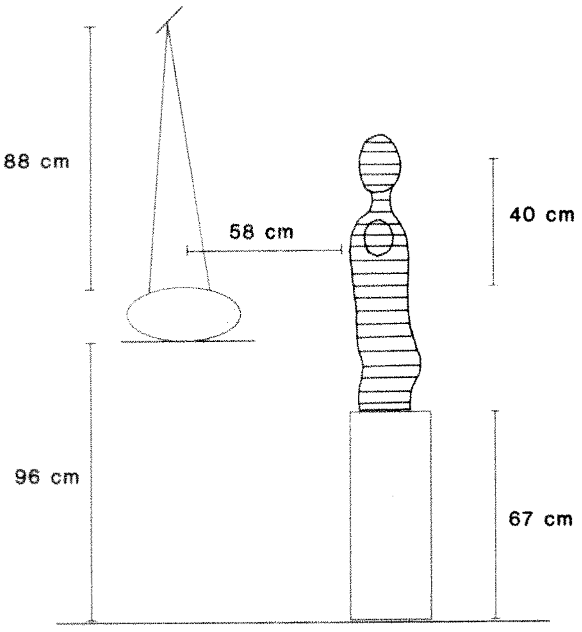

Figure 1. Diagram showing set up of apparatus used to make the measurements

Table I. Percentage dose reduction for eye and brain at 80 kVp and 110 kVp

Protection	80 kVp		110 kVp	
	Brain	Eye	Brain	Eye
Photochromic 1	nsd	50	nsd	39
Lead-glass lens	nsd	86	24	87
Photochromic 2	32	51	19	45
Plastic lens	nsd	nsd	nsd	nsd
Glass lens	33	34	19	30
Moti mask	81	97	81	96

nsd = not statistically different.

Table II. Percentage dose reduction for thyroid and oesophagus at 80 kVp and 110 kVp

Protection	80 kVp	110 kVp
	thyroid/oesophagus	thyroid/oesophagus
Moti mask	97	92
Thyroid collar	84	76

Rando phantom and irradiated under fluoroscopic exposure mode. The scattered radiation distributions used to irradiate the Rando phantom were generated using primary beams of 80 kVp, 1.0 mA and 110 kVp, 1.0 mA. So as to ensure that the lowest dose recorded by the TLD was appreciably above background, the apparatus was irradiated for an extended period. Two irradiations at each tube potential were also performed with the Rando phantom unprotected (*i.e.* without glasses, etc.), thereby establishing a baseline that enabled the attenuation effects of the devices to be compared.

The atomic numbers of the LiF TLD (effective atomic number of 8.1) and soft tissue (effective atomic number of 7.4) are close enough so that the absorbed dose measured with the TLD can be taken to be the body tissue dose without correction (Bergstrom et al, 1972). Calibration of the TLD was performed at the relevant tube potential (*i.e.* 80 kVp and 110 kVp) against a dosemeter whose calibration was traceable to the national standard. Any dependence of measured organ dose on generator output fluctuations was allowed for by expressing the organ dose relative to the dose measured by a TLD placed on the bridge of the nose of the Rando phantom. For the case of protective shields that affected the dose measured on the bridge of the nose, an allowance for the transmission of the shield was made. This factor was experimentally determined using TLDs and scattered radiation and was used in the renormalization of the measured dose to the bridge of the nose.

Results

The percentage dose reduction measured for the brain and eye is presented in Table I and the reduction in dose to the thyroid and upper oesophagus is shown in Table II. Figure 2 is a graph of measured organ dose relative to the dose to the bridge of the nose, for various organs in the head and neck, when no protection is worn.

The repeatability of the experimental technique was estimated by determining one standard deviation as a percentage of the mean of the absorbed dose (normalized to the dose to the bridge of the nose) to organs in the head and neck which were unaffected by the protection used. This value, found to be 7%, includes such uncertainties as positioning errors and TLD readout

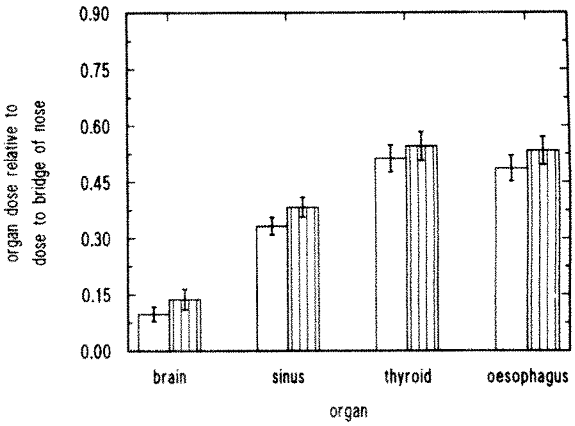

Figure 2. Organ dose relative to dose to bridge of nose, measured at 80 kVp (□) and 110 kVp (▥). The error bars represent one standard deviation.

and calibration errors. The error on the bridge of the nose, eye, thyroid and upper oesophagus doses is therefore approximately 7%. The uncertainty in measured organ dose for tissues in which the dose was close to the background (*e.g.* the brain) will be greater. The uncertainties in the measured brain dose were estimated from the fluctuations in background TLD reading relative to brain dose and were found to be just under 20% at 80 kVp and 13% at 110 kVp.

Discussion

The dose reduction effect of spectacles with various types of lens varies from 0% to 87%, depending on tube potential used and type of lens. The two pairs of spectacles with photochromic lenses provide a similar degree of protection, *i.e.* 50% at 80 kVp and about 40% at 110 kVp. The glass lenses produced a slightly lower dose reduction effect than the photochromic lenses, reducing the eye lens dose by 34% at 80 kVp and by 30% at 110 kVp. The effect of the plastic lensed spectacles was not statistically different from the baseline measurement, being close to zero and therefore confirming the result found by Richman et al (1979). The spectacles with lead-glass lenses had a significant effect on the eye lens dose, reducing the absorbed dose to the eye lens by 86% and 87% at 80 kVp and 110 kVp, respectively.

These figures for reduction in eye lens dose are in good agreement with the values measured by Bergstrom et al (1977) using a similar experimental set up. Day and Forster (1981) quote a limit to dose reduction offered by lead-glass lenses of 89% and 87% (at 62 kVp and 102 kVp, respectively), due to scatter around the lenses from surrounding tissues. The protection offered to the eye lens measured using a realistic phantom is therefore less than would be expected if estimated using the direct irradiation transmission data reported elsewhere (Ardran and Crooks, 1978). This is due, primarily, to the scattering of X rays by the body.

The lead-acrylic mask produced a considerable reduction in eye lens dose of 97% at 80 kVp and 96% at 110 kVp. Such a large reduction in dose may be attributable to the side shields (0.35 mm Pb equivalent) fitted to the face mask which greatly reduce the amount of radiation that is scattered into the eye lens by surrounding tissues. The value found here for the reduction in eye dose is in agreement with that quoted by the manufacturers (Moti Enterprises).

The respective reduction in eye lens dose for each device is greater at 80 kVp than at 110 kVp, consistent with the scattered radiation produced at 110 kVp being more penetrating than that produced at 80 kVp.

Some of the protective devices evaluated here also appear to have had an effect on the measured brain dose. For some of the devices studied, the brain dose differed significantly from the baseline measurement, implying some degree of shielding for the brain. The values of dose reduction measured for the brain for the various pairs of spectacles varied from 0% to 33%, and appeared to be dependent on the composition, as well as the size and shape of the lenses. For the case of lead glass lenses, a reduction in the dose to the brain of 24% was measured at 110 kVp (see Table I) whereas no significant reduction in brain dose was found at 80 kVp. This result is consistent with the larger uncertainties associated with the measurement of brain dose at 80 kVp compared to 110 kVp. The face mask had quite a considerable effect on the brain dose (reducing the dose by 81% at both 80 kVp and 110 kVp).

The thyroid collar had a marked effect on the doses to the thyroid and upper oesophagus, the dose reduction to both these organs being 84% at 80 kVp and 76% at 110 kVp. The lead-acrylic face mask also reduced the thyroid and upper oesophagus doses considerably, with a dose reduction of 97% at 80 kVp and 92% at 110 kVp. Again, for both the lead-acrylic mask and thyroid collar, the dose reduction at 80 kVp was greater than that at 110 kVp.

The graph in Fig. 2 shows the measured relationship between organ dose and dose to the bridge of the nose, for the case of no head protection (and for the geometry shown in Fig. 1). This data may be used to estimate the dose to these radiosensitive organs from a dosemeter worn on the forehead.

Conclusion

The value of eye protection is widely accepted and a high degree of protection is afforded by lead-glass lenses and the face mask with a lead-acrylic window. All the

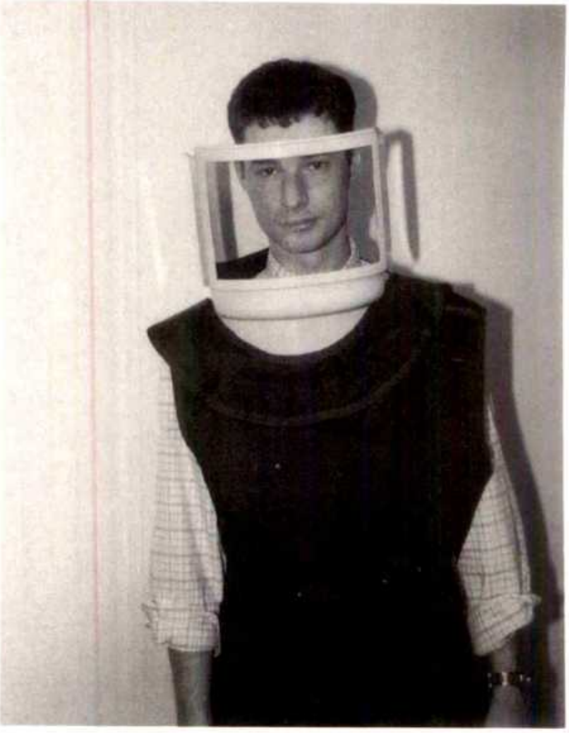

Figure 3. Lead-acrylic face mask used in this study.

protective devices which had an effect on eye dose also provided some degree of shielding for the brain.

The greater protective effect offered by such devices as the lead-acrylic face mask has to be balanced against any physical discomfort or impeding of ease of movement or vision that may be experienced whilst wearing the device. A further factor is the acceptability of such a device to the patient (Fig. 3).

Lead-glass lenses are more widely available and used. They do, however, pose a problem for radiologists requiring refractive correction (perhaps the majority of radiologists in this area). The choice here lies between 'clip on' non-refractive lenses and the purchase of lead-glass lenses ground to individual prescription. In practice, the extra weight of the 'clip on' type lenses is uncomfortable after a short period of time. In addition (especially in a warm environment), the spectacles tend to slip down from the bridge of the nose, which is distracting and interferes with vision. This is a particular problem whilst performing sterile procedures. The second option, prescription lenses, is more acceptable from a user's point of view but the cost is approximately £250.

There is a significant degree of lens and brain dose reduction afforded by the use of glass or photochromic lenses and this should be considered by radiologists when purchasing spectacles. There is, quite rightly, pressure from opticians to purchase plastic lenses, as they result in less ocular damage in the event of facial trauma. These, however, offer no radiation protection. It would not be unreasonable to purchase a spare pair of spectacles with photochromic lenses (typically costing less than £100), which could then be used whilst screening.

Both the thyroid and lead-acrylic face mask have a pronounced effect on the dose to the upper oesophagus and thyroid, reducing the dose to these organs by between 76% and 97%. This observation is particularly important now that the thyroid has an increased tissue weighting factor and the oesophagus has been included in the list of radiosensitive organs for use in the calculation of effective dose (ICRP, 1991).

Acknowledgments

This project was partially supported by a grant from the Commission of European Communities Radiation Protection Programme (Contract Number BI7-0014(3)). The authors would like to thank Professor K. Boddy and Dr R. M. Harrison for their continuing support and encouragement.

References

ARDRAN, G. M. & CROOKS, H. E., 1978. The value of conventional eyeglasses for X-ray protection. *Radiology, 129,* 815–816.

BERGSTROM, K., DAHLIN, H., GUSTAFSSON, M. & NYLEN, O., 1972. Eye lens doses in carotid angiography. *Acta Radiologica Diagnosis, 12,* 134–140.

BERGSTROM, K., JORULF, H. & LOFROTH, P. O., 1977. Eye lens protection for radiological personnel. *Radiology, 124,* 839–840.

DAY, M. J. & FORSTER, E., 1981. Protective effect of spectacles. *British Journal of Radiology, 54,* 137–138.

FAULKNER, K. & HARRISON, R. M., 1988. Estimation of effective dose equivalent to staff in diagnostic radiology. *Physics in Medicine and Biology, 33,* 83–91.

FAULKNER, K. & MOORES, B. M., 1982. An assessment of the radiation dose received by staff using fluoroscopic equipment. *British Journal of Radiology, 55,* 272–276.

ICRP, 1991. *1990 Recommendations of the International Commission on Radiological Protection.* ICRP Publication 60 (Pergamon Press, Oxford).

JEANS, S. P., FAULKNER, K., LOVE, H. G. & BARDSLEY, R. A., 1985. An investigation of the radiation dose to staff during cardiac radiological studies. *British Journal of Radiology, 58,* 419–428.

LAW, J., 1985. Doses to head and arms of radiologists during fluoroscopy. *British Journal of Radiology, 58,* 187–188.

PALMER, K. E. & WRIGHT, I. H., 1985. Eye dose limits and the use of overcouch and undercouch X-ray image intensifier systems. *British Journal of Radiology, 58,* 1221–1223.

RICHMAN, A. H., CHAN, B. & KATZ, M., 1976. Effectiveness of lead lenses in reducing radiation exposure. *Radiology, 121,* 357–359.

1992, *The British Journal of Radiology*, 65, 803–806

Evaluation and skeletal metastases*

By †M. V. Merrick (rapporteur and panel chairman) and members of the panel: ‡J. S. M. Beales, §N. Garvie and ¶R. C. O. Leonard

†Consultant in Nuclear Medicine, Western General Hospital, Edinburgh, ‡Consultant Radiologist, Lister Hospital, Stevenage, §Consultant in Radiology and Nuclear Medicine, The Royal London Hospital and ¶Senior Lecturer and Consultant, Department of Clinical Oncology, Western General Hospital, Edinburgh, UK

(*Received 27 August 1991 and in revised form 29 January 1992, accepted 7 April 1992*)

Keywords: Bone metastases, Carcinoma of breast, Carcinoma of bladder, Carcinoma of prostate

Bone scintigraphy remains one of the commonest isotope imaging investigations employed for the detection of occult skeletal metastases when staging a number of common cancers. The objectives of staging are firstly, to identify patients in whom the disease may be locally curable and secondly, to identify those who may have dissemination, in whom radical local treatment is inappropriate. Increasingly, formal restaging is also repeated at first recurrence. The information considered necessary for clinical management is changing continuously, with developments both in treatment and imaging techniques. The costs must be balanced against those of inappropriate administration or withholding of treatment; in the case of bone scintigraphy, a relatively low-cost procedure, it is not difficult to identify net benefits which offset the costs. The objectives of the panel and its associated floor discussion were to review current practice and to determine, clarify and possibly extend areas in which there is agreement.

Carcinoma of bronchus

Cancer of the lung is the commonest single malignancy in the UK, comprising approximately 25% of all cancers. It is responsible for approximately 40 000 deaths per annum in the UK (Capewell et al, 1987). The case mortality is one of the highest of all tumours, being second only to carcinoma of the pancreas. Untreated, the mean survival from diagnosis is less than 3 months (Capewell et al, 1990). There is a 30% 5 year survival for patients with "locally curable" disease, mostly squamous carcinoma, but these patients constitute only a small percentage of the overall population with lung cancer. In all other types the prognosis is poor. The unfavourable outlook for patients with small cell cancer is reflected in part by the finding of bone marrow involvement, identified immuno-histochemically, but which cannot be identified either by bone or by marrow scintigraphy, in up to 80% of patients at presentation and virtually 100% at post-mortem (Hay et al, 1988).

In many patients, an initial plain chest radiograph is the only imaging investigation indicated. Histological confirmation may be obtained from sputum cytology or at bronchoscopy. If the possibility of resection has been excluded, treatment will be palliative by radiotherapy, chemotherapy or occasionally a combination of both. If more radical treatment has not been excluded, computed tomography is required to assess the degree of involvement of mediastinal and hilar lymph nodes.

In small cell lung cancer, a measurement of clinical performance status and the chest X ray are sufficiently specific indicators of prognosis. Additional information obtained by liver ultrasound and bone scientigraphy does not improve accuracy (Allan et al, 1990). Prior to the advent of computed tomography, bone scintigraphy had some role, to exclude from surgery patients whose disease appeared locally resectable, but which was nevertheless disseminated. With adequate CT staging of the mediastinum, such cases are uncommon. There is probably no indication for routine bone scintigraphy of patients with small-cell tumours if staging includes computed tomography. Nevertheless, if access to CT is restricted, and especially in patients with non-small cell tumours, bone scintigraphy remains a useful screening procedure before surgery (Merrick & Merrick, 1986; Tornyos et al, 1991).

The role of bone scintigraphy in carcinoma of the bronchus is in most other cases limited to identifying whether local pain is of bony origin, with a view to giving palliative radiotherapy. There may however be a case for systematically identifying deposits, particularly in long bones, at a time when they are asymptomatic, because of the risk of subsequent pathological fracture. The economics of this is at present unclear, although for the individual patient there is a substantial benefit from prophylaxis as opposed to repair (Leonard, 1987).

Carcinoma of breast

Carcinoma of the breast is the third commonest malignancy in the UK with an incidence of approximately 25 000 new cases per year, responsible for 16 000 deaths per annum. Bone scintigraphy has been proposed both as part of initial staging, since the early papers from a relatively small number of centres almost 30 years ago (Merrick, 1975), and as a means of defining the response to treatment. However, this view has never been universally accepted and the clinical role remains controversial (Gazet et al, 1985). Achievement of cure and control of local disease are not synonymous. When conducting clinical trials it is important that patients compared are as homogeneous as possible. Such detailed information is not always necessary for the routine management of patients not participating in trials. There is general agreement that endocrine or chemotherapy is appropriate for patients with a high risk of dissemination. The failure to demonstrate the existence of distant metastases is not conclusive and currently tumour size, oestrogen receptor status and above all the state of the axillary lymph nodes are the most important determinants of whether or not systemic therapy should be used. Bone scientigraphy rarely influences this decision.

---

*Report of a consensus panel discussion, Annual Congress of the British Institute of Radiology, Harrogate, 12 June 1990.

Many of the discrepancies noted, particularly those in trials assessing response (Hayward et al, 1977, Coleman et al, 1988a), have been due to lack of uniformity in the criteria used for assessing response in bone, which in general do not strictly comply with the UICC criteria (Bitran et al, 1980). Moreover despite the variable scintigraphic response of metastases to treatment, prolonged survival is possible even with disseminated disease, particularly in patients with "bone-only" metastases (Coombes et al, 1983). Important developments since the early trials include recognition of the importance of oestrogen receptor status and other tumour markers in determining prognosis and response to treatment. There have been substantial changes in both the availability of effective drugs and the surgical approach to this condition, with radical operations largely abandoned in favour of procedures which conserve the breast, combined with radiotherapy, chemotherapy or both (Perren 1991). Lumpectomy has proved as effective as mastectomy and there is clear evidence that non-surgical therapies have a major impact in the control of local disease and prolongation of survival.

The prevalence of occult bone metastases in asymptomatic patients with TNM Stage T0 or T1 tumours is low, certainly less than 3% and probably about 1% (Kunkler et al 1985, Coleman et al 1988b). This rises to 8–9% in T2 tumours and 25% in T4 tumours. The false-positive rate has been estimated at 3%. Consequently, in T0 and T1 tumours the number of false positives found substantially exceeds the number of true positives. There is thus no case for routine bone scintigraphy in patients with clinical T0 or T1 carcinoma of the breast. Although the evidence is more difficult to interpret in the case of T2 tumours, there is no convincing evidence that scintigraphic findings affect management; this examination therefore cannot be recommended on a routine basis in these patients.

In patients with T3 and T4 tumours, treatment is basically concerned with the control of local disease and many of these patients will in any case receive systemic therapy early in the disease management. The findings on bone scintigraphy rarely influence primary management, although it is possible to make out a case that, because of the relatively high prevalence of occult lesions which are of high risk of fracture (for example, in the femoral neck), bone scintigraphy may be indicated in patients with locally advanced disease, in order to permit prophylactic treatment to peripheral metastases likely to progress to overt fracture. The overall value of this remains unproven (Anon 1981, Schunemann et al, 1990). Bone scintigraphy is indicated at any stage of the disease if there are symptoms which could be attributable to bone secondaries, not confirmed by plain radiographs, or if there is a raised alkaline phosphatase which is otherwise unexplained.

During the course of the disease, scintigraphy may be required at any time if symptoms develop which might be attributable to bone metastases, or if the alkaline phosphatase becomes elevated. It is also indicated in patients with an apparent loco-regional occurrence, as up to one-third of these patients have occult bone metastases, treatment of which may prevent pathological fracture (Kunkler & Merrick, 1986). The assessment of change in scintigraphic appearance as a measure of treatment outcome of bone disease (Coleman et al, 1983) is fraught with difficulty. The significance attached to any change must be interpreted with great caution.

Carcinoma of bladder

Carcinoma of bladder is common, with an incidence of approximately 25 per 100 000 per annum in men and half this in women. Under the TNM classification it is categorized into five stages—from T0 (carcinoma *in situ*) to T4, in which there is deep progression through the serosa—'N' staging, depending on whether local or para-aortic nodes are involved and histological grading depending on the degree of differentiation. In the early stages treatment is surgical, with local resection of the tumour or, for multiple T1 disease, topical chemotherapy (bladder installation). In more advanced local disease, radical radiotherapy is now usually the treatment of choice and may in some cases be followed by total cystectomy. Systemic chemotherapy of disseminated disease using cis-platin based regimes now has a place, and a number of trials are currently in progress with some highly active platinum compounds. It is generally considered that chest metastases respond better to chemotherapy than those in other sites but there is no agreement as to how response of bone metastases should be assessed.

Routine staging includes blood chemistry, chest X ray, IVU, cystoscopy and bimanual examination, supplemented by computed tomography if radical radiotherapy is contemplated. Radiologically, skeletal deposits may be lytic or mixed lytic/sclerotic. The prevalence of bone metastases correlates with both the histologic grade and the clinical stage. 70% of patients with invasive carcinoma develop distant metastases within 18 months, mainly to the pelvic lymph nodes, less commonly to the skeleton. Bone scintigraphy is not regarded as a routine staging procedure even though the prevalence of bone metastases is similar, stage for stage, to carcinoma of the breast (Davey et al, 1985).

There is no evidence that routine bone scintigraphy affects management and it therefore cannot be recommended. It is, however, indicated in patients with a raised alkaline phosphatase or with symptoms referable to the skeleton for which no explanation is found on plain radiographs. It may be indicated if a cystectomy is considered as a radical therapeutic manoeuvre, to exclude from this procedure patients who cannot benefit.

Carcinoma of the prostate

This is another common malignancy in which patients frequently suffer metastases to the skeleton. The prevalence of skeletal metastases is related to clinical stage, rising from 5% to 10% in patients with stage 0 disease to 70% in those with stage 4 disease. When surgery is being considered, full TNM staging is normally required. Survival is related both to the histological grading and to the clinical stage, but the most important prognostic indicators are alkaline phosphatase (Merrick et al, 1985) and prostate-specific antigen (Chybowski et al, 1991).

There is as yet no consensus on the value of treating early asymptomatic disease. An MRC trial is in progress, but there seems little prospect that conventional treatment at this stage will improve either total or symptom-free survival. In the UK treatment is for the most part conservative and local therapy is considered only if there is a clinically significant obstruction to urinary outflow. Elsewhere, radical radiotherapy and/or surgery are commonly employed. Where treatment is necessary, there is often a good and prolonged response to ablative (orchidectomy or LHRH analogue) or anti-androgen therapy. Escape from control usually occurs eventually at a distant, rather than at the primary, site.

Overall, about 30% of patients have bone metastases at presentation and about 70% at postmortem, the latter figure possibly reflecting the number of patients whose death is unrelated to the tumour. The majority are sclerotic, the remainder mostly mixed and only a minority lytic. Unlike most tumours which metastasize to bone, pathological fractures are rare in carcinoma of the prostate and they tend to heal well. Primary investigations are more concerned with assessing the severity and extent of bladder outflow obstruction. It was at one time suggested that the bone scan could be used as a prognostic indicator, but it is now clear that alkaline phosphatase and prostate specific antigen (PSA) are considerably more sensitive, the latter being also a better indicator of escape from control. Being a disease of older men, the co-existence of muscular and/or joint pains not related to the carcinoma is, of course, common. Many patients with bone metastases are asymptomatic but, on follow-up, about 10% of initially metastasis-free patients develop skeletal metastases per year.

There is thus only a limited role for bone scintigraphy in the management of this disease. There is a case for performing a bone scan in a patient with a raised PSA or alkaline phosphatase, in order to determine the sites involved and so that Paget's disease can be distinguished from metastases by appropriate radiographs. There is also, as in other diseases, a good case for performing this examination in a patient with local symptoms, especially if there is radiographic doubt as to the presence of metastases. At the present time there is no established place for scintigraphy in the asymptomatic patient with a normal alkaline phosphatase, nor is there any established role for it in routine follow-up.

Conclusions

There is no longer a case for *routine* bone scintigraphy in any of the conditions discussed, but many *specific* indications exist. There is less evidence in other tumours (Leung et al, 1991; Sham et al, 1991), but there is none in which bone scintigraphy can currently be recommended as a routine staging procedure.

References

ALLAN, S. G., STEWART, M. E., LOVE, S., CORNBLEET, M. A., SMYTH, J. F. & LEONARD, R. C. F., 1990. Prognosis of small cell carcinoma of the lung and analysis of clinical, biochemical and haematological factors at presentation. *European Journal of Clinical Oncology*, *26*, 703–705.

ANON., 1981. Pathological fractures due to bone metastases. *British Medical Journal*, *283*, 748.

BITRAN, J. D., BEKERMAN, C. & DESSER, R. K., 1980. The predictive value of isotope bone scans in assessing response to chemotherapy in advanced breast cancer. *Cancer*, *45*, 1562–1568.

CAPEWELL, S. (EDINBURGH LUNG CANCER GROUP), 1987. Patients presenting with lung cancer in South East Scotland. *Thorax*, *42*, 853–857.

CAPEWELL, S. (EDINBURGH LUNG CANCER GROUP), 1990. Performance and prognosis in patients with lung cancer. *Thorax*, *45*, 951–956.

CHYBOWSKI, F. M., JEFFREY, J., KELLER, L., BERGSTRAHL, E. J. & OESTERLING, J. E., 1991. Predicting radionuclide bone scan findings in patients with newly diagnosed, untreated prostate cancer: prostate specific antigen is superior to all other clinical parameters. *Journal of Urology*, *145*, 313–318.

COLEMAN, R. E., MAISEY, M. N., KNIGHT, R. K. & RUBENS, D. R., 1984. Mitoxantrone in advanced breast cancer; a phase II study with special attention to cardiotoxicity. *European Journal of Cancer Clinical Oncology*, *20*, 771–776.

COLEMAN, R. E., MASHITER, G., WHITAKER, K. B., MOSS, D. W., RUBENS, R. D. & FOGELMAN, I., 1988a. Bone scan flare predicts successful systemic therapy for bone metastases. *Journal of Nuclear Medicine*, *29*, 1354–1359.

COLEMAN, R. E., RUBENS, R. D. & FOGELMAN, I., 1988b. Reappraisal of the baseline bone scan in breast cancer. *Journal of Nuclear Medicine*, *29*, 1045–1049.

COOMBES, R. C., DADY, P., PARSON, C., MCREADY, V. R., FORD, H. G., GAZET, J. C. & POWELS, T. J., 1983. Assessment of response of bone metastases to systemic treatment in patients with breast cancer. *Cancer*, *52*, 610–614.

DAVEY, P., MERRICK, M. V., DUNCAN, W. & REDPATH, A. T., 1985. Bladder cancer—the value of routine bone scintigraphy. *Clinical Radiology*, *36*, 77–79.

GAZET, J. C., RAINBURY, R. M., FORD, H. T., POWELL, T. J. & COOMBES, R. C., 1985. Survey of treatment of primary breast cancer in Great Britain. *British Medical Journal, 290,* 1793–1795.

HAY, F. G., FORD, A. & LEONARD, R. C. F., 1988. Clinical applications of immunocytochemistry in the bone marrow in small cell lung cancer. *International Journal of Cancer, (Suppl 2),* 8–11.

HAYWARD, J. L., CARBONE, P. P., HEUSON, J. E. C., KUMOAKA, S., SEGALOFF, A. & RUBENS, R. D., 1977. Assessment of response to therapy in breast cancer. *Cancer, 39,* 1289–1294.

KUNKLER, I. H. & MERRICK, M. V., 1986. The value of non-staging skeletal scintigraphy in breast cancer. *Clinical Radiology, 37,* 561–562.

KUNKLER, I. H., MERRICK, M. V. & RODGER, A., 1985. Bone scintigraphy in breast cancer: a nine year follow-up. *Clinical Radiology, 36,* 279–282.

LEONARD, R. C. F., 1987. Medical complications of malignancy. *Medicine International, 39,* 1639–1643.

LEUNG, S. F., STEWART, I. E. T., TSAO, S. Y. & METREWELI, C., 1991. Staging bone scintigraphy in nasopharyngeal carcinoma. *Clinical Radiology, 43,* 314–315.

MERRICK, M. V., 1975. Bone scanning—Review article. *British Journal of Radiology, 48,* 327–351.

MERRICK, M. V., DING, C. L., CHISHOLM, E. D. & ELTON, R. A., 1985. Prognostic significance of alkaline and acid phosphatase and skeletal scintigraphy in carcinoma of the prostate. *British Journal of Urology, 57,* 715–720.

MERRICK, M. V. & MERRICK, J. M., 1986. Bone scintigraphy in lung cancer—a reappraisal. *British Journal of Radiology, 59,* 1185–1194.

PERREN, T. J., 1991. C erb B2 oncogene as a prognostic marker in breast cancer. Editorial. *British Journal of Cancer, 63,* 328–332.

SCHUNEMANN, H., LANGECKER, P. J., ELLGAS, W., LEONHARD, T. A. & MERKL, H., 1990. The value of bone scanning in the follow up of breast cancer patients. A study of 1000 cases. *Journal of Cancer Research Clinical Oncology, 116,* 486–491.

SHAM, J. S. T., TONG, C. M., CHOY, D. & YEUNG, D. W. C., 1991. Bone scintigraphy in nasopharyngeal carcinoma. *Clinical Nuclear Medicine, 12,* 27–29.

TORNYOS, K., GARCIA, O., KARR, B. & LEBAUD, R., 1991. A correlation study of bone scanning with clinical and laboratory findings in the staging of non-small-cell cancer. *Clinical Nuclear Medicine, 16,* 107–109.

1992, *The British Journal of Radiology*, 65, 807–813

Errors due to non-uniform distribution of fat in dual X-ray absorptiometry of the lumbar spine

By Peter Tothill, BSc, PhD, FRSE and David W. Pye, BSc, PhD

Department of Medical Physics and Medical Engineering, Western General Hospital,
Edinburgh EH4 2XU, UK

(*Received 2 September 1991 and in revised form 9 January 1992, accepted 11 February 1992*)

Keywords: Bone mineral, Fat, Absorptiometry

Abstract. Errors in spinal dual X-ray absorptiometry (DXA) were studied by analysing X-ray CT scans taken for diagnostic purposes on 20 patients representing a wide range of fat content. The mean difference between the fat thickness over the vertebral bodies and that over a background area in antero-posterior (AP) scanning was 6.7±8.1 mm for men and 13.4±4.7 mm for women. For lateral scanning the mean fat thickness difference was only 4 mm for both sexes, but the dispersion was greater, with a standard deviation of 15 mm. To relate these differences to errors in bone mineral, measurements were made of the bone mineral equivalence of fat-equivalent materials on DXA machines from three manufacturers. 10 mm of adipose tissue was equivalent to -0.043 g/cm^2 of hydroxyapatite. For AP scanning a non-uniform fat distribution leads to a mean overestimate of 0.029 g/cm^2 for men and 0.057 g/cm^2 for women. The error exceeded 0.1 g/cm^2 in 10% of slices. For lateral scanning the error exceeded 0.1 g/cm^2 (about 15% of normal) in a quarter of slices.

The measurement of bone mineral has grown in importance with the development and refining of techniques and the realization that there are measures that can be undertaken to reduce bone loss, particularly in post-menopausal women. In particular, dual-photon absorptiometry (DPA) can be used to determine bone mineral in the lumbar spine, hip and whole body with excellent precison. The accuracy of such measurements is less well known, because its determination is more difficult in the absence of a recognized yardstick. Some causes of inaccuracy are inherent in the composition of the human body.

An inherent assumption in dual-energy absorptiometry is that there are only two tissue components—bone mineral and soft tissue of uniform composition—with known attenuation coefficients. The assumption is invalid, since fat is a third component with attenuation characteristics that differ appreciably from those of other soft tissues. With most methods of analysis a uniform layer does not affect bone mineral determination, but in the region of the lumbar spine the distribution of fat, particularly that within the peritoneum, may be very non-uniform.

We and others have previously assessed the likely degree of non-uniformity and have determined the resulting errors in DPA of the lumbar spine using radionuclide sources (Roos et al, 1980; Farrell & Webber, 1989; Tothill et al, 1989). The calculations were based on the known γ-ray energies of the sources and tabulated attenuation coefficients of the tissues involved.

The introduction of dual-energy X-ray absorptiometry (DXA) has brought increased speed of measurement and a precision of better than 1% for the lumbar spine, but introduces uncertainties about the errors due to fat, as the photon beams used are not mono-energetic. The higher photon flux associated with DXA also facilitates lateral scanning of the lumbar spine, permitting measurement of the bone mineral of a vertebral body without overlapping spinous processes. It seemed important to extend our previous assessment of fat-induced errors to DXA. A brief presentation of part of this work has previously been made (Tothill & Pye, 1990).

Methods

The technique of examining the distribution of adipose tissue was the same as that previously used (Tothill et al, 1989). Archived X-ray computed tomographic (CT) scans taken for diagnostic purposes that included the appropriate lumbar vertebrae were selected. Scans of 10 female and 10 male patients were chosen to represent a wide range of fat content.

To examine the distribution relevant to DXA scanning in the antero-posterior (AP) projection, all CT scans including lumbar vertebrae 2 to 4 were examined; this yielded a total of 124 slices. The spacing of slices was such that on average there were two scans per vertebra. For lateral scanning, any slices that included ribs or pelvis were excluded, as these could not be used for lateral DXA. L3 was always included, usually part of L4 and occasionally part of L2. 61 scans were available.

Choice of adipose tissue CT window

The CT image was displayed on the computer monitor and a histogram of number-of-pixels versus CT number (in Hounsfield units, HU) was used to select a window defining the limits of adipose tissue. It was

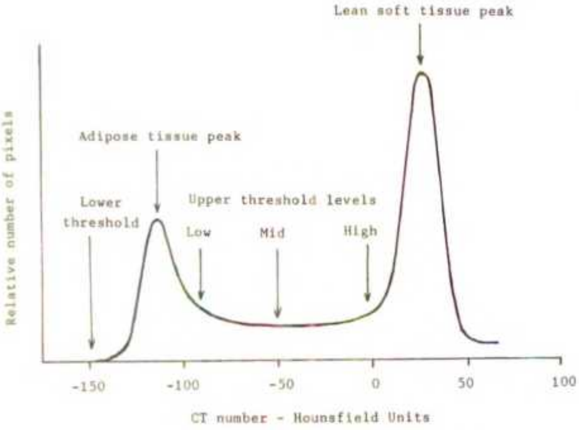

Figure 1. Histogram of number of pixels against CT number in Hounsfield units, with alternative positions of upper threshold.

recognized that a degree of subjectivity might be introduced in this choice, so the effect of changes in this window was investigated. A histogram of HU is illustrated in Fig. 1. It displays two distinct peaks in the soft-tissue range, corresponding to lean and fat tissue, with a broad and relatively flat valley between them. Below the adipose tissue peak there is a sharp cut-off at about −150 HU, so that a fixed lower threshold can be used. The effect of varying the upper threshold was examined by selecting CT scans from three subjects, representing thin, medium and fat individuals. Slices through L1, L3 and L5 were considered and upper threshold levels defined at either end of the histogram valley, just below the lean tissue peak (High) and just above the fat peak (Low), together with a mid-valley value. Fat thicknesses were then determined using these three threshold levels.

Sometimes the partial volume effect led to a non-fat mixture in the gut falling within the chosen window. These areas were edited out before a profile of fat thickness in the AP and lateral projections was computed by summing all adipose tissue pixels along a row. Figure 2 shows a CT scan with the adipose tissue highlighted and the profile of its thickness superimposed.

Background selection

During the processing of an AP scan the DXA apparatus selects a background lateral to the vertebral bodies on either side. The outside edge of this background can be varied, but preferred values are suggested. The computer was used to calculate the mean thickness of adipose tissue on the CT scan in a corresponding background area and also over the width of the vertebral body. Overall background widths of 65, 85, 105 and 125 mm were used, the last being the preferred value of the Hologic machine used in our laboratory.

There is not yet agreement on which area(s) are most appropriate for background selection in lateral scanning, but as examples we took on each CT slice an area anterior and adjacent to the vertebral body of width equal to it and another of twice that width. Figure 2 also shows the background areas associated with the CT slice illustrated.

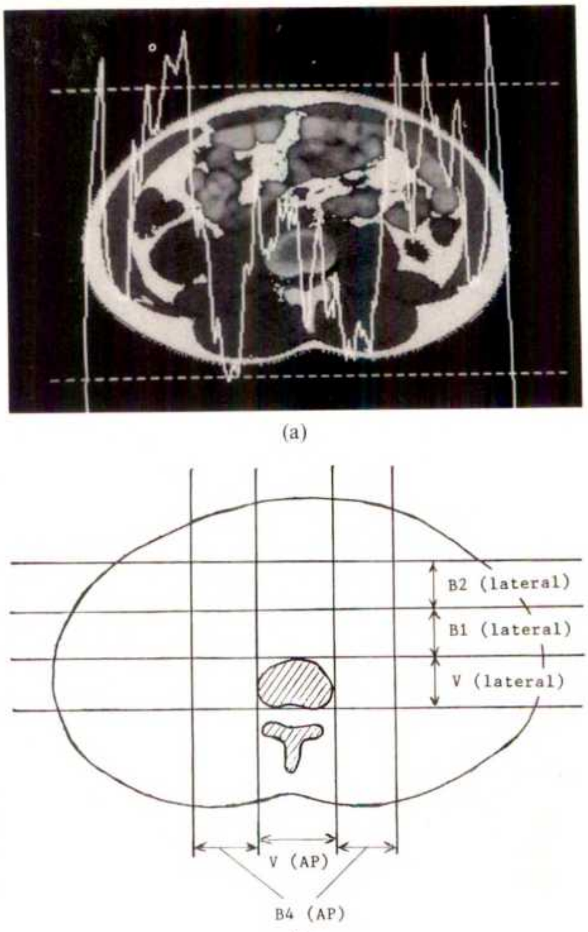

(a)

(b)

Figure 2. (a) CT scan with the adipose tissue highlighted and the profile of its thickness in the AP direction superimposed. (b) Outlines of body and vertebra illustrating the selection of background areas.

Variation of bone mineral density with background width in AP DXA scans

We had previously shown that the position of the selected background area had a profound effect on the error introduced by non-uniform fat distribution in radionuclide DPA (Tothill et al, 1989), so this point was investigated further by analysing a number of patient AP DXA scans using different background widths. Hologic QDR-1000 AP lumbar scans from 20 subjects were chosen, half of them normal volunteers, the remainder patients referred for investigation. There were 16 women and four men. The scans were analysed using overall widths of 85 mm, 105 mm and 125 mm.

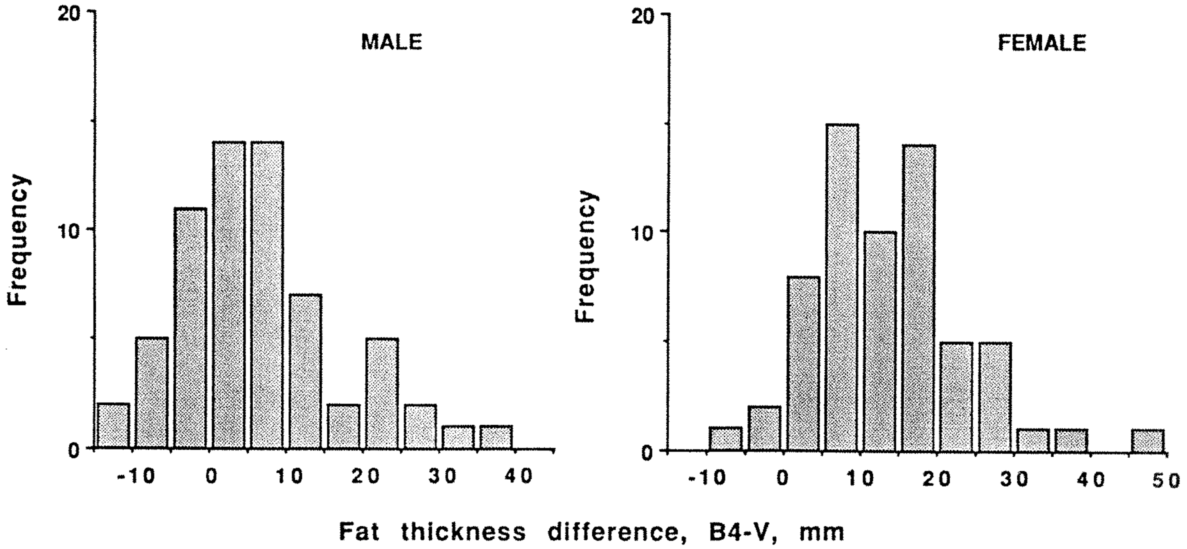

Figure 3. Distributions of differences of thickness of adipose tissue between that over the vertebral bodies and that in a background area of overall width 125 mm, for AP scanning.

Bone mineral equivalence of fat

Owing to the heterogeneous nature of the X-ray spectra used in DXA it was considered necessary to measure, rather than calculate, the bone mineral equivalance of a given thickness of fat, using the apparatus employed for DXA. A water bath was set up on the patient couch and a scan obtained of a slab of bone-mineral-equivalent material (BEM), 5 cm square, placed in the water. The scan was then repeated with the chosen fat-equivalent material (FEM) beneath the bone-equivalent slab. As a variety of materials have been considered as models of fat, measurements were made using polyethylene, paraffin wax, Perspex (methyl methacrylate), stearic acid and lard. Thicknesses of FEM, BEM and water were varied.

The scans were processed in the same way as patient scans, except that a region of interest just inside the slab boundary was chosen manually. The bone mineral equivalence of an FEM layer was taken as the difference between the BMD value with and without the FEM present.

Most measurements were made using a Hologic QDR-1000 machine, which achieves the two X-ray energies by rapid switching of the kVp from 70 to 140. Some measurements were repeated with a Hologic QDR-1000W, used in spine-scanning mode. Measurements were also made on two machines that use absorption edge filtration to split a continuous spectrum into two effective energies, a Lunar DPX and a Norland XR 26.

Results

Effect of CT window on fat thickness estimate

For each of the upper threshold settings on the nine CT slices, the adipose tissue thickness was determined in each of the four background areas and over the vertebral body. As expected, there was a significant increase in deduced adipose tissue thickness with increase in threshold. The relationship was approximately linear, with a threshold difference of 2 HU leading to a change of apparent fat thickness of 1 mm. However, when the difference of fat thickness between that over the vertebral body and that over any of the background areas was considered, there was no relationship with threshold level, so that the setting chosen was not critical.

Fat thickness differences for AP scans

For each CT slice the mean fat thicknesses over the vertebral body (V) and over the background area outside the vertebral body but inside the selected overall width (B) were calculated. B1 refers to a width of 65 mm, B2 to 85 mm, B3 to 105 mm and B4 to 125 mm, most attention being paid to the last as being the preferred value. B − V then constituted the fat thickness difference. The results are illustrated as a frequency distribution for B4 − V for all the slices, separated by sex, in Fig. 3. As mean bone mineral is usually presented for each patient, the mean value of B − V ($\overline{B-V}$) was calculated from all slices for each patient. $\overline{B4-V}$ was positive in all but one of 20 subjects.

The results are summarized in Table I. It can be seen that $\overline{B-V}$ increases with background width, particularly in women. The difference between $\overline{B4-V}$ for men and women was significant at $p < 0.05$. The variance of B4 − V for all slices in individual patients, with a mean standard deviation of 6.3 mm for men and 9.1 mm for women, was similar to the standard deviations of $\overline{B4-V}$ for the groups.

The results were also examined at different levels through the lumbar spine. For each patient a slice was

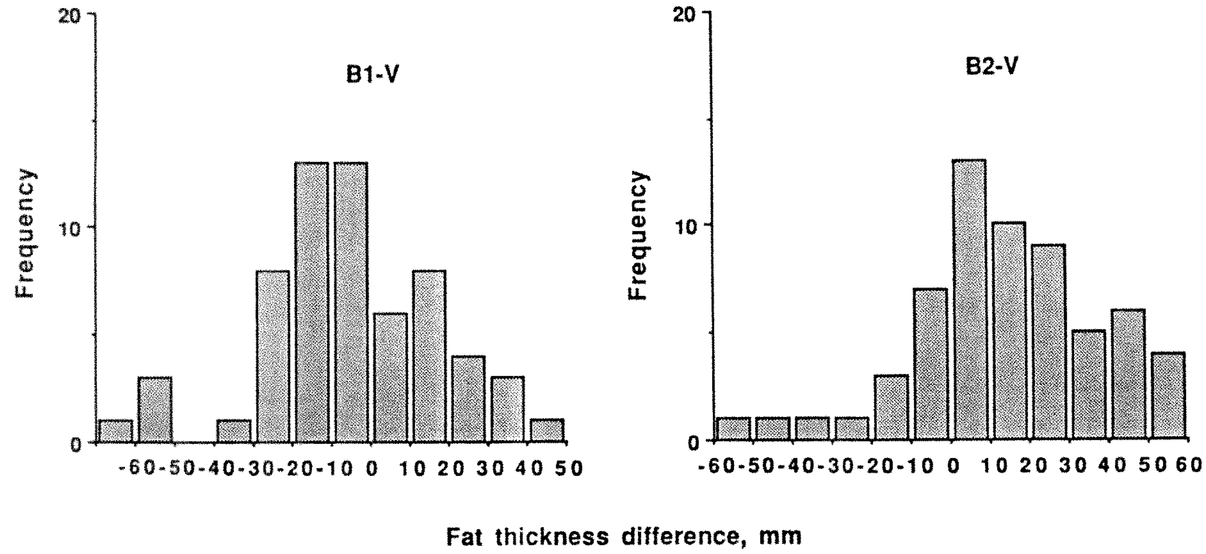

Figure 4. Distributions of differences of thickness of adipose tissue between that over the vertebral bodies and that in anteriorly placed background areas, for lateral scanning.

identified that passed through the vertebral body at L2, L3 and L4. Mean values of B4 − V at the different levels are shown in Table II. For men there were no significant differences of B4 − V for the different vertebrae, but B4 − V was greater at the level of L4 than at either L2 or L3 in women.

The mean value of V was 58.1 ± 28.1 mm for men and 47.7 + 21.4 mm for women. A relationship between B − V and V was sought by linear regression and a somewhat weak one was found, with $\overline{B4-V} = 0.175\overline{V} \pm 1.72$, $r = 0.52$, $p < 0.02$, when results for men and women were considered together.

Fat thickness differences for lateral scans

Mean fat thicknesses were calculated for each slice in the same way as for AP scans. Two values of B were determined, B1 being an area anterior to the vertebral body of the same width and B2 twice that width. There were no significant differences of B − V between men and women, the means being B1 − V = 2.4 ± 16.3 mm for men, 6.7 ± 13.5 mm for women, B2 − V = −1.5 ± 17.0 mm for men, −6.1 ± 14.2 mm for women. The frequency distributions are therefore combined in Fig. 4. There were too few slices through vertebrae other than L3 to permit an investigation of the effect of slice level. It can be seen from Fig. 4 that the mean value of B − V was lower for lateral than AP scanning, but the variance was greater. There was no correlation between B − V and V for lateral scanning.

Bone mineral equivalence of fat-equivalent materials

Most of the measurements were made with a thickness of BEM corresponding to an areal bone mineral density (BMD) of approximately 1 g/cm^2 of calcium hydroxyapatite, near the values found in normal subjects. Thicknesses of FEM ranging from 1 to 7 cm were added and for all three machines the bone mineral equivalence was closely linear when plotted against thickness. The slope of this line then gave the required factor relating fat to apparent bone. The results are presented in Table III. Those for the two Hologic machines and the Norland XR26 were very similar, but the Lunar DPX gave values approximately 11% higher,

Table I. Differences of adipose tissue thickness (B − V) in millimeters for different overall background widths for AP scanning. Means ± standard deviations of all slices covering L2–L4 in 10 subjects of each sex

	Background width (mm)			
	65 (B1 − V)	85 (B2 − V)	105 (B3 − V)	125 (B4 − V)
Men	4.9 ± 6.2	5.1 ± 6.7	5.6 ± 7.7	6.7 ± 8.1
Women	6.9 ± 3.3	8.4 ± 3.0	10.9 ± 3.7	13.4 ± 4.7

Table II. Differences of adipose tissue thickness (B4–V) in millimetres through different lumbar vertebrae for AP scanning. Means ± standard deviations, 10 men, 10 women

	Vertebral level			
	L2	L3	L4	L2–4
B4–V for men	8.2 ± 7.2	3.8 ± 10.5	5.1 ± 6.8	6.7 ± 8.1
B4–V for women	8.5 ± 6.2	9.8 ± 5.4	19.5 ± 8.2*	13.4 ± 4.7**

*Male/female difference significant at $p < 0.001$.
**Male/female difference significant at $p < 0.05$.

in accordance with a similar overestimate of the hydroxyapatite standard, itself scanned without any FEM. Also included in Table III is the density of the FEMs, to permit expression of the bone mineral equivalents for 1 g/cm^2 of material.

The linear relationship between FEM thickness and bone mineral equivalence meant that measurements made with one material could be used to predict results with another by using the factors in Table III. Polyethylene, 34 mm thick, was therefore used as the most convenient material to investigate the effects of different water and BEM thicknesses.

Water depths of 10, 15, 20 and 25 cm were used with a BEM thickness of approximately 1 g/cm^2. Water depth was kept at 15 cm while BEM thickness was varied from 0.4 to 1.3 g/cm^2. The reproducibility of measurements of bone mineral was about 1%. When the difference between measurements of BEM with and without FEM was used to give the bone mineral equivalence of the fat, the uncertainty rose to about 7%. Within this level of uncertainty there was no appreciable dependence of bone mineral equivalence on the thickness of water or bone mineral with any of the apparatus investigated.

Effect of fat thickness differences on error in bone mineral

The measured bone mineral equivalence was used to determine the errors in spine bone mineral measurements introduced by the fat thickness differences reported above. Adipose tissue is not pure fat and indeed probably varies somewhat between sites and subjects. The assumptions were made that adipose tissue is 85% fat and that fat is represented by stearic acid (Nord & Payne, 1990); 1 cm adipose tissue is thus equivalent to -0.043 g/cm^2 of hydroxyapatite. This factor can be used to determine the errors introduced by the differences of adipose thickness $(B-V)$ presented in Table II and Figs 3 and 4.

For AP scanning the mean error in the BMD of L2–L4 taken together was an overestimate of 0.029 ± 0.034 g/cm^2 for men and 0.057 ± 0.020 g/cm^2 for women, or about 3% and 6%, respectively, of normal values. The error exceeded 0.1 g/cm^2 (about 10% of normal) in 10% of slices, but only in one subject out of 20 when taking a mean of L2–L4.

Table III. Bone mineral equivalents for Hologic QDR-1000, Norland XR26 and Lunar DPX

	g/cm^2 hydroxyapatite for 1 cm of material			Density (g/cm^3)
	Hologic	Norland	Lunar	
Polyethylene	0.057	0.058	0.065	0.91
Paraffin wax	0.057	—	—	0.91
Perspex	0.036	0.035	0.042	1.18
Stearic acid	0.050	0.049	0.059	0.95
Lard	0.049	—	—	—

For lateral scanning the mean values of $B-V$ were not significantly different from zero, but the dispersion was greater. Results for each slice are more important, as bone mineral will generally be determined for one vertebra or a part of it. $Bl-V$ exceeded ± 20 mm in a third of slices and ± 40 mm in 8%. The resulting errors in BMD of 0.086 g/cm^2 and 0.172 g/cm^2 represent more than 10% and 20% of normal values.

Variation of BMD with background width in patients

A dependence of total bone mineral content (BMC) and bone mineral density (BMD) on the background width was evident. However, some of this dependence was found to be due to the automatic edge-fitting routine, which defines the extent of the vertebrae. The area selected varied slightly with the overall width included in the analysis. This variation was established by scanning the Hologic spine phantom, in which the "soft-tissue" background is homogeneous plastic. The same scans were used to determine a correction factor for the patient scans. The results are presented in Table IV.

The standard deviations of the patient BMD values show that a wide range was covered, in fact from 0.47 to 1.25 g/cm^2. On the other hand, the standard deviations of the differences in BMD between the different background widths was low, indicating a consistent pattern. The standard deviations for the phantom scans, reflecting only the reproducibility of the measurements, were satisfactorily low. Reducing the analysed scan width below the preferred 125 mm does lead to a small, but significant apparent decrease in BMD, as predicted from the mean fat thickness differences derived from the CT scans. The disparities are greater for the lower lumbar vertebrae, again as predicted.

The variation of BMD with background width, presumably due to non-uniform fat distribution, may be compared quantitatively with that predicted from the

Table IV. BMD values (in g/cm^2) for different overall scan widths (in mm). Means ± standard deviations for 20 patients or 10 repeated scans of Hologic spine phantom

	Overall scan width (mm)		
	85	105	125
L2–L4, patients	0.9111 ±0.2169	0.9224 ±0.2164	0.9287 ±0.2144
L2–L4, phantom	1.0329 ±0.0027	1.0380 ±0.0026	1.0397 ±0.0026
L2–L4, patients, corrected	0.9171	0.9239	0.9287
Corrected difference from 125 mm			
for L2–L4	−0.0116 ±0.0136	−0.0048 ±0.0063	
for L2 only	0.0073	0.0048	
for L3 only	−0.0182	−0.0047	
for L4 only	−0.0194	−0.0126	

CT scans by using the data in Tables I and III. Taking means of the results for men and women for L2–L4, the adipose tissue thickness differences between background widths of 85 mm and 125 mm would be 3.3 mm and between 105 mm and 125 mm, 1.8 mm. These translate into BMD differences, assuming that adipose tissue is equivalent to 85% of stearic acid in water, of 0.014 g/cm^2 and 0.0077 g/cm^2, respectively, values not far from those presented in Table IV.

Discussion

Previous reports of the effect of non-uniform fat on errors of bone mineral measurements in the spine have been concerned with radionuclide source absorptiometry. Roos et al (1980) used measurements on cadavers to deduce that a median error of 7% was introduced into their estimation of bone mineral in L3. Their measurement system is, however, unique.

Farrell and Webber (1989) used CT scans to examine fat distribution. Their conclusions were similar to ours, although the results were expressed in a different way. They deduced that the corresponding error in DPA measurements using a ^{153}Gd source had a median value of 7.9%. This figure has been challenged (Mazess & Sorenson, 1989; Sorenson, 1990) and inconsistencies in their calibration procedures have been pointed out (Pye, 1991). With a consistent treatment, the median error would be 3.6%.

Our own previous investigation regarding fat errors in ^{153}Gd and ^{241}Am/^{137}Cs scanning (Tothill et al, 1989) was based on some of the same CT scans as were used in the present work, so naturally the conclusions are similar. However, different background areas were used, so there are quantitative differences in the fat thickness differences. Our previous finding that a background area far enough from the vertebral bodies to exclude lateral processes increased the fat error substantially, led us to modify our technique of analysis (Tothill et al, 1989). Backgrounds in DXA scanning are usually chosen by edge-detecting algorithms so that the inner edges are close to the vertebral bodies, but the suggested outer edges are quite widely spaced. Table I shows that the fat error can be minimized by reducing the width, but this might have a deleterious effect on precision.

The agreement between the observations of the variation of BMD with background width in patient scans and those predicted from the CT scan data is reassuring, but it must be remembered that the populations were different and so small as to provide no more than an indication of trends.

Our previous bone equivalent factors for radionuclide source scanning, based on assumptions about soft-tissue composition and using tabulated attenuation coefficients, were somewhat lower than the measured values presented here. There have been other estimates of the bone mineral equivalence of fat in DXA. Cullum et al (1989), also using a Hologic QDR-1000, found an apparent 1% change of bone density owing to 3 mm of fat-equivalent material replacing water over bone. They do not indicate what FEM was used, nor the baseline bone density, but their estimate of the error appears to be smaller than ours as presented in Table III.

Hangartner and Johnston (1990) used Lucite to model fat in phantom studies similar to ours. Lucite is methyl methacrylate, similar to Perspex. They accept that it is not a perfect match for fat, as the ratio of attenuation coefficients at the two photon energies is somewhat lower than that for fat. However, the linearity of the effects with thickness of Lucite allows the differences to be taken into account. They found that a fat thickness difference of 1 cm would lead to a bone mineral error of 0.044 g/cm^2 for a Hologic QDR-1000 and 0.051 g/cm^2 for a Lunar DPX. These values are slightly lower than ours for stearic acid (Table I).

Our present communication is the first to combine a survey of fat distribution derived from CT scans with measurements of the bone equivalence of fat in DXA scanning, so no direct comparisons can be made with other results. The examination of errors introduced in lateral scanning is also new. The important finding here is the large variance between patients of fat thickness differences. Errors greater than 10% would be quite common.

Heterogeneity of fat distribution affects precision as well as accuracy. Valkema et al (1990) have shown that heterogeneity of the soft-tissue background increases the standard deviation above that expected from counting statistics using ^{153}Gd DPA. The effect is relatively more important for DXA because the higher photon intensity and greater stability mean that physical limitations of precision are reduced.

The above is concerned with spatial variations of fat distribution. Temporal changes would also be important. It is possible that the pattern of fat distribution changes as the total amount of fat alters. A number of studies of bone mineral changes during weight loss are under way and it could well be that a variable fat error would influence the conclusions.

Intervertebral fat also introduces an error into DPA measurements of spine bone mineral. Its magnitude can be estimated from the composition quoted by Mazess and Vetter (1985). They give a value of 100 mg/cm^3 of fat in the trabecular space of young subjects rising to 300 mg/cm^3 in old subjects. Taking a path length of 2.5 cm, these figures lead to bone mineral errors of 0.013 and 0.038 g/cm^2, respectively, using our equivalence values. These errors are smaller than the average errors resulting from extravertebral fat distributions, but will partially compensate for them for AP scanning.

We have not, as yet, given any attention to possible errors resulting from uneven fat distribution in other parts of the skeleton; it is likely that they will be smaller, as the highly heterogeneous abdominal fat will not be a problem.

Although it is important to appreciate the possibility of errors resulting from fat non-uniformity, there is probably no practical way of making corrections. Multiple-slice CT scanning on all DPA patients would be neither feasible nor justified. Triple-photon scanning has been proposed as a way of providing another equation to solve the third unknown (Jonson et al, 1988). However, the attenuation coefficients are not sufficiently independent, so that the equations are ill conditioned and cannot give an accurate or precise result without a large and impractical increase in photon collection and dose (Farrell & Webber, 1990; Stronach et al, 1990; Kotzki et al, 1991).

The *in vivo* precision of DXA of the lumbar spine, at better than 0.01 g/cm^2 of bone mineral, is excellent and sufficient to permit confidence in longitudinal studies, at least regarding the measurement technique itself. The limitations of accuracy imposed by non-uniform fat distribution will only affect such longitudinal studies if there are appreciable changes of fat. However, the possibility of errors resulting from fat must be borne in mind when assessing the normality of an individual. An error of 0.1 g/cm^2 is possible and this is comparable to the coefficient of variation of the results for normal subjects; indeed, it must contribute to it.

Acknowledgments

We are grateful to Mr Martin Connell for advice and assistance in computing, to Dr David Reid for access to, and help with, the measurements on the Norland DXA apparatus in Aberdeen and to Mrs Kay Fenner for similar assistance with the Lunar apparatus in Glasgow.

References

CULLUM, I. D., ELL, P. J., & RYDER, J. P., 1989. X-ray dual-photon absorptiometry: a new method for the measurement of bone density. *British Journal of Radiology*, *62*, 587–592.

FARRELL, T. J. & WEBBER, C. E., 1989. The error due to fat inhomogeneity in lumbar spine bone mineral measurements. *Clinical Physics and Physiological Measurement*, *10*, 57–64.

—— 1990. Triple photon absorptiometry cannot correct for fat inhomogeneity in lumbar spine bone mineral measurement. *Clinical Physics and Physiological Measurement*, *11*, 77–84.

HANGARTNER, T. N. & JOHNSTON, C. C., 1990. Influence of fat on bone measurements with dual-energy absorptiometry. *Bone and Mineral*, *9*, 71–81.

JONSON, R., ROOS, B. & HANSSON, T., 1988. Triple-photon energy absorptiometry in the measurement of bone mineral. *Acta Radiologica*, *29*, 461–464.

KOTZKI, P. O., MARIANO-GOULART, D. & ROSSI, M., 1991. Theoretical and experimental limits of triple photon energy absorptiometry in the measurement of bone mineral. *Physics in Medicine and Biology*, *36*, 429–437.

MAZESS, R. B. & SORENSON, J. A., 1989. Low influence of fat on spine densitometry? *Clinical Physics and Physiological Measurement*, *10*, 287–288.

MAZESS, R. B. & VETTER, J., 1985. The influence of marrow on measurement of trabecular bone using computed tomography. *Bone*, *6*, 349–351.

NORD, R. H. & PAYNE, R. K., 1990. Standards for body composition calibrations in DEXA. In *Current Research in Osteoporosis and Bone Mineral Measurement*, ed. by E. F. J. Ring (British Institute of Radiology, London), pp. 27–28.

PYE, D. W., 1991. Estimation of the magnitude of the error in bone mineral measurement due to fat: the effect of machine calibration. *Clinical Physics and Physiological Measurement*, *12*, 87–91.

ROOS, B. O., HANSSON, T. H. & SKOLDBORN, H., 1980. Dual photon absorptiometry in lumbar vertebrae: evaluation of the baseline error. *Acta Radiologica Oncologia*, *19*, 111–114.

SORENSON, J. A., 1990. Spine densitometry—further comments on errors. *Clinical Physics and Physiological Measurement*, *11*, 251–253.

STRONACH, I. M., SCOTT, M. C. & SOMERVAILLE, L. J., 1990. Bone density by photon scattering and absorptiometry. In *Current Research in Osteoporosis and Bone Mineral Measurement*, ed. by E. F. J. Ring (British Institute of Radiology, London), pp. 22–23.

TOTHILL, P. & PYE, D. W., 1990. Errors due to fat in lateral spine DPA. In *Current Research in Osteoporosis and Bone Mineral Measurement*, ed. by E. F. J. Ring (British Institute of Radiology, London), p. 19.

TOTHILL, P., PYE, D. W. & TEPER, J., 1989. The influence of extra-skeletal fat on the accuracy of dual photon absorptiometry of the spine. In *Osteoporosis and Bone Mineral Measurement*, ed. by E. F. J. Ring, W. D. Evans and A. S. Dixon (IPSM, York) pp. 48–53.

VALKEMA, R., VERHEIJ, L. F., BLOKLAND, J. A. K., ZWINDERMAN, A. H., BIJVOET, O. L. M., PAPAPOULLOS, S. E. & PAUWELS, E. K. J., 1990. Limited precision of lumbar spine dual-photon absorptiometry by variations in the soft-tissue background. *Journal of Nuclear Medicine*, *31*, 1774–1781.

1992, *The British Journal of Radiology*, 65, 814–815

Technical notes

An afterloading technique utilizing The Royal London Hospital caesium-137 brain needle in an oral obturator

By A. M. Tierney, BSc, B. S. Mantell, FRCP, FRCR

Departments of Medical Physics and Radiotherapy and Oncology, The Royal London Hospital,
London E1 1BB, UK

(*Received 13 September 1991 and in revised form 3 January 1992, accepted 15 January 1992*)

Keywords: Brachytherapy, Oral cancer

The intended use of the brain needle (Fig. 1) is the irradiation of brain tumours using a stereotactic technique (Mantell et al, 1986). We have adapted the needle to suit another purpose.

A patient with a mixed tumour of the right paranasal sinuses was treated by initial chemotherapy followed by maxillectomy, leaving a large cavity extending to the roof of the sphenoid sinus, where histology of the resected specimen showed residual squamous cell carcinoma. Post-operative external irradiation using 8 MV X rays was given to the entire operated volume as a dose of 5000 cGy in 24 fractions over 36 days. It was intended to boost the dose to the region of the sphenoid sinus to minimize the risk of recurrence at this site, while keeping the dose to the brain stem within tolerance. This was achieved by brachytherapy using precisely placed radiation sources (CD12040 miniature cylindrical sources, Amersham International) in the brain needle.

In order to treat the surface of the cavity a closely fitting obturator was constructed by the dental laboratory. The mould was marked via the right nostril to obtain the entry point for the needle. Simulator films were then taken with the patient wearing the obturator. Gastrografin was used to highlight the surfaces of the obturator and the cavity and showed that they matched well. Isodoses of a tandem of sources of combined active length 10 mm and total activity 3020 MBq (81.6 mCi), were obtained from the Philips oncology support system and confirmed by calculations. The isodoses were corrected for magnification and superimposed on the simulator films enabling the desired source position to be determined. A hole was drilled in the obturator from the marked entry point allowing the needle to be inserted through the right nostril to bring the sources to the desired position (Fig. 2).

A final check was made to ensure that the obturator could still be worn comfortably and that the brain needle could locate, with ease, in the obturator. The needle stayed in position and did not slip even when the patient moved so it did not appear necessary to have a method of holding the needle in position. However, a suitable tie was attached for reassurance. Fig. 3 shows the patient wearing the obturator with the needle in position. The patient did not suffer any discomfort and with supervision was able to insert and retract the needle himself.

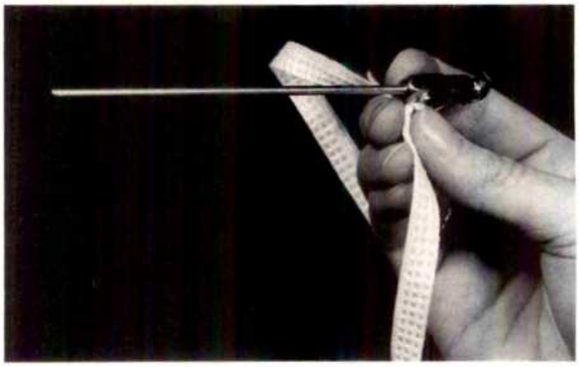

Figure 1. Brain source needle.

The doses was prescribed to the maximum dose-rate on the surface of the obturator, 200 cGy h^{-1} and a dose of 2250 cGy was given with the needle in place for 11 h 15 min over a period of 30 h. This is shown on Fig. 4 (sagittal) from which it was also possible to estimate the dose-rate to the brain stem at 8.5 cGy h^{-1}. Fig. 5 (coronal) shows the estimated dose-rates to the sides of the obturator and that to the left eye at 23 cGy h^{-1} which were considered acceptable.

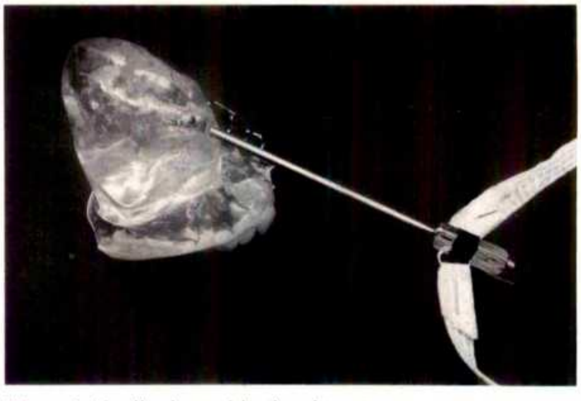

Figure 2. Needle situated in the obturator.

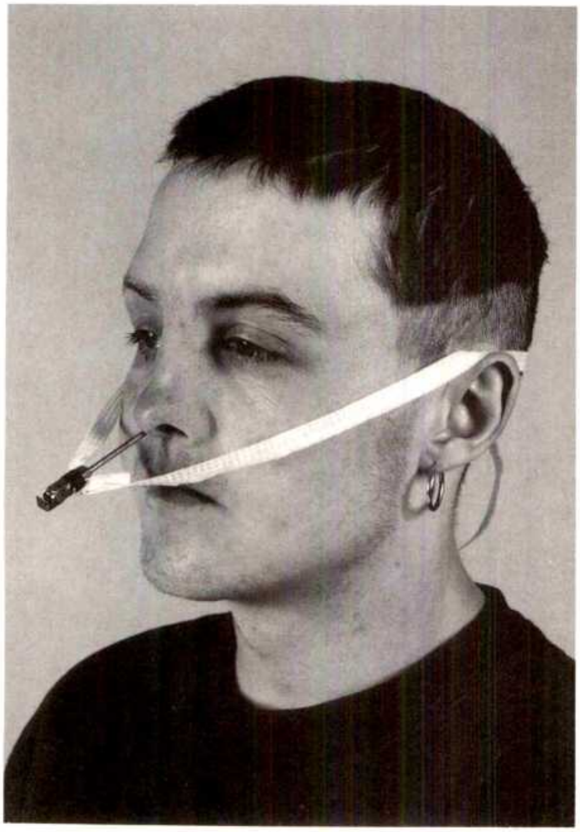

Figure 3. Patient wearing the obturator with the needle inserted and ties to ensure correct source position is maintained.

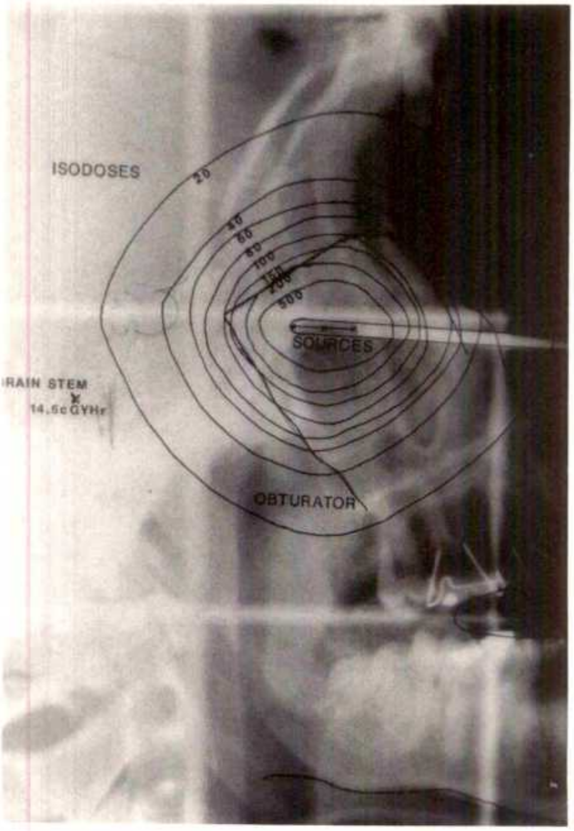

Figure 4. Isodose distribution around the sources indicating the dose-rates on the surface of the obturator.

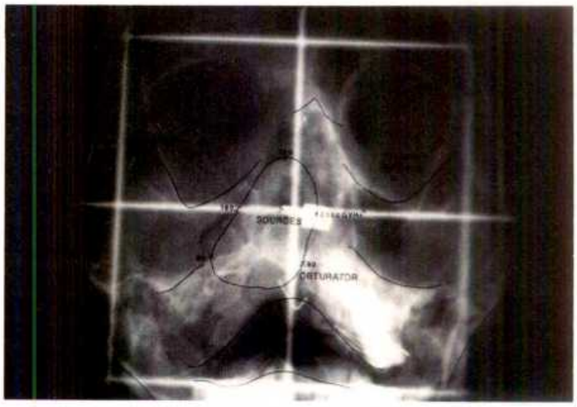

Figure 5. The estimated doses on the sides of the obturator.

Brachytherapy for cavities such as the nasopharynx has long been carried out using gynaecological sources such as a radium pack and more recently high dose-rate afterloading equipment has been available for this purpose. In the absence of such a facility this technique is advantageous for radiation protection, accuracy of dosimetry and a shorter treatment time.

Acknowledgments

The authors wish to thank Mr El Amin and Derek Crome at the dental clinic and Paul Smith, radioactive sealed sources custodian and mould room technician, for their technical contribution.

Reference

MANTELL, B. S., KLEVENHAGEN, S. C., AFSHAR, F., 1986. An afterloaded applicator for the interstitial irradiation of brain tumours. *Clinical Radiology, 37*, 35–38.

1992, *The British Journal of Radiology*, *65*, 816–818

A flexion and extension device for dynamic MR imaging of the neck

By D. M. Hadley, PhD, DMRD, FRCR, B. R. Condon, MSc, PhD, MIPSM and *W. Richardson, CEng, BSc, MIMechE

MRI Unit, Institute of Neurological Sciences, Southern General Hospital, 1345 Govan Road, Glasgow G51 4TF and *Department of Clinical Physics and Bio-engineering, 11 West Graham Street, Glasgow G4 9LF, UK

(*Received 2 December 1991 and in revised form 17 March 1992, accepted 10 April 1992*)

Keywords: MRI Neck, Flexion, Rheumatoid arthritis, Injury

Magnetic resonance (MR) imaging of flexion and extension manoeuvres in the cervical spine has proved useful in the clinical evaluation of bone and joint instability (Hadley & Condon, 1988; Jordan & Enzmann, 1991) as well as providing a research tool into the biomechanics of the living spinal cord (Condon & Hadley, 1988). Unfortunately the image acquisition procedure is time consuming. Difficulties in repositioning are coupled with problems of patient acceptibility caused by discomfort. Images have to be acquired with the patient's neck in flexion, extension and in a neutral position. Images taken at intermediate neck positions may also be necessary for a cine loop to be constructed so that the dynamics of the interactions between the cord and lesions (*e.g.* osteophytes, bone movement etc) can be adequately appreciated. In order to produce an image of sufficient resolution and contrast, each position must be maintained for several minutes. Even in normal volunteers this is rarely practicable if the neck is unsupported, so each position is maintained using various shapes of foam padding with the patient being removed from the imager between scans to alter their position. Repeated lifting and relocation of the patient's neck is required until a good angulation is achieved. Each time the patient also has to be carefully repositioned by the operator to ensure that the patient's midline is in the same plane as the long axis of the magnet. Ensuring correct angulation and positioning simultaneously is difficult and prone to error and scans have often to be repeated.

A device is described which reduces repositioning time and patient discomfort. It permits a calibrated means of ensuring correct angulation for flexion, extension and intermediate positions, as well as standardizing these between patients.

Methods

Figure 1 illustrates the system. The body of the device consists of Tufnol (a resin impregnated cloth) plates and is secured to the end of the patient couch platter using removable Delrin (an acetal plastic) bolts. Delrin and Tufnol were chosen because they contained no ferromagnetic components and produced no significant signal when imaged. The device itself operates by a screw and pulley block system. The pulley system has four cords and the pulley block separation can be changed by a distance of 50 mm using a knurled handwheel. This gives a total range of movement on the canvas head support of 200 mm. A pulley cord leads off the moveable pulley system for a metre in the direction of the patient and is secured to the apex of a triangular plastic plate. From the other two sides of the triangle two cords lead to the Tufnol head rest assembly which is bolted into the magnet end of the patient platter. The assembly consists of two Tufnol plates separated by four Delrin bars. The two cords loop over a tie bar above the patient's forehead, through channels sewn in either side of a canvas sling and are secured to the bottom of the head assembly. The patient's head rests on this sling.

The patient is centred on the couch using standard laser position markers and is positioned with their chin tucked into their chest in the flexed position, *i.e.* with the cord retracted into the block and pulley arrangement. The patient is now loaded into the magnet and the first scan obtained. The patient's head can now be lowered back a calibrated amount without the patient having to be withdrawn from the magnet. To do this the operator rotates the knurled handwheel disc a predetermined number of turns. The triangular plate ensures that both sides of the sling are lowered evenly so that the patient does not have to be repeatedly centred with respect to the median sagittal plane.

A full extension position is achieved because: (a) the

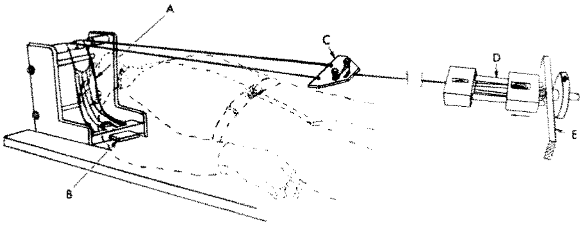

Figure 1 Diagrammatic arrangement of flexion/extension device. A = Canvas head support; B = spigot used to attach head support unit to patient support table; C = triangular support cord adjustment plate; D = screw and pulley block system; E = anchor plate which is firmly attached to the patient support table.

head assembly has no bottom plate, thus allowing the head to lie at a lower level than the patient platter and (b) a cylindrical foam pad is placed under the patient's neck so that their head "droops" over it when the sling is at its lowest point. During the lowering procedure communication with the patient is maintained. The conditions investigated are often too painful to obtain the full range of flexion and extension and it is rather a matter of how much angulation the patient can tolerate.

The images were acquired on a 0.15 T Picker resistive system using an spin-echo (SE) 700/32, 192 view, 2 average, 7 mm thick slice. A single loop surface coil in the shape of a "T" was placed between the sling and the patient's neck. The coil was made from flexible 30 gauge (0.3 mm) copper strip and was covered in plastic wrapping to insulate it electrically and to eliminate sharp edges which might cause discomfort. Flexible surface coils are now being produced commercially by some manufacturers which might be suitable for this purpose.

Scans were performed on a normal volunteer using both the conventional "remove from the magnet and reposition" approach and the new device. The acquisitions were timed and the angulation of brain stem with respect to cervical cord, and the line joining the posterior section of the foramen magnum and clivus with respect to the cord were both used as measures of how closely the device approximated to the conventional repositioning approach.

Results

Figure 2 shows the extension and flexion positions for the conventional positioning approach (upper images) and that for the device (lower images). Angular changes over the flexion and extension manoeuvre between the brain stem and the cervical cord, and between the brain stem and the line joining the posterior extent of the foramen magnum and the tip of the clivus, were the same for both techniques within experimental error (± = 3°). It took an additional 2 min to install the device on the patient couch, but approximately 9 min less for repositioning between scans. This meant a net saving of 7 min in an overall examination time of 51 min. Higher field systems with shorter acquisition and examination times would have a proportionately higher time saving.

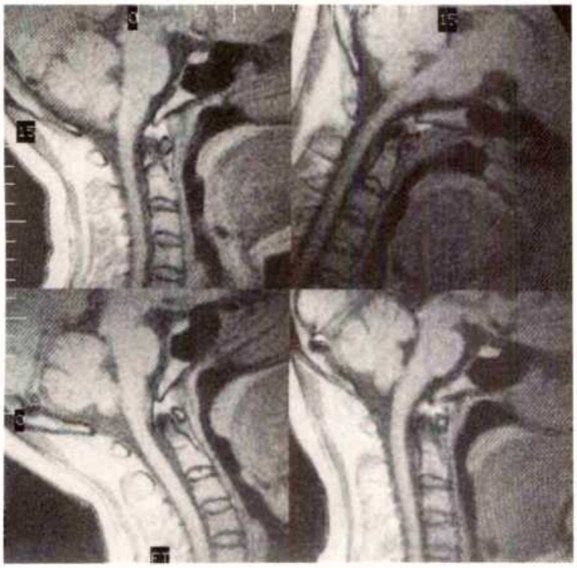

Figure 2. Extension and flexion. Upper figures: conventional positioning technique (extension left, flexion right); lower figures: device positioning technique (extension left, flexion right).

Discussion

It is clear from inspection of the images that the angulation of the skull with respect to the neck is different in the two techniques. In the conventional approach a higher degree of flexion is obtained, whilst better extension is achieved with the device. This apparent discrepancy between the quantitative and visual analyses is due to bending of the neck occurring not just at the atlanto-occipital junction (to which the angulation measurements apply), but also at each cervical level especially at C4/C5.

The winch system has, within error, matched the conventional positioning methods in terms of angular range at the atlanto-occipital junction, but has not managed to mimic the lower components in terms of flexion. It has actually exceeded the conventionally positioned limits of extension because it allows the back of the patient's head to be lower than the level of the platter. We had previously used padding to raise the patient's shoulder during the conventional extension view, erroneously assuming this would allow full extension to be achieved.

The inability to mimic full flexion using the device is not thought to be an intrinsic limitation of the device itself, but of the aperture of the body coil. The older style magnet used has an elliptical bore with a maximum height of 370 mm which limits the height of the tie bar in the head rest assembly over which the drawcords pass. Newer magnets with a round aperture of typically 550 mm or greater will allow a higher support rail and are more likely to allow the full flexion and extension manoeuvre to be performed.

Conclusion

The new device reduces the amount of manipulation to the patient's neck required to produce the correct angulation and position. As well as reducing discomfort it also reduces overall examination time and allows a more calibrated and standardized approach to positioning to be taken. It also allows full extension to be achieved at least as well as the conventional approach and also full flexion at the atlanto-occipital junction. The component of flexion occurring typically at C4/C5 was not achieved, but it is likely that this problem could be overcome in modern magnets. These have body coils with larger vertical internal diameters than the older system used for these measurements, thus allowing the full range of flexion.

References

Condon, B. R. & Hadley, D. M., 1988. Quantification of cord deformation and dynamics during flexion and extension of the cervical spine using MR imaging. *Journal of Computer Assisted Tomography*, *12* (6), 947–955.

Hadley, D. M. & Condon, B., Magnetic resonance imaging cine analysis of flexion and extension manoeuvres in the cervical spine. *British Journal of Radiology*, *61*, 723.

Jordan, M. & Enzmann D., 1991. *Dynamic MR Imaging of the Cervical Spine*. 10th Annual Meeting of the Society of Magnetic Resonance in Medicine (SMRM, Berkeley), p. 156.

Digital cardiac imaging—the death knell of cineangiography?

By J. F. Dyet, FRCR, W. Hartley, FRCR, *A. R. Cowen, BSc and C. P. Aber, FRCP

The Royal Infirmary, Anlaby Road, Hull HU3 2JZ and *Department of Medical Physics, Leeds General Infirmary, The Wellcome Wing, Gt George Street, Leeds LS1 3EX, UK

(*Received 17 May 1991 and in revised form 13 November 1991, accepted 14 January 1992*)

Keywords: Grey scale, Digital, Cineangiography, Image enhancement

Digital X-ray imaging techniques have achieved widespread acclaim in general vascular diagnosis and in the support of interventional procedures. However, in cardiac angiography, acceptability of digital imaging until recently, has been less enthusiastic. To a large extent this has reflected the effectiveness of cine fluorography and the exacting performance standards that it sets to any competing technique. Whereas cine fluorography provides rapid acquisition of dynamic sequences of high (spatio-temporal) fidelty images, the review of these images has to be retrospective and in practice it is necessary to rely heavily on the modest image quality provided by TV fluoroscopy for the on-line evaluation of the procedure.

Early attempts at digital cardiac imaging based upon digital subtraction angiography (DSA) produced results of widely inconsistent quality. This was partly because of the inferior specification of the equipment used at that time. In addition, however, the dynamic nature of the heart itself sets limits to the precision with which subtractive imaging could be performed. Non-subtractive, or grey-scale, digital imaging on the other hand promised several practical advantages over DSA for cardiac studies, provided that the quality of the images could be enhanced using digital imaging techniques (Rouse et al, 1986).

The recent introduction of extremely fast but economical analogue to digital converters and microprocessors now means that the contest between digital and cine fluorography in cardiac imaging can begin in earnest. Viable digital imaging systems which are custom designed for cardiac applications are now available.

This paper compares some of the advantages and disadvantages of an early Philips Digital Cardiac Imaging (DCI) system, with the present cine film "gold standard".

The equipment

In its basic format the DCI operates as a digital cine fluorography system. In this mode it provides rapid acquisition of non-subtracted (grey-scale) digital X-ray images. Digital cine images can be acquired at rates of up to 50 frames per second. Each image comprises a (512 × 512) pixel array with grey-scale discrimination on 256 discrete levels (namely 8 bits or 1 byte of information per pixel).

Correspondingly, each image frame contains approximately one quarter of a megabyte of information. The DCI at Hull utilizes a large diameter triple-field (14″–10″–6″) X-ray image intensifier and an XTV-6 television channel incorporating a 2″ frogs-head Plumbicon camera tube. The image intensifier output is mapped with a degree of overmagnification onto the target of the TV camera. This "overframing" technique, which is often used in cine fluorography, ensures that the digital matrix array is used efficiently. This leads to a corresponding reduction in image field coverage, but this has not proved a problem in cardiac imaging. In DCI the television camera target signal is read out in progressive (non-interlaced) scan mode leading to optimal detail resolution of the moving coronary arteries.

The DCI system also incorporates an enhanced definition mode which provides an increased level of signal-to-noise ratio where the clinical procedure demands better image quality. In this mode the maximum image acquisition speed is reduced to eight frames per second (f.p.s.), while the operating radiation dose is increased by a factor of seven. Subtractive imaging is

---

Address correspondence to Dr J. F. Dyet, Cardiovascular Radiology Unit, Radiology Department, The Royal Infirmary, Hull HU3 2JZ.

also available with the DCI at this reduced image acquisition speed. Other acquisition facilities available with the DCI include high-contrast pulsed fluoroscopy (HCF); the last 5 s of the sequence can be stored for later review and road mapping (two files are provided for multiple road maps).

In its basic form the DCI incorporates a 474 Mbyte magnetic disc; this storage capacity can be increased optionally to 1.42 Gbyte. Digital cardiac imaging inevitably yields prodigious quantities of digital image data. For example, 8 runs at 10 s per run, imaging at 25 f.p.s. yields a volume of data equivalent to the total capacity of the standard hard disc. Under these conditions it would be necessary to review and download the image data to archive after each patient. It is clearly advisable to limit the volume of image data acquired at the outset by optimizing the image acquisition speed; at Hull Royal Infirmary 12.5 f.p.s. is routinely used for coronary examinations. In the DCI, long term archiving may be provided in digital form via an optional streamer tape drive. In practice, the images are archived in their enhanced form on analogue recording media as static frames on a video hard copy imager (Du Pont Opti-Imager) and/or as a dynamic series on VHS video tape. In principle, digital image archival and soft copy review are two of the principal attractions of digital imaging technology.

A major advantage of DCI is that the dynamic sequences of images can be reviewed and analysed immediately following acquisition. The DCI enables this review process to be controlled, either at the patient's side using an infrared hand controlled viewpad or at the separate viewing station, which provides a wider range of image handling and processing facilities. The viewpad enables road map selection, image storage and recall, and instant review of all runs in real-time (or slow motion both forward and reverse). The viewing station console also provides for processing and quantitative analysis of the images.

Image enhancement

Being a computerized system it is possible to perform post-acquisition image enhancement to accentuate certain features. The following programs are available: edge enhancement, window level and width, zoom and loupe (spot magnification).

Analytical programs

The DCI also provides on-line quantification of a number of cardiac functions. These include the following.

Ejection fraction. After identifying the plane of the aortic valve and the apex of the left ventricle, the ventricular outline is automatically traced in end systolic and end diastolic frames. If these tracings appear inaccurate they can be corrected manually. The ejection fraction is then automatically calculated by the area-length method of Sandler & Dodge (1986) (Fig. 1). Using the catheter size as a reference measurement, stroke volume, end systolic and end diastolic volumes can be calculated (Fig. 1).

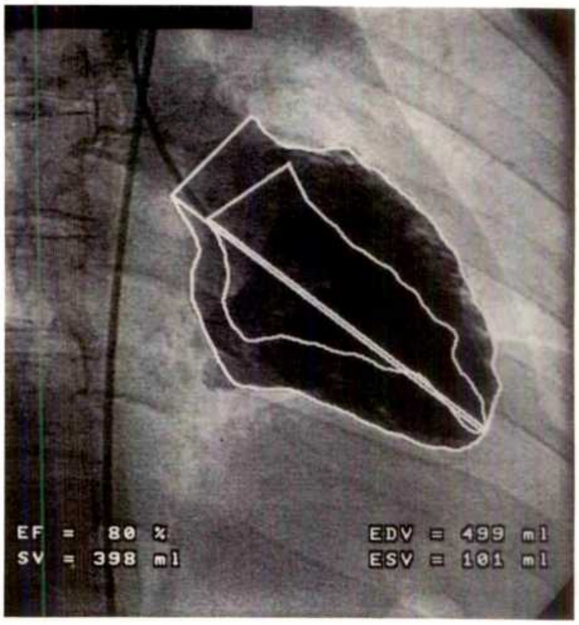

Figure 1. Automatic ejection fraction.

Central line wall motion analysis. Using the information already available the left ventricular wall motion is analysed and reproduced graphically (Fig. 2) (Sheehan, 1986).

Wall motion region of interest. (Fig. 3). This program analyses regional wall motion (Kirkeeide & Gould, 1986).

Coronary analysis. Using the catheter size for calibration, the section of vessel which is of interest is automatically analysed. Edge detection techniques allow the

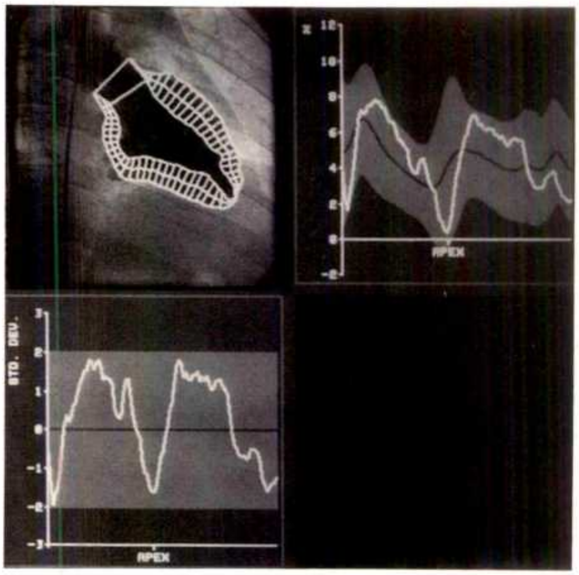

Figure 2. Centre line wall motion.

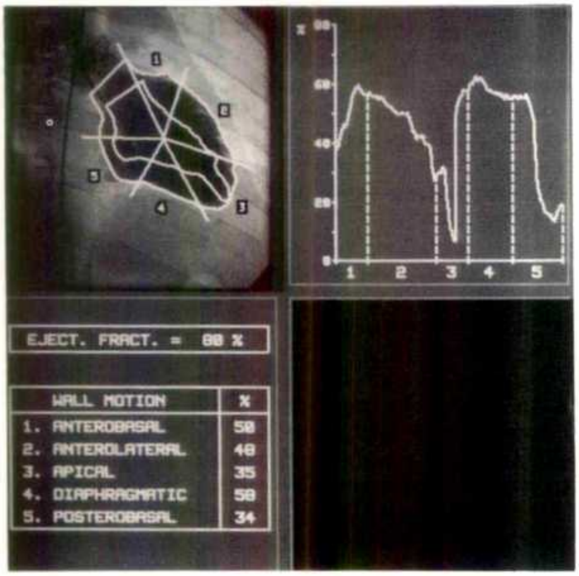

EJECT. FRACT. = 88 %

WALL MOTION	%
1. ANTEROBASAL	50
2. ANTEROLATERAL	40
3. APICAL	35
4. DIAPHRAGMATIC	58
5. POSTEROBASAL	34

Figure 3. Regional wall motion.

contour to be drawn and then the size of the vessel and the percentage of stenosis are calculated (Fig. 4). This facility is particularly useful in sizing angioplasty balloons.

Digital subtraction. We have found this facility useful when investigating extracardiac anomalies. Subtraction may be performed using any frame speed as a pre- or post-acquisition mode. The best images are produced at lower frame rates (less than 8 f.p.s.).

Archiving

Following our initial use of equipment, and after discussion with our surgeons as to what images they found acceptable, we adopted the following methods of archiving, acknowledging a workload of approximately 20 cases per week.

Recording at 12.5 f.p.s. we are able to archive 1 week's work on a C30 standard VHS cassette. This becomes our master copy and never leaves the department. Each case is reported immediately on completion and if intervention is thought to be indicated a separate VHS tape is recorded on a C10 cassette. This tape accompanies the patient to surgery or to angioplasty, but following the intervention is wiped clean and reused. In addition to obtaining the two VHS tapes, selected images are transferred from the photofile onto a hard copy (a standard 35 × 43 cm radiograph) (Fig. 5) using a Dupont Opti-Imager. This is stored in the patient's X-ray envelope. If desired, the digital information can be stored on streamer tape.

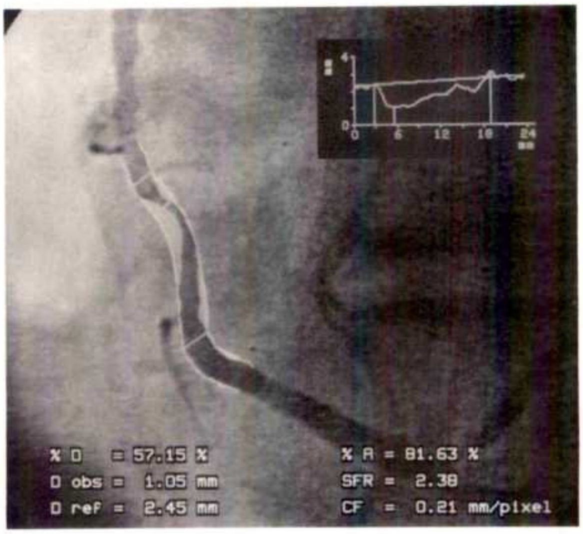

% D = 57.15 %
D obs = 1.05 mm
D ref = 2.45 mm
% A = 81.63 %
SFR = 2.38
CF = 0.21 mm/pixel

Figure 4. Vessel diameter and percentage stenosis.

Comparison with cine film

With use of an optical distributor incorporating a semi-reflective mirror, it is possible to record simultaneous DCI and cine film on each patient. The timing of the frames is identical, as a single pulse of radiation produces both images. In our first 100 coronary angiography patients, simultaneous recordings were made at an acquisition rate of 25 f.p.s. 6 months later, these were re-reported randomly by two radiologists working independently. The number of significant stenotic lesions (those judged to be of more than 50% severity) was noted and each recording was scored for quality, being awarded three (good), two (satisfactory) or one (poor) points. (Tables I & II).

There is no significant difference between the number of lesions reported using DCI and cine film. The slight variation is due to observer interpretation in assessing whether a lesion exceeds 50% severity. Both radiologists scored the quality of the DCI as better than the cine film in a large number of cases, but it is impossible to offer valid statistical evaluation because the viewing of the recordings cannot avoid bias, since the different method of presentation of cine film and DCI recorded on video tape is obvious.

Table I. Number of patients in each stenosis group

Number of stenoses per patient	0	1	2	3	4	5†
DCI	47	43	30	33	24	23
Cine	48	46	28	29	23	26

$\chi^2 = 0.36$ (no significant difference between the two recording modes).

Table II. Quality assessment

	Cine	DCI	Equal
Radiologist 1	6	31	63
Radiologist 2	7	25	68

$\chi^2 = 0.46$ (no significant difference between the two radiologists).

Discussion

One of the main reasons that cine fluoroscopy has been so successful is that the high spatial resolution has given excellent film detail. Theoretically, digital acquisition on a 512 matrix produces poorer spatial resolution, but because the contrast resolution can be controlled directly, it is possible to demonstrate abnormalities more clearly using digital techniques. Digital techniques also allow suppression of unwanted signals such as lung flare, which can be a problem with cine fluoroscopy.

In addition to the analytical programs already referred to, the digital system offers further advantages in radiation reduction, reduction in archiving cost and space, and also in its compatibility with other digital systems which are common in modern radiology departments.

The reduced radiation is of particular importance to interventionists and is achieved by lowering the frame rates from 50 f.p.s or 25 f.p.s. to 12.5 f.p.s.. With digital acquisition it is possible to obtain flicker-free images at this frame rate by using a gap filling technique.

The main disadvantage of the DCI is its cost. A single plane system cost approximately £110 000 more than a comparable cine system. We believe that digital acquisition is the cardiac imaging system of the future. Already, because of its digital control, enhancement facilities and analytical programs, it is considerably more versatile in operation than cine fluoroscopy. Further technological advances will undoubtedly occur, making digital systems even more attractive.

References

KIRKEEIDE, R. L. & GOULD, K., 1986. Computer applications in angiography. In *Cardiac Imaging and Image Processing*, ed by Wai-Hoc (McGraw, Hull).

ROUSE, S., SILVERTON, M. P. & CHANDRA, V. S., 1986. Imaging of the coronary arteries using DGA. *Radiography, 52* (606), 271–273.

SANDLER, H. & DODGE, H. T., 1986. The use of single plane angiocardiograms for the calculation of left ventricular volume in man. *American Heart Journal, 75*, (3), 325–334.

SHEEHAN, F. H., 1986. Advantages and applications of the centerline method for characterizing region ventricular function. *Circulation, 74* (2), 293–305.

1992, *The British Journal of Radiology*, 65, 822–824

Case reports

Tuberculosis of the ribs: computed tomographic findings

By R. FitzGerald, FRCR and *C. E. Hutchinson, BSc, FRCR, FFRRCSI

Department of Radiology, New Cross Hospital, Wolverhampton, UK

(Received 10 September 1991 and in revised form 9 January 1992, accepted 11 February 1992)

Keywords: Osseous tuberculosis, Computed tomography, Mediastinal lymphadenopathy

Tuberculosis (TB) is still endemic in Britain, 5474 cases being notified in England and Wales during 1989 (9:100 000). Eighty-one new cases of TB were notified in Wolverhampton during that year (31:100 000). Despite the introduction of preventative and curative treatment, this is little less than half the 195 new cases of TB in Wolverhampton notified during 1947 (Report of the Director of Public Health, Wolverhampton, 1990). The ethnic minorities in Britain are overrepresented amongst the patients with tuberculosis (Davies et al, 1984). Wolverhampton has a rate three times the national average, and this is considered to be due to the social and ethnic structure of its population.

In the USA the incidence of tuberculosis, which had been previously declining over decades, has since 1985 shown an increase (Buckner et al, 1991). This is considered to be due to the HIV epidemic. Clinical manifestations of tuberculosis in patients with AIDS are often atypical. In approximately 15% of patients without HIV infection TB occurs at extrapulmonary sites, whereas this is seen in 40% of patients who are HIV positive (Goldsmith, 1990).

Bony tuberculosis is classically described in about 1% of patients with tuberculosis (Davidson & Horowitz, 1970). The rib is an uncommon site of osteoarticular tuberculosis.

We present two cases of rib tuberculosis which demonstrate the computed tomographic (CT) appearances and the role of CT in its diagnosis.

Case reports

Case 1

An 80-year-old male Indian farmer presented with lower left chest pain for 6 months. He had smoked until 3 years prior to his admission. Chest radiograph showed a destructive lesion in the left 5th rib with associated soft tissue shadowing. The mediastinum was unremarkable on the chest film. The lesion was initially thought to be malignant, CT was performed and showed right paratracheal, carinal and sub-carinal lymph node enlargement. There was an area of low attenuation with rim enhancement seen deep to serratus anterior and contiguous with a similar lesion in the pleural space (Fig. 1). On bone settings there was destruction of the associated rib. CT attenuation reading of this lesion suggested it to be a fluid density. Aspiration of this lesion yielded pus which grew tuberculous bacilli.

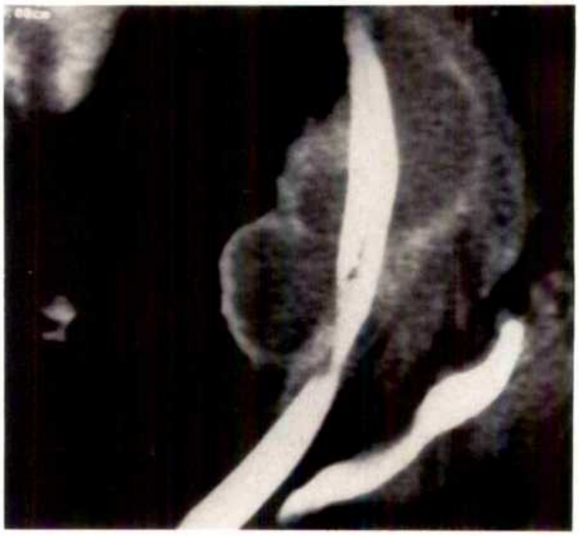

Figure 1. Case 1. Dynamic CT, 100 ml iohexol (300 mgI/ml). Chest wall and pleural soft tissue lesion with rim enhancement and low attenuation centre.

Case 2

A 39-year-old male Indian solicitor was referred with a three month history of pain in the left parasternal region and also interscapular pain. He had a pyrexia, weight loss, anorexia and was experiencing night sweats. On his chest film there was suspicion of right paratracheal nodal enlargement. CT was performed 6 days later in an effort to confirm this. On PA and lateral chest radiographs there was no evidence of chest wall abnormality.

CT showed right paratracheal, carinal and sub-carinal nodal enlargement. The sub-carinal nodes showed peripheral enhancement with central low density (Fig. 2). In the left posterior upper thorax there was a lesion involving the chest wall, rib and pleural space (Fig. 3). Again the CT attenuation suggested fluid density. Biopsy confirmed the presence of tuberculosis bacilli.

Neither patient was thought to be at risk for HIV infection.

Discussion

The ribs are unusual sites for osteo-articular tuberculosis, occurring in none of 36 patients described by

---

*Present address: University of Manchester, Department of Diagnostic Radiology, Stopford Building, Oxford Road, Manchester, M13 9PT, UK.

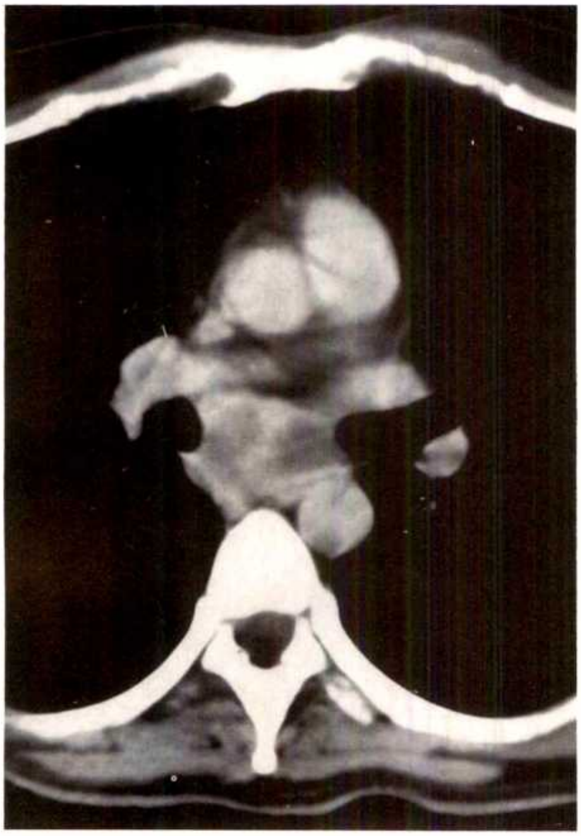

Figure 2. Case 2. Post-contrast CT, 50 ml bolus iohexol (300 mgI/ml). Subcarinal lymph node enlargement exhibiting peripheral enhancement and lower attenuation centre.

Foley-Nolan et al (1991) nor in any of 71 patients reported by Rathakrishnan & Mohd (1989) and in only two of 499 cases described by Goldblatt & Cremin (1978). Newton cited one case of 'chest wall' TB in his series of 74 Manchester patients (Newton et al, 1982) and Nicholson found that 14 of their 176 patients had TB involving 'ribs, manubrium and sternum' (Nicholson, 1974). Brown in Bradford was able to identify and describe seven cases of tuberculosis of the ribs (Brown, 1980).

In the largest series reported, the shaft was the site of infection in the majority of the 23 cases of rib tuberculosis (Tatelman & Drouillard, 1953). Costovertebral involvement was the next most common presentation invariably associated with tuberculous spondylitis.

In our first case, CT images on bone settings demonstrated irregular bone destruction that was not shown on plain radiographs. In our second case, CT demonstrated bony destruction and the associated soft tissue lesion, neither of which were apparent on the plain films.

The nature of bone destruction shown on CT was as one would expect from descriptions in a conventional radiology text (Thijn & Sheensma, 1990), or in previous

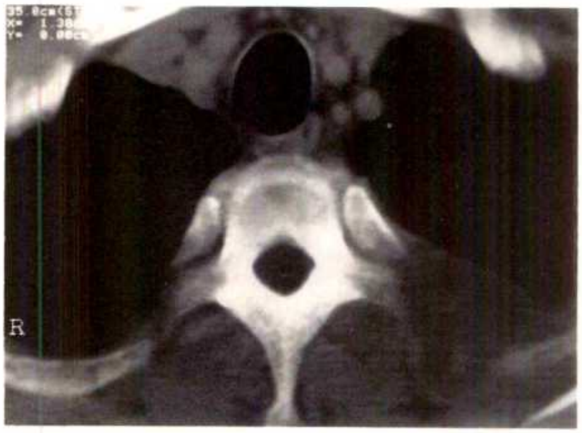

Figure 3. Case 2. Post-contrast CT, 50 ml bolus iohexol (300mgI/ml). Fluid density lesion involving chest wall, rib and pleural space seen in upper left thorax posteriorly.

reports of skeletal tuberculosis demonstrated with CT (Coppola et al, 1987; Ip et al, 1989). The associated soft tissue lesions in our patients had similar features of central low attenuation with rim enhancement which Coppola et al (1987) described in a review paper of CT in musculoskeletal tuberculosis. Similar appearance of TB of the chest wall was shown by Eschelman et al (1991). However, one should be aware of other imaging findings in rib tuberculosis not seen in our patients. Ip et al (1989) described two patients with rib tuberculosis whose associated soft tissue component did not have a low attenuation centre, and relative high attenuation rim. Such an appearance could obviously mimic a tumour and indeed tumour-like tuberculous lesions of bone have been described at other sites (Abdelwahab et al, 1987).

The differential diagnosis of an irregular destructive rib lesion associated with an adjacent soft tissue mass with or without low attenuation change would include metastasis, multiple myeloma, Ewing's and invasive peripheral lung cancer, as well as infective pathology such as actinomycosis and other indolent infections.

Im et al (1987) found the presence of low density areas within enlarged mediastinal nodes to be very helpful in differentiating tuberculosis from other causes of mediastinal lymphadenopathy (22/23 patients). They demonstrated a marked preponderance of enlarged tuberculous mediastinal nodes to be in the right paratracheal, right tracheobronchial and the sub-carinal areas. Our two patients conformed to this pattern.

Low attenuation change in enlarged mediastinal nodes is recognized in lymphoma (North et al, 1990) and metastatic disease, if somewhat unusual (Im et al, 1987). There is overlap in the distribution of enlarged mediastinal nodes in tuberculosis versus neoplastic disease with lymphoma often involving the right paratracheal area. However, sparing of the prevascular and hilar areas is very suggestive of mediastinal TB.

Coloured patients have been shown to exhibit changes of sclerosis and/or florid periosteal reaction associated with their tuberculous bone destruction on plain radiography (Jacobs, 1964; Chapman et al, 1979). Although this was not seen in our patients nor in those of Coppola et al (1987) or Ip et al (1989), one would expect in due course to see such CT findings described.

Because of the AIDS epidemic and the associated increase in the incidence of TB, this is a diagnosis that needs to be considered more frequently than in the recent past. Moreover, given the high rate of extrapulmonary involvement (Goldsmith, 1990), radiologists will need to be attentive to the skeletal manifestations of tuberculosis. Firooznia et al (1973) in a report of 21 cases of disseminated extrapulmonary tuberculosis associated with heroin addiction found that the ribs were the most common site of infection in this group of patients.

Tuberculosis has been shown to occur earlier in the course of HIV infection than other opportunistic infections such as pneumocystic carinii (Goodman, 1990). Delays of many months in the diagnosis of skeletal tuberculosis are well recognized (Newton et al, 1982) but they still occur (Foley-Nolan et al, 1991), but early CT of the thorax and recognition of the features described here may expedite the diagnosis.

In conclusion, the CT findings or irregular rib destruction, with an associated soft tissue lesion which exhibits a low attenuation centre and exhancing rim combined with right-sided mediastinal node enlargement should alert the radiologist to a diagnosis of rib tuberculosis and, if the patient is not of a social group predisposed to tuberculosis, consideration should be given to the possibility of drug abuse or HIV infection.

Acknowledgments

We would like to thank Dr S. J. Connellan and Dr J. S. Mann for their permission to report their patients.

References

Abdelwahale, I., Present, D. A., Zwass, A., Klein, M. J. & Mazzra, J., 1987. Tumour-like tuberculous granulomas of bone. *American Journal of Roentgenology, 149,* 1207–1208.

Brown, T. S., 1980. Tuberculosis of the ribs. *Clinical Radiology, 31,* 681–684.

Buckner, C. B., Leithiser, E., Walker, C. W. & Allison, J. W., 1991. The changing epidemiology of tuberculosis and other mycobacterial infections in the United States: implications for the radiologists. *American Journal of Roentgenology, 156,* 255–264.

Chapman, M., Murray, R. O. & Stoker, D. J., 1979. Tuberculosis of the bones and joints. *Seminars in Roentgenology, 14,* 266–282.

Coppola, J., Muller, N. L. & Connell, D. G., 1987. Computed tomography of musculoskeletal tuberculosis. *Journal of the Canadian Association of Radiologists, 38,* 199–203.

Davidson, P. T. & Horowitz, J., 1970. Skeletal tuberculosis —a review with patient presentations and discussions. *American Journal of Medicine, 48, 77–84.*

Davies, P. D. O., Humphries, M. J., Byfield, S. P., Nunn, A. J., Daryshire, J. H., Citron, K. M. & Fox, W., 1984. Bone and joint tuberculosis; a survey of notifications in England and Wales. *Journal of Bone and Joint Surgery, 66B,* 326–330.

Echelman, D. J., Gibbens, D. T., Fielding, J. R., Romo, L. V., Parker, D. R., Argy, N. & O'Connor, J. F., 1991. Chest case of the day. *American Journal of Roentgenology, 156,* 1295–1300.

Firooznia, H., Selinger, G., Abrams, R. M., Valensi, V. & Shamoun, J., 1973. Disseminated extrapulmonary tuberculosis in association with heroin addiction. *Radiology, 109,* 291–296.

Foley-Nolan, D., Deegan, R. I., Foley-Nolan, A. A., Barry, C., Coughlan, R. J. & Hone, R., 1991. Skeletal tuberculosis. *Irish Medical Journal, 84,* 72–73.

Goldblatt, M. & Cremin, B. J., 1978. Osteo-articular tuberculosis: its presentation in coloured races. *Radiology, 29,* 669–677.

Goldsmith, M. F., 1990. Fogotten (almost) but not gone, tuberculosis suddenly looms large on domestic scene. *Journal of the American Medical Association, 264,* 165–166.

Goodman, P. C., 1990. Pulmonary tuberculosis in patients with acquired immunodeficiency syndrome. *Journal of Thoracic Imaging, 5,* 38–45.

Im, J. G., Song, K. S., Kang, H. S., Park, J. H., Yeon, K. M., Han, M. C. & Kim, C. W., 1987. Mediastinal tuberculosis lymphadenitis: CT manifestations. *Radiology, 164,* 115–119.

Ip, M., Chen, N. K., So, S. Y., Chiei, S. W., & Lam, W. K., 1989. Unusual rib destruction in pleuropulmonary tuberculosis. *Chest, 95,* 242–244.

Jacobs, P., 1964. Osteo-articular tuberculosis in coloured immigrants: a radiological study. *Clinical Radiology, 15,* 59–69.

Newton, P., Sharp, J. & Barnes, K. L., 1982. Bone and joint tuberculosis in Greater Manchester, 1969–1979. *Annals of the Rheumatic Diseases, 41,* 1–6.

Nicholson, R. A., 1974. Twenty years of bone and joint tuberculosis in Bradford. *Journal of Bone and Joint Surgery, 56B,* 760–765.

North, L. B., Libshitz, H. I. & Lorigan, J. G., 1990. Thoracic lymphoma. *Radiologic Clinics of North America, 28* (4), 745–762.

Rathakrishnan, V. & Mohd, T. H., 1989. Osteo-articular tuberculosis. *Skeletal Radiology, 18,* 267–272.

Report of Director of Public Health, Wolverhampton, 1990. Chapter 12, pp. 51–53.

Tatelman, M. & Drouillard, E. J. P., 1953. Tuberculosis of the ribs. *American Journal of Roentgenology, 70,* 923–935.

Thijn, C. J. P., & Sheensma, J. T., 1990. *Tuberculosis of the Skeleton. Focus on Radiology* (Springer-Verlag, Heidelberg), p. 144.

1992, *The British Journal of Radiology*, 65, 825–827

External carotid angioplasty in the treatment of developing stroke

By A. H. Troughton, FRCR, R. A. Morgan, FRCR, R. M. Paxton, FRCR and I. P Wells, FRCR
Department of Neuroradiology, Derriford Hospital, Derriford Road, Plymouth, UK

(*Received 6 August 1991 and in revised form 15 January 1992, accepted 6 March 1992*)

Keywords: Angioplasty, External carotid artery, Stroke

Percutaneous transluminal angioplasty (PTA) is gradually becoming accepted as a method of treatment for internal and common carotid stenoses, although the exact indications, risks and outcomes have not yet been determined (Brown et al, 1990). Angioplasty of atherosclerotic stenoses of the external carotid artery has been performed less often. We present a case where a patient developed increasing hemiparesis since much of the left cerebral circulation was supplied from a stenosed external carotid artery and collaterals. The left internal carotid artery was occluded and the right internal carotid stenosed. The patient's symptoms improved markedly following PTA of the left external carotid artery.

Case report

A 76-year-old woman presented with a 2 month history of slurred speech and increasing weakness of the right arm and leg. She was a lifelong smoker. On examination she was dysarthric, normotensive and in sinus rhythm. The heart sounds were normal but there were bilateral high pitched carotid bruits. On the right side there was mild weakness of the arm and leg, an increased ankle jerk and an extensor plantar reflex. Cranial nerve assessment was normal.

Carotid angiography demonstrated complete occlusion of the left internal carotid and a severe stenosis at the orgin of the left external carotid artery (Fig. 1). There was also a 25% stenosis at the origin of the right internal carotid artery. Although there was some blood flow across the Circle of Willis from the right to left, there was a significant left cerebral supply from the left external carotid via the superficial temporal and supraorbital arteries and then retrogradely along the ophthalmic artery to the carotid syphon.

The patient's condition continued to deteriorate with further weakness of the right arm and leg. It was decided to perform angioplasty of the left external carotid artery to increase the collateral flow to the left hemisphere.

The left common carotid artery was cannulated with a 5 French Mani catheter (W. Cook, Europe) from a right femoral approach. It was not possible to pass a conventional guide wire across the stenosis, but a hydrophilic guide wire passed easily and the diagnostic catheter was placed across the stricture. A 5 mm angioplasty balloon on a straight 5 French catheter was used to dilate the stenosis. The balloon was inflated three times for 20 s on each occasion. Apart from heparinized saline used to flush the catheter no additional heparin was used. A good angiographic result was obtained and no pressure measurements were taken (Fig. 2). The procedure was done under light sedation and the patient suffered neither general nor neurological ill effects throughout.

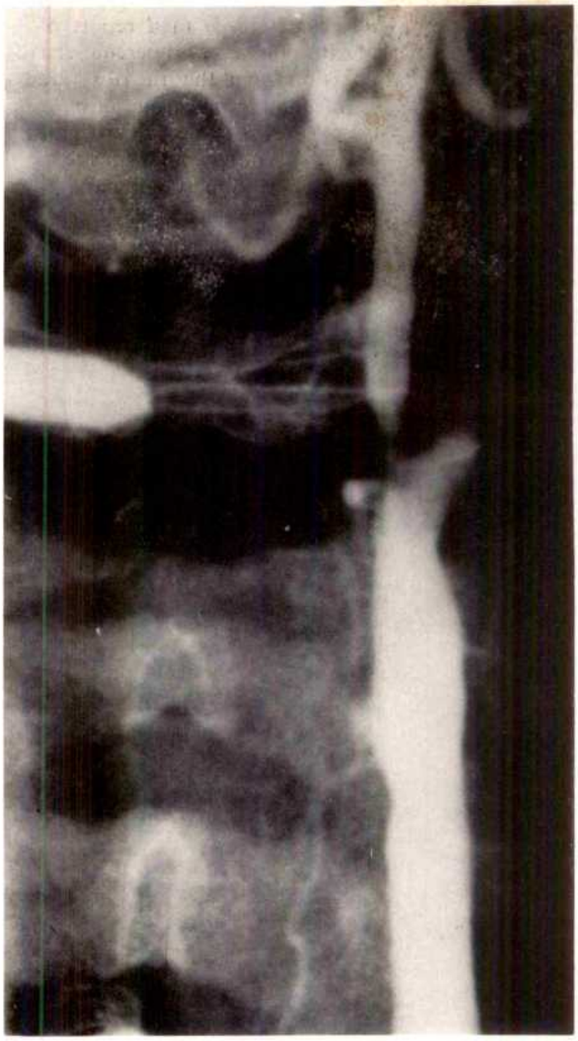

Figure 1. Left carotid angiography demonstrating complete internal carotid occlusion and severe stenosis of the external carotid artery.

By the next day her condition showed marked improvement. She was discharged 1 week later with the strength in her right leg having returned to normal and with only a mild residual weakness of the right arm.

Address correspondence to Dr A. Troughton, Department of Radiology, Bristol Royal Infirmary, Marlborough Street, Bristol BS2 8HW.

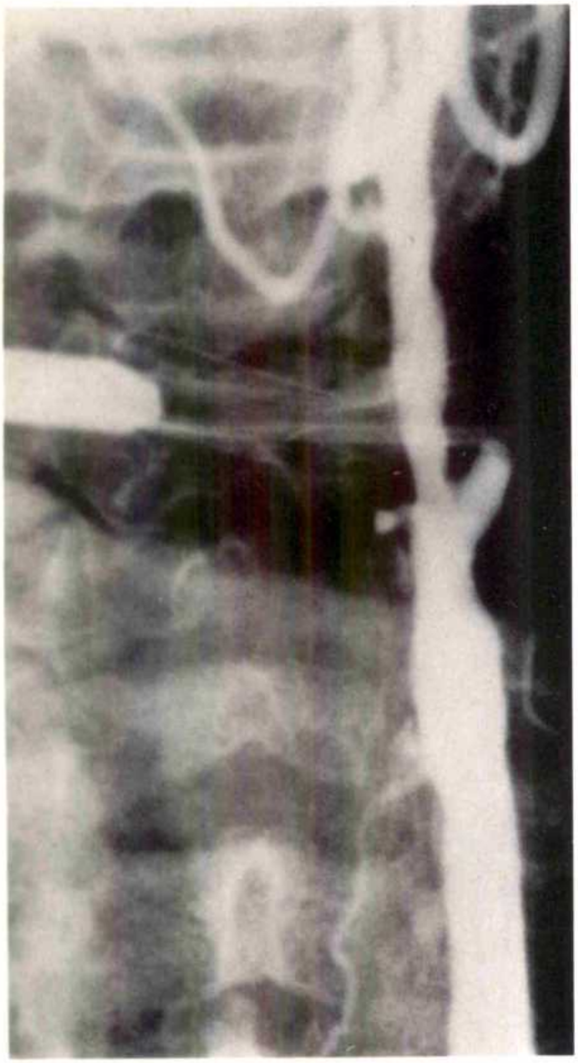

Figure 2. Post-angioplasty appearance of the left external carotid stenosis showing a marked radiographic improvement.

Discussion

Balloon angioplasty of the carotid artery was first described by Kerber and Mullan in separate case reports in 1980 (Kerber et al, 1980; Mullan et al, 1980). Both of these were intraoperative dilatations during carotid endarterectomy. Few case reports followed this because of the perceived risk of causing embolic stroke (Fallon, 1980). Following a retrograde transluminal carotid angioplasty through an arteriotomy, the small amount of debris that was dislodged was collected and analysed (DeMonte et al, 1989). This material was composed of cholesterol crystals and amorphous debris. It is the clinical effect of even a small amount of this material reaching the cerebral circulation that is of concern. Nevertheless, PTA of the supra-aortic arteries has been successfully performed in selected patients and the results have been described in the literature in recent years (Brockenheimer & Mathias, 1983; Wiggli & Gratzl, 1983; Zeitler et al, 1983; Tsai et al, 1986; Vitek et al, 1986; Freitag et al, 1987; Theron et al, 1987; Brown et al, 1990; Kachel, 1991).

The reported success rate of PTA of the supra-aortic arteries is 94–97% (Becker et al, 1989; Kachel et al, 1991) and is similar to that reported from other vascular areas where the technique is more commonly applied (Gruntzig & Kumpe, 1979). No deaths have been described following supra-aortic PTA. The major complication is permanent paresis and this occurs in 0.5% of supra-aortic cases and 1.7% of carotid artery cases. Minor complications include puncture site haematomas, transient neurological symptoms and thromboemboli in the digital arteries. These occur in 2–4% of cases (Becker et al, 1989; Kachel et al, 1991).

Endarterectomy is the established treatment for carotid stenoses in those patients fit for surgery. This has a reported 7.5% risk of death or severe stroke at or within 30 days of surgery (European carotid surgery trial, 1991), although different studies have found risks between 2% and 21% (Easton & Sherman, 1977; Browse & Ross-Russell, 1984). Patients with coexisting symptomatic coronary disease have a 14% mortality rate at surgery (Tsai et al, 1986). Apart from stroke within the territory of the operated vessel, strokes of other areas, myocardial infarcts, pulmonary emboli and local cranial nerve lesions can all occur as surgical complications (Sundt et al, 1975). It is against this technique and its risks that carotid PTA results must be measured. The evidence so far suggests that angioplasty compares favourably.

Most of the reports of carotid angioplasty concern the internal carotid artery. External carotid artery PTA is performed much less commonly, although it has been done prior to temporal artery to middle cerebral artery shunt operations (Motarjeme et al, 1982; Vitek et al, 1986). Although Vitek successfully dilated the external carotid artery in 18 cases, the results of the bypass operations have been disappointing and have failed to prevent ischaemic strokes (EC/IC Bypass Study Group, 1985).

There have been few reports of external carotid PTA to increase collateral flow when the internal carotid artery is occluded (Tsai et al, 1986; Kachel et al, 1991). The three patients described had transient ischaemic attacks but were asymptomatic at the time of the dilatation. The technique was successful and no complications occurred.

External carotid PTA as a treatment of developing hemiparesis has not to our knowledge been reported previously, but may prove useful in cases such as this when no other options are practical.

References

BECKER, G. S., KATZEN, B. T. & DAKE, M. D., 1989. Non coronary angioplasty. *Radiology*, *170*, 921–940.

BROCKENHEIMER, S. A. M. & MATHIAS, K., 1983. Percutaneous transluminal angioplasty in atherosclerotic internal carotid artery stenosis. *American Journal of Neuroradiology*, *4*, 791–792.

1992, *The British Journal of Radiology*, *65*, 827–830

BROWN, M. M., BUTLER, P., GIBBS, J., SWASH, M. & WATERSTON, J., 1990. Feasibility of percutaneous transluminal angioplasty for carotid artery stenosis. *Journal of Neurology, Neurosurgery and Psychiatry*, *53*, 238–243.

BROWSE N. L. & ROSS-RUSSELL, R. W., 1984. Carotid endarterectomy and the Javid Shunt: the early result of 215 consecutive operations for transient ischaemic attacks. *British Journal of Surgery*, *71*, 53–57.

DEMONTE, F., PEERLESS, S. & RANKIN, R., 1989. Carotid angioplasty with evidence of distal embolisation. *Journal of Neurosurgery*, *70*, 138–141.

EC/IC BYPASS STUDY GROUP, 1985. Failure of extracranial-intracranial arterial bypass to reduce the risk of ischaemic stroke. *New England Journal of Medicine*, *313*, 1191–1202.

EASTON, J. D. & SHERMAN, D. G., 1977. Stroke and mortality rate in endarterectomy; 228 consecutive operations. *Stroke*, *8*, 565–568.

EUROPEAN CAROTID SURGERY TRIALLISTS COLLABORATIVE GROUP, 1991. MRC European carotid surgery trial. Interim results for symptomatic patients with severe (70–99%) or with mild (0–29%) carotid senoses. *Lancet*, *337*, 1235–1244.

FALLON, J. T., 1980. Pathology of arterial lesions amenable to percutaneous transluminal angioplasty. *American Journal of Roentgenology*, *135*, 913–916.

FRIETAG, G., FRIETAG, J., KOCH, R. D., HEINRICH, P., WAGEMANN, W., HENNIG, H. P. & DEIKE, R., 1987. Transluminal angioplasty for the treatment of carotid artery stenoses. *Vasa*, *16*, 67–71.

GRUNTZIG, A. & KUMPE, D. A., 1979. Technique of percutaneous transluminal angioplasty with a Gruntzig balloon catheter. *American Journal of Roentgenology*, *132*, 547–552.

KACHEL, R., ST BASCHE, HEERKLOTZ, I., GROSSMANN, K. & ENDLER, S., 1991. PTA of the supra-aortic arteries especially the internal carotid artery. *Neuroradiology*, *33*, 191–194.

KERBER, C., CROMWELL, L. D. & LOEHDEN, E. L., 1980. Catheter dilatation of proximal carotid stenosis during distal bifurcation endarterectomy. *American Journal of Neuroradiology*, *1*, 348–349.

MONTARJEME, A., KEIFER, J. W. & ZUSKER, A. J., 1982. PTA of the brachiocephalic arteries. *American Journal of Roentgenology*, *138*, 457–462.

MULLAN, S., DUDA, E. E. & PATRONAS, N. J., 1980. Some examples of balloon technology in neurosurgery. *Journal of Neurosurgery*, *52*, 321–329.

SUNDT, T. M., SANDOK, B. A. & WHISNANT, J. P., 1975. Carotid endarterectomy: complications and preoperative assessment of risk. *Mayo Cinical Practice*, *50*, 301–306.

THERON, J., RAYMOND, J., CASASCO, A. & COURTHEOUX, F., 1987. Percutaneous angioplasty of atherosclerotic and post surgical stenosis of carotid arteries. *American Journal of Neuroradiology*, *8*, 495–500.

TSAI, F. Y., MATOVICH, V., HIESHIMA, G., SHAH, D. C., MEHRINGER, C. M., TIU, G., HIGASHIDA, R. & PRIBRAM, H. F. W., 1986. Percutaneous transluminal angioplasty of the carotid artery. *American Journal of Neuroradiology*, *7*, 349–358.

VITEK, J. J., KELLER, F. S., DUVAL, J. R., GUPTA, K. L. & CHADRA-SEKAR, B., 1986. Brachiocephalic artery dilatation by PTA. *Radiology*, *158*, 779–785.

WIGGLI, U. & GRATZL, O., 1983. Transluminal angioplasty of stenotic carotid arteries: case reports and protocol. *American Journal of Neuroradiology*, *4*, 793–795.

ZEITLER, E., BERGER, G. & SCHMITT-RUTH, R., 1983. Percutaneous transluminal angioplasty of the supra-aortic arteries. In: *Percutaneous Transluminal Angioplasty*. C. T. Dotter, W. Gruntzig, W. Schoop and E. Zeitler (Springer-Verlag, Berlin), pp. 245–261.

Osteosarcoma metastatic to the kidney with invasion of the inferior vena cava

By C. M. P. King, BSc, MRCP, FRCR, R. H. Reznek, FRCP, FRCR, *A. J. Norton, MRCPath and †J. E. Kingston, BSc, FRCP

Departments of Diagnostic Radiology, *Histopathology and †Paediatric Oncology, St Bartholomew's Hospital, London, UK

(*Received 22 November 1991, accepted 14 January 1992*)

Keywords: Kidney, Metastases, Osteosarcoma

Although renal metastases are found at autopsy in 12% of patients with osteosarcoma (McKenna et al, 1966), antemortem diagnosis is extremely rare. Deposits occur as part of widespread dissemination of the disease and the patients usually die of other effects before their renal disease becomes symptomatic.

We report a patient who presented 5 years after treatment for a femoral osteosarcoma with a renal metastasis involving the renal vein and inferior vena cava which was demonstrated on computed tomography (CT) and ultrasound. This entity has not been previously described and the initial suspicion was that the patient had developed a further primary tumour.

Case report

A 15-year-old male presented in January 1985 with a swelling above the left knee. Radiographs suggested an osteosarcoma and biopsy confirmed the diagnosis.

Address correspondence to: Dr R. H. Reznek, Department of Diagnostic Radiology, St Bartholomew's Hospital, West Smithfield, London, EC1A 7BE.

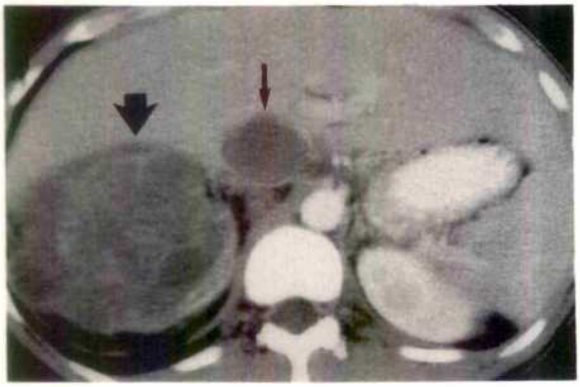

Figure 1. Enhanced CT scan showing replacement of the right kidney by tumour (large arrow). The inferior vena cava is completely filled with tumour (small arrow).

Staging investigations, including CT of the chest and radionuclide bone scan, showed no evidence of metastases. Initial treatment was by limb sparing resection of the primary tumour with pre- and post-operative chemotherapy. Local recurrence a year later necessitated disarticulation of the hip. In March 1989 a left upper lobectomy and wedge resection of the left lower lobe were performed for pulmonary metastases.

Thereafter, he remained well until June 1990 when he presented with a 6 week history of painless haematuria. He failed to attend for investigation of this problem and the haematuria apparently resolved spontaneously. In August 1990 he returned having noticed a lump in the right hypochondrium.

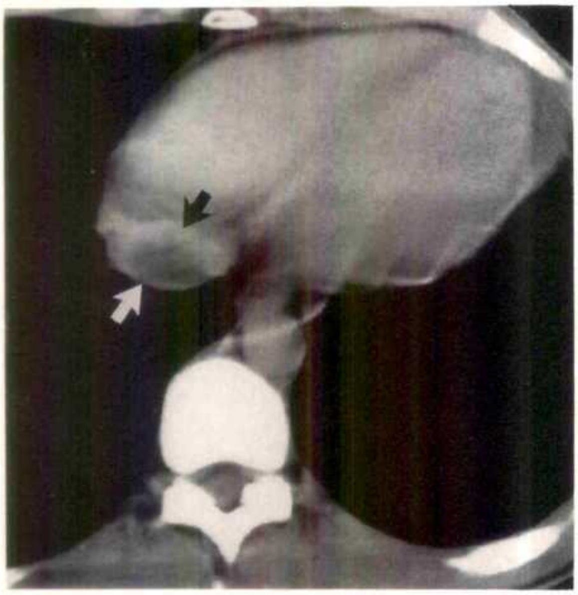

Figure 2. Enhanced CT scan showing extension of the tumour into the supra-diaphragmatic part of the inferior vena cava (arrowed).

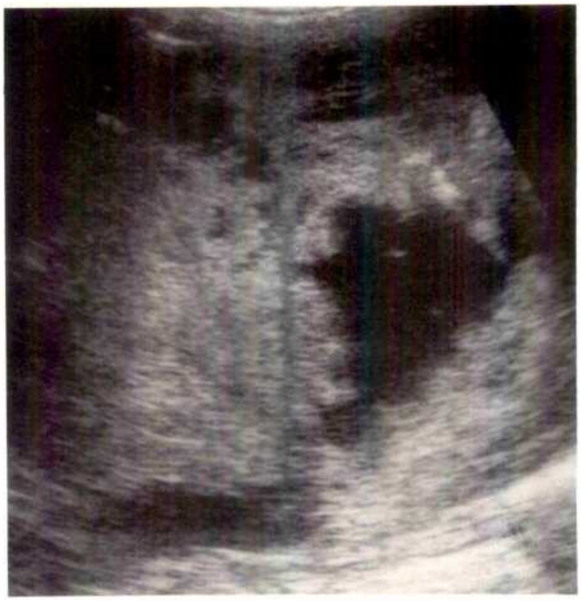

Figure 3. Transverse ultrasound scan of the right kidney showing large partially necrotic tumour mass.

A CT scan showed an inhomogeneous 15 cm mass which showed no calcification or ossification and entirely replaced the right kidney. The mass enhanced after intravenous contast medium (Fig. 1). Dynamic enhanced scans showed massive tumour extension into the inferior vena cava extending superiorly into its supra-diaphragmatic portion (Fig. 2) and into the lower right atrium, and inferiorly to below the pancreatic head. The left kidney appeared normal and no lymph

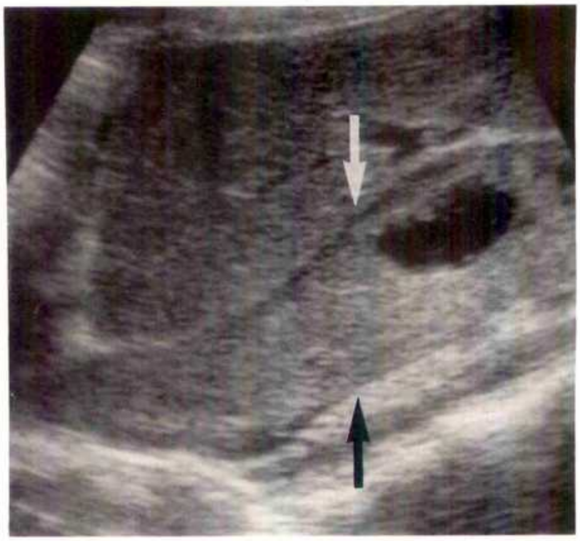

Figure 4. Longitudinal ultrasound scan through the inferior vena cava showing the lumen filled with partially necrotic tumour (arrows) extending above the diaphragm.

node enlargement was found. There were two small pulmonary deposits.

Ultrasound showed a large mass replacing the right kidney with multiple irregular cystic areas presumed to represent necrosis (Fig. 3). Involvement of the inferior vena cava extending above the confluence of the hepatic veins was confirmed (Fig. 4). Under ultrasound guidance two biopsies of the renal mass were obtained using a 14G Trucut needle.

Sections from the biopsies showed a necrotic tumour composed of masses of partly mineralized osteoid containing large, though degenerate, neoplastic cells. Although almost entirely necrotic, the tumour cytology was well demonstrated in Masson's trichrome preparations and the osteoid was readily identified using crossed polarizers. Architecturally the tissue was identical to the primary tumour and subsequent pulmonary metastases.

Discussion

Renal metastases are found at autopsy in 12% of cancer patients, although antemortem diagnosis is much less frequent. The most common primaries are lung, breast, gastrointestinal tract, melanoma and the opposite kidney. Renal metastasis from osteosarcoma is very rare with only eight previous clinical reports of osteosarcoma metastatic to the kidney (Marshall & Drake, 1950; Nelson et al, 1971; Goldstein et al, 1977; Nieh et al, 1977; Gilbert et al, 1983; Hallet et al, 1984; Ayres et al, 1985; Lockhart et al, 1989).

Although invasion of the intrarenal veins by metastases is a recognized postmortem finding (Willis, 1952), there has been only one report of an antemortem diagnosis in the radiological literature. This was in a patient with metastatic squamous cell carcinoma of the lung in whom the diagnosis was made angiographically (Shimkin et al, 1972). Metastatic invasion of the renal vein and cava diagnosed by CT and ultrasound has not been previously reported. It has been stated that such invasion favours a second primary (Pagani, 1983; Choyke et al, 1987; Pollack et al, 1987). It was therefore considered that the tumour in this case might represent a renal adenocarcinoma or a Wilms' tumour, and biopsy was performed.

The absence of calcification within the lesion in our patient did not help in the differential diagnosis because in four of the eight previously reported cases of metastatic renal osteosarcoma, calcification was not present including three in which CT was performed. Renal adenocarcinoma and Wilms' tumour may or may not calcify.

The major site of metastasis from osteosarcoma of the long bones is the lung, with pulmonary deposits present in 93–95% of patients at autopsy (McKenna et al, 1966; Jeffree et al, 1975). The lungs are the first clinical site of recurrence in 90% of those who develop metastases (Bacci et al, 1988). The majority of extrapulmonary metastases are skeletal. In all eight cases of renal metastasis reported previously, and in the case which we present, pulmonary metastases were present before or at the time of diagnosis of renal involvement.

Renal deposits from osteosarcoma have been diagnosed after disease-free intervals of up to 14 years (Hallet et al, 1984). Second primary neoplasms appear to be uncommon after osteosarcoma, and were seen in only one of 172 3-year survivors of childhood osteosarcoma described by Hawkins et al (1987) and in four of 271 patients described by Tucker et al (1984).

Recently, it has been suggested that there has been a change in the pattern of metastasis from osteosarcoma. In patients who have received adjuvant chemotherapy, the first clinical site of recurrence is more frequently extrapulmonary compared with earlier groups of patients who had not received chemotherapy (Giuliano et al, 1984). The basis for this change is not clear and it is not yet substantiated (Bacci et al, 1988). It may be that the increased availability of more sophisticated imaging techniques and more careful monitoring allow earlier detection of extrapulmonary metastases.

Acknowledgment

The authors wish to thank Dr J. A. W. Webb for her assistance in the preparation of this report.

References

AYRES, R., CURRY, N. S., GORDON, L. & BRADFORD, B. F., 1985. Renal metastases from osteogenic sarcoma. *Urologic Radiology*, *7* 39–41.

BACCI, G., AVELLA, M., PICCI, P., BRICCOLI, A., DALLARI, D. & CAMPANACCI, M., 1988. Metastatic patterns in osteosarcoma. *Tumori*, *74*, 421–427.

CHOYKE, P. L., WHITE, E. M., ZEMAN, R. K., JAFFE, M. H. & CLARK, L. R., 1987. Renal metastases: Clinicopathologic and radiologic correlation. *Radiology*, *162*, 359–363.

GILBERT, L. A., WEISS, M. A., GELFAND, M. J., HAWKINS, H. H., NISHIYAMA, H. & ARON, B. S., 1983. Detection of renal metastasis of osteosarcoma by bone scan. *Clinical Nuclear Medicine*, *8*, 325–326.

GIULIANO, A. E., FEIG, S. & EILBER, F. R., 1984. Changing metastatic patterns of osteosarcoma. *Cancer*, *54*, 2160–2164.

GOLDSTEIN, C., AMBOS, M. A. & BOSNIAK, M. A., 1977. Multiple ossified metastases to the kidney from osteogenic sarcoma. *American Journal of Roentgenology*, *128*, 148–149.

HALLET, M. B., WEISS, M. A., ARON, B. S. & BRACKEN, R. B., 1984. Secondary renal osteogenic sarcoma 14 years after primary therapy. *Journal of Urology*, *132*, 752–754.

HAWKINS, M. M., DRAPER, G. J. & KINGSTON, J. E. 1987. Incidence of second primary tumours among childhood cancer survivors. *British Journal of Cancer*, *56*, 339–347.

JEFFREE, G. M., PRICE, C. H. G. & SISSONS, H. A., 1975. The metastatic patterns of osteosarcoma. *British Journal of Cancer*, *32*, 87–107.

LOCKHART, S. K., COAN, J. D., JAFFE, N., EFTEKHARI, F., DAVID, C. & SHIRKHODA, A., 1989. Osteosarcoma metastatic to the kidney. *Clinical Imaging*, *13*, 154–156.

MARSHALL, D. F. & DRAKE, E. H., 1950. Transthoracic nephrectomy for metastatic osteogenic sarcoma of the kidney. *Journal of the Maine Medical Association*, *41*, 320–323.

MCKENNA, R. J., SCHWINN, C. P., SOONG, K. Y. & HIGINBOTHAM, N. L., 1966. Sarcomata of the osteogenic series. *Journal of Bone and Joint Surgery*, *48A*, 1–26.

NELSON, J. A., CLARK, R. E. & PALUBINSKAS, A. J., 1971. Osteogenic sarcoma with calcified renal metastasis. *British Journal of Radiology*, *44*, 802–804.

Nieh, P. T., Waltman, A. C. & Althausen, A. F., 1977. Therapeutic embolisation of symptomatic secondary renal tumours. *Journal of Urology*, *117*, 378–380.

Pagani, J. J., 1983. Solid renal mass in the cancer patient: Second primary renal cell carcinoma versus renal metastasis. *Journal of Computer Assisted Tomography*, *7*, 444–448.

Pollack, H. M., Banner, M. P. & Amendola, M. A., 1987. Other malignant neoplasms of the renal parenchyma. *Seminars in Roentgenology*, *XXII*, 260–274.

Shimkin, P. M., Buchignani, J. S. & Soloway, M. S., 1972. Blood borne metastases to the kidney. *Acta Radiologica (Diagnosis)*, *12*, 387–395.

Tucker, M. A., Meadows, A. T., Boice, J. D., Hoover, R. N. & Fraumeni, J. F., for the Late Effects Study Group, 1984. Cancer risk following treatment of childhood cancer. In *Radiation Carcinogenesis: Epidemiology and Biological Significance*, ed. by J. D. Boice and J. F. Fraumeni (Raven Press, New York), p. 213.

Willis, R. A., 1952. *Spread of Tumours in the Human Body*, 2nd ed. (Butterworth and Co., London), pp. 195–198.

1992, *The British Journal of Radiology*, *65*, 831–832

Case of the month

The third dimension

By A. D. King, MRCP and A. L. Hine, MRCP, FRCR

Department of Radiology, Central Middlesex Hospital, Acton Lane, London NW10 7NS, UK

(Received 10 May 1991, accepted 2 July 1991)

A 31-year-old woman presented with a 6 month history of pain in the neck and 2 months of swelling below the right ear. She had an 8 year history of rheumatoid arthritis for which treatment included prednisolone 5 mg twice a day and monthly gold injections. There was no history of trauma. Physical examination revealed a marked torticollis, pyrexia and a fluctuant mass below the right ear, but no neurological signs. Plain films were difficult to assess because of the torticollis and, therefore, computed tomography (CT) of the neck with bone windows and 3-dimensional (3D) reconstruction was performed.

What abnormalities are demonstrated and what are the two most likely causes of the appearance at the atlas and axis in this patient?

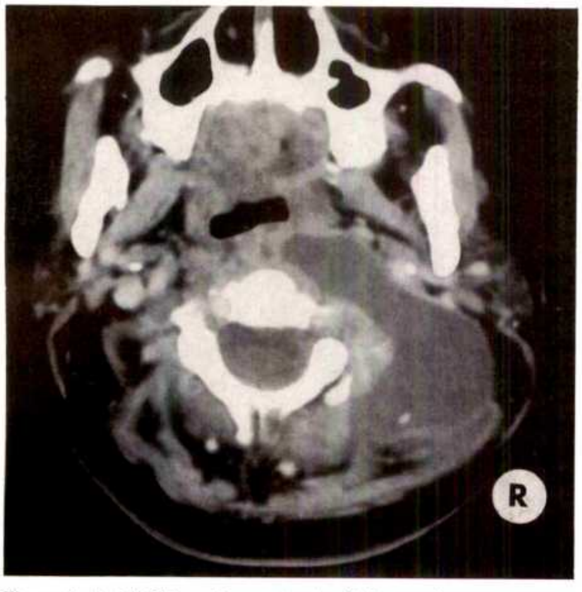

Figure 1. Axial CT section at level of C2 vertebra.

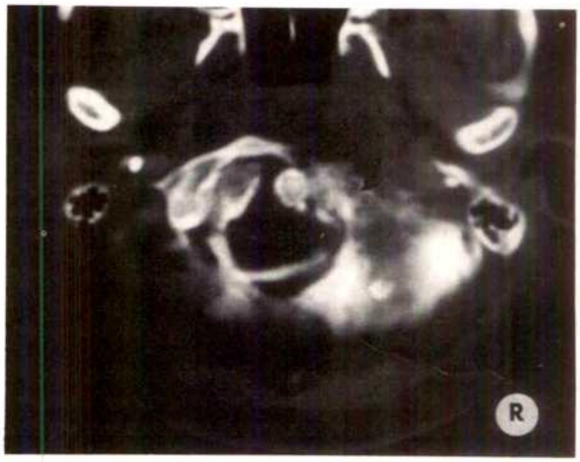

Figure 2. Axial CT bone window section of the atlanto-axial complex.

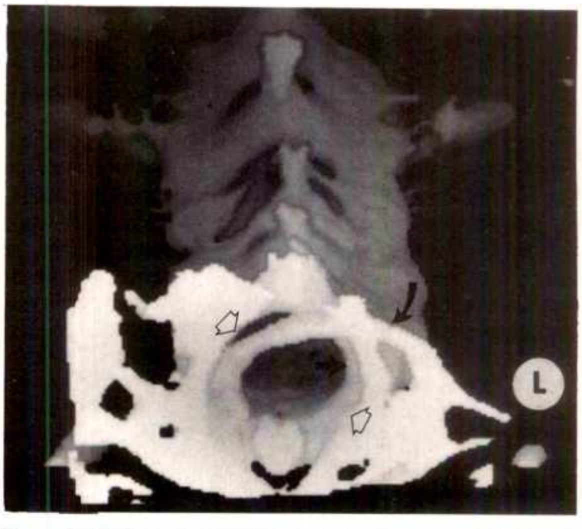

Figure 3. 3D CT reconstruction looking down the cervical spine from the rim of the foramen magnum (open arrows).

The CT scan (Fig. 1) demonstrates an extensive retropharyngeal fluid collection which extends posteriorly on the right to involve the atlas. The bone windows (Fig. 2) show destruction of the right lateral mass of the atlas which is associated with lateral movement of the atlas (curved arrow) to the left and dislocation of the left facet joints. There is also some rotation about the atlanto-axial joint, but no significant anterior subluxation. 3D reconstruction was found to be useful in demonstrating the relationship of the foramen magnum to the atlanto-axial complex. The 3D view (Fig. 3) was taken from the foramen magnum looking down the cervical spine and it demonstrates lateral dislocation of the atlas (curved arrow) to the left with the foramen magnum and remainder of the cervical spine remaining aligned (smaller arrow = axis).

This Indian patient had aspiration of the retropharyngeal abscess from which acid fast bacilli were identified and mycobacterium tuberculosis later cultured. The chest radiograph was normal. Treatment initially involved bed rest, antituberculous chemotherapy and a stiff collar, the latter two being continued for 18 months. Follow-up examination after 1 year demonstrated resolution of the retropharyngeal abscess and normal neurological examination but no change in the degree of bone destruction or subluxation.

Discussion

Tuberculosis of the atlanto-axial joint producing subluxation is rare but well documented (Wang, 1981; Fang et al, 1983; Dowd et al, 1986; Lifeso, 1987). Pain and stiffness in the neck are usually present and may occur before there are any X-ray changes (Shi-Dy, 1989). Constitutional symptoms, dysphagia and a retropharyngeal abscess are also common. Neurological findings range from normal to tetraparesis. Torticollis is well recognized, particularly in atlanto-axial rotation where the head is held in the "cock robin" position (Fielding & Hawkins, 1977).

Tuberculous involvement may be direct from a retropharyngeal abscess or from haematogenous spread. Usually, the pathological process at the atlanto-axial complex initially involves ligaments and bone erosions, particularly around the odontoid. This may lead to subluxation which is usually anterior. Rotatory subluxation, as seen to a minor degree in this case, has also been reported in tuberculosis (Fang et al, 1983), although it is more commonly seen following upper respiratory tract infections, trauma and rheumatoid arthritis (Shi-Dy, 1989). In the later stages of tuberculosis more extensive destruction of bone occurs. At the axis this tends to involve the body and the odontoid, the latter may either fracture just above the base or be completely destroyed. The atlas is usually eroded at the anterior arch or the lateral masses. This is demonstrated in the present case and has resulted in not only rotatory subluxation around an intact odontoid, but also lateral subluxation of the atlas as clearly seen on the 3D scan. This had caused considerable narrowing of the right side of the spinal canal.

Atlanto-axial disease may be caused by other pyogenic infections, trauma, malignancy or the arthritides. The major differential diagnosis of atlanto-axial disease in this patient is rheumatoid arthritis. This most commonly causes anterior subluxation as a result of erosions of the odontoid and may occur with an intact transverse ligament. The synovial process can also involve the lateral facet joints (Halla et al, 1989) producing lateral subluxation, lateral mass collapse and rotatory subluxation. However, in this patient the large tuberculous retropharyngeal abscess adjacent to the extensively destroyed lateral mass of the atlas suggested tuberculosis to be the primary cause, although rheumatoid arthritis may have contributed to the severity of the subluxation.

References

DOWD, C. F., SARTORIS, D. J., HAGHIGHI, P. & RESNICK, D., 1986. Case report 344. *Skeletal Radiology, 15*, 65–68.

FANG, D., LEONG, J. C. Y. & FANG, H. S. Y., 1983. Tuberculosis of the upper cervical spine. *Journal of Bone Joint Surgery, 65* (B), 47–50.

FIELDING, J. W. & HAWKINS, R. J., 1977. Atlanto-axial rotatory fixation. *Journal of Bone Joint Surgery, 59* (A), 37–44.

HALLA, J. T., HARDIN, J. G., VITEK, J. & ALARCON, G. S., 1989. Involvement of the cervical spine in rheumatoid arthritis. *Arthritis and Rheumatism, 32* (5), 652–659.

LIFESO, R., 1987. Atlanto-axial tuberculosis in adults. *Journal of Bone Joint Surgery, 69* (B), 183–187.

SHI-DY, 1989. Early diagnosis of atlanto-axial tuberculosis. *Chung-Hua-Wai-Ko-Tsa-Chih, 27* (2), 78–79, 124.

WANG, L. X., 1981. Peroral focal debridement for treatment of tuberculosis of the atlas and axis. *Chinese Journal of Orthopaedics, 1* (4), 207–209.

1992, *The British Journal of Radiology*, *65*, 833–835

Short communications

Radiation-induced hearing impairment—a pilot study in patients treated for malignant parotid tumours

By P. Kirkbride, MRCP, FRCR, F.-F. Liu, MD, FRCP(C) and M. K. Wax, MD, FRCS(C), FACS

Departments of Radiation Oncology and Surgical Oncology, Princess Margaret Hospital, Toronto, Ontario M4X 1K9, Canada

(*Received 27 August 1991, accepted 12 February 1992*)

Keywords: Radiotherapy, Hearing, Parotid tumours, Sensorineural hearing loss

There are few reports in the literature concerning the long-term effects of radiation on hearing. A recent paper reviewed eight studies which estimated the incidence of post-irradiation hearing loss at 0–54% (Talmi et al, 1989). The nature of the impairment is unclear, since both sensorineural and conductive deafness are reported. Most surveys have studied patients with cancer of the nasopharynx or paediatric tumours, the management of which require bilateral radiotherapy techniques, thus any deterioration in hearing that may occur after radiotherapy (XRT) owing to the lack of controls cannot be definitely ascribed to the effects of ionizing radiation.

Radical radiation of parotid tumours involves unilateral techniques which encompass the entire ear. The 10 year survival from parotid tumours is high—71% at the Princess Margaret Hospital (PMH) (Theriault & Fitzpatrick, 1986)—and, therefore, such patients are ideal candidates to be evaluated for the long-term effects of XRT on the ear. We recently reviewed 269 patients with malignant parotid tumours treated at PMH between 1970 and 1986 and noted that 10 patients out of 202 who received XRT reported unilateral hearing loss during follow-up. This number may be an underestimate of the true incidence because auditory function is not routinely discussed at routine follow-up visits.

Therefore, in an attempt to elucidate the magnitude of this problem, we contacted all patients in the above survey treated between 1978 and 1983, who therefore had at least 7 years of follow-up, and we requested their attendance for a formal audiometric evaluation.

Methods

59 patients who had received unilateral XRT for malignant parotid tumours at PMH between 1978 and 1981 and who were still alive and free of disease were contacted by letter. Patients were treated either using a homolateral wedge pair technique employing megavoltage photons or by a direct mixed beam of photons and electrons. Patients received doses ranging between 4500 cGy in 20 fractions over 4 weeks and 6000 cGy in 30 fractions over 6 weeks. The patients were invited to attend for an audiometric evaluation which included bilateral pure-tone audiograms, to assess bone and air conduction in both ears, and a consultation with an otolaryngologist which included a detailed history and a formal ear, nose and throat (ENT) examination. Any known predisposing factors such as trauma, infection or any structural abnormalites that could affect auditory function were noted. The audiograms were scrutinized for any evidence of hearing loss and those patients with 20 dB of hearing loss at 1 frequency, 15 dB at 2 frequencies or 10 dB at 3 frequencies on the treated side, compared with the unirradiated ear in the absence of a known predisposition, were classified as having a radiation induced loss.

A total of 19 patients replied and agreed to participate. In five cases, audiograms had already been carried out by the patients' own physicians and when possible these were obtained and evaluated.

Results

Of the 19 patients who participated 10 were male and nine were female. Their ages ranged from 40–83 years. All audiograms were performed at least 7 years after the patient received XRT. Two patients were excluded because they had undergone temporal bone surgery on the affected side subsequent to their XRT. Of the remaining 17 patients who were evaluable, 12 had normal audiograms and ear examinations. However, five (29%) patients were found to have significant unilateral hearing losses, mainly at high frequencies, for which no predisposing causes could be elucidated. These losses were regarded as being compatible with a radiation induced effect. Two examples are illustrated in Fig. 1. In all cases the deficit was predominantly sensorineural, with both air and bone conduction being affected equally. There was no evidence in any patient of a chronic secretory otitis media caused by XRT.

Two of the five patients with positive tests reported a noticeable loss of hearing in the affected ear, both of whom dated it to a time following their XRT. One patient thought the impairment began soon after her treatment, the other noted a gradual loss over a period of years. One of these patients was already using a hearing aid, the other is now also wearing one.

Of the five patients with unilateral loss, three received 5000 cGy in 20 fractions, one received 5500 cGy in 26 fractions and the remaining patient received 6000 cGy over 30 fractions.

Discussion

In this study, the incidence of significant unilateral hearing impairment of almost 30% is considerably greater than is conventionally expected. Although the incidence of idiopathic unilateral sensorineural hearing loss is not known, it has been estimated that the annual incidence of idiopathic hearing loss is 10.7 in 100 000 people (Byl, 1975). Although there have been previous published reports on radiation induced hearing loss, the data are confusing.

Whilst there are studies that have examined models (Keleman, 1963; Bohne et al, 1985; Tokimoto & Kanagawa,

---

Address reprints to Dr P. Kirkbride, Department of Radiation Oncology, Princess Margaret Hospital, 500 Sherbourne Street, Toronto, Ontario M4X 1K9, Canada.

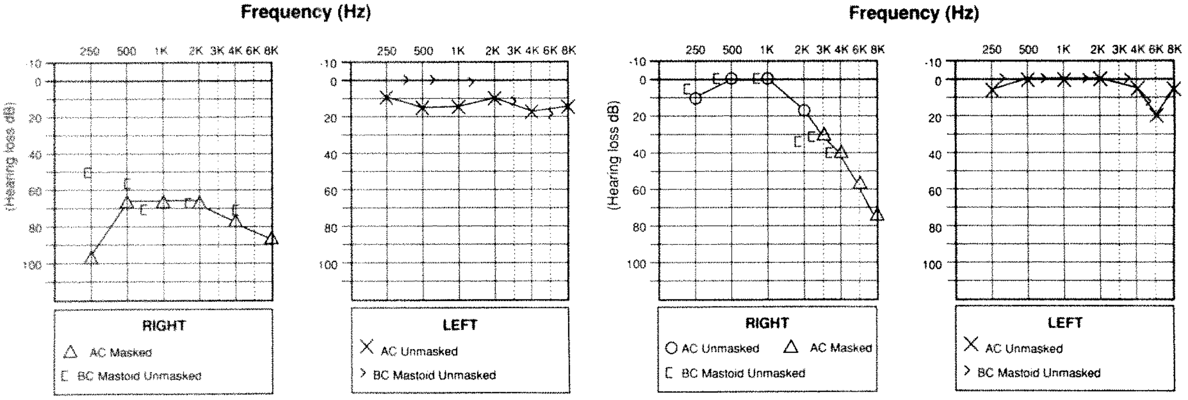

(a) (b)

Figure 1. Audiograms showing significant unilateral sensorineural hearing loss in patients after radiotherapy for parotid tumours. In (a) the patient received 5500 cGy in 26 fractions to the right parotid gland in 1978 and in (b) the patient received 5000 cGy in 20 fractions to the right parotid in 1980. In both cases there is a unilateral loss of bone and air conducted hearing implying sensorineural defects.

1985), few have concerned human subjects. Those that have examined human subjects only evaluated short-term losses, conductive or mixed losses, or lacked adequate controls. The first report of any effect of ionizing radiation upon auditory function in humans was in 1961 when Borsanyi et al reported an acute loss of hearing following XRT given to 14 patients with nasopharyngeal tumours. The defect was principally conductive in nature and ascribed to radiation otitis media. In 1965 Leach first described late hearing loss following XRT for head and neck cancers in 36% of patients studied and noted sensorineural as well as conductive hearing loss. Since then there have been sporadic reports on the subject in the literature, which were reviewed by Talmi et al in 1989. They noted that rates of sensorineural loss of 0–54% following XRT had been reported.

Recently, a prospective study on 22 patients receiving external beam XRT for nasopharyngeal cancer showed a significant loss of sensorineural hearing when pre- and post-treatment audiograms were compared (Grau et al, 1991). A latent period of at least 12 months before the onset of the detectable deficit was noted, as was a significant dose–response relationship. Other recent publications have included surveys of patients with parotid tumours similar to our own and, although one reported significant hearing deficit on the irradiated side in 15 of 28 patients (Singh & Slevin, 1991), the other failed to demonstrate any significant effect (Evans et al, 1988). It is clear that further work is needed to clarify the situation.

The use of unilateral XRT techniques has allowed us to use the contralateral ear as a control. In nasopharyngeal carcinoma both ears are irradiated and one would expect any treatment induced hearing loss to be bilateral. There are few known causes of unilateral sensorineural loss and an idiopathic aetiology is rare (vide supra). We have examined patients with parotid neoplasms which, by their nature, would rarely have any effect on the mechanism of hearing. Any loss that was detected could, therefore, be attributed to the treatment rather than the disease.

Although the aetiologies of most cases of unilateral hearing loss are not known, any such loss requires full otolaryngological work-up. It is difficult to discern from the literature what the true incidence of such pathology is, as many reports are from tertiary referral centres and deal with selected populations. The differential diagnosis may be subdivided into conductive losses, sensorineural losses and combined losses, each of which may have several different causes and many patients will have treatable pathology.

Most diagnoses can be made after a full history and physical examination, although ancillary testing consisting of auditory brainstem responses, computed tomography (CT) scanning and magnetic resonance imaging (MRI) may be useful. Of the 19 patients in our study who received unilateral XRT following complete work-up as outlined above, five had hearing loss confined to the irradiated side, after patients who had undergone subsequent temporal bone resection or other determinable causes of hearing loss were excluded.

Any conductive or mixed hearing loss should be detected by the otolaryngologist's examination. Furthermore, additional investigations would detect most known causes of sensorineural loss. In a retrospective study of this nature it is impossible to document a definite causal relationship between radiation and sensorineural hearing loss, but our results seem to imply this.

It appears that a relationship may exist between radiation exposure and sensorineural hearing loss. The mechanism of this is not known presently. Only a few studies have been done in which the temporal bone has been examined and these demonstrated damage to the Organ of Corti, with atrophy of the basilar membrane, spinal ligaments and stroma vascularis. Hair cell atrophy throughout was also noted (Gyorki & Pollock, 1960, Leach, 1965; Schaknecht & Carmody, 1966). Whether the damage is due to a direct effect of ionizing radiation upon the components of the inner ear by a secondary endarteritis obliterans of the stria vascularis will require further clarification.

It might be expected that patients with any form of hearing problem would be more willing to participate in this study than patients without any perceived hearing loss, although all except one patient in whom definite contact was made agreed to participate. Nevertheless, the number of patients with hearing impairment is such that we feel further investigation is warranted. We are, therefore, proposing to study prospectively all patients at this institution treated with XRT to areas close to the ear. In addition to patients with parotid malignancies, we also hope to include patients with benign parotid tumours, skin tumours and other lesions such as glomus tumours. We hope to be able to estimate the radiation dose to the inner ear of each individual patient, so that the incidence of radiation induced hearing loss could be confirmed. We also hope to be able to establish a dose–response relationship, as the inner ear doses may differ depending on the technique used and the dose prescription, both of which may vary with the type and location of the lesion.

The observations made in this study, if confirmed, may have considerable impact on radiotherapeutic practice. Although a possible interaction between radiation and Cis-platinum has led to proposals that treatment techniques for tumours such as nasopharyngeal carcinoma, which may require XRT to areas encompassing the inner ear in addition to platinum-based chemotherapy, be modified (Kirkbride & Plowman, 1989); yet there is little convincing evidence that radiation alone has significant deleterious effects on the normal function of the ear. However, if clinically significant hearing loss does occur in patients receiving XRT in the region of the inner ear, then some conventional techniques for treating tumours in certain parts of the head and neck may need to be reappraised.

References

BOHNE, B. A., MARKS, J. E. & GLASGOW, G. P., 1985. Delayed effects of ionising radiation on the ear. *Laryngoscope*, *86*, 598–602.

BORSANYI, S., BLANCHARD, C. L. & THORN, B., 1961. The effects of ionising radiation on the ear. *Annals of Otology, Rhinology and Laryngology*, *70*, 255–262.

BYL, F. M., 1975. Seventy six cases of presumed sudden hearing loss occurring in 1973: prognosis and incidence. *Laryngoscope*, *87* (5 pt 1), 817–825.

EVANS, R. A., LIU, K. C., AZHAR, T. & SYMONDS, R. P., 1988. Assessment of hearing impairment following radical megavoltage radiotherapy. *Journal of Laryngology and Otology and Supplements*, *102*, 588–589.

GRAU, C., MOLLER, K., OVERGAARD, M., OVERGAARD, J. & ELBROND, O., 1991. Sensori-neural hearing loss in patients treated with irradiation for nasopharyngeal carcinoma. *International Journal of Radiation Oncology Biology Physics*, *21*, 723–728.

GYORKI, J. & POLLOCK, F. J., 1960. Radiation necrosis of the ossicles. *Archives of Otolaryngology—Head and Neck Surgery*, *71*, 793–796.

KELEMAN, G., 1963. Radiation and the ear. *Acta Otolaryngologica*. Suppl. 184.

KIRKBRIDE, P. & PLOWMAN, P. N., 1989. Platinum chemotherapy, radiotherapy and the inner ear: implications for "standard" radiotherapy portals. *British Journal of Radiology*, *62*, 457–462.

LEACH, W., 1965. Irradiation of the ear. *Journal of Laryngology and Otology and Supplements*, *769*, 870–880.

SINGH, I. P. & SLEVIN, N. J., 1991. Late audiovestibular consequences of radical radiotherapy to the parotid. *Clinical Oncology*, *3*, 217–219.

SCHAKNECHT, H. F. & CARMODY, C. S., 1966. Radionecrosis of the temporal bone. *Laryngoscope*, *76*, 1416–1428.

TOKIMOTO, T. & KANAGAWA, K., 1985. Effects of X-ray irradiation on hearing in guinea pigs. *Acta Oto Laryngologica and Supplements*, *100*, 266–272.

THIERAULT, C. & FITZPATRICK, P. J., 1986. Malignant parotid tumors. *American Journal of Clinical Oncology*, *9*, 510–516.

TALMI, Y. P., FINKELSTEIN, Y. & ZOHAR, Y., 1989. Post-irradiation hearing loss. *Audiology*, *28*, 121–126.

Historical experiments predating commercially available computed tomography*

By S. Webb

Joint Department of Physics, Institute of Cancer Research and Royal Marsden Hospital, Downs Road, Sutton, Surrey SM2 5PT, UK

(Received 12 September 1991, accepted 8 October 1991)

Keywords: Computed tomography, History, Classical tomography

Abstract

Computed tomography (CT) was a revolution in radiology. Commercially available CT scanners appeared in 1972, a joint effort between the EMI Company, Atkinson Morley's Hospital, London and the Department of Health and Social Security (DHSS). The name of Sir Godfrey Hounsfield will always be associated with these developments.

Like most developments in science the breakthrough came by standing on the shoulders of giants and many experiments can, with the curious wisdom of hindsight, be considered precursors to CT. Gabriel Frank's patent in 1940 showed apparatus for back-projection CT and Takahashi developed equipment in the 1940s for reconstructing from a sinogram; in both cases using an optical "computer". A medical CT scanner was reportedly constructed in 1957 in Kiev. Transmission CT was performed by Kuhl in 1965. Cormack built an experimental scanner in 1963. Oldendorf identified what was needed for successful CT as early as 1960. Throughout the 1960s a host of independent workers were busy on the mathematical problems of reconstructing from projections with both medical scanning and non-medical applications in mind.

Experiments in early emission tomography influenced the development of CT. With imagination one can even see how close "classical" tomography, as started even before 1920, came to the realization of CT. The pioneering British radiographer Watson stands out from a galaxy of inventors.

The lecture at Radiology and Oncology '91 in Brighton was

---

*Based on a paper presented at Radiology and Oncology '91 in Brighton on 29 April 1991.

a thumbnail sketch of the origins of radiological CT. A fuller story is told elsewhere (Webb, 1990).

Classical tomography

Commercial CT is now nearly 20 years old. CT is regarded as a standard radiological procedure and it is perhaps hard for younger radiologists to imagine what diagnosis was like without it. Extraordinary efforts were made to visualize tomographic slices by "classical" or "blurring" tomography. Bocage (1921/22) was the first to patent the method of producing an image of a single plane in focus with others blurred out. In the 1920s a small number of people were working quite independently, with no knowledge of each other's work on putting these principles into practice. Those best known included Ziedses des Plantes, Pohl, Vallebona, Kieffer, Grossmann, Bartelink, Baese, Andrews and Mayer. By 1934 they began to find out about each other. Some rather personal writing emerged from these workers prosecuting their rights of invention! The detailed story is told in full elsewhere (Webb, 1990).

Pioneers of computed tomography

In 1940 a remarkable patent appeared from Gabriel Frank (1940) in which he explained the principles of CT. He drew equipment which would form the sinogram and apparatus for reconstructing by an optical backprojection. He forgot about the necessary convolution filter but had he built this device it would have nearly worked. Later, in Japan, in the mid 1940s Takahashi built equipment to make a tomographic slice by backprojection methods. He published an account of this work (Takahashi, 1957) when he became aware that his work was totally unknown in the West. In the year war broke out the British radiographer Watson (1937/1939) patented a method of axial transverse tomography, which using grazing incidence X rays was again not far short of achieving CT.

A group of Russian papers, recently "discovered" in the West and translated (Tetel'Baum et al, 1956, 1957; Korenblyum et al, 1985; Barrett et al, 1983) recounted that a CT scanner was built around 1957 for medical purposes in Kiev. The papers discussed the filtered backprojection method of reconstruction and have drawings, though not photographs, of equipment.

The beginnings of emission computed tomography (ECT) can be traced to the late 1950s. Among the pioneering workers was Kuhl who constructed (with Edwards) a series of machines for ECT. These comprised detectors which rotated and translated about the patient receiving radiation. On 14 May 1965 Kuhl replaced one set of detectors by a low-activity radiation source and made one of the first transmission CT scans of a live patient (Fig. 1). Cormack (1963, 1964) was also able to make such images on a table-top CT scanner, but when he published results in 1963 no one was really very interested. Oldendorf (1960/63) patented principles which related to CT and showed how combining rotation with translation movements could isolate signals from specific brain locations. His famous "Oldendorf's experiment" is often quoted as an early CT apparatus, but it did not reconstruct images. However, the patent described how such images could be made. Once again the time was not right and one of his approaches to an X-ray company led to one of the understatements of all time: "We cannot imagine a market for such an expensive apparatus which would do nothing but make a radiographic cross-section of a head".

Towards the end of the 1960s there were plenty of papers detailing reconstruction from projections in fields as diverse as radioastronomy, electron microscopy, and optics and radiology. Indeed it is well known that the basic principles were described as early as 1917 by Radon (1917).

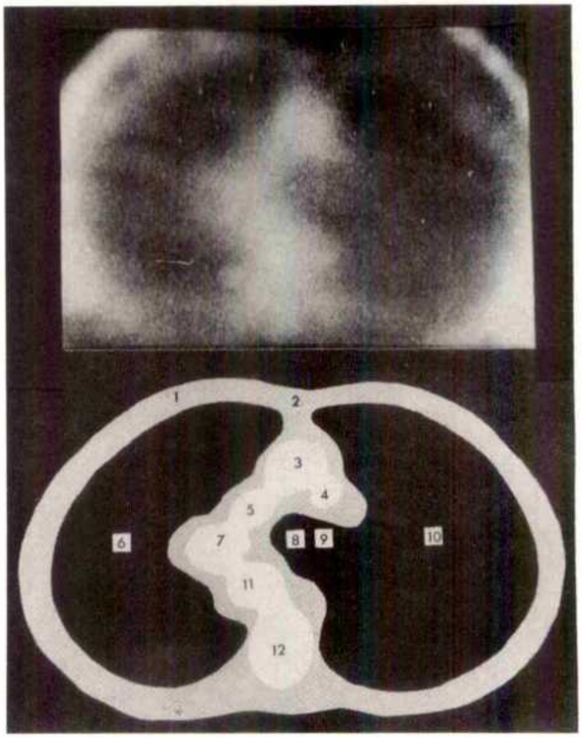

Figure 1. Probably the first transmission CT scan of a live human thorax, taken by Dr David Kuhl on 14 May 1965 with a modification of the "Kuhl Mark 2 scanner" (photograph courtesy of David Kuhl).

Commercial CT was a product of a unique collaboration between Hounsfield and the EMI Company, the DHSS and Atkinson Morley's Hospital, London. Work at EMI had started as early as 1967 (Hounsfield, 1968/72; Bull, 1981) and progressed through laboratory stages until a prototype could be installed at the hospital, taking the first image on 1 October 1971. The work was kept secret until the 1972 BIR Congress (New Scientist, 1972). Whatever view one forms of the precursors to CT, this collaboration achieved a practical technique of monumental significance in radiology.

The history of the development of CT seems a good example of the remarks of Sir Isaac Newton, who wrote "If I have seen a little further it is by standing on the shoulders of giants".

References

Barrett, H. H., Hawkins, W. G. & Joy, M. L. G., 1983. Historical note on computed tomography. *Radiology, 147* (1), 172.

Bocage, A. E. M., 1921/22. *Procèdè et Dispositifs de Radiographie sur Plaque en Mouvement.* French Patent 536464 (a translation to English by J. D. Bricker appeared in *Classic Descriptions in Diagnostic Röntgenology, 1964,* ed. by A. J. Bruwer (Charles C. Thomas, Springfield) pp. 1414–1417).

Bull, J., 1981. History of computed tomography. In *Radiology of the Skull and Brain: Technical Aspects of Computed Tomography,* ed. by T. H. Newton and D. G. Potts (C.V. Mosby Co, St Louis), pp. 3835–3849.

CORMACK, A. M., 1963. Representation of a function by its line integrals, with some radiological applications. *Journal of Applied Physics, 34,* 2722–2727.

—— 1964. Representation of a function by its line integrals, with some radiological applications 2. *Journal of Applied Physics, 35,* 2908–2913.

FRANK, G., 1940. *Verfahren zur Herstellung von Körperscnittbildern mittels Röntgenstrahlen.* German Patent 693374.

HOUNSFIELD, G. N., 1968/72. *A Method of and Apparatus for Examination of a Body by Radiation Such As X or Gamma Radiation.* UK Patent 1283915.

KORENBLYUM, B. I., TETEL'BAUM, S. I. & TYUTIN, A. A., 1958. About one scheme of tomography. *Izvestia Vyshikh Uchebnykh Zavedenii, Radiofizika, 13,* 151–157 (translated from the Russian by H. H. Barrett, Tucson, Arizona).

NEW SCIENTIST, 1972. *X-ray Diagnosis Peers Inside the Brain.* 27 April, 1972.

OLDENDORF, W. H., 1960/63. *Radiant Energy Apparatus for Investigating Selected Areas of the Interior of Objects Obscured by Dense Material.* US Patent 3106640.

RADON, J., 1917. Über die Bestimmung von Functionen durch ihre Integralwerte längs gewisser Mannigfaltigkeiten (On the determination of functions from their integrals along certain manifolds) *Ber Verb Sachs Akad Wiss Leipzig Math Phys Kl, 69,* 262–277.

TAKAHASHI, S., 1957. *Rotation Radiography.* Japan Society for the Promotion of Science.

TETEL'BAUM, S. I., 1956. About the problem of improvement of images obtained with the help of optical and analogue instruments. *Bulletin of Kiev Polytechnic Institute, 21,* 222.

—— 1957. About a method of obtaining volume images with the help of X-rays. *Bulletin of the Kiev Polytechnic Institute, 22,* 154–160 (Translated from the Russian by J. W. Boag, Institute of Cancer Research, 1987).

WATSON, W., 1937/39. *Improvements in or Relating to X-ray Apparatus.* British Patent 508381.

WEBB, S., 1990. *From the Watching of Shadows: the Origins of Radiological Tomography* (Adam Hilger, Bristol).

1992, *The British Journal of Radiology*, *65*, 838

Erratum — letter to the Editor

The Publisher apologizes to both the authors and the readers for an error which appeared in this letter which was published in the May 1992 issue of the *British Journal of Radiology*. The error occurred in the paragraph which covered the creatinine clearance values pre- and post-administration of contrast media. In the interests of clarity the letter has been reprinted.

The use of theophylline, an adenosine antagonist in the prevention of contrast media induced nephrotoxicity

THE EDITOR—SIR,

Impaired renal perfusion has been implicated in the pathogenesis of contrast media (CM) induced nephrotoxicity (El-Sayed et al, 1991). Animal and, more recently, clinical studies have suggested that endogenous adenosine may mediate the renal haemodynamic response to intravascular CM (Arend et al, 1987; Katholi et al, 1991). We have recently attempted to evaluate the protective effect of an adenosine antagonist, theophylline against CM-induced nephrotoxicity. 21 patients (14 males, 7 females; mean age 54 [±9.0] years) undergoing coronary angiography were randomly selected to receive either theophylline 125 mg tds or placebo. Treatment commenced a day before angiography and continued for 48 h afterwards. Iopramide 300 or Ioxaglate 320 was used for the examination. Creatinine clearances were measured before and 72 h after the examination. No significant change in the creatinine clearance was demonstrated following angiography in both groups. In the placebo group (n=8) the mean dose of CM was 131.9 (±34.3) mls, the creatinine clearance before the examination was 86.9 (±25.4) ml/min, and 86.5 (±45.1) ml/min 3 days post-examination. In the theophylline group (n=13) the mean CM dose was 146.5 (±25) mls, the mean creatinine clearance before the examination was 89.7 (±16.0) ml/min and 83 (±40.1) ml/min 3 days after. The mean serum theophylline concentration immediately before angiography was 5.8 (±3.1) mg/l. Three patients (mean age 52.7 [±5.3] years) in this study developed significant renal impairment with marked falls in creatinine clearance from 78 (±29) ml/min to 24.7 (±7.4) ml/min post-examination. Two of these patients were on theophylline. Two of the patients had received Ioxaglate 320 and one had received Iopramide 300. The mean CM dose was 133.3 (±2.4) mls. None of these patients was taking nephrotoxic drugs.

In this small series a protective effect of theophylline, with these doses, was not evident. However, the incidence of nephrotoxicity was 14% which is comparable with that reported in the literature (Burns, 1989). Larger studies using bigger doses of theophylline are required to reach a firm conclusion on the role of adenosine antagonists in preventing CM induced nephrotoxicity.

Yours etc.,

M. R. GANDHI
P. BROWN
C. A. J. ROMANOWSKI
S. K. MORCOS
*S. CAMPBELL
§A. M. EL NAHAS
#T. A. GRAY

Departments of Radiodiagnosis,
*Cardiology, §Renal Medicine
and #Chemical Pathology,
Northern General Hospital,
Herries Road,
Sheffield
S5 4LH, UK

(Received 22 January 1992, accepted 30 January 1992)

References

AREND, L. J., BAKRIS, G. L., BURNETT, J. C., MEGERIAN, C. & SPIELMAN, W. S., 1987. Role for intrarenal adenosine in the haemodynamic response to contrast media. *Journal of Laboratory and Clinical Medicine*, *110*, 406–411.

BURNS, A. S., 1989. Nephrotoxicity of contrast media. *Kidney International*, *36*, 730–740.

EL-SAYED, A., HAYLOR, J. L., EL-NAHAS, A. L., FALZANO, S. & MORCOS, S. K., 1991. Haemodynamic effect of water soluble contrast media on the isolated perfused rat kidney. *British Journal of Radiology*, *64*, 435–439.

KATHOLI, R. E., TAYLOR, G. J., MCCANN, W. P., WOODS, W. T., WOMACK, K. A. & MIKELL, F. L., 1991. Contrast medium nephrotoxicity in humans is mediated by intrarenal adenosine and related to osmotic load. *Radiology* (suppl), *181*, 285.

1992, *The British Journal of Radiology*, *65*, 839–844

Proceedings of the British Institute of Radiology

Progress in MRI: scientific and clinical developments in the United Kingdom

Abstracts of papers presented at an all day meeting organized by the BIR Diagnostic Methods Committee and supported by Premise Engineering and Schering Health Care Ltd, held at the Scientific Societies Lecture Theatre, New Burlington Place, London W1 on Monday 14 October 1991

UV generated spin-trapped hydrosyl free radicals imaged by proton-electron double-resonance imaging, by D. J. Lurie, I. Nicholson, J. McLay and J. R. Mallard
Observation of MT effects in human subjects—assesment of changes in tissue parameters and design of imaging sequences, by J. V. Hajnal, C. J. Baudouin, A. Oatridge and I. R. Young
Sequence choice for image segmentation via dual thresholding, by M. Paley, I. D. Wildinson, M. Hall-Craggs and K. Chong
Measurement of fetal growth *in utero* by magnetic resonance imaging, by N. Roberts, A. S. Garden, P. A. Martin and R. H. T. Edwards
In vitro evaluation of phase difference MR flow measurements, by P. Summers, M. J. Graves, M. Tarnawashi, M. G. Taylor and T. S. Padayachee
Visualization of complex blood flow patterns using computerized vector analysis of MR velocity maps, by P. J. Kilner, G. Z. Yang, R. H. Mohiaddin, D. N. Firmin, P. Burger and D. B. Longmore
Initial experience with abdominal MRA, by D. J. Lomas
Gadolinium-DTPA enhanced turboFLASH imaging in advanced aortic iliac disease—results and comparison with conventional angiography, by U. M. Sivananthan, J. Ridgway, K. Bann and M. R. Rees
Magnetic resonance velocity mapping in aortic coarctation: what should be measured, flow or velocity? by R. H. Mohiaddin, P. J. Kilner, R. S. O. Rees and D. B. Longmore
Magnetic resonance imaging in adult congenital heart disease—does it compare well with echocardiography and angiography? by U. M. Sivananthan, A. R. Essop, J. Ridgway, K. Bann and M. R. Rees
Analysis of ventricular diastolic regional wall velocity in patients with stable ischaemic heart disease, by S. Karwatowski, R. Underwood, R. Mohiaddin and D. Longmore
An evaluation of fast spin echo in patients with multiple sclerosis, by R. J. Gibson and J. V. Byrne
Combination of MRI, MRA and CT data for improved skull-base surgery planning, by G. P. Robinson, D. L. G. Hill, P. E. Summers, S. E. M. Green, J. E. Crossman, A. J. Strong, T. S. Padayachee, D. J. Hawkes and M. J. Gleeson
Knee imaging in arthritis, by G. Sherman
MRI of the carpal tunnel before and after treatment for carpal tunnel syndrome, by C. W. Heron, C. R. Smith, A. G. White and E. Paice
Rapid dynamic contrast-enhanced imaging of the liver and portal vein, by J. Ward, D. Martinex, A. G. Chalmers, J. Ridgway and P. J. Robinson
MRI study of rat liver tumours following high intensity ultrasound therapy, by I. J. Rowland, I. Rivens, I. Chen, G. H. Lebozer, D. J. Collins, G. R. ter Haar and M. O. Leach
Magnetic resonance imaging of the uterine cervix using intravaginal coils, by C. J. Baudouin, W. P. Soutter, A. Oatridge and D. J. Gilderdale

UV generated spin-trapped hydroxyl free radicals imaged by proton-electron double-resonance imaging

*D. J. Lurie, *I. Nicholson, J. McLay and J. R. Mallard
**Department of Biomedical Physics and Department of Medicine, University of Aberdeen, Foresterhill, Aberdeen AB9 2ZD, UK*

Endogenous free radicals such as hydroxyl (OH) are widely acknowledged to be implicated in many disease states. In this work we have used proton-electron double-resonance imaging (PEDRI) together with a technique called spin-trapping to image the hydroxyl free radicals formed by the action of UV light on phantoms containing hydrogen peroxide. In PEDRI a nuclear magnetic resonance (NMR) image is collected while the erythrocyte sedimentation rate (ESR) resonance of a free radical solute is irradiated. The result is an enhancement of the NMR signal in regions of the sample containing free radical; these regions then exhibit greater intensity in the final image. A quartz tube was filled with a solution of H_2O_2 and DMPO spin-trap. An ultraviolet source was placed 15 cm from the sample inside the NMR imager, which operated at 0.01 T. The ESR resonance of the free radical was irradiated at 223 MHz while a series of images was obtained. After switching on the UV source, the images showed that the free radical concentration increased to a peak of 200 μM and then decayed slowly. We have demonstrated that PEDRI can be used to image the production of endogenous type free radicals. This work paves the way for both biological and *in vivo* studies.

Observation of MT effects in human subjects—assessment of changes in tissue parameters and design of imaging sequences

J. V. Hajnal, C. J. Baudouin, A. Oatridge and I. R. Young
NMR Unit, Hammersmith Hospital, Du Cane Road, London W12 OHS, UK

Objective: To determine the changes in M_z and T_1 that can be induced by magnetization transfer (MT) and to use this information to develop imaging sequences that display increased and/or novel contrast. *Introduction:* The signals observed in *in vivo* ^{1}H nuclear magnetic resonance (NMR) derive from only a fraction of the protons in tissue. Many spins, for example those bound in large proteins and other macromolecules, remain invisible because of their short transverse relaxation tissues. Magnetization is constantly exchanged between the visible and invisible pools of spins (conventionally labelled A and B, respectively). In consequence both M_z and T_1 of the visible (A) pool are modified by the presence of the B pool. Selective saturation of the B pool, achieved using off resonance r.f. irradiation, results in changes in M_z and T_1 of the A pool due to magnetization transfer. *Methods:* We have measured NMR tissue parameters modified by MT in the brain and leg of normal volunteers by observing the changes in signal strength as a function of the duration for which the B pool is held at saturation. At 0.15 T the most striking change is to the T_1 of muscle, which is reduced by almost a factor of 3 to approximately 150 ms. Grey and white matter also show significant changes, whereas the signal from fat is virtually unaffected. *Sequence design:* The changes in both M_z and T_1 of some tissues suggest that a reappraisal of standard imaging sequences may yield startling new results. For example, at 0.15 T, the reduced T_1 of muscle is almost equal to that of fat, allowing both to be suppressed using short T_1 inversion recovery sequences. The result is a form of angiogram, which displays high contrast between blood and surrounding tissue.

Sequence choice for image segmentation via dual thresholding

M. Paley, I. D. Wilkinson, *M. Hall-Craggs and K. Chong
*Department of Medical Physics and Bioengineering, University College London and *Department of Radiology, Middlesex Hospital, Mortimer Street, London, UK*

A widespread clinical requirement is to measure volumes of tissue *in vivo* to monitor, for example, brain atrophy or increase in cerebrospinal fluid with age or disease process. The use of the multidimensional nature of magnetic resonance (MR) data to achieve better separation of tissues has recently been investigated by several groups. A two dimensional "scatter plot" can be produced by plotting pixel intensity from two images with different T_1 and T_2-weighting. Tissues of different type cluster into regions of the scatter plot and by selecting out these pixels it is possible to produce an image of a particular tissue. A segmentation scheme using dual thresholds acquired from the standard deviation of a histogram of values for each image pair of a tissue type has been investigated. A simulation programme has been developed which produces scatter plots for two arbitrary imaging sequences allowing user change of imaging parameters to optimize the separation of tissue data clusters. Measurements of volume of tissues in the brains of normal volunteers and patients with HIV infection are now underway using dual echo spin echo and dual echo STIR sequences.

Measurement of fetal growth *in utero* by magnetic resonance imaging

N. Roberts, A. S. Garden, P. A. Martin and R. H. T. Edwards
Magnetic Resonance Research Centre, University of Liverpool, PO Box 147, Liverpool L69 3BX, UK

Fast scan magnetic resonance (MR) imaging techniques (*e.g.* gradient recalled acquisition in the steady state (GRASS)) provide the possibility for "freezing" fetal motion and offer the opportunity for three dimensional measurements of fetal development to be made *in utero*. Quantitation by automatic image analysis is made difficult in view of the variety of features (*e.g.* head, thorax, abdomen and limbs) that need to be segmented. However, unbiased estimates of fetal, and fetal organvolume can be obtained manually in 3–4 min using the ancient stereological method known as the Cavalieri Principle. Of the order of 10–15 points of intersection between a systematically arranged, but randomly orientated, sampling grid must be obtained with the feature of interest in each image. Our trials have shown that wth five or more sections through the fetus, or organ, a coefficient of error (CE) of better than 10% can be obtained. If 10 sections are obtained the CE can be reduced to 2% and of the order of 20 sections are required for an accuracy of 1%. A 27-year-old female who had developed complications during an earlier pregnancy was imaged on five occasions between weeks 35 and 40 of a second normal pregnancy. Linear regression analysis of the stereological data revealed that fetal volume increased by 33 ± 3 cm^3 per day, while the volume of the fetal liver increased by 2.3 ± 0.3 cm^3 per day during this time. Measurements made in three dimensions are likely to be far more reliable and sensitive indicators of change than those currently made in two dimensions from ultrasound images. The prospect of "real-time" MR imaging adds to our expectation for these studies and it is possible that in the future fetal growth will be studied in detail via the use of an MR imaging system in the antenatal department.

In vitro evaluation of phase difference MR flow measurements

P. Summers, M. J. Graves, M. Tarnawaski, M. G. Taylor and T. S. Padayachee
MR Flow Group, Department of Radiological Services, UMDS, Guy's Hospital, London SE1 9RT, UK

Continuous and ECG-gated gradient-echo phase contrast MR flow measurements were compared with Doppler ultrasound (US) and electromagnetic (EM) flowmetry for pulsatile flow in a phantom. We also examined the effects of a number of imaging parameters on the accuracy of gated measurements. The measurement techniques were compared for flow in large and small diameter (19 mm id, 6.5 mm id, respectively) tubes generated by a pulsatile pump at rates between 1.0 and 6.0 l/min. Gated magnetic resonance (MR) measurements were in excellent agreement with those obtained by US and EM. When compared with timed collection, R2 values of 1.00, 0.98 and 0.99 respectively were obtained for the large tube; while for the smaller tube the R2 values were 0.96, 0.98 and 1.00. The continuous acquisition flow measurements were found to depend upon the systolic period and pulsatility index (PI) of the flow. Agreement with timed collection (systole $\simeq$ 50%, PI $\simeq$ 3) yielded R2 values of 0.99 in the large tube and 0.84 in the smaller tube. The dependence of measurement accuracy on echo time (TE), slice thickness (SLT), in-plane pixel size (PIX), percent of phase encoding acquired (PACQ) r.f. flip angle (FLIP), velocity sensitivity (VS), slice orientation (SLO) and slice position (SLP) was investigated. Variations in TE, FLIP and VS were found to have minimal effect on the measured flows. Variations in SLT were noted to have variable effects on the measurement, whilst changes in PIX, PACQ and SLP demonstrated a more linear behaviour. Changes in SLO revealed effects related to the implemented gradient sequence. These preliminary results suggest that ECG-gated techniques are well suited to pulsatile flows whereas continuous acquisition may be employed for "non-pulsatile" or slowly varying flows. In either application, the limitations and effects of imaging parameters must also be considered.

Visualization of complex blood flow patterns using computerized vector analysis of MR velocity maps

P. J. Kilner, G. Z. Yang, R. H. Mohiaddin, D. N. Firmin, P. Burger and D. B. Longmore
Magnetic Resonance Unit, Royal Brompton National Heart Hospital, London and Department of Computing, Imperial College, London, UK

Objectives: Magnetic resonance (MR) velocity mapping is capable of providing multidirectional velocity data in the heart and blood vessels, but conventional grey-scale MR velocity maps are unsuitable for representation of complex, multidirectional flow. Therefore, we set out to develop software to render normal and abnormal blood velocity patterns in a graphic form immediately recognizable as flow. *Methods:* We performed multidirectional cine MR phase shift velocity mapping using a 0.5 Tesla Picker machine in 10 healthy volunteers and nine patients. Diagnoses: atrial septal defect (2); ventricular septal defect (1); pulmonary stenosis (1) and aorto-iliac atheroma (5). Velocity information in the flow field was then represented by multiple computer generated "particles" whose length, direction and movement corresponded to velocities in the chosen image plane. *Results:* Computer graphic representation of MR velocity data as moving "particles" allowed immediate recognition of patterns of secondary flow. The technique reveals coherent, vortical patterns of blood movement during normal right atrial and left ventricular filling and during systolic ejection into the aortic root. In septal defects and stenoses, jet formation was seen to be associated with varied patterns of secondary parajet flow reversal.

Initial experience with abdominal MRA

D. J. Lomas
Department of Radiology, University of Cambridge School of Medicine, Addenbrooke's Hospital, Hills Road, Cambridge CB2 2QQ, UK

The use of a flow compensated gradient echo sequence (MAST FAST) for breath holding abdominal magnetic resonance angiography is described. Image artefacts including ghostin and signal losses from turbulence are discussed and demonstrated in volunteers. Examples of potential clinical applications are demonstrated in patients being assessed for liver and small bowel transplantation, in a patient with suspected Budd Chiari syndrome and in a patient with renal malignancy.

Gadolinium-DTPA enhanced turboFLASH imaging in advanced aortic ilac disease—results and comparison with conventional angiography

U. M. Sivananthan, *J. Ridgway, *K. Bann and M. R. Rees
*Department of Cardiac Radiology and Cardiac Research, Killingbeck Hospital, York Road, Leeds and *MRI Unit, St James' University Hospital, Leeds, UK*

Fast MR imaging has matured in the last few years and is now of established value for several aspects of clinical magnetic resonance (MR) imaging. Preliminary studies suggest that MR angiography may have a useful role in atherosclerotic aortoiliac disease. We have employed 2-D turboFLASH gradient echo sequences with Gadolinium-DTPA enhancement to image advanced aortoiliac disease in 12 patients. The MR images were obtained on a Siemens Magnatom imaging system with a 1 Tesla superconducting magnet. A sagittal localizer was initially obtained and preliminary unenhanced coronal images—using the same turboFLASH sequences were acquired to determine the ideal scanning planes of the aorta and the iliac arteries. Once this was established three sets of 10 5 mm thick slices were acquired simultaneously while the patient was breath holding, 10 s after bolus intravenous Gadolinium-DTPA. A 400 mm field of view with 256×256 acquisition matrix was used. TR of approximately 100 ms amd a fixed TE of 4 ms were employed. The images were then post-processed by using the maximum intensity projection (MIP) algorithm to produce projection images. Satisfactory results were achieved in all our patients. The total time per patient was less than 10 min. The images compared well with conventional angiography in the eight patients in whom it was performed. We feel that this imaging sequence promises to be an alternative non-invasive method to conventional angiography for evaluating advanced aortoiliac disease. We will present the technique, advantages and limitations of this promising new sequence.

Magnetic resonance velocity mapping in aortic coarctation: what should be measured, flow or velocity?

R. H. Mohiaddin, P. J. Kilner, R. S. O. Rees and D. B. Longmore
The Royal Brompton National Heart and Lung Hospital, London, UK

A non-invasive method for evaluation of aortic coarctation is highly desirable in the pre- and post-operative management of patients. A common way of assessing the haemodynamic significance of coarctation is to calculate pressure gradient across the diseased segment from peak velocity measurement. However, there are technical and physiological problems with this approach. In this study we used magnetic resonance imaging with velocity mapping (TE 3.6 ms) to characterize flow in the thoracic aorta of 10 patients with aortic coarctation and 10 healthy volunteers. Flow waveforms were studied in an oblique plane perpendicular to the ascending aorta and to the descending thoracic aorta 1 cm distal to the coarcation segment. Instantaneous flow was calculated from mean velocity and the cross sectional area of the vessel. The cardiac output and the flow curves in the ascending aorta differed significantly: peak flow rate (patients 10.4 ± 3.4 l/min, controls 17.8 ± 2.7 l/min, $p < 0.001$); mean flow rate (patients 2.6 ± 0.9 l/min, controls 3.5 ± 0.7 l/min $p < 00.5$) and the ratio of descending to ascending aortic flow (patients 0.47 ± 0.18, controls 0.62 ± 0.07, $p < 00.5$). These differences are most likely related to the resistance imposed on flow by the coarctation and could be an additional index for monitoring patients with coarctation of the aorta.

Magnetic resonance imaging in adult congenital heart disease—does it compare well with echocardiography and angiography?

U. M. Sivananthan, A. R. Essop, *J. Ridgway, *K. Bann and M. R. Rees
*Department of Cardiac Radiology and Cardiac Research, Killingbeck Hospital, York Road, Leeds and *MRI Unit, St James' University Hospital, Beckett Street, Leeds*

The purpose of this study is to investigate the adequacy of magnetic resonance imaging (MRI) in the display of anatomy and flow in adult congenial heart disease and to compare the results with that of echocardiography and conventional angiography. *Materials and methods:* 25 adult patients with congenital heart disease were studied using a 1 Tesla Siemens Magnatom scanner. Gated spin echo images in three orthogonal as well as selected oblique planes and gradient cine angiography measurements were obtained. The results were compared with those of echoradiography and angiography in cases where they were performed. Two major groups of patients studied included coarctations of the aorta and patients who had right ventricular outflow obstruction (nine in each group). MR images were adequated in the post-operative cases and the need for angiography was avoided in the patients with coarctation and in the four other patients who had corrections of the right ventricular outflow tract obstructions. In total 10 additional lesions were demonstrated. MRI also gave significant additional information of the abdominal situs, and the anatomy of the major vessels. Four Blalock shunts were studied which could not be catheterized. MR images were satisfactory and, in addition, flow and anatomical information of the pulmonary vasculature were obtained. We will present the technique and limitations of the MR Imaging. In conclusion, MR should at least be considered as a first line investigation in adult congenital heart disease.

Analysis of ventricular diastolic regional wall velocity in patients with stable ischaemic heart disease

S. Karwatowski, R. Underwood, R. Mohiaddin and D. Longmore
Magnetic Resonance Unit, National Heart and Lung Institute, London, UK

Global diastolic ventricular function can be studied by a number of techniques, but regional function is more difficult to quantify. Since ischaemic heart disease produces regional effects we used magnetic resonance (MR) velocity mapping to examine regional left ventricular wall motion. We studied 11 patients with ischaemic heart disease (IHD) and 14 control subjects. All underwent an MRI scan using a field even echo rephasing protocol to measure the velocity of the myocardium in the long axis of the heart. The plane selected was 1 cm below the mitral annulus at end systole. The last B-blocker dose was 72 h before the study, short acting preparations were withheld on the day of the study. The myocardium was divided into six segments for regional analysis, temporal resolution was 27–35 ms. The peak diastolic velocity (PDV) was identified, at the same time interval measurements of minimum diastolic velocity (MDV) and range of diastolic velocity (RDV) expressed as a percentage of the peak velocity were compared between the two groups. The table below shows the means of these values, standard deviations are given in brackets. Thus magnetic resonance velocity mapping of diastolic ventricular wall velocities can detect regional wall motion abnormalities in patients with IHD.

	PDV	MDV	RDV
Control	136 (39)	76 (27)	44 (9)
IHD	80 (29)	9 (27)	84 (24)

All values were signficantly different at the 0.001 level.

An evaluation of fast spin echo patients with multiple sclerosis

R. J. Gibson and J. V. Byrne
Department of Neuroradiology, Radcliffe Infirmary, Oxford, UK

A comparison of conventional spin echo (SE) and fast spin echo (FSE) sequences was made based on the brain scans of ten patients with multiple sclerosis (MS). FSE is a derivative of the rapid acquisition relaxation enhanced (RARE) fast imaging technique, in which multiple echoes are acquired per time to repeat (TR) interval. All scans were performed in a Signa Advantage 1.5 T scanner. Two similar dual echo protocols were used, where scan plane, slice thickness and gap, field of view, matrix size and number of excitations were standardized. The study time for FSE imaging was 30% of the time needed for conventional SE imaging. Comparisons were made of the numbers of plaques seen on each technique. The MR studies were reviewed in random order by two radiologists who were blinded to the technique used. No statistical difference was found between the numbers of lesions demonstrated, nor was there significant interobserver error for either technique. There is a clear advantage in the new technique in terms of scanning time and patient throughput. The potential disadvantages are an increase in acoustic noise within the bore of the magnet and a theoretical heating effect because of the increased radiofrequency deposition. Our experience has shown that the fast spin echo technique is a rapid and reliable method for detecting plaques in the brains of patients with MS.

Combination of MRI, MRA and CT data data for improved skull-base surgery planning

G. P. Robinson, D. L. G. Hill, P. E. Summers, S. E. M. Green, J. E. Crossman, A. J. Strong, T. S. Padayachee, D. J. Hawkes and M. J. Gleeson
Departments of Neurology, Radiological Sciences and Surgery, UMDS—Guy's Hospital, London SE1 9RT, UK

In preparation for skull-base surgery, patients at this Institution undergo magnetic resonance imaging (MRI) for pathology detail and computed tomography (CT) scans for bone detail during surgical planning. Conventionally, the images are printed onto film, and displayed side-by-side on a light box. We present an improved display method which involves combining the MRI and CT images and incorporating vascular information from MRA. The surgeon can interact with this composite patient representation on an imaging workstation using volumetric display techniques. Images are acquired using normal clinical protocols, and are transferred digitally to Sun workstations for processing. The MRI, CT and MRA images are registered to an accuracy of within 2 mm by identifying between 6 and 12 equivalent point-like structures in the three modalities. The image data sets are then transformed to a common co-ordinate frame by trilinear interpolation. Bone is segmented from the CT by thresholding, the tumour is segmented from the MRI by thresholding and masking of fat signal and blood vessels are segmented from the MRA by thresholding and application of morphological operators. The segmented image information is combined using image algebra to produce a composite volume data-set. Volume rendering is performed using the Sunvision software package (on loan from Sun Microsystems) which allows interactive control of tissue opacities, volume orientation and cut surface positioning. A prospective clinical trial of the technique is in progress. Initial results will be presented.

Knee imaging in arthritis

G. Sherman
Department of Physics, University of Exeter, Stocker Road, Exeter EX4 4QL, UK

A new targetted magnetic resonance imaging (MRI) system based on a 560 mm diameter 0.5 T superconducting magnet (overall length 1 m) has been developed. The system uses an actively screened gradient set to make maximum use of the available space, resulting in a clear access of 500 mm. The system was designed for high-resolution imaging of the knee (for arthritis research). However, it has proved excellent for imaging the brain and we are investigating possibilities for imaging the cervical and lumbar spine. All this work requires specialized radiofrequency coil design. To this end the brain images were obtained using a standard birdcage coil. For high-resolution knee imaging a coil that can be fitted to patients (with arthritis) outside the magnet is required. This needs to be in two halves so that optimum filling factor can be obtained—this could not be achieved if the foot has to pass through the coil to locate the knee. An inductively coupled split birdcage coil has been designed for this purpose. In this paper a brief outline of the system will be given and particular attention will be paid to the design and implementation of the inductively coupled knee coil.

MRI of the carpal tunnel before and after treatment for carpal tunnel syndrome

*C. W. Heron, C. R. Smith, A. G. White and E. Paice
**Department of Radiology, St George's Hospital, London SW17 and Rheumatology Department, Whittington Hospital, London N19, UK*

The cause and pathogenesis of carpal tunnel syndrome (CTS) are often undetermined and diagnosis is based on clinical findings and electromyography (EMG). Patients may be treated with either local injections of steroids or surgical decompression. The aim of this study was to examine two groups of patients undergoing one or other type of therapy and to compare the magnetic resonance imaging (MRI) appearances on pre- and post-treatment scans with the clinical outcome and the EMG findings. Scans of both wrists were obtained using spin echo and gradient echo pulse sequences. Of the 12 patients examined to date, the carpal tunnel was decompressed surgically in seven cases and five patients received steroid injections. Pre-treatment MRI showed enlarged flexor tendon sheaths in 10 hands, palmar bowing of the flexor retinaculum in seven, swelling of the median nerve in five and flattening in two. Post-surgery MRI confirmed disruption of the flexor retinaculum in all patients with a satisfactory response but one patient who made a poor recovery was shown to have a fibrous nodule pressing on the nerve. A poor clinical response was seen in three conservatively treated patients who had persistent abnormalities on the post-treatment scan whereas the two patients with normal scans responded well.

Rapid dynamic contrast-enhanced imaging of the liver and portal vein

J. Ward, D. Martinez, A. G. Chalmers, J. Ridgway and P. J. Robinson
MRI Unit, St James' University Hospital, Beckett Street, Leeds LS9 7TF, UK

The purpose of this study was firstly to show the diagnostic value of a rapid acquisition multislice sequence (TurboFLASH) during bolus injection of Gd-DTPA by comparing it with the pulse sequences currently used for abdominal studies and secondly to develop improved scanning protocols for the liver. Patients were referred for upper abdominal studies including portal vein assessment. Each patient was imaged in the coronal plane using a multislice TurboFLASH sequence (TR = 100, TE = 4) acquired during a breath hold period of 19 s. The short echo time allows up to 11 slices of 5 mm thickness to be acquired simultaneously. Images were obtained during and after bolus administration of Gd-DTPA. The slices from each acquisition were combined using a maximum intensity projection algorithm to include all the vessels on a single image. Initially each patient was also scanned using a conventional axial T_2-weighted spin echo sequence (TR 2000, TE = 45/90) and a coronal T_1-weighted spin echo sequence (TR 450, TE = 15). Each sequence was compared by two independent viewers for lesion conspicuity and number of lesions, lesion characterization, vessel patency and local spread to adjacent structures. The clarity of the demonstration of vessel anatomy was also scored for all sequences. Analysis of the first 10 patients enabled us to identify those sequences which provided the least information. The protocol was refined to exclude these sequences and further patients have been studied with the revised protocol. Lesion conspicuity was significantly improved on the post-contrast images. Patency of the main portal vein was better assessed with the dynamic sequence and MIP whilst patency of the right and left portal veins was equally well assessed on the dynamic images, T_2-weighted SE images and MIP images. The anatomy of the main portal vein was better seen on the MIP images. All other vessels were equally well seen on both T_2-weighted SE sequences and the dynamic sequences.

MRI study of rat liver tumours following high intensity ultrasound therapy

I. J. Rowland, I. Rivens, L. Chen, G. H. Lebozer, D. J. Collins, G. R. ter Haar and M. O. Leach
CRC Clinical Magnetic Resonance Research Group and Joint Department of Physics, Institute of Cancer Research and Royal Marsden Hospital, Downs Road, Sutton, Surrey SM2 5PT, UK

Magnetic resonance imaging (MRI) has been used to investigate the physiological and morphological changes in both tumour bearing and normal liver lobes of rats treated invasively using high intensity focused beam ultrasound surgery. The potentially non-invasive, high intensity, focused beam ultrasound therapy is currently being developed as a novel treatment for discrete liver metastases. HSN tumours were grown in the middle hepatic lobes of female CBH rats and were imaged, before and after treatment, using a head coil in a Siemens Magnetom 1.5 T whole body imaging system. Proton density MR images were obtained using a FLASH gradient echo sequence (TR = 200 ms, TE = 11 ms, F1 = 70°) together with a T_1 and T_2-weighted sequences. Images were obtained before and after the intravenous administration of contrast agent. Before ultrasound treatment and using the FLASH sequence, the tumours appeared hypointense with respect to normal rat liver. Immediately following treatment, the damaged region appeared hyperintense with respect to the normal liver. With time, the treated region appeared homogenous, whilst the periphery of treated normal liver appeared as a hypointense rim and enhanced preferentially following injection of Gd-DTPA. A distinct boundary region between normal and damaged liver was confirmed by histology.

Magnetic resonance imaging of the uterine cervix using intravaginal coils

C. J. Baudouin, W. P. Soutter, A. Oatridge and D. J. Gilderdale
NMR Unit, Hammersmith Hospital, Du Cane Road, London W12 OHS, UK

Objective: The aim of the study was to assess the feasibility of using intravaginal receive coils to obtain high resolution images of the uterine cervix. *Methods and patients:* Intravaginal coils were designed for use at 0.15 and 1.6 Tesla. Solenoid and saddle coils mounted on cylindrical Delryn formers were used. Both passive and active decoupling circuits were employed. T_1- and T_2-weighted spin echo and STIR sequences were used in transverse, sagittal and oblique planes. 15 patients were studied, 12 had no known abnormality of the cervix, one had a cervical polyp and two had cervical intra-epithelial neoplasia Grade III. *Results:* Patient tolerance of the procedure was excellent. Good zonal anatomy of the cervix could be identified on all three sequences used but useful information was still seen from the fringing field, *i.e.* the parametrium and vagina. Benign abnormalities including Naboithian follicle and cervical polyp were visualized. In one patient with CIN III the endocervical canal appeared irregular and thickened but marked variation in normal appearances was seen. *Conclusion:* Detailed images of the cervix can be obtained using intravaginal coils. This technique may be useful to assess local extent of early cervical carcinoma.

The professional difference

The Clinac® 600C

Take the concept:
Its simplicity is still unmatched. Its beam stability gains new relevance when treating exceptionally small fields used in stereotactic radiosurgery.

Take the isocenter:
It's a careful balance between working height and positioning space.

Take the cost:
Low running costs, no source replacements, higher throughput make it the ideal workhorse.

Varian International AG
Medical Equipment
Kollerstrasse 38, CH-6300 Zug, Switzerland
Phone (042) 44 88 44

Varian – the Predictable Future

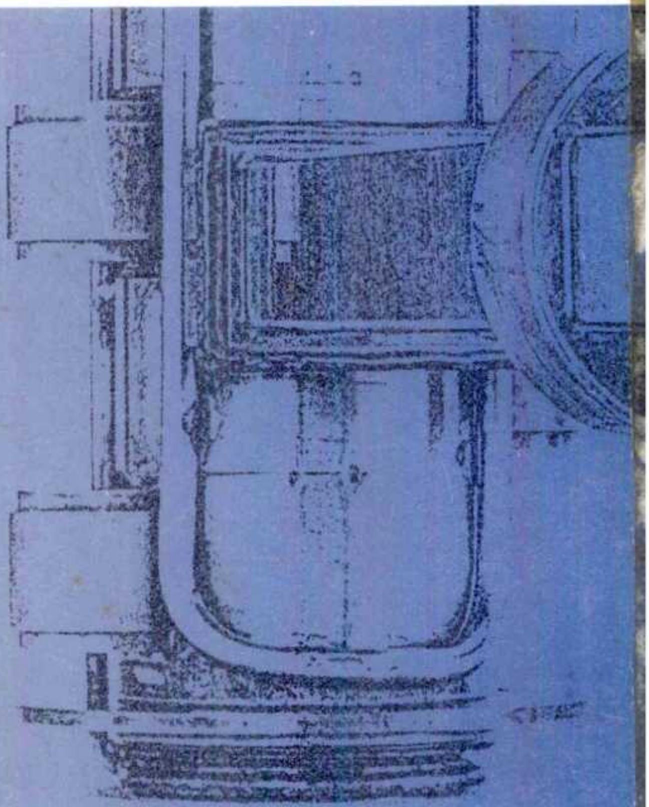

varian